Imaging for physicists

Welcome and introduction

Tufve Nyholm

Evaluation - Certificates

Evaluation
Very important for us to be able to contiously imporve and adapt the course to the needs

Evaluation forms: Sent to you from Survey Monkey (If any problem contact Miika)

Certificates
Will be handed out by Miika at the last day

Case assignments

A list of topics has been distributed

Group size: Ideal: 4-5 people
Study the topic and give a short presentation (x min) on Thursday

Use the suggested literature as a starting point – much more information can be found on the web

Presentation: Not only a literature review - the focus should be on own reflections.

Social program

Course dinner: Today (Sunday). We leave from Lobby at 19.00
Dinner starts at 20.00 - El Pimpi
Free afternoon: Tuesday

Imaging for physicists

Introduction

Tufve Nyholm

UMEÅ UNIVERSITET

ESTRO School

Imaging for physicists

- The role of imaging in radiotherapy
- The goals, learning objectives and content of the course

Pre-treatment imaging

CT

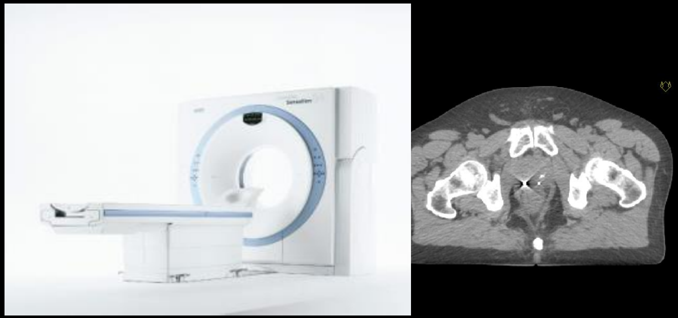

PET

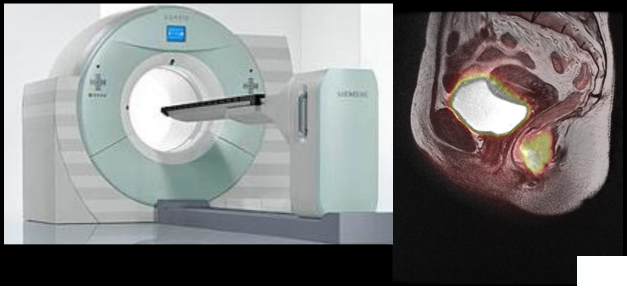

MR

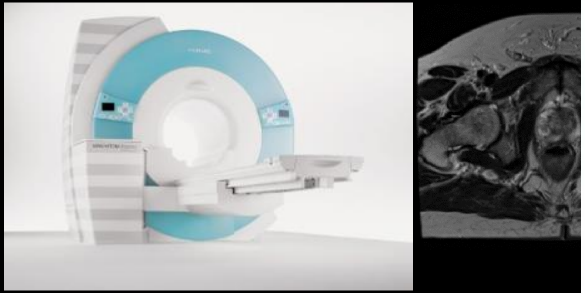

1977

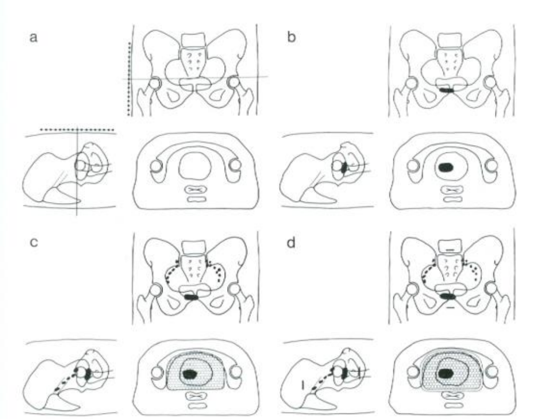

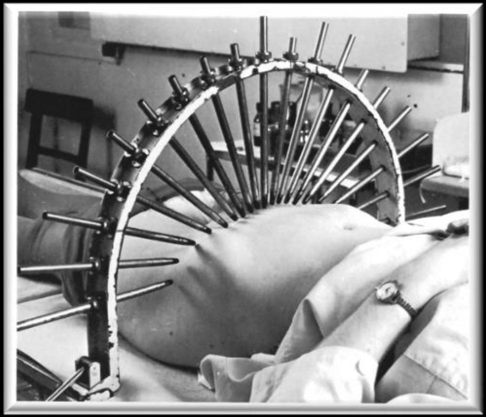

Planning

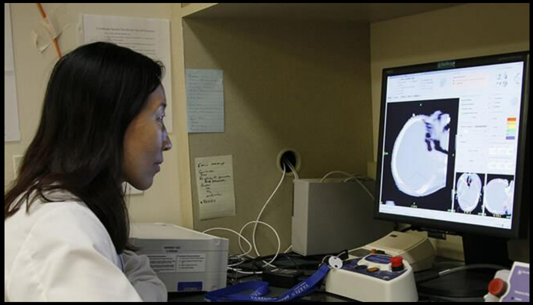

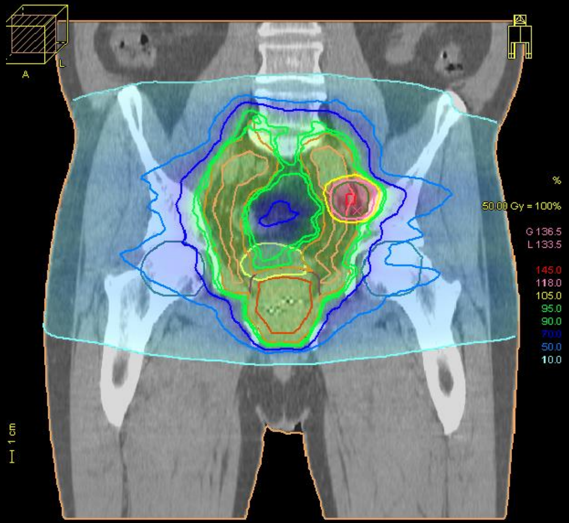
A
L
%
50.00 Gy = 100%
G 136.5
L 133.5
145.0
118.0
105.0
95.0
90.0
70.0
50.0
10.0
1 cm

1975

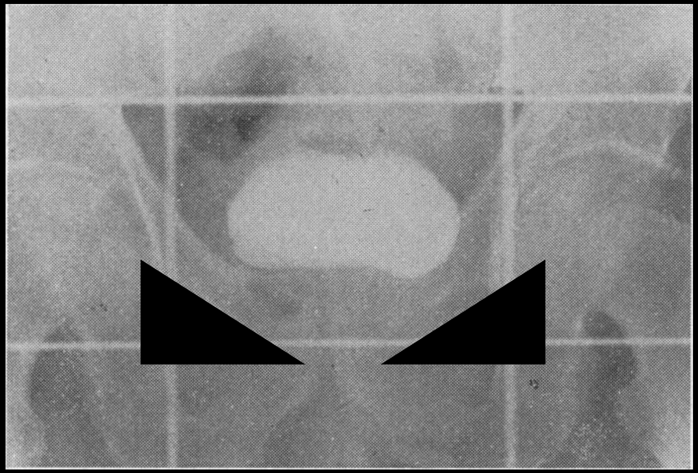

Treatment

Imaging in radiotherapy

Right dose
Right place

- Target definition
- Treatment planning
- Dose calculation
- Positioning

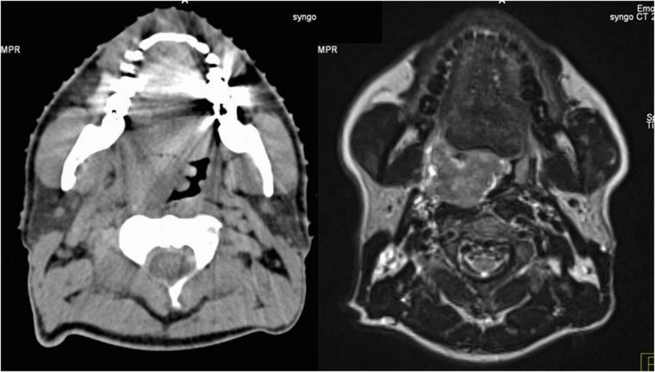
A
syngo
MPR
A
MPR

Imaging in radiotherapy

Right dose
Right place

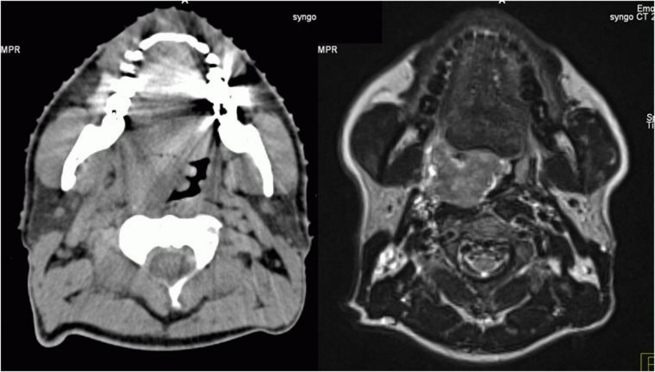
syngo
MPR
MPR
syngo CT

ELEKTA
ATLANTIC
CONSORTIUM

Imaging in radiotherapy

Right dose
Right place

- Target definition
- Treatment planning
- Dose calculation
- Positioning

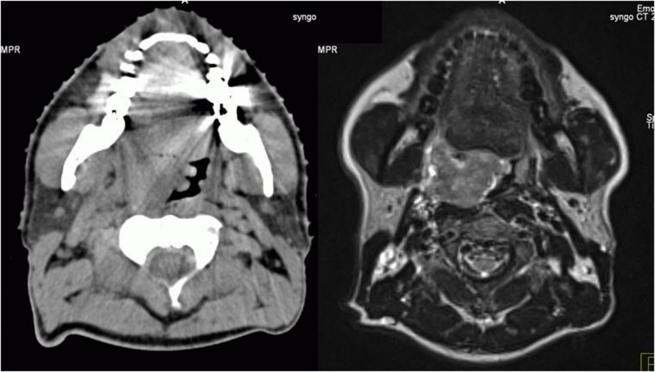
syngo
MPR
MPR

ELEKTA
ATLANTIC CONSORTIUM

Imaging in radiotherapy

Right dose
Right place

- Target definition -> Voxel prescription/constraints
- Treatment planning →Daily automatic process
- Dose calculation
- Positioning –> real time →Re-optimization

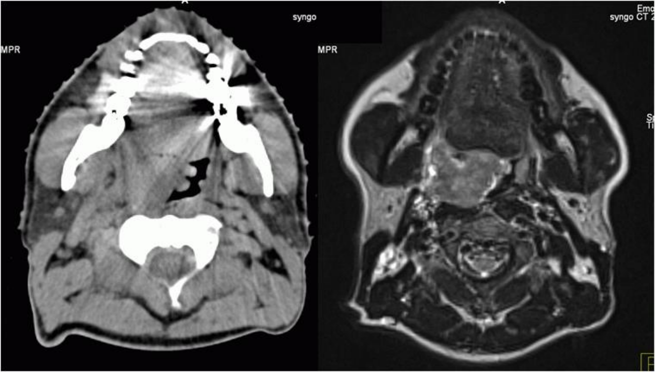
syngo
MPR
MPR
syngo CT

ATLANTIC CONSORTIUM
ELEKTA

- Target definition
- Treatment planning
- Dose calculation
- Positioning
- Dose prescription
- Response assessment

Target definition

CT

PET

MR

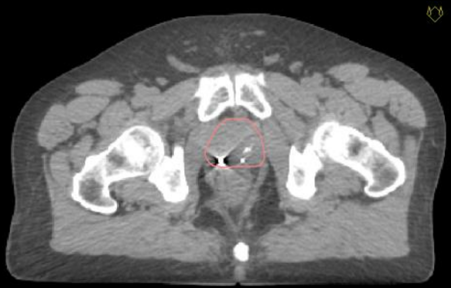

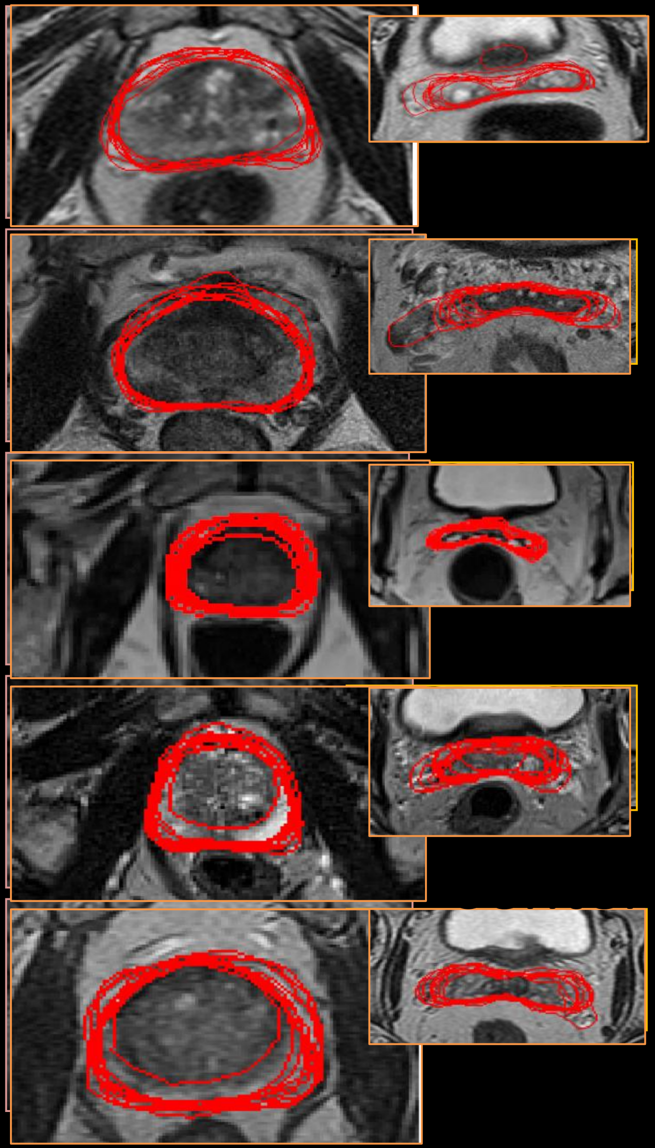

CT/MR workflow

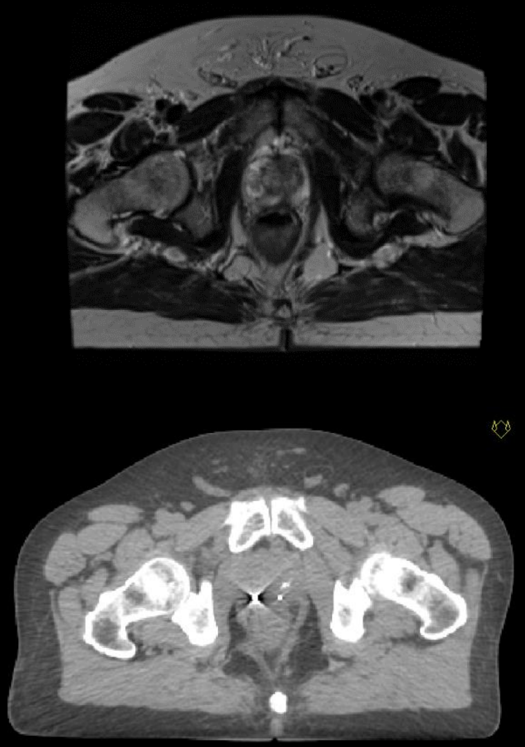

Images

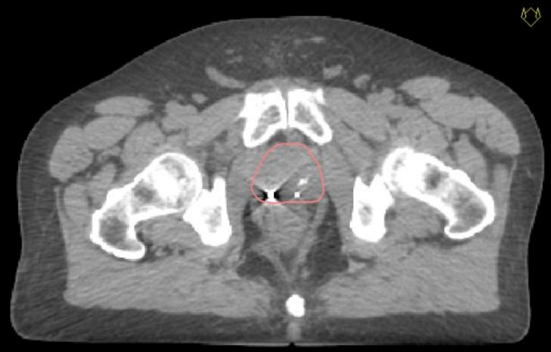

Registration /
Target definition

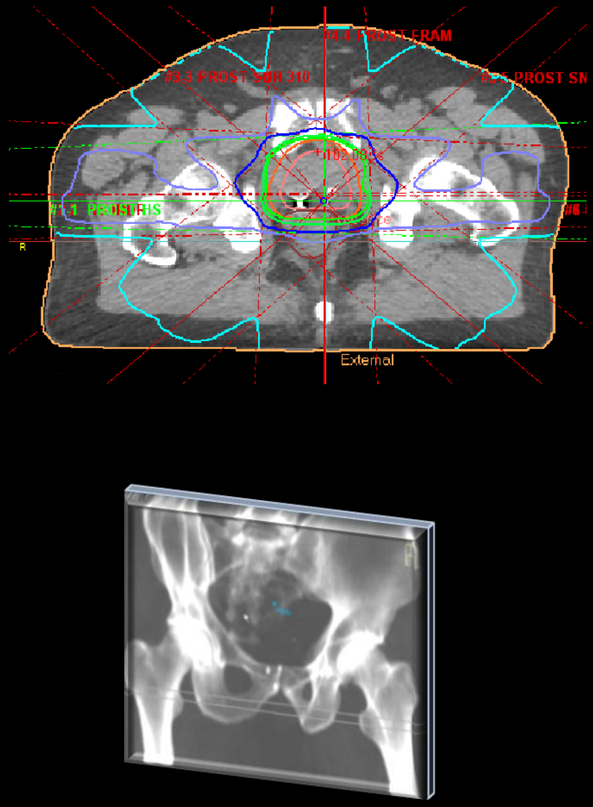
#4.4 PROST FRAM
#3.3 PROST SBH 310
PROST SN
+102.08 %
R
External

Treatment planning

Dose calculation

MRCAT Algorithm Overview

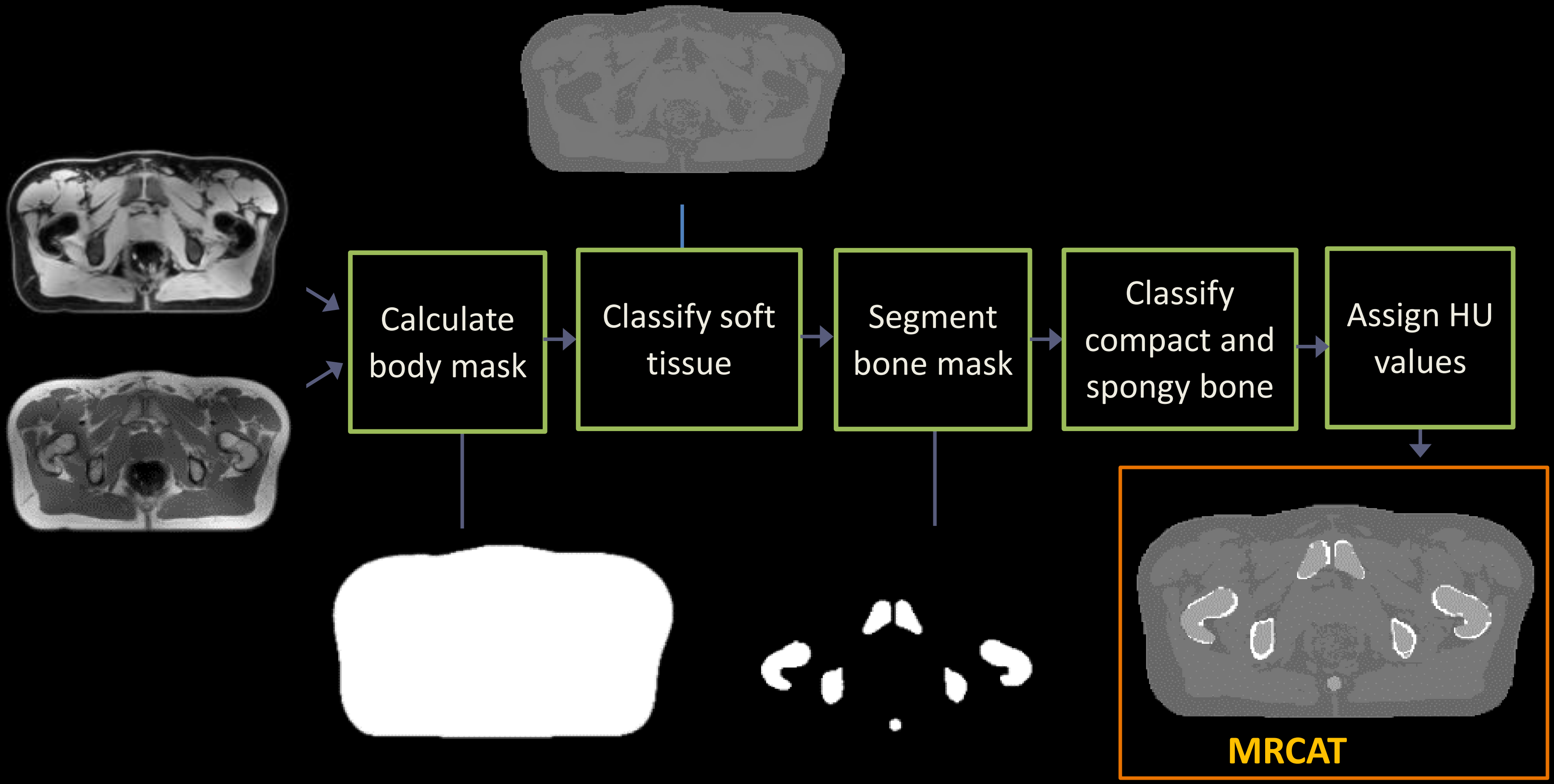

Calculate body mask

Classify soft tissue

Segment bone mask

Classify compact and spongy bone

Assign HU values

Courtesy: Neelam Tyagi

Philips; white paper Kohler et al 2015

Positioning

RoboCouch
CyberKnife

Cyberknife.com

Halcyon

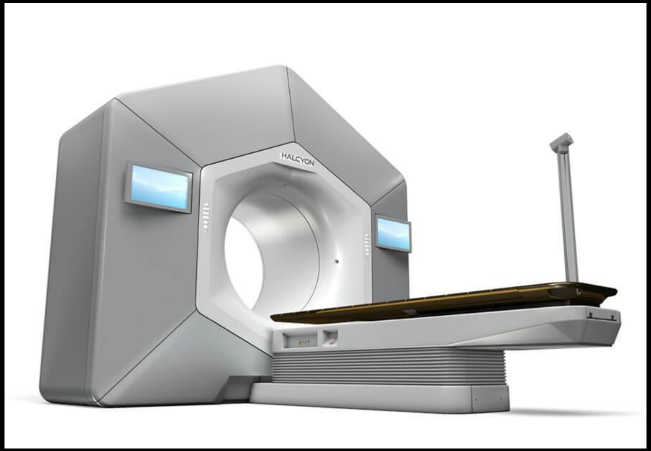

Tomotherapy

Positioning

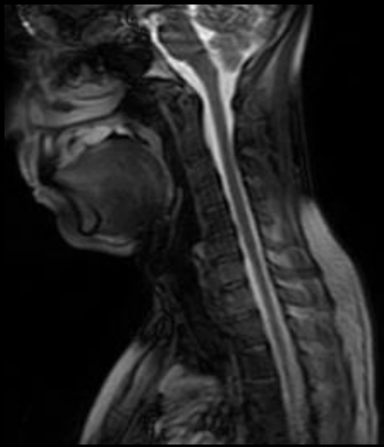

ViewRay

Edmonton

Sydney

ELEKTA
ATLANTIC CONSORTIUM

Elekta

Prescription

Biological target volume

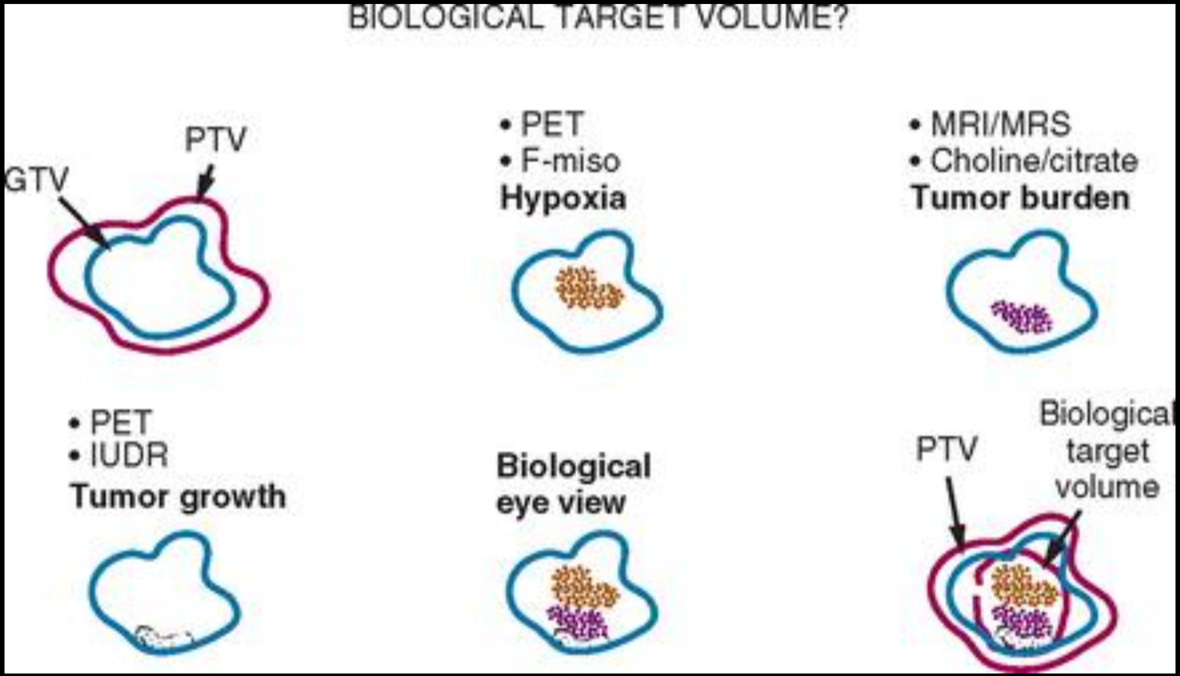
BIOLOGICAL TARGET VOLUME?
PTV
GTV
• PET
• F-miso
Hypoxia
• MRI/MRS
• Choline/citrate
Tumor burden
• PET
• IUDR
Tumor growth
Biological
eye view
PTV
Biological
target
volume

Ling, IJROBP 2000

Prescription

Functional imaging

ADC map

DWI (b=1000 s/mm^2)

[^{68}Ga]PSMA

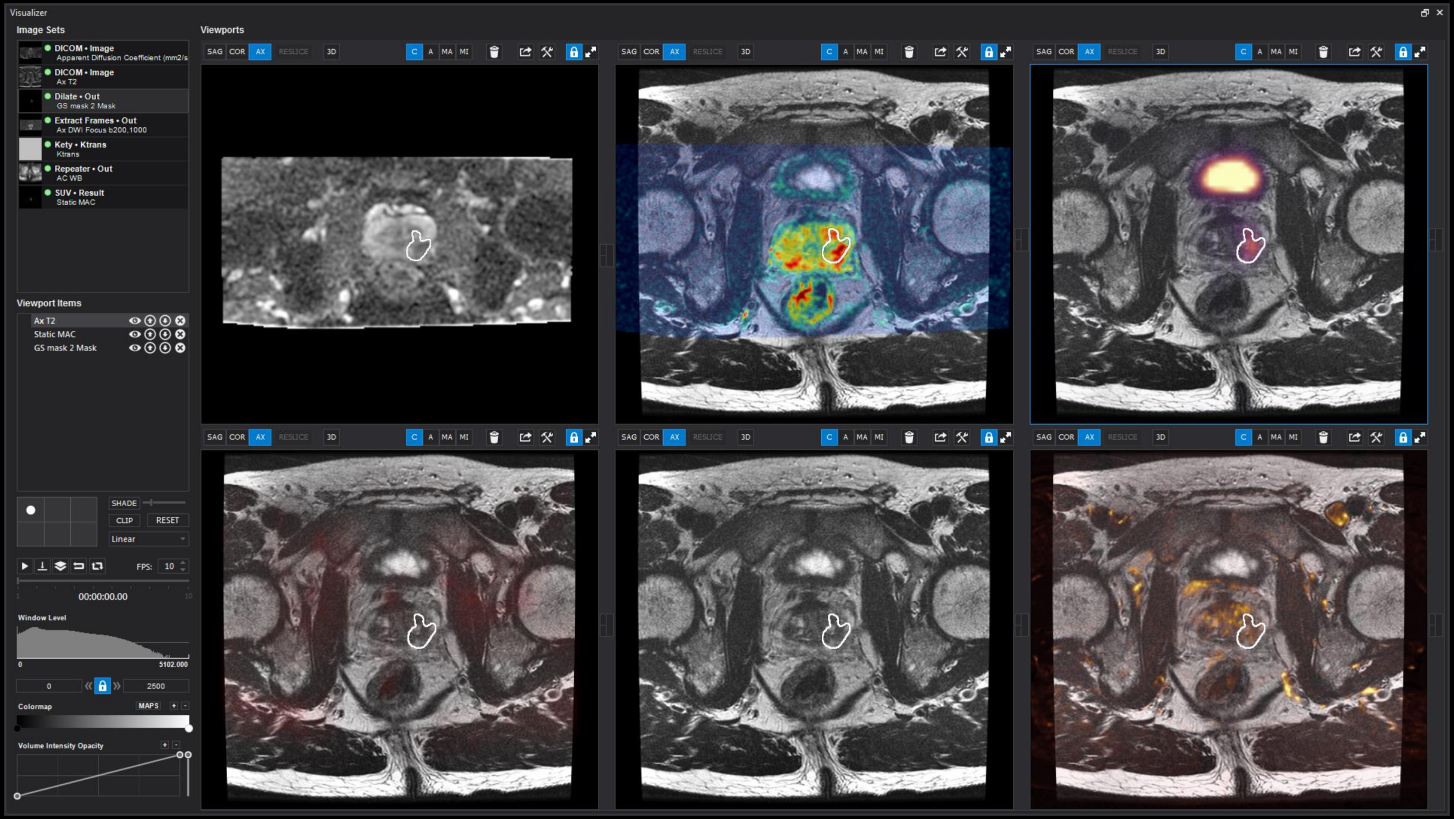
Visualizer
Image Sets
DICOM • Image
Apparent Diffusion Coefficient (mm2/s
DICOM • Image
Ax T2
Dilate • Out
GS mask 2 Mask
Extract Frames • Out
Ax DWI Focus b200,1000
Kety • Ktrans
Ktrans
Repeater • Out
AC WB
SUV • Result
Static MAC
Viewport Items
Ax T2
Static MAC
GS mask 2 Mask
Viewports
SAG
COR
AX
RESLICE
3D
C
A
MA
MI
SHADE
CLIP
RESET
Linear
FPS: 10
00:00:00.00
Window Level
0
5102.000
0
2500
Colormap
MAPS
Volume Intensity Opacity

[^{11}C]Acetate

T2w

DCE (K^{trans})

Prescription

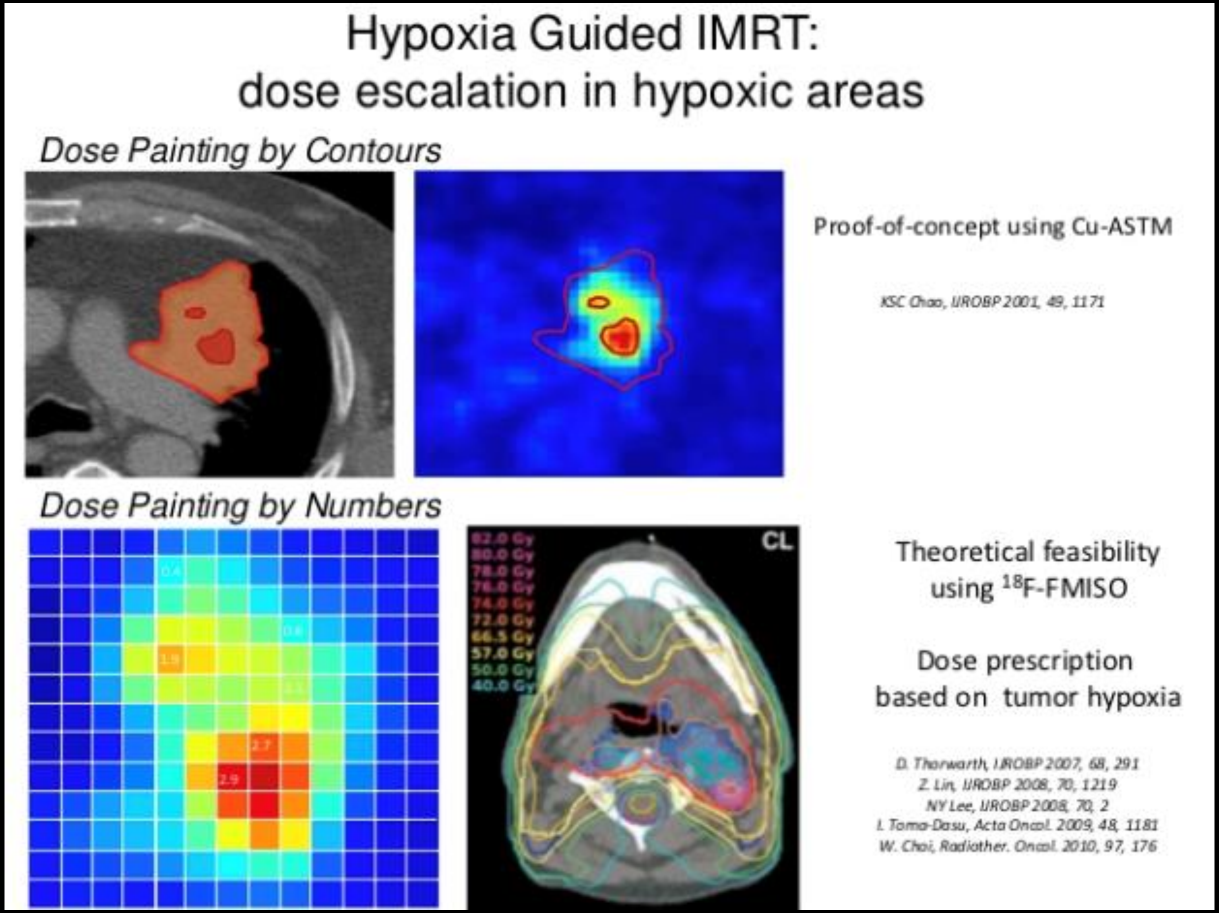

Hypoxia Guided IMRT:
dose escalation in hypoxic areas

Dose Painting by Contours

Proof-of-concept using Cu-ASTM

KSC Chao, IJROBP 2001, 49, 1171

Dose Painting by Numbers

0.4
0.8
1.9
2.7
2.9
82.0 Gy
80.0 Gy
78.0 Gy
76.0 Gy
74.0 Gy
72.0 Gy
66.5 Gy
57.0 Gy
50.0 Gy
40.0 Gy
CL

Theoretical feasibility
using ^{18}F-FMISO

Dose prescription
based on tumor hypoxia

D. Thorwarth, IJROBP 2007, 68, 291
Z. Lin, IJROBP 2008, 70, 1219
NY Lee, IJROBP 2008, 70, 2
I. Toma-Dasu, Acta Oncol. 2009, 48, 1181
W. Choi, Radiother. Oncol. 2010, 97, 176

Image

↓

Dose

Borrowed from slideshare - Lambin

Response assessment

FDG

Baseline

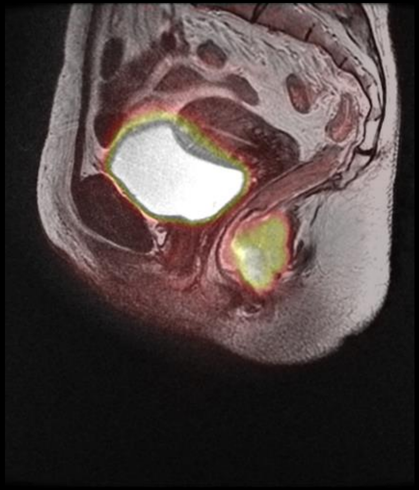

1 w CRT

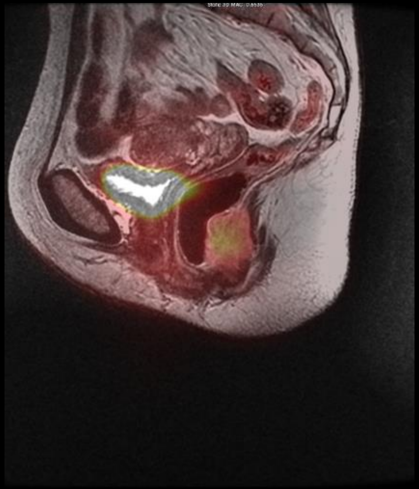

Diffusion

Baseline

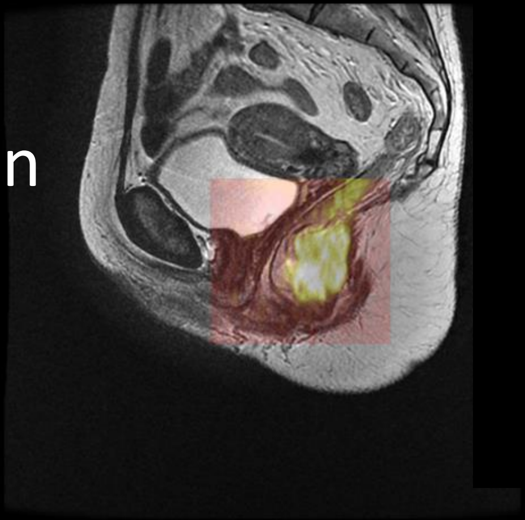

1 w CRT

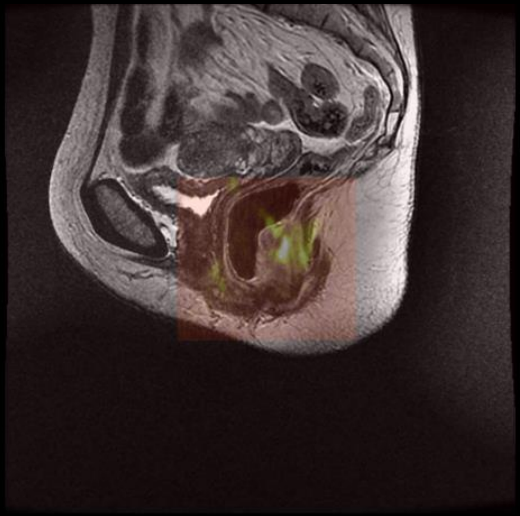

ESTRO School

Imaging for physicists

Goals

- Improve the understanding of the physics principles of MRI, PET and CT
- Explore potential applications of these imaging modalities in clinical practice.

Learning outcomes

- Understand the basic concepts of MRI, PET and CT physics
- Understand the key technical challenges and solutions unique to the application of MRI, PET and advanced CT in radiotherapy
- Understand the potential and challenges of biological imaging methods in radiotherapy treatment planning and follow-up.

ESTRO School

Imaging for physicists

Rational

- Imaging is a fundamental part of radiotherapy today
- The importance will likely increase further

RT physics

ESTRO School

Imaging for physicists

Rational

- Imaging is a fundamental part of radiotherapy today
- The importance will likely increase further

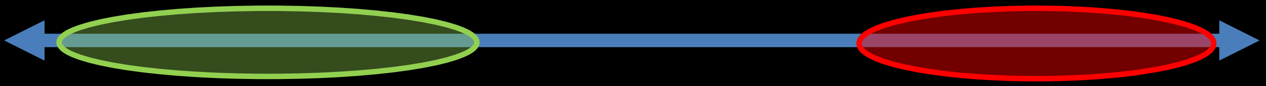

Imaging physicist

Radiotherapy physicist

Imaging physics

RT physics

ESTRO School

Imaging for physicists

Rational

- Imaging is a fundamental part of radiotherapy today
- The importance will likely increase further

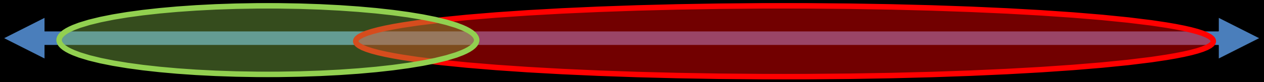

Imaging physicist

Radiotherapy physicist

Imaging physics

RT physics

ESTRO School

Imaging for physicists

Rational

- Imaging is a fundamental part of radiotherapy today
- The importance will likely increase further

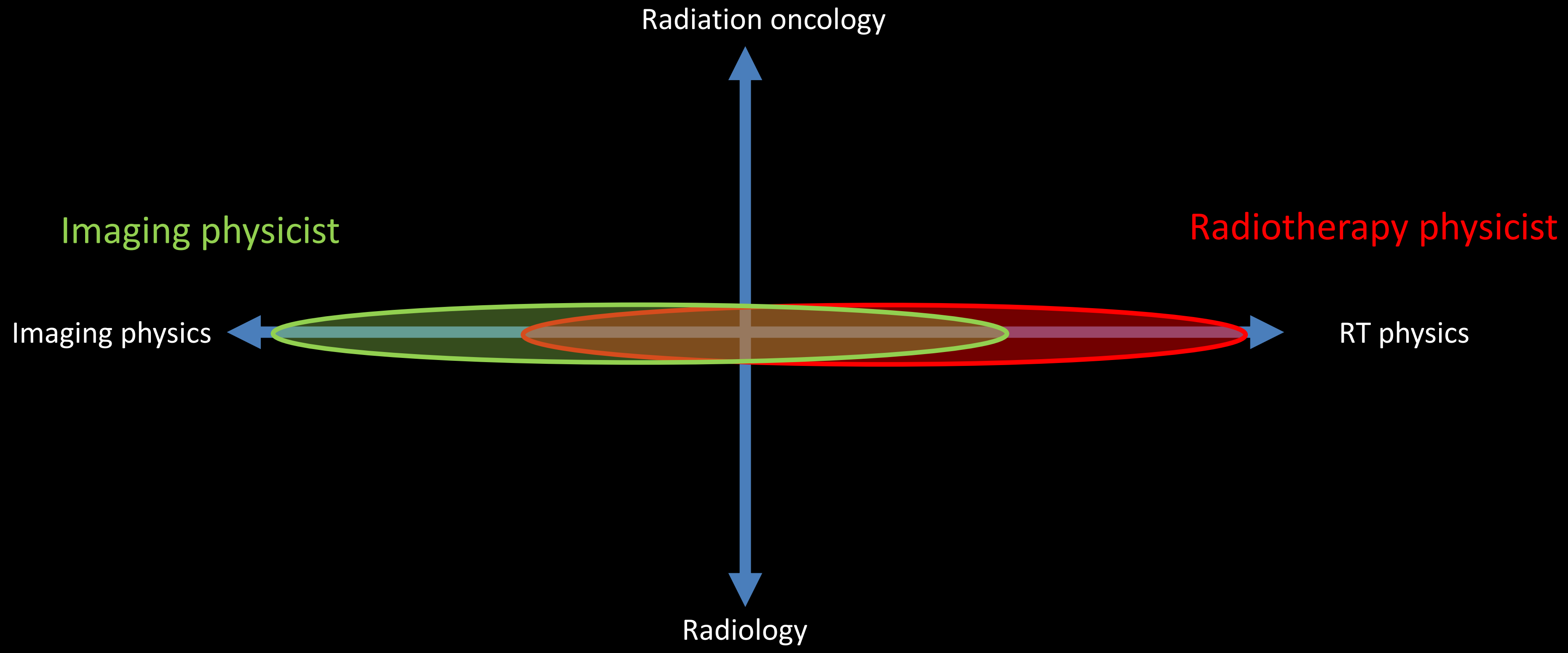
Radiation oncology
Imaging physicist
Radiotherapy physicist
Imaging physics
RT physics
Radiology

ESTRO School

Imaging for physicists

Rational

- Imaging is a fundamental part of radiotherapy today
- The importance will likely increase further

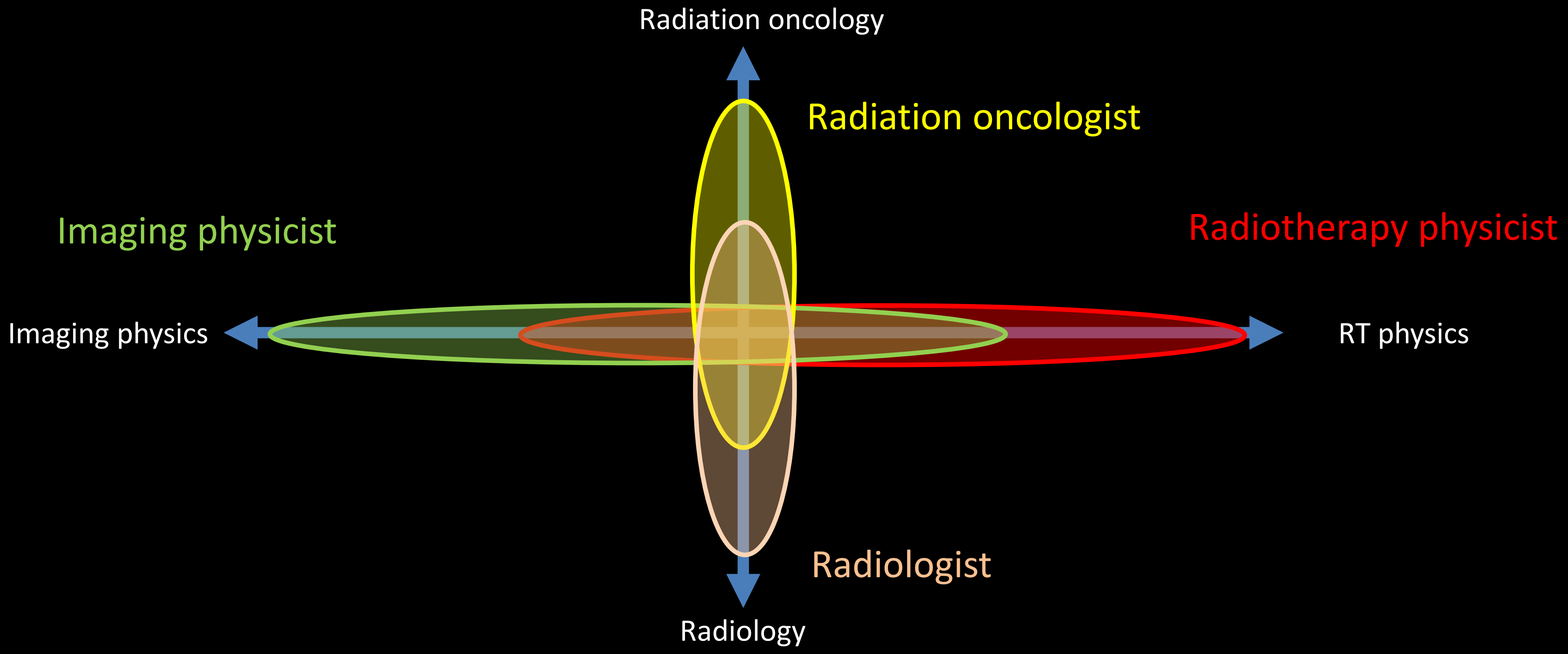

Radiation oncology

Radiation oncologist

Imaging physicist

Radiotherapy physicist

Imaging physics

RT physics

Radiologist

Radiology

ESTRO School

Imaging for physicists

Rational

- Imaging is a fundamental part of radiotherapy today
- The importance will likely increase further

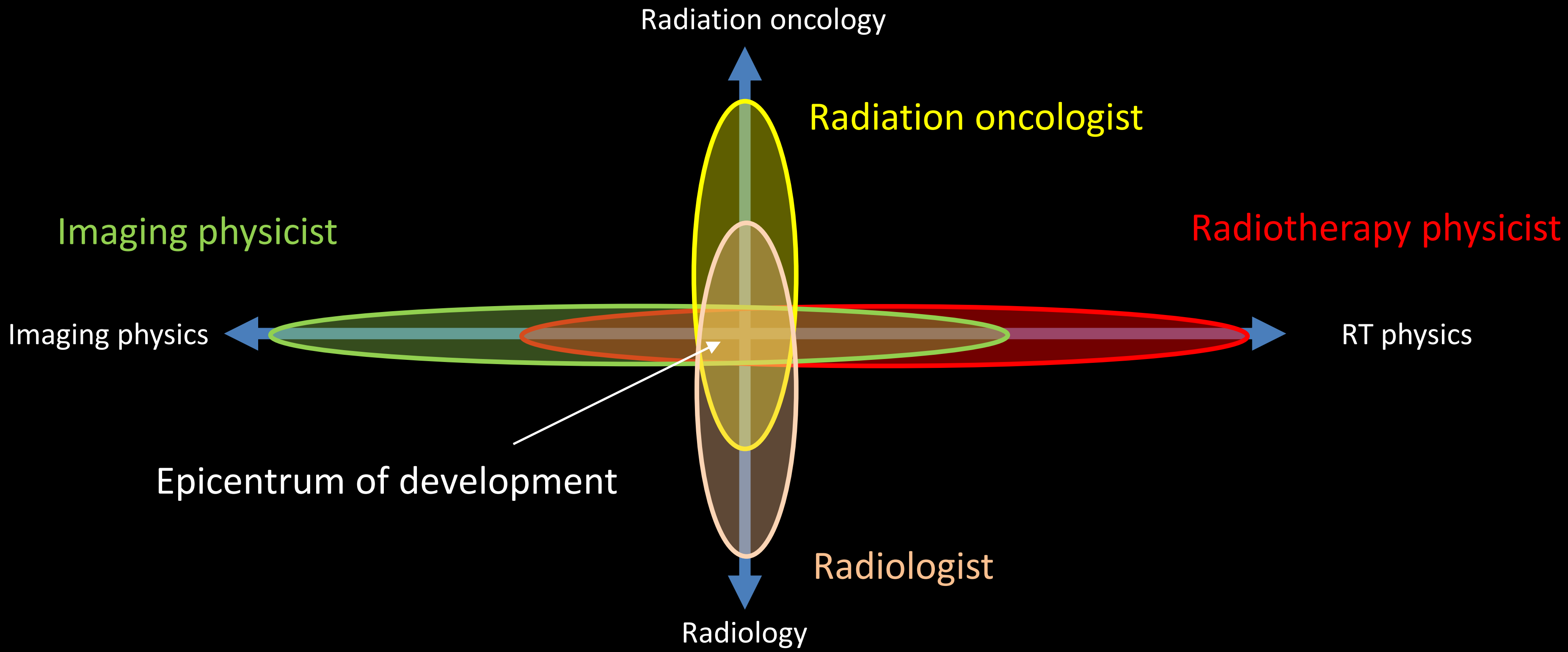
Radiation oncology
Radiation oncologist
Imaging physicist
Radiotherapy physicist
Imaging physics
RT physics
Epicentrum of development
Radiologist
Radiology

ESTRO School

Imaging for physicists

Rational

- Imaging is a fundamental part of radiotherapy today
- The importance will likely increase further

MR

PET

CT

Fundamental principals

Radiotherapy physicist

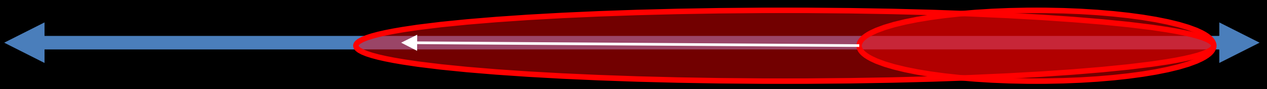

Imaging physics

RT physics

Possibilities

Communication

Limitations

ESTRO School

Imaging for physicists

Rational

- Imaging is a fundamental part of radiotherapy today
- The importance will likely increase further

Clinical lectures

- Prostate
- Cervix
- Brain
- Head&Neck

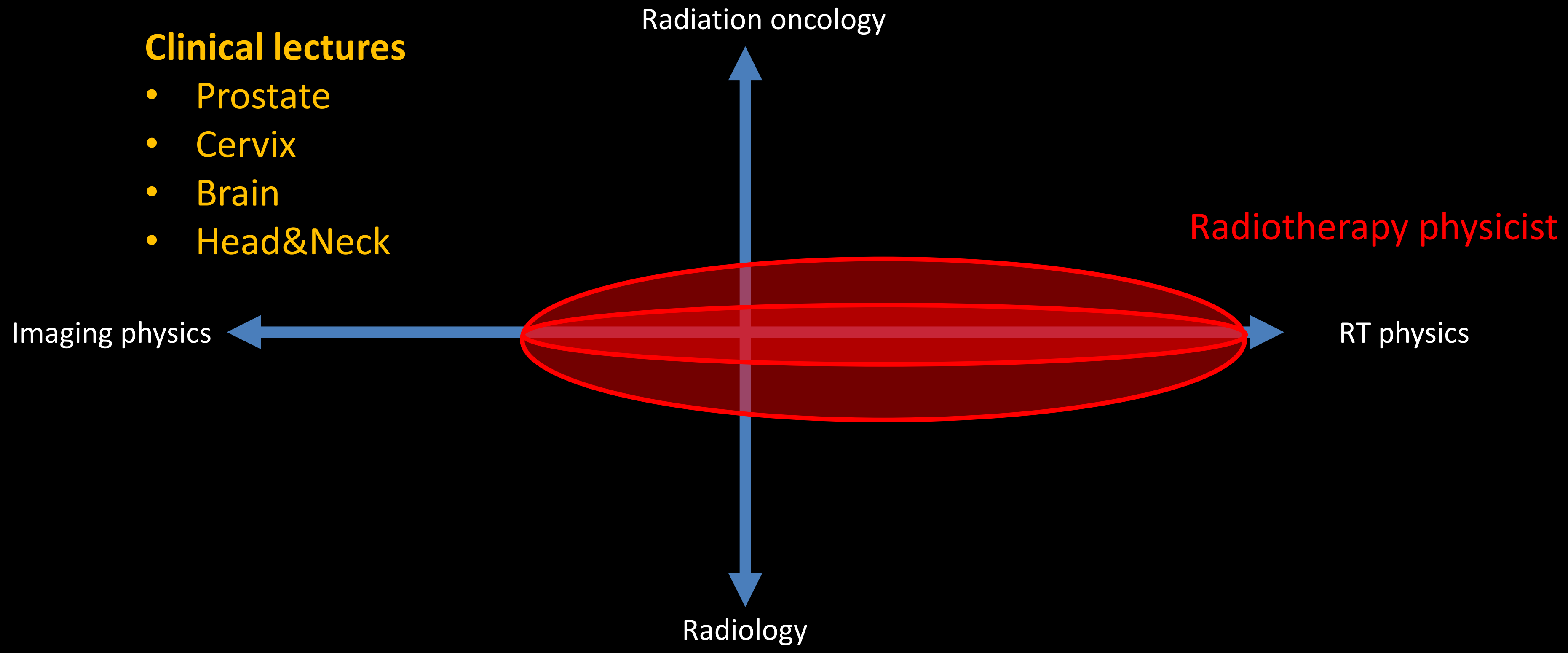
Radiation oncology
Radiotherapy physicist
Imaging physics
RT physics
Radiology

Thank you!

Acknowledgments

Uulke Van der Heide

Per Nilsson

ESTRO School

Imaging for physicists

Rational

- Imaging is a fundamental part of radiotherapy today
- The importance will likely increase further

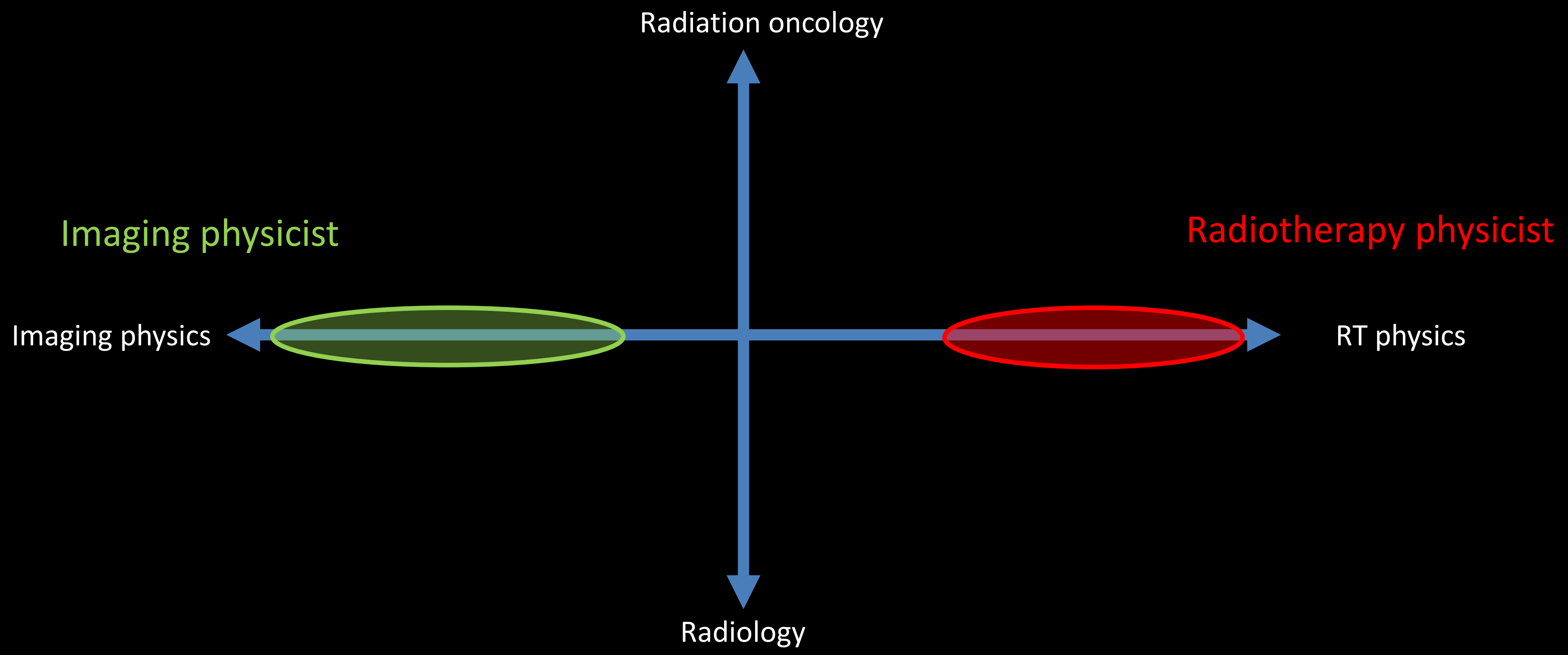
Radiation oncology
Imaging physicist
Radiotherapy physicist
Imaging physics
RT physics
Radiology

UiO : Department of Physics
University of Oslo

Oslo
University Hospital

MRI physics - basic principles

Eirik Malinen

Background

- All clinical applications of MRI today are based on magnetic properties of the hydrogen nucleus
- Body tissues contains lots of water and fat, and hence hydrogen

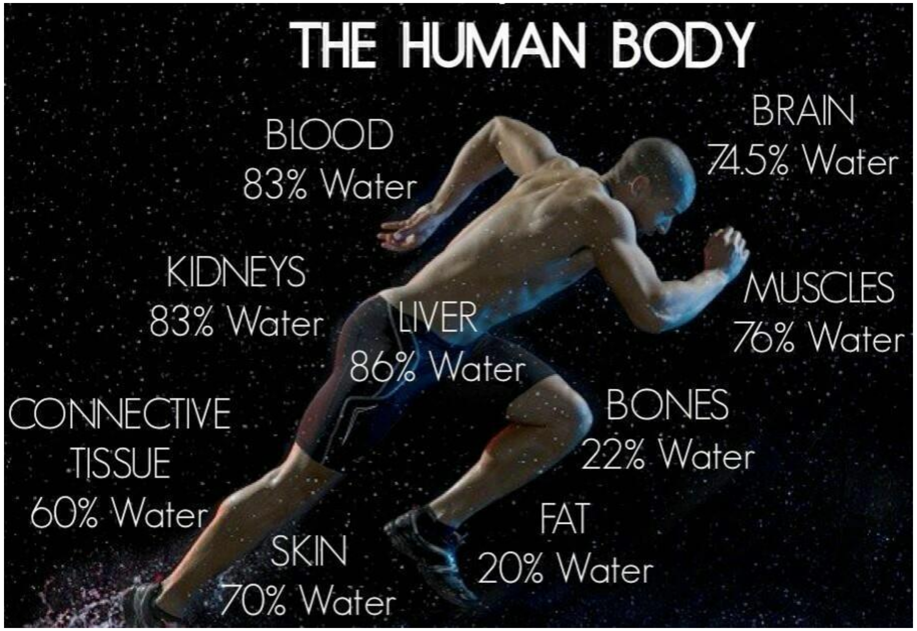
THE HUMAN BODY
BLOOD
83% Water
BRAIN
74.5% Water
KIDNEYS
83% Water
LIVER
86% Water
MUSCLES
76% Water
CONNECTIVE
TISSUE
60% Water
BONES
22% Water
SKIN
70% Water
FAT
20% Water

Nuclear magnetic moment

- Stern-Gerlach experiment:

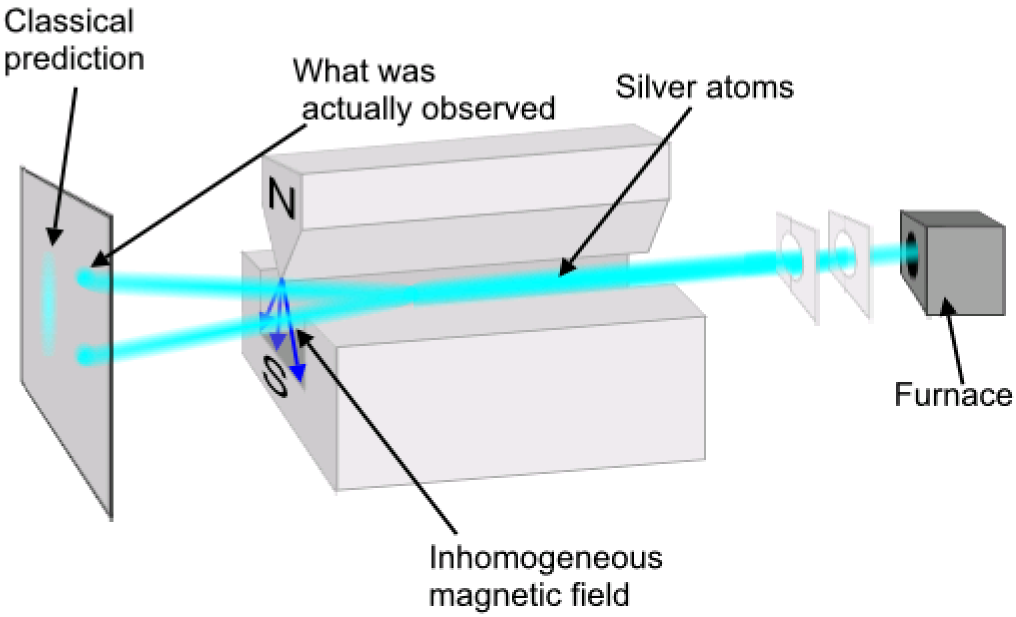
Classical prediction
What was actually observed
Silver atoms
N
S
Furnace
Inhomogeneous magnetic field

Otto Stern

Walter Gerlach

→ Atomic nuclei has a quantized magnetic moment

Magnetic moment and spin

- Consider charge *q* in circular motion:

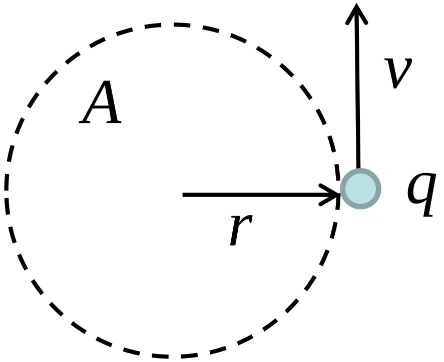

Current:

$$i = \frac{\Delta q}{\Delta t} = \frac{qv}{2\pi r}$$

Magnetic moment:

$$\mu = iA = \frac{q}{2m} L \quad , \quad L = mvr$$

- Rotating charged sphere with uniform charge:

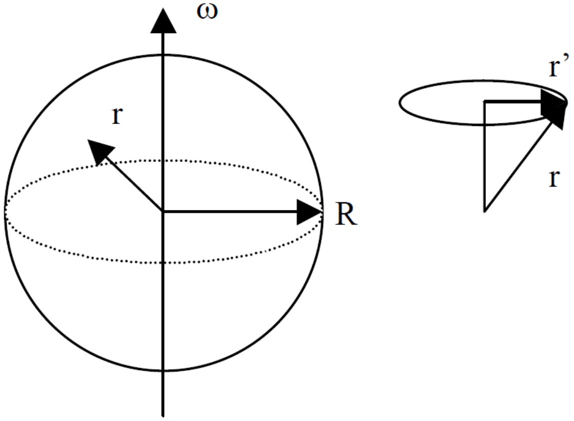

$$\mu = \frac{q}{2m} S$$

↖

Spin!

Quantized nuclear spin

- Nuclear spin is a form of angular momentum
- Nuclear spin, $\mathbf{I}$, is quantized in units of $\hbar$
- Nuclear quantum number depends on nuclear configuration; I=1/2, 1…
- Hydrogen has spin I=1/2, with spin projection numbers m_I=+1/2 , -1/2; spin ‘up’ or ‘down’
- Magnetic moment is $\boldsymbol{\mu}=\gamma\mathbf{I}$

$\nwarrow$

Gyromagnetic ratio

Unpaired nucleons, spin and γ

Nucleus	Unpaired Protons	Unpaired Neutrons	Spin	γ (MHz/T)
^{1}H	1	0	1/2	42.58
^{2}H	1	1	1	6.54
^{31}P	1	0	1/2	17.25
^{23}Na	1	2	3/2	11.27
^{14}N	1	1	1	3.08
^{13}C	0	1	1/2	10.71
^{19}F	1	0	1/2	40.08

Potential energy in magnetic field

- In an external magnetic field, the potential energy is:

$$E_{pot} = -\boldsymbol{\mu} \cdot \mathbf{B}$$

$$= -\gamma\hbar m_I B = \mp\frac{1}{2}\gamma\hbar B$$

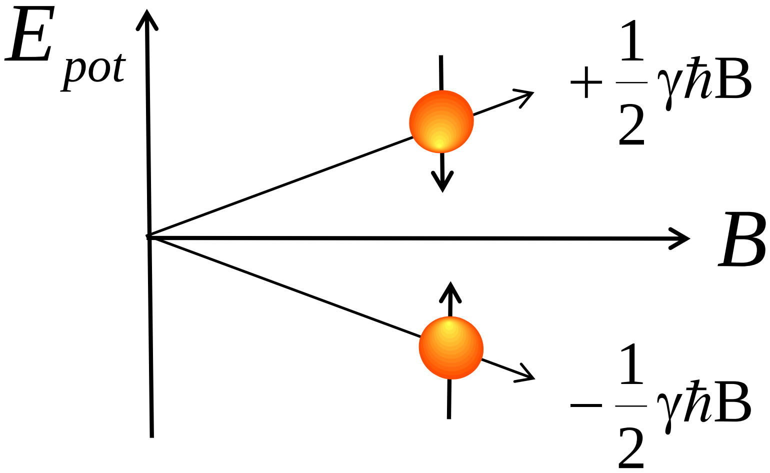

E_{pot}
$+\frac{1}{2}\gamma\hbar B$
B
$-\frac{1}{2}\gamma\hbar B$

→ Two energy states are possible

- *Zeeman effect*

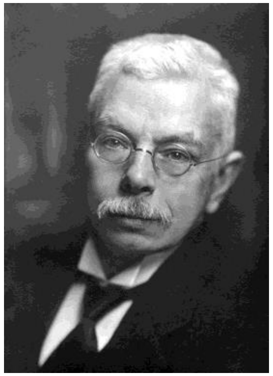

Pieter Zeeman

Magnetic resonance

- Spin system under an external magnetic field exposed to electromagnetic radiation

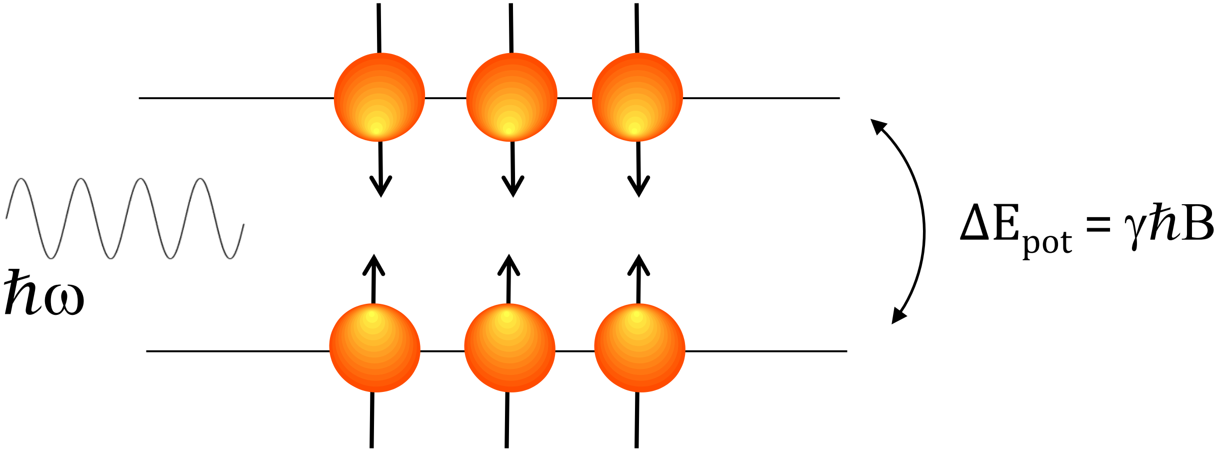

Isidor Isaac Rabi

- Transitions from spin down to spin up or vice versa may occur if $\underline{\underline{\hbar\omega = \Delta E_{pot} = \gamma\hbar B}}$

Magnetic resonance

- $\hbar\omega = \underline{\underline{\gamma\hbar B \rightarrow \omega=\gamma B}}$; *resonance condition*

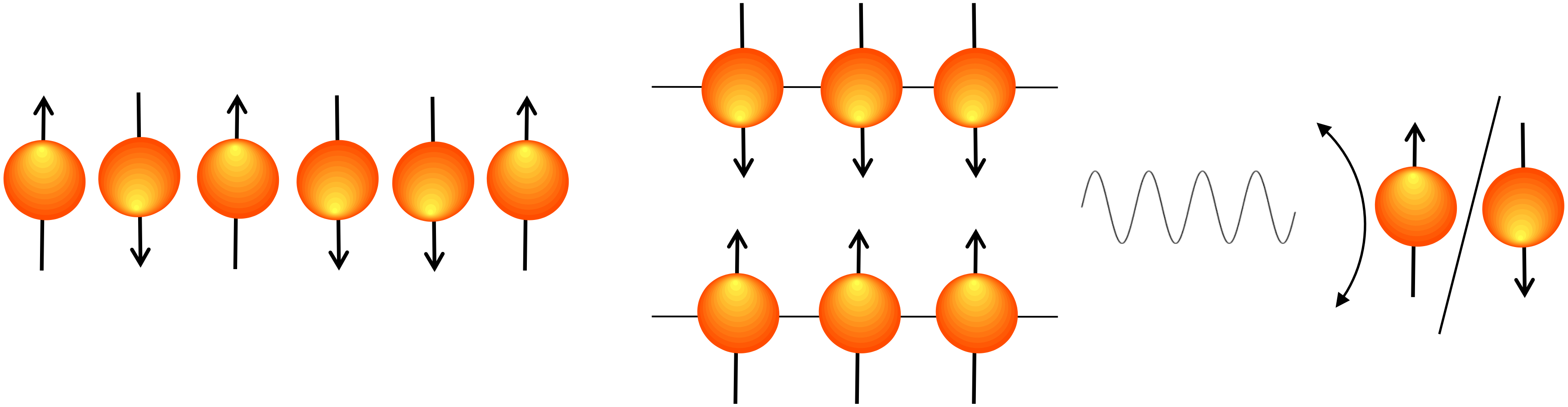

Without external field

With external field

With external field + electromagnetic radiation

- Resonance frequency, ^{1}H, B=1T: $\omega \approx 43$ MHz
  → radiofrequency !

Macroscopic considerations

- Spin transition probability is equal for *up*→*down* and *down*→*up*

- How can a net energy absorption be observed?

- Distribution of spins follows Boltzmann:

$$\frac{N_\downarrow}{N_\uparrow} = e^{-\Delta E_{pot}/kT} = e^{-\hbar\gamma B/kT}$$

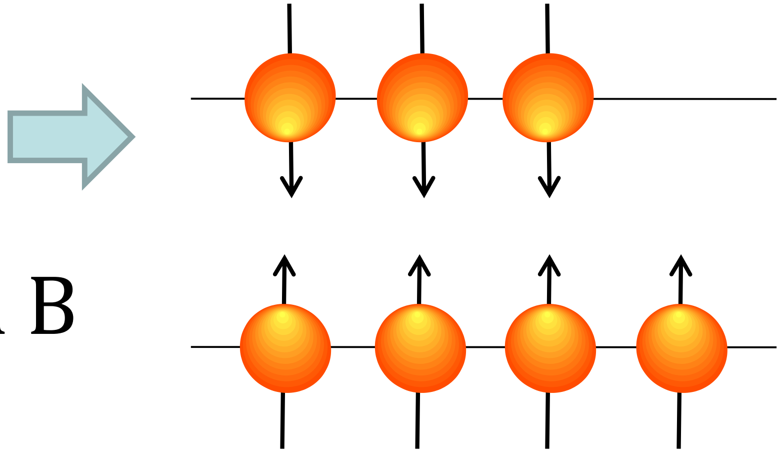

- Difference increases with B and decreases with T

Macroscopic magnetization

- Population difference generates a net magnetization

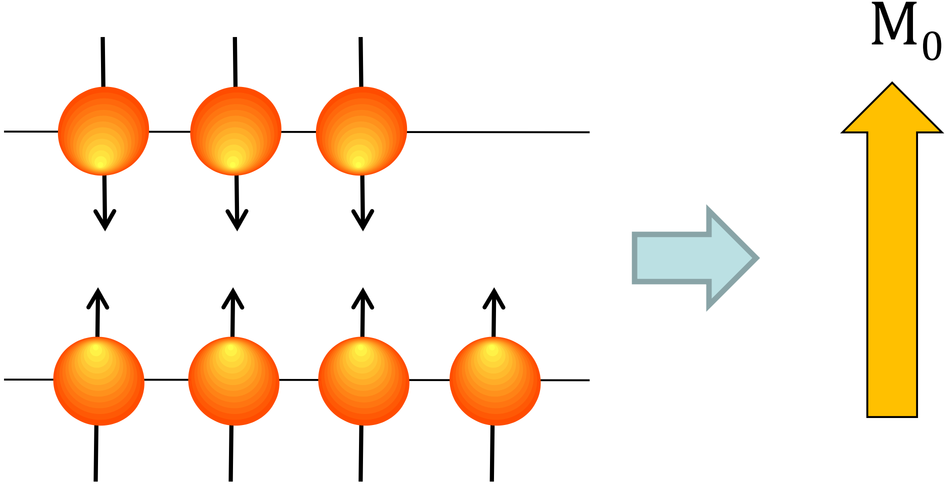

- The more spins, the stronger the magnetization

- Torque exerted on a magnet by a magnetic field:

$$\boldsymbol{\tau} = \frac{d\mathbf{M}}{dt} = \gamma \mathbf{M} \times \mathbf{B}$$

Bloch equations

$$\boldsymbol{\tau} = \frac{d\boldsymbol{M}}{dt} = \gamma \boldsymbol{M} \times \boldsymbol{B}$$

$$\Rightarrow \frac{\mathrm{dM_x}}{\mathrm{dt}} = \gamma \mathrm{BM_y} \quad , \quad \frac{\mathrm{dM_y}}{\mathrm{dt}} = -\gamma \mathrm{BM_x} \quad , \quad \frac{\mathrm{dM_z}}{\mathrm{dt}} = 0$$

$$\Rightarrow$$

$$\mathrm{M_x(t) = M_x^0 \cos(\omega_L t)} \;,\; \mathrm{M_y(t) = M_y^0 \sin(\omega_L t)}$$

$$\mathrm{M_z(t) = M_0}$$

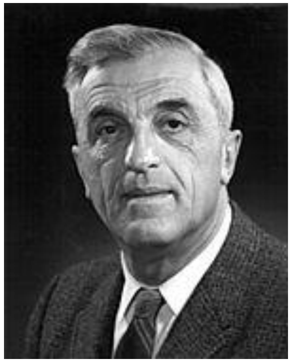

Felix Bloch

Joseph Larmor

- $\omega_L = \gamma B$; *Larmor frequency*
- Set of equations describing a *precession* around the axis defined by ***B*** (z-axis)

Spin precession

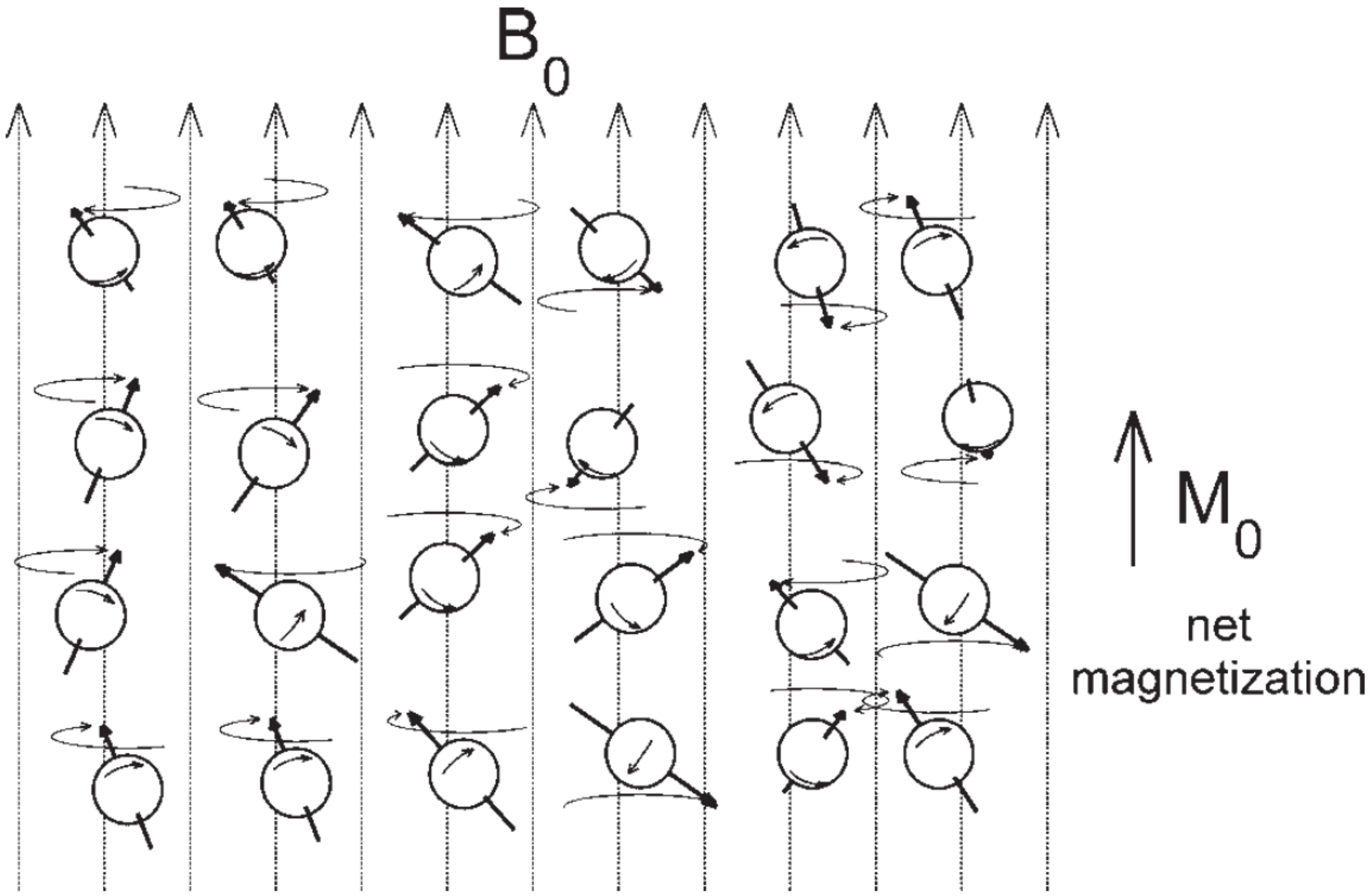
B
0
M
0
net
magnetization

Spin precession

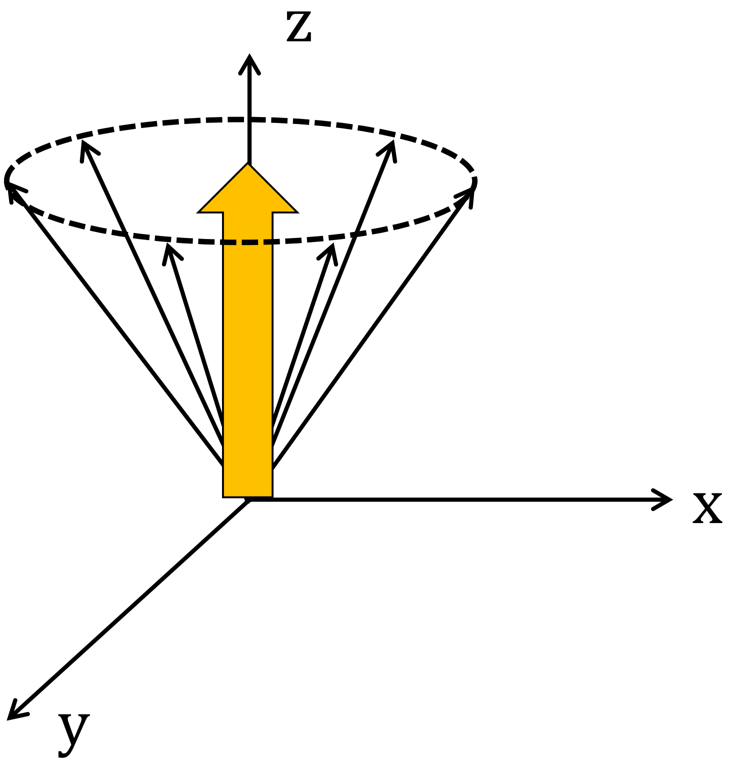

Spins out of phase

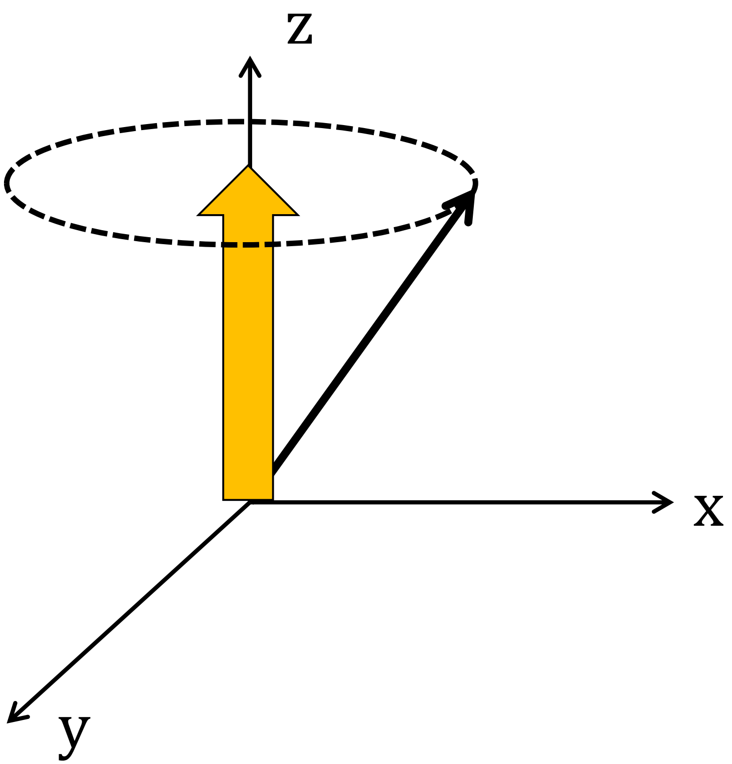

All spins in phase with
same Larmor frequency

Introducing the RF field

- How can the magnetization be altered?
- Introduce oscillating (RF) magnetic field in the xy-plane

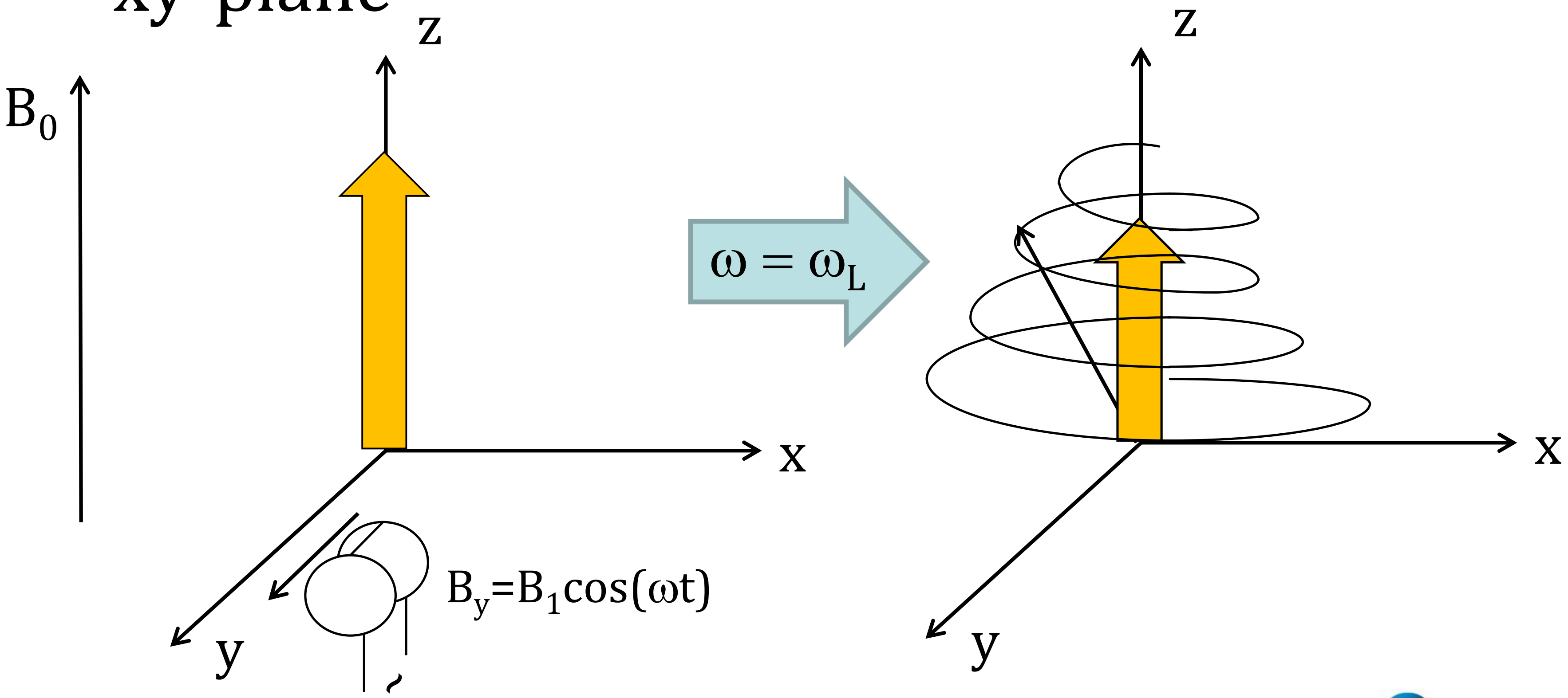
z
B_0
x
y
$B_y = B_1 \cos(\omega t)$
$\omega = \omega_L$
z
x
y

Flip angle

- The degree of which the magnetization is tipped relative to B_0 due to an excitation pulse
- From Bloch's considerations:

$$\theta = 2\pi\gamma\tau B_1$$

- t: duration of pulse
- B1: ~RF power

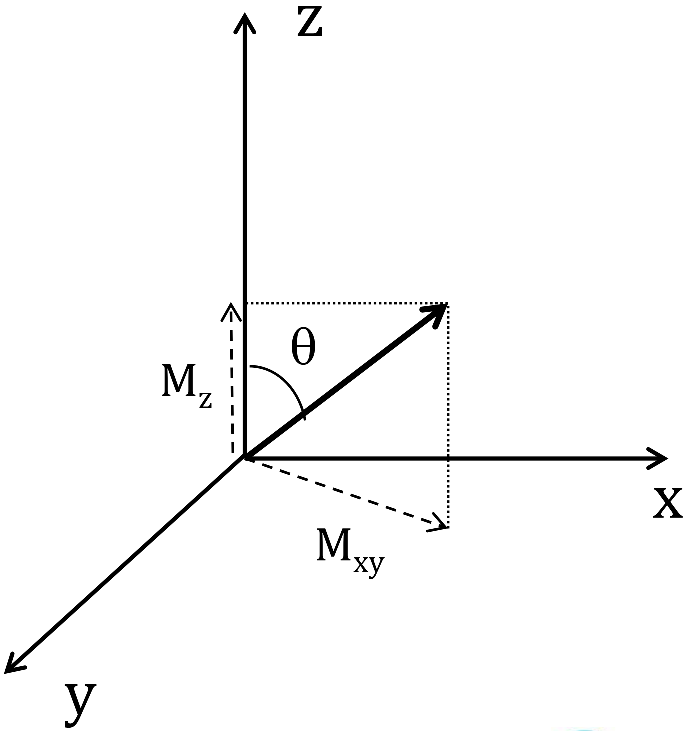

T1 relaxation

- Fluctuating magnetic fields from the molecular environment may have Larmor frequency→ stimulated transitions may occur
- After an RF-pulse, the z-component of M relaxes back to equilibrium via such stimulated transitions
- Longitudinal relaxation, Spin lattice relaxation, T1 relaxation
- Rate of relaxation: R1=1/T1

↑

Varies between tissues

T2 relaxation

- The *transverse* component of the magnetization also decays
- Local, microscopic field inhomogeneities causes each spin to precess with a frequency slightly different from ω_L
- An excitation pulse initially causes all spins to precess in phase, but a dephasing then occurs
- transverse- or spin-spin relaxation; T2
- T2<T1

T2 relaxation cont'd

- However, transverse relaxation is also caused by B_0 inhomogeneities and tissue magnetic susceptibility
- Actual T2 time is denoted T2*:

$$\frac{1}{T2*} = \frac{1}{T2} + \gamma \Delta B_0$$

- T2*<T2

Relaxation

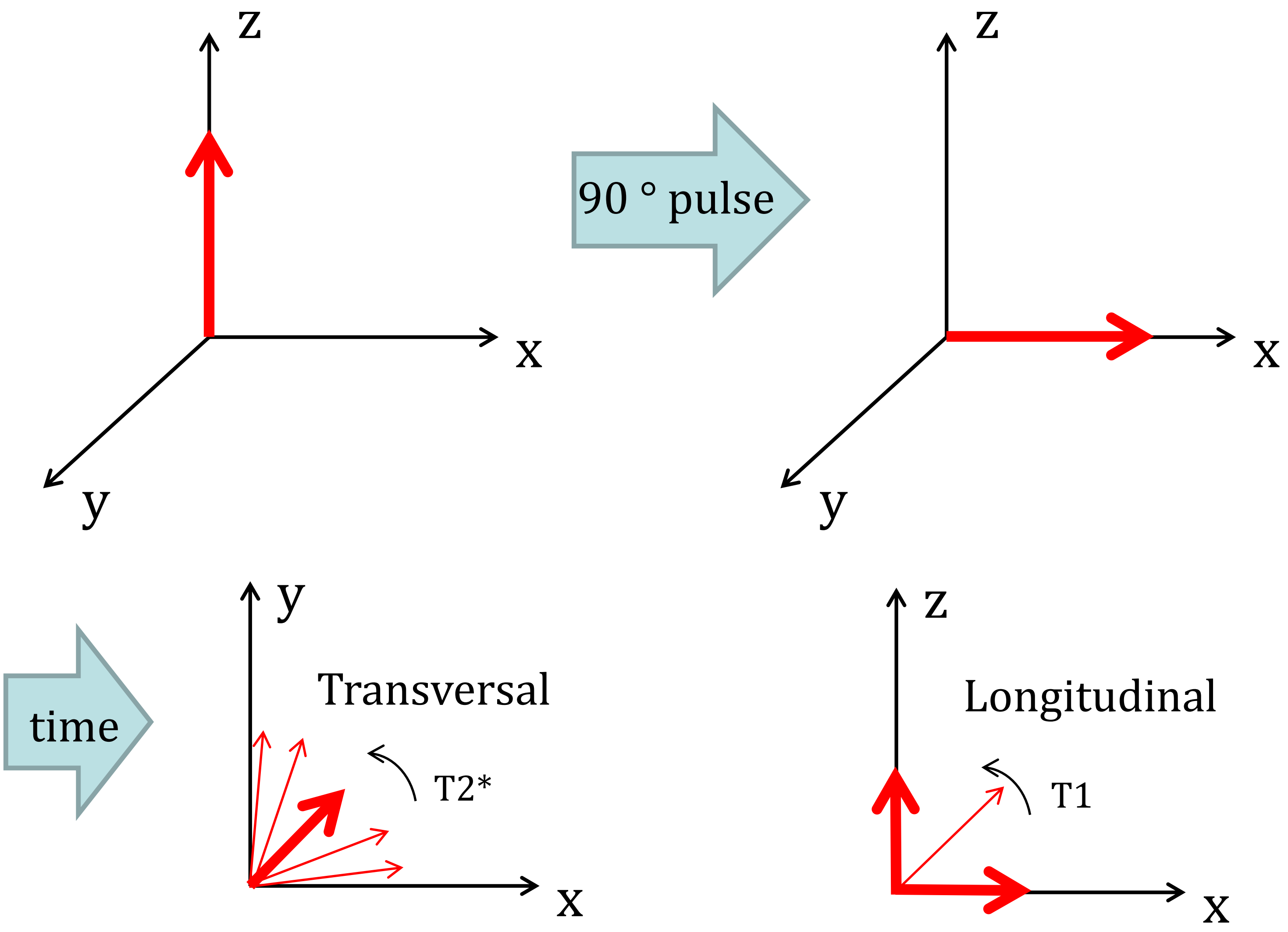

90 ° pulse

time

Transversal

Longitudinal

z
x
y
z
x
y
y
x
T2*
z
x
T1

Relaxation – 90° pulse and T1

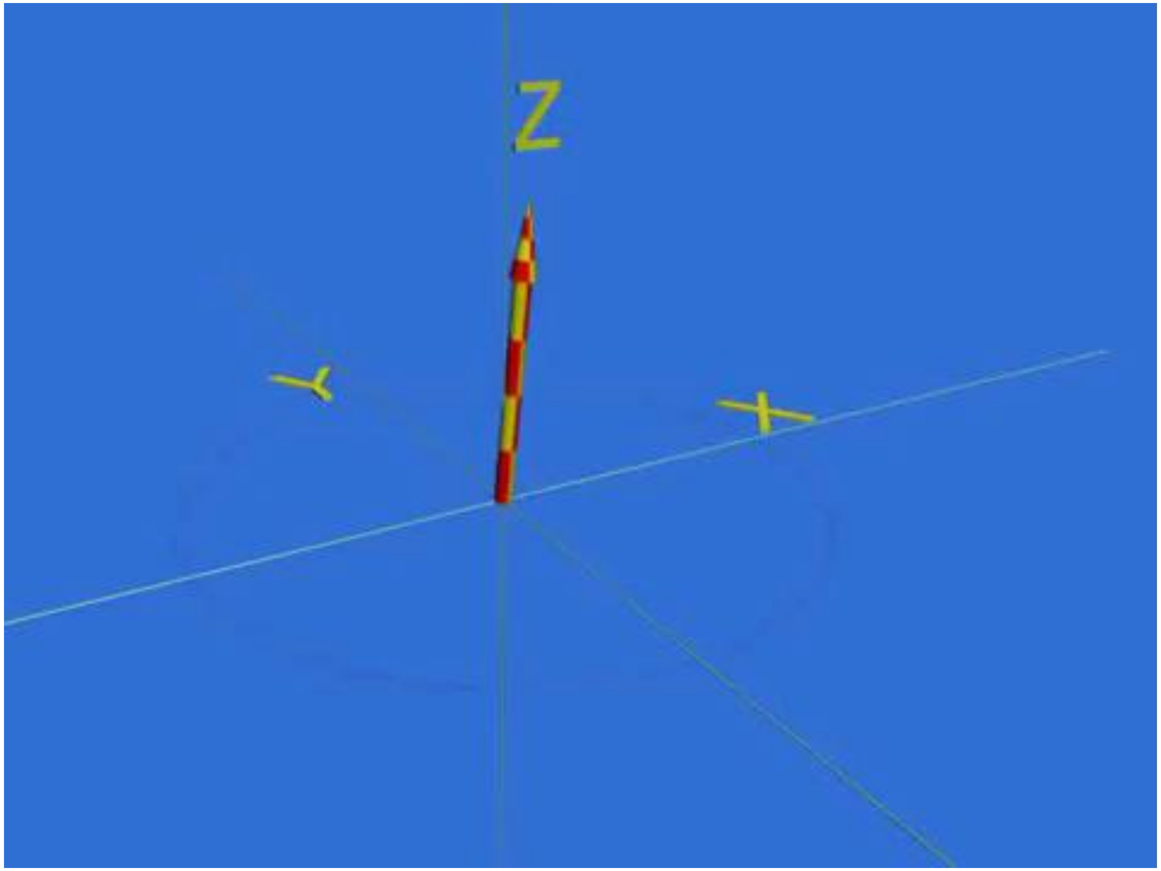

Relaxation - 90° pulse and T2

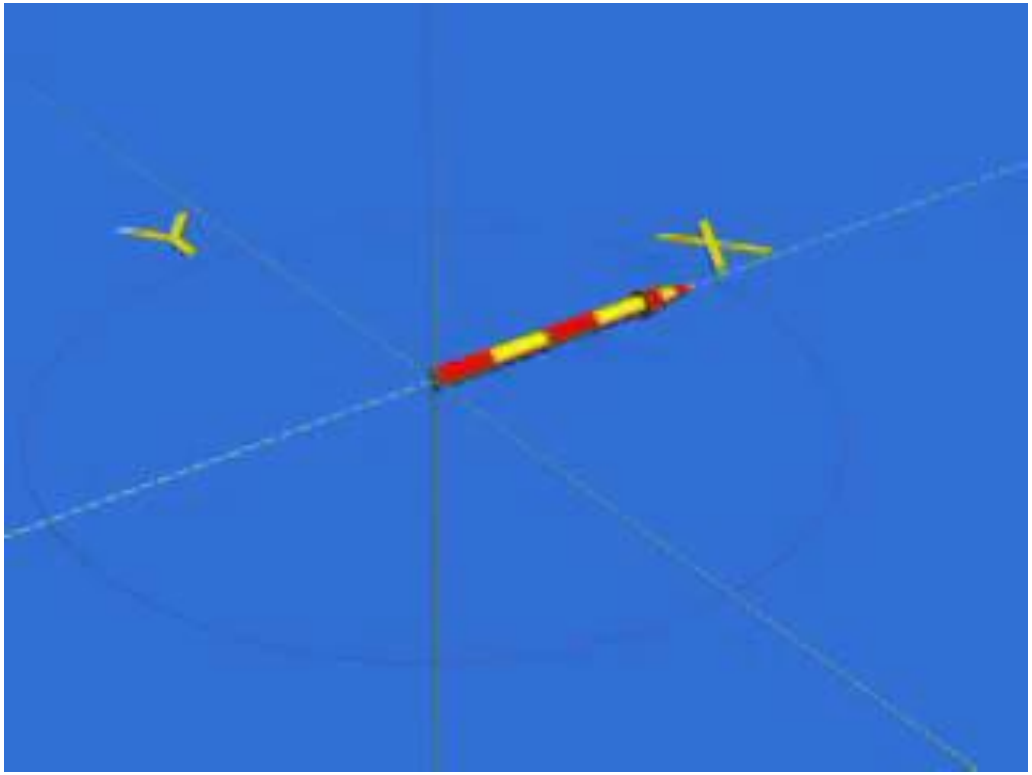

Relaxation dynamics

- Bloch's equations expanded with relaxation components; $M_{xy}/T2^*$ and $(M_z-M_0)/T1$
- May be shown that:

$$M_z(t) = M_0(1-e^{-t/T1}) \longrightarrow$$

$$t = T1 \Rightarrow \; M_z = 0.63 M_{z,\infty}$$

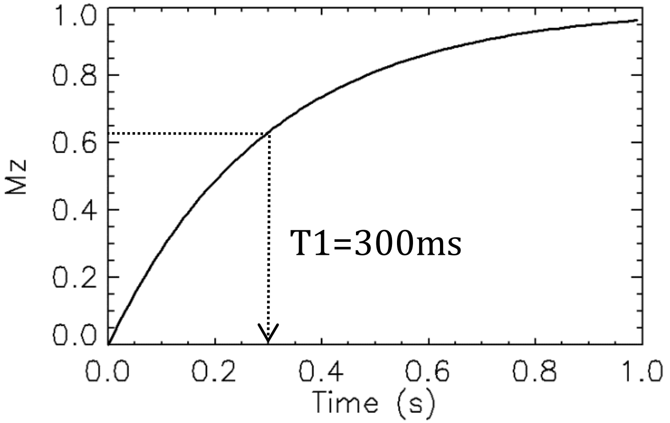

$$M_{xy}(t) = M_{xy,0} e^{-t/T2^*} \longrightarrow$$

$$t = T2^* \Rightarrow \; M_{xy} = 0.37 M_{xy,0}$$

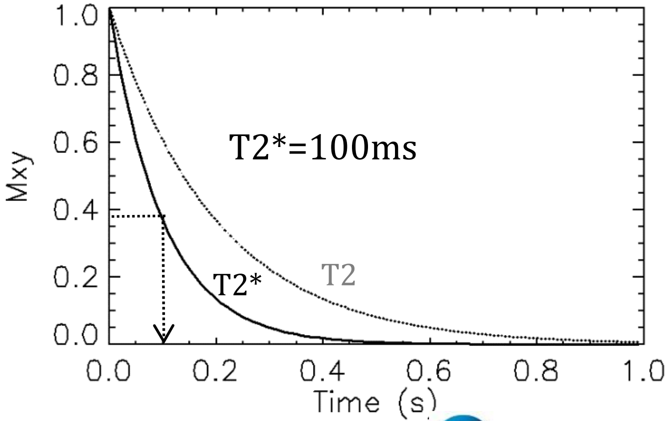

Relaxation times

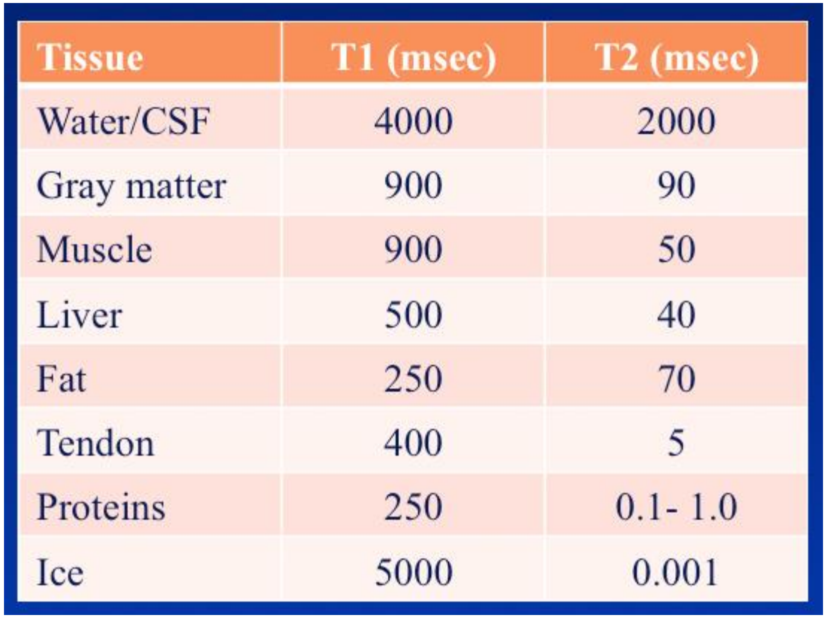

Tissue	T1 (msec)	T2 (msec)
Water/CSF	4000	2000
Gray matter	900	90
Muscle	900	50
Liver	500	40
Fat	250	70
Tendon	400	5
Proteins	250	0.1- 1.0
Ice	5000	0.001

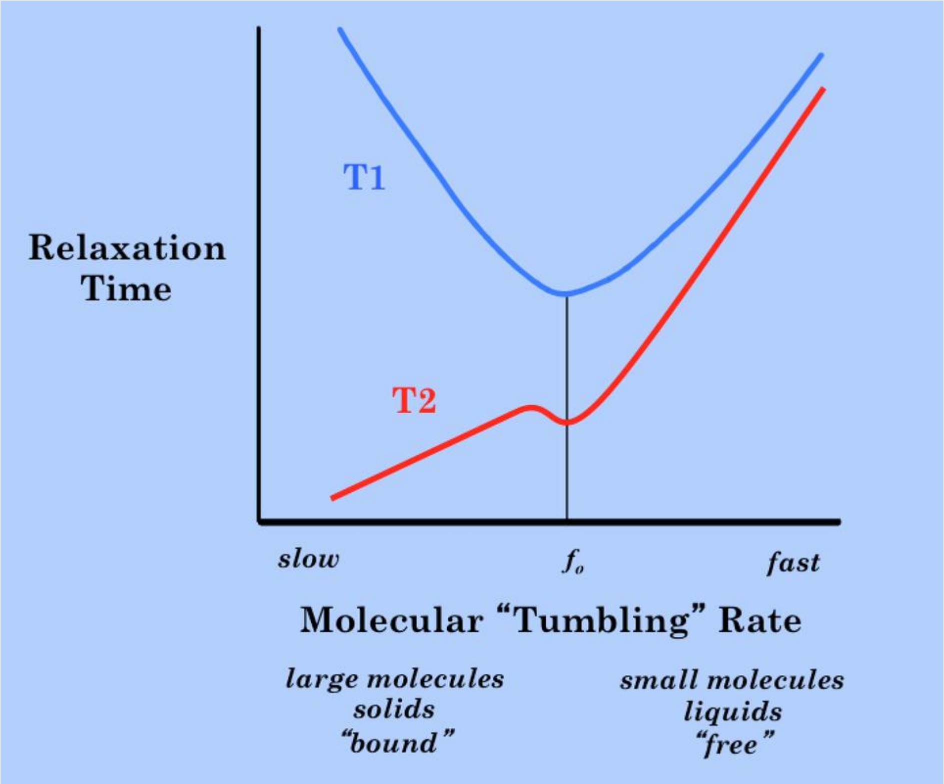

Allen D. Elster, http://mriquestions.com/

Relaxation dynamics and contrast

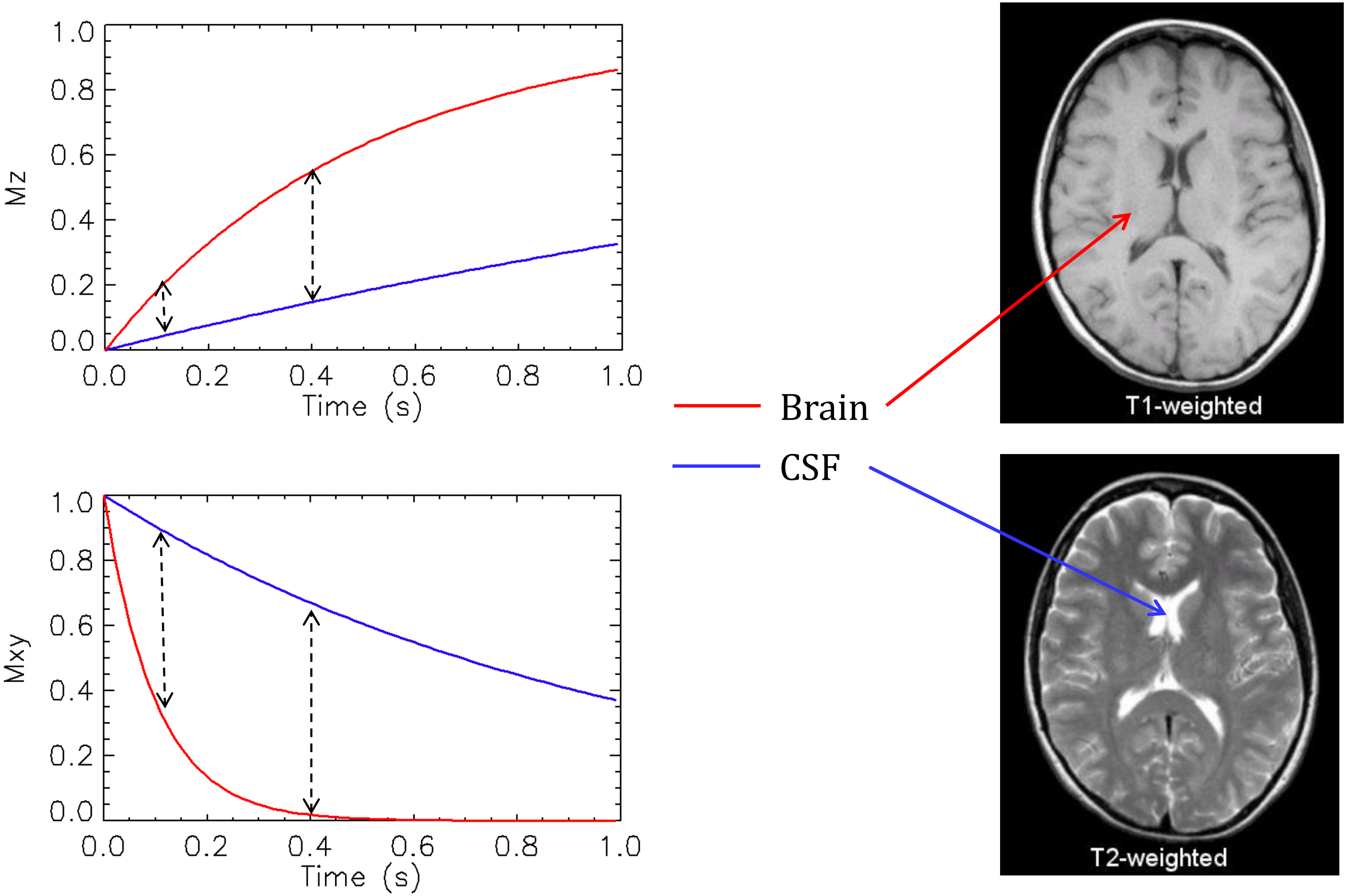

Brain

CSF

Detection

- Changes in magnetization give rise to a current in a wire loop (Faraday's law of induction)
- Receiver coil perpendicular to B_0:

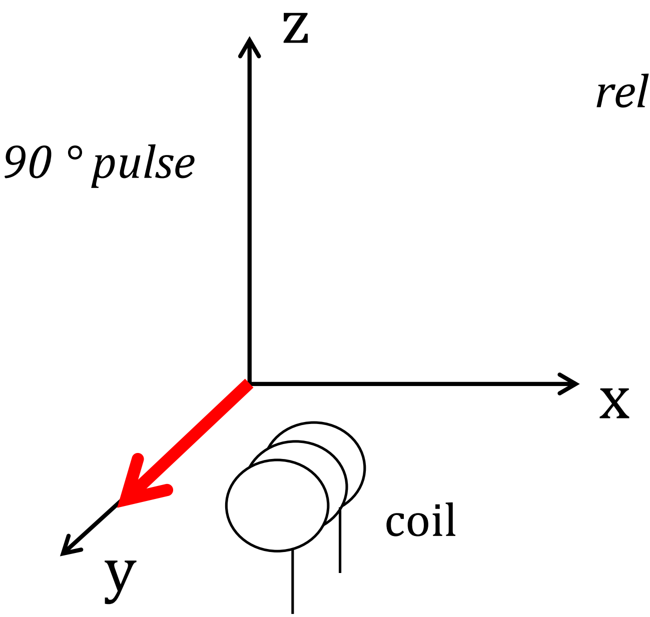
z
90 ° pulse
x
y
coil

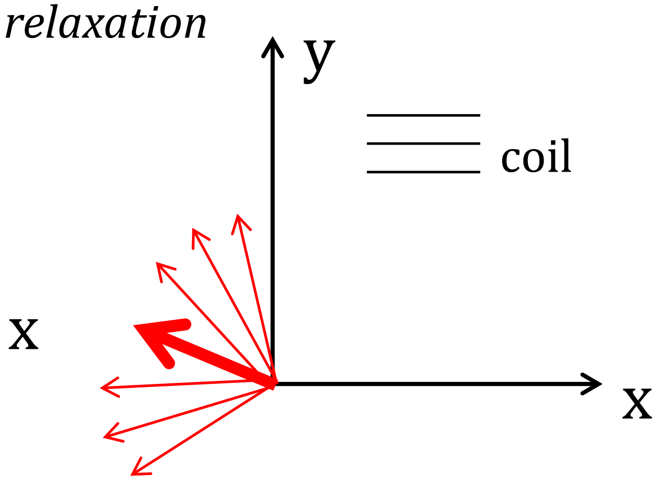
relaxation
y
coil
x

Coil signal; "FID"

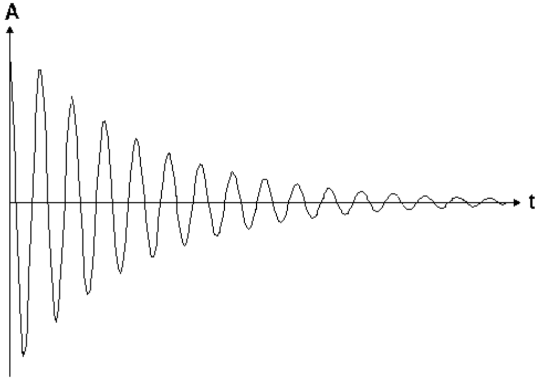

Free induction decay

- Envelope of FID describes the T2*-decay:

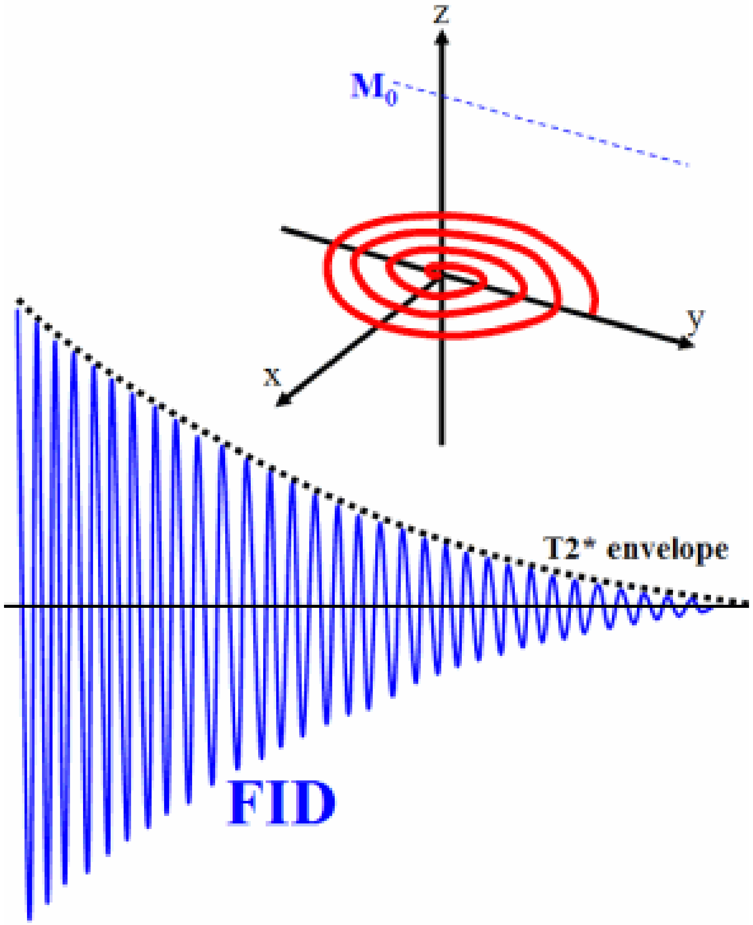
z
M_0
y
x
T2* envelope
FID

Fourier transform

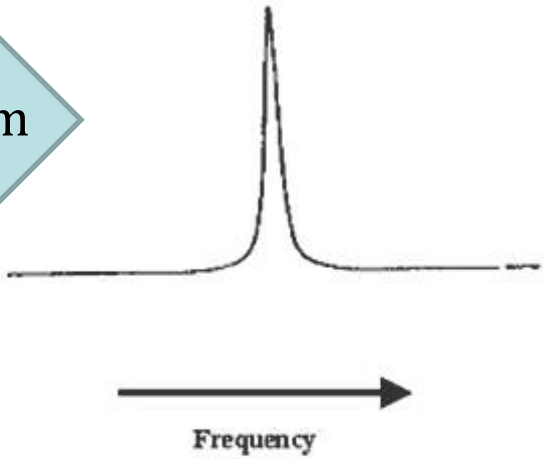

Summary

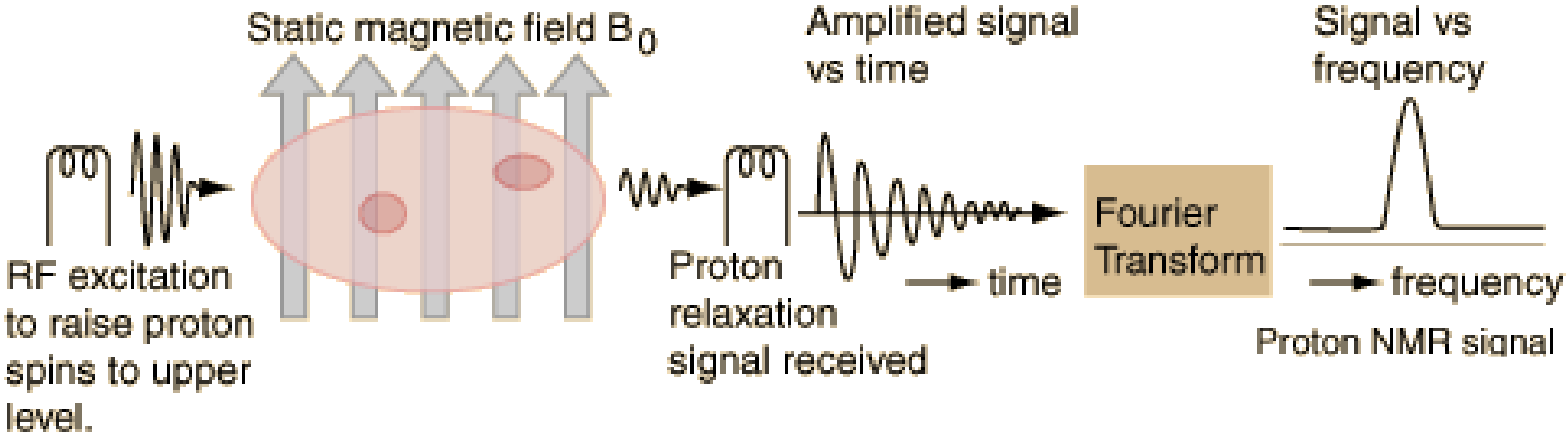
Static magnetic field B_0
Amplified signal vs time
Signal vs frequency
RF excitation to raise proton spins to upper level.
Proton relaxation signal received
time
Fourier Transform
frequency
Proton NMR signal

MRI physics: Contrast formation

Tufve Nyholm

Content

- Relaxation
  - T1, T2, T2*
- Contrasts
  - T1, T2, Proton density
- Sequences
  - Ordinary Spin-echo, Inversion recovery, Gradient echo

Entire talk is based on classical macroscopic physics

Precession

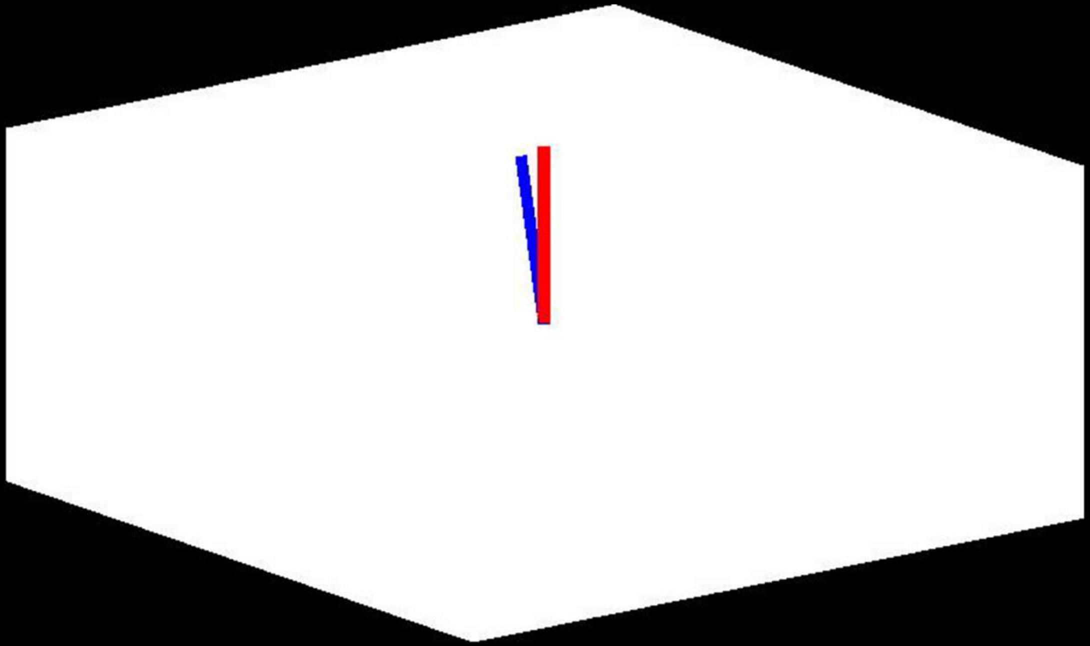

Spin’s (net magnetization) precession around the local magnetic field:

Larmor frequency

$$\omega = -\gamma B$$

42.576 MHz/T

Magnetic field

Flip

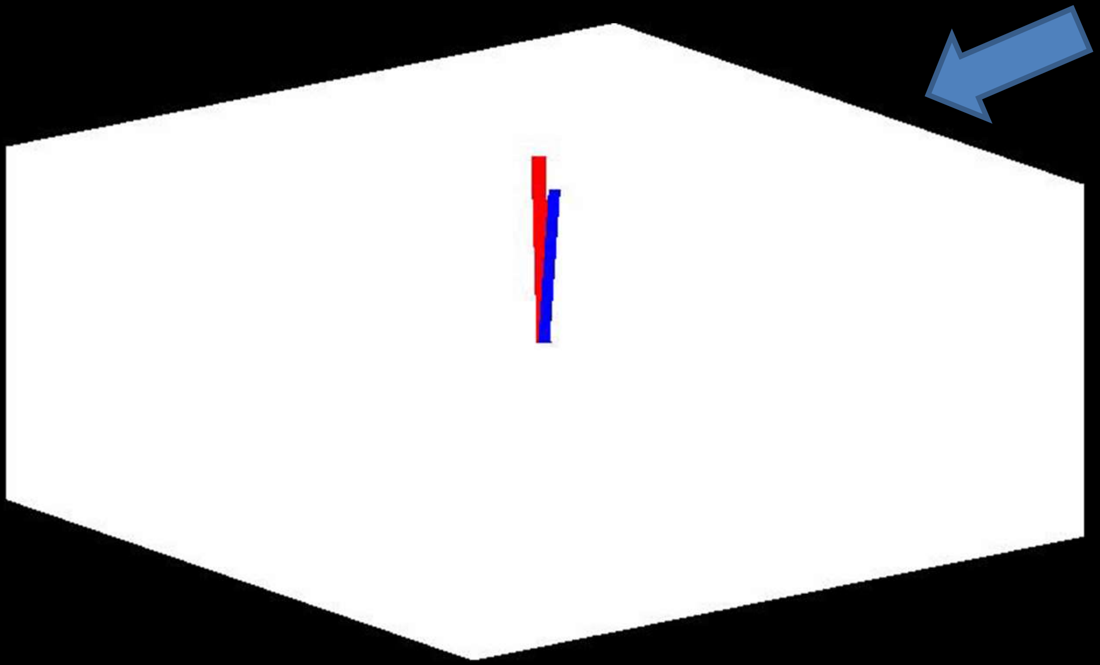

RF pulse

Spin’s (net magnetization) precession around the local magnetic field:

Larmor frequency

$$\omega = -\gamma B$$

42.576 MHz/T

Magnetic field

Relaxation

T1 relaxation
Parallel plane

Rotating coordinate system

T2 relaxation
Transversal plane

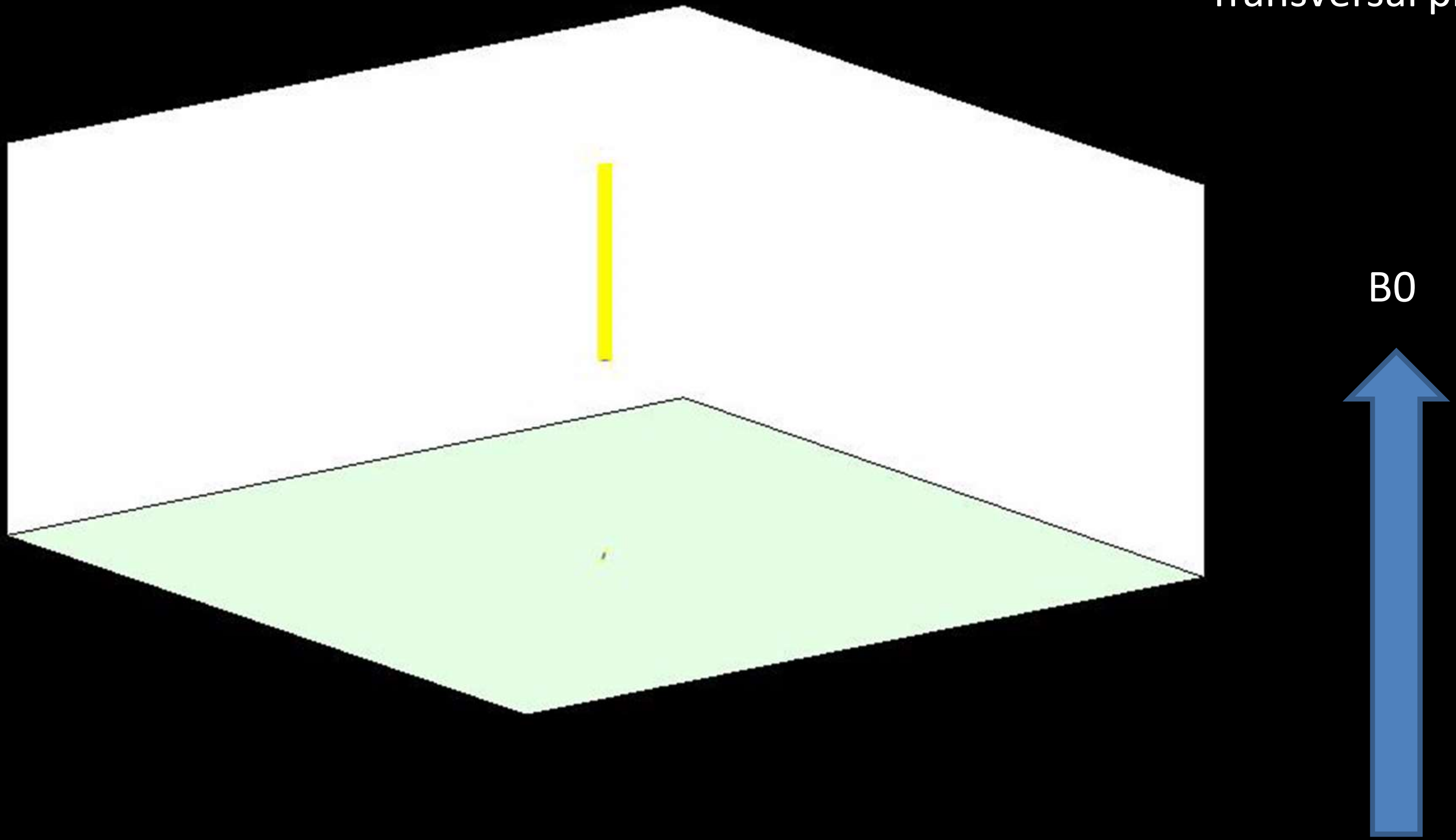

The transversal component gives signal

T1 relaxation

- Spin-lattice or longitudinal relaxation
- Restoring longitudinal magnetization after RF excitation
- T1 – Time until 63% of the initial magnetization M0 is restored

Adipose tissue – 240ms
Spinal fluid – 4300ms
Gray matter – 980ms
White matter – 780ms
Muscles – 880ms

$$M(t)_z = M_0\left[1 - e^{-t/T1}\right]$$

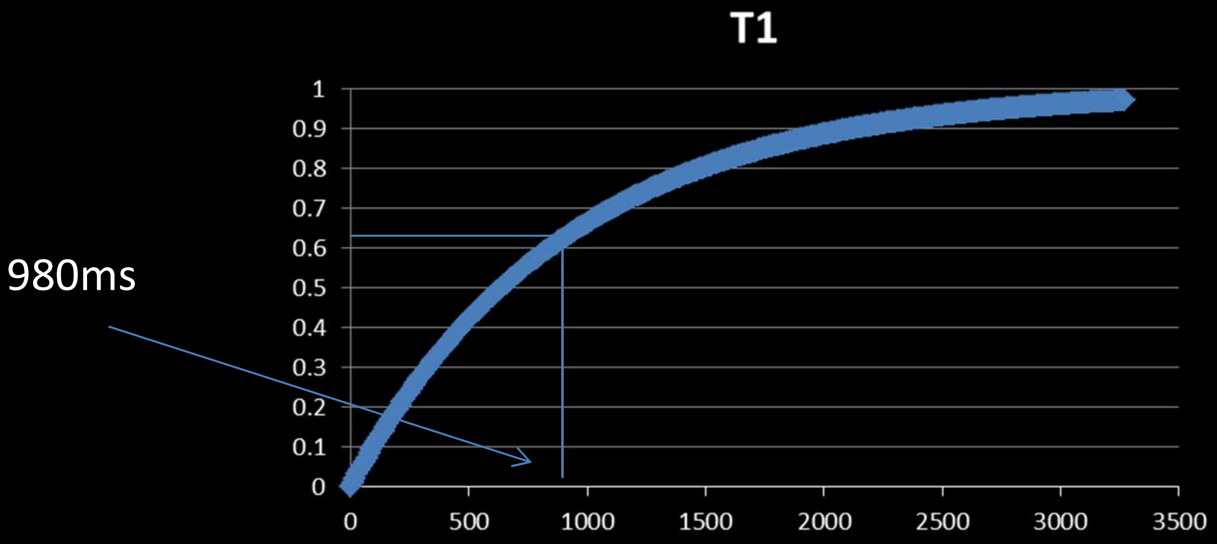

T2 relaxation

- Spin-spin or transversal relaxation
- Loss of transversal magnetization after RF excitation
- T2 – time until 63% of the transversal magnetization is lost

Adipose tissue – 70ms
Spinal fluid – 2200ms
Gray matter – 100ms
White matter – 90ms
Muscles – 50ms

$$M(t)_r = M_{r,t=0} e^{-t/T2}$$

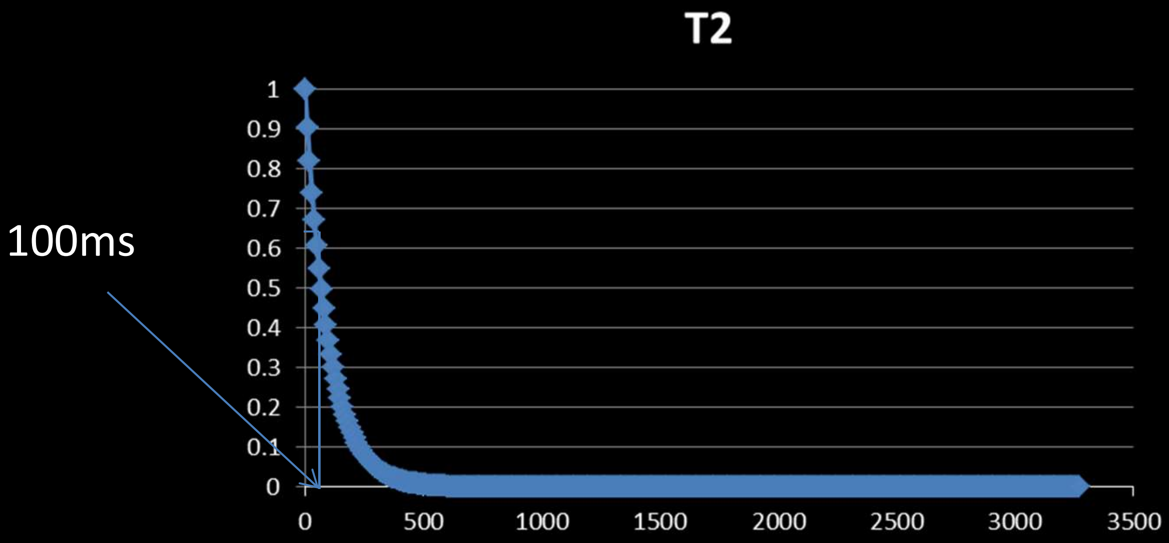

T2* relaxation

$$M(t)_r = M_{r,t=0}e^{-t/T2^*}$$

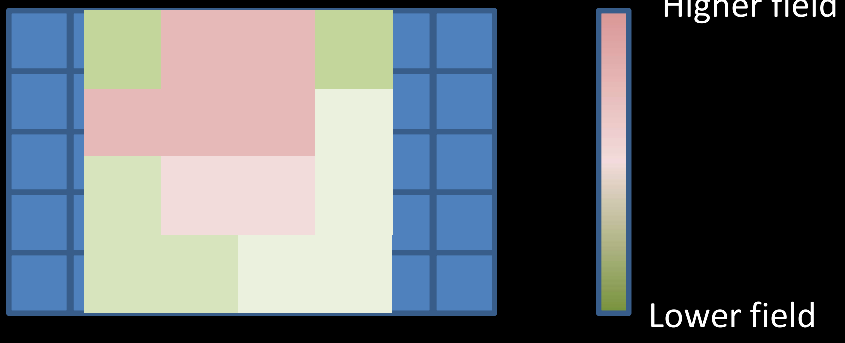
Higher field
Lower field

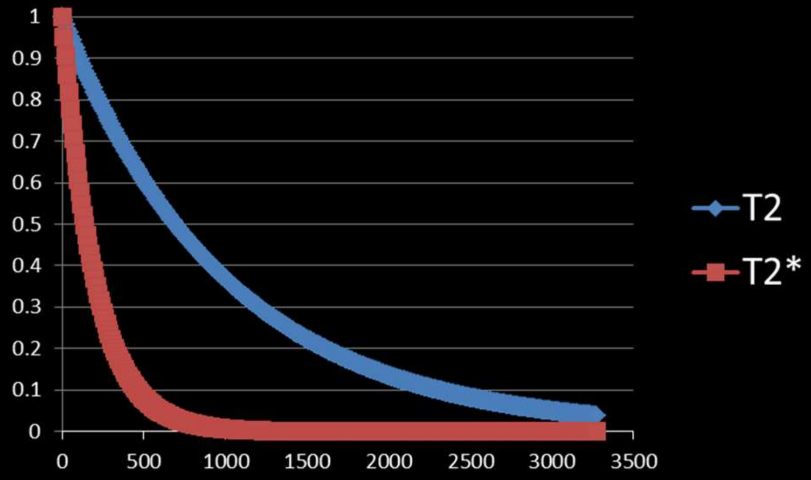

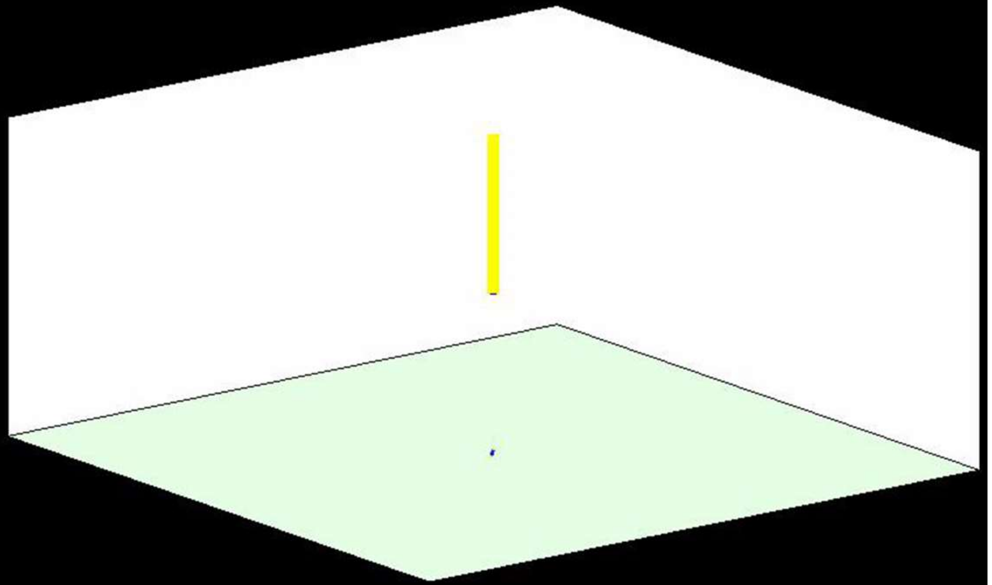

Spin-Echo sequence

- 180 degree pulse refocus the spins
- Signal independent of T2*

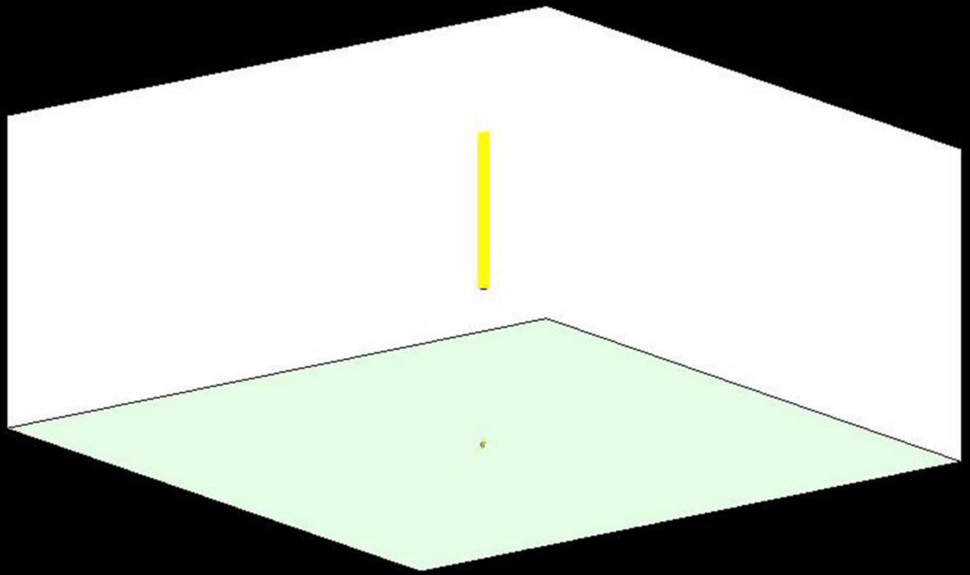

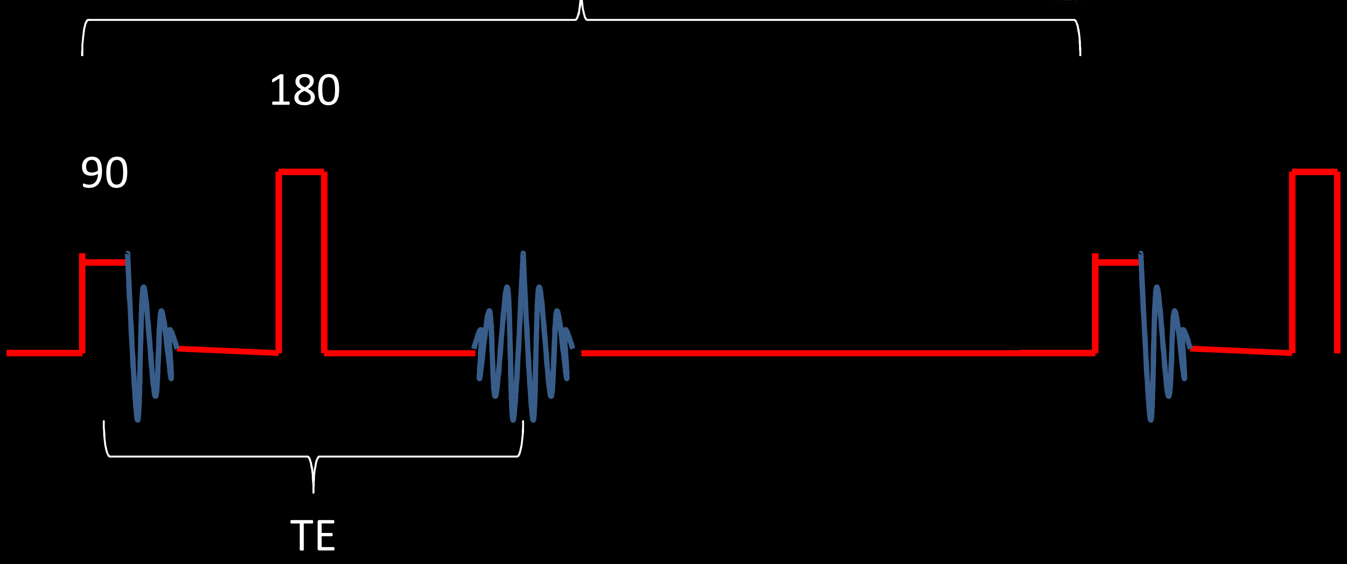

Spin-Echo sequence

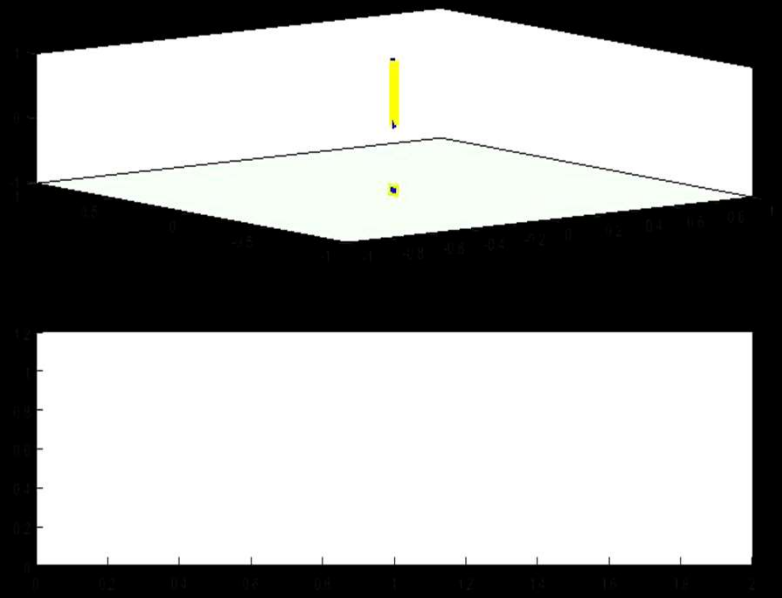

🟩 Parallel component

🟦 Transversal component

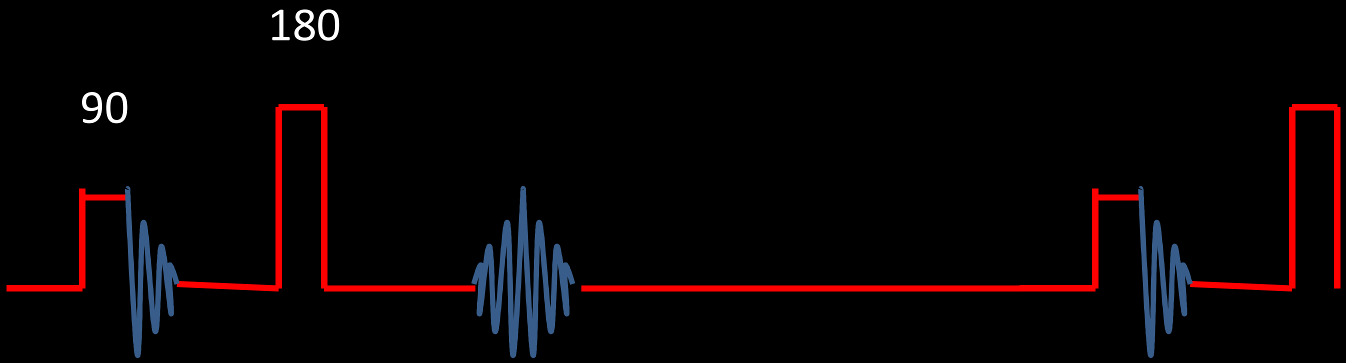

Spin-Echo sequence

T1 relaxation

$$M(t)_z = M_0\left[1 - e^{-t/T1}\right]$$

T2 relaxation

$$M(t)_r = M_{r,t=0}e^{-t/T2}$$

Signal equation

$$S = k\rho\left(1 - e^{-TR/T1}\right)e^{-TE/T2}$$

Constant depending on

- Coils
- Temperature
- etc

Proton density

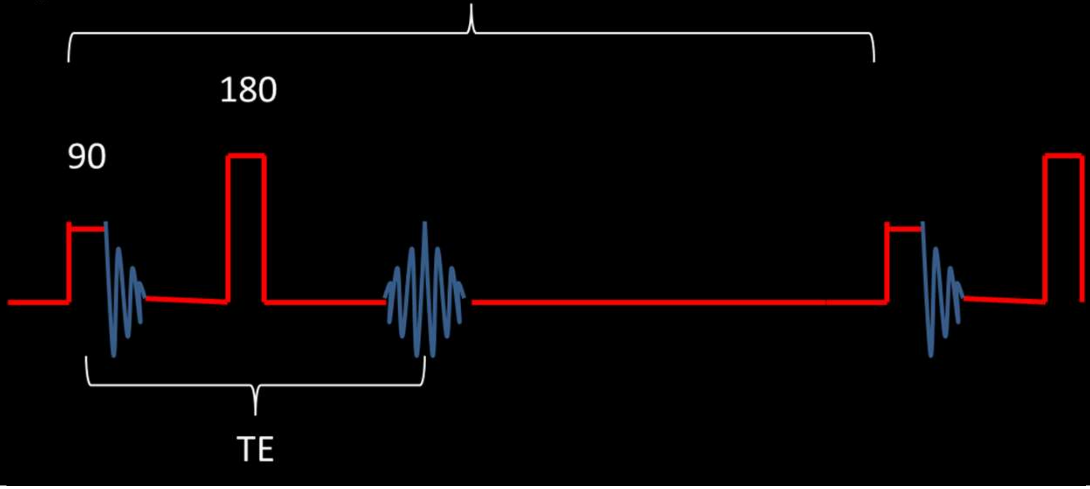

T2 contrast

$$S = k\rho \underbrace{\left(1 - e^{-TR/T1}\right)}_{\text{Minimize influence i.e. Long TR}} \underbrace{e^{-TE/T2}}_{\text{Focus}}$$

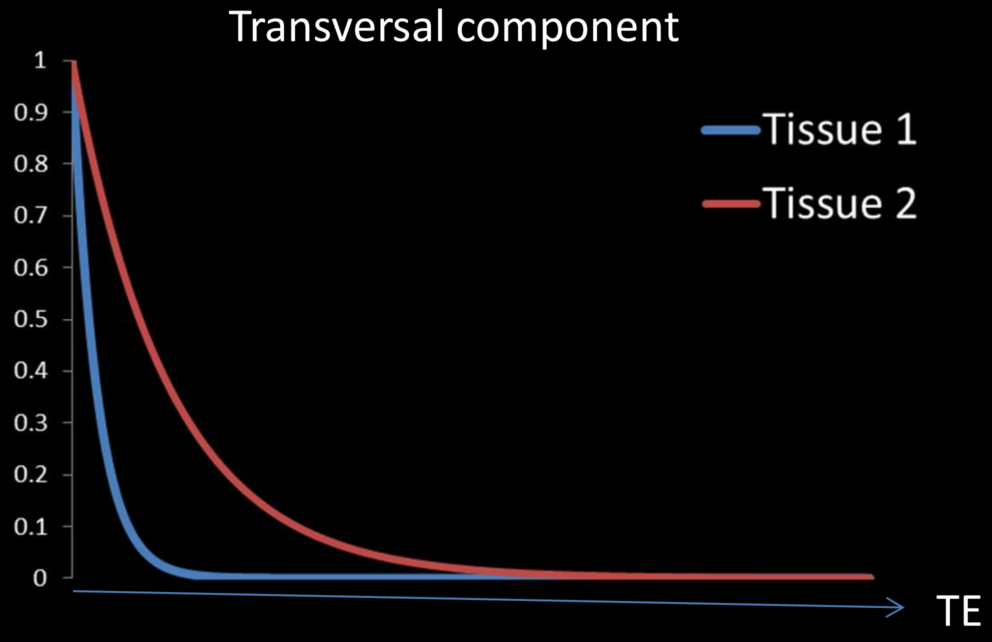
Transversal component

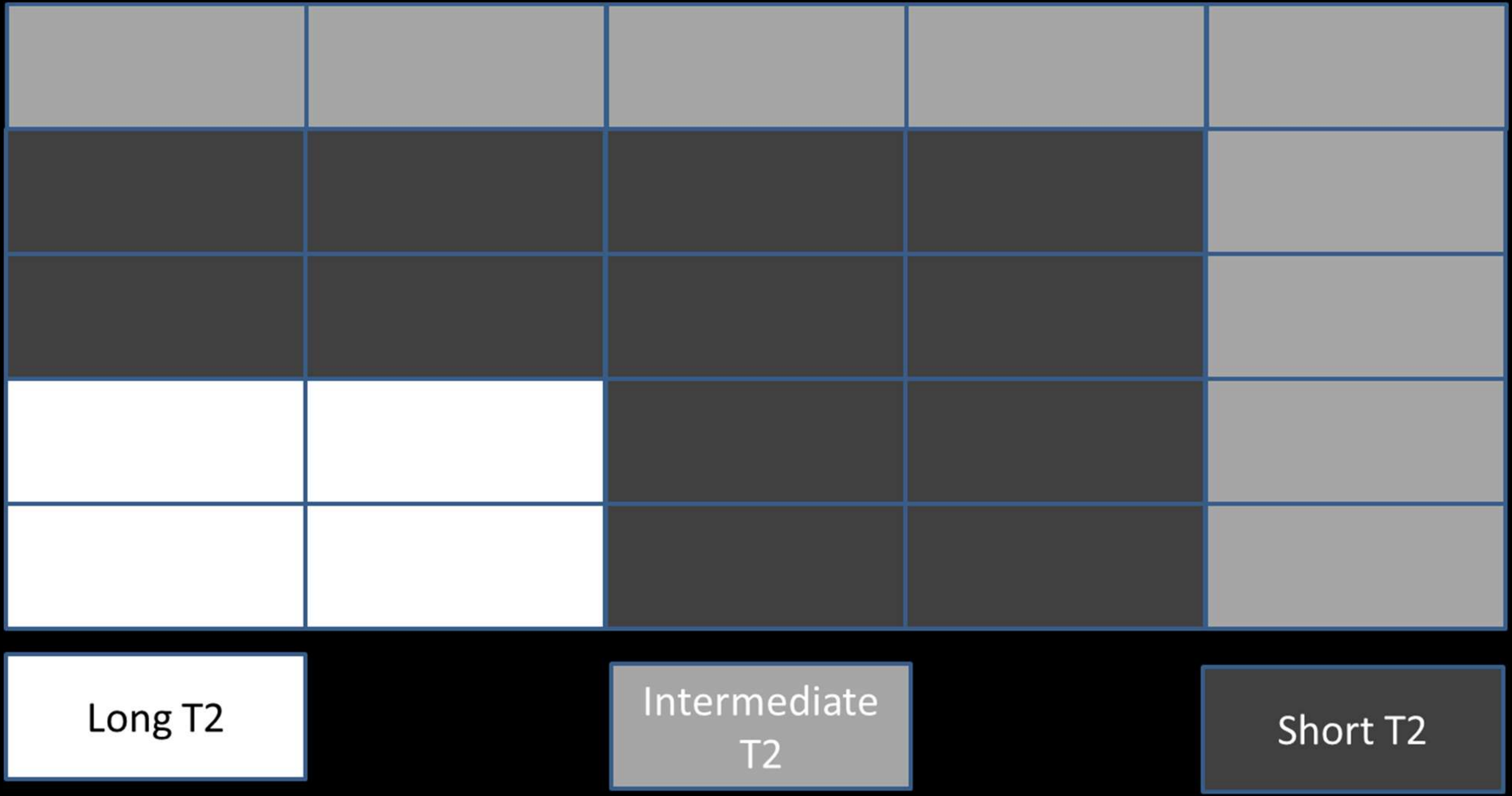

Long T2

Intermediate T2

Short T2

T2 contrast

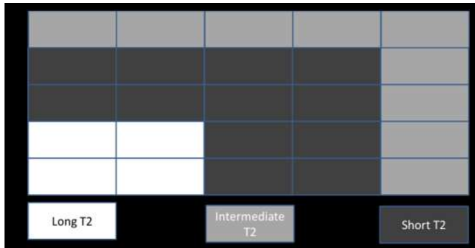
Long T2
Intermediate T2
Short T2

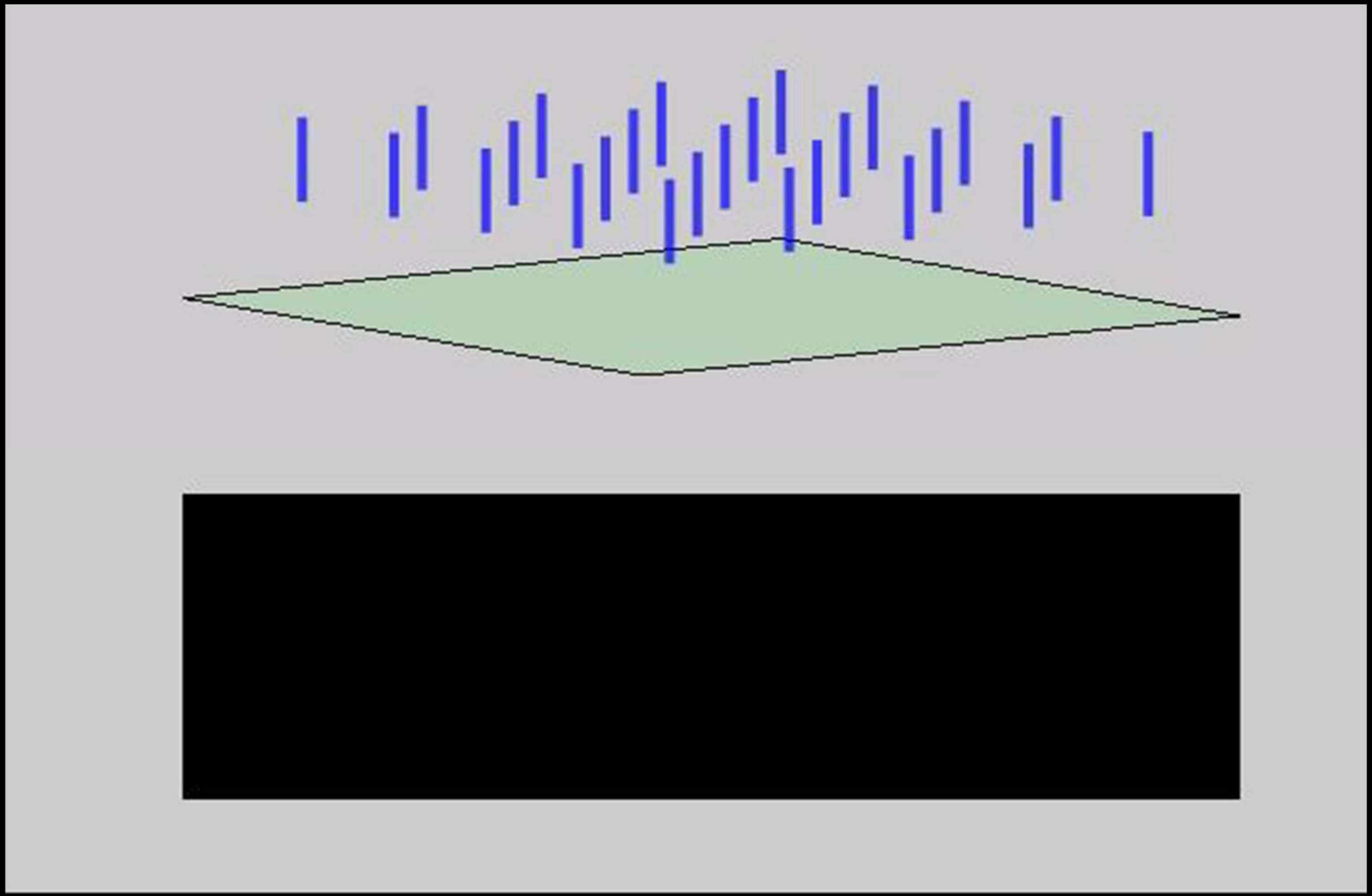

Examples

T2 Contrast

Adipose tissue – 70ms
Spinal fluid – 2200ms
Gray matter – 100ms
White matter – 90ms
Muscles – 50ms

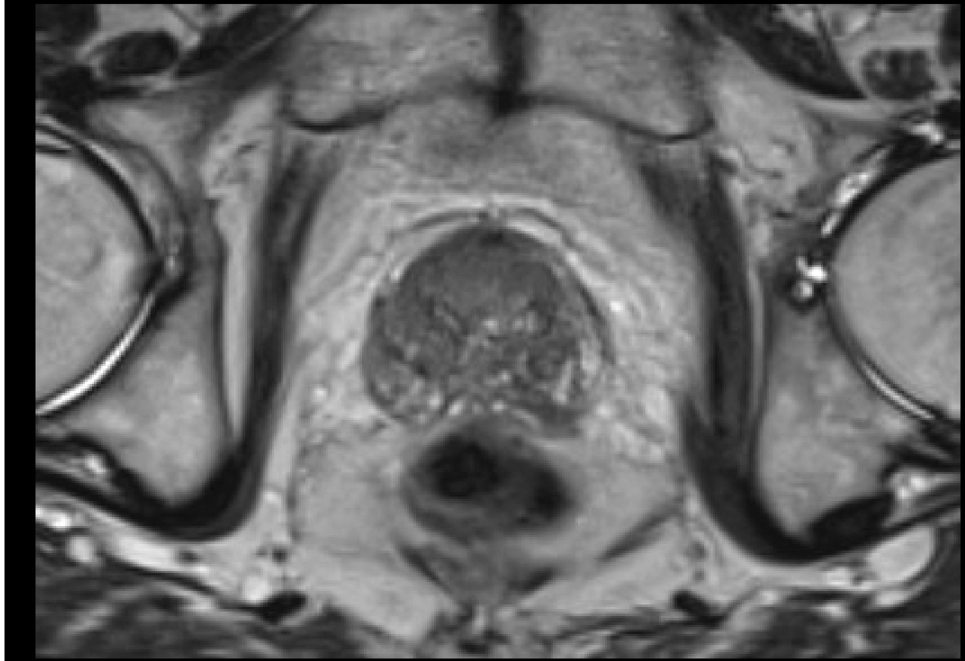

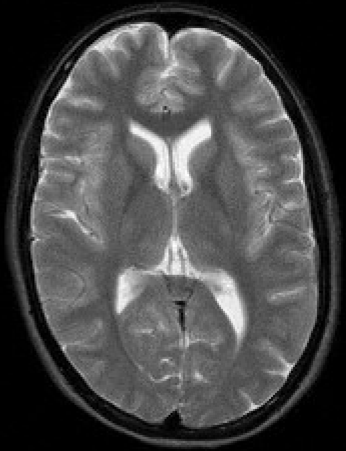

TE=90ms

T1 contrast

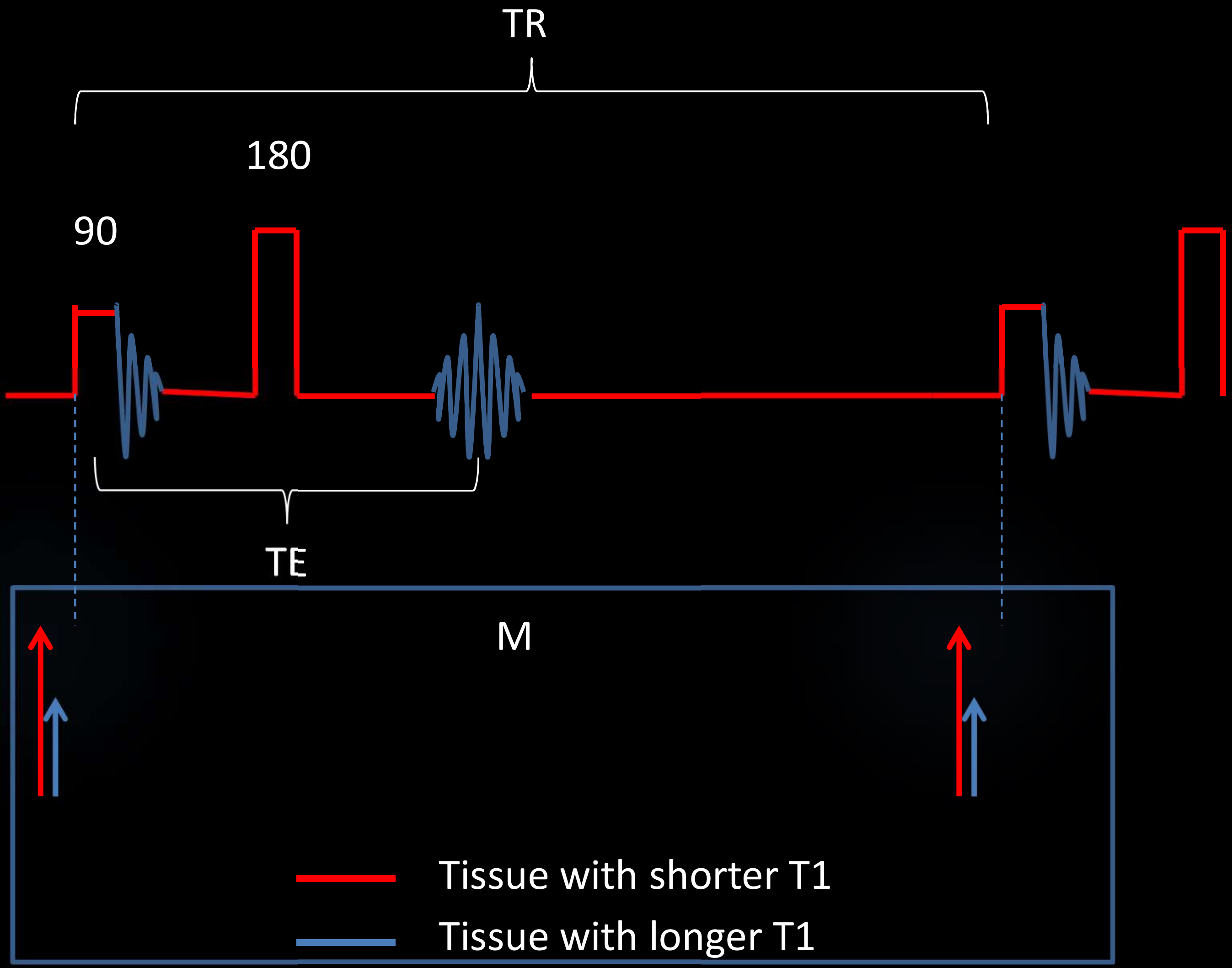
TR
180
90
TE
M
Tissue with shorter T1
Tissue with longer T1

T1 contrast

Long T1

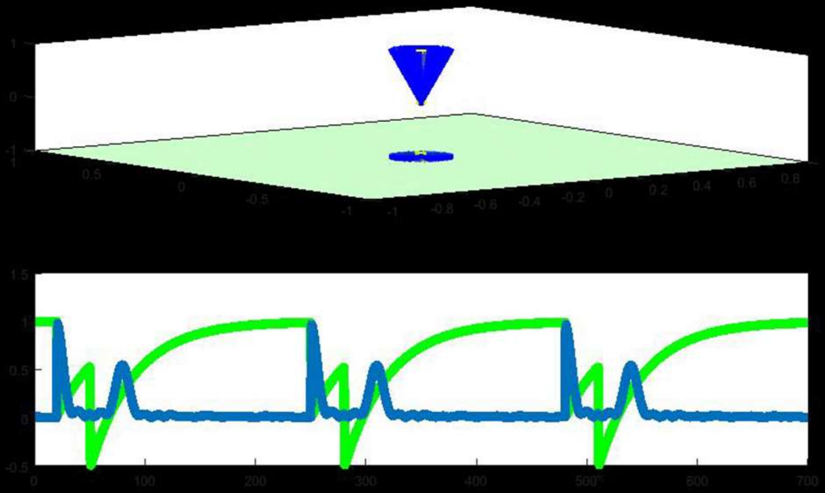

Short T1

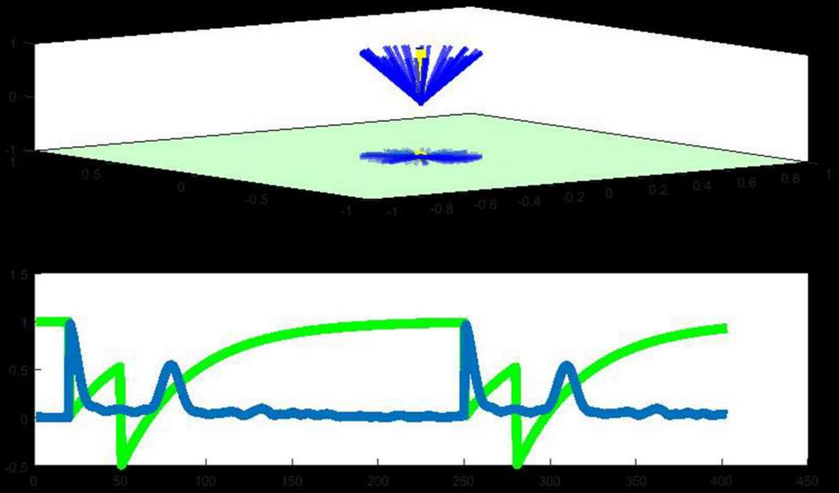

🟩 Parallel component

🟦 Transversal component

T1 Contrast

$$S = k\rho \underbrace{\left(1 - e^{-TR/T1}\right)}_{\text{Focus}} \underbrace{e^{-TE/T2}}_{\text{Minimize influence i.e. Short TE}}$$

Parallel component

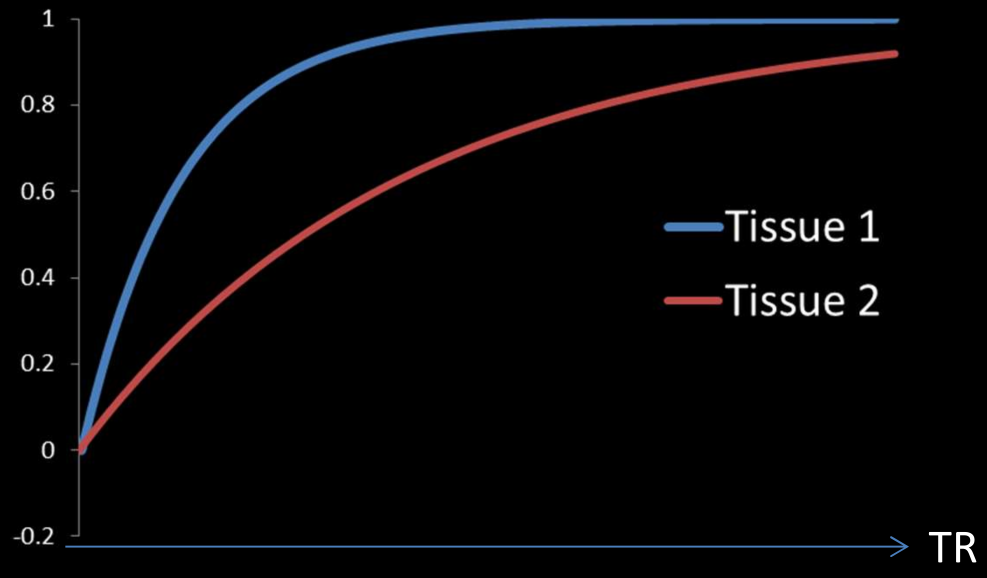

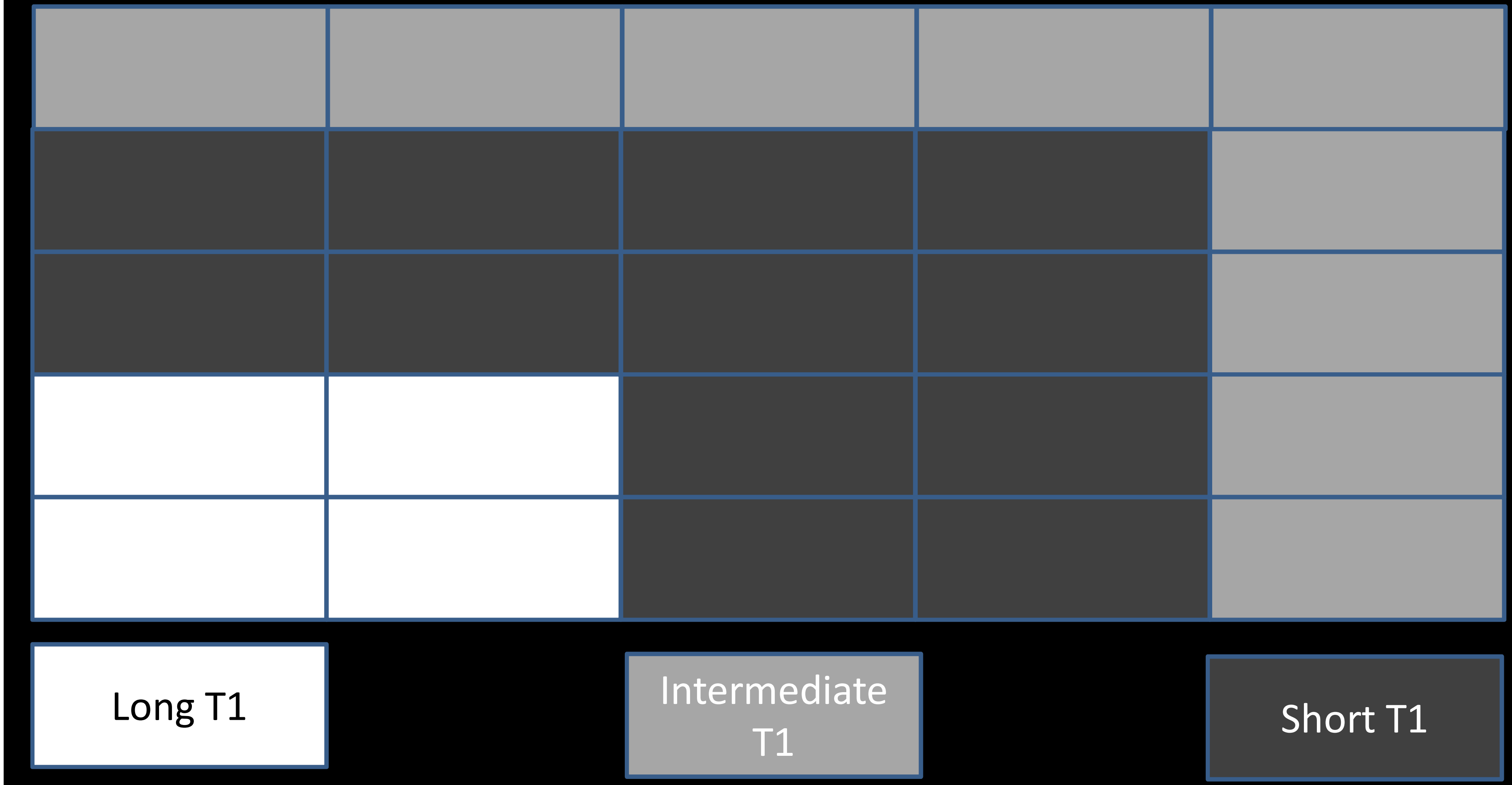
Long T1
Intermediate T1
Short T1

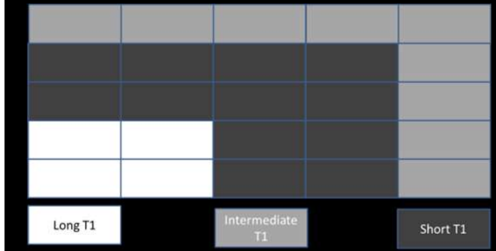
Long T1
Intermediate T1
Short T1

T1 contrast

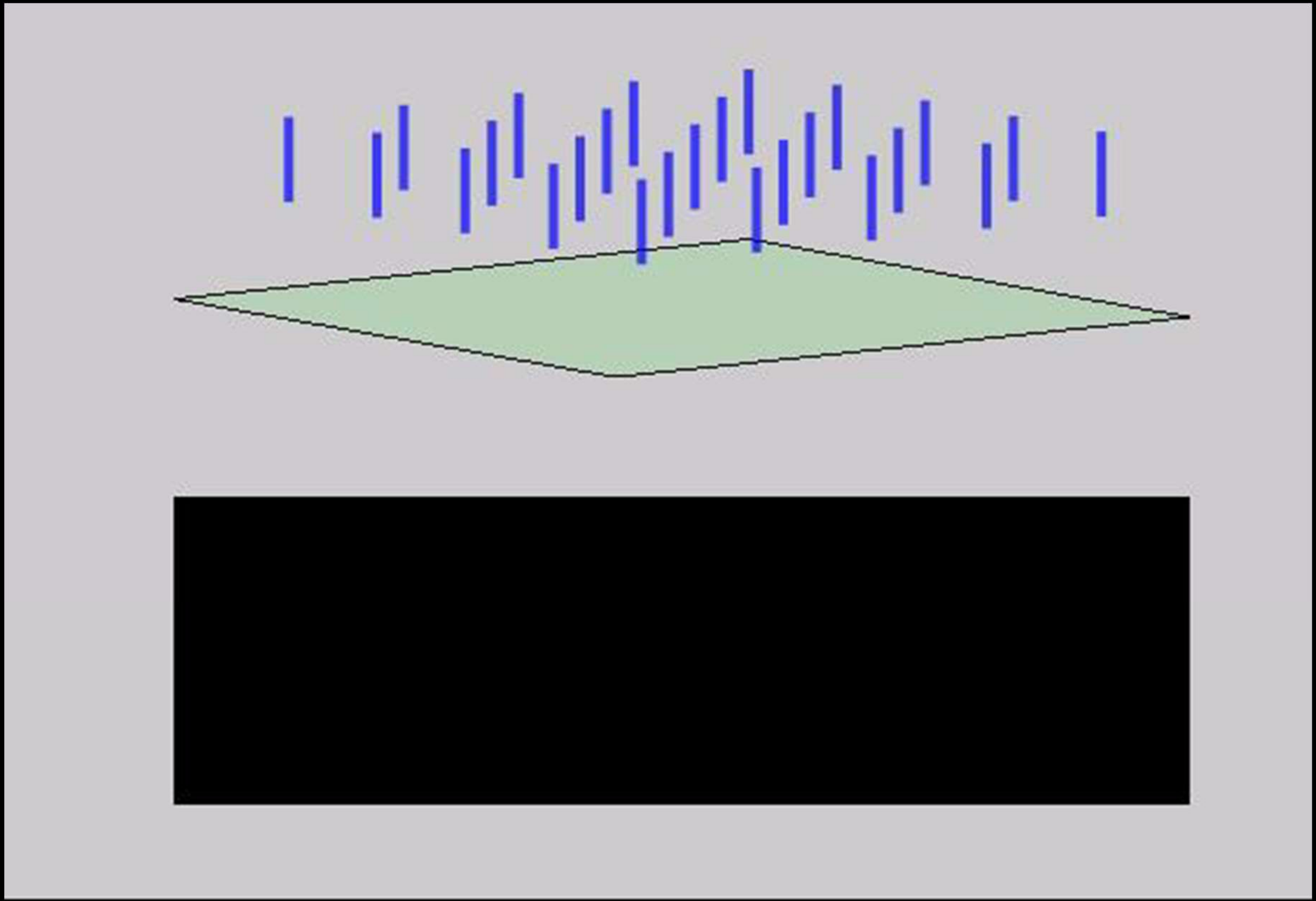

Examples

T1 contrast

Adipose tissue – 240ms
Spinal fluid – 4300ms
Gray matter – 980ms
White matter – 780ms
Muscles – 880ms

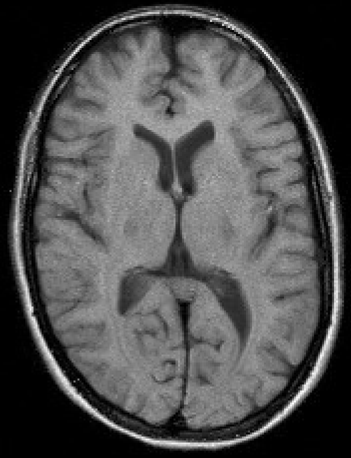

TR=450ms

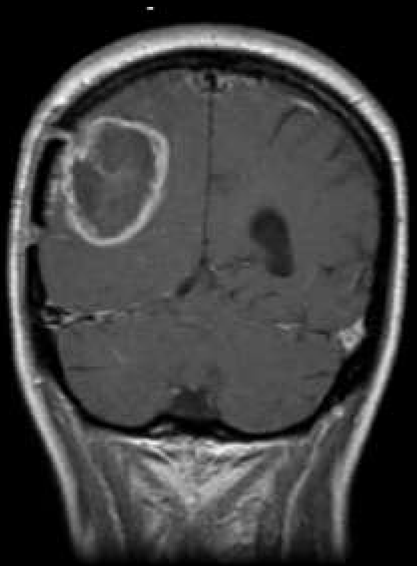

Inversion-recovery (IR)

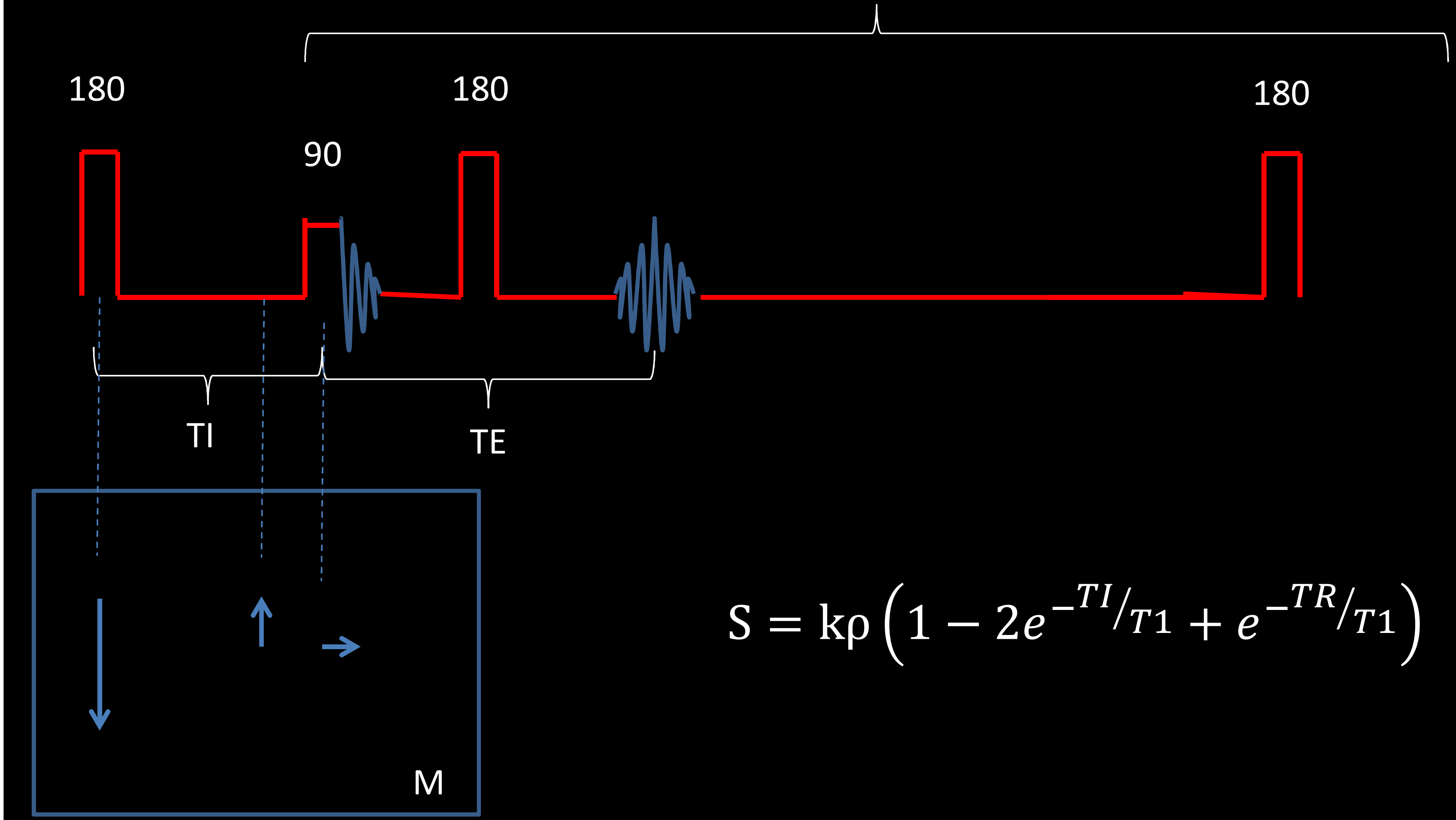
TR
180
180
90
180
TI
TE
M

$$S = k\rho\left(1 - 2e^{-TI/T1} + e^{-TR/T1}\right)$$

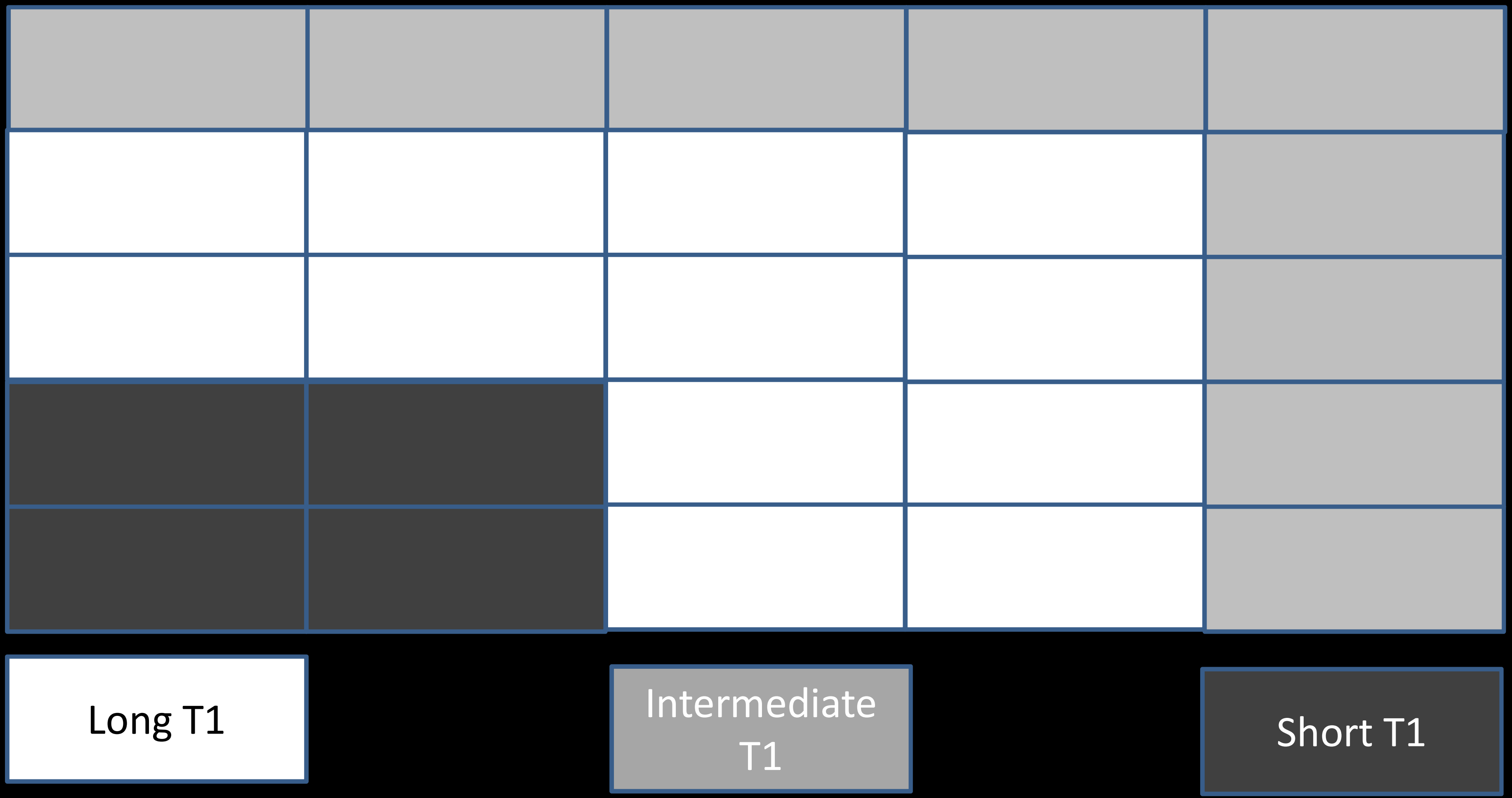

Long T1

Intermediate T1

Short T1

IR

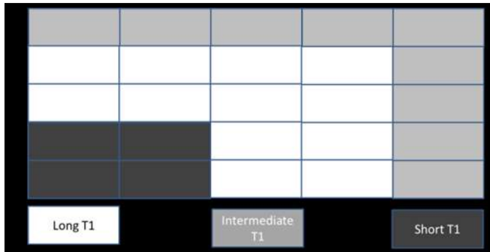
Long T1
Intermediate T1
Short T1

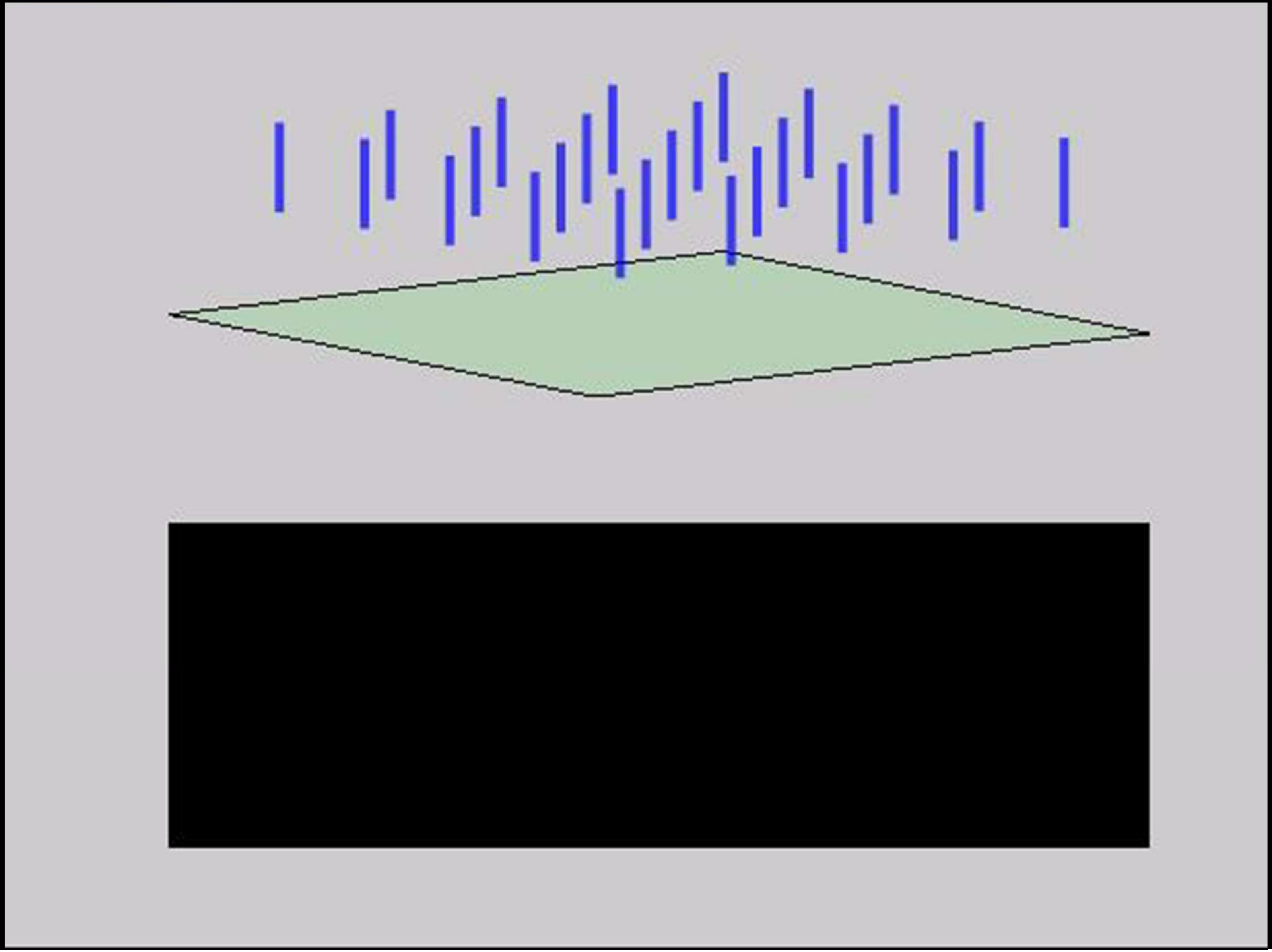

Example Inversion recovery

FLAIR

Dark fluid

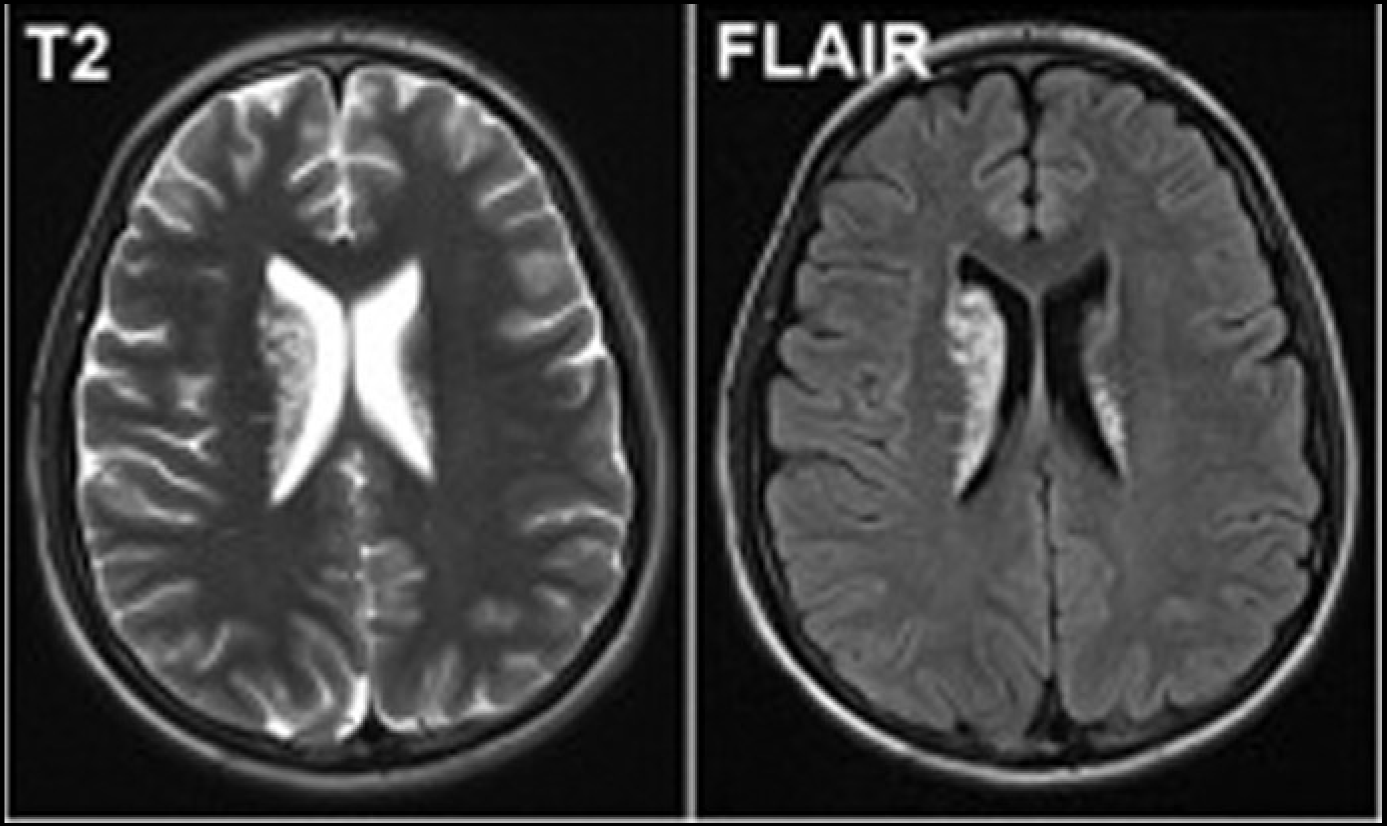

Summary

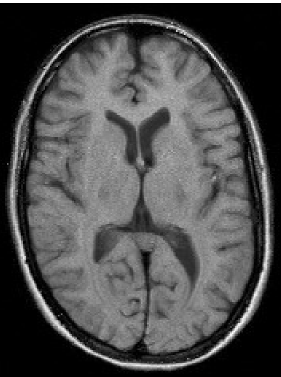

T1 contrast

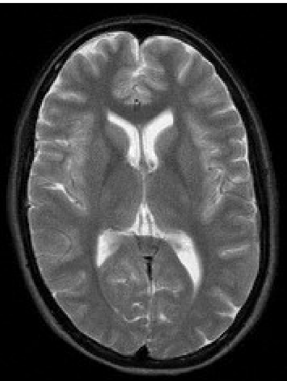

T2 contrast

TE - Short
TR – Optimized

Inversion recovery
TI - Optimized

- Use for anatomical imaging
- For pathology together with contrast agent

TE - Optimized
TR – Long

- Use for pathology
- Use for anatomical imaging

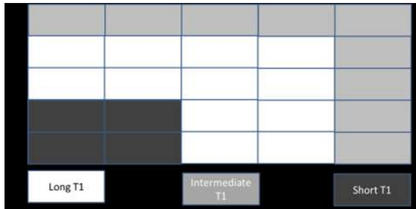
Long T1
Intermediate T1
Short T1

IR

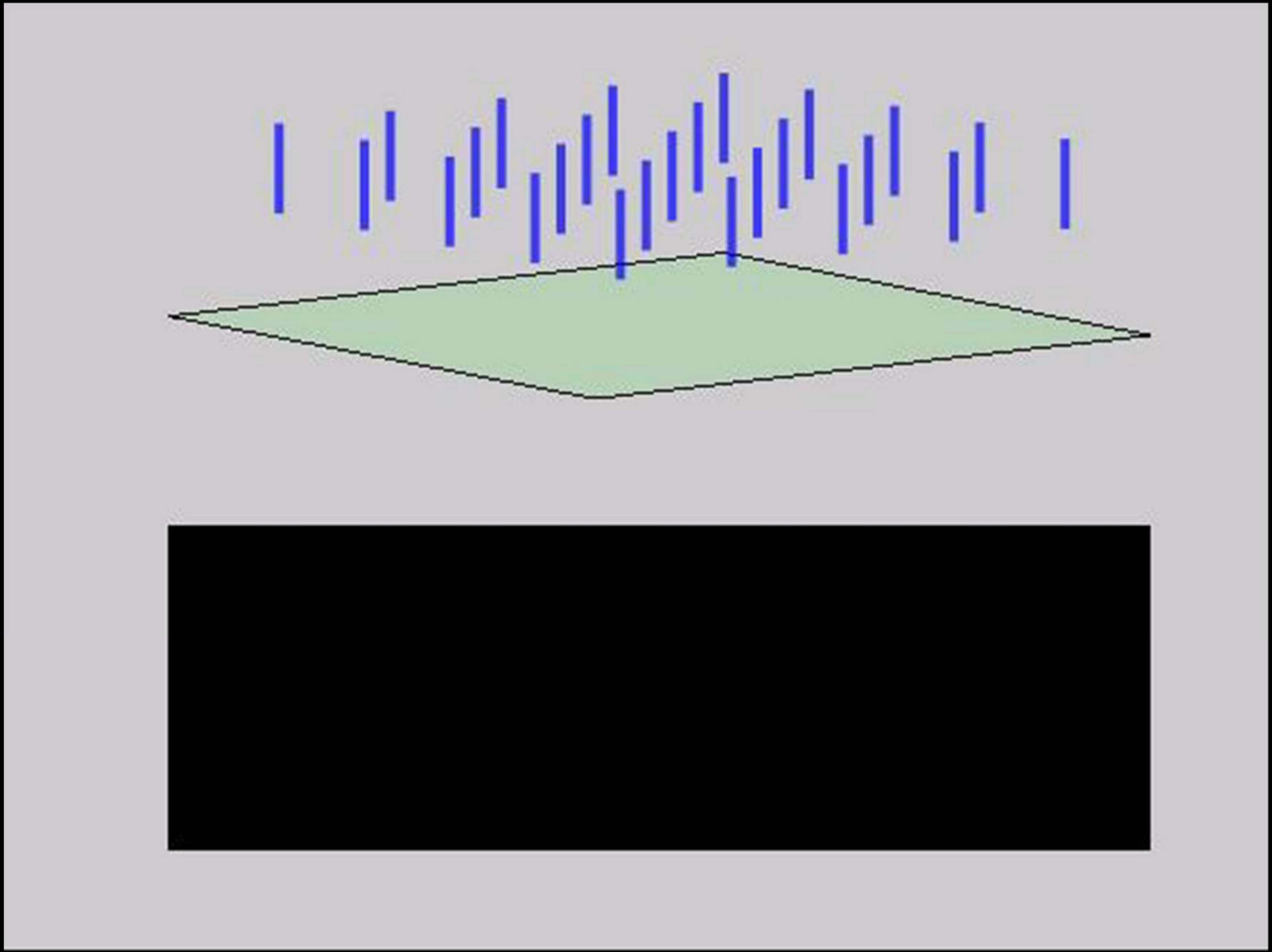

Proton contrast

$$S = k\rho\underbrace{\left(1 - e^{-TR/T1}\right)}_{\substack{\text{Minimize influence}\\ \text{i.e. Long TR}}}\underbrace{e^{-TE/T2}}_{\substack{\text{Minimize influence}\\ \text{i.e. Short TE}}}$$

Focus

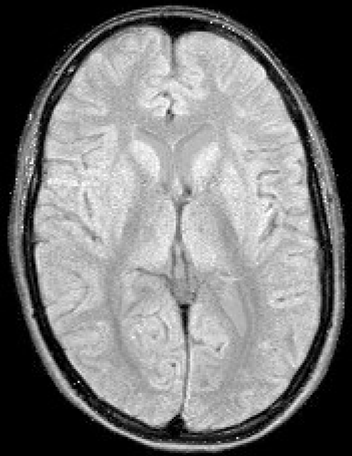

Turbo spin echo
Fast spin echo

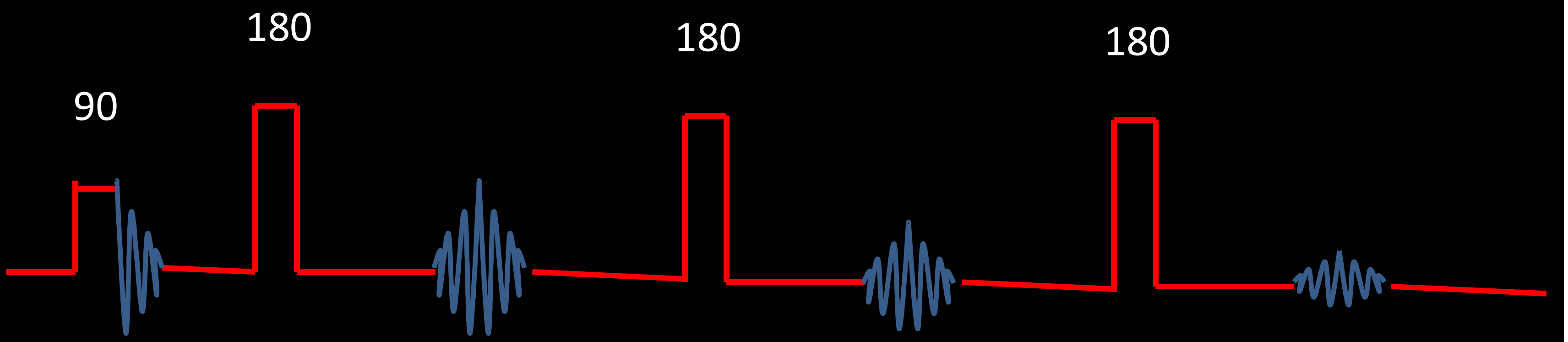
180
180
180
90

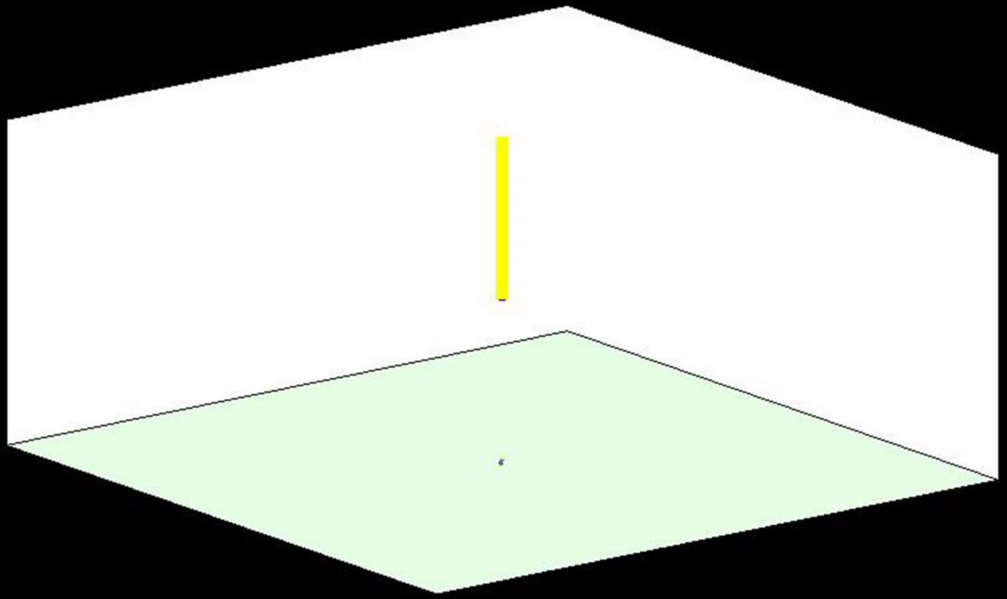

Gradient echo sequences

- No refocusing pulse → sensitive to T2*
- Gradients used to generate an echo
- Main benefit: Faster than Spin-Echo

Gradient echo (T2*)

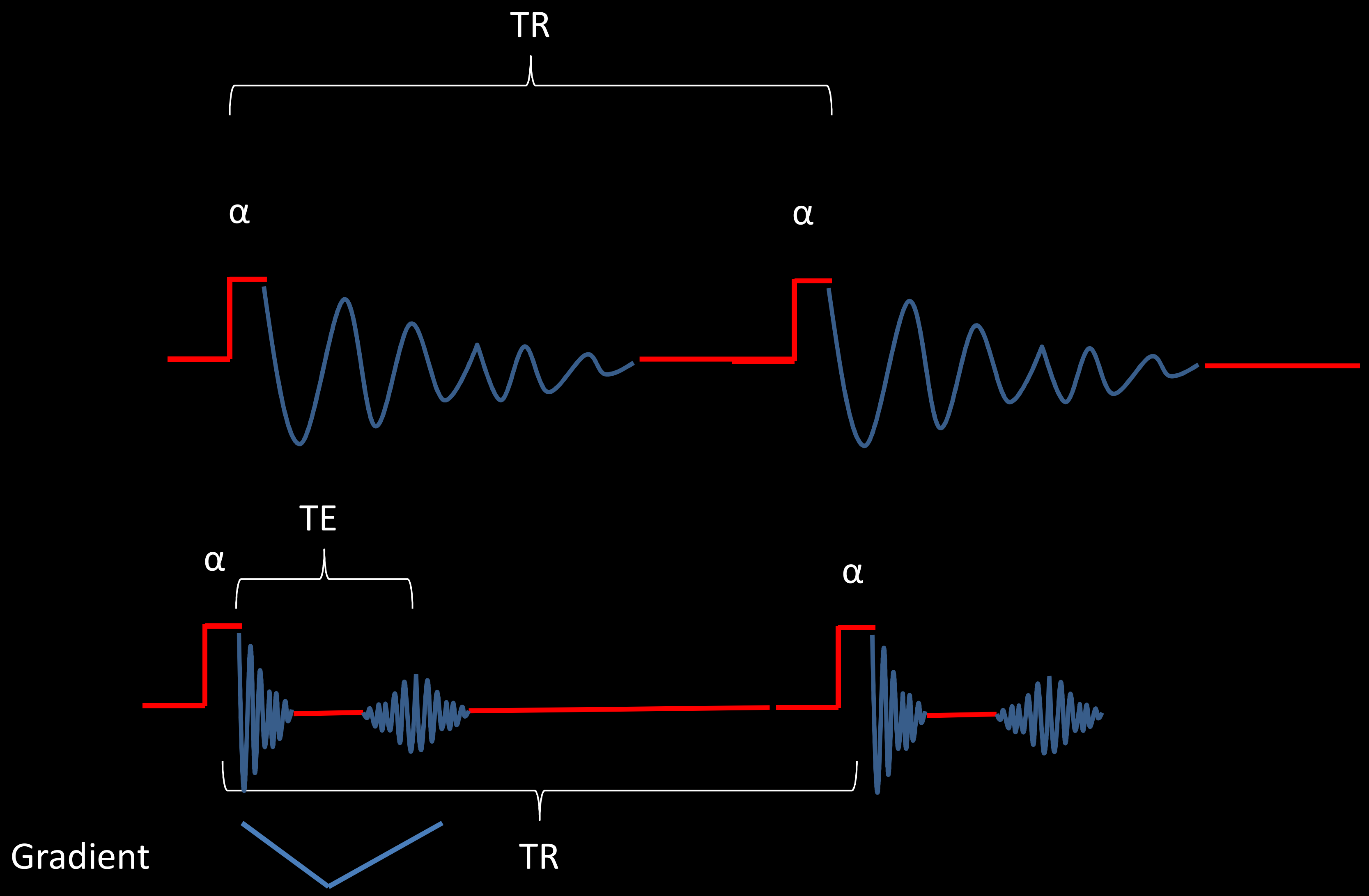
TR
α
α
TE
α
α
TR
Gradient

Gradient echo (T2*)

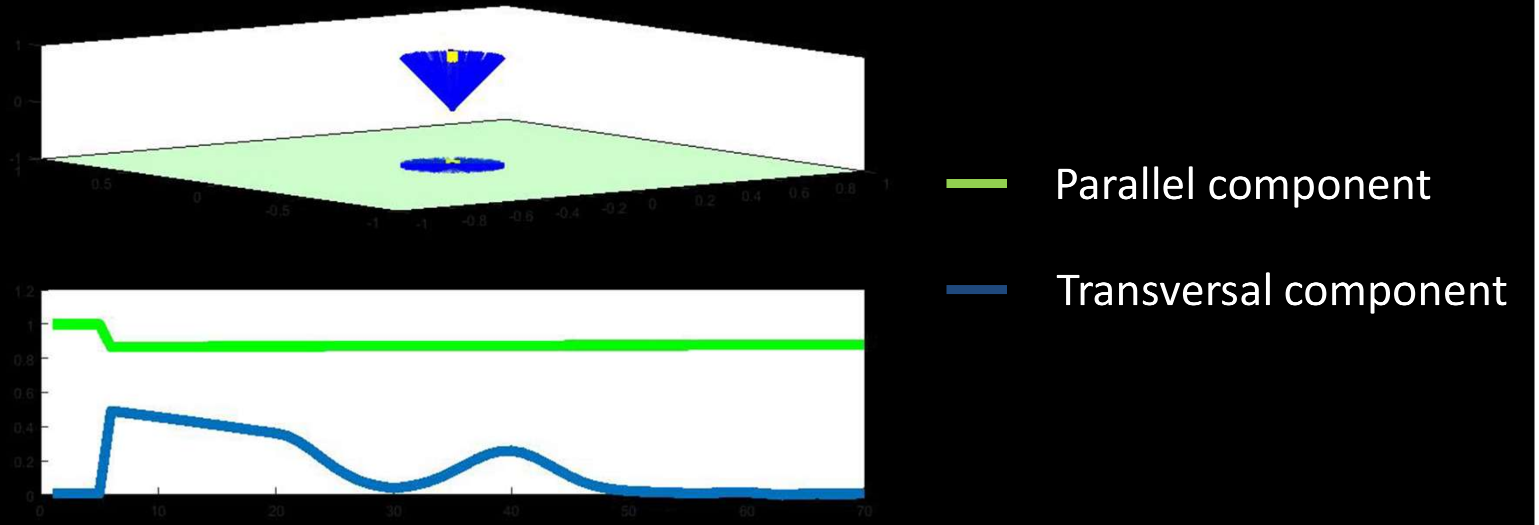

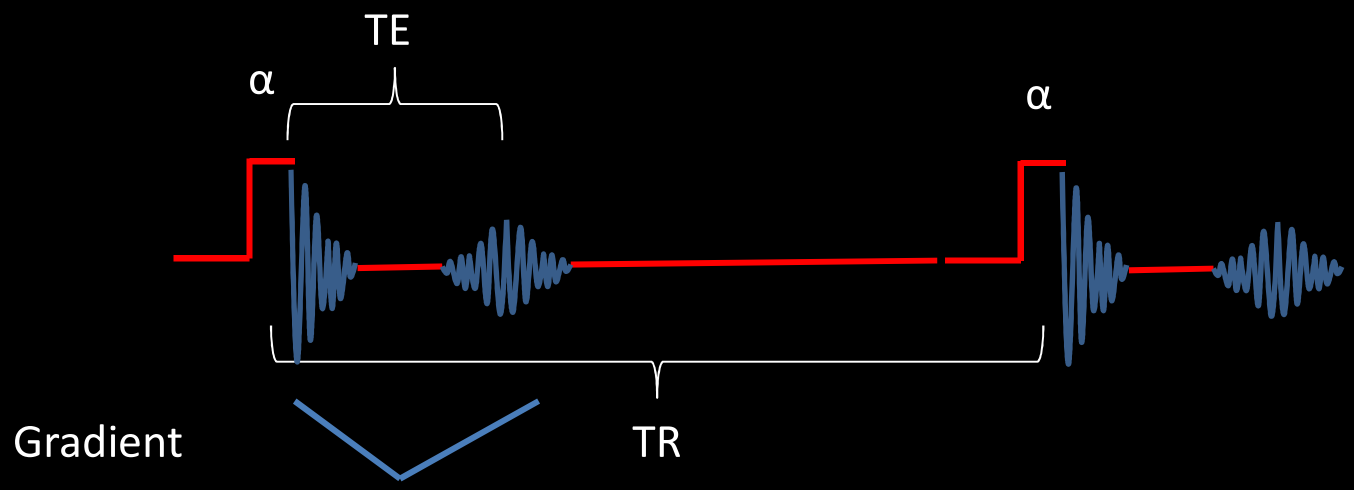
TE
α
α
Gradient
TR

Spooling

Without spooling

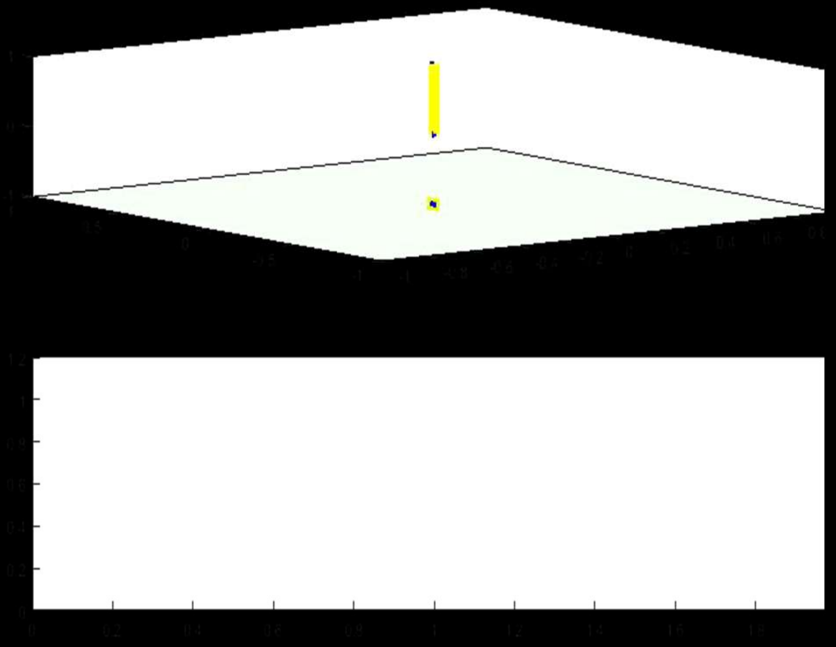

With spooling

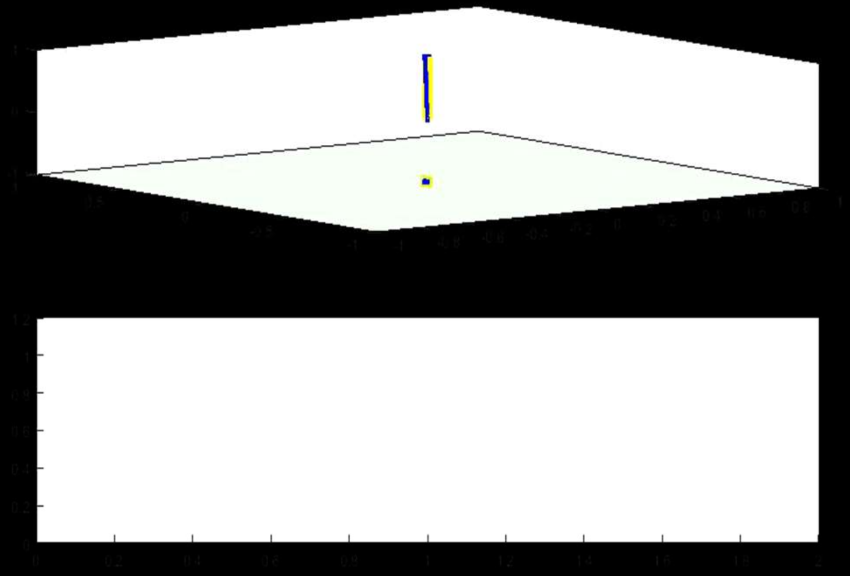

▬ Parallel component

▬ Transversal component

Spooling

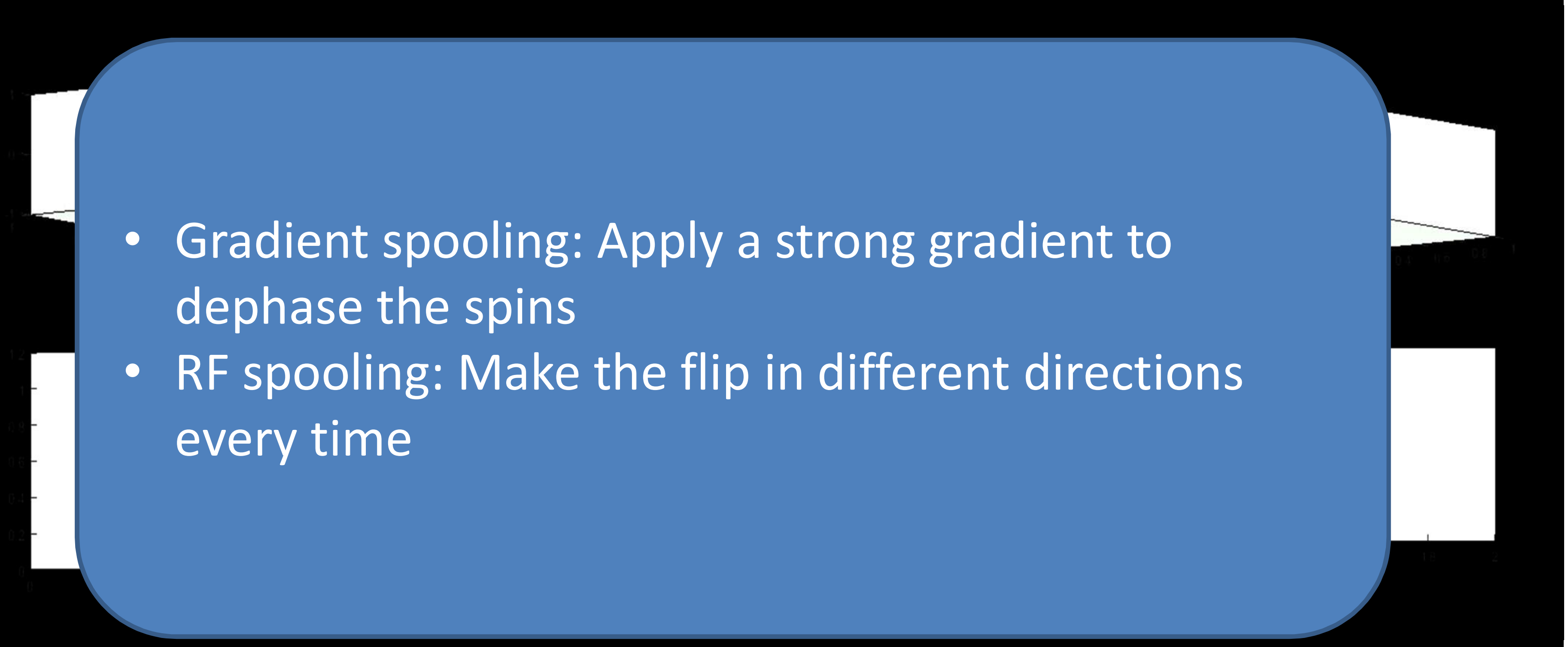

- Gradient spooling: Apply a strong gradient to dephase the spins
- RF spooling: Make the flip in different directions every time

🟩 Parallel component

🟦 Transversal component

Gradient echo

$$\mathrm{S} \sim \rho\left(\sin(\theta) e^{-TE/_{T2*}}\right) \frac{1 - e^{-TR/_{T1}}}{1 - \cos(\theta) e^{-TR/_{T1}}}$$

Small angle - reduces T1 weighting and yielding proton density weighting
Large flip - yields T1 weighting
Short TR - increases T2* weighting (residual transverse magnetization is dominant)
Long TR - enhances T1 weighting
Short TE - reduces T2* weighting and increases T1 or PD weighting
Long TE - enhances T2* weighting

$$\theta_{Ernst} = \cos^{-1}\left(e^{-TR/_{T1}}\right)$$

Optimal flip angle

🟩 Parallel component

🟦 Transversal component

Very small angle

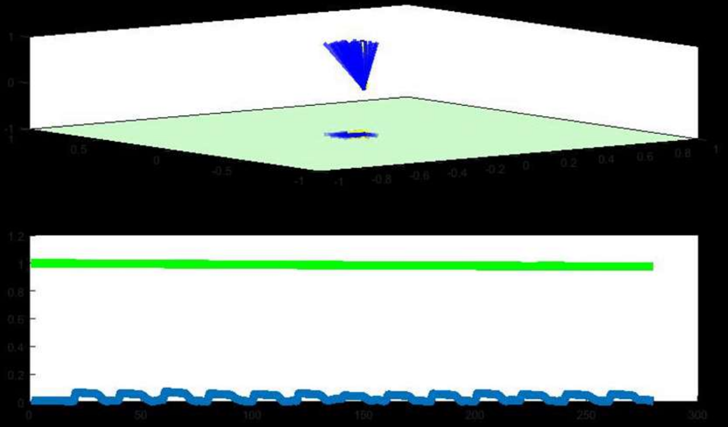

Small angle

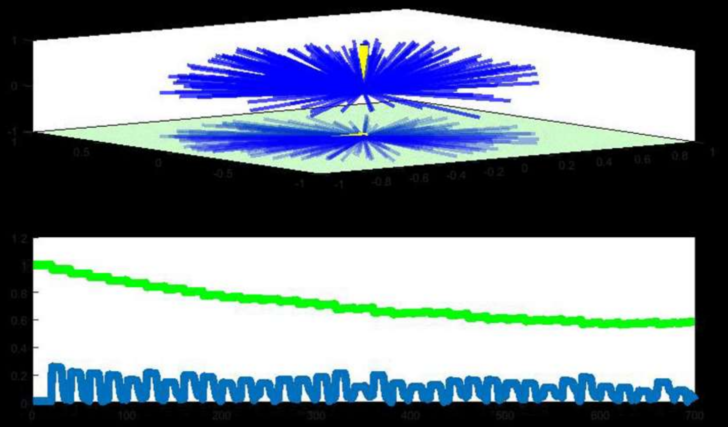

Large angle

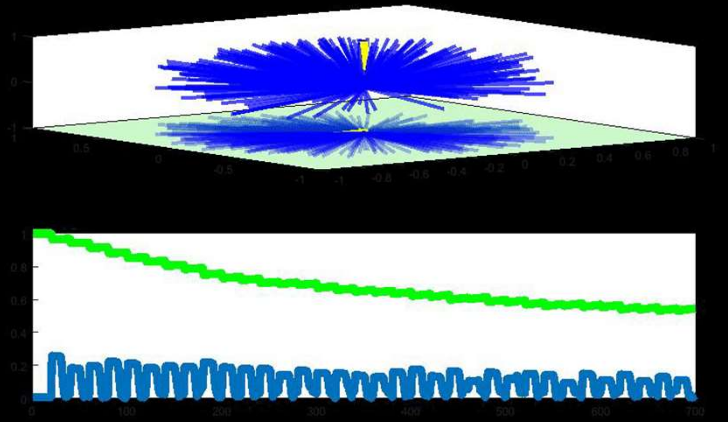

Very large angle

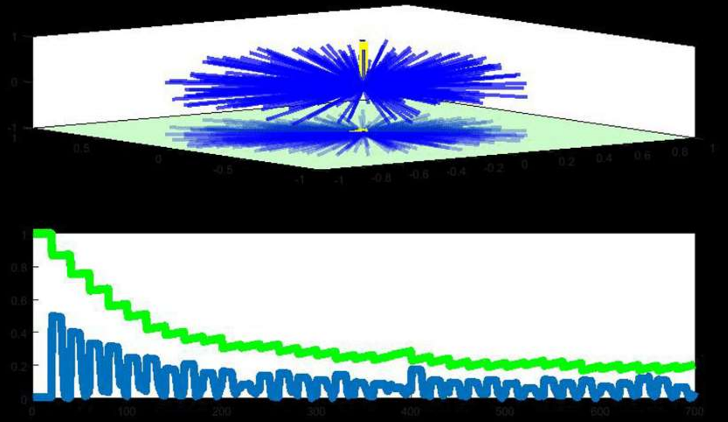

Phase contrast

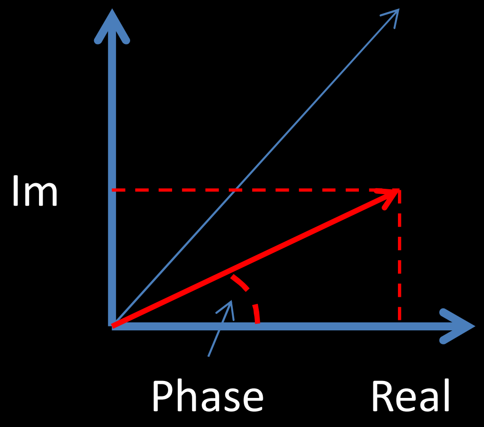
Im
Phase
Real

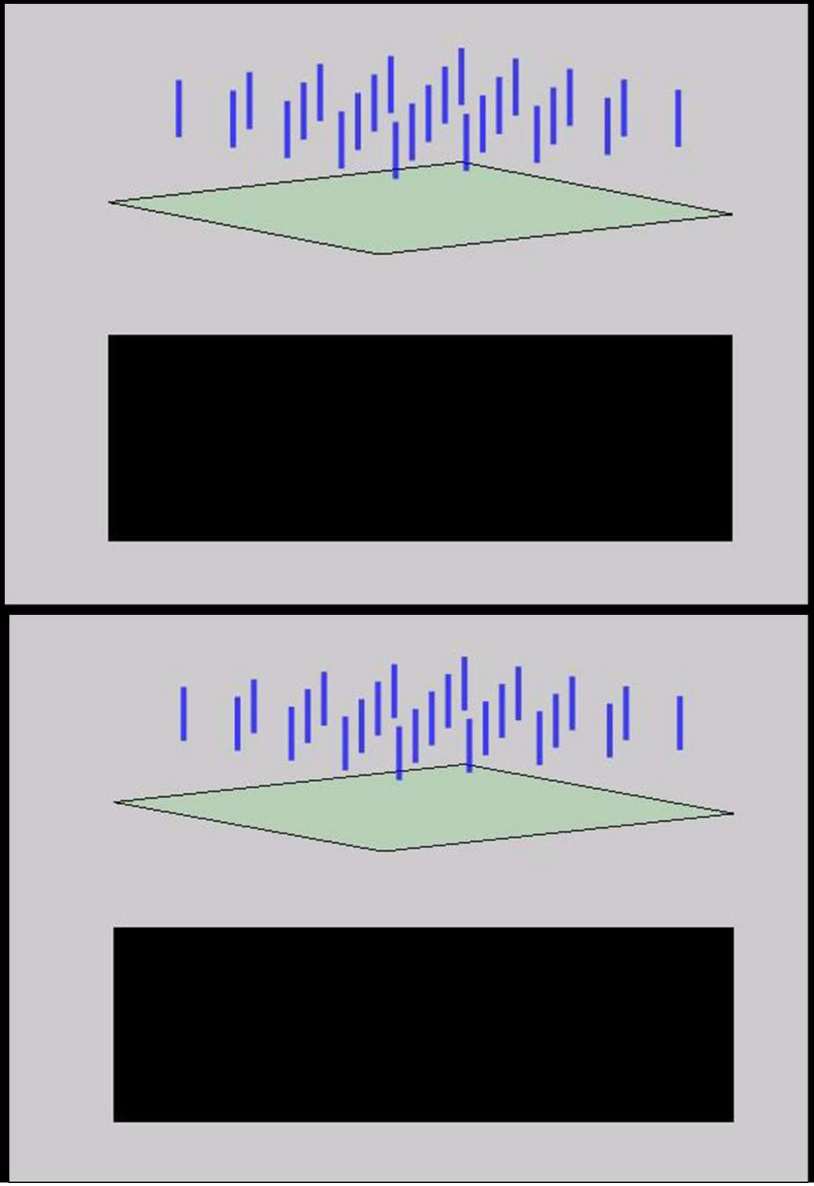

$Phase \sim TE * \Delta B$

A little bit more about phase in the DCE lecture

Summary again (Spin-echo)

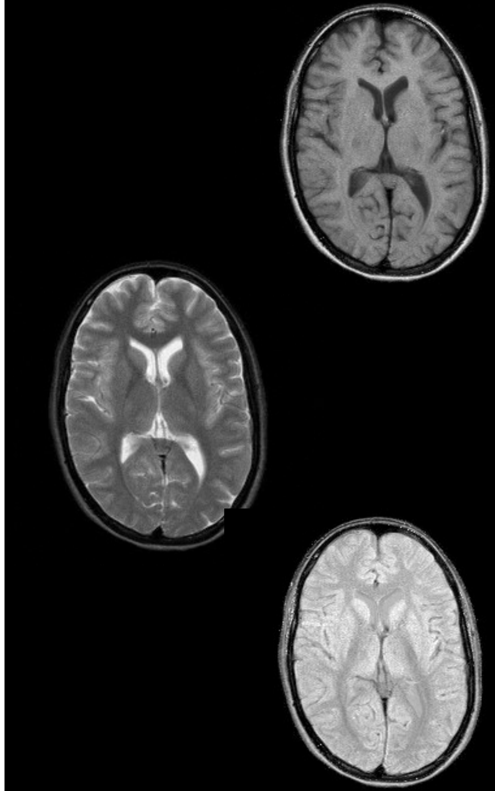

- **T1 Weighting**
  - Maximizing T1 → short TR
  - Minimizing T2 → short TE
- **T2 Weighting**
  - Maximizing T2 → long TE
  - Minimizing T1 → long TR
- **Proton weighting**
  - Minimizing T2 → short TE
  - Minimizing T1 → long TR

Thank you

If you want this presentation with animations – Just ask and bring USB stick

MRI Physics: Space Encoding

A/Prof Gary Liney

5th November 2017

ESTRO Imaging for Physicists

Introduction

- MRI extremely flexible spatial localisation
  - Orientation easily altered
- Gradients used to modulate phase and frequency
  - In-plane directions always ‘phase’ and ‘frequency’
- Signal is reconstructed with 2D or 3D Fourier Transformation

Spin Echo Sequence

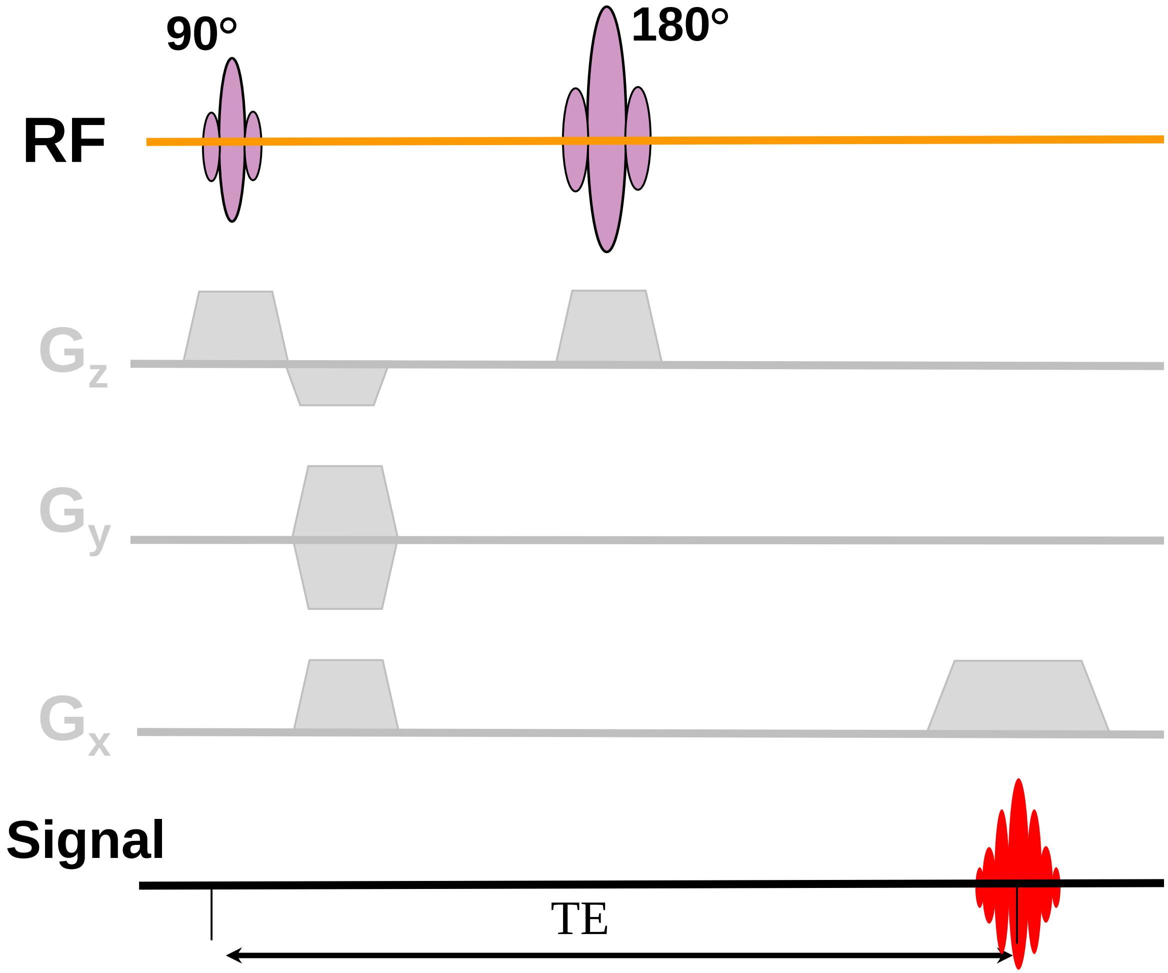
90°
180°
RF
G_z
G_y
G_x
Signal
TE

Slice Selection

Phase Encoding

Frequency Encoding

Spin Echo Sequence

Slice Selection

Phase Encoding

Frequency Encoding

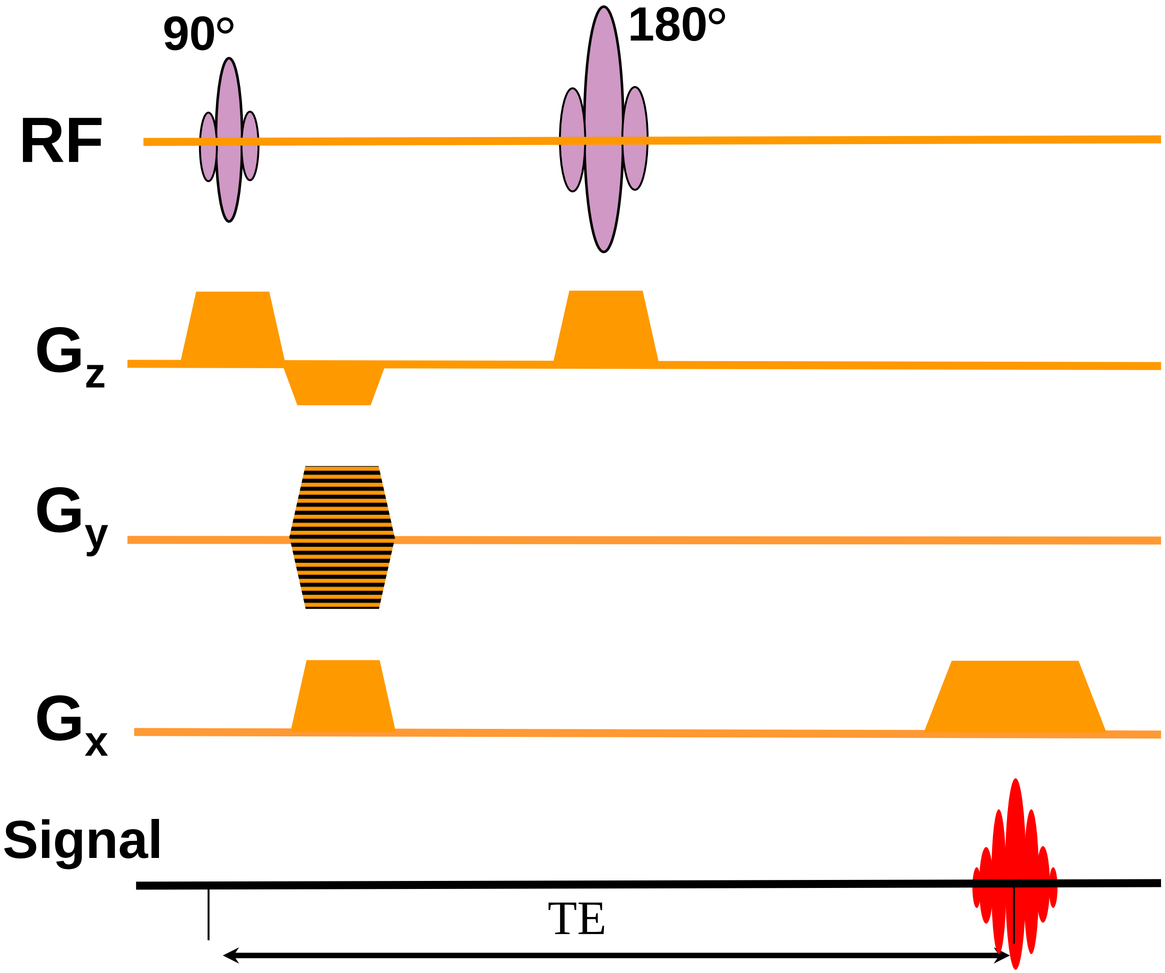
90°
180°
RF
G_z
G_y
G_x
Signal
TE

An axial image..

Fourier Transform (FT)

- Time signal can be decomposed into sum of sinusoids of different frequencies, phases and amplitudes

$$s(t) = a_0 + a_1\sin(\omega_1 t + \varphi_1) + a_2\sin(\omega_2 t + \varphi_2) + \dots$$

- Fourier series may be represented by frequency spectrum
- Time and frequency domain data can be thought of as FT pairs

Fourier Transform (FT)

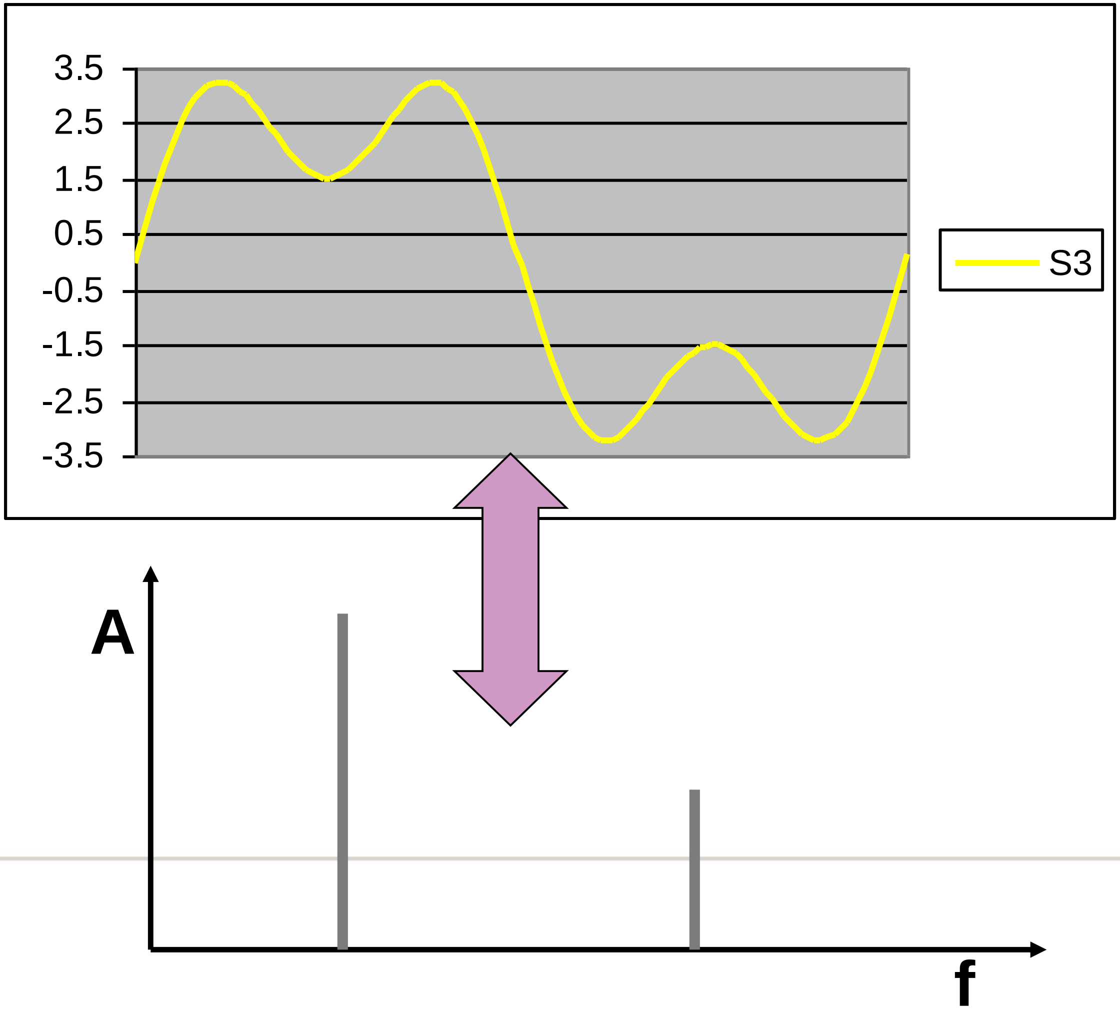

- S1 has amplitude *a* and frequency *f*
- S2 has *a*/2 and 3*f*
- S3 = S1 + S2
- S3 is two sine waves of different *frequency* and *amplitude*

The FT is shown

FT Pairs

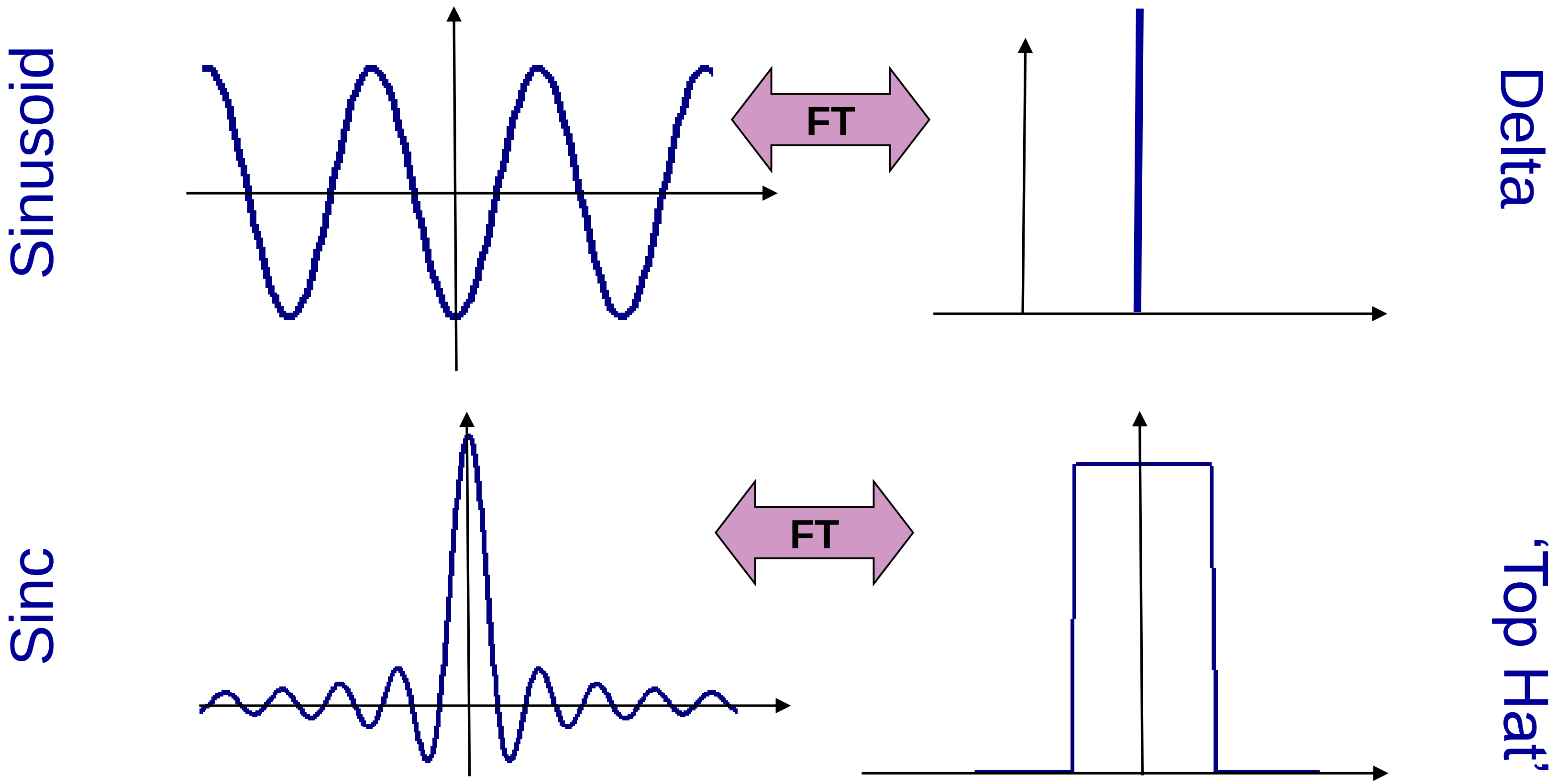

Sinusoid

FT

Delta

Sinc

FT

'Top Hat'

Time

Frequency

FT Pairs

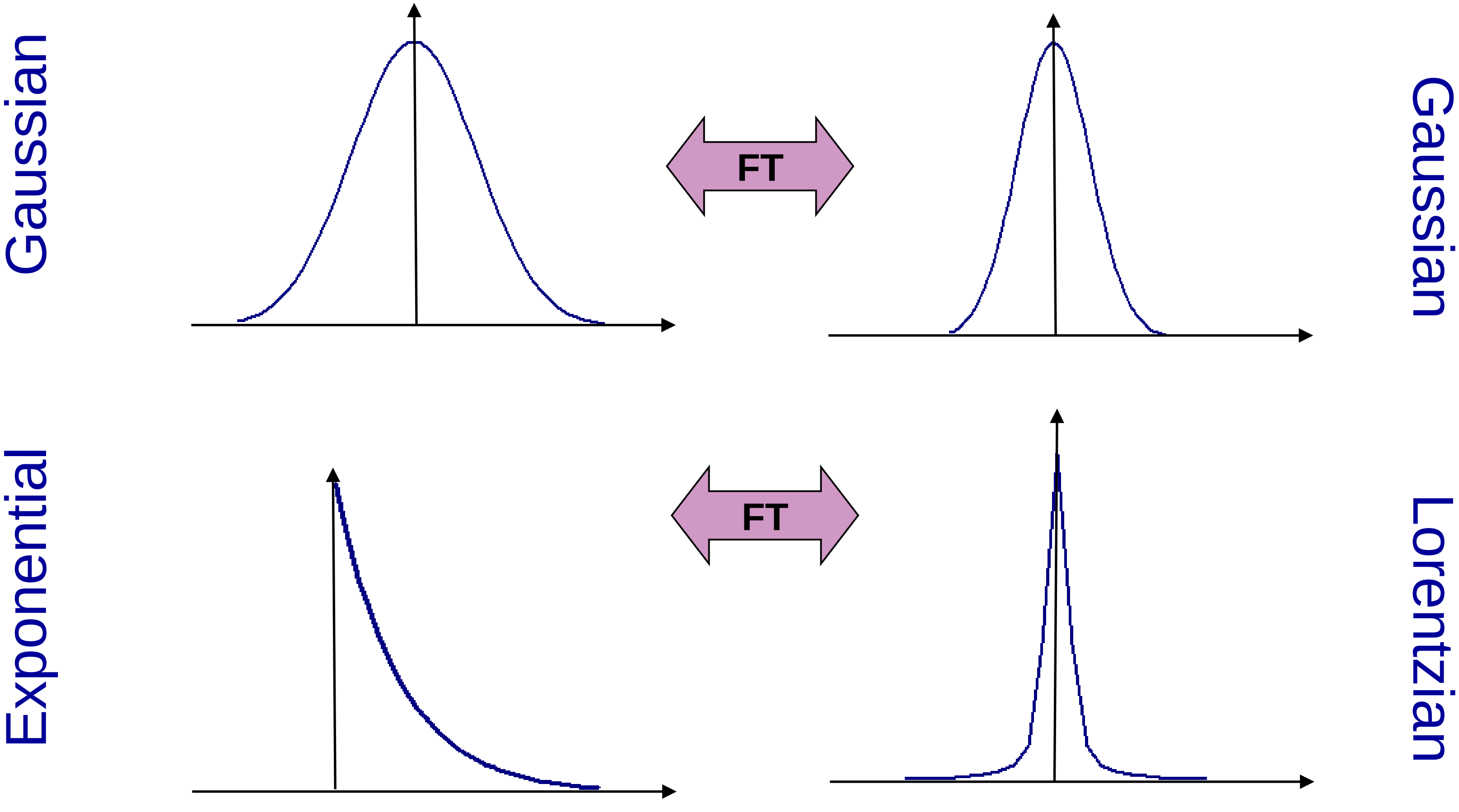

Gaussian

FT

Gaussian

Exponential

FT

Lorentzian

Time

Frequency

Gradients

- Recall that the resonant frequency is proportional to field strength

$$\boxed{\omega_0 = \gamma B_0}$$

- Magnetic gradient changes B_0 field strength over distance
- In MRI a linear gradient changes the resonant frequency in a given direction

$$\boxed{\omega = \gamma(B_0 + xG_x)}$$

$$\left\{ \begin{array}{l} \boxed{G_x = {dB_0}/{dx}} \\ \boxed{G_y = {dB_0}/{dy}} \\ \boxed{G_z = {dB_0}/{dz}} \end{array} \right.$$

Slice Selection

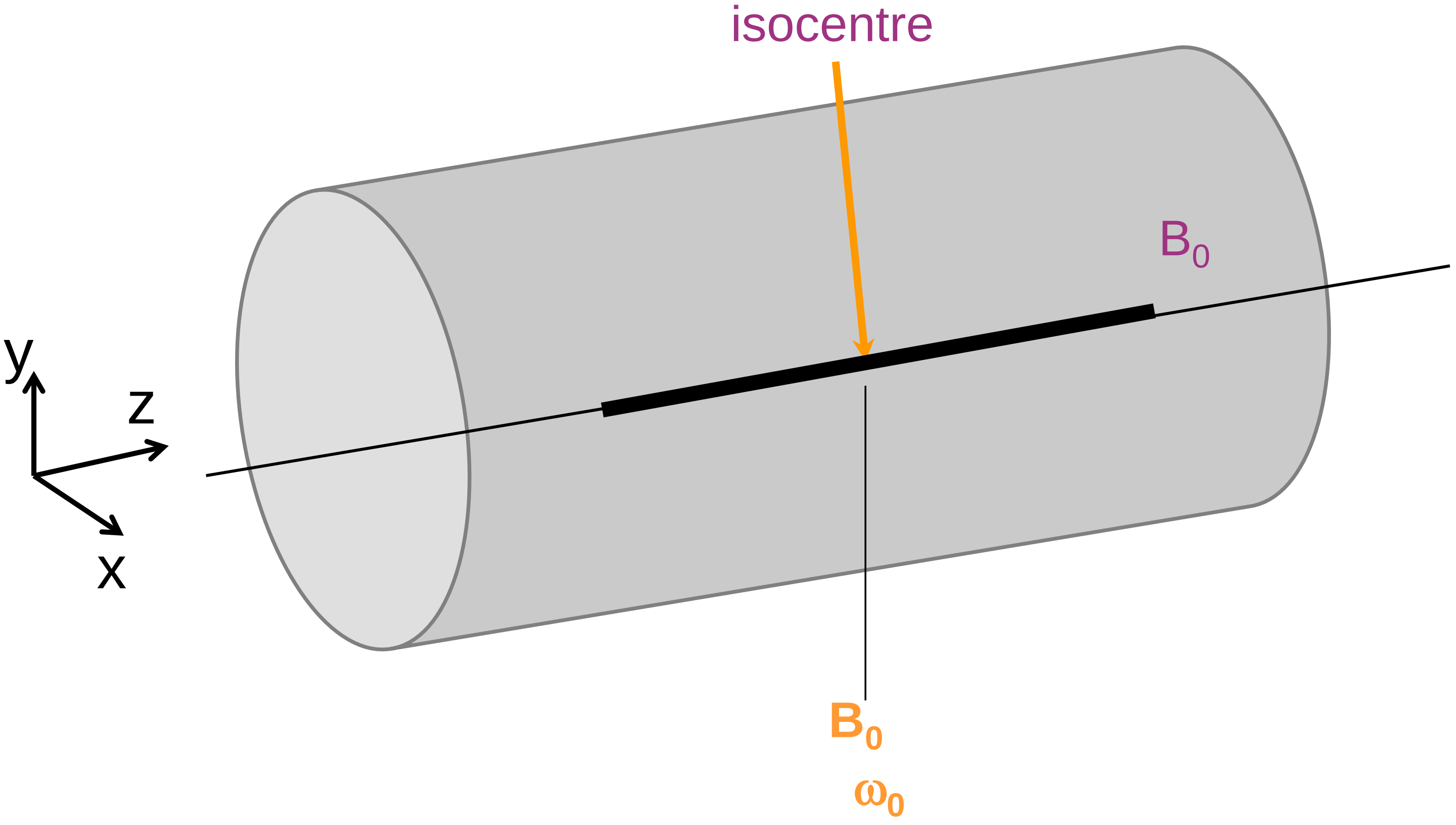
isocentre
B_0
y
z
x
B_0
ω_0

Slice Selection

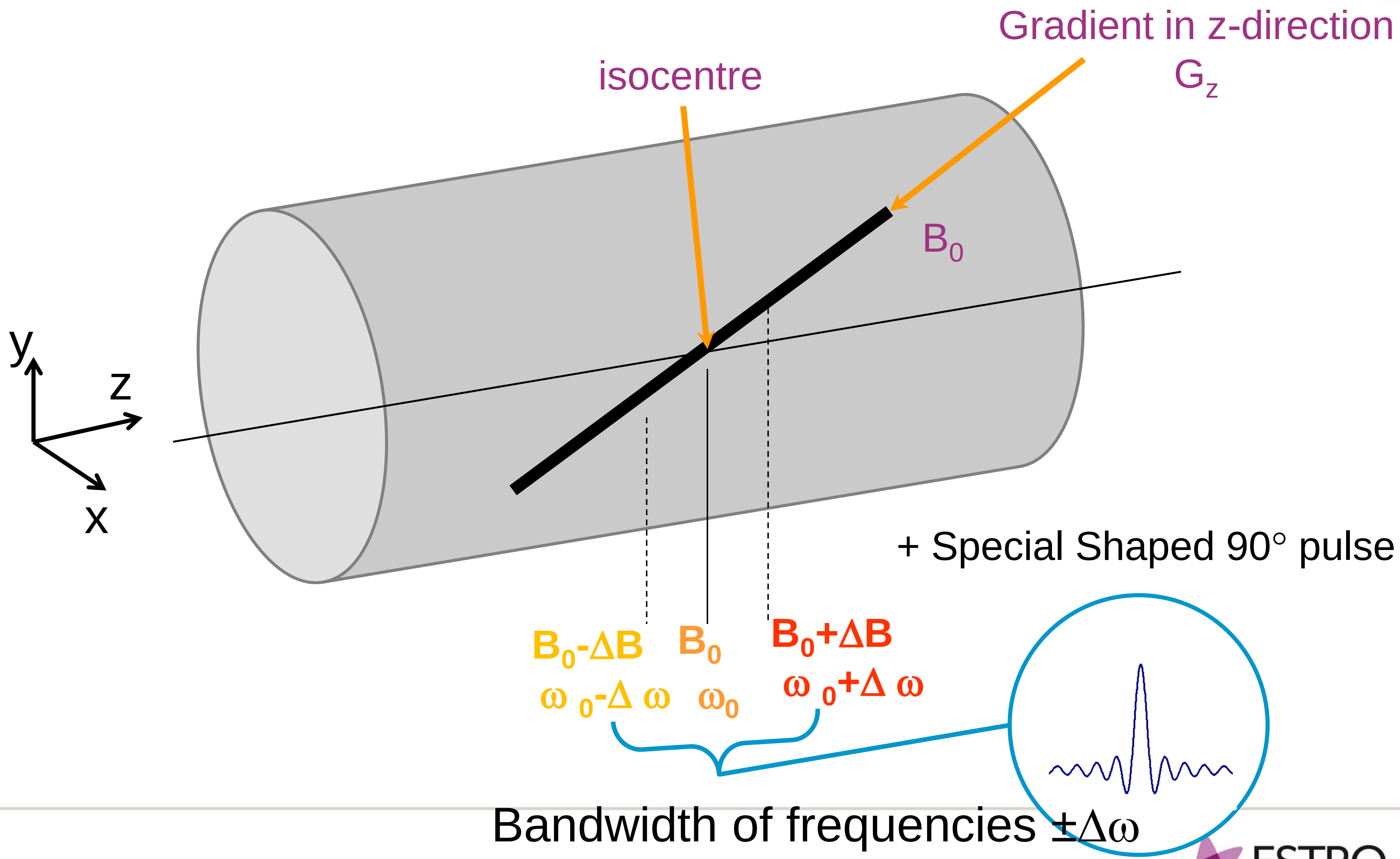
Gradient in z-direction
G_z
isocentre
B_0
y
z
x
B_0-ΔB
B_0
B_0+ΔB
$\omega_0 - \Delta\omega$
ω_0
$\omega_0 + \Delta\omega$

+ Special Shaped 90° pulse

Bandwidth of frequencies ±Δω

Slice Selection

Only this section can be ‘seen’ by the RF coil

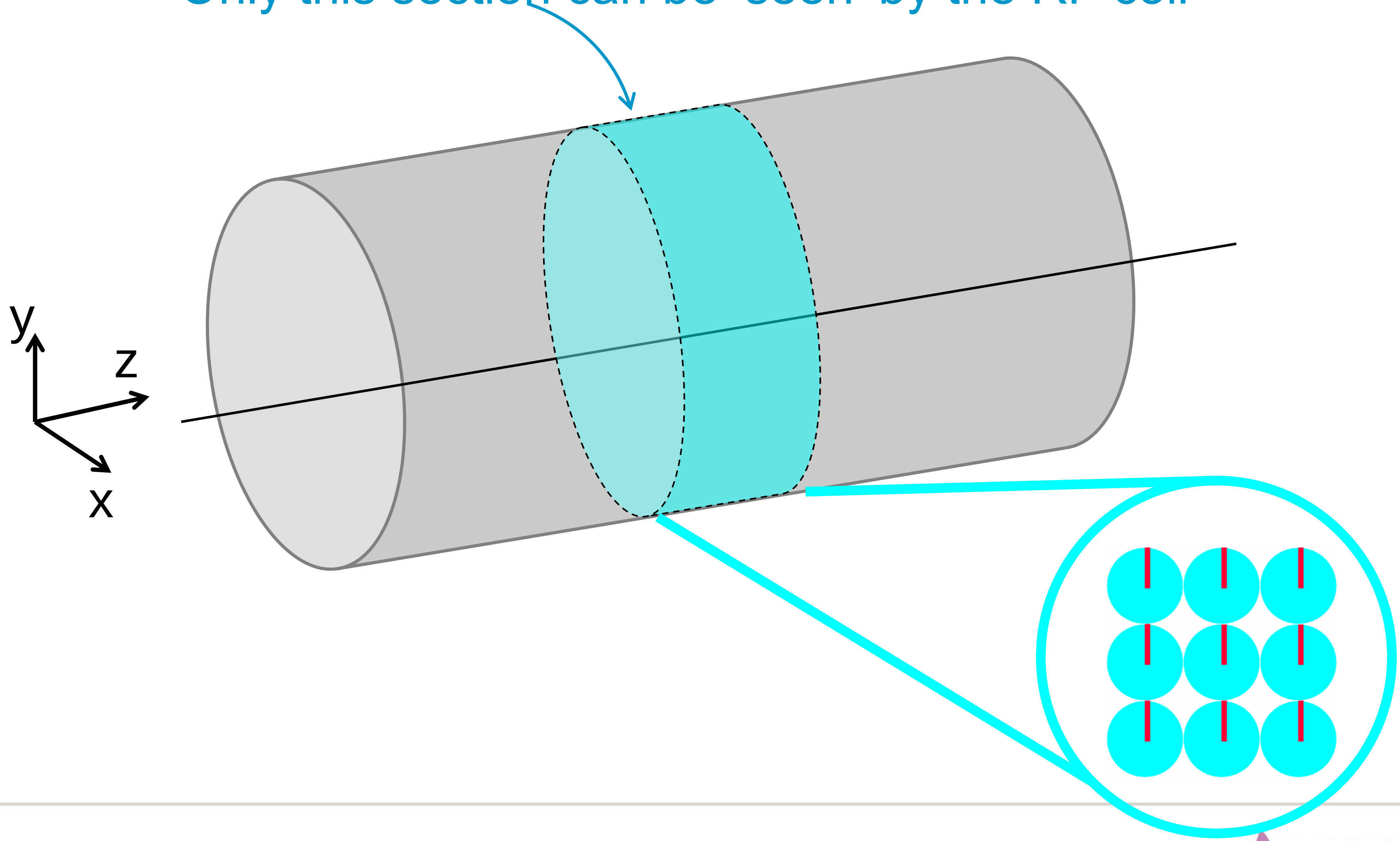

Slice Selection

- Gradient used to change resonant frequency in slice direction
- Excite spins using (*sinc-shaped*) 90° RF pulse containing a bandwidth of frequencies
- Only a particular section of spins are excited into transverse plane
- Signal has been discriminated in one dimension
- Can change orientation, slice thickness and position

Slice Selection

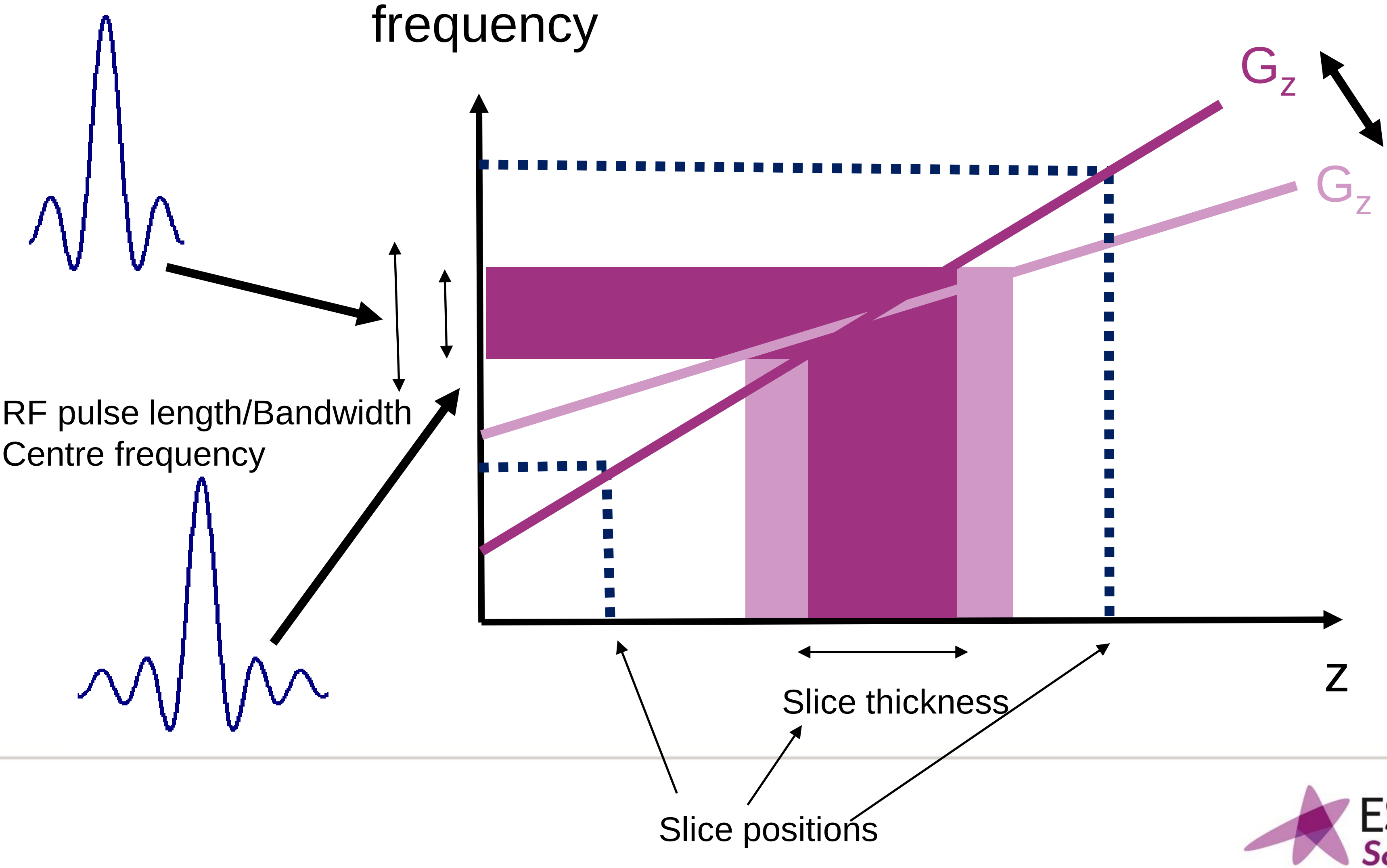
frequency
G_z
G_z
RF pulse length/Bandwidth
Centre frequency
z
Slice thickness
Slice positions

Phase & Frequency Encoding

- Need to still encode signal in remaining directions (x & y)
  - Use changes of frequency & phase
- When a gradient is applied the spins will be at different phases once the gradient has been turned off
- This is the role of the phase encoding gradient
- Used in combination with frequency encoding gradient in the 2nd direction...

In-plane Encoding

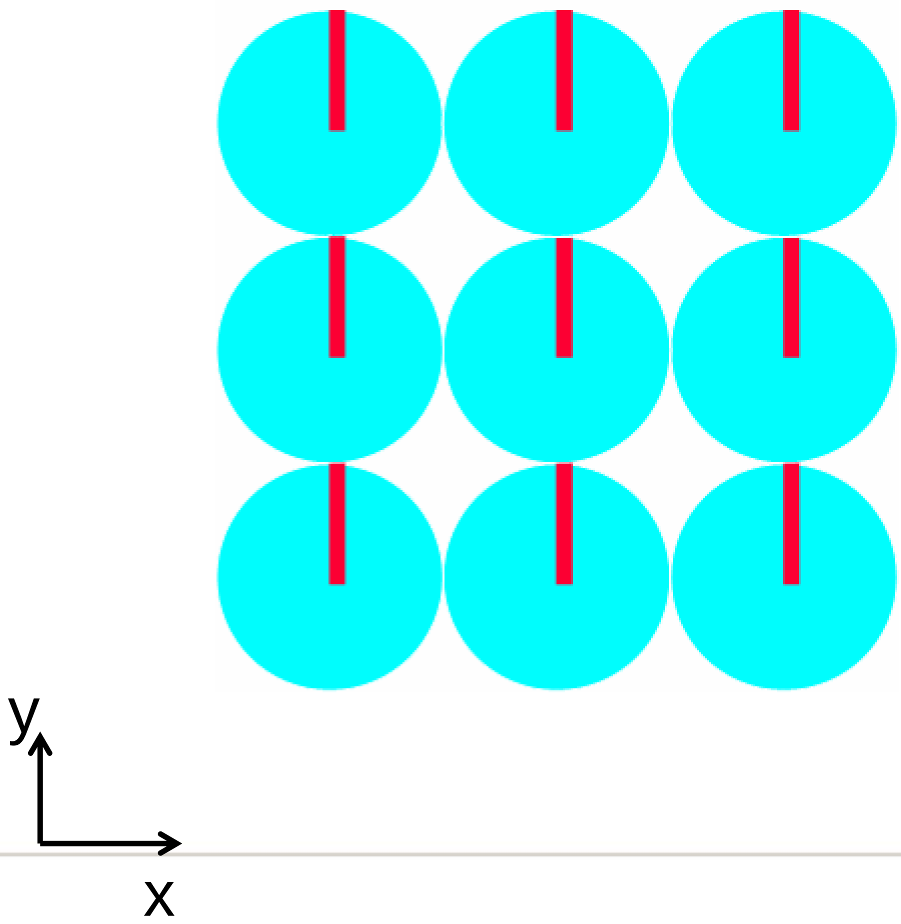

Initially, all spins have **same frequency**

In-plane Encoding

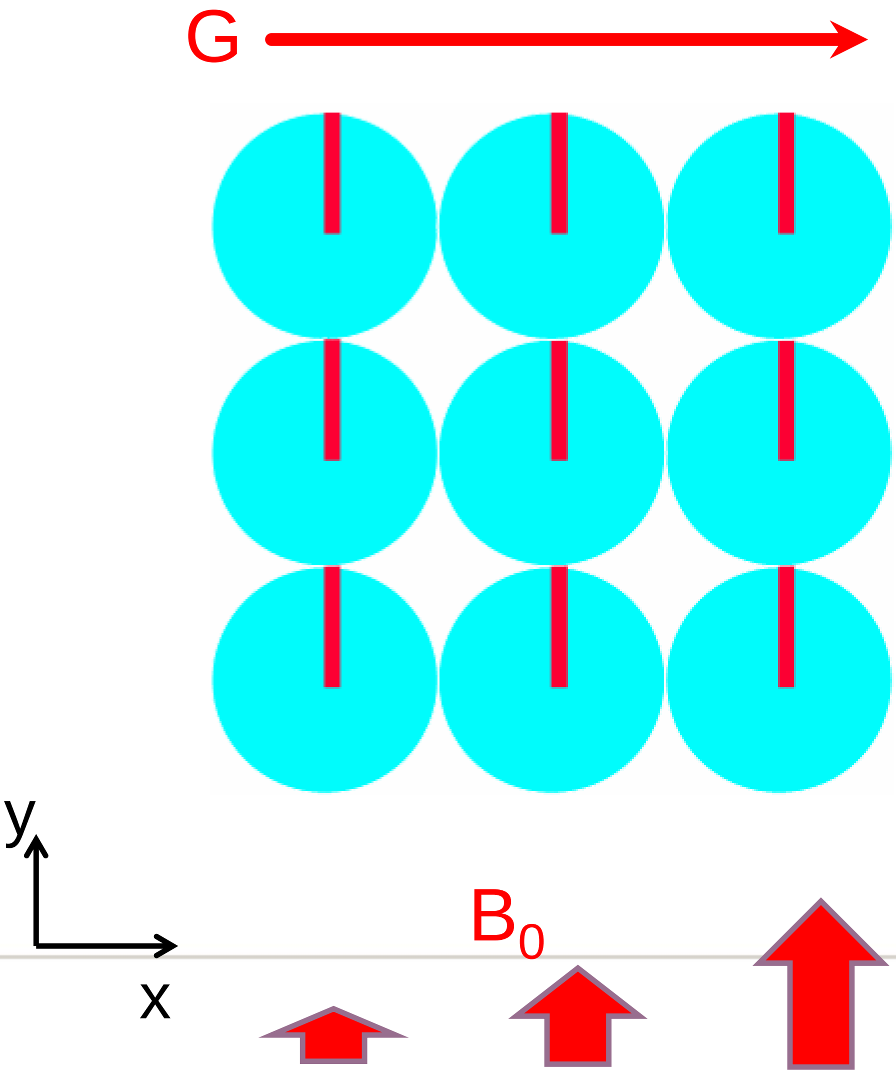

- Apply a gradient left to right
- Linear change in B_0

In-plane Encoding

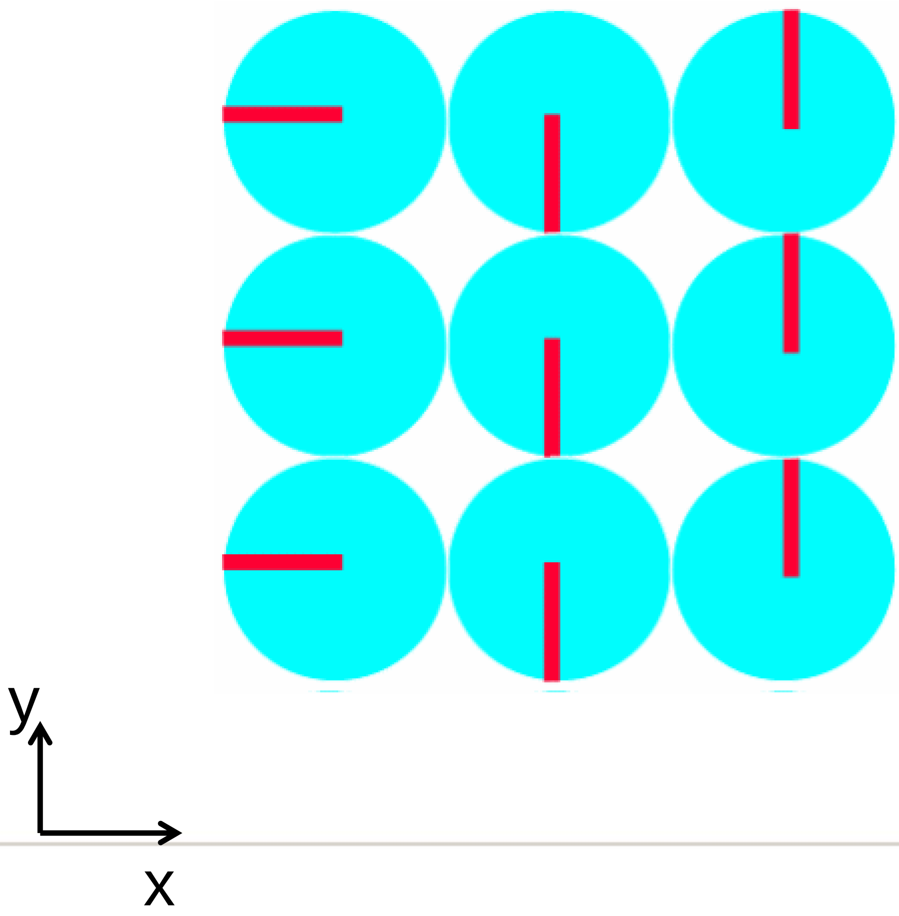

- After gradient is removed
- Spins revert to same frequency
- Phase is different between columns
- This gradient is applied n times with different amplitudes

In-plane Encoding

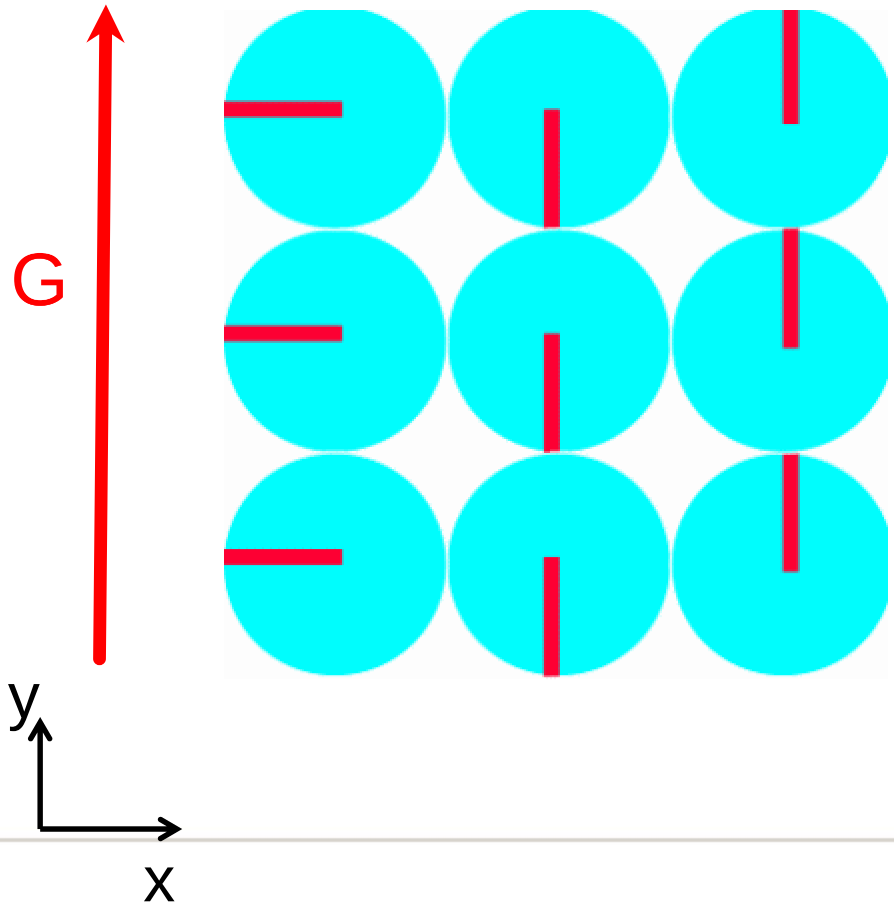

- Apply a further gradient bottom to top
- This gradient is applied once
- Sample the data m times
- Create m×n pixel image

Phase Encoding

- Each pixel is assigned a unique phase and frequency
- FT decodes unique frequency but only measures summation of phase
- Individual phase contributions cannot be detected
- Need multiple increments of PE gradient to provide enough information about phase changes
- Number of PE increments depends on image matrix

Spin Echo Sequence

Resonance condition

$\omega = \gamma (B_0 + zG_z)$

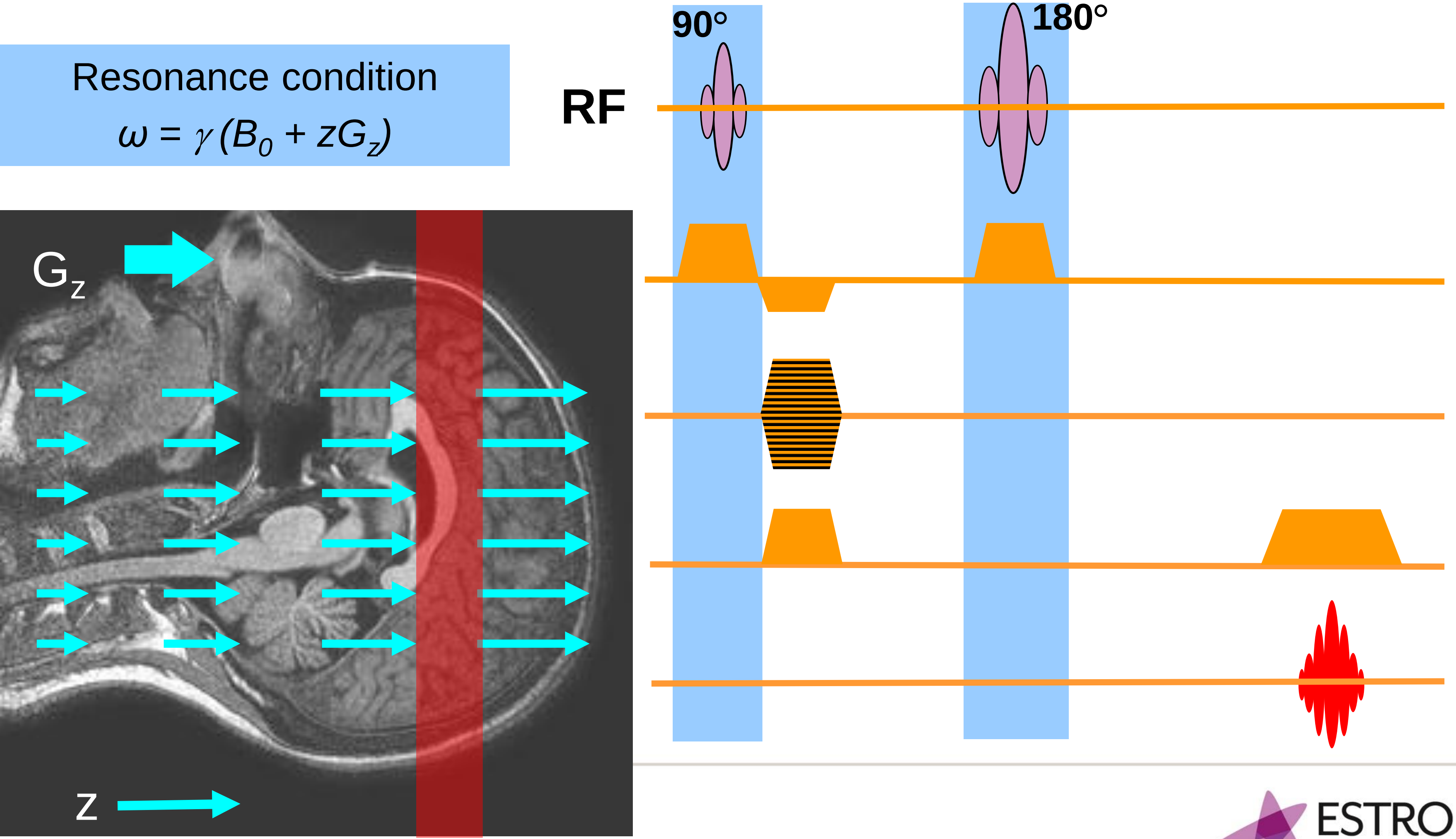

G_z
z
90°
180°
RF

Spin Echo Sequence

Increment gradient after RF pulse and before read-out

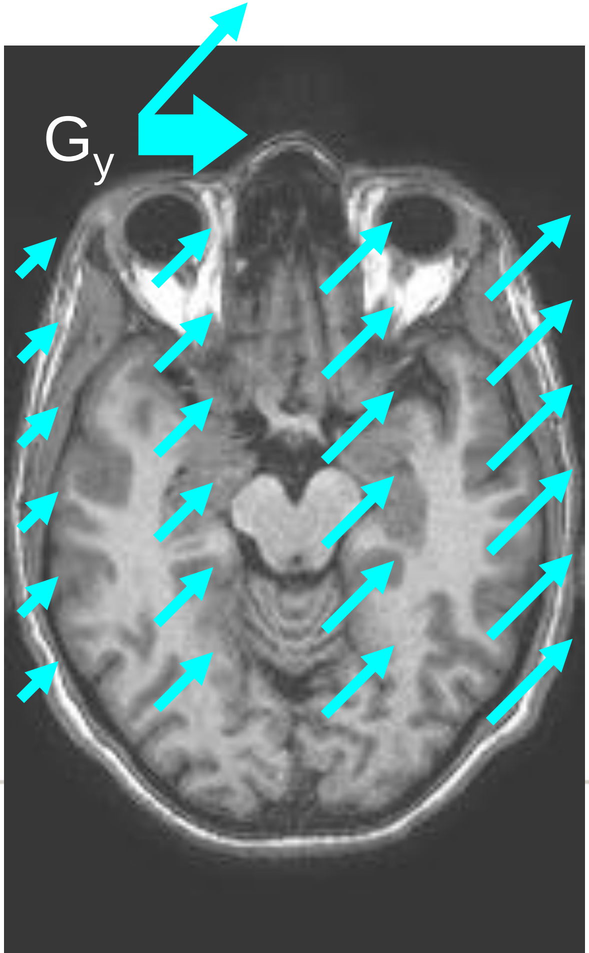

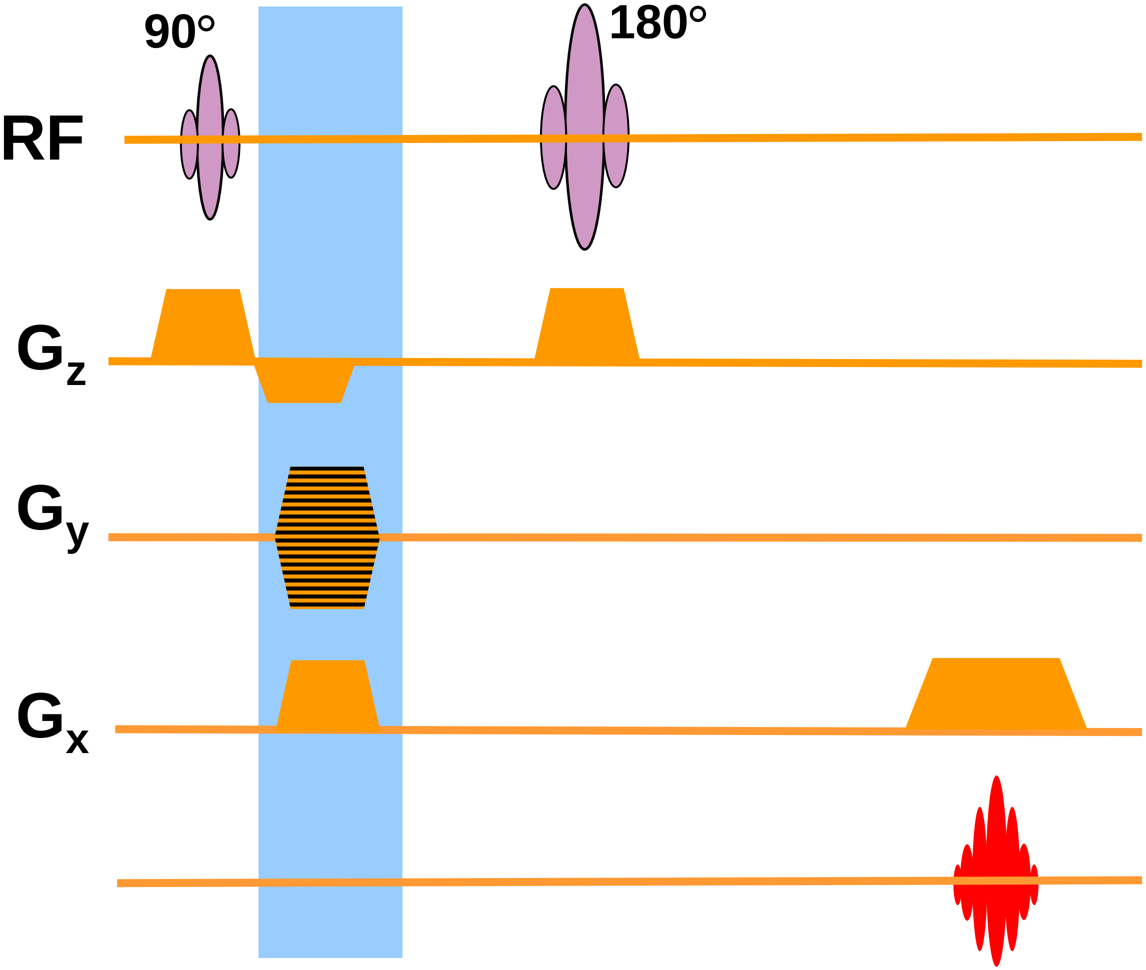
90°
180°
RF
Gz
Gy
Gx

Spin Echo Sequence

Apply gradient during read-out

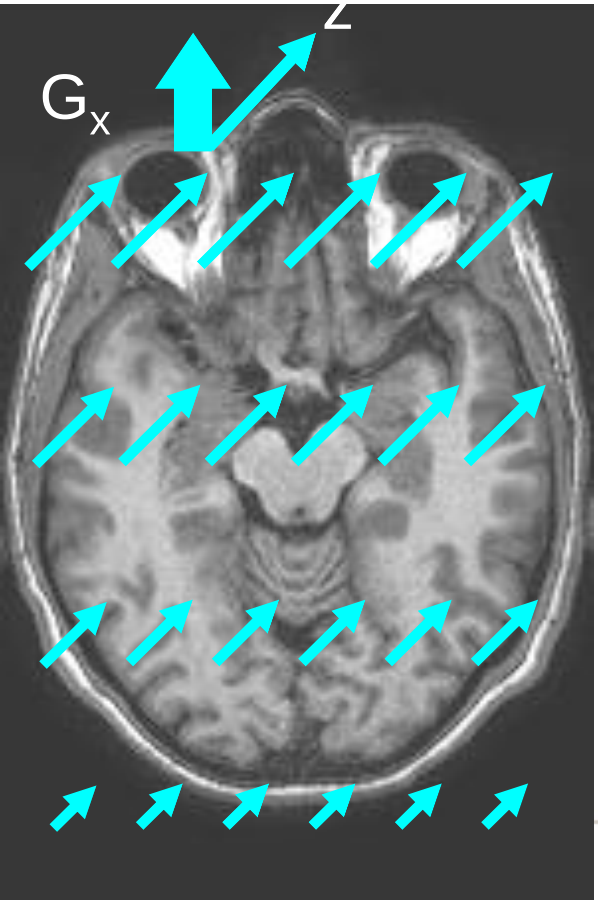

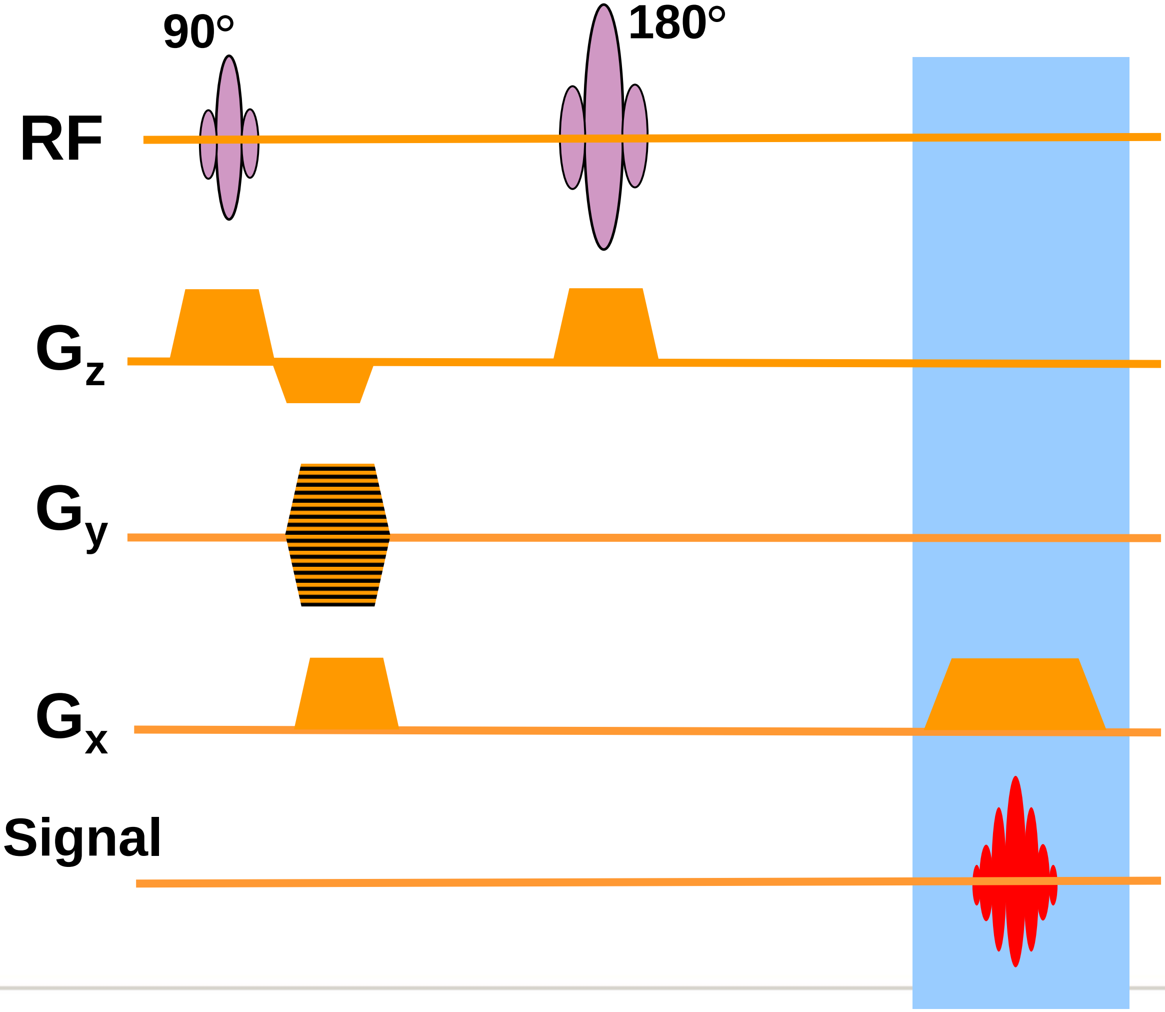

90°
180°
RF
G_z
G_y
G_x
Signal

Multi-Slice Imaging

- Period between the echo and the next RF pulse is called *dead time*
- Used to excite a separate slice
- Multiple slices are acquired in each TR
- Slice profiles are not rectangular leading to cross-excitation
- Slices are acquired with gaps or interleaved

Scan Time

- Frequency encoding done at time of echo
- Phase encoding done over many TRs
- Time between TR-TE is dead time

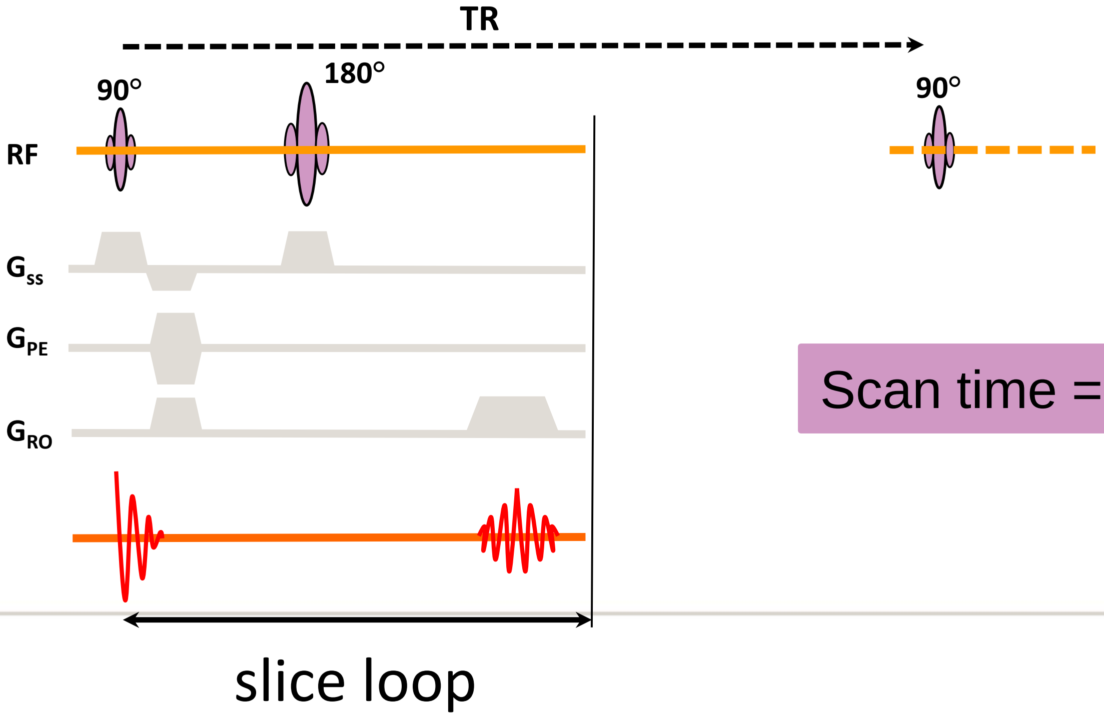
TR
90°
180°
90°
RF
G_{SS}
G_{PE}
G_{RO}
slice loop

Scan time = TR × N_{av} × N_{PE}

‘3D’ Sequences

- True 3D volume rather than multiple 2D slices
- A slab or multiple-slabs are selected
- Phase encoding also in the ‘slice’ dimension
  - Through-plane resolution can be comparable to in-plane
  - Phase wrap in ‘slice’ direction
- SNR is improved, scan time longer:

$$N_{PE} \times TR \times NEX \times N_s$$

Volumetric Imaging

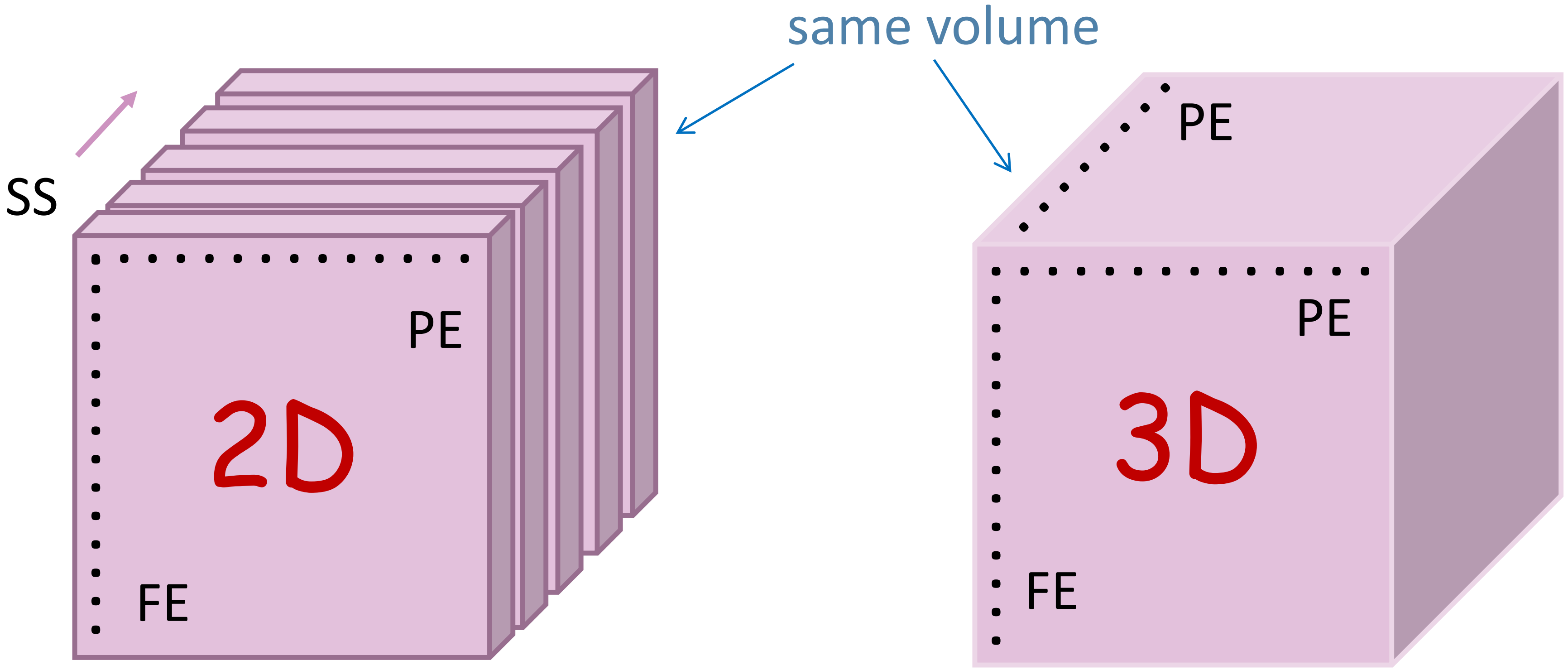
same volume
SS
PE
FE
2D
PE
PE
FE
3D

Scan time = TR × N_{av} × N_{PE}

Scan time = TR × N_{av} × N_{PE1} × N_{PE2}

Typical gradient resolution parameters (45 mT/m):
(2D) in-plane 0.012 mm; slice thickness 0.1 mm
(3D) partition 0.05 mm

What is k-space?

- ‘k’ is wave-number: number of cycles per unit distance
  - Spatial analogue to ‘cycles per second’ (frequency)
- k-space is the raw data
  - An array of numbers whose FT is the MR image
- Each row in k-space corresponds to the echo data obtained from a single application of the PE gradient
  - Rows near centre correspond to low-order PE steps (small gradients)
  - Rows at edges correspond to high-order steps

What is k-space?

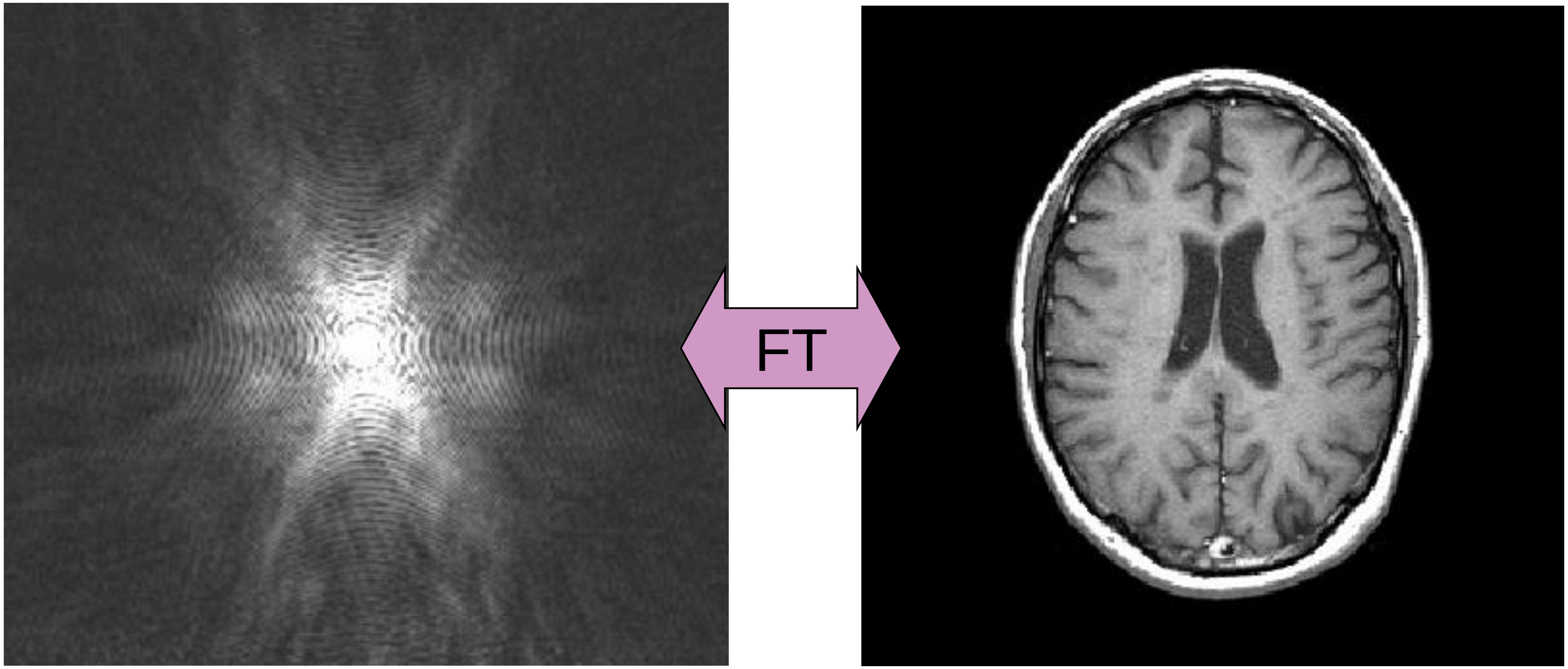

k-space and image-space of the brain

What is k-space?

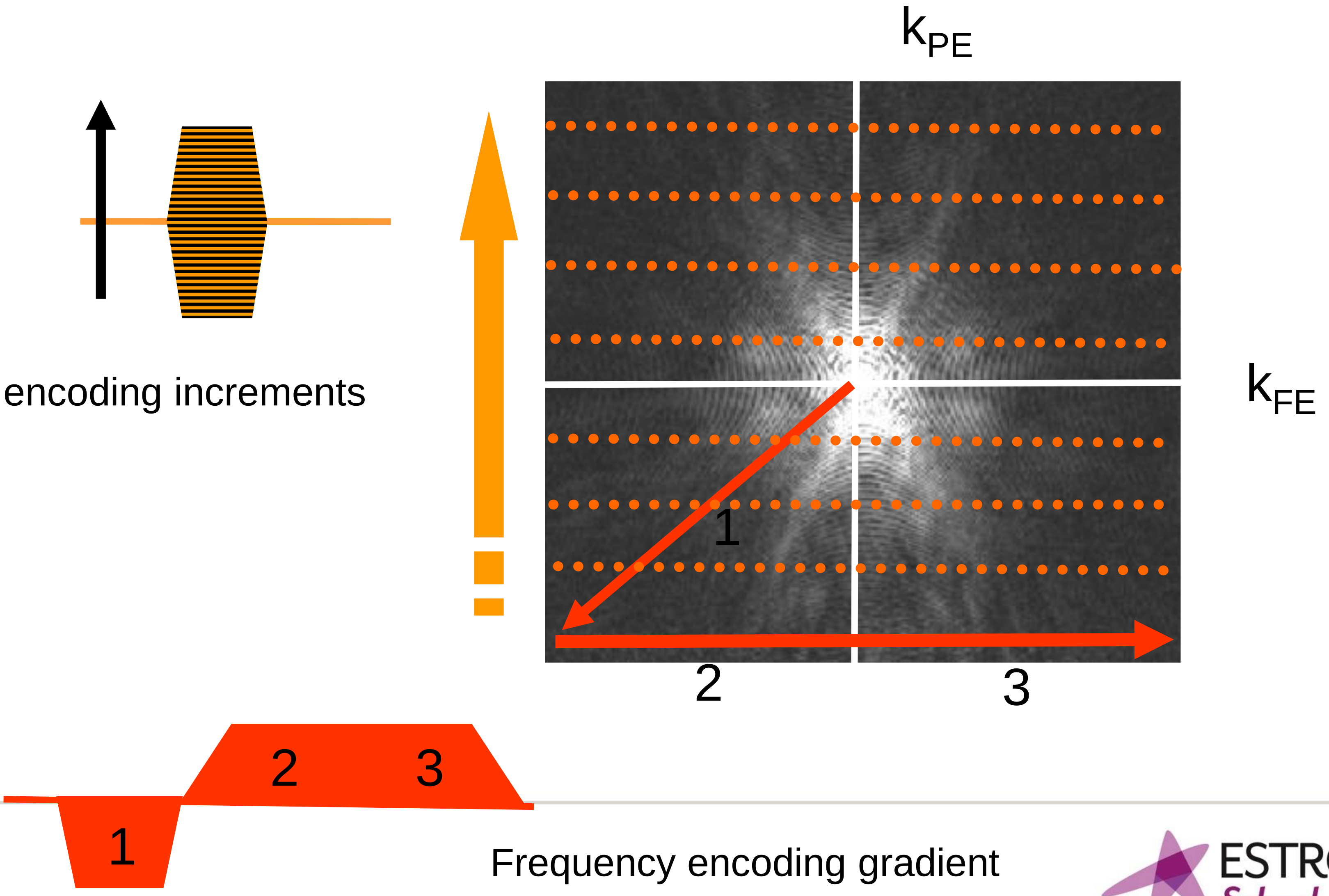
k_{PE}
k_{FE}
1
2
3
2
3
1

Phase encoding increments

Frequency encoding gradient

k-space

- All of k-space needs to be filled to create an image
  - ✓ Centre: bulk signal/contrast information
  - ✓ Edge: image detail
- Individual cells do not correspond one-to-one with individual pixels in image
- Each cell has information about every image pixel: *explains why motion artefacts propagate through whole image*

k-space

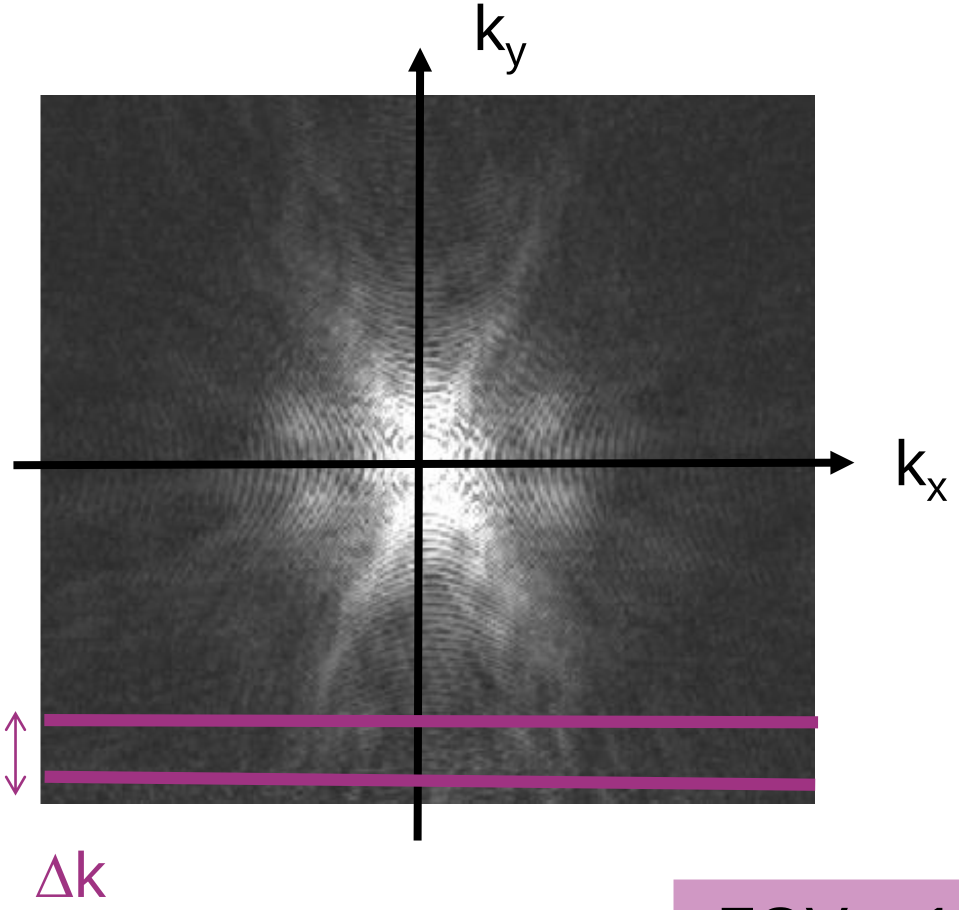
k_y
k_x
Δk

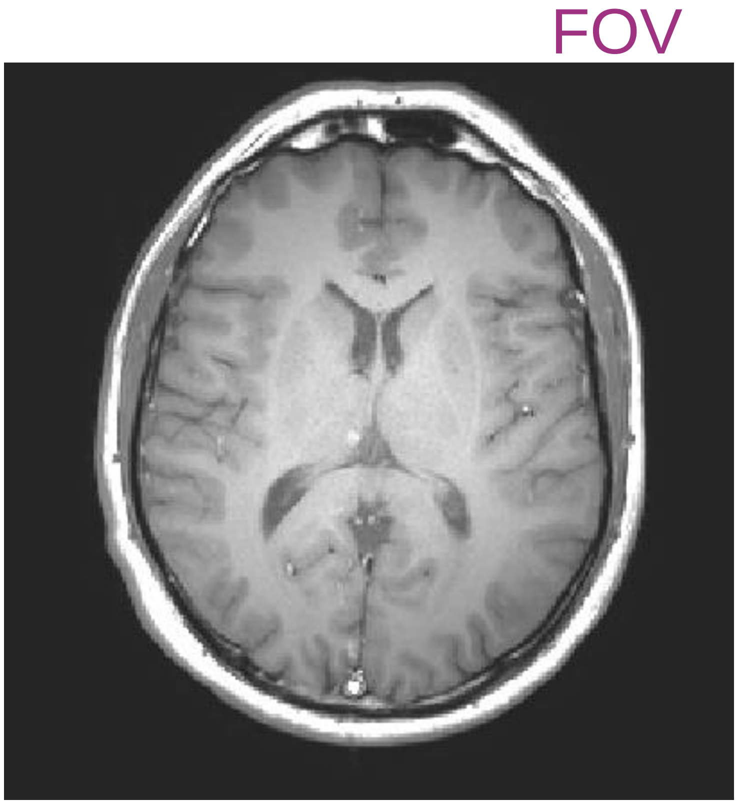

$\text{FOV} = 1/\Delta k$

$\Delta x = 1/\text{FOV}_k$

k-space

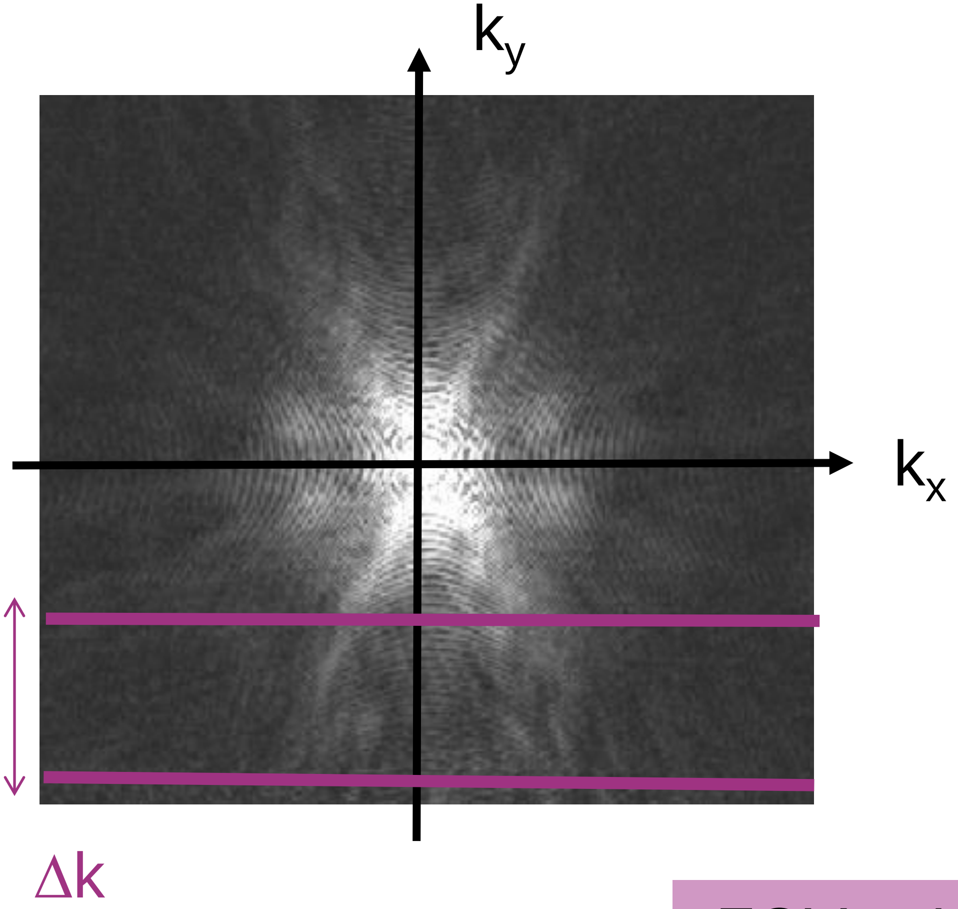
k_y
k_x
Δk

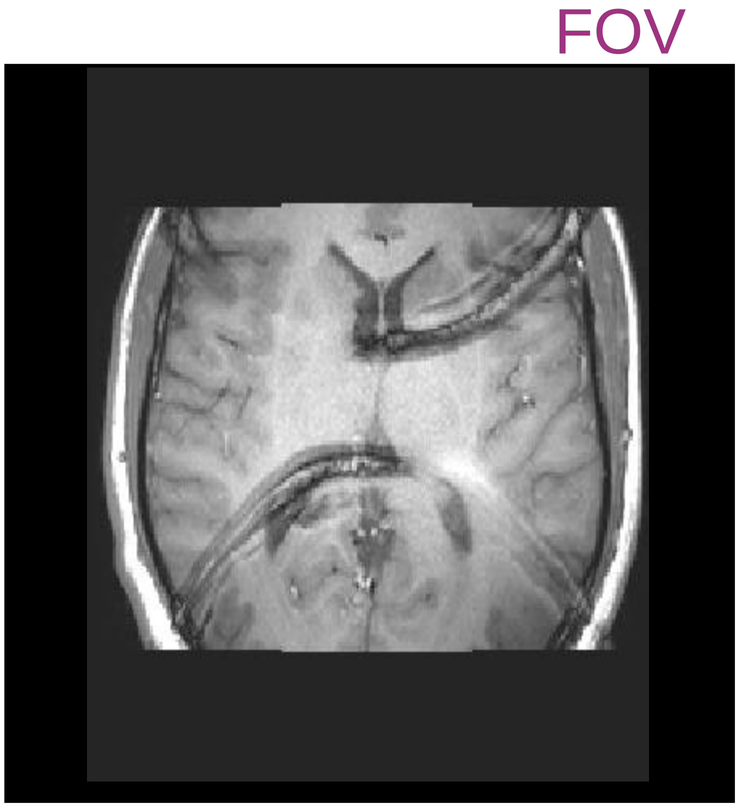

$$\mathrm{FOV} = 1/\Delta k$$
$$\Delta x = 1/\mathrm{FOV}_k$$

k-space

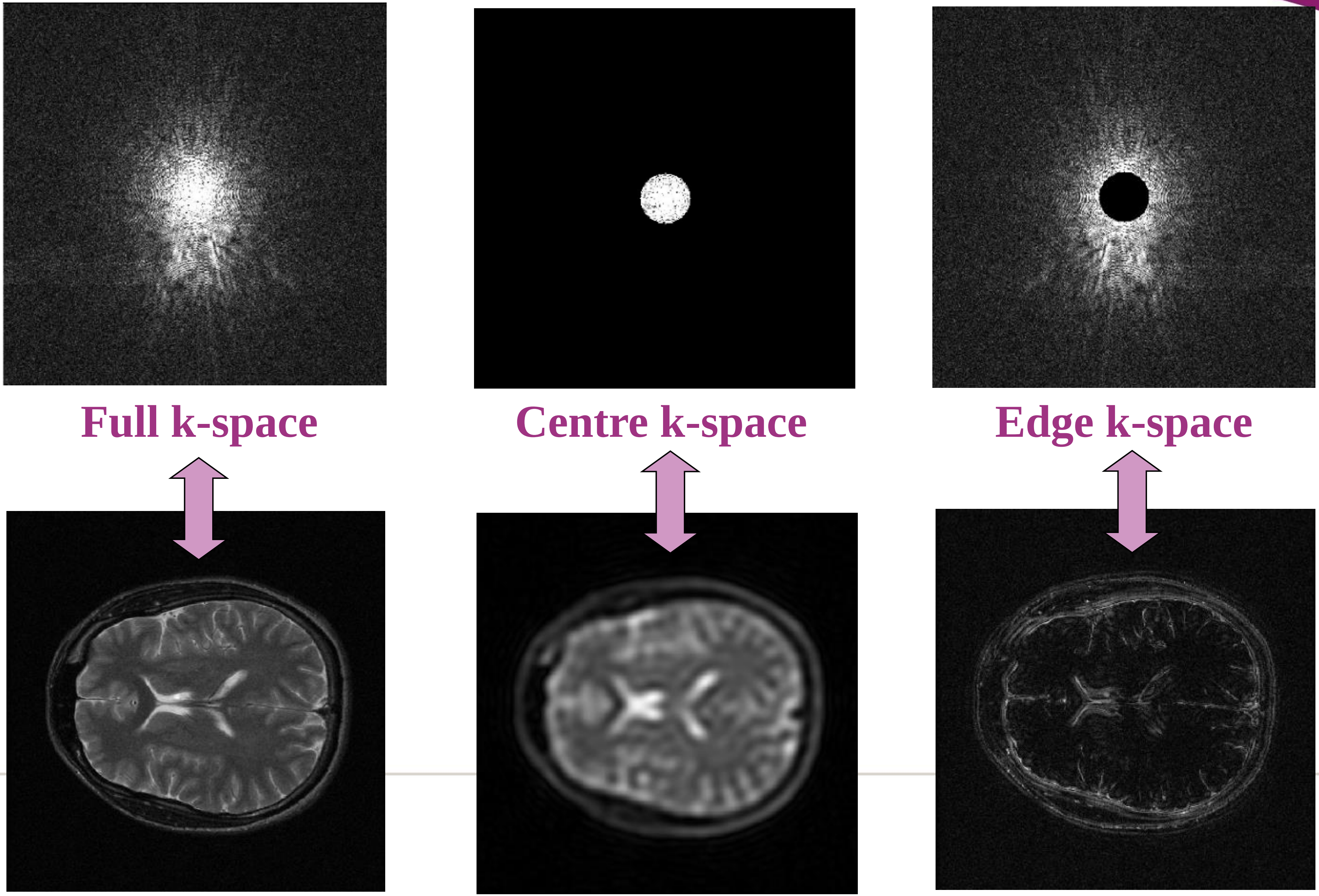

Full k-space

Centre k-space

Edge k-space

k-space: Acquisition strategies

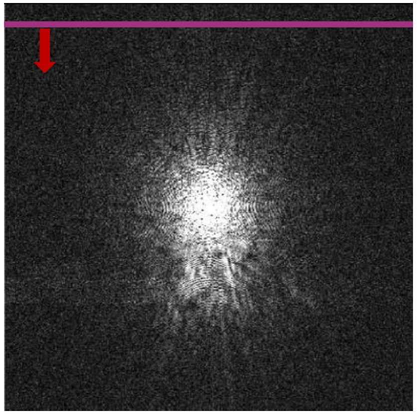

One line per TR

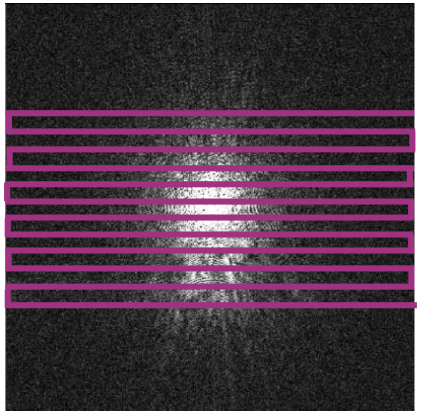

Single-Shot

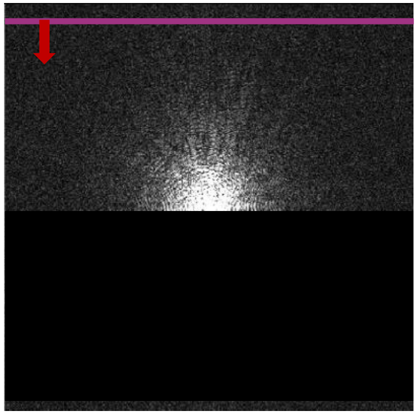

Partial Data

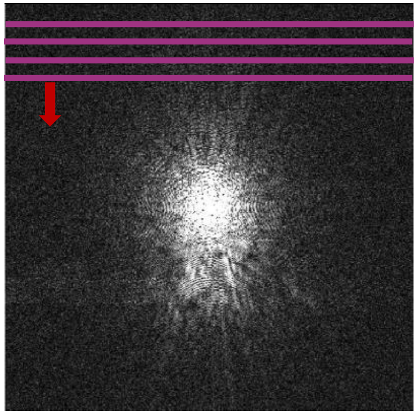

Multiple lines per TR

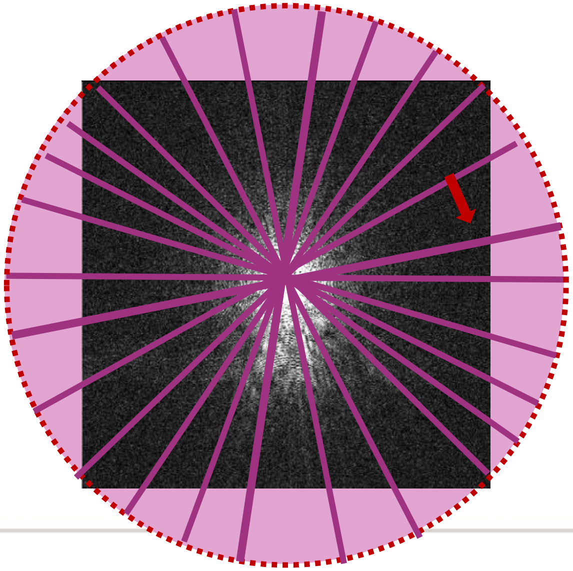

Radial

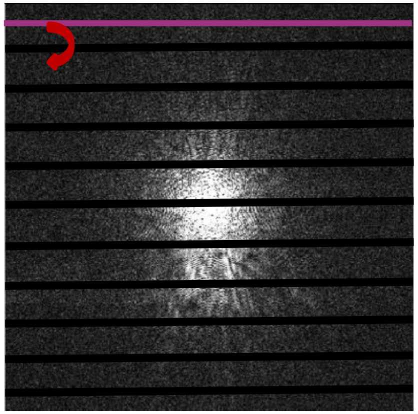

Skip lines

k-space: Acquisition strategies

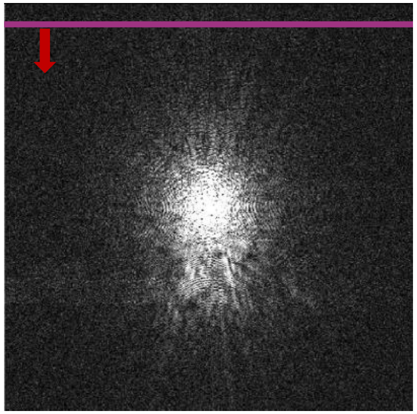

One line per TR

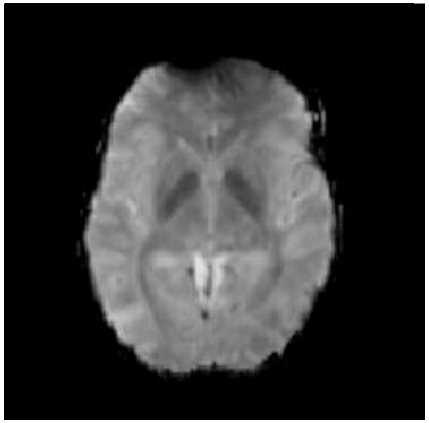

Single-Shot

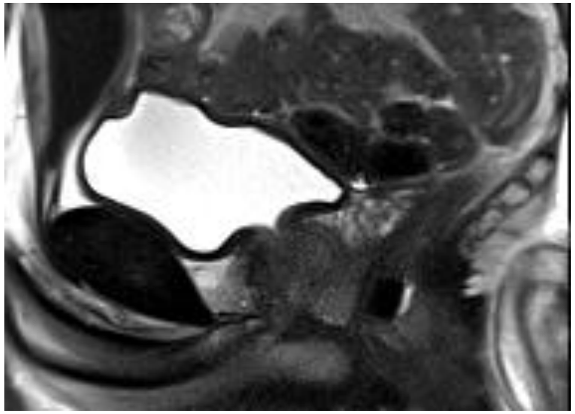

Partial Data

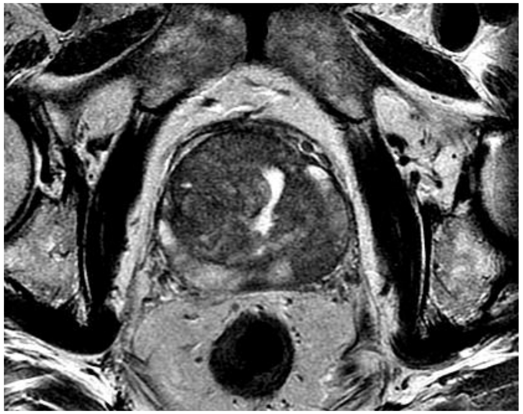

Multiple lines per TR

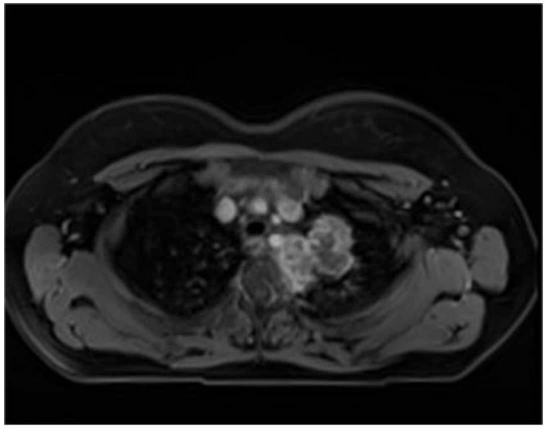

Radial

Skip lines

MRI Physics: Equipment & Safety

A/Prof Gary Liney

5th November 2017

ESTRO Imaging for Physicists

Historical Perspective

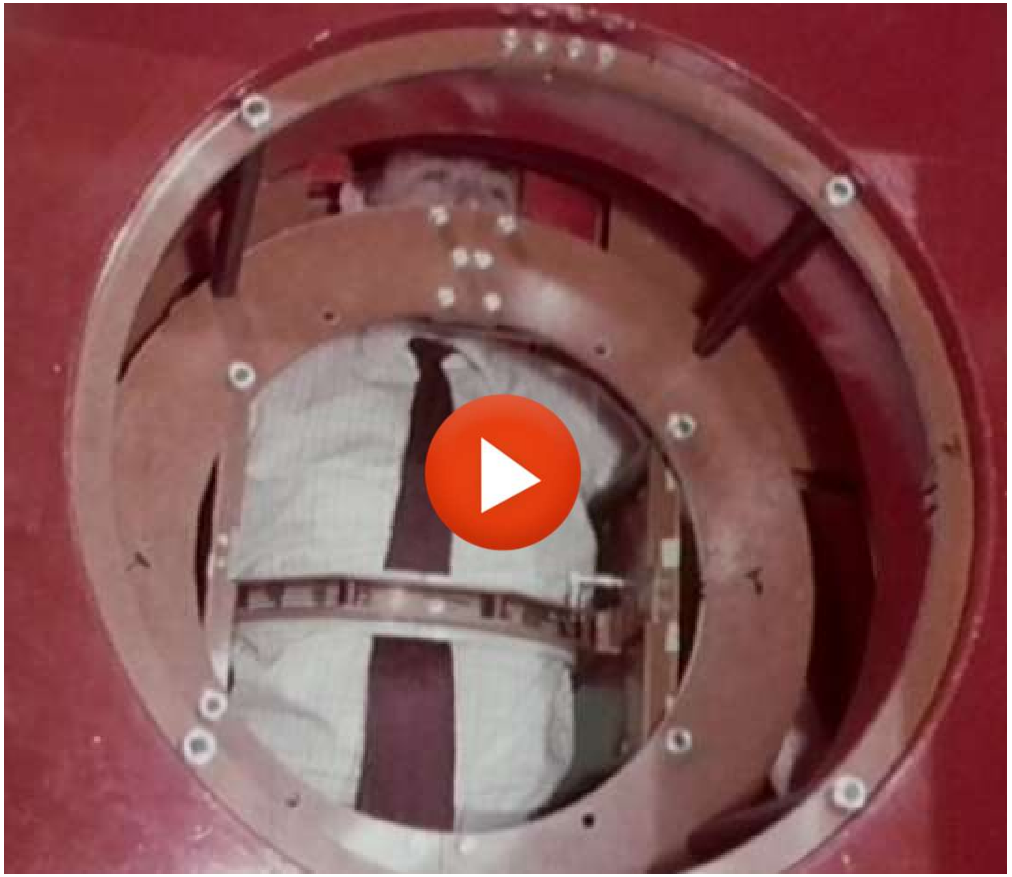

(short video)

The MRI Controlled Area

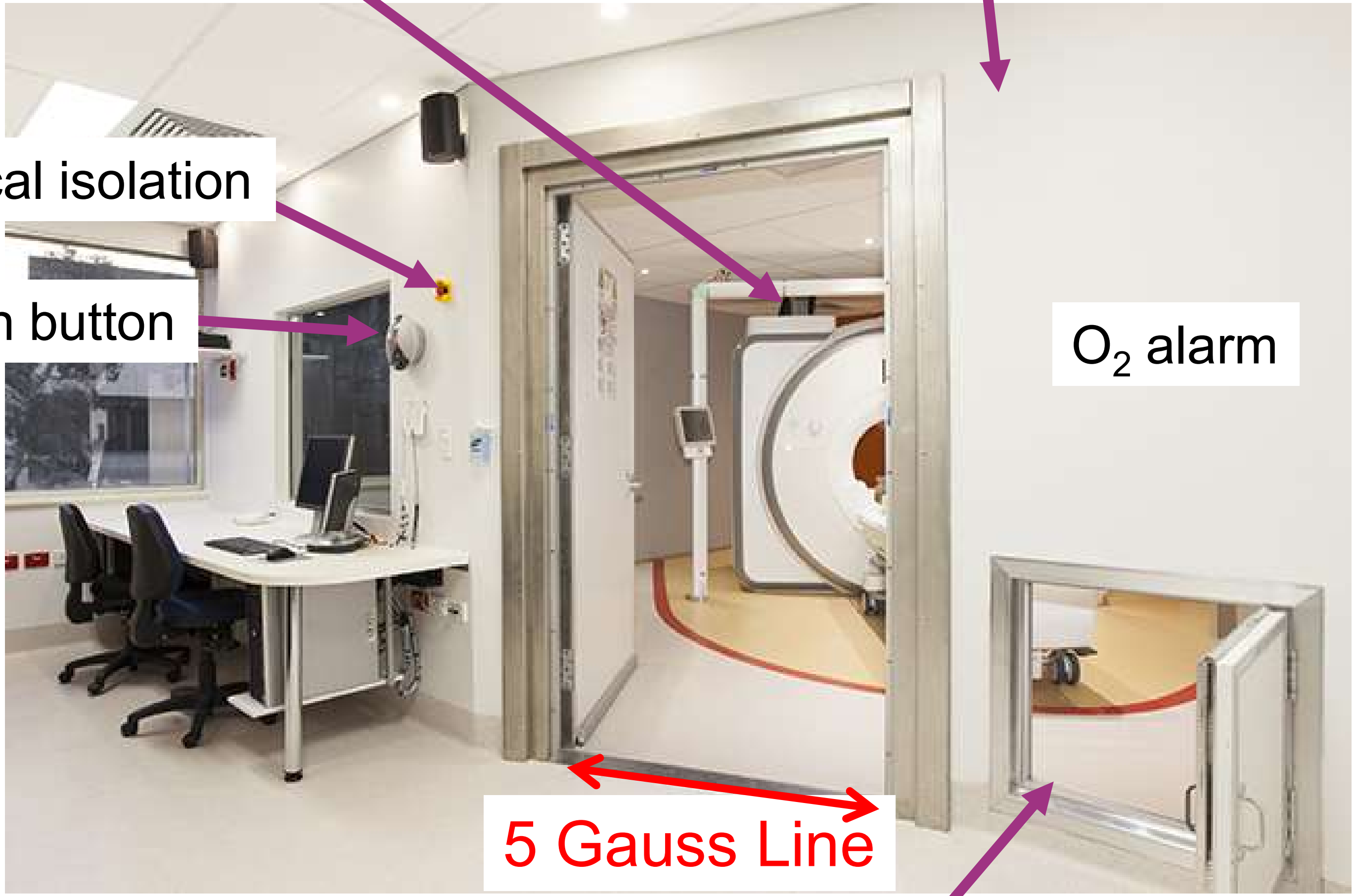

RF Cage

Quench pipe

Electrical isolation

Quench button

O_2 alarm

5 Gauss Line

Control Room

Pressure release hatch

RF Cage

- MRI inherently low (RF) signal technique
- Faraday cage
  - All 6 sides enclosed in copper
  - Electromagnetic shielding
  - Examples microwave oven, coax cable
- Integrity must be maintained

  Penetration panel

  Mesh window, waveguide

  Closed scan room door, no fluorescent lights

RF Cage Construction

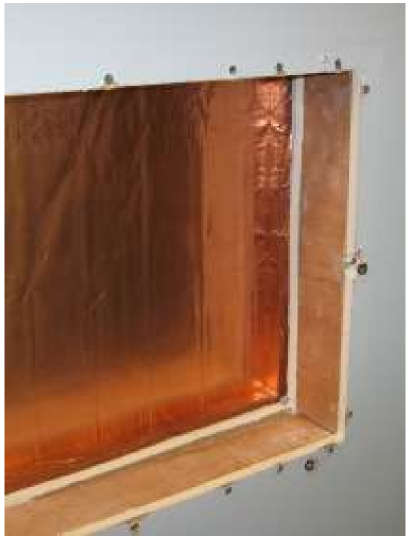

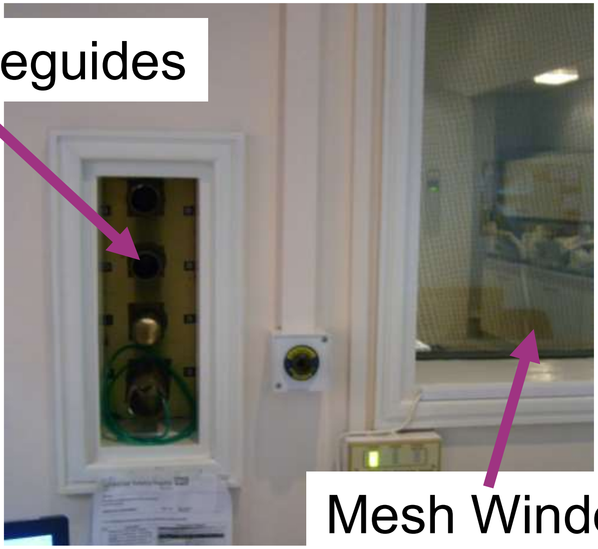

Waveguides

Mesh Window

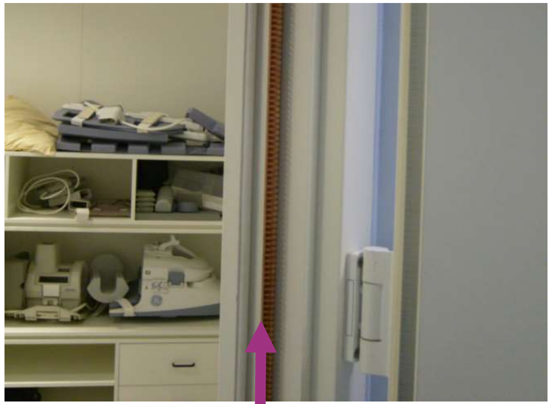

Door surround

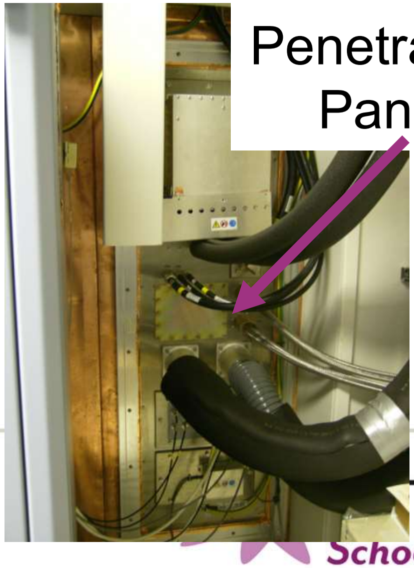

Penetration Panel

The Scanner

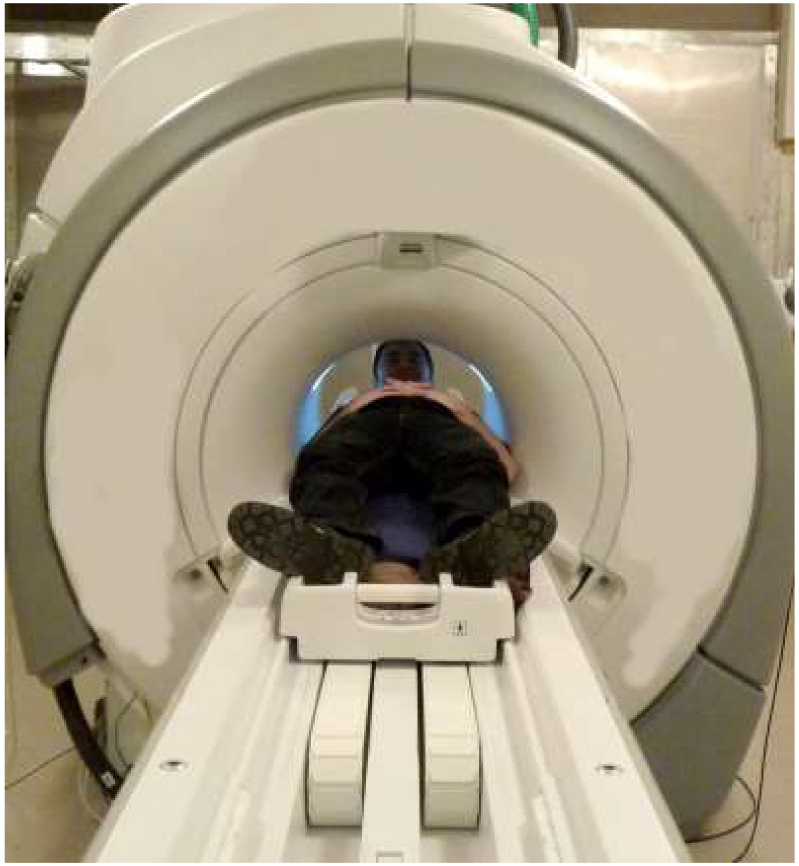

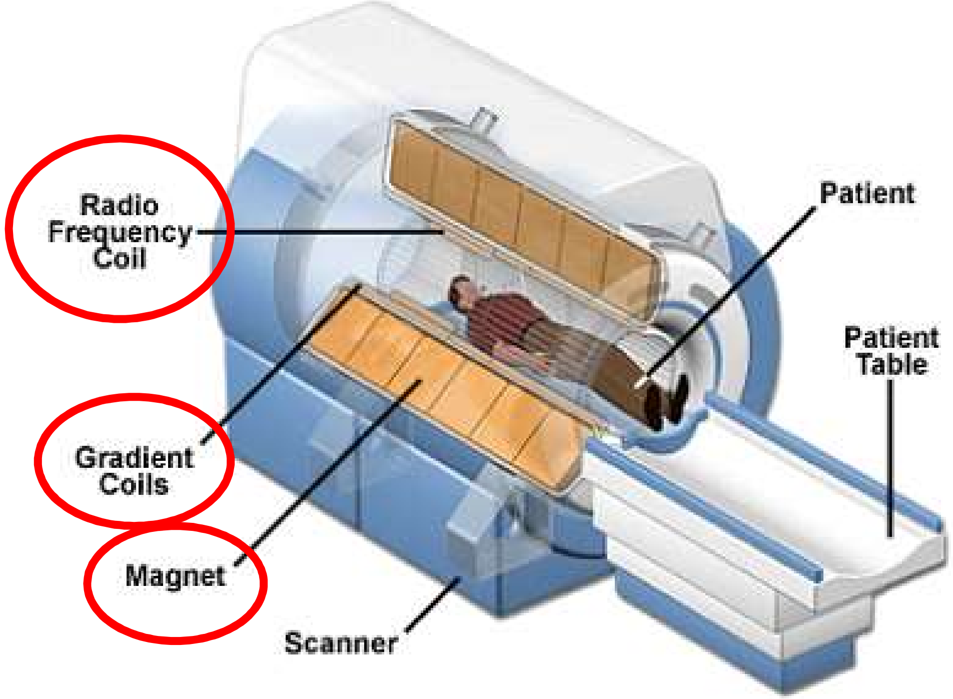
Radio Frequency Coil
Patient
Patient Table
Gradient Coils
Magnet
Scanner

…plus shielding coils, shim coils and cryostat!

Equipment & Safety

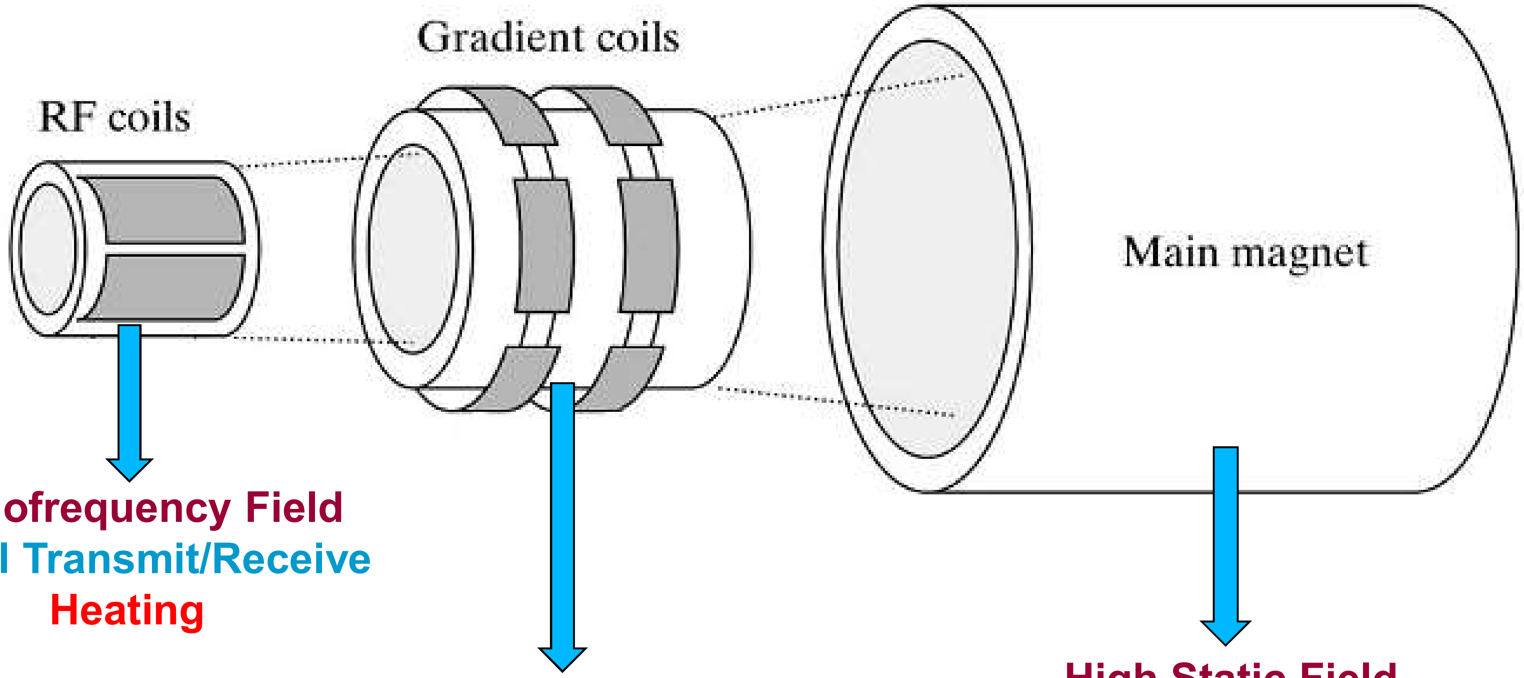
Gradient coils
RF coils
Main magnet

Radiofrequency Field
Signal Transmit/Receive
Heating

Rapid changes to Field
Spatial Encoding
Noise
Stimulation

High Static Field
Establish magnetisation
Projectiles
Bioeffects

Three magnetic field interactions to consider

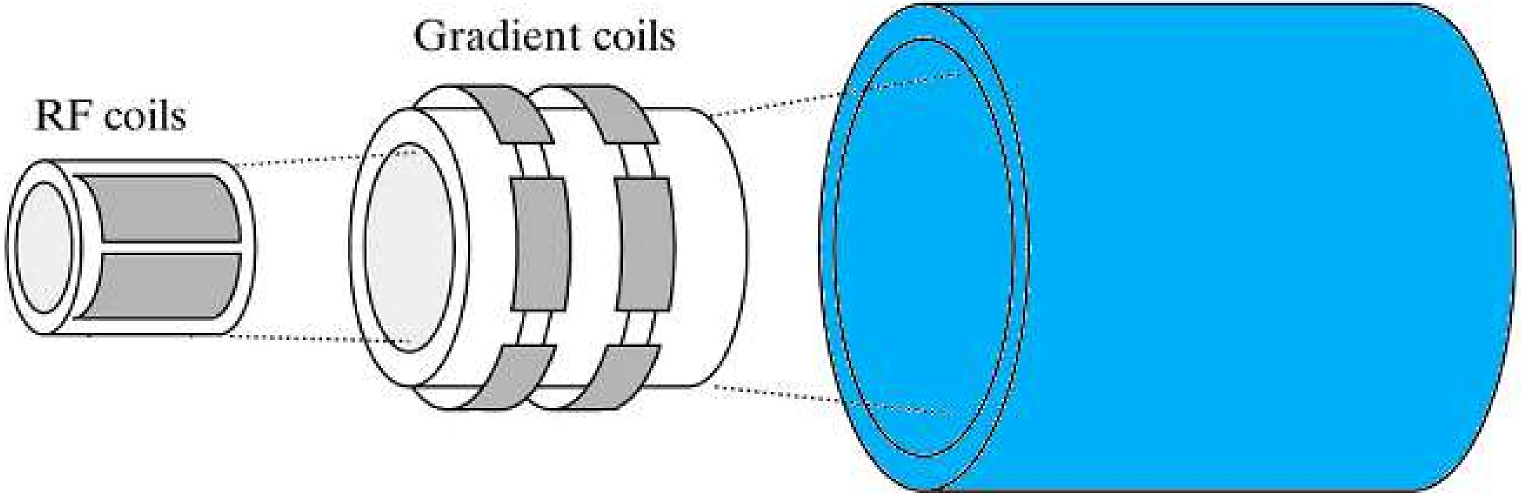
Gradient coils
RF coils

Main Magnet

Magnet Field (B0)

- Low sensitivity requires very high field
- 1 Tesla = 10,000 Gauss

  cf. 0.3-0.7 G earth's field
- Mostly superconductors

  Niobium-titanium (9.5 K)

  field decay: 5-10 G y^{-1}

  field stability: <0.1 ppm h^{-1}

1987: Elscint's Gyrex System

Philips' vertical HFO System

Homogeneity (Inside the Magnet)

Uniform imaging
volume
at isocentre

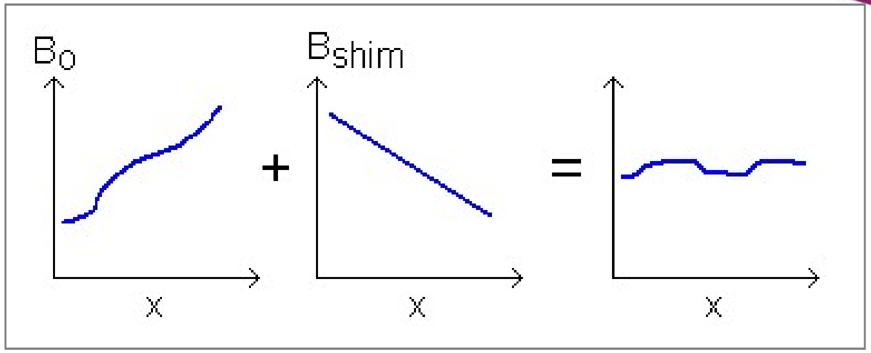

B_o
B_{shim}
+
=
x
x
x

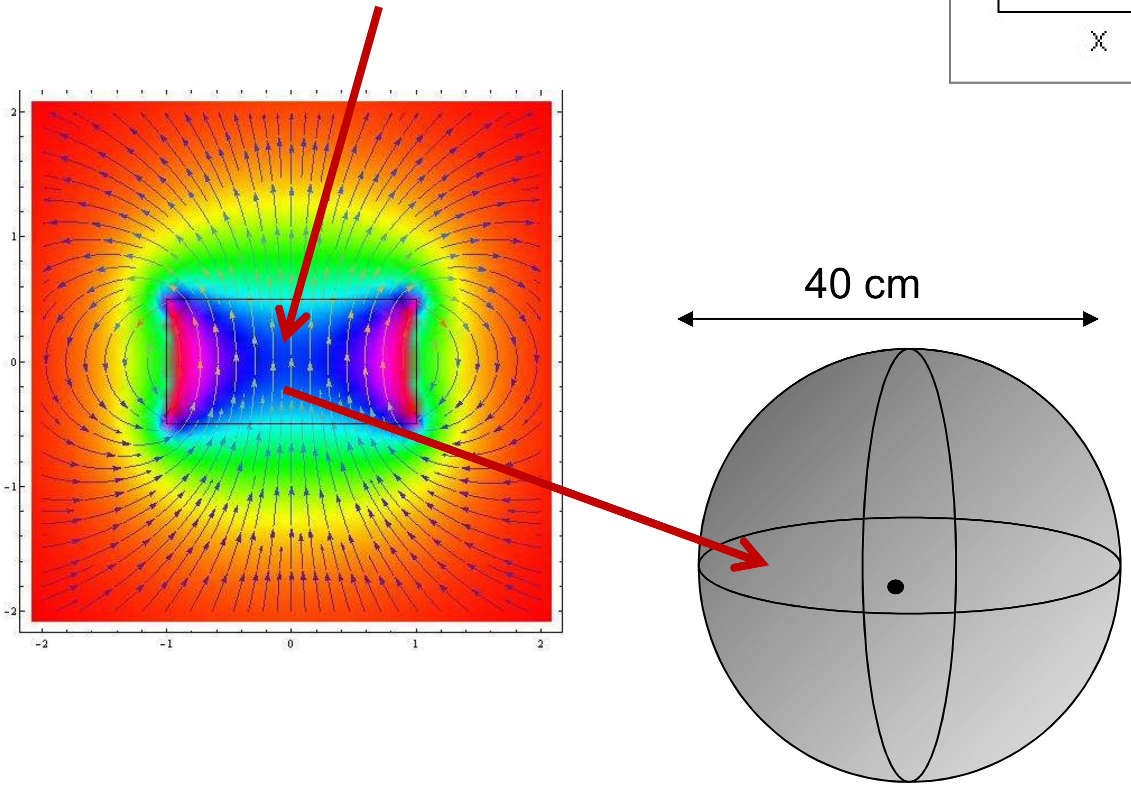

40 cm
2
1
0
-1
-2
-2
-1
0
1
2

e.g. DSV_{40cm} = 0.2 ppm

(at 1.5 T):
0.2 x 63.87 MHz = 12.8 Hz

- Magnet is shimmed at installation- additional (dynamic) shimming may be required

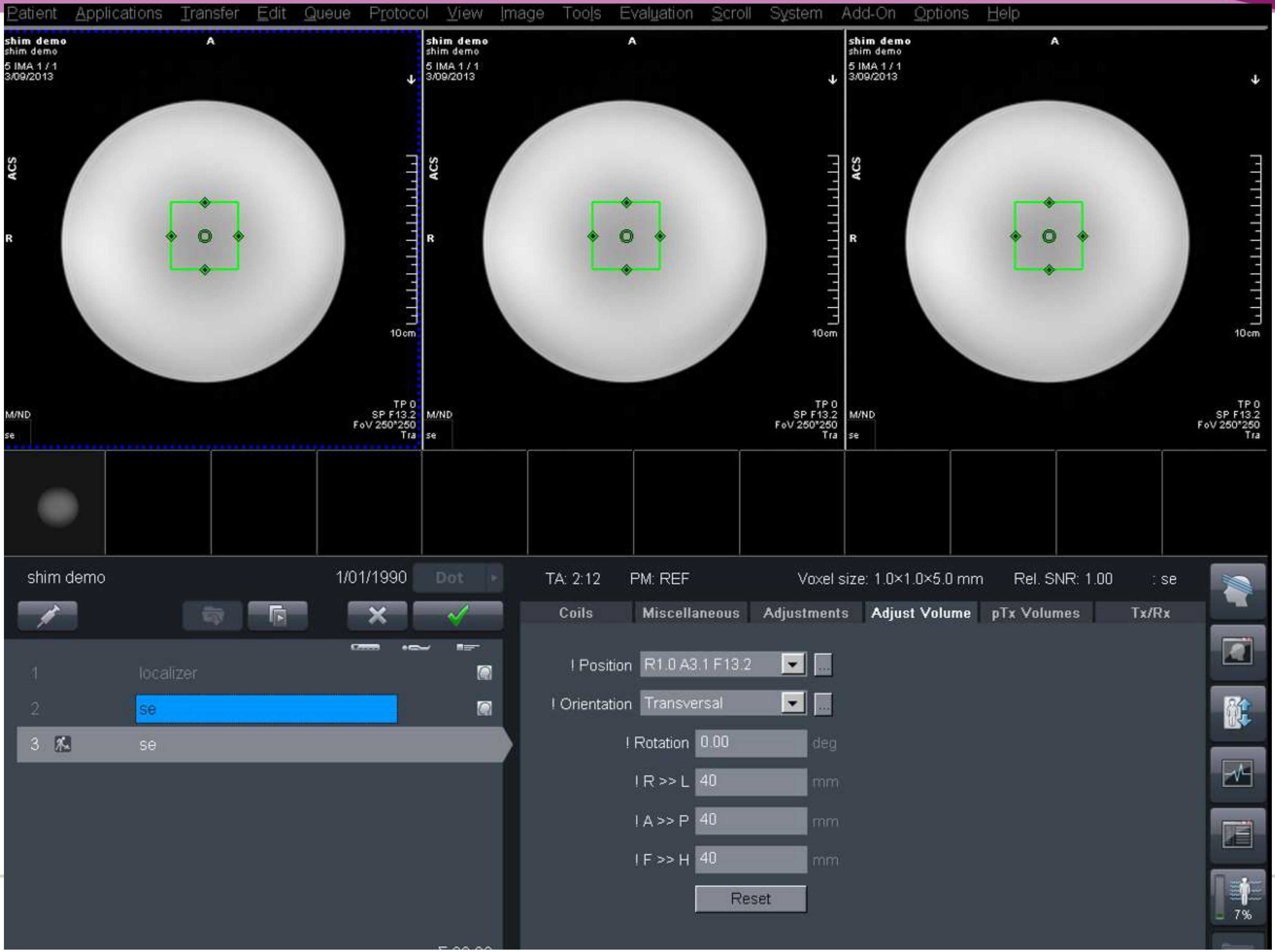
Patient Applications Transfer Edit Queue Protocol View Image Tools Evaluation Scroll System Add-On Options Help
shim demo
shim demo
5 IMA 1 / 1
3/09/2013
A
ACS
R
10cm
M/ND
se
TP 0
SP F13.2
FoV 250*250
Tra
Dot
Coils
Miscellaneous
Adjustments
Adjust Volume
pTx Volumes
Tx/Rx
Reset
7%

shim demo 1/01/1990

1 localizer

2 se

3 se

TA: 2:12 PM: REF Voxel size: 1.0×1.0×5.0 mm Rel. SNR: 1.00 : se

! Position R1.0 A3.1 F13.2

! Orientation Transversal

! Rotation 0.00 deg

! R >> L 40 mm

! A >> P 40 mm

! F >> H 40 mm

FID

FT

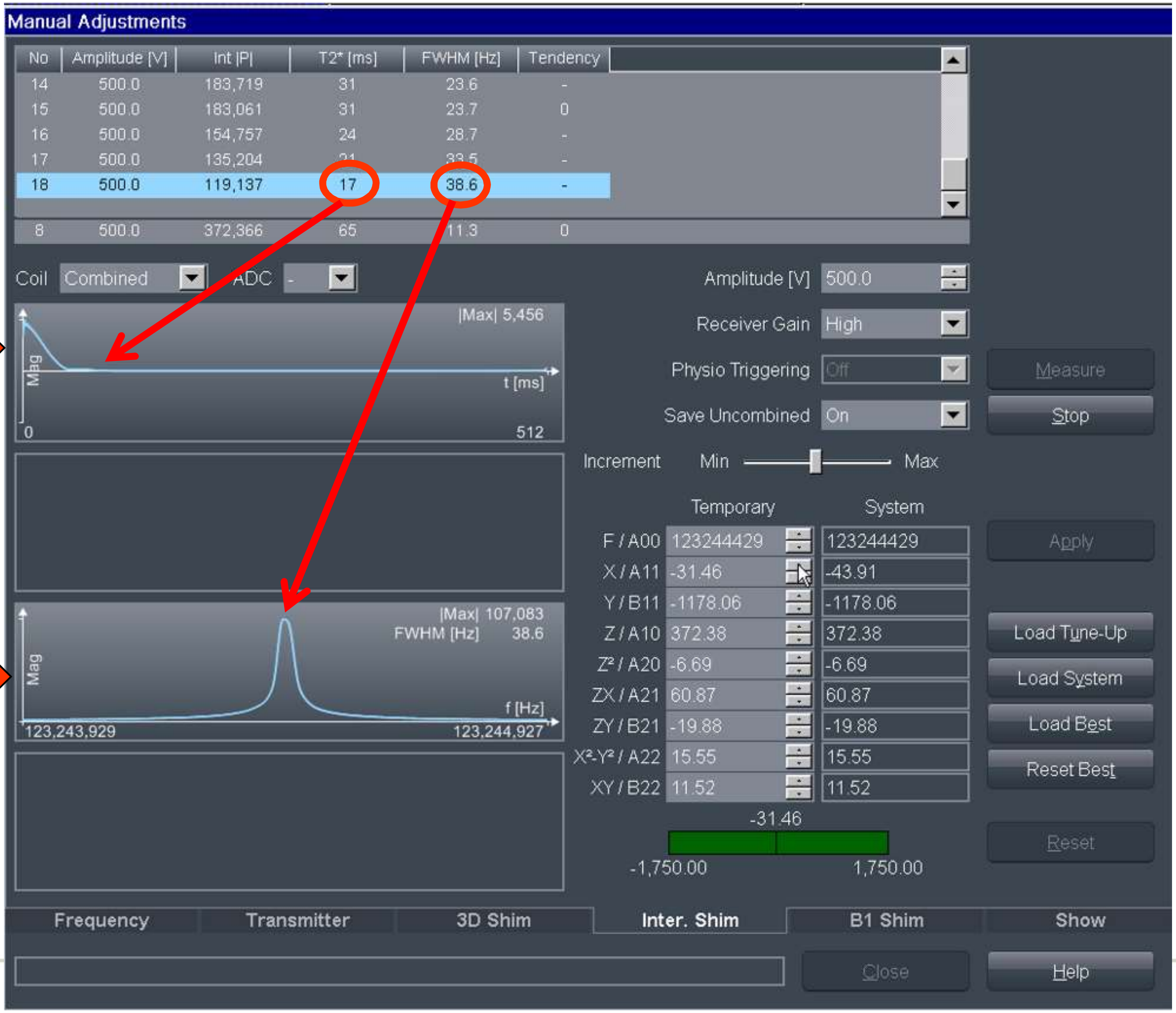

Manual Adjustments

No	Amplitude [V]	Int |P|	T2* [ms]	FWHM [Hz]	Tendency
14	500.0	183,719	31	23.6	-
15	500.0	183,061	31	23.7	0
16	500.0	154,757	24	28.7	-
17	500.0	135,204	21	33.5	-
18	500.0	119,137	17	38.6	-
8	500.0	372,366	65	11.3	0

Coil Combined

ADC -

Amplitude [V] 500.0

Receiver Gain High

Physio Triggering Off

Save Uncombined On

	Temporary	System
F / A00	123244429	123244429
X / A11	-31.46	-43.91
Y / B11	-1178.06	-1178.06
Z / A10	372.38	372.38
Z² / A20	-6.69	-6.69
ZX / A21	60.87	60.87
ZY / B21	-19.88	-19.88
X²-Y² / A22	15.55	15.55
XY / B22	11.52	11.52

|Max| 5,456
Mag
t [ms]
0
512
|Max| 107,083
FWHM [Hz] 38.6
Mag
f [Hz]
123,243,929
123,244,927
Increment
Min
Max
-31.46
-1,750.00
1,750.00
Measure
Stop
Apply
Load Tune-Up
Load System
Load Best
Reset Best
Reset
Frequency
Transmitter
3D Shim
Inter. Shim
B1 Shim
Show
Close
Help

FID

FT

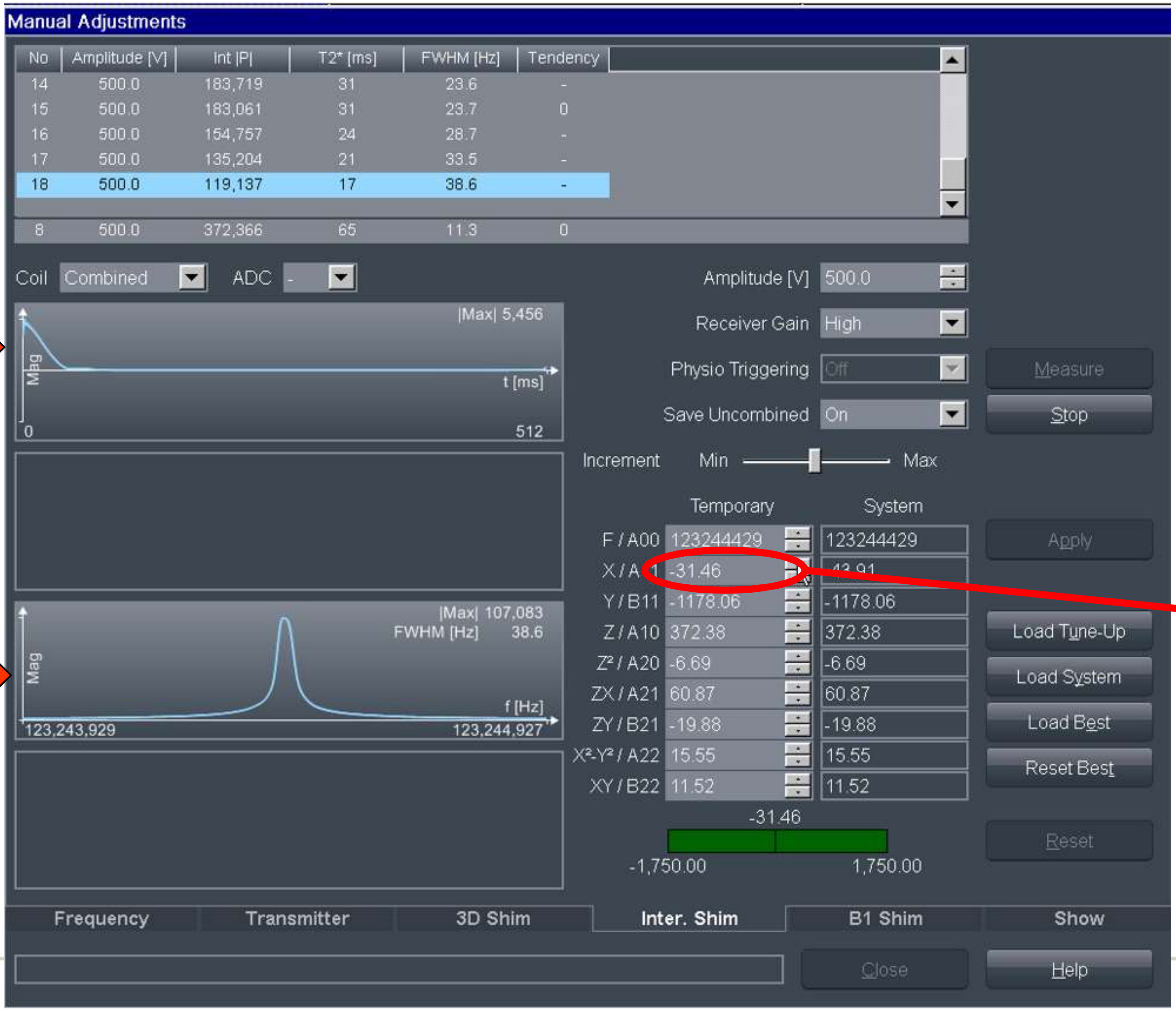
Manual Adjustments
|Max| 5,456
Mag
t [ms]
0
512
|Max| 107,083
FWHM [Hz] 38.6
Mag
f [Hz]
123,243,929
123,244,927
Measure
Stop
Apply
Load Tune-Up
Load System
Load Best
Reset Best
Reset
Frequency
Transmitter
3D Shim
Inter. Shim
B1 Shim
Show
Close
Help

No	Amplitude [V]	Int [P]	T2* [ms]	FWHM [Hz]	Tendency
14	500.0	183,719	31	23.6	-
15	500.0	183,061	31	23.7	0
16	500.0	154,757	24	28.7	-
17	500.0	135,204	21	33.5	-
18	500.0	119,137	17	38.6	-
8	500.0	372,366	65	11.3	0

Coil Combined ADC -

Amplitude [V] 500.0

Receiver Gain High

Physio Triggering Off

Save Uncombined On

Increment Min Max

	Temporary	System
F / A00	123244429	123244429
X / A 1	-31.46	-43.91
Y / B11	-1178.06	-1178.06
Z / A10	372.38	372.38
Z² / A20	-6.69	-6.69
ZX / A21	60.87	60.87
ZY / B21	-19.88	-19.88
X²-Y² / A22	15.55	15.55
XY / B22	11.52	11.52

-31.46

-1,750.00 1,750.00

Gx

FID

FT

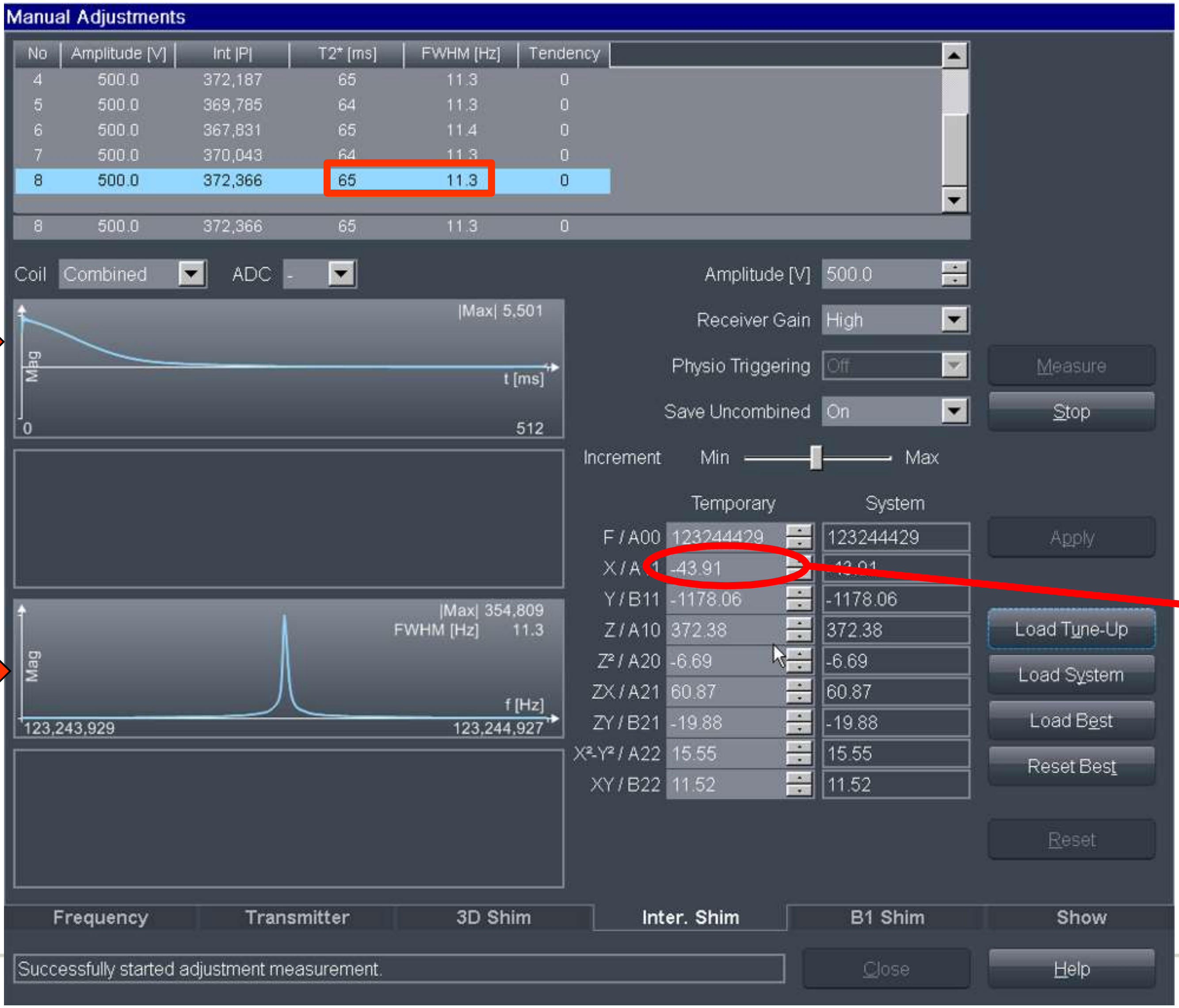

Gx

Manual Adjustments

No	Amplitude [V]	Int [P]	T2* [ms]	FWHM [Hz]	Tendency
4	500.0	372,187	65	11.3	0
5	500.0	369,785	64	11.3	0
6	500.0	367,831	65	11.4	0
7	500.0	370,043	64	11.3	0
8	500.0	372,366	65	11.3	0
8	500.0	372,366	65	11.3	0

Coil: Combined
ADC: -
Amplitude [V]: 500.0
Receiver Gain: High
Physio Triggering: Off
Save Uncombined: On
Increment: Min – Max

	Temporary	System
F / A00	123244429	123244429
X / A11	-43.91	-43.91
Y / B11	-1178.06	-1178.06
Z / A10	372.38	372.38
Z² / A20	-6.69	-6.69
ZX / A21	60.87	60.87
ZY / B21	-19.88	-19.88
X²-Y² / A22	15.55	15.55
XY / B22	11.52	11.52

Successfully started adjustment measurement.

|Max| 5,501
Mag
t [ms]
0
512
|Max| 354,809
FWHM [Hz] 11.3
Mag
f [Hz]
123,243,929
123,244,927
Measure
Stop
Apply
Load Tune-Up
Load System
Load Best
Reset Best
Reset
Frequency
Transmitter
3D Shim
Inter. Shim
B1 Shim
Show
Close
Help

Outside the Magnet: Fringe Field

- Magnet is shielded to reduce extent of fringe field

  5 G line for an unshielded 7 T is 23m away!

- Active & passive shielding is use
- Active shielding causes a sharp field gradient

  Magnitude and variation of field need to be understood

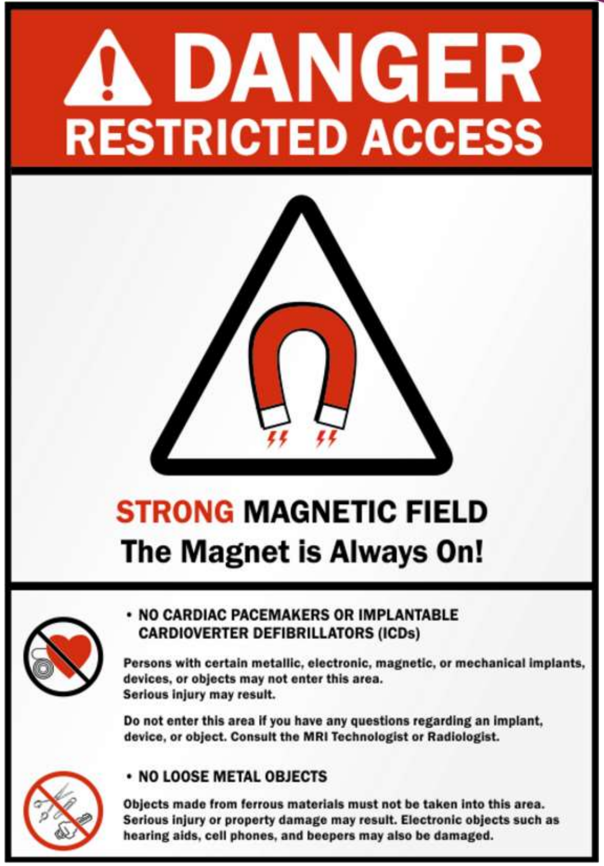

DANGER

RESTRICTED ACCESS

STRONG MAGNETIC FIELD

The Magnet is Always On!

- NO CARDIAC PACEMAKERS OR IMPLANTABLE CARDIOVERTER DEFIBRILLATORS (ICDs)

Persons with certain metallic, electronic, magnetic, or mechanical implants, devices, or objects may not enter this area.
Serious injury may result.

Do not enter this area if you have any questions regarding an implant, device, or object. Consult the MRI Technologist or Radiologist.

- NO LOOSE METAL OBJECTS

Objects made from ferrous materials must not be taken into this area. Serious injury or property damage may result. Electronic objects such as hearing aids, cell phones, and beepers may also be damaged.

Note: ‘Magnetic Shielding’ is also sometimes used to describe RF shielding (Faraday cage)

Proximity Limits

- Each scanner has its ‘footprint’
- ‘5 Gauss line’ (0.5 mT) should be confined to scan room
- Radial & axial components

  Typically axial 1.6 times larger
- May be measured with handheld gaussmeter

> 30 G	Stainless steel, non-ferromagnetic objects
< 30 G	ECG monitors, unrestrained ferromagnetic objects
< 10 G	Credit cards, x-ray tubes
< 5 G	Pacemakers, general public
< 3 G	Moving cars etc
< 1 G	TVs, CT & PET scanners
< 0.5 G	Railways, gamma cameras

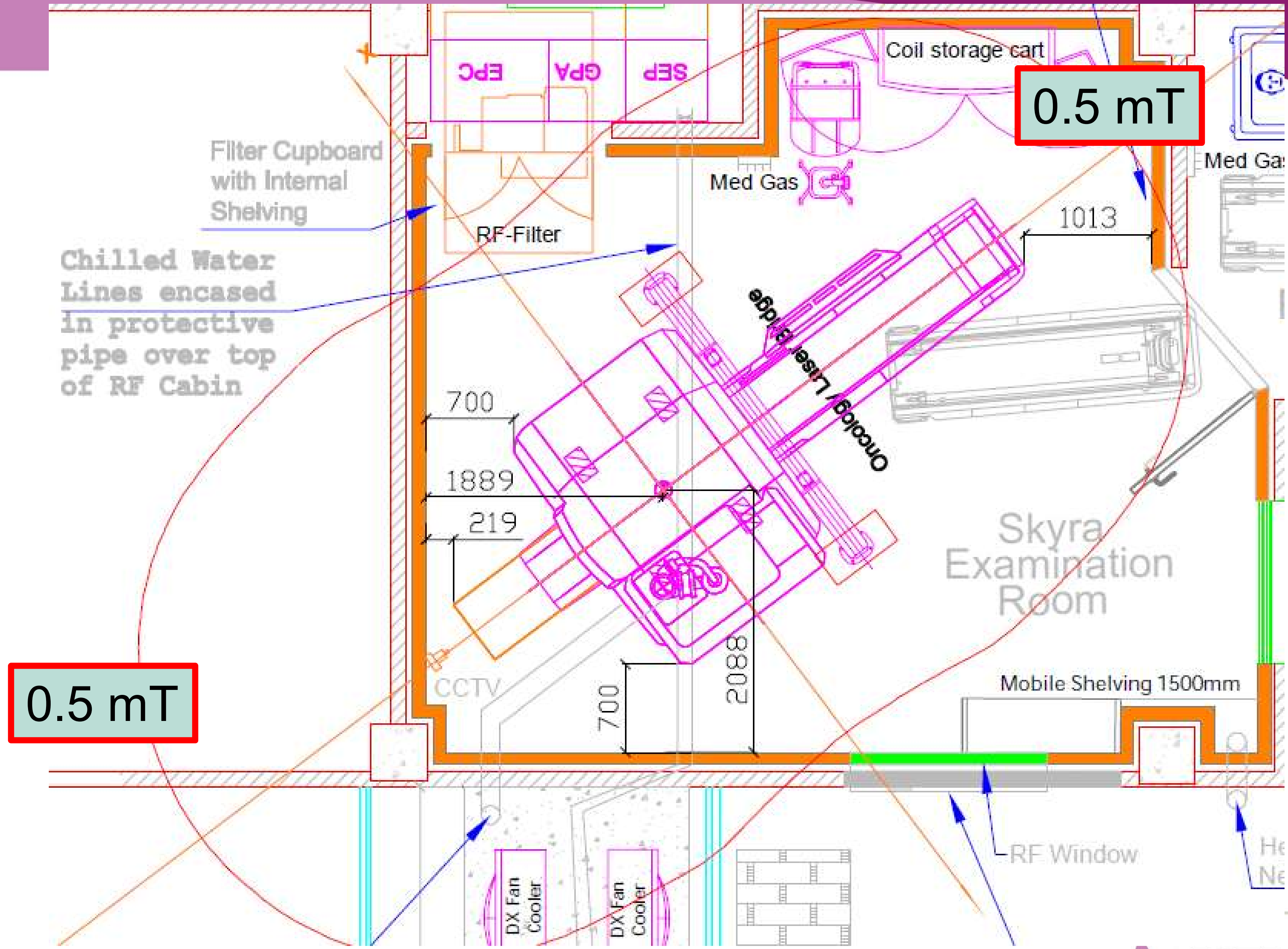
EPC
GPA
SEP
Coil storage cart
Med Gas
Med Gas
Filter Cupboard with Internal Shelving
RF-Filter
Chilled Water Lines encased in protective pipe over top of RF Cabin
1013
Oncolog / Laser Bridge
700
1889
219
CCTV
700
2088
Skyra Examination Room
Mobile Shelving 1500mm
RF Window
DX Fan Cooler
DX Fan Cooler

0.5 mT

0.5 mT

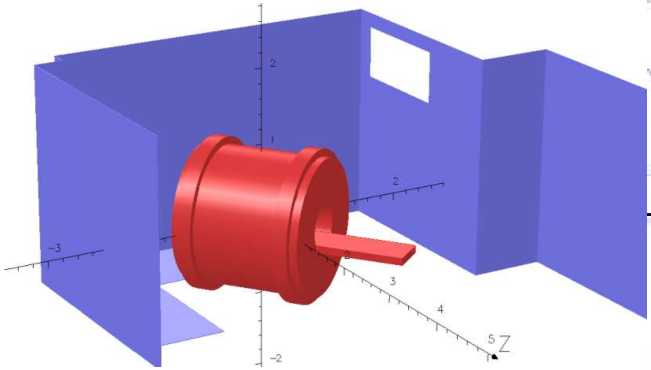

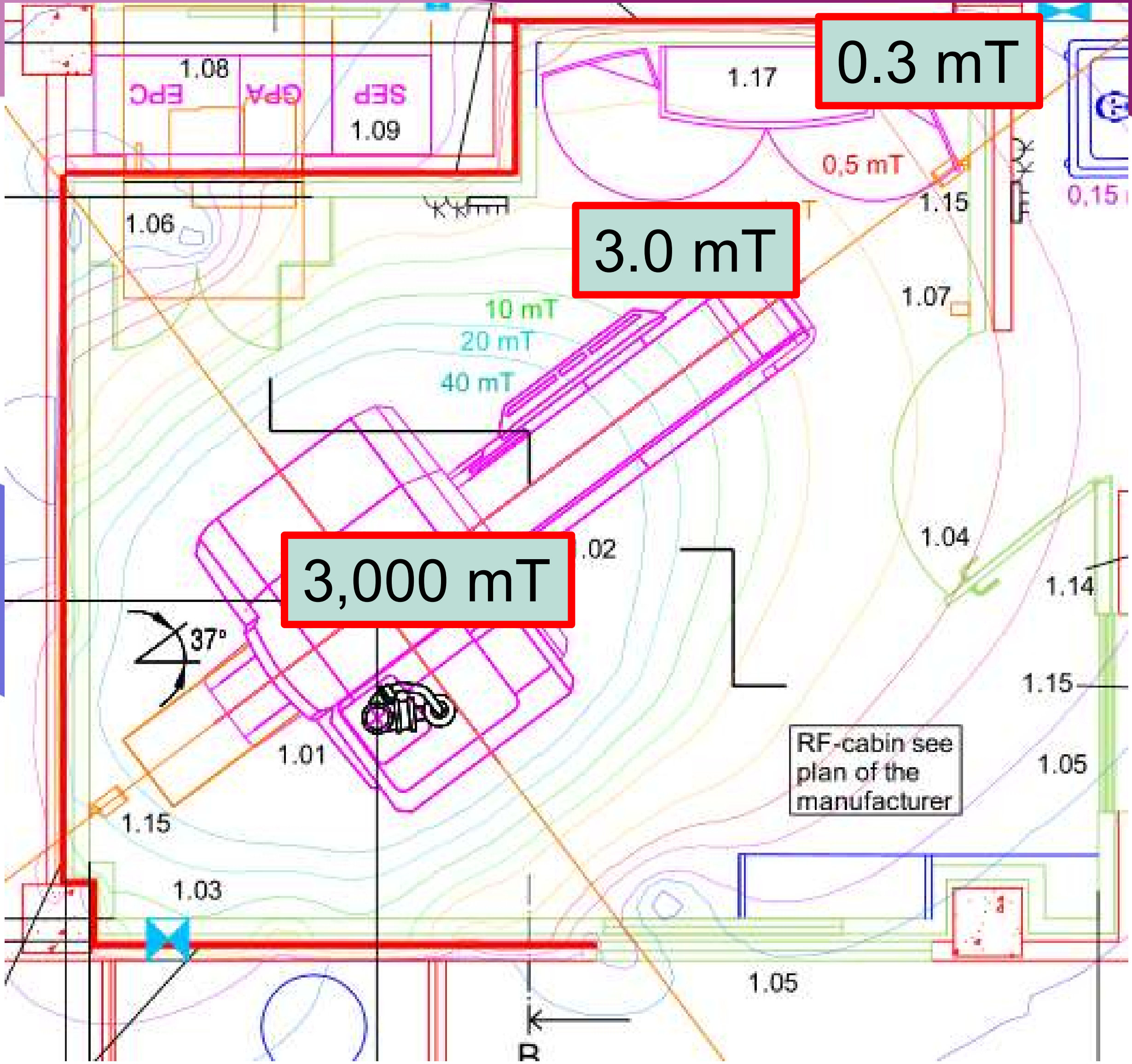
1.08
EPC
GPA
SEP
1.09
1.17
0,5 mT
1.15
0,15
1.06
1.07
10 mT
20 mT
40 mT
1.04
.02
1.14
37°
1.15
RF-cabin see plan of the manufacturer
1.05
1.01
1.15
1.03
1.05
B

0.3 mT

3.0 mT

3,000 mT

The Inner Controlled Area

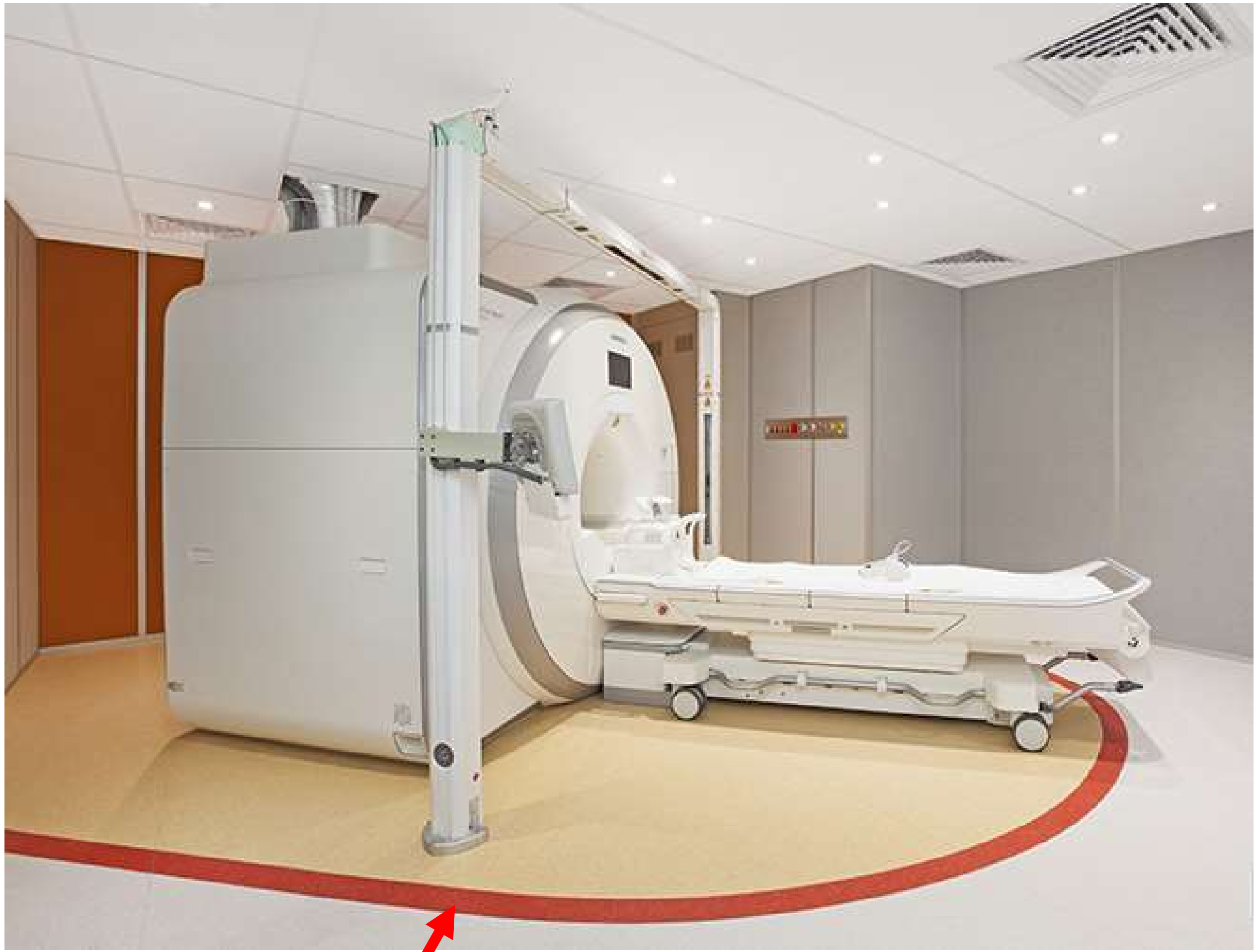

30 Gauss (3 mT)

Static Field (B_0) Effects

- Translational Force (Projectiles)
  - Force product ($B_0 \times dB_0/dz$)
  - Ferromagnetic objects
- Torque
  - Proportional to B_0^2
- Bioeffects?
  - Some transient effects (magnetophosphenes, metallic taste, vertigo) at 4.0 Tesla
  - No known long term effects

STATIC Field Gradient

$$F_z = \frac{V\chi}{\mu_0} B_0 \frac{\partial B_0}{\partial z}$$

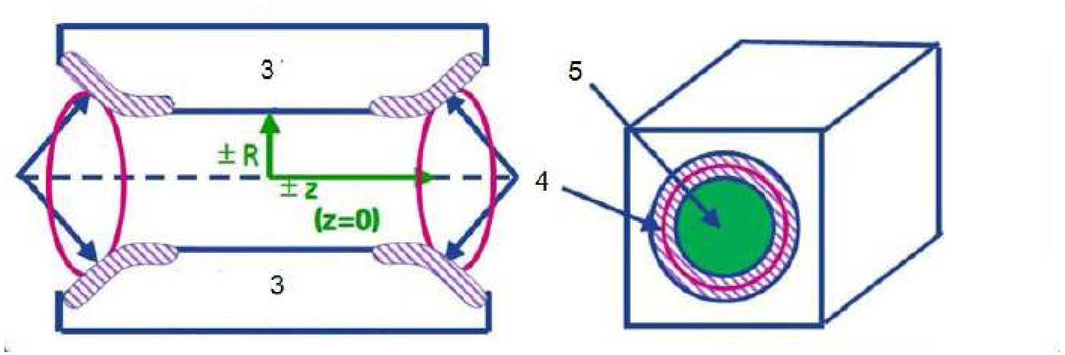

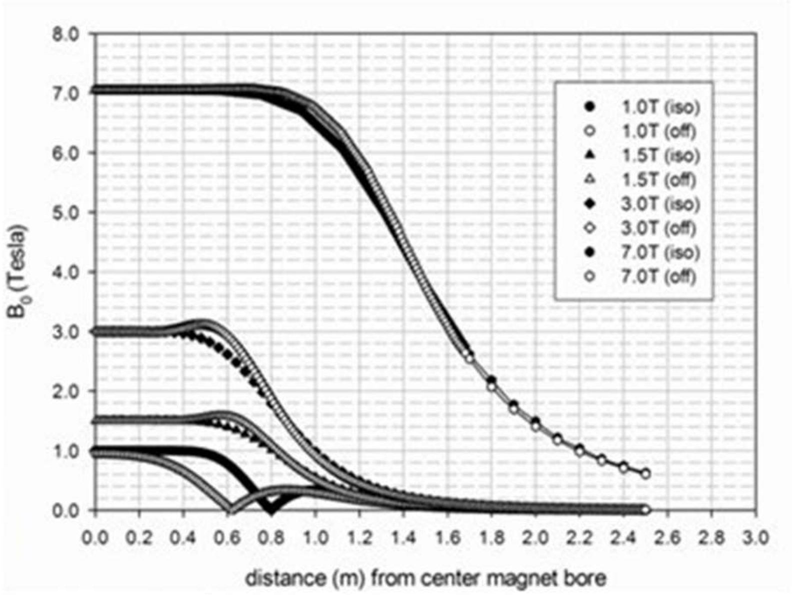

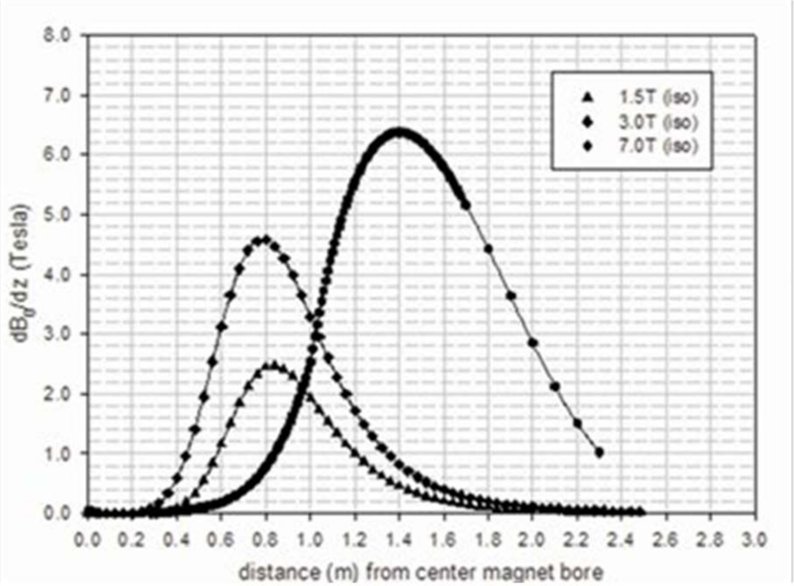

- Peak areas around the bore ends (field, spatial gradient)
- Field can be as high as 1.7-2.4 Tesla on a 1.5 T scanner

The Projectile Effect

Field Gradient Map

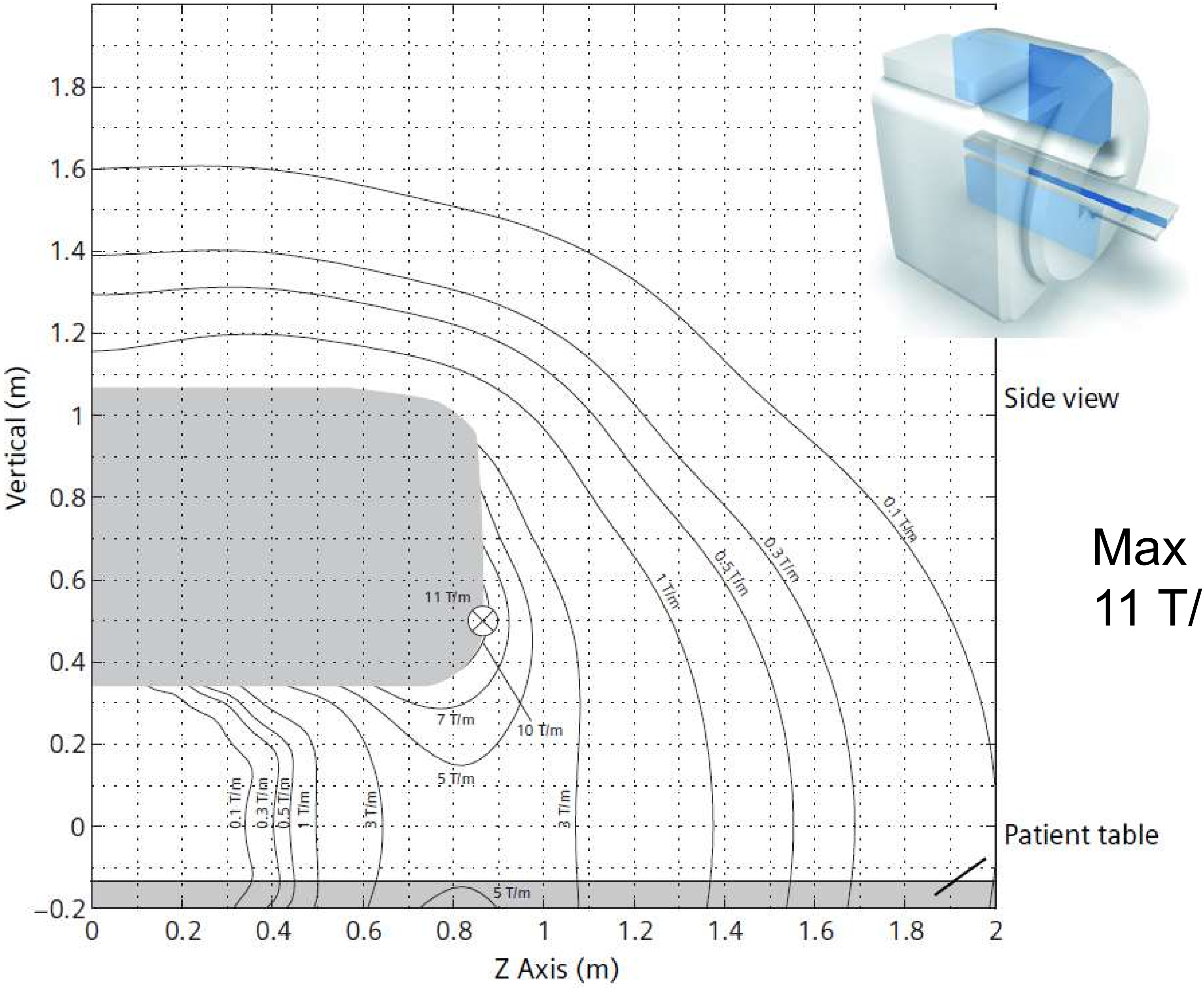

Max is
11 T/m

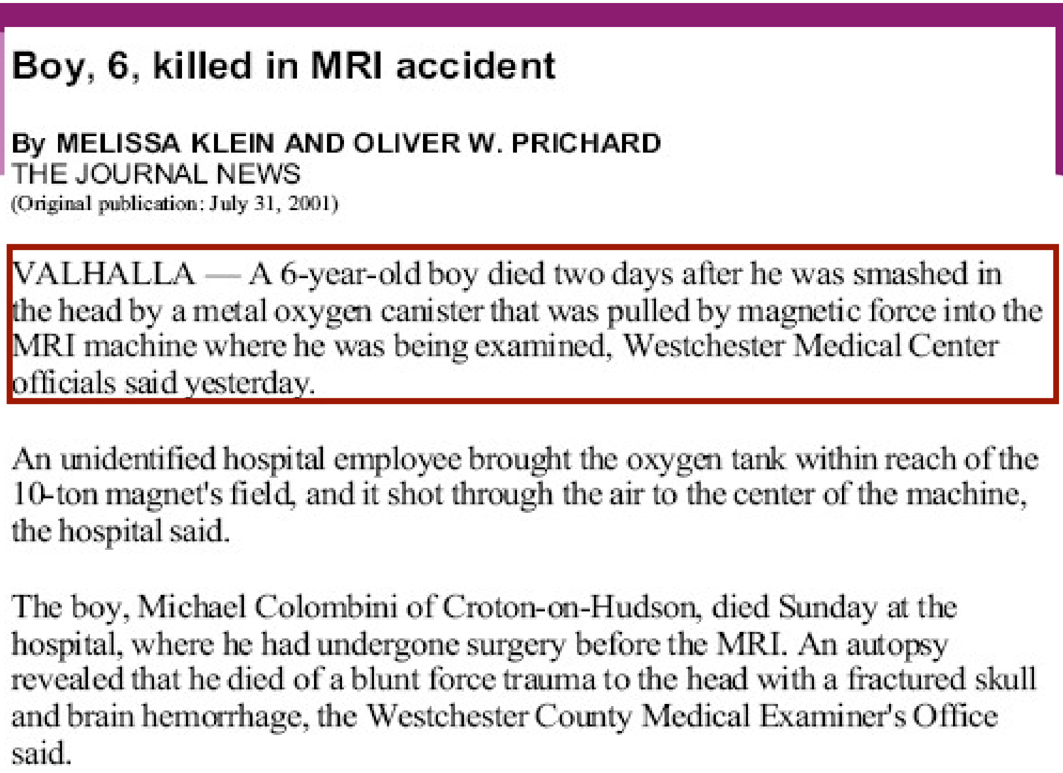

Boy, 6, killed in MRI accident

By MELISSA KLEIN AND OLIVER W. PRICHARD
THE JOURNAL NEWS
(Original publication: July 31, 2001)

VALHALLA — A 6-year-old boy died two days after he was smashed in the head by a metal oxygen canister that was pulled by magnetic force into the MRI machine where he was being examined, Westchester Medical Center officials said yesterday.

An unidentified hospital employee brought the oxygen tank within reach of the 10-ton magnet's field, and it shot through the air to the center of the machine, the hospital said.

The boy, Michael Colombini of Croton-on-Hudson, died Sunday at the hospital, where he had undergone surgery before the MRI. An autopsy revealed that he died of a blunt force trauma to the head with a fractured skull and brain hemorrhage, the Westchester County Medical Examiner's Office said.

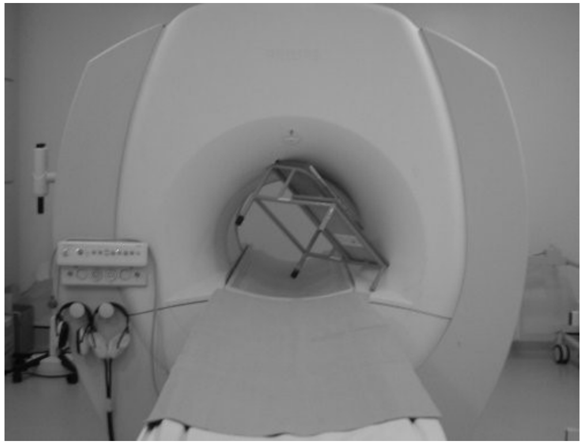

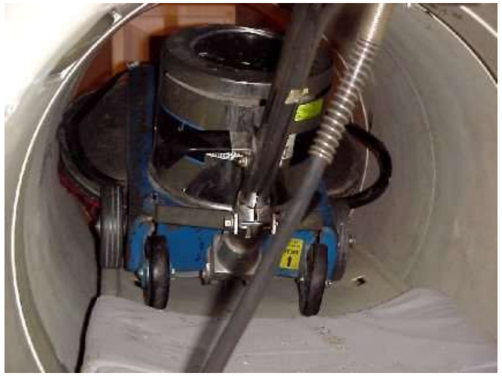

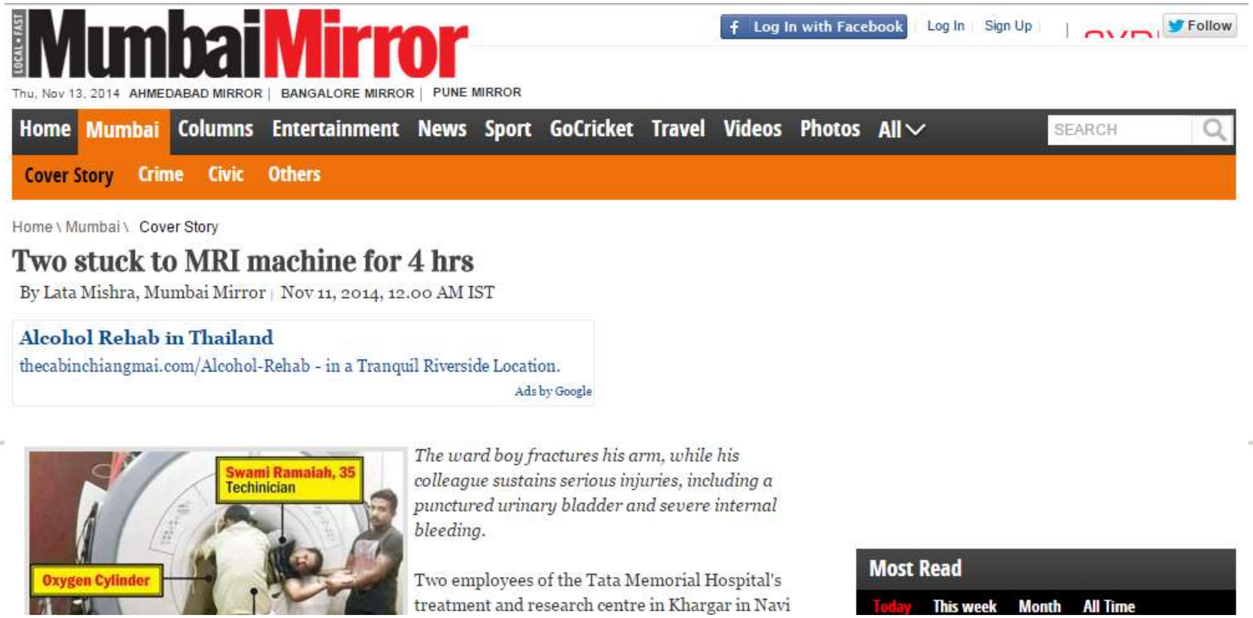
MumbaiMirror
LOCAL • FAST
Log In with Facebook
Log In
Sign Up
Follow
Thu, Nov 13, 2014 AHMEDABAD MIRROR | BANGALORE MIRROR | PUNE MIRROR
Home
Mumbai
Columns
Entertainment
News
Sport
GoCricket
Travel
Videos
Photos
All
SEARCH
Cover Story
Crime
Civic
Others
Home \ Mumbai \ Cover Story

Two stuck to MRI machine for 4 hrs

By Lata Mishra, Mumbai Mirror | Nov 11, 2014, 12.00 AM IST

Alcohol Rehab in Thailand
thecabinchiangmai.com/Alcohol-Rehab - in a Tranquil Riverside Location.
Ads by Google

Swami Ramaiah, 35
Techinician
Oxygen Cylinder

The ward boy fractures his arm, while his colleague sustains serious injuries, including a punctured urinary bladder and severe internal bleeding.

Two employees of the Tata Memorial Hospital's treatment and research centre in Khargar in Navi

Most Read
Today
This week
Month
All Time

Implants & Devices

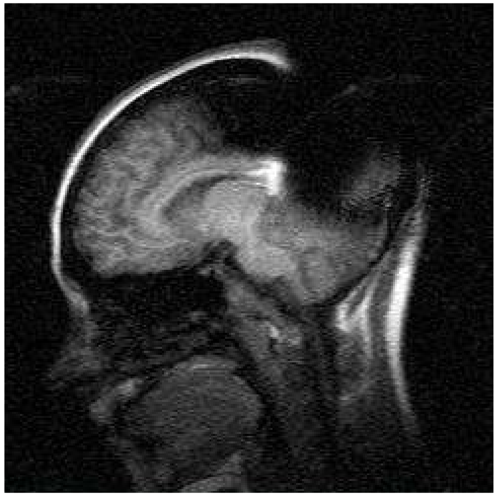

- 1 April, 2000 Australia: Patient with pacemaker scanned and died as a result of malfunction
- Another accident left a patient blinded from a minute metal fragment in his eye
- Ex-vivo testing of devices required at *appropriate field strength*
- Deflection Angle Test *(see next)*

Is it 'Magnetic'?

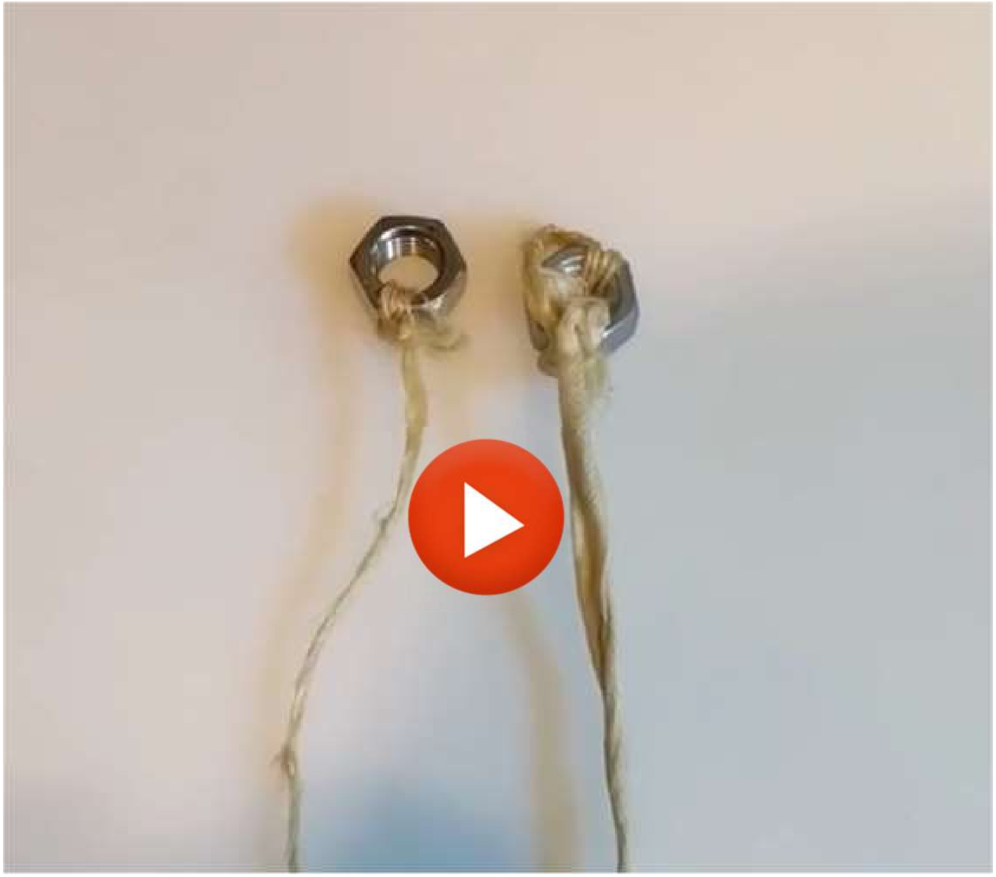

ASTM Labels

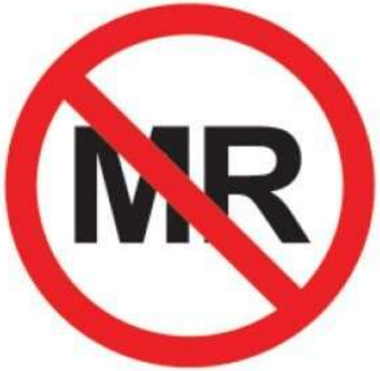

MR Unsafe

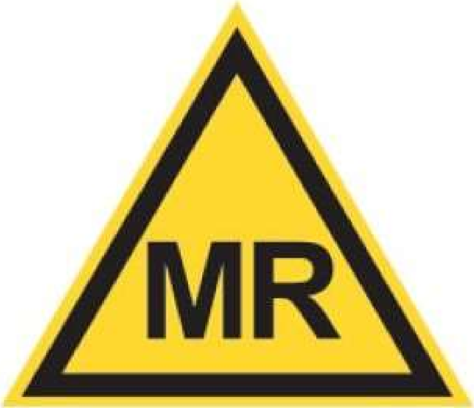

MR Conditional

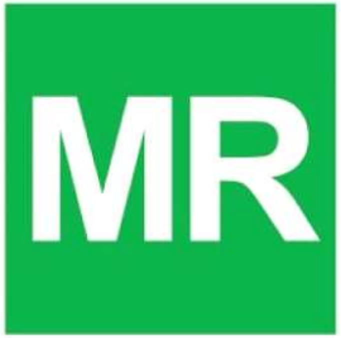

MR Safe

2005: Replaced terms ***MR Compatible*** and ***MR Unsafe***

MR Conditional Pacemakers

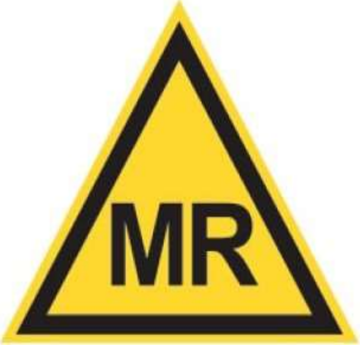

- Up to 75% pacemaker patients will need MRI
- Main concerns are function & heating

- MR conditional types exist
  - *Reduced ferromagnetic components*
  - *MR specific mode*
  - *Radiopaque marking*
  - *Replaced read switch*
  - *Power supply protection*

Patient Screening

- ✓ Operate controlled area
- ✓ Screen patients/helpers
- ✓ Orbit x-ray if required
- ✓ Check compatibility of device (all 3 fields!)

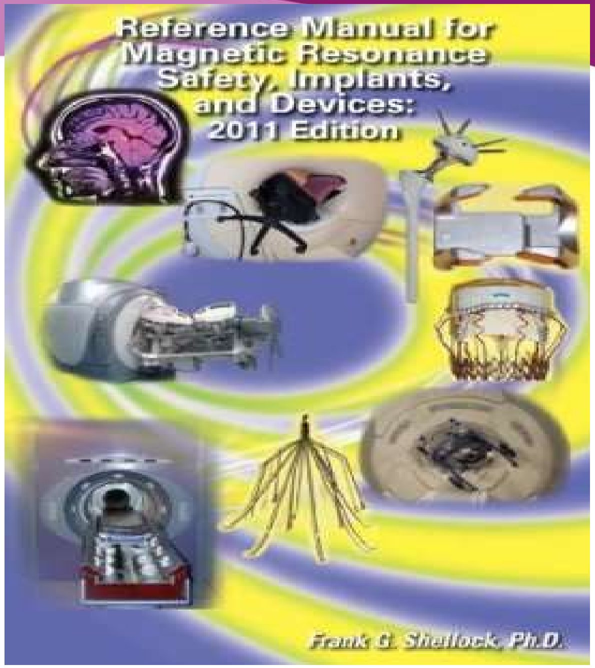

Reference Manual for Magnetic Resonance Safety, Implants, and Devices: 2011 Edition

Frank G. Shellock, Ph.D.

If in doubt DO NOT scan

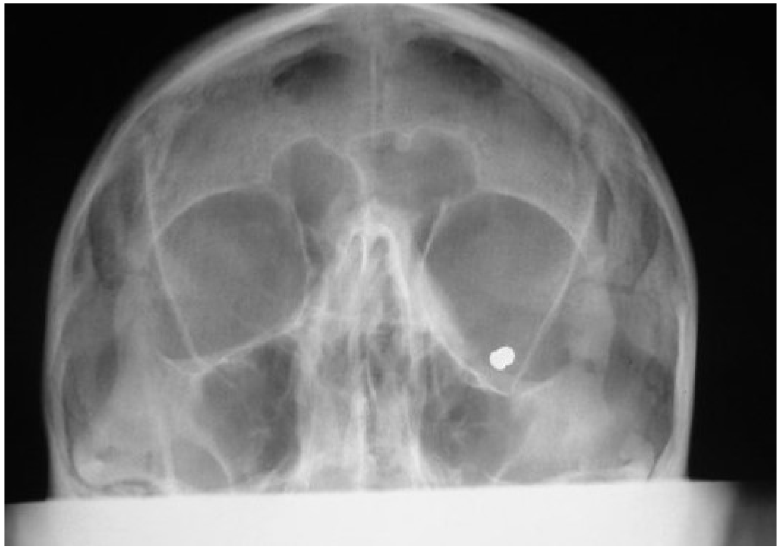

Quench

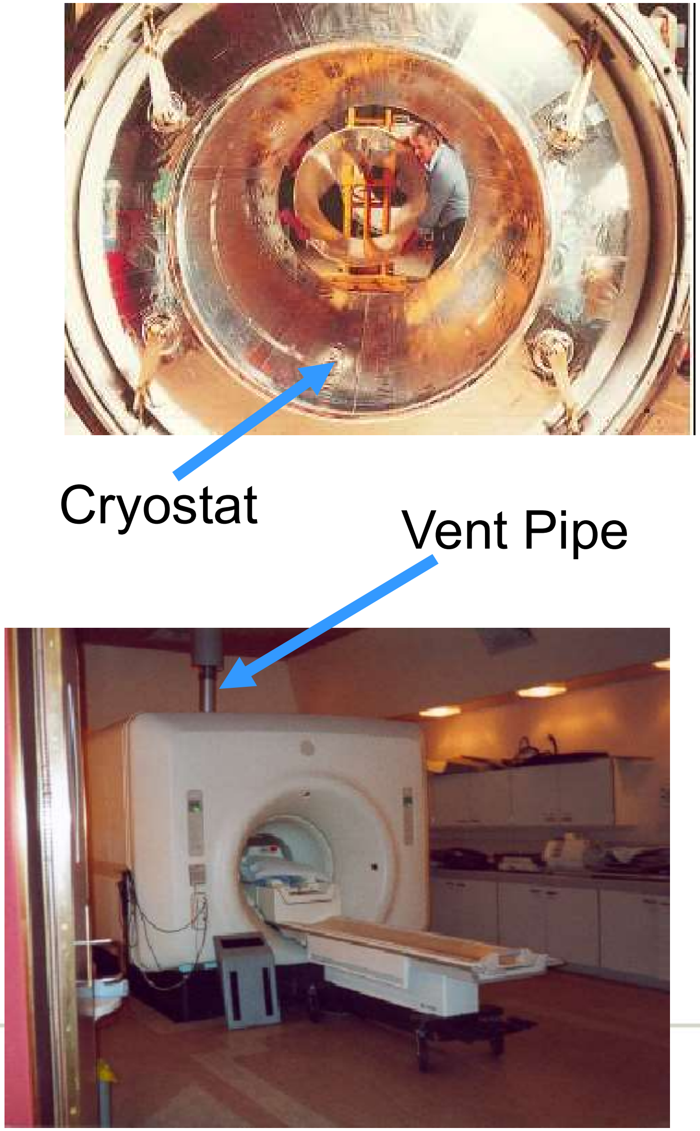
Cryostat
Vent Pipe

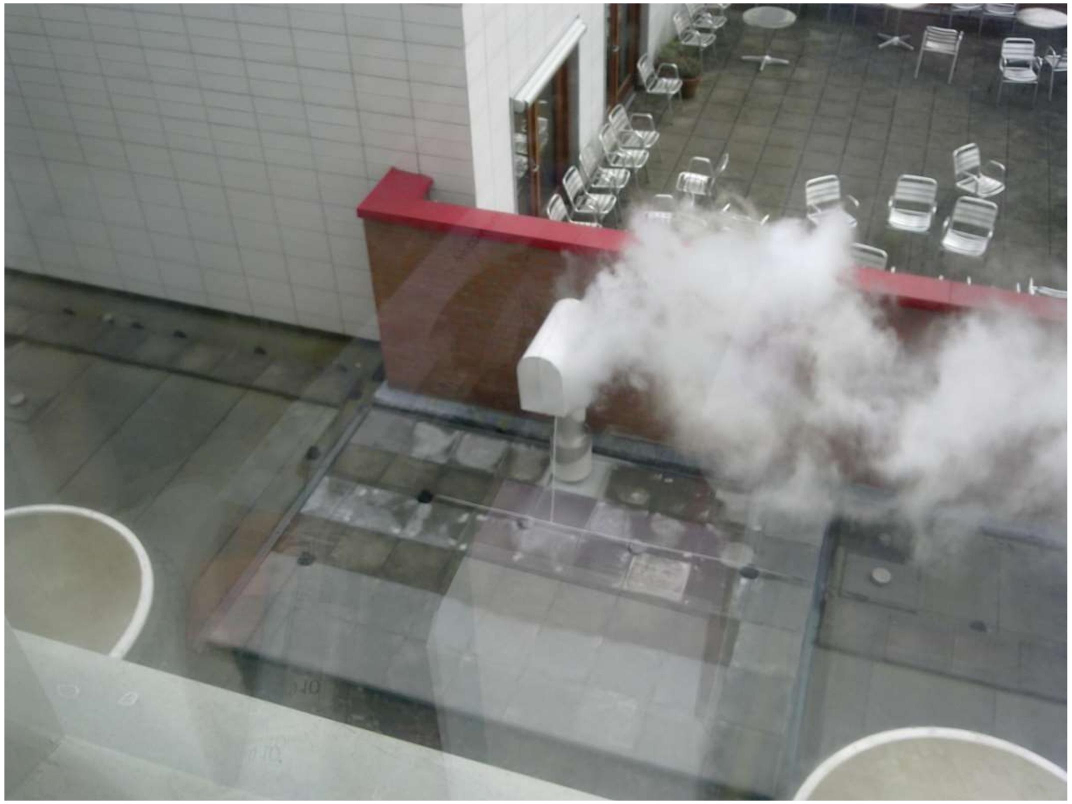

Liquid helium (boiling point 4.2 K) cryogen

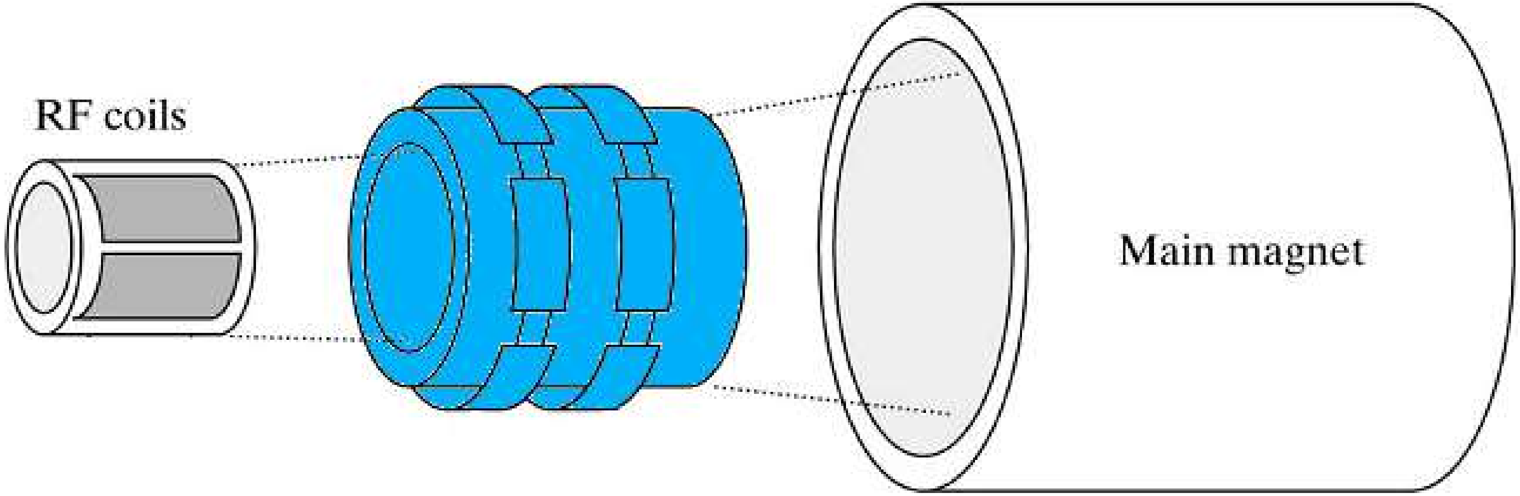
RF coils
Main magnet

Gradient Coils

Imaging Gradients

- 3 orthogonal or in combination
  - ✓ Spatially encode image
- Higher amplitudes mean:
  - ✓ Better resolution
  - ✓ greater diffusion weighting
- Faster switching rates mean:
  - ✓ Faster scans

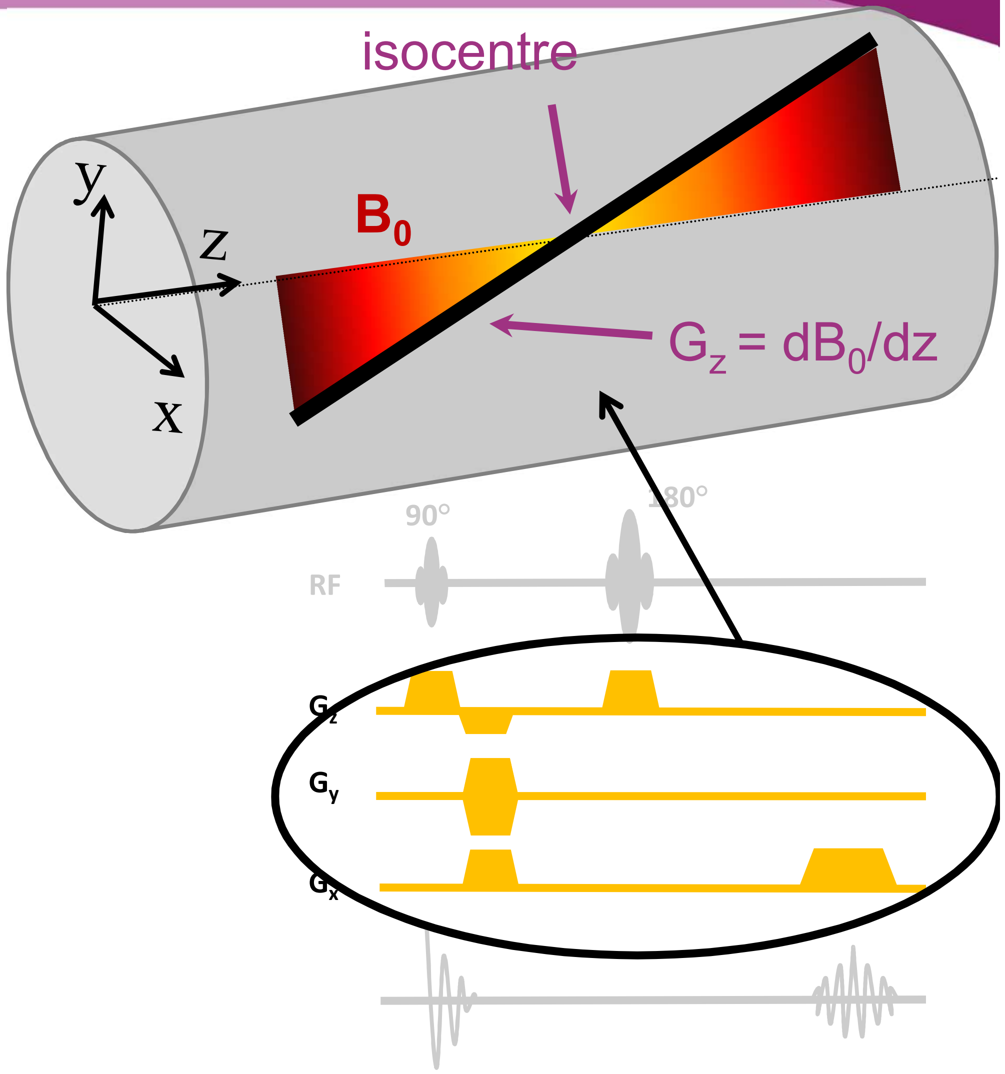
isocentre
B_0
y
z
x
$G_z = dB_0/dz$
90°
180°
RF
G_z
G_y
G_x

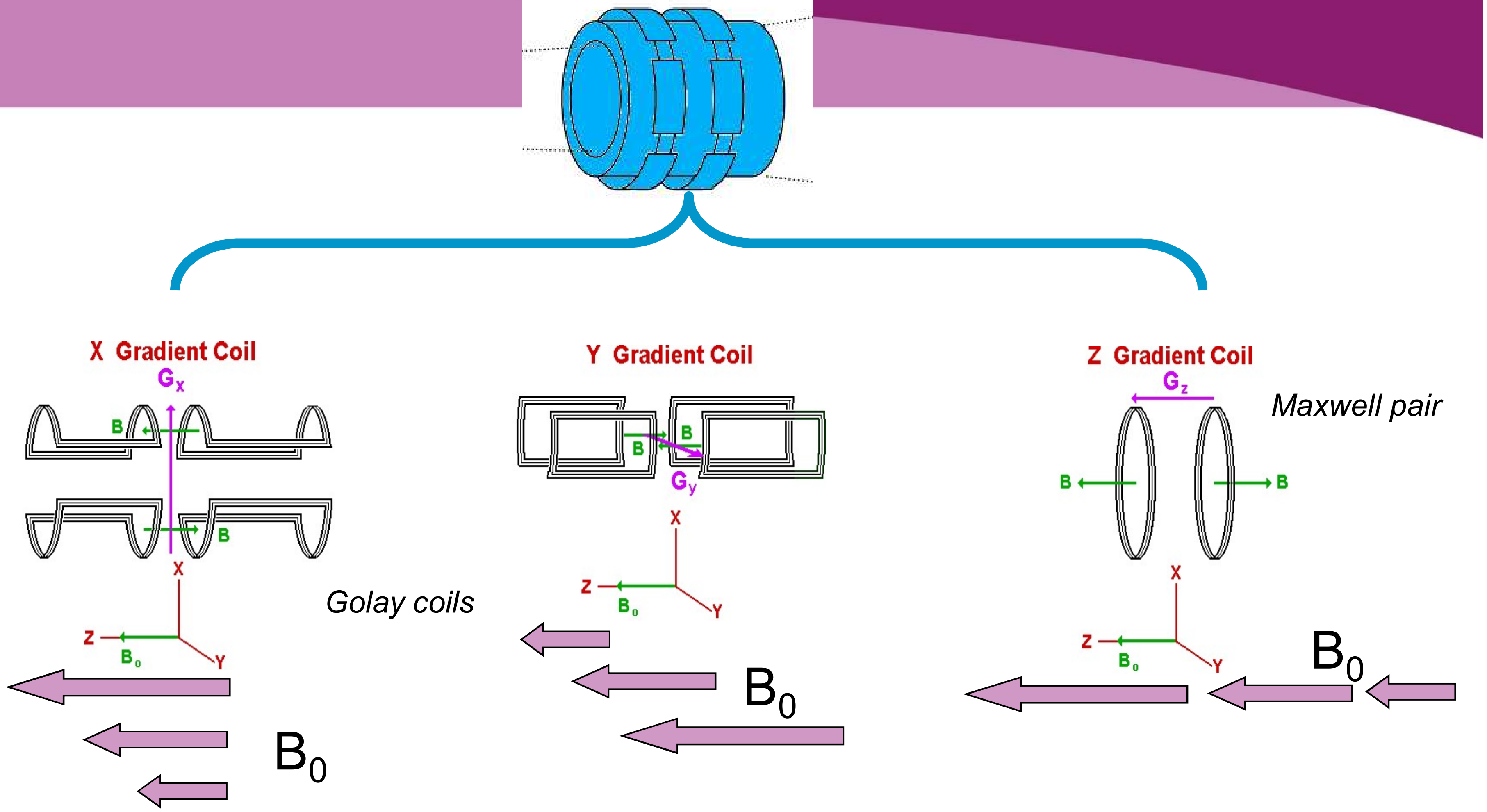
X Gradient Coil
G_x
B
B
X
Z
B_0
Y
Golay coils
B_0
Y Gradient Coil
B
B
G_y
X
Z
B_0
Y
B_0
Z Gradient Coil
G_z
Maxwell pair
B
B
X
Z
B_0
Y
B_0

$$\omega_x = \gamma(B_0 + xG_x)$$

$$\omega_y = \gamma(B_0 + yG_y)$$

$$\omega_z = \gamma(B_0 + zG_z)$$

Gradient Linearity

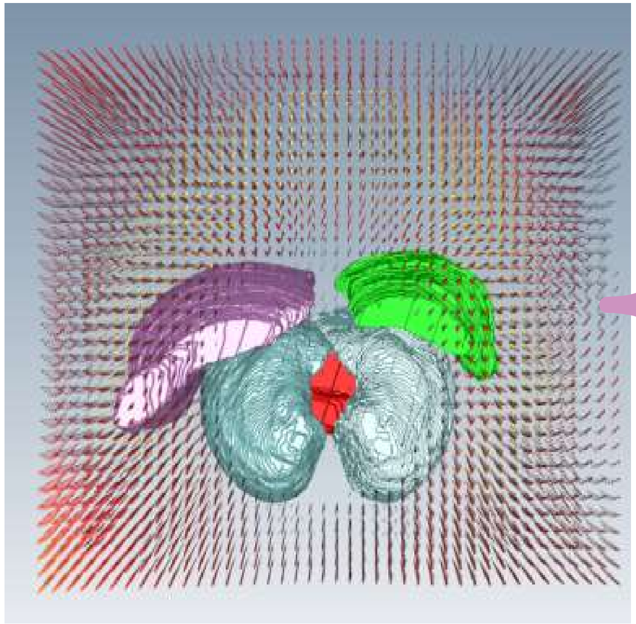

No system distortion on RT Planning

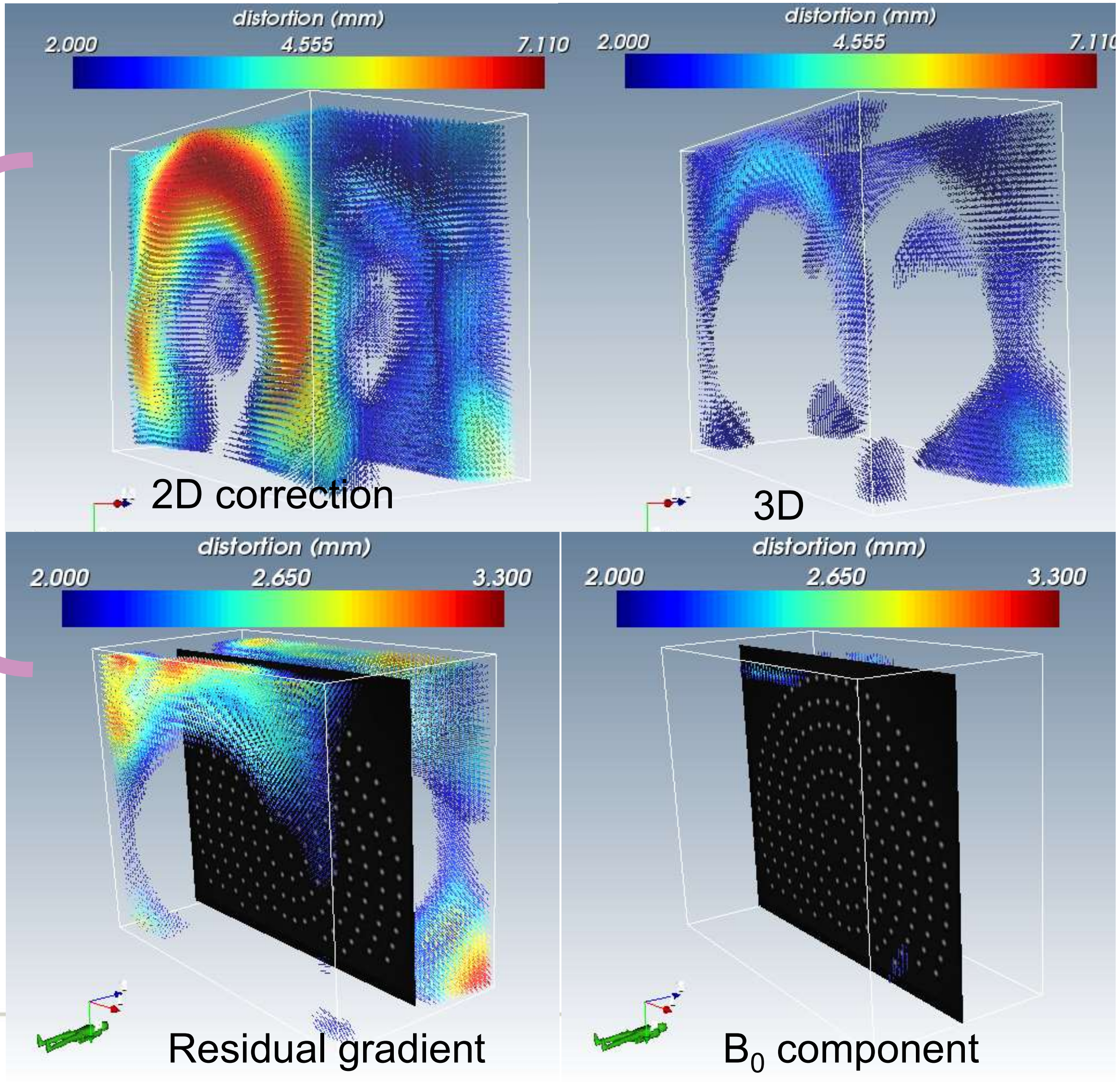
distortion (mm)
2.000
4.555
7.110
2D correction
distortion (mm)
2.000
4.555
7.11
3D
distortion (mm)
2.000
2.650
3.300
Residual gradient
distortion (mm)
2.000
2.650
3.300
B_0 component

‘db by dt’

- Gradient waveform trapezoidal
- Amplitude, Rise time, Slew rate

  e.g. 40 mT/m & 200 μs = 200 T/m/s
- Rapid changes (‘db/dt’) potential safety aspects

$$\text{Slew Rate (T/m/s)} = \frac{\text{Amplitude (mT/m)}}{\text{Rise Time } (\mu\text{s})}$$

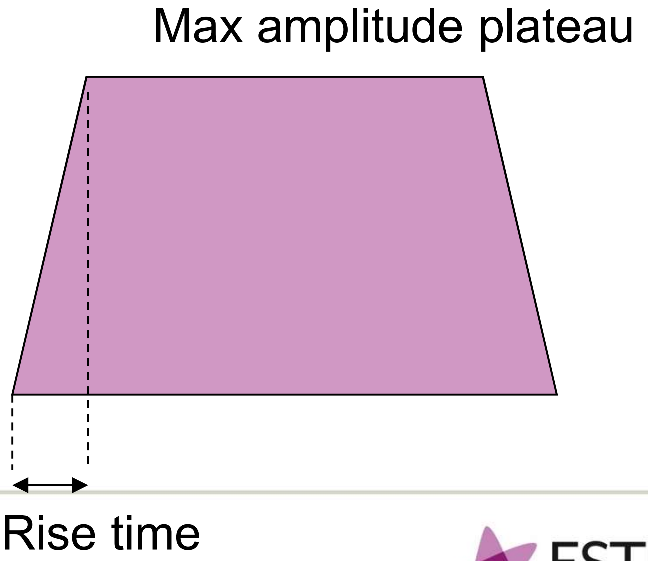
Max amplitude plateau
Rise time

Acoustic Noise

Lorentz force causes gradient coils to vibrate

- Sequence dependent
- Increases with B_0

Manufacturer	**Field Strength (T)**	**SPL (dB(A))**
Philips	1.5	112
Siemens	1.5	106
GE	1.5	110
Varian	3.0	118
Bruker	3.0	113

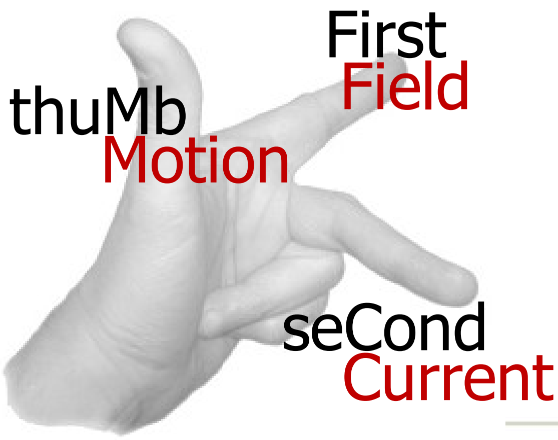
First
Field
thuMb
Motion
seCond
Current

Painful at 134 dB
Permanent damage at 120 dB

$$\vec{F}_L = I d\vec{l} \times \vec{B}_0$$

Peripheral Nerve Stimulation (PNS)

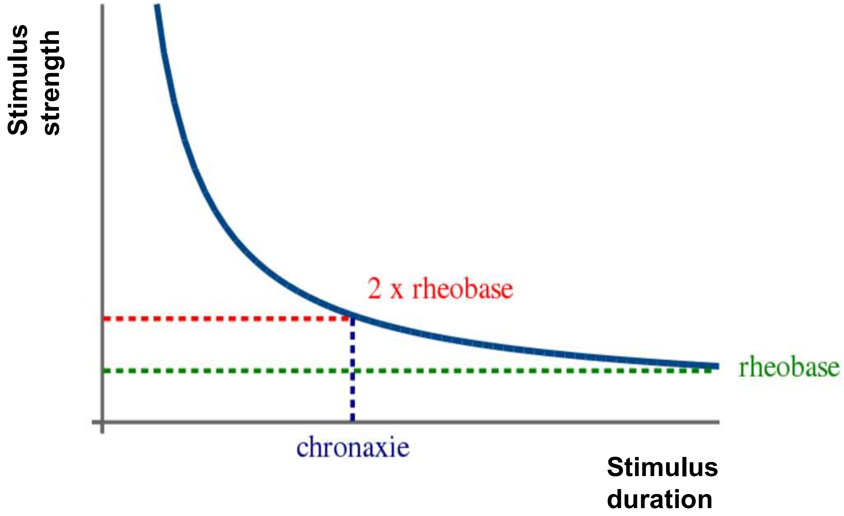

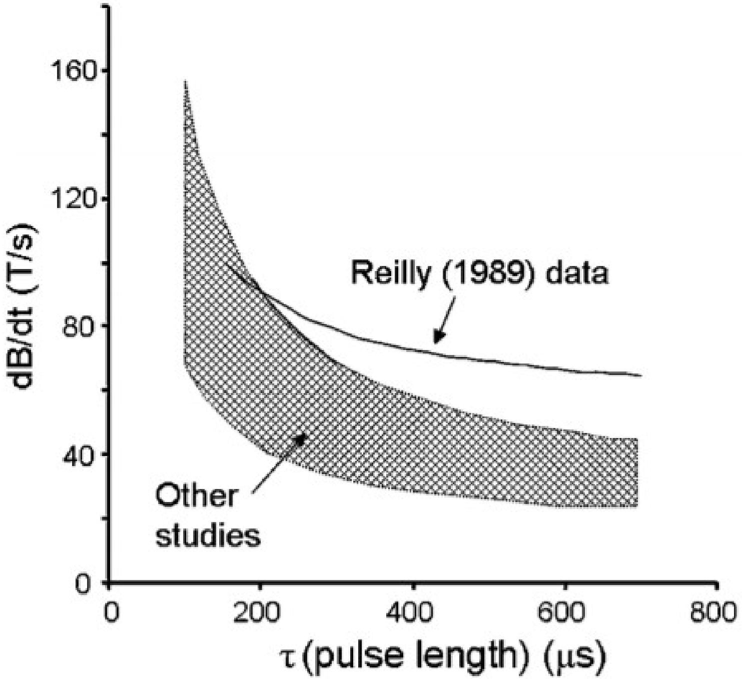

Depolarisation of nerve cells from electrical field stimulation

Empirically measured; Cardiac stimulation should not occur

PNS threshold used as basis of scanner limit

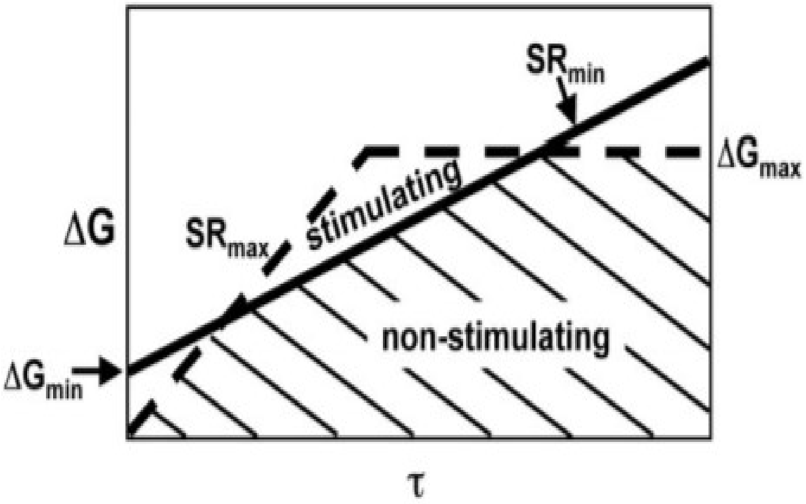
SR$_{min}$
ΔG_{max}
ΔG
SR$_{max}$
stimulating
non-stimulating
ΔG_{min}
τ

Common to set limit at 20 cm radius

More useful to consider ΔB & ΔG: linear with rise time

	N	Axis	db/dt (T/s)	ΔB (mT)	SR (T/m/s)	ΔG (mT/m)	τ (µs)
Reilly (1989)	-			54	7.5		138
Bourland (1999)	84	y z	14.9 26.2	5.4 9.9			365 378
Ham (1997)	4	xyz			41.5	34	810
Hebrank (2000)	65	y xy xyz	16.3 18.6 20.1	8.6 8.7 10.2			526 467 507
Zhang (2003)	20	xy	25.1	13.2	77.0	40.5	526

Literature PNS thresholds (Adapted from *Zhang et al MRM 50:50-58; 2003*)

Solutions

- Noise
  - ✓ Bore liner, gradients mounted to floor & inside vacuum
  - ✓ Ear plugs or ear defenders

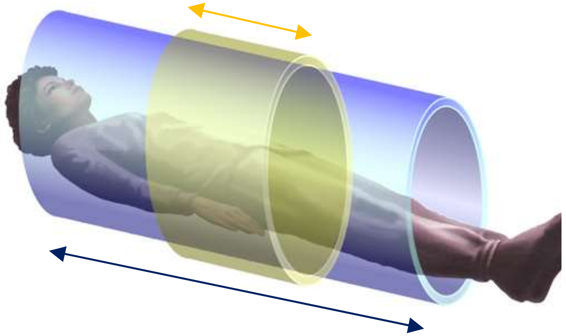

- PNS
  - ✓ Dual gradients
  - ✓ Parallel imaging (RF coil encoding)

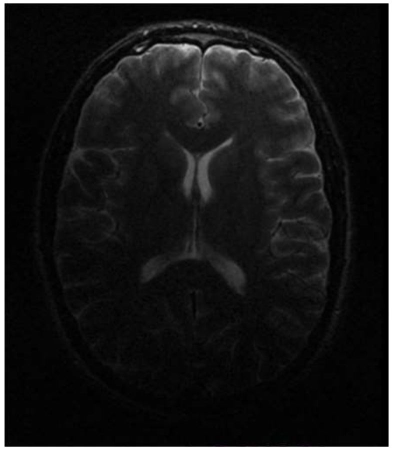

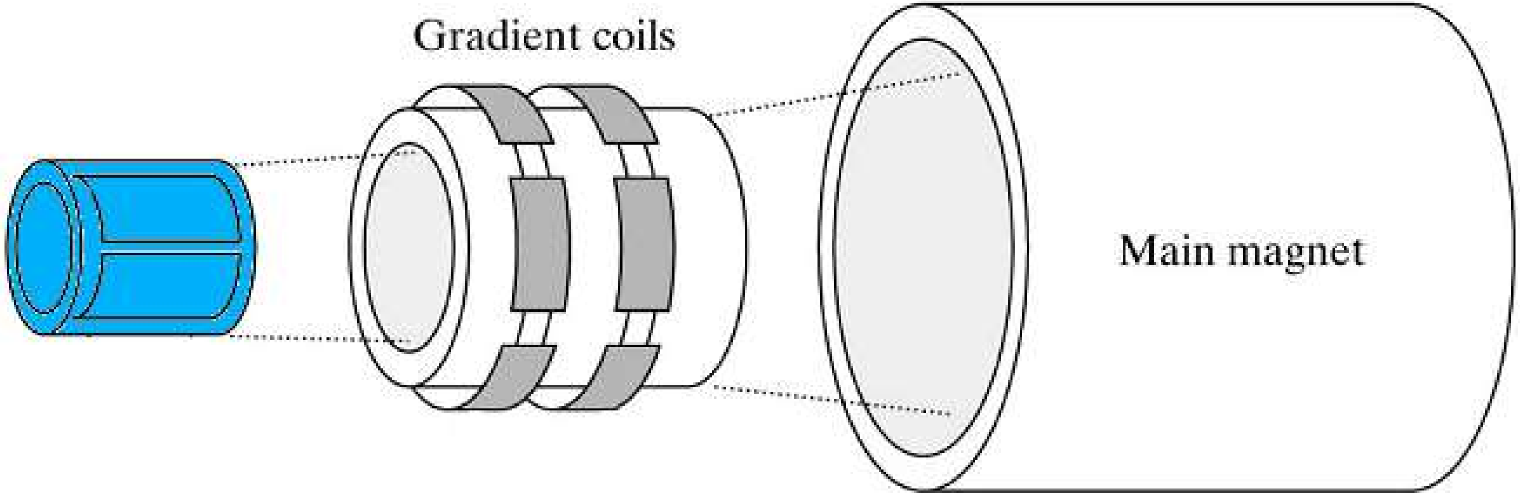
Gradient coils
Main magnet

RF Coils

RF Coil Designs

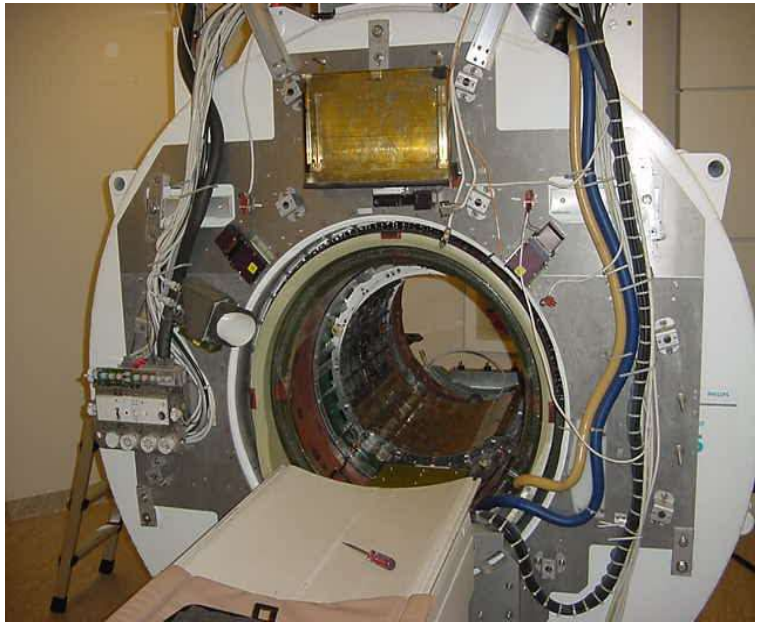

Coils used as Rx or Tx/Rx

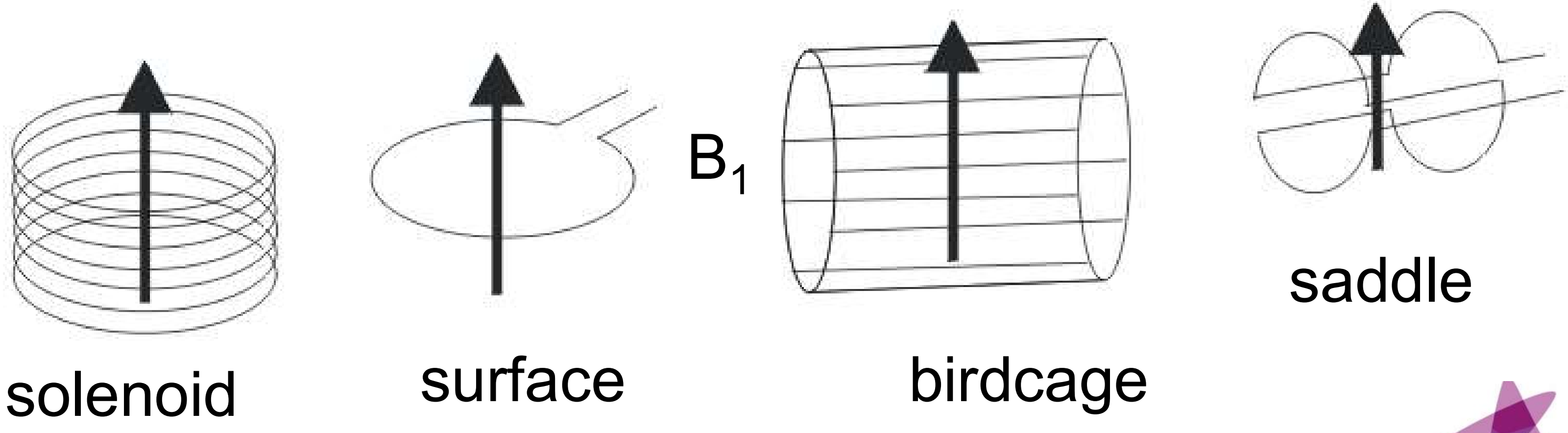
B$_1$
solenoid
surface
birdcage
saddle

Signal Characteristics

$$B = \frac{\mu_0 I 2\pi a^2}{\left(\quad \right)^{3/2}}$$

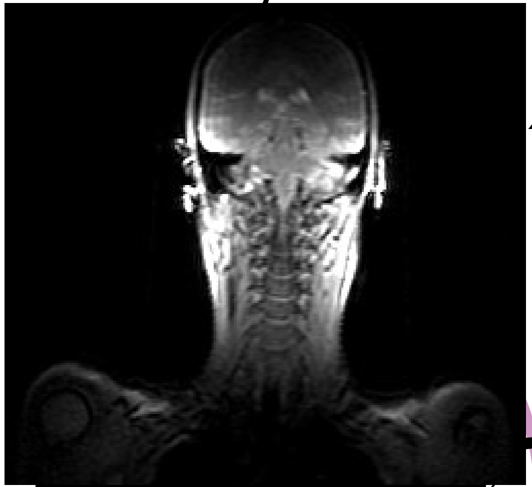

Surface Coil:
Excellent SNR
close to coil

Poor uniformity

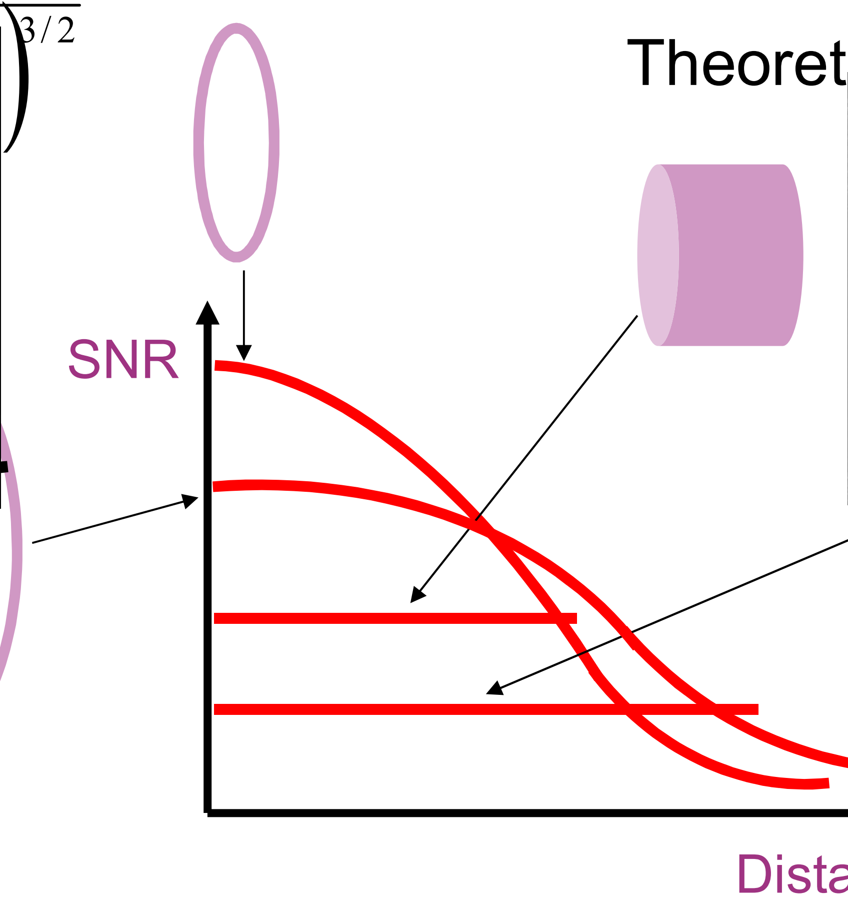

Theoretical cylinder coils

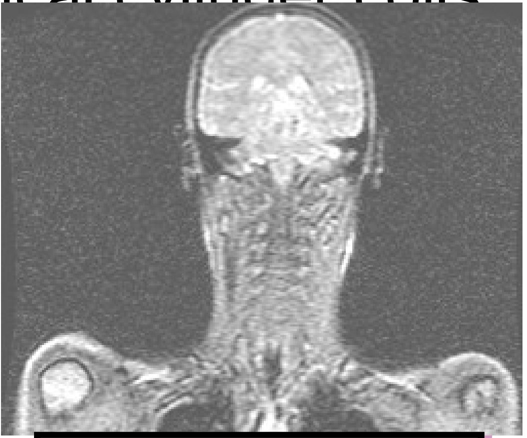

Body Coil:
Poor SNR

Excellent
uniformity

Finite Element Modelling used for
complicated designs

B$_1$ Uniformity

- Surface coils require intensity correction

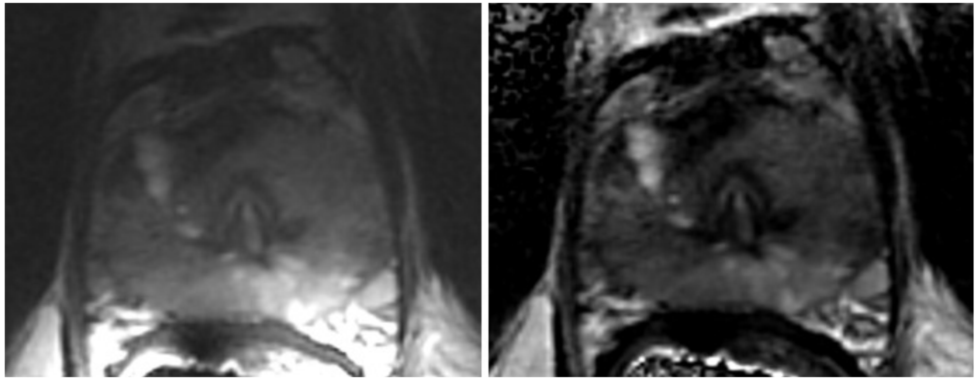

original corrected

- At 3T $\lambda \approx 26$ cm, leads to dielectric artefacts
- Dual transmit body coil used to remedy signal variation

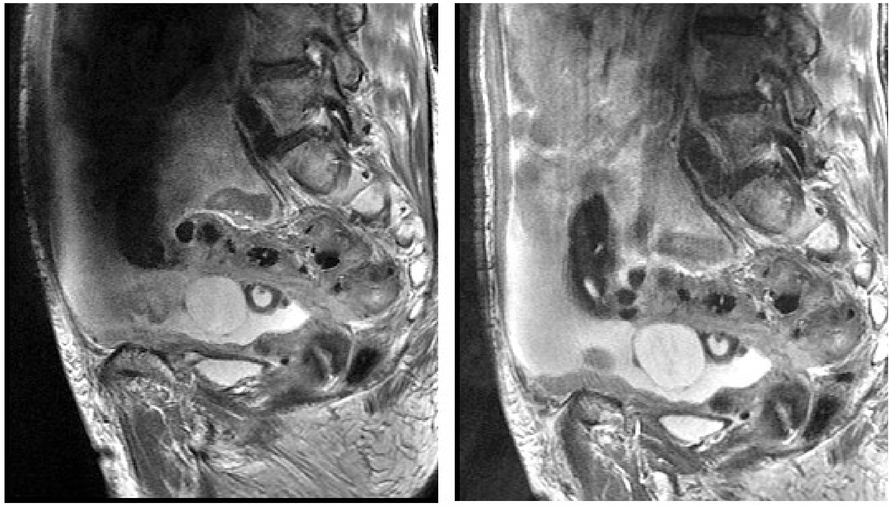

Coil Arrays

- Extend surface coil coverage
  Small coil excellent SNR
- Overlap to prevent mutual inductance
- Separate Rx channels
  Noise not correlated, further increase SNR
- Can be used in parallel imaging*

18 channel body coil

64 channel H&N coil

**covered in 'Speed-up & specialised sequences'*

RF Heating

- RF power deposition expressed as **Specific Absorption Rate** or **SAR** (in W/Kg)
- Up to 3.0 T, SAR $\propto B^2$
- heat stress (Testis, Foetus etc), implants/devices
- At higher field the body is more conductive and leads to weaker penetration
- SAR depends on RF pulses per unit time, patient weight, flip angle, RF wave form, field strength, transmit coil design (quadrature or linear)
- Scanner calculates SAR and also performs real time monitoring (time average and peak)

RF Heating Effect

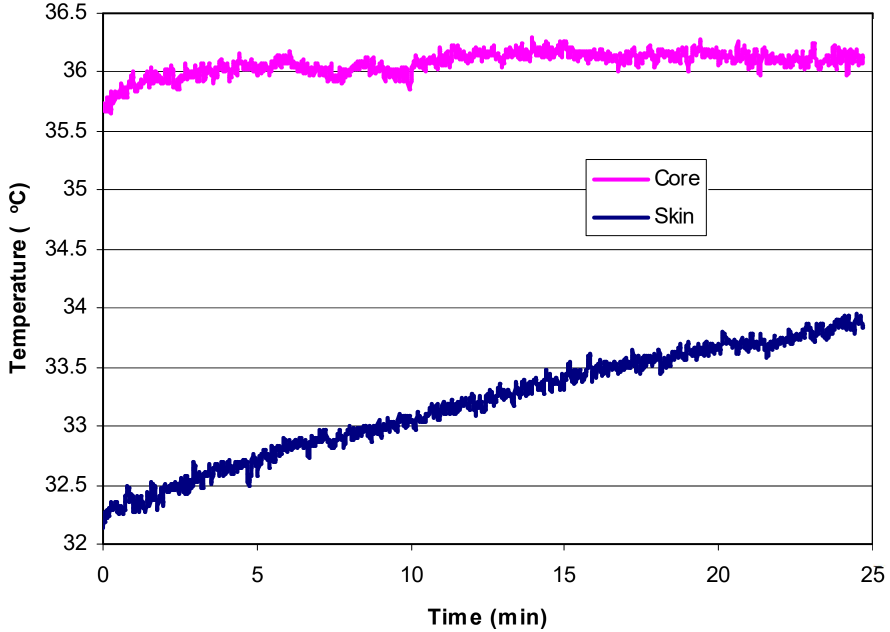

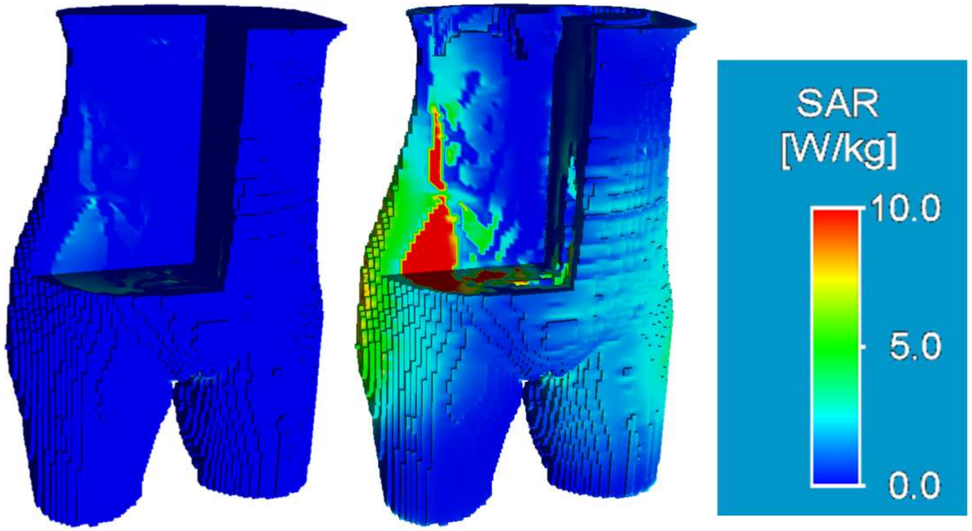
SAR
[W/kg]
10.0
5.0
0.0

3.0 Tesla 7.0 Tesla

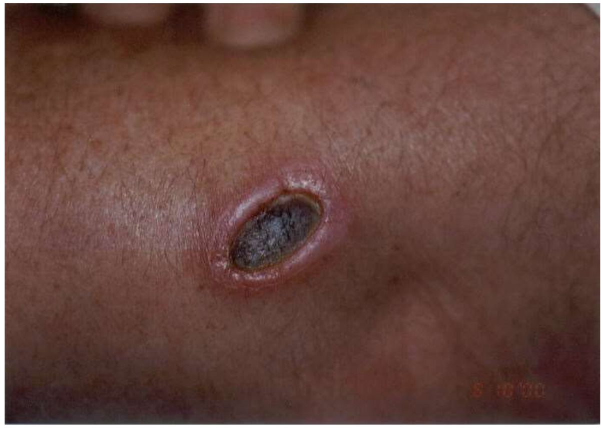

hotspots and in extreme cases **RF burns**

Avoid crossed cables, patient loops

Quadrature Coils

- Linear polarisation- only half RF power effective
- Circularly polarised

  Signal has 90° phase
- Efficient transmission

  Power halved, reduced SAR
- Receiver coils

  SNR increases √2

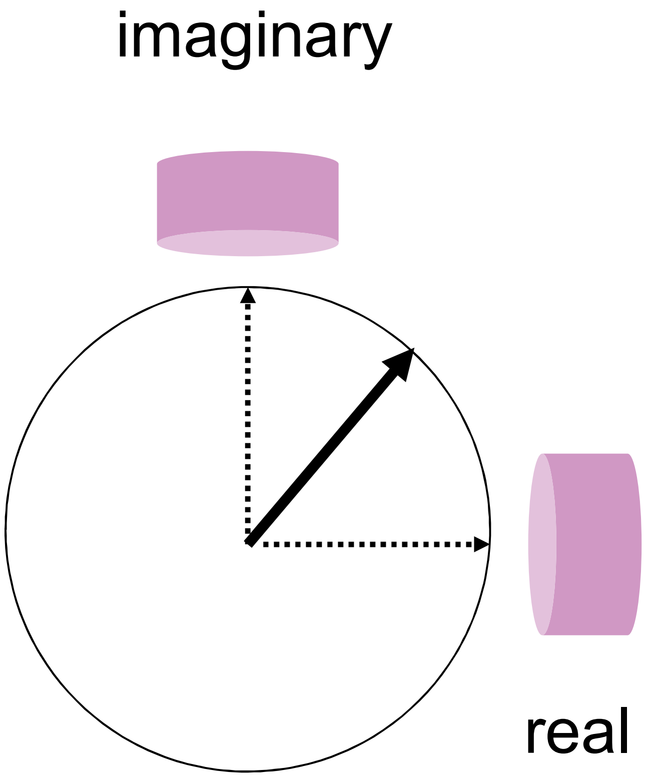

Exposure Limits*

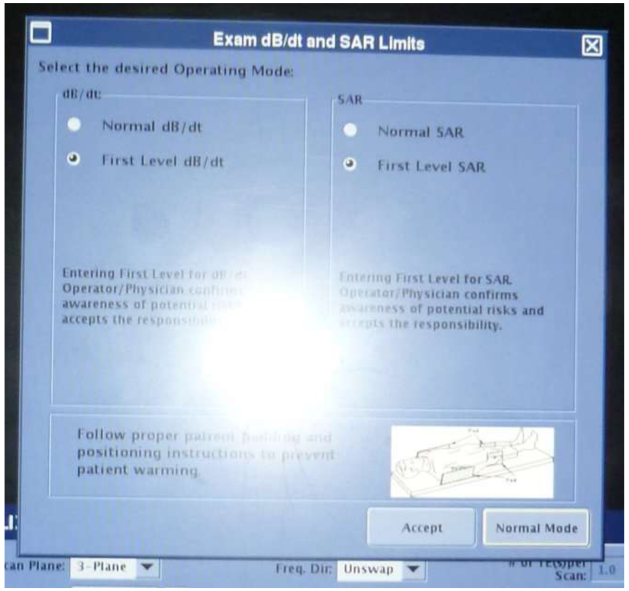
Exam dB/dt and SAR Limits

Select the desired Operating Mode:

dB/dt:

○ Normal dB/dt

● First Level dB/dt

Entering First Level for dB/dt Operator/Physician confirms awareness of potential risks and accepts the responsibility.

SAR

○ Normal SAR

● First Level SAR

Entering First Level for SAR. Operator/Physician confirms awareness of potential risks and accepts the responsibility.

Follow proper patient handling and positioning instructions to prevent patient warming.

Scan Plane: 3-Plane

Freq. Dir: Unswap

# of TE(s) per Scan: 1.0

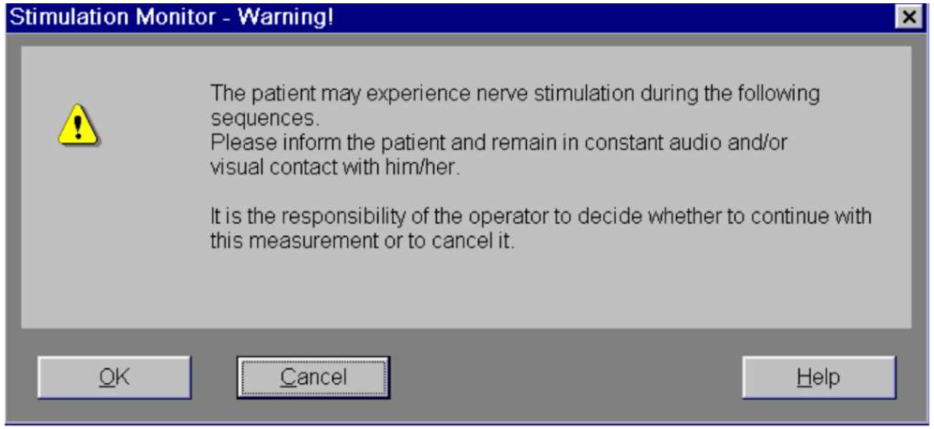
Stimulation Monitor - Warning!

The patient may experience nerve stimulation during the following sequences.
Please inform the patient and remain in constant audio and/or visual contact with him/her.

It is the responsibility of the operator to decide whether to continue with this measurement or to cancel it.

Stratify operation (and safe limits) into 3 modes

(1) Normal: No effects

(2) Controlled or First Level: Transient/mild effects

(3) Research/Experimental: Unrestricted & requires monitoring

**Detailed exposure limits at the end of this talk*

Pregnancy

No harmful effects- better than ionising radiation. Pregnant women normally excluded in first trimester.

Foetus expected to be more susceptible to MRI.
Contrast agents can pass placenta- no breast feeding for 24hrs

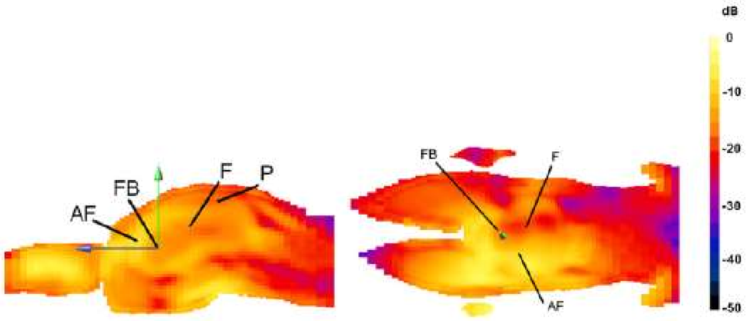

Figure 3. Distributions of SAR_{10g} at 64 MHz in sections $x = 0.008$ m (left) and $y = 0.008$ m (right). The origin of coordinates, located in the foetal brain, is shown. The dB scale is relative to the maximum SAR_{10g} which occurs in the left wrist. The relatively low SAR in the foetus (F), foetal brain (FB) and placenta (P), and high SAR in the amniotic fluid (AF) are evident.

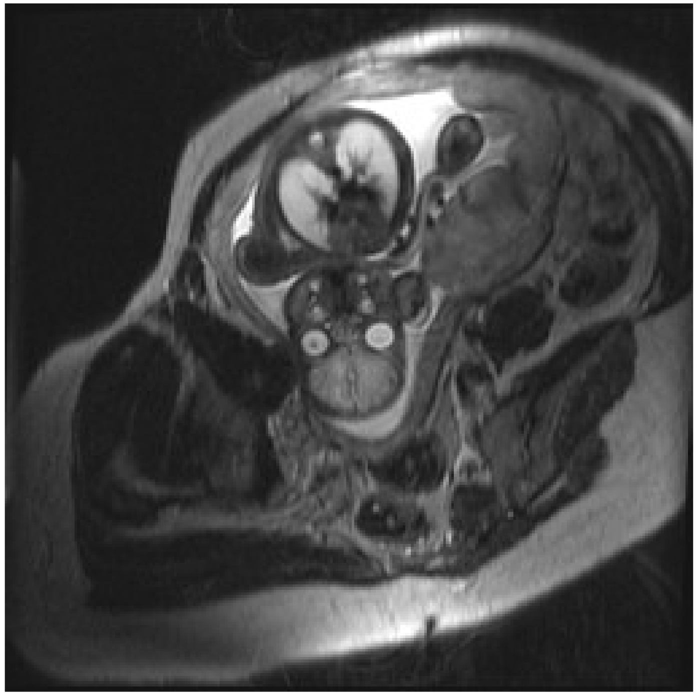

Questions?

MRI-Linac= Equipment & Safety of the Future!

Exposure Limits: Static Field

	Normal mode	Controlled mode	Research mode	Movement limit
HPA	≤ 4 T	4-8 T	> 8 T	1 Ts^{-1}
IEC 2002	< 2 T	2-4 T	> 4 T	-
IEC 2010	≤ 3 T	3-4 T	> 4 T	3 Ts^{-1}
ICNIRP 2009	≤ 4 T	4-8 T	> 8 T	1 Ts^{-1}

Exposure Limits: Gradients

	Normal mode	Controlled mode	Research mode
Percentage (%) of perceptible threshold*: $= 20(1 + 0.36t^{-1})$	< 80	80-100	100-120
Ts^{-1} limit to prevent cardiac stimulation*	$< \frac{20}{\left\{1 - exp\left(-\frac{t}{3}\right)\right\}}$		

Above are IEC 2010 limits with following notes:
*t is effective stimulus duration in ms

Exposure Limits: RF

SAR

	Whole body	head	Partial body*	Local Body**	Local Extremity**
Normal	2 W/kg	3.2	2-10	10	20
Controlled	4	3.2	4-10	20	40
Research	> 4	> 3.2	> 10	> 20	> 40

Above are IEC 2010 limits with following notes:
Over a time average 6 min; 10 s duration cannot exceed ×2
*scales as 10-8×r where r is ratio of exposed mass to whole body mass
**local SAR based on 10g tissue mass
Assumes normal ambient temperature and humidity

Body Temperature

	Max increase (°C)
Normal	0.5
Controlled	1.0
Research	> 1.0

Contrast Agents

Gadolinium agents better tolerated than iodinated (CT) agents

Gd-DTPA (Magnevist) safety record:
5 million uses, 1,234 AEs (1992)
Anaphylactic shock and death in 1 case

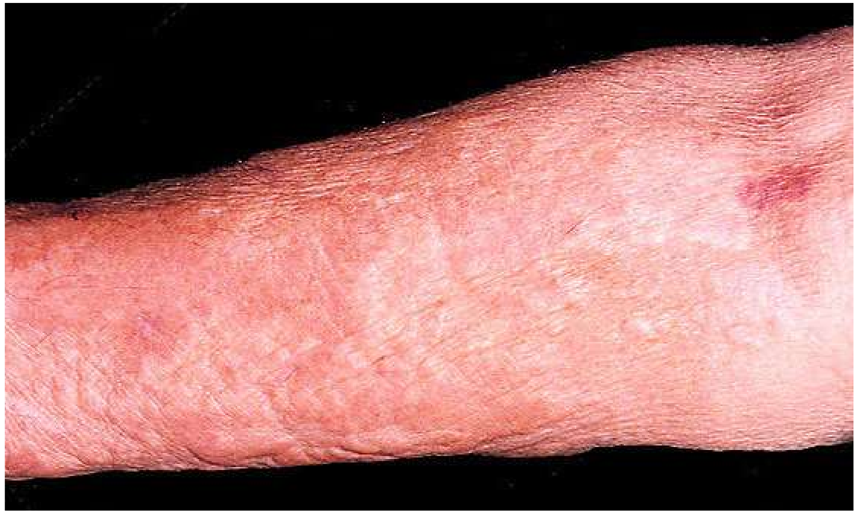

nephrogenic systemic fibrosis (NSF) in kidney dysfunction

Macrocyclic agents (Dotarem, Prohance, Gadovist) more commonly used IV

EMA recently suspended linear agents (Magnevist, Optimark, Omniscan)

Positron Emission Tomography

Physics - Basic Principles

ESTRO Teaching Course on Advanced Imaging Technologies

November 5-9, 2017 in Malaga, Spain

Daniela Thorwarth
Section for Biomedical Physics,
University Hospital for Radiation Oncology, Tübingen

Eberhard-Karls-Universität
UKT
Universitätsklinikum Tübingen

Molecular Imaging with Positron Emission Tomography (PET)

PET imaging adds molecular information to morphology and function imaged with CT and/or MRI.

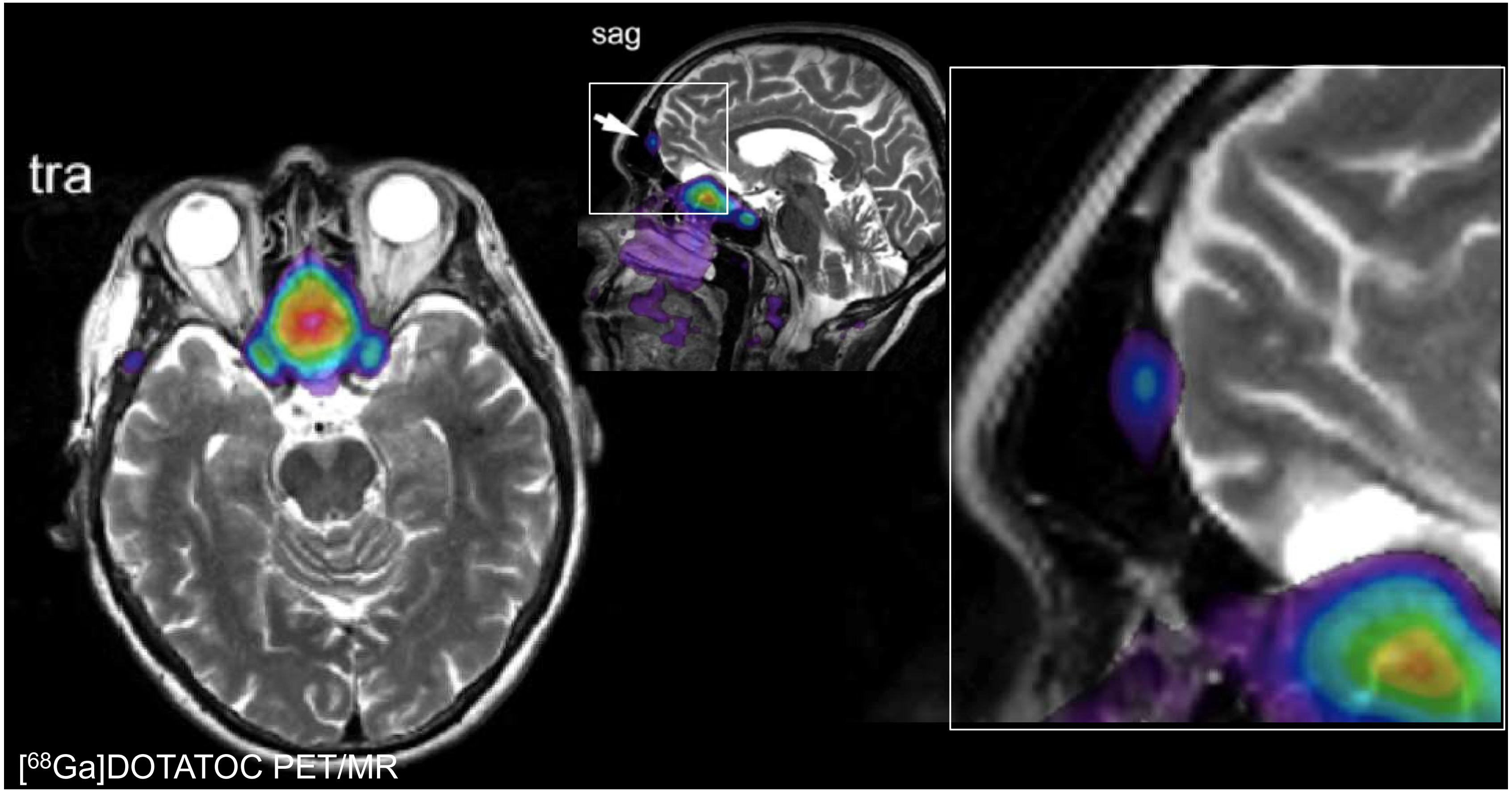

T2w MRI and PET (BrainPET) show small satellite in dorsal area of frontal sinus (detected on PET).

Boss et al, JNM 2010; 51.

Basic principle of PET

- Positron emitters (β+) used as biomarkers
- Positron-electron annihilation
  ⇒ Two γ-quanta with 511 keV each are emitted under approx. 180°
- Coincidence detection in a detector ring

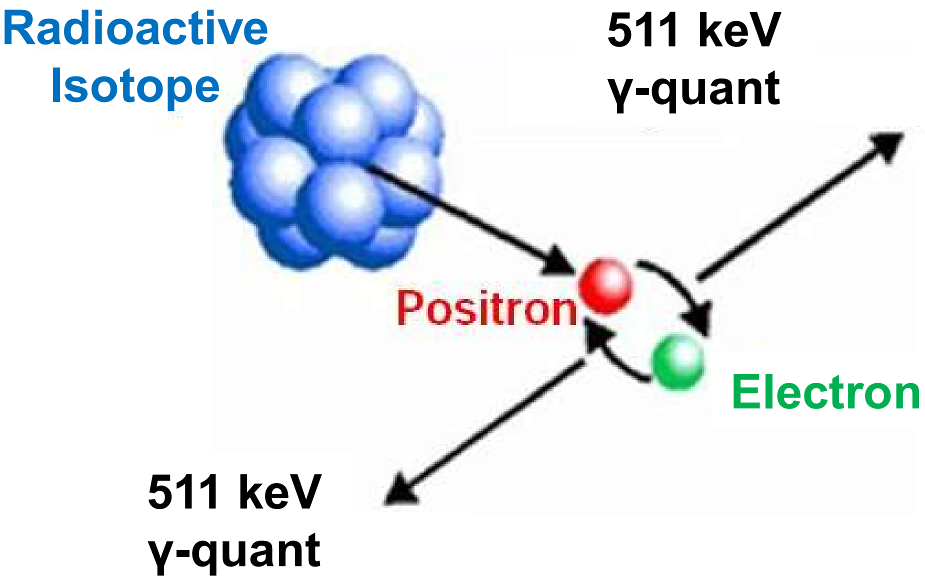
Radioactive Isotope
511 keV γ-quant
Positron
Electron
511 keV γ-quant

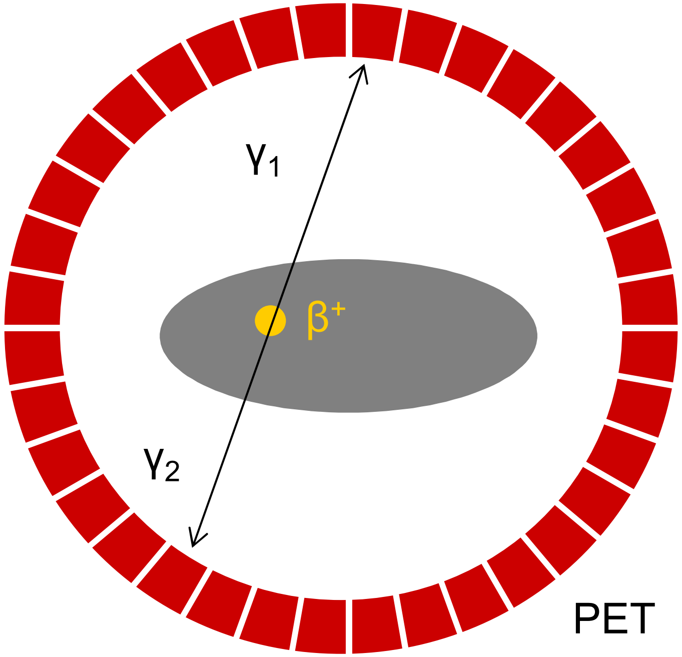

Today: Combined PET/CT

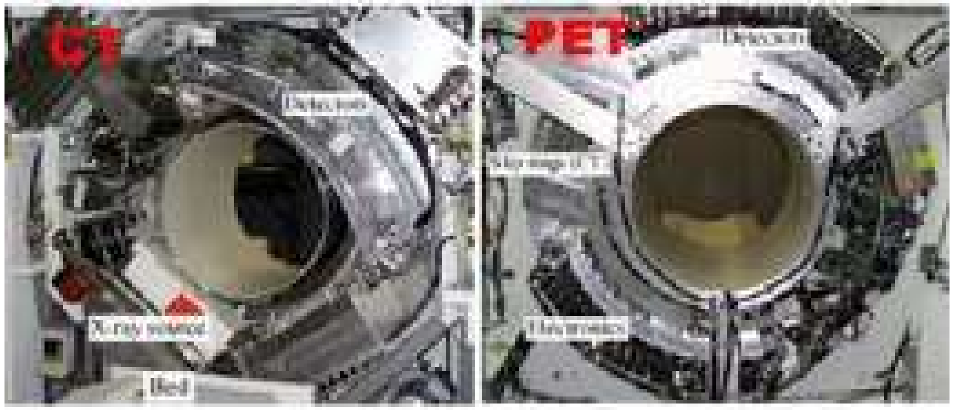
CT
PET
Detectors
X-ray source
Bed
Detectors
Electronics

PET/CT: combination of structure and function

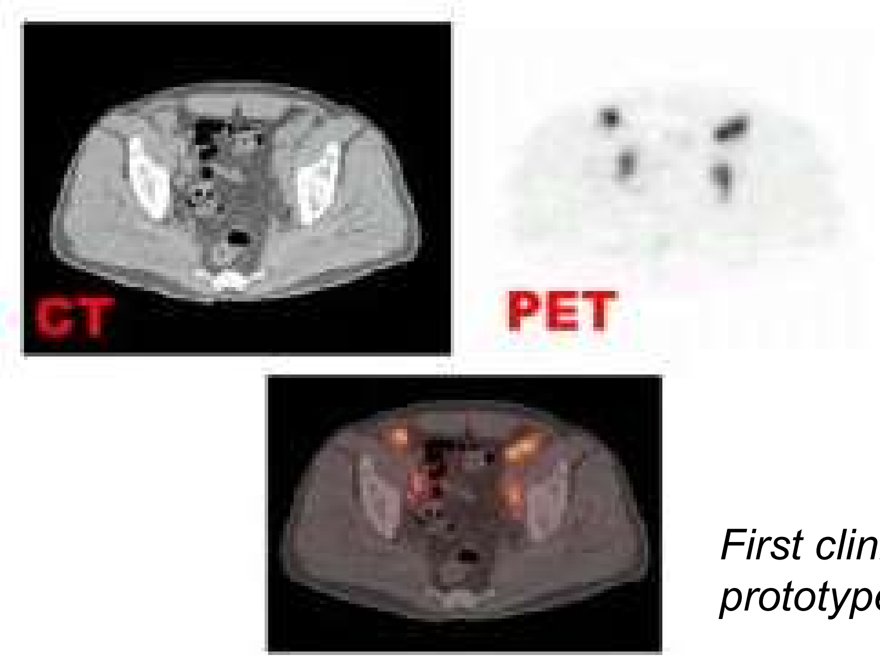

First clinical PET/CT prototype (mid 1990s) [3]

State-of-the-art PET/CT Designs

(a)

Gemini series, Philips Healthcare Systems

(b)

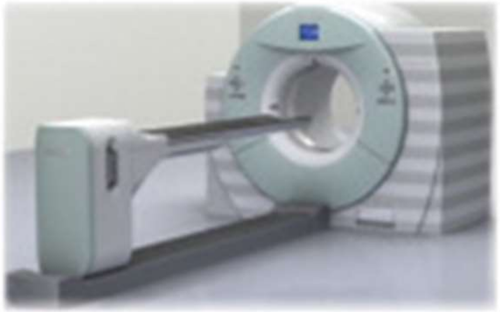

Biograph series, Siemens Healthcare Solutions

(c)

Discovery series, GE Healthcare

(d)

Aquiduo series, Toshiba Medical Systems

(e)

Sceptre series, Hitachi Medical Systems

(f)

Anyscan series, Mediso

! All PET/CT tomographs combine diagnostic PET and CT components and a dedicated patient support system. **!**

Courtesy T. Beyer, cmi-experts Zürich

PET/CT

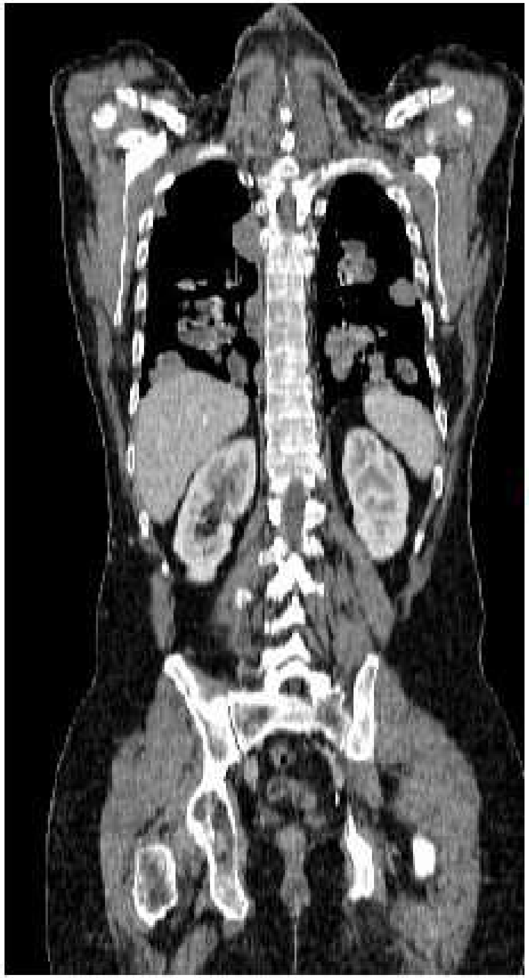

CT

+

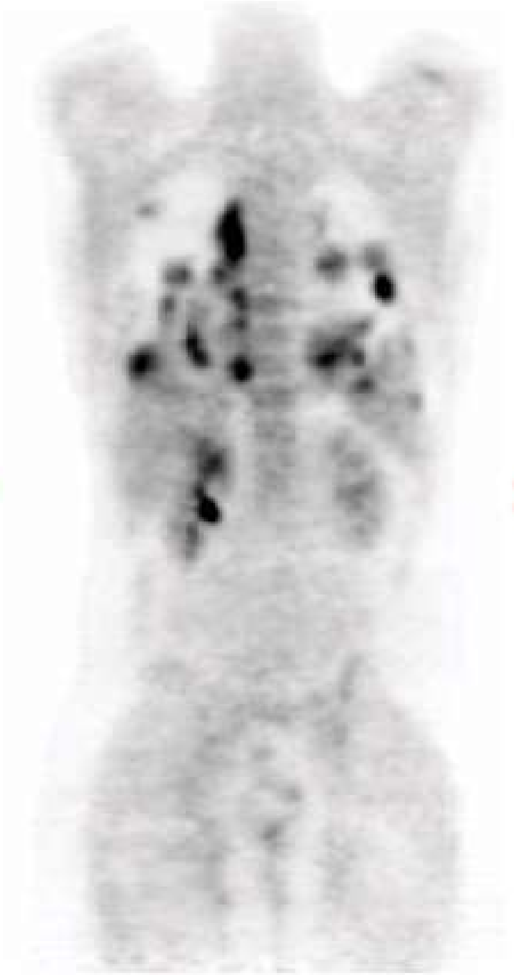

PET

=

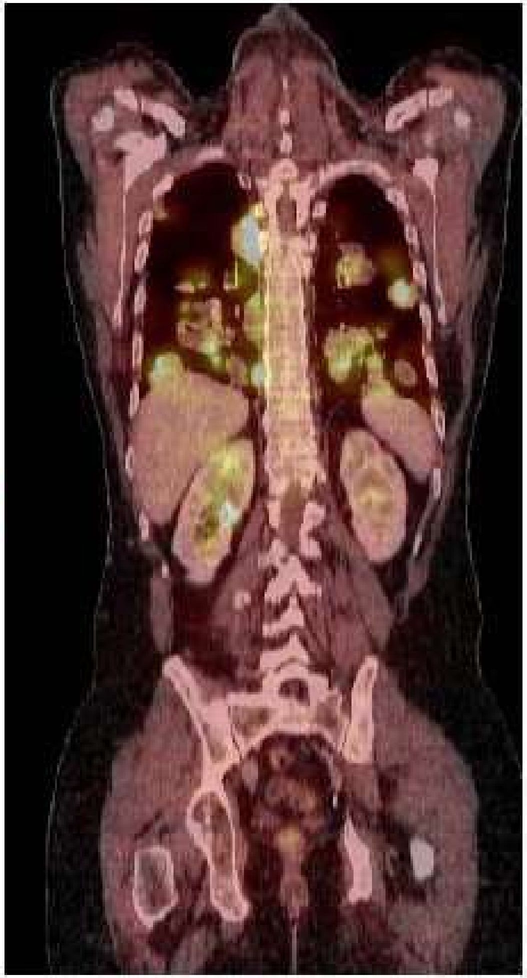

PET/CT

Raw data stored in sinograms

Sinograms:
Measurement of the activity distribution of a radioactive tracer.

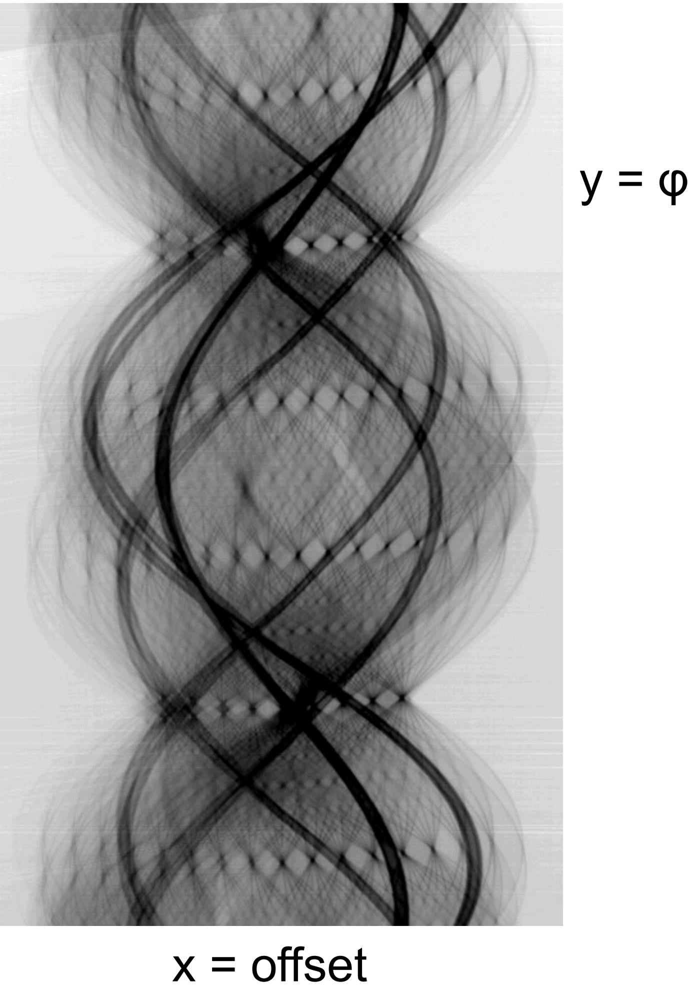

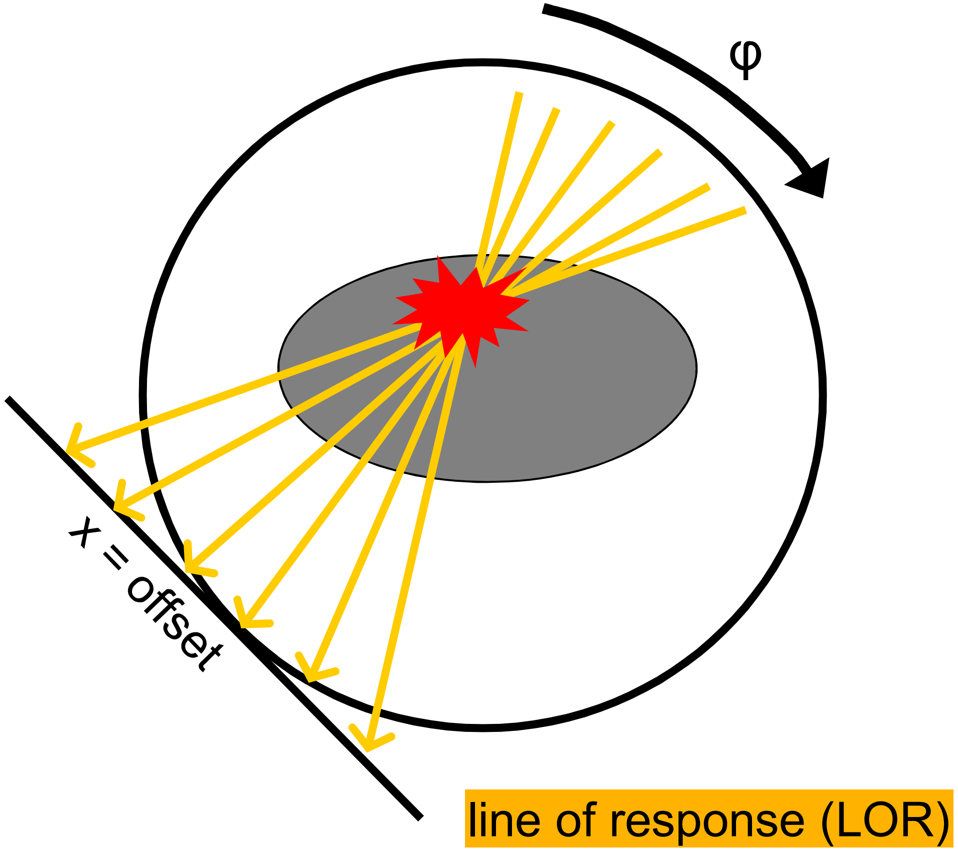
φ
x = offset
line of response (LOR)

Radial Sampling

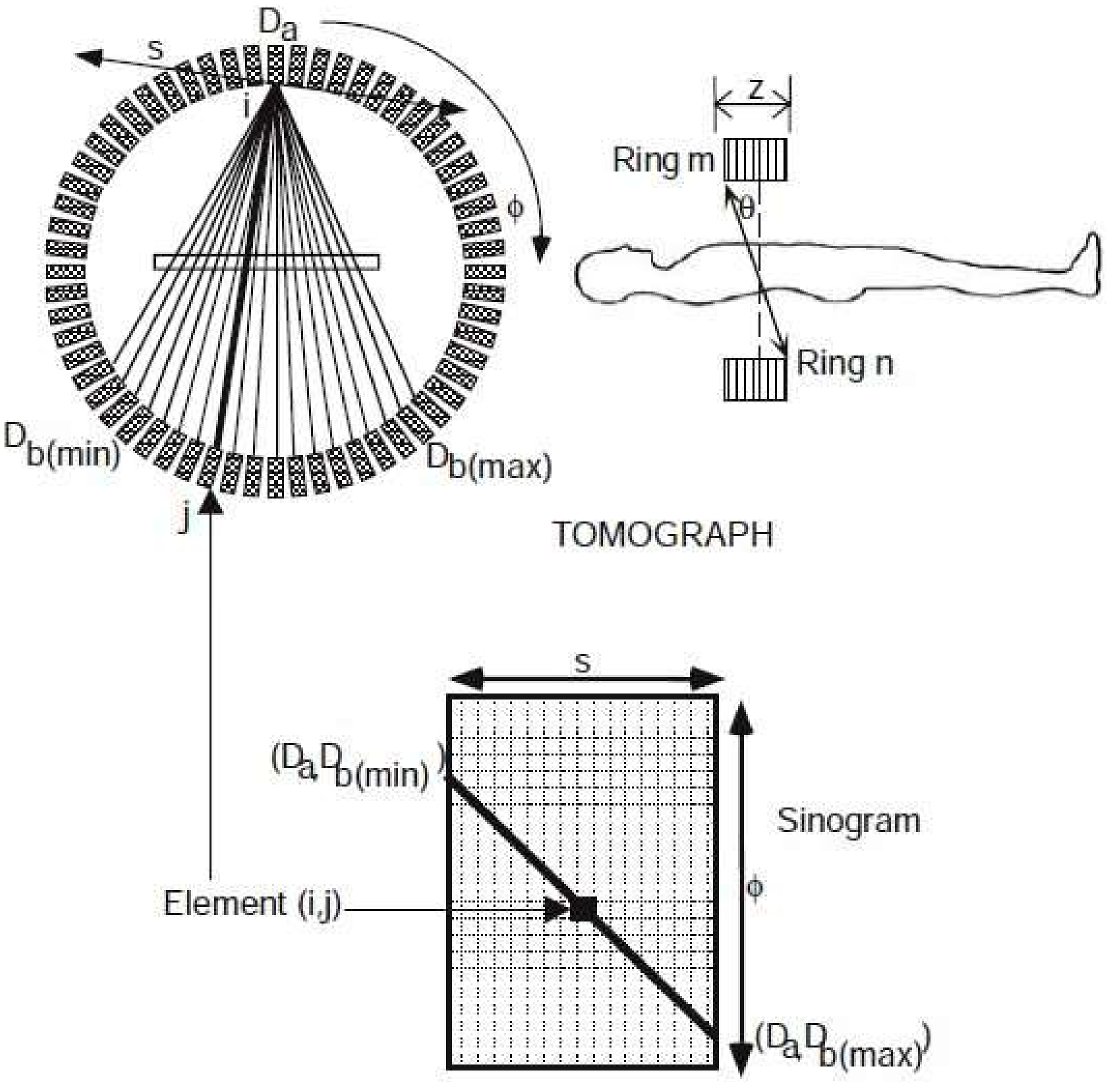
D$_a$
s
i
ϕ
Z
Ring m
θ
Ring n
D$_{b(min)}$
D$_{b(max)}$
j
TOMOGRAPH
s
(D$_a$D$_{b(min)}$)
Sinogram
ϕ
Element (i,j)
(D$_a$D$_{b(max)}$)

Mapping from sampling projections to sinograms [2].

Transaxial field of view of a PET tomograph is defined by the acceptance angle in the plane.

2D-/3D-PET

2D-PET

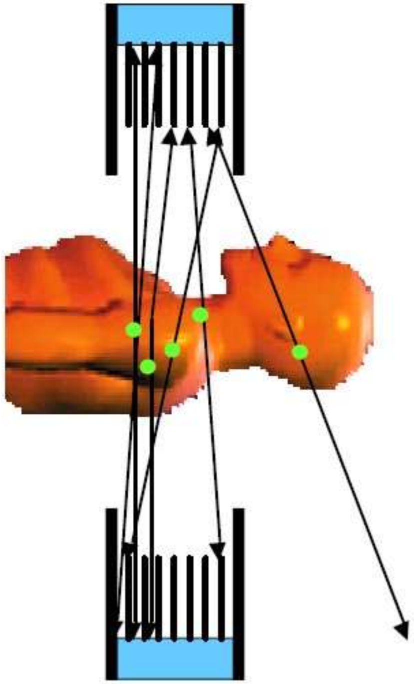

- Geometric collimation with septa
- Data sampling only with θ=0°
- Lower overall sensitivity
- Lower fraction of scattered photons

3D-PET

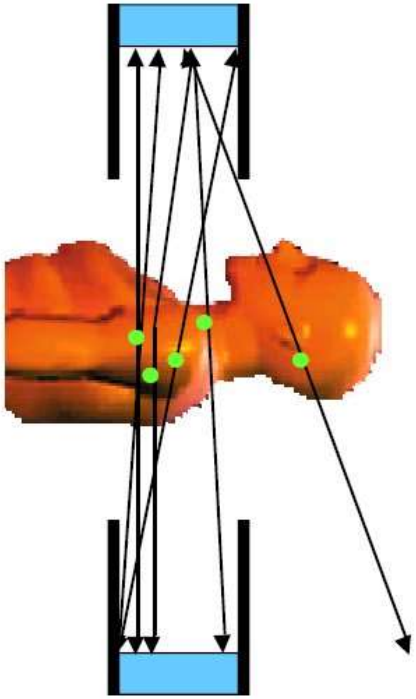

- Projections at polar angles θ>0° measured
- Increased sensitivity
- Higher scatter fraction
- Special reconstruction algorithms are necessary

2D/3D-PET acquisition

2D acquisition: the entire FOV is sampled.

3D acquisition: truncation of projections occurs for θ > 0°.
This results in loss of data corresponding the ends of the tomograph [2].

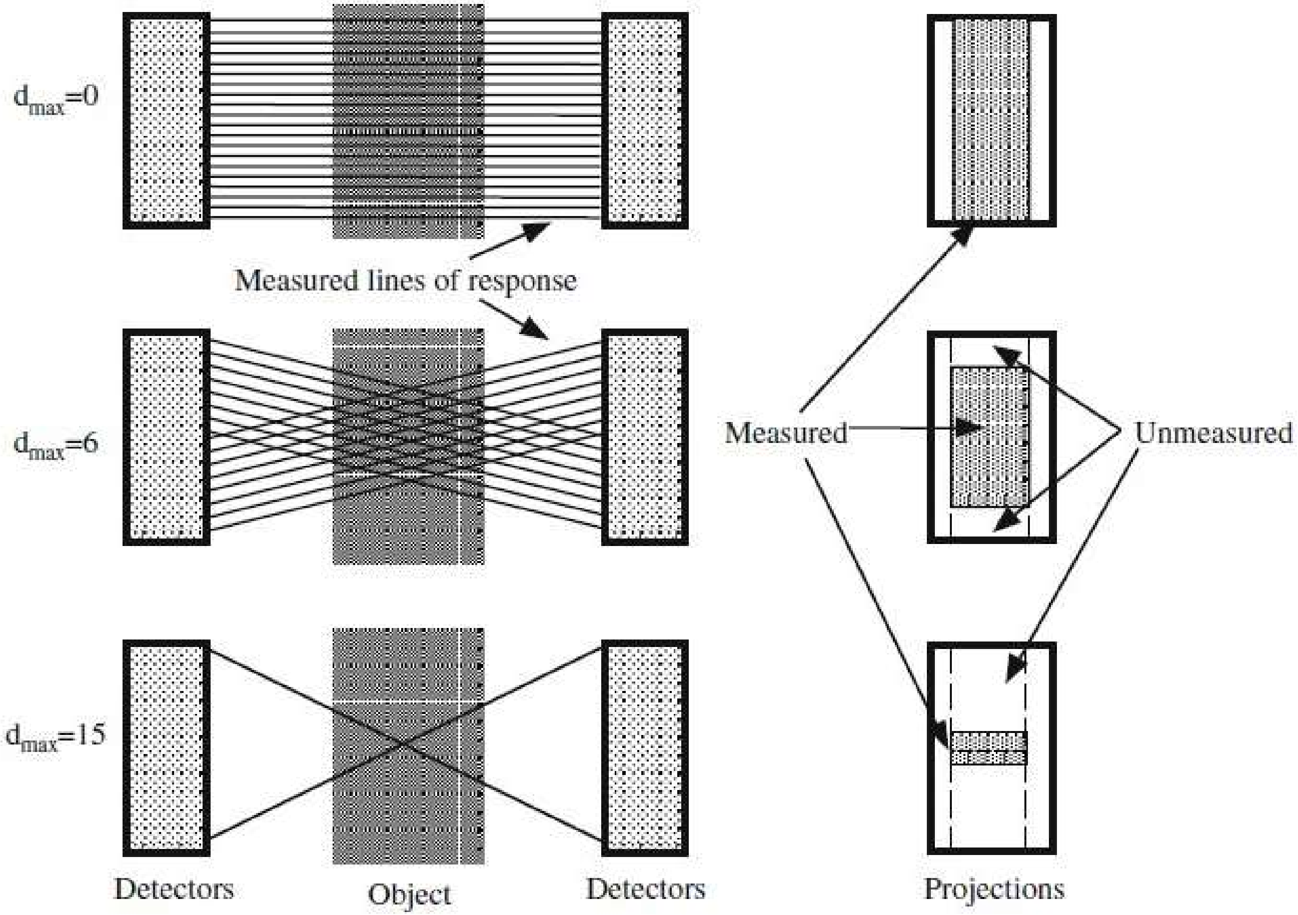
d_{max}=0
Measured lines of response
d_{max}=6
Measured
Unmeasured
d_{max}=15
Detectors
Object
Detectors
Projections

Axial Sensitivity

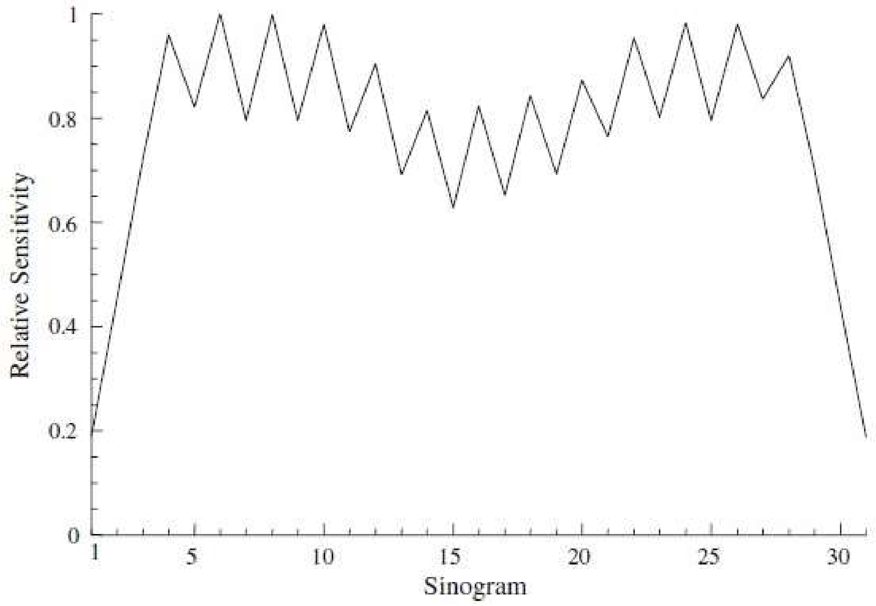

2D axial sensitivity profile for a line source in air in a 16-ring tomograph [2].

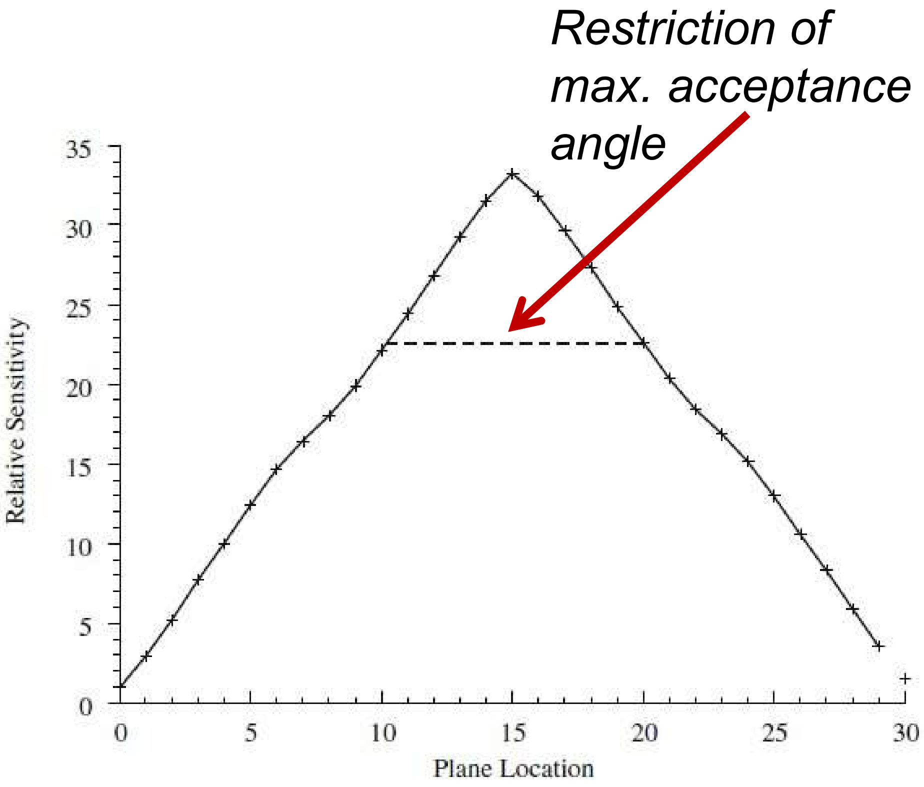

Axial sensitivity variation for 3D acquisition in a 16-ring tomograph [2].

Image Formation

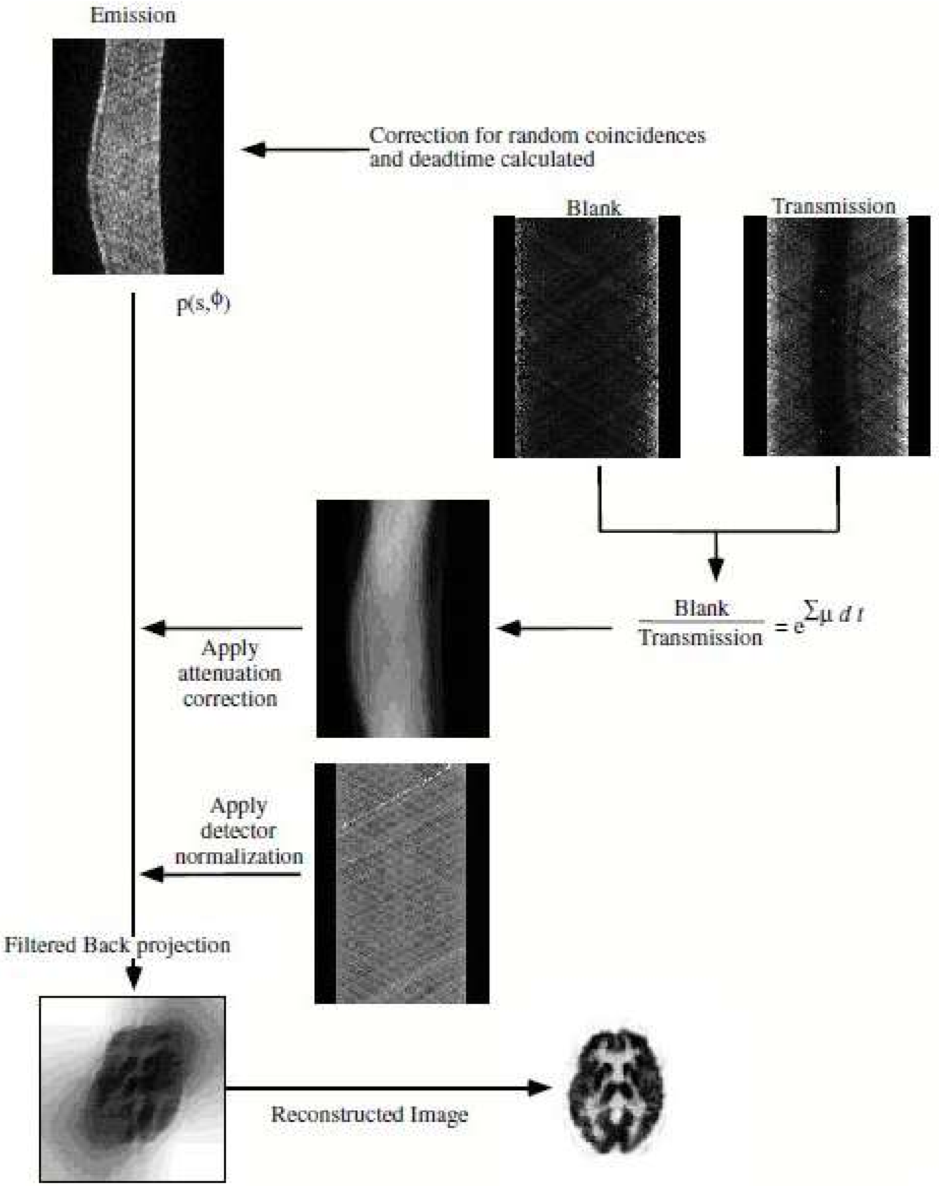
Emission
Correction for random coincidences
and deadtime calculated
Blank
Transmission
p(s,ϕ)
Blank
Transmission
$= e^{\Sigma \mu \, d\, t}$
Apply
attenuation
correction
Apply
detector
normalization
Filtered Back projection
Reconstructed Image

(1) Emission scan

(2) Normalization scans (one per plane in 2D) to correct for differential detector efficiencies and geometric effects related to the detector ring

(3) Set of sinograms of attenuation correction factors to correct of photon attenuation (self-absorption or scattering) by the object

Radiation detection

Desired for PET:

1. High stopping efficiency
2. Good energy resolution

→ **Scintillation detectors**

- Inorganic crystal that emits visible light photons after interaction of photons with detector.
- # of scintillation photons is proportional to the energy deposited in the crystal.
- Important properties for application in PET:
  - Stopping power for 511 keV photons
  - Signal decay time
  - Light output
  - Intrinsic energy resolution

Properties of scintillaton detectors applied in PET

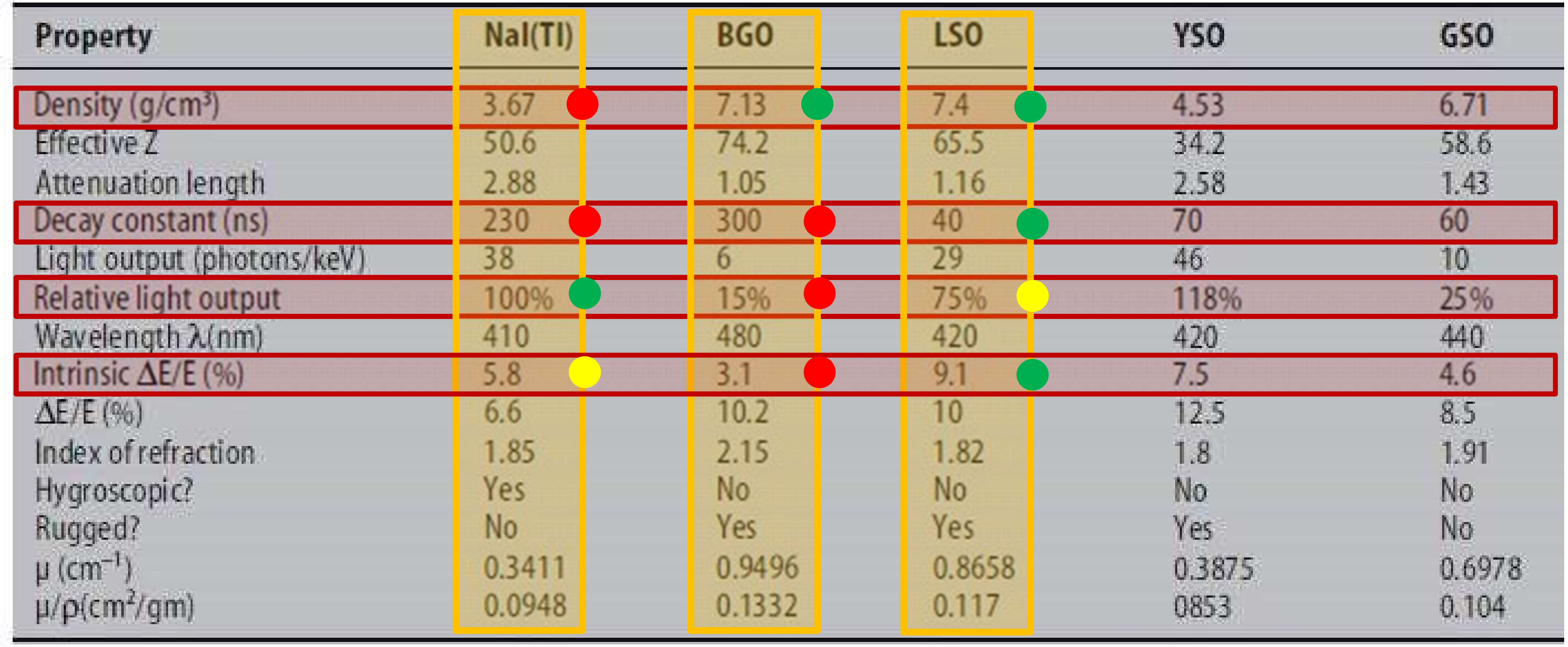

Property	NaI(TI)	BGO	LSO	YSO	GSO
Density (g/cm³)	3.67 🔴	7.13 🟢	7.4 🟢	4.53	6.71
Effective Z	50.6	74.2	65.5	34.2	58.6
Attenuation length	2.88	1.05	1.16	2.58	1.43
Decay constant (ns)	230 🔴	300 🔴	40 🟢	70	60
Light output (photons/keV)	38	6	29	46	10
Relative light output	100% 🟢	15% 🔴	75% 🟡	118%	25%
Wavelength λ(nm)	410	480	420	420	440
Intrinsic ΔE/E (%)	5.8 🟡	3.1 🔴	9.1 🟢	7.5	4.6
ΔE/E (%)	6.6	10.2	10	12.5	8.5
Index of refraction	1.85	2.15	1.82	1.8	1.91
Hygroscopic?	Yes	No	No	No	No
Rugged?	No	Yes	Yes	Yes	No
μ (cm^{-1})	0.3411	0.9496	0.8658	0.3875	0.6978
μ/ρ(cm^2/gm)	0.0948	0.1332	0.117	0853	0.104

NaI(TI):	sodium iodide deoped with thallium
BGO:	bismuth germanate ($Bi_4Ge_3O_{12}$)
LSO:	lutetium oxyorthosilicate doped with cerium(Lu_2SiO_5:Ce)
YSO:	yttrium oxyorthosilicate doped with cerium(Y_2SiO_5:Ce)
GSO:	gadolinium oxyorthosilicate doped with cerium(Gd_2SiO_5:Ce)

New: LYSO

Photo-multiplier tubes (PMTs)

PMTs: photo-detectors used in scintillation detectors for PET

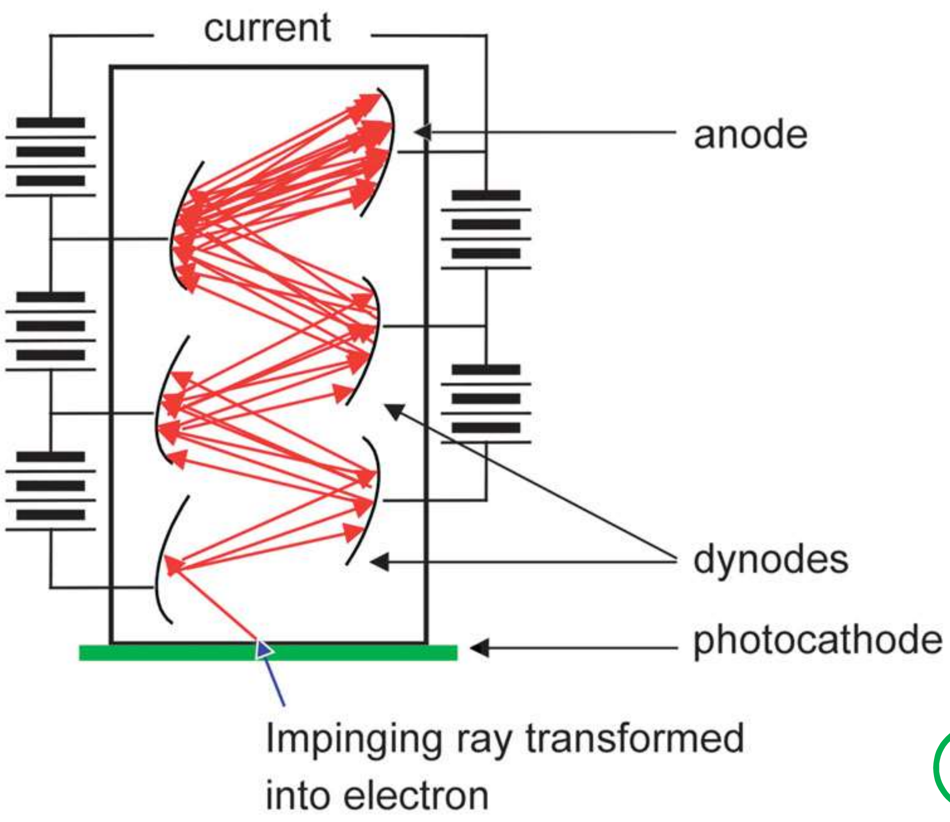
current
anode
dynodes
photocathode
Impinging ray transformed into electron

(1) Incoming photon deposits its energy at the photocathode, release of a photo-electron

(2) Applied electric field accelerates the electron to the first dynode

(3) Emission of multiple secondary electrons due to increased electron energy

(4) …

☺ **Good signal-to-noise ratio (SNR)**

☹ **Low quantum efficiency (QE) ~ 25%**

Detector Designs used in PET

One-to-one coupling:

- Single crystals glued to individual photo-detector
- Spatial resolution limited by discr crystal size

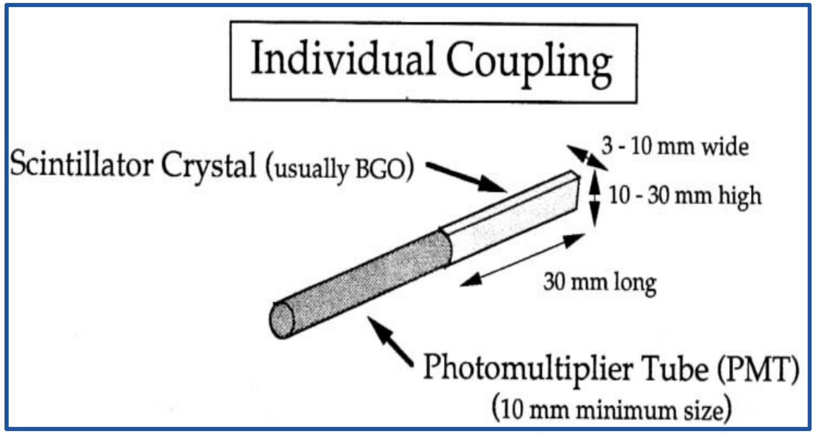
Individual Coupling
Scintillator Crystal (usually BGO)
3 - 10 mm wide
10 - 30 mm high
30 mm long
Photomultiplier Tube (PMT)
(10 mm minimum size)

Block detector design:

- Rectangular scintillator block sectioned by partial saw cuts of different depth into discrete elements
- Usually 4 attached PMTs
- Anger positioning

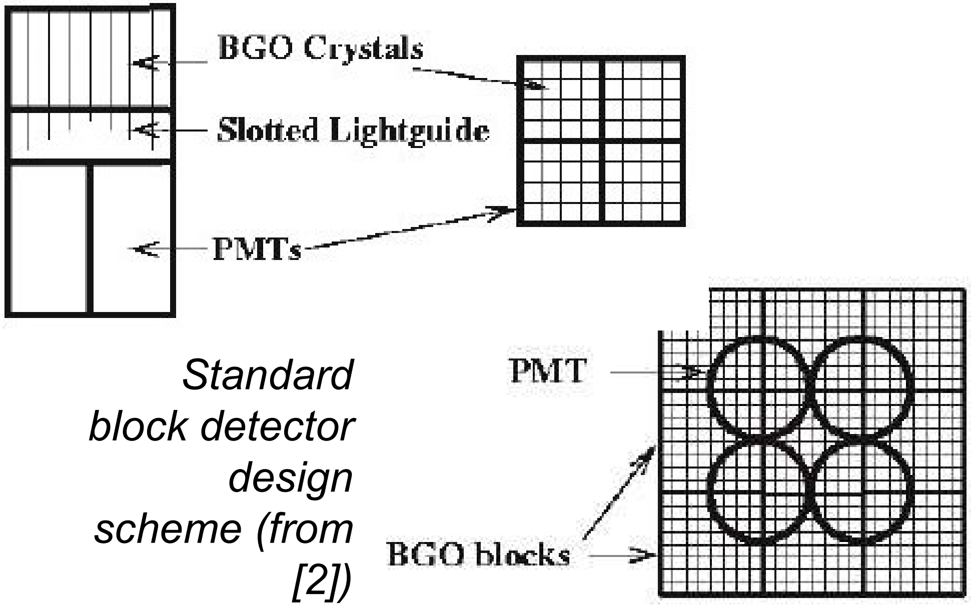
BGO Crystals
Slotted Lightguide
PMTs
PMT
BGO blocks

Standard block detector design scheme (from [2])

Detector Designs used in PET

Anger detector:

- Large scintillator crystal glued to array of PMTs
- Weighted centroid positioning algorithm used to estimate interaction position within the detector

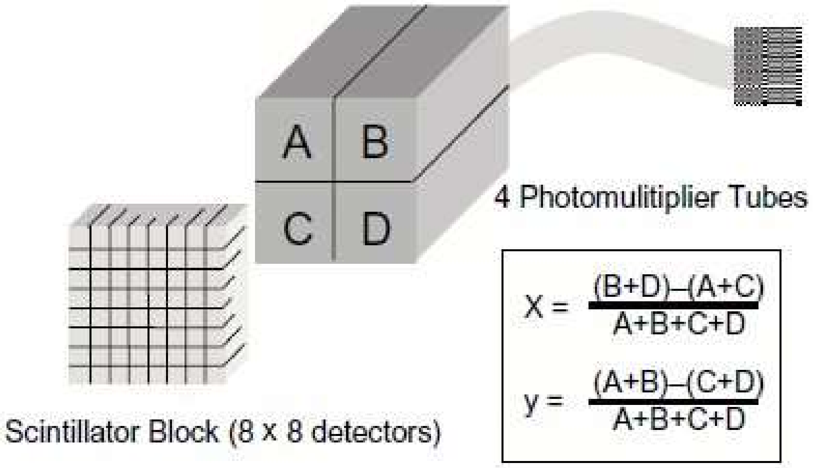
A
B
C
D
4 Photomulitiplier Tubes
Scintillator Block (8 x 8 detectors)

$$X = \frac{(B+D)-(A+C)}{A+B+C+D}$$

$$y = \frac{(A+B)-(C+D)}{A+B+C+D}$$

Block detector system + Anger logic [3]

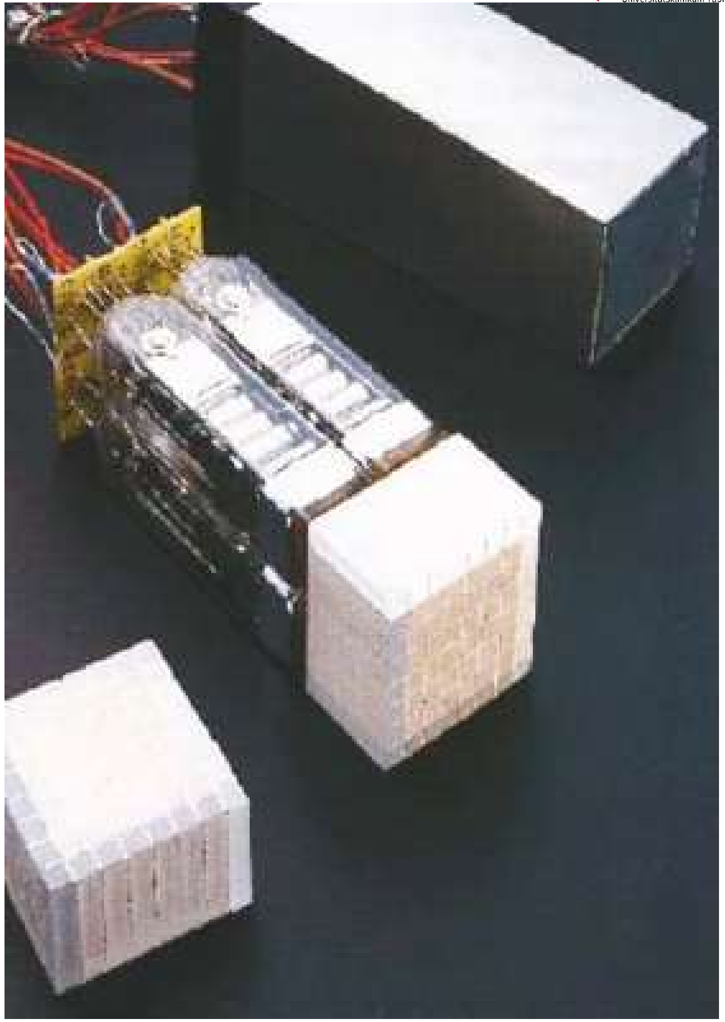

Block detector Siemens-CTI ECAT 951, 8x8 block BGO with 4 PMTs (from [2])

Timing Resolution and Coincidence Detection

Coincidence time window: 2τ

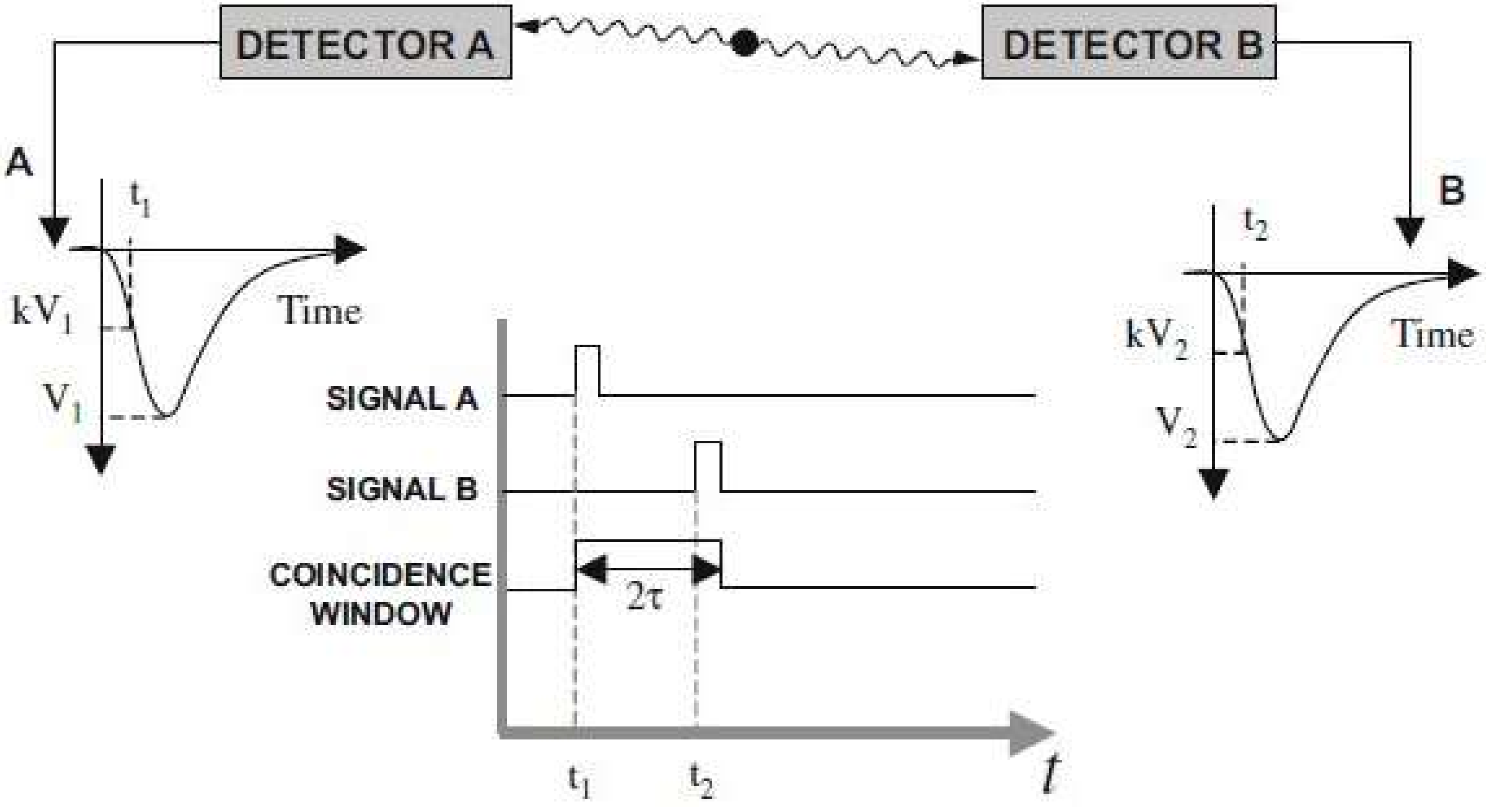
DETECTOR A
DETECTOR B
A
B
t_1
kV_1
V_1
Time
t_2
kV_2
V_2
Time
SIGNAL A
SIGNAL B
COINCIDENCE WINDOW
2τ
t_1
t_2
t

Time-of-flight (TOF) PET

- In addition to the coincidence information, the difference in flight time is registered

$$\Delta t = \frac{2\Delta x}{c}$$

- Better SNR

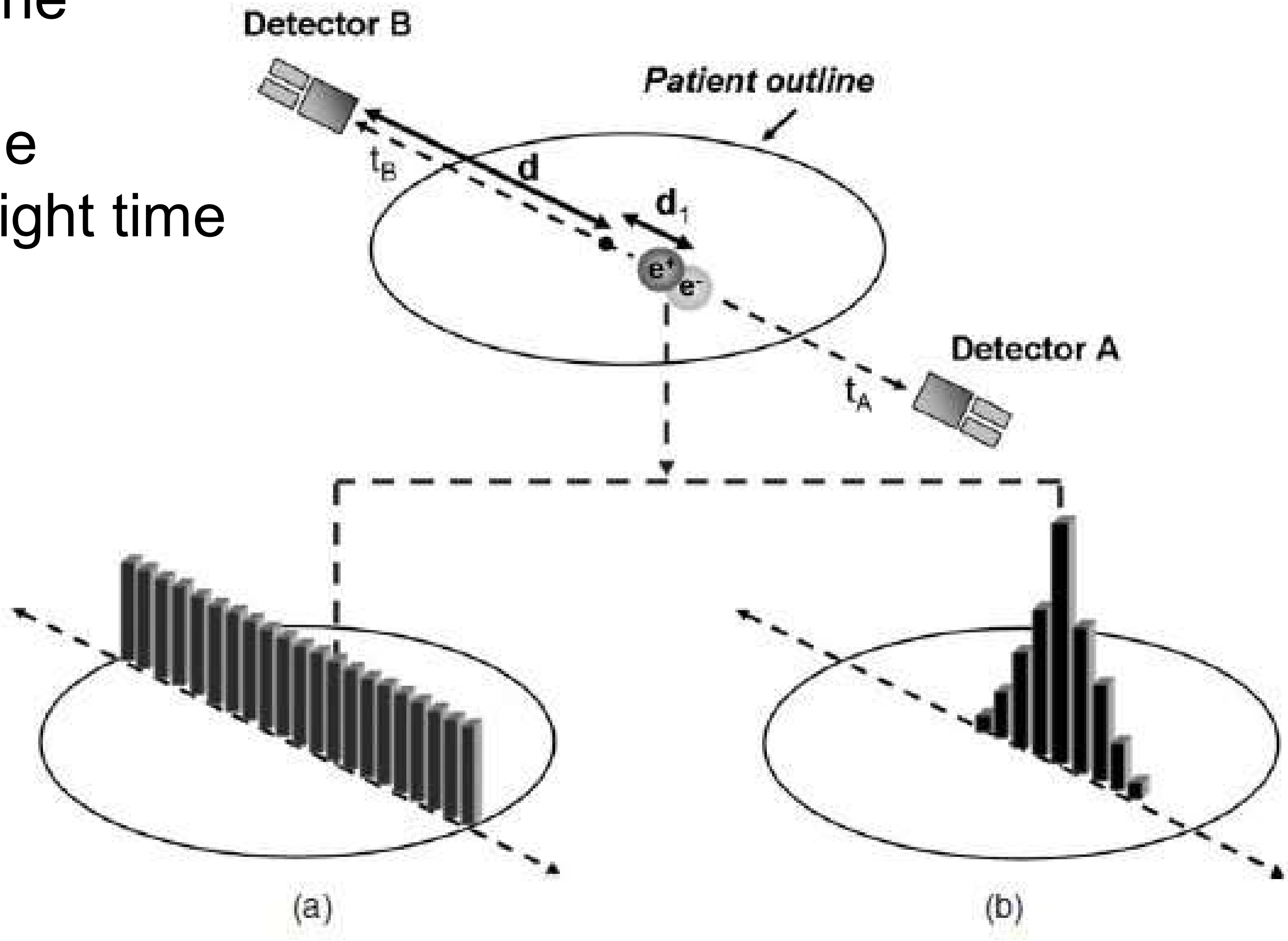
Detector B
Patient outline
t_B
d
d_1
e^+
e^-
Detector A
t_A
(a)
(b)

(a) Localization without TOF,
(b) with TOF. Townsend, PMB 2008 [3]

Detected Events in PET

- Detection event is valid (= **prompt** event) if
  - Two photons are detected in coincidence window
  - LOR is within valid acceptance angle
  - Energy of both photons within selected energy window

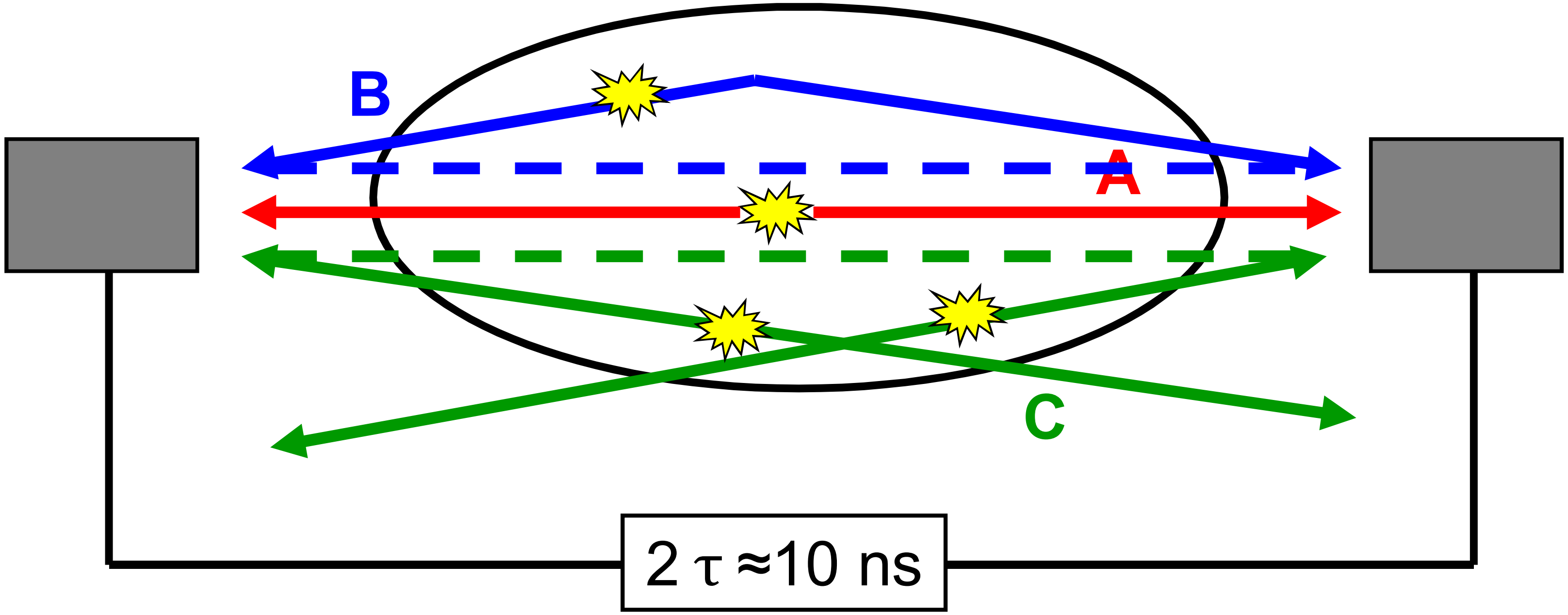

True coincidence (A) , scattered coincidence (B), random coincidence (C)

Prompt Events

- **Single** event
  - single photon is counted by detector (1-10%)
- **True** coincidence
  - event derives from single positron-electron annihilation
  - both photons reach tomograph without interaction
- **Random** coincidence
  - two nuclei decay at approximately the same time
  - random event count rate (R_{ab}) between two detectors *a* and *b*:

$$R_{ab} = 2\tau \cdot N_a N_b \propto N^2$$

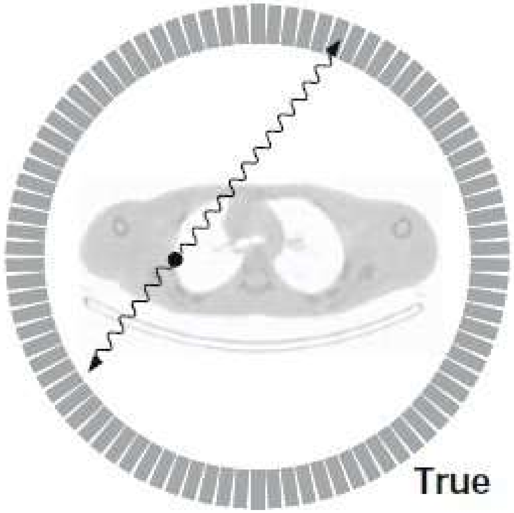

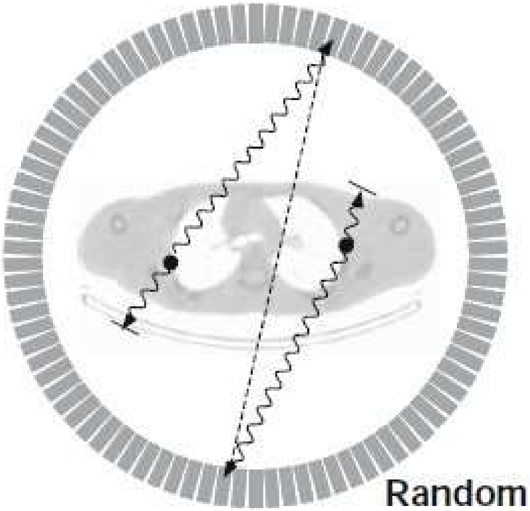

Prompt Events (II)

- **Scattered** events
  - One or both photons detected have undergone a Compton interaction
  - Loss in energy and change in direction
  - Due to poor energy resolution, many scattered photons cannot be discriminated
  - Wrong LOR assigned

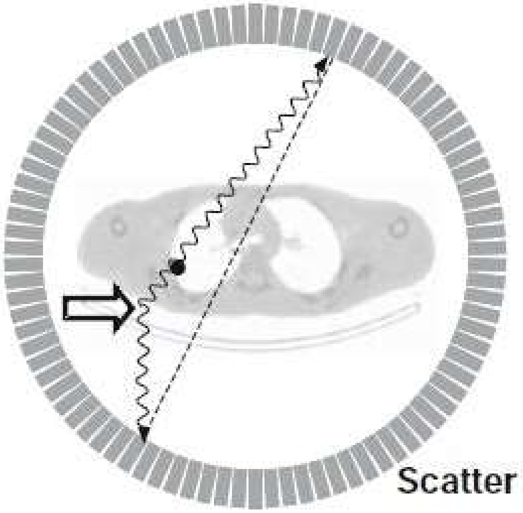

- **Multiple** (triple) events
  - Three events from two annihilations detected
  - Event is disregarded
  - Proportional to count rate

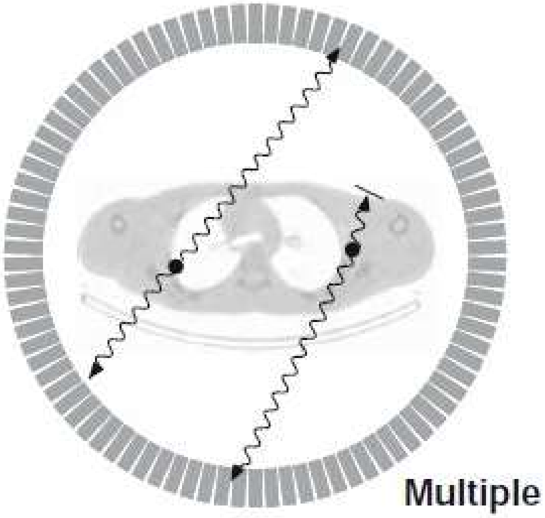

Performance of PET Systems

- Sensitivity

$$S = \frac{c}{t \cdot A} = \left[\frac{\text{counts}}{\sec \cdot kBq} \right]$$

  - Good systems reach *S=7-9 counts/(sec.kBq)*
- Spatial Resolution
- Energy Resolution
- Count Rate Performance
- Scatter Fraction

Performance of PET Systems: Spatial Resolution

- Determined by *full width half maximum* (FWHM) of *point spread function* (PSF): $FWHM = \sqrt{8\ln(2\sigma)}$

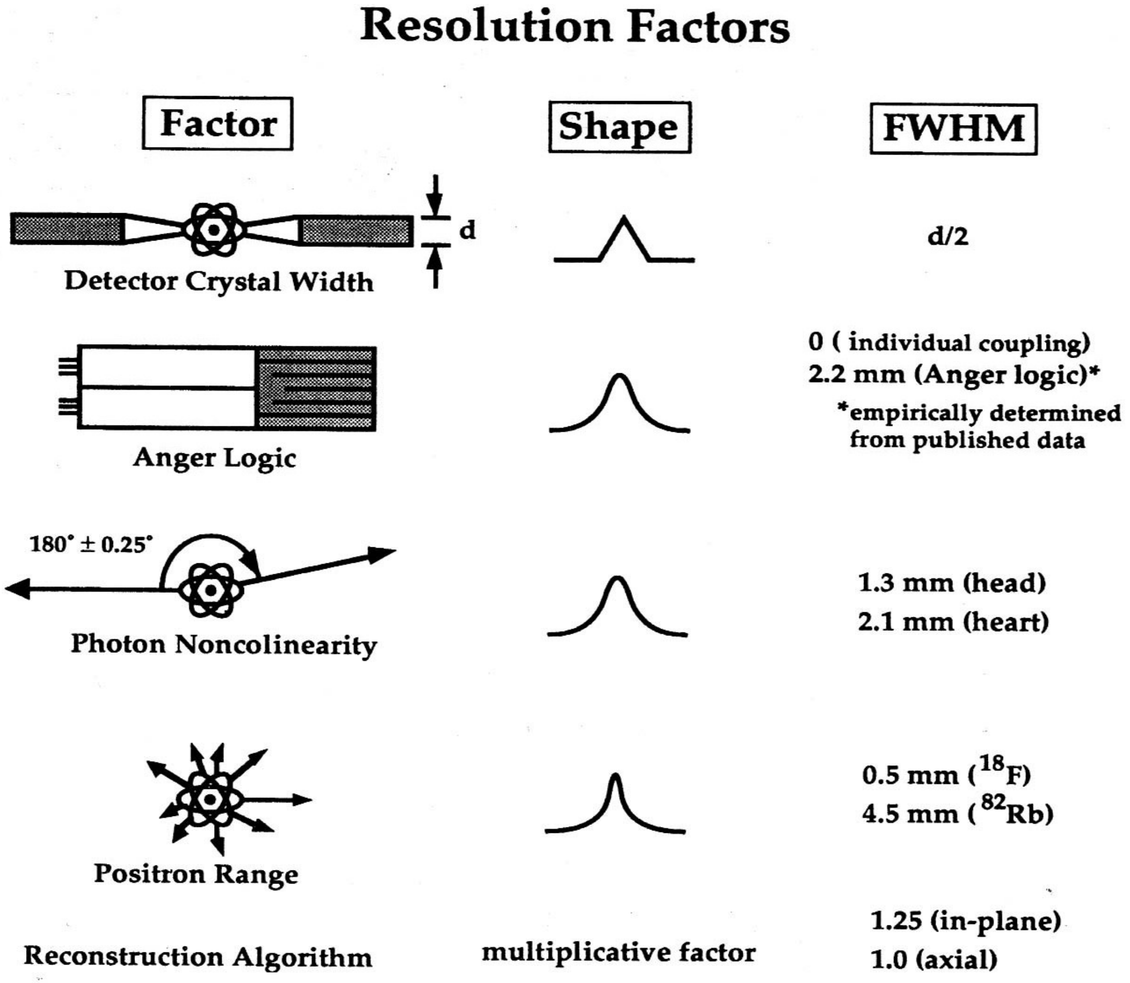

Resolution Factors

Factor	Shape	FWHM
Detector Crystal Width		d/2
Anger Logic		0 (individual coupling) 2.2 mm (Anger logic)* *empirically determined from published data
Photon Noncolinearity		1.3 mm (head) 2.1 mm (heart)
Positron Range		0.5 mm (^{18}F) 4.5 mm (^{82}Rb)
Reconstruction Algorithm	multiplicative factor	1.25 (in-plane) 1.0 (axial)

Performance of PET Systems: Energy Resolution

- Statistical uncertainty of energy determination due to limited light yield of scintillator crystal
- Two methods for determination of energy resolution:
  - *Single event* energy resolution
  - *Coincidence* (i.e. both events) energy resolution

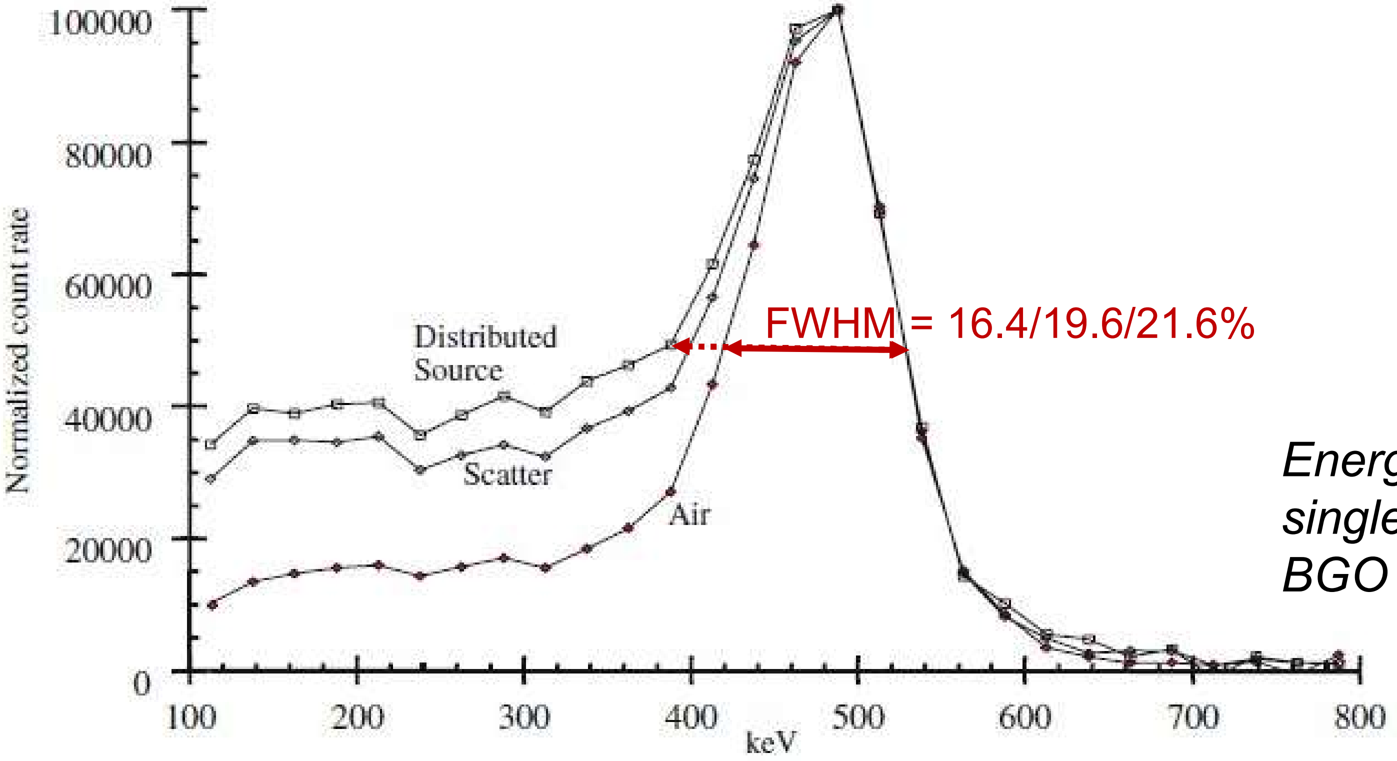

Energy spectra for single photons for a BGO PET system [2].

Performance of PET Systems: Count Rate Performance

- Ratio Trues/Randoms unbalanced for high Activities
- Processing of detected photons takes finite time
- Noise Equivalent Count Rate:

$$NECR = \frac{T^2}{T + S + 2fR}$$

T: trues
S: scattered
R: randoms
f: rel. area of object on proj. surface

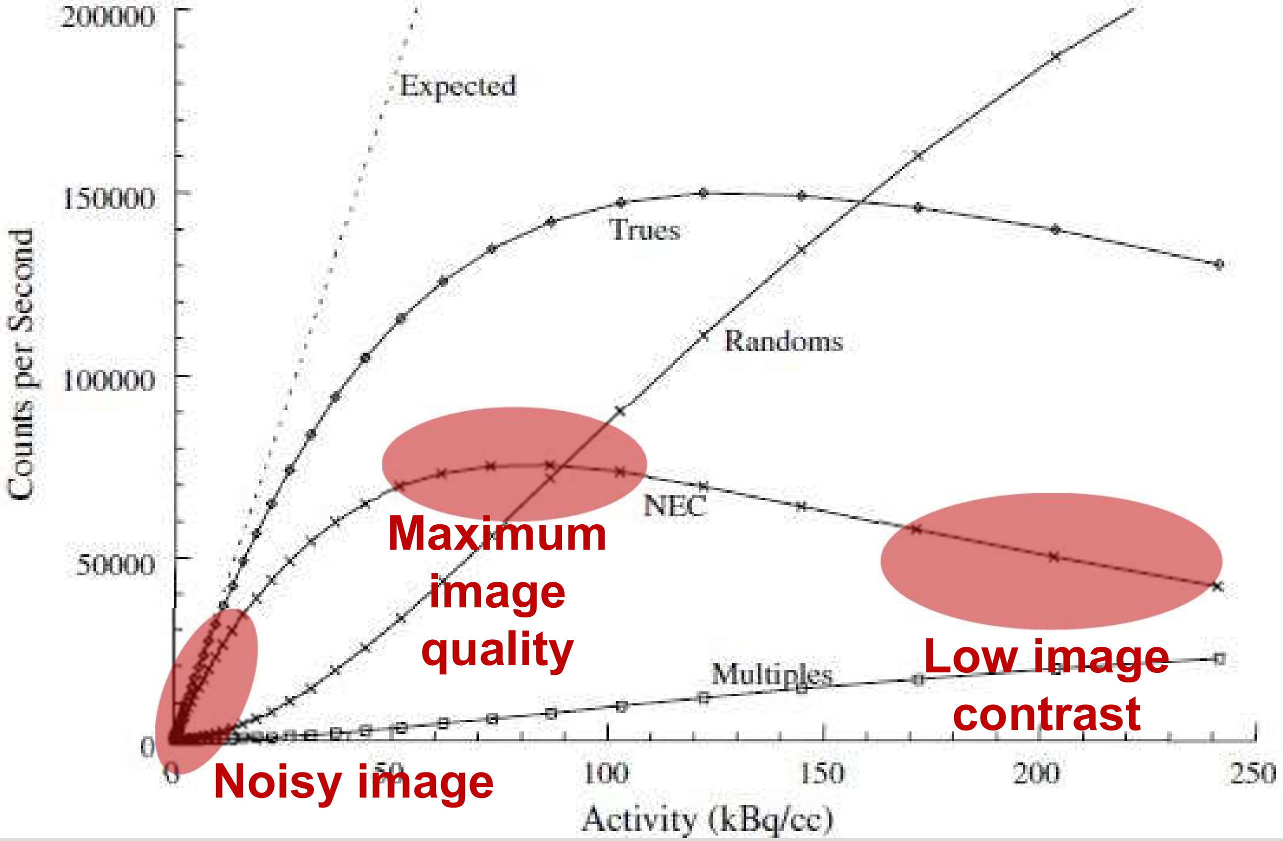

Count rate curves for true, random and multiple coincidences. Derived curves for expected and noise equivalent count rate [2]. Data recorded on a CTI ECAT 953B PET using a ^{11}C-filled cylinder in water.

Performance of PET Systems: Scatter Fraction

- Fraction of the total coincidences recorded in the photopeak window that have been scattered
- Sources of scattering
  - Scattering within the object containing the radionuclide
  - Scattering off the gantry components (lead septa/side shields)
  - Scattering within the detectors

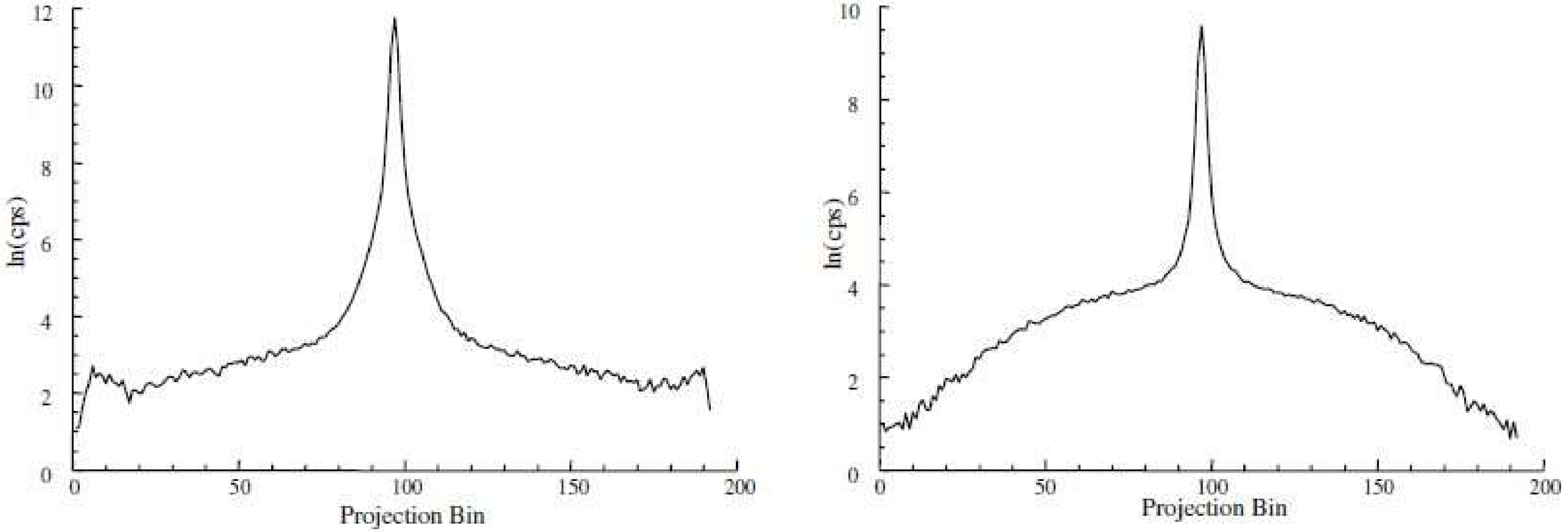

Log-lin count rate profiles of line source in air/water show additive scatter component outside of central peak [2].

Performance of PET Systems: Scatter Fraction

- Fraction of the total coincidences recorded in the photopeak window that have been scattered
- Sources of scattering
  - Scattering within the object containing the radionuclide
  - Scattering off the gantry components (lead septa/side shields)
  - Scattering within the detectors

- Scatter fraction can be reduced by
  - TOF
  - Usage of a powerful iterative reconstruction method
  - Shielding of scattered photons by septa and endshiels
  - Small coincidence window
  - Good energy resolution

Summary

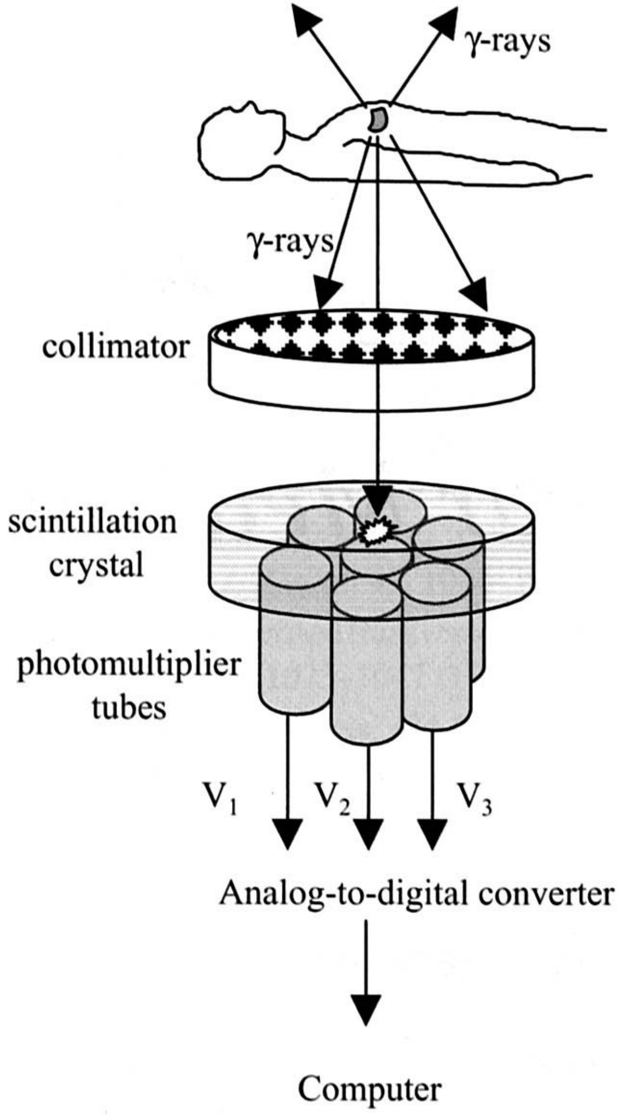
γ-rays
γ-rays
collimator
scintillation crystal
photomultiplier tubes
V_1
V_2
V_3
Analog-to-digital converter
Computer

- Positron emitter used as radioactive tracer in the patient
- Use of collimators to generate ‚image slices‘
- Detection of γ-quanta in scintillation crystal
- Better resolution due to Anger logic
- Signal amplification using PMTs
- Image reconstruction

Literature

[1] DL Bailey, JS Karp, S Surti. Physics and Instrumentation in PET. In: Positron Emission Tomography: Basic Science and Clinical Practice. Editors: PE Valk, DL Bailey, DW Townsend, MN Maisey. Springer London 2003, pp. 13-39.

[2] DL Bailey. Data Acquisition and Performance Characterization in PET. In: Positron Emission Tomography: Basic Science and Clinical Practice. Editors: PE Valk, DL Bailey, DW Townsend, MN Maisey. Springer London 2003, pp. 41-61.

[3] DW Townsend. Multimodality imaging of structure and function. Phys Med Biol 2008; 53: R1-R39.

[4] B Sattler, JA Lee, M Lonsdale, E Coche. PET/CT (and CT) instrumentation, image reconstruction and data transfer for radiotherapy planning. Radiother Oncol 2010; 96: 288-297. Review.

Imaging for Physicists

Artifacts 1

Uulke van der Heide

Artifacts in MRI

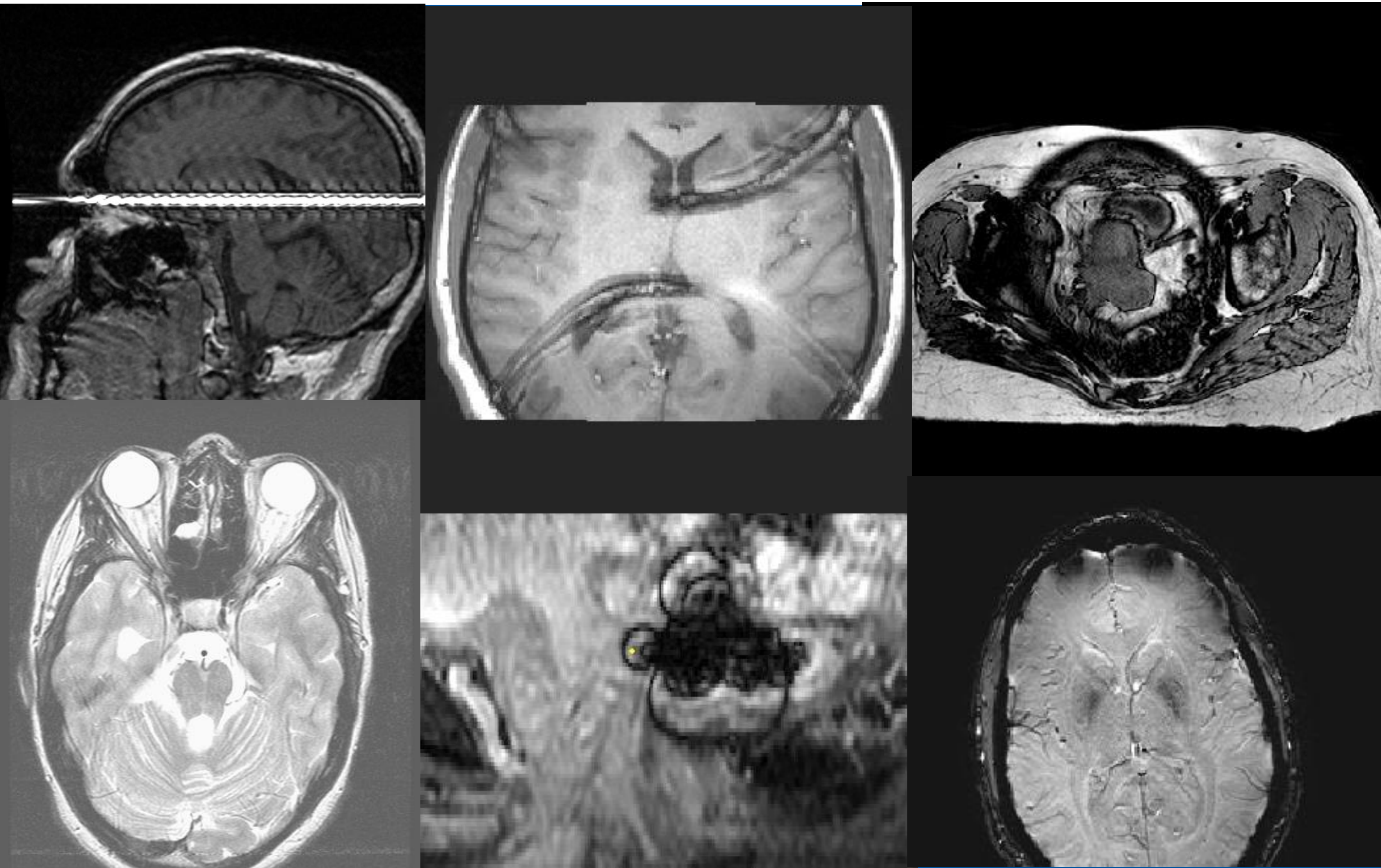

Artifacts in MRI

- An image artifact is any property or effect observed in an image that does not appear in the original object

- Images can be distorted in many ways
  - Signal loss
  - Deformations
  - Poor resolution
  - Ghosting
  - Aliasing
  - …..

- Consequences for use
  - Interpretation is difficult
  - Geometrical accuracy may be compromised

Outline

- Origin of geometrical artifacts
    - Fold-over artifacts
    - Ringing
    - Impact of field distortions

Origin of various artifacts

- Sampling of k-space
  - Sample k-space in too large steps
  - Don’t sample high k-values

- Magnetic field errors
  - Inhomogeneous B_0 field
  - non-linear gradients
  - Susceptibility
  - Chemical shift

- Motion

Imaging artifact

- T_1-weighted SE image of a brain
- What is wrong?

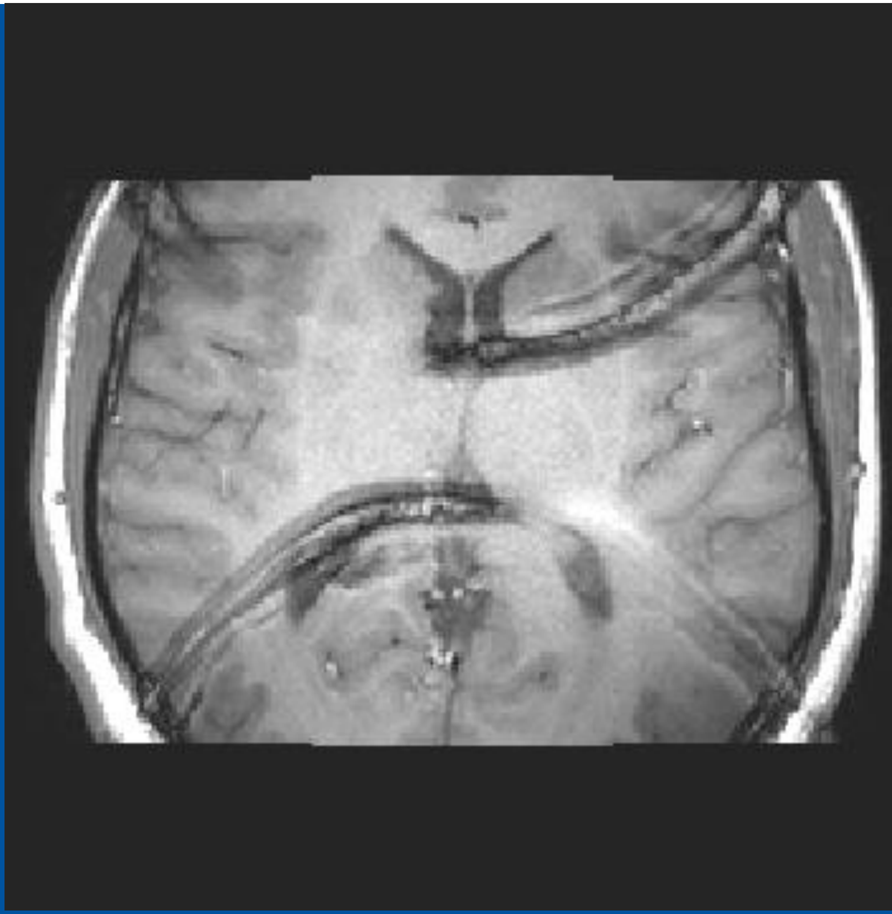

Sampling the MR signal

- Nyquist criterium: signal must be sampled at at least twice the rate of the highest frequency component

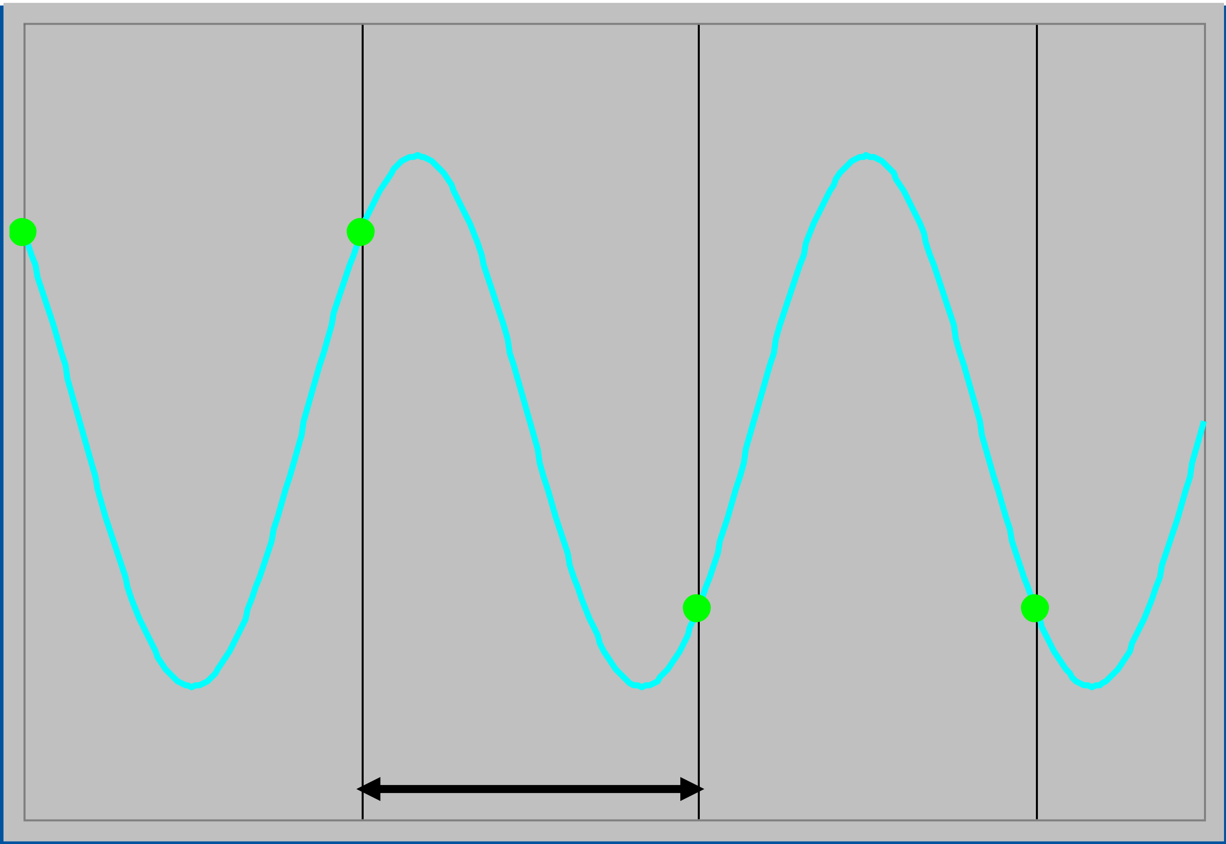

Sampling the MR signal

- Nyquist criterium: signal must be sampled at at least twice the rate of the highest frequency component

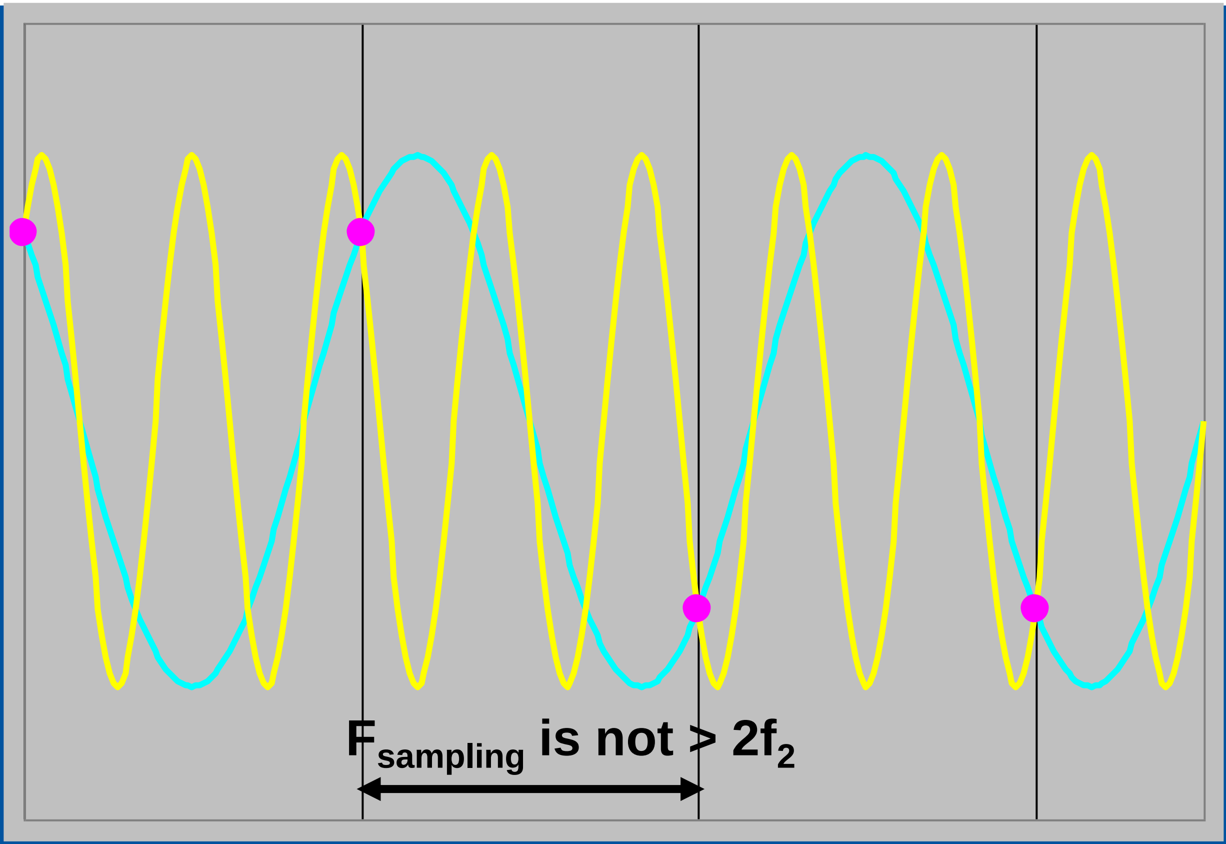

- If the signal contains higher frequency components, aliasing occurs

Resolve aliasing by increasing sampling frequency

- Nyquist criterium: signal must be sampled at at least twice the rate of the highest frequency component

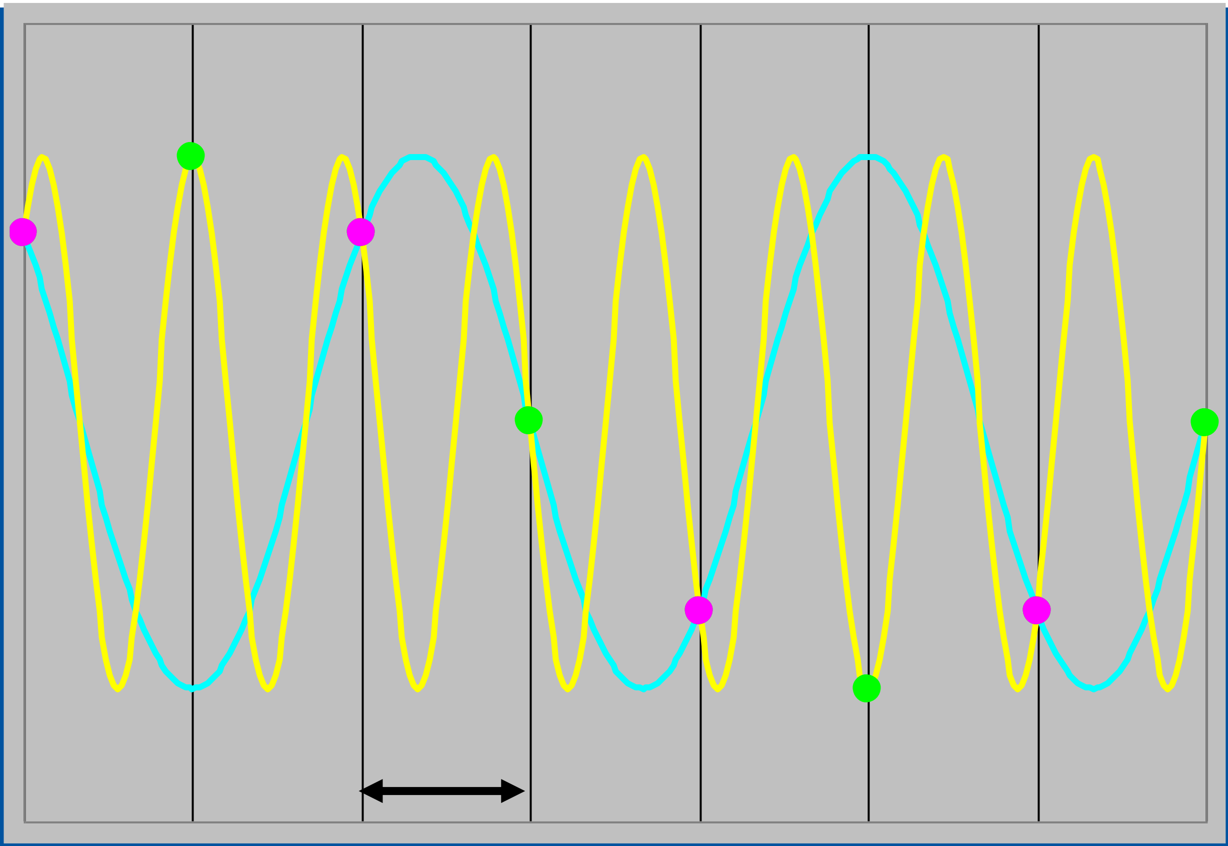

- By increasing the sample frequency, the higher frequency components can be resolved and aliasing is avoided

Field Of View covers entire object: no fold-over

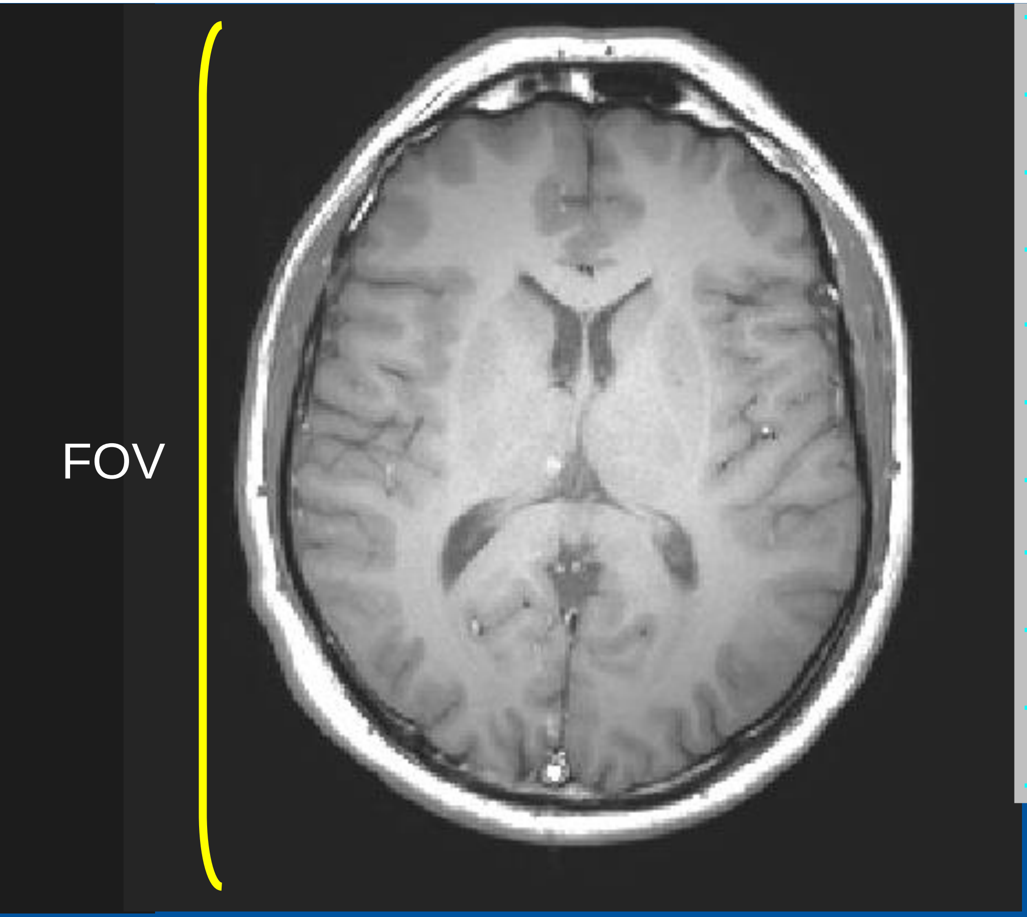

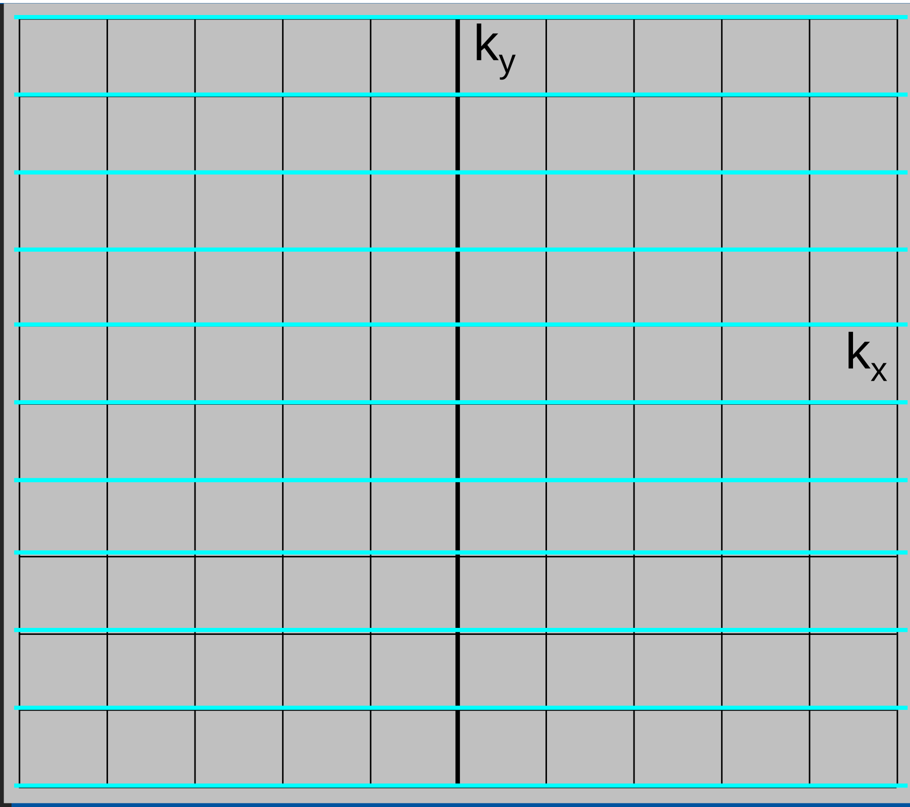

What happens with the distance between lines in k-space, if you reduce the field of view by a factor of 2?

1. ★ The distance between k-lines is increased by a factor of 2
2. The distance between k-lines is reduced by a factor of 2
3. The distance between k-lines remains the same (but the extent of k-space is reduced by a factor of 2

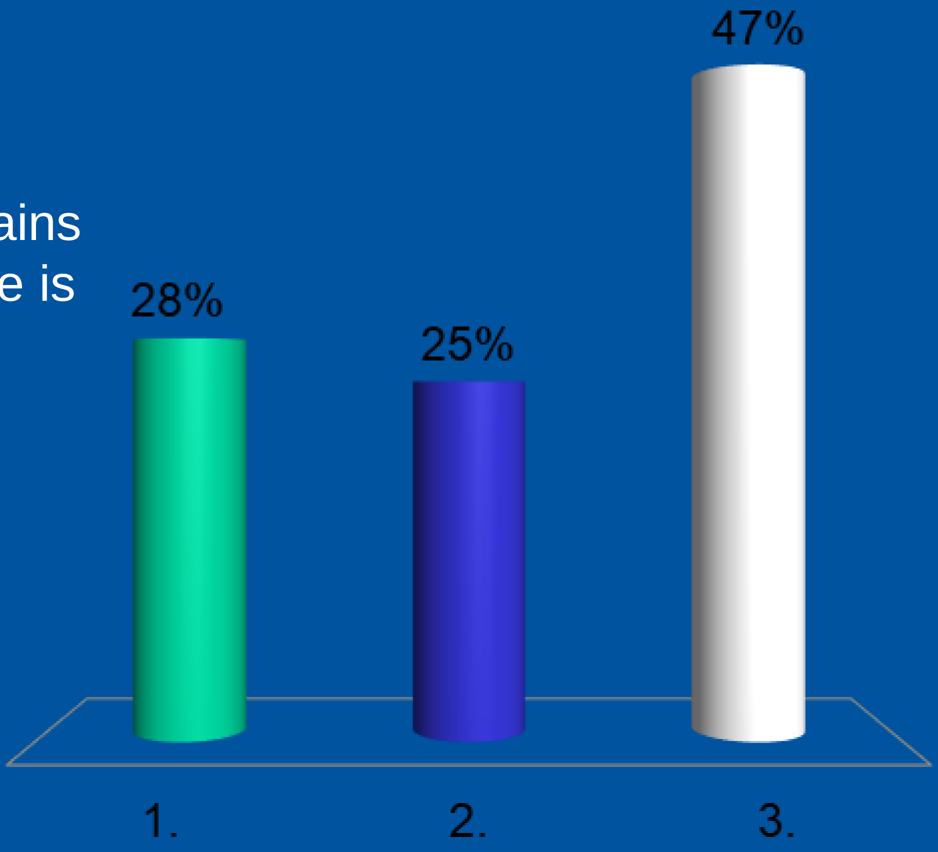

Field Of View covers entire object: no fold-over

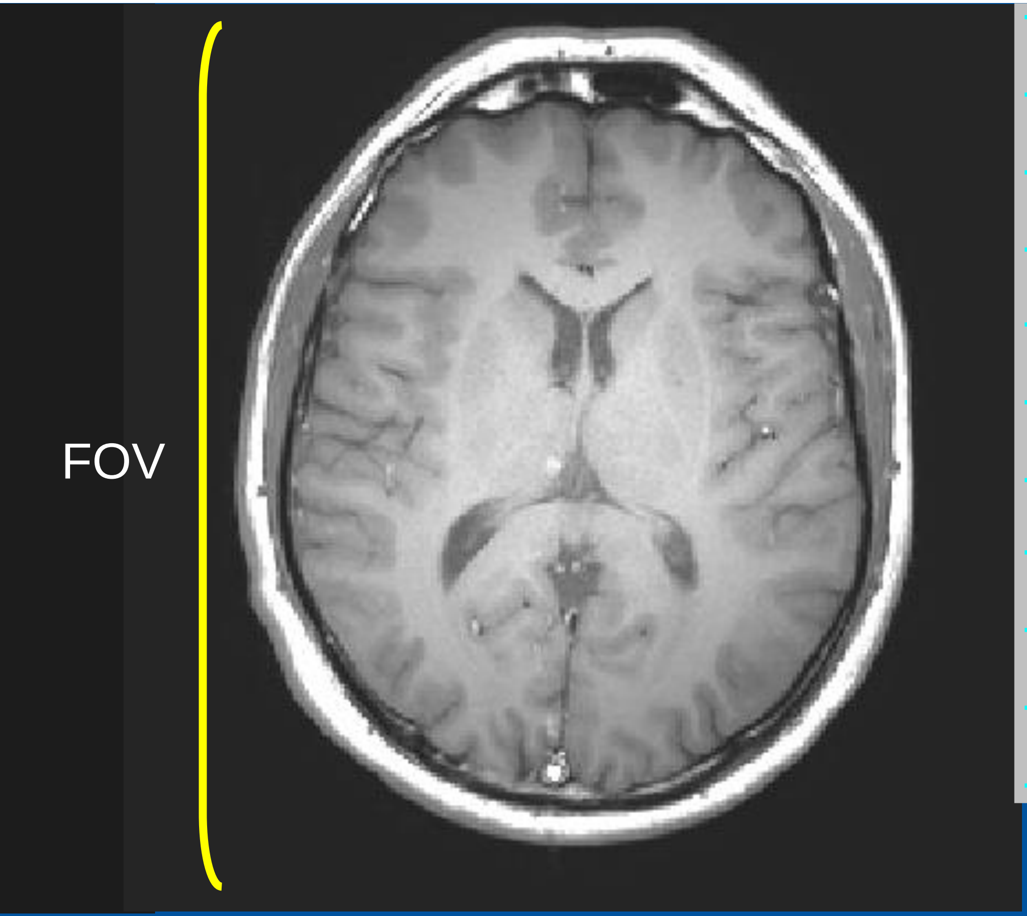

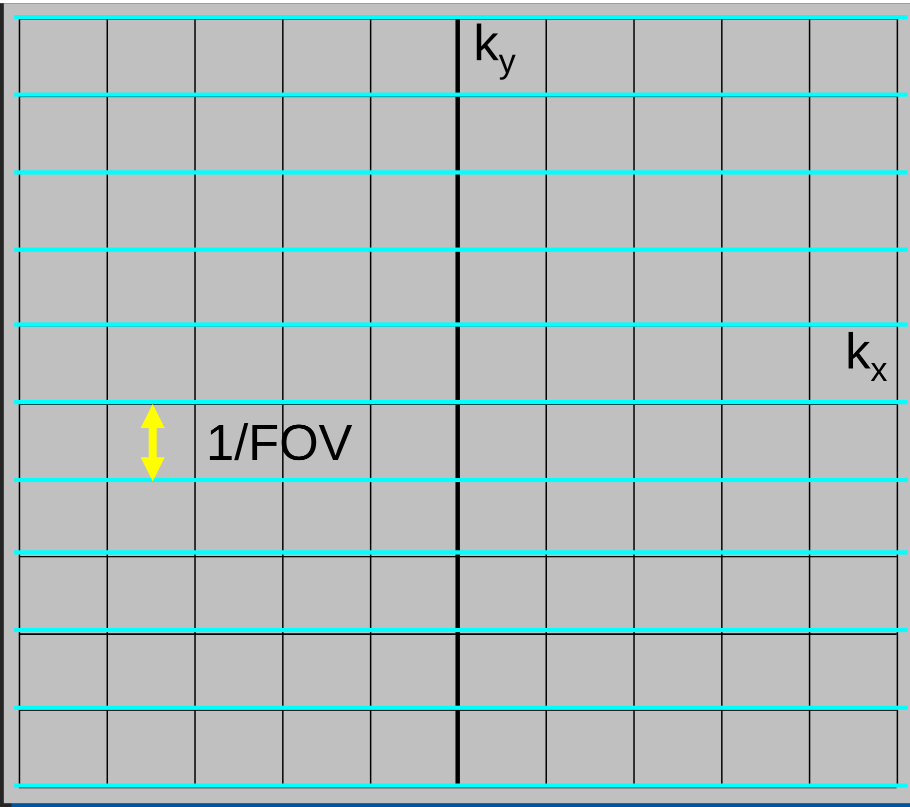

FOV too small: fold-over

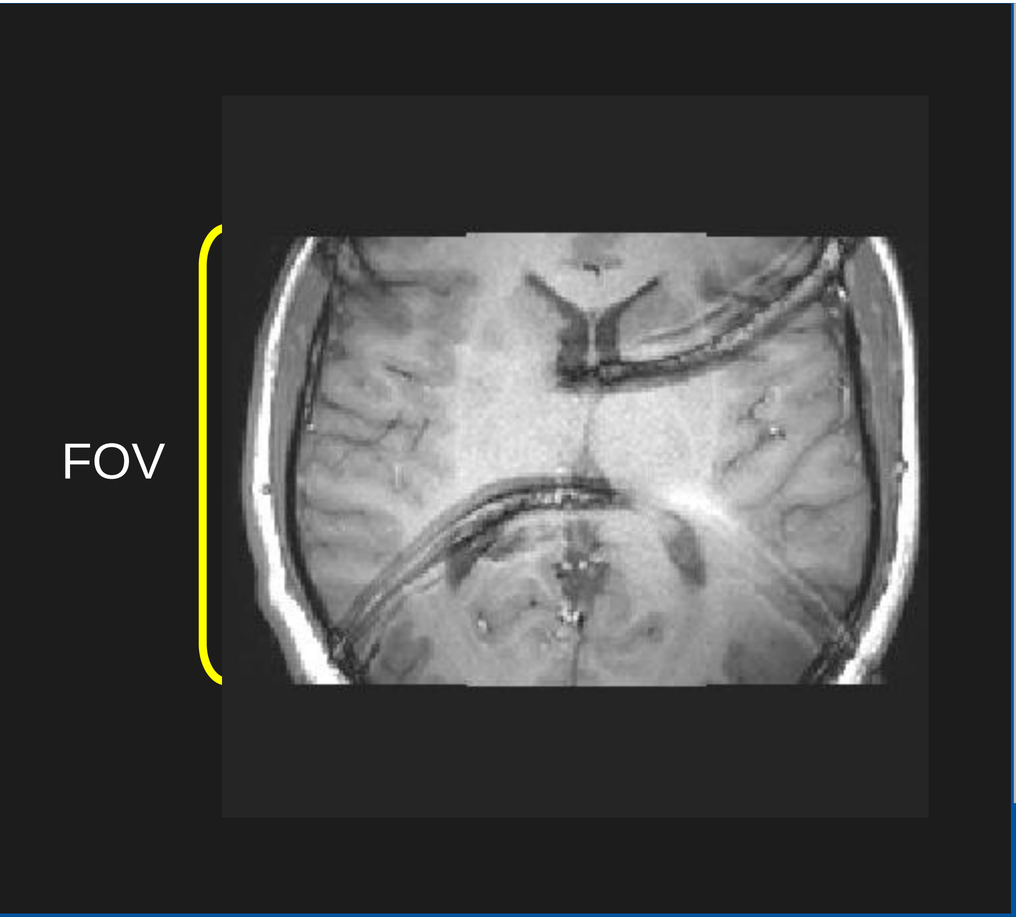

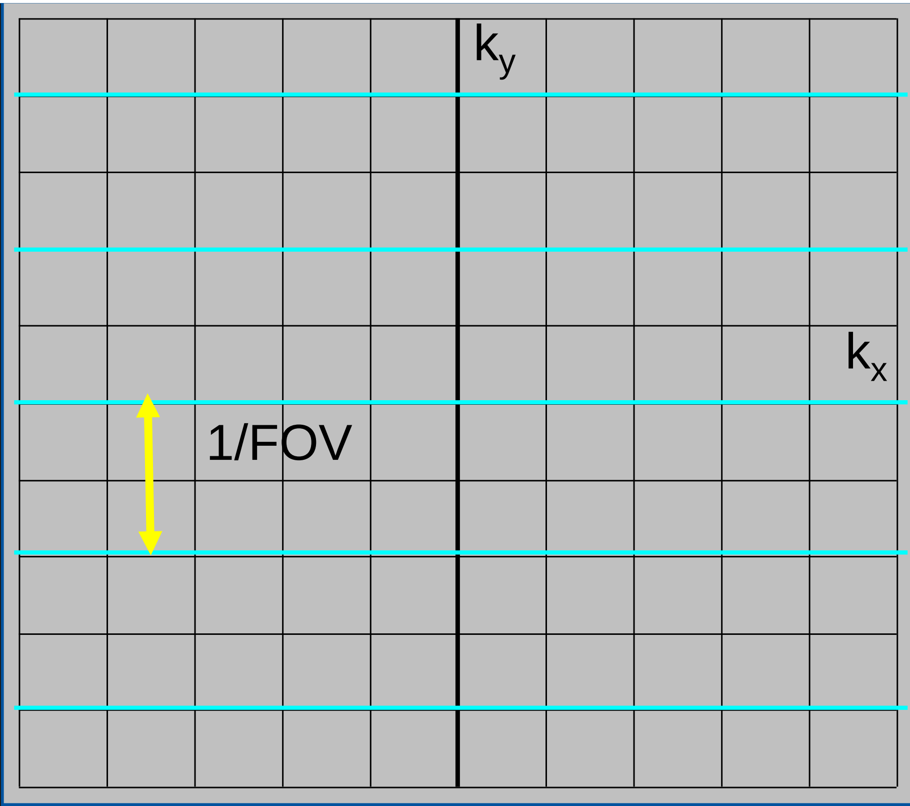

How to suppress fold-over artifacts?

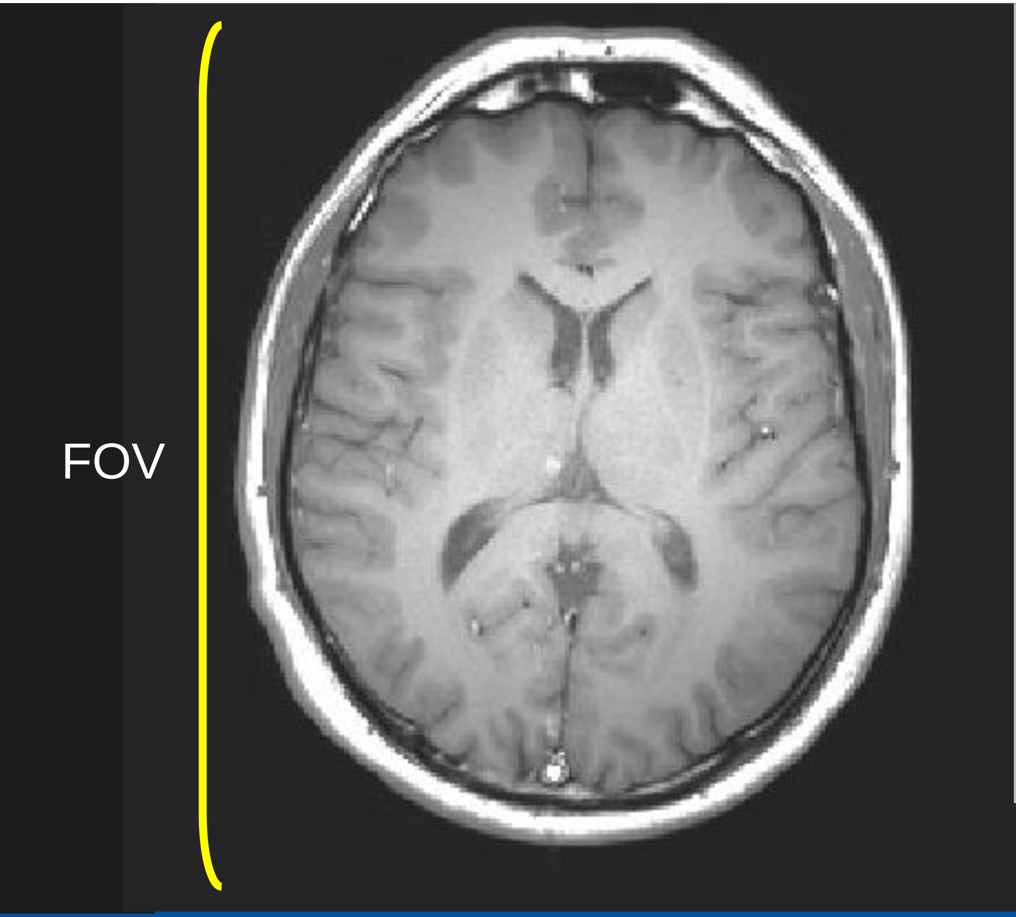

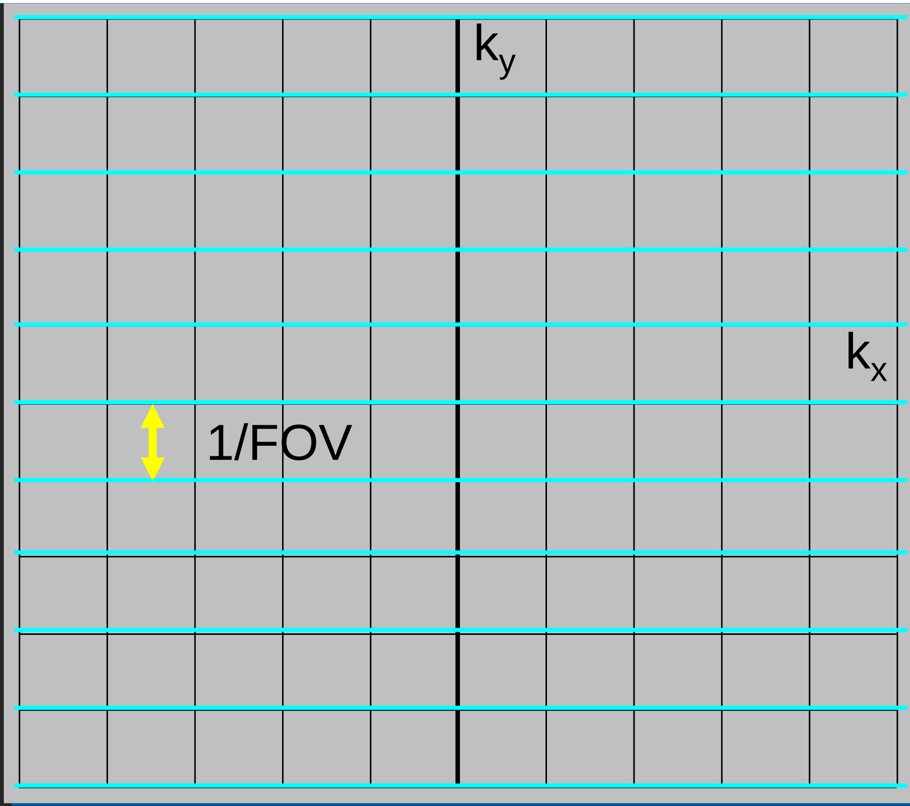

- If NSA>1: Measure all k-lines (full FOV), but reconstruct only half of the image

How to suppress fold-over artifacts?

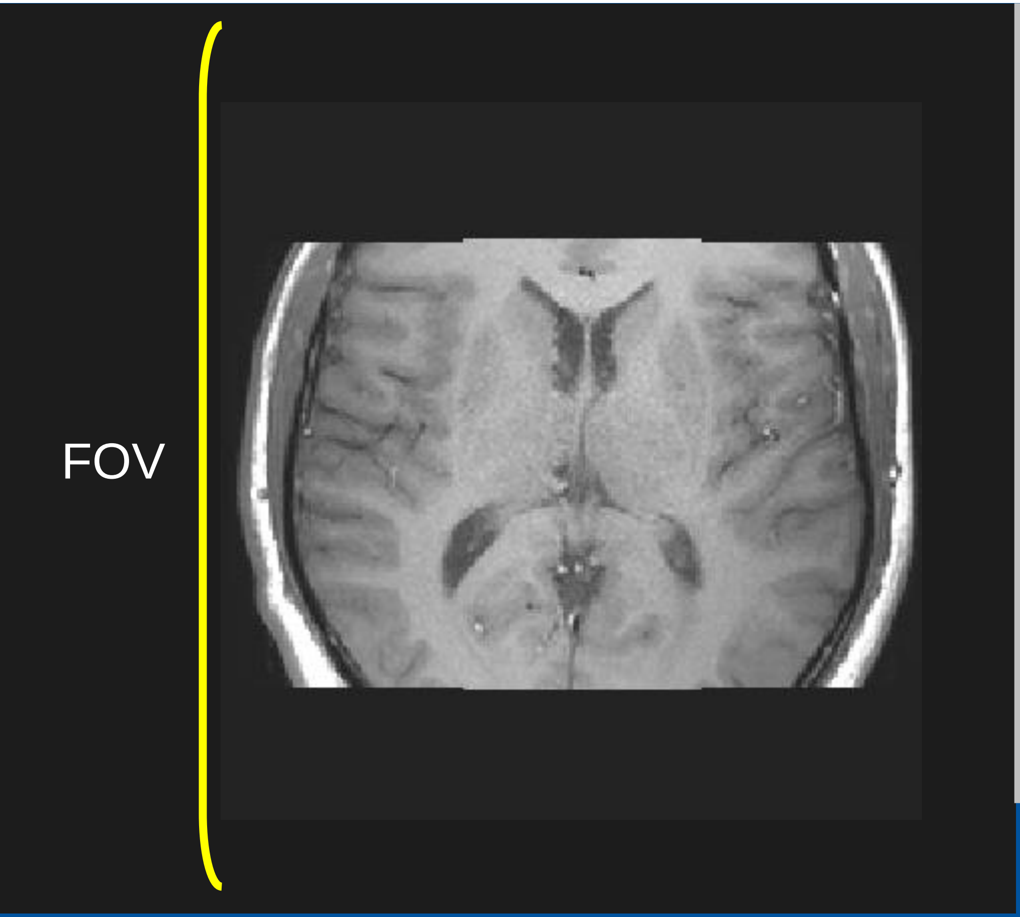

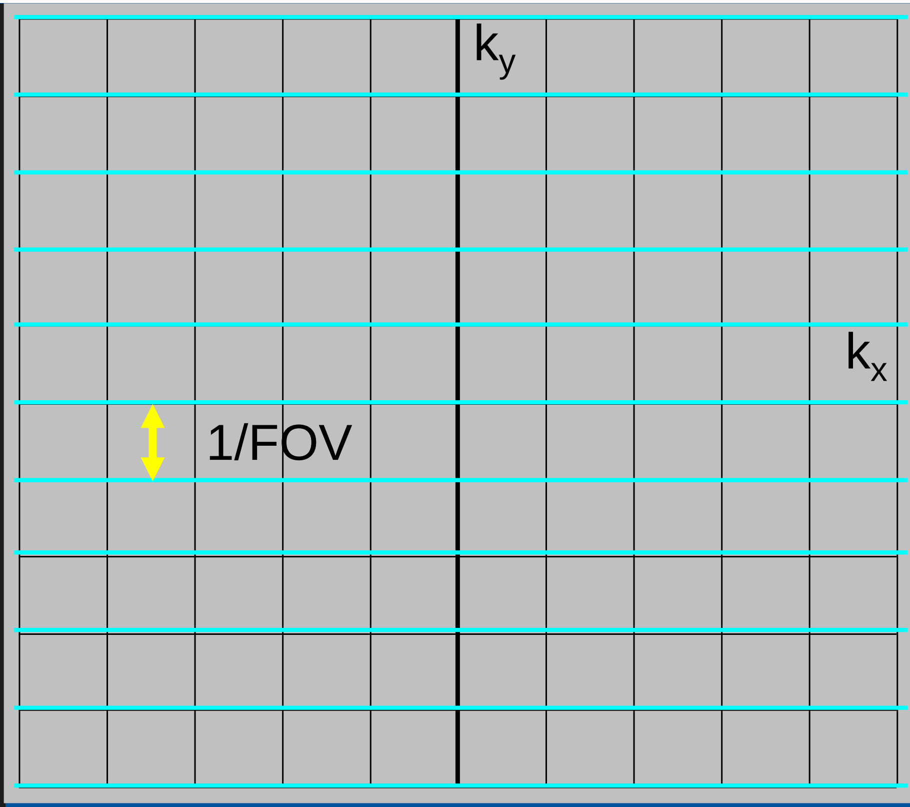

- If NSA>1: Measure all k-lines (full FOV), but reconstruct only half of the image

How to suppress fold-over artifacts?

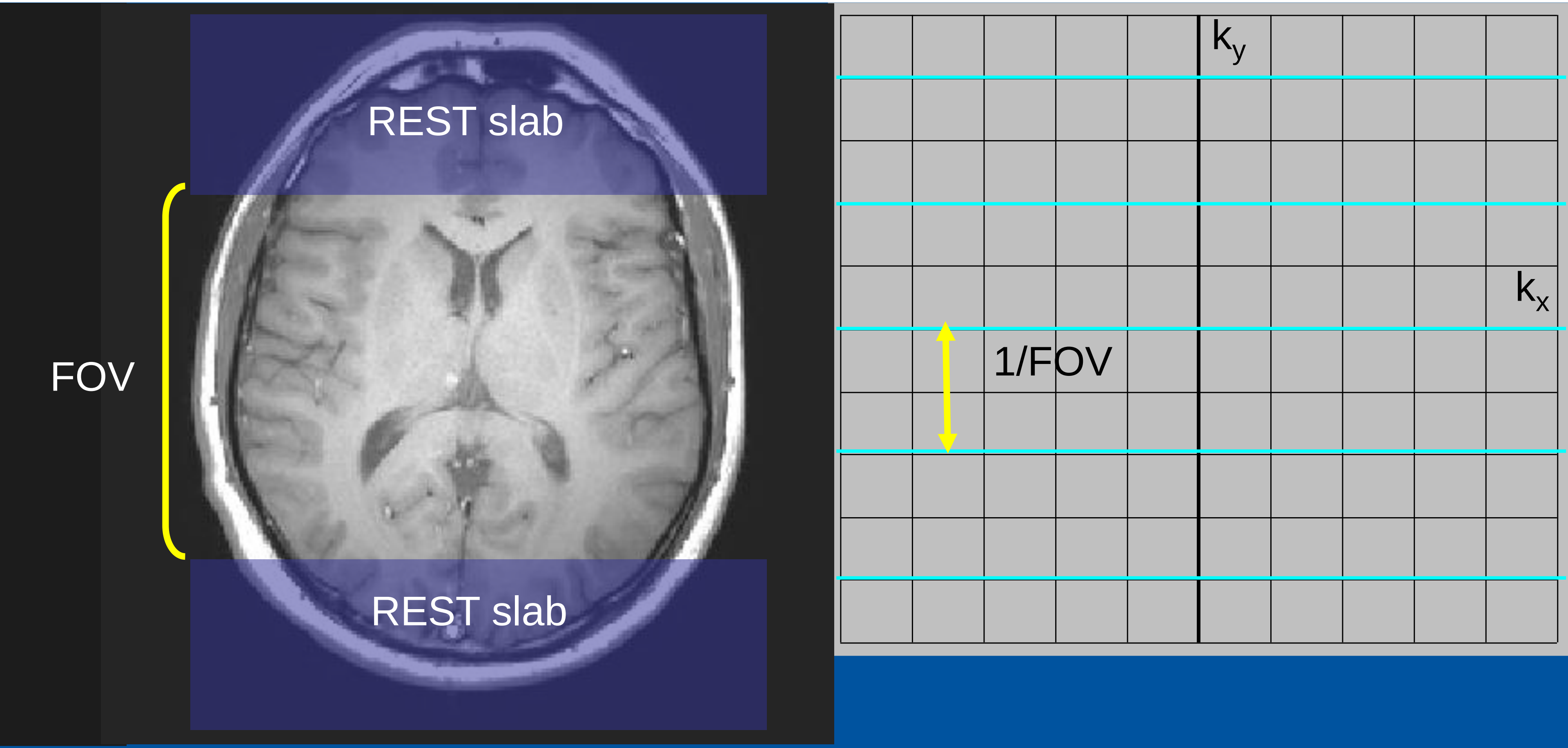
REST slab
FOV
REST slab
k_y
k_x
1/FOV

- If NSA=1: Saturate the signal from outside the field-of-view with REST slabs

Saturate signal from outside FOV

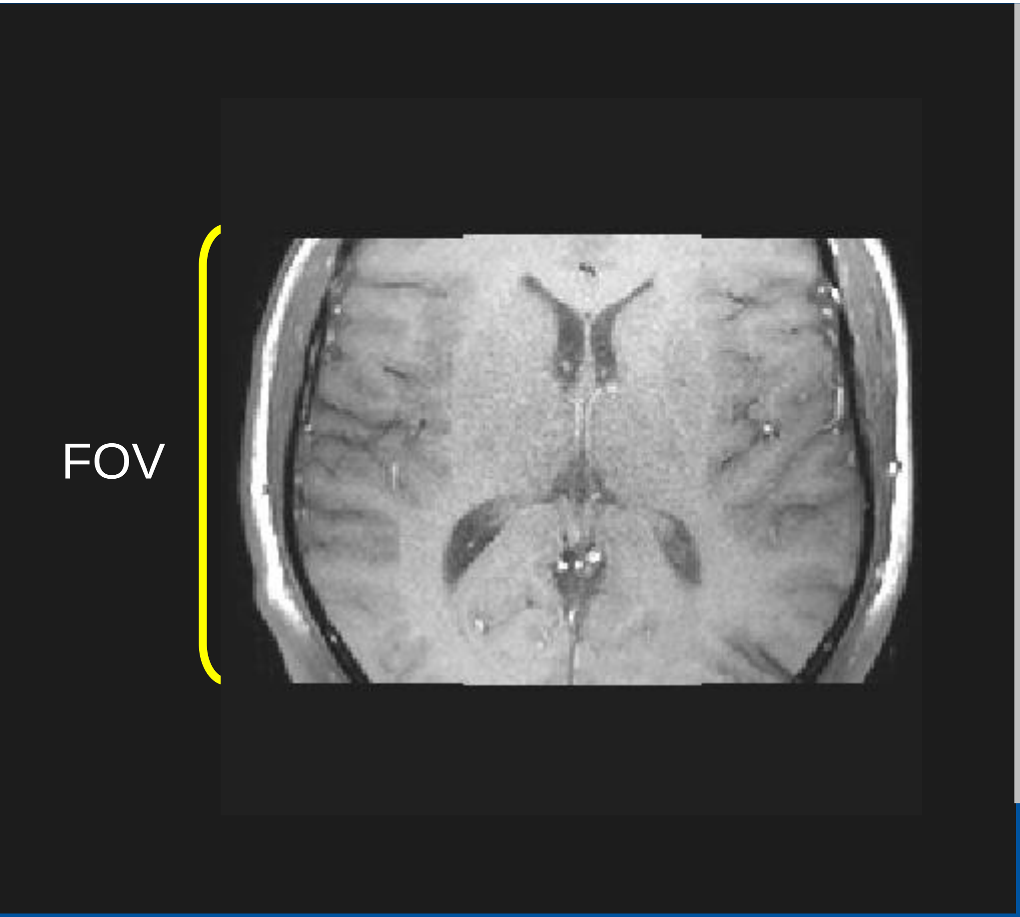

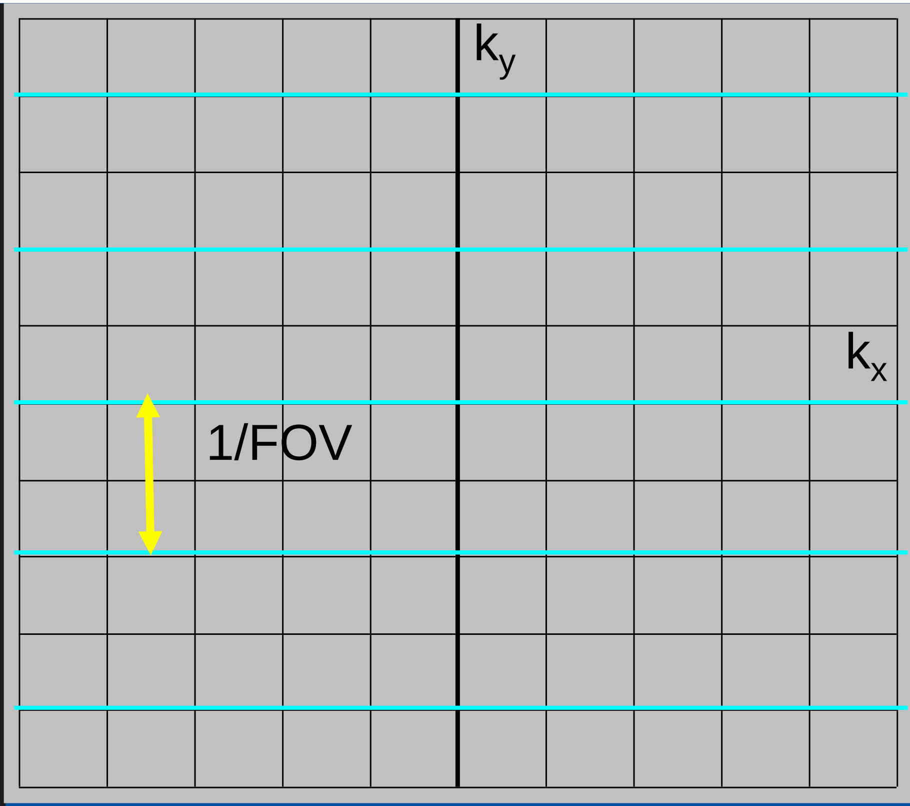

Imaging artifact

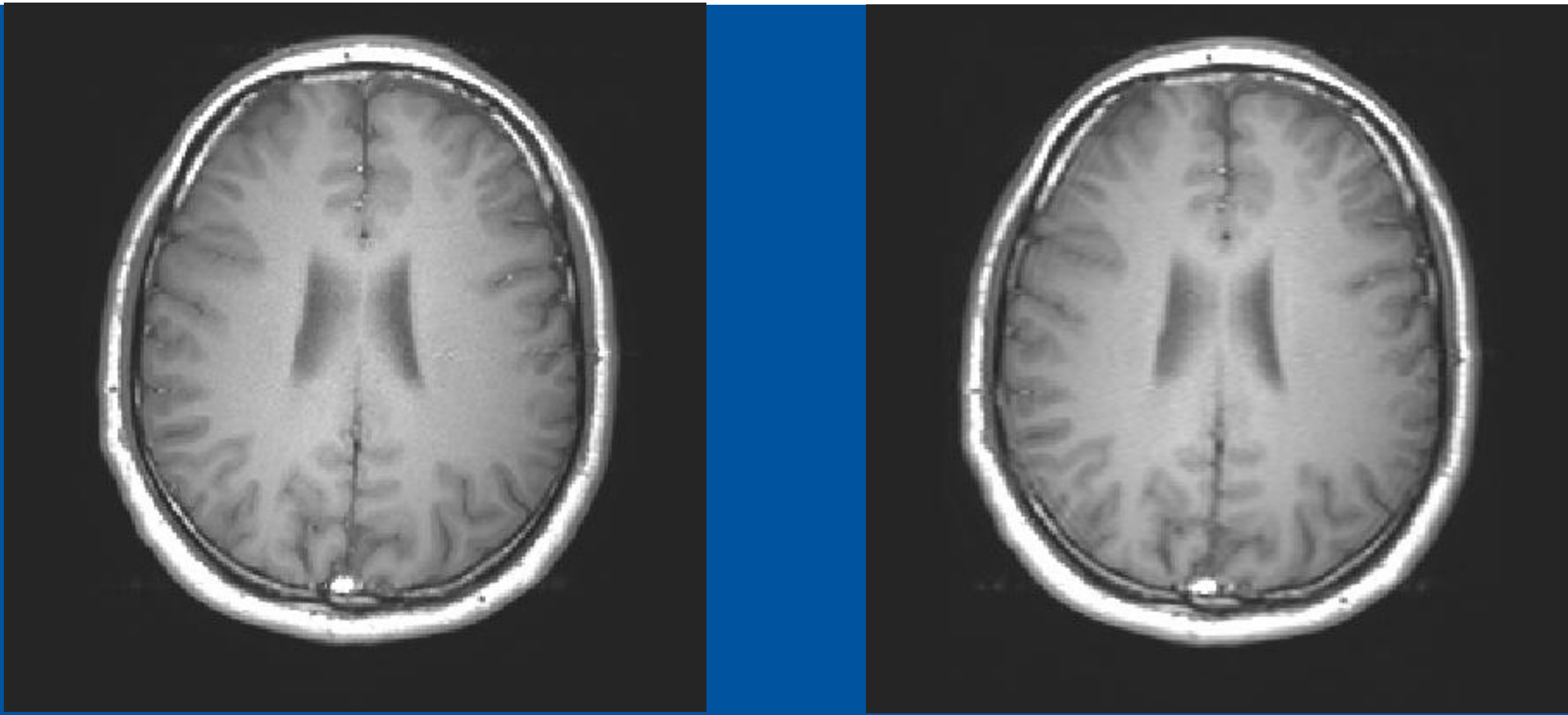

- T_1-weighted SE image of a brain
- What is the difference between the left and right image?

Imaging artifact

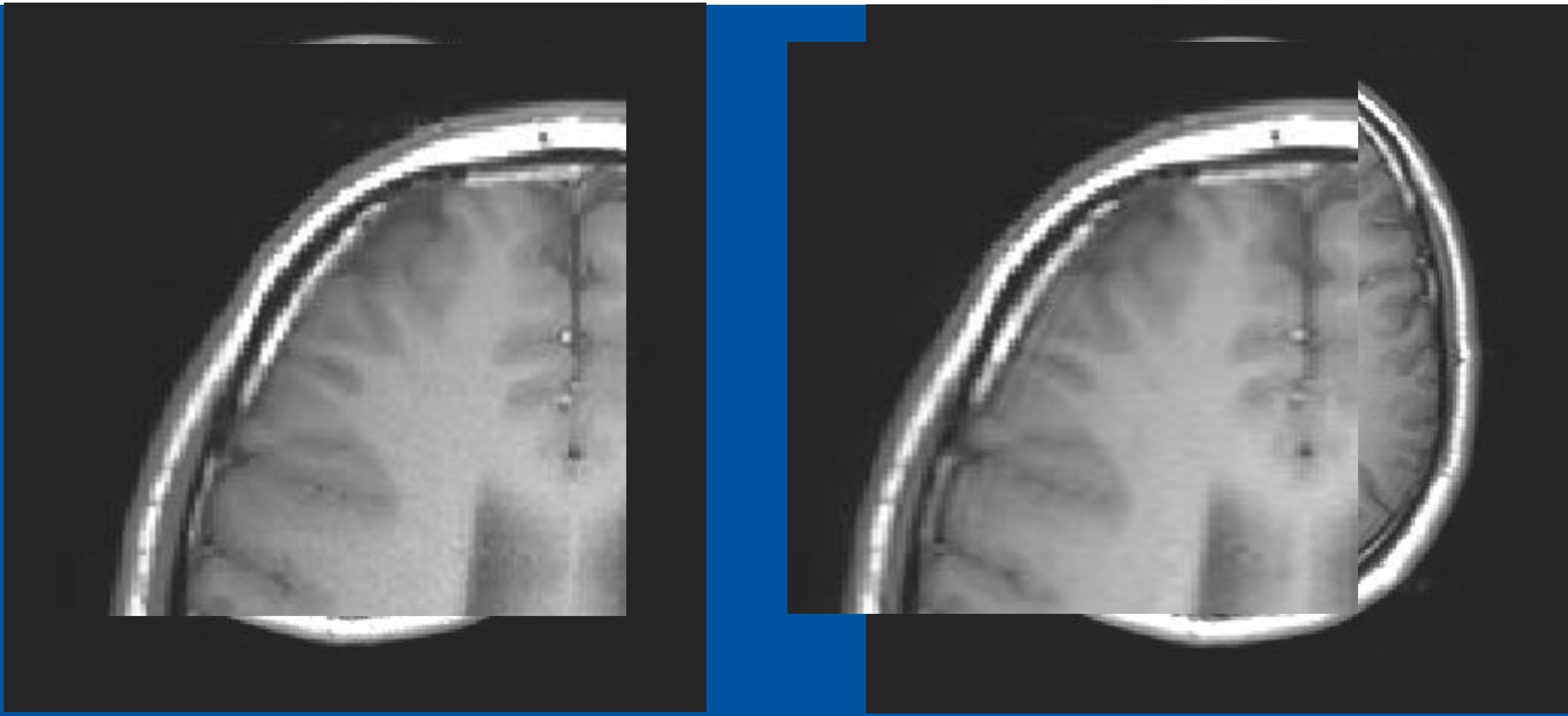

- T_1-weighted SE image of a brain
- What is the difference between the left and right image?

Truncation errors (ringing)

- Imaging sharp edges requires high frequency components in k-space
- Cutting off the high-frequency k-lines causes oscillations in the image

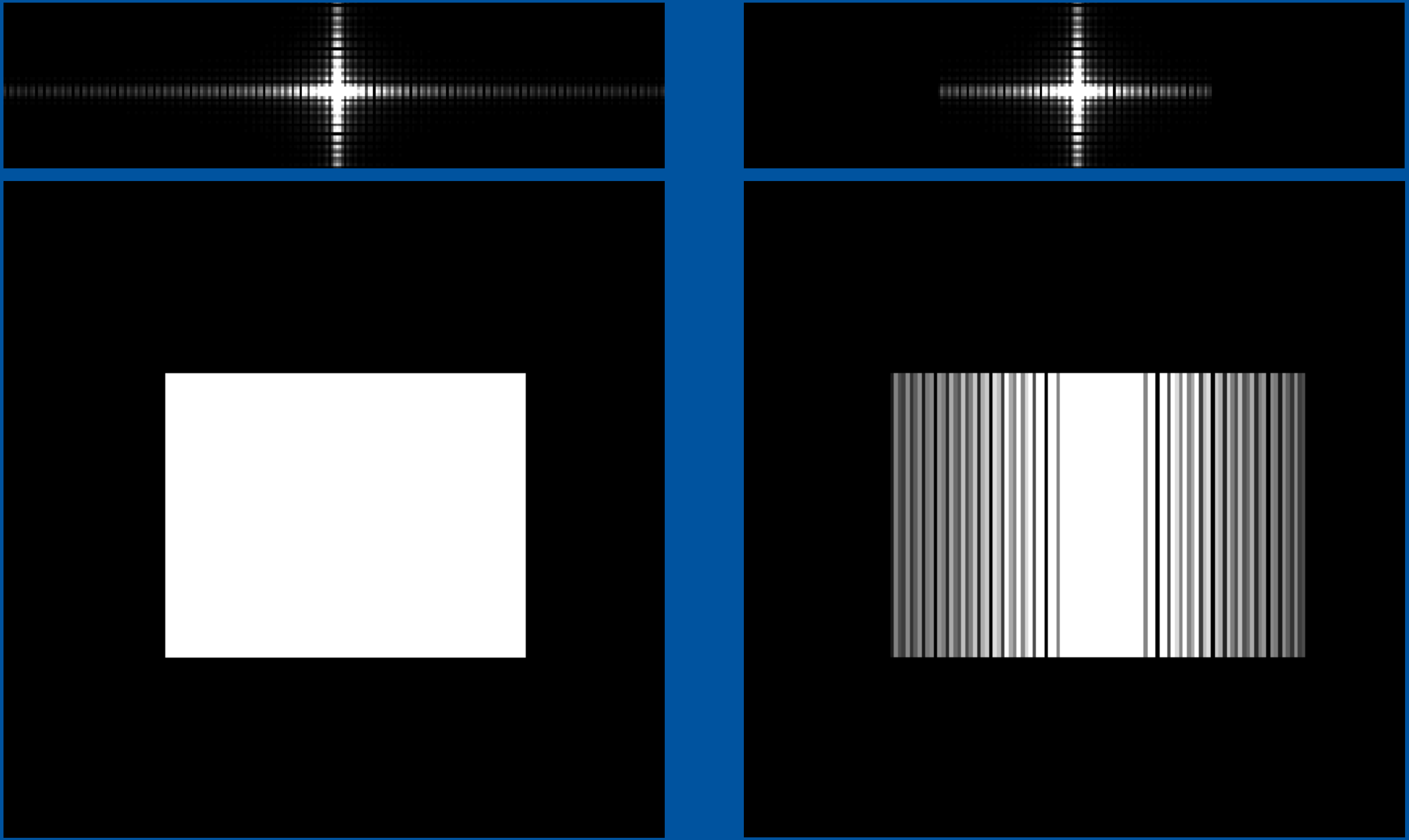

How to avoid truncation errors (Ringing)

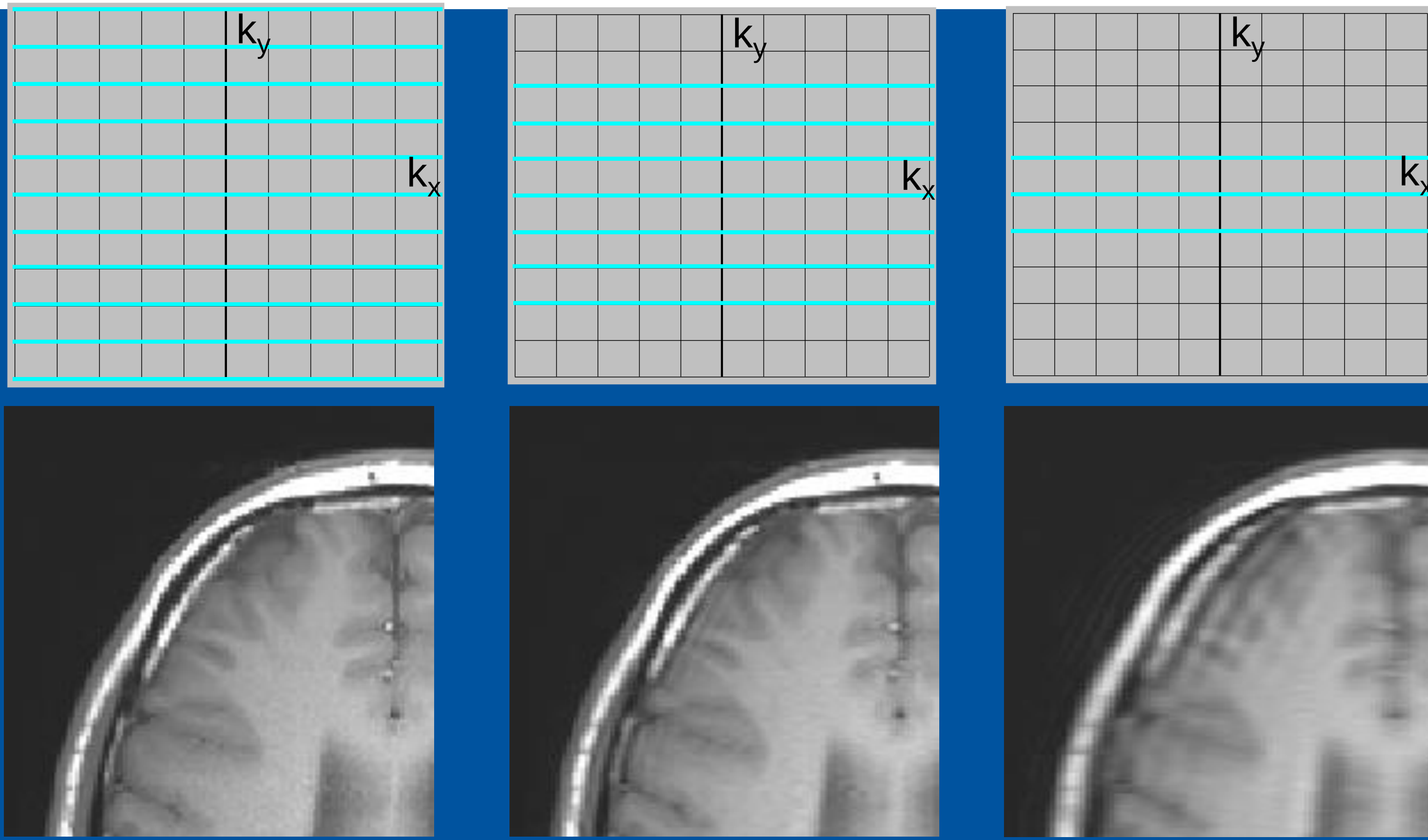

- sample k-space up to sufficiently high frequencies (use sufficiently small voxels during acquisition)
- filtering; the ringing may disappear, but the spatial resolution of the image, and sharpness of edges tends to be compromised

Sampling of k-space

Aliasing/Fold-over artifact:

- Fold-over of signal from outside field-of-view into the image
- Appears in phase-encoding direction

What to do about it:

- Increase FOV in phase-encoding direction
  - (decrease the distance between k-lines)
- Suppress signal from outside FOV

Sampling of k-space

Ringing artifact:

- Oscillating pattern next to sharp edges in an image

What to do about it:

- Decrease voxel size
  - (sample higher k-values)
- Filter the image

Sampling k-space in practice

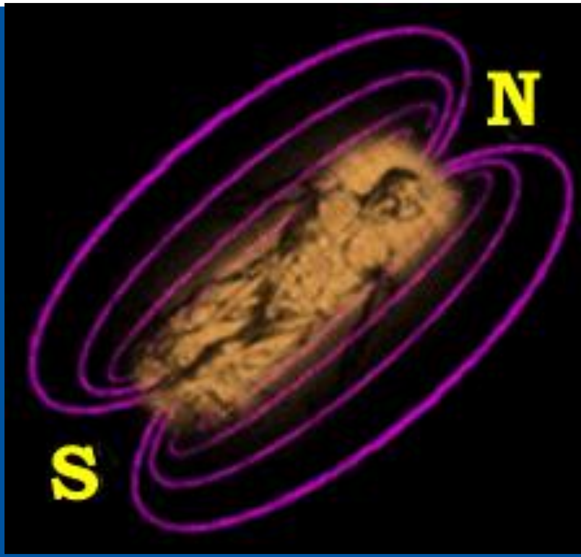

- Let’s assume we sample k-space well. Do we really sample, what we thought we sampled?
- Spatial encoding occurs by switching gradients to modulate frequency and phase
- How can this process lead to artifacts?

$$\omega = \gamma \boldsymbol{B}_0$$

Linear magnetic gradient fields (x, y, z) create spatial differentation of the signals

$\rightarrow$ 3D images

Position encoding in a spin-echo sequence

RF pulse

Slice selection gradient

Phase encoding gradient

Frequency encoding gradient

Signal detection

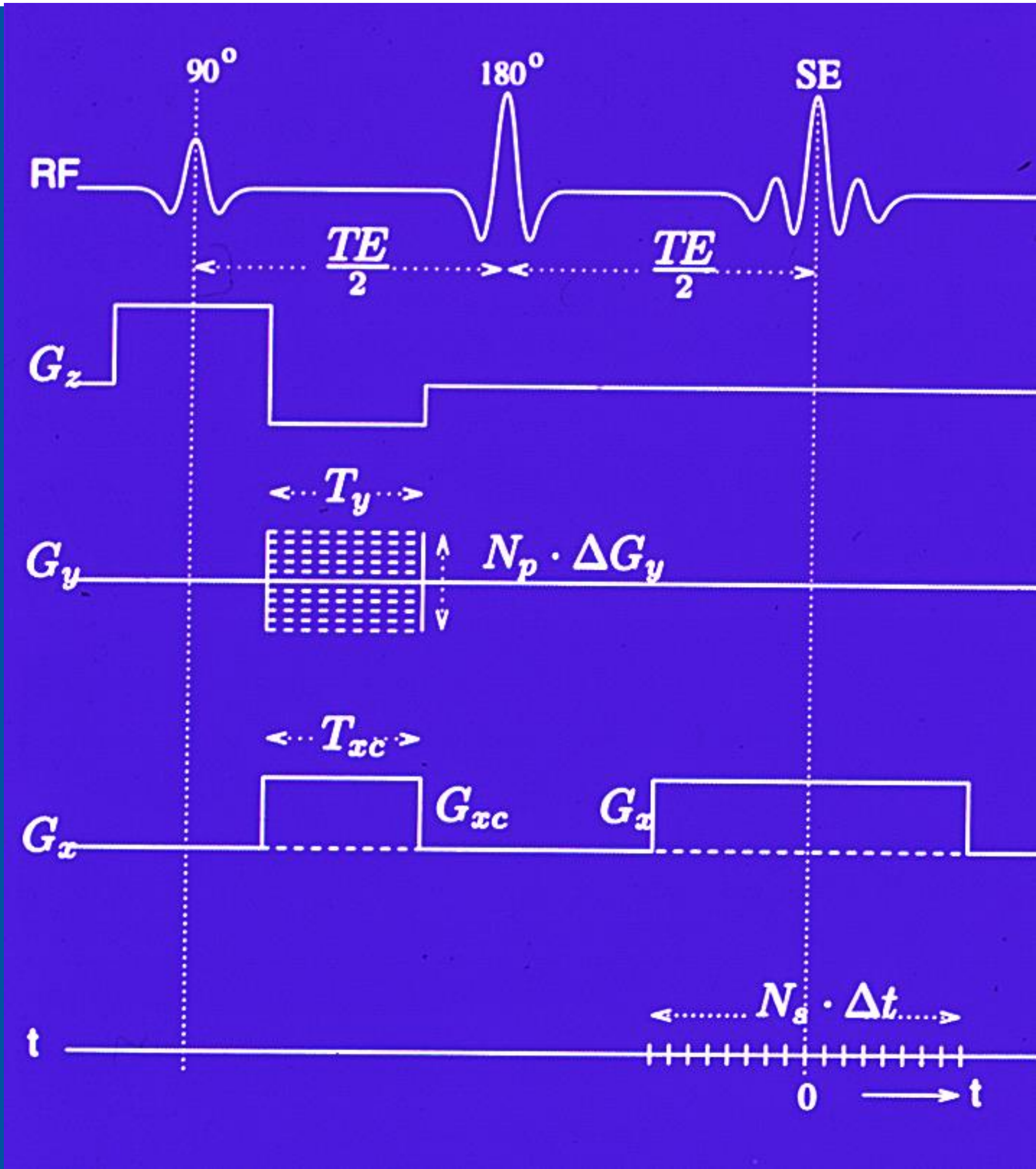
90°
180°
SE
RF
$\frac{TE}{2}$
$\frac{TE}{2}$
G_z
T_y
G_y
$N_p \cdot \Delta G_y$
T_{xc}
G_{xc}
G_x
G_x
t
$N_s \cdot \Delta t$
0
t

Slice selection: transversal

Resonance condition

$$\omega = \gamma (B_0 + zG_z)$$

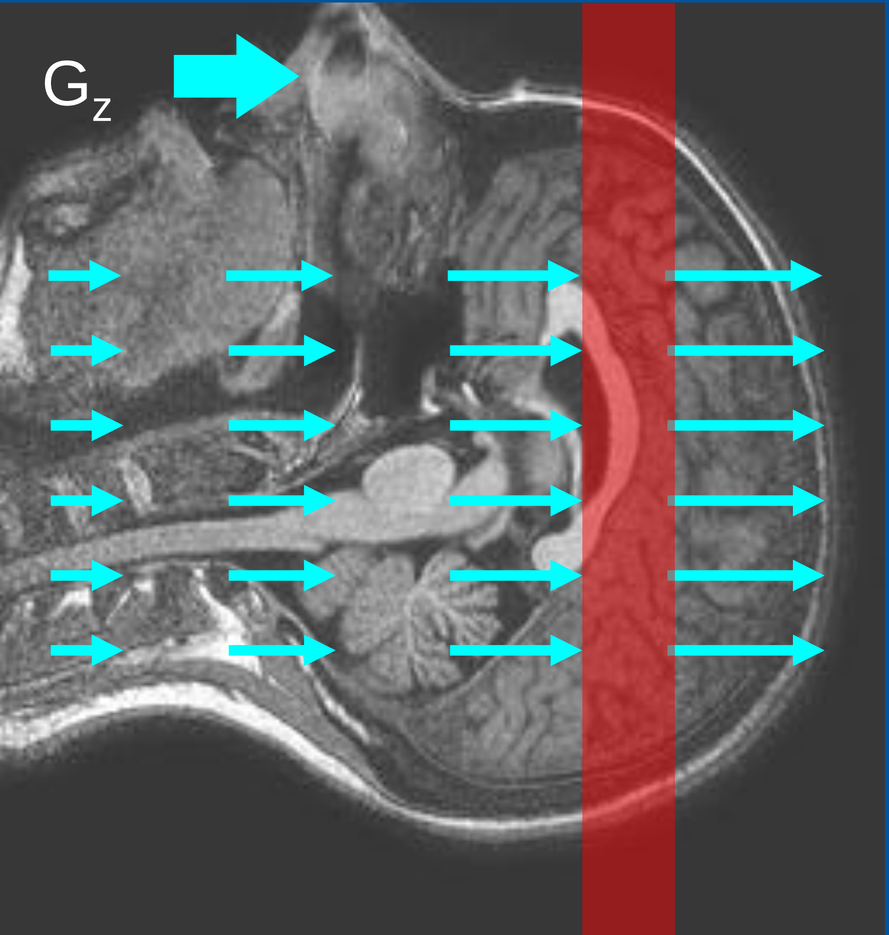

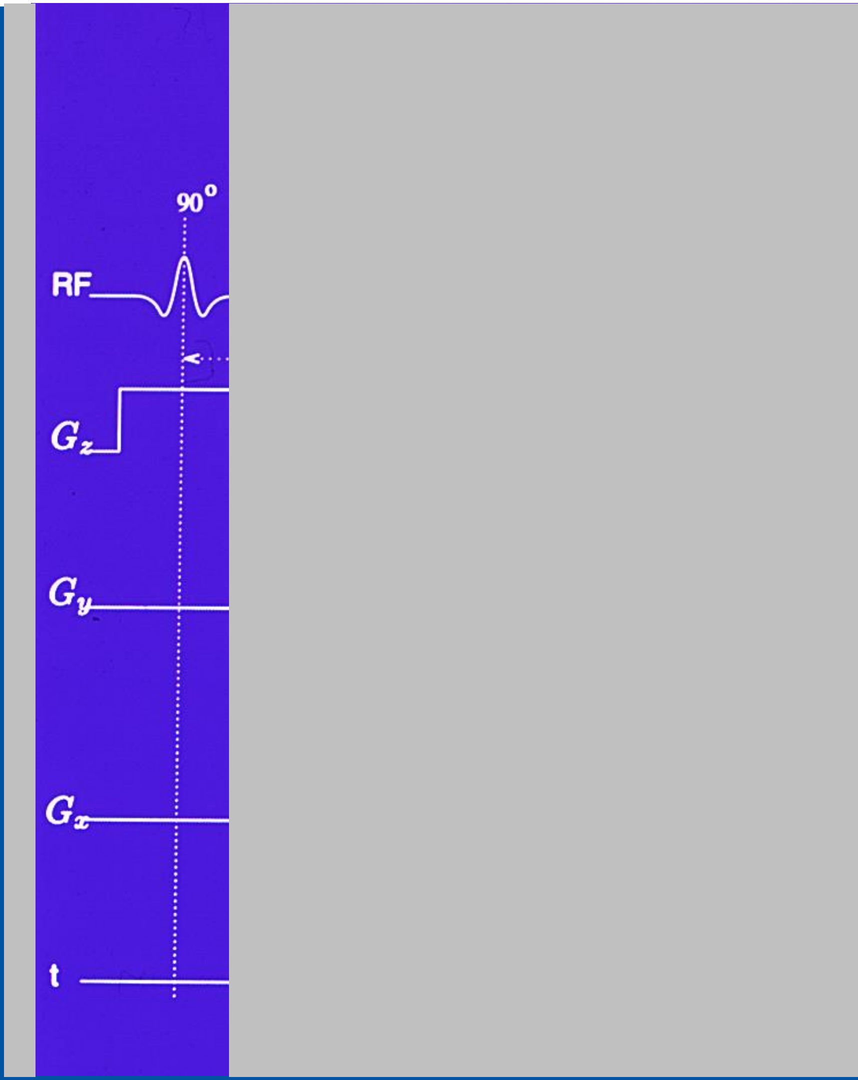
90°
RF
G_z
G_y
G_x
t

Phase encoding

Apply gradient after RF pulse and before read-out

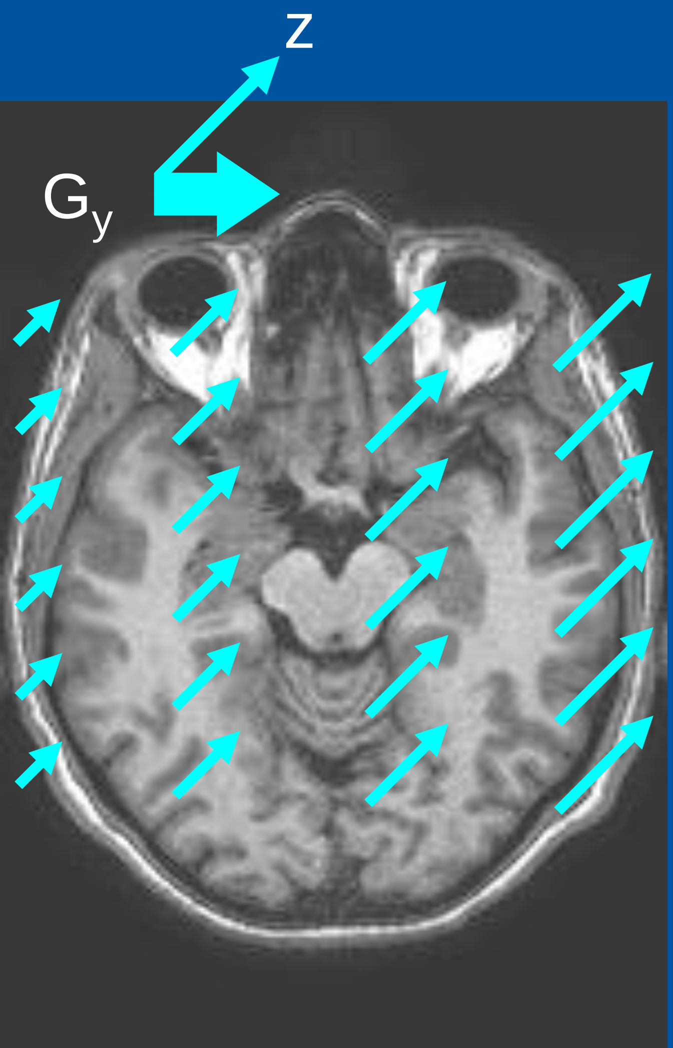

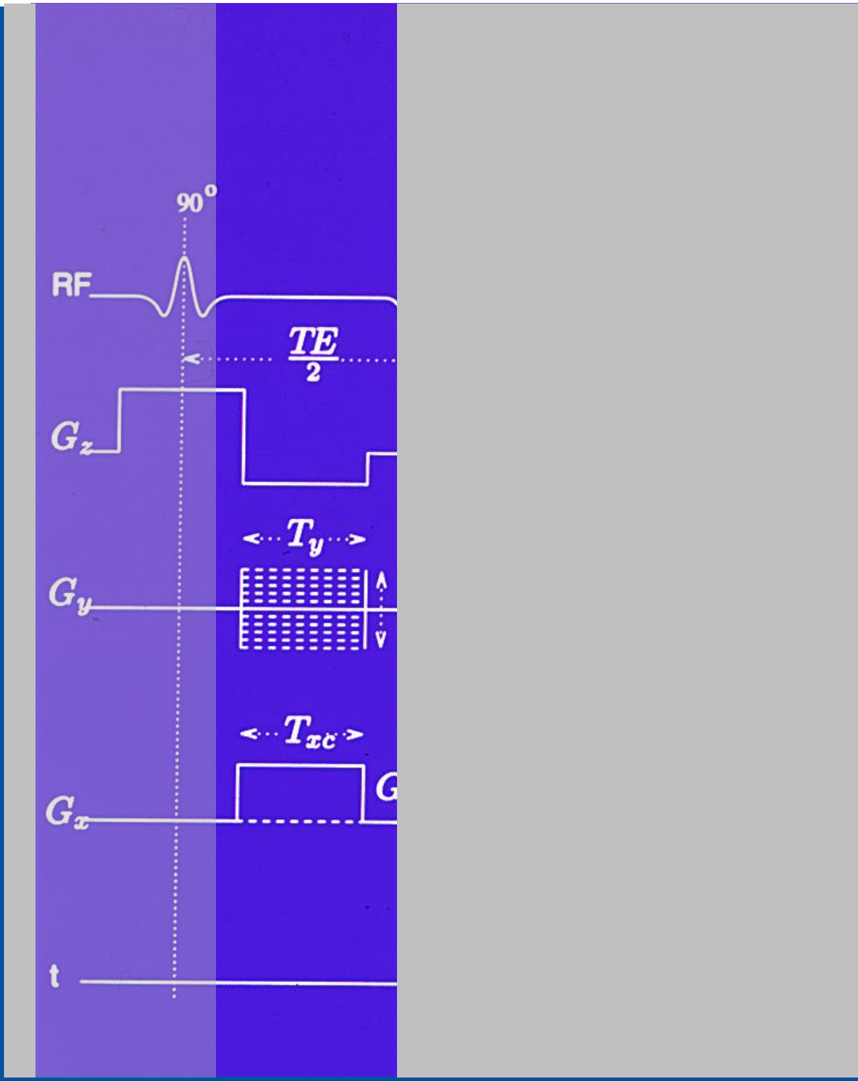
90°
RF
$\frac{TE}{2}$
G_z
T_y
G_y
T_{xc}
G_x
G
t

Phase encoding

$$\omega = \gamma B_0$$

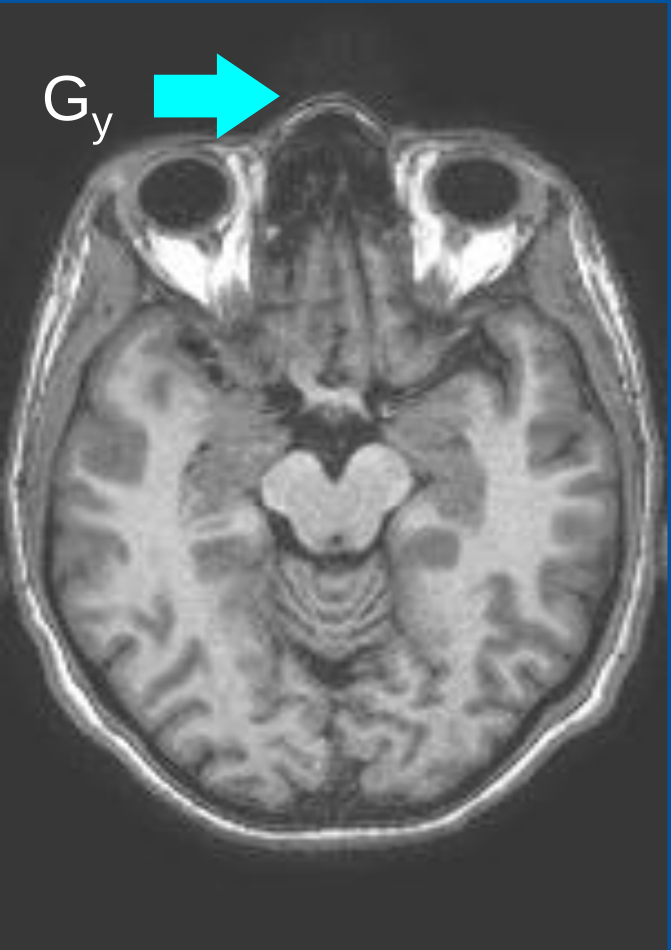

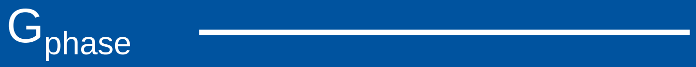

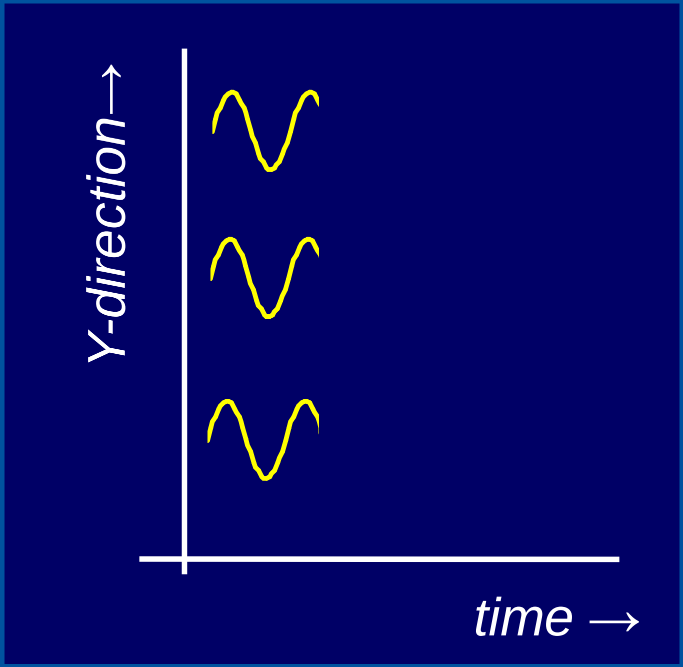
Y-direction ⟶
time ⟶

Phase encoding

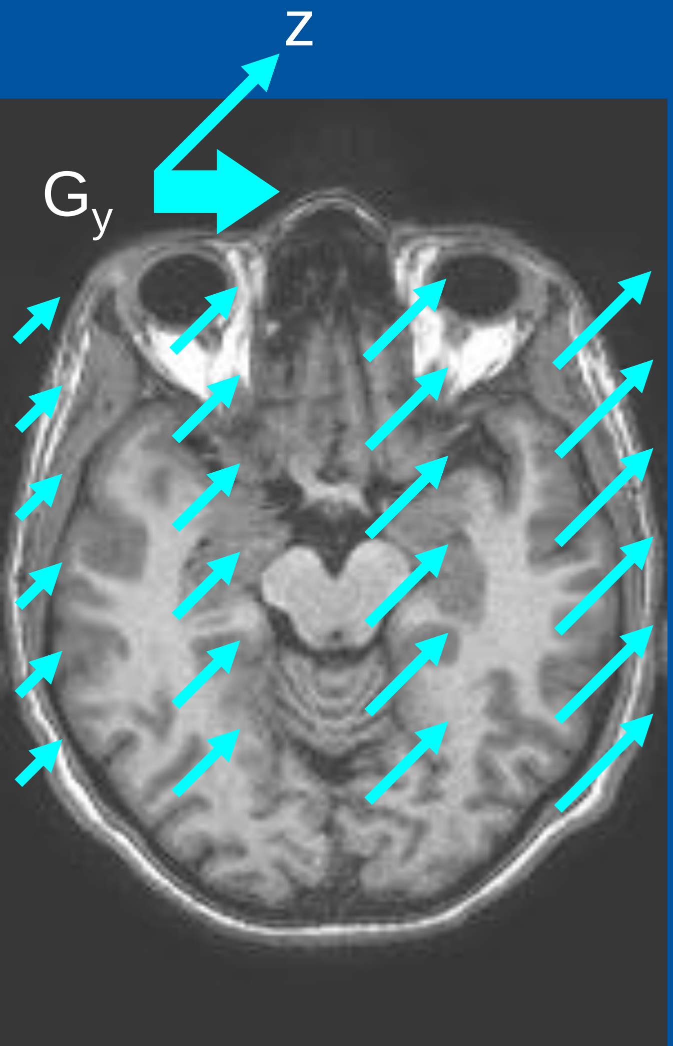

$$\omega = \gamma\,(B_0+yG_y)$$

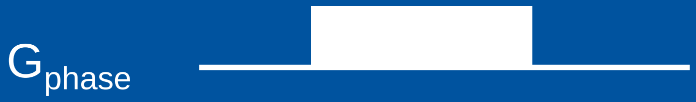

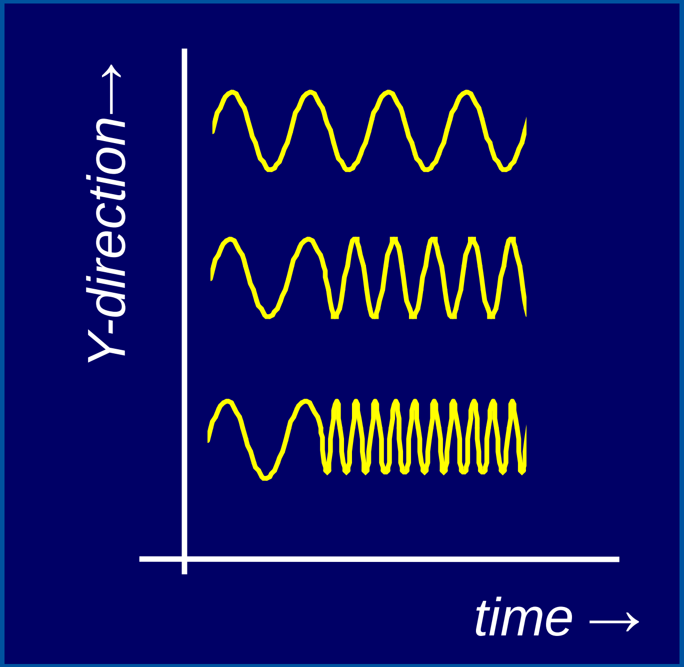
Y-direction ⟶
time ⟶

Phase encoding

$$\omega = \gamma B_0$$

G_{phase}

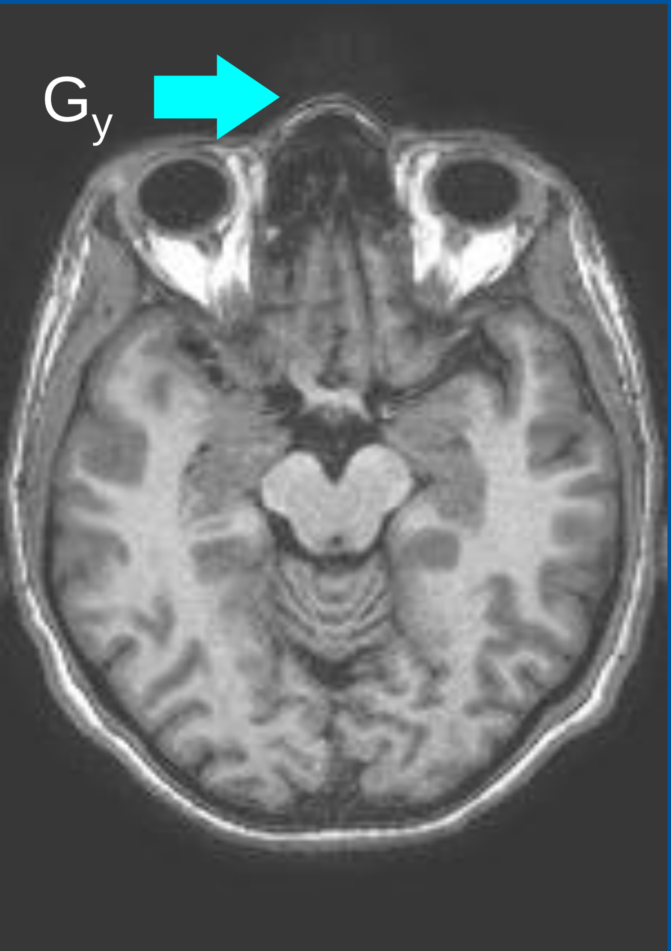

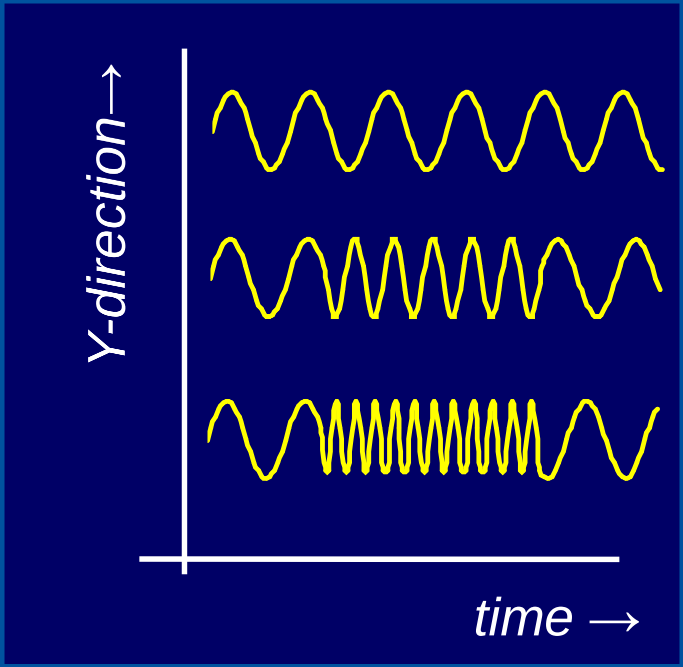
Y-direction→
time →

Frequency encoding (read-out)

Apply gradient during read-out

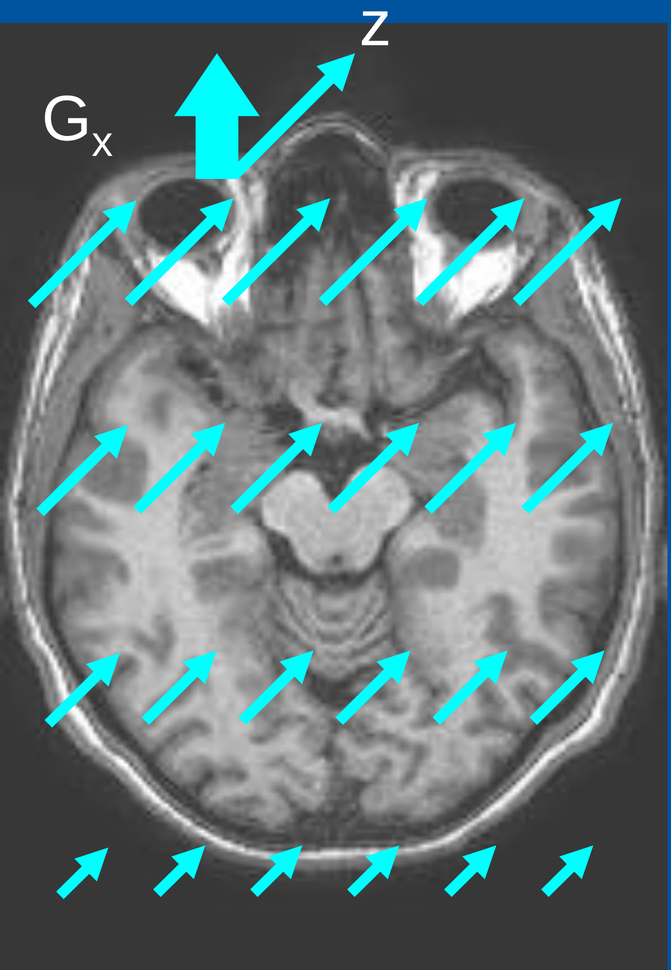

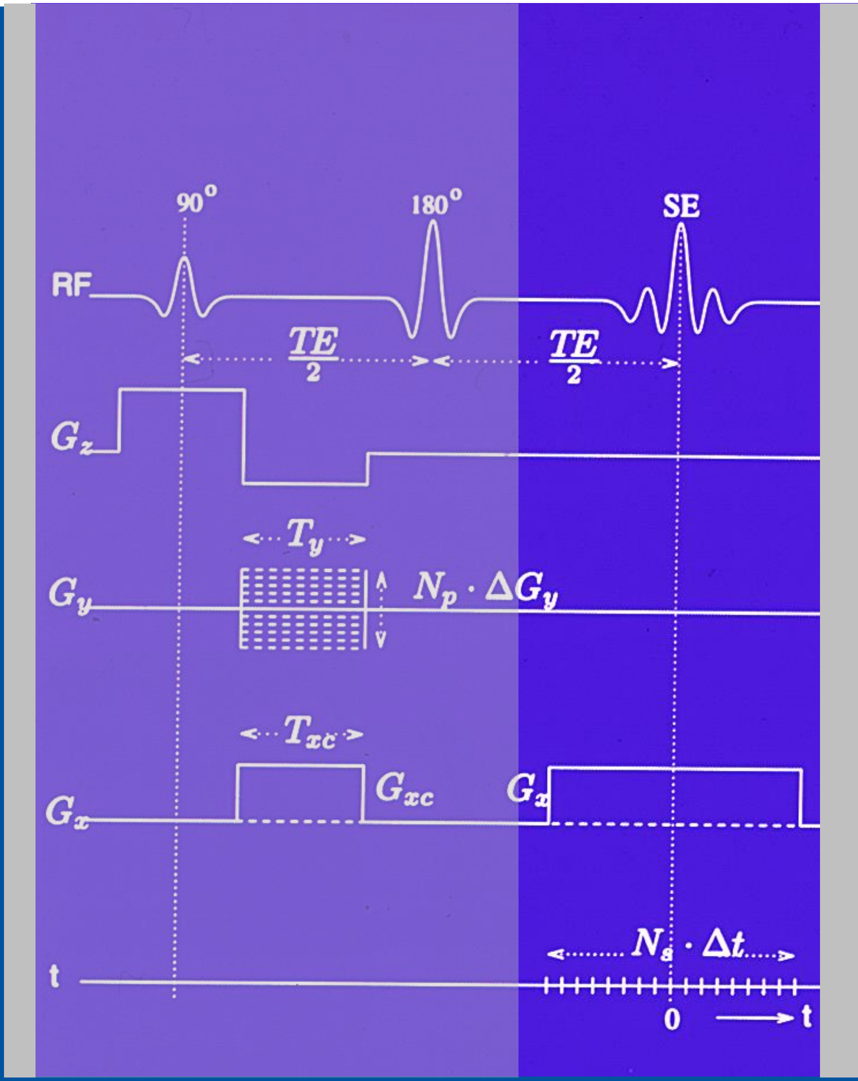
90°
180°
SE
RF
$\frac{TE}{2}$
$\frac{TE}{2}$
G_z
T_y
G_y
$N_p \cdot \Delta G_y$
T_{xc}
G_{xc}
G_x
G_x
$N_s \cdot \Delta t$
t
0
t

Frequency encoding (read-out)

$$\omega = \gamma\,(B_0 + xG_x)$$

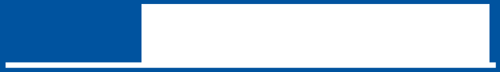

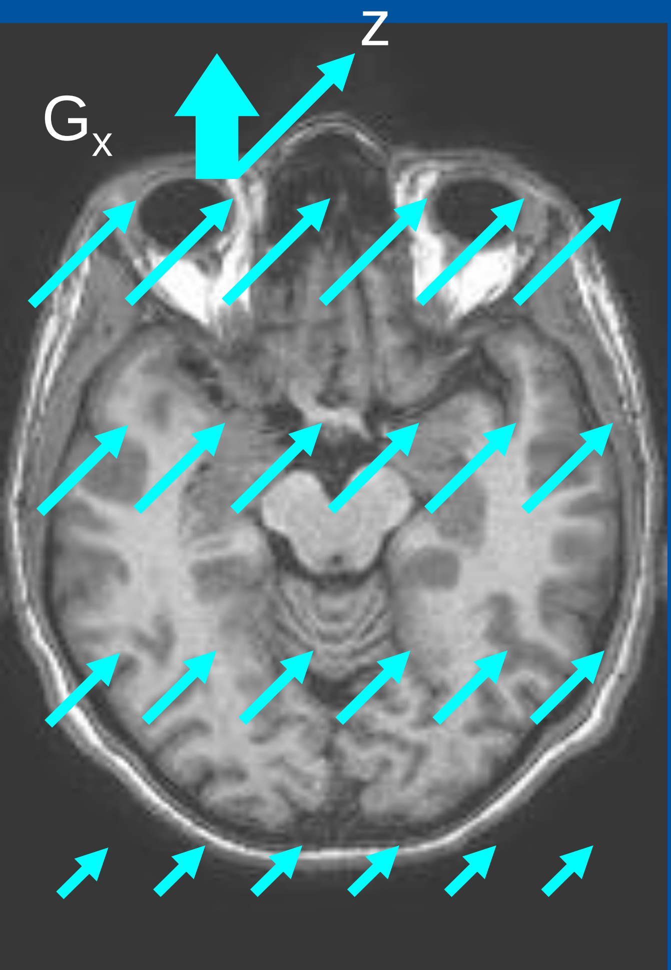

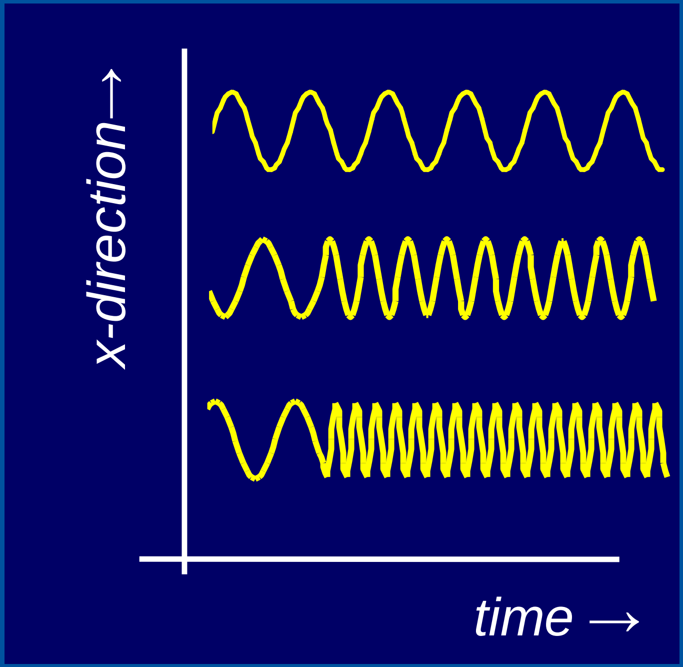
x-direction →
time →

Position encoding in a spin-echo sequence

2D Fourier transform imaging

nth time sample of the signal after the mth phase encoding step:

$$S(n,m) = \int_{-\infty}^{\infty}\int_{-\infty}^{\infty}\int_{-\infty}^{\infty} A(x,y,z)\, e^{i\Phi(x,y,z,n,m)}\, \mathrm{d}x\, \mathrm{d}y\, \mathrm{d}z,$$

Discrete 2D inverse Fourier transformation:

$$A'(u,v) = \sum_{n=-\frac{N_s}{2}}^{\frac{N_s}{2}-1} \sum_{m=-\frac{N_p}{2}}^{\frac{N_p}{2}-1} S(n,m)\, e^{-i\Phi(u,v,n,m)},$$

with

$$n \in [-\tfrac{N_s}{2}, \tfrac{N_s}{2} - 1] \text{ and } m \in [-\tfrac{N_p}{2}, \tfrac{N_p}{2} - 1].$$

gives complex image *A'(u,v).*

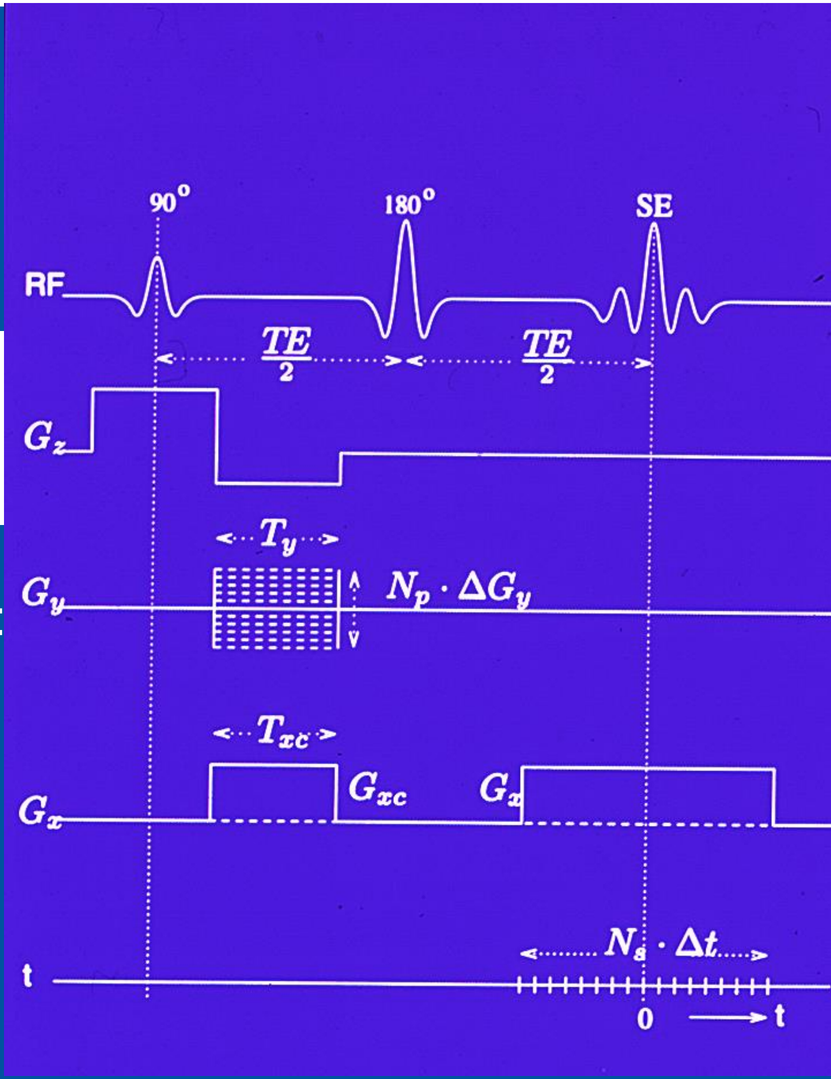
90°
180°
SE
RF
$\frac{TE}{2}$
$\frac{TE}{2}$
G_z
T_y
G_y
$N_p \cdot \Delta G_y$
T_{xc}
G_{xc}
G_x
G_x
$N_s \cdot \Delta t$
t
0
t

A spin-echo sequence in k-space

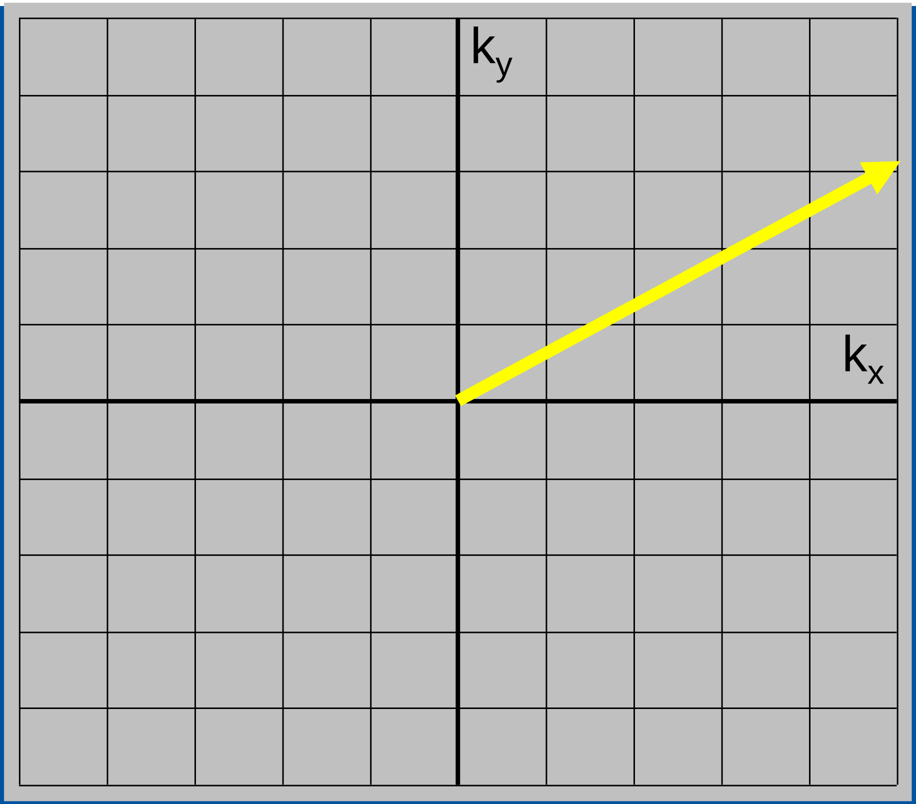

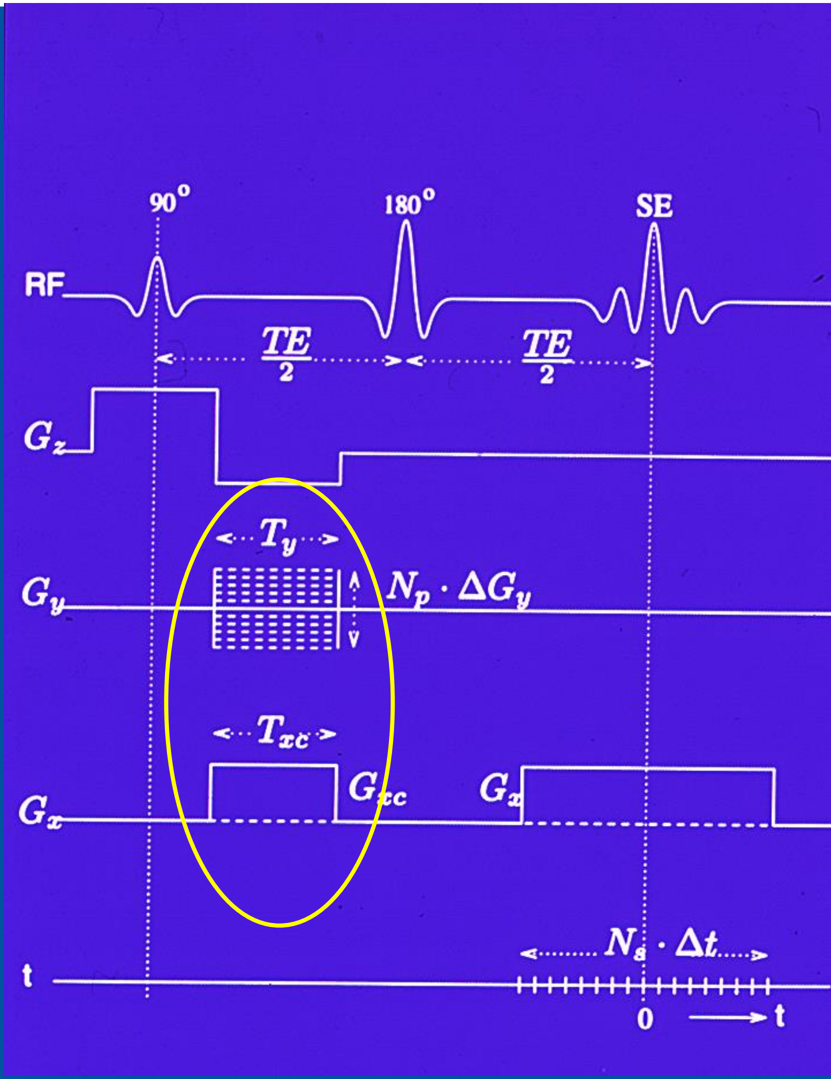
90°
180°
SE
RF
$\frac{TE}{2}$
$\frac{TE}{2}$
G_z
T_y
G_y
$N_p \cdot \Delta G_y$
T_{xc}
G_x
G_{xc}
G_x
$N_s \cdot \Delta t$
t
0
t

A spin-echo sequence in k-space

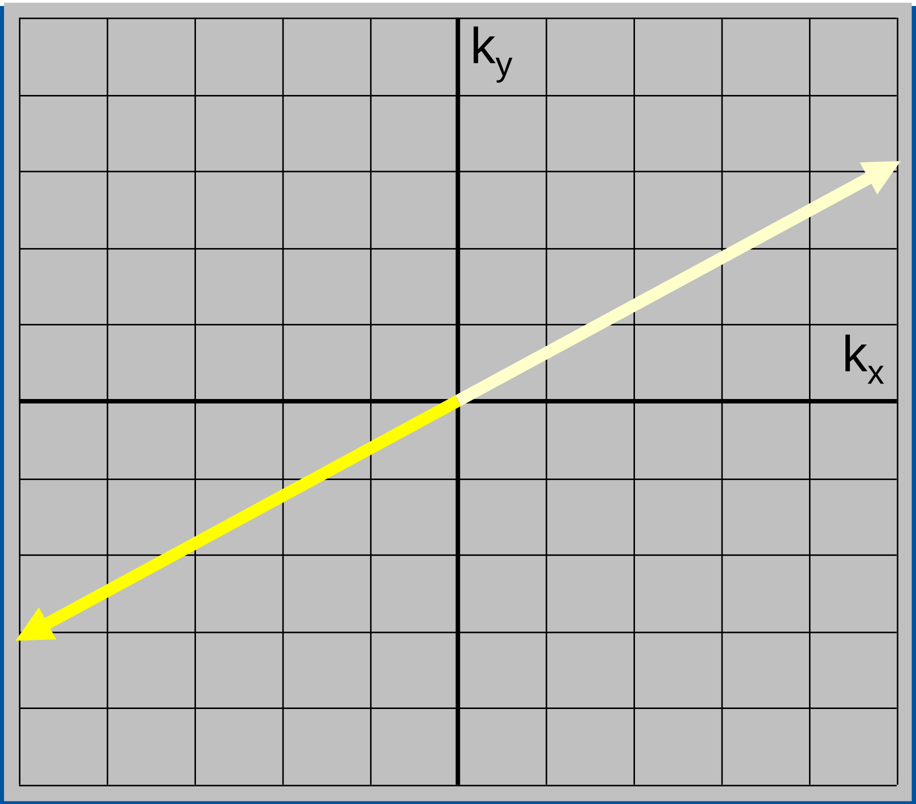

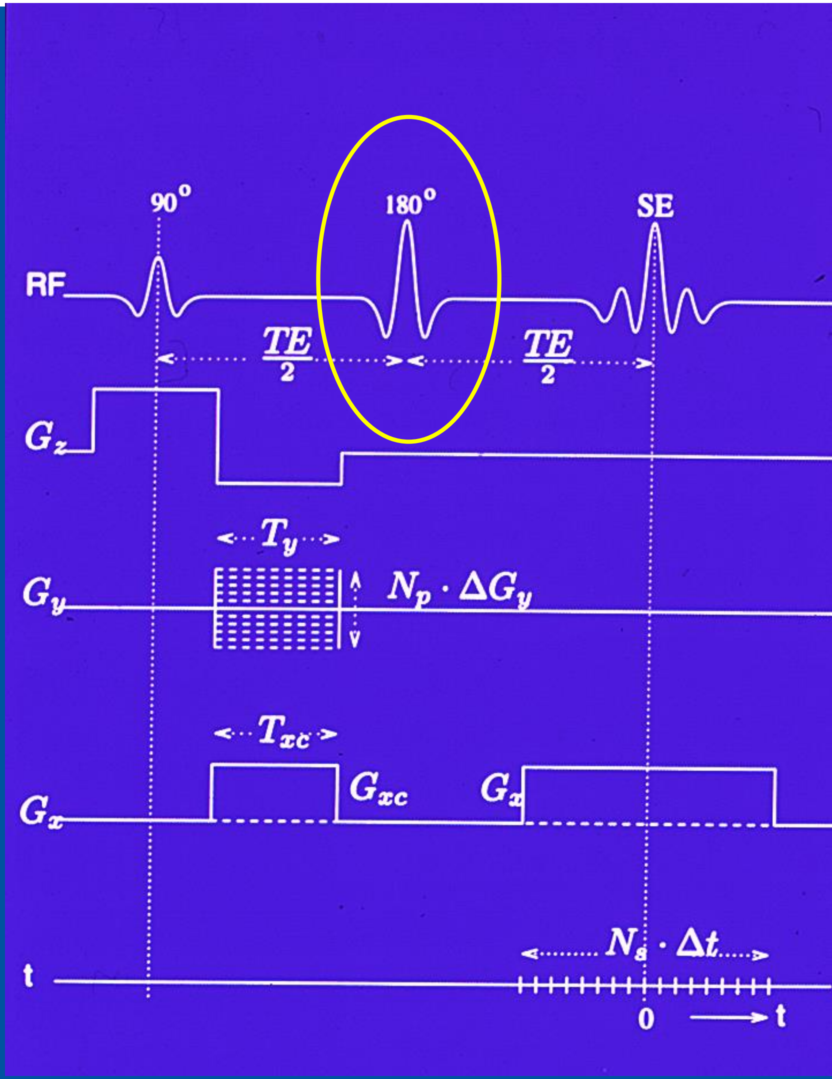
RF
90°
180°
SE
$\frac{TE}{2}$
$\frac{TE}{2}$
G_z
T_y
G_y
$N_p \cdot \Delta G_y$
T_{xc}
G_{xc}
G_x
G_x
$N_s \cdot \Delta t$
t
0
t

A spin-echo sequence in k-space

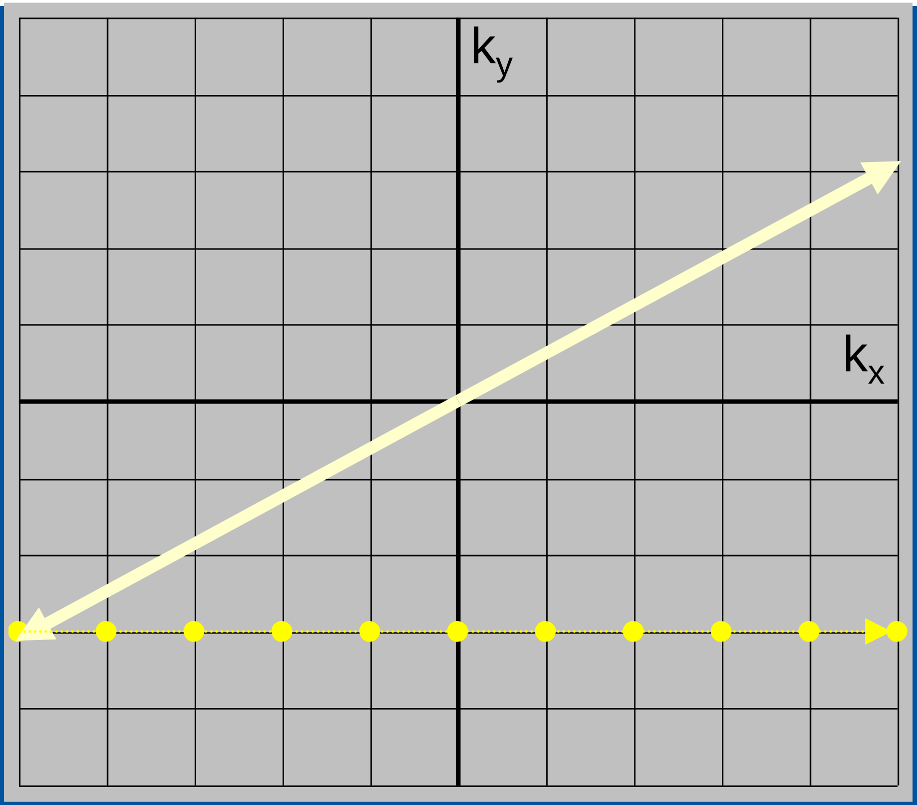

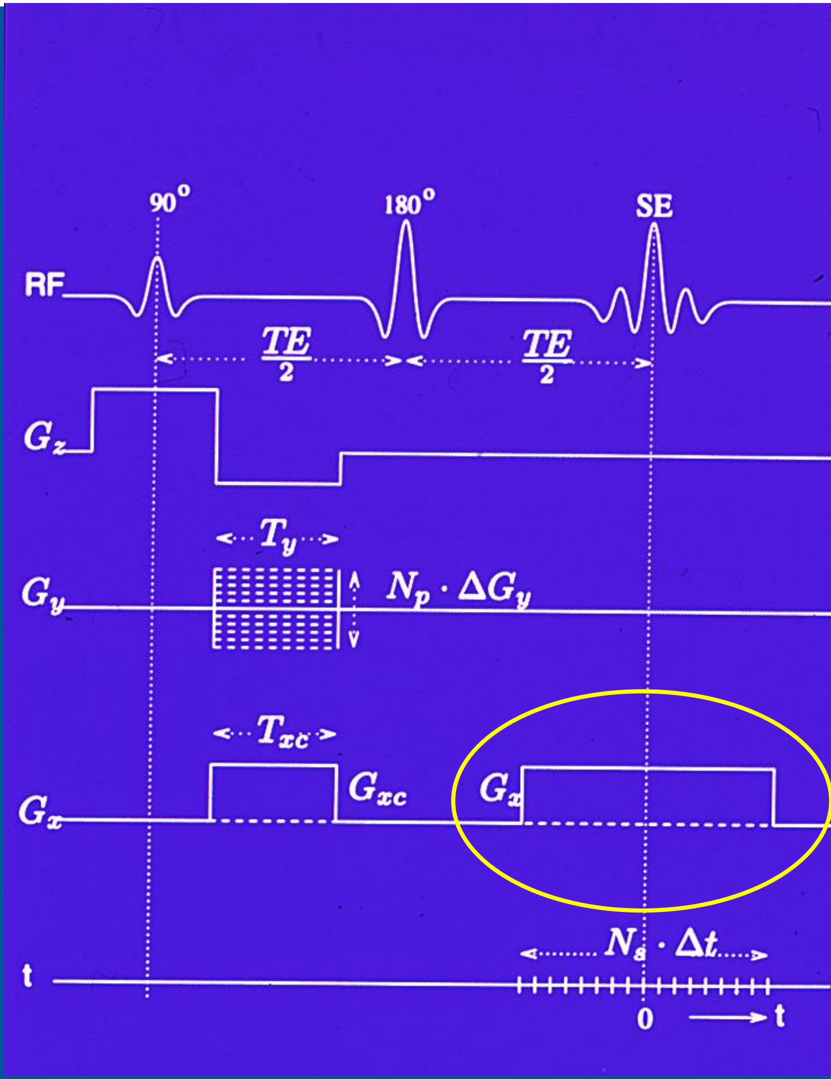

90°
180°
SE
RF
$\frac{TE}{2}$
$\frac{TE}{2}$
G_z
T_y
G_y
$N_p \cdot \Delta G_y$
T_{xc}
G_{xc}
G_x
G_x
$N_s \cdot \Delta t$
t
0
t

Phase evolution

$$\Phi_0(t) = \omega_0 t$$

- The phase shift depends on the strength and duration of the gradient applied;

$$\Delta\Phi(T) = \Delta\omega T = \gamma\Delta B T$$

- For the phase-encoding (y) and read-out (x) gradients, this means:

$$\Delta\Phi_m = \gamma y m \Delta G_y T_y$$

and

$$\Delta\Phi_n = \gamma x G_x n \Delta T_x$$

- In a spin-echo sequence, the spins flip 180° during the 180° pulse. Thus, a phase difference created before the 180° pulse has the opposite effect during read-out

Phase evolution

$$\Phi(x,y,z,n,m) = -\gamma x G_{xc} T_{xc} + \gamma x G_x (n + \frac{N_s}{2}) \Delta t - \gamma y m \Delta G_y T_y.$$

With a balanced read-out gradient:

$$-G_{xc} T_{xc} + G_x \Delta t \tfrac{N_s}{2} = 0,$$

And in the absence of field inhomogeneities:

$$\Phi(x,y,z,n,m) = \gamma x G_x n \Delta t - \gamma y m \Delta G_y T_y.$$

with

$$n \in [-\tfrac{N_s}{2}, \tfrac{N_s}{2} - 1] \text{ and } m \in [-\tfrac{N_p}{2}, \tfrac{N_p}{2} - 1].$$

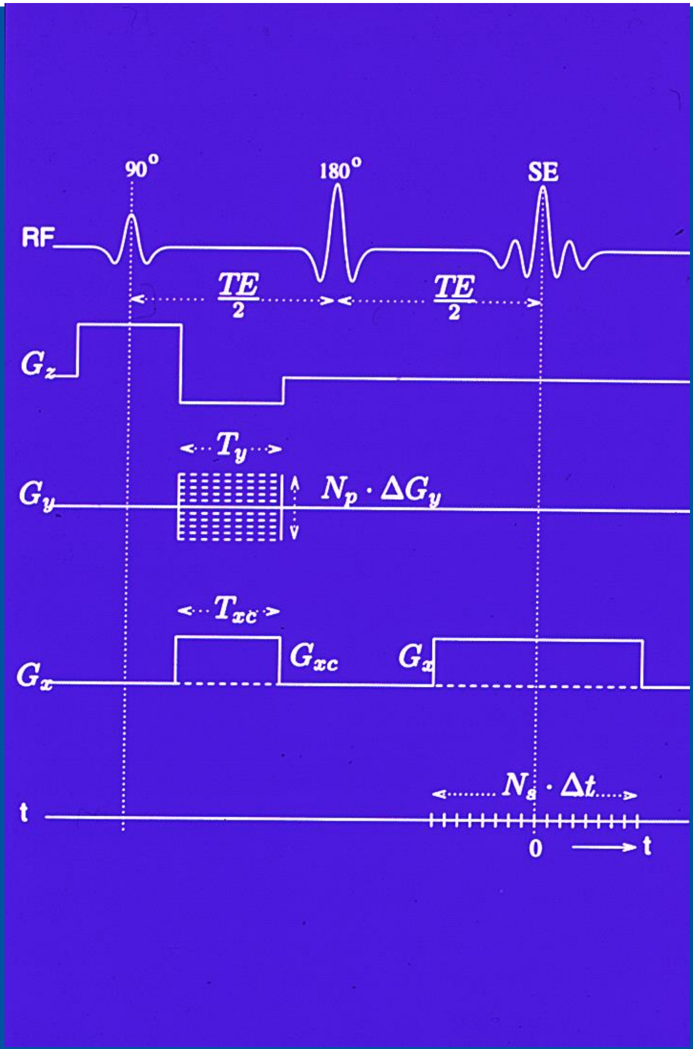
90°
180°
SE
RF
$\frac{TE}{2}$
$\frac{TE}{2}$
G_z
T_y
G_y
$N_p \cdot \Delta G_y$
T_{xc}
G_{xc}
G_x
G_x
$N_s \cdot \Delta t$
t
0
t

echo centered in the acquisition window at *t=0* (*n=0, m=0*)

A spin-echo sequence in k-space

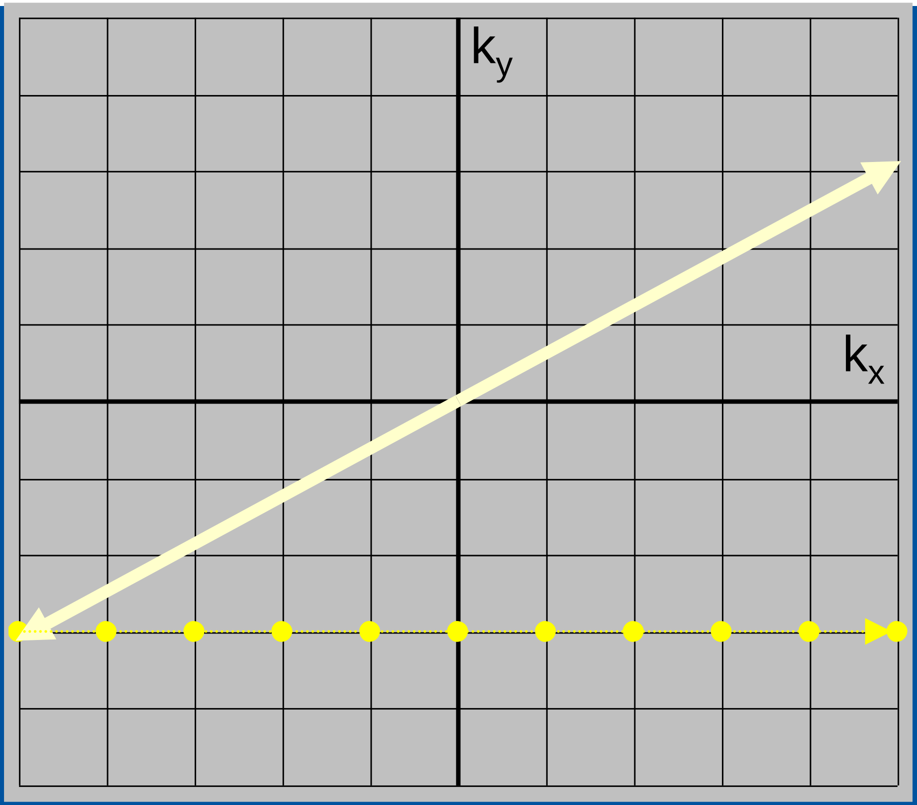

$$k_y = \gamma y m \Delta G_y T_y$$

$$k_x = \gamma x G_x n \Delta T_x$$

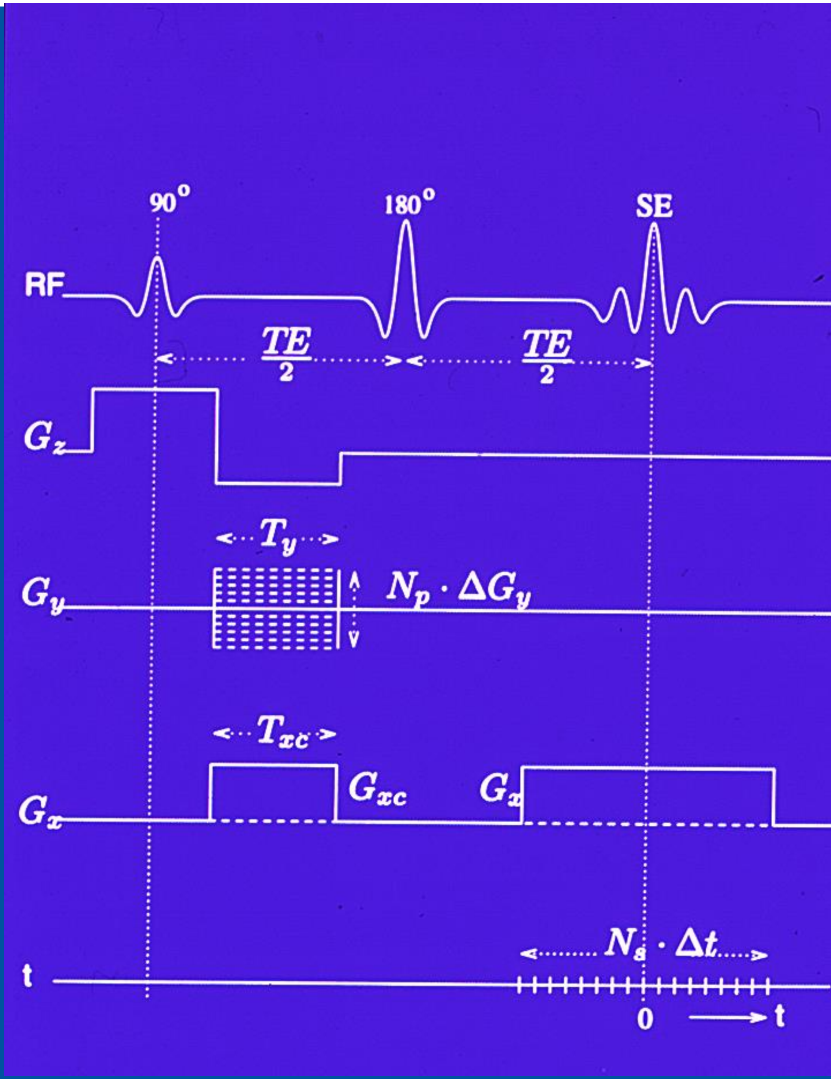
90°
180°
SE
RF
$\frac{TE}{2}$
$\frac{TE}{2}$
G_z
T_y
G_y
$N_p \cdot \Delta G_y$
T_{xc}
G_{xc}
G_x
G_x
$N_s \cdot \Delta t$
t
0
t

Do we really sample k-space the way we think we do?

Many reasons why the phase evolution can be distorted

- Hardware
  - non-linear gradients
- Patient
  - chemical shift
  - Susceptibility

Imperfections of B_0 and gradient fields

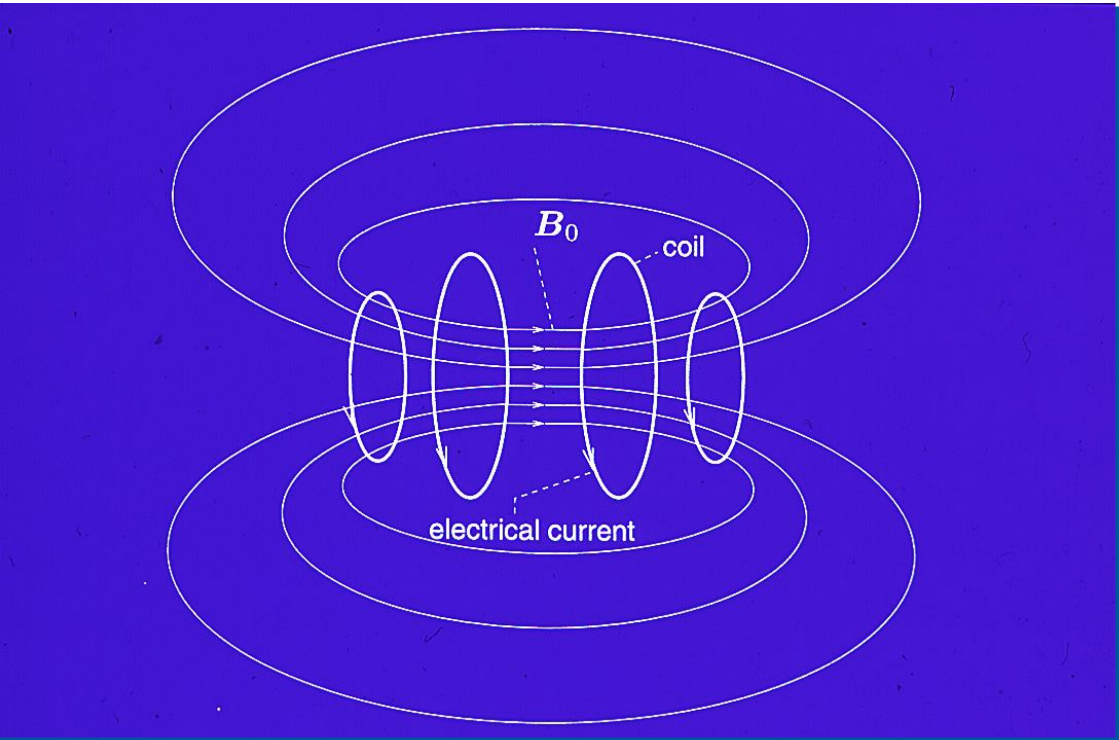

Imperfect magnetic field homogeneity:

- divergence of the magnetic field lines at the end of the coil
- imperfect winding the superconducting wire
- variations of current densities in the wire
- Distortion of the magnetic field by metal close to the scanner

Non-linear gradients cause position distortions

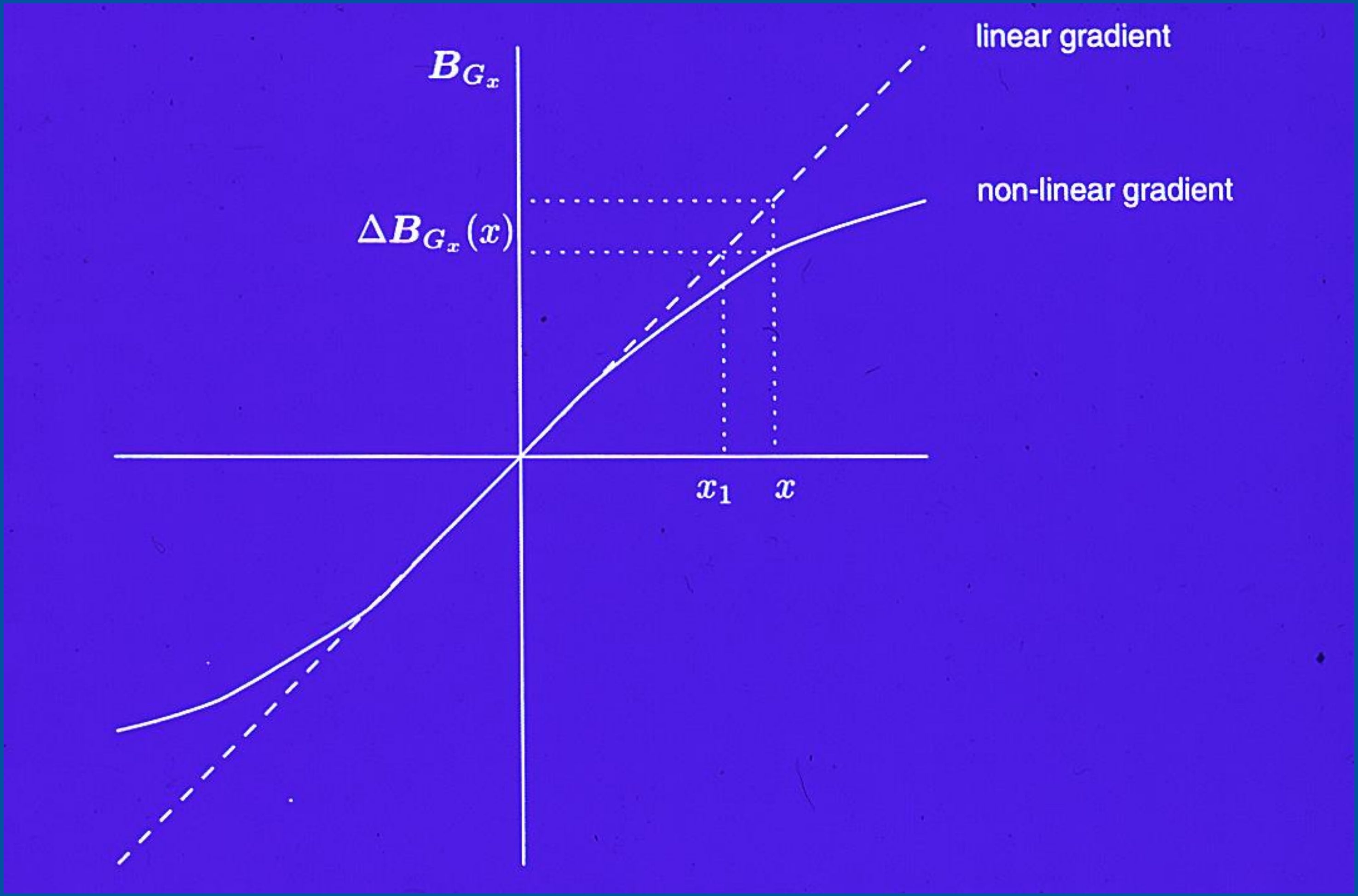
linear gradient
B_{G_x}
non-linear gradient
$\Delta B_{G_x}(x)$
x_1
x

Magnetic susceptibility

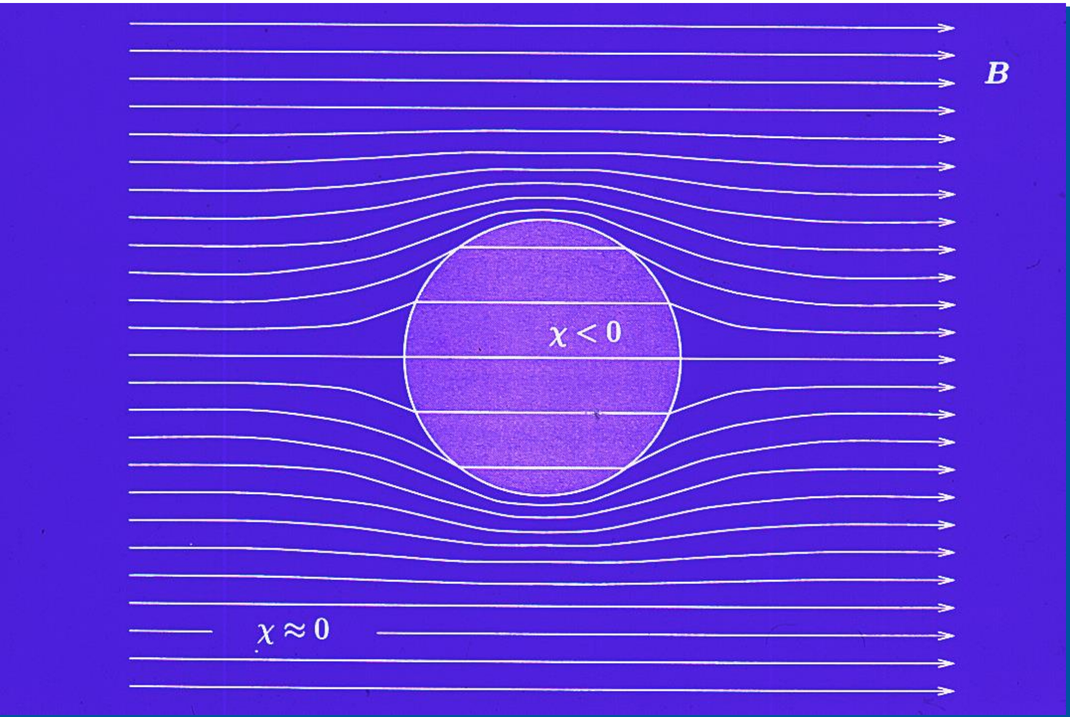

Magnetic susceptibility χ : M=χH

M = magnetization, H = magnetic field

- diamagnetic materials: χ< 0 (tissues ca. -9.10^{-6})
- paramagnetic materials: χ > 0
- ferromagnetic materials: very large susceptibility
- air: χ = 0

Water-fat shift

Magnetic field at the nucleus depends on magnetic shielding of surrounding electron clouds, depends on molecular environment

example:
resonant frequencies of protons in fat and water differ by 3.4 ppm

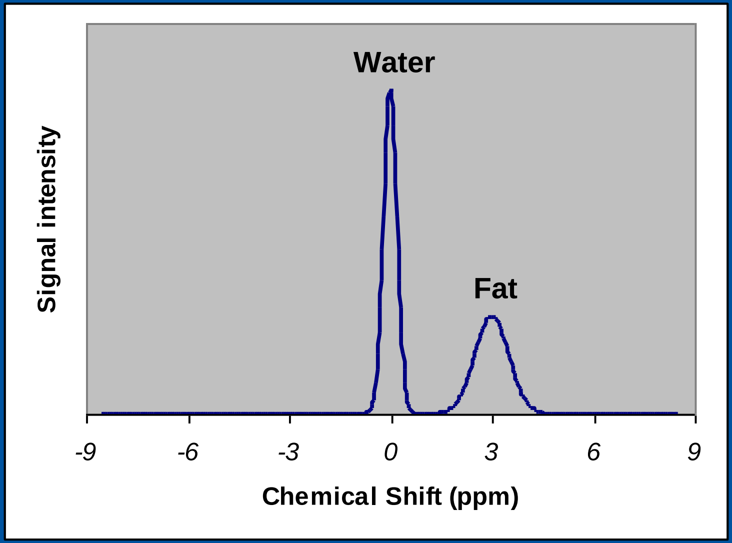

Erroneous sampling of k-space

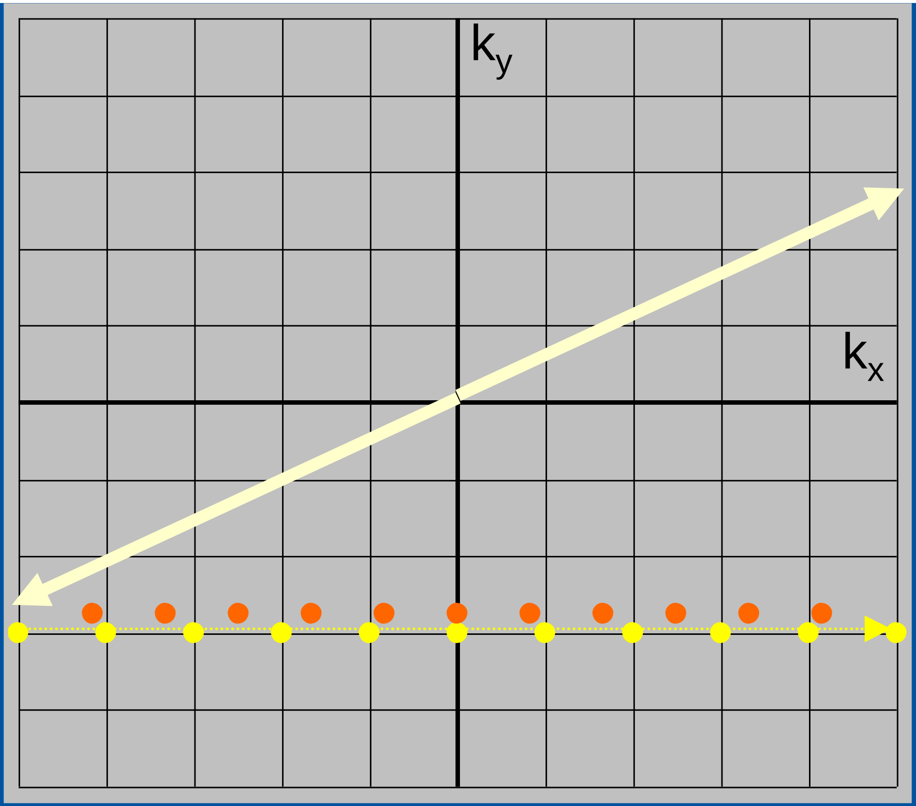

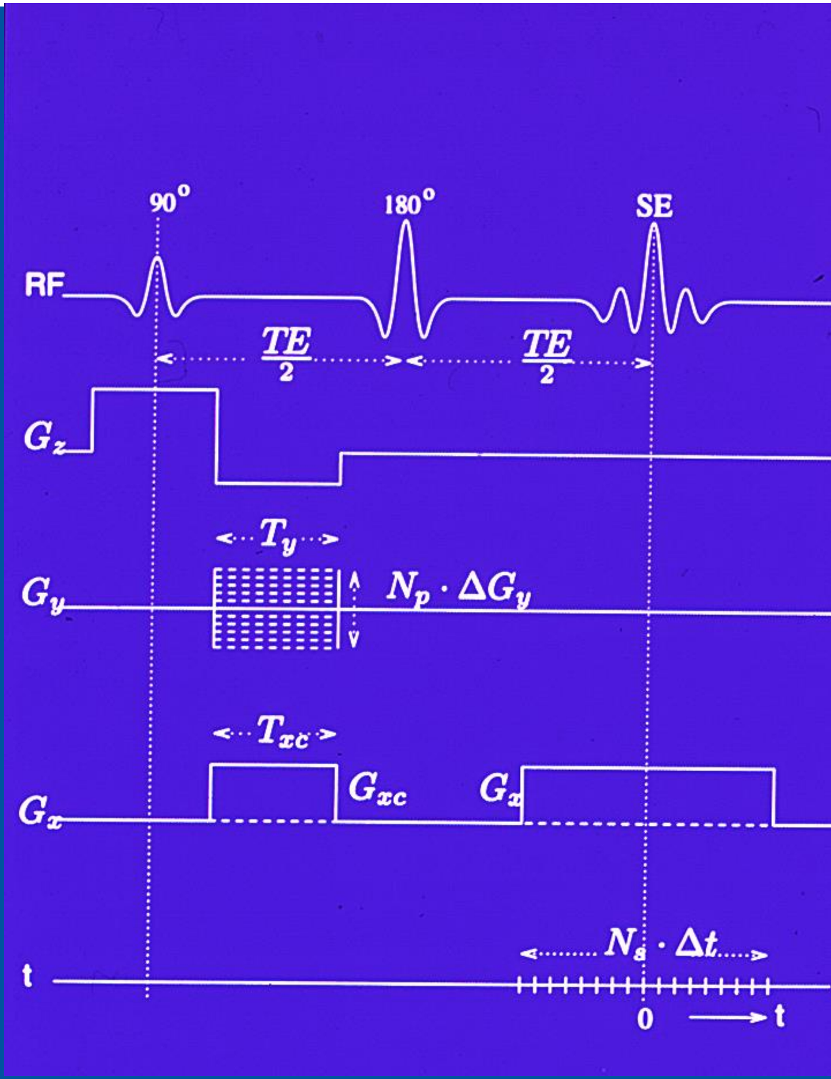
90°
180°
SE
RF
$\frac{TE}{2}$
$\frac{TE}{2}$
G_z
T_y
G_y
$N_p \cdot \Delta G_y$
T_{xc}
G_x
G_{xc}
G_x
$N_s \cdot \Delta t$
t
0
t

Position errors: slice selection

A deviation of the magnetic field during the 90° pulse results in a shift in the selected slice:

$$z_1 = z - \frac{\Delta B_0}{G_z} - \frac{\Delta B_{G_z}}{G_z}$$

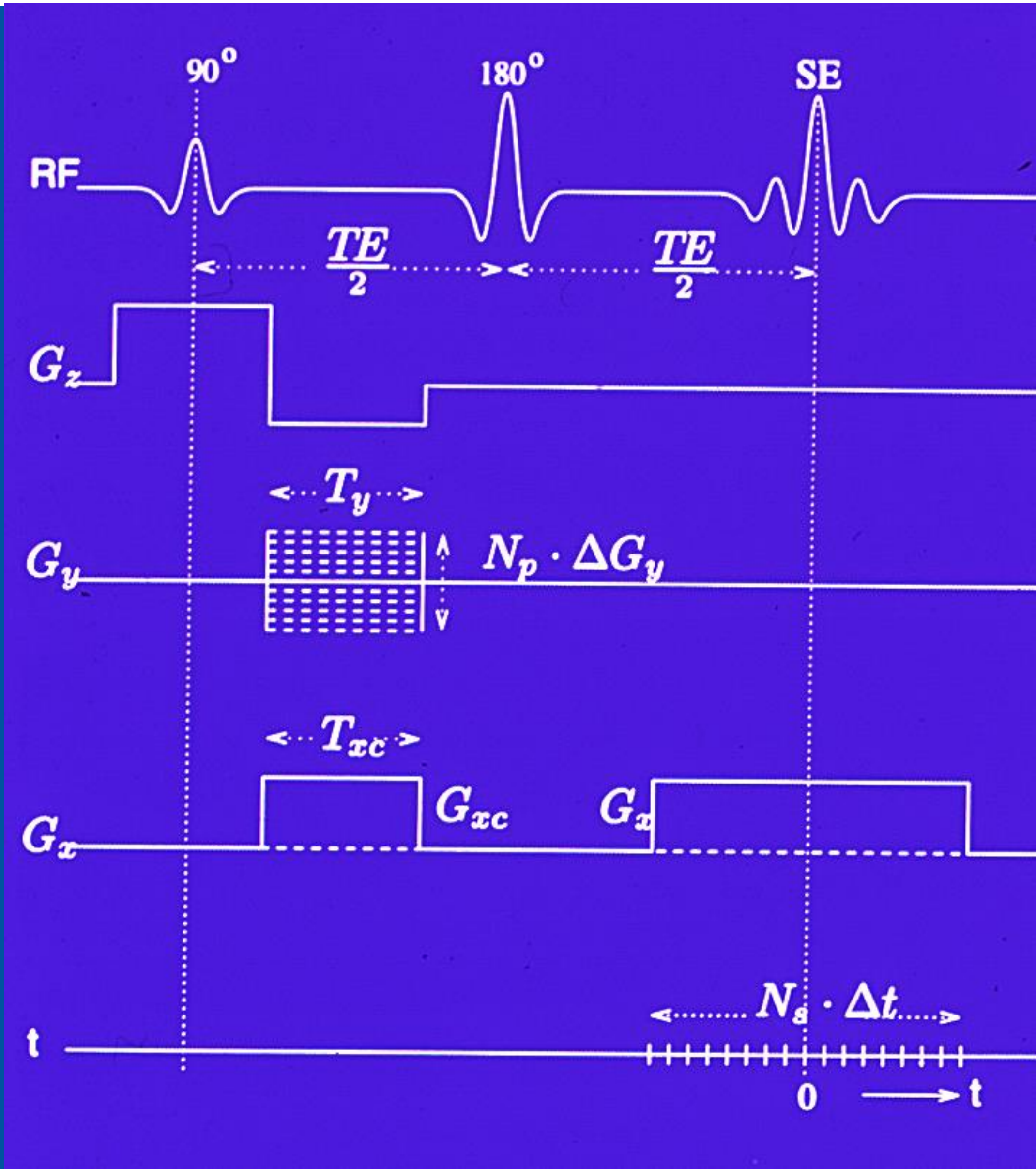

90°
180°
SE
RF
TE/2
TE/2
G_z
T_y
G_y
$N_p \cdot \Delta G_y$
T_{xc}
G_{xc}
G_x
G_x
$N_s \cdot \Delta t$
t
0
t

Distortion of phase evolution

$$\begin{aligned}\Phi^{distorted}(x,y,z,n,m) = \Phi(x,y,z,n,m) \\ + \gamma\Delta B_0(x,y,z)n\Delta t \\ + \gamma\Delta B_{G_x}(x,y,z)n\Delta t \\ - \gamma m\Delta B_{\Delta G_y}(x,y,z)T_y\end{aligned}$$

With:

$\Phi^{\text{distorted}}$ the distorted phase evolution

Φ the ideal phase evolution:

$$\Phi(x,y,z,n,m) = \gamma x G_x n\Delta t - \gamma y m\Delta G_y T_y$$

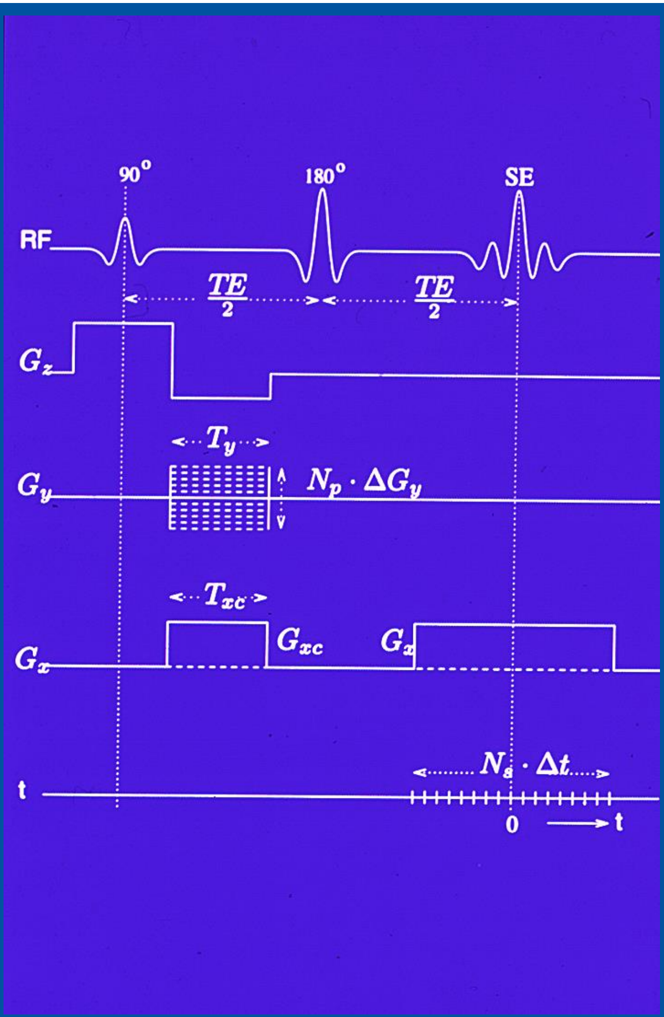
90°
180°
SE
RF
$\frac{TE}{2}$
$\frac{TE}{2}$
G_z
T_y
G_y
$N_p \cdot \Delta G_y$
T_{xc}
G_x
G_{xc}
G_x
$N_s \cdot \Delta t$
t
0
t

Impact on geometrical accuracy

Interpretation of the effect of disturbances:

$$\Phi^{distorted}(x,y,z,n,m)=\Phi(x_1,y_1,z_1,n,m)$$

Group x-terms for distortions in read-out direction:

$$\gamma x G_x n\Delta t+\gamma\Delta B_0(x,y,z)n\Delta t+\gamma\Delta B_{G_x}(x,y,z)n\Delta t=\gamma x_1 G_x n\Delta t$$

and solve for x_1

$$x_1=x+\frac{\Delta B_0(x,y,z)}{G_x}+\frac{\Delta B_{G_x}(x,y,z)}{G_x}$$

Impact on geometrical accuracy

Group y-terms for distortions in fase-encoding direction:

$$-\gamma y m \Delta G_y T_y - \gamma m \Delta B_{\Delta G_y}(x, y, z) T_y = -\gamma y_1 m \Delta G_y T_y$$

and solve for y_1

$$y_1 = y + \frac{\Delta B_{\Delta G_y}}{\Delta G_y}$$

Assuming that the errors in the gradient are independent of the gradient step, this is equal to

$$y_1 = y + \frac{\Delta B_{G_y}}{G_y}$$

Result: geometrical distortion in spin-echo imaging

$$x_1 = x + \frac{\Delta B_0(x,y,z)}{G_x} + \frac{\Delta B_{G_x}(x,y,z)}{G_x}$$

In the frequency-encoding direction, both the non-linearity of the frequency-encoding gradient and static field inhomogeneity cause geometric distortions

$$y_1 = y + \frac{\Delta B_{G_y}}{G_y}$$

In the phase-encoding direction, distortions are solely caused by the non-linearity of the phase-encoding gradient

Water and fat have a slightly different resonance frequency. This results in a shift between the water and the fat in an image, called ‘water-fat shift’

In what direction does this shift occur?

1. Slice direction
2. Phase-encoding direction
3. ★ Read-out direction

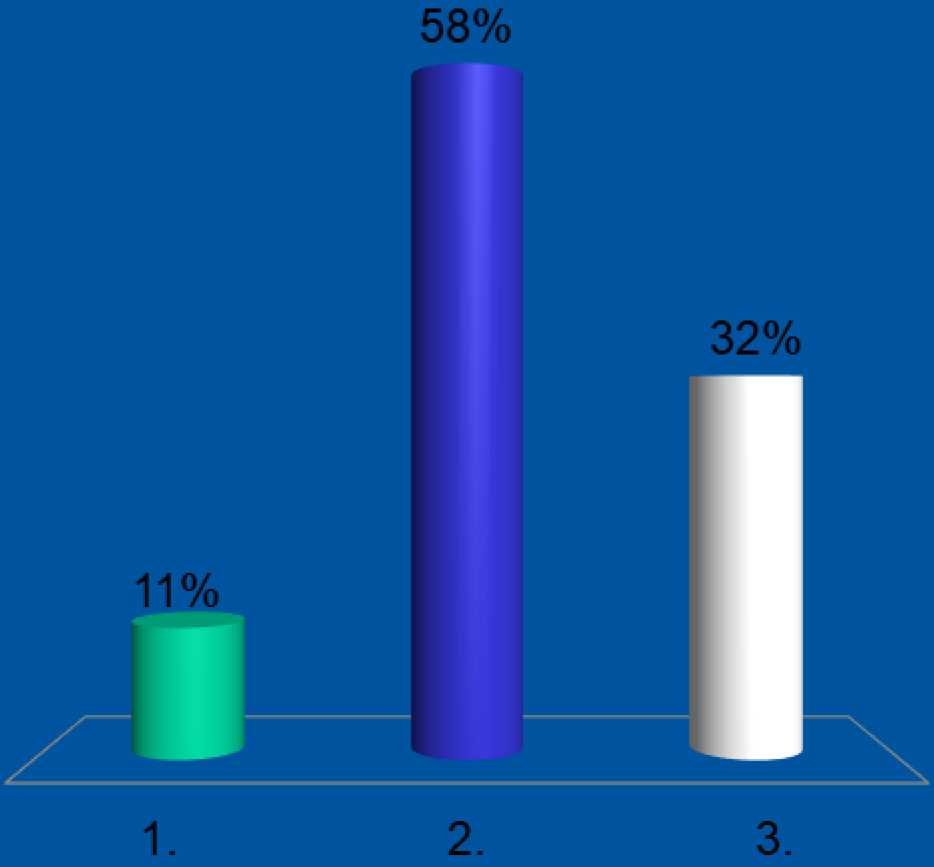

Result: geometrical distortion in spin-echo imaging

$$x_1 = x + \frac{\Delta B_0(x,y,z)}{G_x} + \frac{\Delta B_{G_x}(x,y,z)}{G_x}$$

frequency-encoding (read-out) direction:
- non-linearity of the gradient
- static field inhomogeneity
  (= static difference in resonance frequency)

$$y_1 = y + \frac{\Delta B_{G_y}}{G_y}$$

phase-encoding direction:
- non-linearity of the gradient

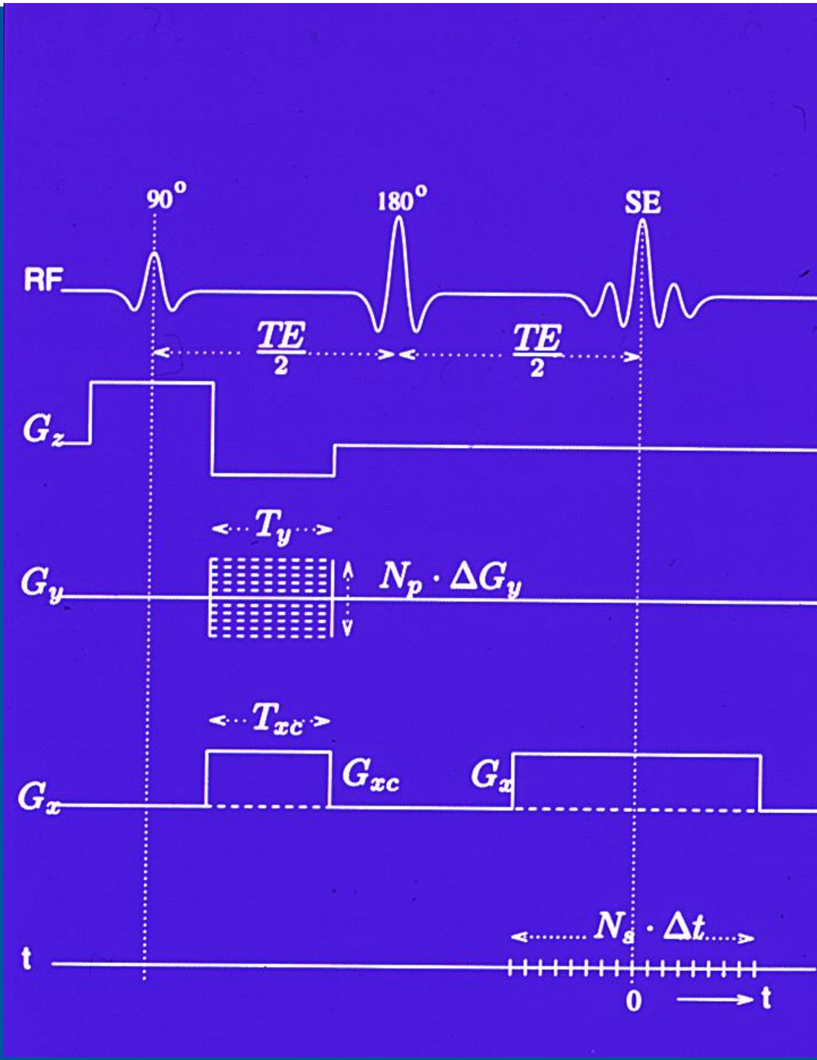
90°
180°
SE
RF
$\frac{TE}{2}$
$\frac{TE}{2}$
G_z
T_y
$N_p \cdot \Delta G_y$
G_y
T_{xc}
G_{xc}
G_x
G_x
t
$N_s \cdot \Delta t$
0
t

Distortions in a Gradient Echo sequence

In Gradient Echo imaging, the same distortions occur.

However, in the frequency-encoding direction also dephasing occurs, resulting in signal loss:

$$\Delta\Phi(x,y,z) = \gamma TE \Delta B_0(x,y,z)$$

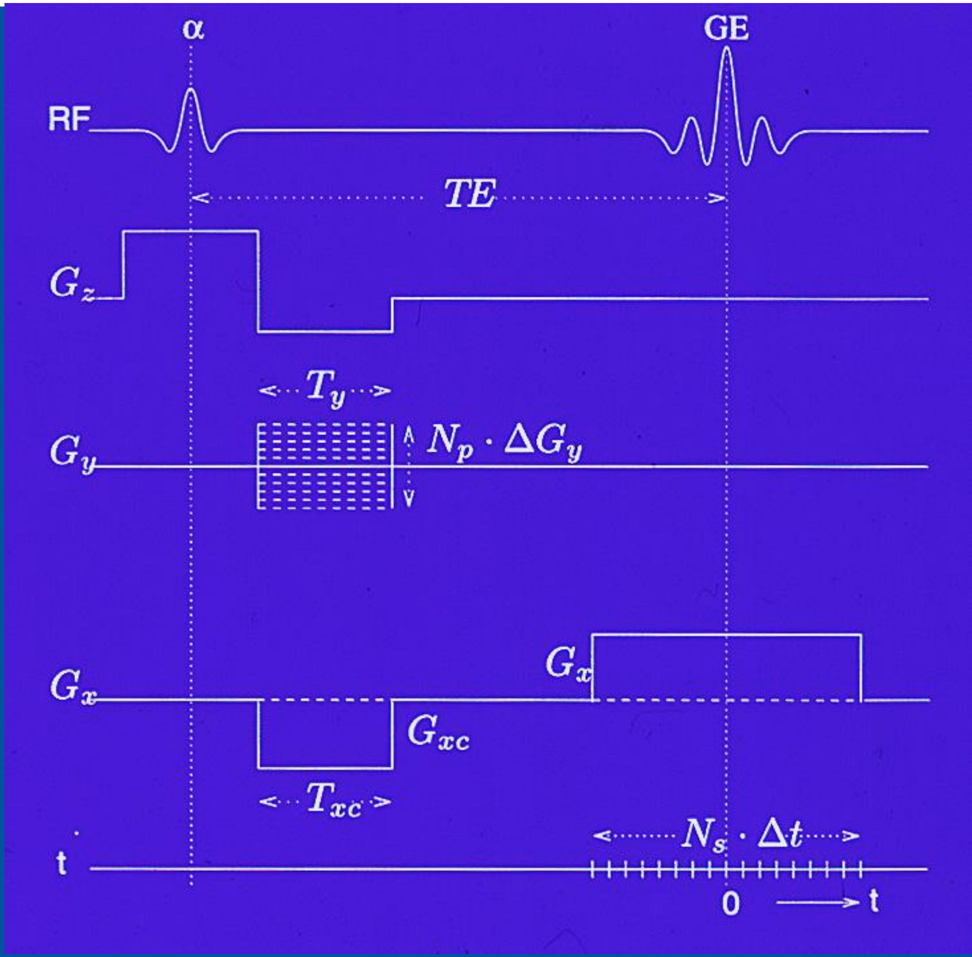
α
GE
RF
TE
G_z
T_y
G_y
$N_p \cdot \Delta G_y$
G_x
G_x
G_{xc}
T_{xc}
$N_s \cdot \Delta t$
t
0
t

Dephasing due to static field inhomogeneities

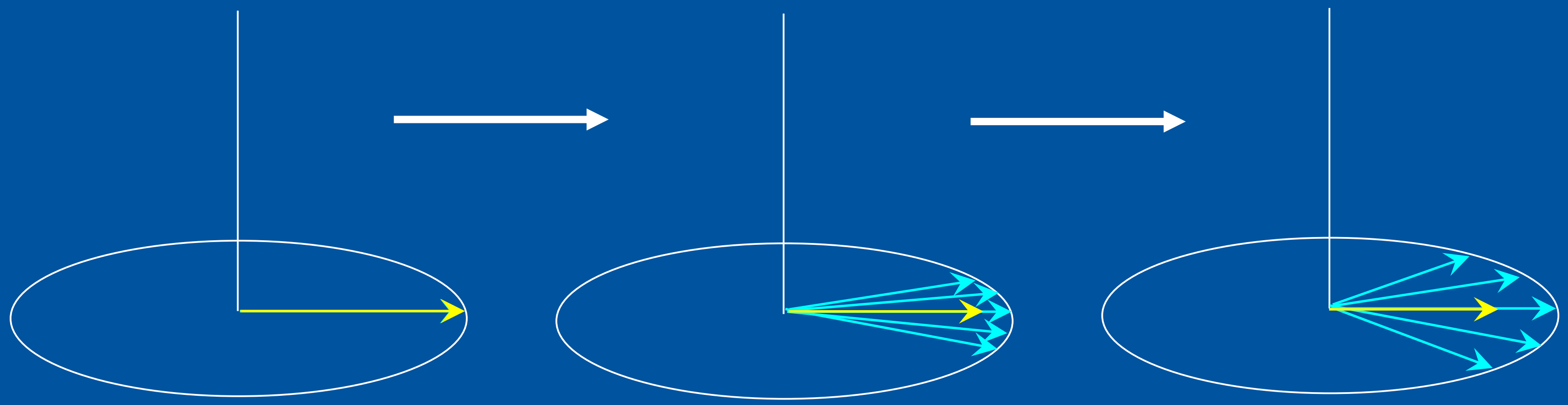

Rephasing in a Spin Echo sequence

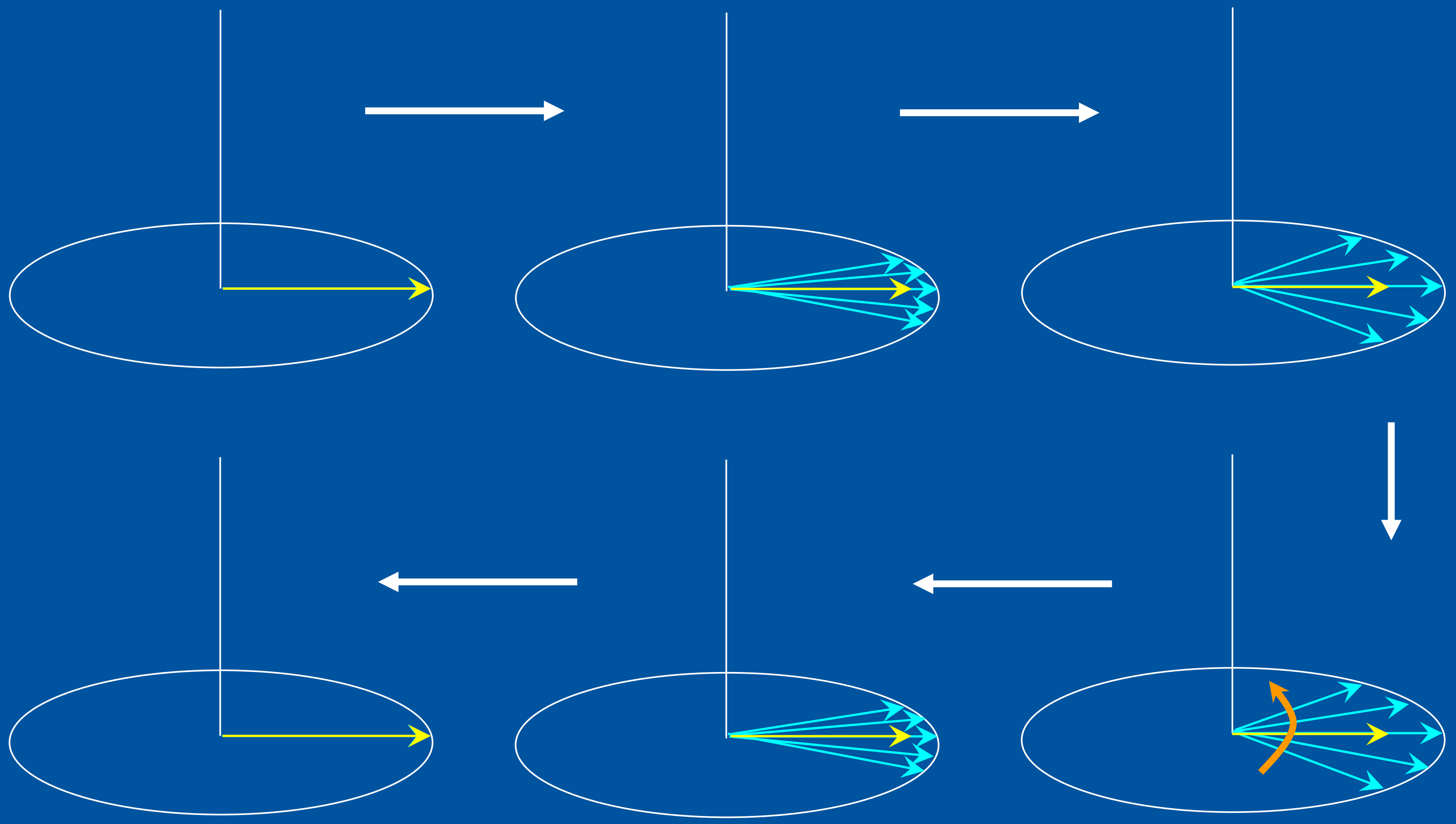

Continued dephasing in a Gradient Echo sequence

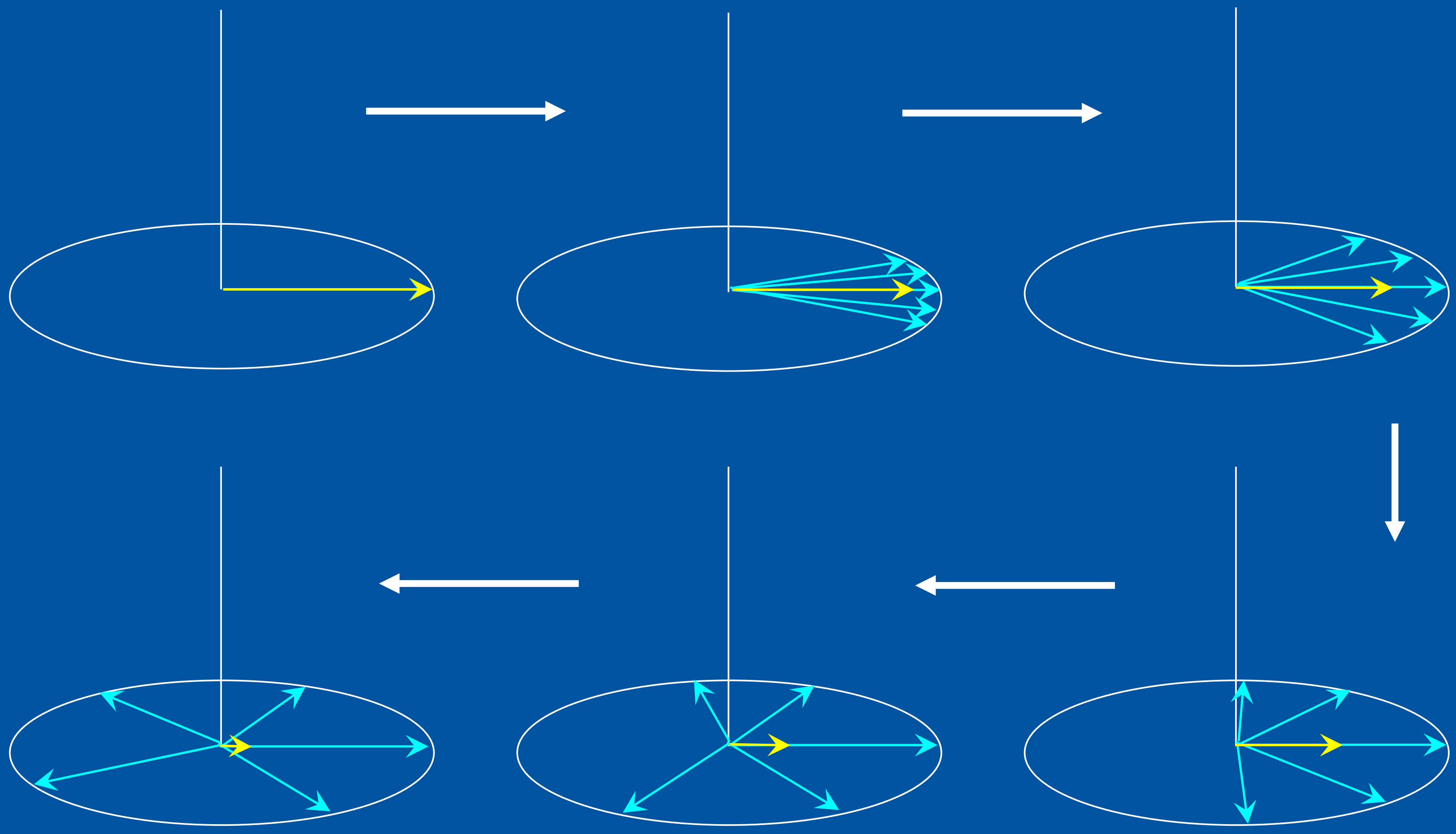

Phantom experiments

Some qualitative experiments with coaxial cylinder (water air susceptibility difference):

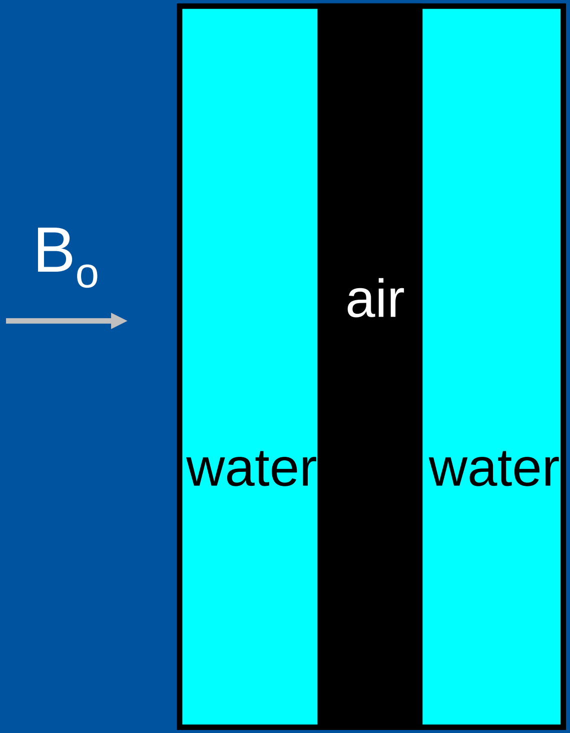
B_o
air
water
water

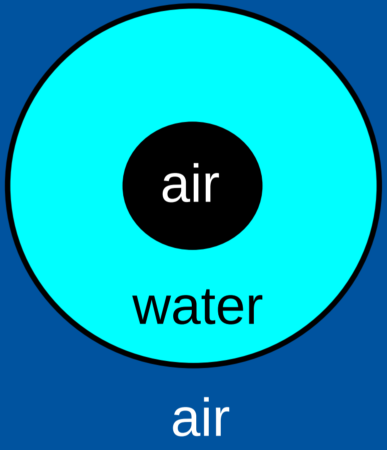
air
water
air

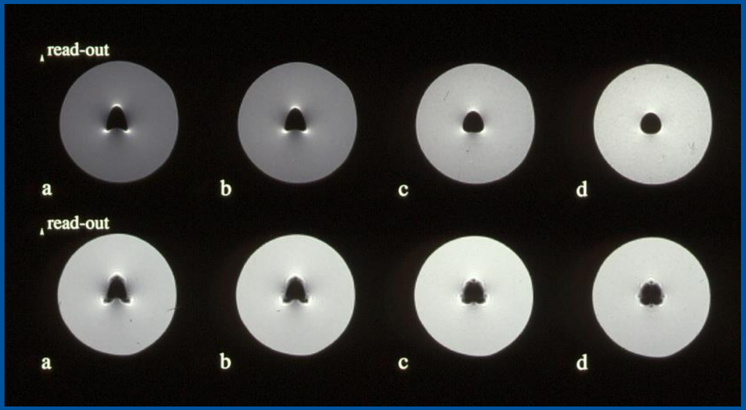
read-out
a
b
c
d
read-out
a
b
c
d

air: $\chi \approx 0$

water: $\chi \approx -9.10^{-6}$

Dephasing effects increase with TE in gradient echo imaging

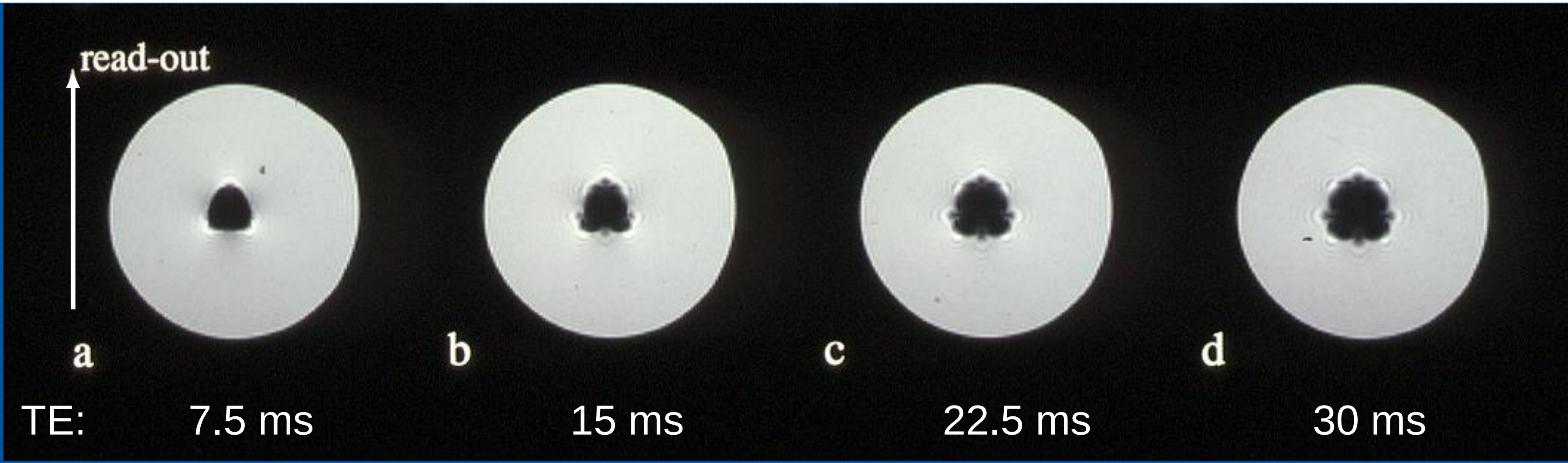
read-out
a
b
c
d
TE:
7.5 ms
15 ms
22.5 ms
30 ms

- Dephasing artifacts increase with Echo Time

Dephasing effects increase with TE in gradient echo imaging

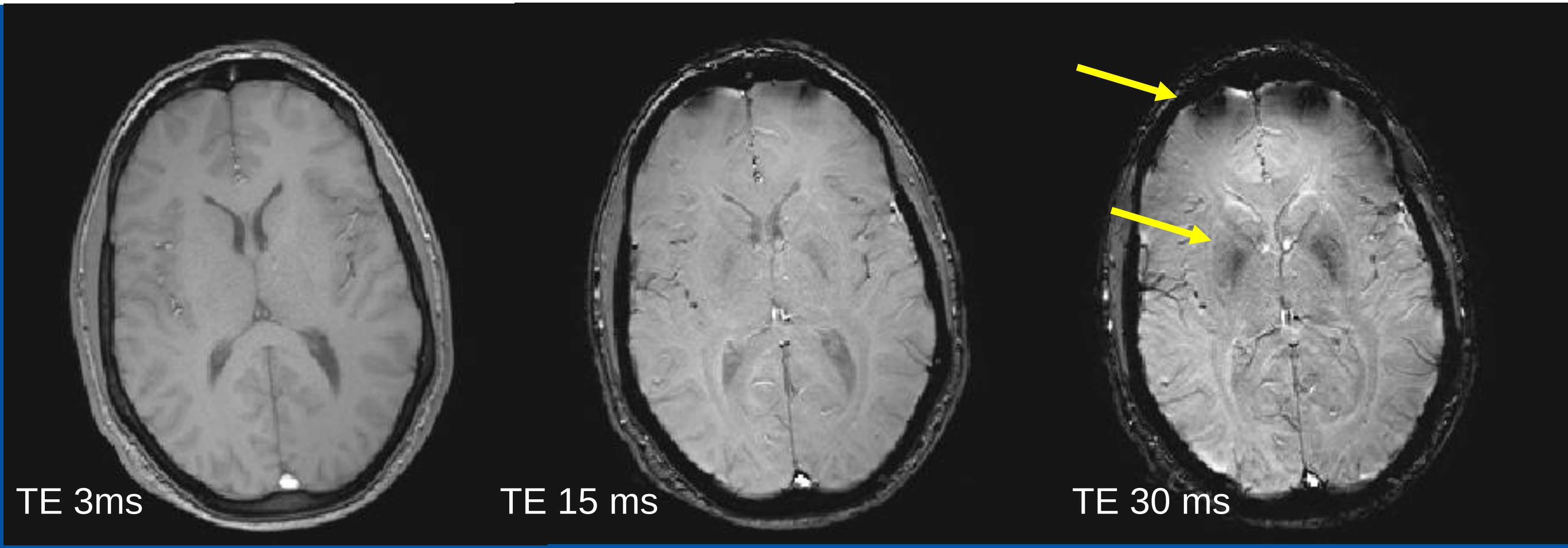
TE 3ms
TE 15 ms
TE 30 ms

- 3T scanner
- FFE sequence; TR = 100 ms, FA 45º

Summary 1

- Many reasons exists for artifacts in images
  - Erroneous sampling of k-space
    - Aliasing
    - Ringing
  - Magnetic field errors
    - Gradient artifacts
    - Susceptibility artifacts
    - Water-fat shift

- Geometrical artifacts show up in a particular direction
  - Phase encoding direction: aliasing
  - Read-out direction: susceptibility, water-fat shift

- Dephasing results in signal loss in gradient echo sequences

MRI Physics: Speed-up and Specialised Sequences

A/Prof Gary Liney

6th November 2017

ESTRO Imaging for Physicists

ESTRO School

Introduction

- MRI slow technique (compared to CT)
- Desirable to cover anatomy quickly
  - ✓ Patient comfort
  - ✓ Reduce artefacts
  - ✓ Image physiological
- Some sequences specific for RT

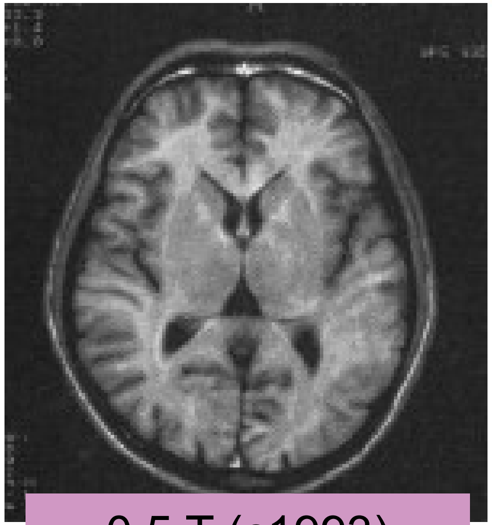

0.5 T (c1993)
32 x 4 mm in 5 min

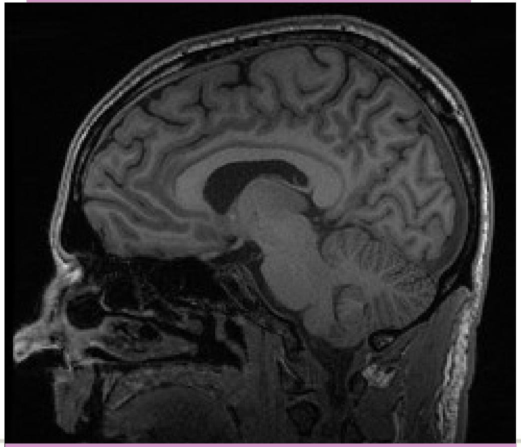

3.0 T (2010)
148 x 1 mm in 3.5 min

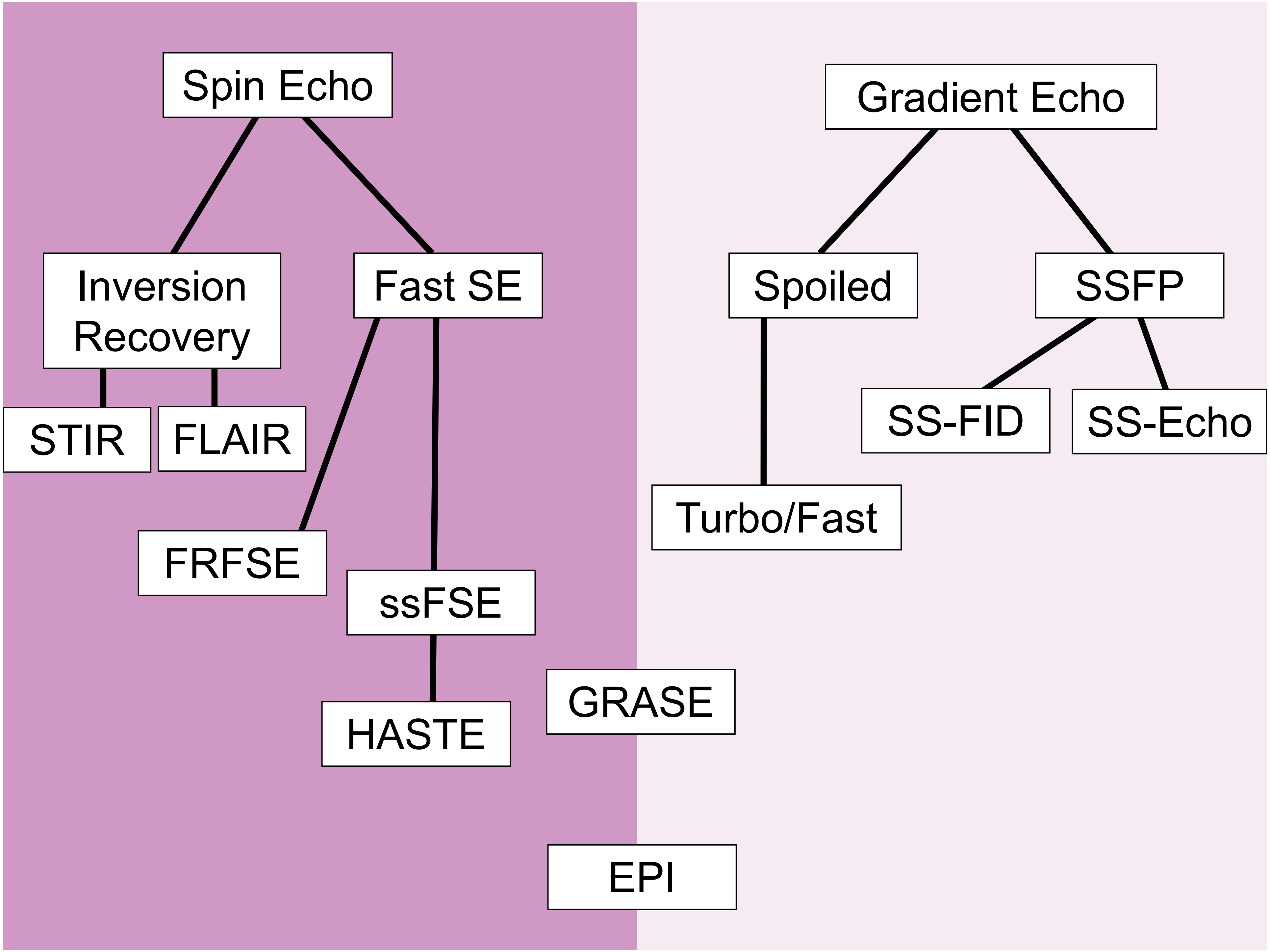

Spin Echo

Inversion Recovery

Fast SE

STIR

FLAIR

FRFSE

ssFSE

HASTE

GRASE

EPI

Gradient Echo

Spoiled

SSFP

SS-FID

SS-Echo

Turbo/Fast

Spin-echoes…

- T_2-weighted essentially limited by long TR
- Increase speed by:

  Segmented k-space

  Acquire more than one line of k-space per TR

  Partial k-space

  Acquire less than full k-space

k-space: Acquisition strategies

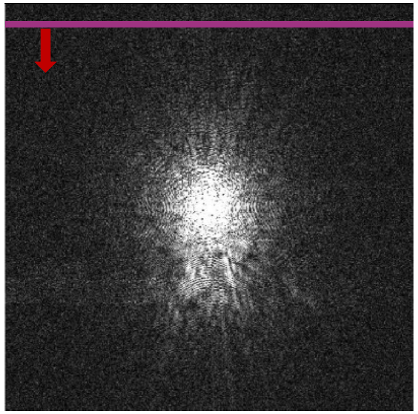

Spin-echo

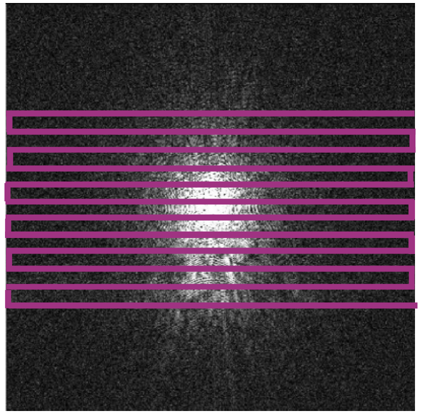

Single-Shot

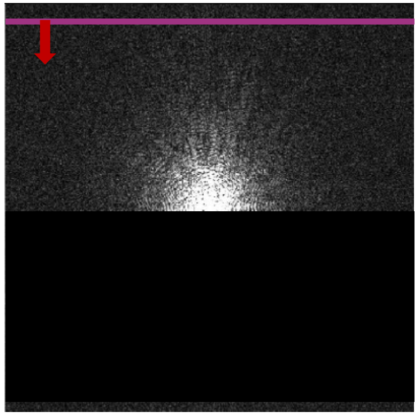

Partial Data

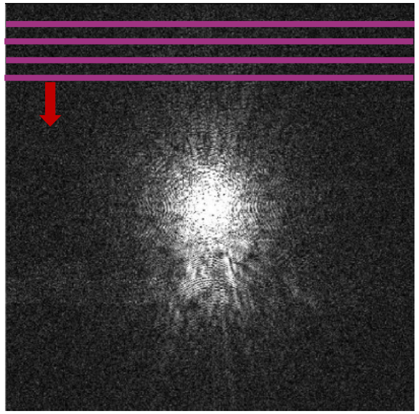

Segmented

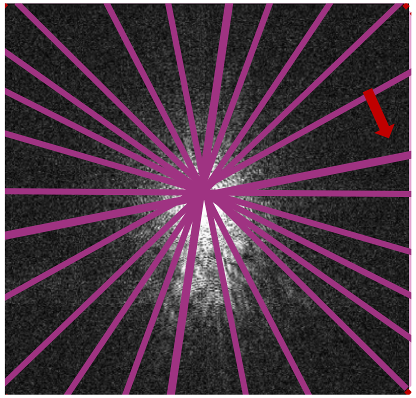

Radial

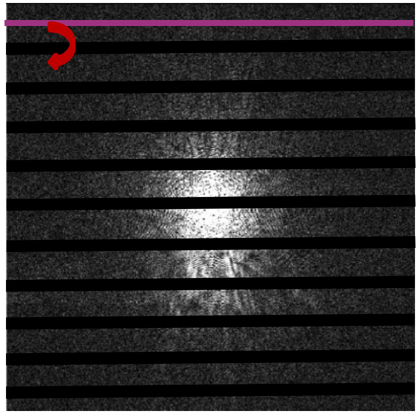

Parallel imaging

k-space: Scan Time

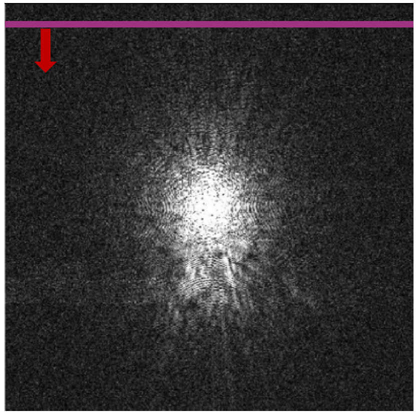

$TR \times N_{AV} \times N_{PE}$

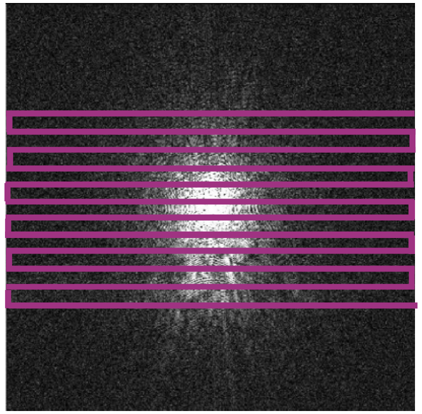

$TR \times N_{AV}$

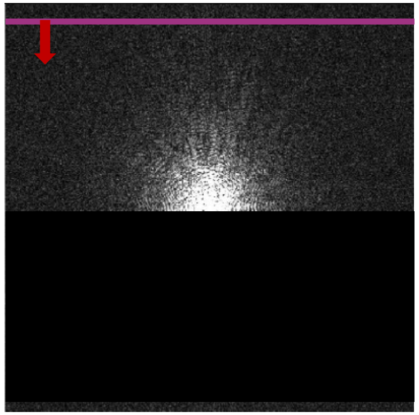

$TR \times N_{AV} \times (N_{PE}/2)$

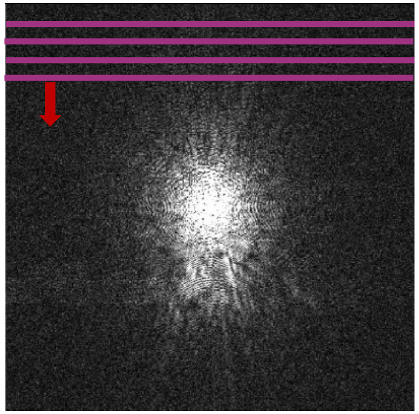

$(TR \times N_{AV} \times N_{PE})/ETL$

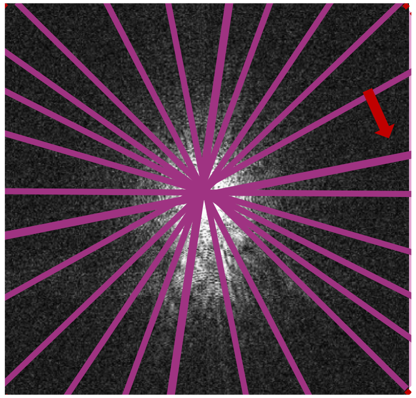

$TR \times N_{AV} \times N_{PE} \times 2\pi$

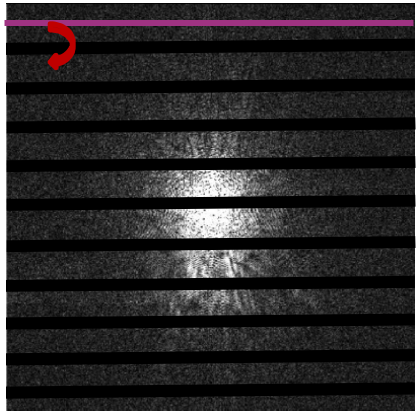

$(TR \times N_{AV} \times N_{PE})/R$

Fast (Turbo) Spin Echo

- Multiple SEs but individually phase encoded
- Scan time reduced by ETL ('Turbo factor')
- Effective TE
- Image quality trade-off

  If ETL or ESP too large blurring
- Characteristic bright fat

  J-coupling breakdown caused by use of echo trains

Aka:
FSE
TSE
RARE

$$\text{Scan time} = (TR \times N_{AV} \times N_{PE})/ETL$$

FSE (TSE)

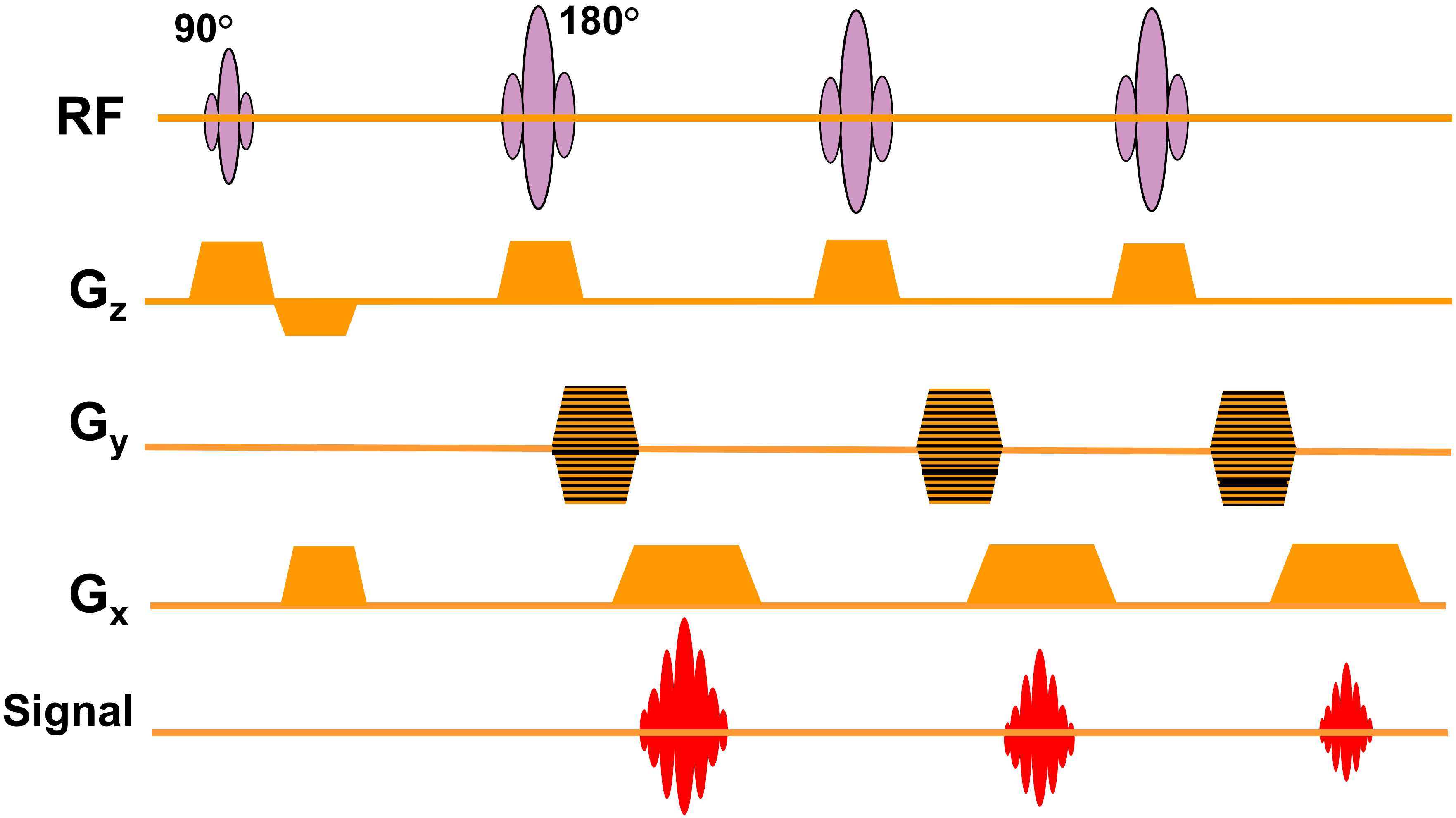
90°
180°
RF
G_z
G_y
G_x
Signal

Example: FSE

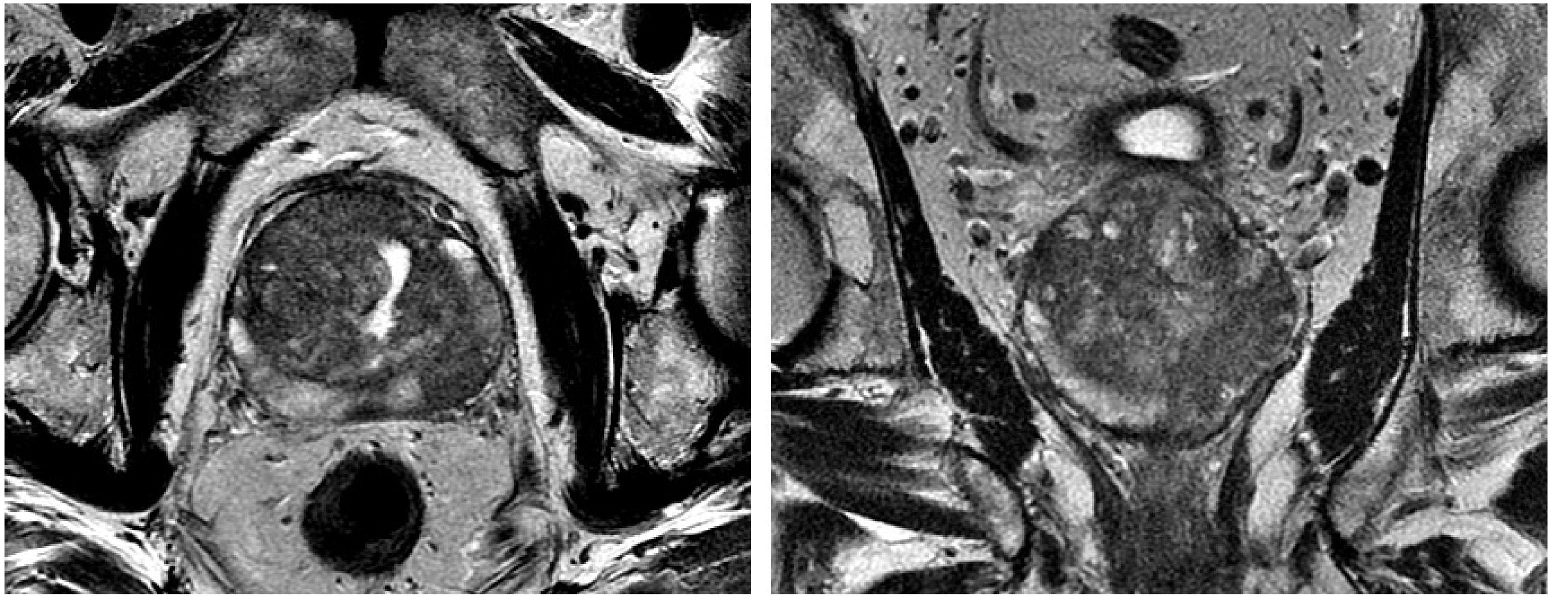

FSE extensively used in prostate: axial and coronal planes at 3.0 Tesla without ER coil and excellent T2-weighting

Partial k-Space

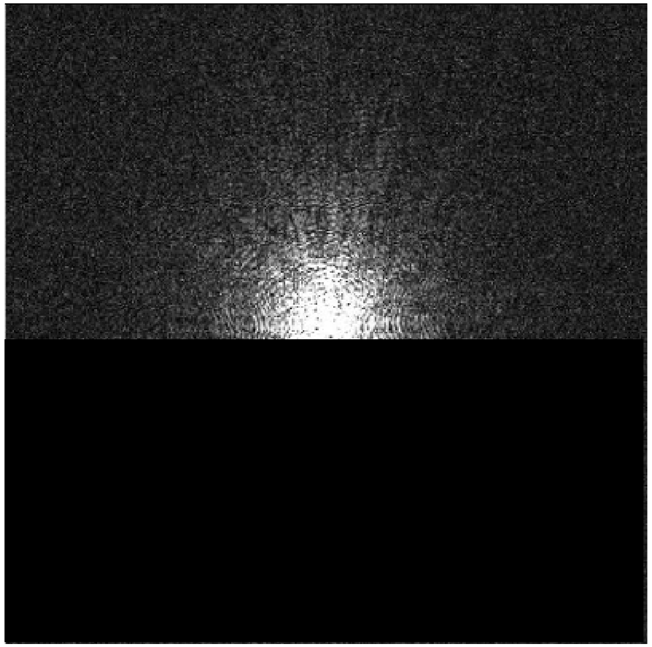

Partial Fourier/ Fractional NEX

- Half of phase encoding
- **Reduced scan time**
- Other reduction fractions possible

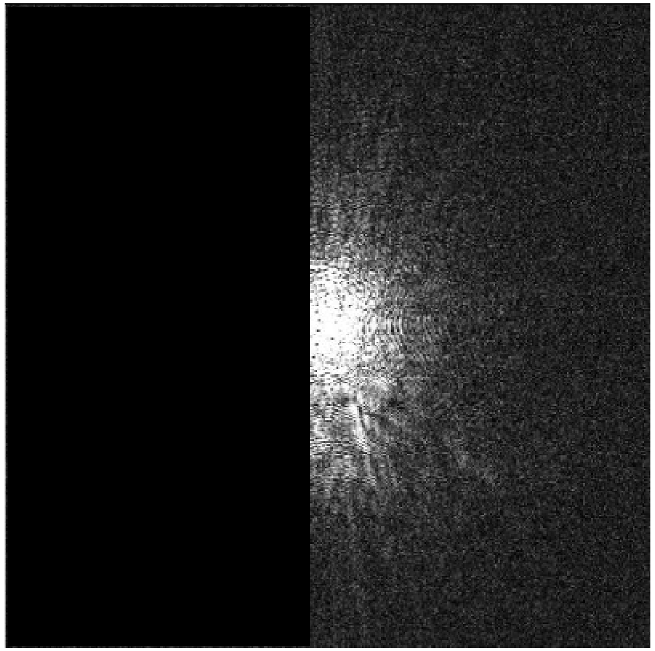

Partial Echo

- Half of echo
- Reduced minimum TE
- No effect on scan time

ssFSE and HASTE

Single shot FSE (ssFSE)

- All k-space in one TR
- Good for high contrast and volume coverage
- MRCP exam right

HASTE

- Single shot AND partial k-space
- Just over half k-space acquired
- Reasonable temporal & spatial resolution (prostate right)

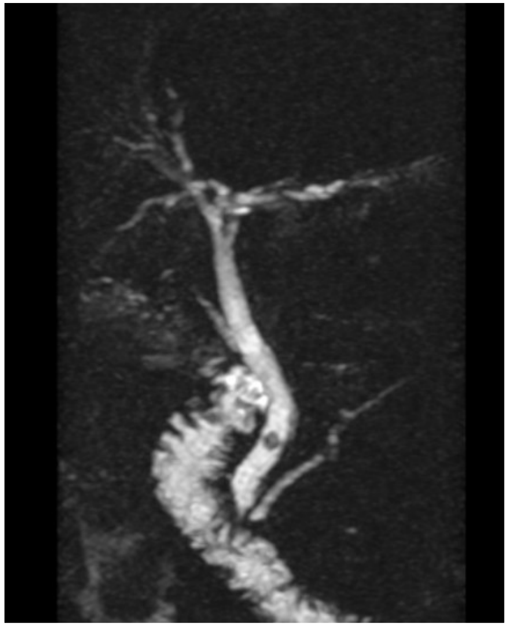

MIP from ssFSE
(TE/TR = 260 ms/12 s)

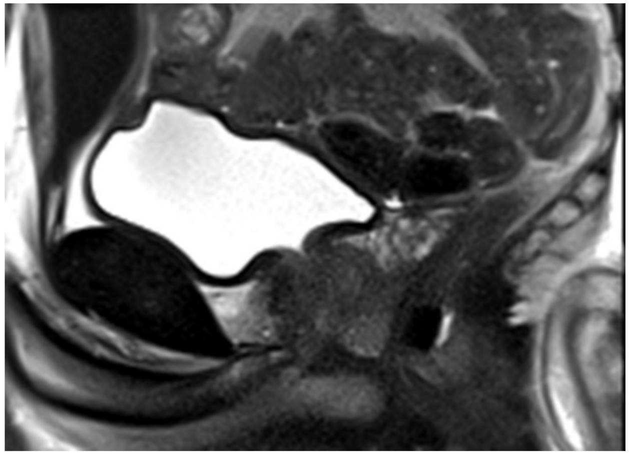

HASTE

Echo Planar Imaging (EPI)

- Implemented by Peter Mansfield (1977)
- Single-shot (can be run multi-shot)
  - ➢ Scan time = TR
- Blipped, spiral and constant versions
- Inherently noisy
- Limited resolution (e.g. 64 or 128 matrix)
- Can be SE or GRE based
- Widespread use in fMRI & DWI

EPI

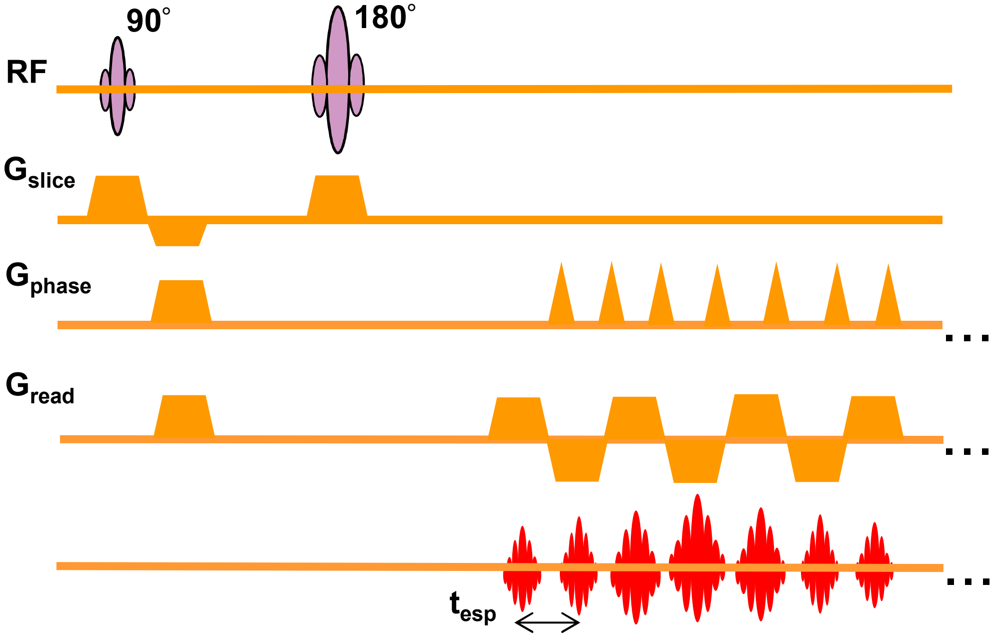
90°
180°
RF
G_{slice}
G_{phase}
G_{read}
…
…
…
t_{esp}

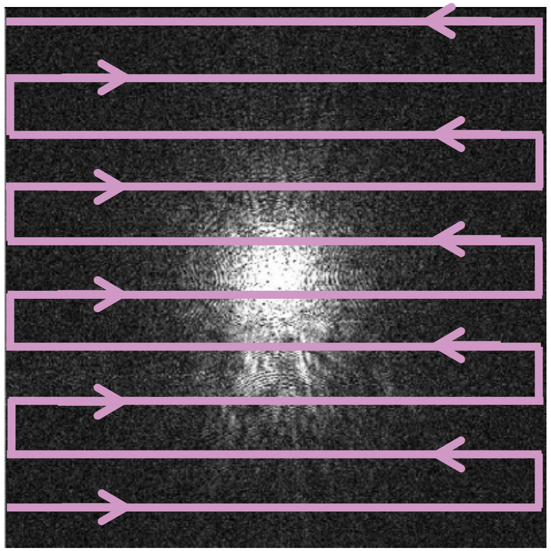

Effective 'phase-encoding' bandwidth is very small

$$\Delta \nu_{phase} = \frac{N_{shot}}{t_{esp}}$$

(e.g. 1 ms $t_{esp} \Rightarrow$ 1 kHz)

EPI

Prone to artefacts:

- N/2 ghosting (switching between lines)
- Distortions (eddy currents)
- Large chemical shift requires fat suppression
- Huge susceptibility effects along PE

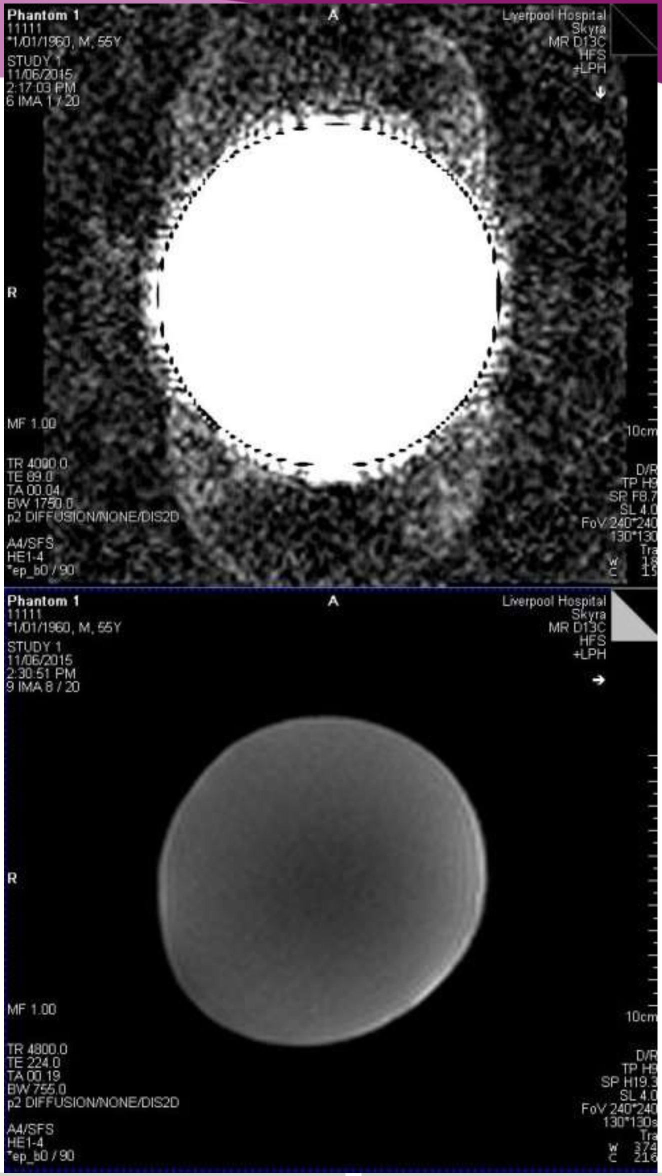
Phantom 1
11111
*1/01/1960, M, 55Y
STUDY 1
11/06/2015
2:17:03 PM
6 IMA 1 / 20
A
Liverpool Hospital
Skyra
MR D13C
HFS
+LPH
R
MF 1.00
TR 4000.0
TE 89.0
TA 00:04
BW 1750.0
p2 DIFFUSION/NONE/DIS2D
A4/SFS
HE1-4
*ep_b0 / 90
10cm
Phantom 1
11111
*1/01/1960, M, 55Y
STUDY 1
11/06/2015
2:30:51 PM
9 IMA 8 / 20
A
Liverpool Hospital
Skyra
MR D13C
HFS
+LPH
R
MF 1.00
TR 4800.0
TE 224.0
TA 00:19
BW 755.0
p2 DIFFUSION/NONE/DIS2D
A4/SFS
HE1-4
*ep_b0 / 90
10cm

EPI with B_0 Correction

Non corrected

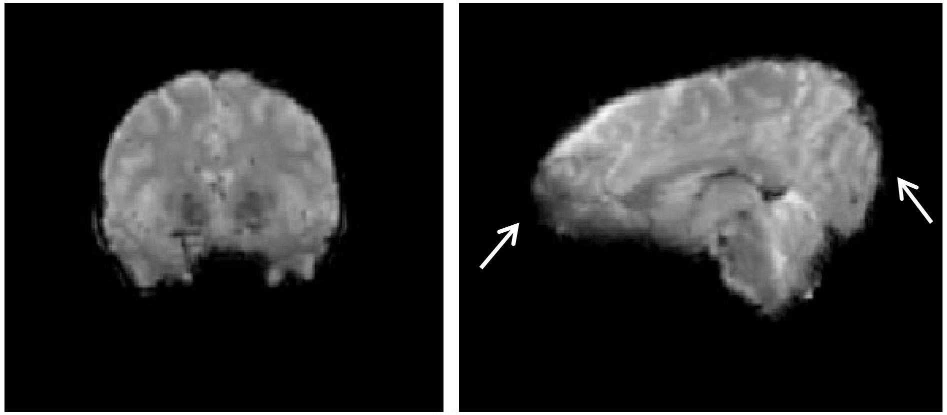

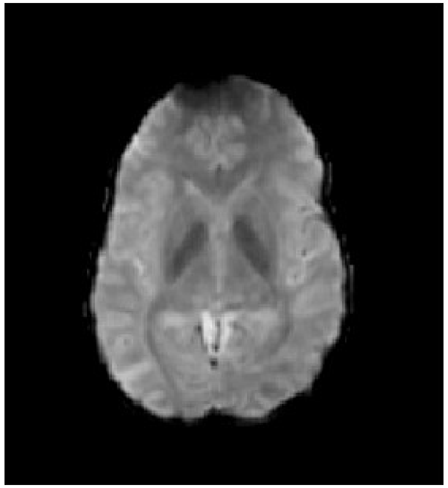

Susceptibility effects are particularly noticeable in frontal and occipital lobes.

Corrected

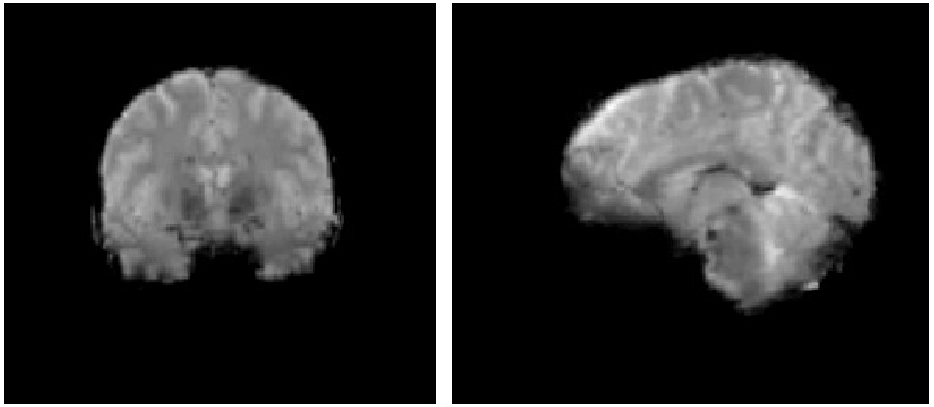

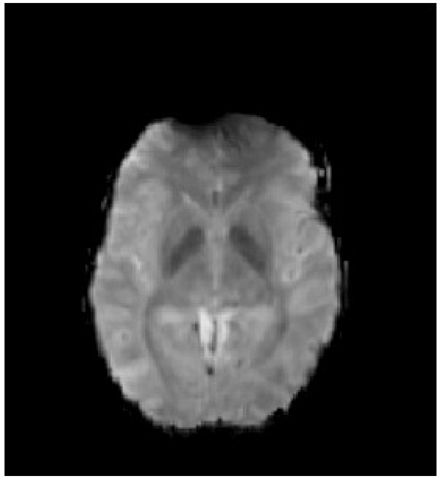

Courtesy of
Roberto Garcia-Alvarez,
GE Healthcare

Robust DWI

Conventional single shot EPI

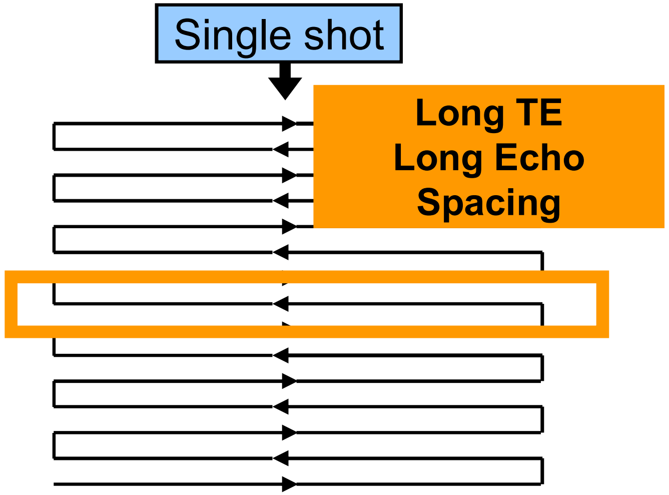
Single shot
Long TE
Long Echo
Spacing

RESOLVE

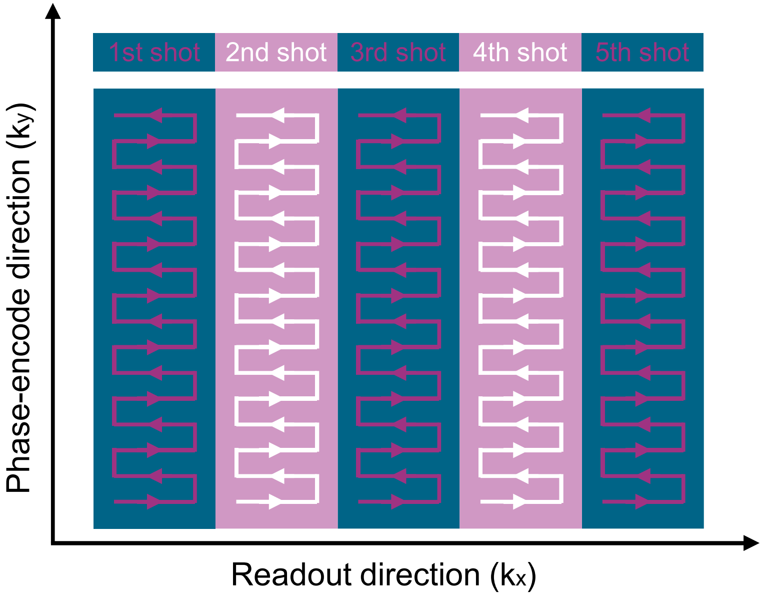
1st shot
2nd shot
3rd shot
4th shot
5th shot
Phase-encode direction (ky)
Readout direction (kx)

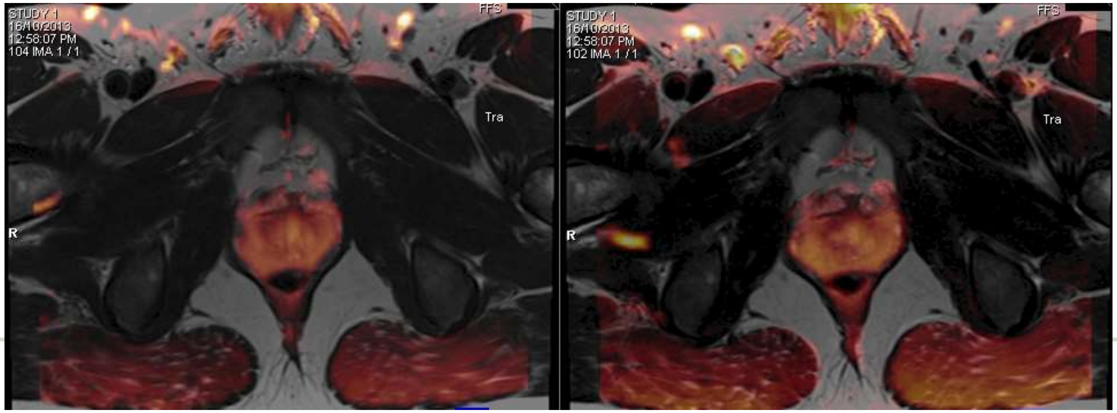
STUDY 1
16/10/2013
12:58:07 PM
104 IMA 1 / 1
FFS
Tra
R
STUDY 1
16/10/2013
12:58:07 PM
102 IMA 1 / 1
FFS
Tra
R

EPI RESOLVE

GRASE

- Hybrid sequence
- Gradient And Spin Echo
- Also known as TurboGSE
- Multiple spin-echoes and gradient echoes at each spin-echo
  - ‘Gradient’ AND ‘Turbo’ factors to consider
- Each echo phase encoded

$$\text{Scan time} = (TR \times N_{AV} \times N_{PE}) / (N_{GRE} \times N_{SE})$$

GRASE (TGSE)

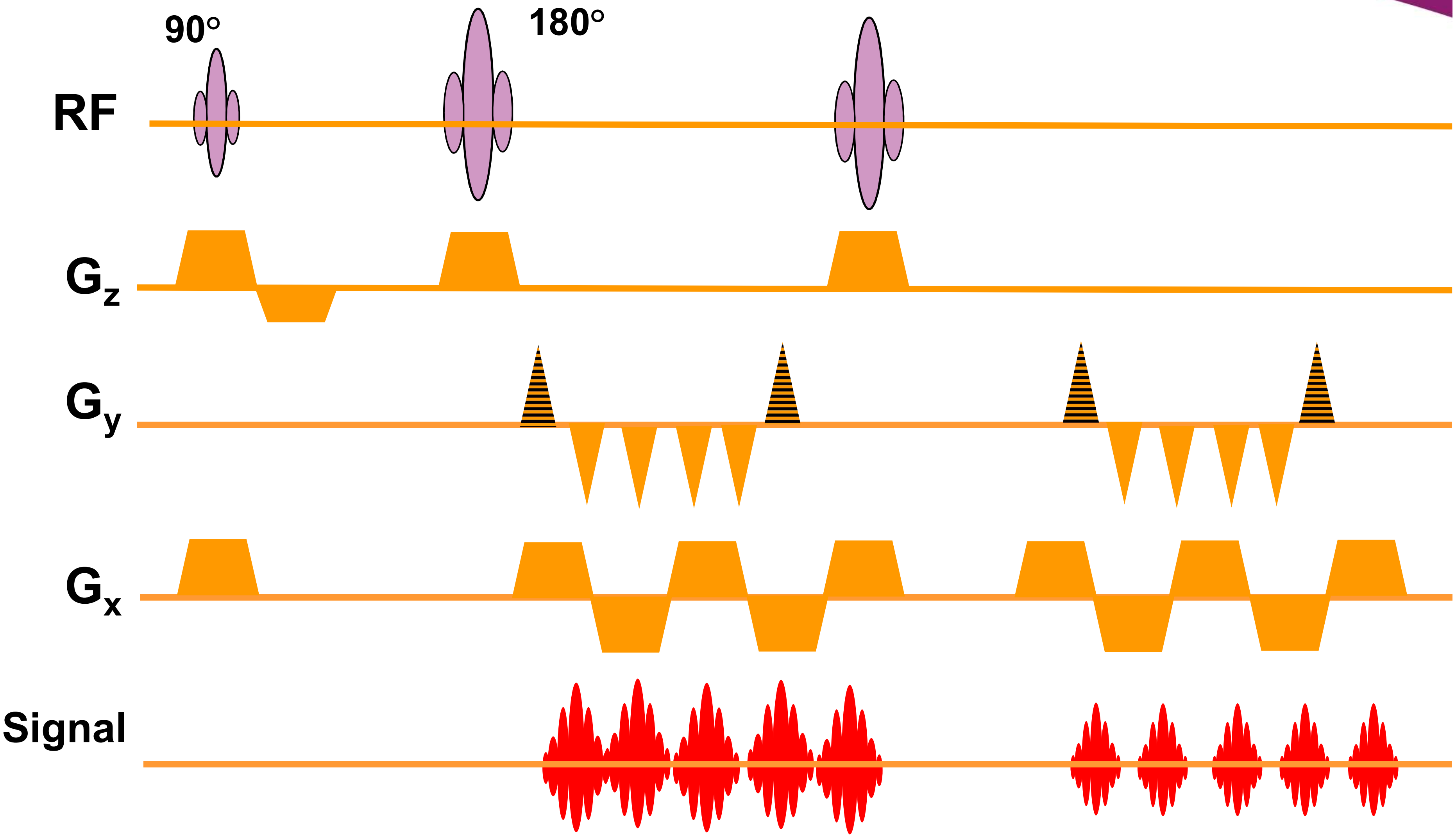
90°
180°
RF
G_z
G_y
G_x
Signal

Example: TGSE

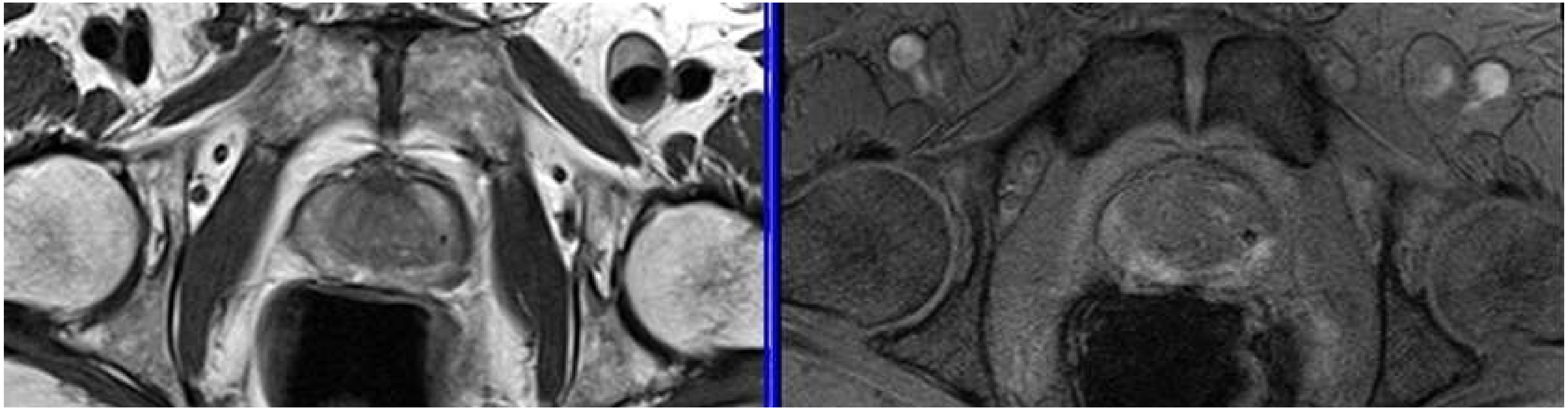
TGSE GE

- TGSE in prostate with gold seeds compared to GE
- T_2-w contrast and seed visualisation in one sequence

Gradient-echoes…

- Inherently fast due to lack of 180° and short TR
- Partially excite using reduced flip (Ernst) angle
  - Not restricted by relaxation
- If we further reduce TR…
  - Steady-state magnetisation when TR << T_2

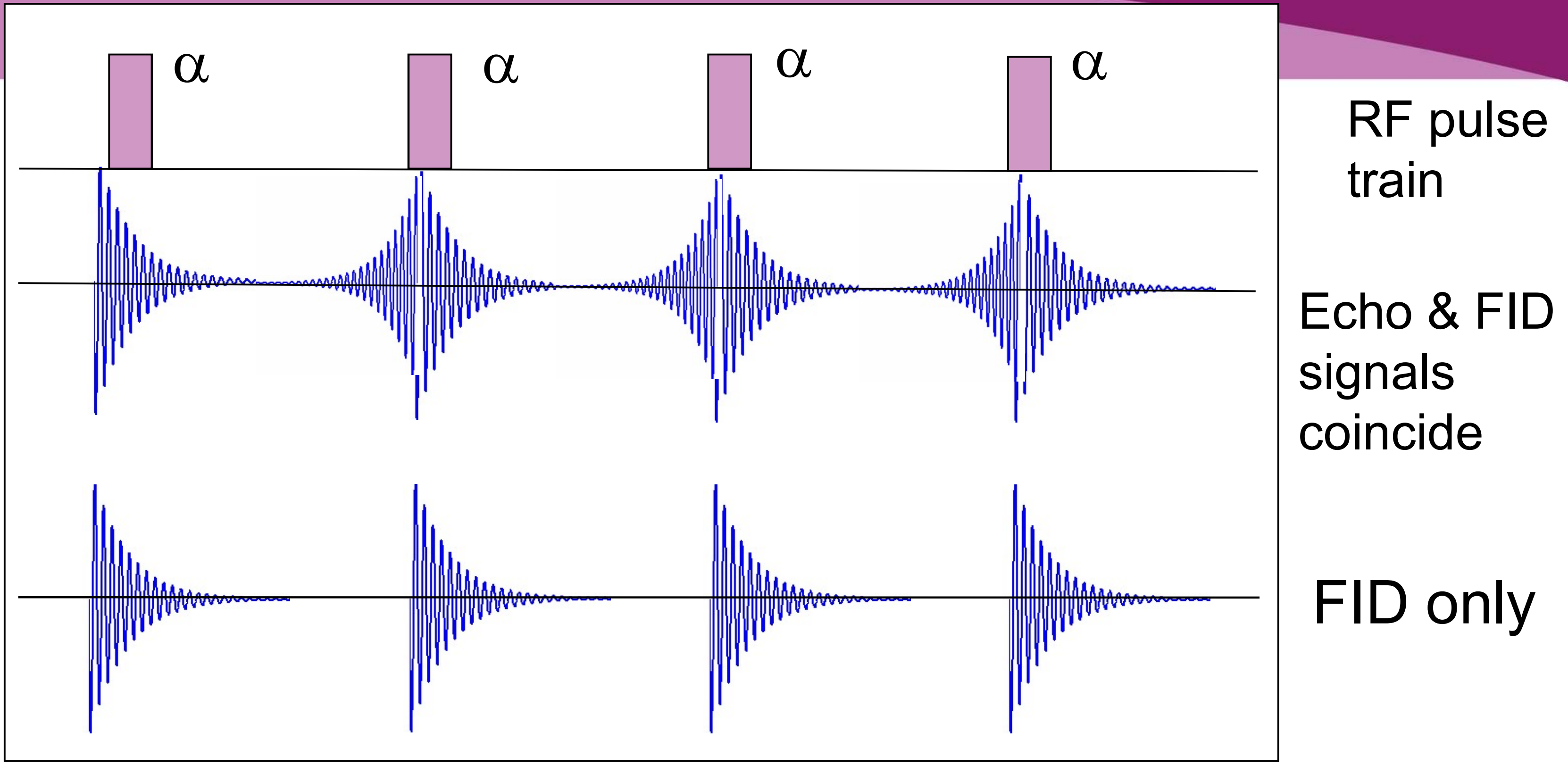
α
α
α
α
RF pulse train
Echo & FID signals coincide
FID only

- Rapid successive RF pulses
- Refocus residual transverse magnetisation into ‘Hahn’ echoes
- Using or destroying these alters contrast

Steady State Sequences

- Spoiling (or ‘incoherent steady state’)
  - Removes residual transverse signal
  - Use RF (or gradient) spoiling
    - RF phase angle increased to produce net cancellation of transverse magnetization
  - Incomplete spoiling leads to ‘FLASH-bands’

FLASH (Turbo-FLASH)
SPGR (FSPGR)
RF-FAST

$$S \propto \frac{\sin\alpha\left[1-\exp\left(-TR/T_1\right)\right]\exp\left(-TE/T_2^{\ast}\right)}{1-\cos\alpha\exp\left(-TR/T_1\right)}$$

Steady State Sequences

- Rewinding (SS-FID)
  - Maintains coherent transverse magnetisation
  - FISP, GRASS rewind phase encoding only
  - ‘True’ FISP or bFFE rewind all 3 gradient directions
    - Have to additionally phase cycle RF (ROAST)
- Time Reversed sequences (SS-Echo)
  - PSIF
  - Use (Hahn) echo -essentially T_2-weighted

FAST
FISP
GRASS
bFFE/bSSFP
FIESTA

CE-FAST
PSIF
SSFP

Signals depend on:
flip angle, T_1/T_2

Steady-State Sequences

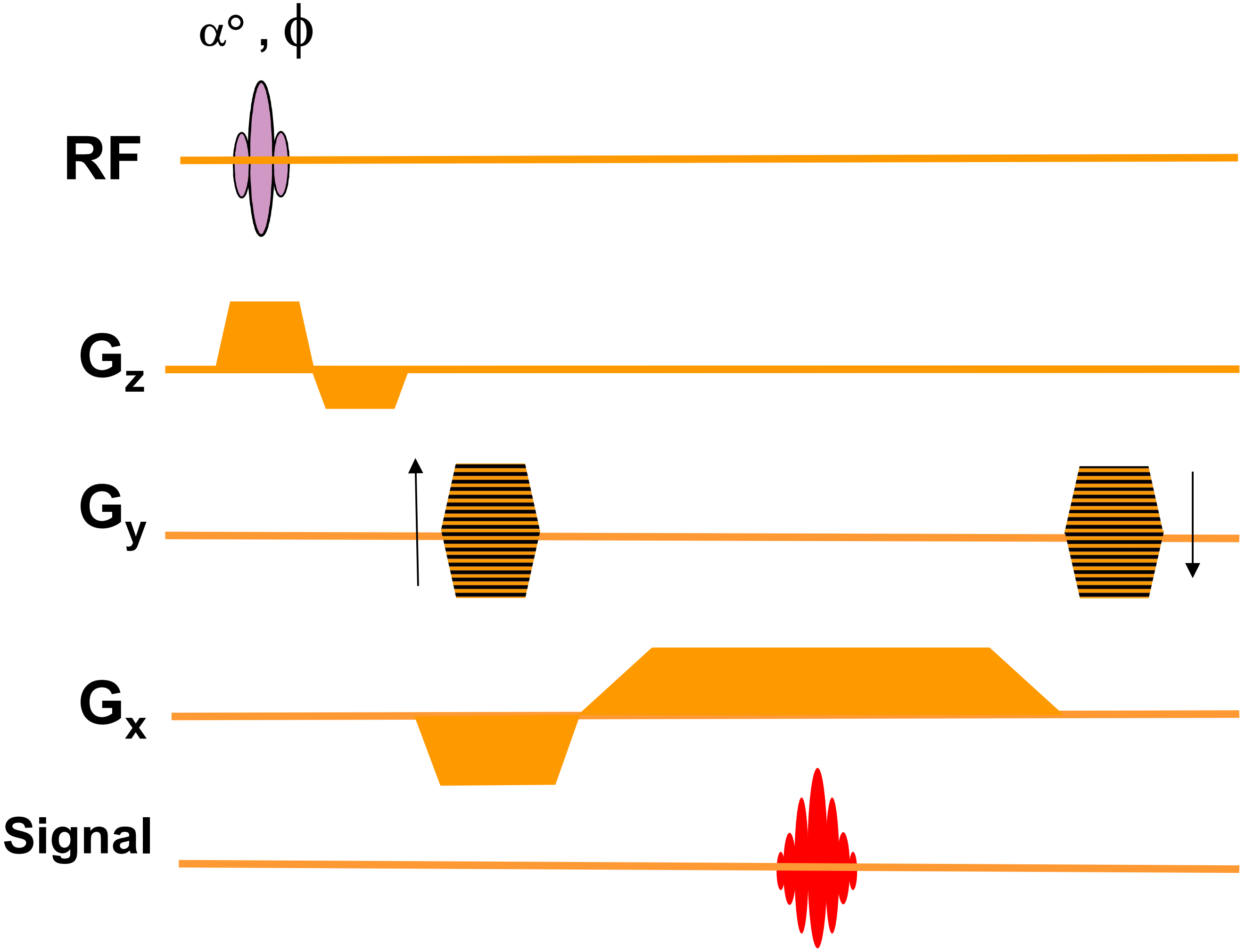
α° , ϕ
RF
G_z
G_y
G_x
Signal

RF spoiled:
phase (ϕ) is increased

Example: TrueFISP

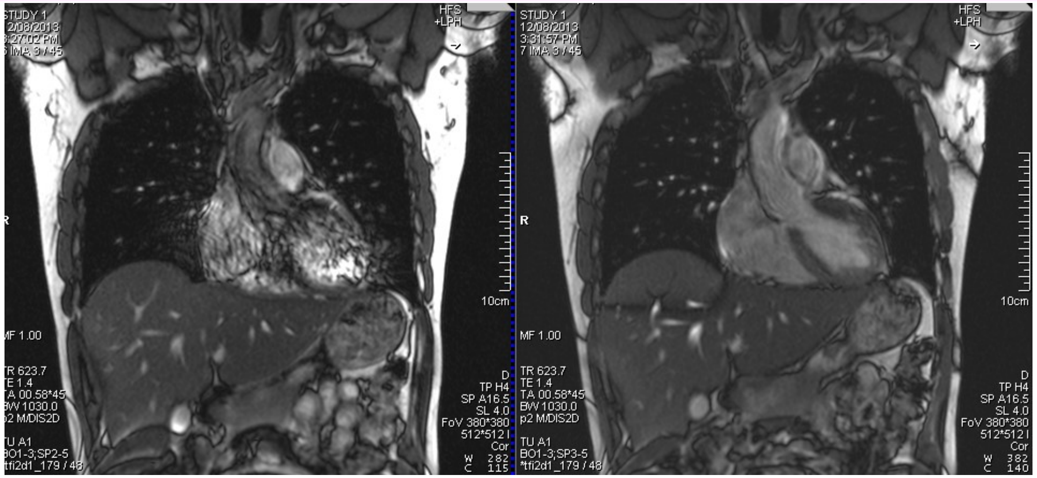
STUDY 1
12/08/2013
HFS
+LPH
R
10cm
MF 1.00
TR 623.7
TE 1.4
TA 00.58*45
BW 1030.0
p2 M/DIS2D
TU A1
TP H4
SP A16.5
SL 4.0
FoV 380*380
512*512 I
Cor
STUDY 1
12/08/2013
3:31:57 PM
7 IMA 3 / 45
HFS
+LPH
R
10cm
MF 1.00
TR 623.7
TE 1.4
TA 00.58*45
BW 1030.0
p2 M/DIS2D
TU A1
BO1-3;SP3-5
*tfi2d1_179 / 48
D
TP H4
SP A16.5
SL 4.0
FoV 380*380
512*512 I
Cor
W 382
C 140

Reduced artefacts with cardiac shim

Real time free breathing lung scans using TrueFISP

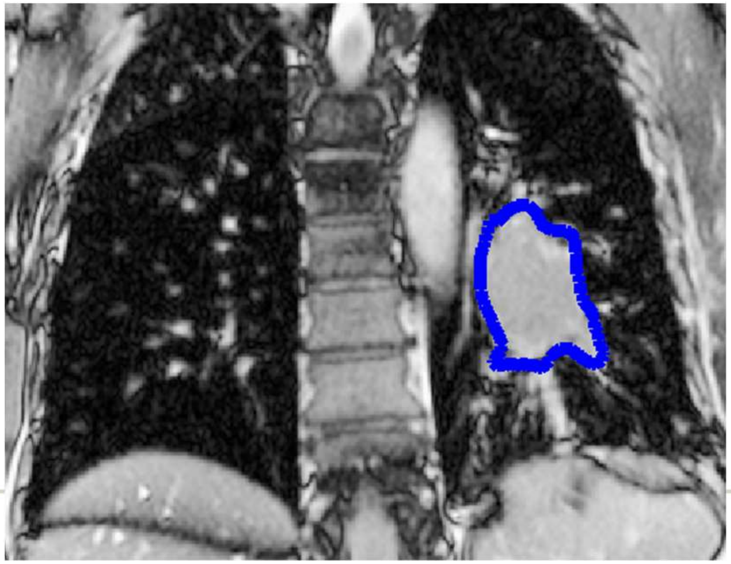

Gradient-Speed Limit

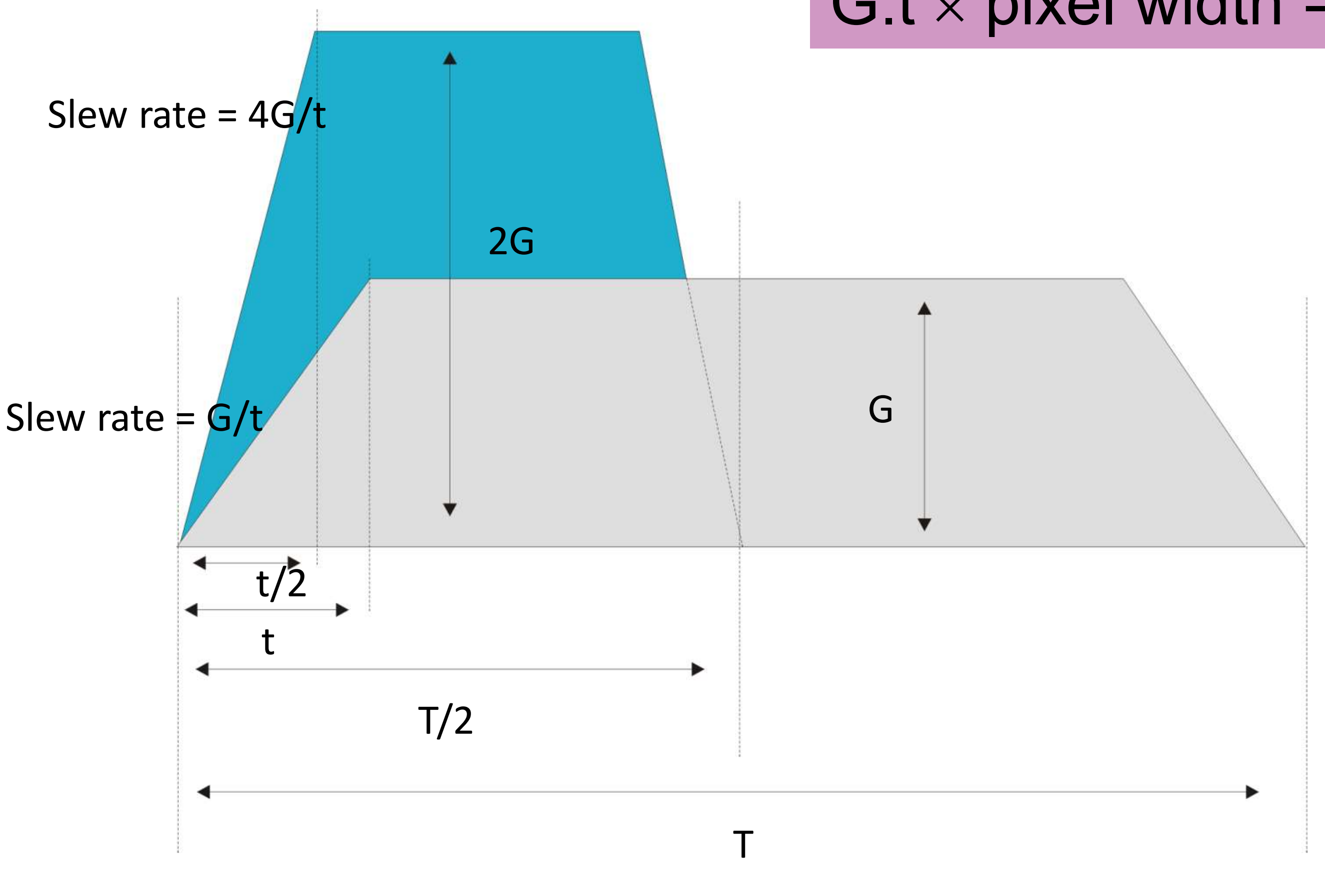
Slew rate = 4G/t
2G
Slew rate = G/t
G
t/2
t
T/2
T

G.t × pixel width = constant

Gradients can be made to run faster

but

Physiological limit = PNS

Parallel Imaging

- Acquire fewer k-space lines
  - ✓ Speed up scanning
- Use Coil Arrays to:

Unwrap aliased images (image space) ‘SENSE’ -like

OR

Generate missing lines (k-space) ‘SMASH’ -like

Scan time = $(TR \times N_{AV} \times N_{PE})/R$

‘Coil Encoding’

Multi-channel RF coils:
Signal strength from one coil
with respect to another
provides
alternative localisation method

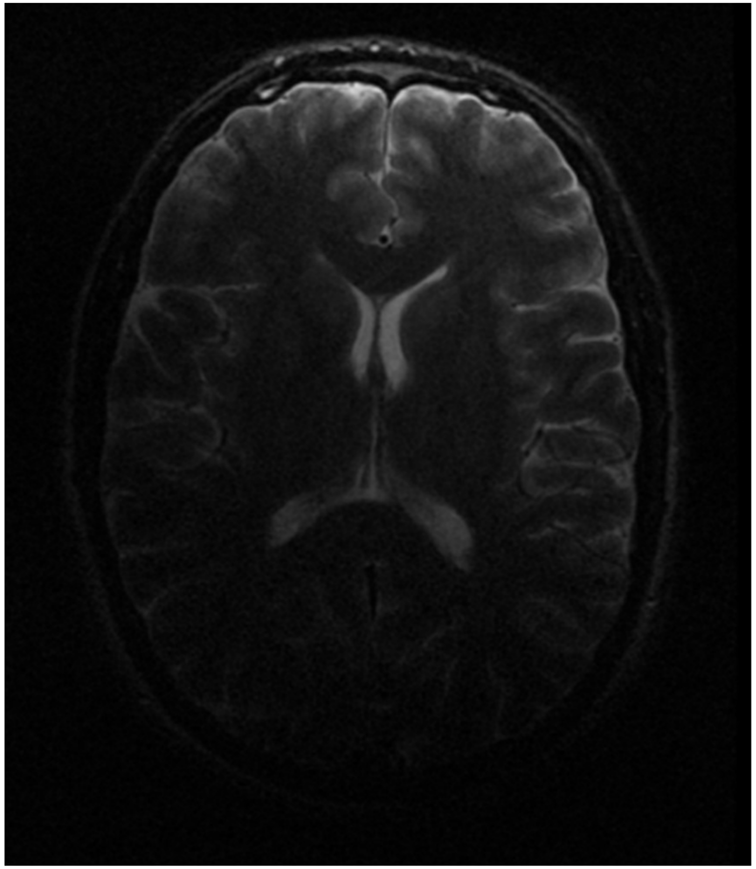

Parallel Imaging

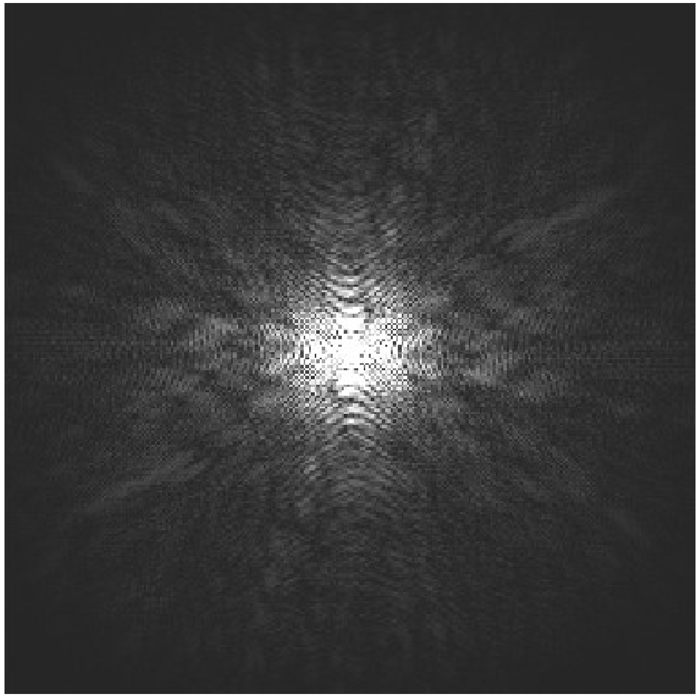

Full k-space
(takes time!)

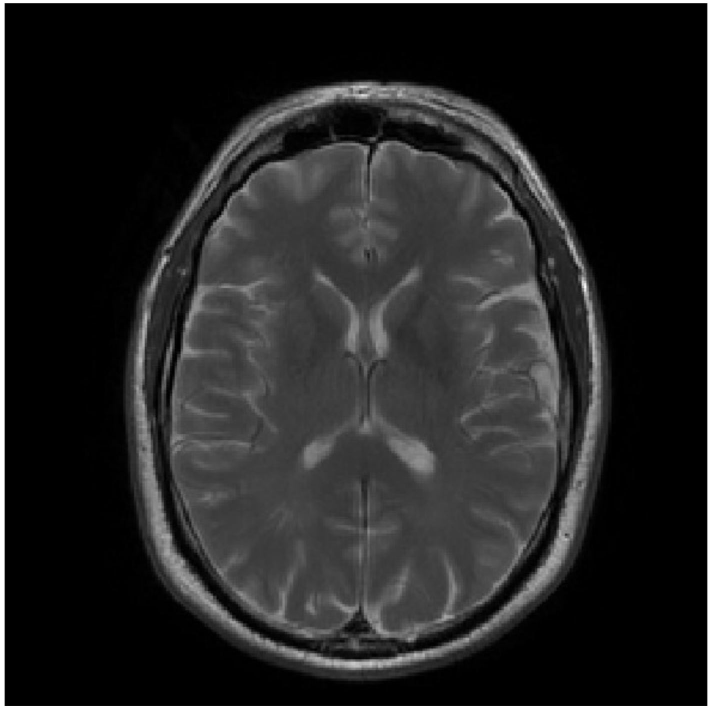

Whole image

Parallel Imaging

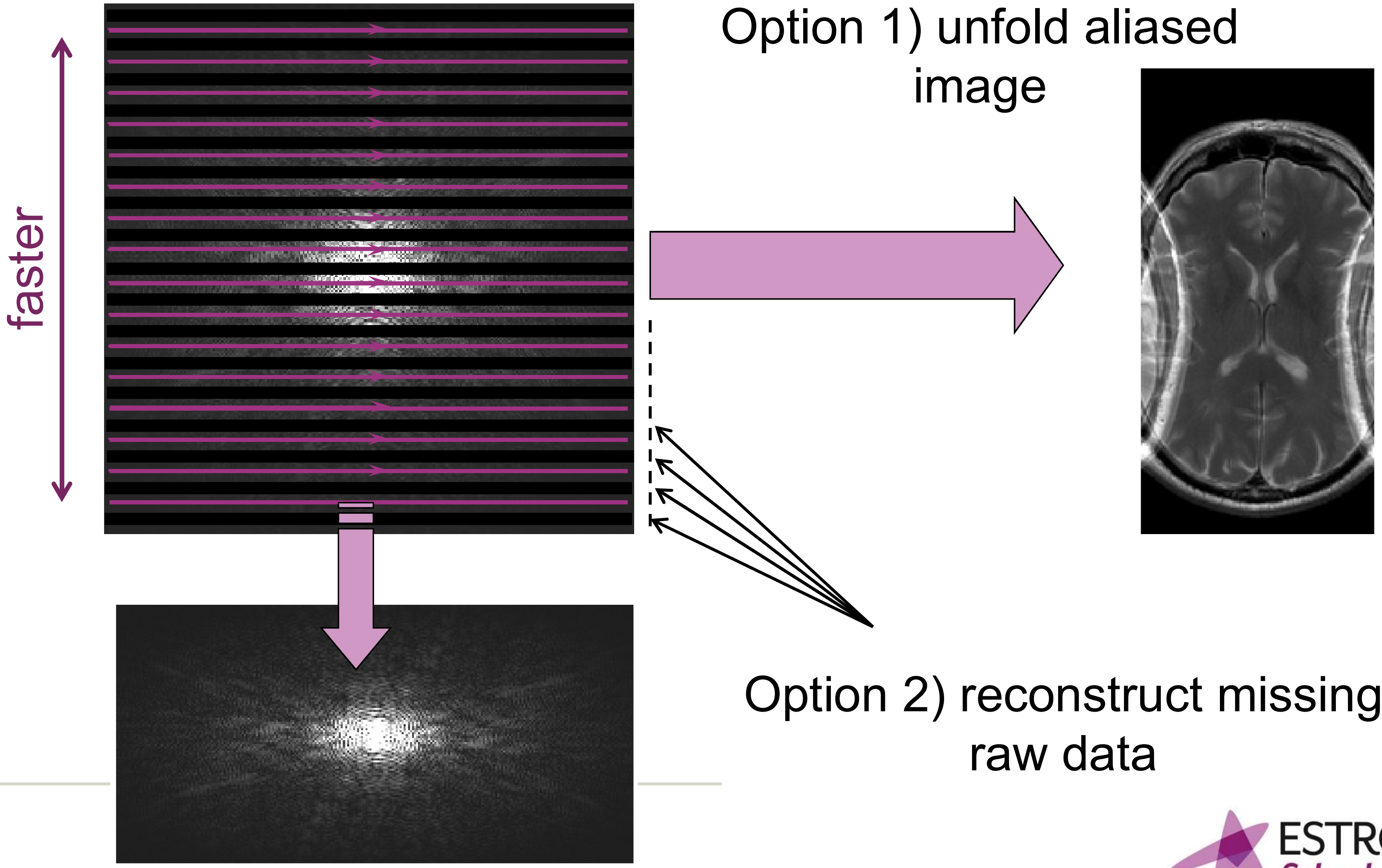

Option 1) unfold aliased image

Option 2) reconstruct missing raw data

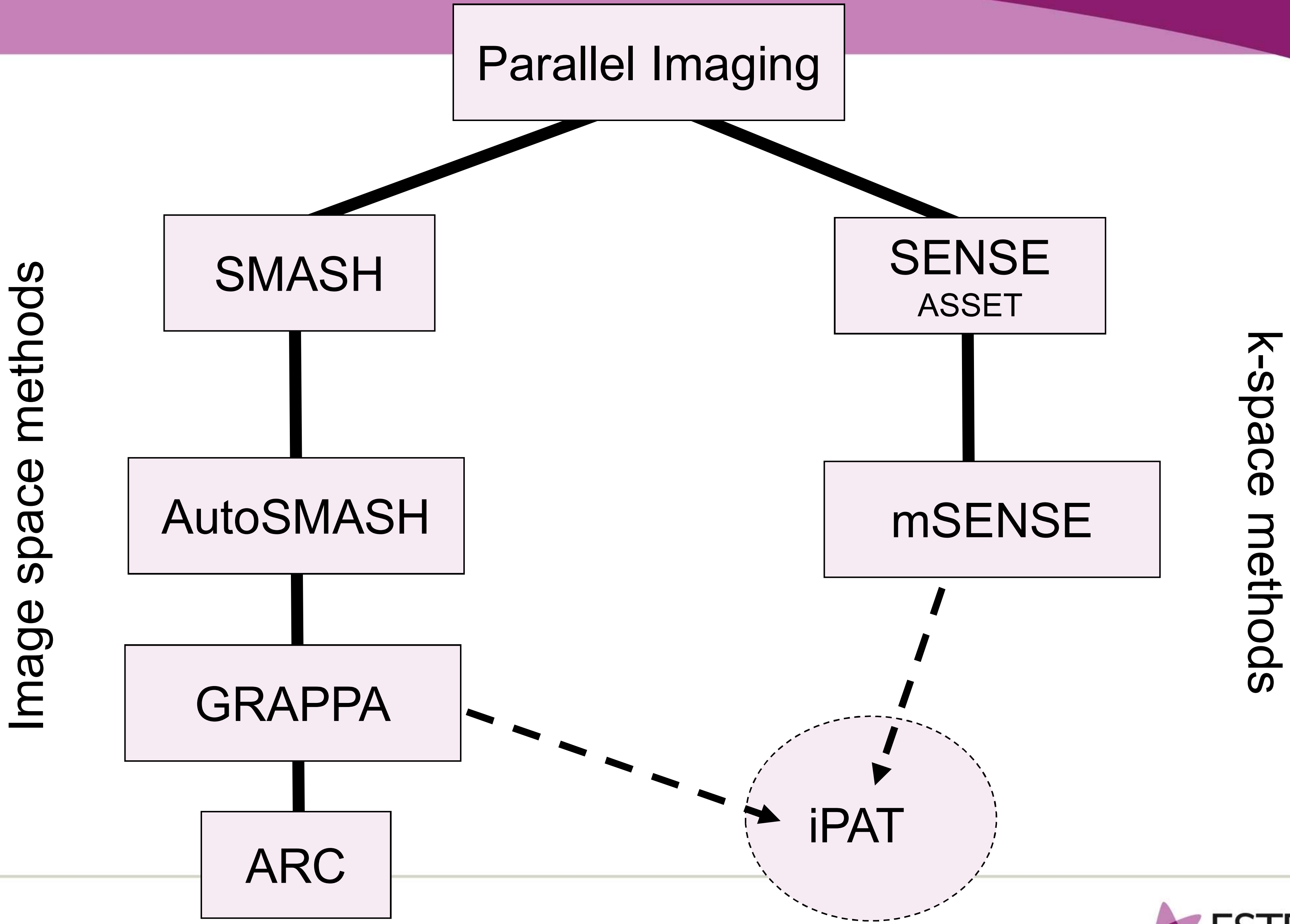

Parallel Imaging

Image space methods

SMASH

AutoSMASH

GRAPPA

ARC

k-space methods

SENSE
ASSET

mSENSE

iPAT

SENSE

- SENSitivity Encoding
- Commercially implemented by Philips
- Other Implementations:
  - ASSET (GE), SPEEDER (Toshiba), RAPID (Hitachi)
- Apply knowledge of coil sensitivity profiles to calculate aliased signal component
- Can be applied in through-plane phase encoding (3D)
- Reduction Factor = 1 to number of coils (+non integers)
- Cannot handle inherent aliasing (FOV must encompass object)

Where $\Delta y = FOV_{rec}/R$

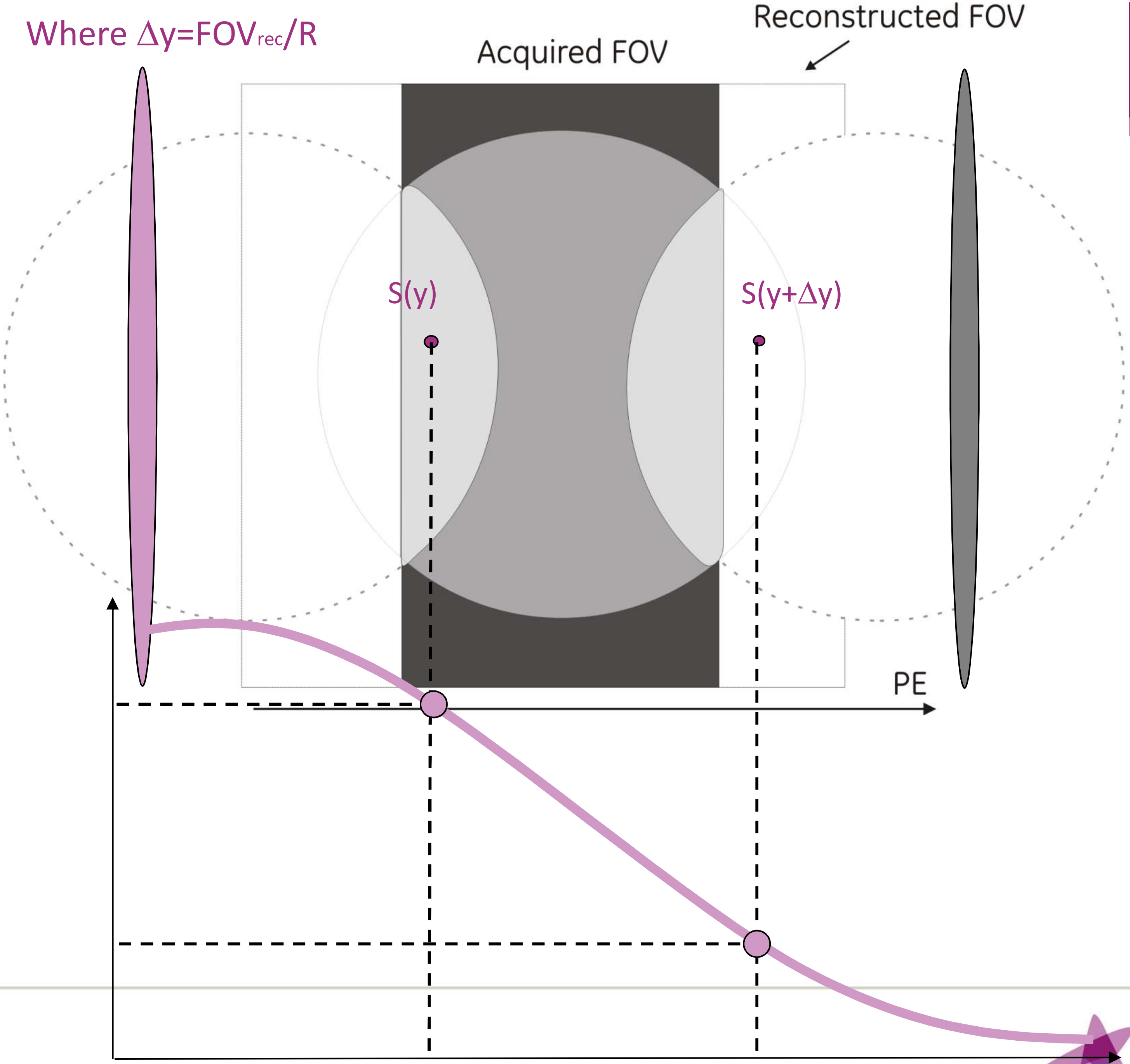
Reconstructed FOV
Acquired FOV
S(y)
S(y+Δy)
PE

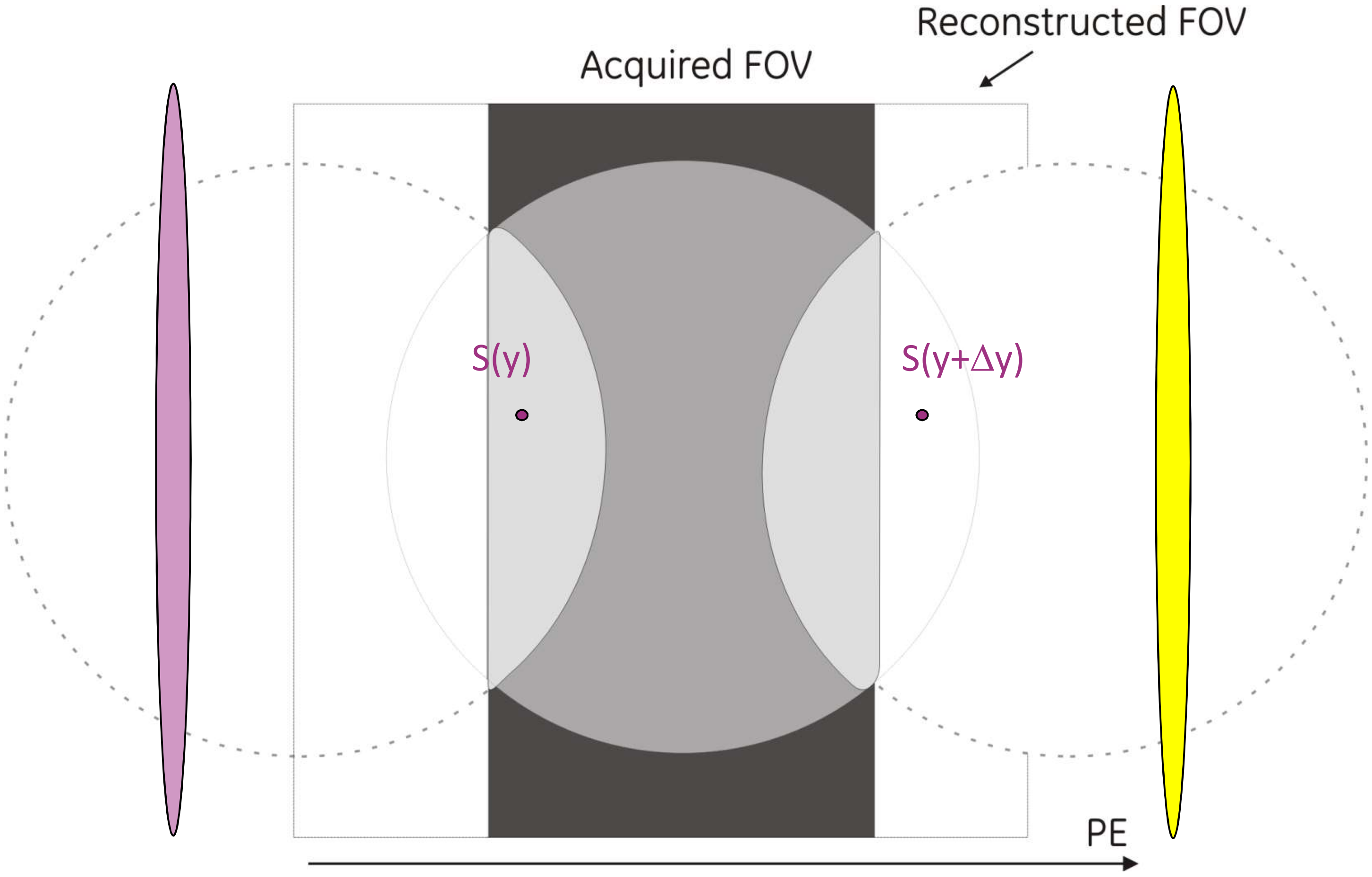
Reconstructed FOV
Acquired FOV
S(y)
S(y+∆y)
PE

$I(y)_1 = C_1(y)S(y) + C_1(y + FOV_{rec}/R)\, S(y + FOV_{rec}/R)$

$I(y)_2 = C_2(y)S(y) + C_2(y + FOV_{rec}/R)\, S(y + FOV_{rec}/R)$

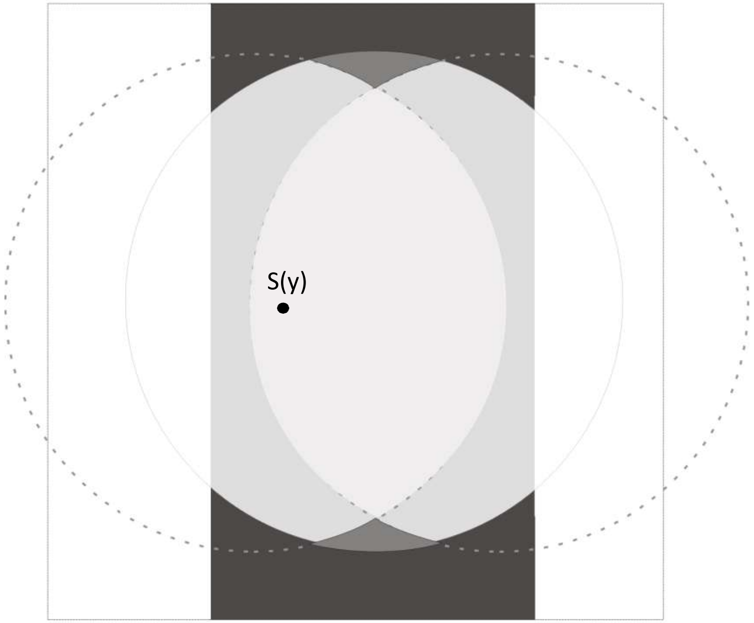

$$I_j(x,y)=\sum_{n=0}^{n_A-1} C_j(x,y+n\Delta Y)\,S(x,y+n\Delta Y)$$

$$I_j(y)=C_j(y)\,S(y)+C_j(y+\Delta Y)\,S(y+\Delta Y)+\ldots+C_j(y+(n_A-1)\Delta Y)\,S(y+(n_A-1)\Delta Y)$$

$$\begin{pmatrix} I_1(x,y)\\ I_2(x,y)\\ .\\ .\\ .\\ I_L(x,y)\end{pmatrix}_{L\,x\,1}=\begin{pmatrix} C_1(x,y) & C_1(x,y+\Delta Y) & . & . & . & C_1\left(x,y+\left(n_A-1\right)\Delta Y\right)\\ C_2(x,y) & C_2(x,y+\Delta Y) & . & . & . & C_2\left(x,y+\left(n_A-1\right)\Delta Y\right)\\ . & & . & & & .\\ . & & & . & & .\\ . & & & & . & .\\ C_L(x,y) & C_L(x,y+\Delta Y) & & & & C_L\left(x,y+\left(n_A-1\right)\Delta Y\right)\end{pmatrix}_{L\,x\,n_A}\begin{pmatrix} S(x,y)\\ S(x,y+\Delta Y)\\ .\\ .\\ .\\ S\left(x,y+\left(n_A-1\right)\Delta Y\right)\end{pmatrix}_{n_A\,x\,1}$$

$$I=C\,S$$

SENSE

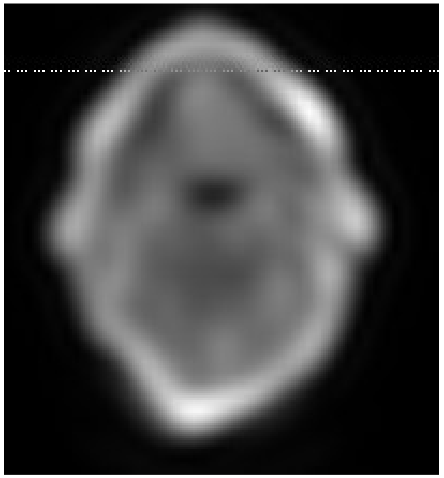

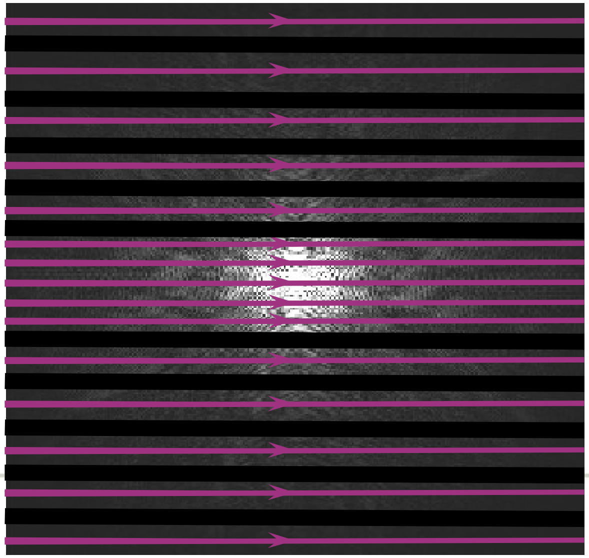

- Calibration scan (sensitivity maps) required
- Typically 20 s
- single scan only
- Relies on no patient motion between calibration and speed-up scans
- Modified SENSE uses calibration from oversample k-space

$$SNR' = \frac{SNR}{g\sqrt{R}}$$

SMASH

- SiMultaneous Acquisition of Spatial Harmonics
- Re-create sinusoidal signal variation from ‘missing’ phase encoding

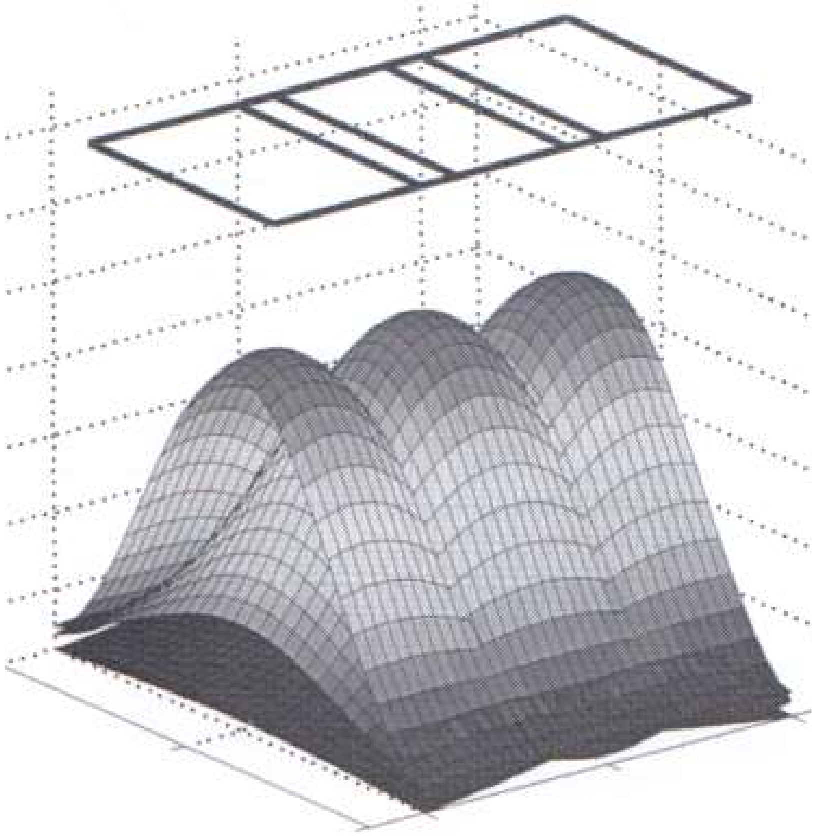

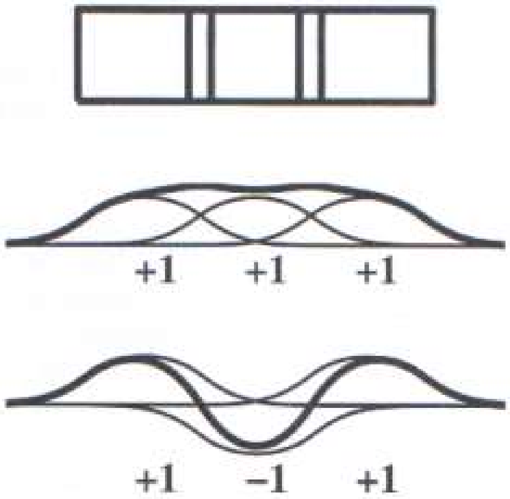

Empirical self calibration:

AutoSMASH

GRAPPA

ARC

Example: iPAT

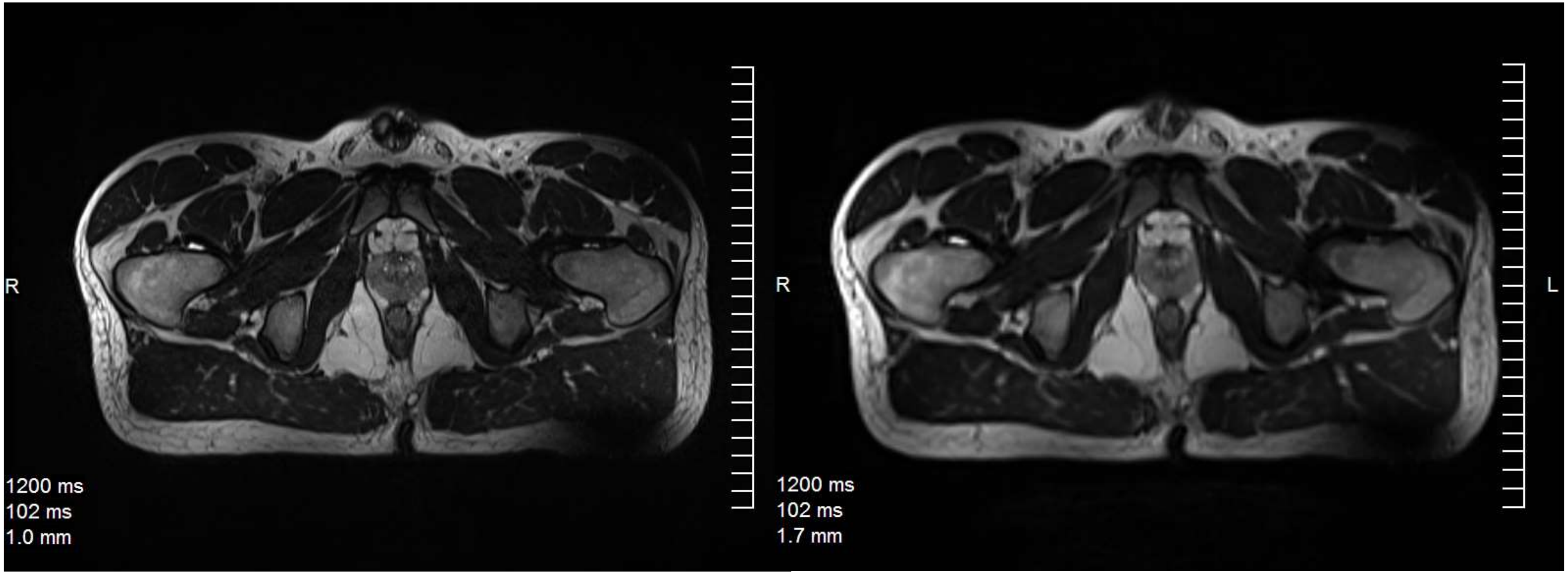
R
1200 ms
102 ms
1.0 mm
R
L
1200 ms
102 ms
1.7 mm

iPAT (4): 5 min 17 s

5 min 42 s

DIXON Imaging

- Fat and water have different resonance frequencies (220 Hz at 1.5 T)
- At specific echo times (TE) fat and water are either in phase (=1/220 Hz or every 4.6 ms) or put of phase
- Total of 4 Image contrasts are obtained (useful in MR-only)

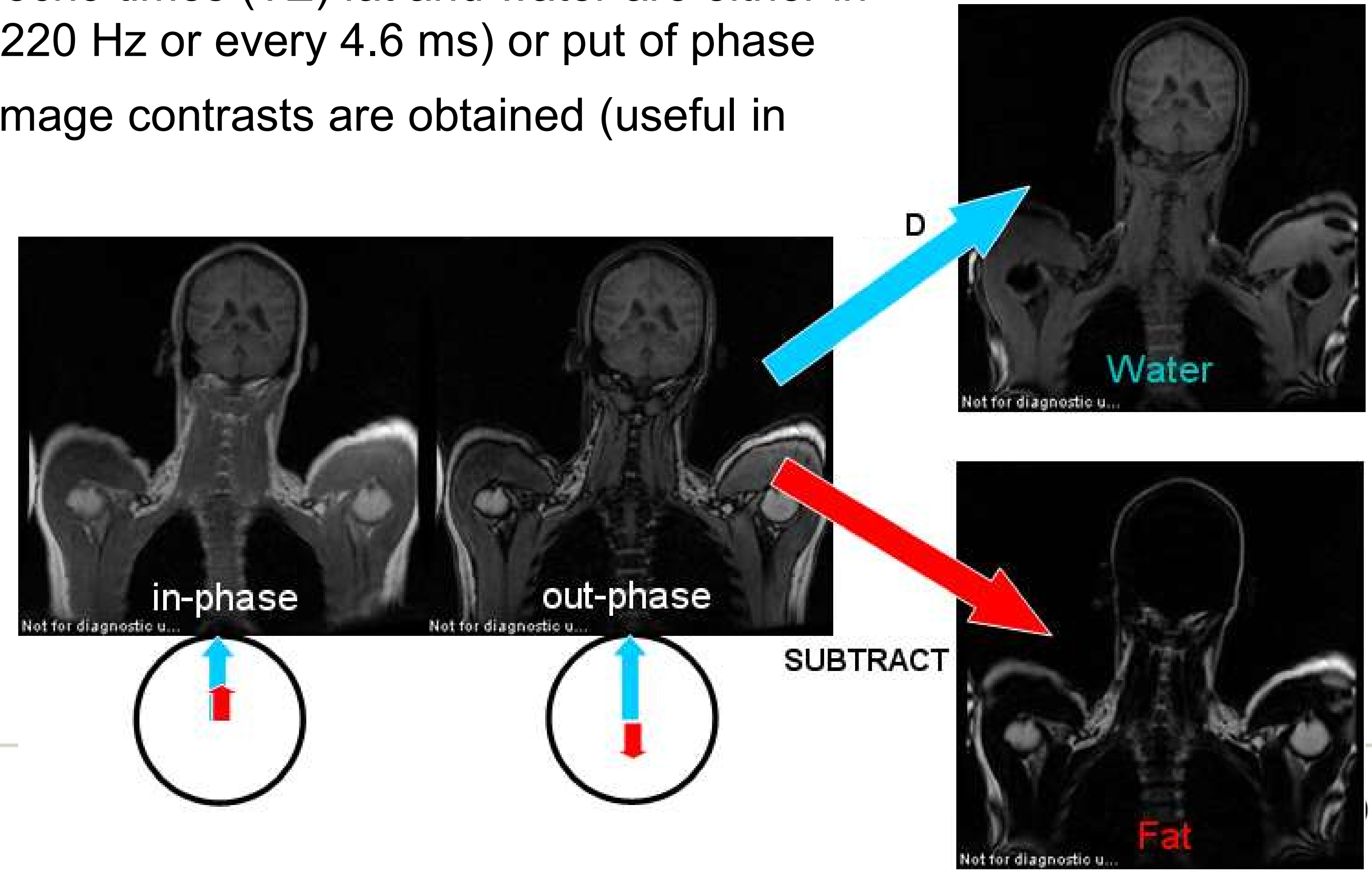
D
Water
Not for diagnostic u...
in-phase
Not for diagnostic u...
out-phase
Not for diagnostic u...
SUBTRACT
Fat
Not for diagnostic u...

k-space: Acquisition strategies

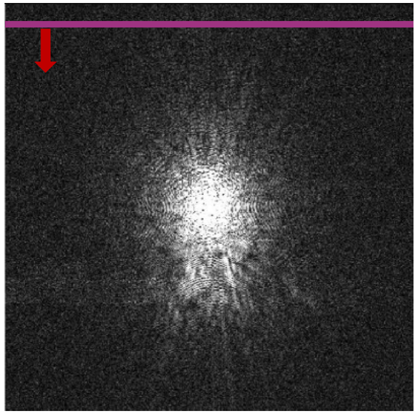

Spin-echo

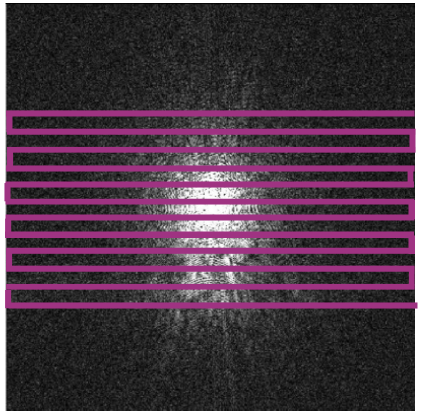

Single-Shot

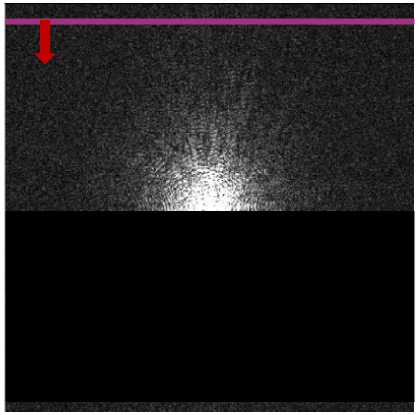

Partial Data

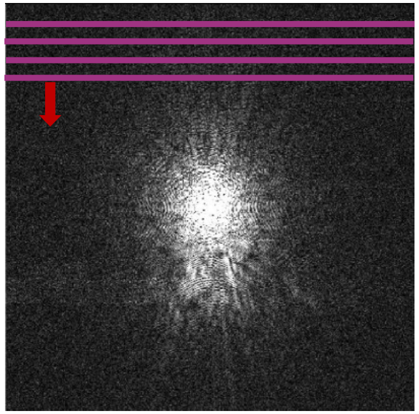

Segmented

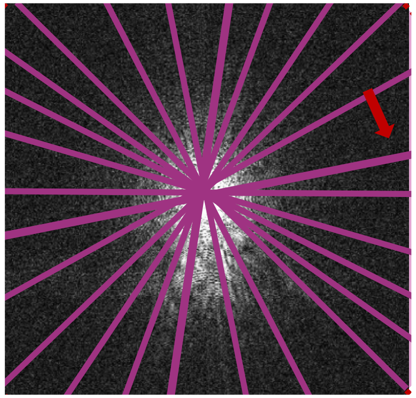

Radial

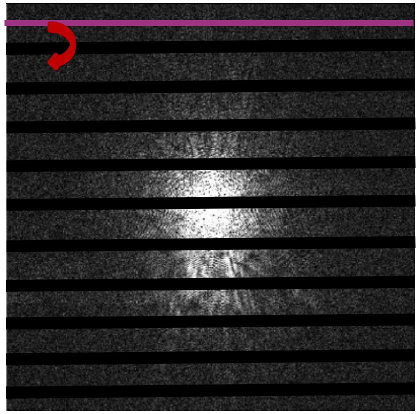

Parallel imaging

Radial Acquisition

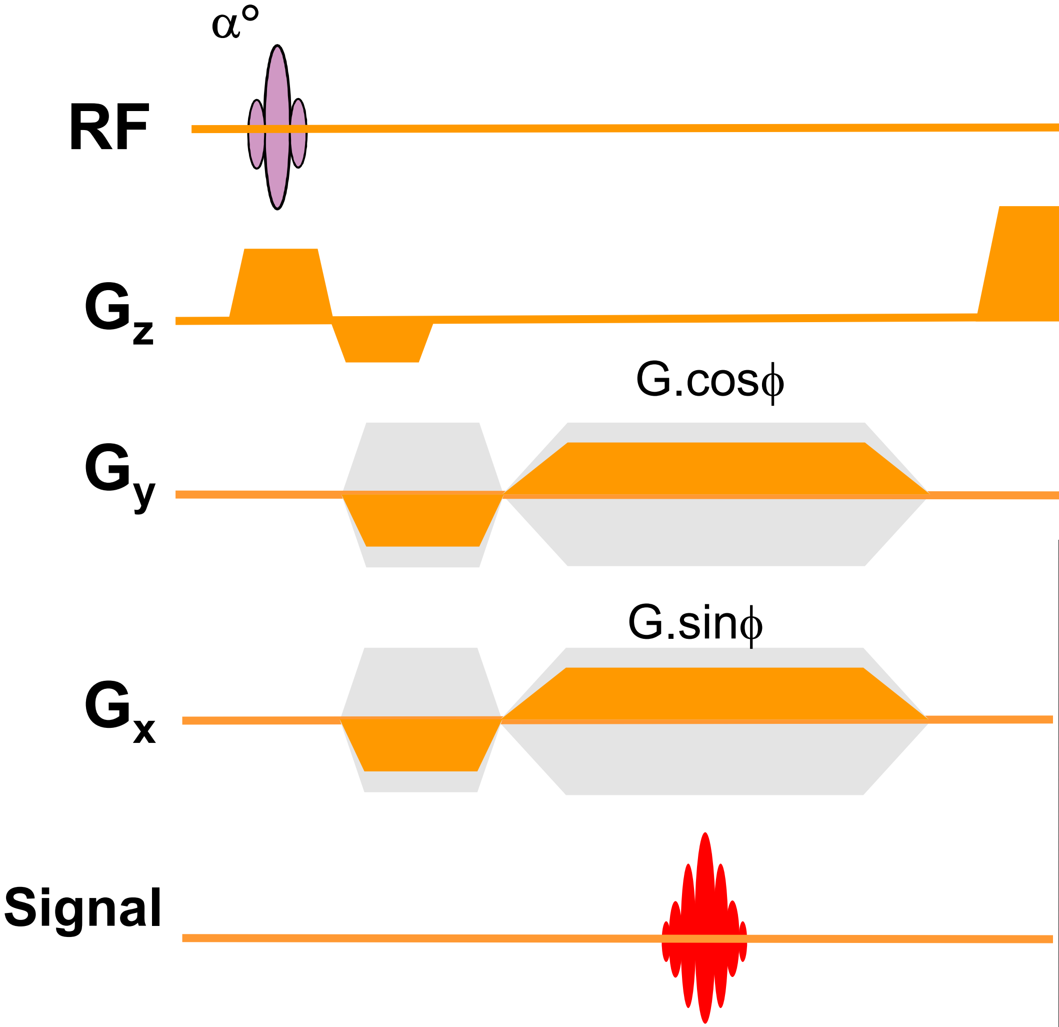
α°
RF
G_z
G_y
G.cosϕ
G_x
G.sinϕ
Signal

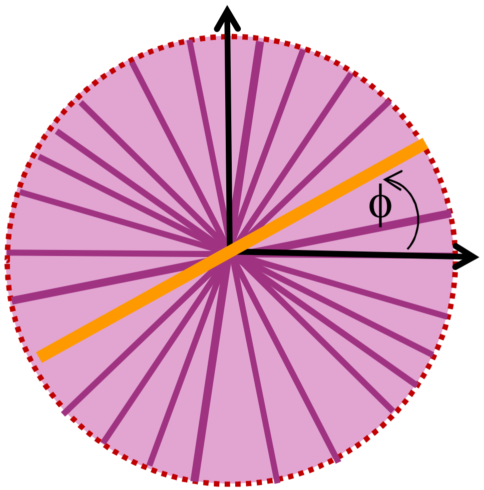

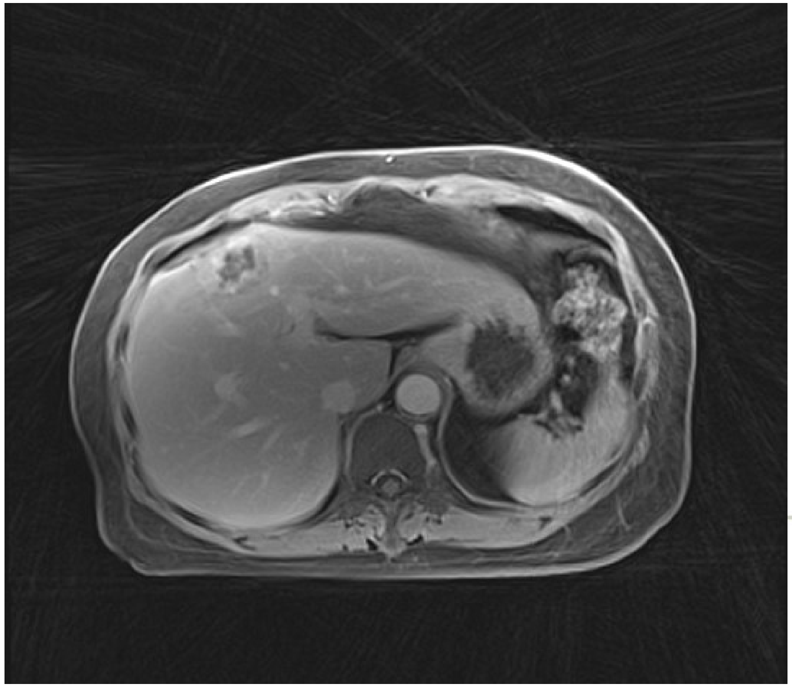

Ultra-short TE

- Radial (and spiral) trajectory very fast and efficient
- TE can be further minimised with non-selective or half RF pulses and ramp sampling
- TE can be limited to switching capability of Tx/Rx
- TE ≤ 0.1 ms (100 μs) said to be ‘ultrashort’

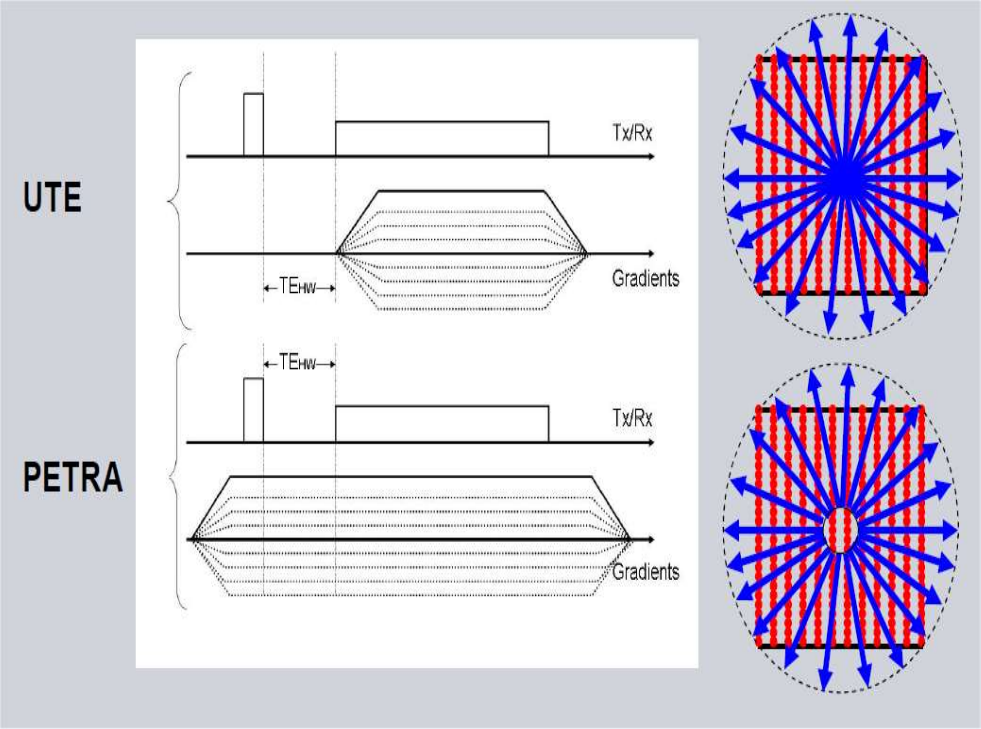
UTE
Tx/Rx
Gradients
TEHW
PETRA
TEHW
Tx/Rx
Gradients

- In some methods (ZTE and PETRA) gradients ramped up prior to sampling

Ultra-short TE

T2 values
Water: 4000 ms
Soft-tissue: 90 ms
Achiles tendon: 5 ms
Cortical bone: 0.5 ms
Ice: 0.015 ms

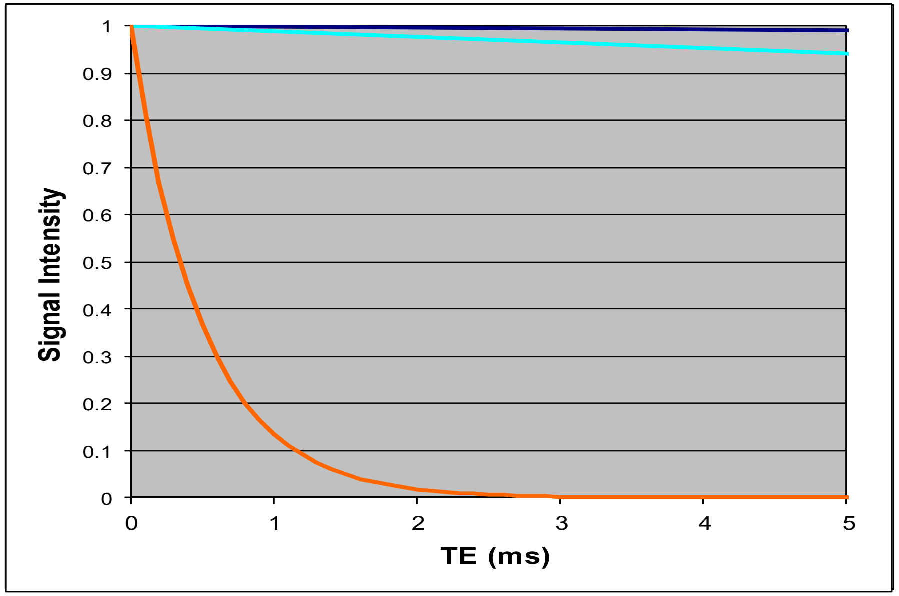

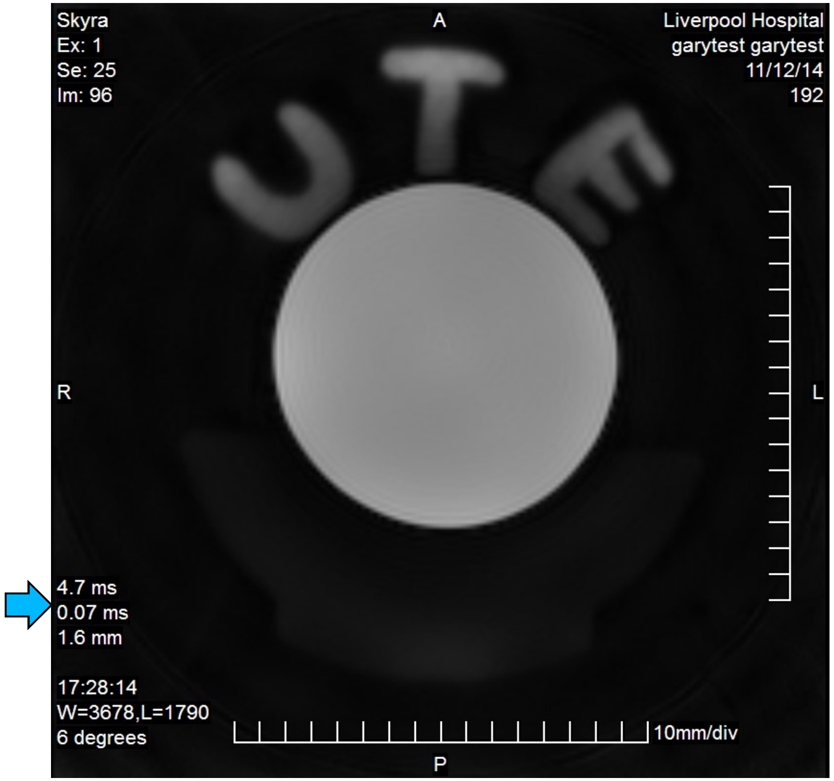
Skyra
Ex: 1
Se: 25
Im: 96
A
Liverpool Hospital
garytest garytest
11/12/14
192
UTE
R
L
4.7 ms
0.07 ms
1.6 mm
17:28:14
W=3678,L=1790
6 degrees
10mm/div
P

Solid material becomes **visible** if we can encode signal **rapidly**

UTE Examples

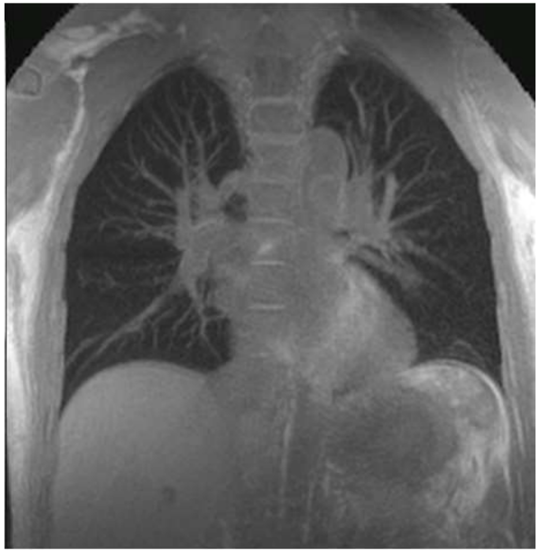

Lung

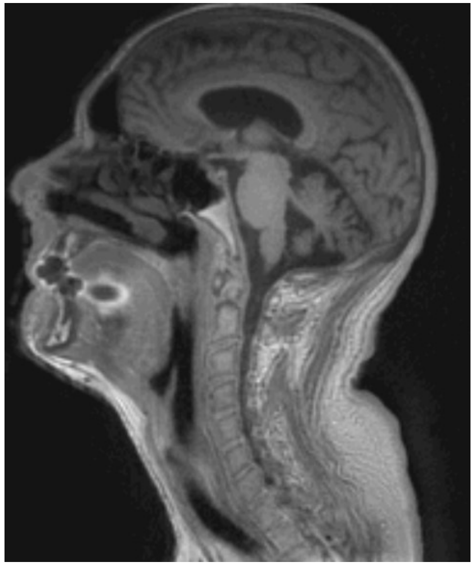

H&N

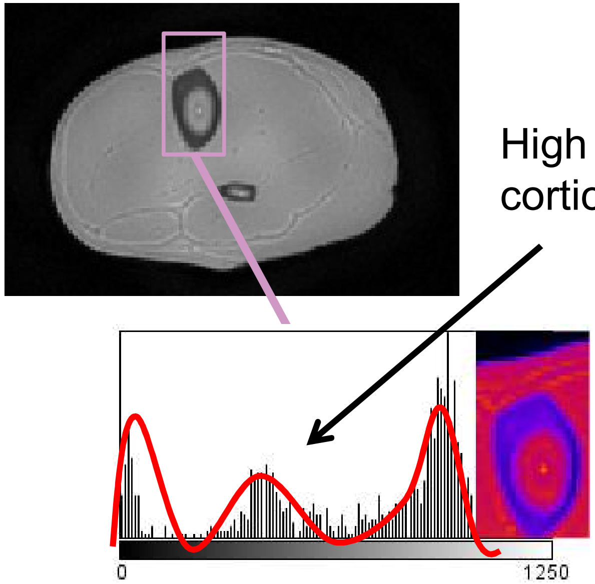

High SNR in cortical bone

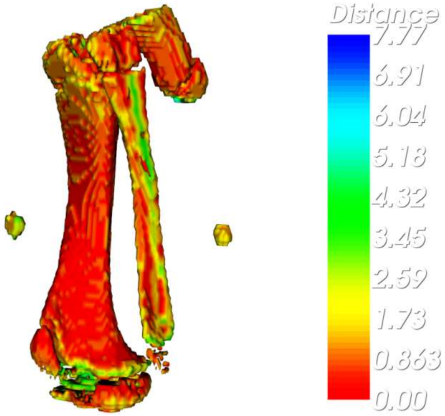
Distance
7.77
6.91
6.04
5.18
4.32
3.45
2.59
1.73
0.863
0.00

Bone segmentation

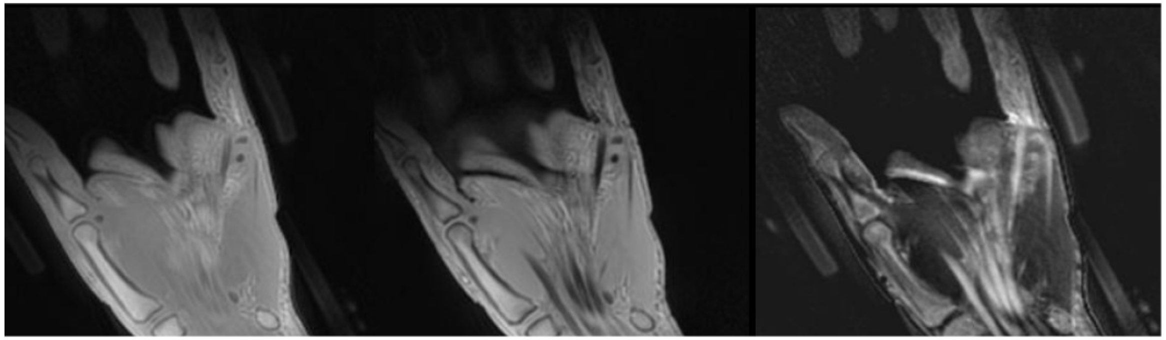

0.07 ms - 2.3 ms = subtraction

Questions?

Positron Emission Tomography

Physics – Image Reconstruction, Contouring

ESTRO Teaching Course on Advanced Imaging Technologies

November 5 – 9, 2017 in Malaga, Spain

Daniela Thorwarth
Section for Biomedical Physics,
University Hospital for Radiation Oncology, Tübingen

Eberhard-Karls-Universität
UKT
Universitätsklinikum Tübingen

PET Image Formation

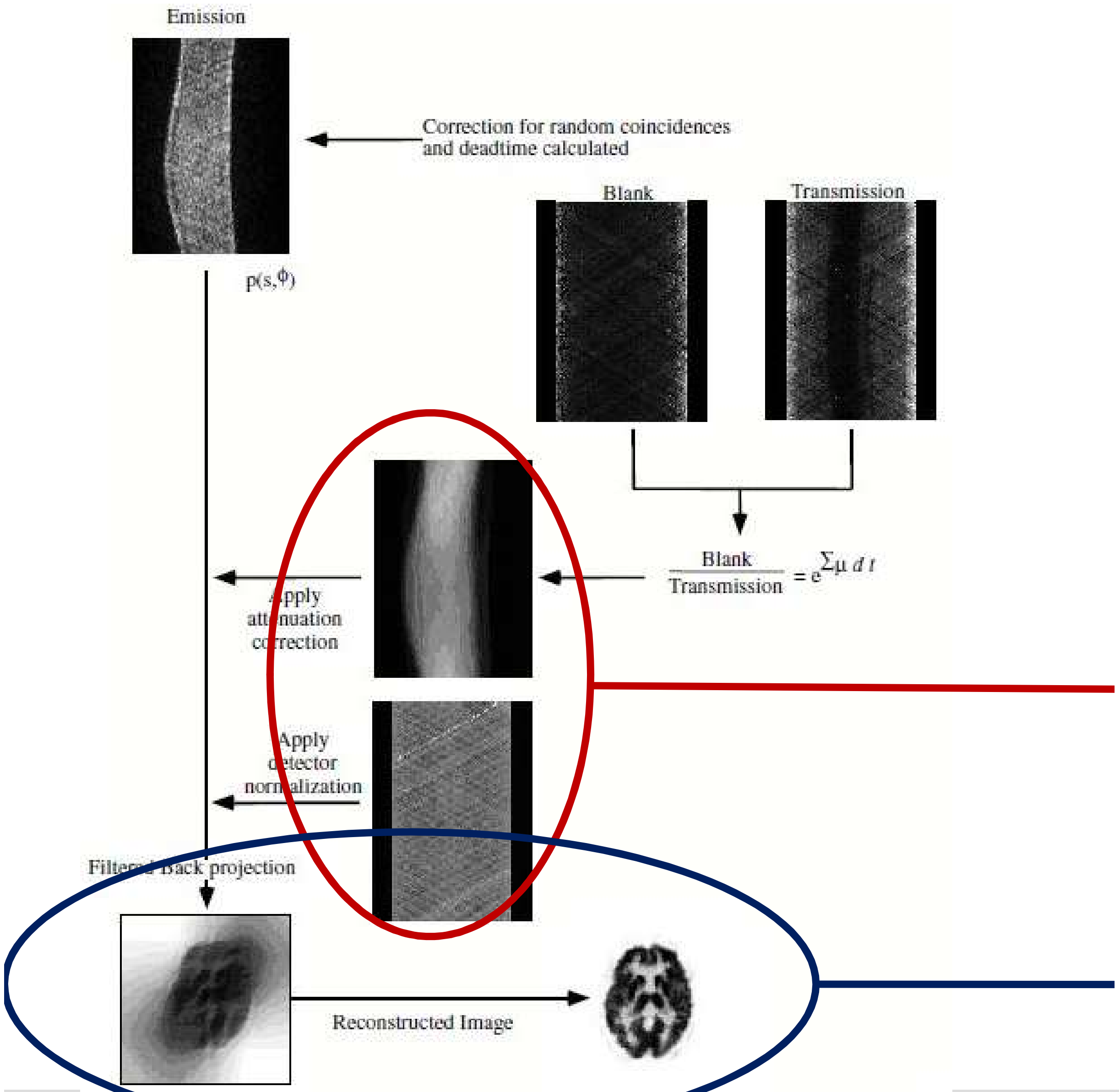
Emission
Correction for random coincidences and deadtime calculated
Blank
Transmission
p(s,φ)
Blank / Transmission = e^Σμ d t
Apply attenuation correction
Apply detector normalization
Filtered Back projection
Reconstructed Image

1. Raw data correction

2. Image Reconstruction

Random Correction

- Randoms: $R_{ab} = 2\tau \cdot N_a N_b \propto N^2$

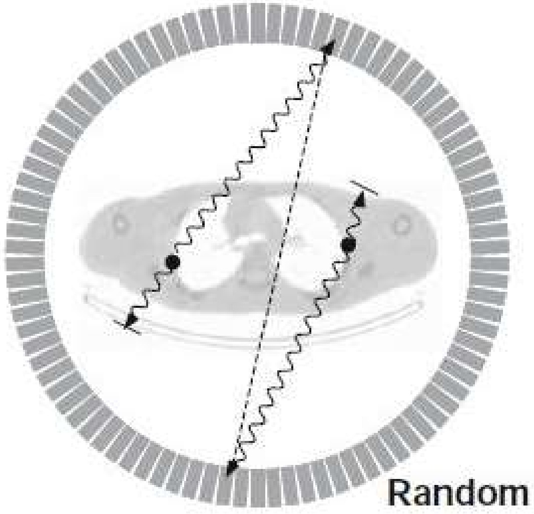

Correction Methods:

- Tail Fitting
  - Estimate random distribution in the object by fitting the tails outside the object
- Estimation from Single Rates
  - Direct determination from single rates N_a and N_b
- Delayed Coincidence Channel Estimation
  - Data stream containing signals from one channel is delayed for several times the coincidence window
  - Removal of all annihilation events
  - Any coincidences detected are random
  - Subtraction from coincidences in the prompt channel

Normalization

- LORs have different sensitivities
- Individual correction factor for each LOR

Correction Methods:

- Direct Normalization
  - Illumination of all possible LORs with planar or rot. line source
  - Long scan times necessary
  - Sources must have very uniform activity distribution

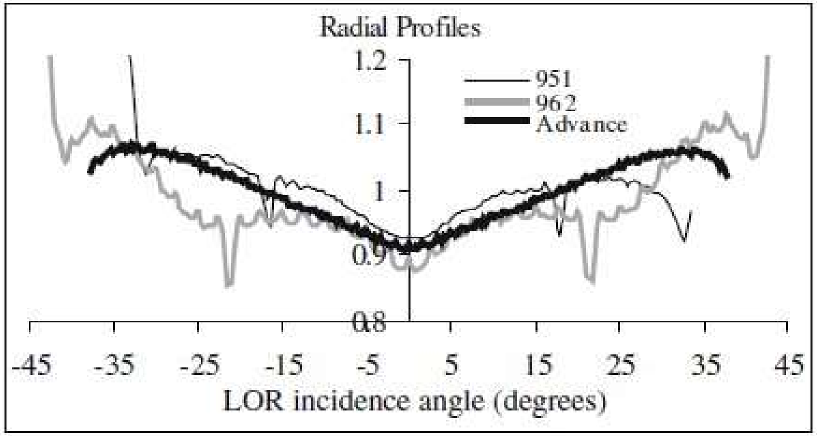

Mean radial geometric profiles for three block-detectors. Asymmetry due to the fact that centre of rotation of sources not coincident with center of detector ring (from [2]).

- Component-based Model for Normalization

Dead Time Correction

- Measurement of dead time with ‘decaying source’
  - Uniform source (^{18}F, ^{11}C) of known activitiy
  - Measurements of singles, prompt and random coincidence rates

- Construction of look-up tables for dead time correction factors

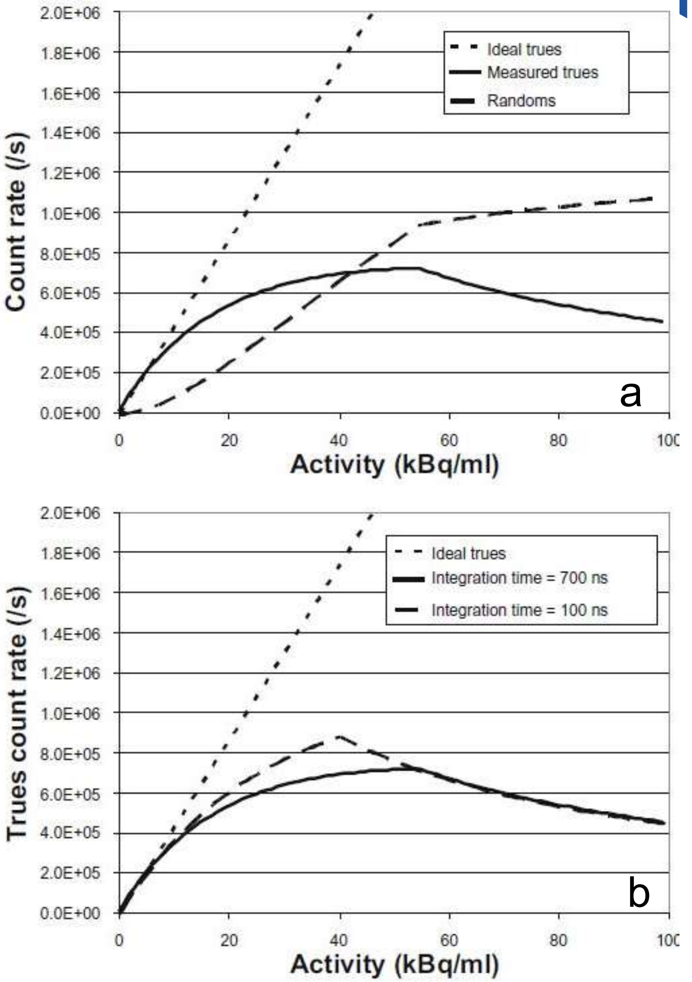

(a) Effect of dead time on count rate linearity.

(b) Effect of shortening the signal integration time (from [2]).

Scatter Correction

- Most likely: Compton scattering
- Compton equation $$E_{sc} = \frac{E}{1+\frac{E}{m_0c^2}(1-\cos\Omega)}$$
  - Relates photon energy before (*E*) and after scattering (E_{sc}) to scattering angle *Ω*
  - m_0c^2: resting energy of electron before scattering

Correction strategies:

- Fitting scatter tails
- Direct measurement
- Dual energy window methods
- Multiple energy window methods
- Simulation-based methods

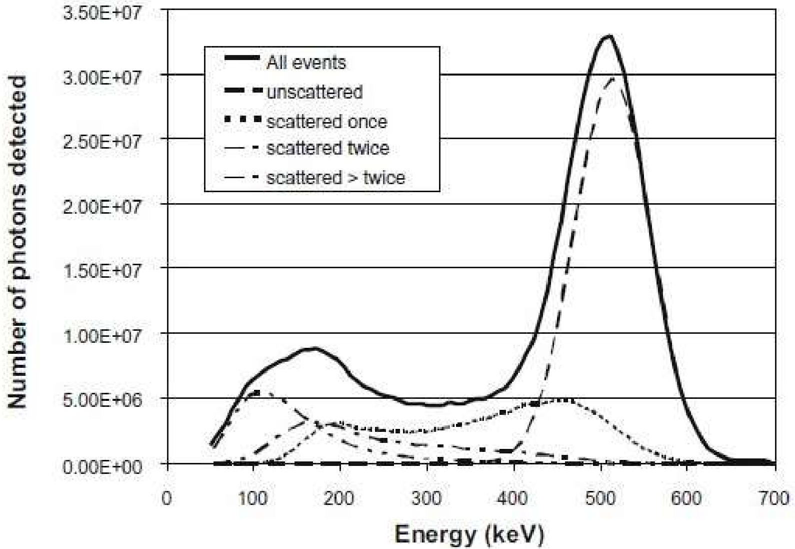

Spectral distribution of scattered 511 keV photons [2].

Improved image quality due to random and scatter correction

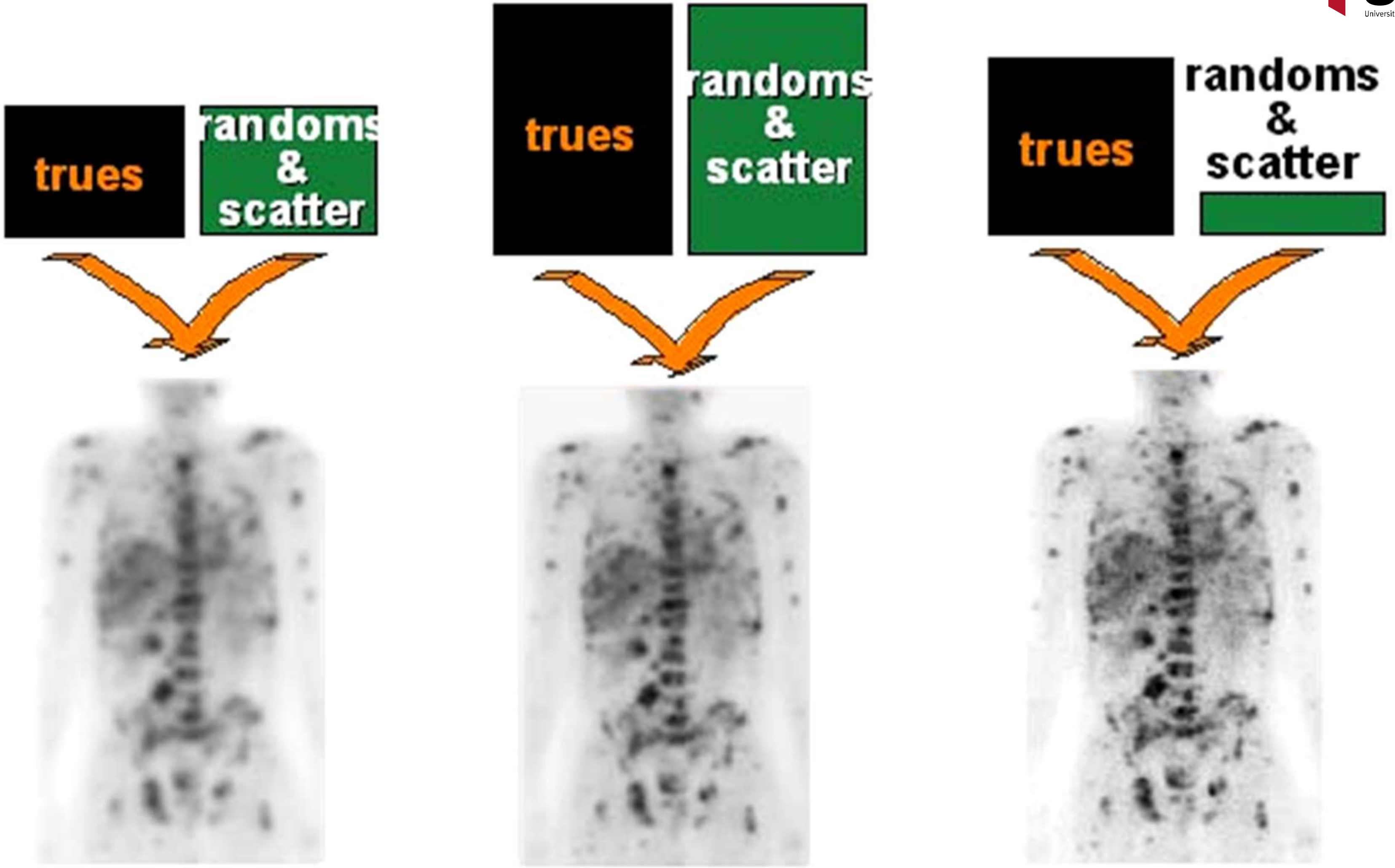
trues
randoms & scatter
trues
randoms & scatter
trues
randoms & scatter

Attenuation Correction

Probability P_1 for quant γ$_1$ to reach a detector:

$$P_1 = k_1 \cdot e^{-\int_{x}^{x_O} \mu(x)dx}$$

Accordingly P_2 for quant γ$_2$:

$$P_2 = k_2 \cdot e^{-\int_{x_u}^{x} \mu(x)dx}$$

Probability for a coincidence event:

$$P_{tot} = P_1 \cdot P_2 = k_1 \cdot k_2 \cdot e^{-\int_{x_u}^{x_O} \mu(x)dx}$$

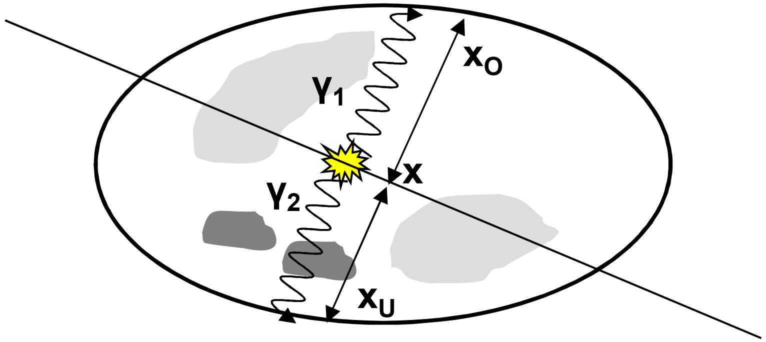

Accurate attenuation correction is possible if the line integral $\int_{x_u}^{x_o} \mu(x)dx$ can be obtained from a transmission measurement.

➡ **CT is used for attenuation correction!**

CT-based attenuation correction

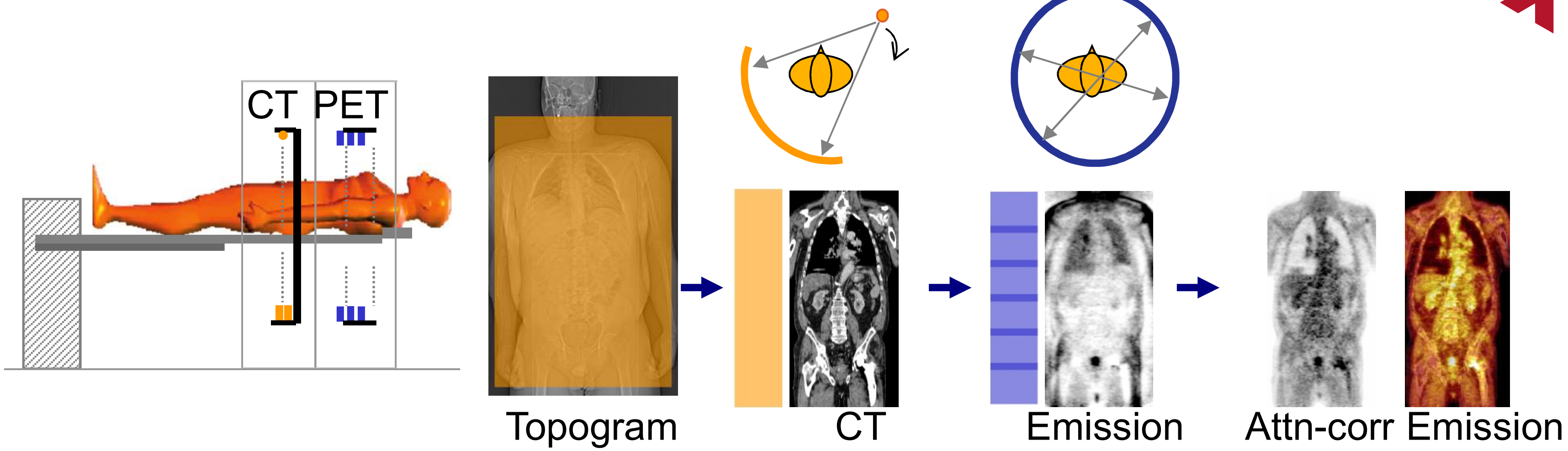
CT
PET
Topogram
CT
Emission
Attn-corr Emission

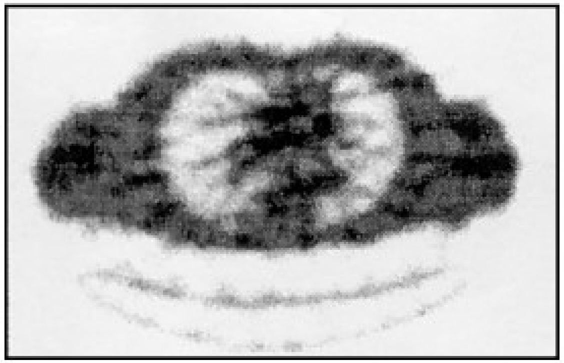

(a) ^{68}Ge/^{68}Ga positron source

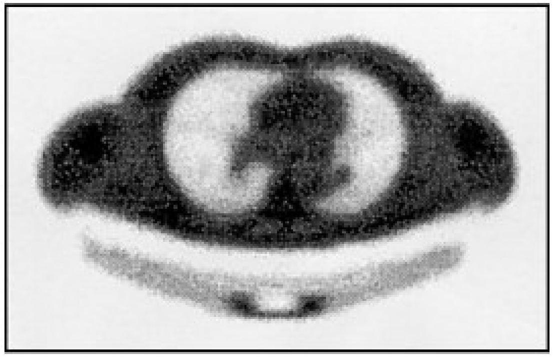

(b) ^{137}Cs gamma-ray source

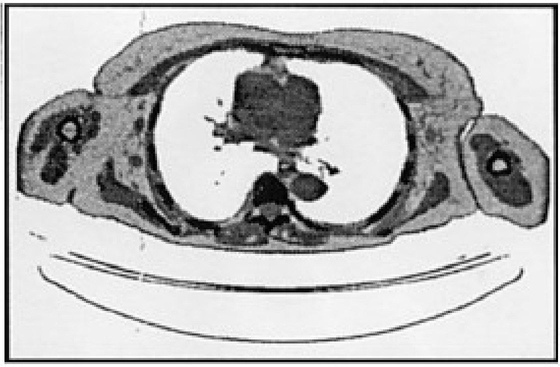

(c) 120 kVp x-ray source

CT-transmission imaging: fast, low noise, not affected by emission.

Kinahan et al, Sem Nucl Med 2003.

Artifacts due to CT-based attenuation correction

Breathing…

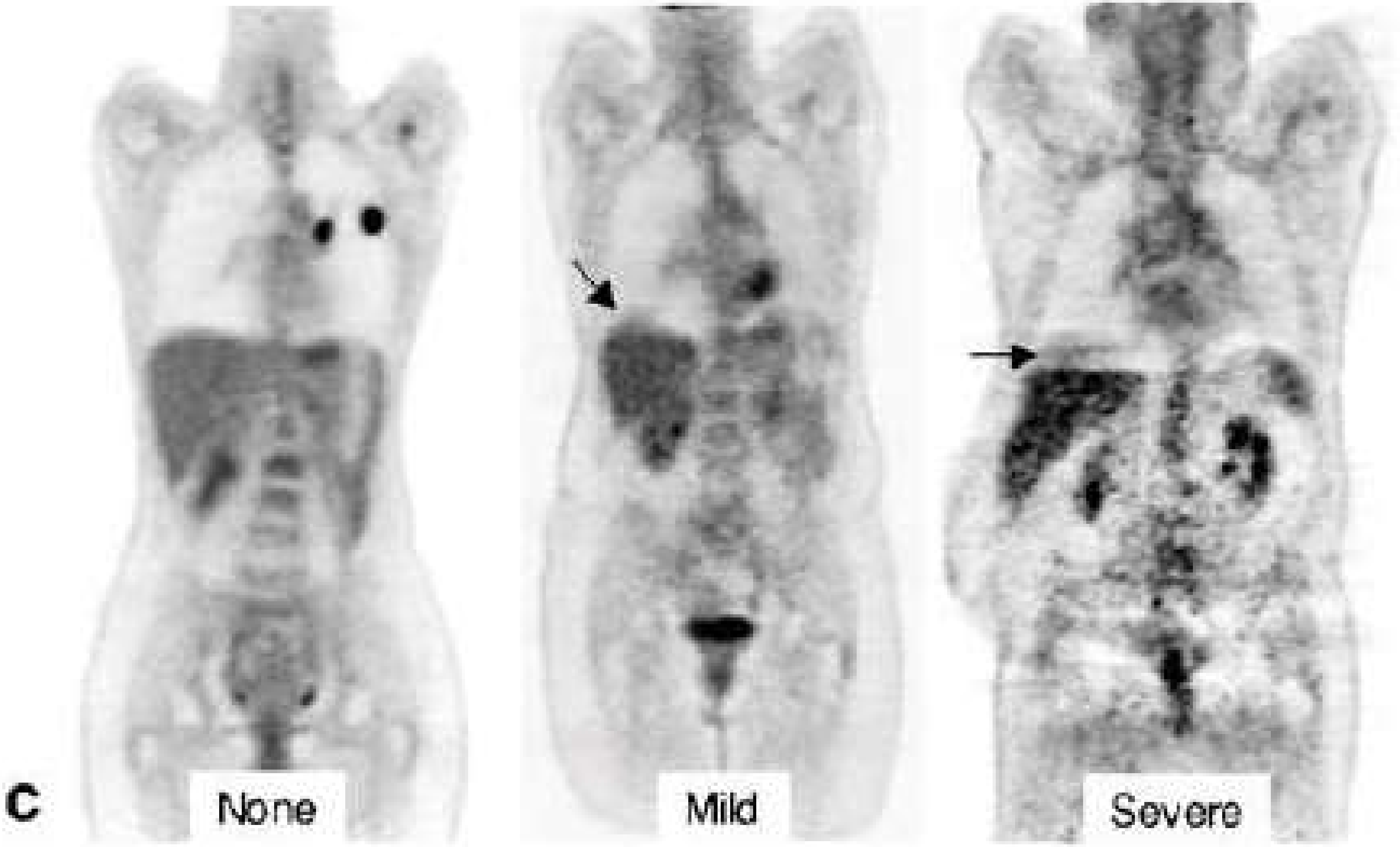

Beyer et al, EJNMMI 2005; 32: 1429-1439.

...and their consequences

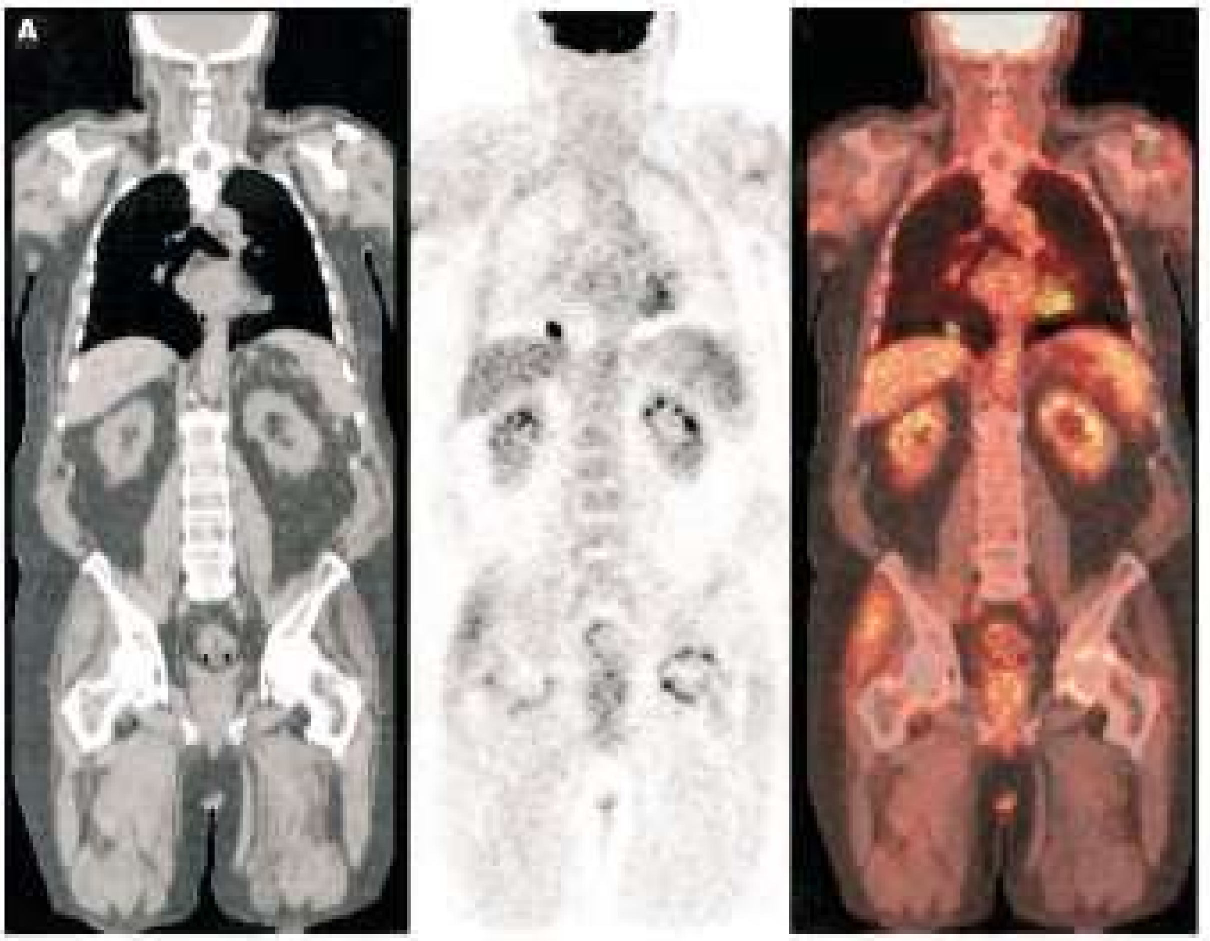

CT PET (CTAC) Fused (PET CTAC -CT)

Osmann et al, JNM 2003; 44: 240-243.

FIGURE 2. Coronal (A) and transaxial (B) PET/CT fusion images of 70-y-old man with colon cancer and MRI-proven liver metastases (arrow) but no lung lesions. Lesion is seen in right lung base, but no lung lesion is seen on CT; on both NAC and GeAC images without CT fusion, lesion was correctly localized to liver. Fused (PET CTAC-CT) = PET CTAC fused with CT; fused (PET GeAC-CT) = PET GeAC fused with CT.

4D-PET/CT

- Respiratory organ or lesion motion induces degradation effects on PET/CT data
- 4D-PET/CT acquisition improves image quality and quantitative accuracy

Breathing Signal:

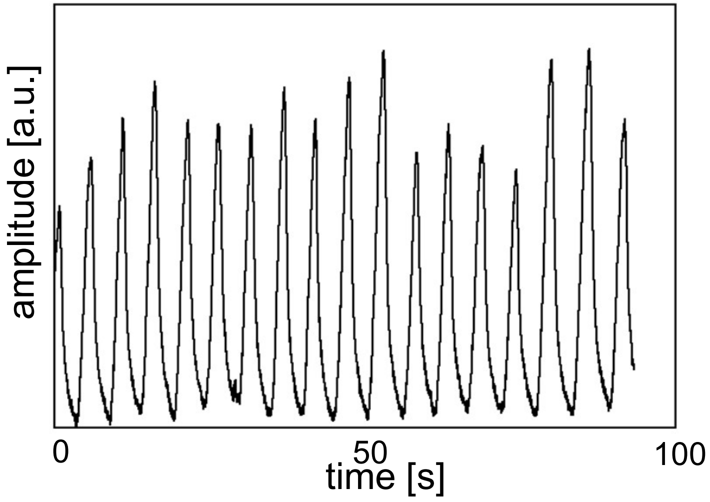

PET acquisition time:

$$T = N_p \cdot t$$

- Respiratory monitoring synchronized to 4D-PET and 4D-CT
  - Pressure sensor
  - Spirometry system, …
- 4D-PET
  - Preferentially recorded in 3D mode
  - data sorted into different phases of the breathing cycle
    - Prospective sorting
    - Retrospective (list mode acq.)
- 4D-CT for phase-sensitive attenuation correction!

4D-PET/CT vs. 3D-PET/CT

Aristophanous et al, IJROBP 2012; 82(1): e99-105.

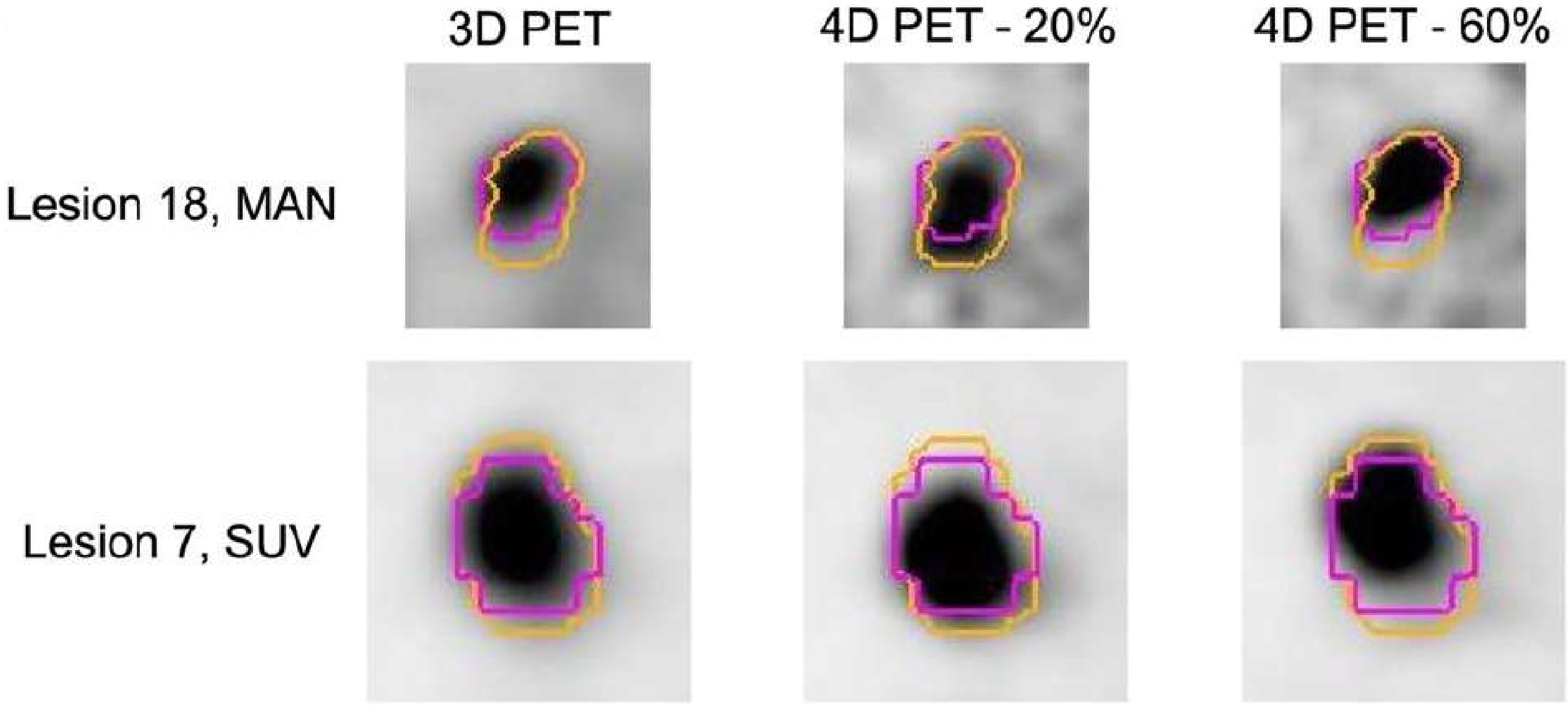
3D PET
4D PET - 20%
4D PET - 60%
Lesion 18, MAN
Lesion 7, SUV

- Comparison of PET-based GTV contouring on 3D- vs. 4D PET (different phases: 20%, 60%)
- RT volumes contoured on 4D-PET (orange) were larger than 3D-PET volumes (pink)

Image Reconstruction

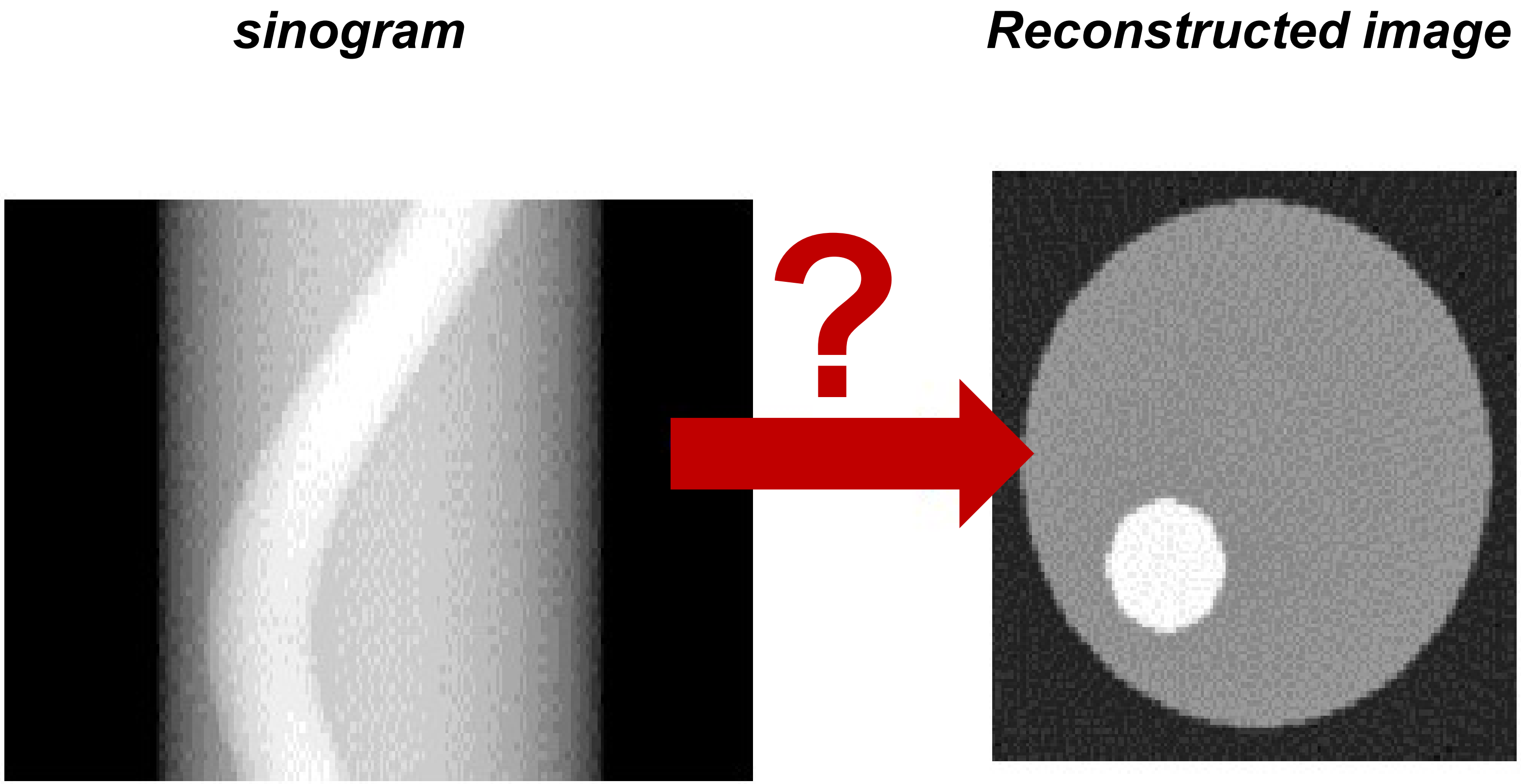
sinogram
Reconstructed image
?

1. Filtered Backprojection
2. Iterative Reconstruction Methods

Analogue to CT reconstruction: Filtered Backprojection

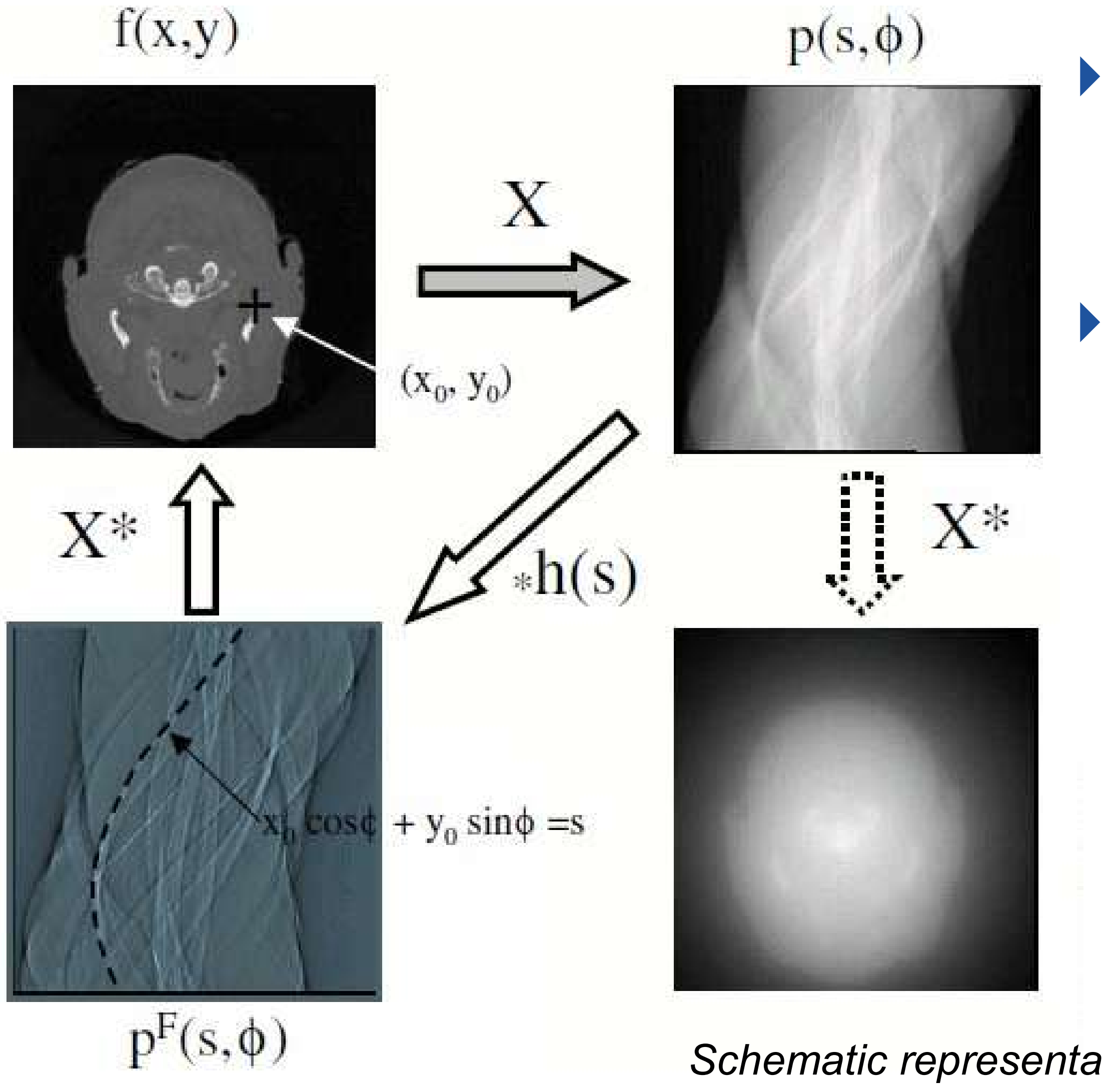

$f(x,y)$
$p(s,\phi)$
X
(x_0, y_0)
X*
$*h(s)$
X*
$x_0 \cos\phi + y_0 \sin\phi = s$
$p^F(s,\phi)$

- Works well for lower noise environment of brain
- Not optimal for whole-body imaging

Schematic representation of FBP [1].

Fourier Slice Theorem

The Fourier transform of the projection equals the Fourier transform of the density distribution along a line in polar coordinates.

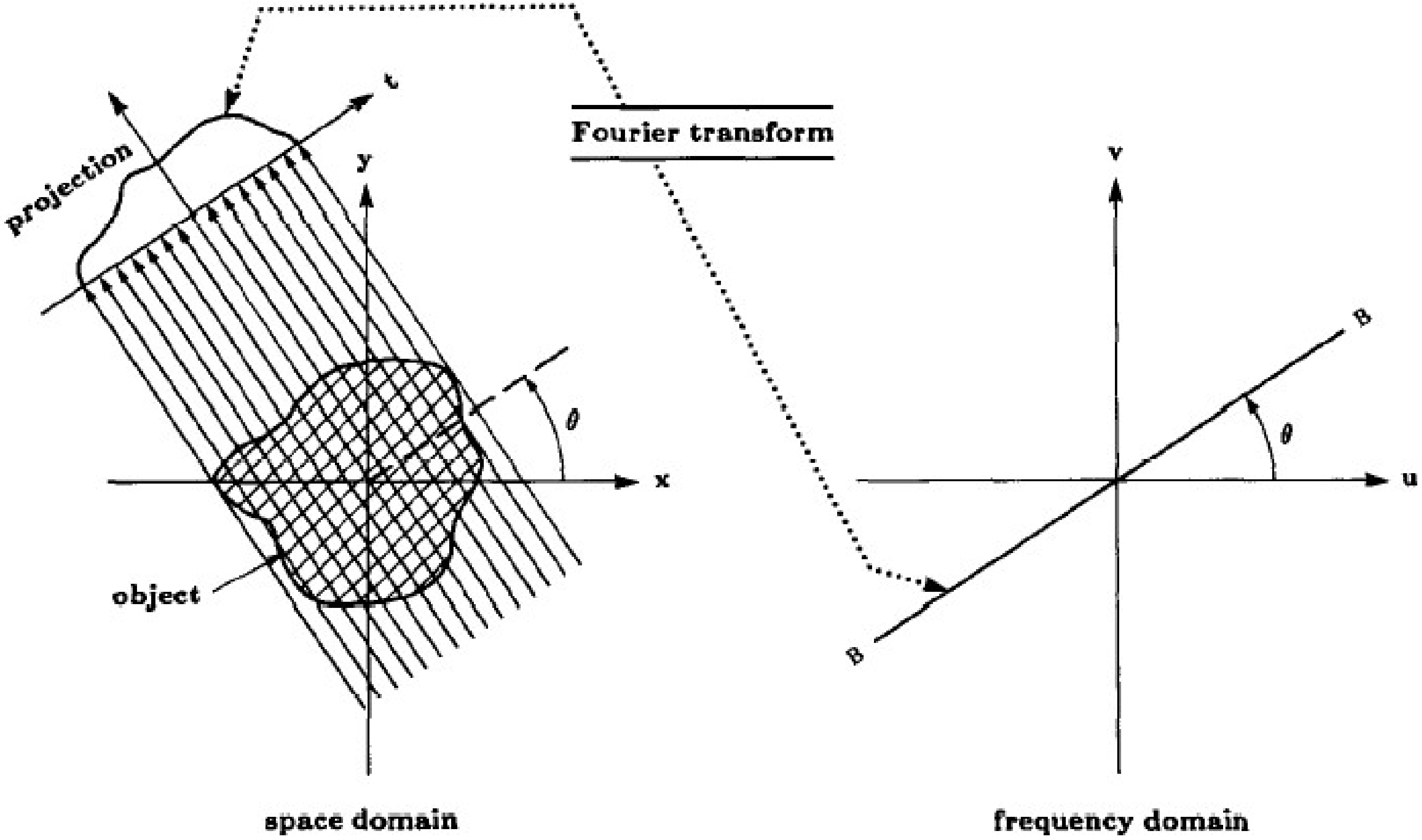
projection
t
y
Fourier transform
v
θ
x
B
θ
u
object
B
space domain
frequency domain

Filtered Backprojection (FBP)

Projection:

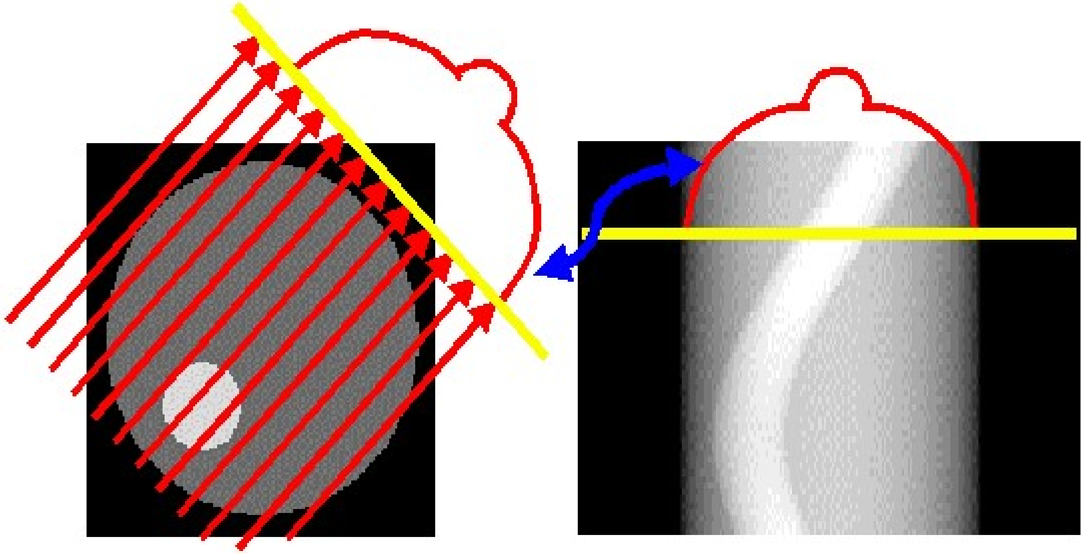

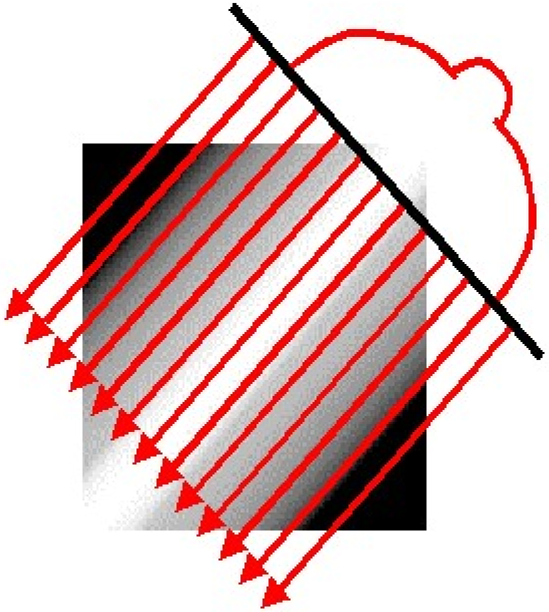

and Backprojection

Note: Blurring effect of line integration!

Filtered Backprojection FBP

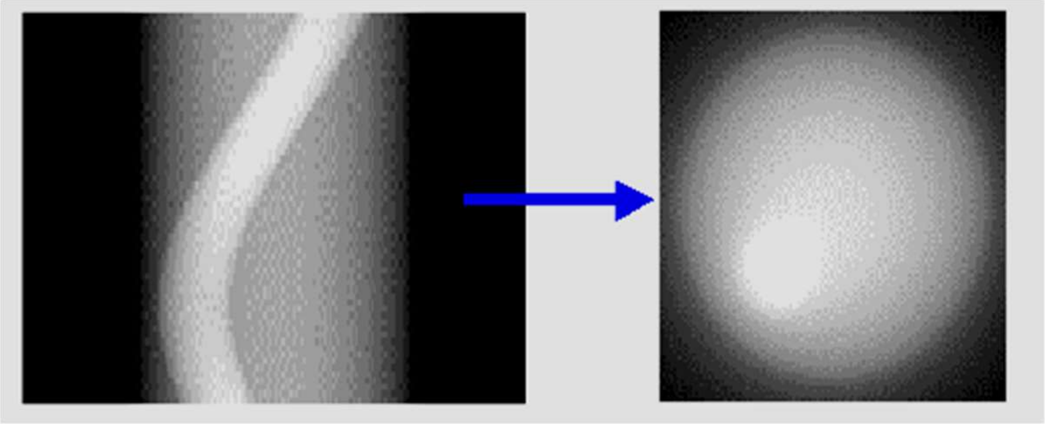

- Backprojection of all projections yields a blurred image.
- Unblurring Operation = convolution with an edge enhancing filter
- 1D-convolution of the sinogram with a ramp filter that enhances high frequencies (Linearity of projection operation allows to convolve projection data with a filter!)

Filtered Backprojection

To increase edge definition, the projections are convolved with an edge enhancement filter:

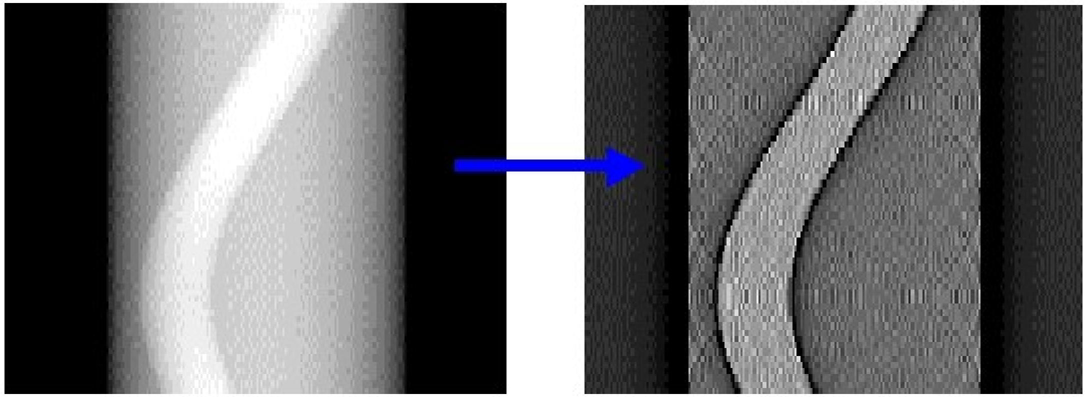
filtered Sinogram

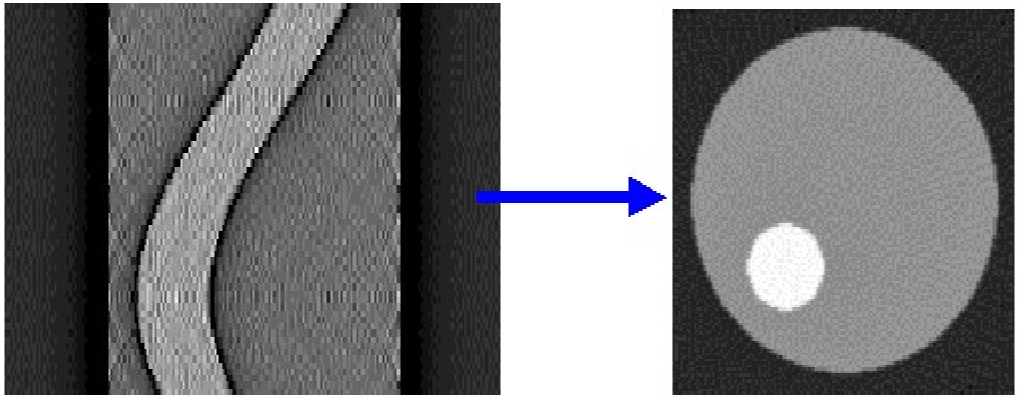
filtered Backprojection

Iterative reconstruction: ML-EM

- Iterative reconstruction
  - Discrete representation of data and image
- **Expectation maximization (EM)** algorithm offers determination of **maximum likelihood (ML)** estimate of the image

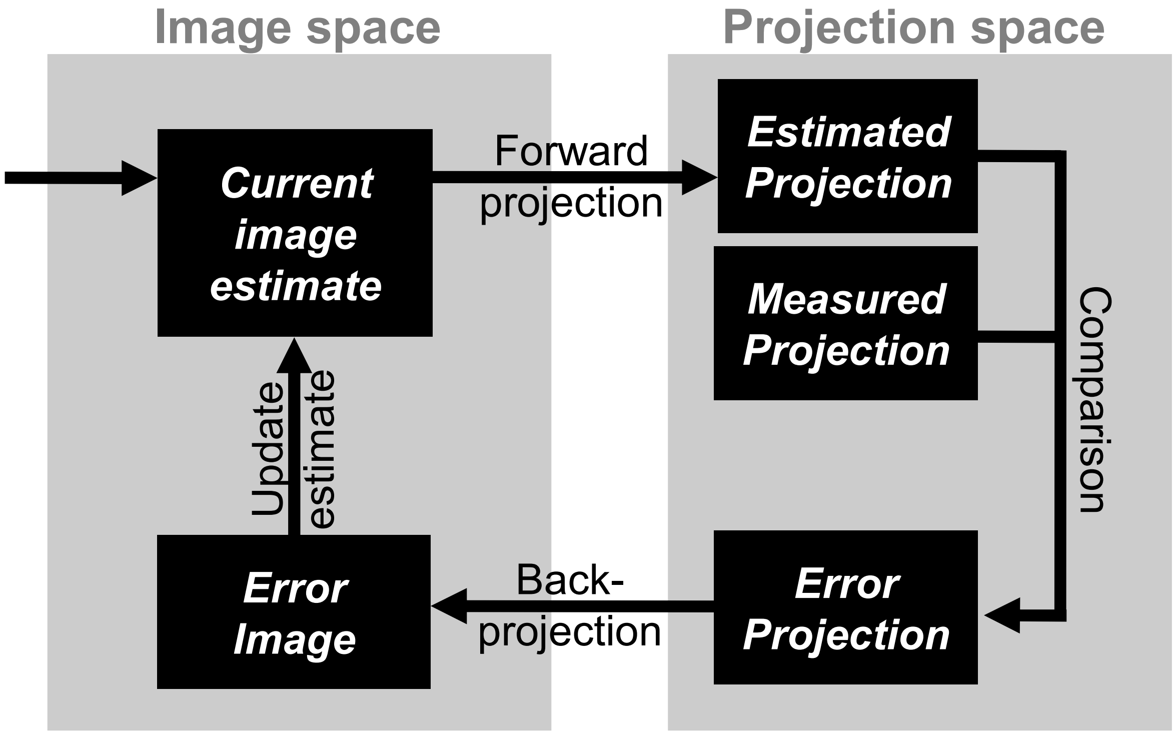
Image space
Projection space
Current image estimate
Forward projection
Estimated Projection
Measured Projection
Comparison
Error Projection
Back-projection
Error Image
Update estimate

ML-EM: noisy data introduce instabilities

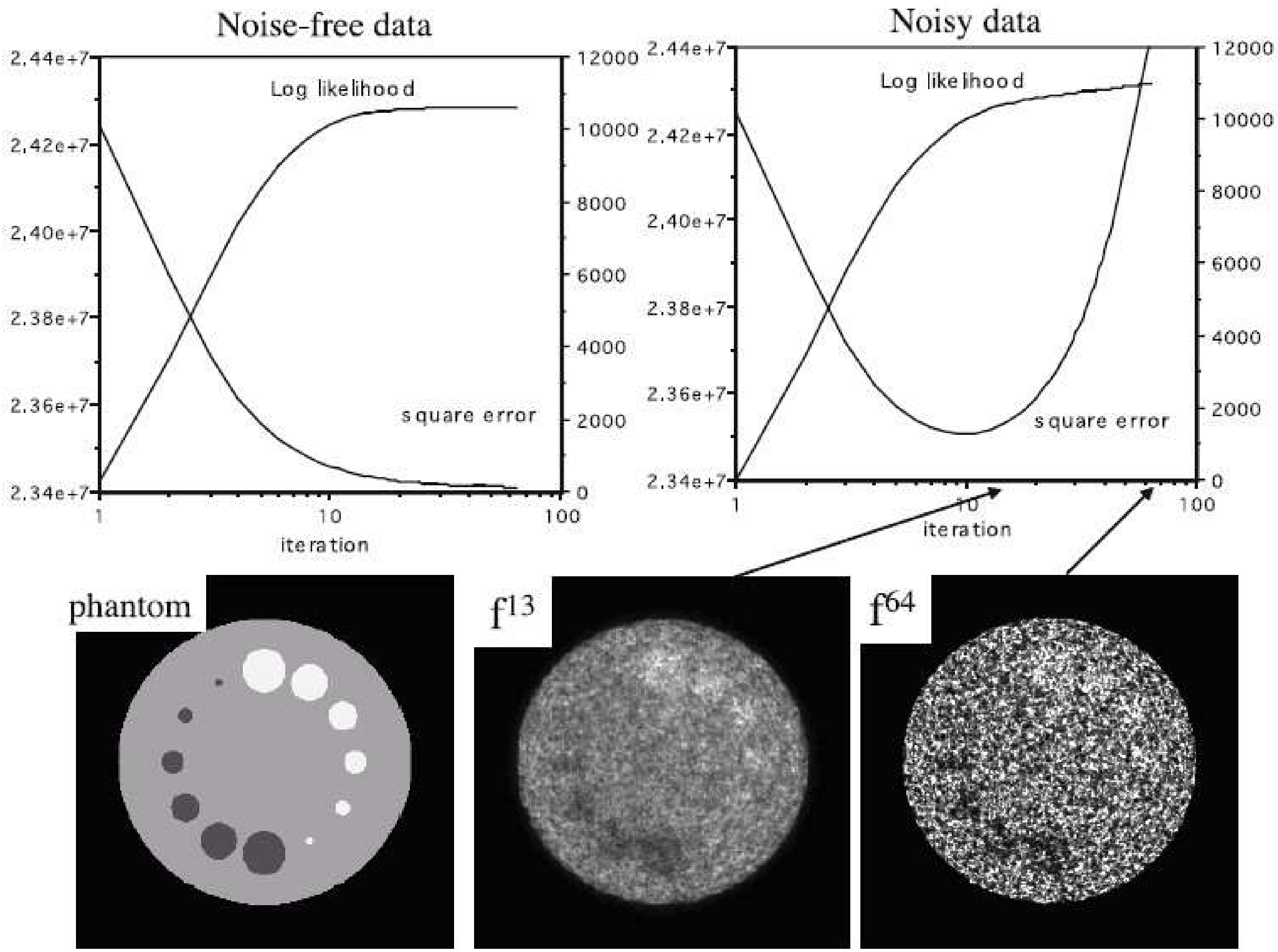

2D reconstruction of math. phantom with ML-EM. Poisson log-likelihood and square reconstruction error with regard to reference image versus number of iterations [1].

OSEM (ordered subset EM)

- Accelerated version of ML-EM
- LOR data are partitioned in *S* disjoint subsets

$$J_1, \ldots, J_S \subset [1, \ldots, N_{LOR}]$$

- Commonly, projections are divided into subsets with different views, or azimuthal angles
- ML-EM algorithm for data from one subset only
- Each subset processed in well-defined order
- Convergence accelerated by factor ≈ *S*

OSEM (ordered subset EM)

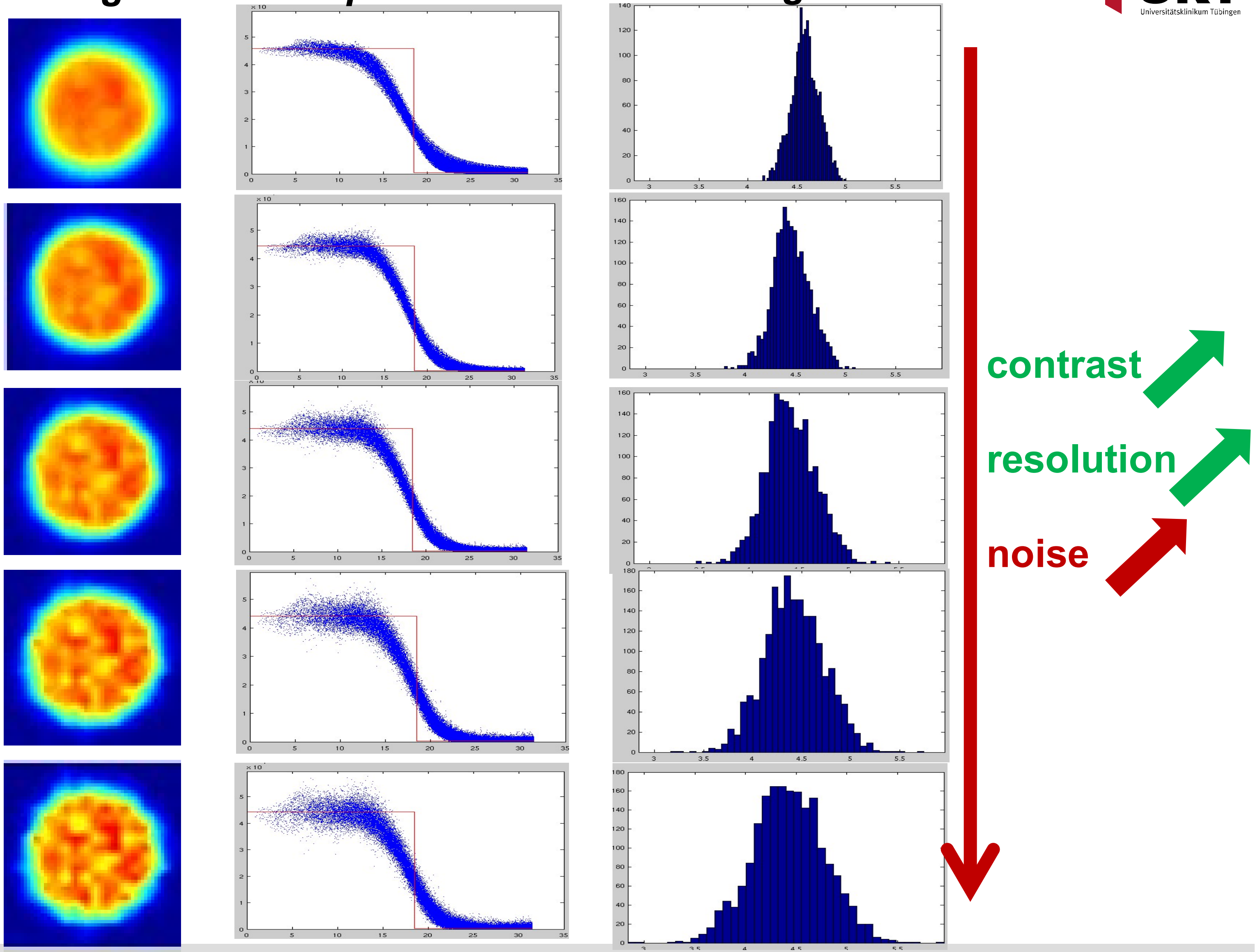

2 iterations,
4 subsets:

2 iterations,
8 subsets:

4 iterations,
8 subsets:

8 iterations,
8 subsets:

8 iterations,
16 subsets:

contrast ↗

resolution ↗

noise ↗

3D Iterative Reconstruction

- Fully 3D PET measurements and reconstruction
- Increasing computational demands
- Rebinning 3D data into 2D transaxial slices

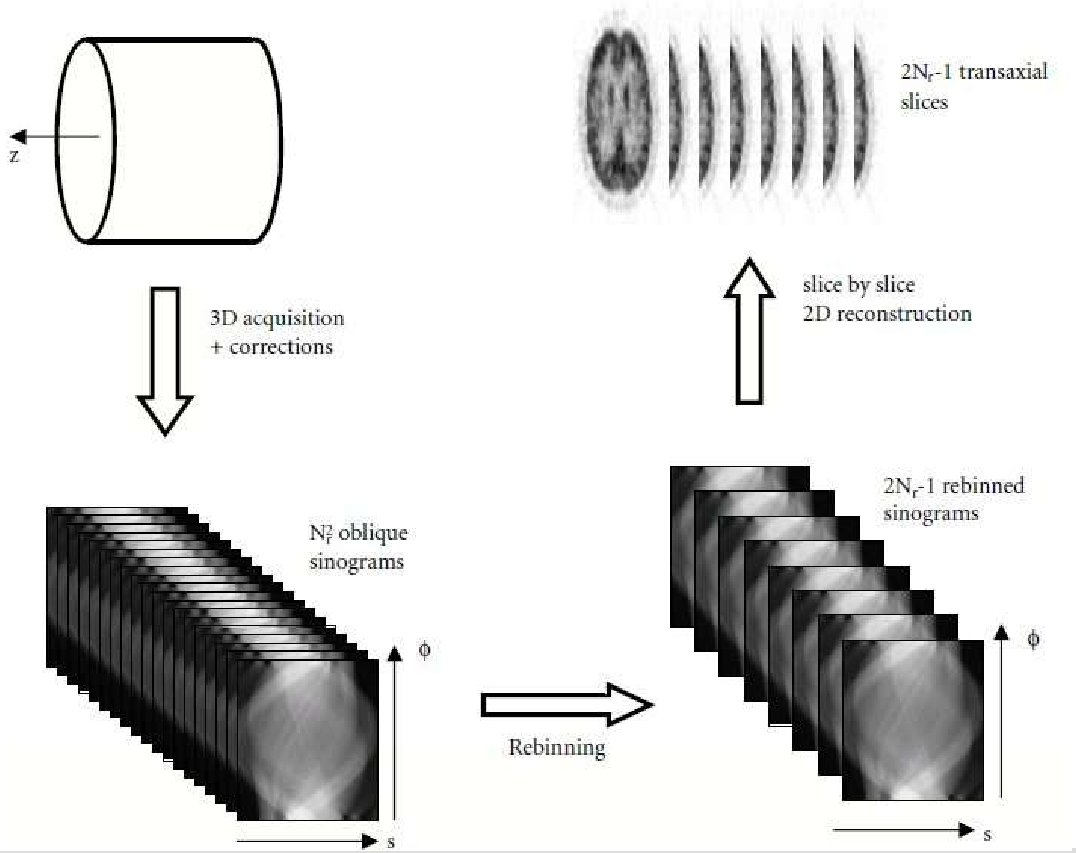
z
3D acquisition + corrections
N_r^2 oblique sinograms
ϕ
s
Rebinning
$2N_r$-1 rebinned sinograms
ϕ
s
slice by slice 2D reconstruction
$2N_r$-1 transaxial slices

Time-of-Flight (TOF) PET

- Difference in flight time of photons is registered

$$\Delta t = \frac{2\Delta x}{c}$$

- Probability of event occurrence is limited to a certain area along the LOR

- Better SNR
  - Especially in the abdomen / heavy patients

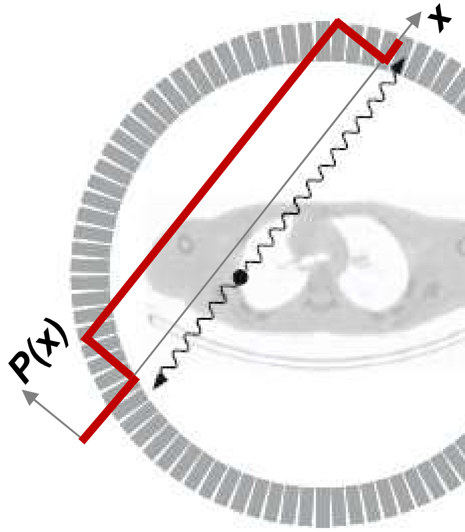

no TOF

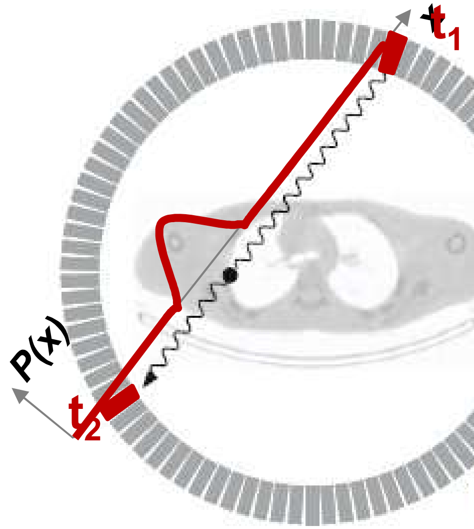

TOF

Resolution Modeling - PSF

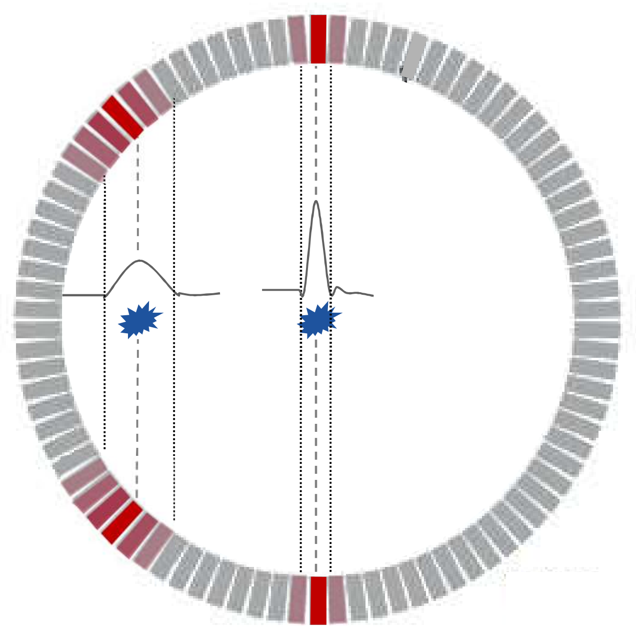

- Deconvolution of local **point-spread functions (PSF)** during iterative reconstruction
- Enhanced resolution
- Reduction of blurring and distortions

Iterative reconstruction with resolution modeling

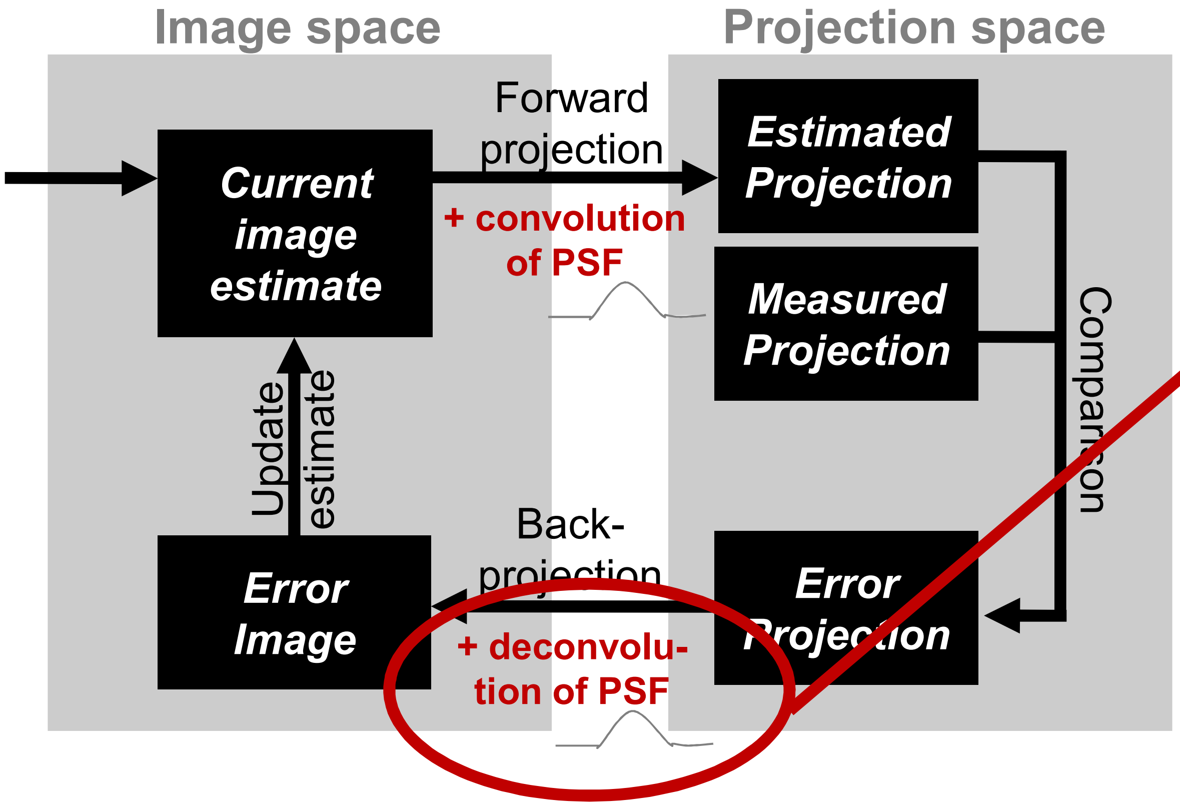
Image space
Projection space
Forward projection
+ convolution of PSF
Current image estimate
Estimated Projection
Measured Projection
Comparison
Update estimate
Back-projection
+ deconvolution of PSF
Error Image
Error Projection

- May introduce Gibbs-artifacts
- Not necessarily activity conservation

Improvement of PET/CT Image Quality

[18F]-FDG PET study performed on a PET-only BGO system:

[18F]-FDG PET study performed on a state-of-the art PET/CT system:

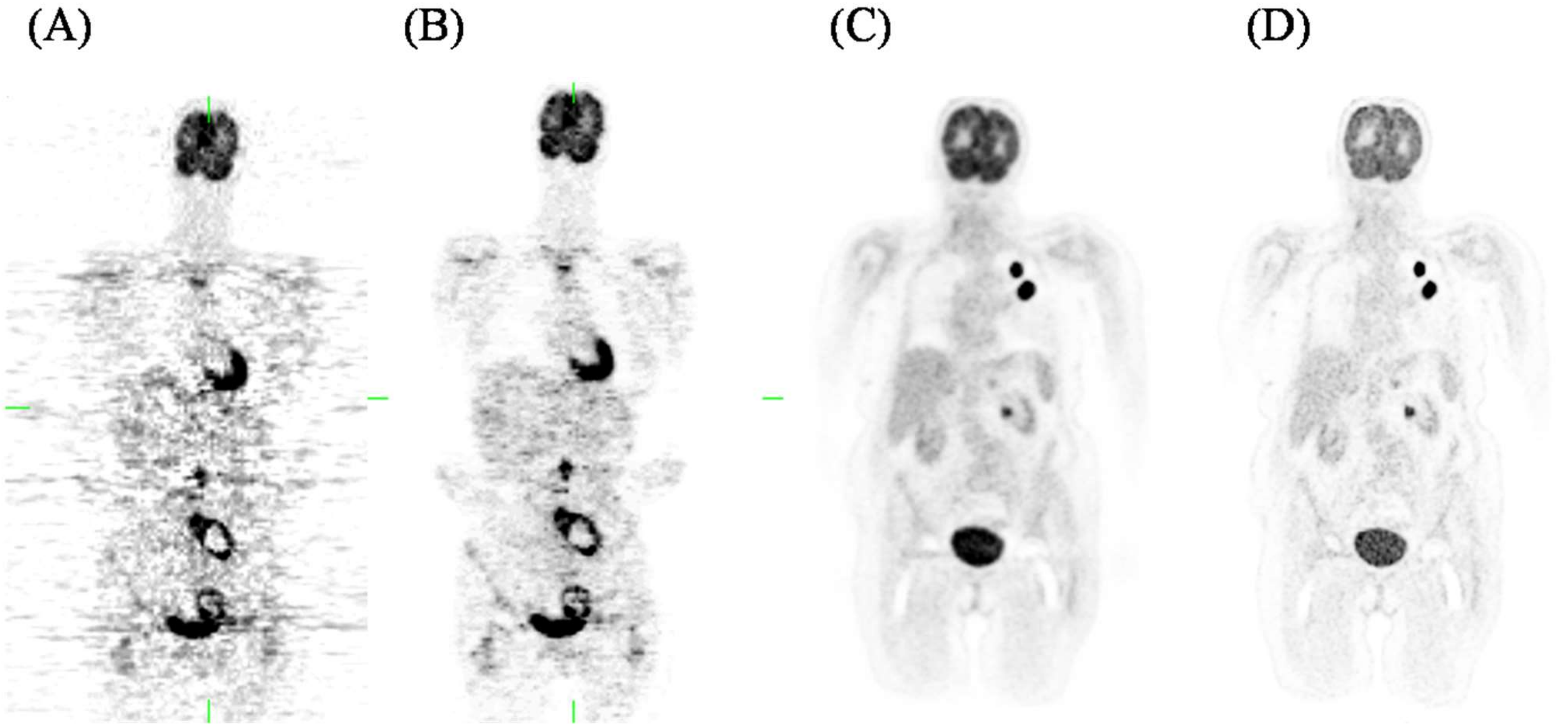

FBP Reconstruction

Iterative Reconstruction

Iterative Reconstruction

TOF+PSF Iterative Reconstruction

Coutesy R. Boellaard, Amsterdam

Summary: Reconstruction

- Today, iterative reconstruction (IR) algorithms are standard on all PET/CT systems
- Superior image quality when compared to filtered back projection
- Iteratively reconstructed images are characterized by
  - number of iterations and subsets
  - matrix and voxel size
  - image zoom
  - image smoothing, smoothing filter size or kernel (FWHM).
- IR methods employing a sufficient number of iterations and subsets to ensure sufficient amount of convergence are preferred.
- Reconstructed with and without AC recommended to allow inspection of AC artifacts.

Quantitative analysis of PET images

Tracer uptake is frequently quantified by the

Standardized uptake value (SUV)

$$SUV = \frac{C}{A} w$$

with *C:* tumor/voxel activity concentration [Bq/ml]

A: injected activity [Bq]

w: body weight [g]

!!! *SUV=1 means that the tracer is equally distributed in the whole body*

Radiotherapy target volume delineation (TVD) based on PET

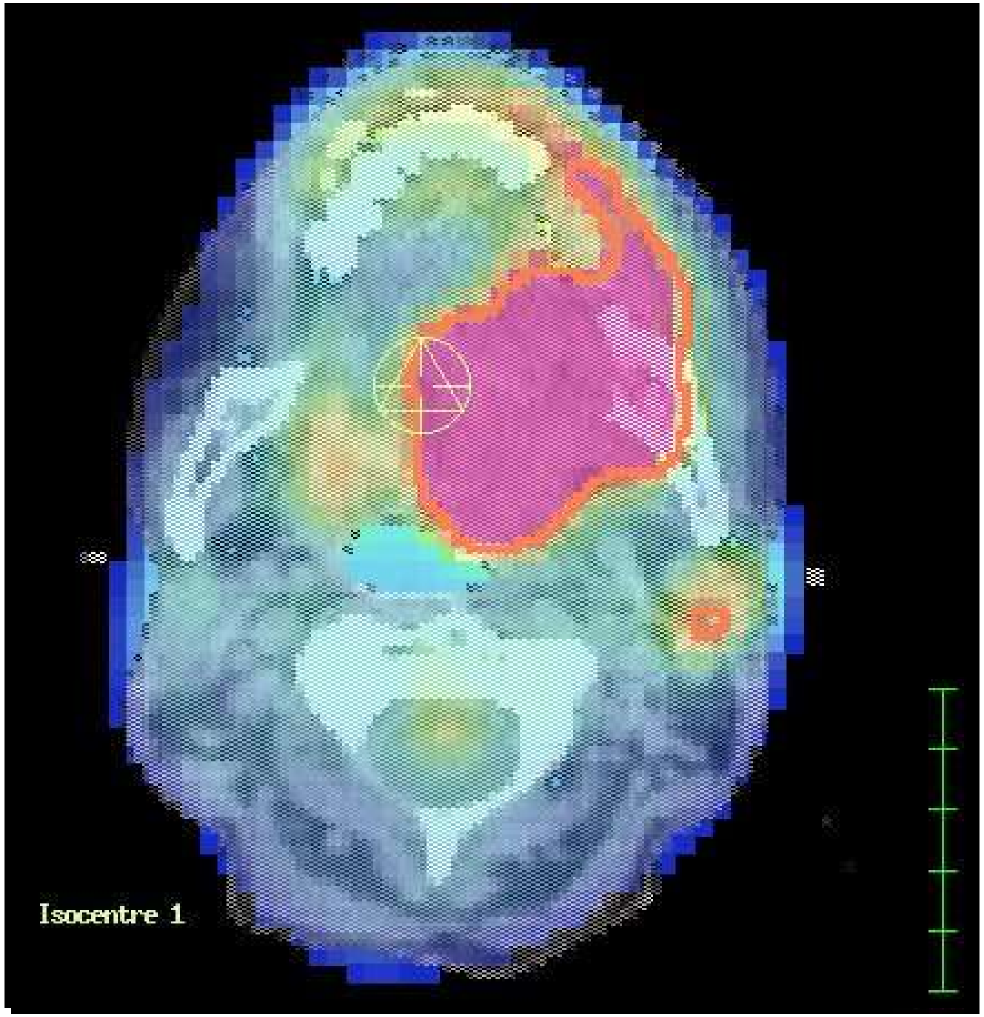

Floor of mouth carcinoma, 45 y, w

- Most commonly used for TVD: [^{18}F]FDG
- Image Registration / Patient Positioning very important issue
- **Which is the correct theshold to use?**

Absolute Thresholding

PET image

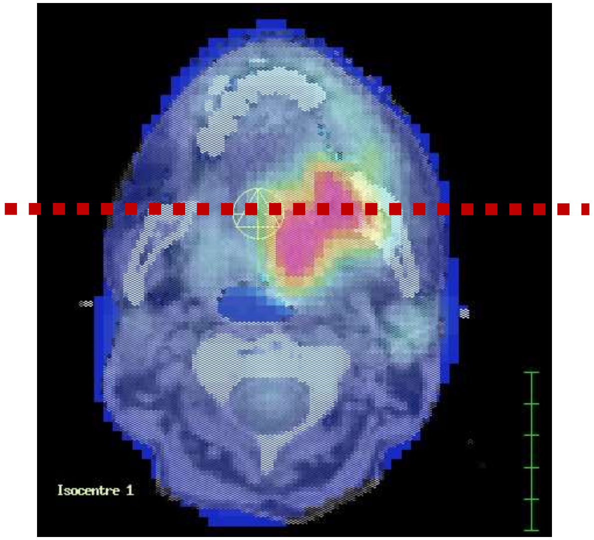

Line profile

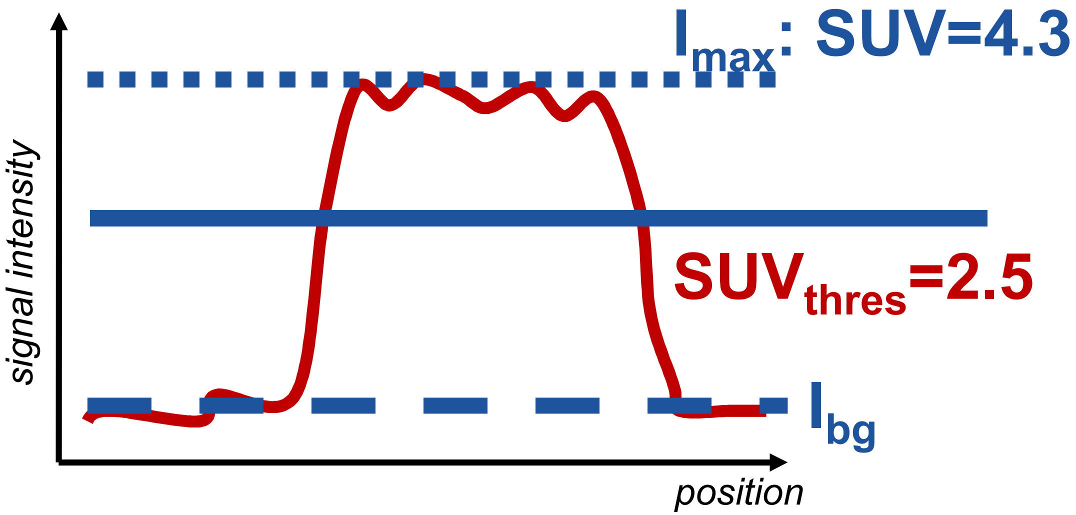

- Fix SUV-threshold of 2.0/2.5
- Easy to implement
- Often fails when the physiologic background activity lies above the threshold
- Absolute SUVs are strongly influenced by various technical factors (scan protocol, image acquisition, reconstruction, scanner calibration, etc.)

Relative Thresholding

PET image

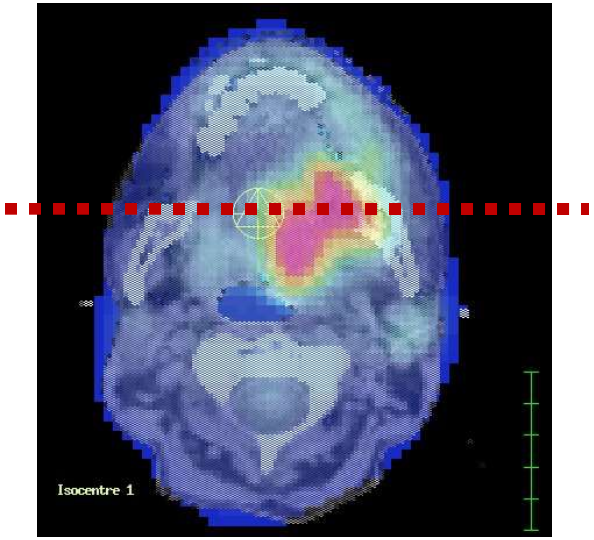
Isocentre 1

Line profile

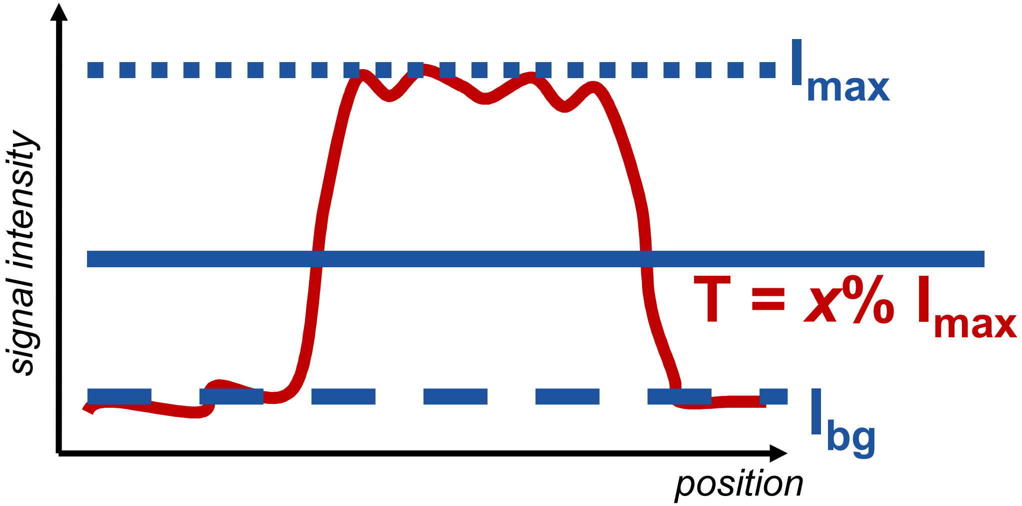
I_{max}
T = x% I_{max}
I_{bg}
signal intensity
position

- Relative Threshold T, depending on the max. intensity
- Commonly used: x=42% (40-50%)
- Easy to implement
- Calibration with phantom measurements possible
- Frequently used in clinical routine

Iterative Thresholding

PET image

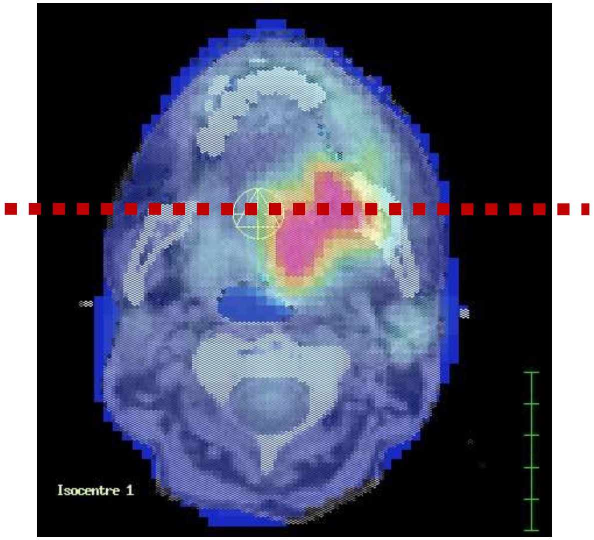
Isocentre 1

Line profile

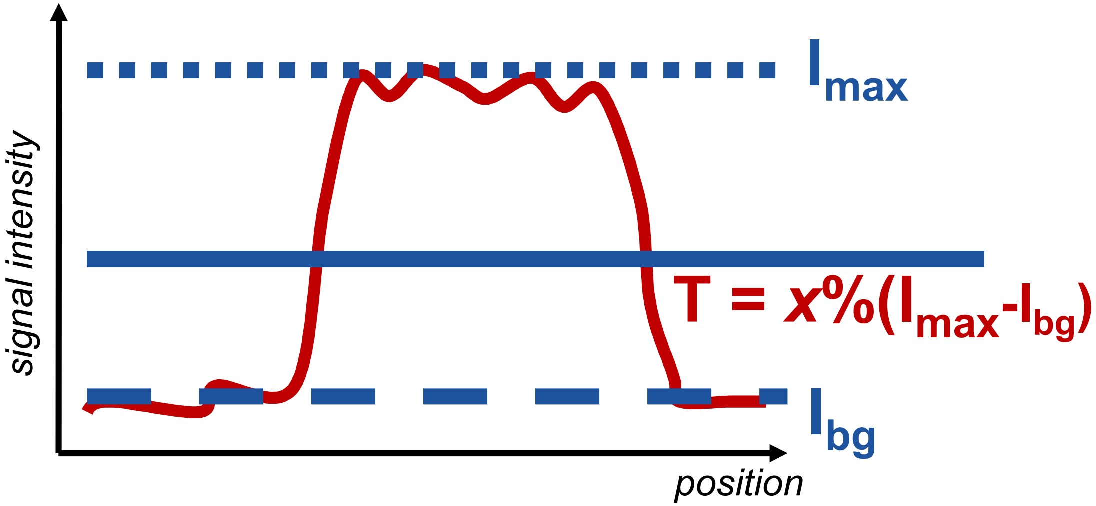
signal intensity
I_{max}
$T = x\%(I_{max}-I_{bg})$
I_{bg}
position

- Background-subtracted relative threshold level
- Adjustable threshold *x*
- Iterative approach based on phantom measurements

Source-to-Background Algorithms

PET image

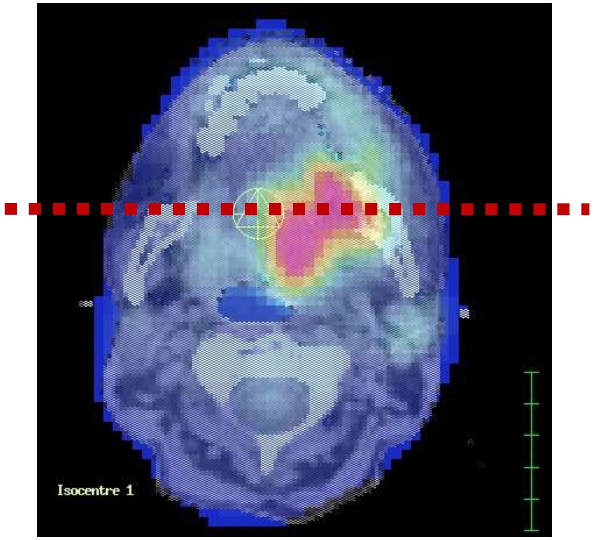
Isocentre 1

Line profile

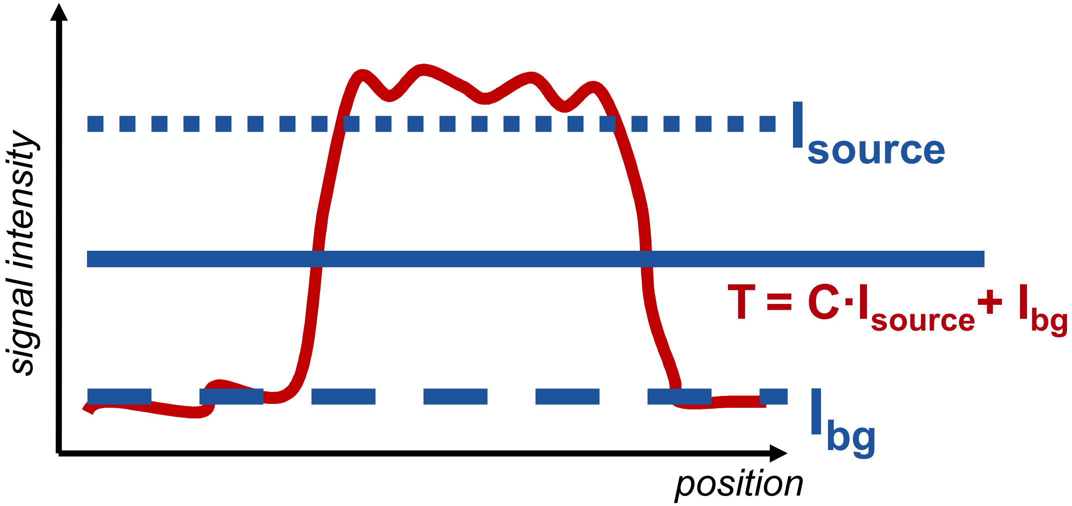
signal intensity
I_{source}
$T = C \cdot I_{source} + I_{bg}$
I_{bg}
position

- Constant C determined from phantom measurements
- Works very well for quasi-spherical lesions
- *Value of C depending of different factors:*
  - *Lesion size and shape*
  - *Scanner type and calibration*
  - *Reconstruction protocol*
  - *Image analysis software*

Schaefer et al, EJNMMI 2008; 35(11): 1989-99.

Comparison of different contouring approaches

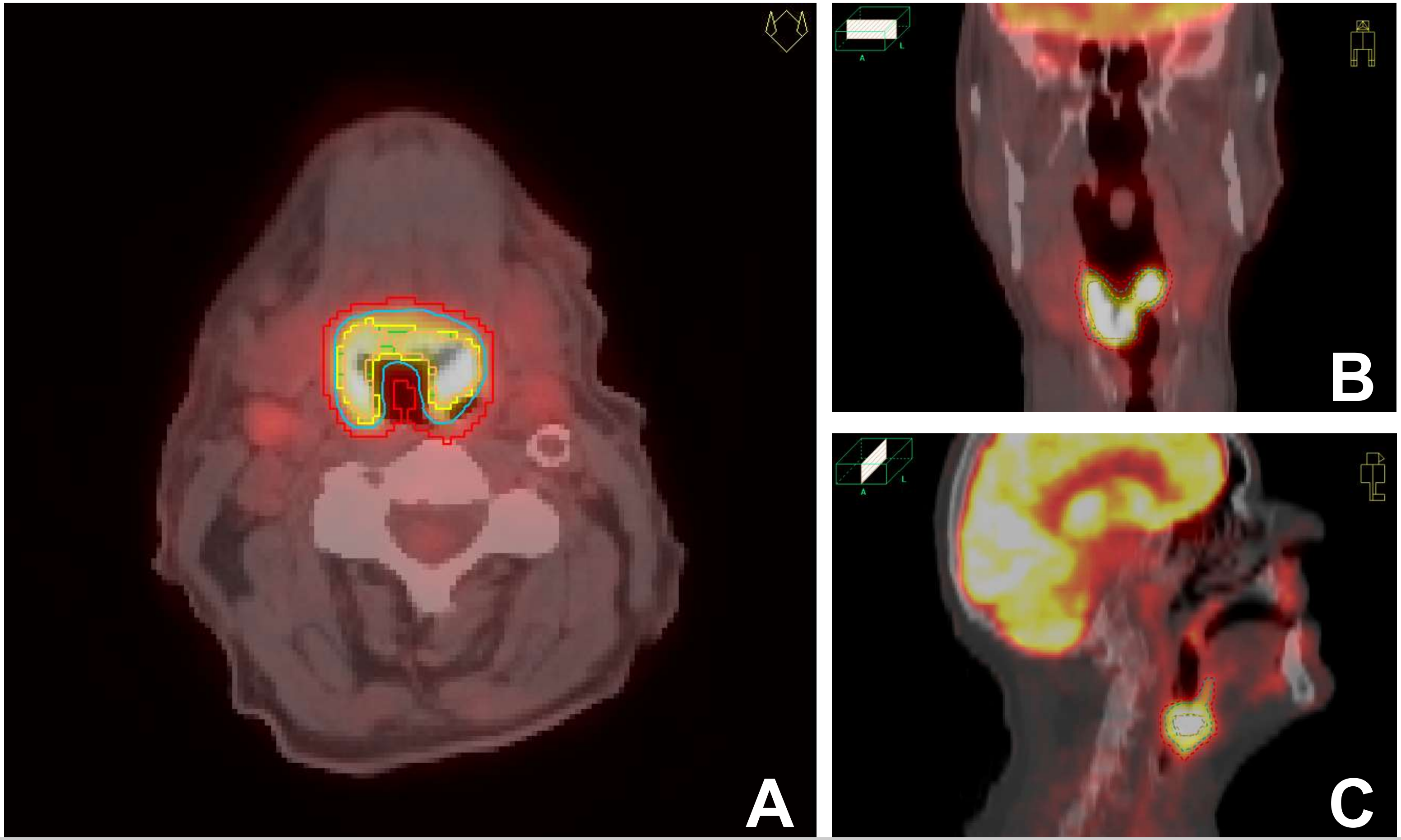

Contours created with different segmentation algorithms: manual delineation (21.8 ccm), absolute threshold SUV=2.5 (35.0 ccm), relative threshold 42% of maximum PET intensity (11.5 ccm), adaptive thresholding (10.6 ccm), source-to-background based algorithm of Schaefer *et al* (13.0 ccm)

Gradient-based auto-contouring

1. Image processing

- **Denoising** by bilateral edge-preserving filter

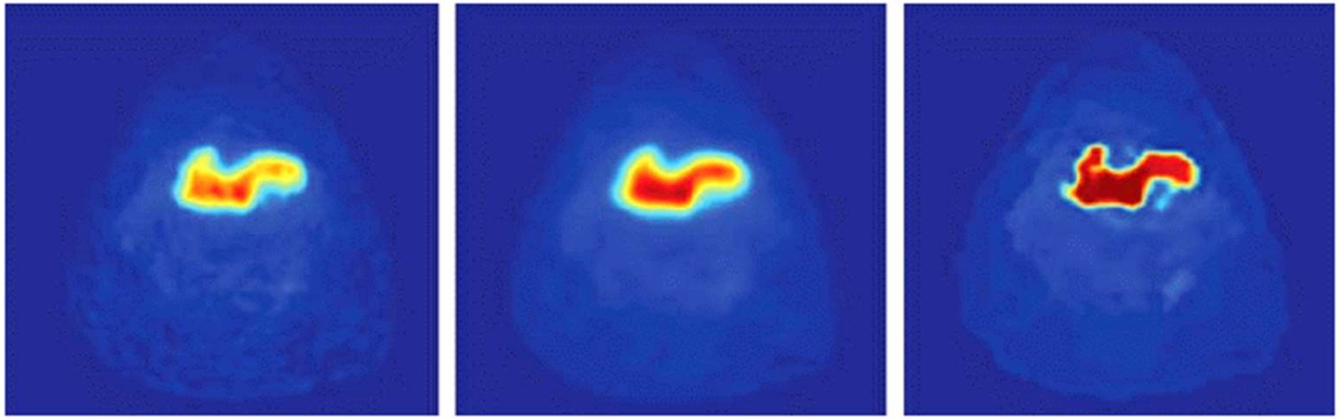

Fig. 2 Axial PET images from a patient with a hypopharyngeal tumour. On the *left panel*, the PET image corresponds to the raw image reconstructed with 3D OSEM algorithm. The application of the bilateral filter and the deconvolution algorithm restored the intensity gradient (*right panel*) in comparison with the classical 4-mm Gaussian filter (*middle panel*)

Geets et al, EJNMMI 2007; 34: 1427-1438.

Gradient-based auto-segmentation

2. Gradient-based segmentation

- Derive a gradient-intensity image:
  Plains & Plateaus → Mountain chains & Valleys
- Crest detection by applying Watershed Transformation
- Cluster analysis

PET image

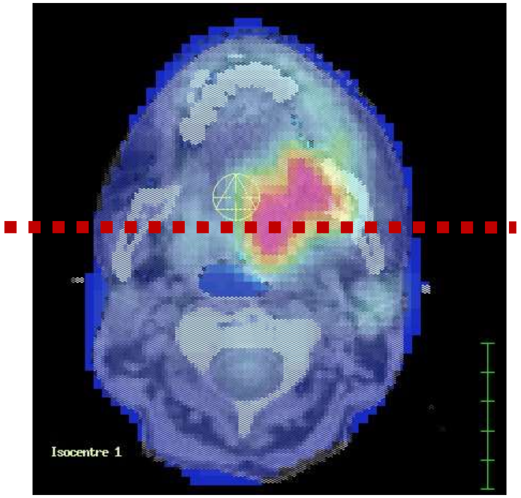

Line profile

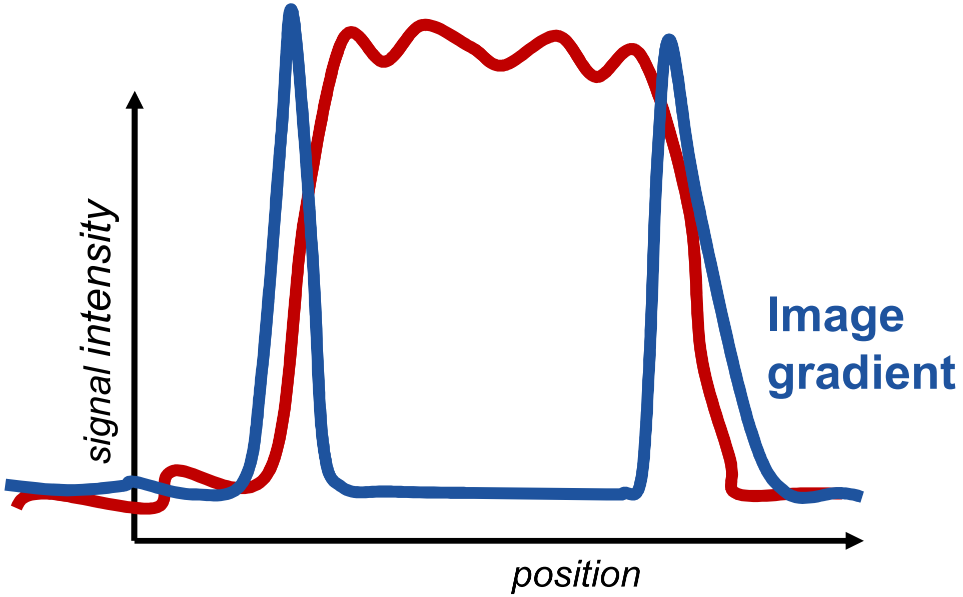

Gradient-based segmentation improves target volume definition in NSCLC

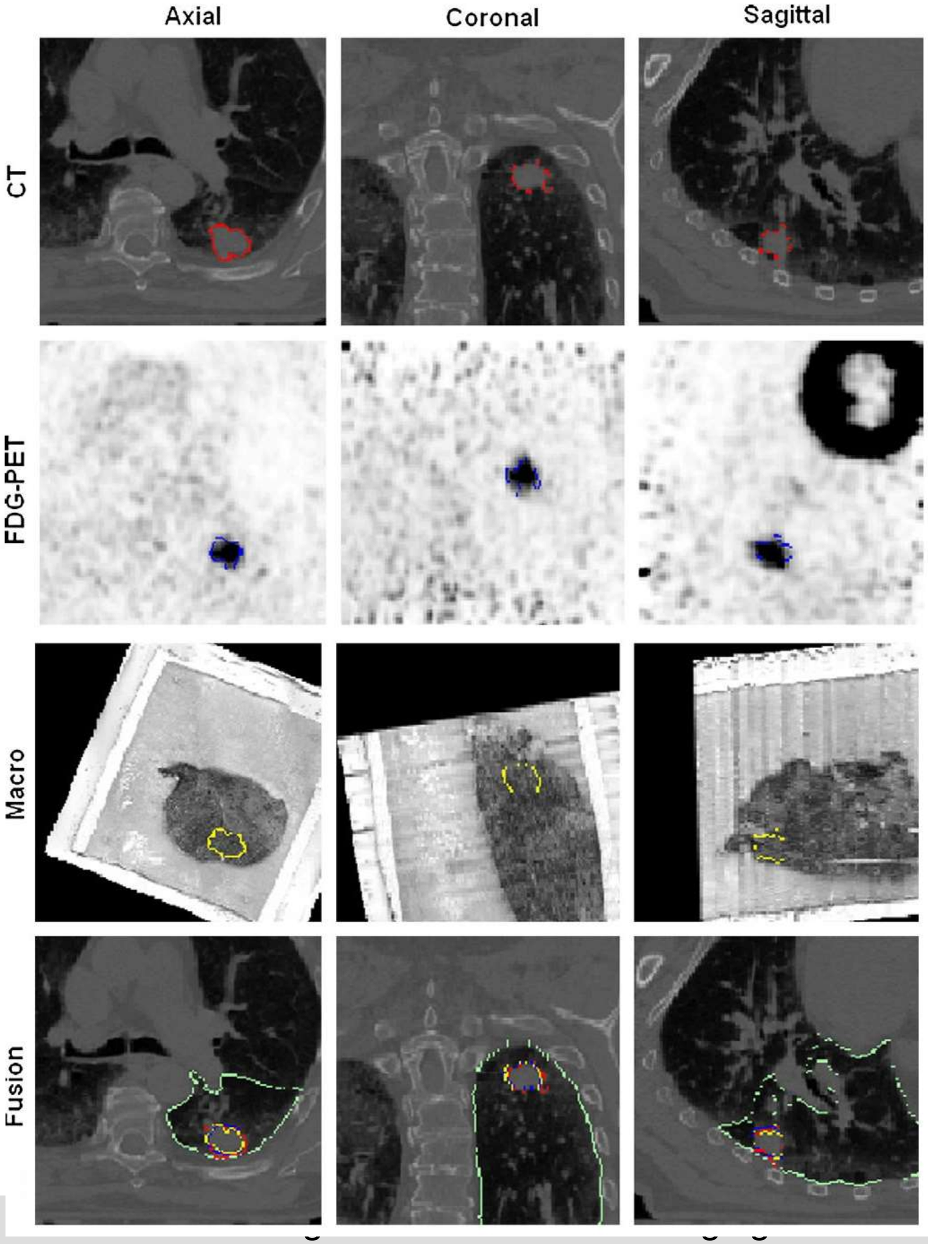

Wanet M et al. Radiother Oncol 2011;98:117-25.

- N=10 NSCLC patients
- GTV delineation on CT±PET
- Comparison with surgical specimen
- PET yields more robust delineation in poorly defined tumors
- Gradient based seg. outper-formed threshold method in terms of accuracy and robustness

Activity Recovery, Partial Volume Effect: The Smaller the Volume, the Darker it Appears

^{68}Ga Phantom measurements:

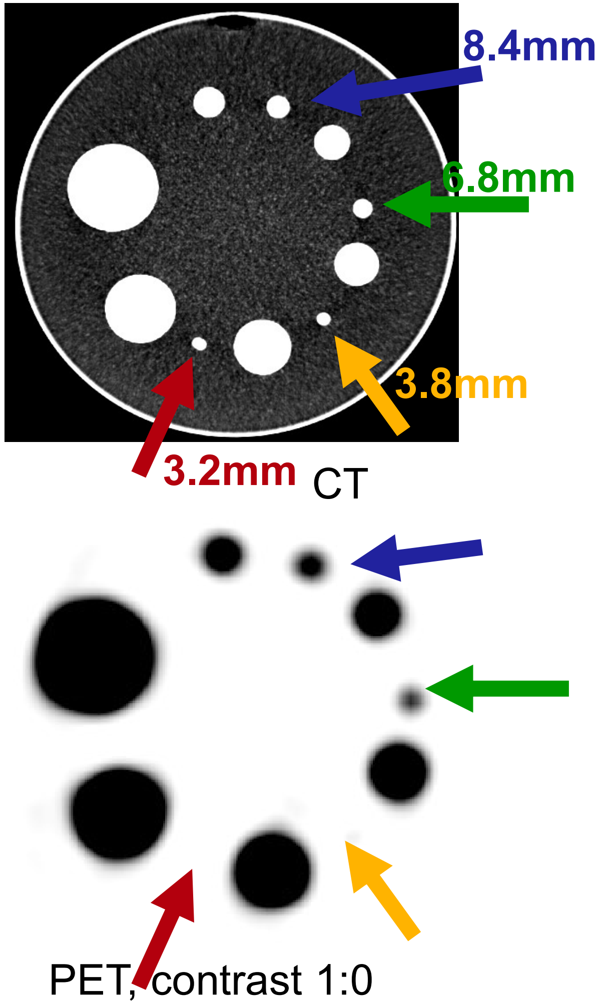

CT

PET, contrast 1:0

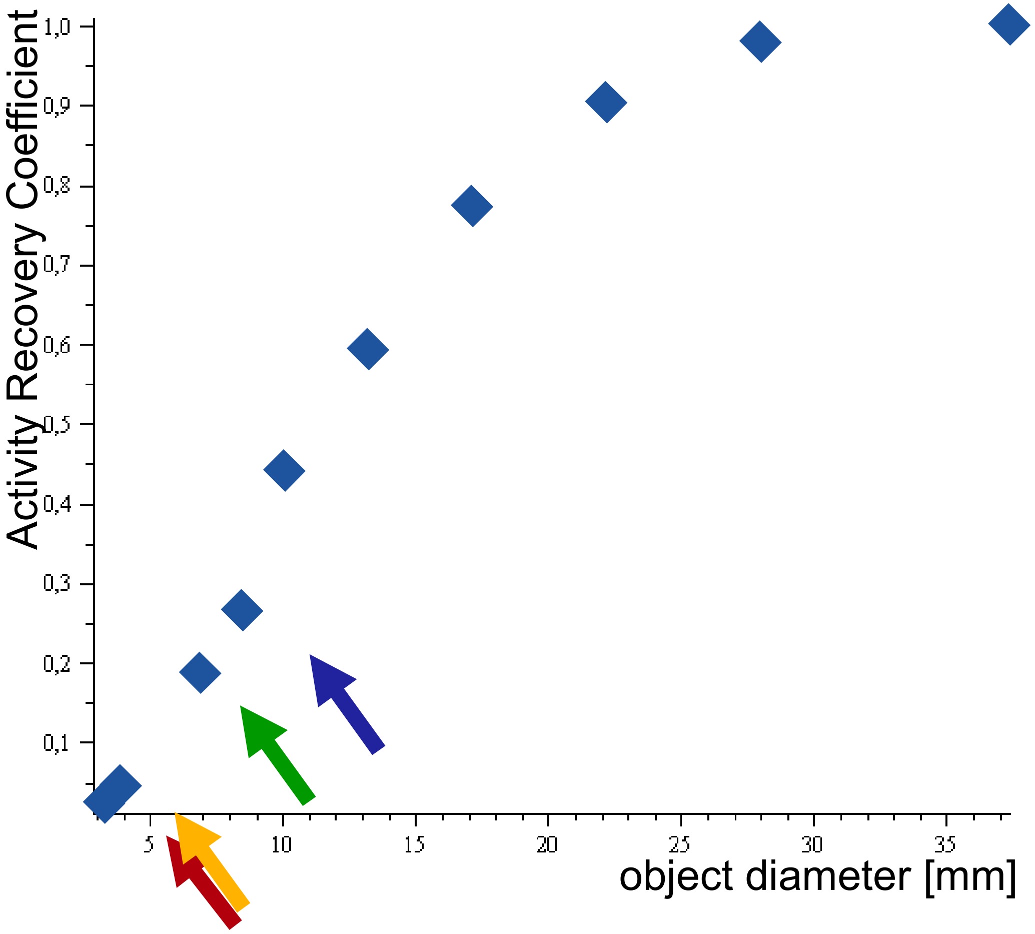

Influence of PET reconstruction

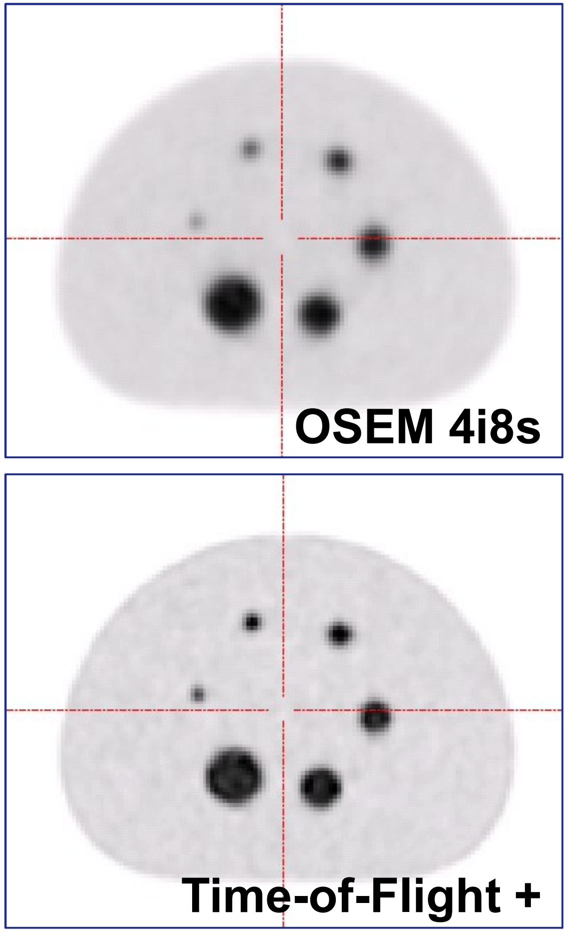

OSEM 4i8s

Time-of-Flight + res. modeling 2i21s

Contrast 6:1, constant concentration

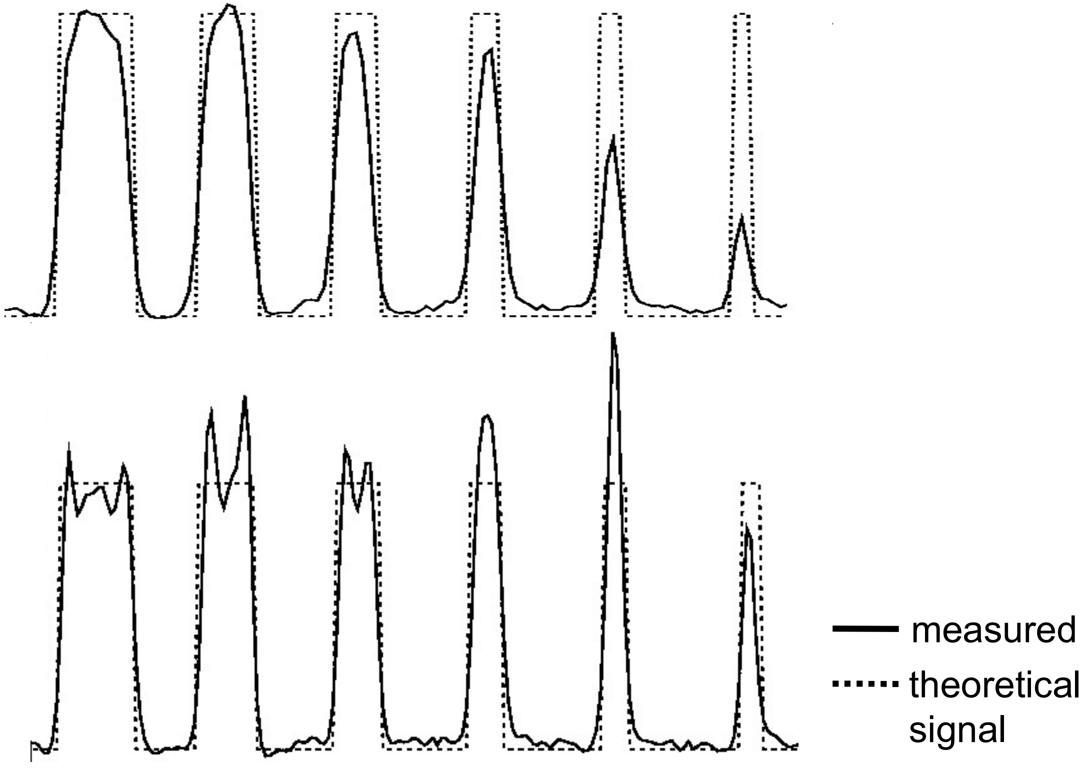

Effect of reconstruction on PET-based contouring

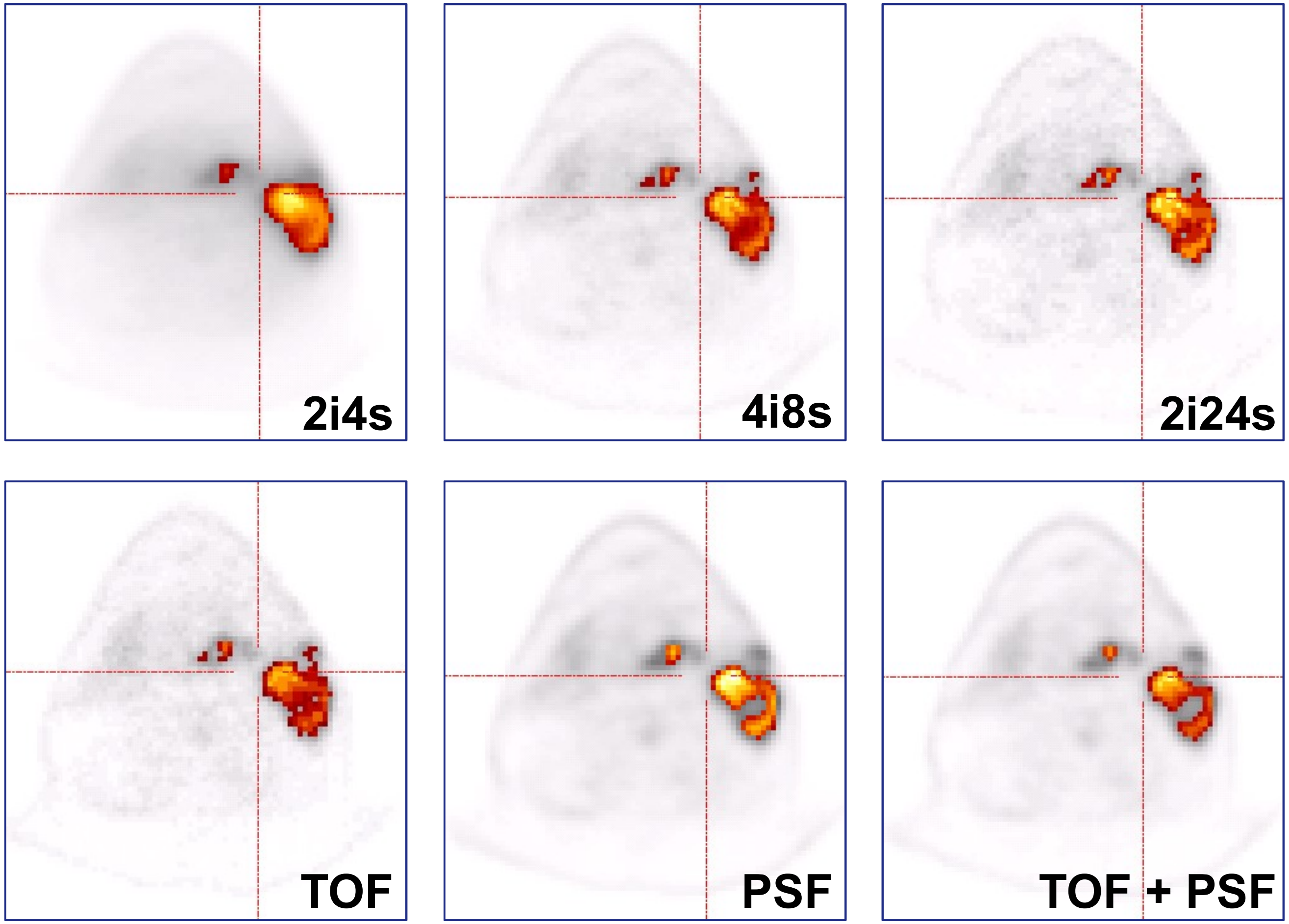
2i4s
4i8s
2i24s
TOF
PSF
TOF + PSF

Threshold:
40% SUV$_{max}$

Comparison of auto-contouring methods with „intelligent“ manual delineation

Bayne M et al. Int J Radiother Oncol Biol Phys 2010; 77: 1151-7.

- GTVs contoured by 6 experts using a **highly standardized protocol**
- Autocontouring with SUV=2.5, 3.5, 4.0, and 40% SUV_{max}
- Automatic delineations differed widely
- Visual contouring protocol gave reproducible results

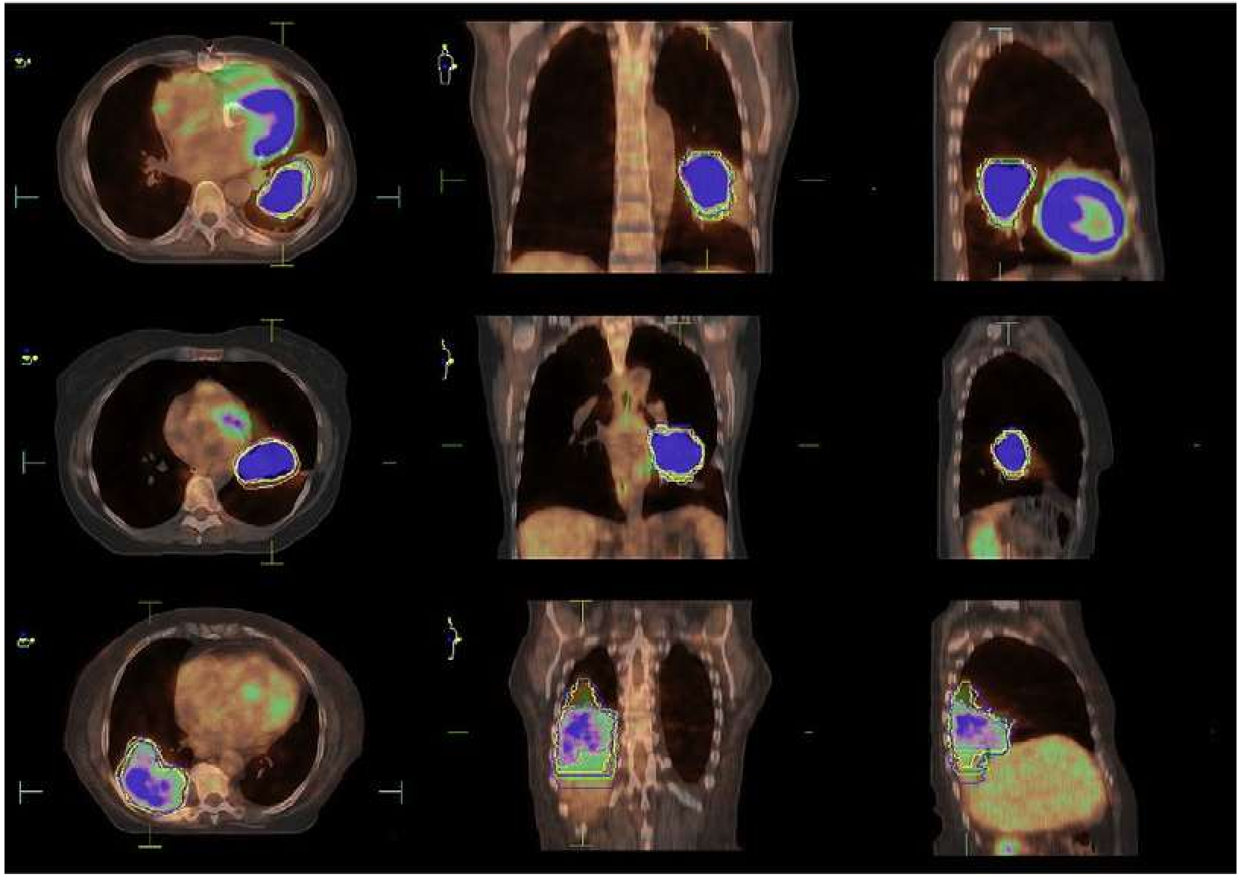

EARL: Standardization of clinical PET scanners

Guideline of the EANM (European Assoc. of Nuclear Medicine:

"FDG PET and PET/CT: EANM procedure guideline for tumour PET imaging: version 1.0." (Boellaard R et al, EJNMMI 2010; 37(1):181-200)

Objectives of EARL:

- to provide a minimum standard of PET/CT scanner performance in order to harmonise the acquisition and interpretation of PET scans
- ensure similar performance of PET/CT systems within a multicentre setting
- characterisation of imaging site by continuing quality control, making it highly eligible as a participant in multicentre studies
- high quality of routine patient examinations

EARL: Multicenter QC and calibration

- Calibration
  - Minimum allowable deviation: +/- 10%

- SUV recovery
  - For SUV_{max}
  - For SUV_{mean}

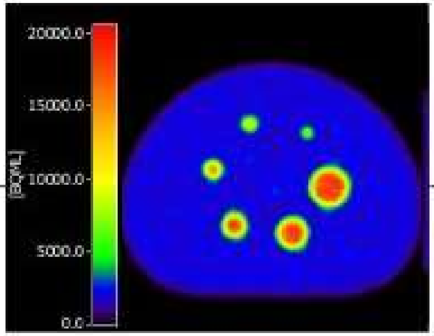
20000.0
15000.0
10000.0
5000.0
0.0
[BQ/ML]

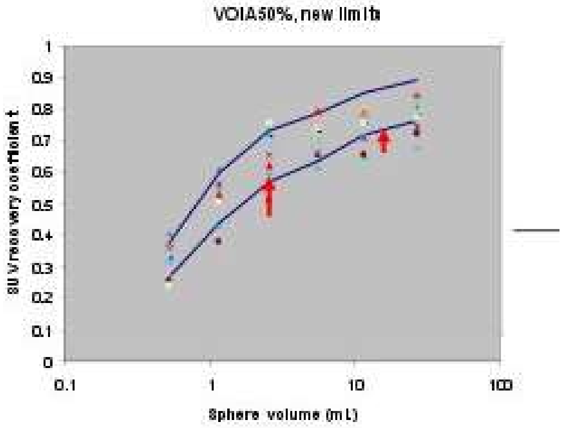

http://www.earl.eanm.org

Summary / Conclusion

- For quantitative PET imaging, raw data correction is necessary
  - Random, scatter and dead time correction
  - Normalization
  - Attenuation correction with CT!
- Image reconstruction
  - FBP, ML-EM, OSEM, 3D-reconstruction protocols

- Automatic contouring algorithms for RT
  - Absolute / relative thresholding
  - Iterative thresholding
  - Source-to-background
  - Gradient-based algorithm

Literature

[1] M Defrise, PE Kinahan, CJ Michel. Image Reconstruction. In: Positron Emission Tomography: Basic Science and Clinical Practice. Editors: PE Valk, DL Bailey, DW Townsend, MN Maisey. Springer London 2003, pp. 63-91.

[2] SR Meikle, RD Badawi. Quantitative Techniques in PET. In: Positron Emission Tomography: Basic Science and Clinical Practice. Editors: PE Valk, DL Bailey, DW Townsend, MN Maisey. Springer London 2003, pp. 93-126.

[3] DW Townsend. Multimodality imaging of structure and function. Phys Med Biol 2008; 53: R1-R39.

[4] JA Lee. Segmentation of positron emission tomography images: Some recommendations for target volume delineation in radiation oncology. Radiother Oncol 2010; 96: 302-307. Review.

[5] D. Thorwarth, A. Schaefer. Functional radiotherapy target volume delineation on the basis of Positron Emission Tomography and the correlation to histopathology. *QJNMMI 2010; 54(5):490-499.*

Applications: MRI in Brain

Cynthia Ménard, M.D.

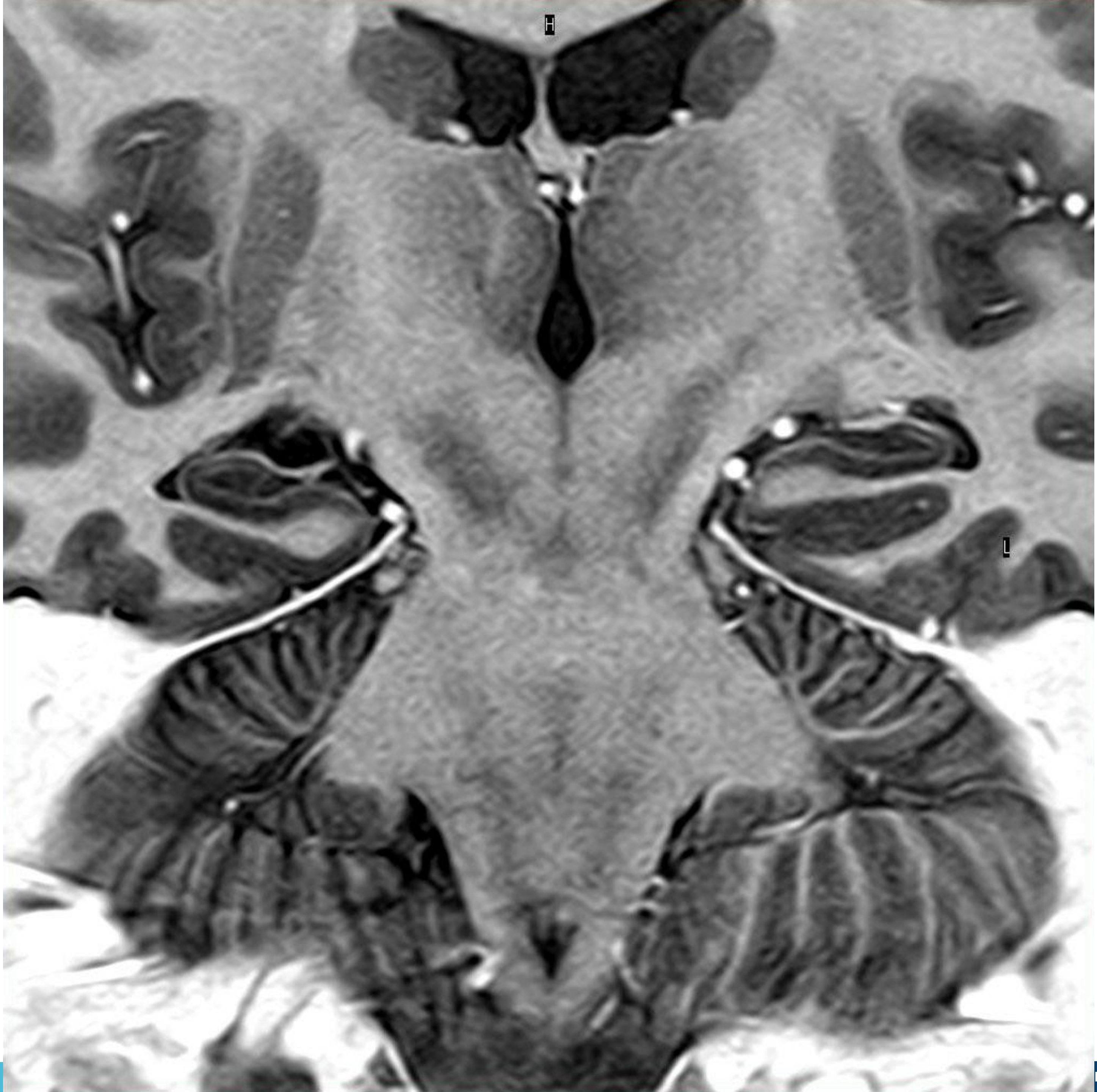
H
L

Goal – MRI Simulation

- Build ideal patient model for radiotherapy planning
  - Accurate and precise depiction of target and organ boundaries (reduce observer uncertainty, enable autosegmentation)
  - Representative of therapy conditions (+ motion)
  - Geometrically accurate
  - Inform on tissue composition / dose attenuation
  - Bridge to online guidance tools
  - Predictive of response (guide dose prescriptions)

Brain Applications

- High precision
  - – SRT / SRS
  - – Brain metastasis
  - – Base of skull benign lesions

- Poor prognosis
  - – Glioblastoma(GBM)

Neuro-Oncology

Neuro-Oncology 17(9), 1188–1198, 2015
doi:10.1093/neuonc/nov095
Advance Access date 6 August 2015

Consensus recommendations for a standardized Brain Tumor Imaging Protocol in clinical trials

Benjamin M. Ellingson, Martin Bendszus, Jerrold Boxerman, Daniel Barboriak, Bradley J. Erickson, Marion Smits, Sarah J. Nelson, Elizabeth Gerstner, Brian Alexander, Gregory Goldmacher, Wolfgang Wick, Michael Vogelbaum, Michael Weller, Evanthia Galanis, Jayashree Kalpathy-Cramer, Lalitha Shankar, Paula Jacobs, Whitney B. Pope, Dewen Yang, Caroline Chung, Michael V. Knopp, Soonme Cha, Martin J. van den Bent, Susan Chang, W.K. Al Yung, Timothy F. Cloughesy, Patrick Y. Wen, Mark R. Gilbert, and the Jumpstarting Brain Tumor Drug Development Coalition Imaging Standardization Steering Committee

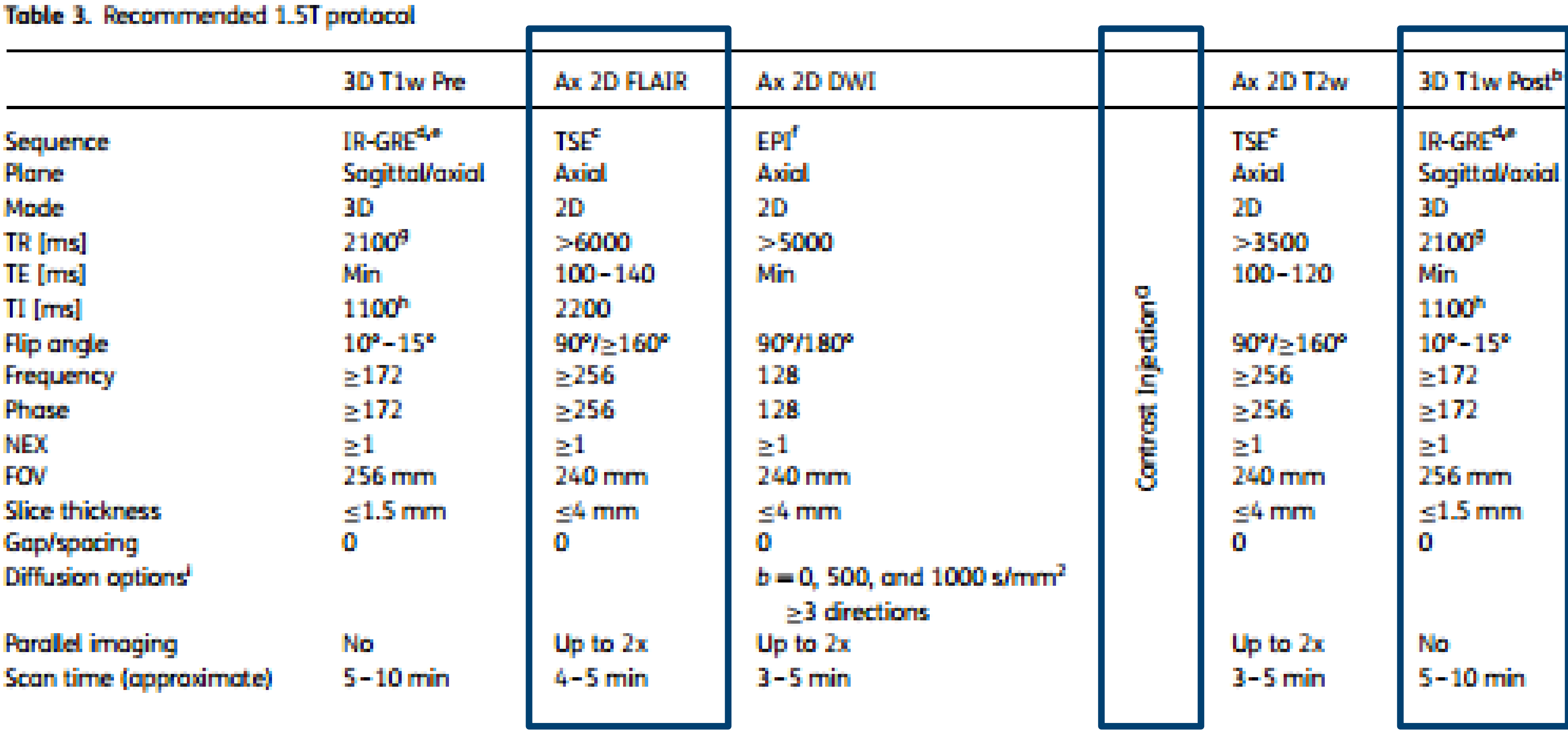

Table 3. Recommended 1.5T protocol

	3D T1w Pre	Ax 2D FLAIR	Ax 2D DWI	Contrast Injection[a]	Ax 2D T2w	3D T1w Post[b]
Sequence	IR-GRE[d,e]	TSE[c]	EPI[f]		TSE[c]	IR-GRE[d,e]
Plane	Sagittal/axial	Axial	Axial		Axial	Sagittal/axial
Mode	3D	2D	2D		2D	3D
TR [ms]	2100[g]	>6000	>5000		>3500	2100[g]
TE [ms]	Min	100–140	Min		100–120	Min
TI [ms]	1100[h]	2200				1100[h]
Flip angle	10°–15°	90°/≥160°	90°/180°		90°/≥160°	10°–15°
Frequency	≥172	≥256	128		≥256	≥172
Phase	≥172	≥256	128		≥256	≥172
NEX	≥1	≥1	≥1		≥1	≥1
FOV	256 mm	240 mm	240 mm		240 mm	256 mm
Slice thickness	≤1.5 mm	≤4 mm	≤4 mm		≤4 mm	≤1.5 mm
Gap/spacing	0	0	0		0	0
Diffusion options[i]			b = 0, 500, and 1000 s/mm^2 ≥3 directions			
Parallel imaging	No	Up to 2x	Up to 2x		Up to 2x	No
Scan time (approximate)	5–10 min	4–5 min	3–5 min		3–5 min	5–10 min

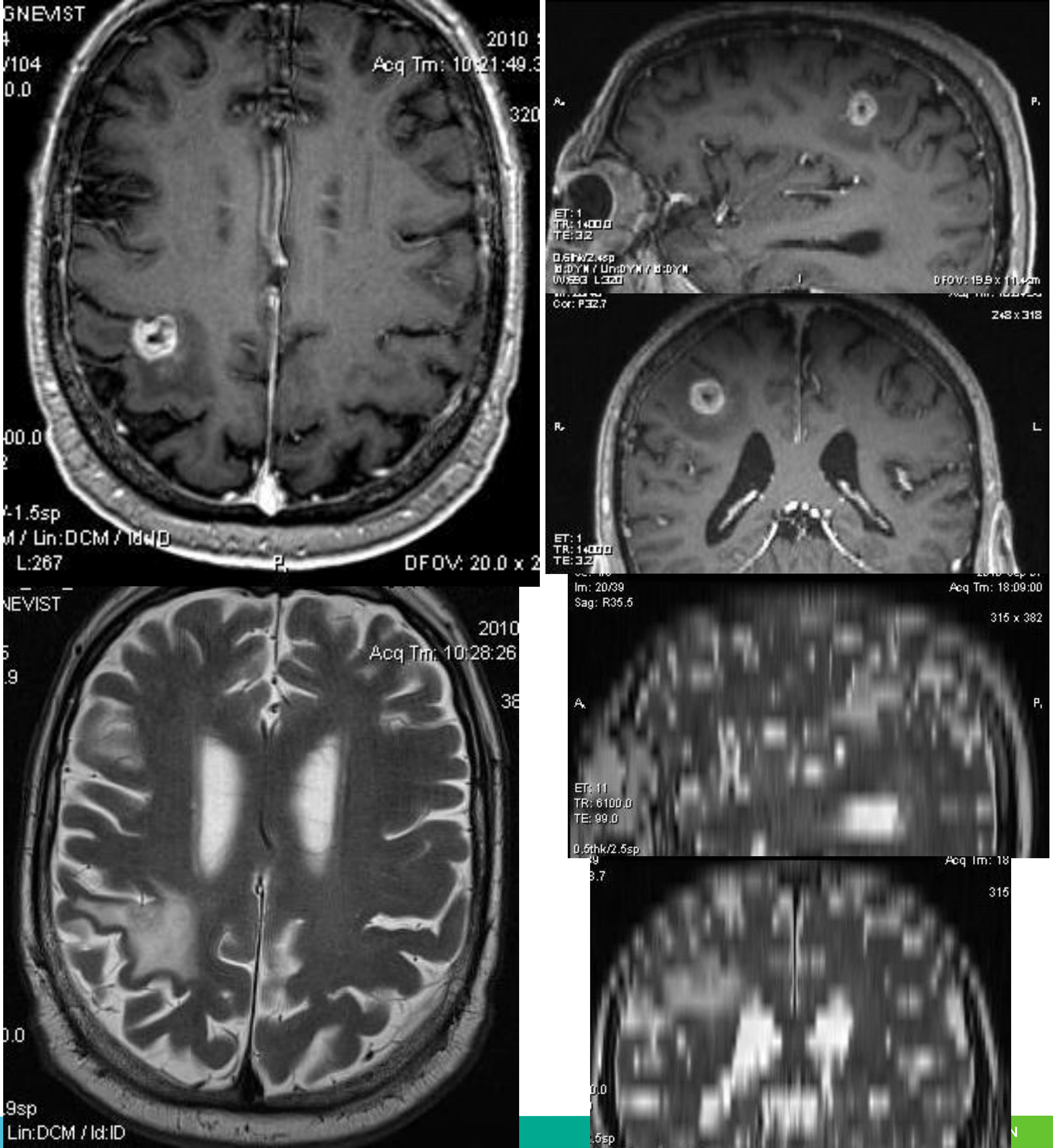
GNEVIST
2010
Acq Tm: 10:21:49.3
320
-1.5sp
L:267
DFOV: 20.0 x 2
ET: 1
TR: 1400.0
TE: 3.2
DFOV: 19.9 x 11.4cm
Cor: P32.7
248 x 318
Im: 20/39
Sag: R35.5
Acq Tm: 18:09:00
315 x 382
ET: 11
TR: 6100.0
TE: 99.0
0.5thk/2.5sp
NEVIST
2010
Acq Tm: 10:28:26
9sp
Lin:DCM / Id:ID

3D

1.5mm slice thickness

2D

3mm slice thickness

Timing of Injection – Brain Metastases

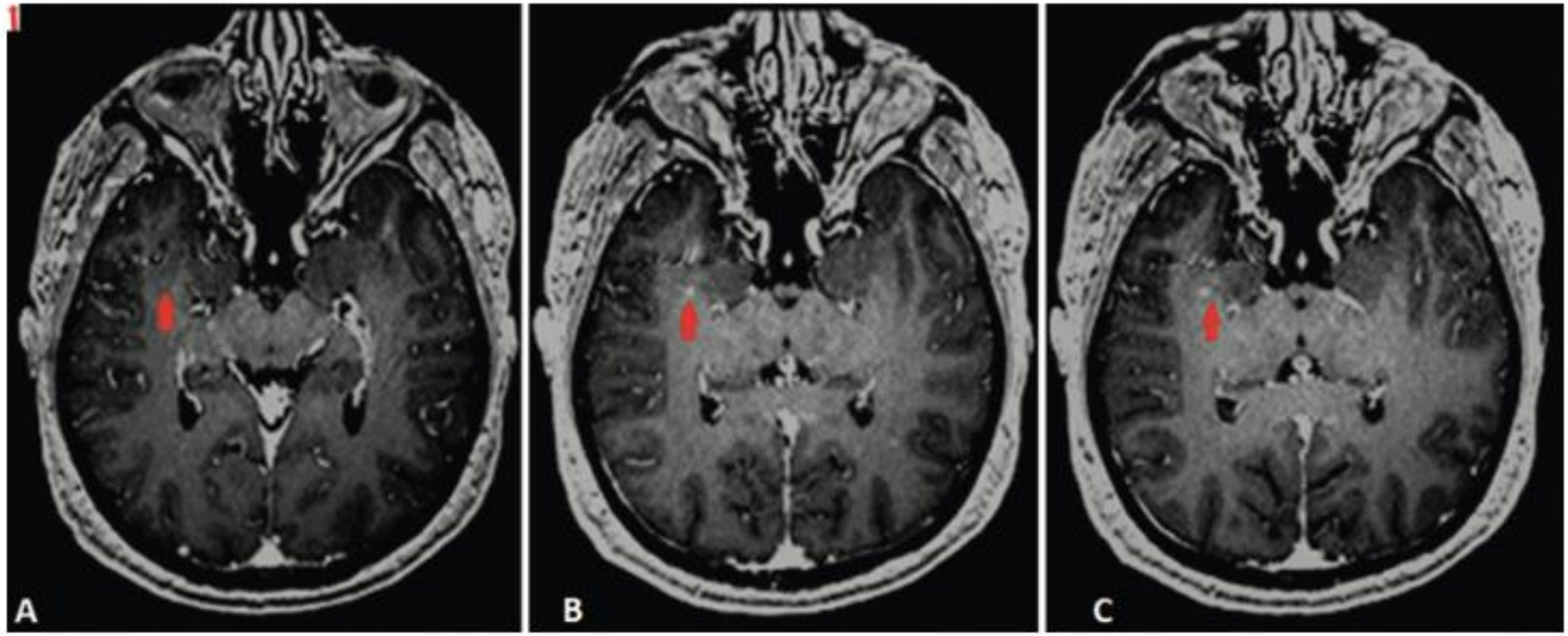

G. 1. In a study performed immediately after contrast injection **(A)**, there is no lesion visible in the right parahippocampal region. wever, a treatable tumor becomes visible at 10-minute **(B)** and 15-minute **(C)** delays. *Red arrows* denote where a lesion is not ualized **(A)** and where it becomes manifest **(B and C)**. Figure is available in color online only.

Kushnirsky et al., JNS 2016

Detection / Segmentation

A convolutional neural network-based automatic delineation strategy for brain metastases

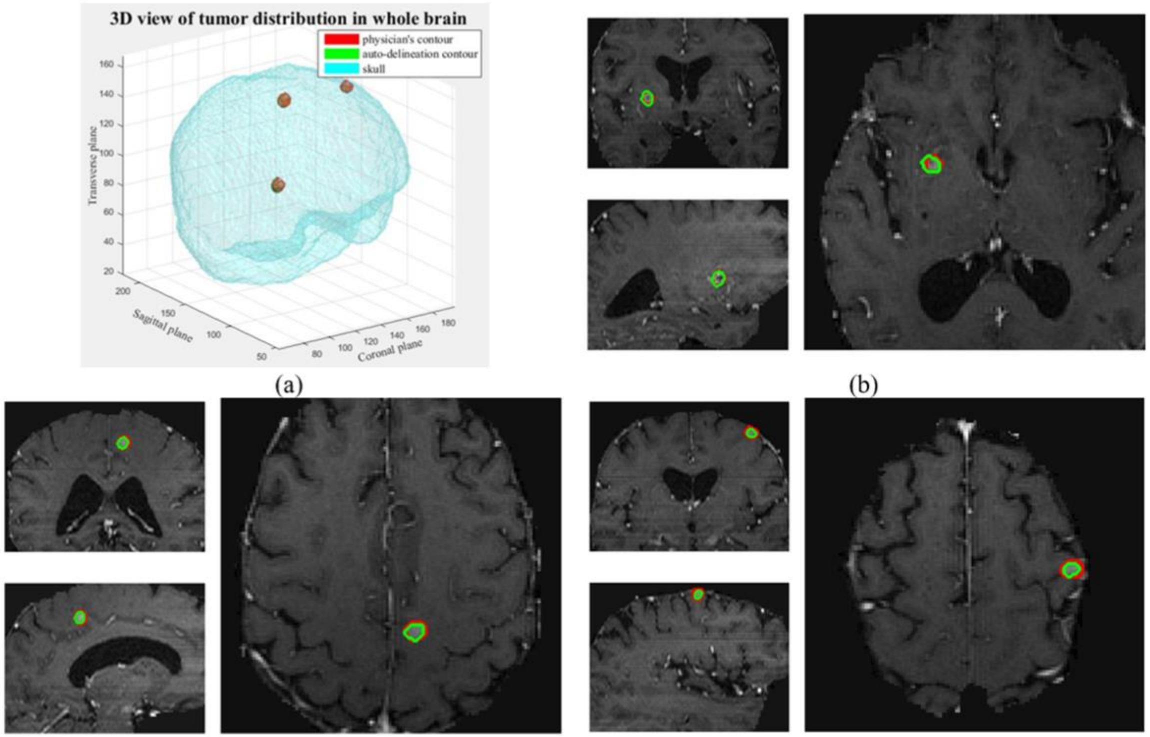
3D view of tumor distribution in whole brain
🟥 physician's contour
🟩 auto-delineation contour
🟦 skull
Transverse plane
160
140
120
100
80
60
40
20
Sagittal plane
200
150
100
50
Coronal plane
80
100
120
140
160
180
(a)
(b)

Liu et al., PLOS One 2017

CHUM

Tissue Contrast

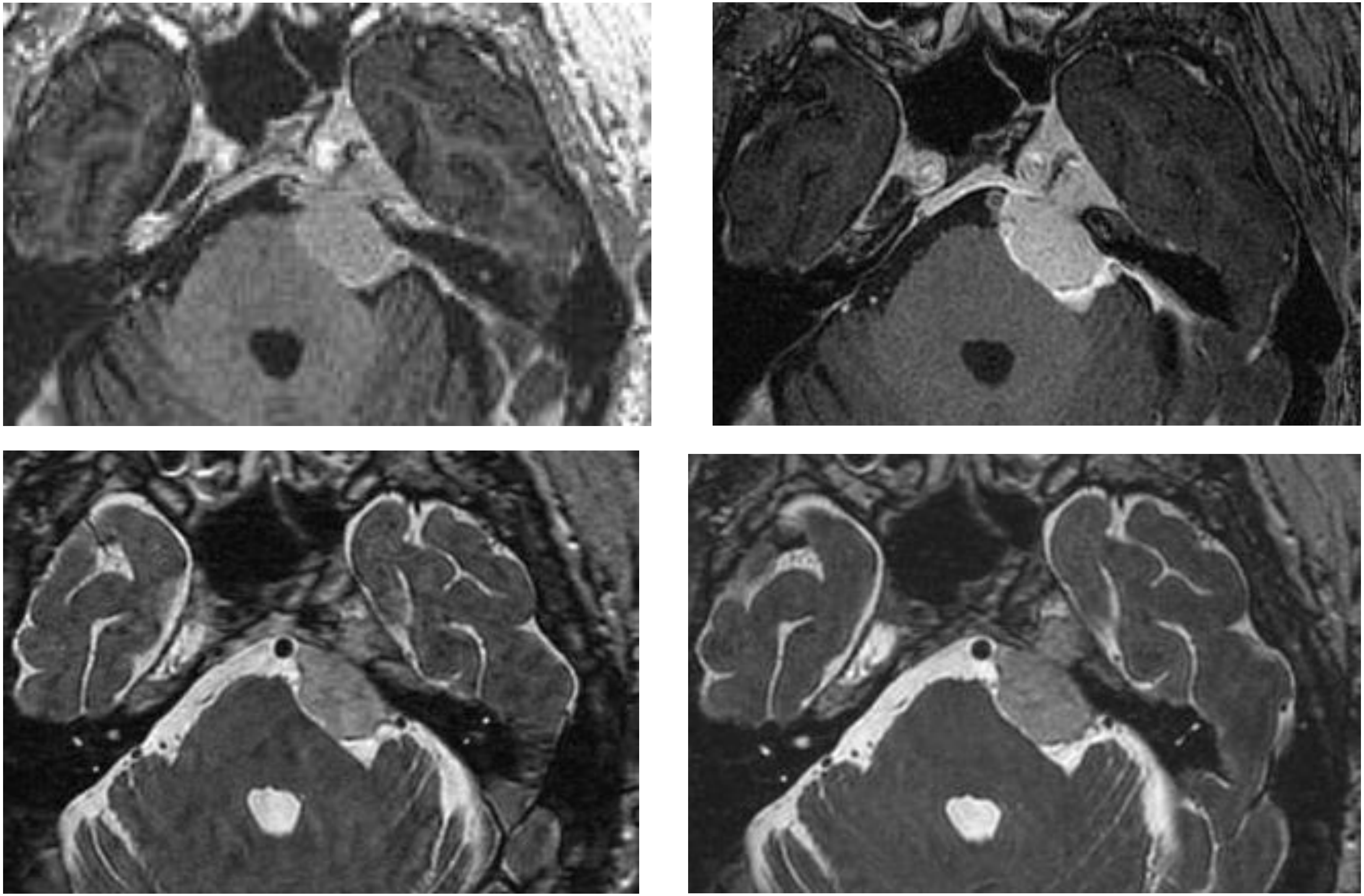

MacFadden et al., IJROBP 76:5:1472-1479, 2010

MR-Only Simulation

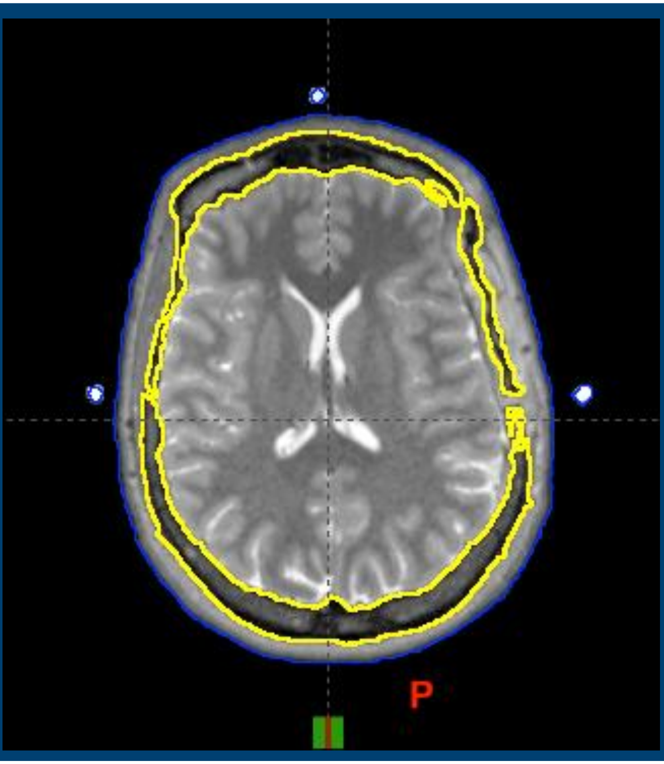

- Imaging
- Bone segmentation
- Body contour segmentation
- Density override

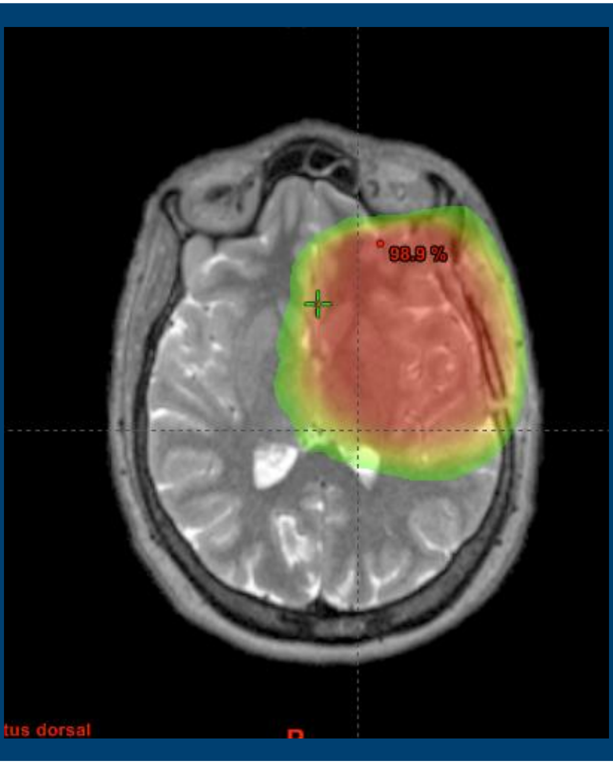

- Dose calculation

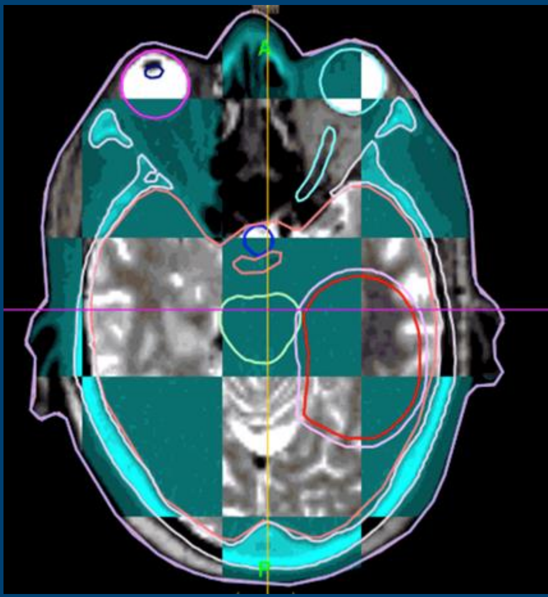

- IGRT
- Dose re-calculation

Delineation – Visible Tumor

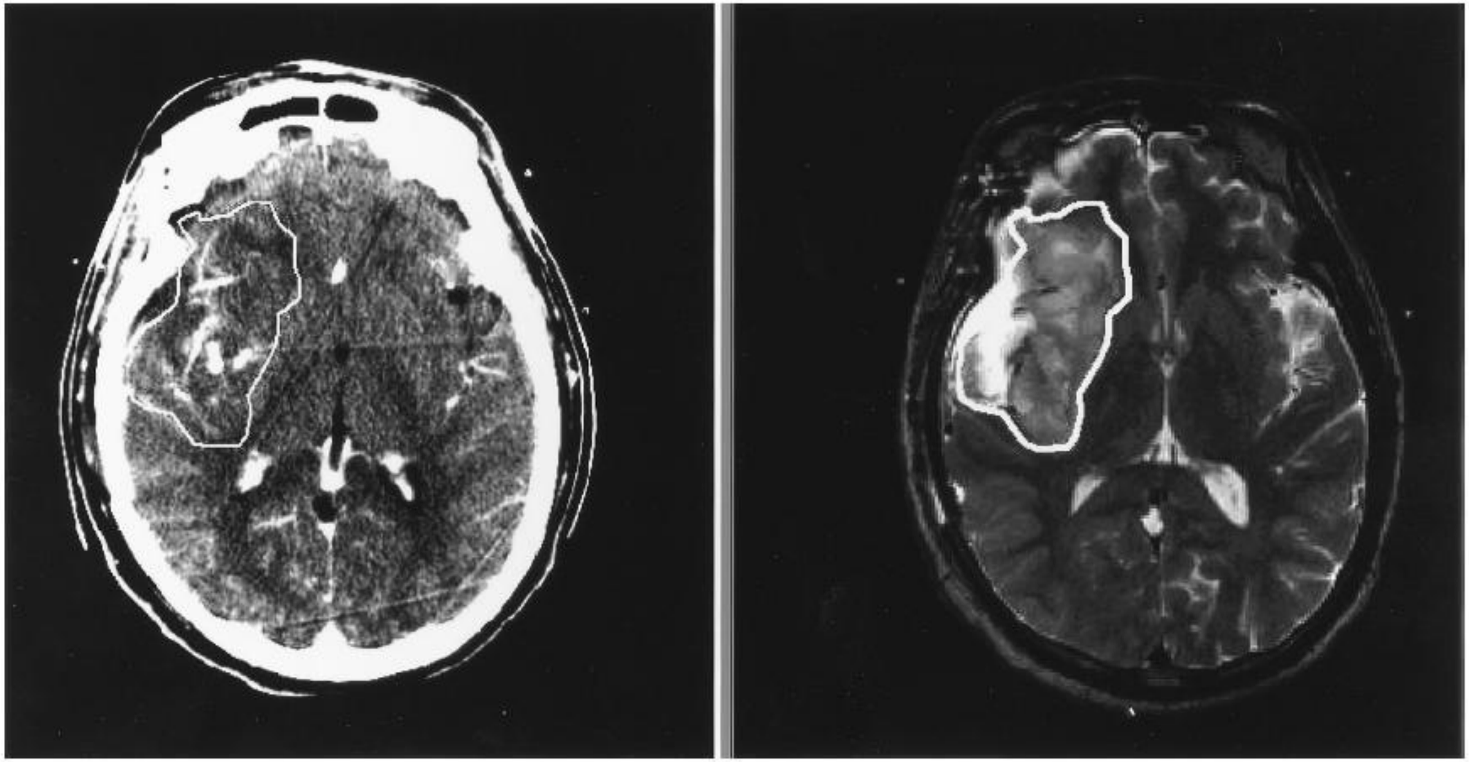

- 🕮 Ten Haken et al., Radiot Oncol, 1992
- 🕮 Khoo et al., IJROBP 2000
- 🕮 Aoyama et al., IJROBP 2001

IDH1 - MRSI

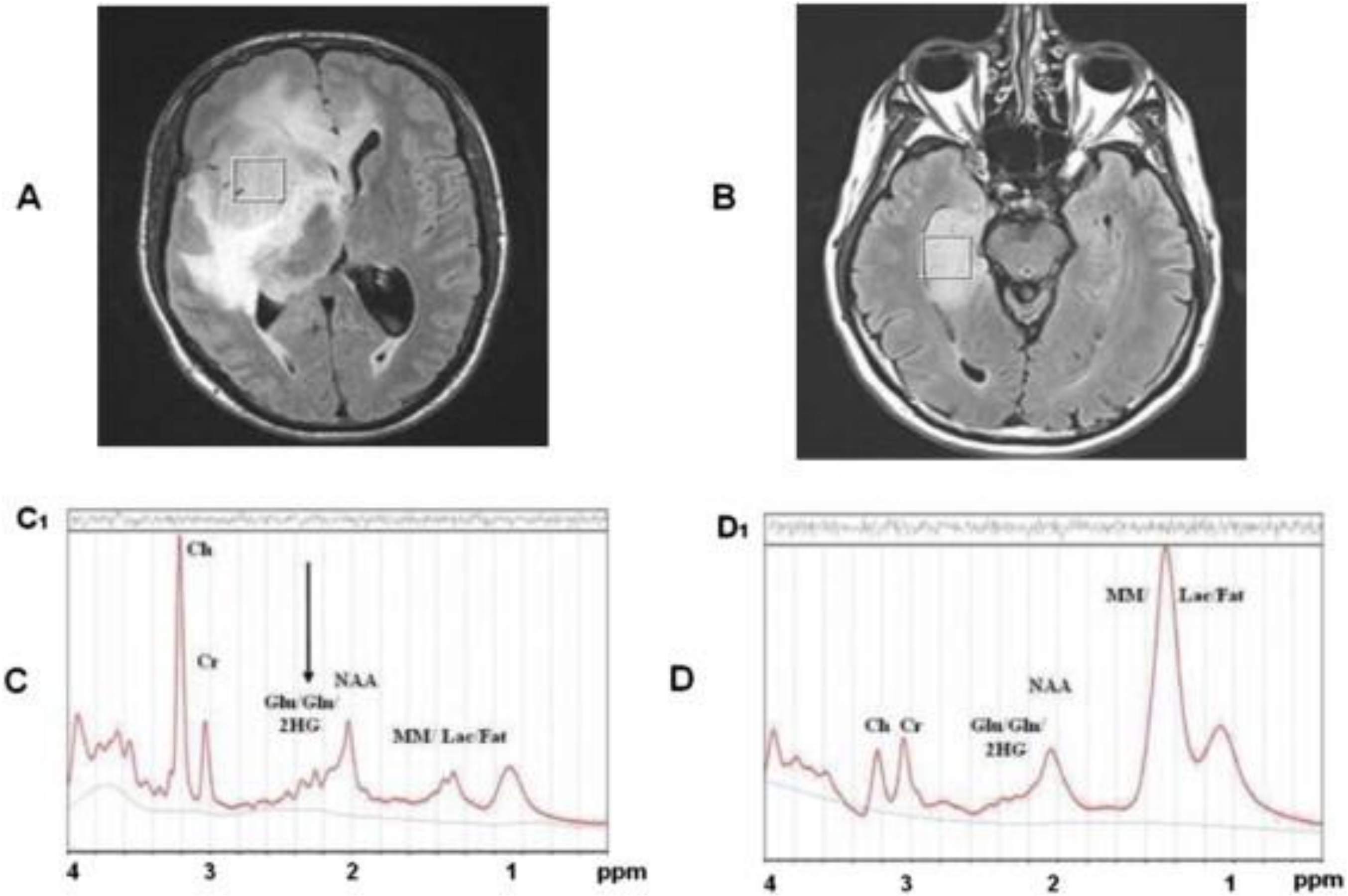
A
B
C1
C
Ch
Cr
NAA
Gln/Glu/
2HG
MM/ Lac/Fat
4
3
2
1
ppm
D1
D
MM/
Lac/Fat
NAA
Ch
Cr
Gln/Glu/
2HG
4
3
2
1
ppm

Chung et al., Sem Rad Oncol 2014

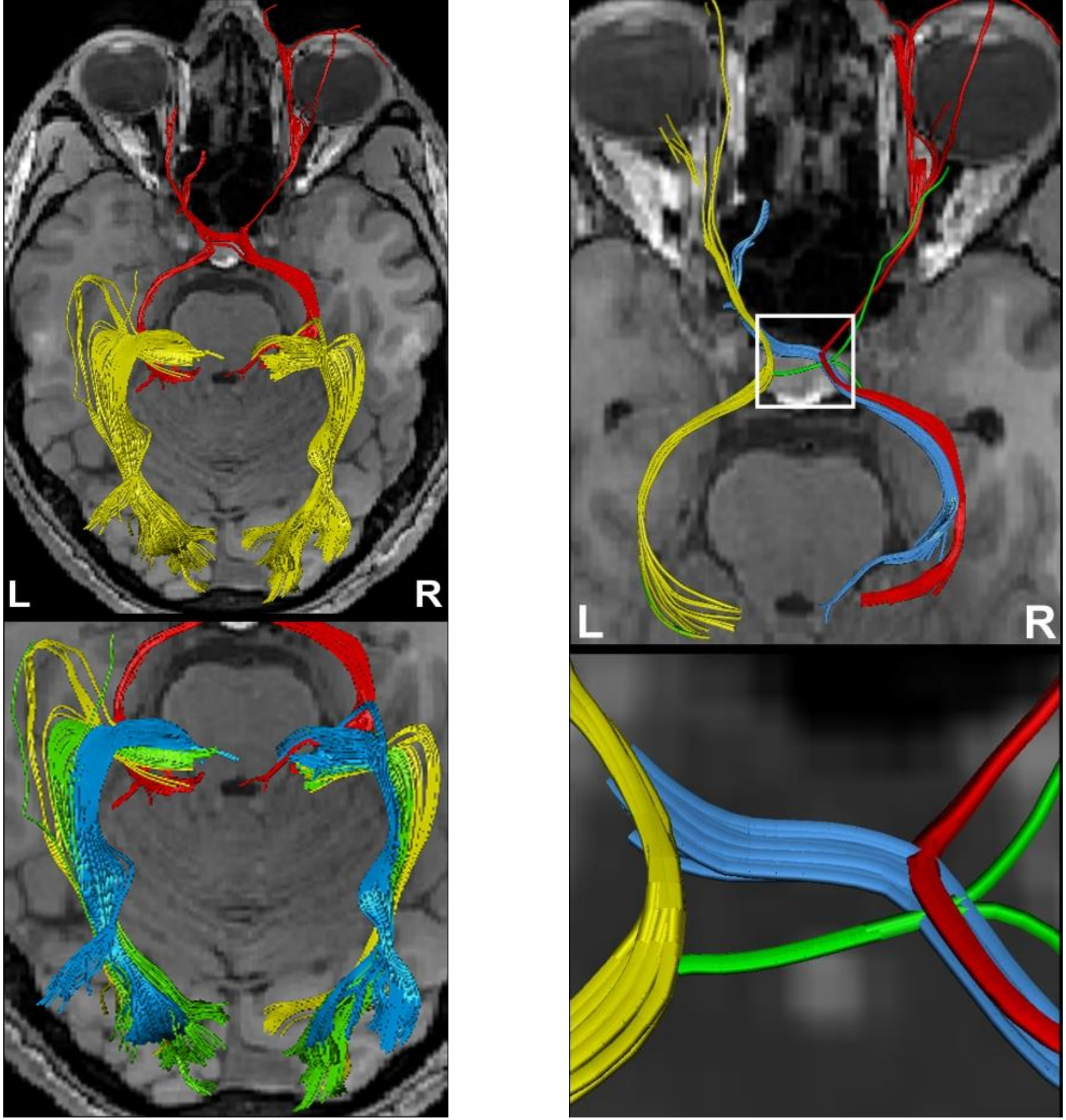

📖 Hofer et al., Front Neur 4: 15, 2010

FA map for CTV delineation

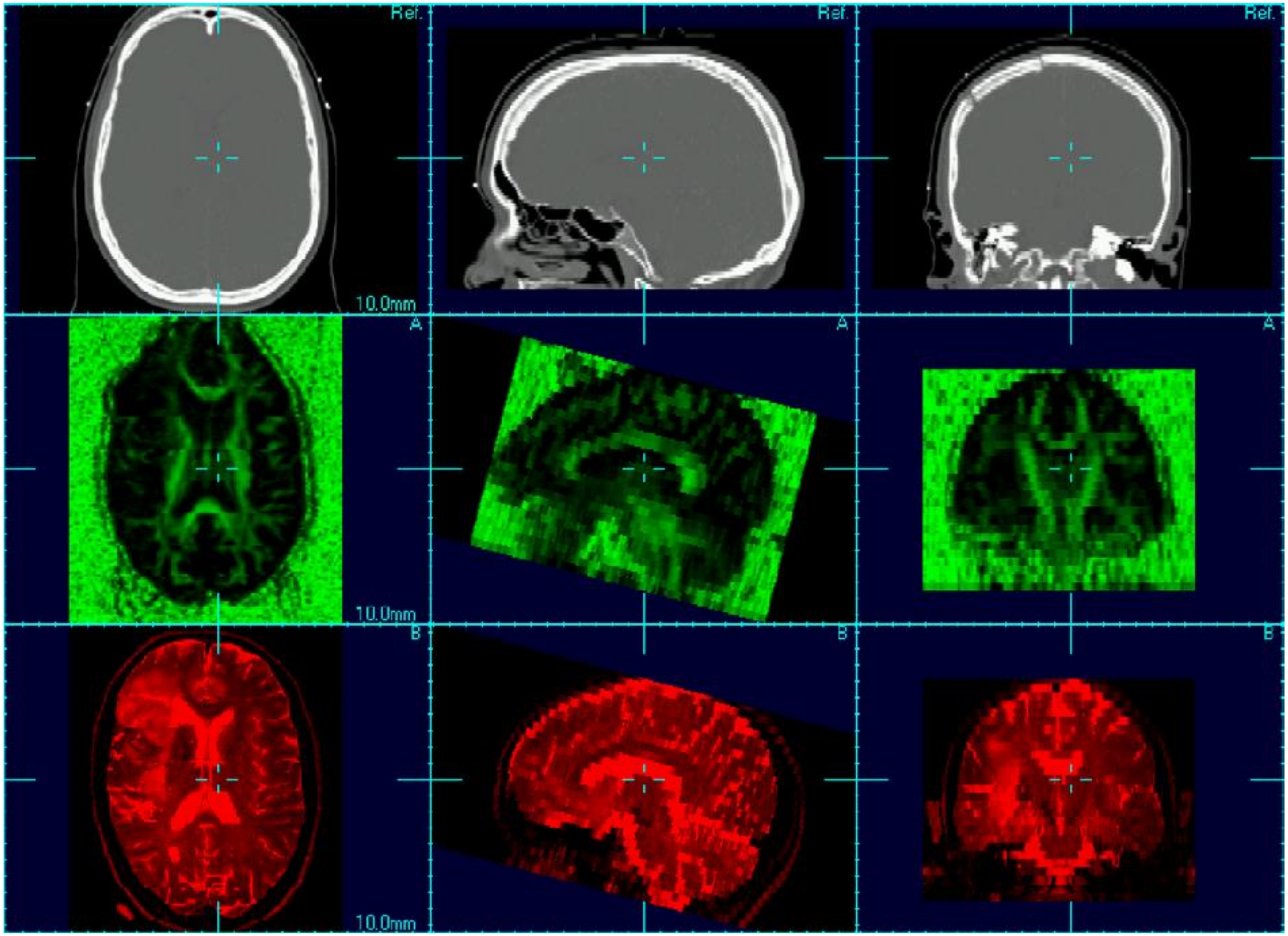
Ref.
Ref.
Ref.
10.0mm
A
A
A
10.0mm
B
B
B
10.0mm

Jena et al., Clin Oncol 2005

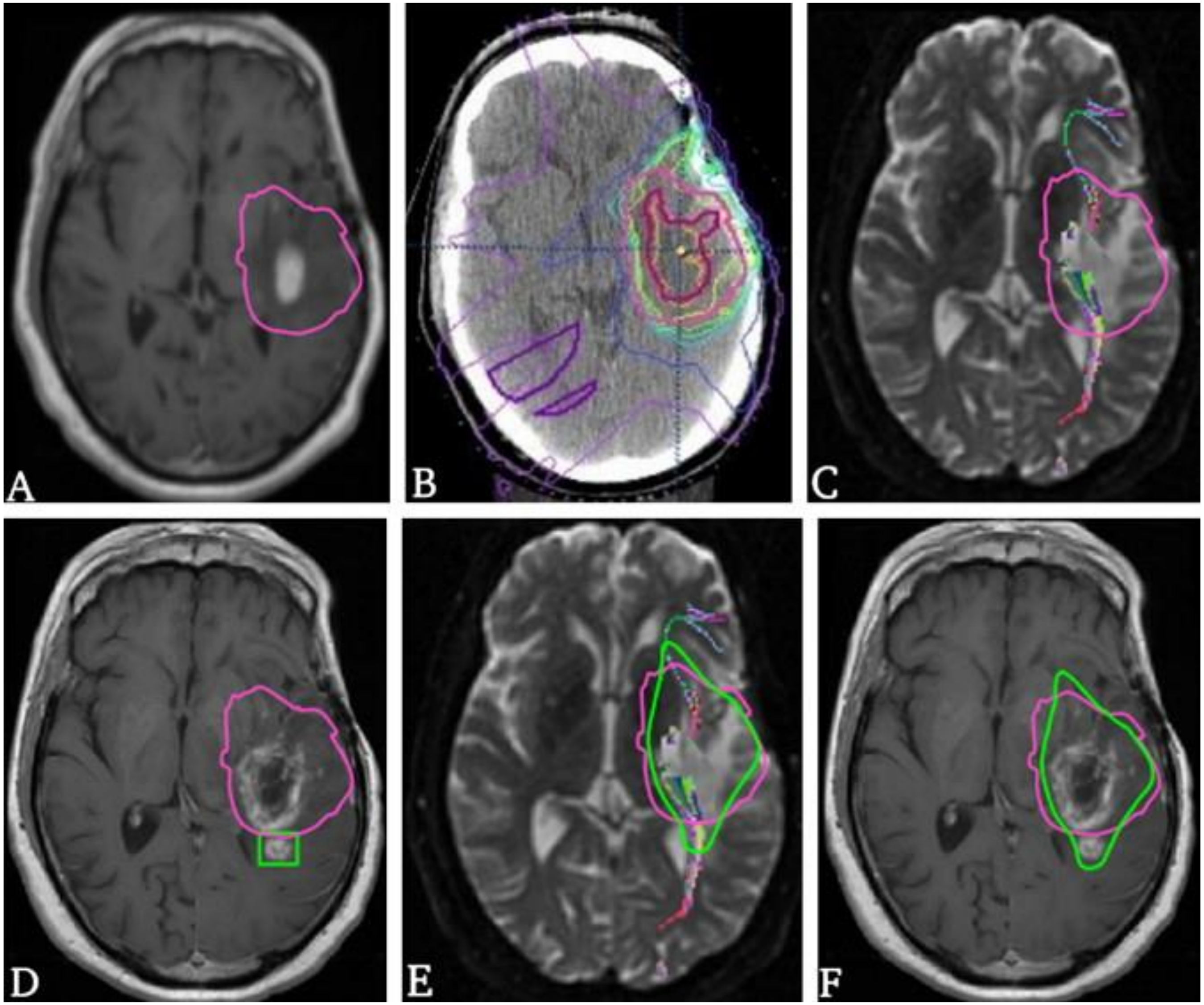

📖Krishnan et al., IJROBP, 2008;

📖Berberat et al., Strahlenther Oncol 2014

Optic Radiation – SRS Injury

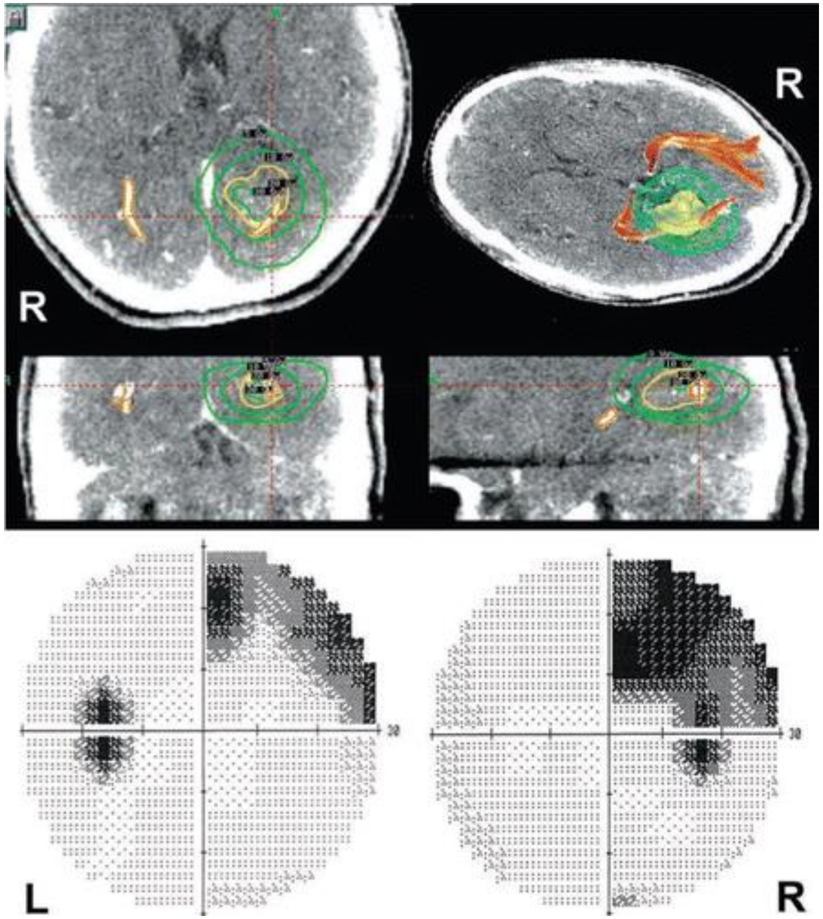

Maruyama et al, J Neurosurg, 2007

DTI – OAR Sparing

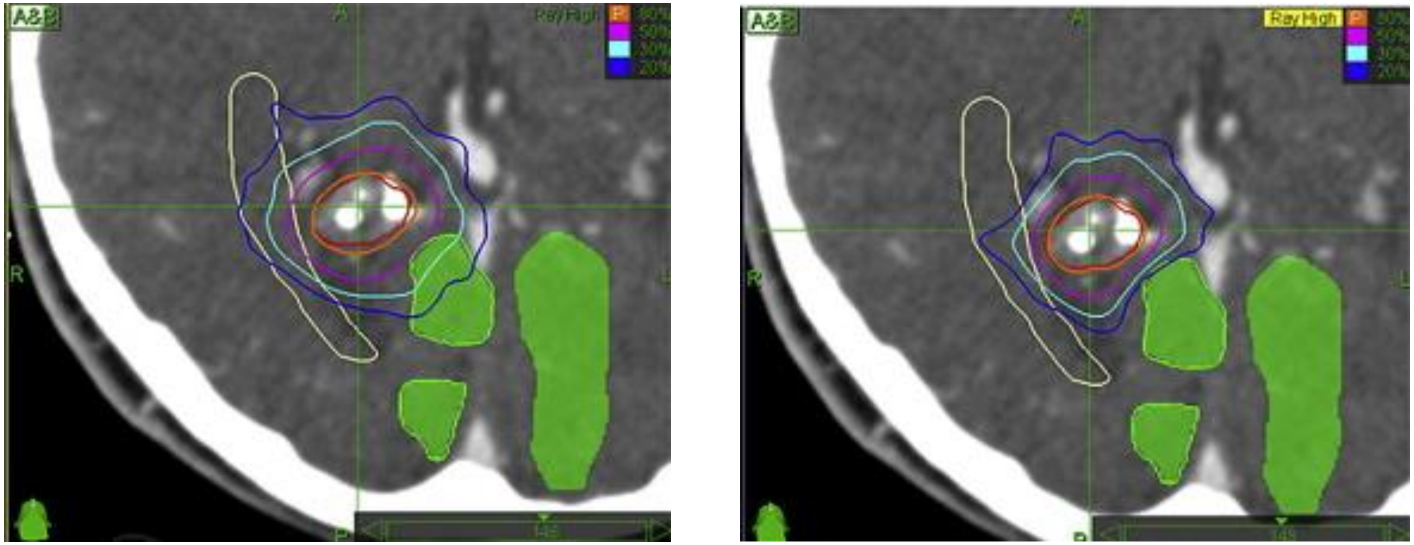
A&B
A
Ray High
P
80%
50%
30%
20%
R
L
P

Pantelis et al, IJROBP, 2010

Pyramidal Tract / Speech

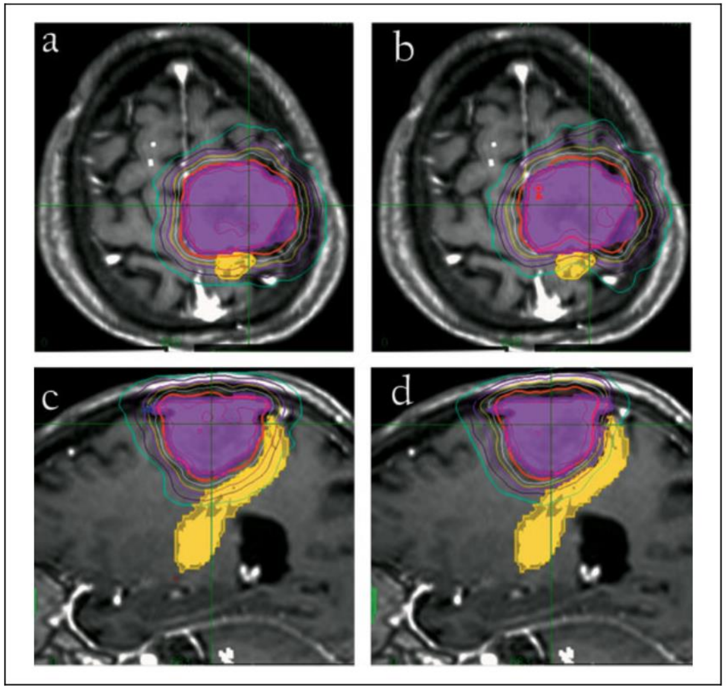

Figure 2. Treatment plans developed without (left side) and with (right side) the introduction of the pyramidal tracts in the optimization process for the meningioma case, plotted in axial and sagittal planes. This patient received 21 Gy units of radiation in 7 Gy fractions. The radiation dose to pyramidal tract is lowered from 2396.97 to 1460.96 cGy after the optimized process with pyramidal tract.

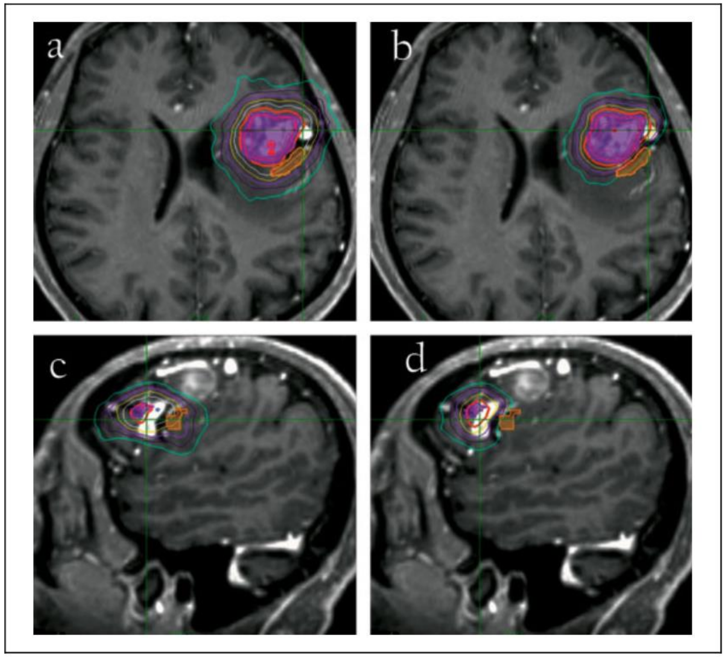

Figure 3. Treatment plans developed without (left side) and with (right side) the introduction of the language area in the optimization process for the AVM case, plotted in axial and sagittal planes. This patient received 16 Gy in single fraction. The maximum radiation dose to the language area is lowered from 1587.55 to 1273.88 cGy after the optimized process with language area. AVM indicates arteriovenous malformation.

Sun et al., Tech Can Res Treat 2017

DTI Map

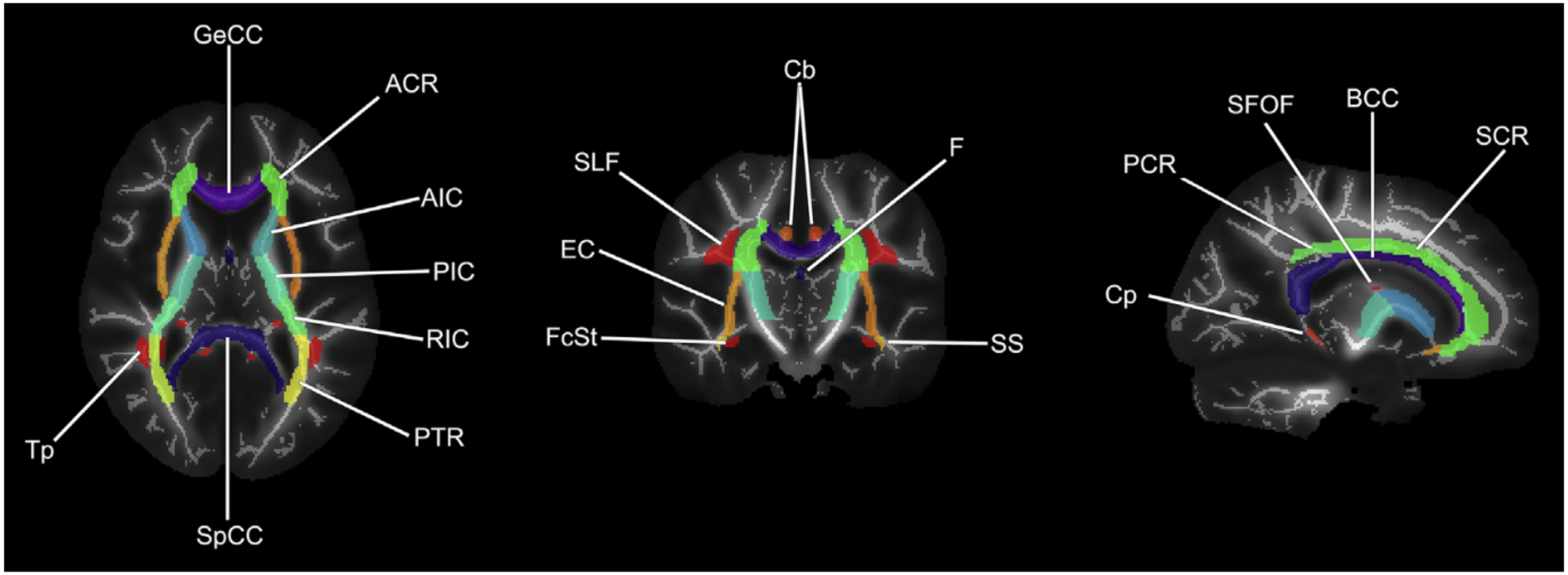

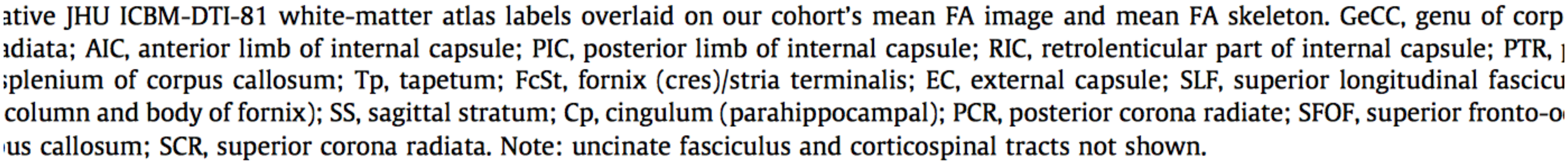
ative JHU ICBM-DTI-81 white-matter atlas labels overlaid on our cohort's mean FA image and mean FA skeleton. GeCC, genu of corp
adiata; AIC, anterior limb of internal capsule; PIC, posterior limb of internal capsule; RIC, retrolenticular part of internal capsule; PTR,
splenium of corpus callosum; Tp, tapetum; FcSt, fornix (cres)/stria terminalis; EC, external capsule; SLF, superior longitudinal fascicu
column and body of fornix); SS, sagittal stratum; Cp, cingulum (parahippocampal); PCR, posterior corona radiate; SFOF, superior fronto-o
us callosum; SCR, superior corona radiata. Note: uncinate fasciculus and corticospinal tracts not shown.

Connor Rad Oncol 2017

Atlas-based Segmentation

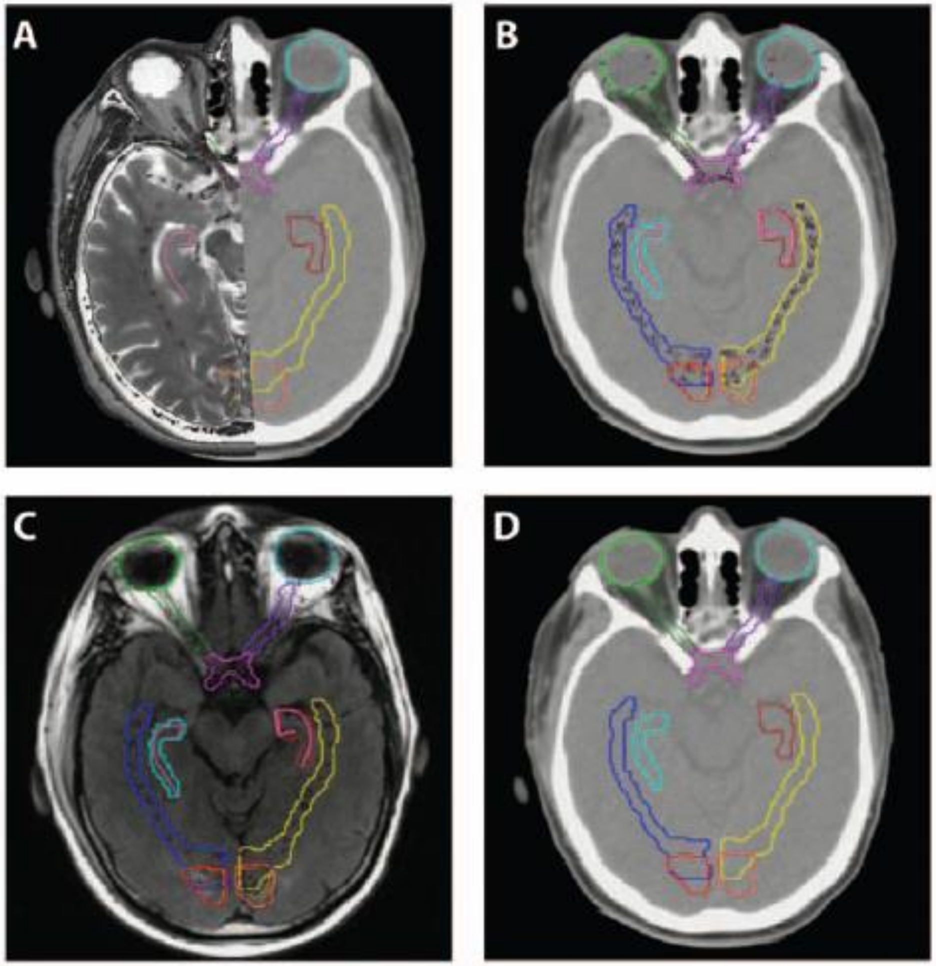

Weksberg et al., 2012, PLoS One

Eloquent Cortex

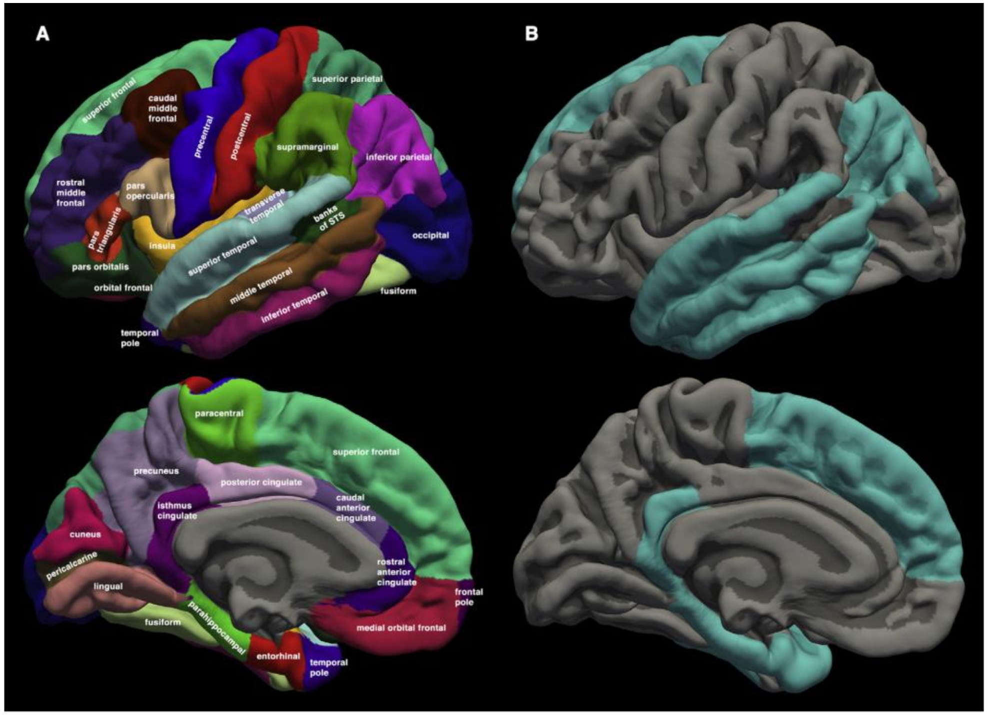
A
superior frontal
caudal middle frontal
precentral
postcentral
superior parietal
supramarginal
inferior parietal
rostral middle frontal
pars opercularis
pars triangularis
transverse temporal
banks of STS
occipital
insula
pars orbitalis
superior temporal
orbital frontal
middle temporal
inferior temporal
fusiform
temporal pole
B
paracentral
superior frontal
precuneus
posterior cingulate
isthmus cingulate
caudal anterior cingulate
cuneus
pericalcarine
rostral anterior cingulate
lingual
frontal pole
fusiform
parahippocampal
medial orbital frontal
entorhinal
temporal pole

Fig. 1. (A) Cortical regions from the Desikan-Killiany atlas available in the FreeSurfer neuroimaging software suite. Regions are displayed on the FreeSurfer average brain for illustration, but statistical analyses were carried out using the corresponding regions delineated in the native magnetic resonance imaging space of each patient. Average radiation dose and average cortical thickness change were calculated for each region. (B) Cortical regions with significant radiation dose-dependent cortical atrophy in linear mixed-effects model. FreeSurfer average brain surface shown in gray (light gray for gyrus, dark gray for sulcus). Regions statistically significant after correction for multiple comparisons are colored. Only the left hemisphere is shown for convenience, but statistical tests included bilateral observations.

📖 Seibert et al., Int J Rad Oncol Biol Phys 2017

Stereotactic Reference - Deviation

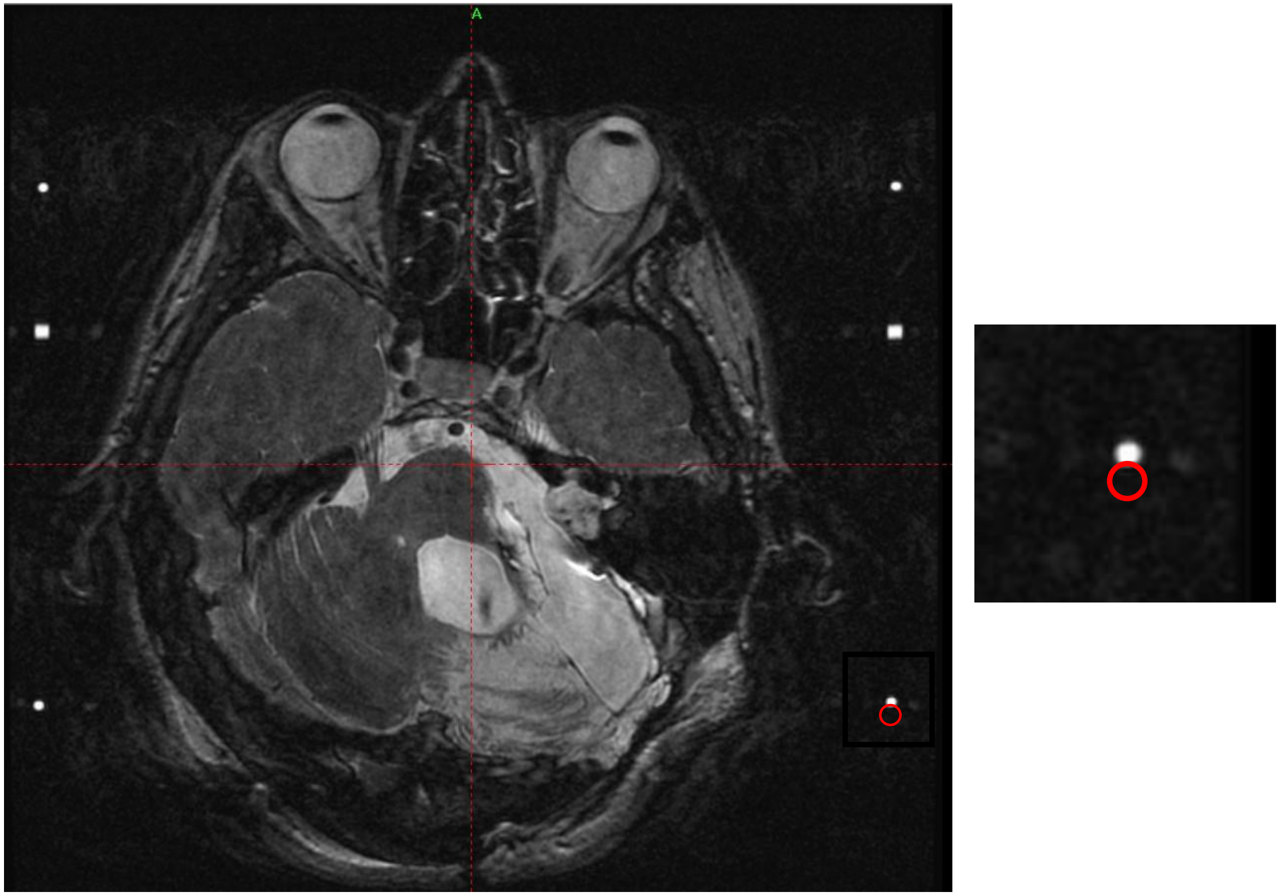

📖Zhang et al. PMB 55:22:6601-6615, 2010

3T T2 FRFSE

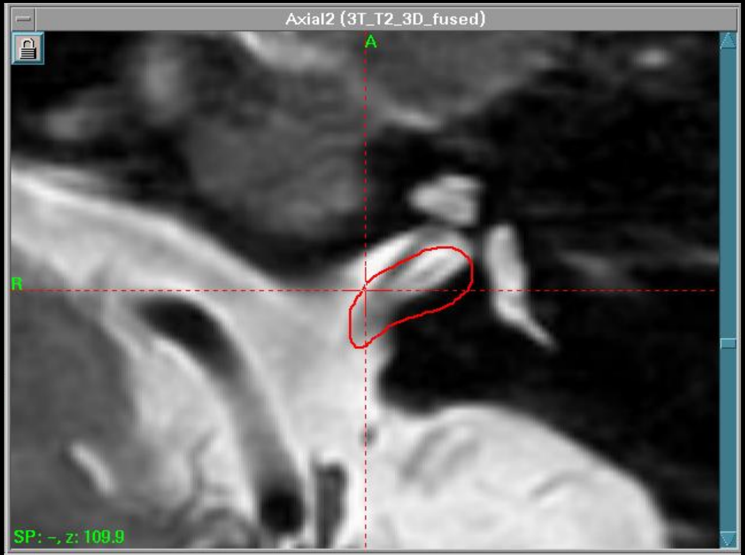
Axial2 (3T_T2_3D_fused)
A
R
SP: –, z: 109.9

CT

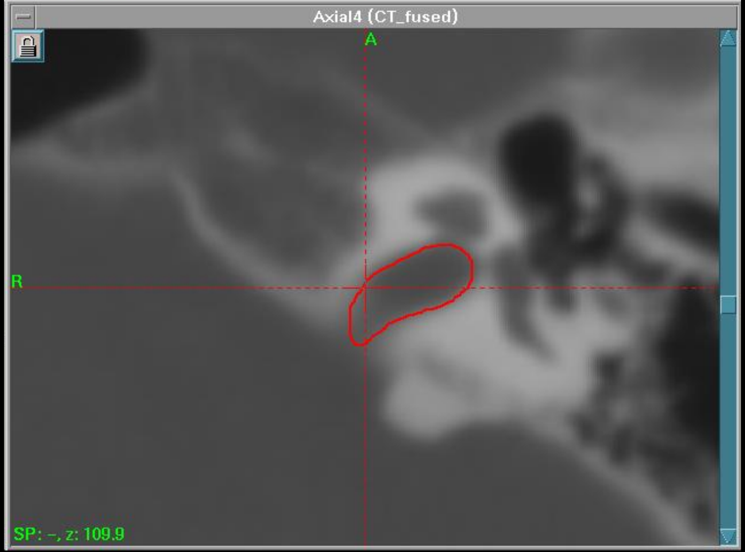
Axial4 (CT_fused)
A
R
SP: –, z: 109.9

Zhang et al. PMB 55:22:6601-6615, 2010

Hemorhagic Metastasis

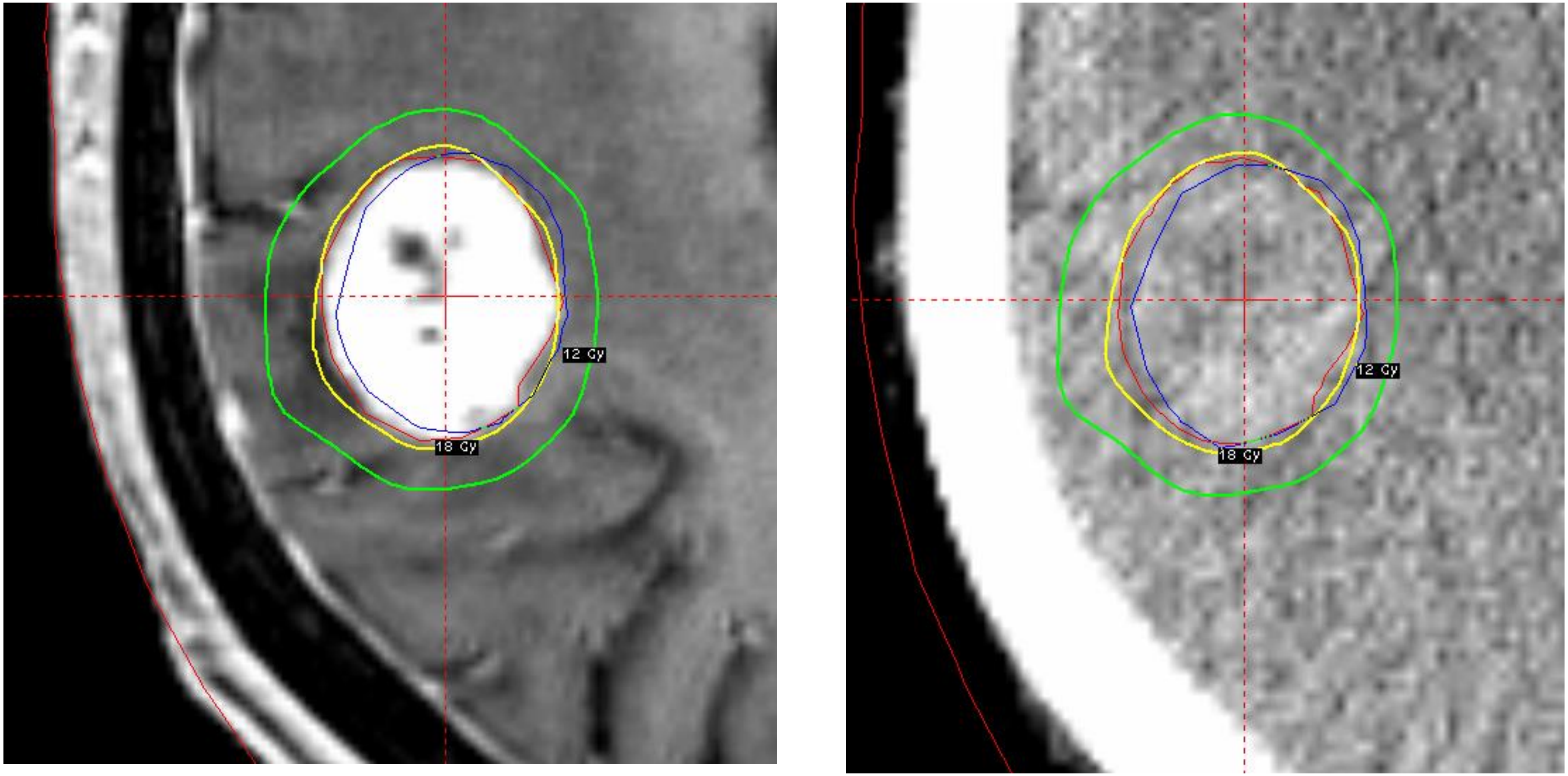
12 Gy
18 Gy
12 Gy
18 Gy

📖 Chung et al., ISRS, 2011

CHUM

Tumor Geometry ROC for 2y OS

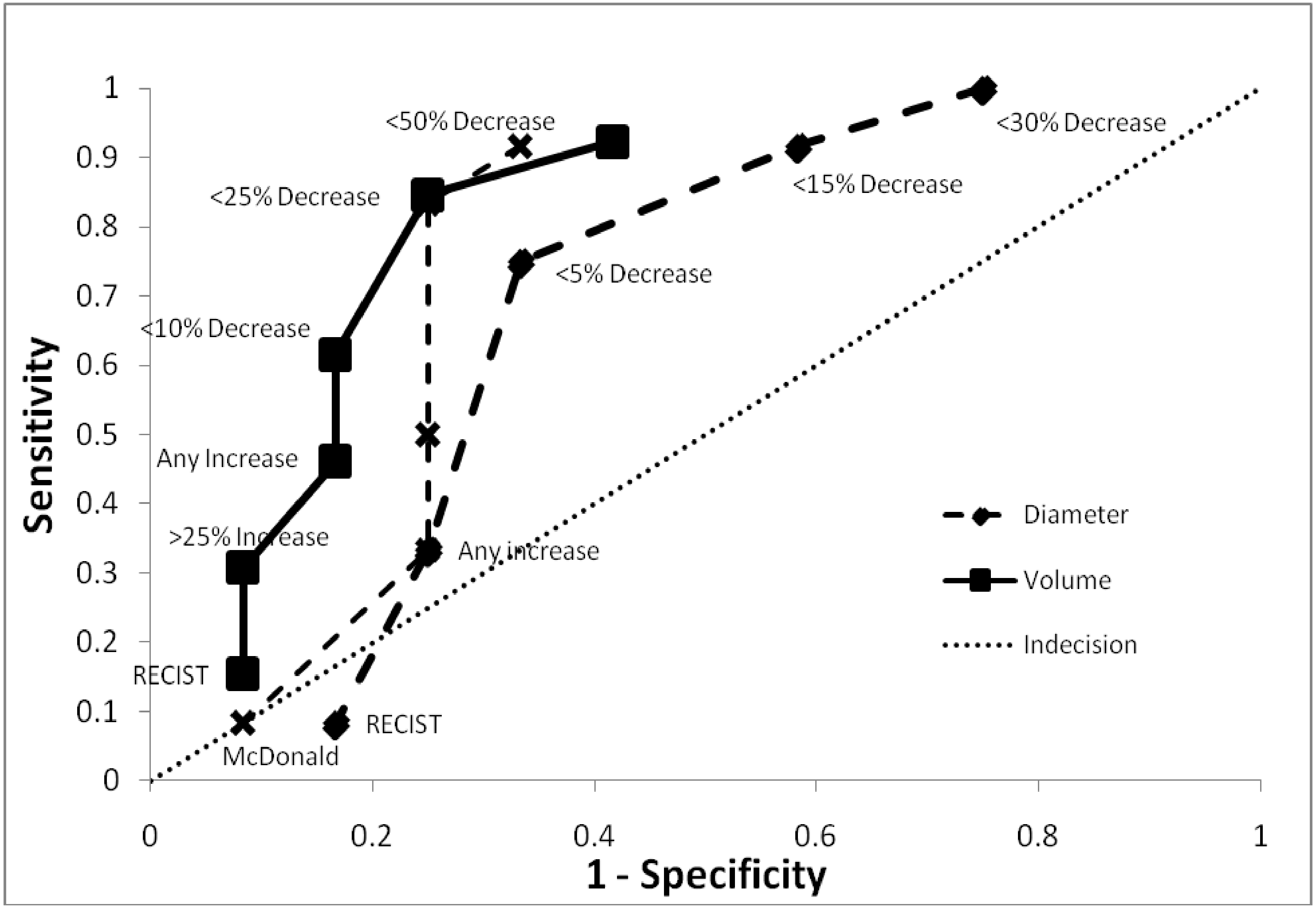

Gladwish et al., Radiat Oncol 2011

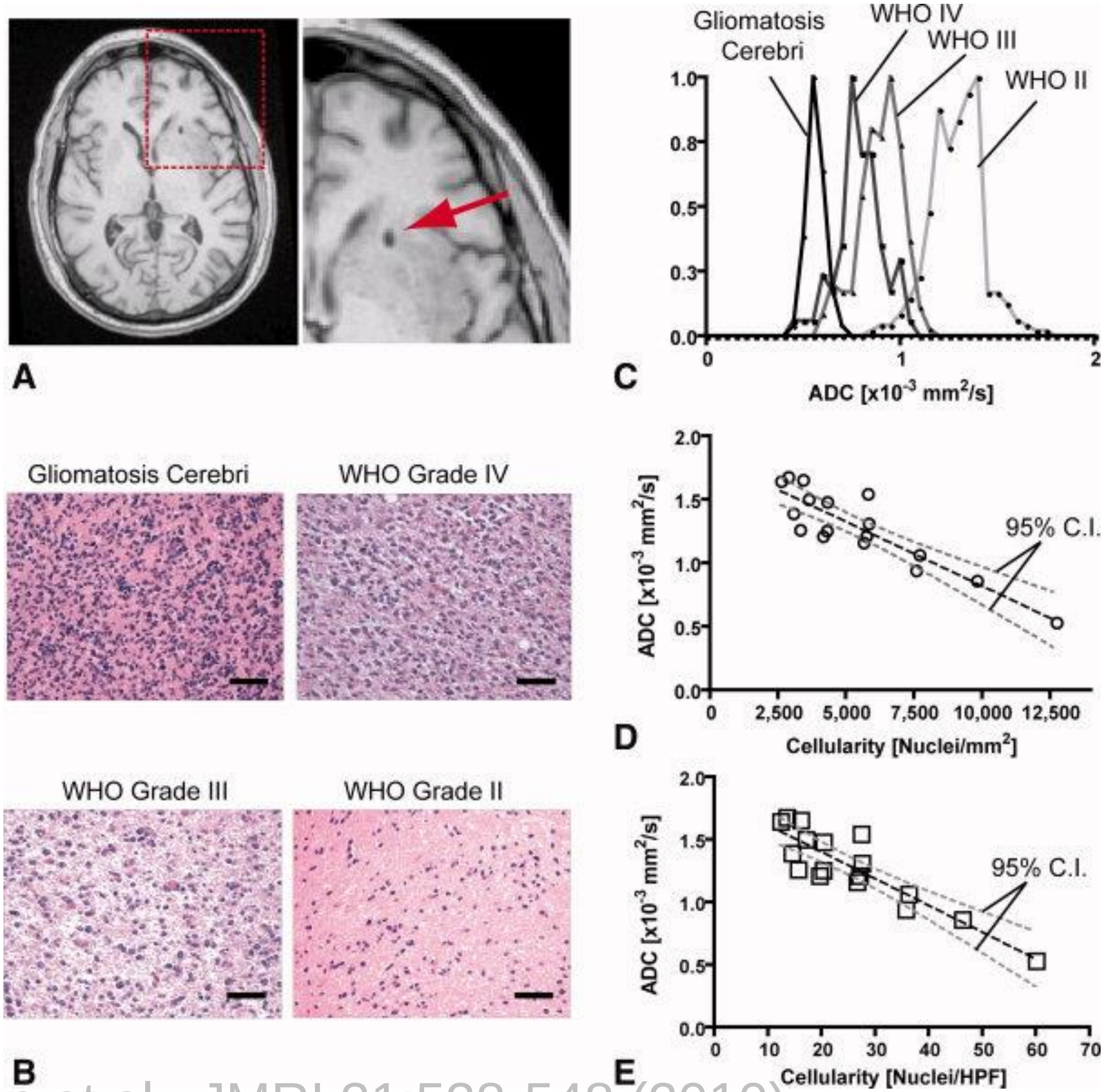
A
C
Gliomatosis Cerebri
WHO IV
WHO III
WHO II
1.0
0.8
0.5
0.3
0.0
0
1
2
ADC [x10⁻³ mm²/s]
Gliomatosis Cerebri
WHO Grade IV
WHO Grade III
WHO Grade II
B
D
ADC [x10⁻³ mm²/s]
2.0
1.5
1.0
0.5
0.0
0
2,500
5,000
7,500
10,000
12,500
Cellularity [Nuclei/mm²]
95% C.I.
E
ADC [x10⁻³ mm²/s]
2.0
1.5
1.0
0.5
0.0
0
10
20
30
40
50
60
70
Cellularity [Nuclei/HPF]
95% C.I.

Ellingson et al., JMRI 31:538-548 (2010)

ADC Response

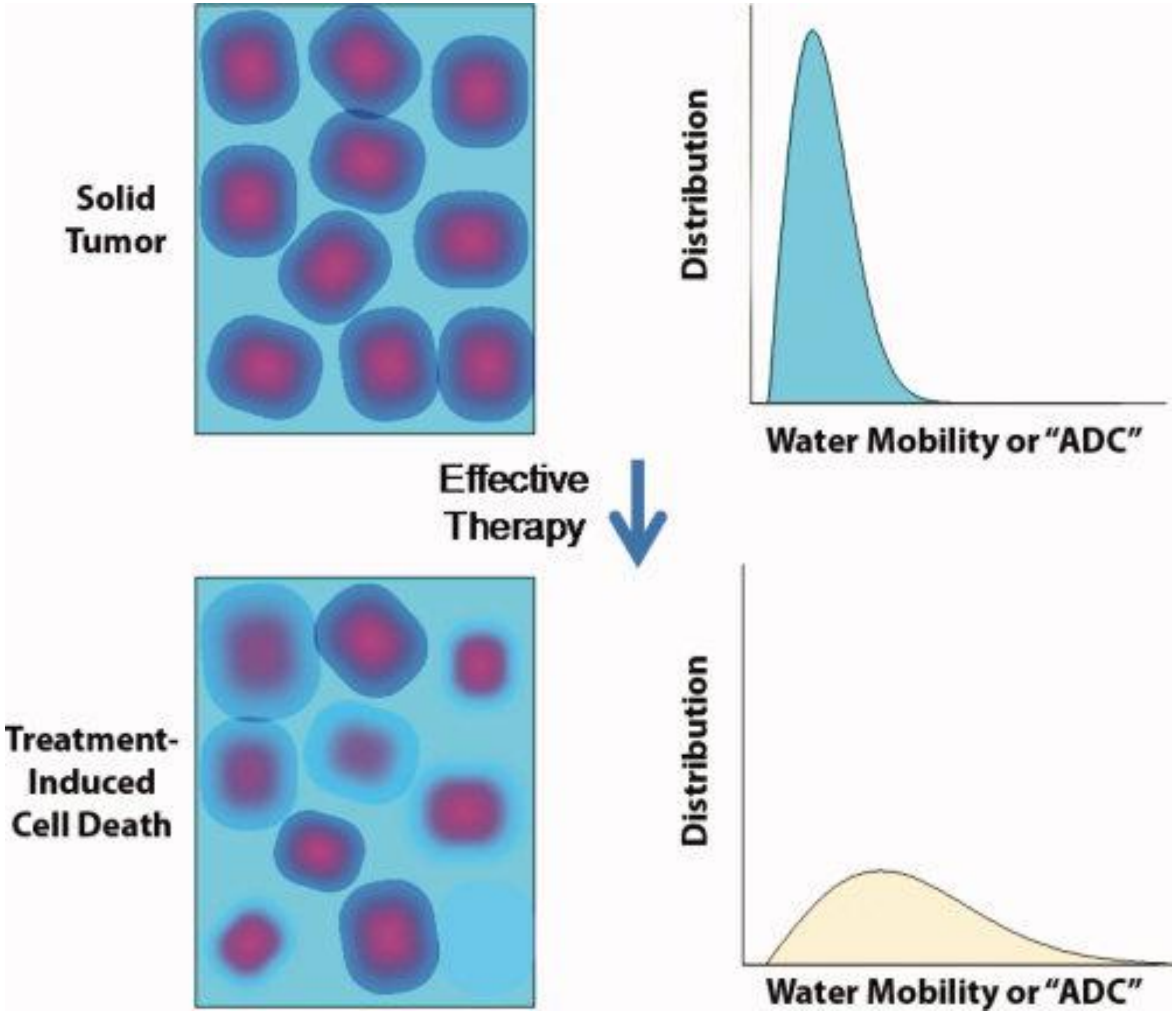
Solid Tumor
Distribution
Water Mobility or "ADC"
Effective Therapy
Treatment-Induced Cell Death
Distribution
Water Mobility or "ADC"

📖 Thoeny et al., JMRI 32:2-16, 2010

ADC Dynamics

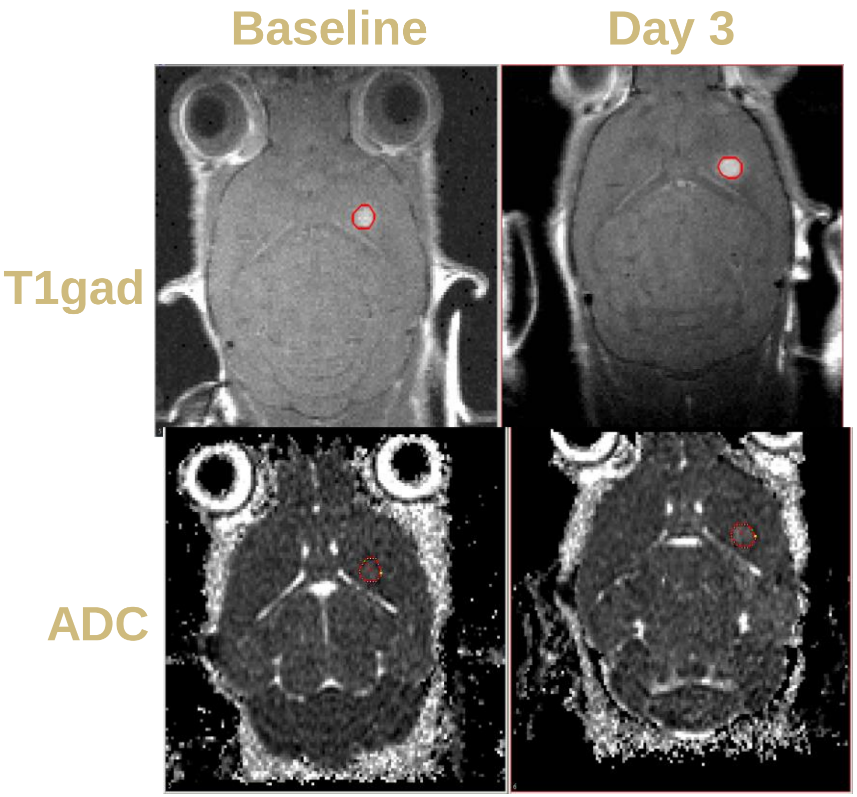
Baseline
Day 3
T1gad
ADC

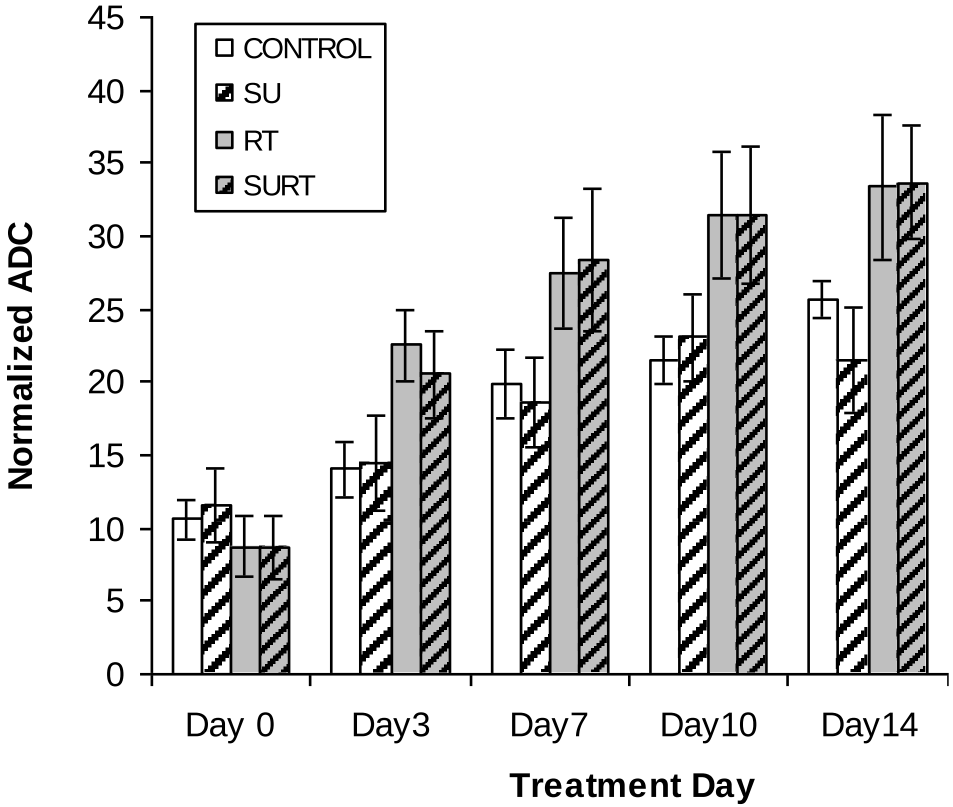

Chung et al., IJROBP, 2012

ADC Response vs Tumor Growth Rate

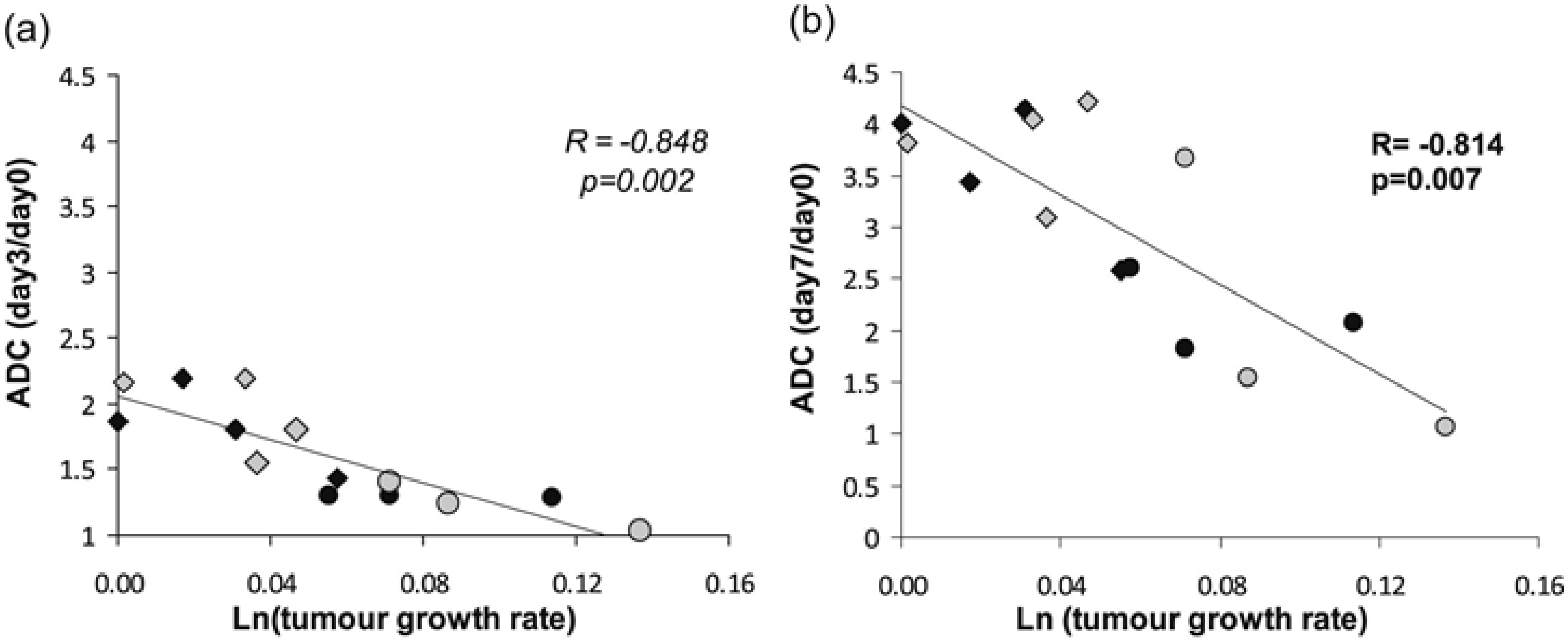

Chung et al., IJROBP, 2012

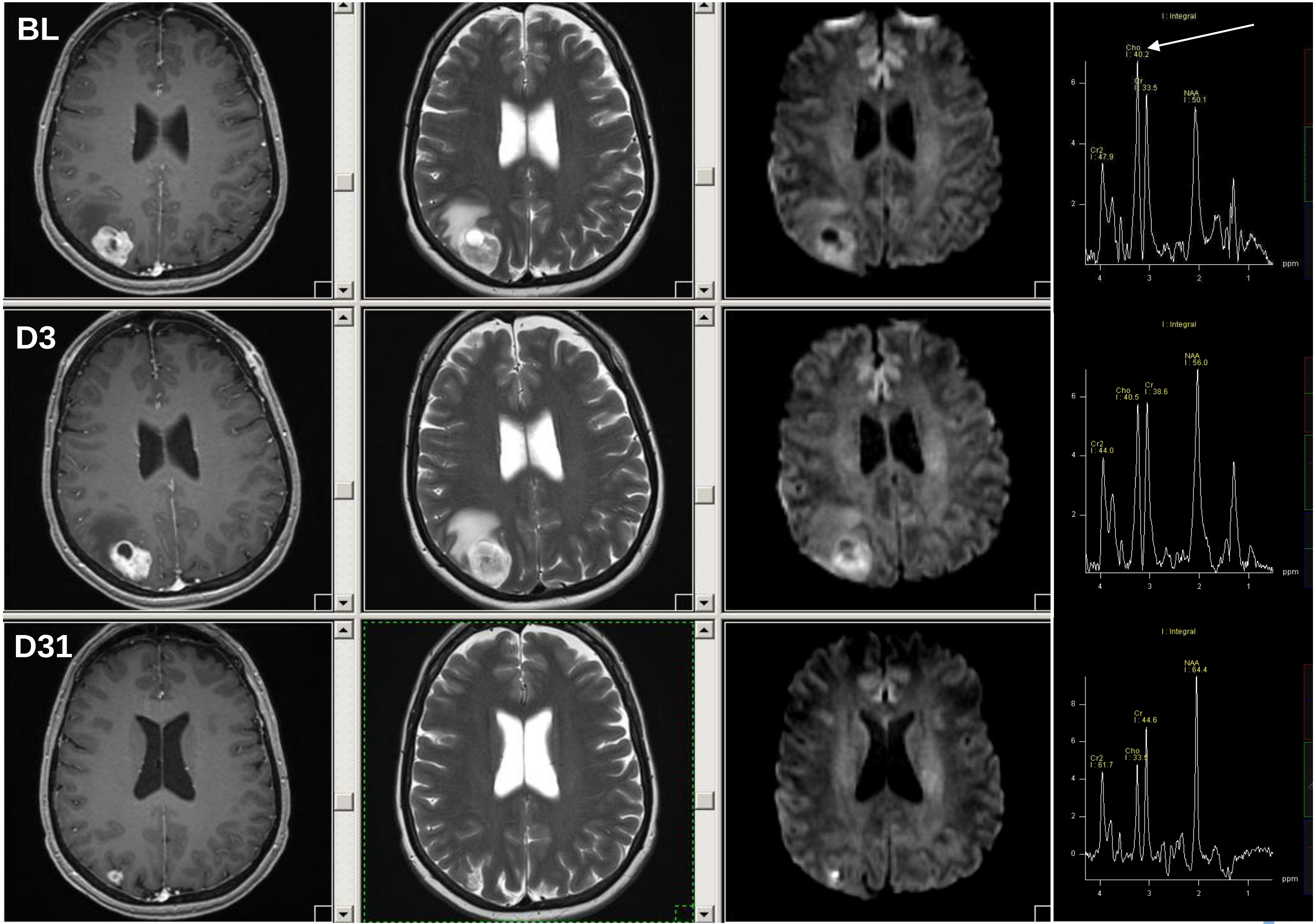
BL
D3
D31
I : Integral
Cho
I : 40.2
Cr
I : 33.5
NAA
I : 50.1
Cr2
I : 47.9
Cho
I : 40.5
Cr
I : 38.6
NAA
I : 56.0
Cr2
I : 44.0
NAA
I : 64.4
Cr
I : 44.6
Cho
I : 33.5
Cr2
I : 61.7
ppm

Menard et al., Chapter in Technical Basis of RT

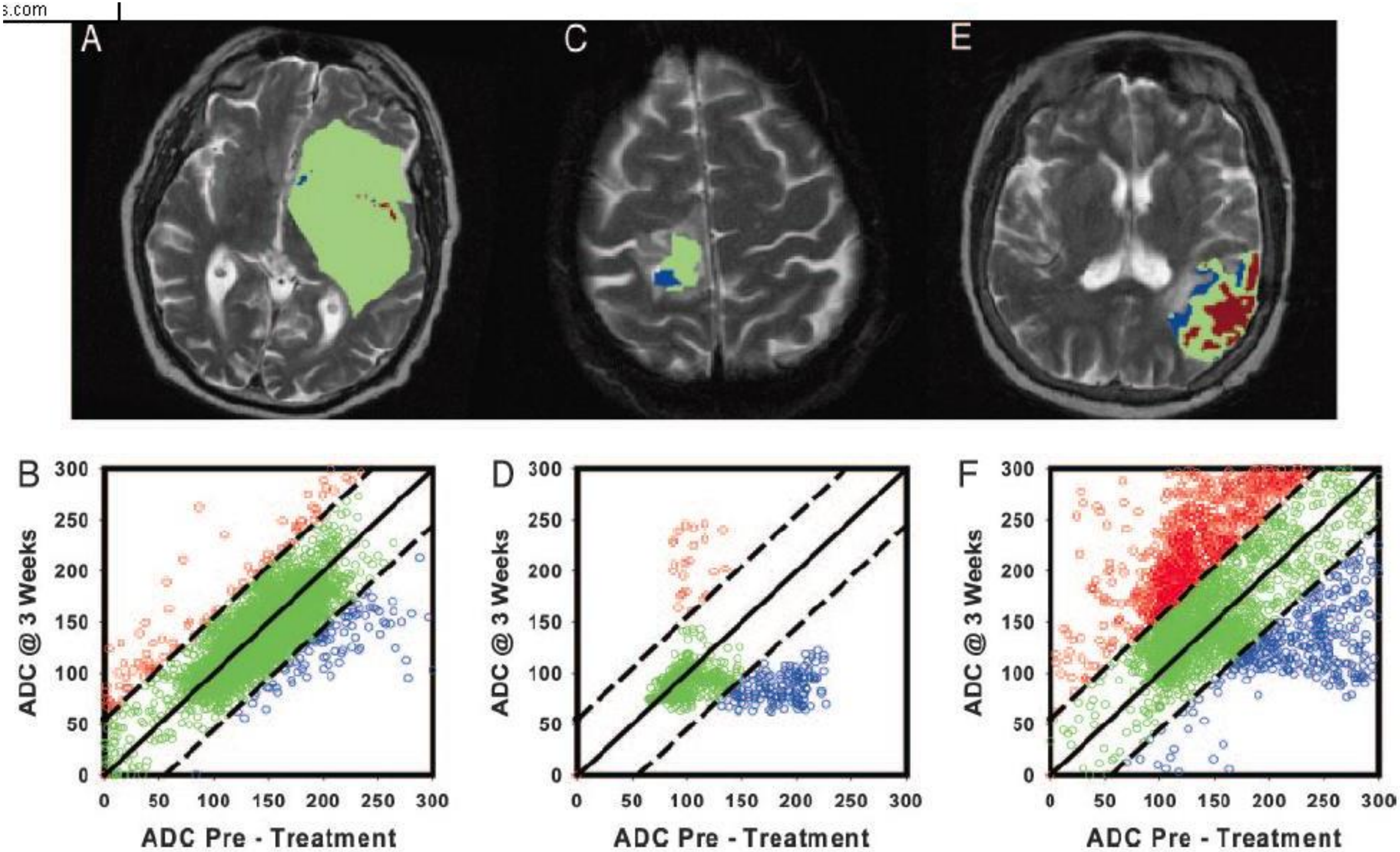
s.com
A
C
E
B
D
F
300
250
200
150
100
50
0
0
50
100
150
200
250
300
ADC @ 3 Weeks
ADC Pre - Treatment

Moffat et al.

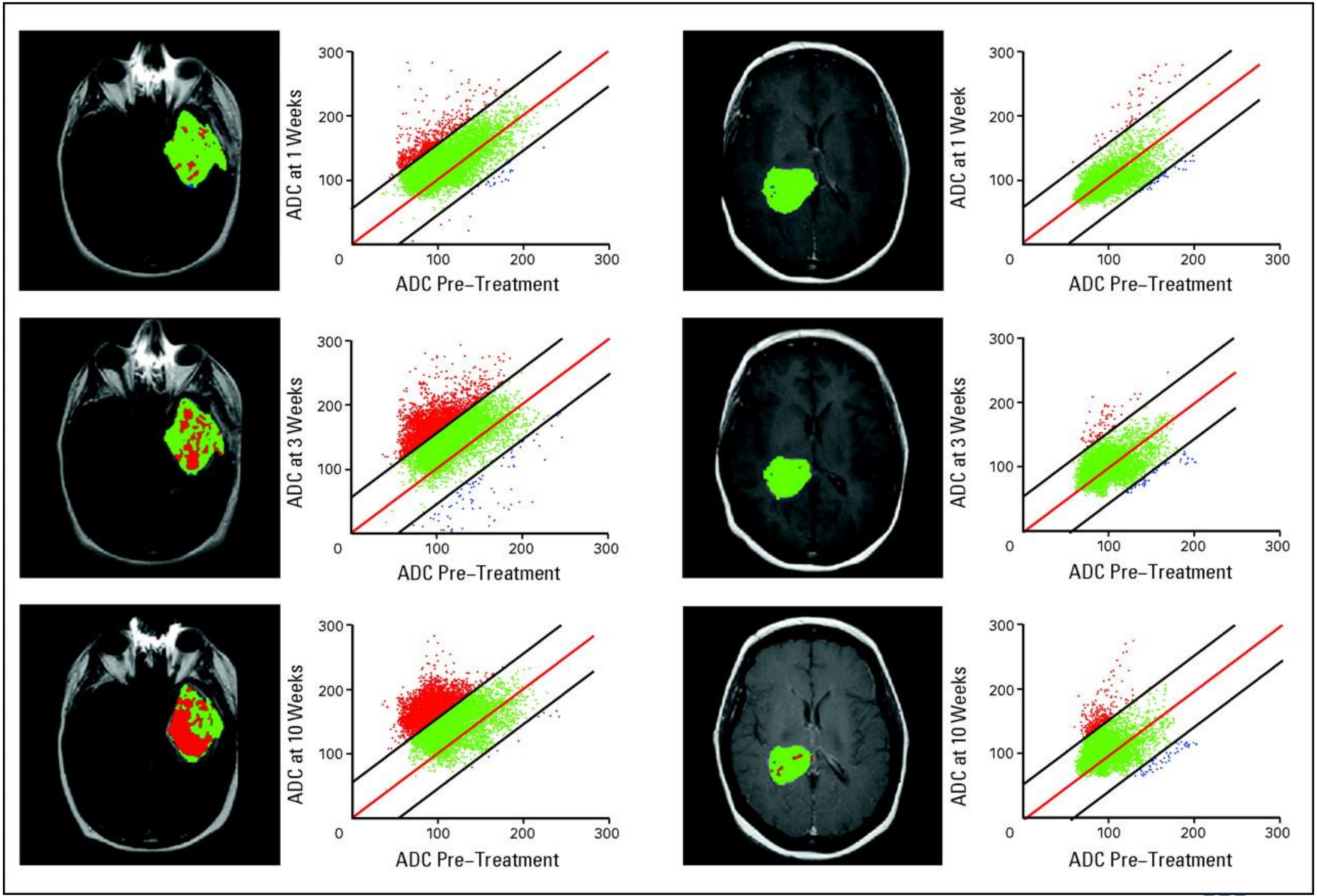
ADC at 1 Weeks
300
200
100
0
100
200
300
ADC Pre–Treatment
ADC at 1 Week
300
200
100
0
100
200
300
ADC Pre–Treatment
ADC at 3 Weeks
300
200
100
0
100
200
300
ADC Pre–Treatment
ADC at 3 Weeks
300
200
100
0
100
200
300
ADC Pre–Treatment
ADC at 10 Weeks
300
200
100
0
100
200
300
ADC Pre–Treatment
ADC at 10 Weeks
300
200
100
0
100
200
300
ADC Pre–Treatment

Diffusion Abnormality Index

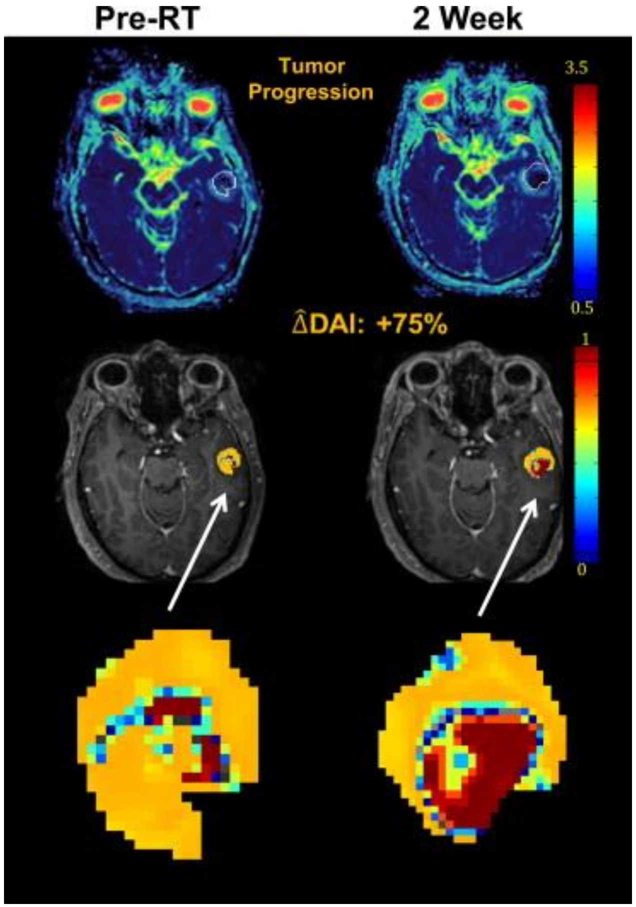
Pre-RT
2 Week
Tumor Progression
3.5
0.5
ΔDAI: +75%
1
0

Tsien et al., Sem in Rad Oncol 2014

DTI in RT

- Several studies track FA and diffusivities longitudinally post-RT in normal appearing white matter

- Early DTI changes now being related to functional consequences

DTI & radiation effects

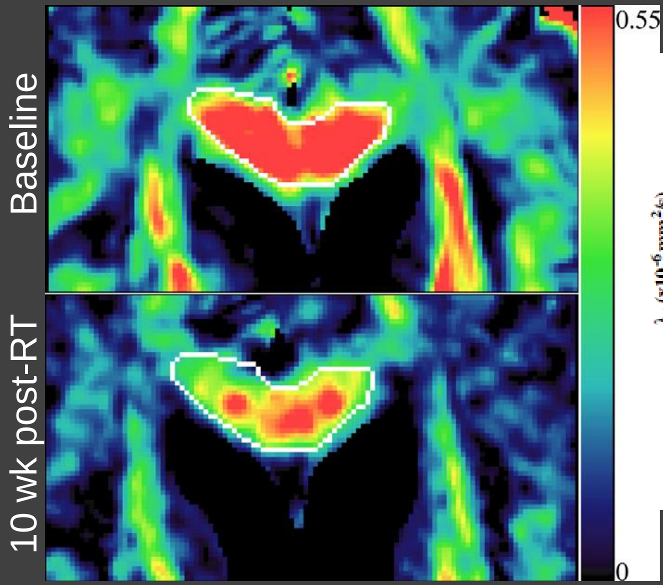

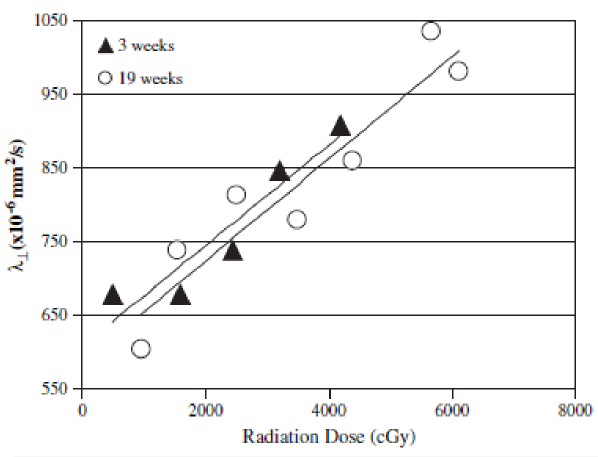

DTI & late cognitive decline

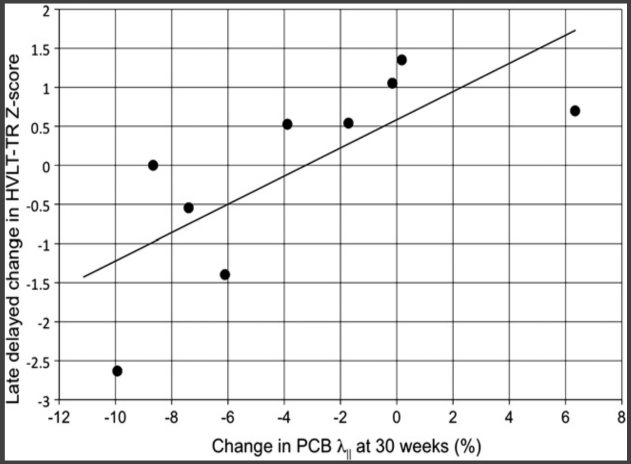

Nagesh, IJROBP, 2008; Chapman, IJROBP, 2012

Increased radial diffusion in parahippocampal cingulum white matter at end of RT predicts for decline in verbal fluency at 18 months.

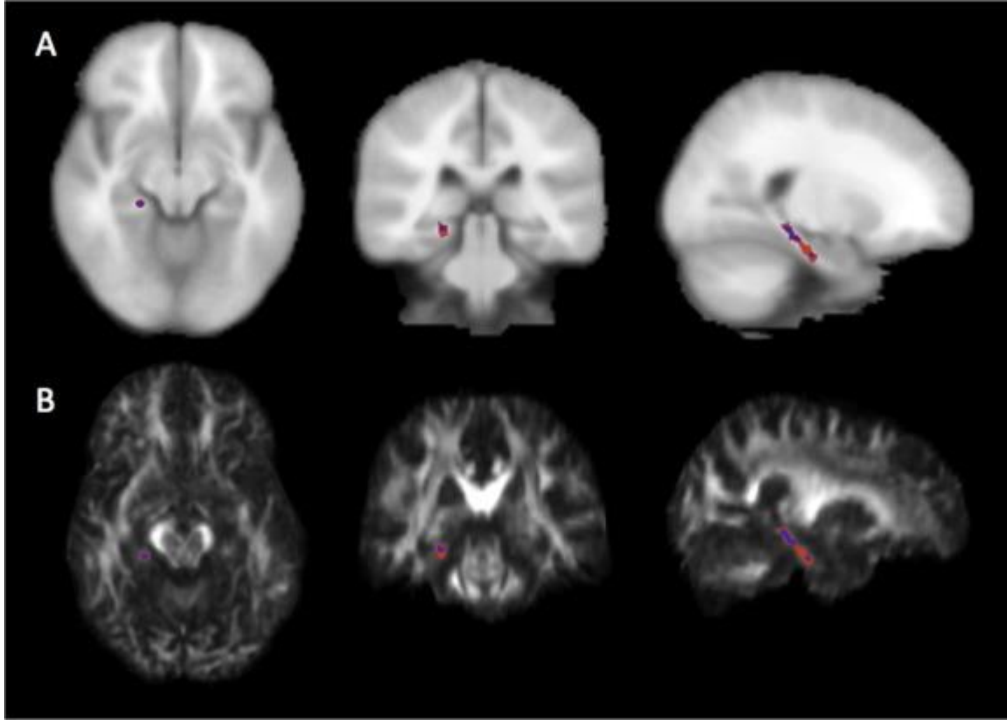

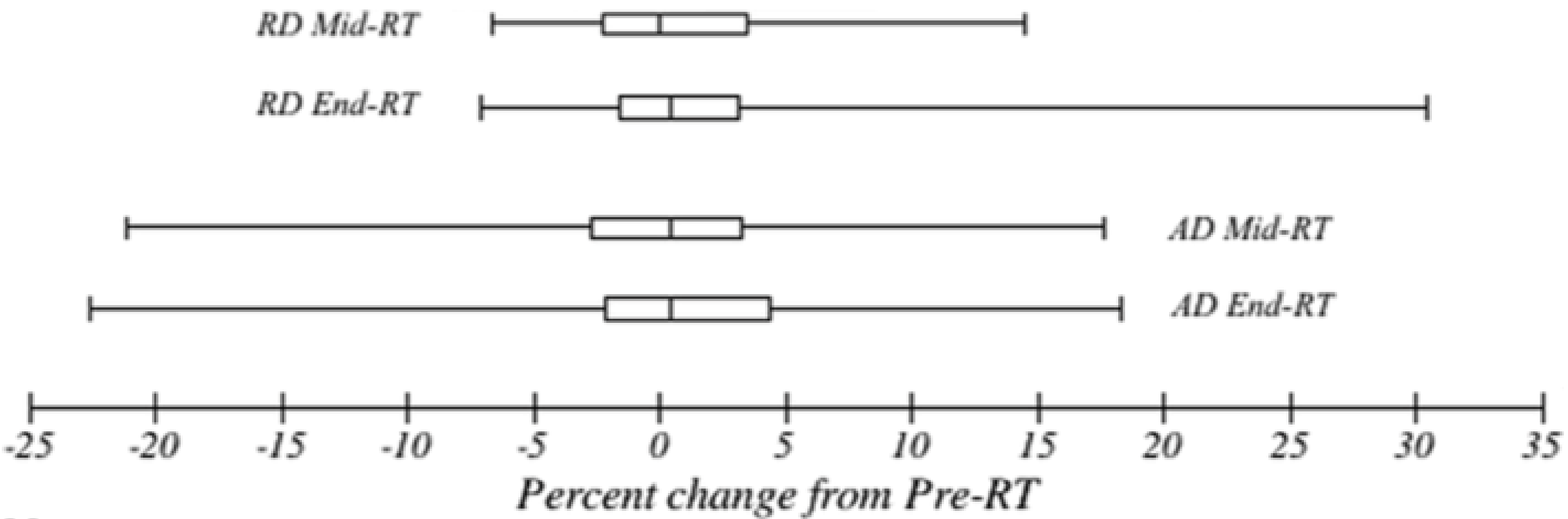

Chapman et al., Radio Oncol 2016

Parametric Response Map

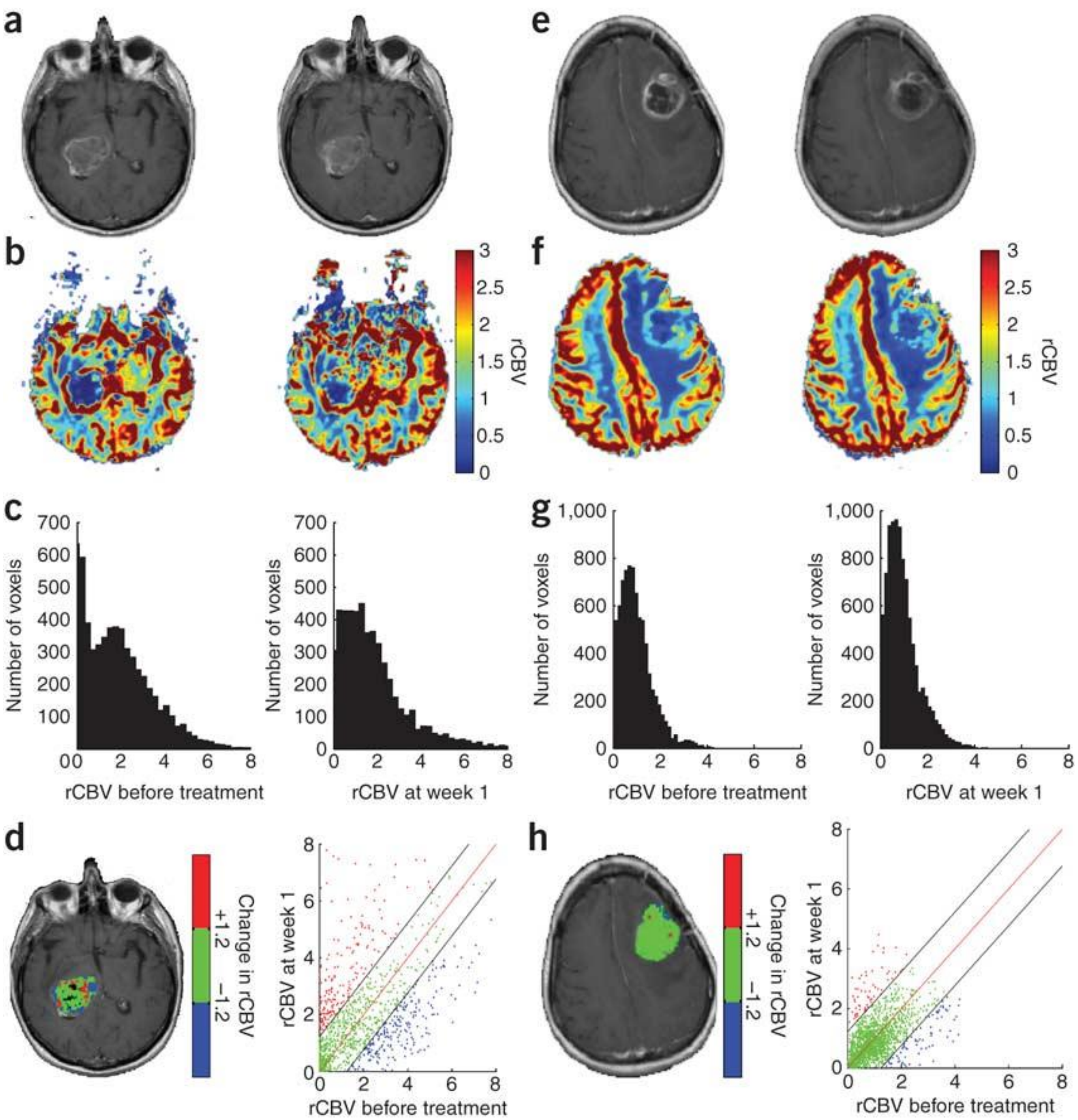
a
b
c
d
e
f
g
h
rCBV
3
2.5
2
1.5
1
0.5
0
Number of voxels
rCBV before treatment
rCBV at week 1
700
600
500
400
300
200
100
0
1,000
800
600
400
200
2
4
6
8
Change in rCBV
+1.2
−1.2

Galban et al., Nat Med, 2009

Radionecrosis - Structure

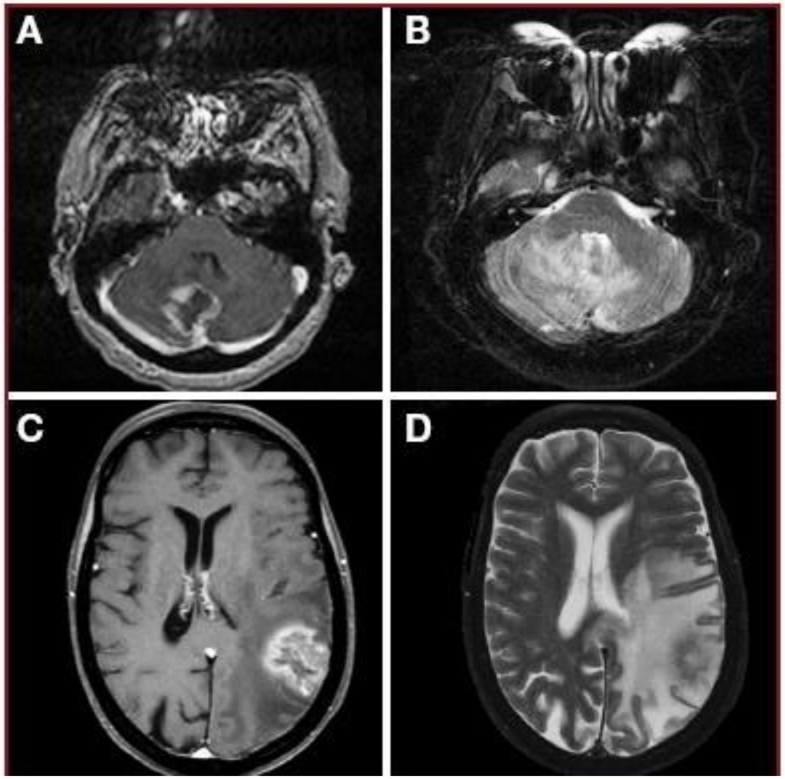

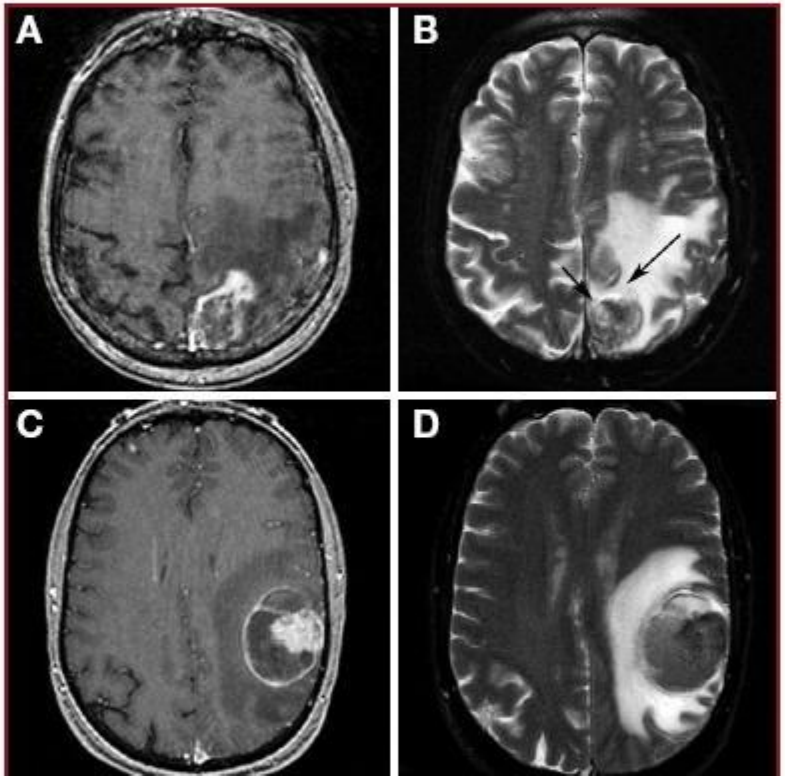

Kano et al., Neurosurg, 2010

Radionecrosis - DSC

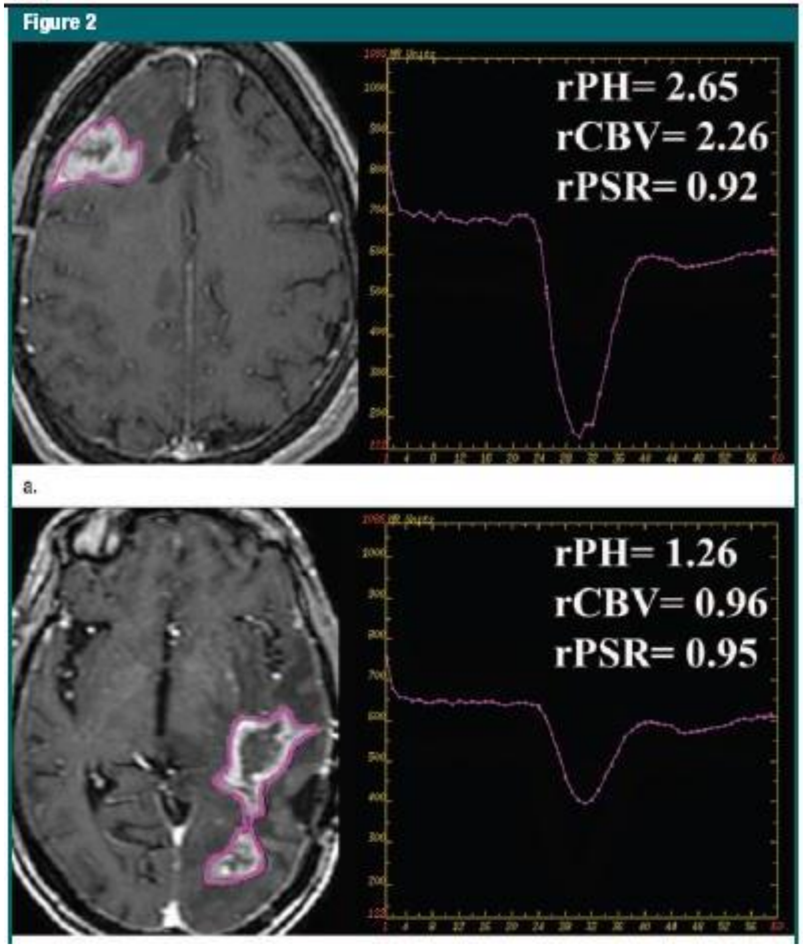
Figure 2
rPH= 2.65
rCBV= 2.26
rPSR= 0.92
a.
rPH= 1.26
rCBV= 0.96
rPSR= 0.95

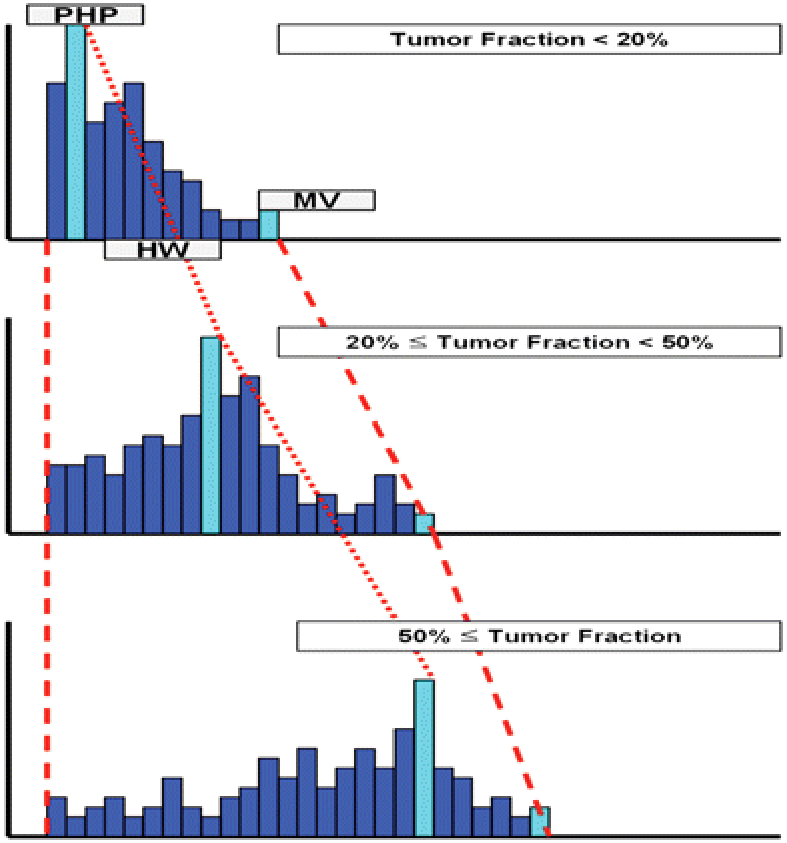

📖 Barajas et al., Radiology 253(2), 2009; Kim et al., Radiology 256(3), 2010; Alexiou et al., MRI 2014; Larsen et al., Neuroradiology 2013

Radionecrosis vs. Recurrent Tumor

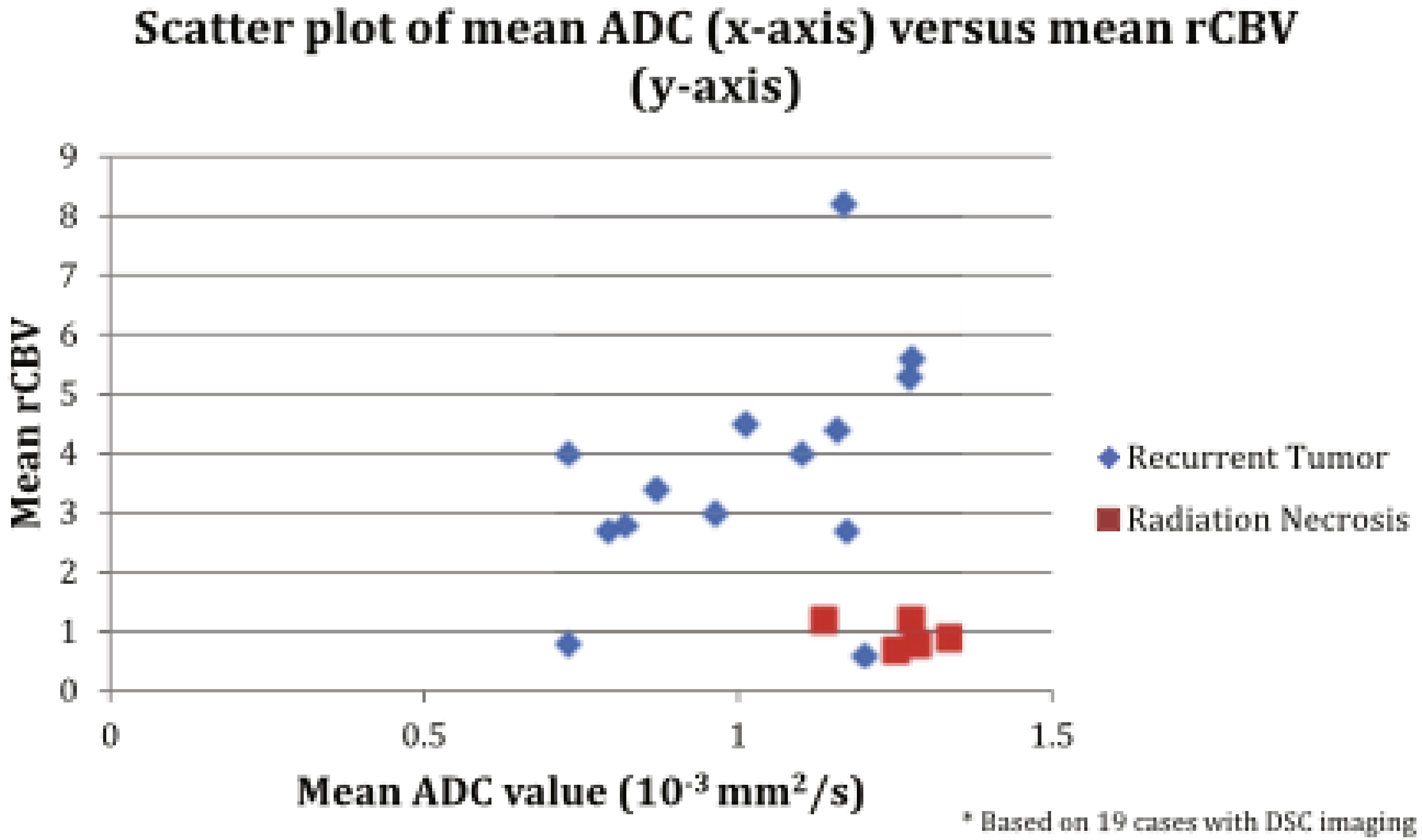

Masch et al, Acad Radio 2016

Radiation Injury: Post RT Benign Tumor

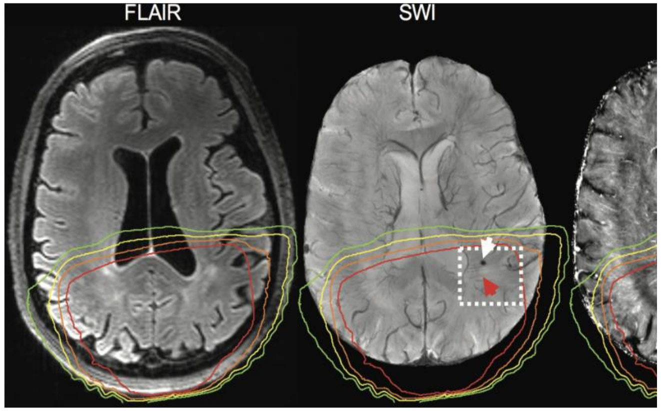

FIG 3. Patient 3 showing microbleeds on SWI and R_2^* (*white arrow*) a
(*red arrow*). *Isodose lines* are same as in Fig 1.

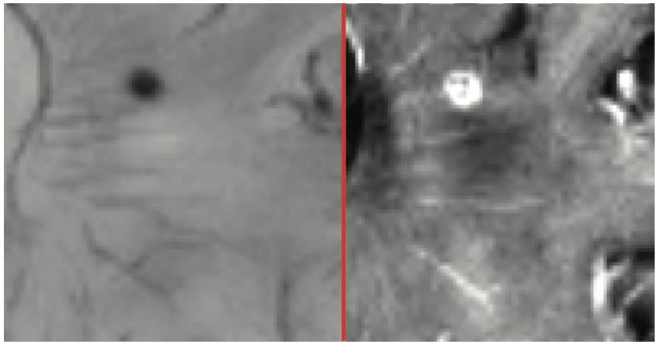

FIG 4. Zoomed-in view of Fig 3 (within the *white box* in Fig 3). Venous vasculature is seen through the suspected white matter lesion.

- Microbleeds 70% within 1 year
- White matter changes 40%
- Venocentric
- Neuroinflammatory mechanism
- Occurs in high-dose region

Beliveau et al., AJRN Sept 2017

SWI after WBRT

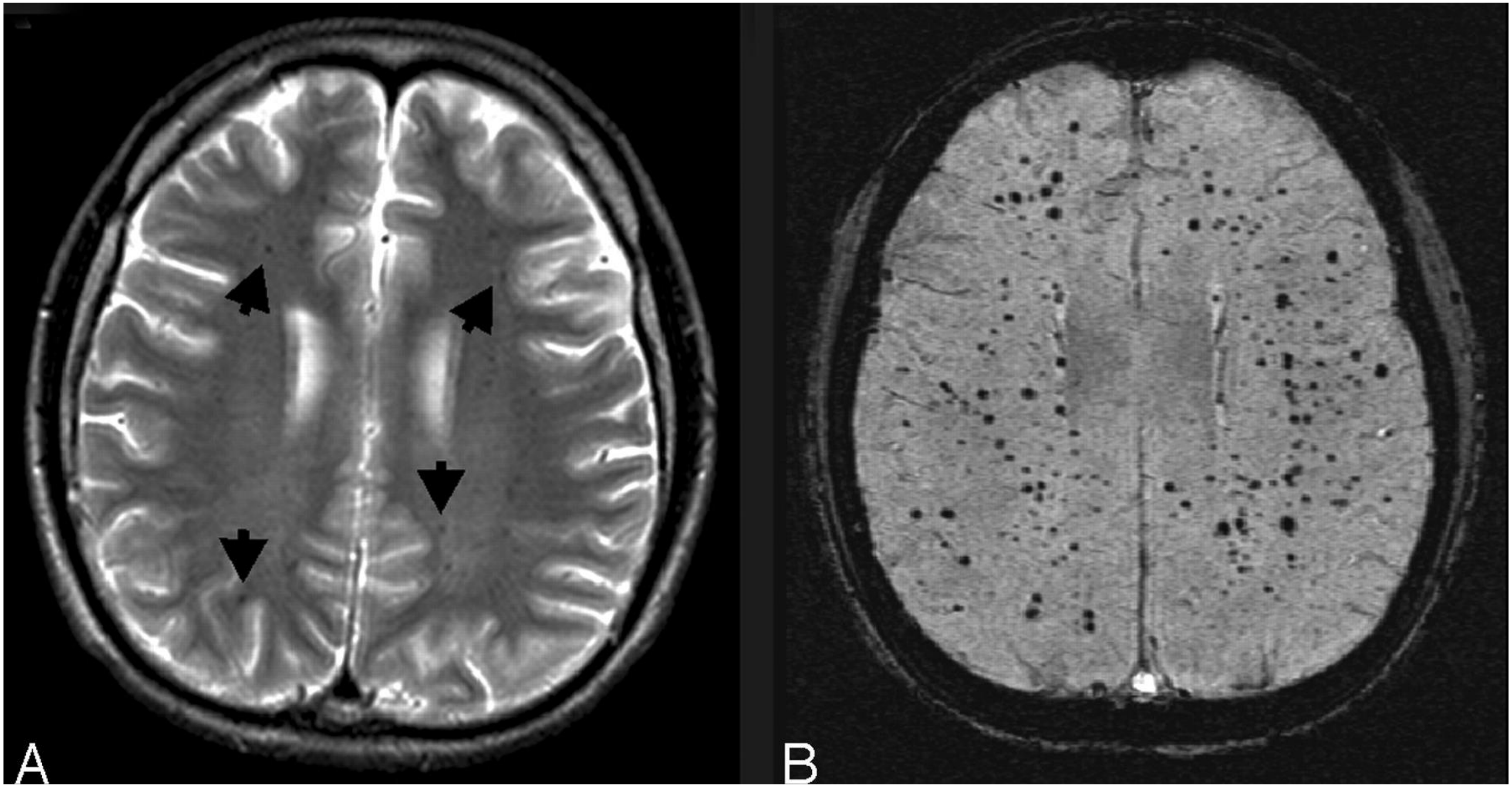

Conclusions

- MRI is central to radiotherapy planning and response assessment.
- Geometric fidelity relevant in high-precision treatments (SRS) and base of skull.
- Emphasis on image quality
- Consider expanding planning protocol (diffusion) to assist response assessment.

- Cao et al, Neuro Oncol 2017
- Langen et al, Nat Rev Neurol 2017

CHUM

Shepherd the Technology

CHUM

UMC Utrecht

EPI & Diffusion

Rob Tijssen, Dphil
Dept. of Radiotherapy
University Medical Center Utrecht

Outline

- Introduction 10 mins
  - Why Diffusion Weighted Imaging
  - What is diffusion (physiology)
- How do we measure Diffusion? 30 mins
  - Generating DWI constrast
  - Echo Planar Imaging
  - Typical DWI acquistion
- Some Body DWI examples 10 mins

Why do we measure Diffusion MRI?

Meso scale:
Enormous complexity, making tissues diverse & functionally distinct

Macro – meso gap:
~3 orders of magnitude (1000x!)

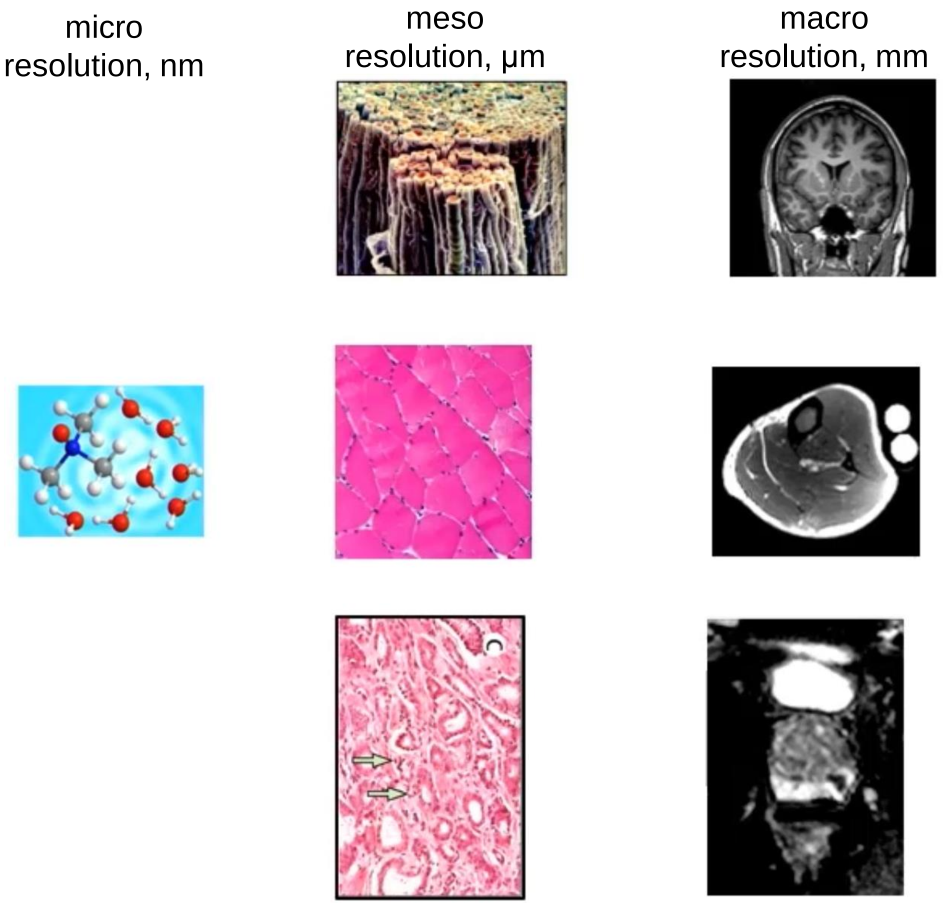
micro
resolution, nm
meso
resolution, µm
macro
resolution, mm

Els Fieremens, ISMRM weekend edu, 2017

Scaling of resolution

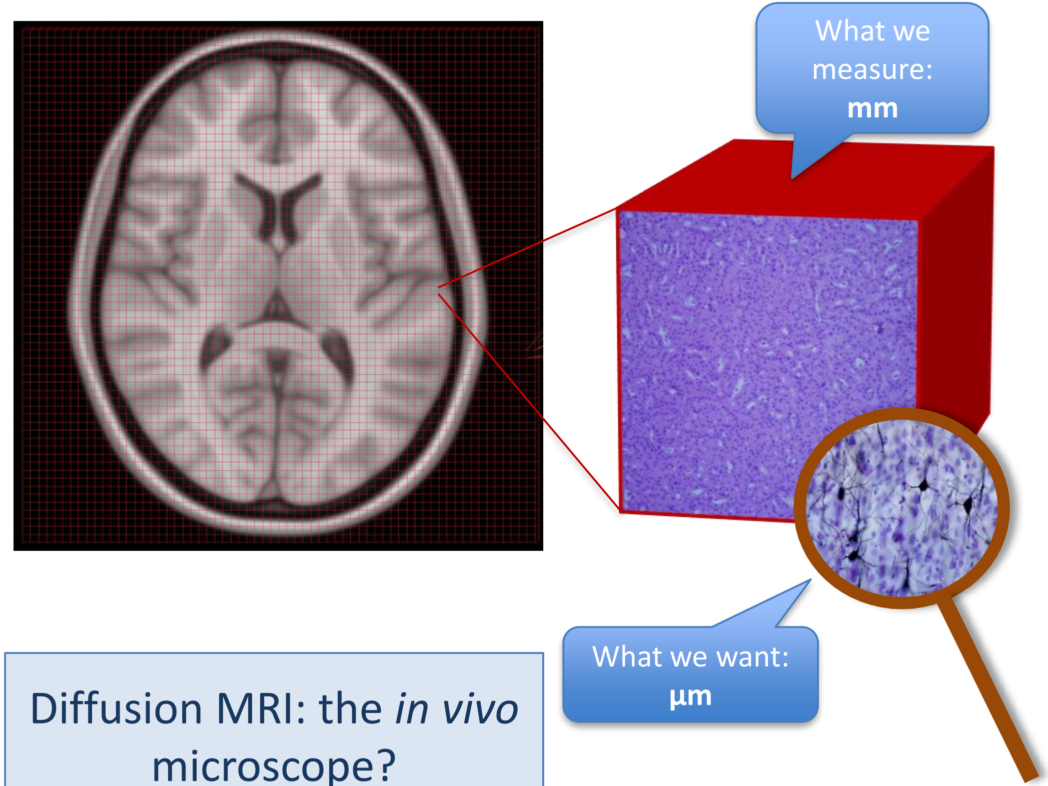

What we measure: **mm**

What we want: **µm**

Diffusion MRI: the *in vivo* microscope?

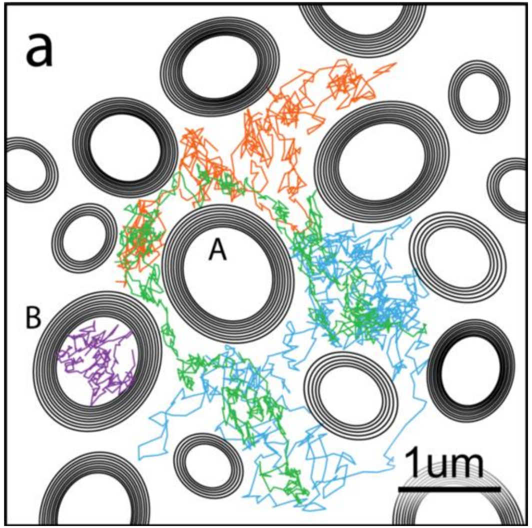

Michiel Kleinnijenhuis, PhD thesis

Diffusion probes length scales on the order of 1 – 50 µm

Els Fieremens, ISMRM weekend edu, 2017

Diffusion basics

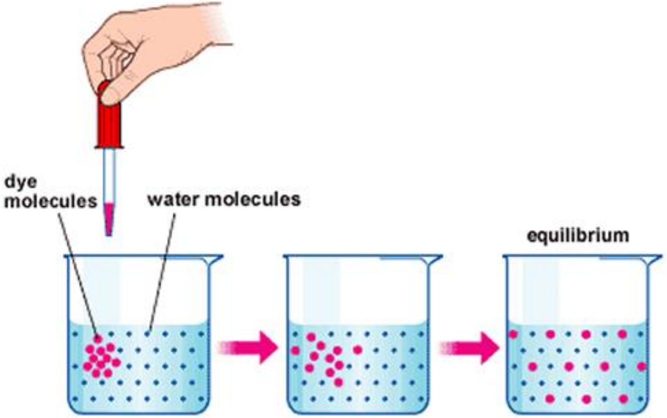
dye
molecules
water molecules
equilibrium

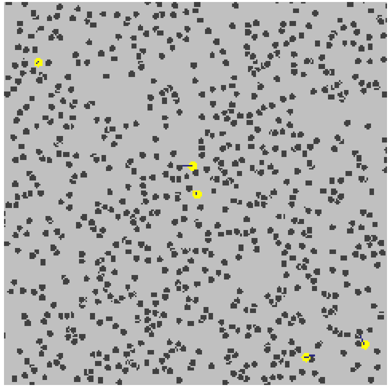

Robert
Brown
1827

Louis
Bachelier
1900

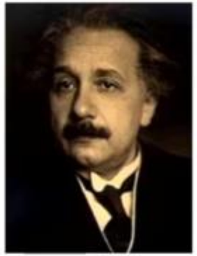

Albert
Einstein
1905

Marian
Schmoluchowski
1906

Diffusion basics

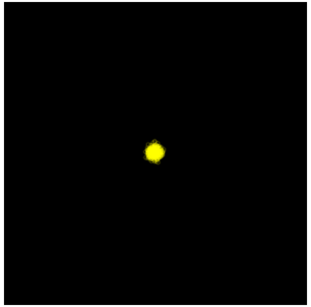

Einstein's Diffusion formula:

$$\langle (r - r_0)^2 \rangle = 2Dt$$

Brownian motion random walk: $(r - r_0)^2 = \frac{t}{\delta t}\varepsilon^2$

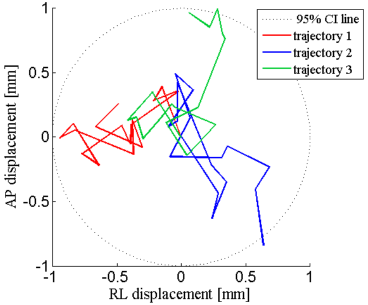

PDF of displacements

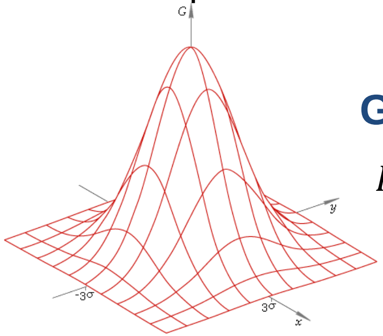

Gaussian PDF

$$P(r|r_0,t) = \frac{1}{\sqrt{4\pi Dt}} exp\left(\frac{(r - r_0)^2}{4\pi Dt}\right)$$

What do we probe with Diffusion MRI?

$$D(t) = \frac{\langle (r - r_0)^2 \rangle}{2dt}$$

Free diffusion
true Brownian motion

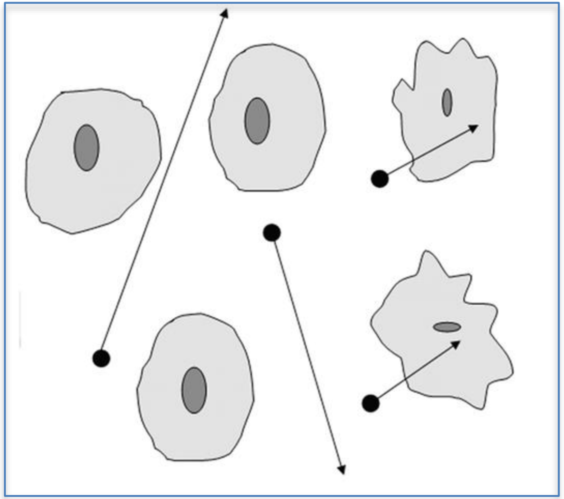

Unrestricted *in vivo* diffusion
low cellularity & defective membranes

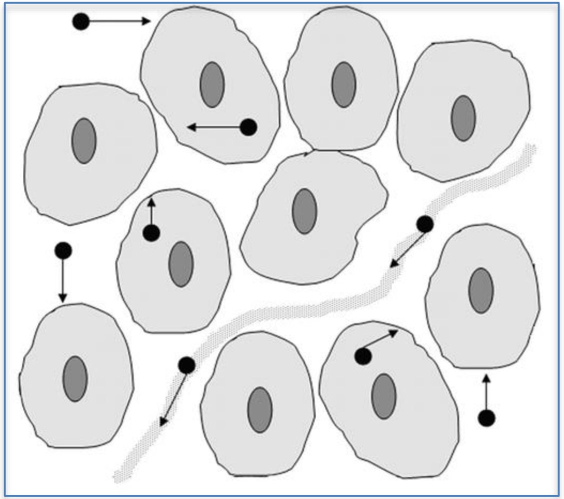

Restricted *in vivo* diffusion
high cellularity & intact membranes

$D_{\text{pure water}}$ = 3 μm²/ms @ 37°

$D_{\text{in-vivo}}$ ≈ 1 μm²/ms @ 37° (depending on restrictions)

Koh et al., AJR, 2007

Cellularity in lung tumors

Apparent Diffusion Coefficient

ADC $= 1\ [\mu m^2/ms]$

$= 1000\ [10^{-6} mm^2/s]$

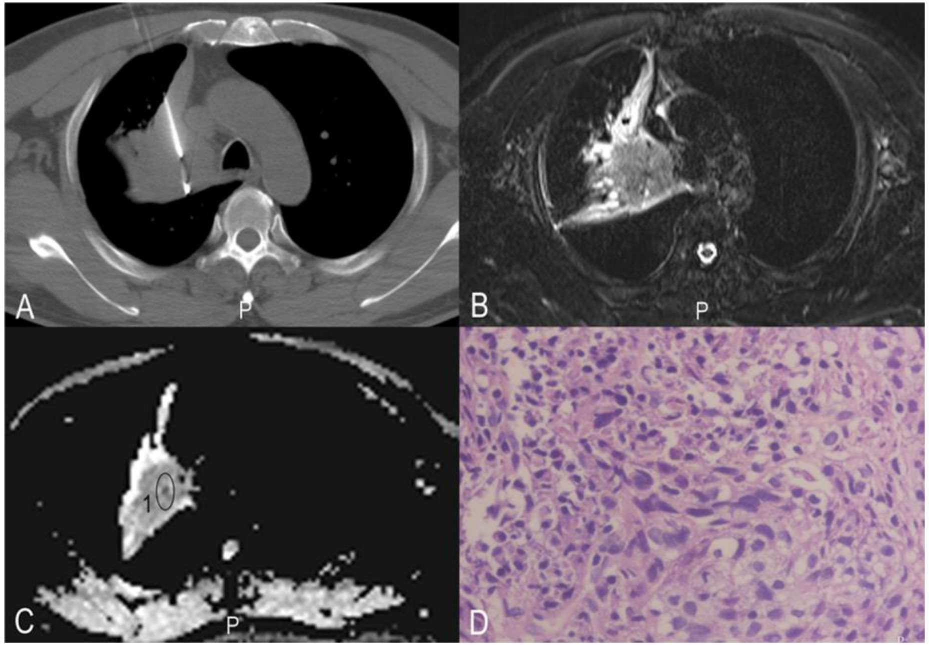

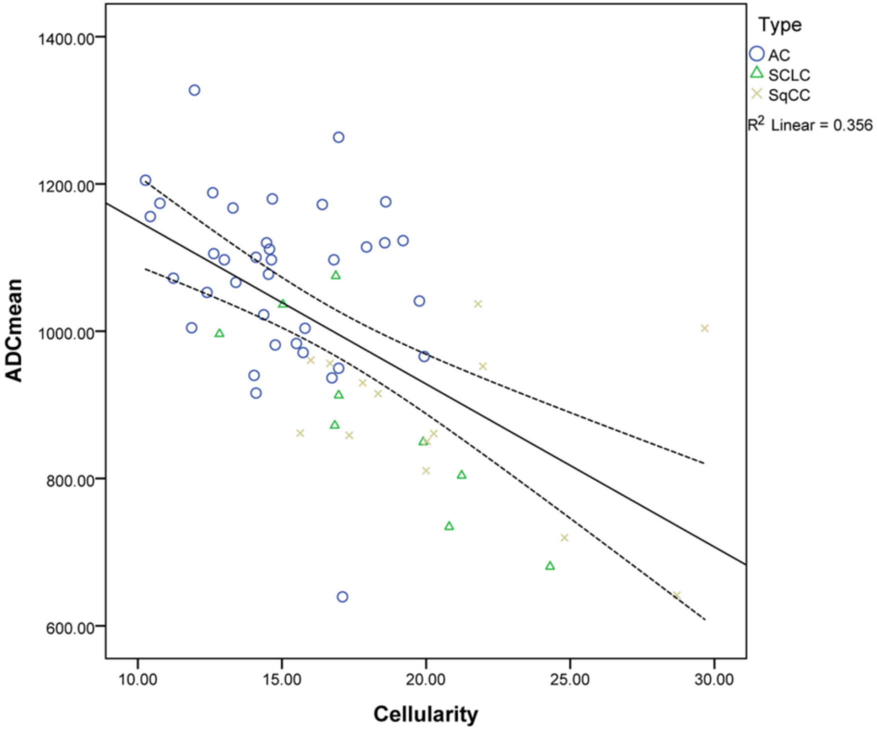

Chen et al., PLOS ONE, 2014

What is Diffusion: Summary

- The motion of water molecules *in vivo*
- In biological tissues the observed or “apparent” diffusion of water with tissues typically <<< pure water
- Interactions with intracellular elements, membranes, and macromolecules restrict water diffusion
- The DWI signal is derived from the motion of water molecules in the extracellular space, the intracellular space and the intravascular space

Le Bihan et al., Radiology, 1988
Koh et al., AJR, 2007

How do we measure DWI?

Quick MR physics refresher

How to create Diffusion Weighting?

Echo Planar Imaging

A typical DWI acquisition

How do we measure DWI?

Quick MR physics refresher

How to create Diffusion Weighting?

Echo Planar Imaging

A typical DWI acquisition

A simple MRI pulse sequence

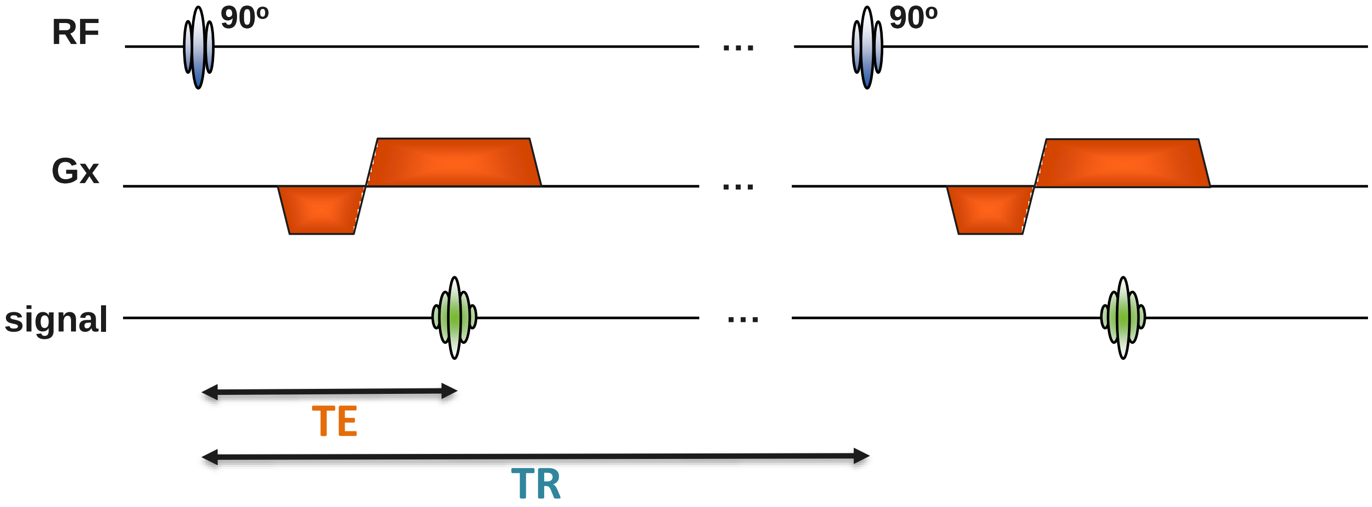
RF
90º
…
90º
Gx
…
signal
…
TE
TR

TE = echo time

Determines how much T2 decay before signal is acquired

TR = repetition time

Determines how much T1 relaxation occurs before next RF pulse

MRI Pulse Sequence = Sheet Music

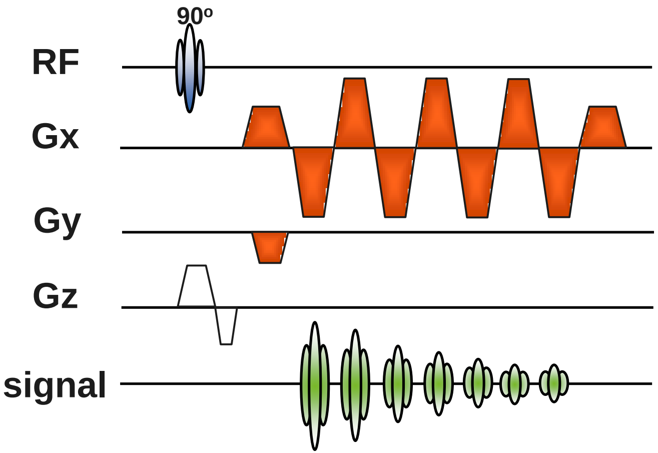
90°
RF
Gx
Gy
Gz
signal

EPI 🔊

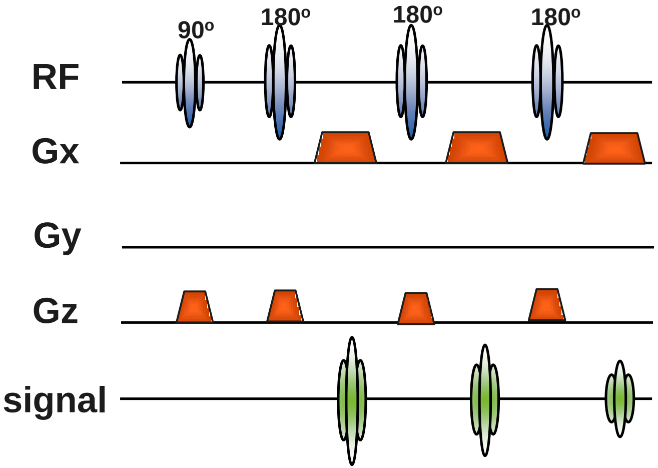
90°
180°
180°
180°
RF
Gx
Gy
Gz
signal

TSE 🔊

Sebastian Bach sequence 🔊

Sound files: Ma et al., MRM 2016;75:2303–2314.

MR Signal

$$S = M_0 \cdot (1 - e^{-TR/T1}) \cdot (e^{-TE/T2})$$

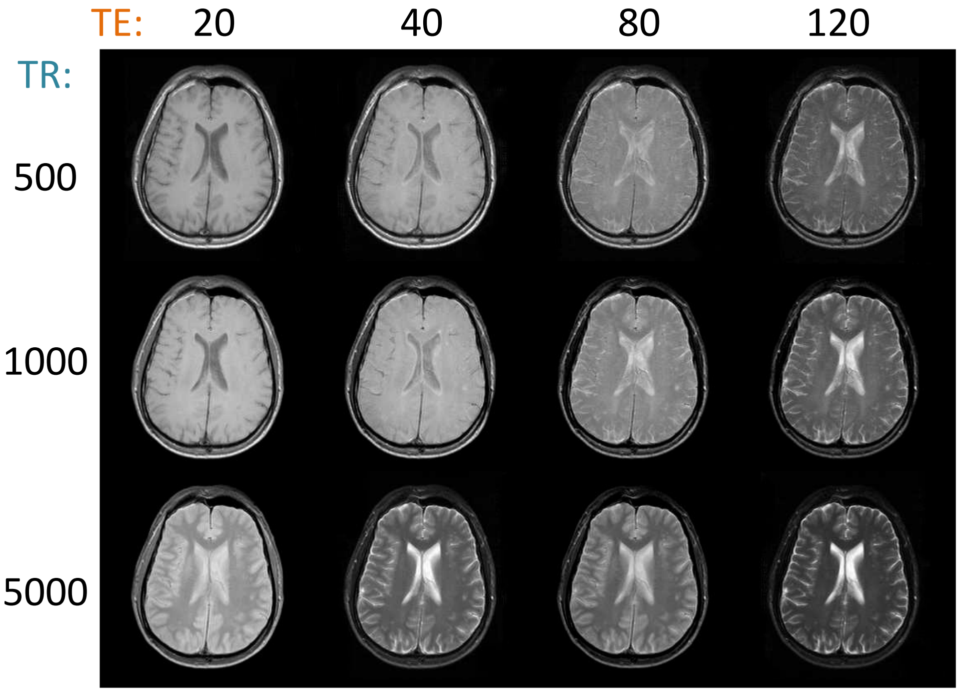
TE:
20
40
80
120
TR:
500
1000
5000

Gradient Echo vs. Spin Echo

GRE

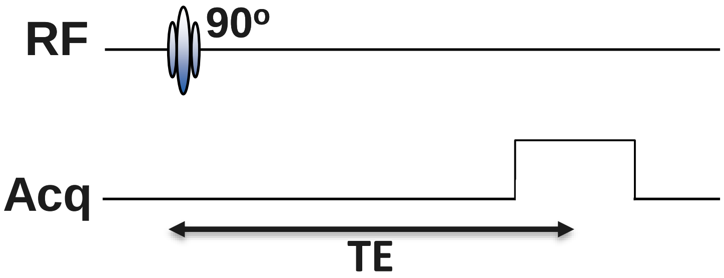
RF
90º
Acq
TE

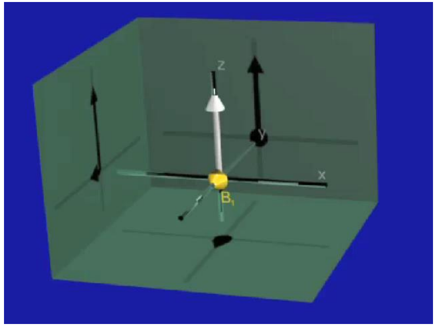

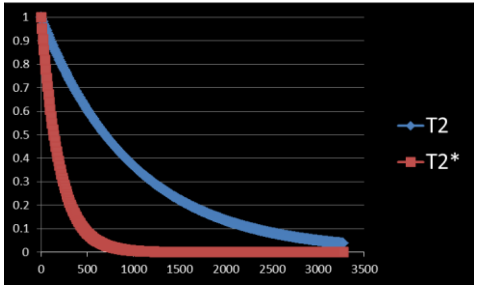

SE

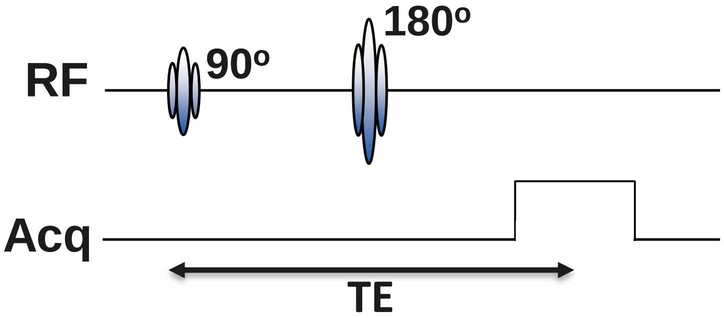
RF
90º
180º
Acq
TE

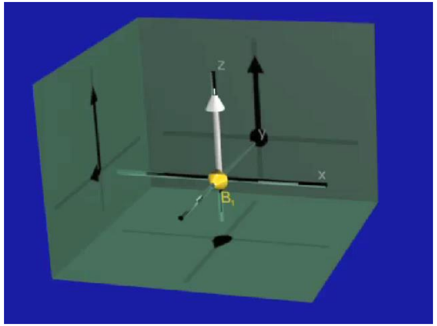

Spin Echo Diffusion-weighted imaging

Stejskal & Tanner 1965

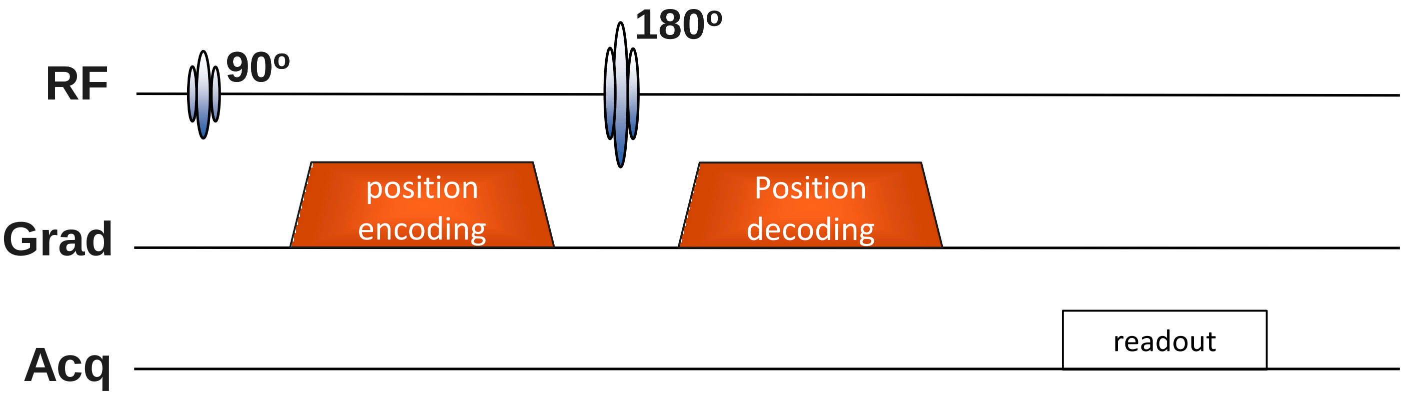

RF
90°
180°
Grad
position encoding
Position decoding
Acq
readout

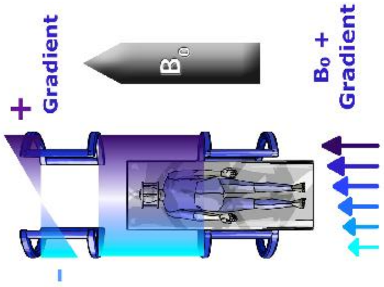

Gradient
+
B_0
B_0 + Gradient
-

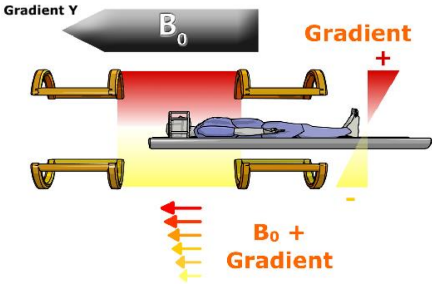

Gradient Y
B_0
Gradient
+
-
B_0 + Gradient

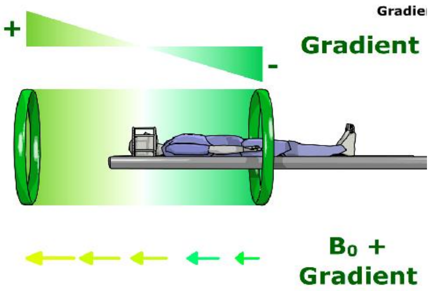

+
-
Gradie
Gradient
B_0 + Gradient

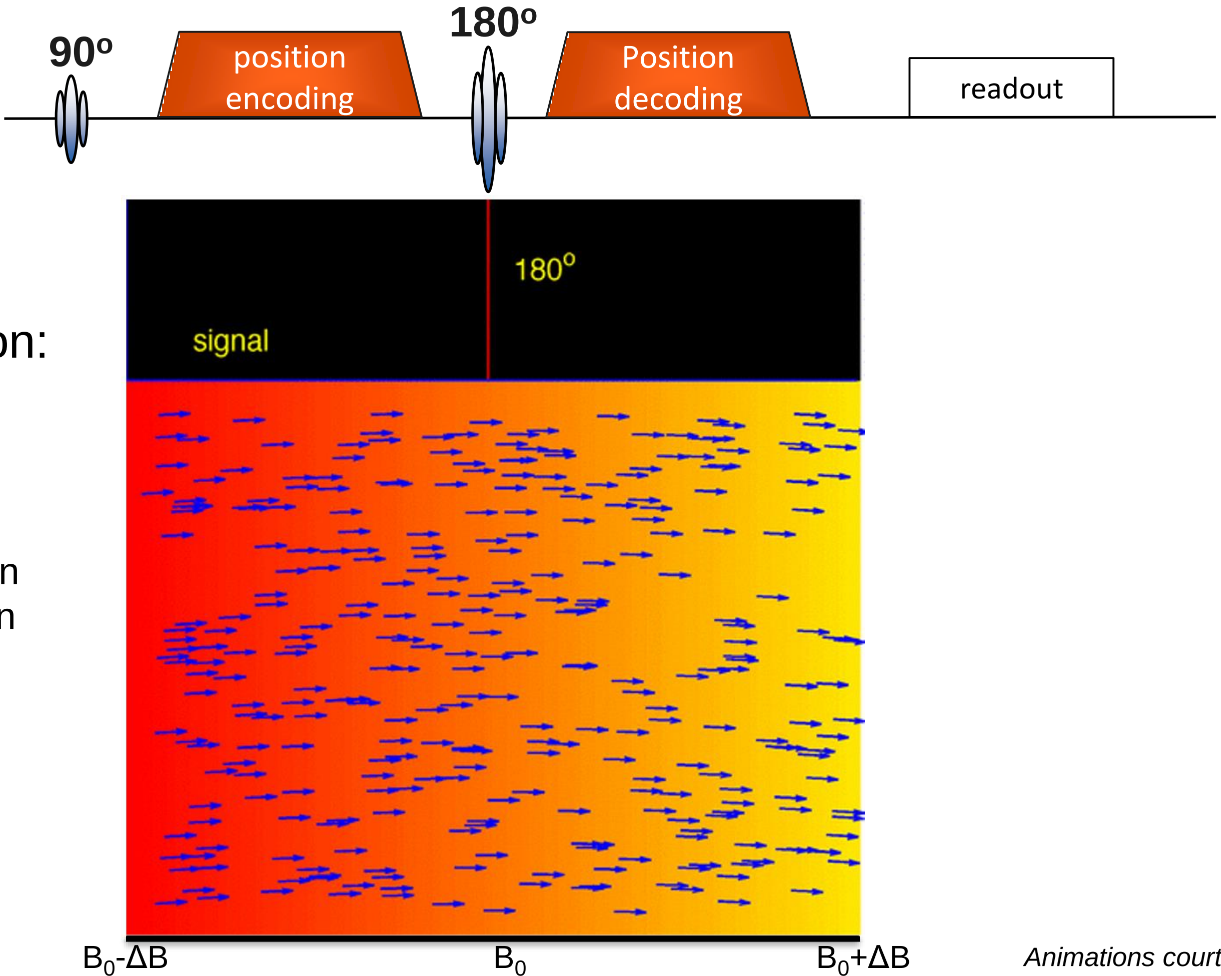
90º
position encoding
180º
Position decoding
readout
180º
signal
B0-ΔB
B0
B0+ΔB

Without diffusion:

all spins have fixed position

1. All spins accrue phase depending on their (static) position

2. 180° pulse flips magnetization

3. All spins realign

Animations courtesy of Karla Miller, Oxford

Without diffusion:

all spins have fixed position

1. All spins accrue phase depending on their (static) position

2. 180° pulse flips magnetization

3. All spins realign

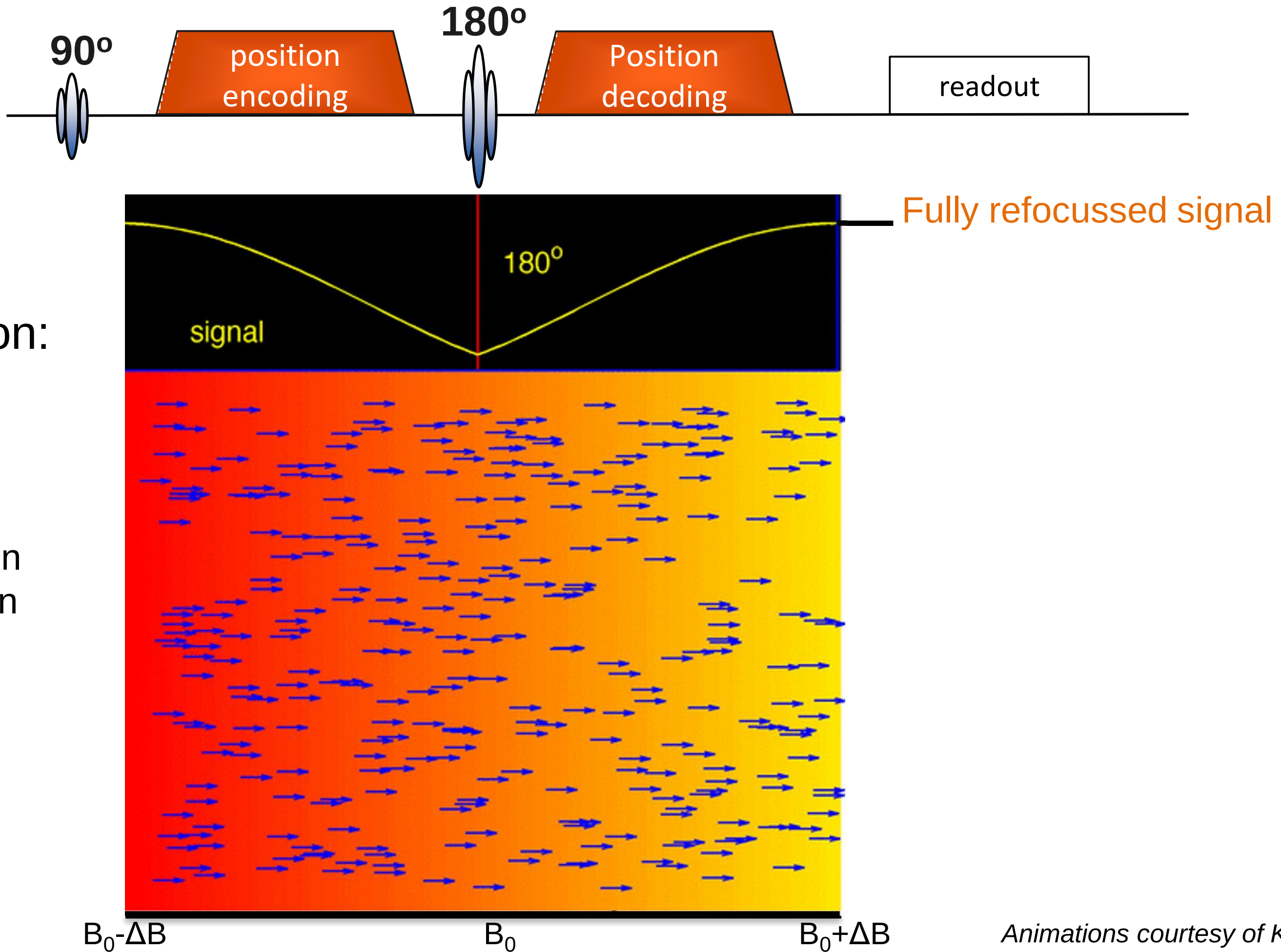

90º
position encoding
180º
Position decoding
readout
Fully refocussed signal
180º
signal
B_0-ΔB
B_0
B_0+ΔB

Animations courtesy of Karla Miller, Oxford

With diffusion:

spins undergo continuous motion

1. All spins accrue phase (with varying speed) according to changing position

2. 180° pulse flips magnetization

3. No complete realignment

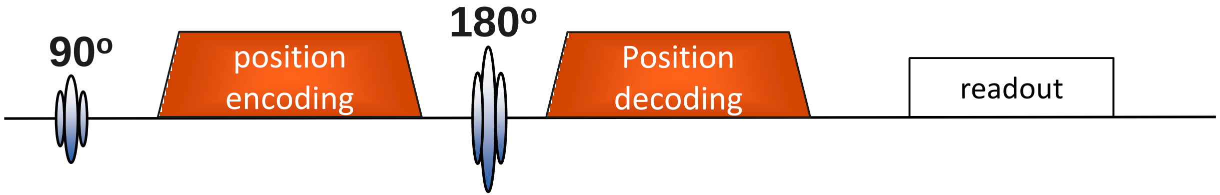
90°
position encoding
180°
Position decoding
readout

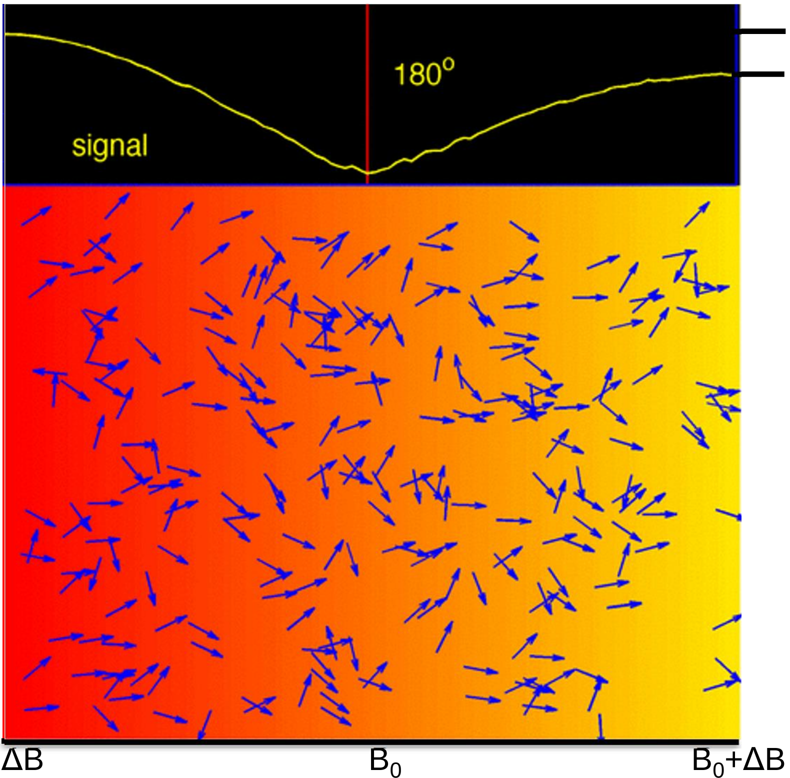
signal
180°
B_0-ΔB
B_0
B_0+ΔB

Fully refocussed signal

Diffusion-weighted signal

In the presence of diffusion, the resulting signal will be lower.

More diffusion

=

Less signal

Animations courtesy of Karla Miller, Oxford

Diffusion parameters (the options you have)

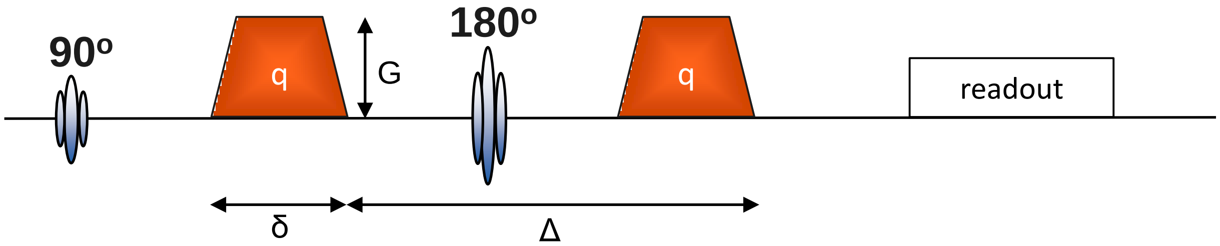
90°
q
G
180°
q
readout
δ
Δ

By adjusting the *time spacing* and *strength* of the gradients we can change the amount of Diffusion Weighting
(i.e., “making the sequence more or less sensitive to molecular motion”)

The amount DW is expressed as the b-value: $b \propto q^2 * \Delta$

$$b = (\gamma G \delta)^2 \cdot \left(\Delta - {}^{\delta}/_{3}\right)$$

low b-value = bright image

high b-value = dark image

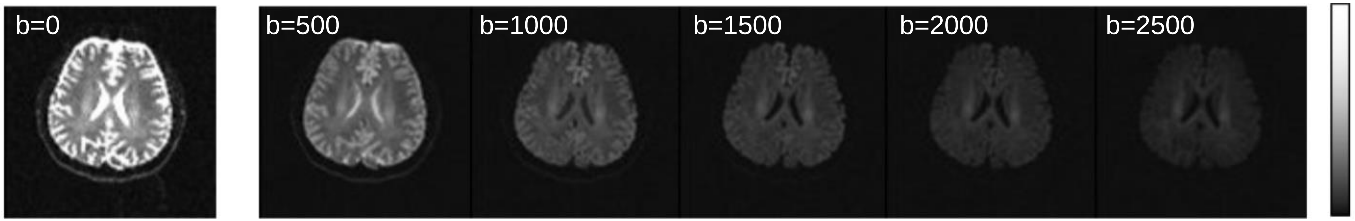
b=0
b=500
b=1000
b=1500
b=2000
b=2500

MR physics refresher: contrast

$$S = \underline{M_0 \cdot (1 - e^{-TR/T1}) \cdot (e^{-TE/T2})} \cdot e^{-bD}$$

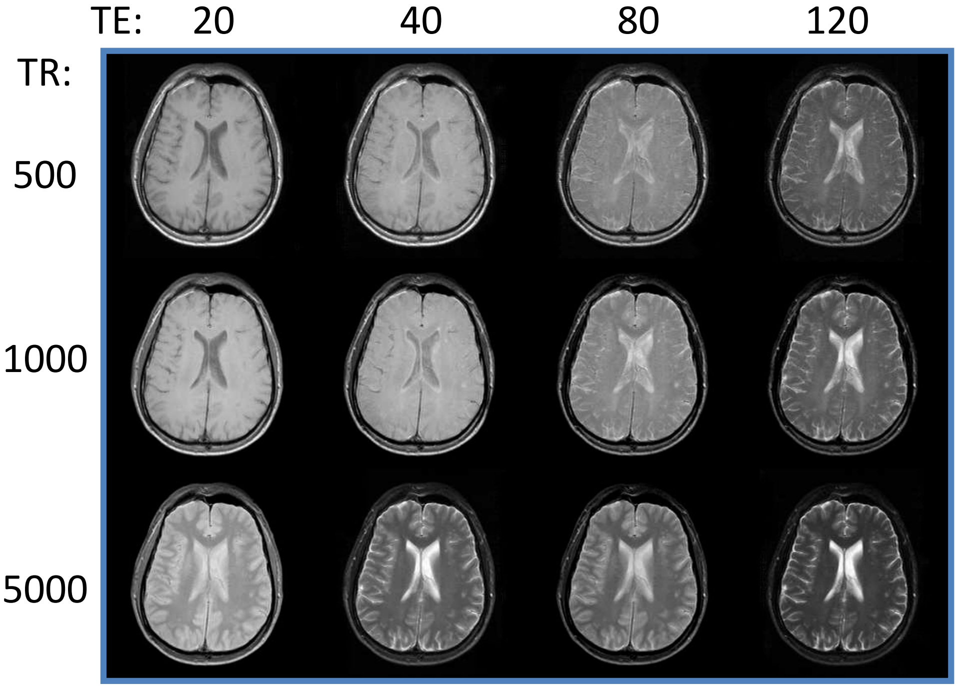
TE:
20
40
80
120
TR:
500
1000
5000

b = diffusion gradient

D = diffusion coefficient

MR physics refresher: contrast

$$S = \underline{M_0 \cdot (1 - e^{-TR/T1}) \cdot (e^{-TE/T2})} \cdot e^{-bD}$$

$$S = \underline{S_0} \cdot e^{-bD}$$

b = diffusion gradient

D = diffusion coefficient

S_0 (T2w)

$S_0 * e^{-bD}$

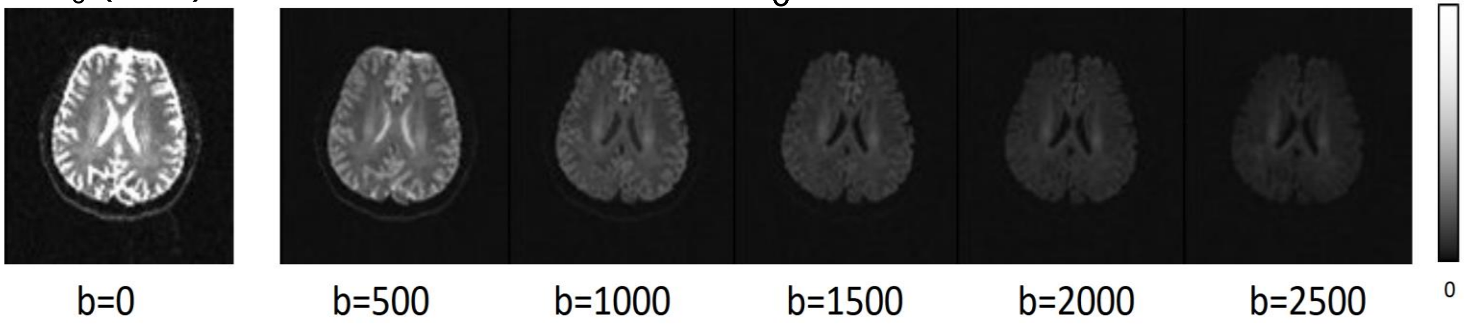
b=0
b=500
b=1000
b=1500
b=2000
b=2500
0

Diffusion weighted contrast

Gaussian distribution of diffusion

If DW signal comes from free diffusion, gradient magnetic pulse would decay DW signal mono-exponentially with b-value

Diffusivity (-bD) decreases linearly across b-value

Diffusion coefficient is constant

$S = S_0 \cdot e^{-bD}$ → $-bD = \ln(S/S_0)$ → $D = \ln(S/S_0) / -b$

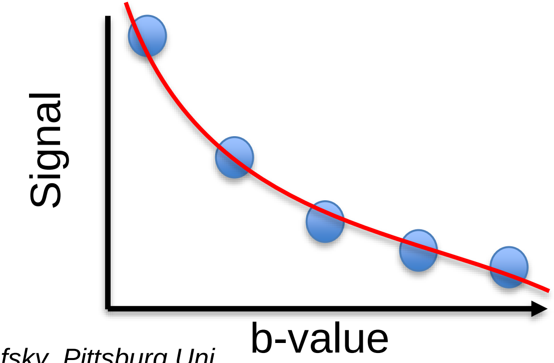

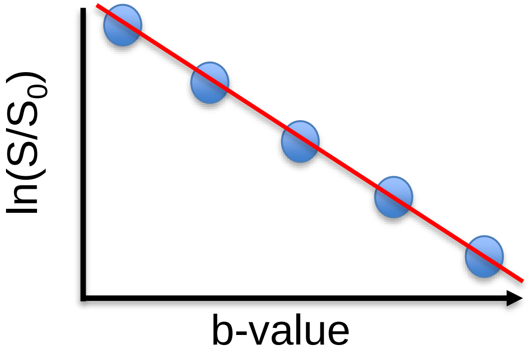

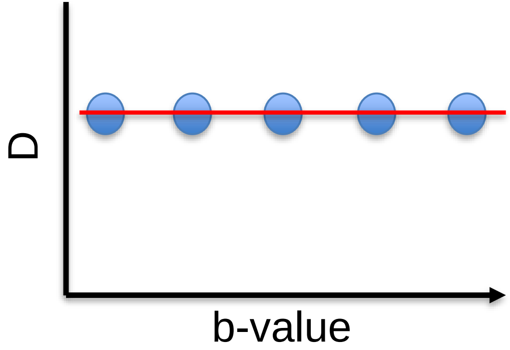

Litcofsky, Pittsburg Uni

Effect of b-values on DWI: free diffusion

Water phantom
(NiS04.6H20/NaCL)

Mean DWI (50 directions)

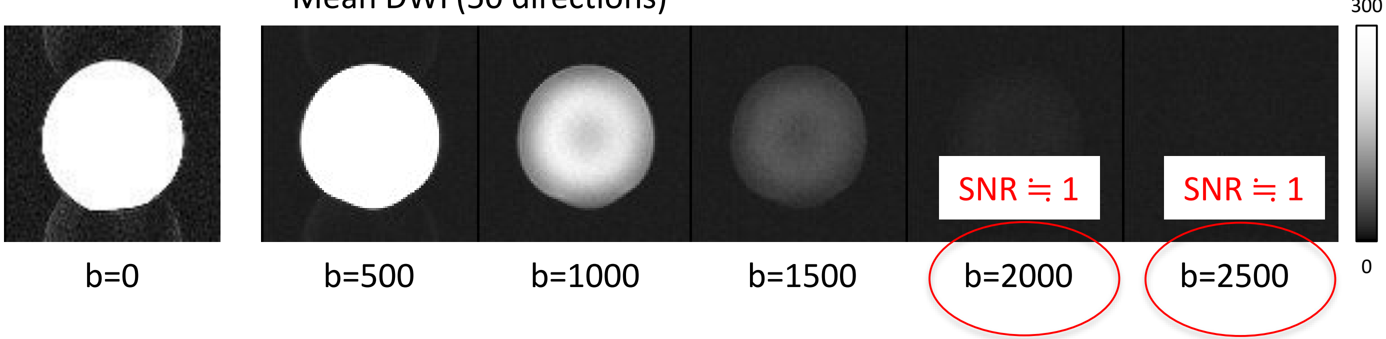
SNR ≒ 1
SNR ≒ 1
b=0
b=500
b=1000
b=1500
b=2000
b=2500
300
0

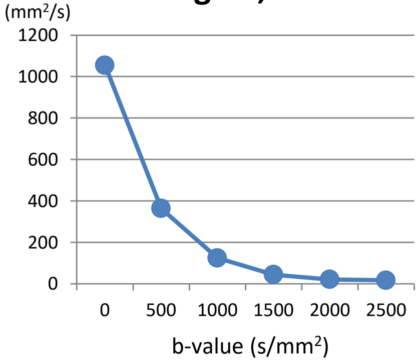

Signal, DWI

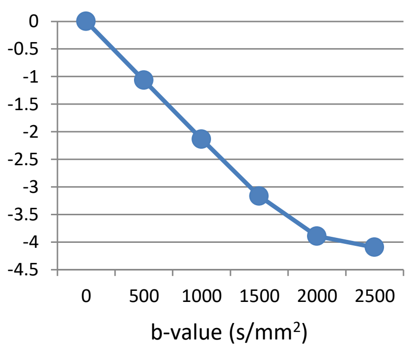

ln S/S0

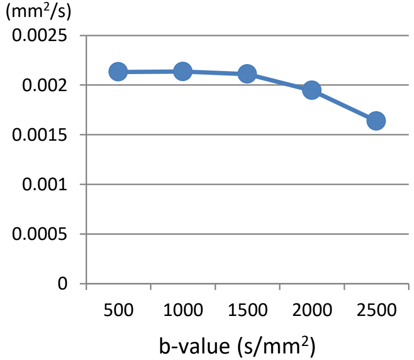

ADC

Litcofsky & Tazoe, Pittsburg University

Effect of b-values on DWI: restricted diffusion at high b-vals

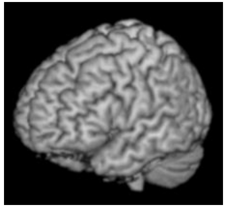

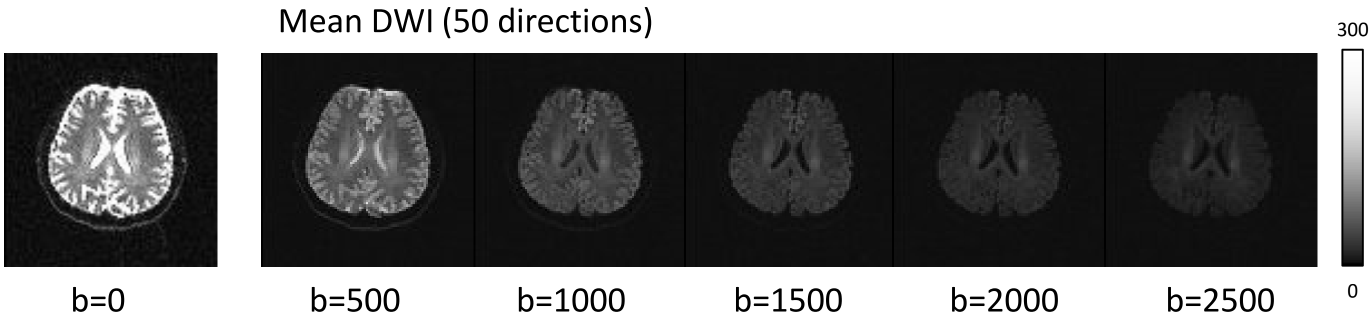
Mean DWI (50 directions)
300
0
b=0
b=500
b=1000
b=1500
b=2000
b=2500

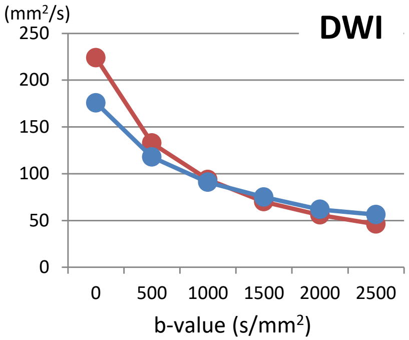

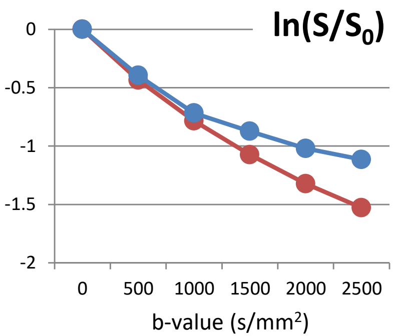

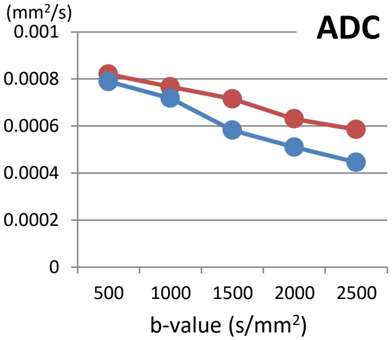

WM ▬ GM ▬

Litcofsky & Tazoe, Pittsburg University

The effect of b-values on DWI:

perfusion at low b-vals

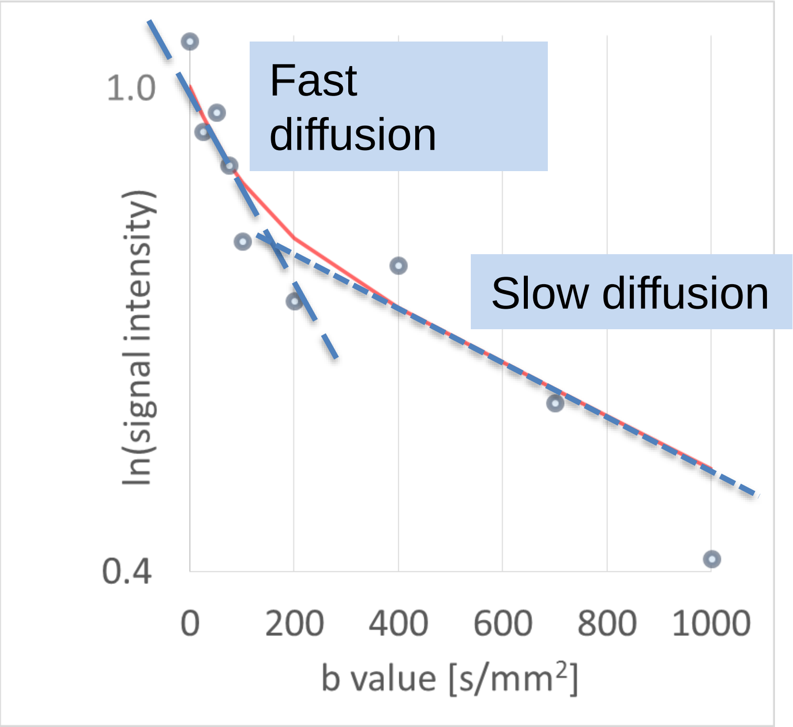

Fast diffusing component;
@ b-values < ~150 s/mm2
'Perfusion'

Slow diffusing component;
@ b-values > ~150 s/mm2
'Diffusion'

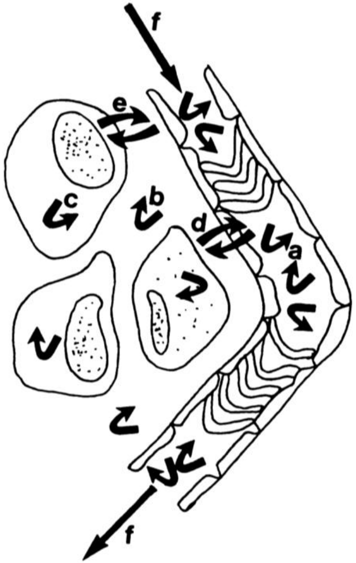

Figure 4. Model of biologic tissue. A tissue can be described by a volume fraction *f* of water flowing (*f*) and diffusing (*a*) in capillaries. This fraction involves only perfused capillaries, which are a part of total capillaries, depending on the current physiologic or pathologic situations. The rest of the voxel water, occupying a volume fraction 1 − *f*, is involved in diffusion only. This volume fraction corresponds to extracellular (*b*) and intracellular (*c*) spaces. There are exchanges between those two compartments (*e*). In a simple approach, exchanges between water inside capillaries and outside capillaries (*d*) during the measurement time (100 msec) are neglected. Another assumption is that the diffusion coefficient in sectors *a*, *b*, and *c* is nearly the same.

Le Bihan et al., Radiology, 1988

The effect of b-values on DWI:

perfusion at low b-vals

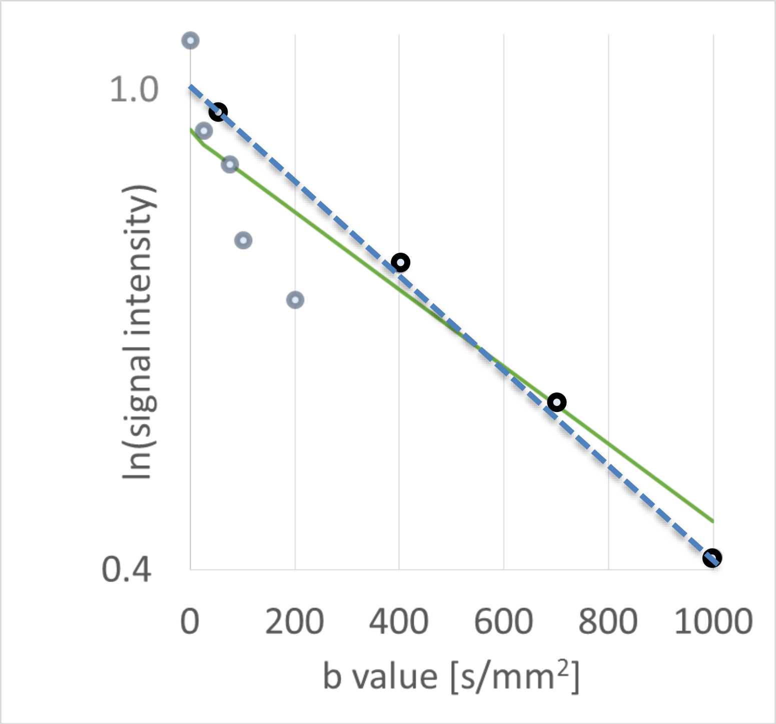

Fast diffusing component;
@ b-values < ~150 s/mm2
'Perfusion'

Slow diffusing component;
@ b-values > ~150 s/mm2
'Diffusion'

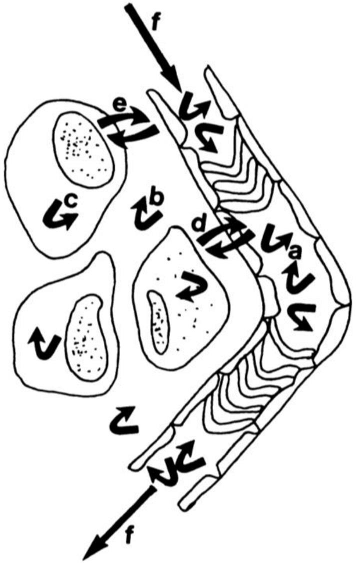

Figure 4. Model of biologic tissue. A tissue can be described by a volume fraction *f* of water flowing (*f*) and diffusing (*a*) in capillaries. This fraction involves only perfused capillaries, which are a part of total capillaries, depending on the current physiologic or pathologic situations. The rest of the voxel water, occupying a volume fraction 1 − *f*, is involved in diffusion only. This volume fraction corresponds to extracellular (*b*) and intracellular (*c*) spaces. There are exchanges between those two compartments (*e*). In a simple approach, exchanges between water inside capillaries and outside capillaries (*d*) during the measurement time (100 msec) are neglected. Another assumption is that the diffusion coefficient in sectors *a*, *b*, and *c* is nearly the same.

Le Bihan et al., Radiology, 1988

The effect of b-values on DWI:

perfusion at low b-vals

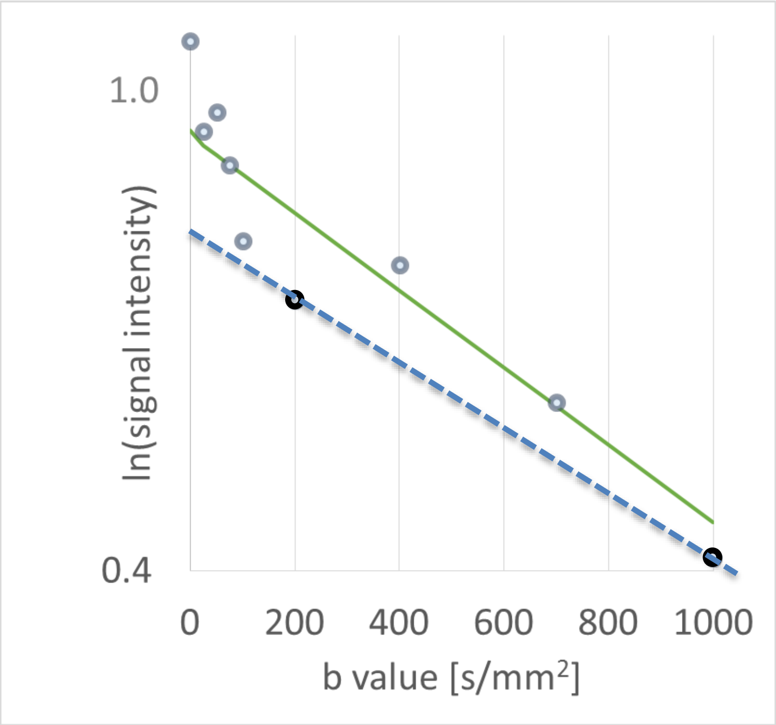

Fast diffusing component;
@ b-values < ~150 s/mm2
'Perfusion'

Slow diffusing component;
@ b-values > ~150 s/mm2
'Diffusion'

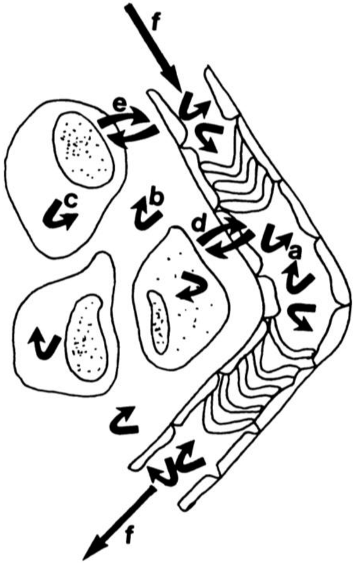

Figure 4. Model of biologic tissue. A tissue can be described by a volume fraction *f* of water flowing (*f*) and diffusing (*a*) in capillaries. This fraction involves only perfused capillaries, which are a part of total capillaries, depending on the current physiologic or pathologic situations. The rest of the voxel water, occupying a volume fraction 1 − *f*, is involved in diffusion only. This volume fraction corresponds to extracellular (*b*) and intracellular (*c*) spaces. There are exchanges between those two compartments (*e*). In a simple approach, exchanges between water inside capillaries and outside capillaries (*d*) during the measurement time (100 msec) are neglected. Another assumption is that the diffusion coefficient in sectors *a*, *b*, and *c* is nearly the same.

Le Bihan et al., Radiology, 1988

The effect of b-values on DWI:

perfusion at low b-vals

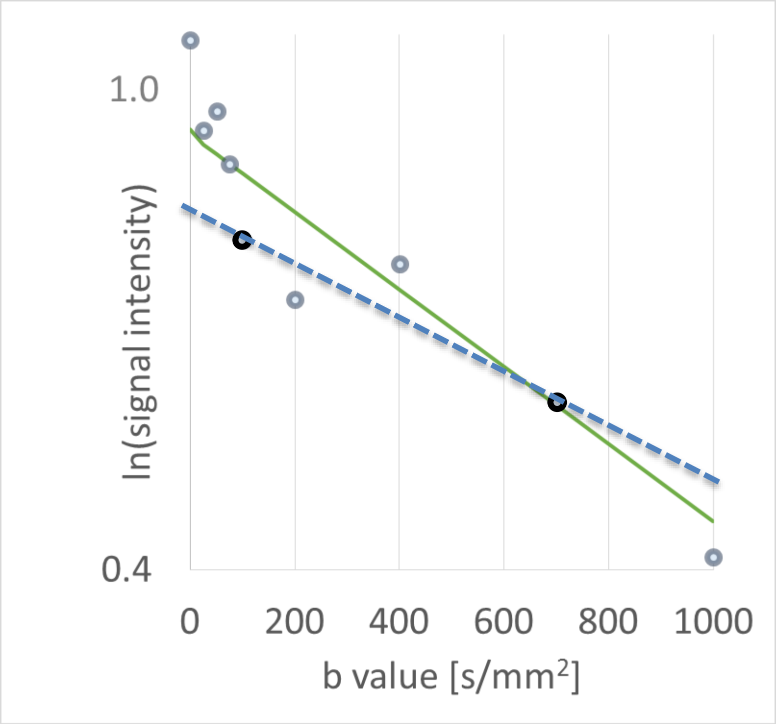

Fast diffusing component;
@ b-values < ~150 s/mm2
'Perfusion'

Slow diffusing component;
@ b-values > ~150 s/mm2
'Diffusion'

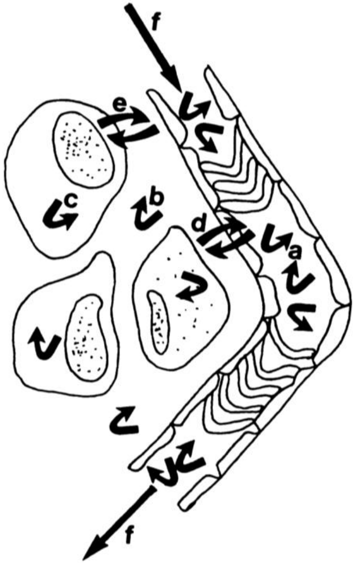

Figure 4. Model of biologic tissue. A tissue can be described by a volume fraction *f* of water flowing (*f*) and diffusing (*a*) in capillaries. This fraction involves only perfused capillaries, which are a part of total capillaries, depending on the current physiologic or pathologic situations. The rest of the voxel water, occupying a volume fraction 1 − *f*, is involved in diffusion only. This volume fraction corresponds to extracellular (*b*) and intracellular (*c*) spaces. There are exchanges between those two compartments (*e*). In a simple approach, exchanges between water inside capillaries and outside capillaries (*d*) during the measurement time (100 msec) are neglected. Another assumption is that the diffusion coefficient in sectors *a*, *b*, and *c* is nearly the same.

Le Bihan et al., Radiology, 1988

The effect of b-values on DWI:

perfusion at low b-vals

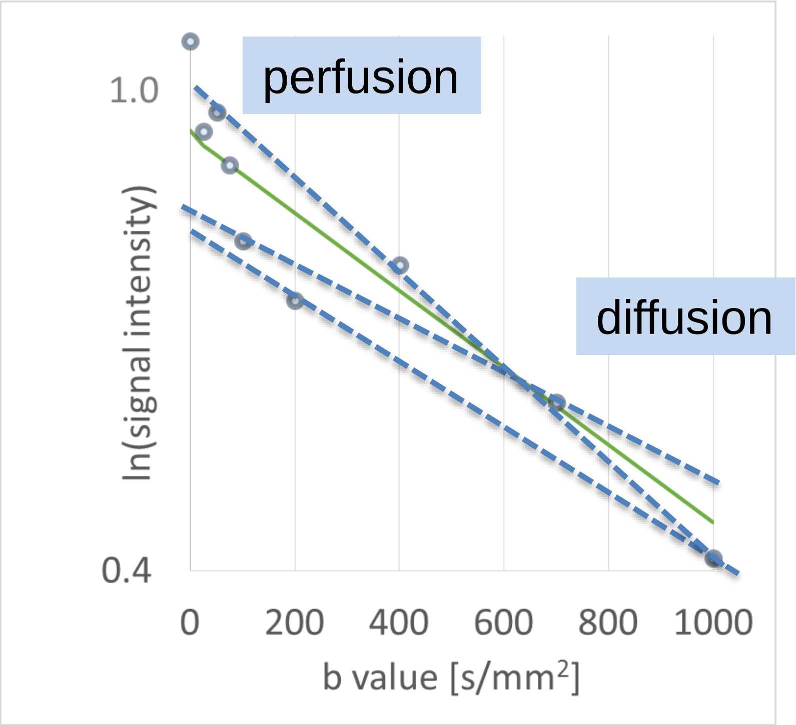

Fast diffusing component;
@ b-values < ~150 s/mm2
'Perfusion'

Slow diffusing component;
@ b-values > ~150 s/mm2
'Diffusion'

Always measure range of b-values to capture both

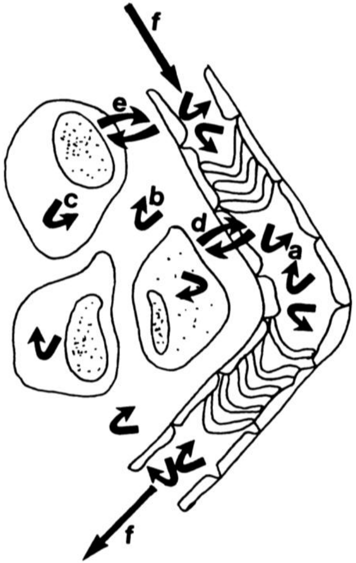

Figure 4. Model of biologic tissue. A tissue can be described by a volume fraction *f* of water flowing (*f*) and diffusing (*a*) in capillaries. This fraction involves only perfused capillaries, which are a part of total capillaries, depending on the current physiologic or pathologic situations. The rest of the voxel water, occupying a volume fraction 1 − *f*, is involved in diffusion only. This volume fraction corresponds to extracellular (*b*) and intracellular (*c*) spaces. There are exchanges between those two compartments (*e*). In a simple approach, exchanges between water inside capillaries and outside capillaries (*d*) during the measurement time (100 msec) are neglected. Another assumption is that the diffusion coefficient in sectors *a*, *b*, and *c* is nearly the same.

Le Bihan et al., Radiology, 1988

How will the choice of b-values influence the calculated b-value?

A. only low b-values will results in a lower ADC

B. only high b-values will result in a lower ADC

C. the calculated ADC is independent of the b-value

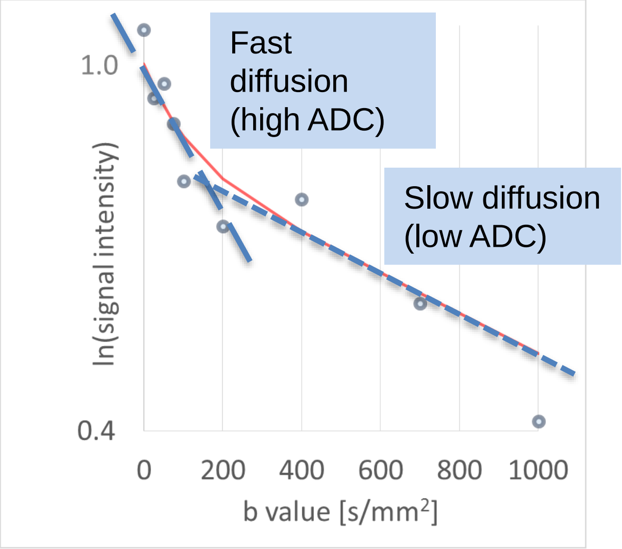

Summary: DWI contrast

- Diffusion is not free / Gaussian distributed in biological tissues.
  - ADC value dependent on chosen b-values
- Low b-values (< 150 s/mm^2) probe for perfusion effects
- Intermediate b-values (up to 1000 s/mm^2, or 1/ADC) best for evaluating diffusion metrics (ADC, FA, etc.) Jones & Basser, 2004
- Higher b-values (e.g., 2500 s/mm^2) may be more beneficial for tractography, likely as a result of greater sensitivity in detecting smaller fibers Rane, Nair & Duong, 2010

How do we measure DWI?

Quick MR physics refresher

How to create Diffusion Weighting?

Echo Planar Imaging

A typical DWI acquisition

Choosing the right readout strategy

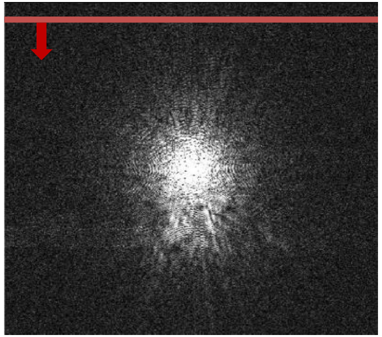

2DFT
(one line per TR)

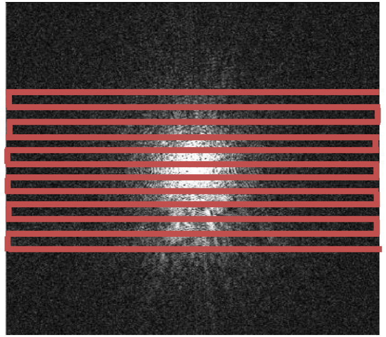

Single-shot
Echo Planar Imaging

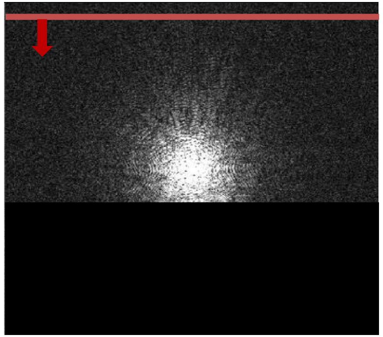

Partial Data

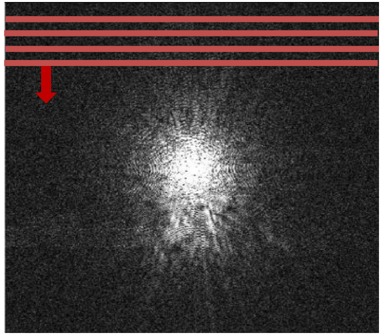

Multiple lines per TR

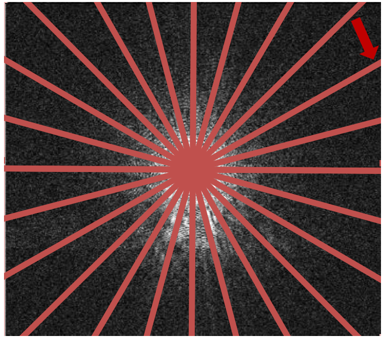

Radial

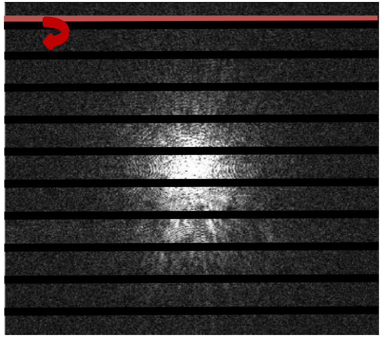

Skip lines

Choosing the right readout strategy

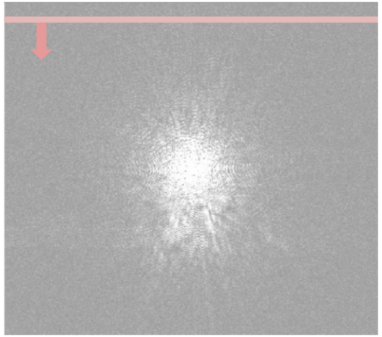

2DFT
(one line per TR)

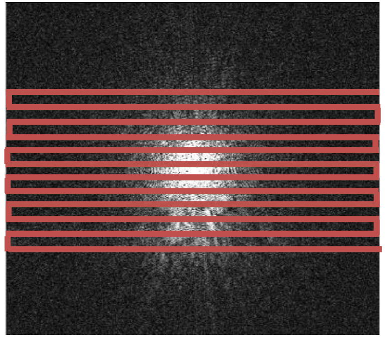

Single-shot
Echo Planar Imaging

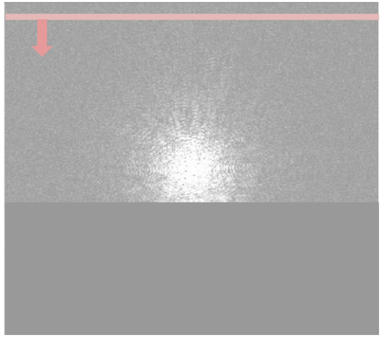

Partial Data

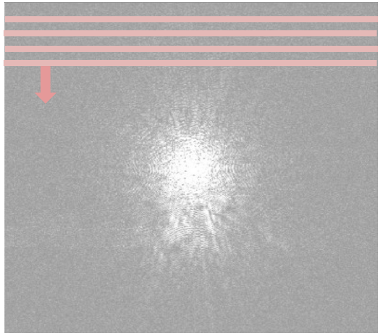

Multiple lines per TR

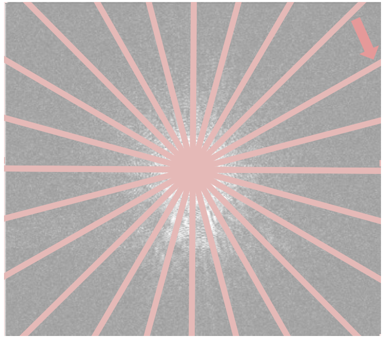

Radial

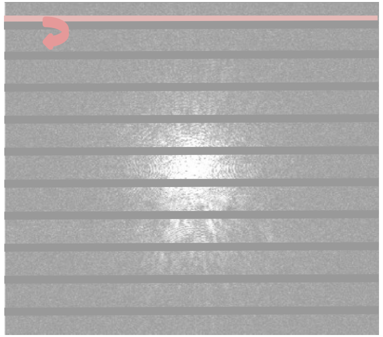

Skip lines

Echo Planar Imaging (EPI)

Invented by Sir Peter Mansfield, 1977
Nottingham, UK

Many gradient echoes after single excitation

- High SNR/time
- Low SAR
- Ideal for quantitative MRI
- “snapshot MRI”

Many applications:
Perfusion MRI (ASL)
fMRI (BOLD)
Diffusion MRI
Real-time imaging
..

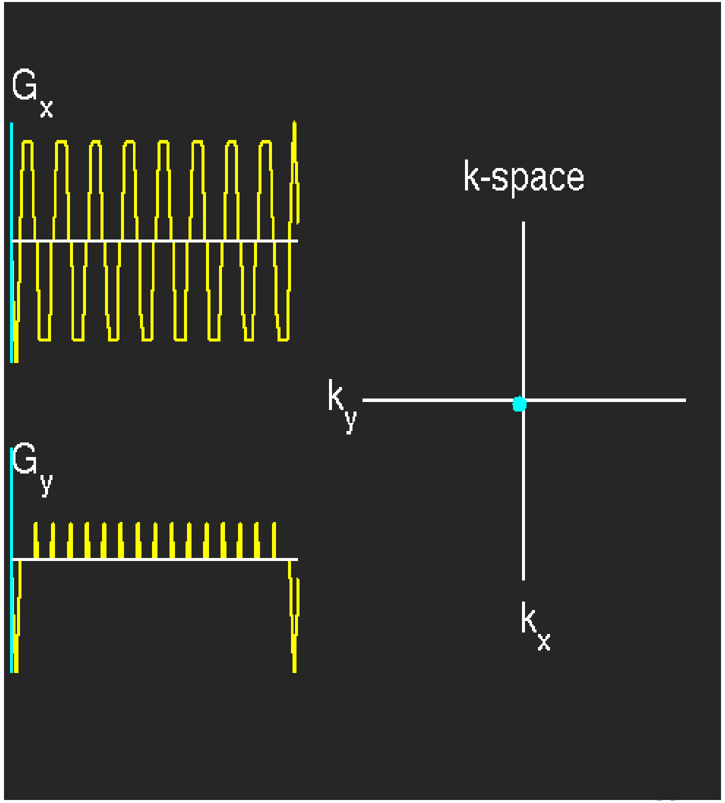

Gradient-Echo EPI

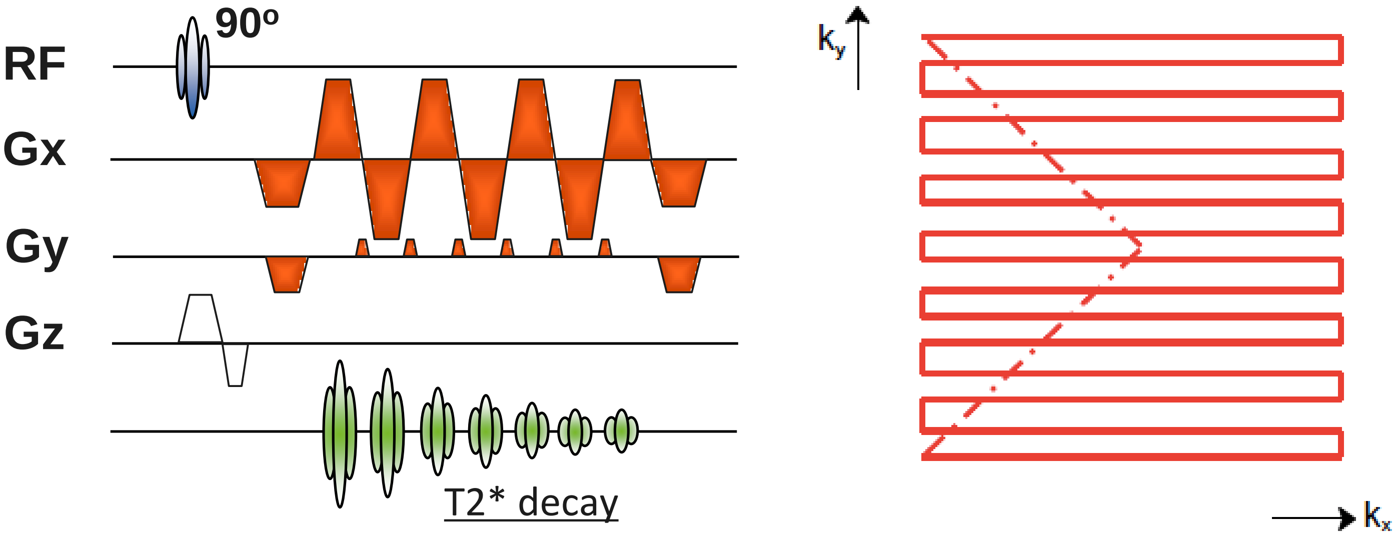
90º
RF
Gx
Gy
Gz
T2* decay
k_y
k_x

- Entire k-space acquired in one shot
- Fastest Cartesian readout available (~50 ms)
- No 180 pulses => gradient echo instead of spin echo (BOLD, ASL, RT-MRI)

Spin-Echo EPI

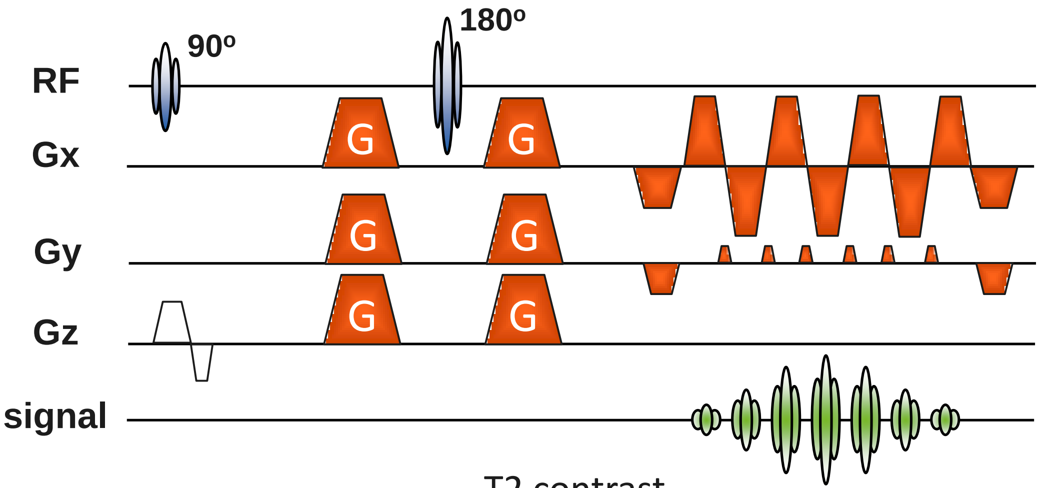
90°
180°
RF
Gx
Gy
Gz
signal
G
G
G
G
G
G

T2 contrast

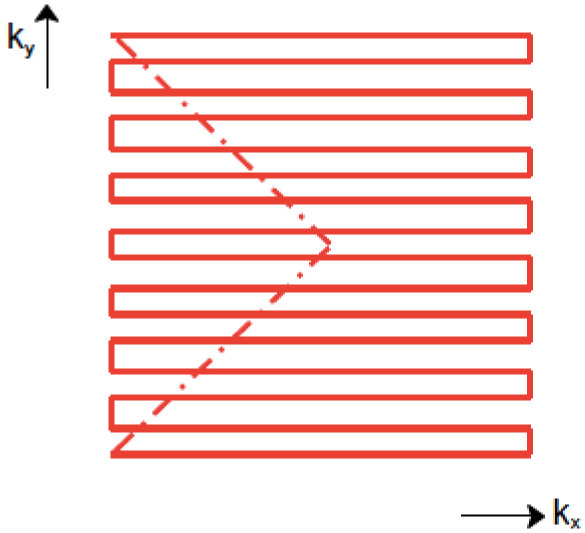

- Entire k-space acquired in one shot
- Fastest Cartesian readout available (~50 ms)
- **DWI:** Append 180 refocussing pulse & DW gradients

The Pitfalls of EPI: Distortion

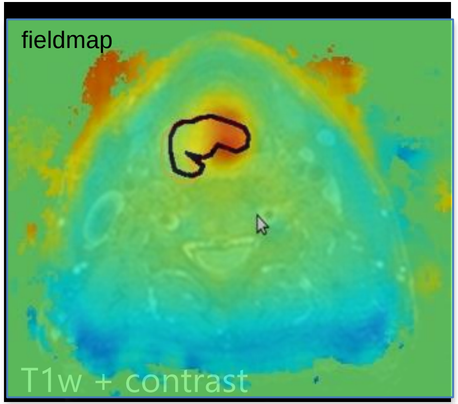
fieldmap
T1w + contrast

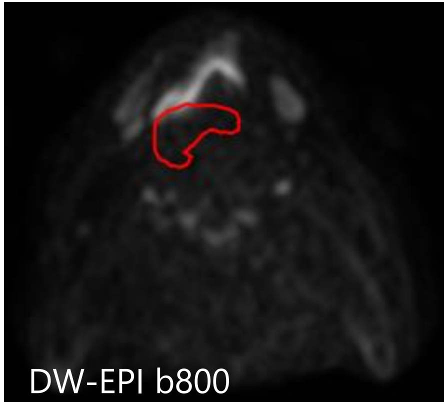

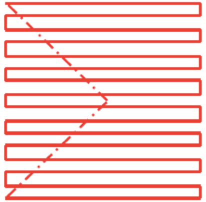

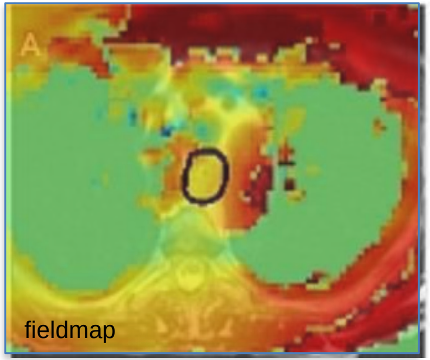

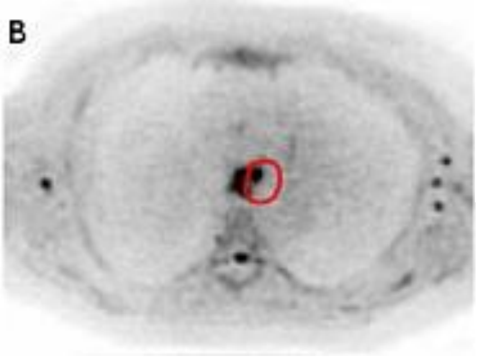

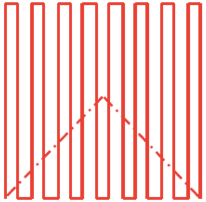

- Geometric displacements along EPI phase encode direction
- Caused by field inhomogeneities (susceptibility artefacts)
- Can be partly corrected as a post processing step

Tim Schakel & Astrid van Lier

Calculate amount of displacement

No distortion

$$\omega = \gamma(B_0 + G_x x)$$

$$\boxed{G_x x = \frac{\omega}{\gamma} - B_0}$$

$$x = \frac{\frac{\omega}{\gamma} - B_0}{G_x}$$

With susceptibility offset

$$\omega = \gamma(B_0 + G_x x \boxed{+ \Delta B(x, y)})$$

$$\boxed{G_x x = \frac{\omega}{\gamma} - B_0 - \Delta B(x, y)}$$

$$x = \frac{\frac{\omega}{\gamma} - B_0}{G_x} \boxed{- \frac{\Delta B(x, y)}{G_x}}$$

$$\Delta x = \frac{\Delta B(x, y)}{G_x}$$

small gradient gives large displacement!

EPI Distortion

Simplified EPI readout to understand appearance of image distortions in EPI…

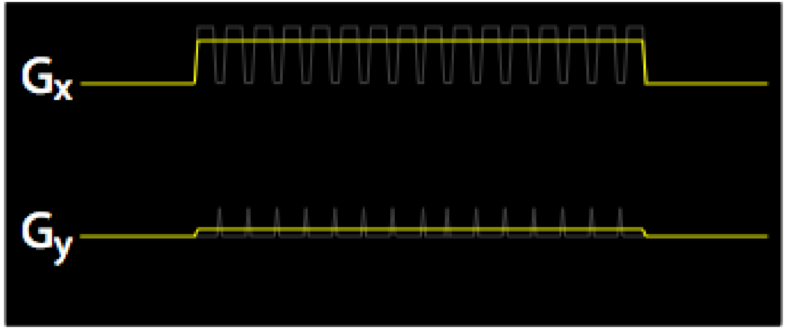

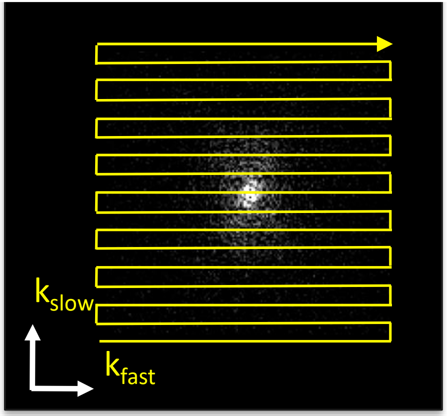

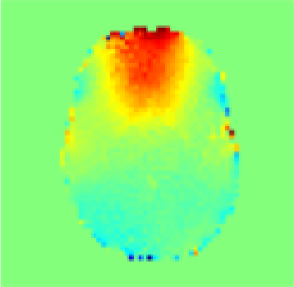
field

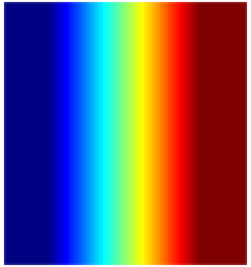
fast gradient

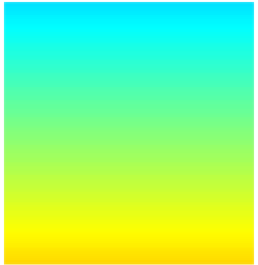
slow gradient

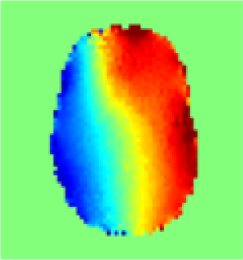
net (fast)

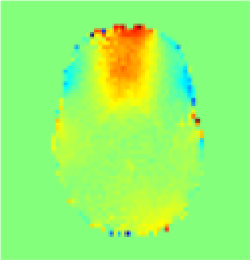
net (slow)

Images courtesy of Karla Miller, Oxford

Distortion correction

distorted image

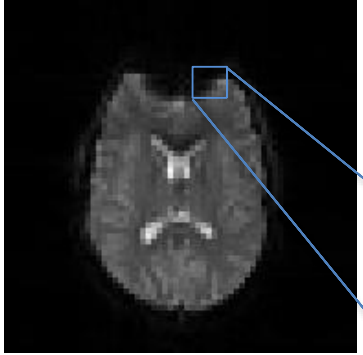

Displacement map (px)

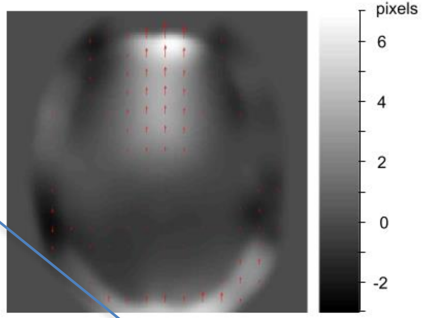

undistorted image

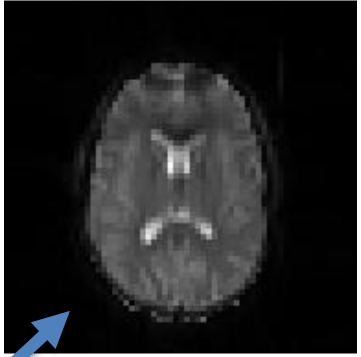

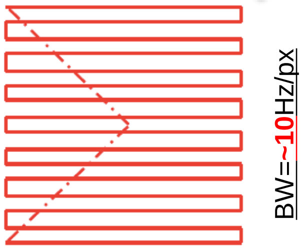

BW=1000Hz/px

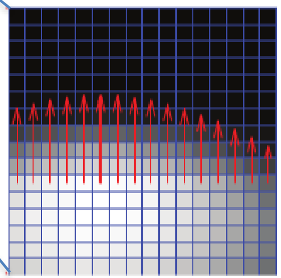

Processing steps

1. Acquire fieldmap
2. Convert to displacement map
3. Calculate inverse transform
4. Warp original image

Images courtesy of Jesper Andersson, Oxford

Corrections in Head & Neck

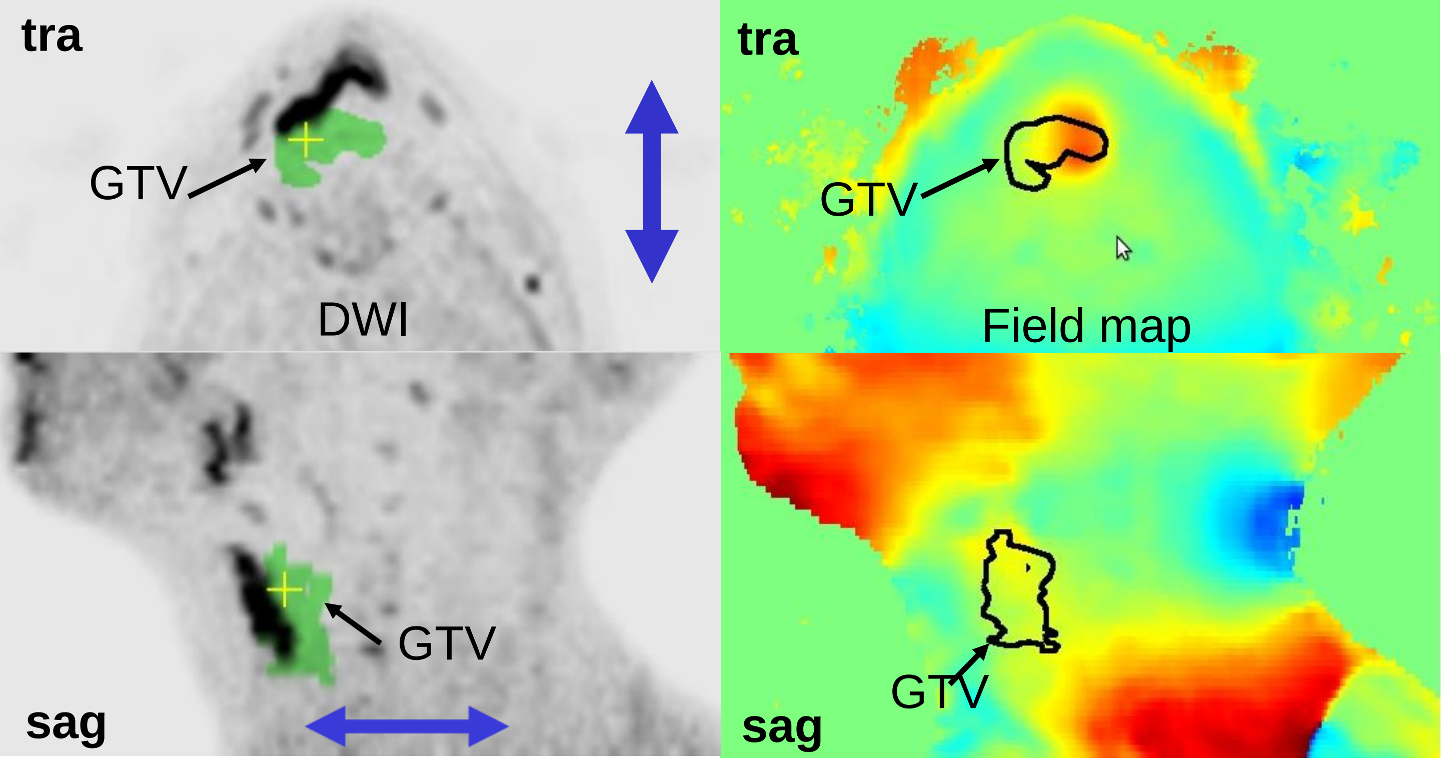
tra
GTV
DWI
tra
GTV
Field map
GTV
sag
GTV
sag

Schakel, RadOnc, 2013

Corrections in Head & Neck

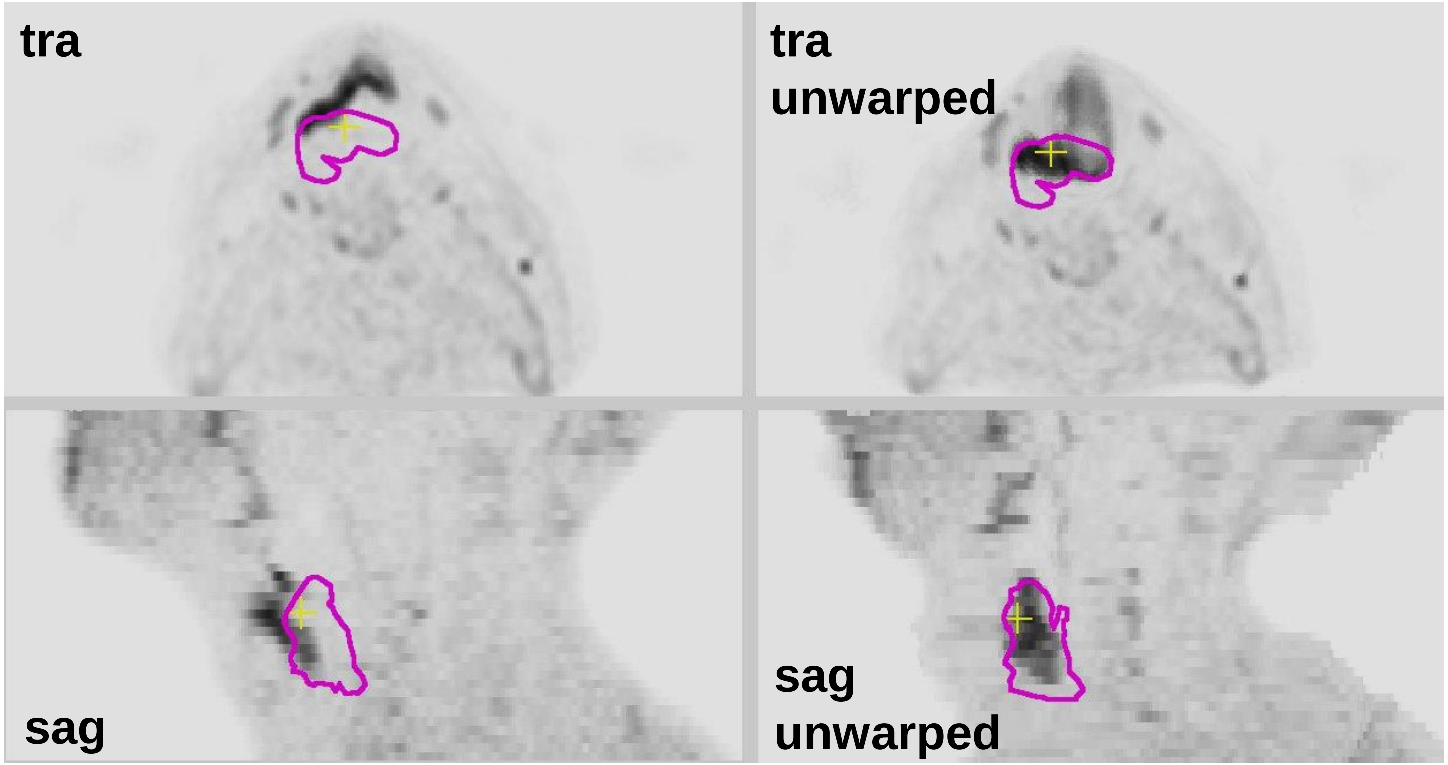
tra
tra unwarped
sag
sag unwarped

Schakel, RadOnc, 2013

Summary: EPI

- Many benefits
  - Single-shot EPI prevents motion corrupted images
  - Very efficient acquisition scheme (fast!)
- Longer readout = more image artifacts
  - Image distortions occur along the slow (Phase Encode) direction, because the effective gradient strength is low
- Dealing with distortions
  - Shimming (homogenize the magnetic field)
  - Acquire a field-map (measure the field to correct distortions)
  - Reduce readout length (high BW, parallel imaging)

How do we measure DWI?

Quick MR physics refresher

How to create Diffusion Weighting?

Echo Planar Imaging

A typical DWI acquisition

Measuring diffusion: b-vals & diffusion dirs

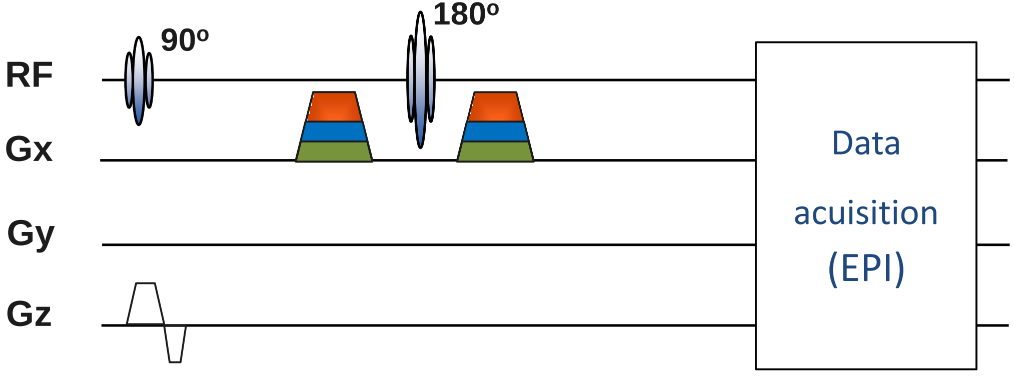
180o
90o
RF
Gx
Gy
Gz
Data
acuisition
(EPI)

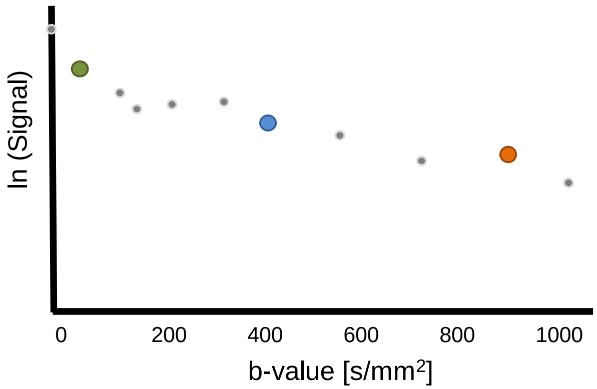

Diffusion anisotropy => Diffusion Tensor Imaging

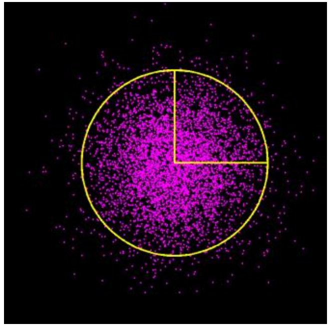
Isotropic diffusion

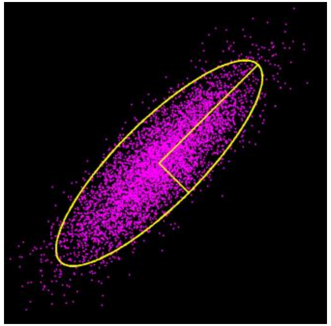
Anisotropic diffusion

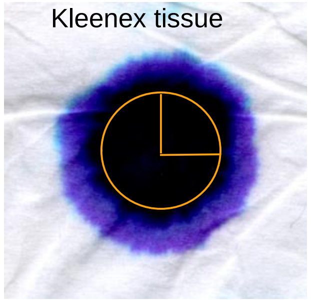
Kleenex tissue

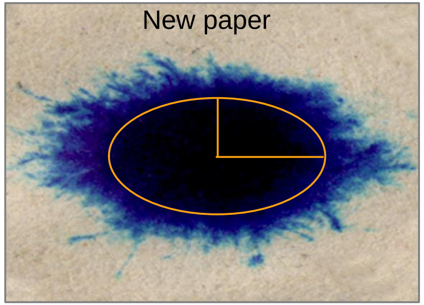

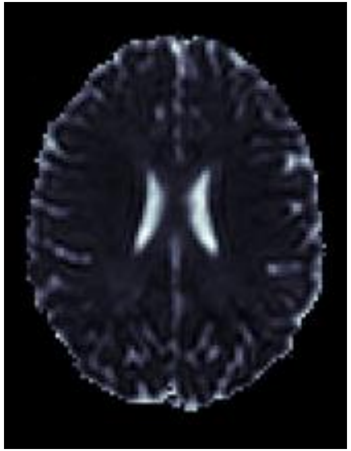
Mean Diffusivity (MD)

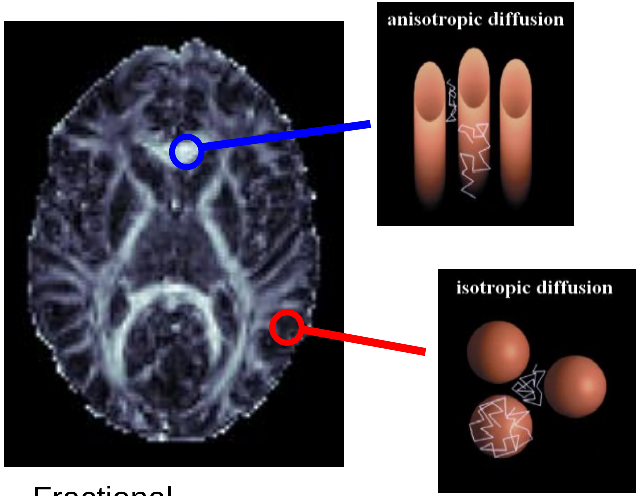
anisotropic diffusion
isotropic diffusion
Fractional Anisotropy (FA)

Mean diffusivity: average of all ADC measurements sensitive to cellularity, edema, and necrosis

Fractional Anisotropy: summary measure of structural integrity., sensitive to microstructural changes

Gordon Kindlimann

DTI post-processing

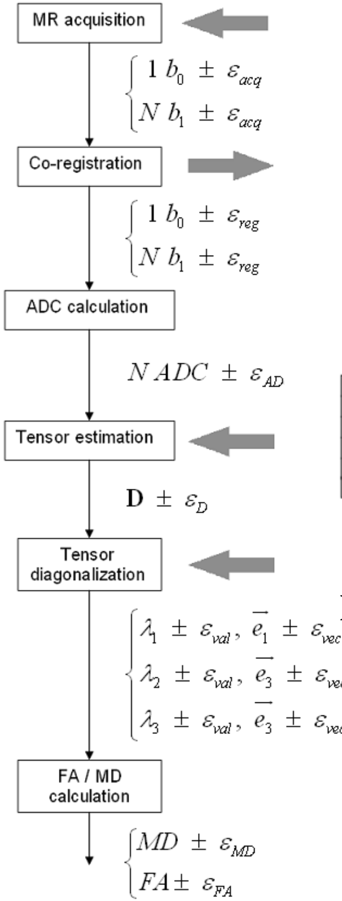

MR acquisition

$$\begin{cases} 1\ b_0 \pm \varepsilon_{acq} \\ N\ b_1 \pm \varepsilon_{acq} \end{cases}$$

Co-registration

$$\begin{cases} 1\ b_0 \pm \varepsilon_{reg} \\ N\ b_1 \pm \varepsilon_{reg} \end{cases}$$

ADC calculation

$$N\ ADC \pm \varepsilon_{AD}$$

Tensor estimation

$$\mathbf{D} \pm \varepsilon_D$$

Tensor diagonalization

$$\begin{cases} \lambda_1 \pm \varepsilon_{val},\ \vec{e}_1 \pm \varepsilon_{vec} \\ \lambda_2 \pm \varepsilon_{val},\ \vec{e}_3 \pm \varepsilon_{vec} \\ \lambda_3 \pm \varepsilon_{val},\ \vec{e}_3 \pm \varepsilon_{vec} \end{cases}$$

FA / MD calculation

$$\begin{cases} MD \pm \varepsilon_{MD} \\ FA \pm \varepsilon_{FA} \end{cases}$$

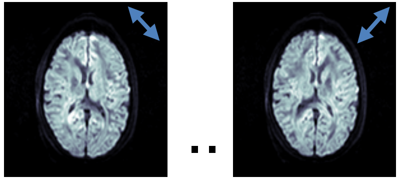

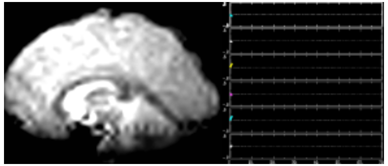

$$\begin{bmatrix} ADC_1 \\ ADC_2 \\ \vdots \\ ADC_N \end{bmatrix} = \begin{bmatrix} g_{x1}^2 & g_{y1}^2 & g_{z1}^2 & 2g_{x1}g_{y1} & 2g_{x1}g_{z1} & 2g_{y1}g_{z1} \\ g_{x2}^2 & g_{y2}^2 & g_{z2}^2 & 2g_{x2}g_{y2} & 2g_{x2}g_{z2} & 2g_{y2}g_{z2} \\ \vdots & \vdots & \vdots & \vdots & \vdots & \vdots \\ g_{xN}^2 & g_{yN}^2 & g_{zN}^2 & 2g_{xN}g_{yN} & 2g_{xN}g_{zN} & 2g_{yN}g_{zN} \end{bmatrix} \cdot \begin{bmatrix} Dxx \\ Dyy \\ Dzz \\ Dxy \\ Dxz \\ Dyz \end{bmatrix}$$

$$\mathrm{D} = \begin{bmatrix} D_{xx} & D_{xy} & D_{xz} \\ D_{yx} & D_{yy} & D_{yz} \\ D_{zx} & D_{zy} & D_{zz} \end{bmatrix} = \mathrm{E}^{\mathrm{T}} \begin{bmatrix} \lambda_1 & 0 & 0 \\ 0 & \lambda_1 & 0 \\ 0 & 0 & \lambda_1 \end{bmatrix} \mathrm{E}$$

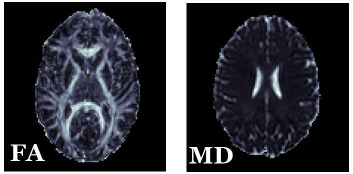

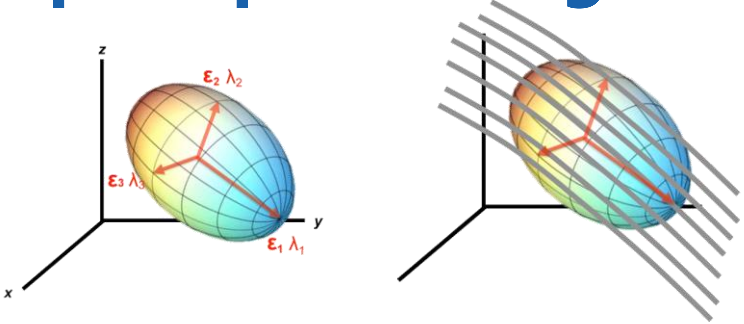

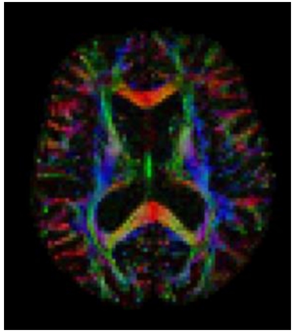

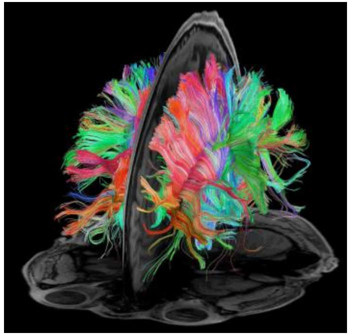

Tijssen et al., HBM 2007

Measuring diffusion

- Diffusion dataset
  - Multiple diffusion directions
    - Oncology application: 3 orthogonal directions (isotropic diffusion)
    - Diffusion Tensor Imaging (DTI): up to 128+ directions
  - Multiple b-values
    - At least 2: b=0 & b>0
      - Calculate ADC
    - IVIM: up to 10 b-values

→ Lots of data to acquire

Some body DWI examples

UMC Utrecht

The ‘apparent’ diffusion map

$$S_b = S_{T2}\, e^{-b\, ADC}$$

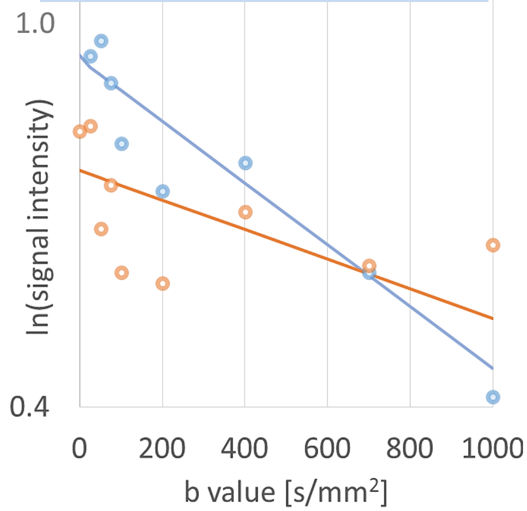

ADC =
slope of b-val vs ln(SI)

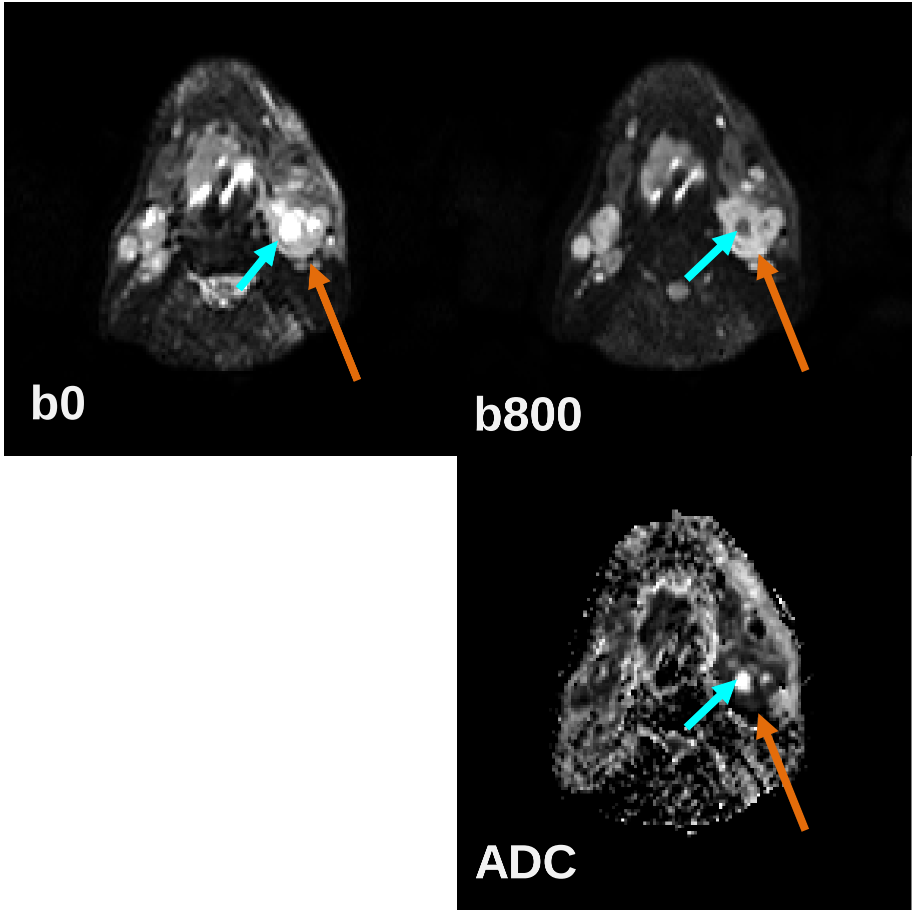

Dense structure (LN, tumour, nerves):

High SI on T2 w MRI

high SI on b800

Low ADC

Necrosis:

High SI on T2w MRI

low SI on b800

high ADC

Diffusion in response to therapy

Negative correlation between ADC and cell density

Validated with histology in preclinical animal studies

Also observed in patients

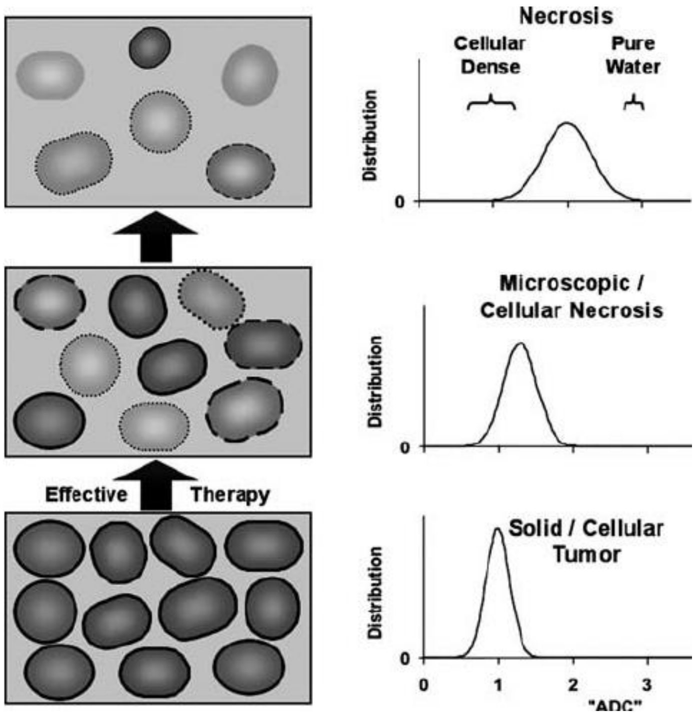
Effective
Therapy
Necrosis
Cellular Dense
Pure Water
Microscopic / Cellular Necrosis
Solid / Cellular Tumor
Distribution
0
0
1
2
3
"ADC"

Moffat et al., MAGMA, 2004

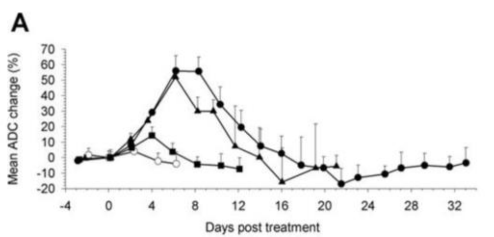

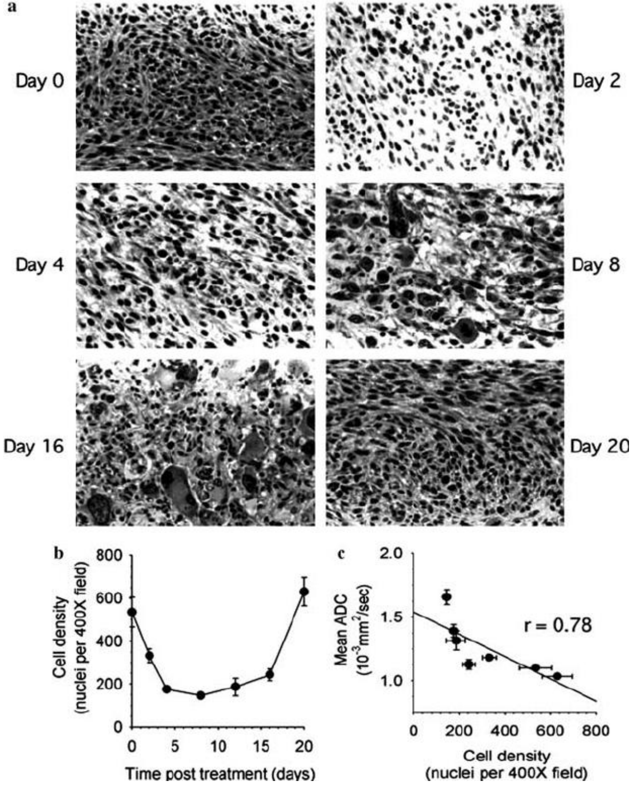
a
Day 0
Day 2
Day 4
Day 8
Day 16
Day 20
b
Cell density (nuclei per 400X field)
800
600
400
200
0
0
5
10
15
20
Time post treatment (days)
c
Mean ADC (10^{-3}mm^2/sec)
2.0
1.5
1.0
r = 0.78
0
200
400
600
800
Cell density (nuclei per 400X field)

Chenevert et al., J Natl Cancer, 2000

DWI for response monitoring: esophagus

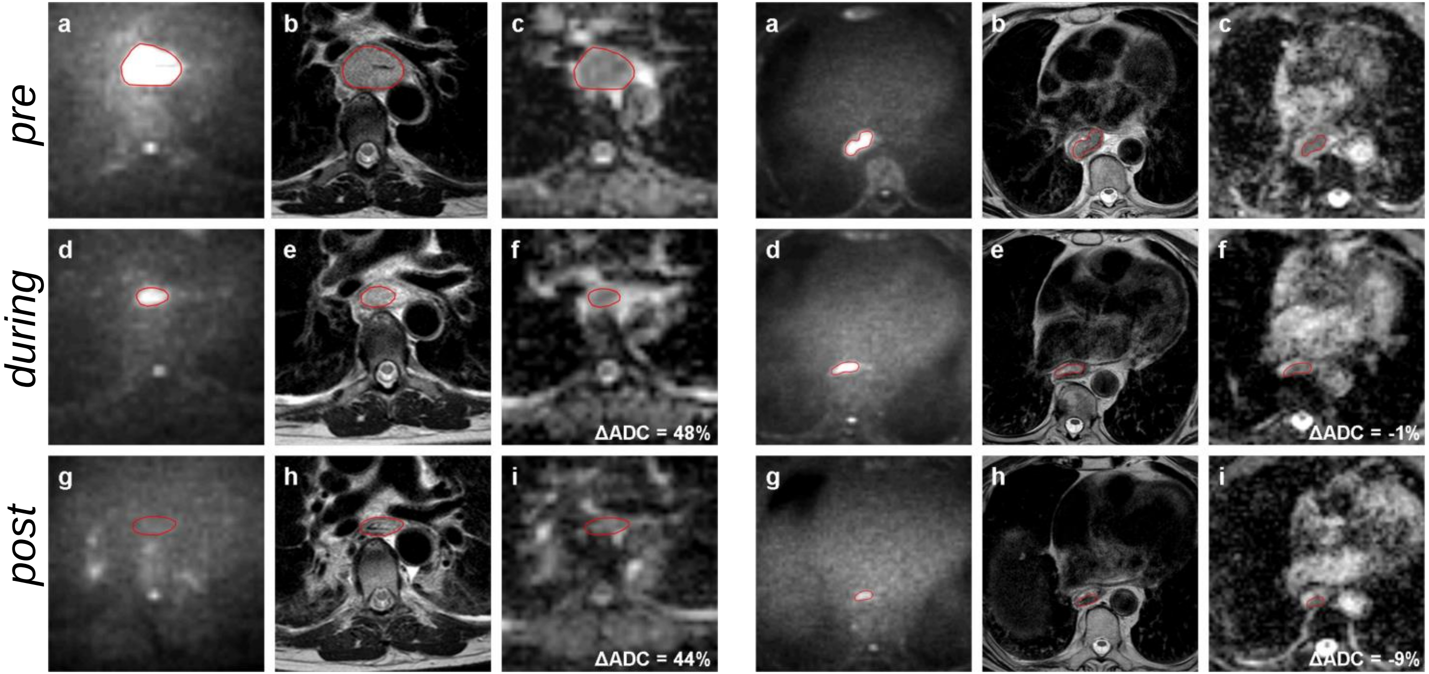
pre
during
post
a
b
c
d
e
f
ΔADC = 48%
g
h
i
ΔADC = 44%
a
b
c
d
e
f
ΔADC = -1%
g
h
i
ΔADC = -9%

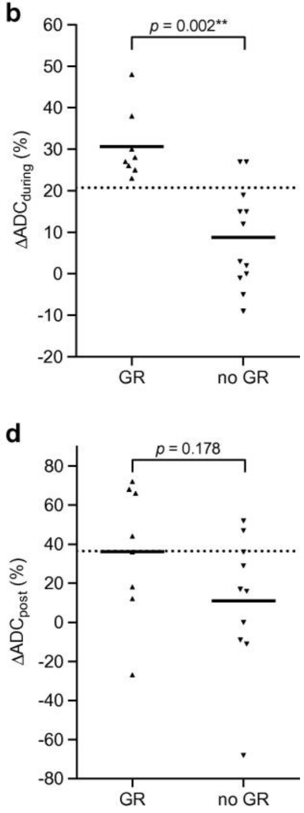

Identify good responders based on early ADC changes (wk 2)

Van Rossum et al., RadOnc, 2015

Questions?

References

Kingsley et al.,
Concepts in MR. 28(2), 101—179 (2006)

Padhani et al.,
Neoplasia 11(2), 102—125, (2009)

Bihan et al.,
JMRI 24:478—488 (2006)

Jezzard et al.,
HBM 8:80—85 (1999)

Jones et al.,
MRM 51(4): 807—815 (2004)

Acknowledgements

Els Fieremans
Karla Miller
Tim Schakel
Marielle Philippens

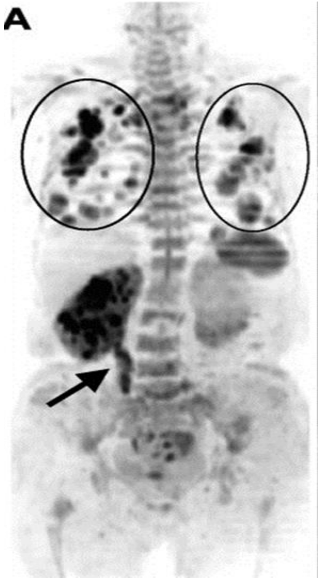

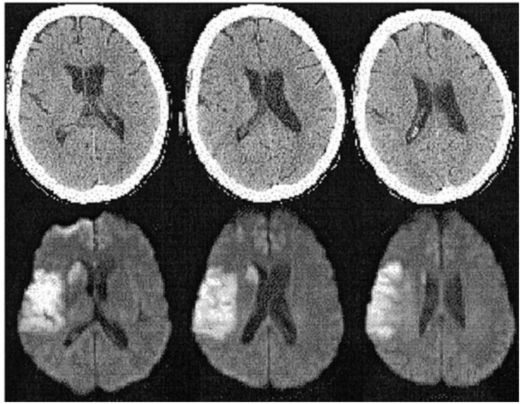

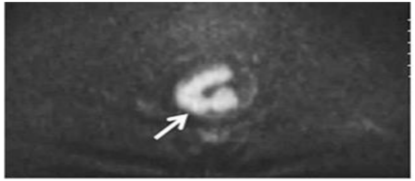

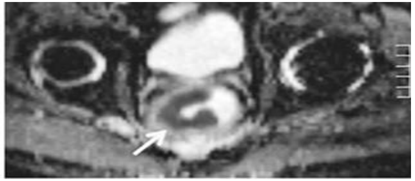

APPLICATIONS:
MRI IN CERVICAL CANCER

Piet Dirix MD, PhD

Dpt. of Radiation Oncology, Iridium Cancer Network

Associate Professor, University of Antwerp

www.iridiumkankernetwerk.be

Cervical cancer

Age-standardised death rates from cervical cancer by country (per 100,000 inhabitants).

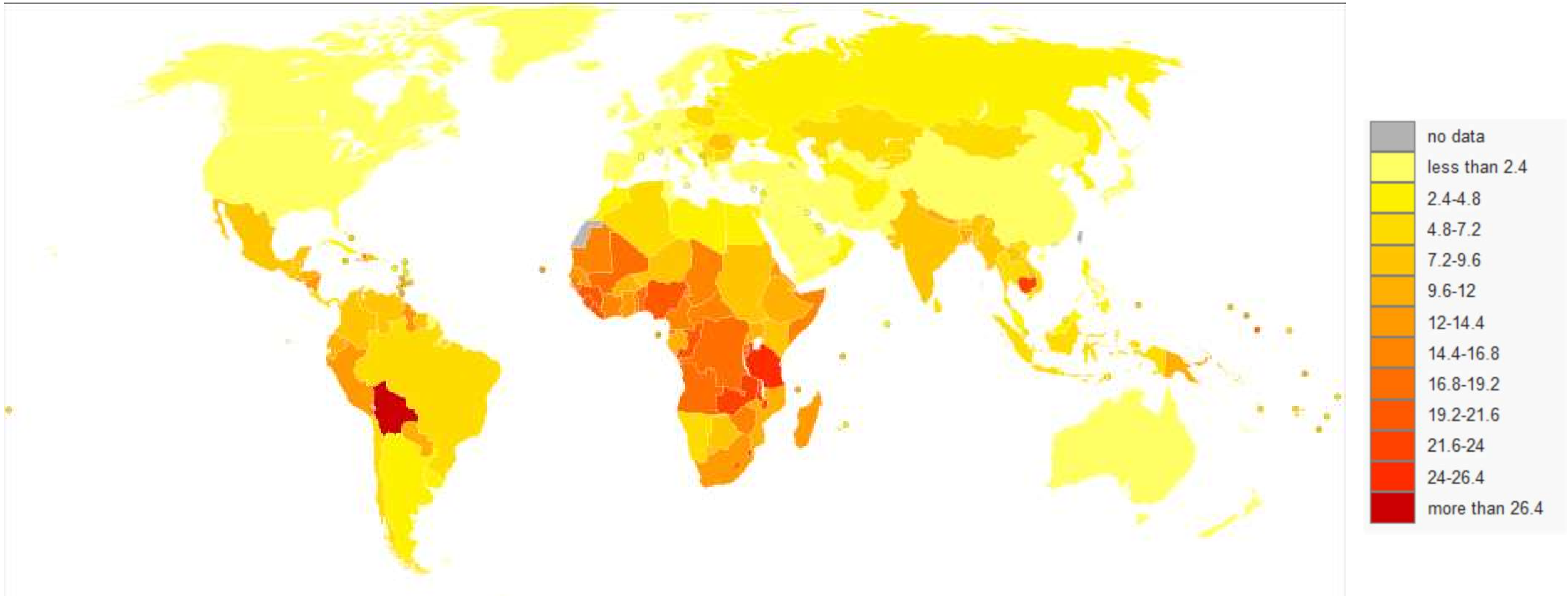
no data
less than 2.4
2.4-4.8
4.8-7.2
7.2-9.6
9.6-12
12-14.4
14.4-16.8
16.8-19.2
19.2-21.6
21.6-24
24-26.4
more than 26.4

Incidence & motality dependent on screening & vaccination:
+/- 75% decrease in developed countries
+/- 80% of all cases of cervical cancers now occur in developing countries

Vaccination

- Persistent viral infection with carcinogenic HPV types causes virtually all cancer of the cervix and most cases of anal cancer. The carcinogenic types, HPV 16 and HPV 18 cause approximately 70 percent of all cervical cancers worldwide and 72 percent of anal cancers. HPV types 31, 33, 45, 52, and 58 are estimated to cause an additional 19 percent of invasive cervical cancers. HPV 6 and HPV 11 cause approximately 90 percent of genital warts.
- Available vaccines:
  - Gardasil, a quadrivalent HPV vaccine, targets HPV types 6, 11, 16, and 18.
  - Gardasil 9, a 9-valent vaccine, targets the same HPV types as the quadrivalent vaccine (6, 11, 16, and 18) as well as types 31, 33, 45, 52, and 58.
  - Cervarix, a bivalent vaccine, targets HPV types 16 and 18.
- HPV immunization is most effective among individuals who have not yet been infected with HPV (i.e. before sexual debut).
- Routine immunization should be offered to girls 11 to 12 years of age, but can be administered as early as nine years. Catch-up vaccination should be offered for females aged 13 to 26 years who have not been previously vaccinated. If cost and availability are not issues, the 9-valent vaccine should be used for females in whom HPV vaccination is indicated.

MRI in radiotherapy for cervical cancer

1. Cervical cancer
2. MRI & FDG-PET/CT for pre-treatment assessment of cervical cancer
3. MRI for external beam radiotherapy (EBRT) planning
4. MRI for brachytherapy planning
5. MRI for response assessment

MRI in radiotherapy for cervical cancer

1. **Cervical cancer:**
   1. **FIGO staging**
   2. **Treatment**

2. MRI & FDG-PET/CT for pre-treatment assessment of cervical cancer

3. MRI for external beam radiotherapy (EBRT) planning

4. MRI for brachytherapy planning

5. MRI for response assessment

Normal anatomy

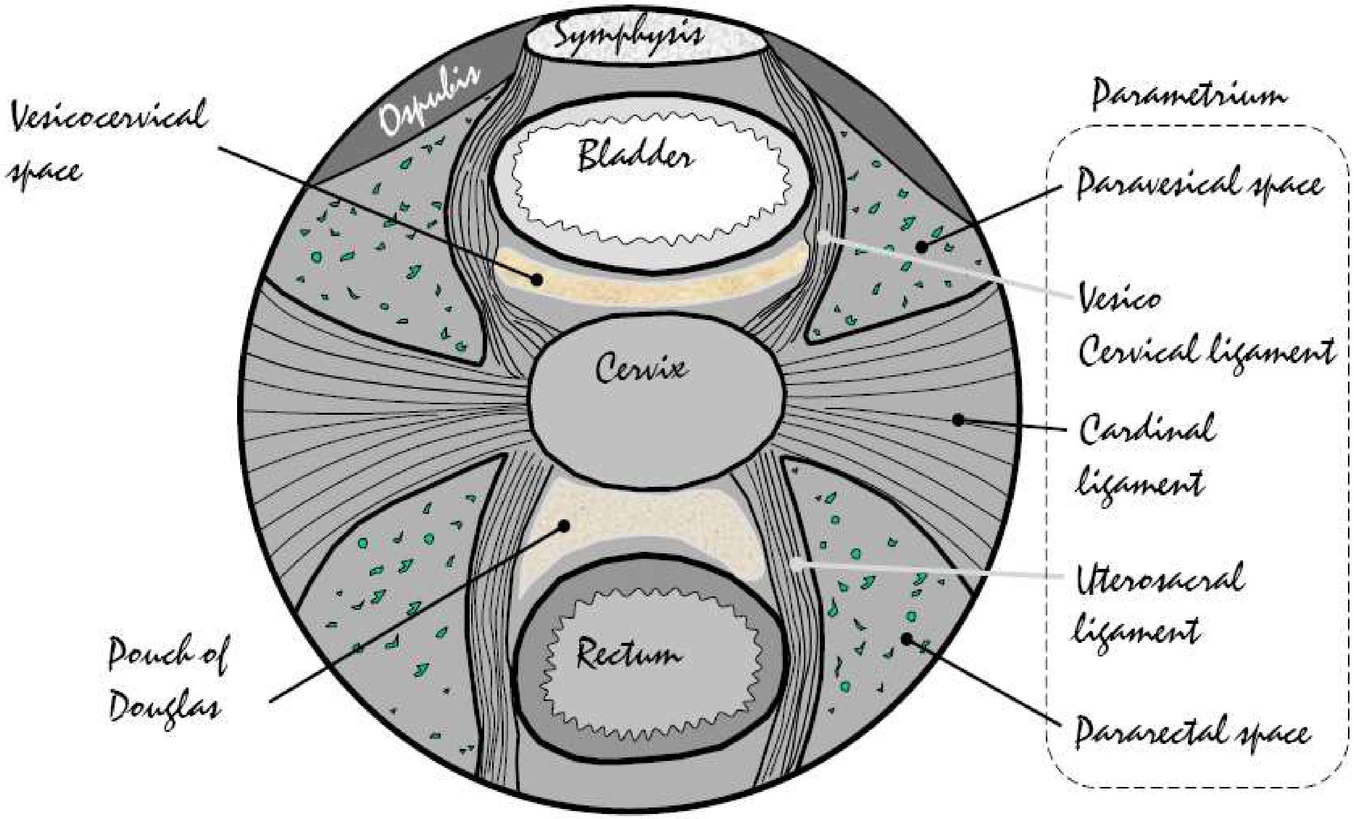
Symphysis
Os pubis
Bladder
Vesicocervical space
Parametrium
Paravesical space
Vesico Cervical ligament
Cervix
Cardinal ligament
Uterosacral ligament
Pouch of Douglas
Rectum
Pararectal space

MRI features

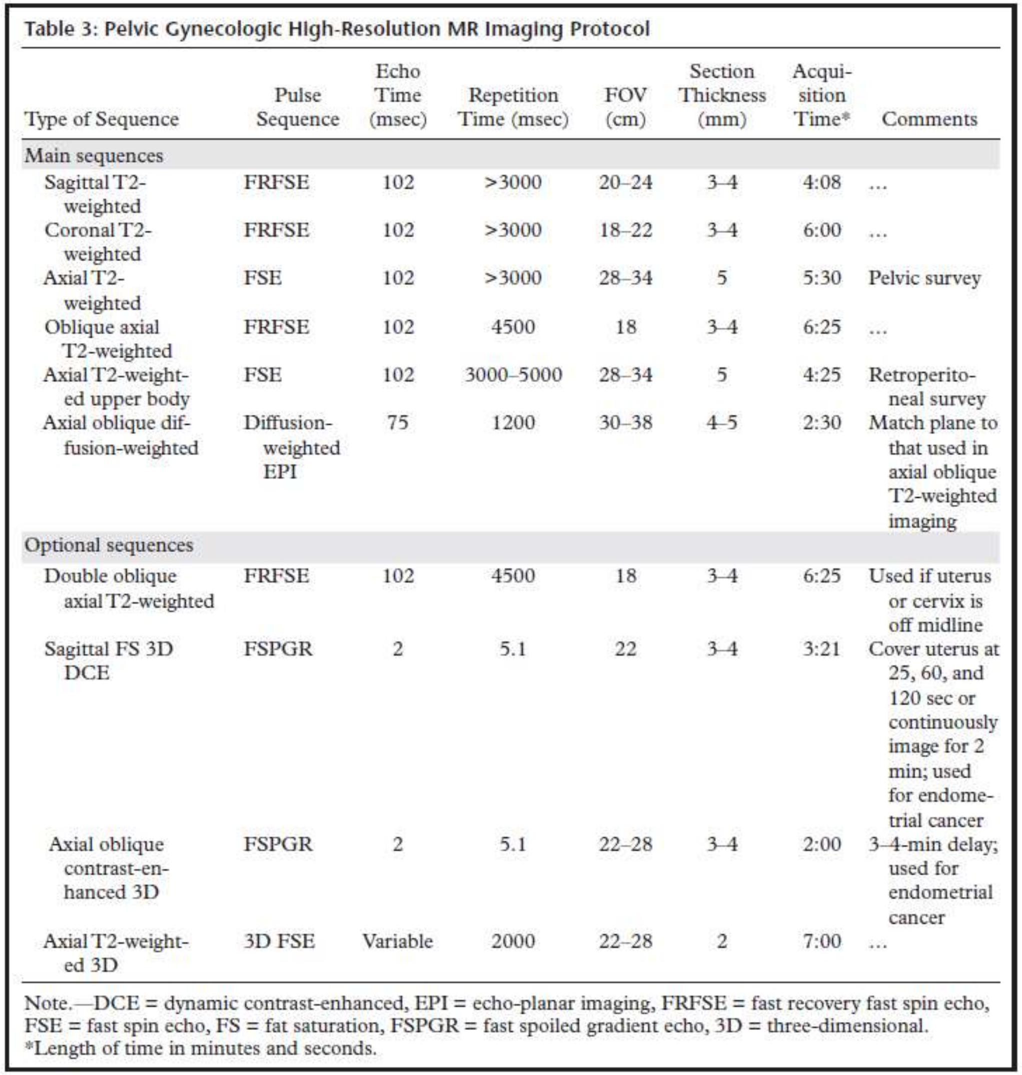

Table 3: Pelvic Gynecologic High-Resolution MR Imaging Protocol

Type of Sequence	Pulse Sequence	Echo Time (msec)	Repetition Time (msec)	FOV (cm)	Section Thickness (mm)	Acquisition Time*	Comments
Main sequences							
Sagittal T2-weighted	FRFSE	102	>3000	20–24	3–4	4:08	…
Coronal T2-weighted	FRFSE	102	>3000	18–22	3–4	6:00	…
Axial T2-weighted	FSE	102	>3000	28–34	5	5:30	Pelvic survey
Oblique axial T2-weighted	FRFSE	102	4500	18	3–4	6:25	…
Axial T2-weighted upper body	FSE	102	3000–5000	28–34	5	4:25	Retroperitoneal survey
Axial oblique diffusion-weighted	Diffusion-weighted EPI	75	1200	30–38	4–5	2:30	Match plane to that used in axial oblique T2-weighted imaging
Optional sequences							
Double oblique axial T2-weighted	FRFSE	102	4500	18	3–4	6:25	Used if uterus or cervix is off midline
Sagittal FS 3D DCE	FSPGR	2	5.1	22	3–4	3:21	Cover uterus at 25, 60, and 120 sec or continuously image for 2 min; used for endometrial cancer
Axial oblique contrast-enhanced 3D	FSPGR	2	5.1	22–28	3–4	2:00	3–4-min delay; used for endometrial cancer
Axial T2-weighted 3D	3D FSE	Variable	2000	22–28	2	7:00	…

Note.—DCE = dynamic contrast-enhanced, EPI = echo-planar imaging, FRFSE = fast recovery fast spin echo, FSE = fast spin echo, FS = fat saturation, FSPGR = fast spoiled gradient echo, 3D = three-dimensional.
*Length of time in minutes and seconds.

Rauch G.M. et al. Radiographics 2014.

Normal anatomy on MRI

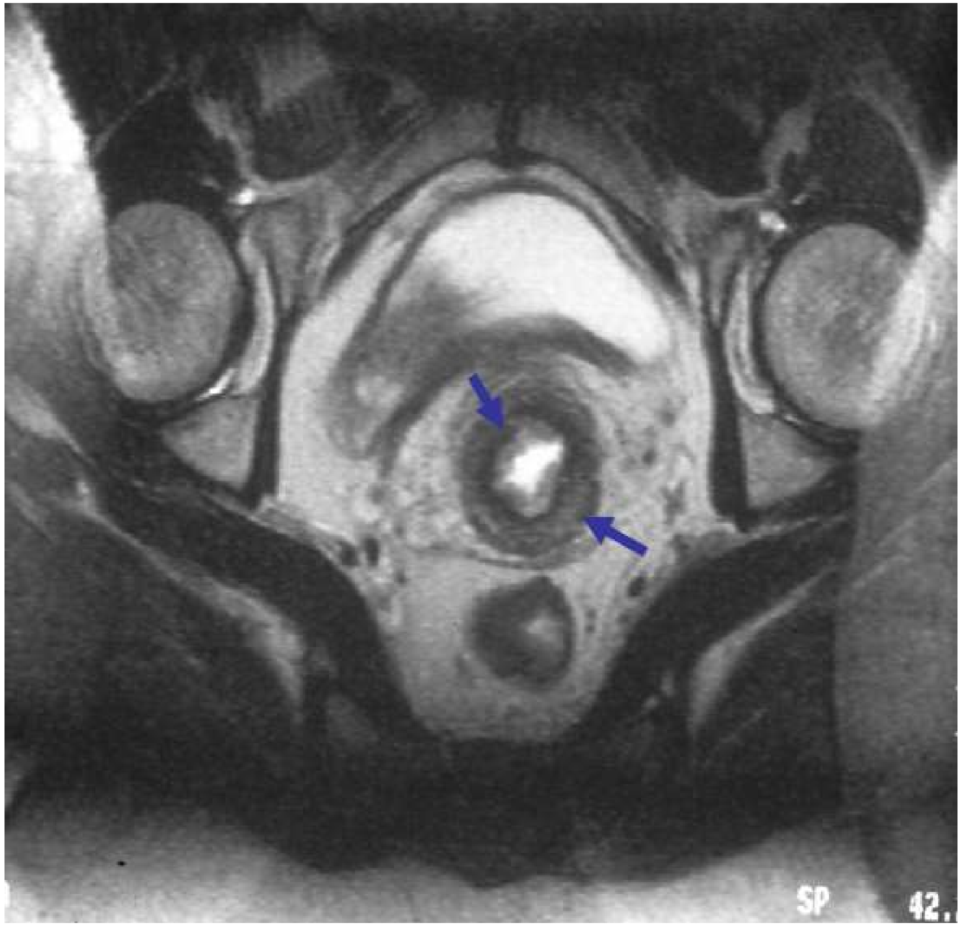

T2-weighted images:

Endocervical canal: high SI

Mucosa: intermediate SI

Cervical rim: low SI

Outer zone: intermediate SI

T1-weighted images:

Homogeneous low SI

FIGO I (confined to uterus)

IB1: < 4 cm

IB2: > 4 cm

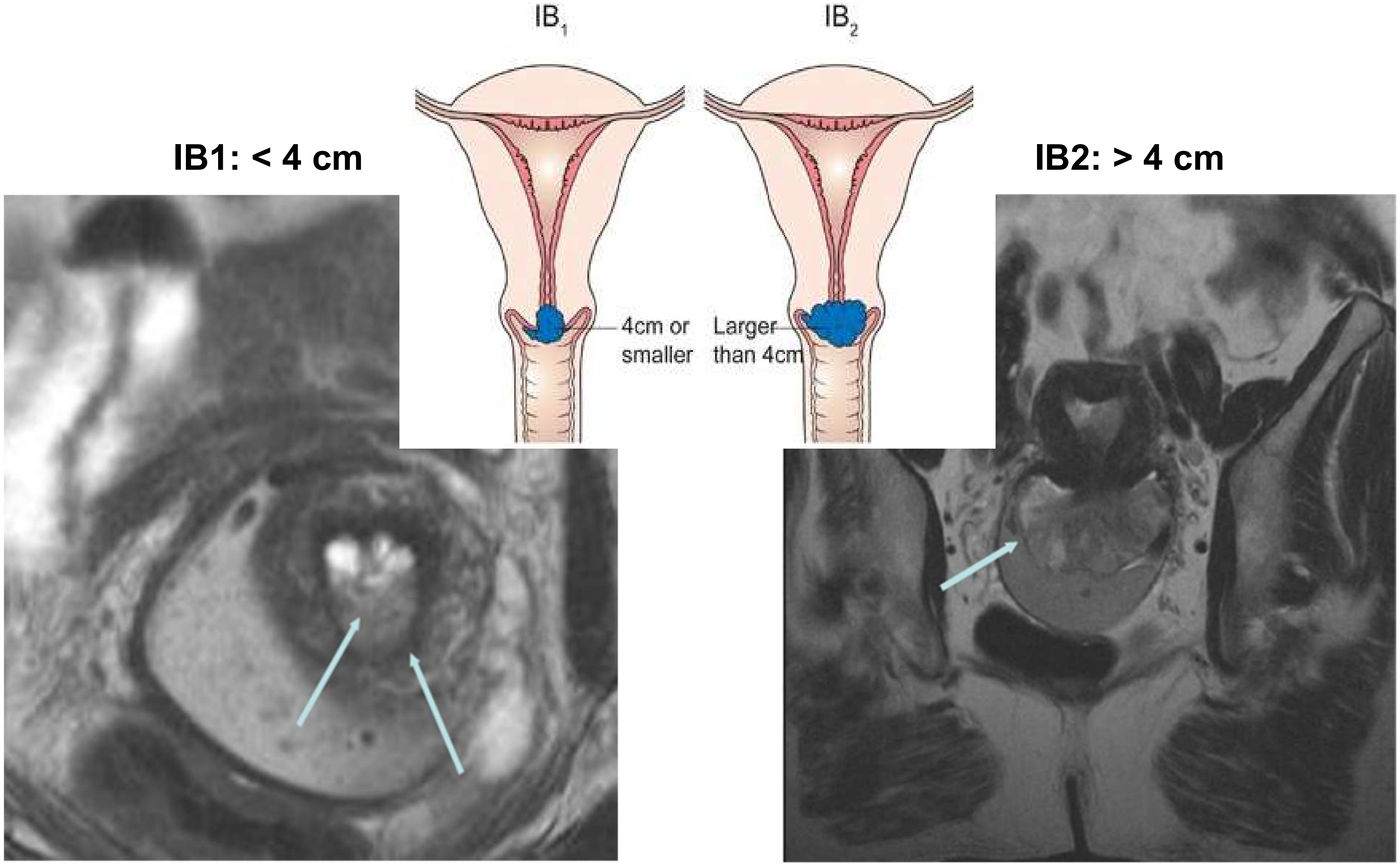
IB1
IB2
4cm or smaller
Larger than 4cm

FIGO II (beyond uterus)

IIA: upper 2/3 of vagina

IIB: parametrial invasion

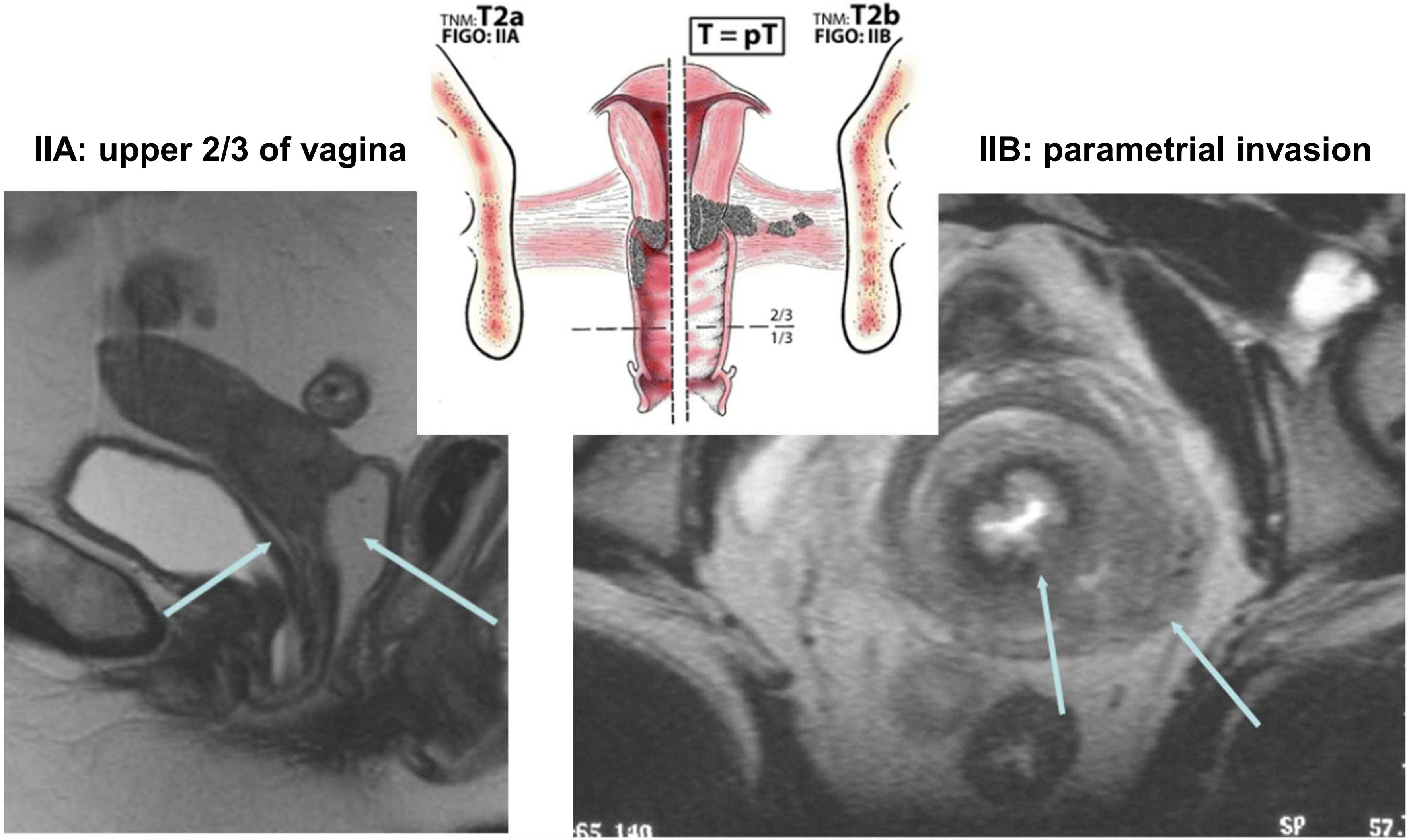
TNM: T2a
FIGO: IIA
T = pT
TNM: T2b
FIGO: IIB
2/3
1/3
65 140
SP
57.

FIGO III

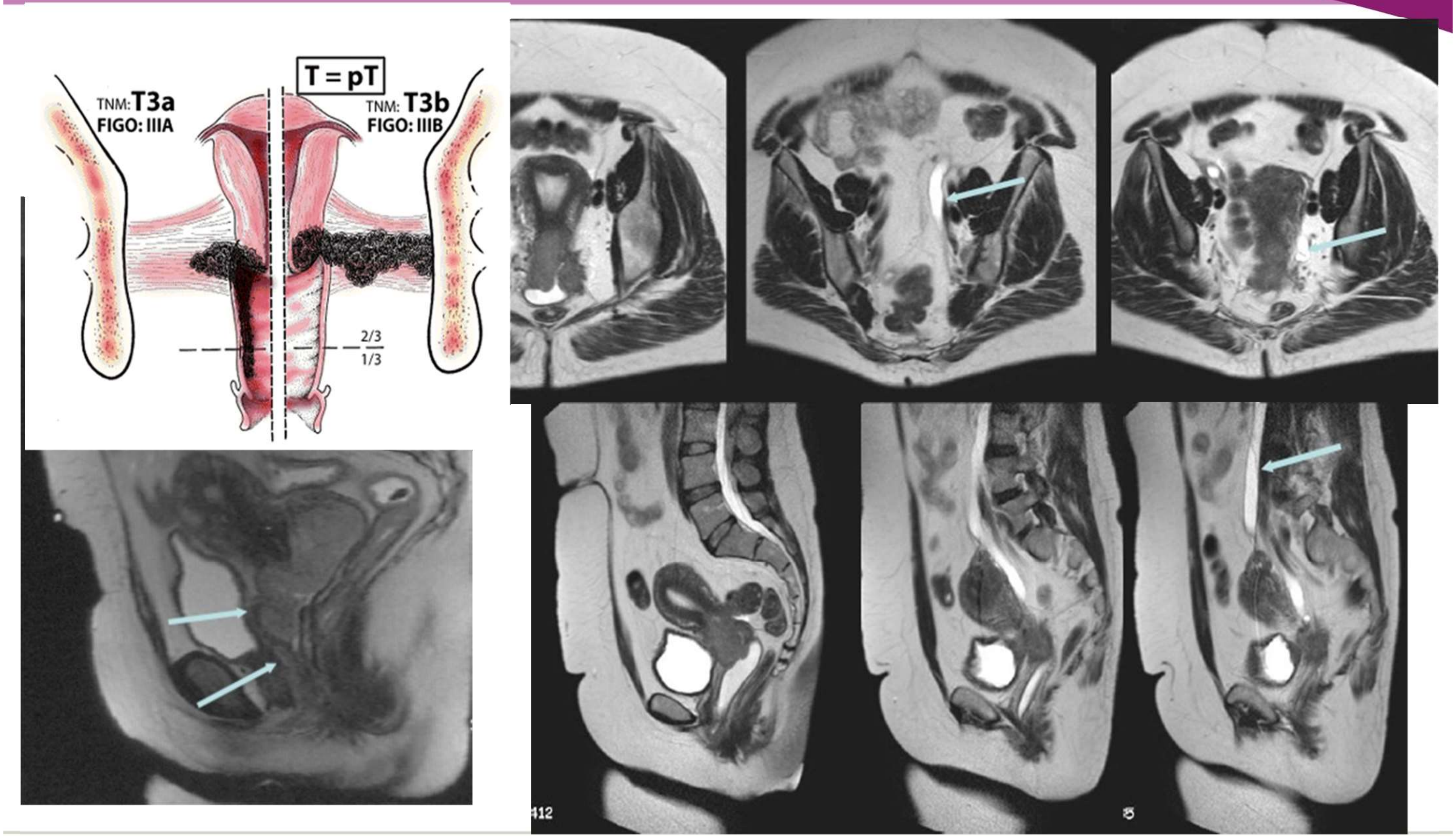
T = pT
TNM: T3a
FIGO: IIIA
TNM: T3b
FIGO: IIIB
2/3
1/3
412
5

IIIA: lower third of vagina

IIIB: to pelvic wall (hydronephrosis)

FIGO IVA (to adjacent organs)

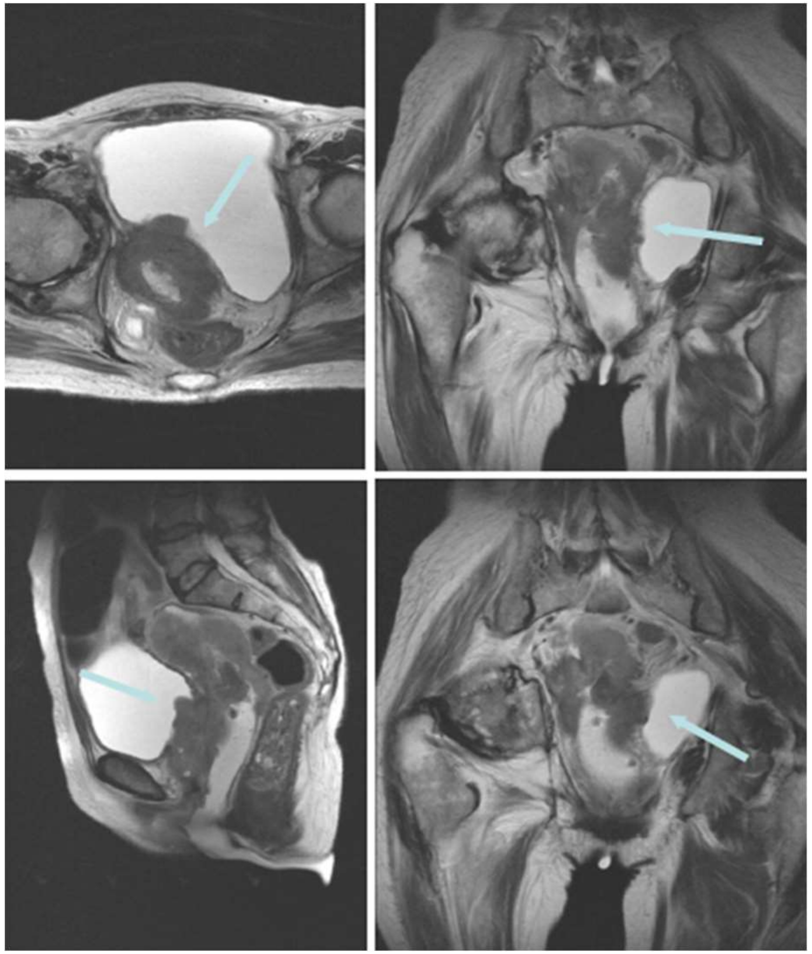

Invasion of bladder

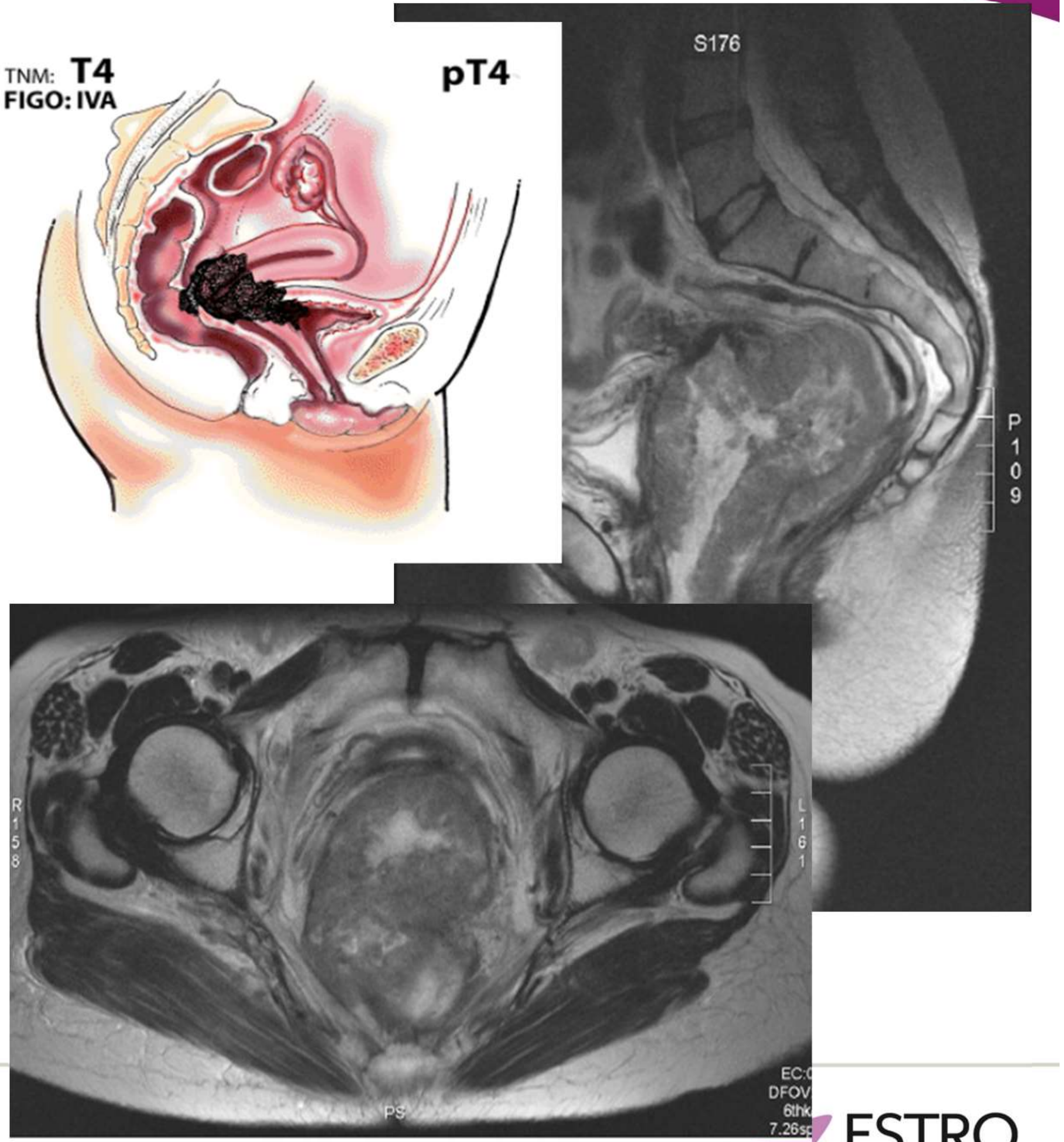
TNM: T4
FIGO: IVA
pT4
S176
P
1
0
9
R
1
5
8
L
1
6
1
PS
EC:
DFOV
6thk
7.26sp

Invasion of rectum

Treatment

- EARLY STAGE (IA & IB1):
  - Surgery (radical hysterectomy with pelvic lymphadenectomy)
  - Primary chemoradiation

- LOCALLY ADVANCED STAGE (IB2 - IVA):
  - Primary chemoradiation

Primary chemoradiation

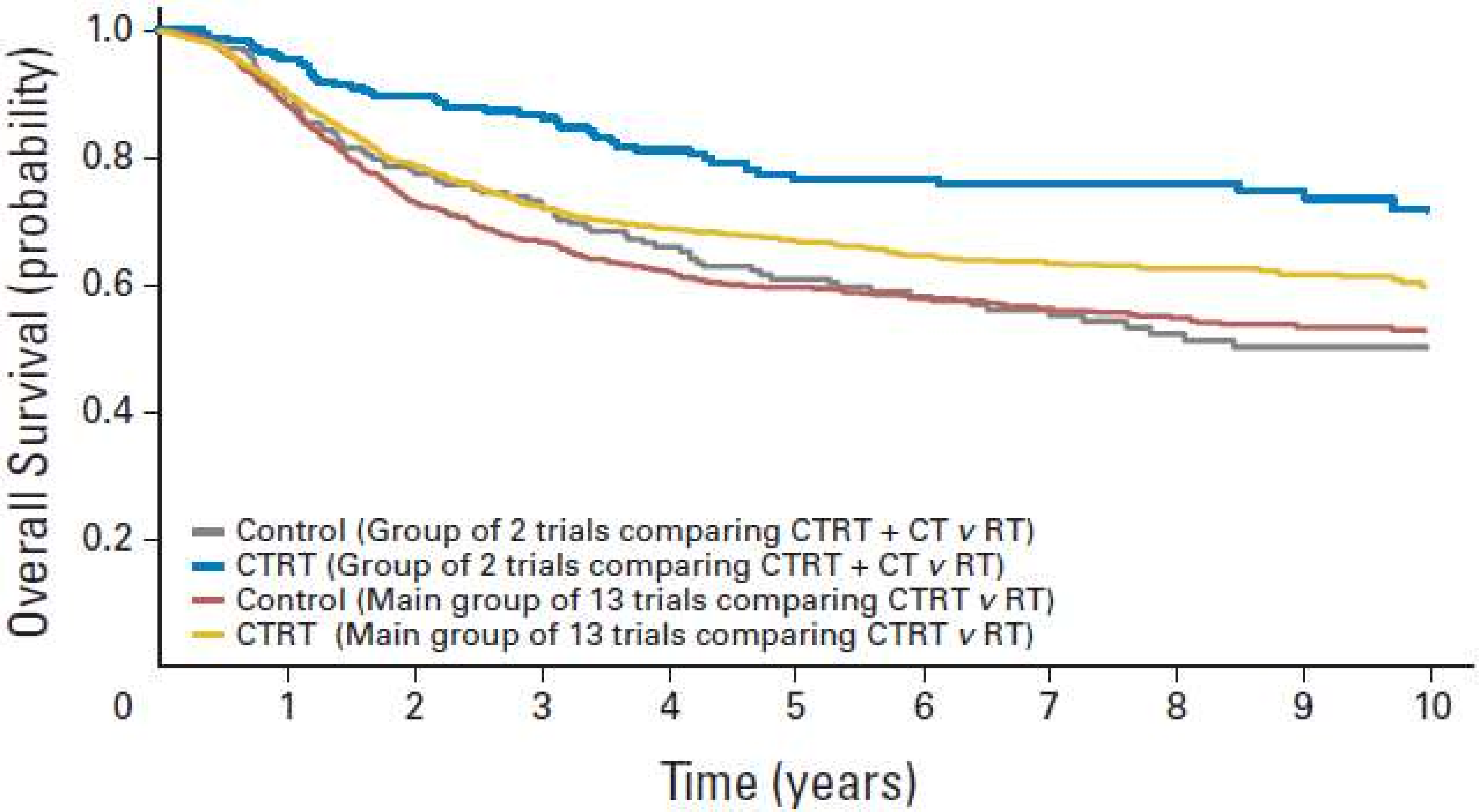

Chemoradiotherapy for cervical cancer meta-analysis collaboration 2010

EORTC 55994
Treatment scheme

Eligibility check
FIGO IB2 – IIA - IIB

Randomization

Treatment 1 (343 patients)

Neoadjuvant chemotherapy (3 courses Cisplatin based)

Followed by Surgery

Treatment 2 (343 patients)

Concomitant chemotherapy and radiotherapy

MRI in radiotherapy for cervical cancer

1. Cervical cancer
2. **MRI & FDG-PET/CT for pre-treatment assessment of cervical cancer:**
    1. **Parametrial invasion (PMI)**
    2. **Nodal staging**
3. MRI for external beam radiotherapy (EBRT) planning
4. MRI for brachytherapy planning
5. MRI for response assessment

Question 1: PMI?

Especially in small tumors (< 4 cm), confined to the cervix:

Determine the right patients for surgery vs. CRT

To avoid tri-modality treatment with its known complications

ACRIN 6651 – GOG 183

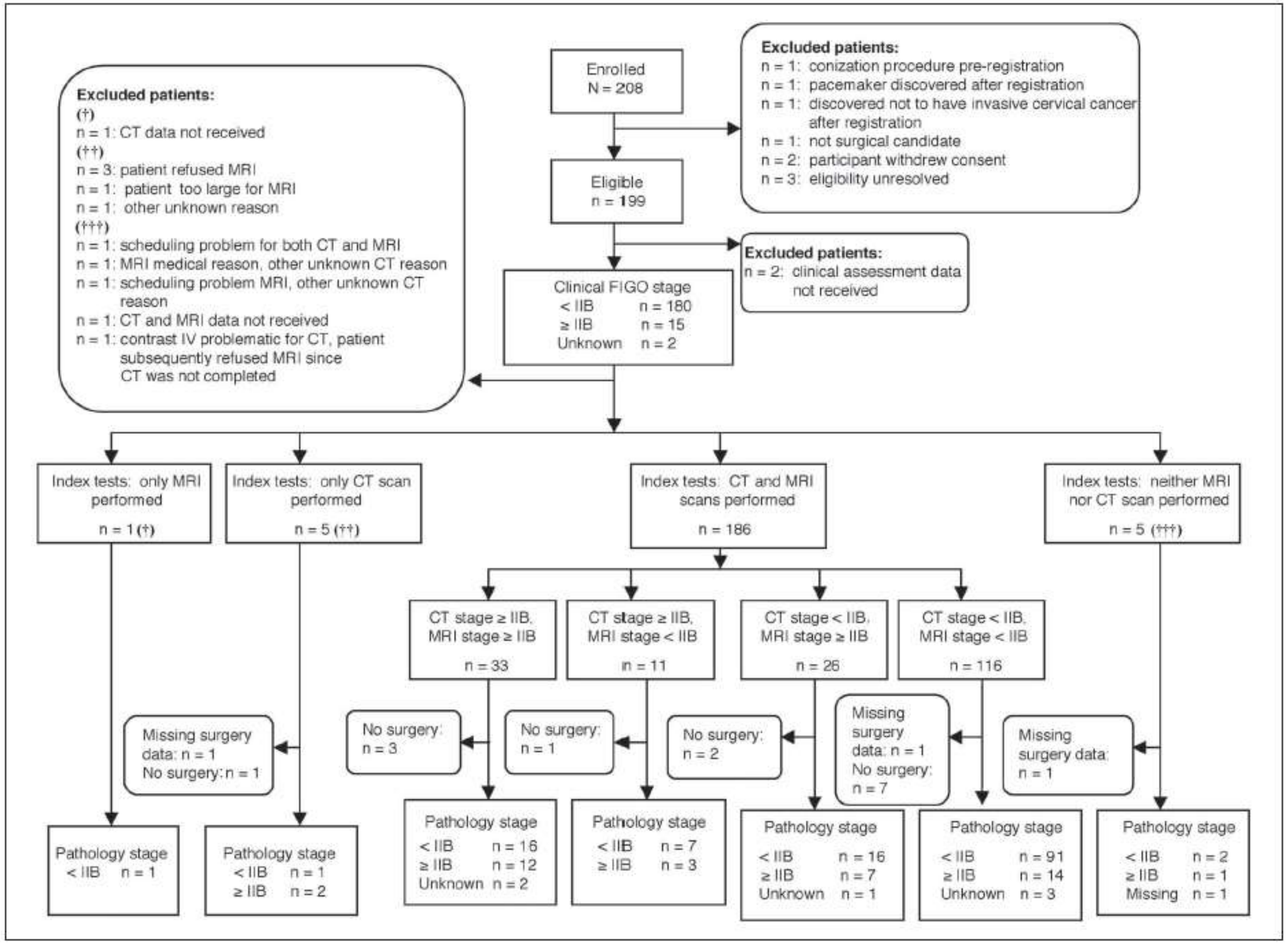
Enrolled
N = 208
Excluded patients:
n = 1: conization procedure pre-registration
n = 1: pacemaker discovered after registration
n = 1: discovered not to have invasive cervical cancer after registration
n = 1: not surgical candidate
n = 2: participant withdrew consent
n = 3: eligibility unresolved
Eligible
n = 199
Excluded patients:
n = 2: clinical assessment data not received
Clinical FIGO stage
< IIB n = 180
≥ IIB n = 15
Unknown n = 2
Excluded patients:
(†)
n = 1: CT data not received
(††)
n = 3: patient refused MRI
n = 1: patient too large for MRI
n = 1: other unknown reason
(†††)
n = 1: scheduling problem for both CT and MRI
n = 1: MRI medical reason, other unknown CT reason
n = 1: scheduling problem MRI, other unknown CT reason
n = 1: CT and MRI data not received
n = 1: contrast IV problematic for CT, patient subsequently refused MRI since CT was not completed
Index tests: only MRI performed
n = 1 (†)
Index tests: only CT scan performed
n = 5 (††)
Index tests: CT and MRI scans performed
n = 186
Index tests: neither MRI nor CT scan performed
n = 5 (†††)
CT stage ≥ IIB, MRI stage ≥ IIB
n = 33
CT stage ≥ IIB, MRI stage < IIB
n = 11
CT stage < IIB, MRI stage ≥ IIB
n = 26
CT stage < IIB, MRI stage < IIB
n = 116
Missing surgery data: n = 1
No surgery: n = 1
No surgery: n = 3
No surgery: n = 1
No surgery: n = 2
Missing surgery data: n = 1
No surgery: n = 7
Missing surgery data: n = 1
Pathology stage
< IIB n = 1
Pathology stage
< IIB n = 1
≥ IIB n = 2
Pathology stage
< IIB n = 16
≥ IIB n = 12
Unknown n = 2
Pathology stage
< IIB n = 7
≥ IIB n = 3
Pathology stage
< IIB n = 16
≥ IIB n = 7
Unknown n = 1
Pathology stage
< IIB n = 91
≥ IIB n = 14
Unknown n = 3
Pathology stage
< IIB n = 2
≥ IIB n = 1
Missing n = 1

Fig 1. Patient flowchart. Of 208 patients enrolled in the study, nine were subsequently deemed ineligible; of the remaining 199 patients, 172 (86%) had complete data sets for inclusion in the data analysis. CT, computed tomography; MRI, magnetic resonance imaging; FIGO, International Federation of Gynecology and Obstetrics.

Hricak H. et al. J Clin Oncol 2005.

ACRIN 6651 – GOG 183

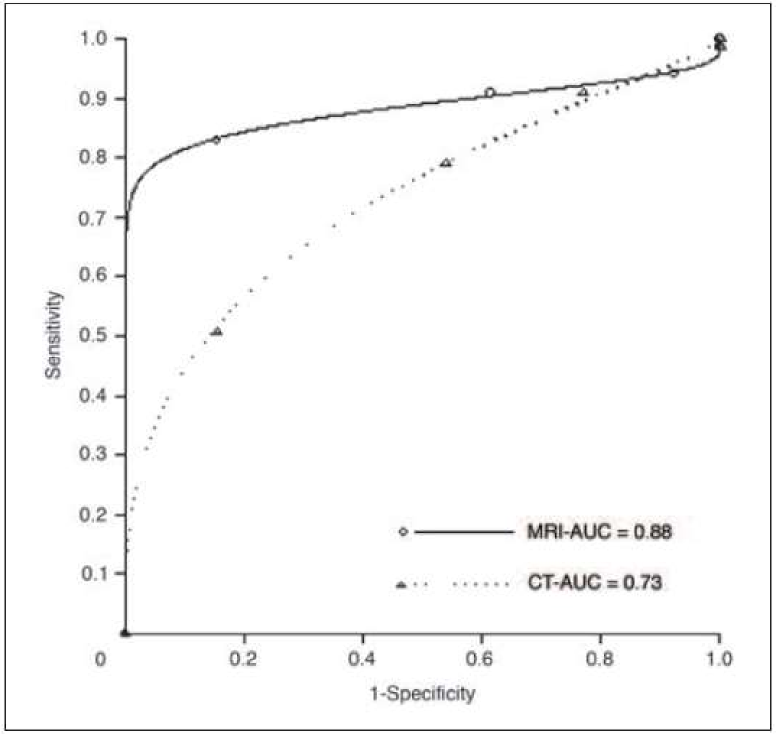

Fig 2. Plots of receiver operating characteristic (ROC) curves for the assessment of cervical involvement by magnetic resonance imaging (MRI) and computed tomography (CT). For each modality, the estimated area under the ROC curve is reported. MRI was significantly better than CT for detecting cervical tumor, as measured by the respective areas under the ROC curves (AUC).

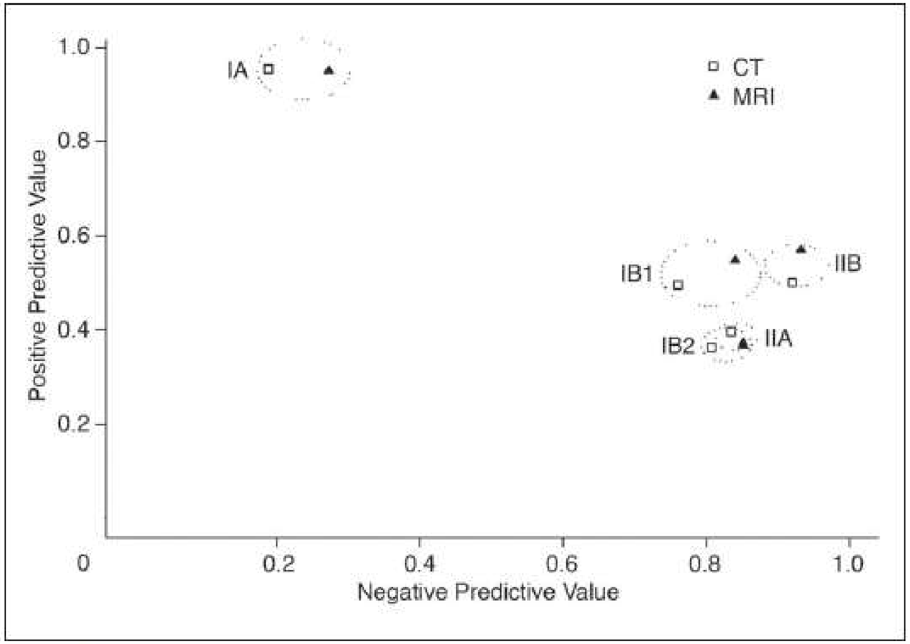

Fig 4. Positive and negative predictive values of computed tomography (CT) and magnetic resonance imaging (MRI) for different stage thresholds. When the threshold was set at stage IA, CT and MRI had high positive predictive value (PPV; 0.95; 0.90 to 0.98 for both modalities) and low negative predictive value (NPV; 0.19; 0.08 to 0.35; and 0.27; 0.11 to 0.50; respectively). PPV decreased and NPV increased as the stage threshold increased.

MRI correlated more closely with surgicopathological findings than CT or clinical examination

Hricak H. et al. J Clin Oncol 2005.

ACRIN 6651 – GOG 183

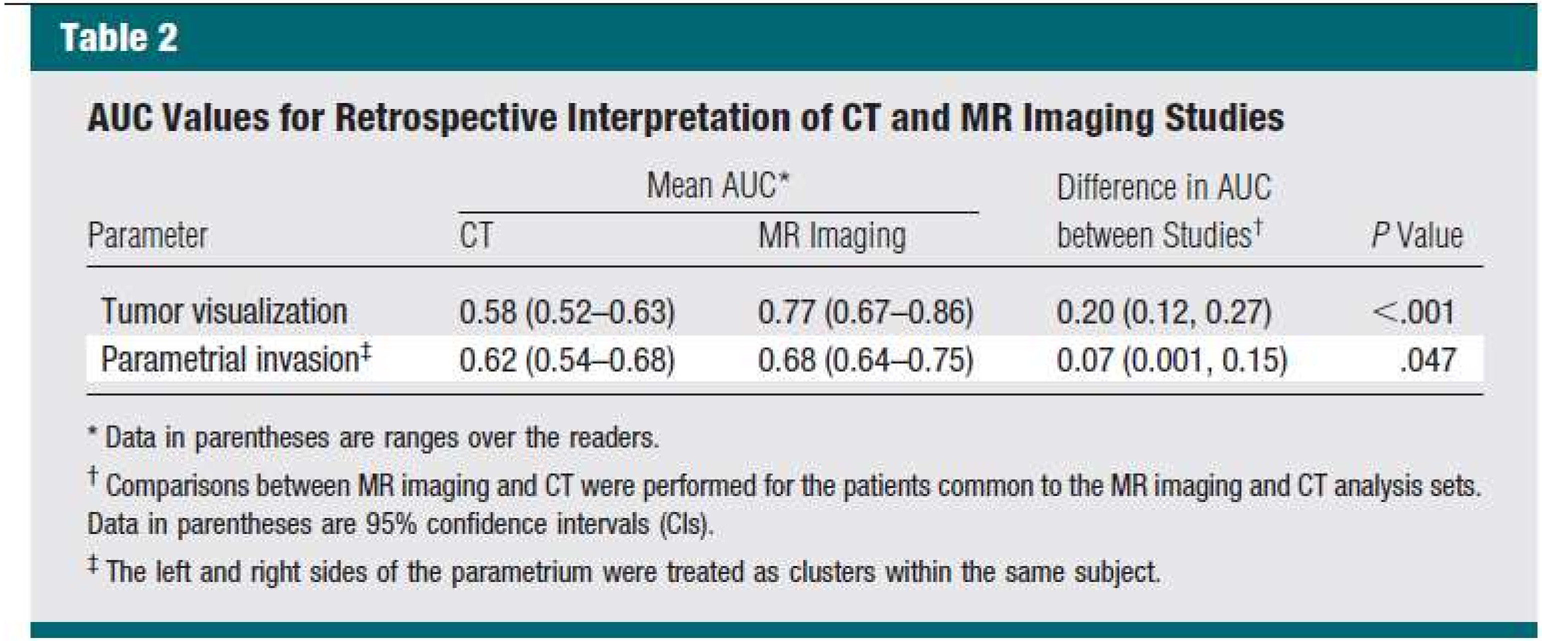

Table 2

AUC Values for Retrospective Interpretation of CT and MR Imaging Studies

Parameter	Mean AUC*		Difference in AUC between Studies[†]	*P* Value
	CT	MR Imaging		
Tumor visualization	0.58 (0.52–0.63)	0.77 (0.67–0.86)	0.20 (0.12, 0.27)	<.001
Parametrial invasion[‡]	0.62 (0.54–0.68)	0.68 (0.64–0.75)	0.07 (0.001, 0.15)	.047

* Data in parentheses are ranges over the readers.

[†] Comparisons between MR imaging and CT were performed for the patients common to the MR imaging and CT analysis sets. Data in parentheses are 95% confidence intervals (CIs).

[‡] The left and right sides of the parametrium were treated as clusters within the same subject.

MRI is better than CT for tumor visualization and depiction of parametrial invasion.

MRI has 94% accuracy and 95% NPV for determining PMI.

Hricak H. et al. Radiology 2007.

PMI: need for multiplanar FSE-T2

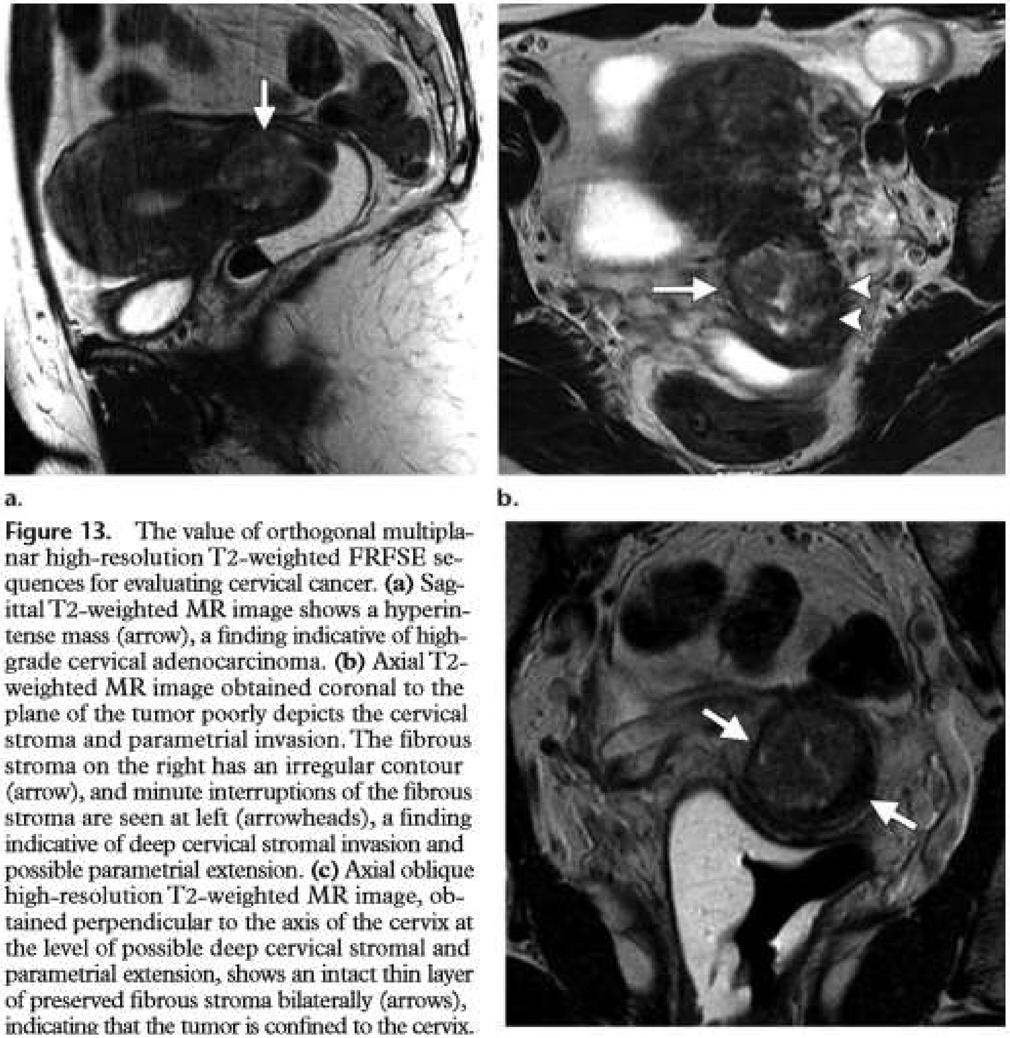
a.

b.

Figure 13. The value of orthogonal multiplanar high-resolution T2-weighted FRFSE sequences for evaluating cervical cancer. **(a)** Sagittal T2-weighted MR image shows a hyperintense mass (arrow), a finding indicative of high-grade cervical adenocarcinoma. **(b)** Axial T2-weighted MR image obtained coronal to the plane of the tumor poorly depicts the cervical stroma and parametrial invasion. The fibrous stroma on the right has an irregular contour (arrow), and minute interruptions of the fibrous stroma are seen at left (arrowheads), a finding indicative of deep cervical stromal invasion and possible parametrial extension. **(c)** Axial oblique high-resolution T2-weighted MR image, obtained perpendicular to the axis of the cervix at the level of possible deep cervical stromal and parametrial extension, shows an intact thin layer of preserved fibrous stroma bilaterally (arrows), indicating that the tumor is confined to the cervix.

Rauch G.M. et al. Radiographics 2014.

DWI to predict PMI

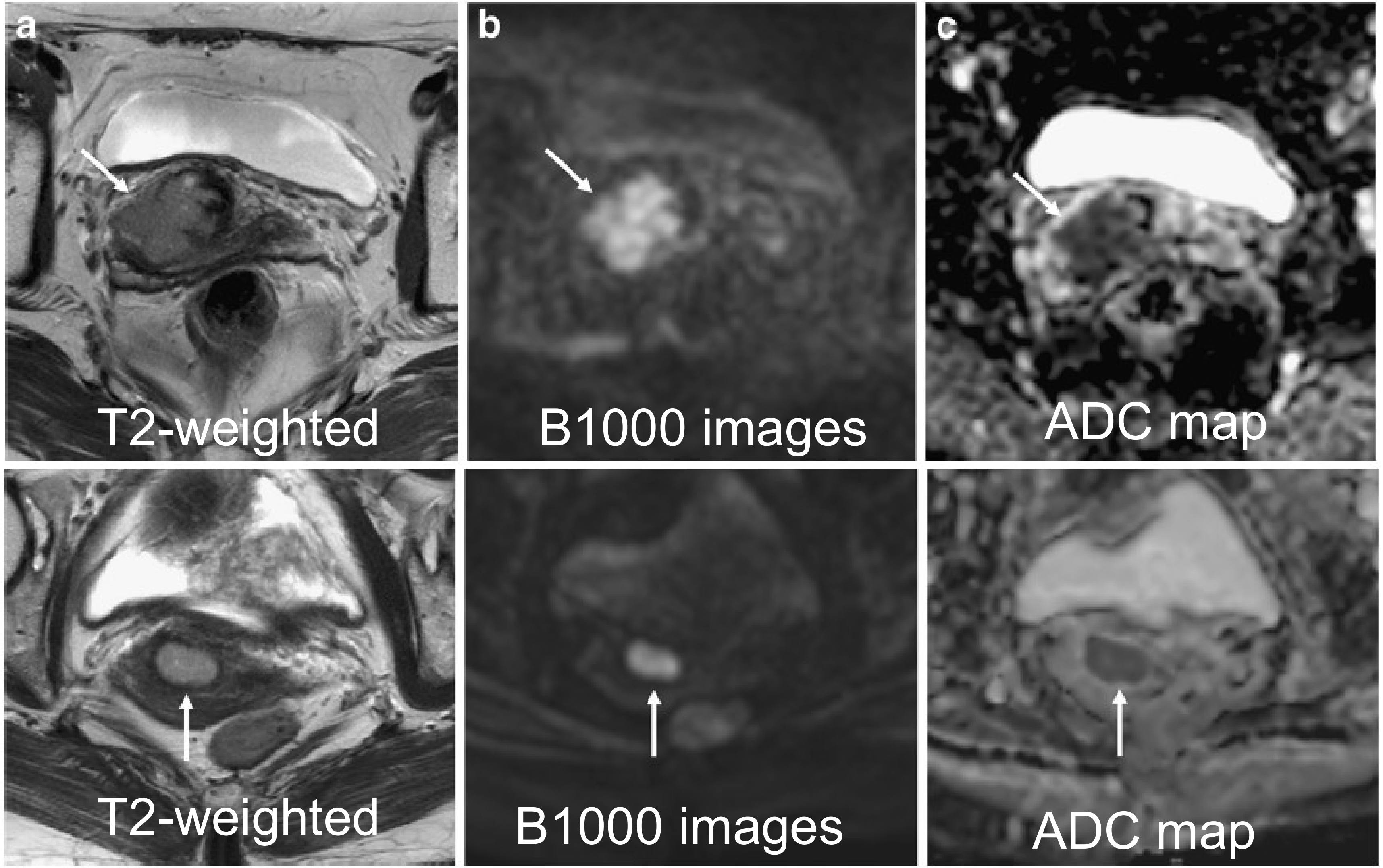
a
b
c
T2-weighted
B1000 images
ADC map
T2-weighted
B1000 images
ADC map

Park J.J. et al. Eur Radiol 2014.

Question 2: LNI?

Pelvic nodal involvement is noted in 30–50% of patients.

Para-aortic nodes are involved in 10–25% of patients.

Nodal staging: PET-CT

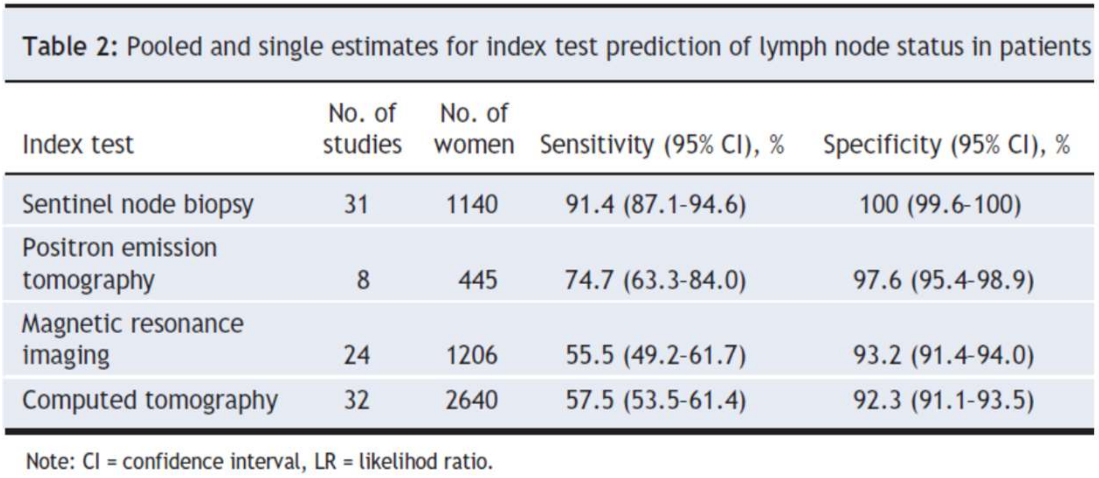

Table 2: Pooled and single estimates for index test prediction of lymph node status in patients

Index test	No. of studies	No. of women	Sensitivity (95% CI), %	Specificity (95% CI), %
Sentinel node biopsy	31	1140	91.4 (87.1-94.6)	100 (99.6-100)
Positron emission tomography	8	445	74.7 (63.3-84.0)	97.6 (95.4-98.9)
Magnetic resonance imaging	24	1206	55.5 (49.2-61.7)	93.2 (91.4-94.0)
Computed tomography	32	2640	57.5 (53.5-61.4)	92.3 (91.1-93.5)

Note: CI = confidence interval, LR = likelihod ratio.

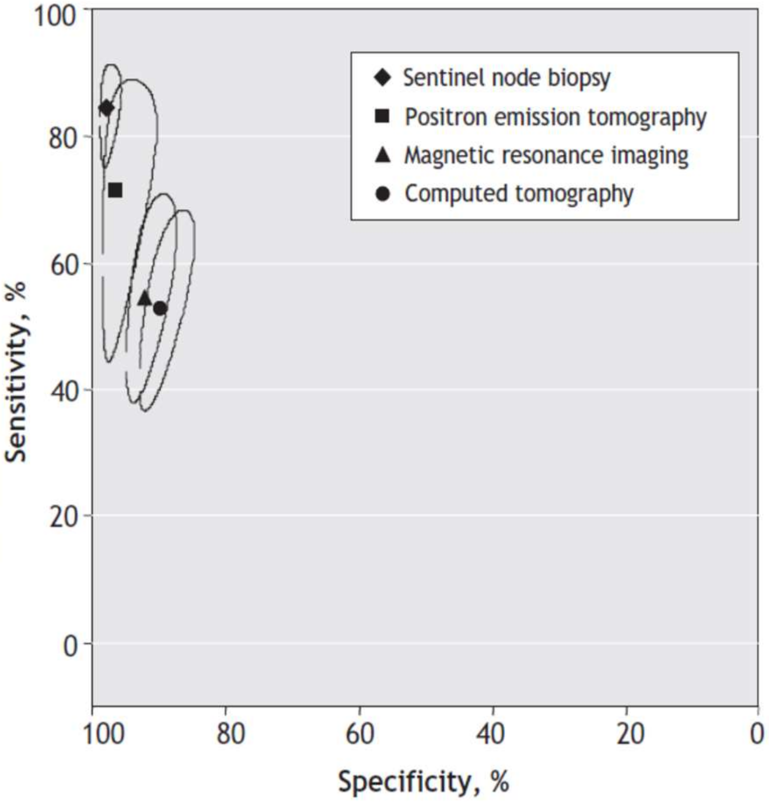

Meta-analysis of 72 studies including 5042 women:

PET: sens 75% and spec 98%

MRI: sens 56% and spec 93%

CT: sens 58% and spec 92%

Selman T. J. et al. CMAJ 2008.

Pelvic LN staging: added value of DWI

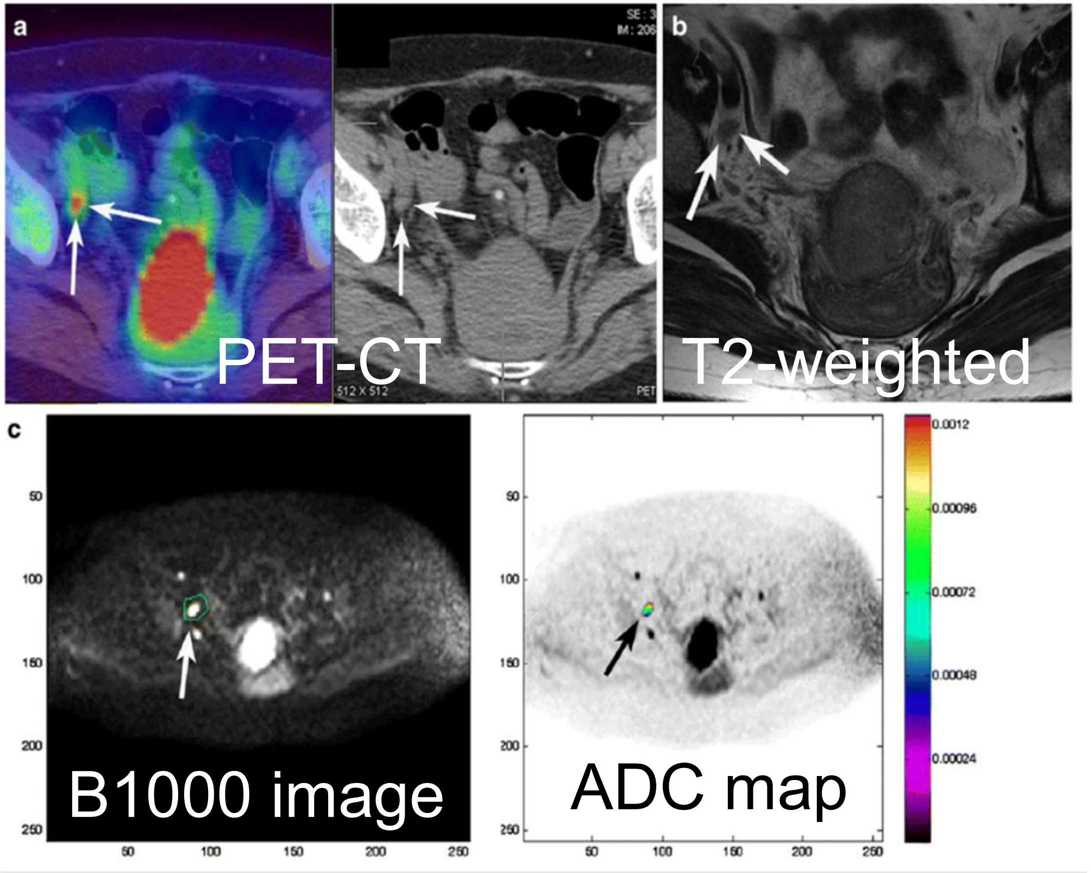
a
b
c
PET-CT
T2-weighted
B1000 image
ADC map
0.0012
0.00096
0.00072
0.00048
0.00024
50
100
150
200
250

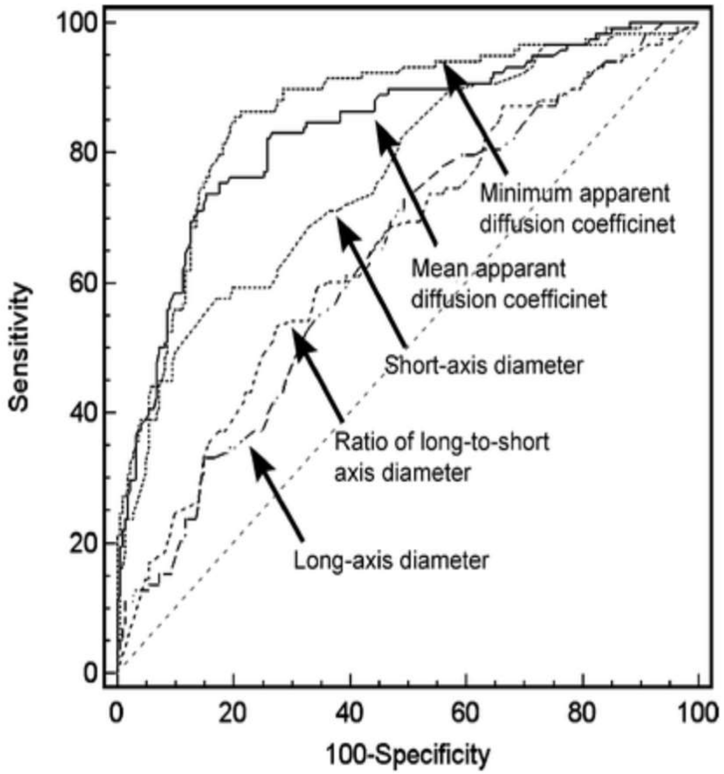

ADC showed superior correlation with PET-CT compared with conventional size-based criteria on T2-TSE.

Choi E. K. et al. Eur Radiol 2009.

Meta-analysis on DWI for nodal staging

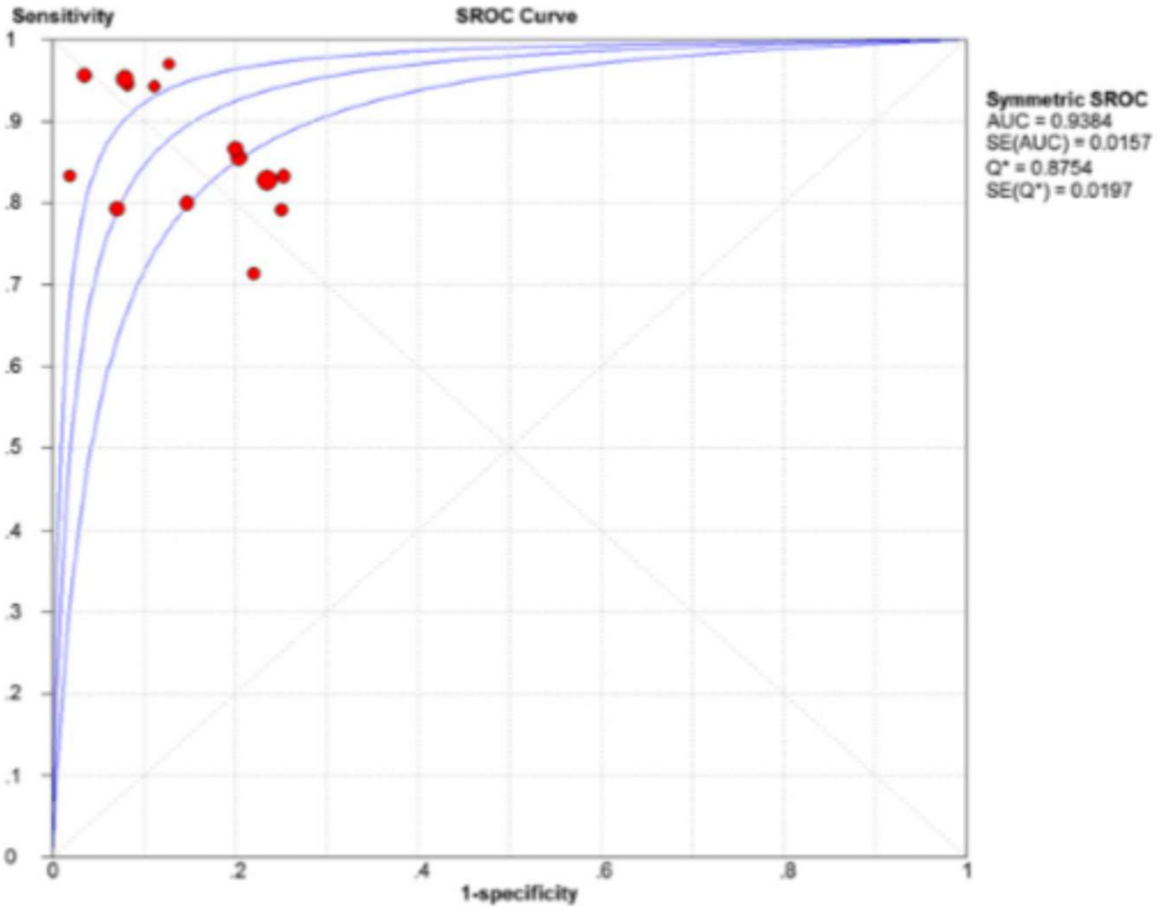

The pooled sensitivity and specificity of DWI were 0.86 and 0.84, respectively.

Shen G. et al. Br J Radiol 2015.

Meta-analysis on DWI for nodal staging

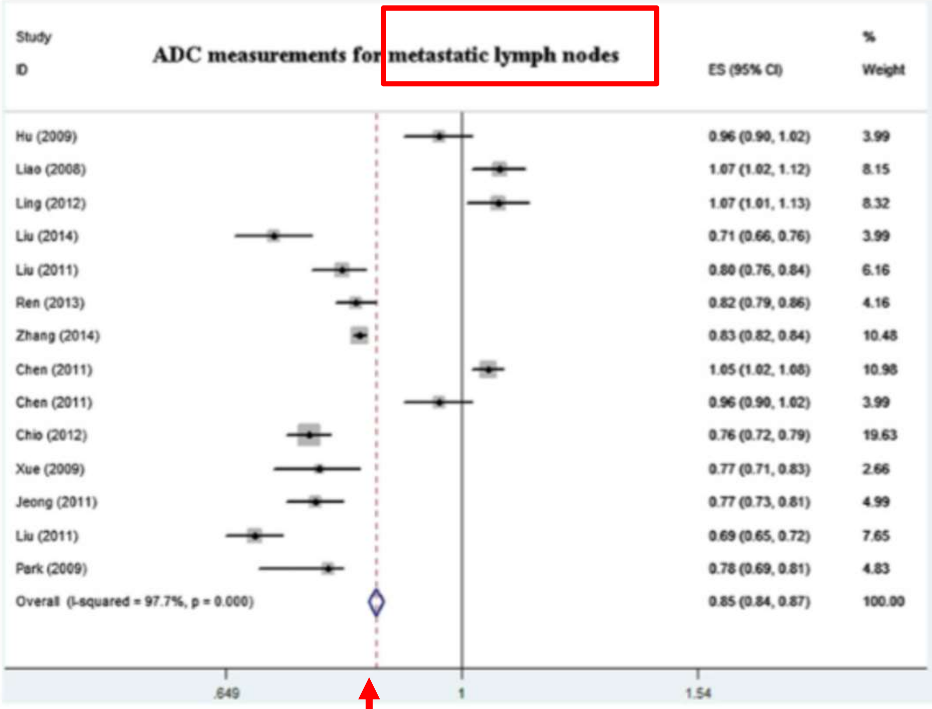

Study ID	ES (95% CI)	% Weight
Hu (2009)	0.96 (0.90, 1.02)	3.99
Liao (2008)	1.07 (1.02, 1.12)	8.15
Ling (2012)	1.07 (1.01, 1.13)	8.32
Liu (2014)	0.71 (0.66, 0.76)	3.99
Liu (2011)	0.80 (0.76, 0.84)	6.16
Ren (2013)	0.82 (0.79, 0.86)	4.16
Zhang (2014)	0.83 (0.82, 0.84)	10.48
Chen (2011)	1.05 (1.02, 1.08)	10.98
Chen (2011)	0.96 (0.90, 1.02)	3.99
Chio (2012)	0.76 (0.72, 0.79)	19.63
Xue (2009)	0.77 (0.71, 0.83)	2.66
Jeong (2011)	0.77 (0.73, 0.81)	4.99
Liu (2011)	0.69 (0.65, 0.72)	7.65
Park (2009)	0.78 (0.69, 0.81)	4.83
Overall (I-squared = 97.7%, p = 0.000)	0.85 (0.84, 0.87)	100.00

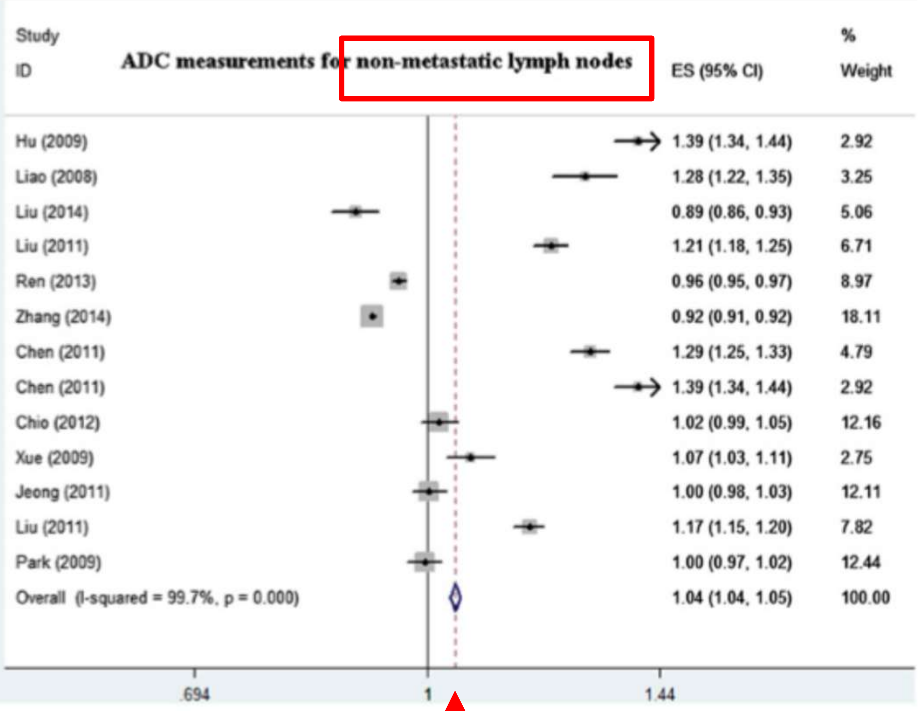

Study ID	ES (95% CI)	% Weight
Hu (2009)	1.39 (1.34, 1.44)	2.92
Liao (2008)	1.28 (1.22, 1.35)	3.25
Liu (2014)	0.89 (0.86, 0.93)	5.06
Liu (2011)	1.21 (1.18, 1.25)	6.71
Ren (2013)	0.96 (0.95, 0.97)	8.97
Zhang (2014)	0.92 (0.91, 0.92)	18.11
Chen (2011)	1.29 (1.25, 1.33)	4.79
Chen (2011)	1.39 (1.34, 1.44)	2.92
Chio (2012)	1.02 (0.99, 1.05)	12.16
Xue (2009)	1.07 (1.03, 1.11)	2.75
Jeong (2011)	1.00 (0.98, 1.03)	12.11
Liu (2011)	1.17 (1.15, 1.20)	7.82
Park (2009)	1.00 (0.97, 1.02)	12.44
Overall (I-squared = 99.7%, p = 0.000)	1.04 (1.04, 1.05)	100.00

0,85 (95% CI 0,84 – 0,87)

1,04 (95% CI 1,04 – 1,05)

The heterogeneity was relatively high between studies.
Large-scale, high-quality trials with standard protocols are required.

$p < 0,05$

Shen G. et al. Br J Radiol 2015.

ESTRO School

Para-aortic nodes

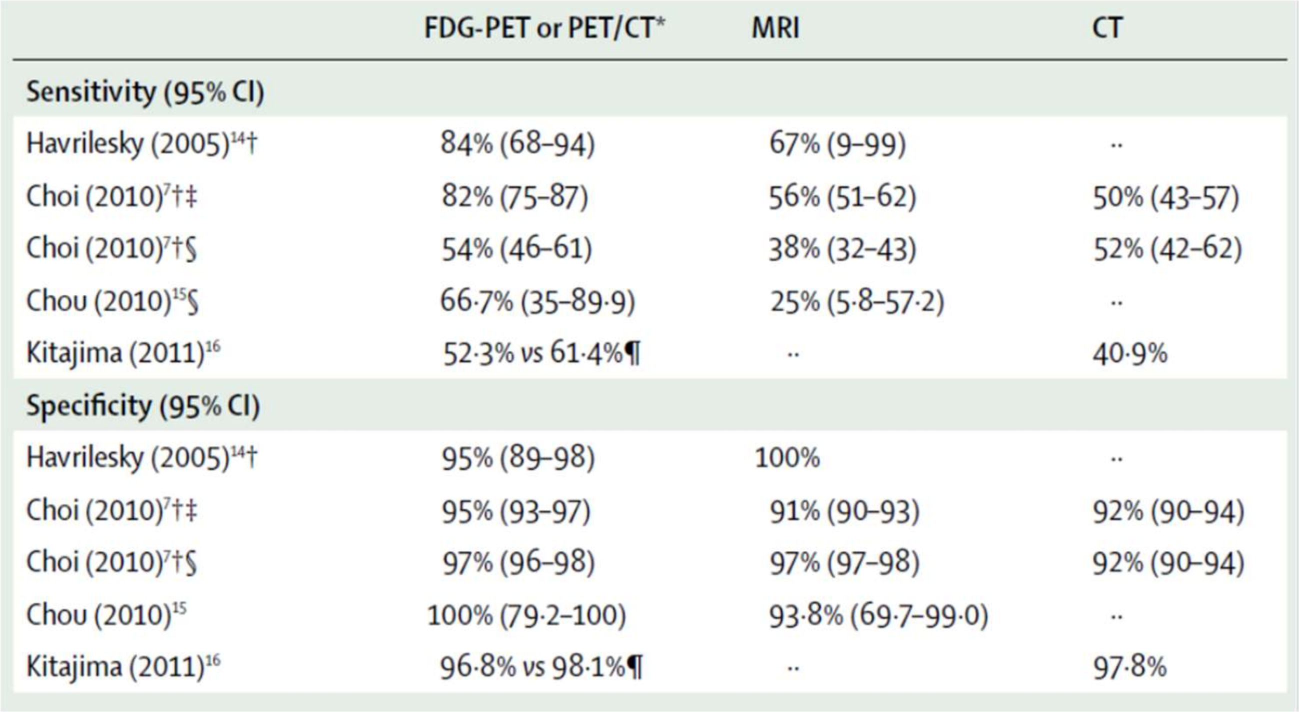

	FDG-PET or PET/CT*	MRI	CT
Sensitivity (95% CI)			
Havrilesky (2005)[14]†	84% (68–94)	67% (9–99)	··
Choi (2010)[7]†‡	82% (75–87)	56% (51–62)	50% (43–57)
Choi (2010)[7]†§	54% (46–61)	38% (32–43)	52% (42–62)
Chou (2010)[15]§	66·7% (35–89·9)	25% (5·8–57·2)	··
Kitajima (2011)[16]	52·3% vs 61·4%¶	··	40·9%
Specificity (95% CI)			
Havrilesky (2005)[14]†	95% (89–98)	100%	··
Choi (2010)[7]†‡	95% (93–97)	91% (90–93)	92% (90–94)
Choi (2010)[7]†§	97% (96–98)	97% (97–98)	92% (90–94)
Chou (2010)[15]	100% (79·2–100)	93·8% (69·7–99·0)	··
Kitajima (2011)[16]	96·8% vs 98·1%¶	··	97·8%

The prevalence of para-aortic nodal metastasis locally-advanced disease is 10–25%.
The true-positive rate of PET is high, suggesting that surgical staging is not necessary if uptake takes place in the para-aortic region.
However, false-negative results (in the para-aortic region) have been recorded in 12% of patients, rising to 22% in those with uptake during PET of the pelvic nodes.

Gouy S. et al. Lancet Oncol 2012.

Pre-treatment assessment: conclusions

- Local staging: MRI
  - If suspect for bladder invasion: cystoscopy
  - If suspect for rectal invastion: rectoscopy

- Nodal and distant staging: PET-CT
  - If pelvic LN+, consider surgical para-aortic staging

MRI in radiotherapy for cervical cancer

1. Cervical cancer

2. MRI & FDG-PET/CT for pre-treatment assessment of cervical cancer

3. **MRI for external beam radiotherapy (EBRT) planning:**
    1. **Target volume delineation**
    2. **Image-guidance**

4. MRI for brachytherapy planning

5. MRI for response assessment

Question 1: target volume delineation

The most clinically relevant benefit of MRI for cervical cancer planning lies in the clear visualization of the cervical tumor in multiple planes allowing for a reliable volumetric definition of the target volume.

GTV delineation

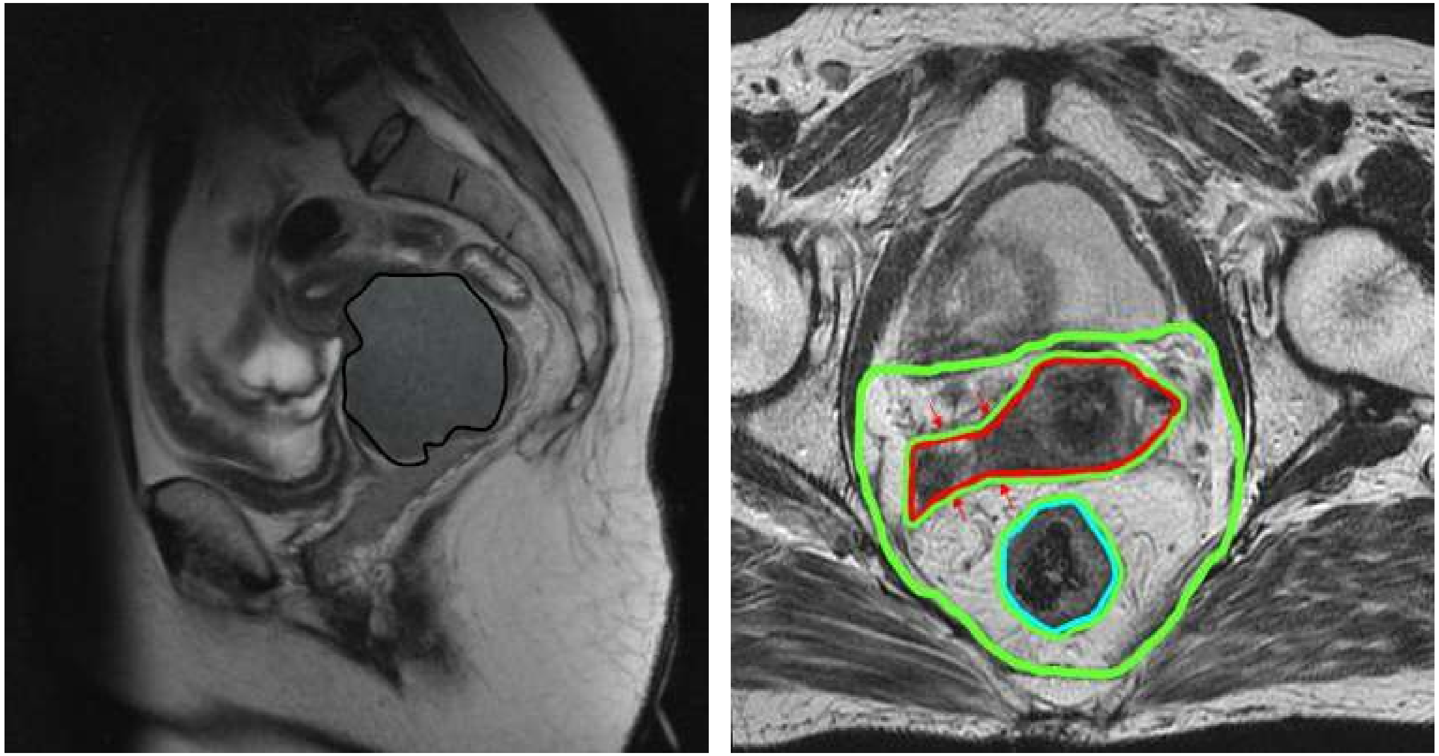

GTV = high SI zones in cervix & surroundings on T2

Lim K. et al. Int J Radiat Oncol Biol Phys 2011.

PET/MRI for GTV

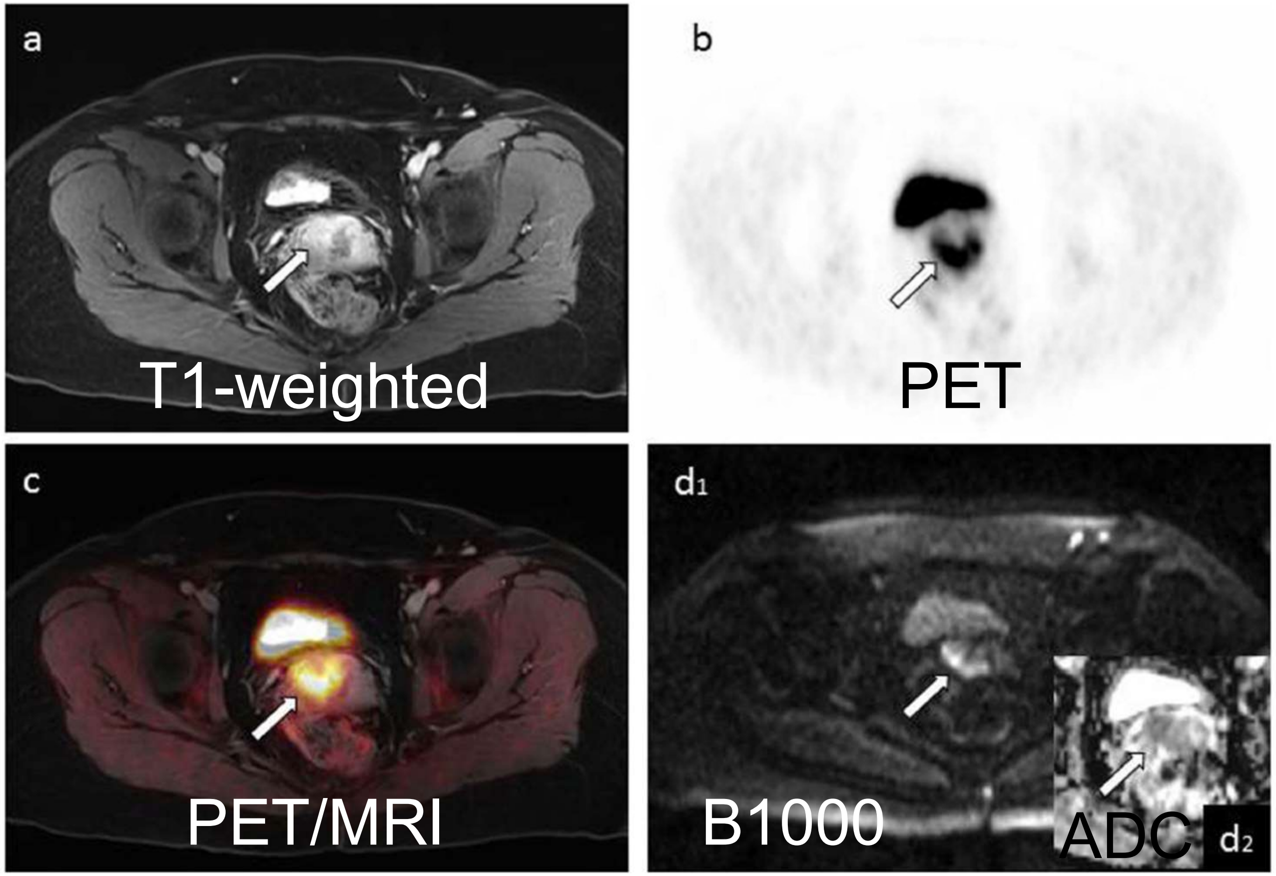
a
T1-weighted
b
PET
c
PET/MRI
d1
B1000
ADC
d2

Grueneisen J. et al. Plos One 2014.

Correlation between SUV_{max} & ADC_{min}

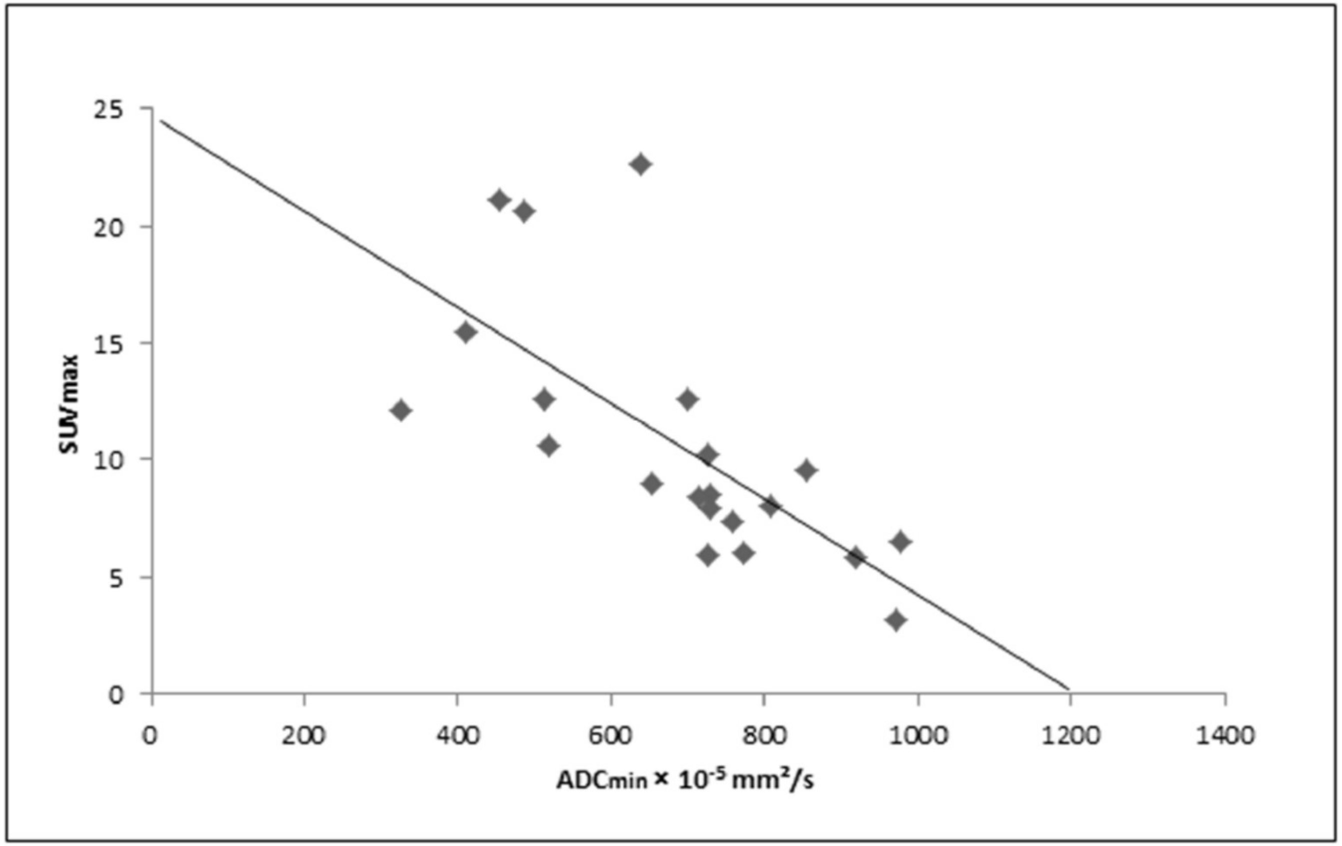

Grueneisen J. et al. Plos One 2014.

CTV delineation

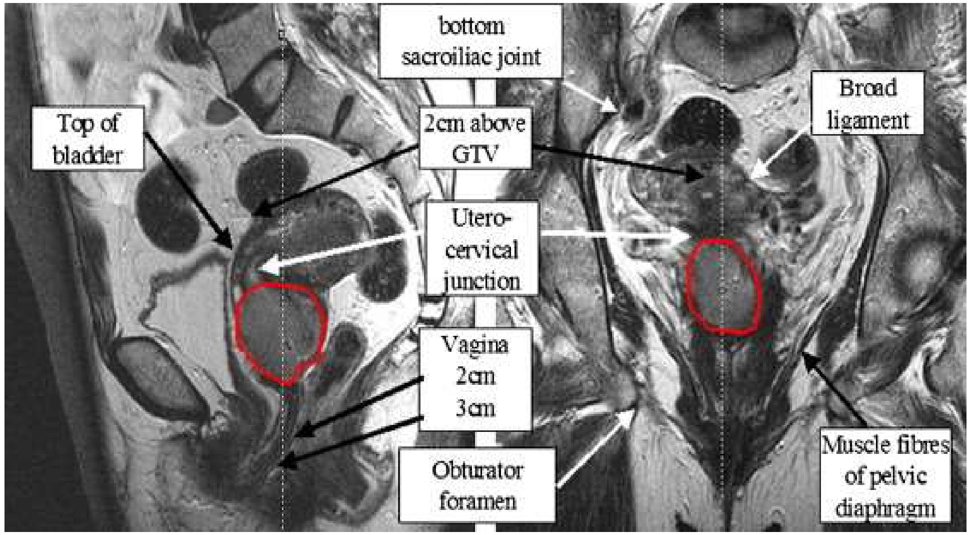
bottom sacroiliac joint
Top of bladder
2cm above GTV
Broad ligament
Utero-cervical junction
Vagina 2cm 3cm
Obturator foramen
Muscle fibres of pelvic diaphragm

GTV + margin of at least 10 mm, unless safe barriers (bone, muscle).

Parametria, uterus & (part of) vagina (at least 20 mm below GTV).

Pelvic LN: parametrial, pararectal, internal iliac, external iliac, presacral & common iliac.

Inguinal LN if stage IIIA. Para-Aortic LN only if involved?

Nodal volumes should follow the relevant vessels with a margin of 7 mm in the loose connective tissue.

Lim K. et al. Int J Radiat Oncol Biol Phys 2011.

CTV consensus guidelines (1)

Tumoral CTV:

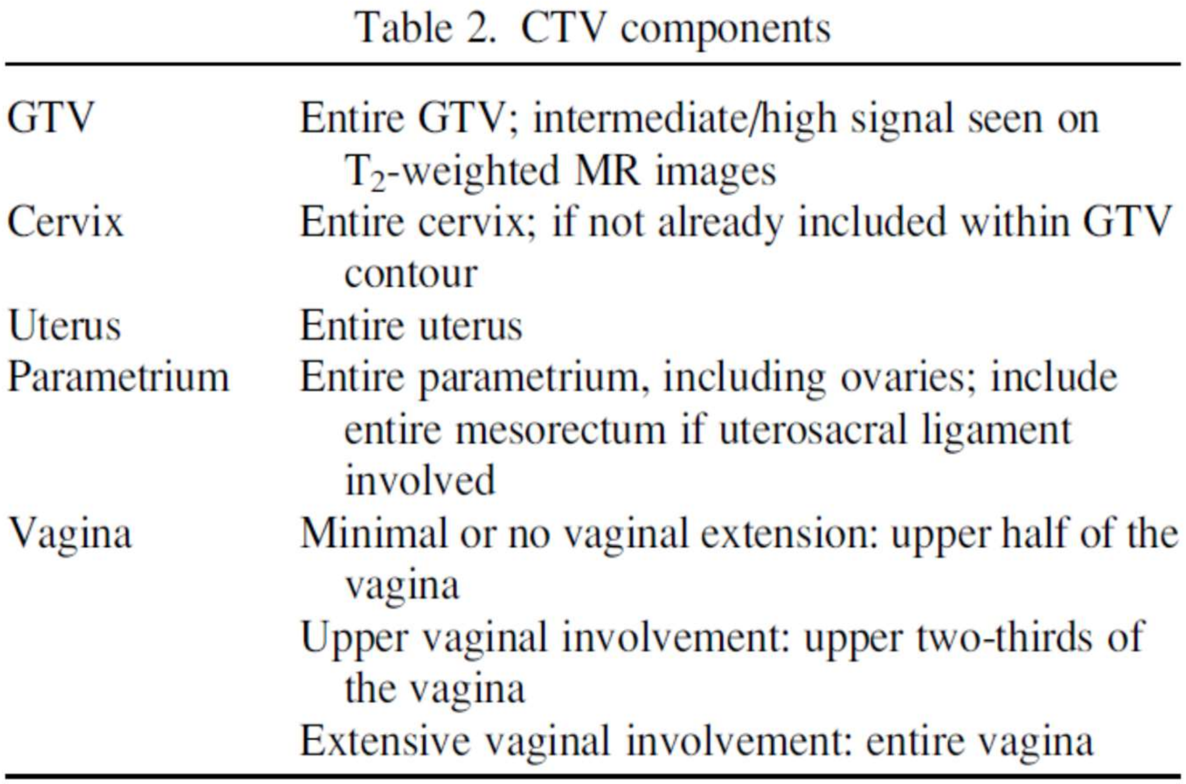

Table 2. CTV components

GTV	Entire GTV; intermediate/high signal seen on T_2-weighted MR images
Cervix	Entire cervix; if not already included within GTV contour
Uterus	Entire uterus
Parametrium	Entire parametrium, including ovaries; include entire mesorectum if uterosacral ligament involved
Vagina	Minimal or no vaginal extension: upper half of the vagina Upper vaginal involvement: upper two-thirds of the vagina Extensive vaginal involvement: entire vagina

Lim K. et al. Int J Radiat Oncol Biol Phys 2011.

CTV consensus guidelines (2)

Nodal CTV:

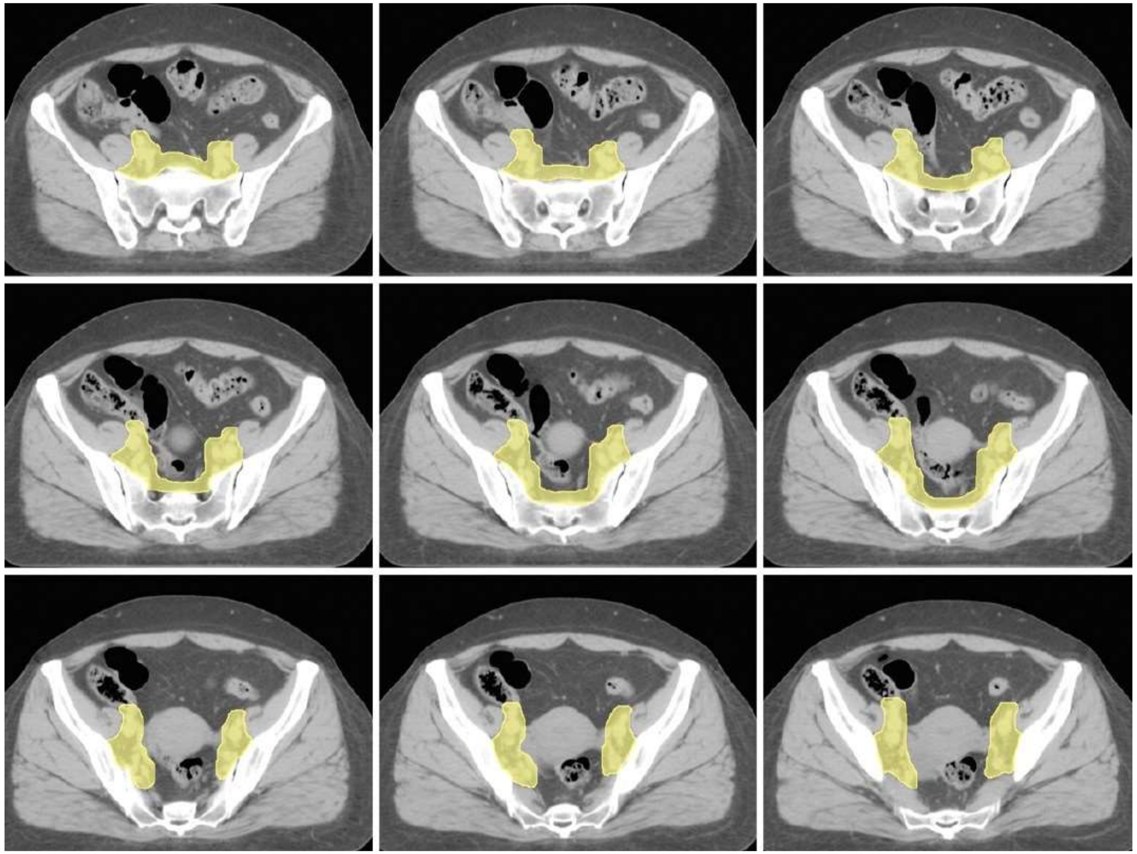

Toita T. et al. Jpn J Clin Oncol 2010.

PTV delineation

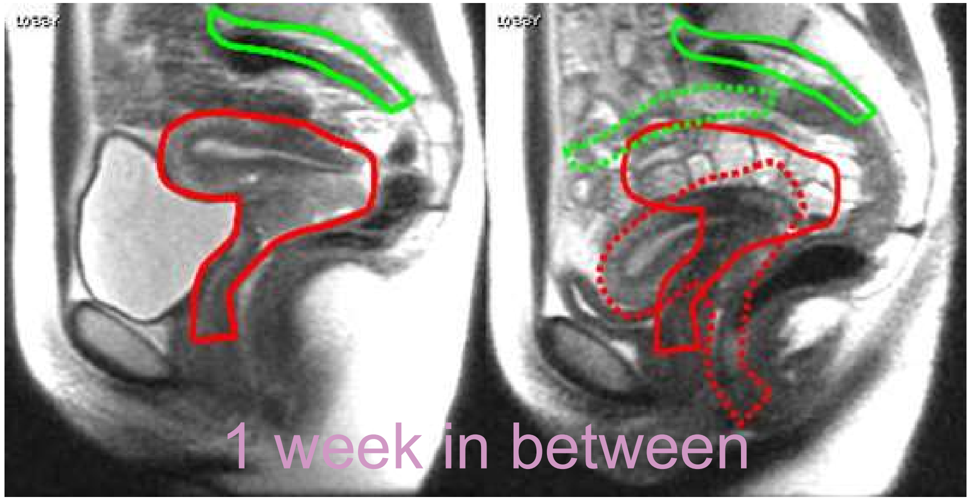

The combination of 2 problems:

- unpredictable organ motion
- substantial tumor regression

resulted in conservative margin recommendations by the Consortium.

PTV margins of 1.5 to 2 cm around the CTV were recommended if good quality daily soft tissue verification was available during treatment.

A PTV margin of 7 mm around the nodal CTV was agreed upon in line with previous recommendations in the postoperative cervix cancer setting (e.g., RTOG 0418).

Lim K. et al. Int J Radiat Oncol Biol Phys 2011.

Question 2: inter- and intrafraction mobility

MRI is particularly useful to measure motion variability due to its excellent soft tissue visualization, the absence of radiation, the availability of multiplanar imaging and fast 4D imaging. Using serial MRIs during external beam radiation for cervical cancer demonstrates that the uterus, cervix, vagina and even pelvic lymph nodes have considerable motion between treatments due to changes in bladder filling, rectal filling and other internal motion.

— GTV — CTV — PTV

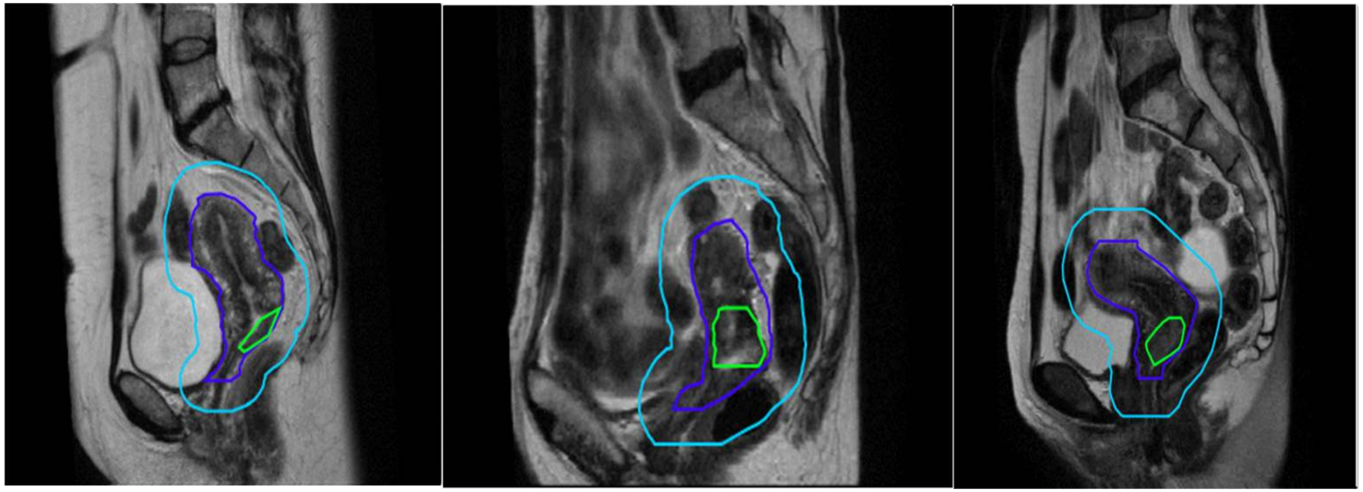

Slide courtesy of U. van der Heide

MRI-guided IMRT: organ motion (1)

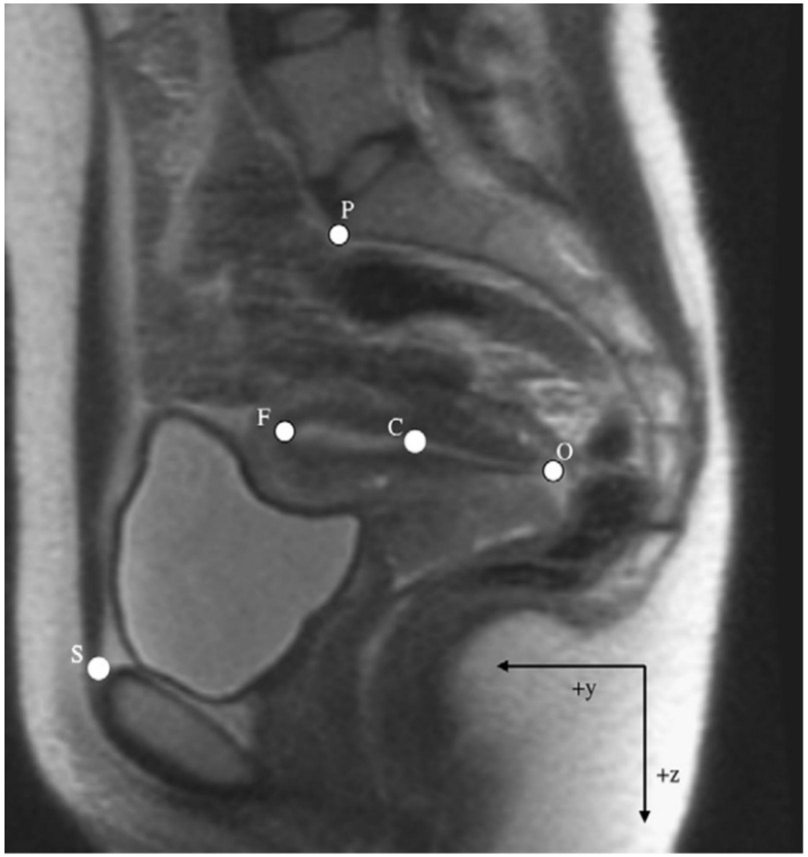

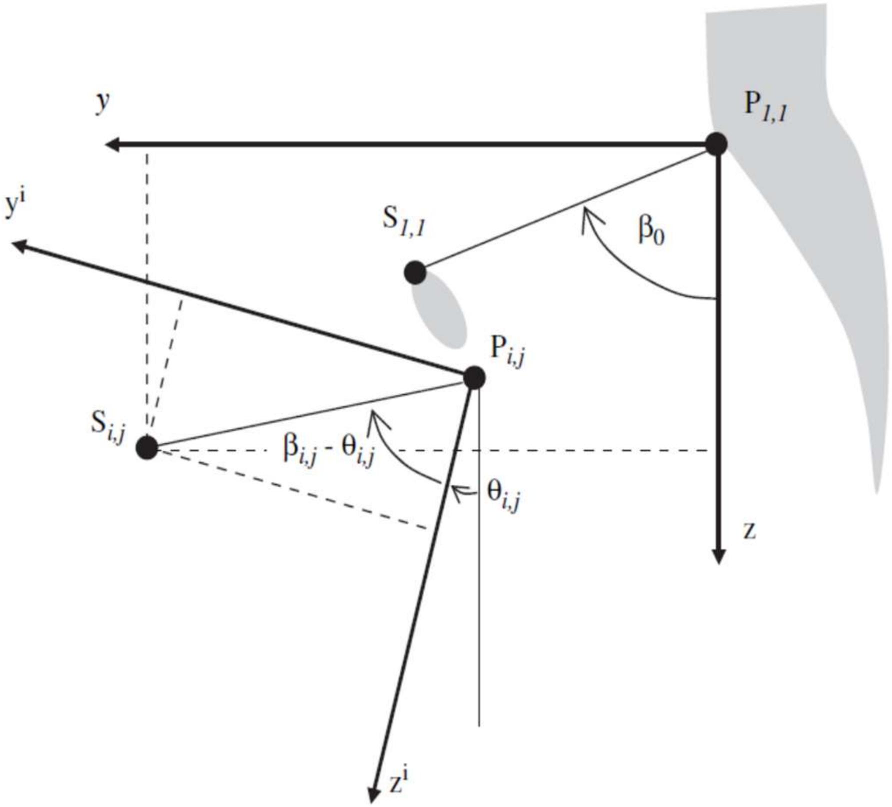
y
$P_{1,1}$
y^i
$S_{1,1}$
β_0
$P_{i,j}$
$S_{i,j}$
$\beta_{i,j} - \theta_{i,j}$
$\theta_{i,j}$
z
z^i

Large interscan motion was found for all 3 POI, only partially explained by variations in bladder and rectal filling. The margins required to encompass 90% of the interscan motion were 4 cm at the fundus and 1.5 cm at the external cervical os.

Chan P. et al. Int J Radiat Oncol Biol Phys 2008.

MRI-guided IMRT: organ motion (2)

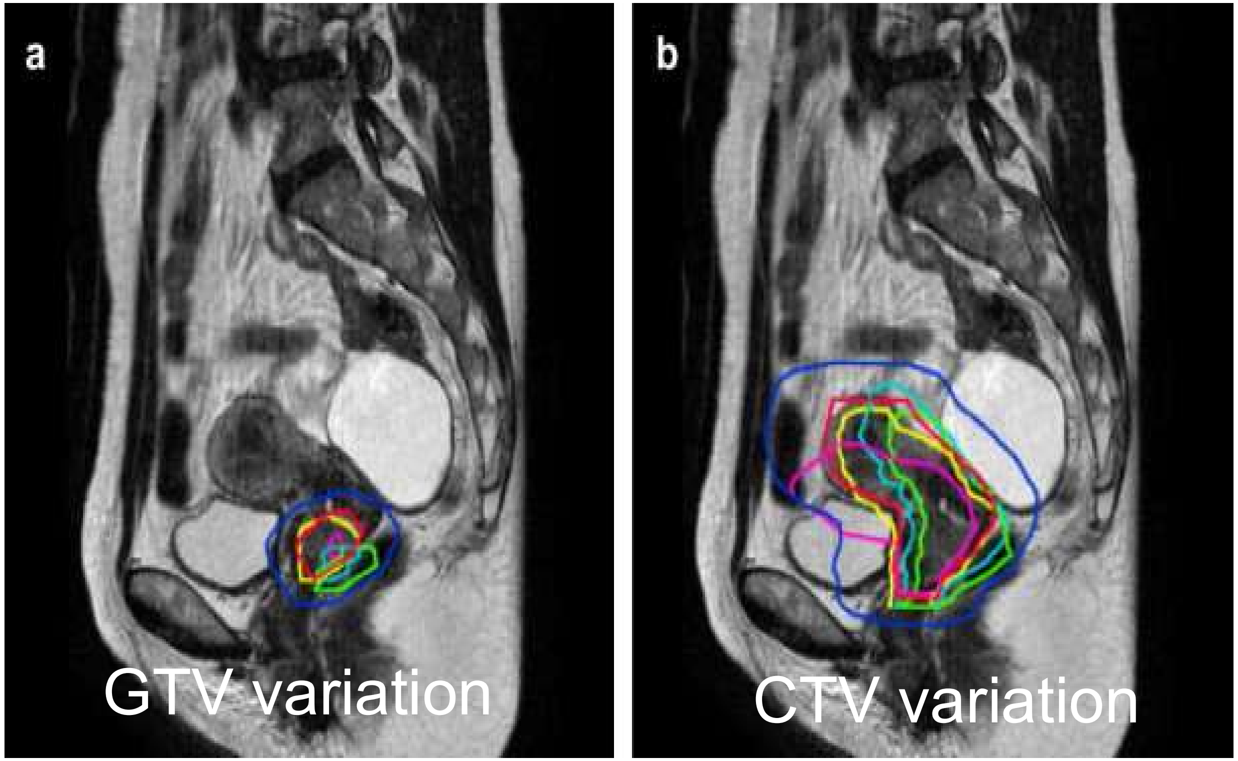
a
b
GTV variation
CTV variation

The CTV required margins of 24, 17, 12, 16, 11 and 8 mm. The shift of the GTV and CTV in the AP directions correlated weakly with the change in rectal volume. For the bladder, the correlations were even weaker.

---

van de Bunt L. et al. Radiother Oncol 2008.

MRI-guided IMRT: organ motion (3)

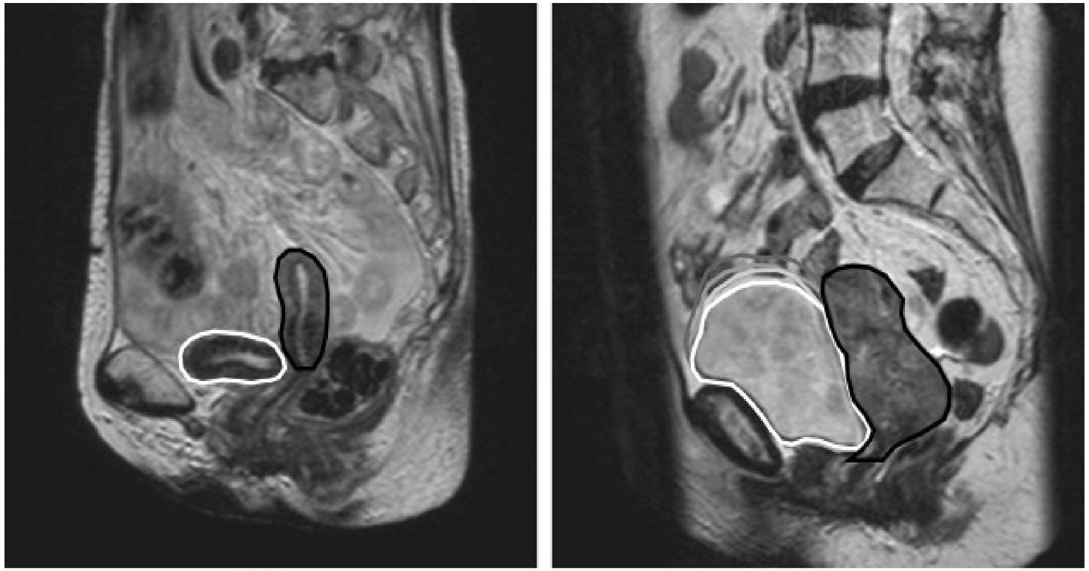

- Twenty-two patients underwent 2–3 offline MRI exams before and during their radiation treatment.
- Each MRI exam included four sagittal and four axial MRI scans alternately within 16 min.
- The maximum (residual) motions within 16 min for all points on the CTV contour for 90% of the MRI exams without registration, with rigid bony anatomy registration, and with rigid soft tissue registration were 10.6, 9.9, and 4.0 mm.
- A significant but weak correlation was found between intrafraction bladder filling and CTV motion.

Kerkhof E.M. et al. Radiother Oncol 2009.

Online MRI guidance

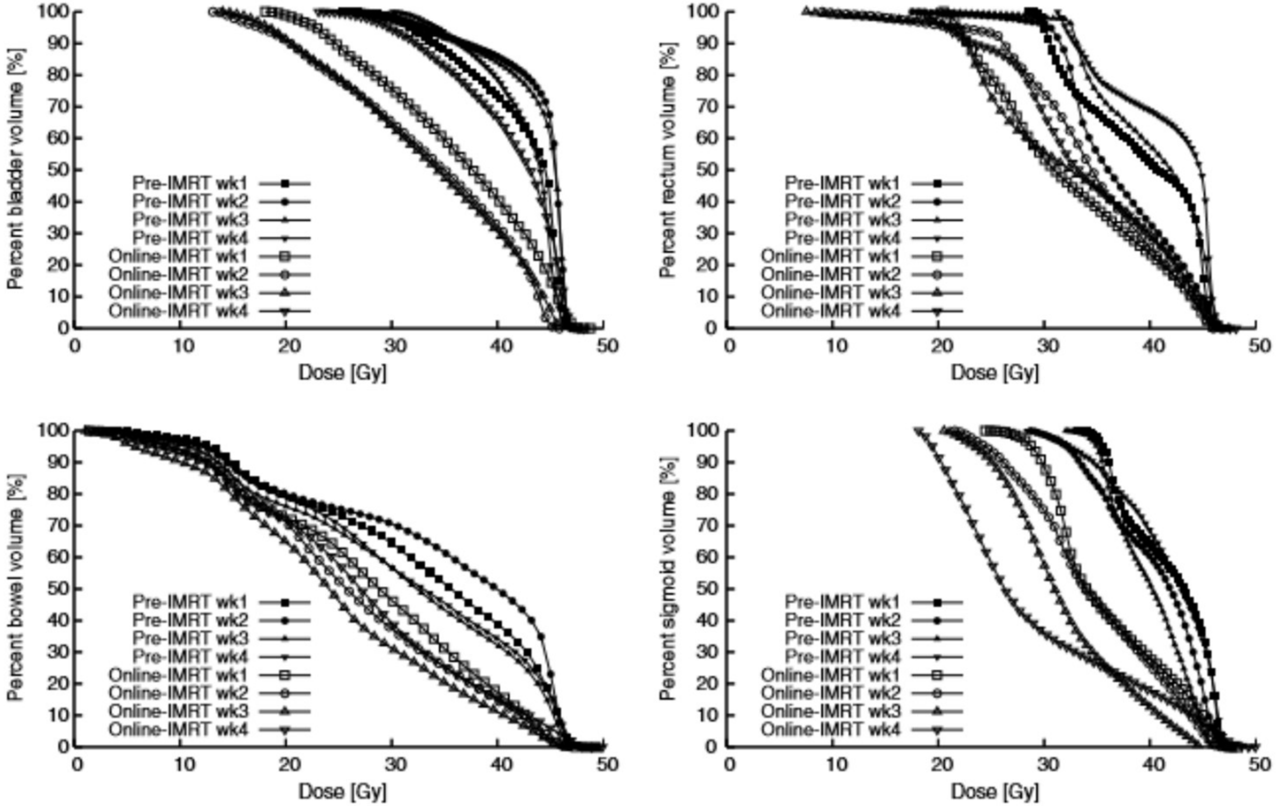

Fig. 5. Dose volume histograms of the bladder, rectum, bowel, and sigmoid for patient 3 for both pre-IMRT and online-IMRT.

Online-IMRT compared to pre-IMRT significantly reduced the volume of healthy tissue irradiated to all dose levels, except V10$_{Gy}$.

Kerkhof E. M. et al. Radiother Oncol 2008.

UCLA

GYN: Endometrial

VIEWRAY | Visibly Different

Confidential Information

GYN- Endometrial

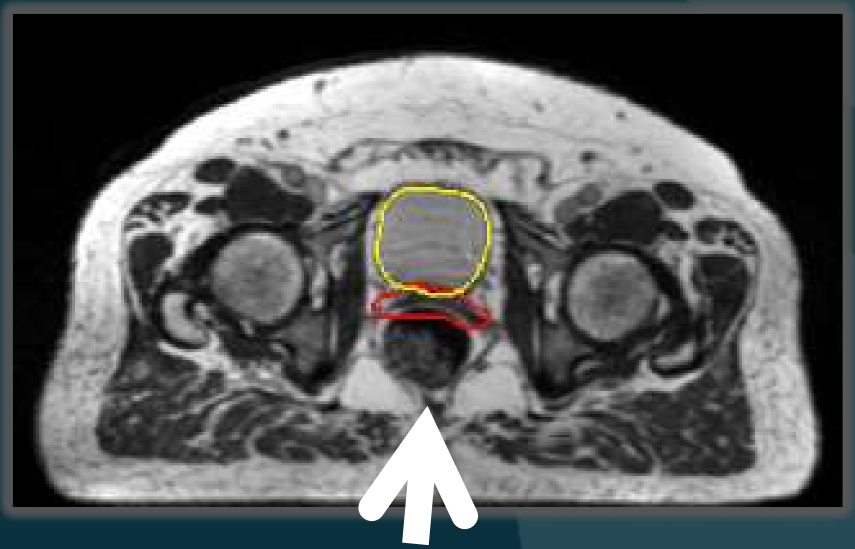

Planning MRI: Note Rectal Fill

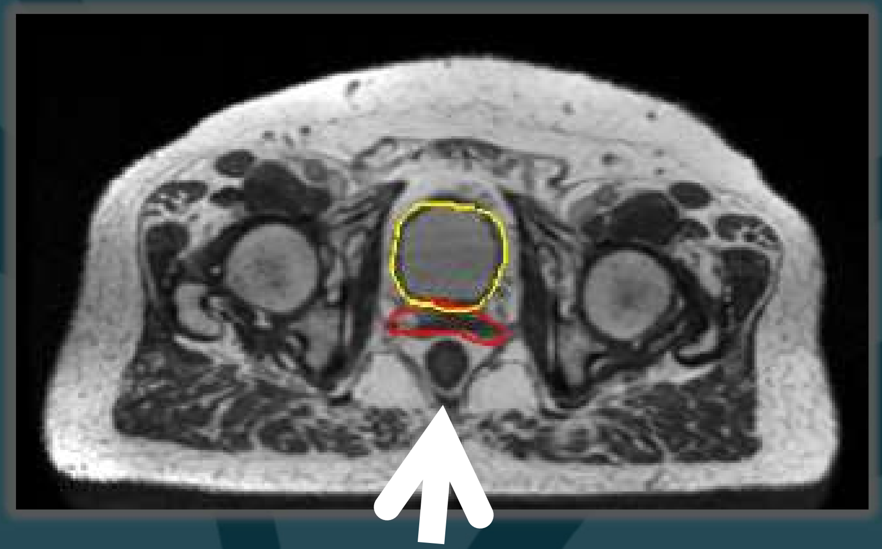

Daily MRI: Note Rectal Fill Change

GYN- Endometrial

Fraction #5

PTV coverage affected up to 20% of Beam-on time

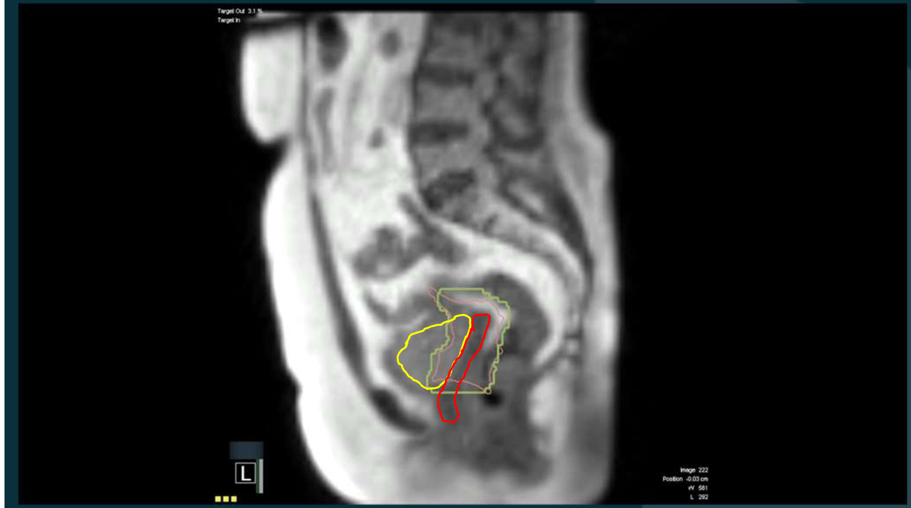

Fraction #7

PTV coverage affected up to 25% of Beam-on time

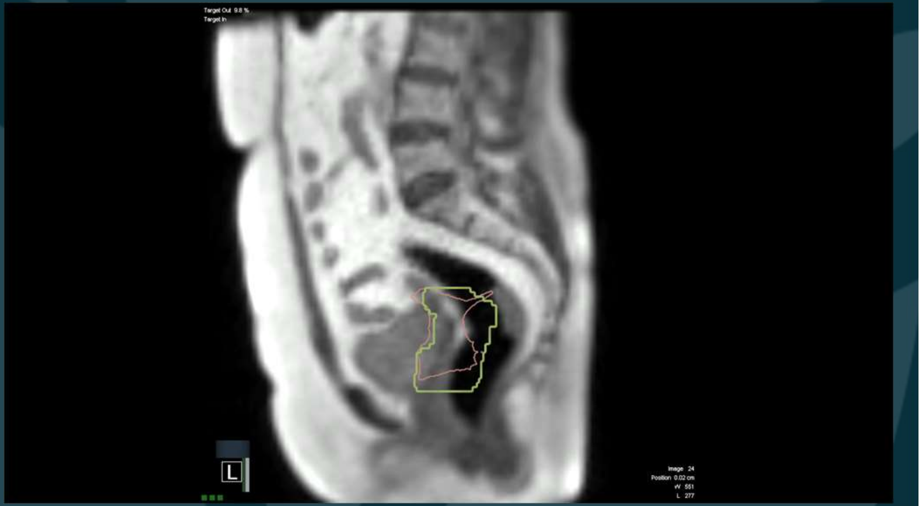

GYN- Endometrial

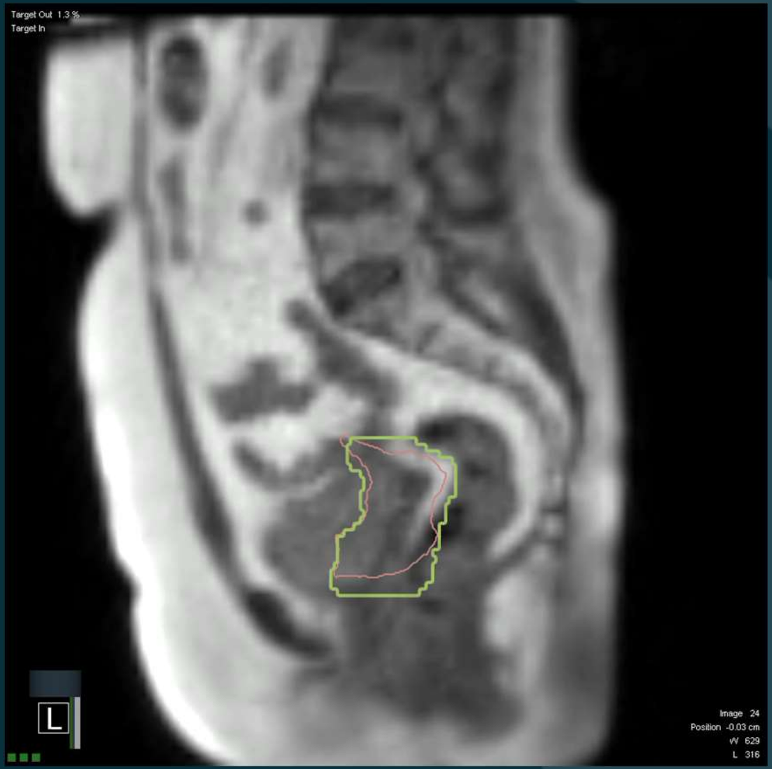
Target Out 1.3 %
Target In
L
Image 24
Position -0.03 cm
W 629
L 316

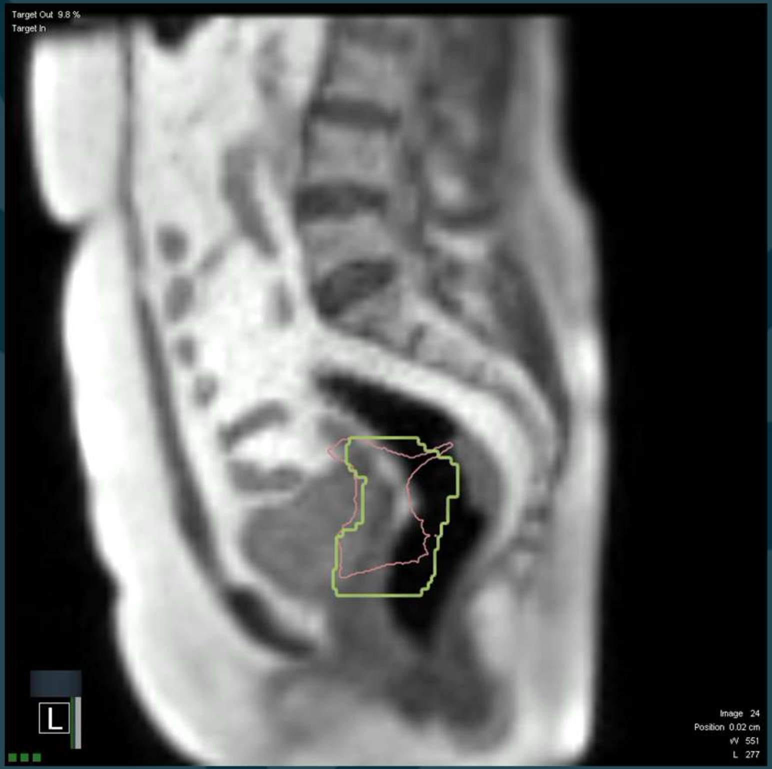
Target Out 9.8 %
Target In
L
Image 24
Position 0.02 cm
W 551
L 277

MRI-guided IMRT: what about LN?

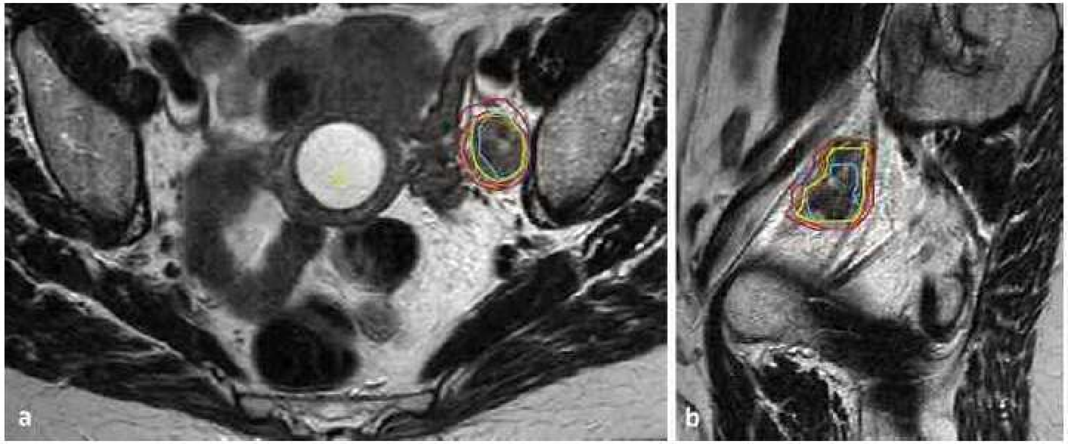

Fig. 1. Pre-treatment transversal (a) and sagittal (b) T2-weighted MR image of a patient with an enlarged lymph node in the left obturator region. The delineations of the node on the pre-treatment scan (yellow line), scan in week 1 (green line), week 2 (orange line), week 3 (purple line) and week 4 (blue line) are all overlaid on the pre-treatment MR image. The red line represents the manually derived margin to encompass the node in all weeks.

Nodal volume regression from the pre-treatment situation to week 4 was 58% on average. Nodal volumes partly increased between the pre-treatment scans and the scans in weeks 1–3, but in week 4 all nodes except one had regressed.
Around the nodal volumes ITV margins accounting for volume changes and position shifts of 7.0, 4.0, 7.0, 8.0, 7.0 and 9.0 mm to the medial, lateral, anterior, posterior, superior and inferior directions were needed to cover 95% of all nodes.

Schippers M. et al. Radiother Oncol 2014.

MRI-guided IMRT: tumor shrinkage

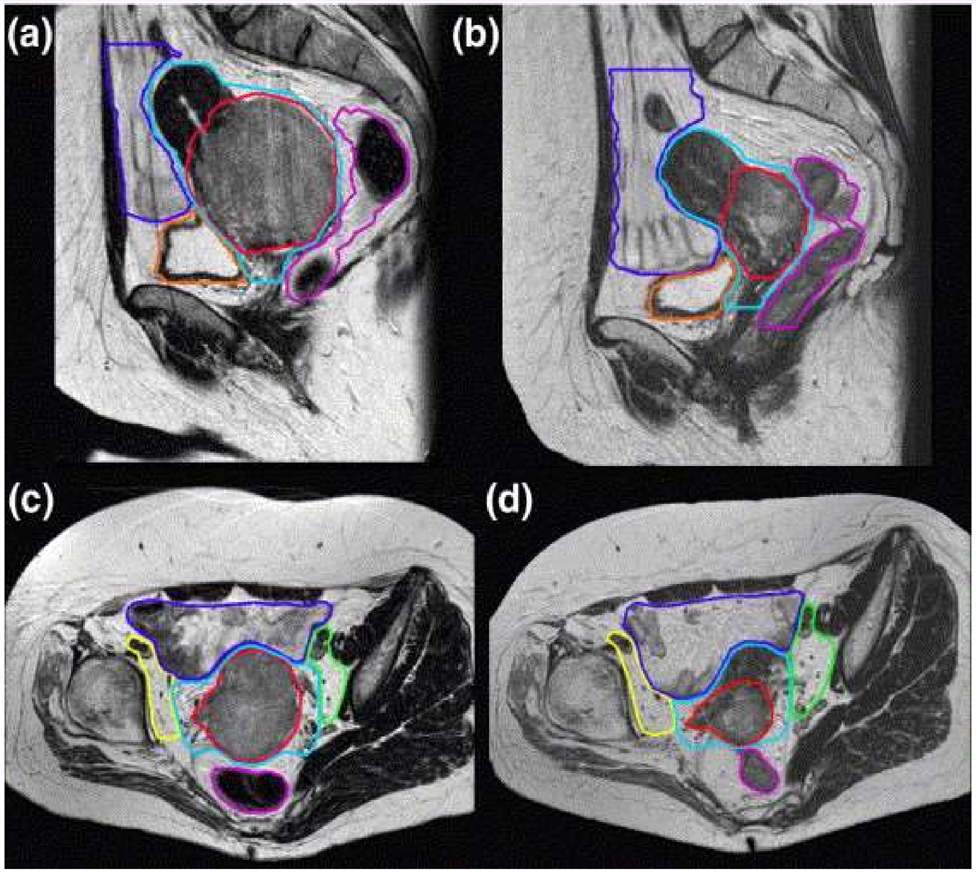

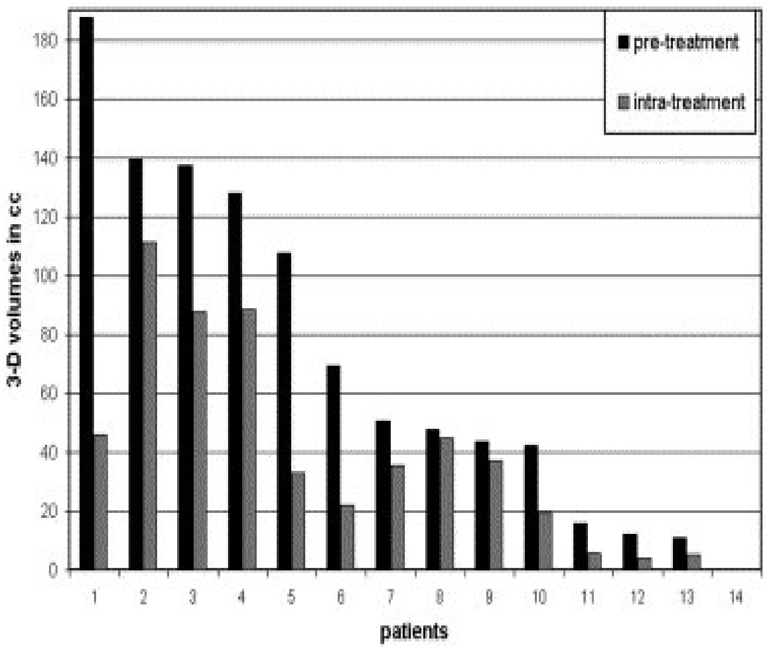

After 30 Gy, the GTVs decreased an average of 46% (6.1–100%). The TVs on the intratreatment MRI remained sufficiently covered by the 95% isodose. Repeated IMRT planning can improve the sparing of the bowel and rectum in patients with substantial tumor regression.

van de Bunt L. et al. Int J Radiat Oncol Biol Phys 2006.

MRI in radiotherapy for cervical cancer

1. Cervical cancer
2. MRI & FDG-PET/CT for pre-treatment assessment of cervical cancer
3. MRI for external beam radiotherapy (EBRT) planning
4. **MRI for brachytherapy planning**
5. MRI for response assessment

Brachytherapy is not optional

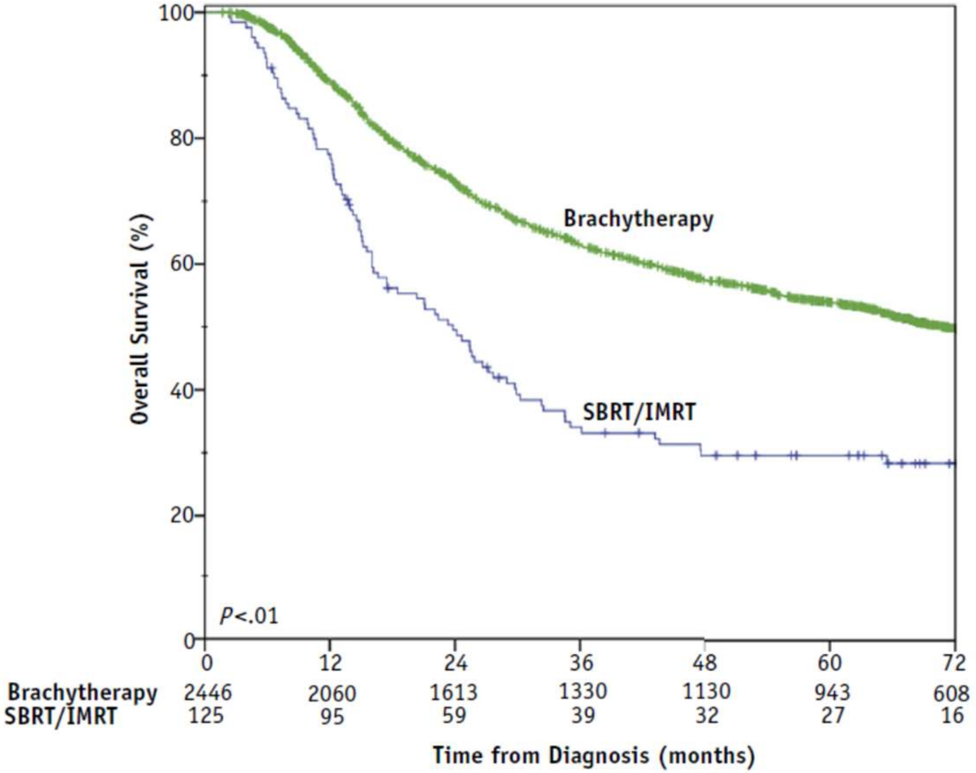

Fig. 2. Kaplan-Meier overall survival estimate stratified by boost modality. IMRT = intensity modulated radiation therapy; SBRT = stereotactic body radiation therapy.

Gill B.S. et al. Int J Radiat Oncol Biol Phys 2014.

MRI-guided, adaptive brachyherapy

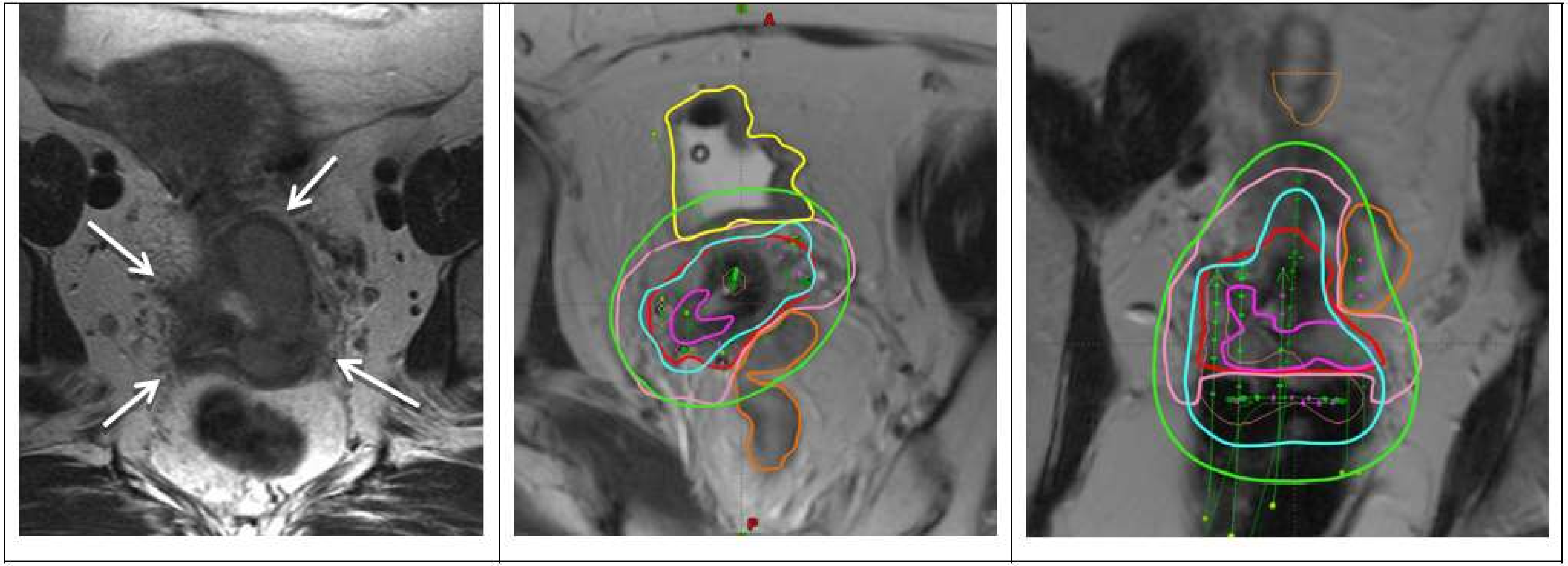

Left panel shows transverse MRI at time of diagnosis with PMI (left and right). At the time of BT, there was still residual PMI. A combined intracavitary- interstitial applicator (5 needles) was used. Middle and right panel show paratransverse and coronal MRI at the time of BT. The volumes are as follows: residual GTV (magenta), CTV HR (red), CTV IR (pink), bladder (yellow), and sigmoid (orange). Isodoses 15 Gy (cyan) and 7.5 Gy (green) correspond to 84 Gy and 60 Gy in terms of total EQD2.

Tanderup K. et al. Semin Radiat Oncol 2014.

GEC-ESTRO target definitions (1)

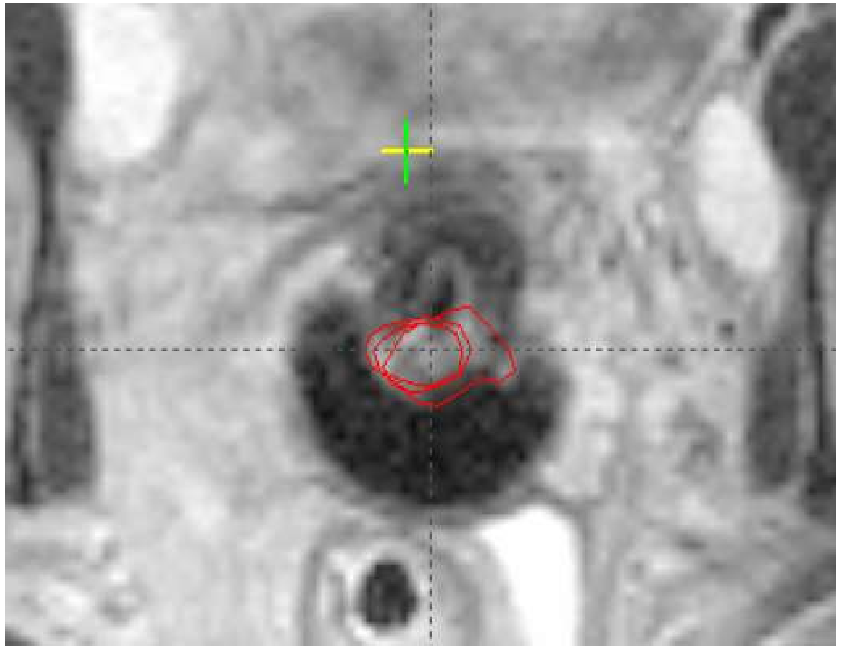

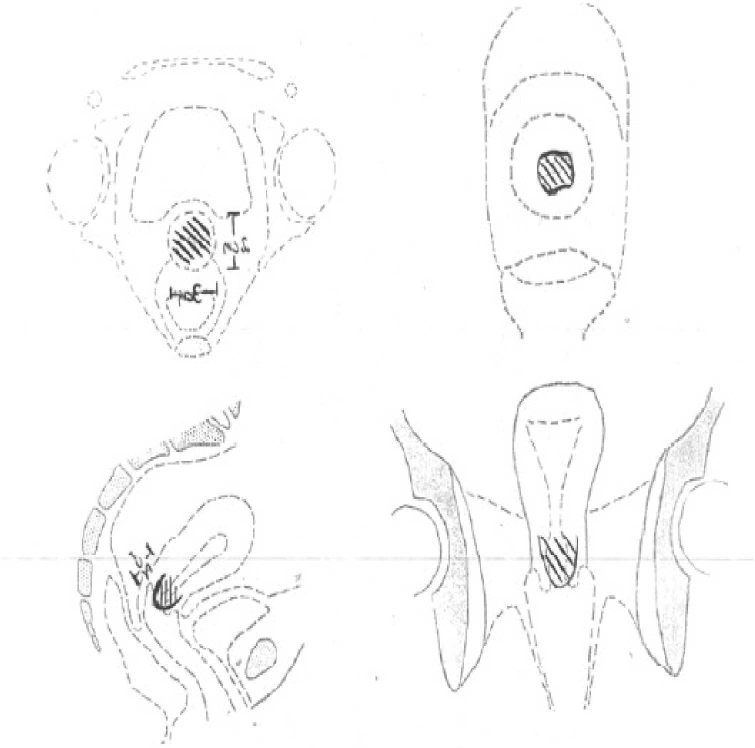

GTV_B: macroscopic tumor at BT

Clinical examination

MRI: high SI zones in cervix and surroundings

Haie-Meder C. et al. Radiother Oncol 2005.

GEC-ESTRO target definitions (2)

- **HR CTV:** whole cervix (assumed residual tumor)
  - Persistent GTV
  - Always whole cervix
  - Presumed extracervical tumor extension:
    - Residual clinically edematous zones
    - Residual grey zones on MRI
  - No safety margins are added
  - Dose high enough to sterilize macroscopic tumor

- **IR CTV:** significant microscopic disease at BT
  - Encompasses HR CTV
  - Safety margins (5 – 15 mm) depending on tumor spread

- **LR CTV:** presumed treated with EBRT, not treated with BT

Haie-Meder C. et al. Radiother Oncol 2005.

GEC-ESTRO target definitions (3)

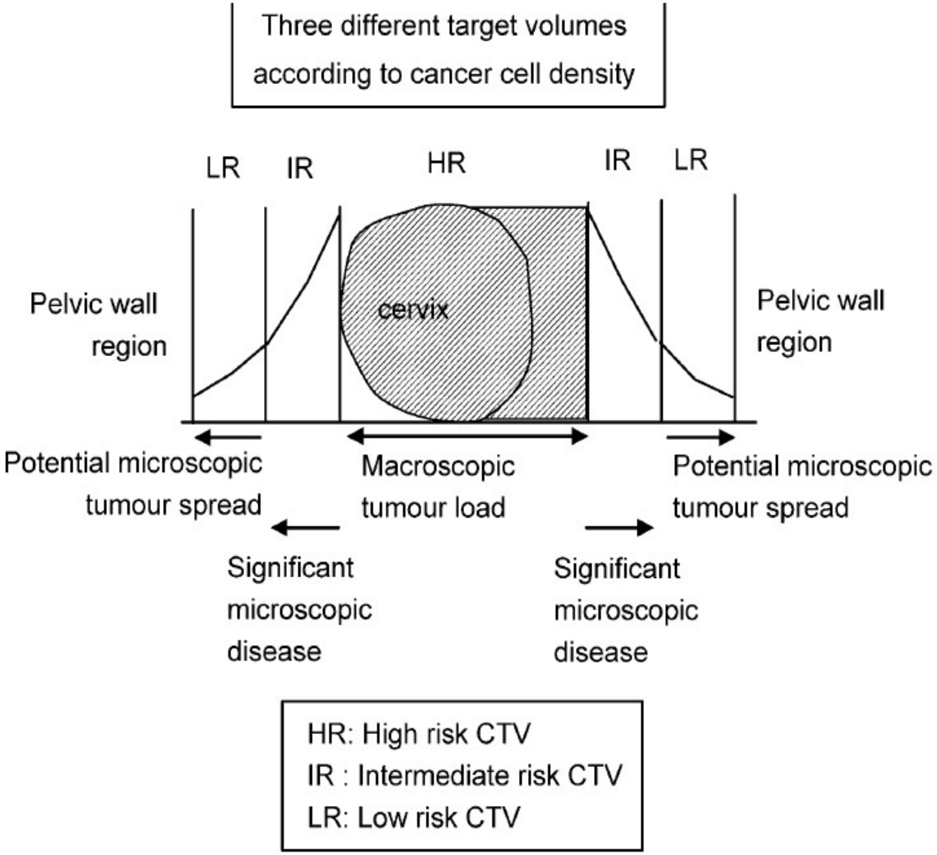
Three different target volumes according to cancer cell density
LR
IR
HR
IR
LR
Pelvic wall region
cervix
Pelvic wall region
Potential microscopic tumour spread
Macroscopic tumour load
Potential microscopic tumour spread
Significant microscopic disease
Significant microscopic disease
HR: High risk CTV
IR : Intermediate risk CTV
LR: Low risk CTV

Haie-Meder C. et al. Radiother Oncol 2005.

Allows for an "adaptive" boost

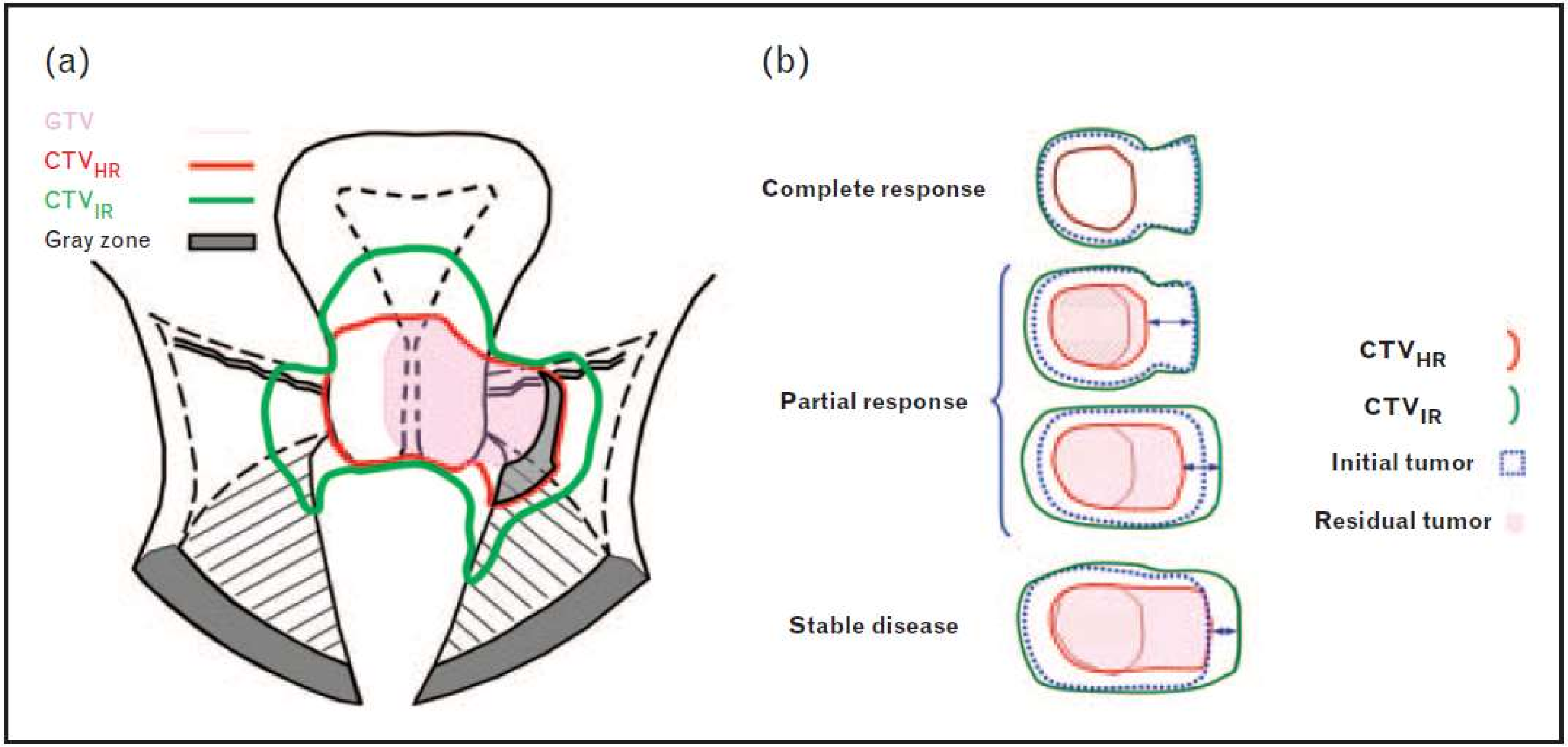
(a)
GTV
CTV_{HR}
CTV_{IR}
Gray zone
(b)
Complete response
Partial response
Stable disease
CTV_{HR}
CTV_{IR}
Initial tumor
Residual tumor

Castelnau-Marchand P. et al. Curr Opin Oncol 2016.

IODV in IGABT

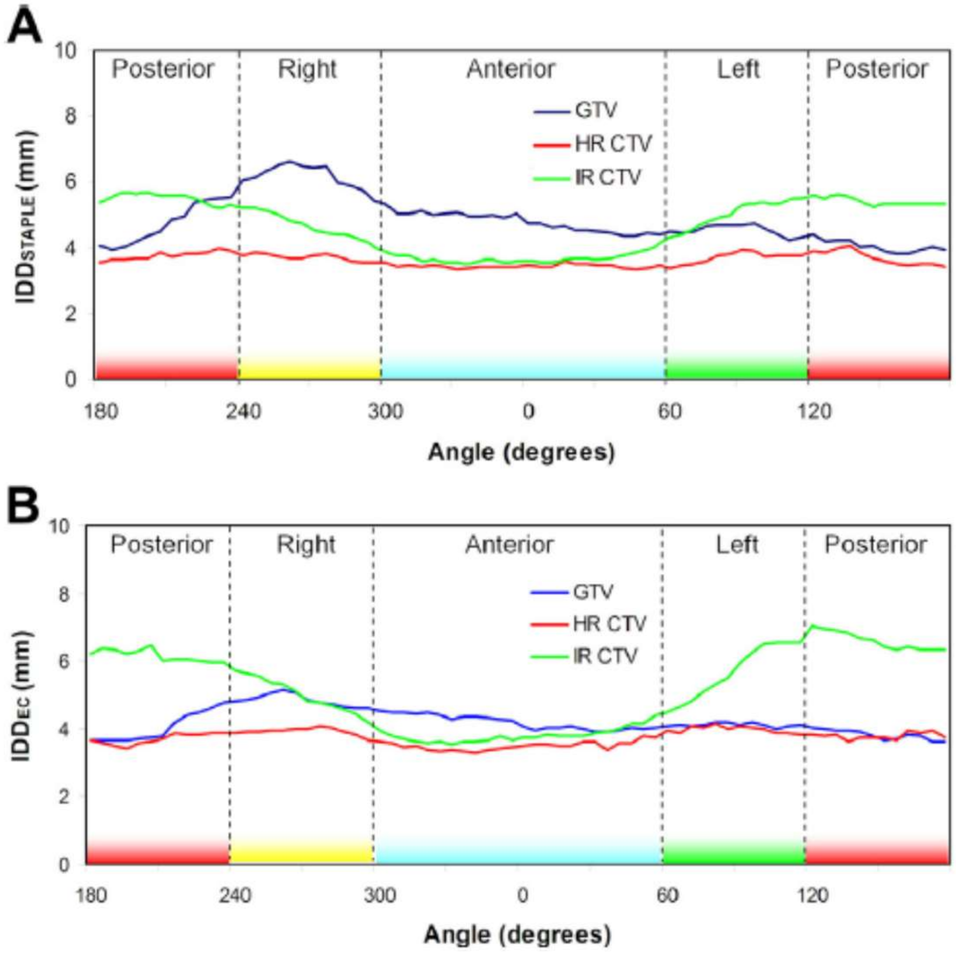

Due to lower delineation uncertainties when compared to GTV and IR CTV, HR CTV may be considered most robust volume

Petric P. et al. Radiother Oncol 2013.

Dosimetric impact of IODV

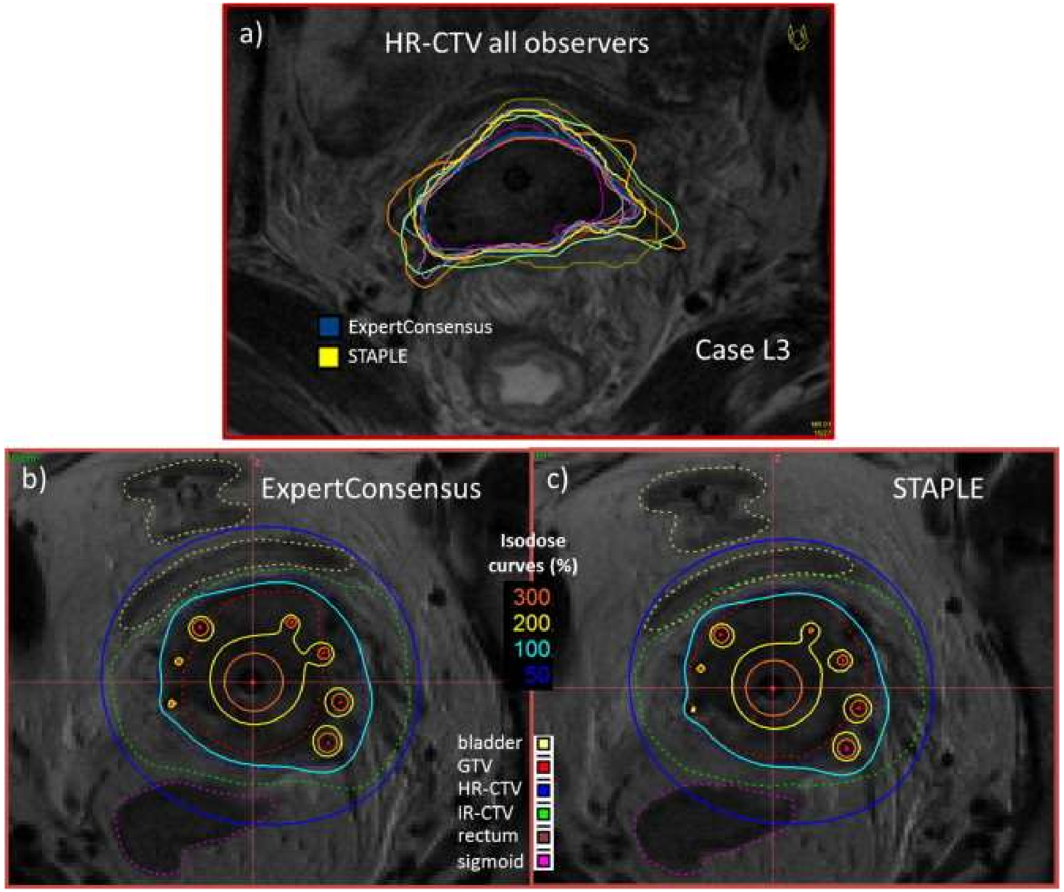
a)
HR-CTV all observers
ExpertConsensus
STAPLE
Case L3
b)
ExpertConsensus
c)
STAPLE
Isodose curves (%)
300
200
100
50
bladder
GTV
HR-CTV
IR-CTV
rectum
sigmoid

For the target volumes the dosimetric impact of IODV was smallest for the GTV and HR-CTV, while IODV had an even smaller impact on the bladder and rectum.

Hellebust T. et al. Radiother Oncol 2013.

DWI/DCE/FDG-PET decreases IODV

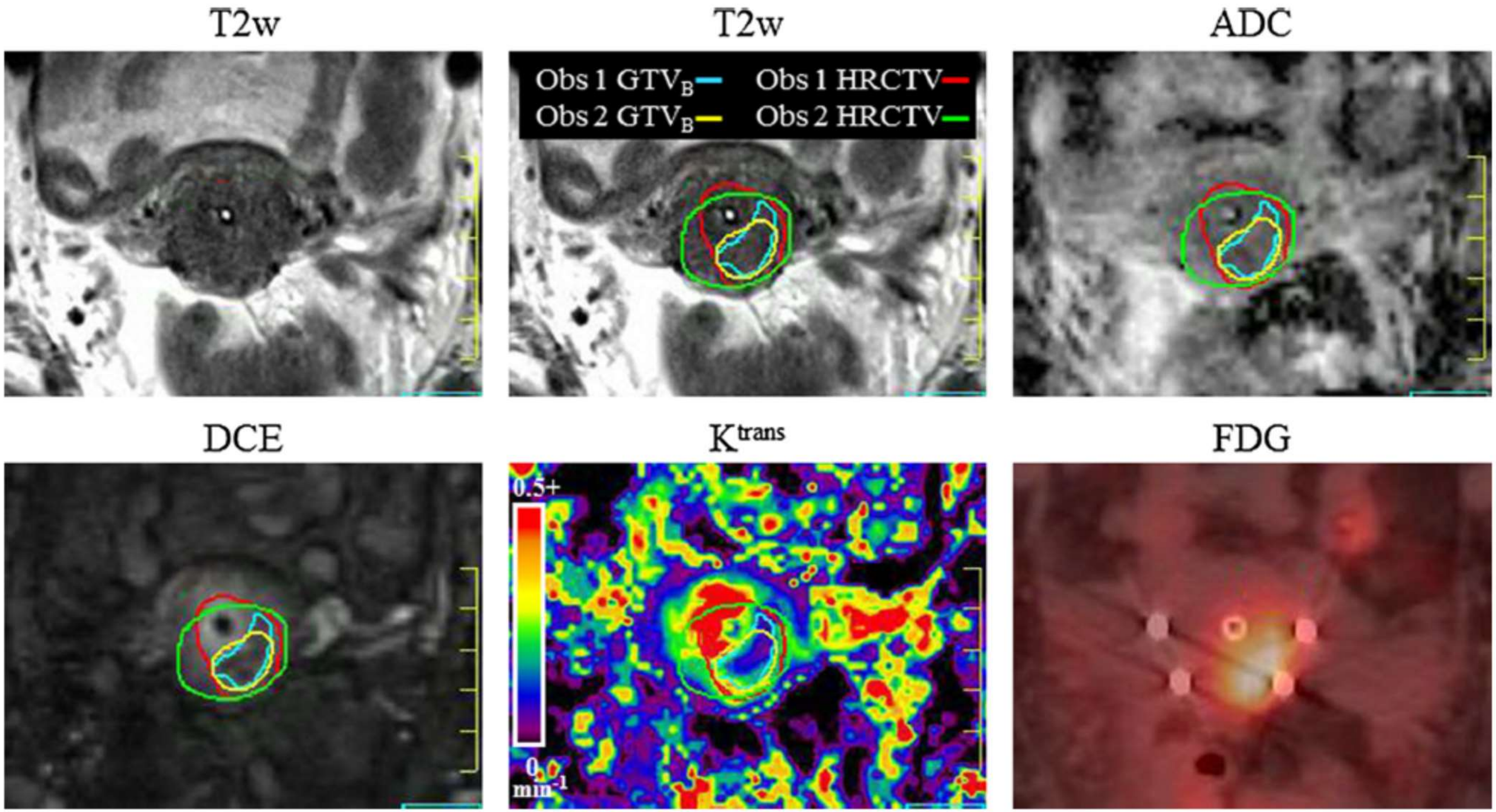
T2w
T2w
Obs 1 GTV$_B$
Obs 2 GTV$_B$
Obs 1 HRCTV
Obs 2 HRCTV
ADC
DCE
K^{trans}
0.5+
0
min^{-1}
FDG

Han K. et al. Radiother Oncol 2016.

GEC-ESTRO treatment planning

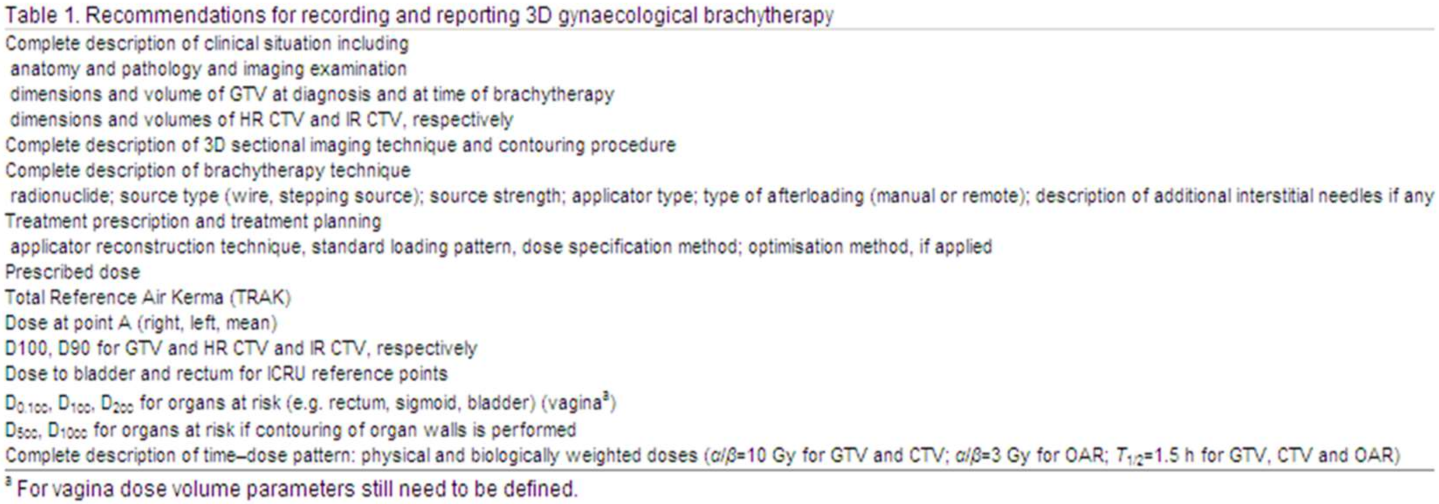

Table 1. Recommendations for recording and reporting 3D gynaecological brachytherapy

Complete description of clinical situation including
- anatomy and pathology and imaging examination
- dimensions and volume of GTV at diagnosis and at time of brachytherapy
- dimensions and volumes of HR CTV and IR CTV, respectively

Complete description of 3D sectional imaging technique and contouring procedure

Complete description of brachytherapy technique
- radionuclide; source type (wire, stepping source); source strength; applicator type; type of afterloading (manual or remote); description of additional interstitial needles if any

Treatment prescription and treatment planning
- applicator reconstruction technique, standard loading pattern, dose specification method; optimisation method, if applied

Prescribed dose

Total Reference Air Kerma (TRAK)

Dose at point A (right, left, mean)

D100, D90 for GTV and HR CTV and IR CTV, respectively

Dose to bladder and rectum for ICRU reference points

$D_{0.1cc}$, D_{1cc}, D_{2cc} for organs at risk (e.g. rectum, sigmoid, bladder) (vagina[a])

D_{5cc}, D_{10cc} for organs at risk if contouring of organ walls is performed

Complete description of time–dose pattern: physical and biologically weighted doses (α/β=10 Gy for GTV and CTV; α/β=3 Gy for OAR; $T_{1/2}$=1.5 h for GTV, CTV and OAR)

---

[a] For vagina dose volume parameters still need to be defined.

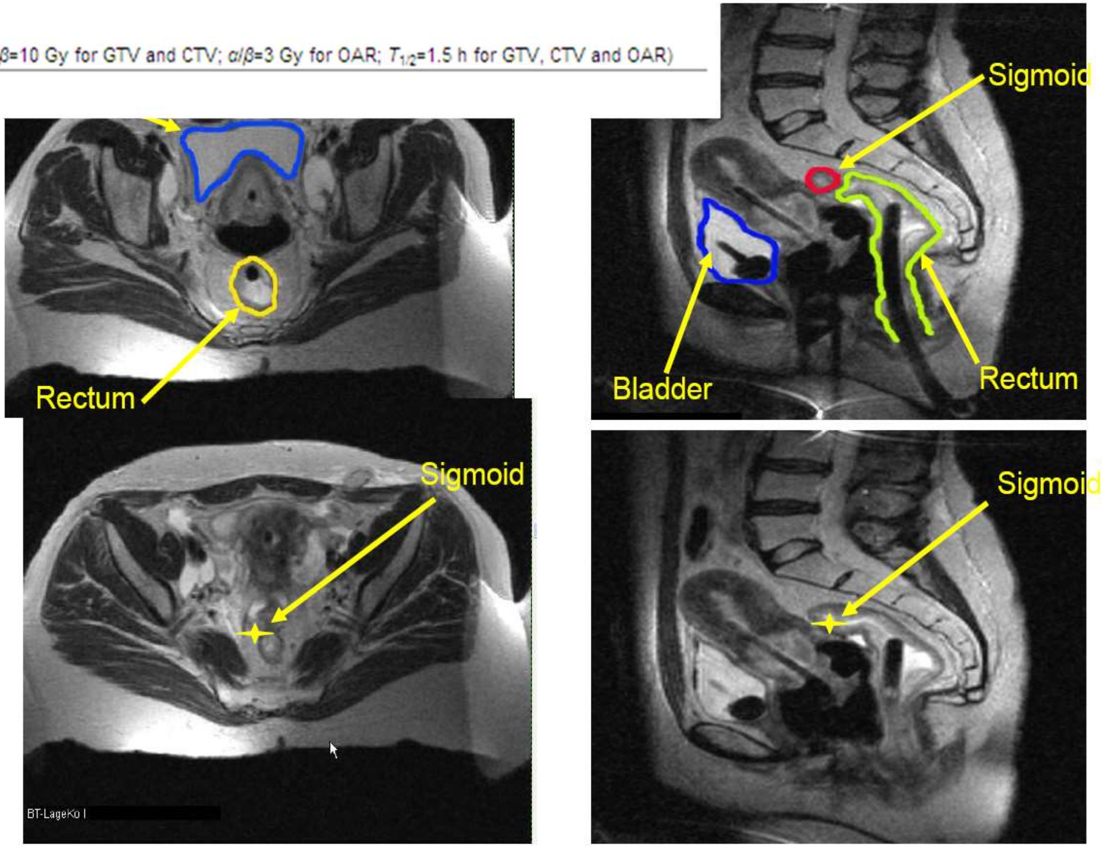

Pötter R. et al. Radiother Oncol 2006.

GEC-ESTRO EQD2 spreadsheet

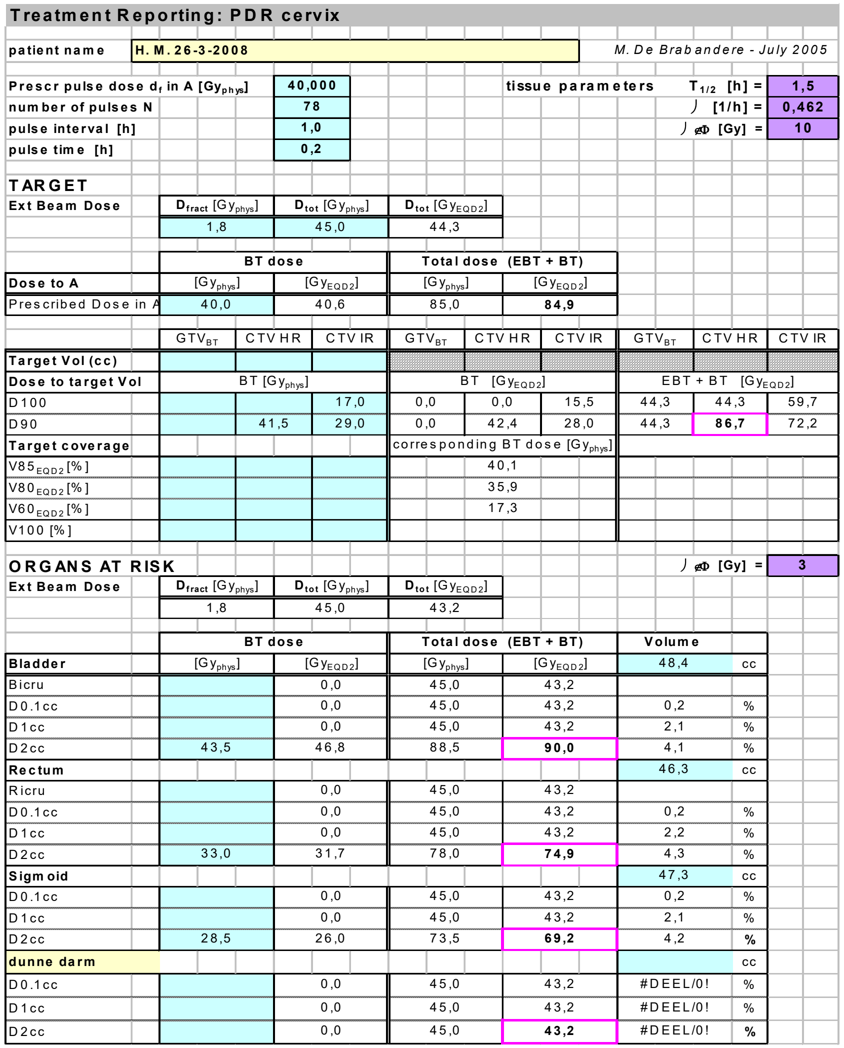

Treatment Reporting: PDR cervix

patient name	H. M. 26-3-2008	*M. De Brabandere - July 2005*

Prescr pulse dose d_f in A [Gy_{phys}]	**40,000**	**tissue parameters** $T_{1/2}$ **[h] =**	**1,5**
number of pulses N	**78**	**λ [1/h] =**	**0,462**
pulse interval [h]	**1,0**	**α/β [Gy] =**	**10**
pulse time [h]	**0,2**		

TARGET

Ext Beam Dose	**D_{fract}** [Gy_{phys}]	**D_{tot}** [Gy_{phys}]	**D_{tot}** [Gy_{EQD2}]
	1,8	45,0	44,3

	BT dose		**Total dose (EBT + BT)**	
Dose to A	[Gy_{phys}]	[Gy_{EQD2}]	[Gy_{phys}]	[Gy_{EQD2}]
Prescribed Dose in A	40,0	40,6	85,0	**84,9**

	GTV_{BT}	CTV HR	CTV IR	GTV_{BT}	CTV HR	CTV IR	GTV_{BT}	CTV HR	CTV IR
Target Vol (cc)				▨	▨	▨	▨	▨	▨
Dose to target Vol	BT [Gy_{phys}]			BT [Gy_{EQD2}]			EBT + BT [Gy_{EQD2}]		
D100			17,0	0,0	0,0	15,5	44,3	44,3	59,7
D90		41,5	29,0	0,0	42,4	28,0	44,3	**86,7**	72,2
Target coverage				corresponding BT dose [Gy_{phys}]					
$V85_{EQD2}$ [%]				40,1					
$V80_{EQD2}$ [%]				35,9					
$V60_{EQD2}$ [%]				17,3					
V100 [%]									

ORGANS AT RISK α/β [Gy] = **3**

Ext Beam Dose	**D_{fract}** [Gy_{phys}]	**D_{tot}** [Gy_{phys}]	**D_{tot}** [Gy_{EQD2}]
	1,8	45,0	43,2

	BT dose		**Total dose (EBT + BT)**		**Volume**	
Bladder	[Gy_{phys}]	[Gy_{EQD2}]	[Gy_{phys}]	[Gy_{EQD2}]	48,4	cc
Bicru		0,0	45,0	43,2		
D0.1cc		0,0	45,0	43,2	0,2	%
D1cc		0,0	45,0	43,2	2,1	%
D2cc	43,5	46,8	88,5	**90,0**	4,1	%
Rectum					46,3	cc
Ricru		0,0	45,0	43,2		
D0.1cc		0,0	45,0	43,2	0,2	%
D1cc		0,0	45,0	43,2	2,2	%
D2cc	33,0	31,7	78,0	**74,9**	4,3	%
Sigmoid					47,3	cc
D0.1cc		0,0	45,0	43,2	0,2	%
D1cc		0,0	45,0	43,2	2,1	%
D2cc	28,5	26,0	73,5	**69,2**	4,2	%
dunne darm						cc
D0.1cc		0,0	45,0	43,2	#DEEL/0!	%
D1cc		0,0	45,0	43,2	#DEEL/0!	%
D2cc		0,0	45,0	**43,2**	#DEEL/0!	%

LQ modeled

Tumor: α/β = 10 Gy

$T_{½}$ = 1,5 h

OAR: α/β = 3 Gy

$T_{½}$ = 1,5 h

GEC-ESTRO MRI recommendations

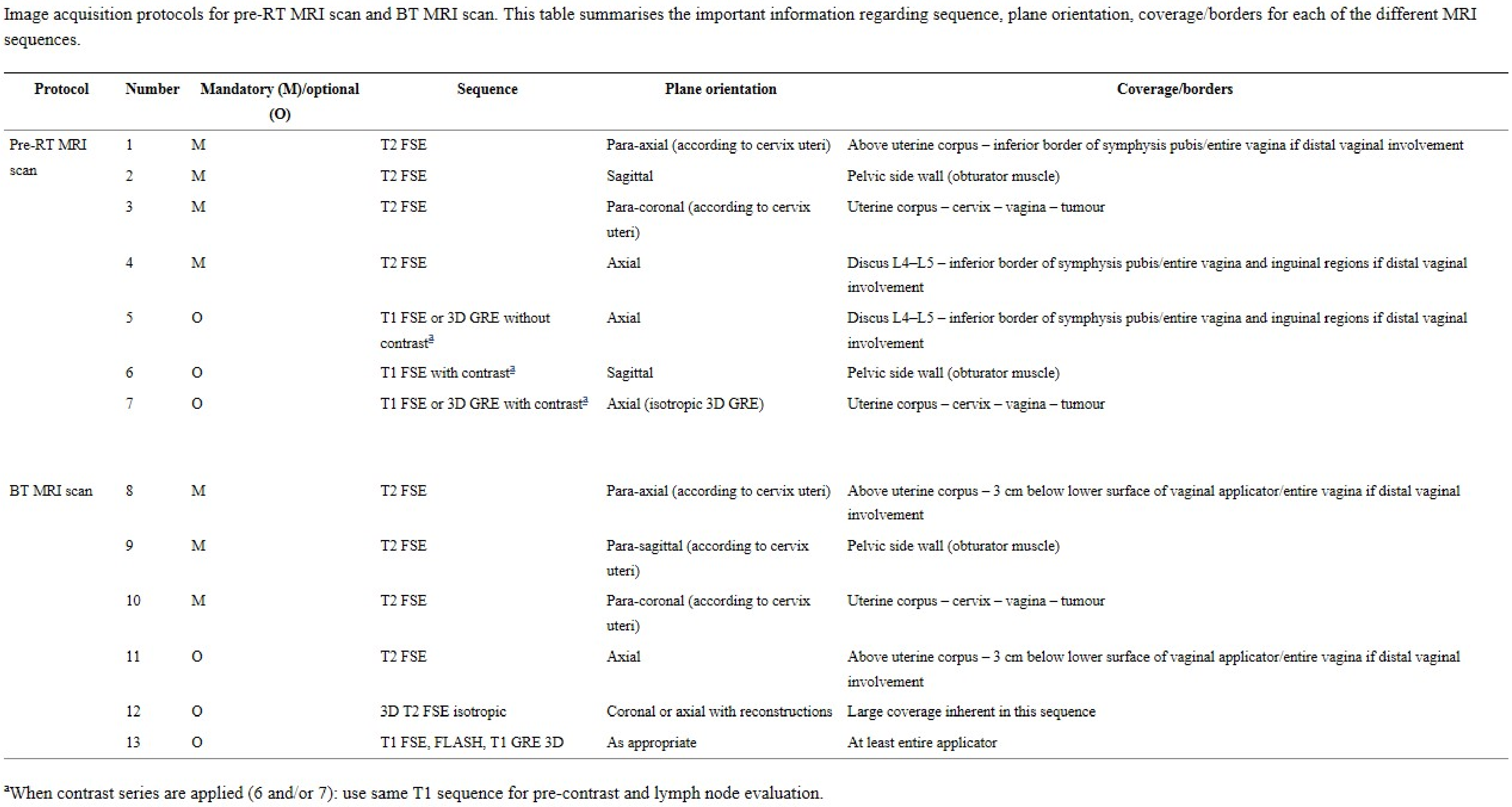

Image acquisition protocols for pre-RT MRI scan and BT MRI scan. This table summarises the important information regarding sequence, plane orientation, coverage/borders for each of the different MRI sequences.

Protocol	Number	Mandatory (M)/optional (O)	Sequence	Plane orientation	Coverage/borders
Pre-RT MRI scan	1	M	T2 FSE	Para-axial (according to cervix uteri)	Above uterine corpus – inferior border of symphysis pubis/entire vagina if distal vaginal involvement
	2	M	T2 FSE	Sagittal	Pelvic side wall (obturator muscle)
	3	M	T2 FSE	Para-coronal (according to cervix uteri)	Uterine corpus – cervix – vagina – tumour
	4	M	T2 FSE	Axial	Discus L4–L5 – inferior border of symphysis pubis/entire vagina and inguinal regions if distal vaginal involvement
	5	O	T1 FSE or 3D GRE without contrast[a]	Axial	Discus L4–L5 – inferior border of symphysis pubis/entire vagina and inguinal regions if distal vaginal involvement
	6	O	T1 FSE with contrast[a]	Sagittal	Pelvic side wall (obturator muscle)
	7	O	T1 FSE or 3D GRE with contrast[a]	Axial (isotropic 3D GRE)	Uterine corpus – cervix – vagina – tumour
BT MRI scan	8	M	T2 FSE	Para-axial (according to cervix uteri)	Above uterine corpus – 3 cm below lower surface of vaginal applicator/entire vagina if distal vaginal involvement
	9	M	T2 FSE	Para-sagittal (according to cervix uteri)	Pelvic side wall (obturator muscle)
	10	M	T2 FSE	Para-coronal (according to cervix uteri)	Uterine corpus – cervix – vagina – tumour
	11	O	T2 FSE	Axial	Above uterine corpus – 3 cm below lower surface of vaginal applicator/entire vagina if distal vaginal involvement
	12	O	3D T2 FSE isotropic	Coronal or axial with reconstructions	Large coverage inherent in this sequence
	13	O	T1 FSE, FLASH, T1 GRE 3D	As appropriate	At least entire applicator

[a] When contrast series are applied (6 and/or 7): use same T1 sequence for pre-contrast and lymph node evaluation.

Dimopoulos J. et al. Radiother Oncol 2012.

MRI-guided BT: manual optimization

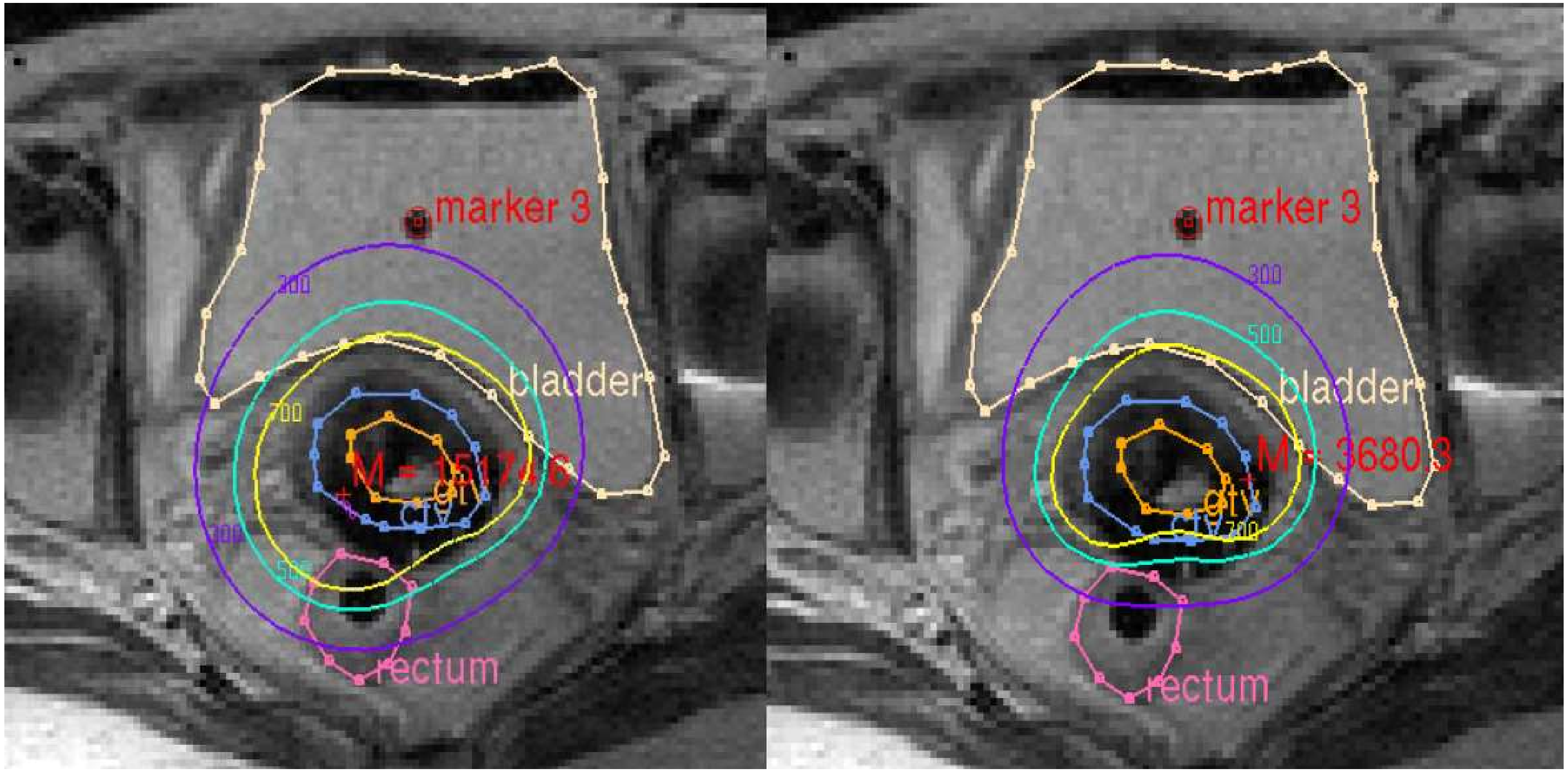
marker 3
300
500
700
bladder
M = 15174.6
gtv
ctv
rectum
marker 3
300
500
700
bladder
M = 3680.3
gtv
ctv
rectum

= Individual shaping of isodose lines to spare OAR without lowering target dose.

MRI-guided BT: when things go wrong…

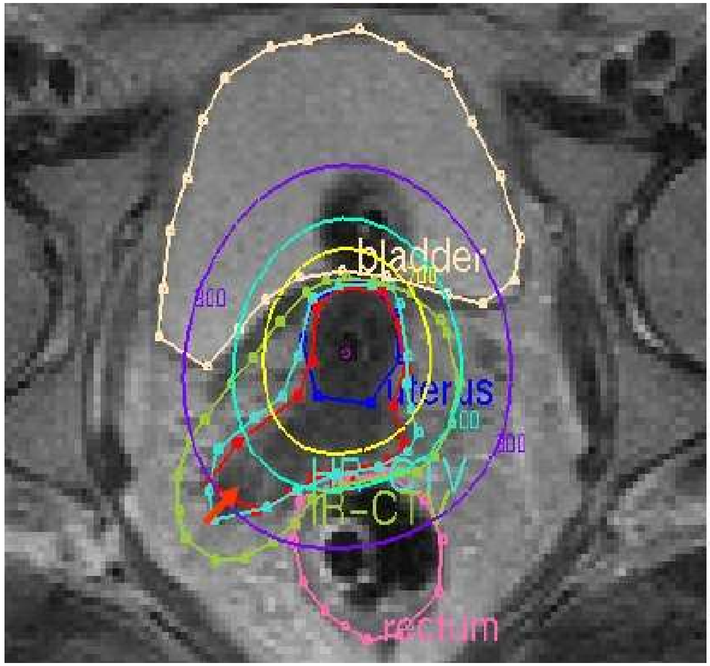
bladder
uterus
HR-CTV
IR-CTV
rectum

09-2000: stage IIIB cervical ca.

EBRT + 3D BT boost with insufficient optimization (D90 < 70 Gy HR CTV)

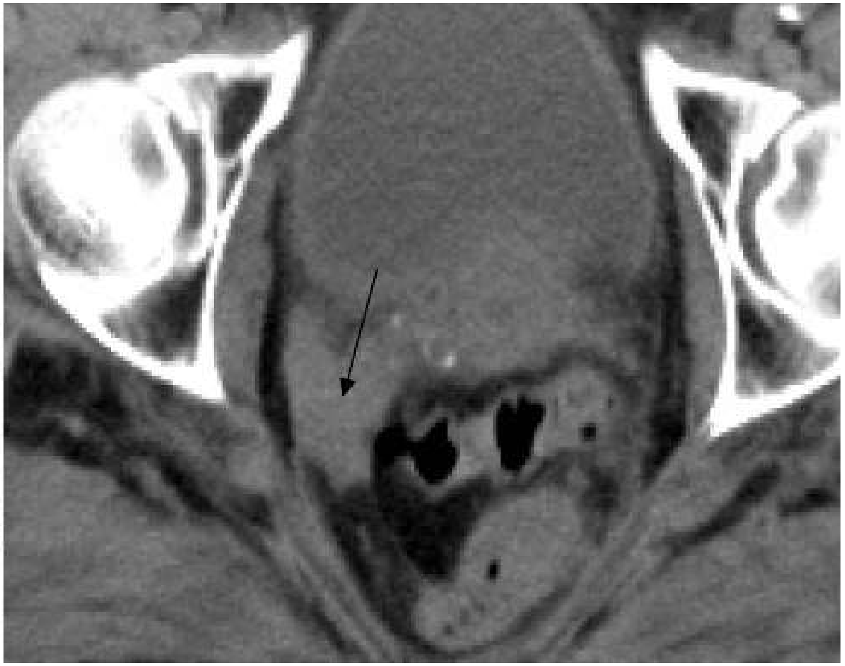

08-2001: parametrial/pelvic wall recurrence

Results

Group	Year	N	Dose rate	Interstitial BT (%)	LC	OS	Grade 3-4 tox
Vienna	2011	156	HDR	44%	95% at 3 yrs	68% at 3 yrs	6%
Aarhus	2013	140	PDR	43%	91% at 3 yrs	79% at 3 yrs	7%
Pittsburg	2014	128	HDR	0%	92% at 2 yrs	88% at 2 yrs	1%
Paris	2015	225	PDR	2%	86% at 3 yrs	76% at 3 yrs	7%
Leuven	2016	154	PDR	16%	96% at 3 yrs	65% at 5 yrs	11%
Retro-EMBRACE	2016	731	mixed	23%	91% at 3 yrs	74% at 3 yrs	11%

Conclusion: 86 – 96% local control at 2 – 3 years, with severe late toxicity ≤ 10%.

2D vs. IGABT (1)

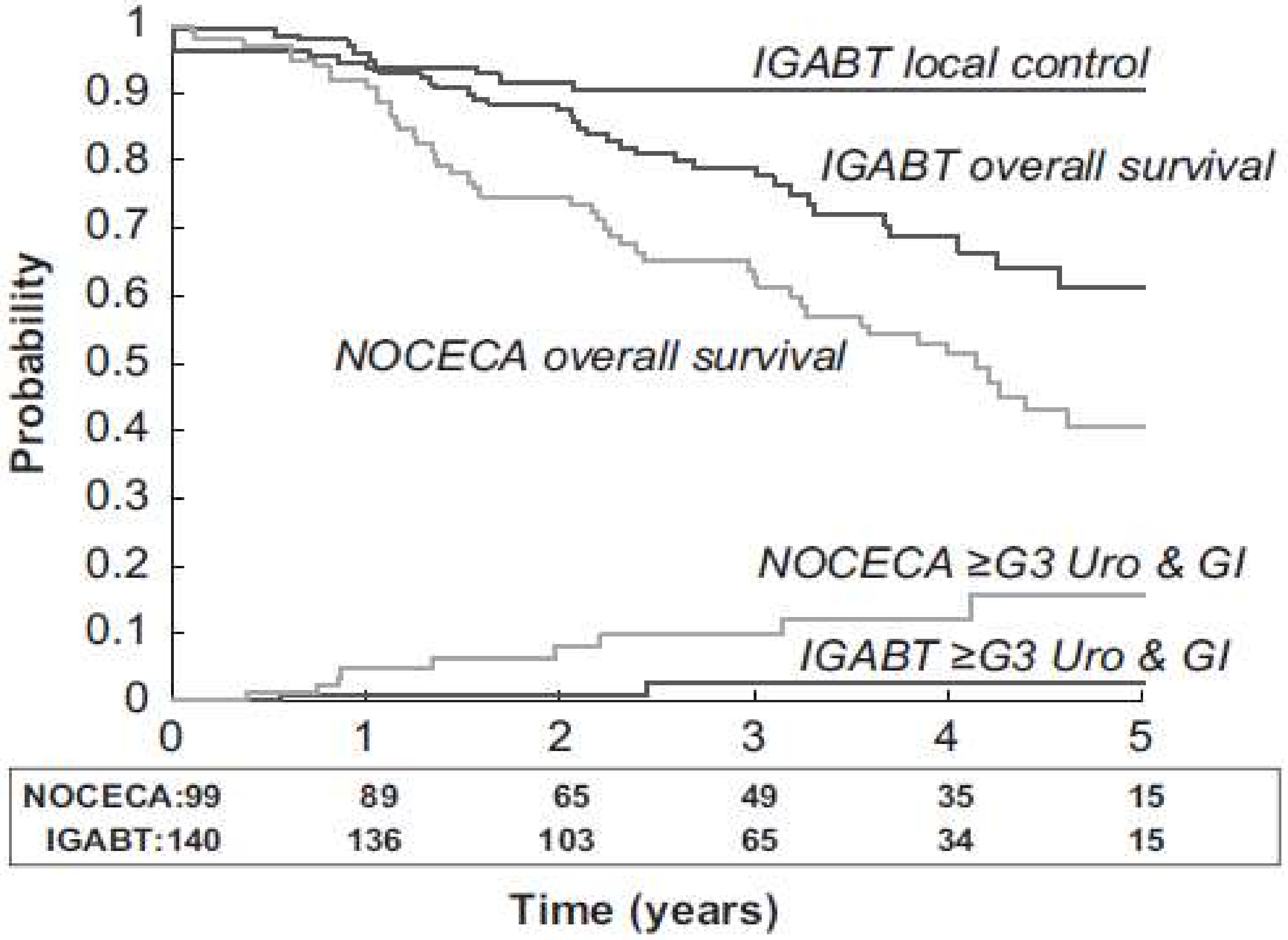

Lindegaard J. et al. Acta Oncol 2013.

2D vs. IGABT (2)

Group	Year	Type	Arms	N	OS	Grade 3-4 tox
Vienna	2007	Retrospective	IGABT 2D	72 73	64% at 3 yrs, p = 0,03 53%	10%, p = NS 22%
STIC trial	2012	Prospective	IGABT 2D	117 118	74% at 2 yrs, p = NS 55%	3%, p = 0,004 23%
Aarhus	2013	Retrospective	IGABT 2D	140 99	79% at 3 yrs, p = 0,005 63%	7%, p = 0,02 15%
Leiden	2014	Retrospective	IGABT 2D	83 43	86% at 3 yrs, p < 0,01 43%	3%, p < 0,01 21%

IGABT provides higher LC and lower tocity rates compared to classical radiographs-based BT.

EMBRACE trial (1)

intErnational study on Mri-guided BRachytherapy in locally Advanced CErvical cancer.

European study on MRI-guided brachytherapy in locally advanced cervical cancer (GEC-ESTRO) started in 2008.

Accrual ended in December 2015, with > 1400 patients included.

Prospective observational multicenter setting

Primary endpoints: LC and morbidity.

Secondary endpoints: RC, DFS, OS and QoL.

Correlation between image-based DVH and outcome.

FIGO IB to IVA

EBRT + BT

EMBRACE trial (2)

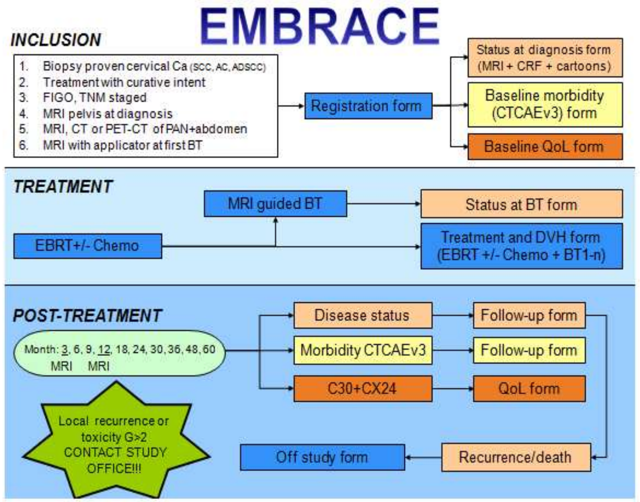
EMBRACE
INCLUSION
1. Biopsy proven cervical Ca (SCC, AC, ADSCC)
2. Treatment with curative intent
3. FIGO, TNM staged
4. MRI pelvis at diagnosis
5. MRI, CT or PET-CT of PAN+abdomen
6. MRI with applicator at first BT
Registration form
Status at diagnosis form (MRI + CRF + cartoons)
Baseline morbidity (CTCAEv3) form
Baseline QoL form
TREATMENT
MRI guided BT
Status at BT form
EBRT+/- Chemo
Treatment and DVH form (EBRT +/- Chemo + BT1-n)
POST-TREATMENT
Month: 3, 6, 9, 12, 18, 24, 30, 36, 48, 60
MRI MRI
Disease status
Follow-up form
Morbidity CTCAEv3
Follow-up form
C30+CX24
QoL form
Local recurrence or toxicity G>2 CONTACT STUDY OFFICE!!!
Off study form
Recurrence/death

Quality of Life sub-study

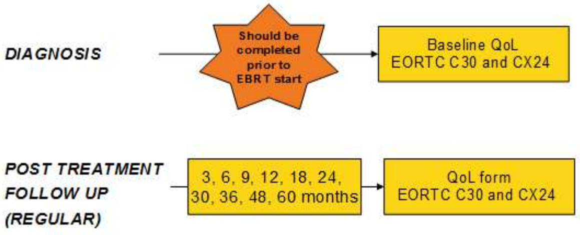
DIAGNOSIS
Should be completed prior to EBRT start
Baseline QoL EORTC C30 and CX24
POST TREATMENT FOLLOW UP (REGULAR)
3, 6, 9, 12, 18, 24, 30, 36, 48, 60 months
QoL form EORTC C30 and CX24

Centre	Code	Principal Investigator	Physicist
Aarhus	AAR	Jacob Lindegaard	Kari Tanderup
Arnhem	ARN	Elzbieta van der Steen Banasik	Bernard Oosterveld
Paris	PAR	Christine Haie-Meder	Isabelle Dumas
Leiden	LEI	Karen Neelis	Martijn Ketelaars
Leuven	LEU	Erik van Limbergen	Marisol de Brabandere
Ljubljana	LJU	Primoz Petric	Robert Hudej
Milwaukee	MIL	Beth Erickson	Jason Rownd
London	LON	Peter Hoskin	Gerry Lowe
Mumbai	MUM	Umesh Mahantshetty	Jamema Swamidas
Pittsburgh	PIT	Sushil Beriwal	Hayeon Kim
Utrecht	UTR	Ina Maria Jurgenliemk-Schulz	Astrid De Leeuw
Vienna	VIE	Richard Pötter	Christian Kirisits
Edmonton	EDM	Robert Pearcey	Geetha Menon
Kaposvar	KAP	Janaki Hadzsiev	Gergely Antal
Leeds	LEE	Rachel Cooper	Peter Bownes
Maastricht	MAA	Ludy Lutgens	Brigitte Reniers
Oslo	OSL	Kolbein Sundfor	Taran Paulsen Hellebust
Trondheim	TRO	Marit Sundset	Anne Beate Langeland Marthinsen

https://www.embracestudy.dk/

Dose-volume effect for OAR

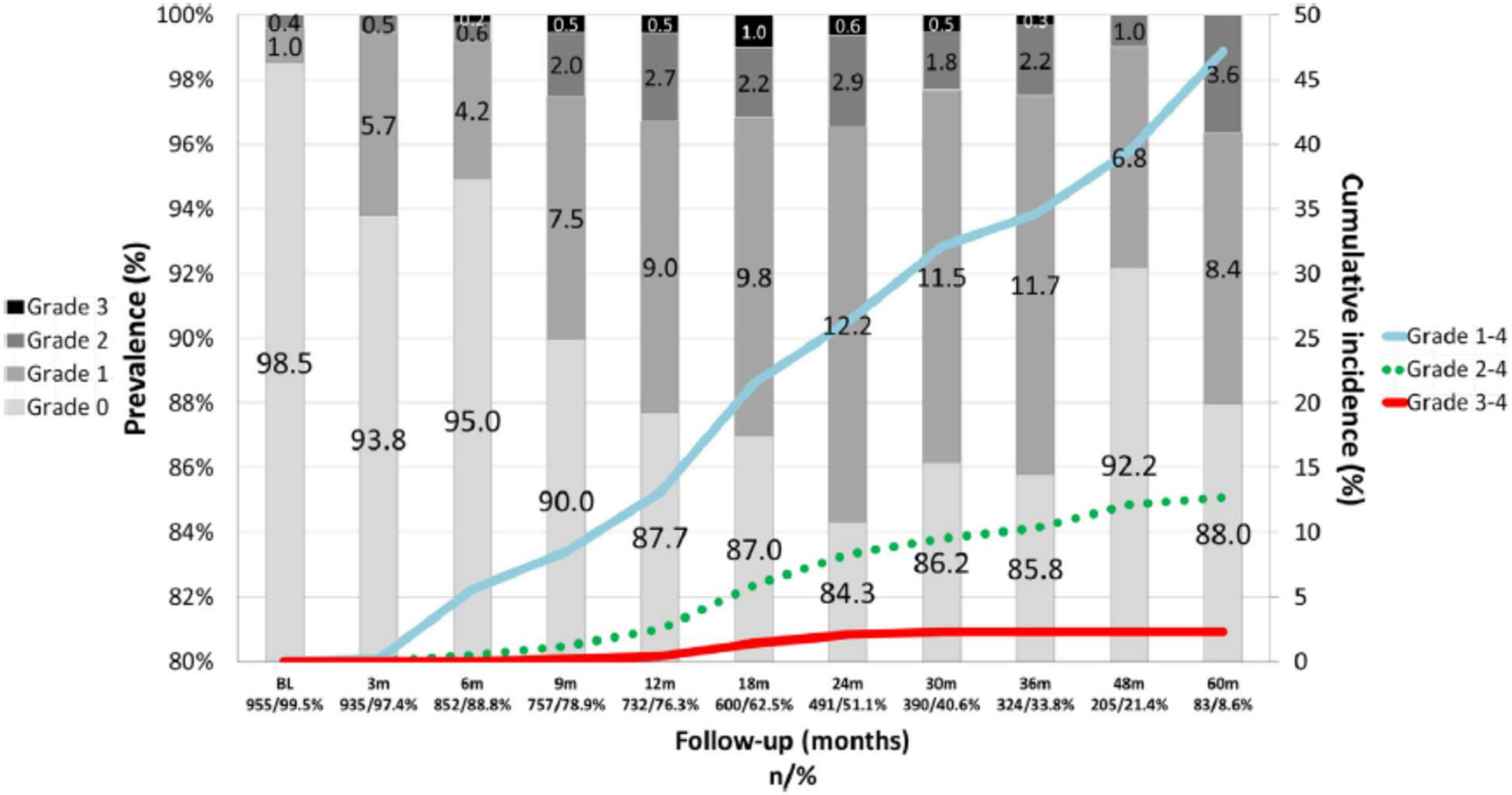

Mazeron R. et al. Radiother Oncol 2016.

Dose-volume effect for tumor response

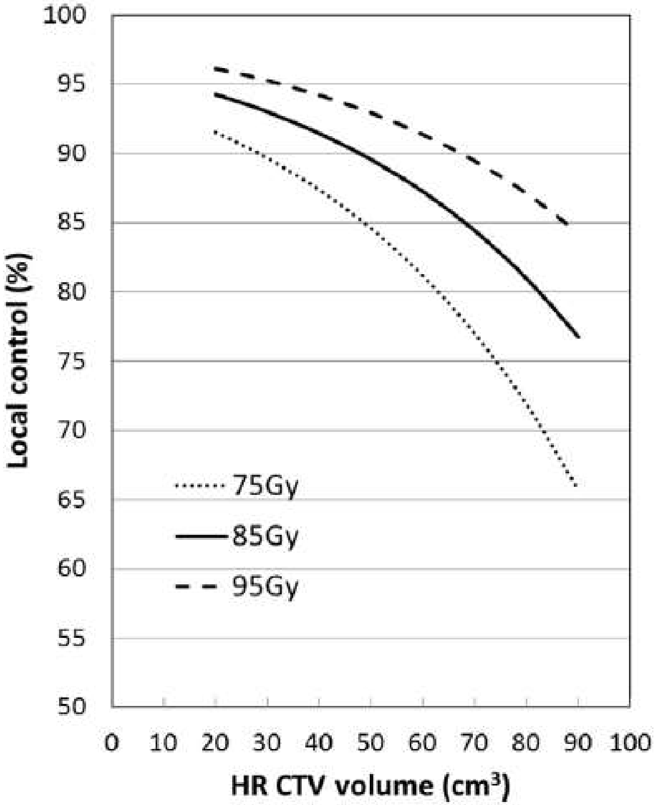

Fig. 2. Local control as depending on CTV_{HR} dose and volume according to the multivariate Cox regression model. The figure shows predicted 3-year actuarial local control as a function of CTV_{HR} volume for three different dose levels: 75 Gy, 85 Gy and 95 Gy and for the median OTT of 49 days.

Tanderup K. et al. Radiother Oncol 2016.

MRI in radiotherapy for cervical cancer

1. Cervical cancer
2. MRI & FDG-PET/CT for pre-treatment assessment of cervical cancer
3. MRI for external beam radiotherapy (EBRT) planning
4. MRI for brachytherapy planning
5. **MRI for response assessment:**
    1. **Volume measurements**
    2. **Functional imaging**

Response assessment: T2w MRI

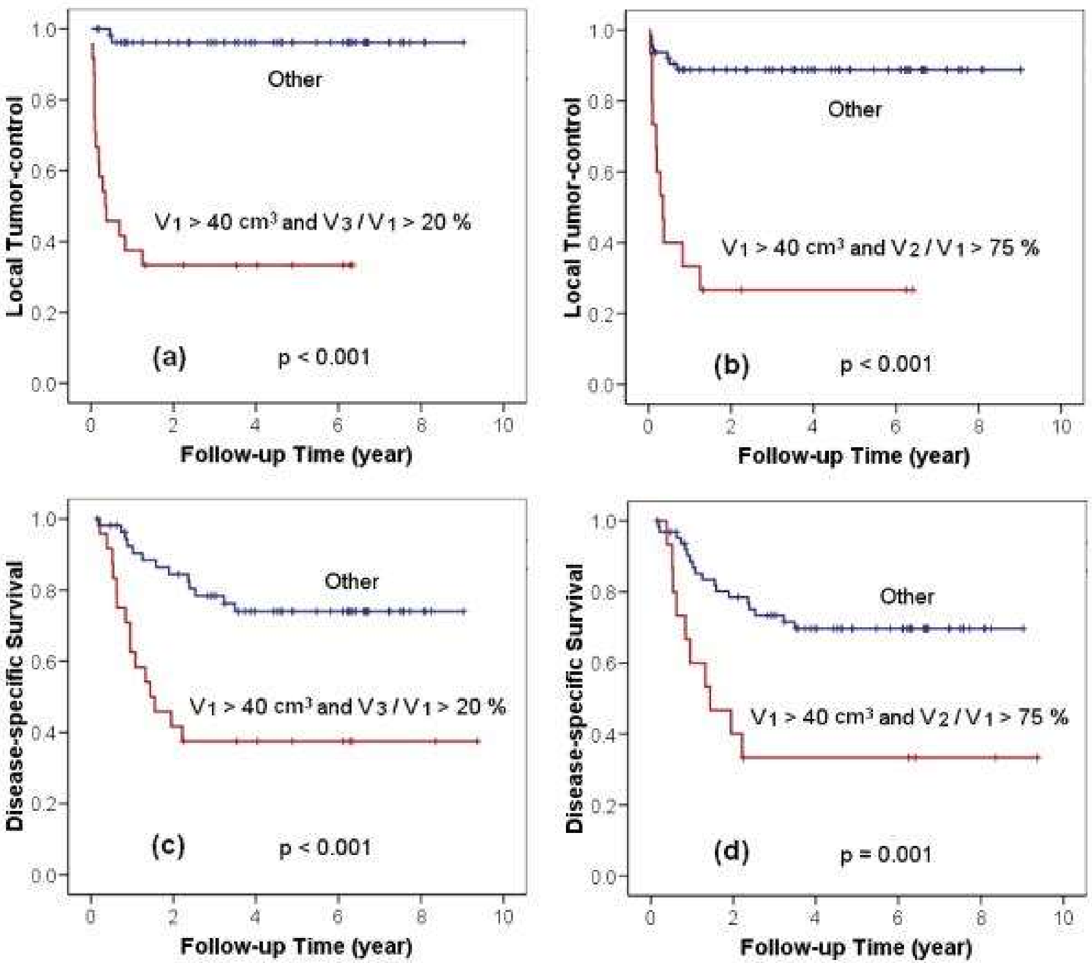

Wang J. et al. Cancer 2010.

Response assessment: functional imaging

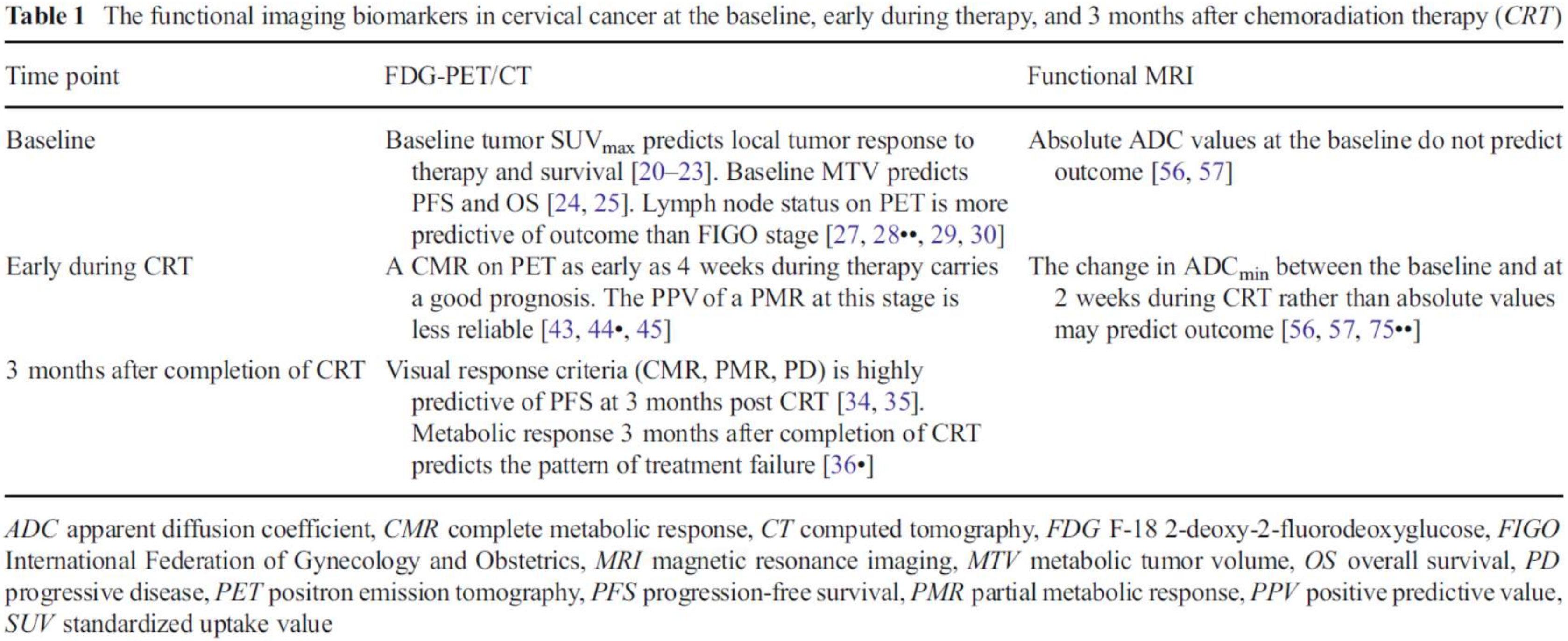

Table 1 The functional imaging biomarkers in cervical cancer at the baseline, early during therapy, and 3 months after chemoradiation therapy (*CRT*)

Time point	FDG-PET/CT	Functional MRI
Baseline	Baseline tumor SUV_{max} predicts local tumor response to therapy and survival [20–23]. Baseline MTV predicts PFS and OS [24, 25]. Lymph node status on PET is more predictive of outcome than FIGO stage [27, 28••, 29, 30]	Absolute ADC values at the baseline do not predict outcome [56, 57]
Early during CRT	A CMR on PET as early as 4 weeks during therapy carries a good prognosis. The PPV of a PMR at this stage is less reliable [43, 44•, 45]	The change in ADC_{min} between the baseline and at 2 weeks during CRT rather than absolute values may predict outcome [56, 57, 75••]
3 months after completion of CRT	Visual response criteria (CMR, PMR, PD) is highly predictive of PFS at 3 months post CRT [34, 35]. Metabolic response 3 months after completion of CRT predicts the pattern of treatment failure [36•]	

ADC apparent diffusion coefficient, *CMR* complete metabolic response, *CT* computed tomography, *FDG* F-18 2-deoxy-2-fluorodeoxyglucose, *FIGO* International Federation of Gynecology and Obstetrics, *MRI* magnetic resonance imaging, *MTV* metabolic tumor volume, *OS* overall survival, *PD* progressive disease, *PET* positron emission tomography, *PFS* progression-free survival, *PMR* partial metabolic response, *PPV* positive predictive value, *SUV* standardized uptake value

Barwick T. et al. Curr Oncol Rep 2013.

DWI/DCE for response assessment

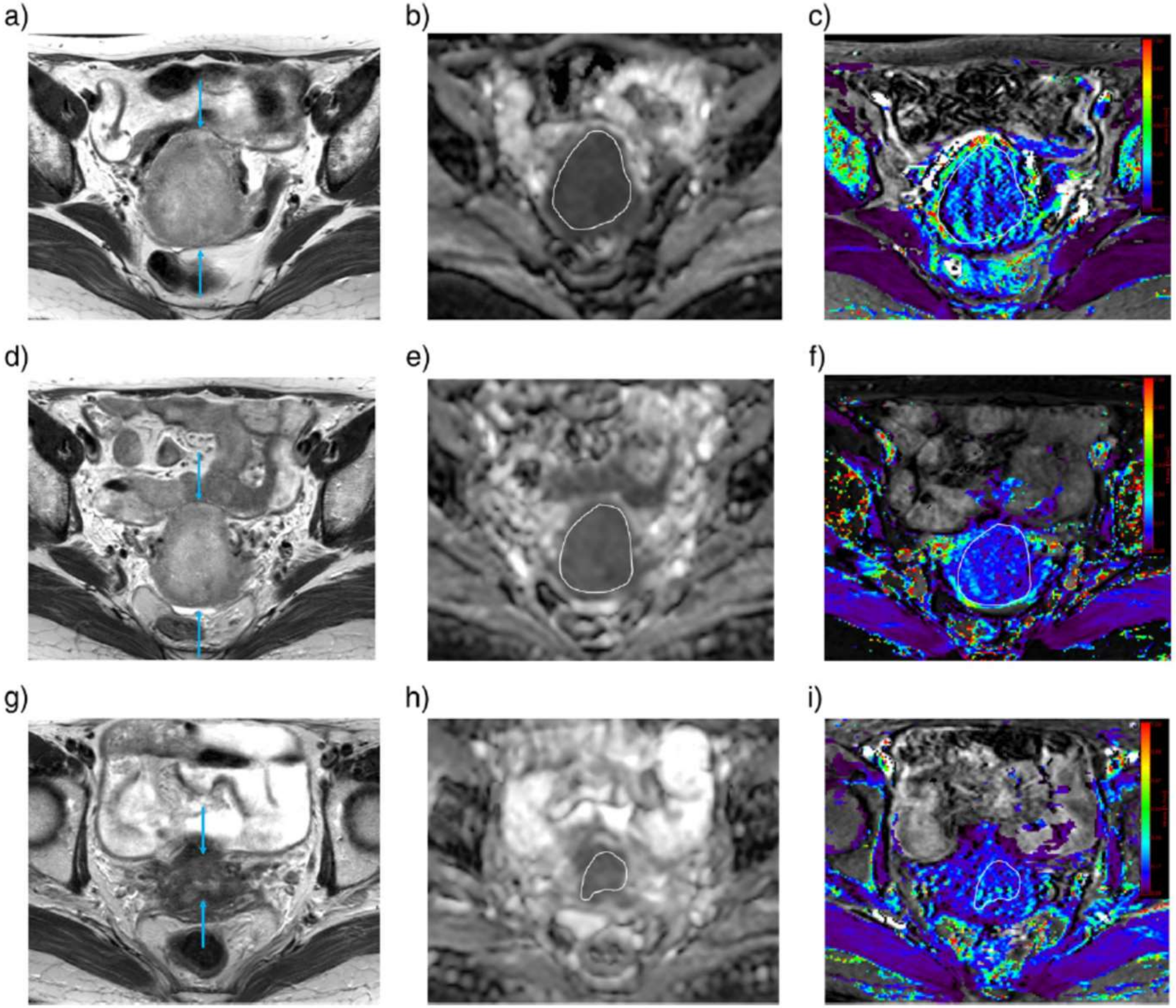

Before CRT

1 week into CRT

1 month after CRT

Park J.J. et al. Magnetic Resonance Imaging 2014.

Response assessment: DWI

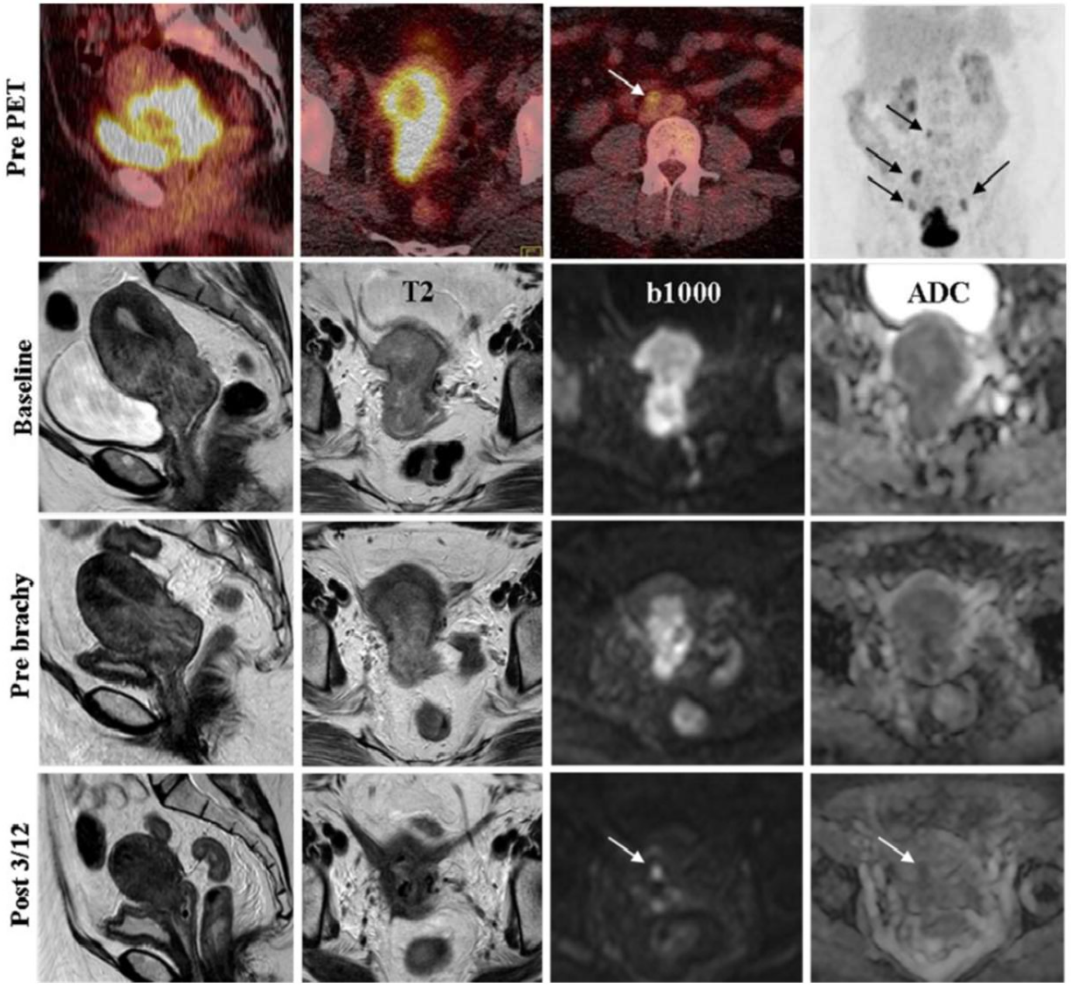
Pre PET
Baseline
Pre brachy
Post 3/12
T2
b1000
ADC

Barwick T. et al. Curr Oncol Rep 2013.

DWI for response assessment

Meta-analysis of 9 studies with 231 patients (Ib1 – IVB)

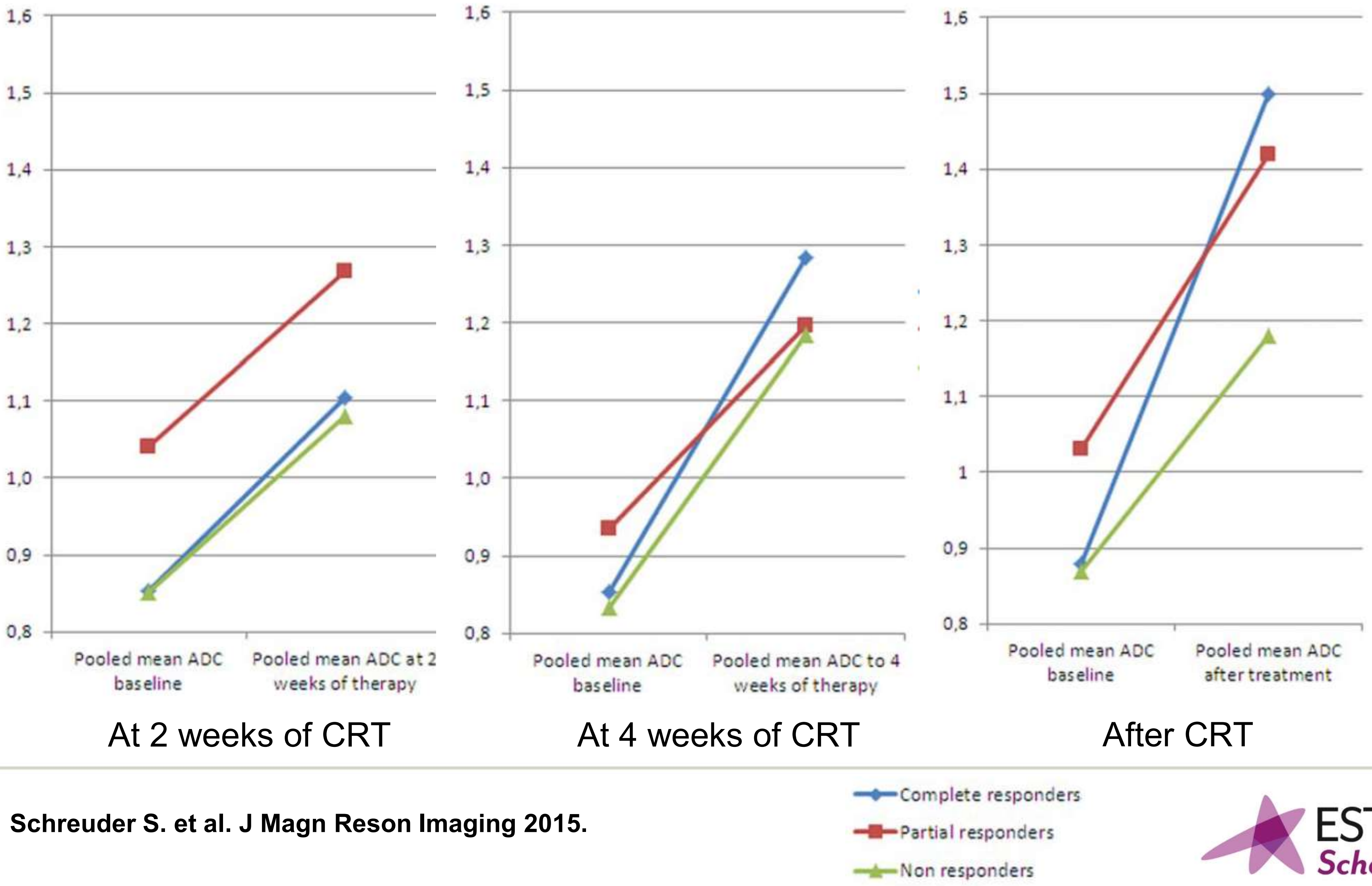

At 2 weeks of CRT

At 4 weeks of CRT

After CRT

Schreuder S. et al. J Magn Reson Imaging 2015.

Response assessment: PET/MRI

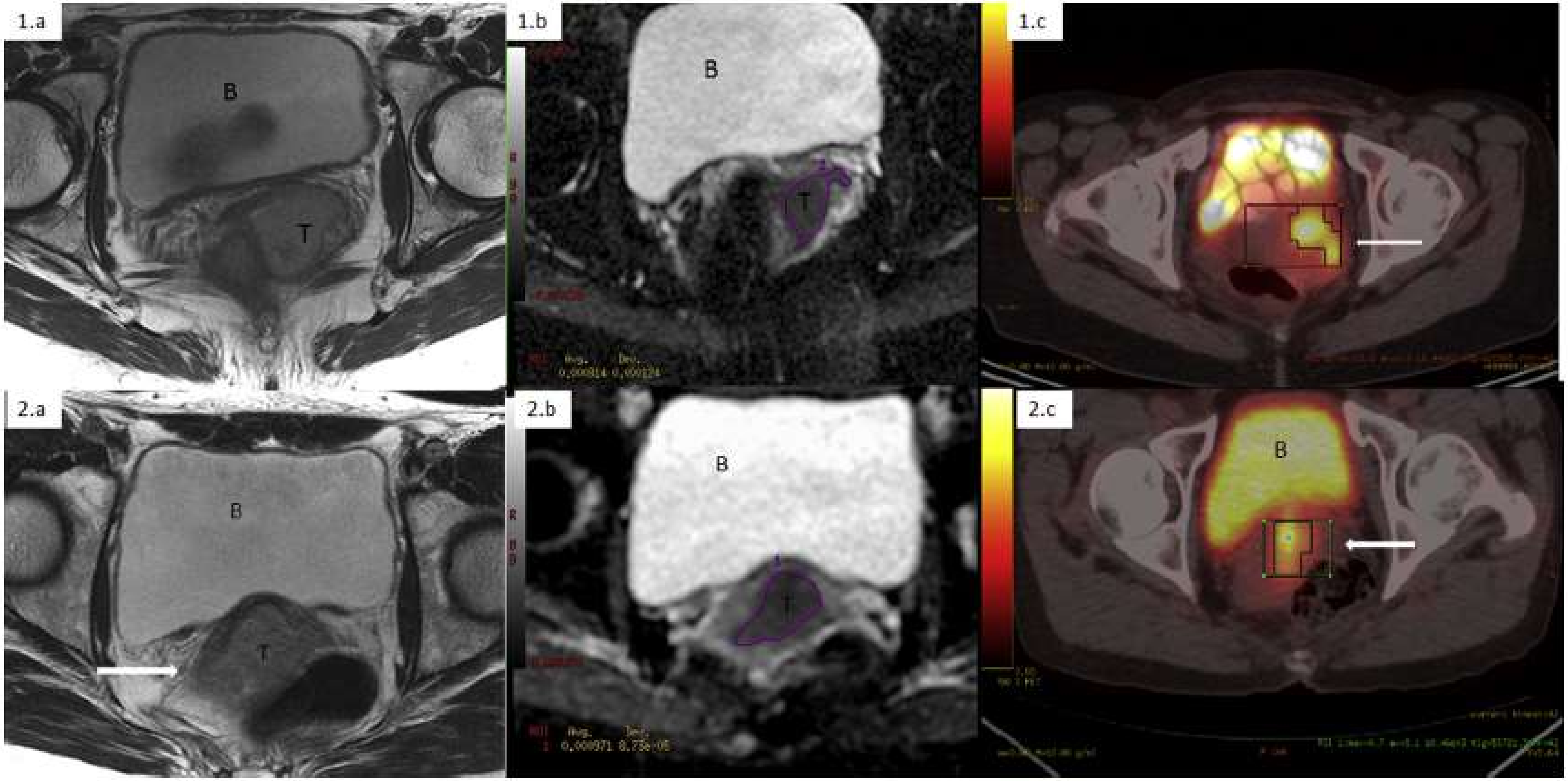
1.a
B
T
1.b
B
T
1.c
2.a
B
T
2.b
B
T
2.c
B

Micco M. et al. Eur J Radiol 2014.

Take home messages

- Using MRI, patients can be more accurately staged and guided towards the correct management options.
- For patients that require radiation therapy, MRI shows excellent soft tissue delineation and should be incorporated into both external beam and brachytherapy treatment planning.
- Image-based BT allows for individualization of the applicator with possible incorporation of interstitial needles, leading to adapted treatment planning, optimized prescription dose and limitation of dose to OAR.
- In the future, MRI will likely become even more prevalent as deformable dose registration, adaptive imaging for external beam and functional imaging become more established.

MRI throughout cervical cancer treatment

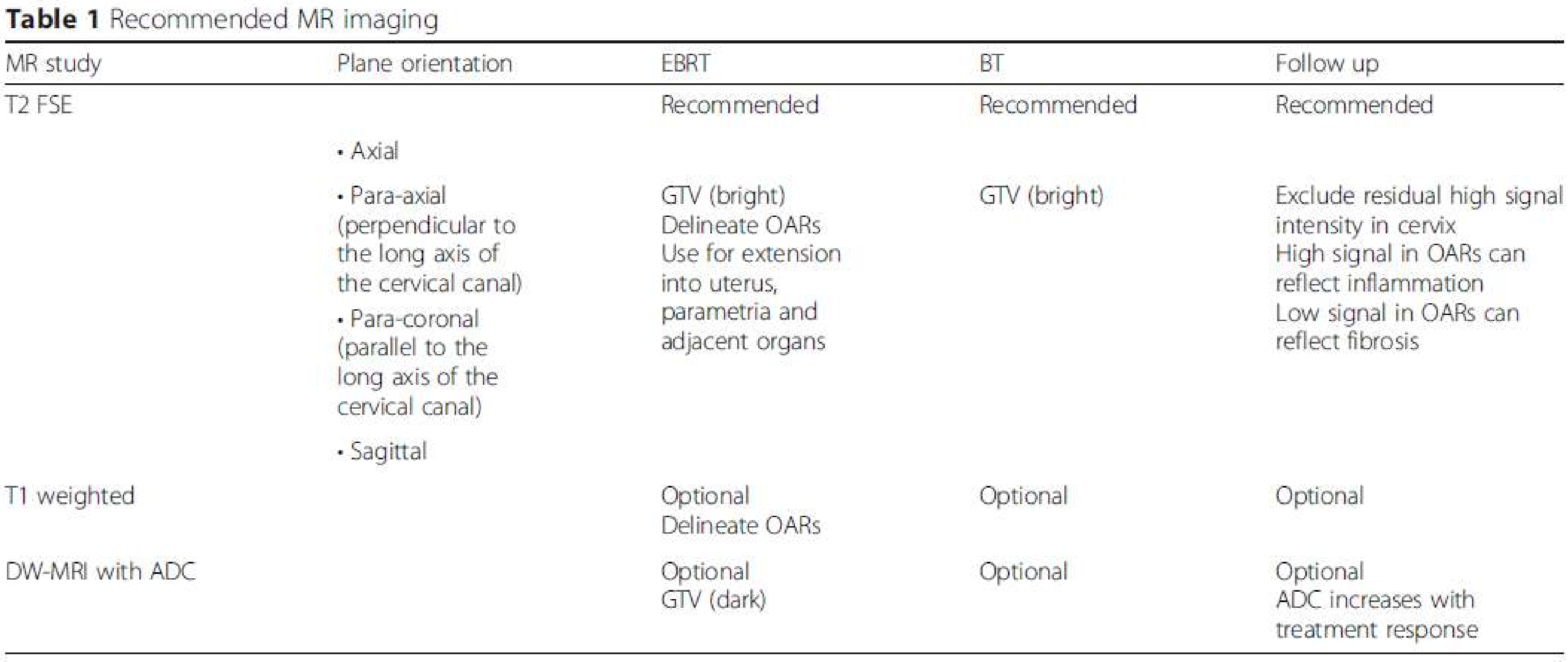

Table 1 Recommended MR imaging

MR study	Plane orientation	EBRT	BT	Follow up
T2 FSE		Recommended	Recommended	Recommended
	• Axial			
	• Para-axial (perpendicular to the long axis of the cervical canal) • Para-coronal (parallel to the long axis of the cervical canal)	GTV (bright) Delineate OARs Use for extension into uterus, parametria and adjacent organs	GTV (bright)	Exclude residual high signal intensity in cervix High signal in OARs can reflect inflammation Low signal in OARs can reflect fibrosis
	• Sagittal			
T1 weighted		Optional Delineate OARs	Optional	Optional
DW-MRI with ADC		Optional GTV (dark)	Optional	Optional ADC increases with treatment response

Fields E. et al. Radiat Oncol 2016.

Applications: MRI in Prostate

Cynthia Ménard, M.D.

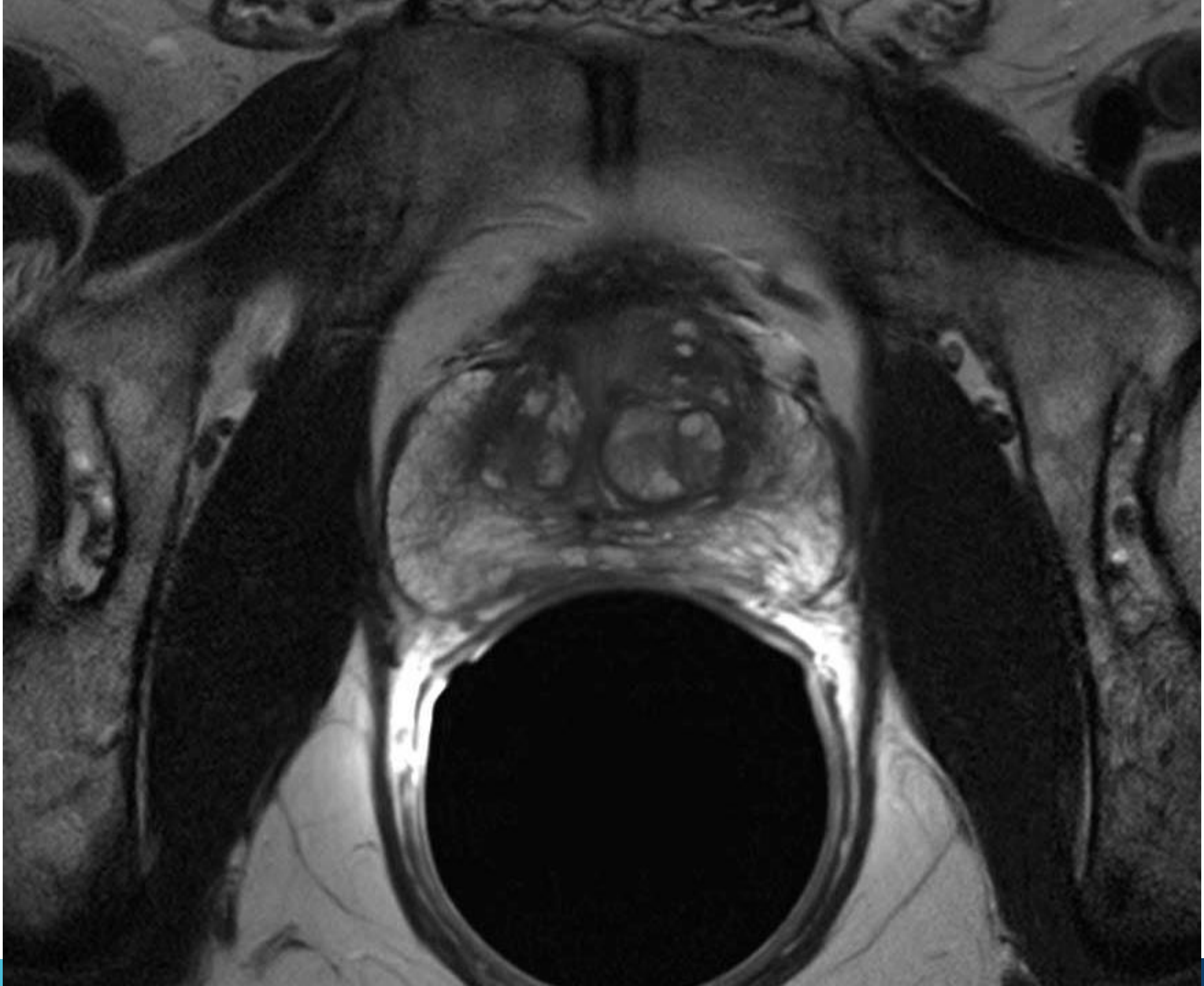

MRI – Target Delineation

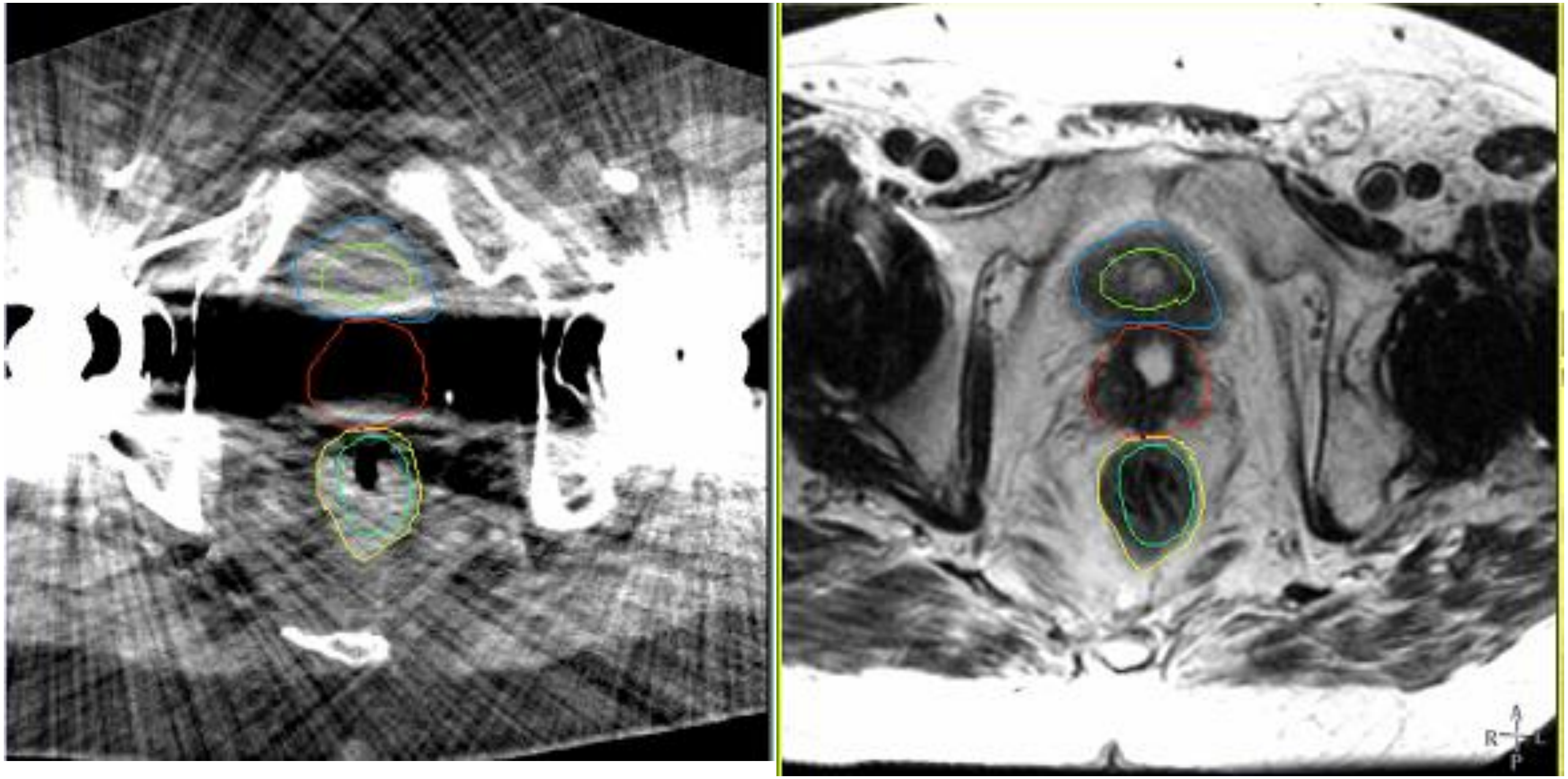

📖 Rosewall et al., Radiother Oncol. 2009 Mar;90(3):325-30.

MRI Integration Improves Prostate Delineation Accuracy?

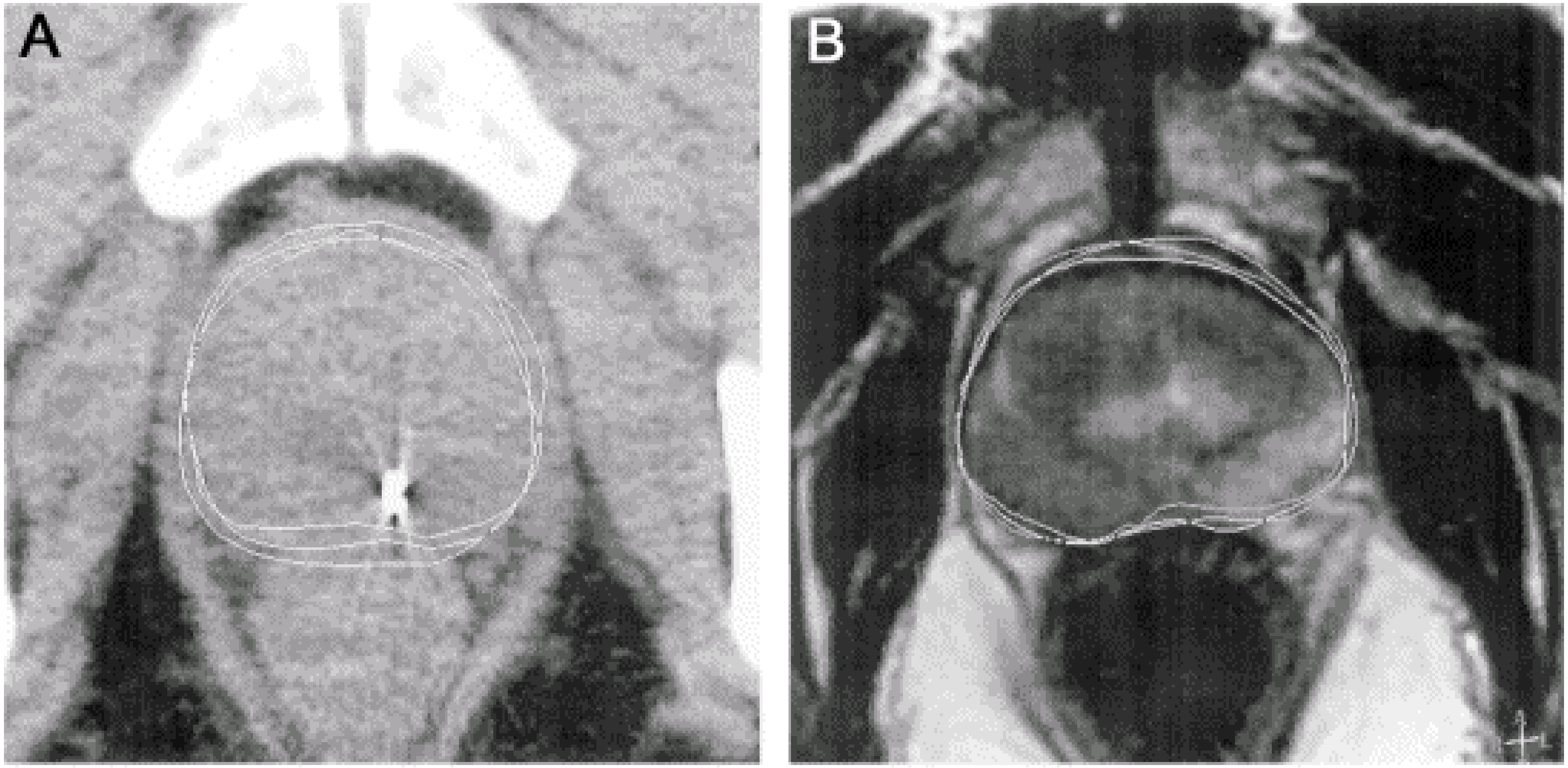

- 🕮 Milosevic et al., Radiother Oncol, 1998
- 🕮 Wachter, et al., Strahlenther Onkol, 2002
- 🕮 Parker et al, Radiot Oncol, 2003
- 🕮 Villeirs et al., Int J Radiat Oncol Biol Phys, 2004
- 🕮 Villeirs et al., Strahlenther Onkol, 2005
- 🕮 Nyholm et al., Radiat Oncol 2013

CHUM

Smaller CTV

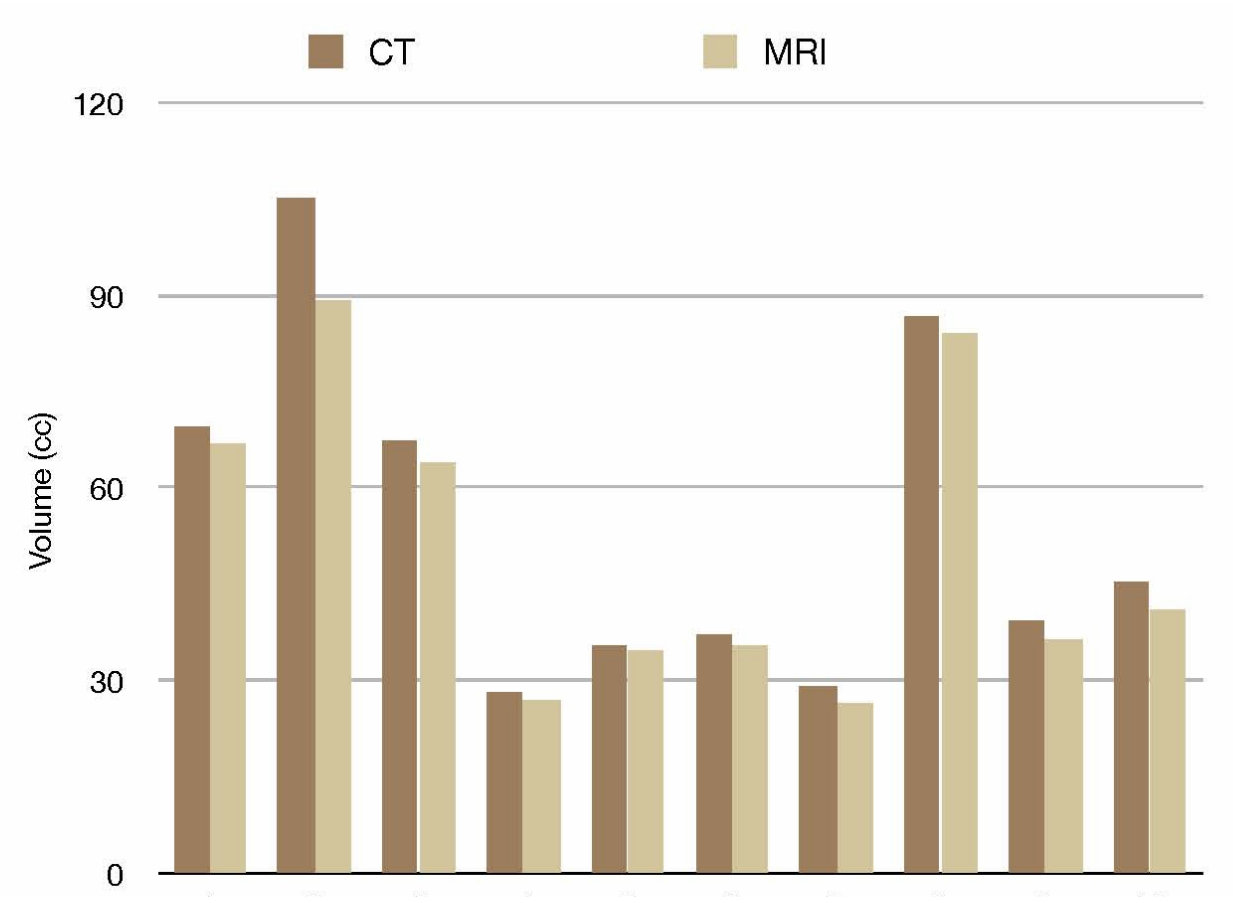

Roach, M., 3rd, et al., Int J Radiat Oncol Biol Phys, 1996
Kagawa, K., et al., Int J Radiat Oncol Biol Phys, 1997
Debois et al., Int J Radiat Oncol Biol Phys, 1999
Rasch, C., et al., Int J Radiat Oncol Biol Phys, 1999
Smith, W.L., et al., Int J Radiat Oncol Biol Phys, 2007

Better Dosimetry

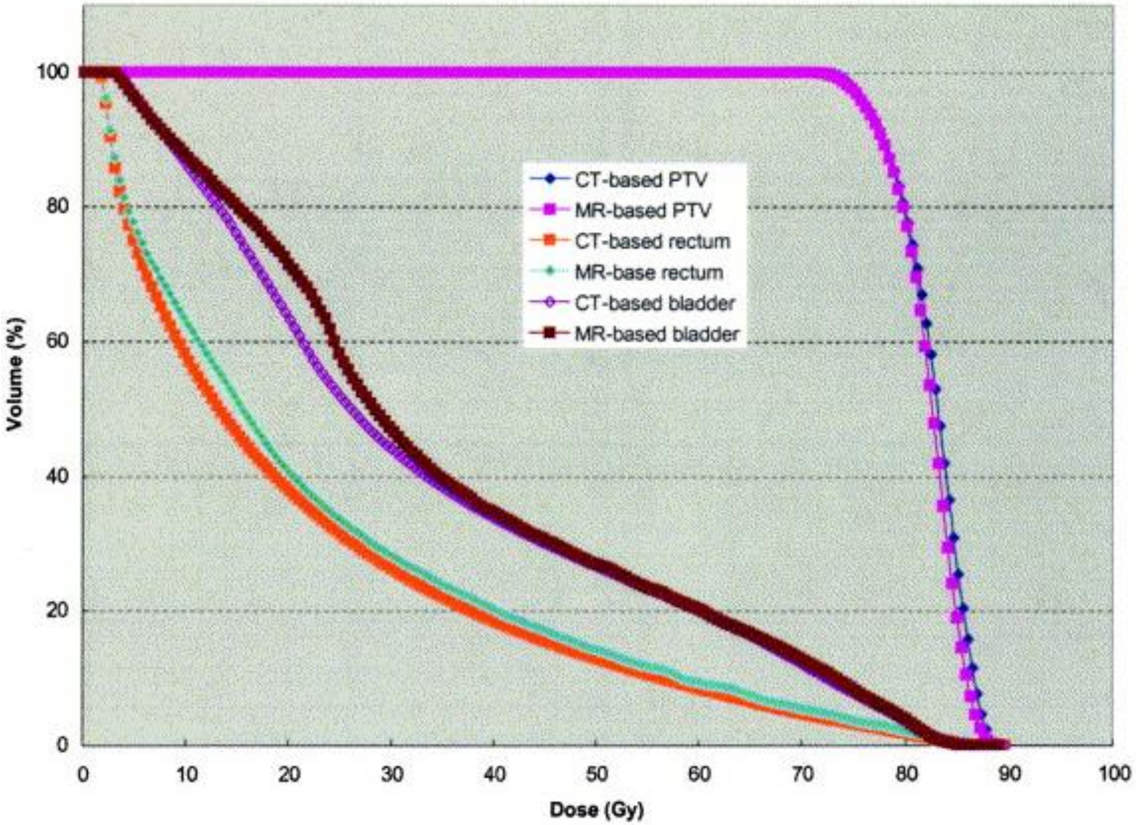

- 🕮 Sannazzari, G.L., et al., Br J Radiol, 2002. (b)
- 🕮 Chen et al., 2004
- 🕮 Buyyounouski, M.K., et al., Int J Radiat Oncol Biol Phys, 2004
- 🕮 McLaughlin, P.W., et al., Int J Radiat Oncol Biol Phys, 2005

CHUM

Better Outcomes?

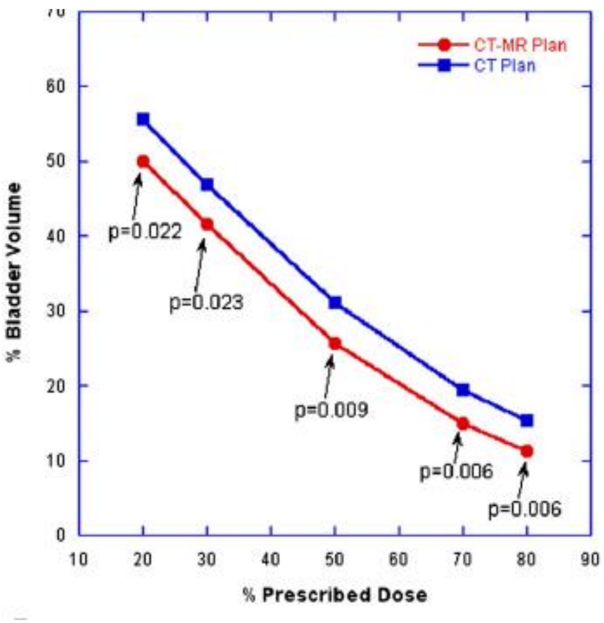

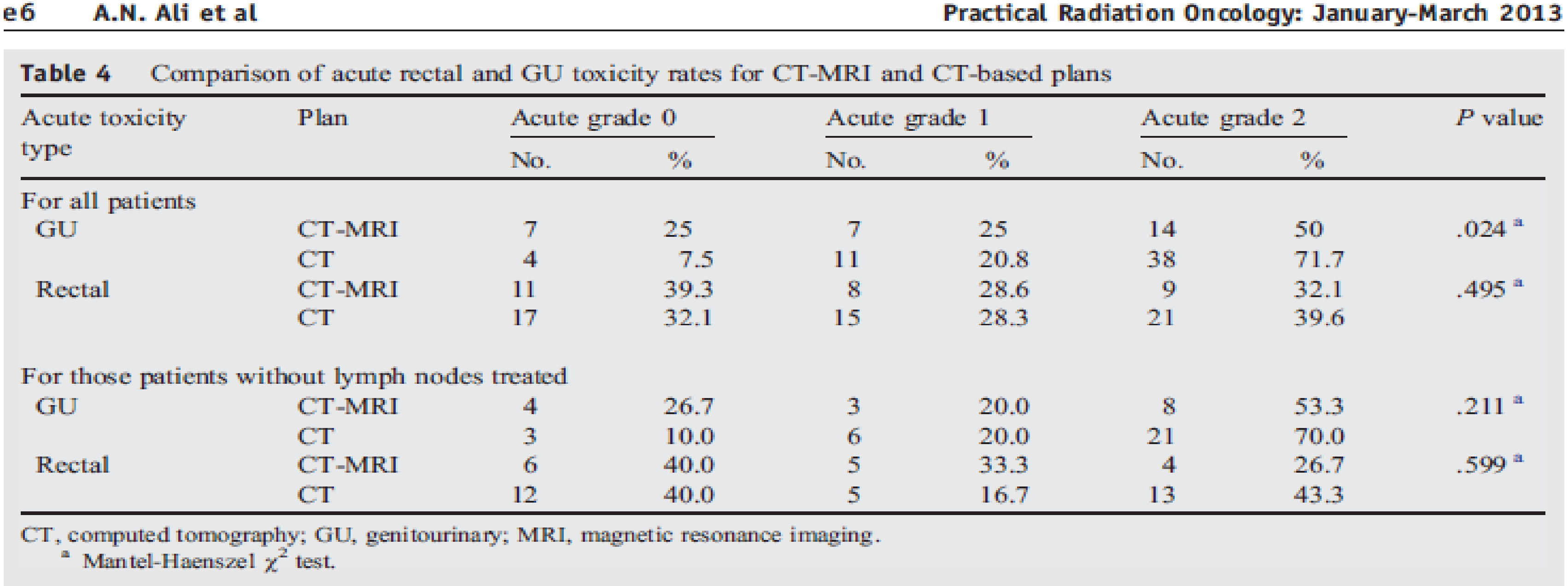

e6 **A.N. Ali et al** **Practical Radiation Oncology: January-March 2013**

Table 4 Comparison of acute rectal and GU toxicity rates for CT-MRI and CT-based plans

Acute toxicity type	Plan	Acute grade 0		Acute grade 1		Acute grade 2		*P* value
		No.	%	No.	%	No.	%	
For all patients								
GU	CT-MRI	7	25	7	25	14	50	.024 [a]
	CT	4	7.5	11	20.8	38	71.7	
Rectal	CT-MRI	11	39.3	8	28.6	9	32.1	.495 [a]
	CT	17	32.1	15	28.3	21	39.6	
For those patients without lymph nodes treated								
GU	CT-MRI	4	26.7	3	20.0	8	53.3	.211 [a]
	CT	3	10.0	6	20.0	21	70.0	
Rectal	CT-MRI	6	40.0	5	33.3	4	26.7	.599 [a]
	CT	12	40.0	5	16.7	13	43.3	

CT, computed tomography; GU, genitourinary; MRI, magnetic resonance imaging.

[a] Mantel-Haenszel χ^2 test.

Dominant Tumors

- Need to further improve *radio-*therapeutic ratio in prostate cancer
- Cancer outcomes related to gross tumor-bearing sub-regions
- Approach → Tumor-targeting
- Need → Accurate technique

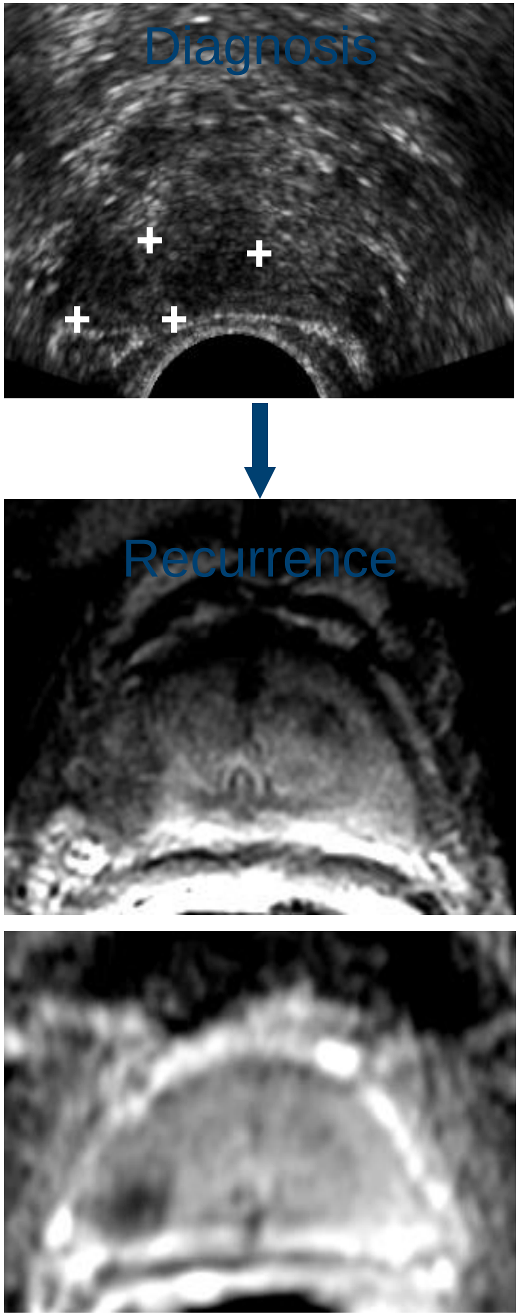

🕮Pucar *et al.* IJROBP 69(1) 2007

🕮Joseph *et al.* IJROBP 73(3) 2009

🕮Arrayeh et al. IJROBP 82(5) 2012

Local Failure

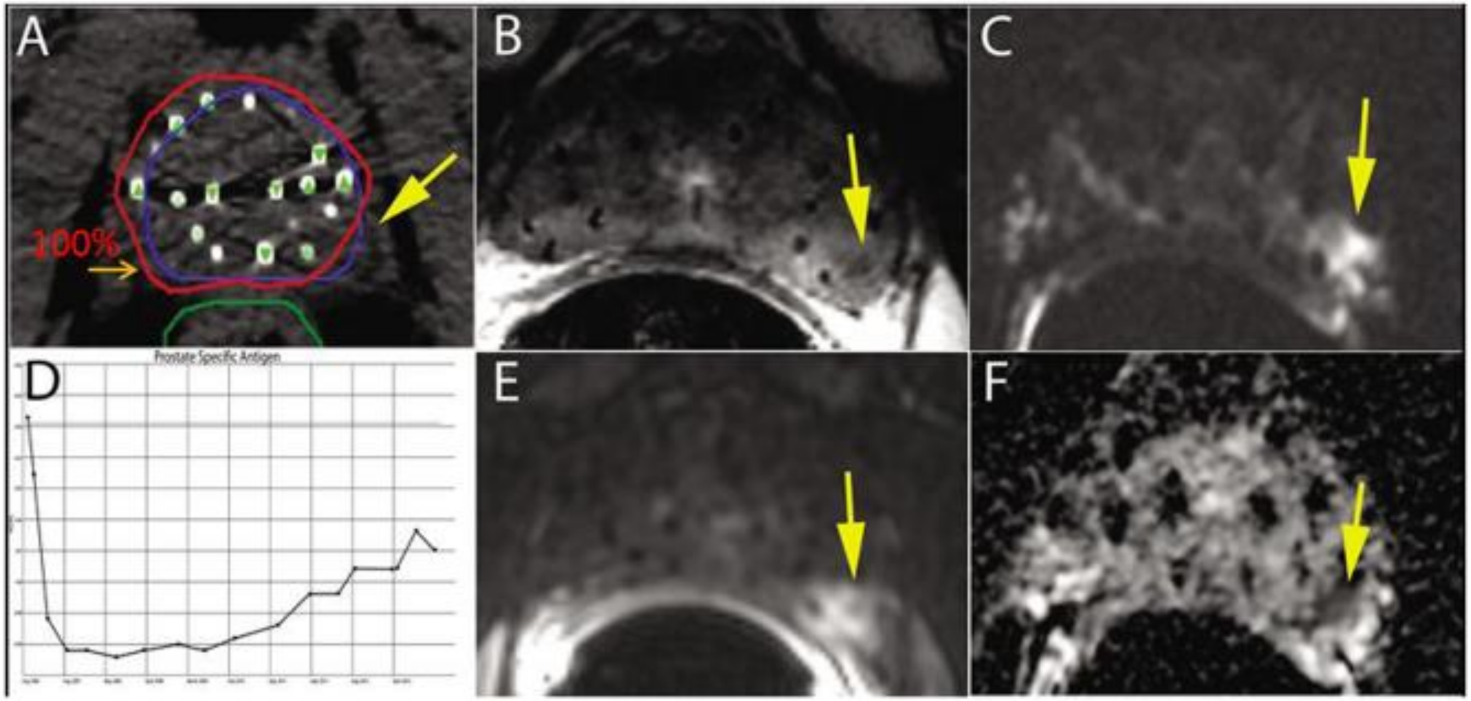

Figure 5 A 75-year-old male presented with a small nodule at the left base of the gland (ie, clinical T2a), PSA of 6 ng/mL, and Gleason Score (GS) of 7 (3 + 4) and was treated with a prostate brachytherapy implant alone to 144 Gy with 125-I (A). Postimplant dosimetry demonstrated a V100 = 97% and a D90 = 177 Gy; however, the left midgland was not covered with the 100% isodose line (A). The patient's PSA reached a nadir of 0.3 ng/mL 18 months after the implant. At 6 years after treatment, he had a PSA of 2.3 ng/mL with a PSA doubling time greater than 12 months (D). Multiparametric 1.5T MRI including T2W (B), DWI (C), DCE (E), and ADC maps (F) localized the recurrence at the left midgland. Metastatic workup showed negative result. Biopsy of the left midgland confirmed adenocarcinoma with a GS of 7 (4 + 3). ADC, apparent diffusion coefficient. (Color version of figure is available online.)

Tanderup et al., Sem Rad Oncol 2014

Imaging Tumours

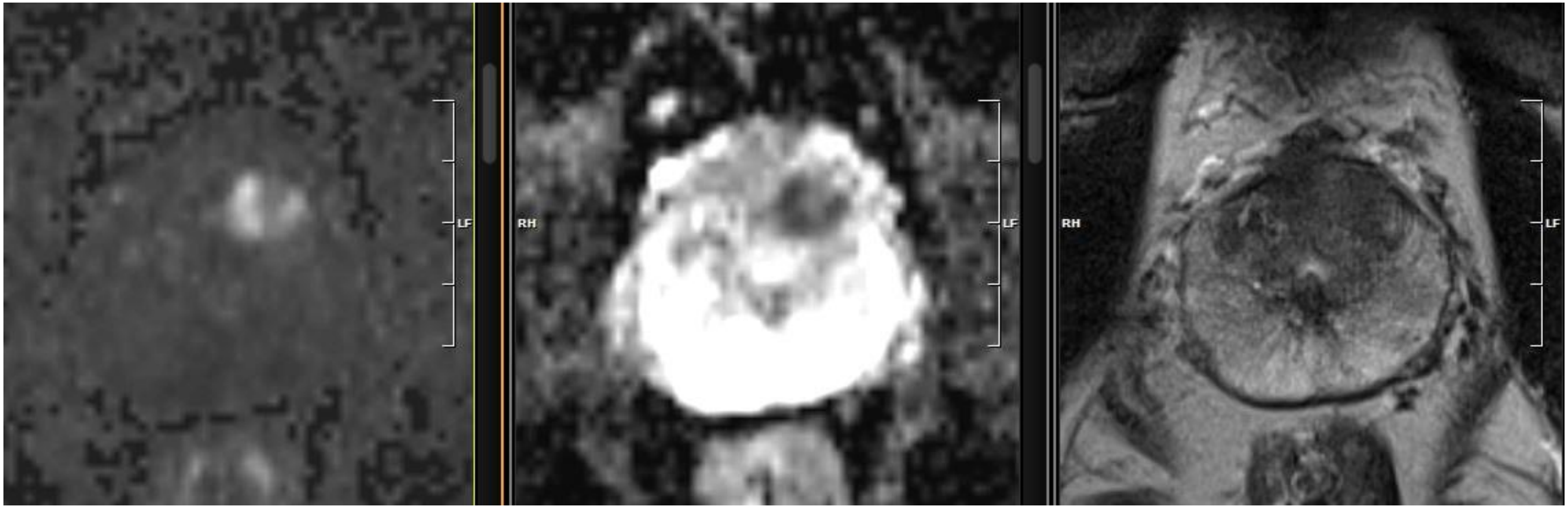
LF
RH
LF
RH
LF

PIRADS v2.0, ACR, 2015

Cancer is Not Confided to the Prostate Gland

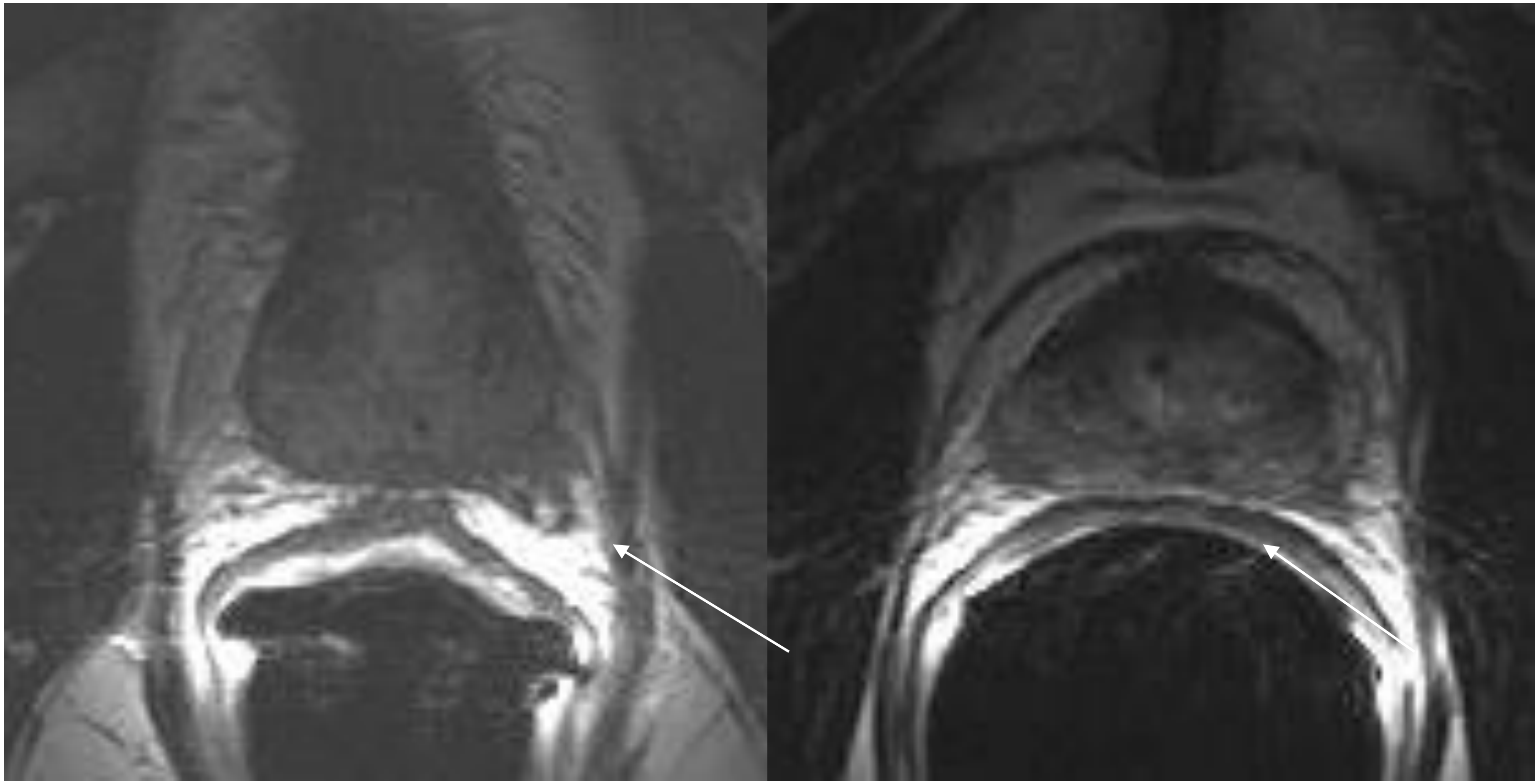

Courtesy P. Choyke

Independent Predictive Factor

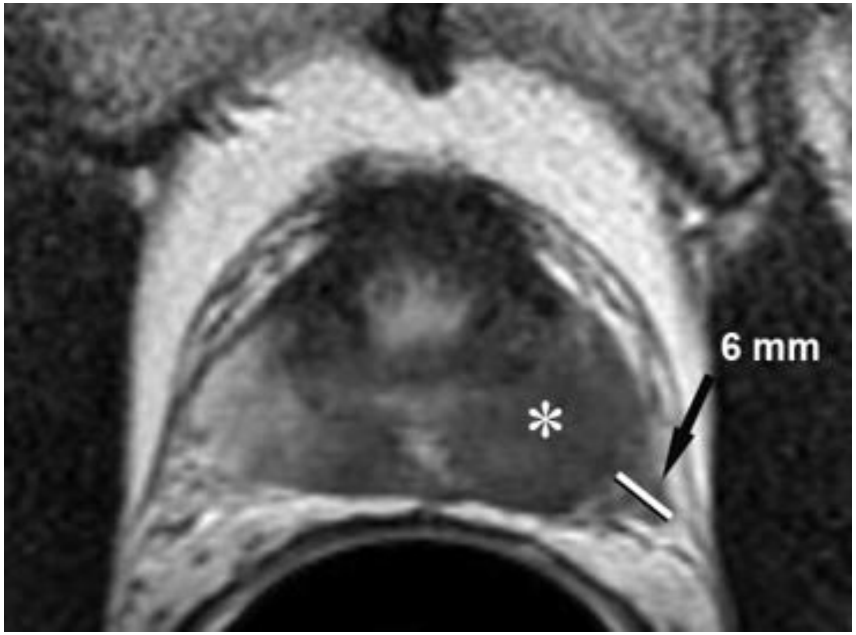

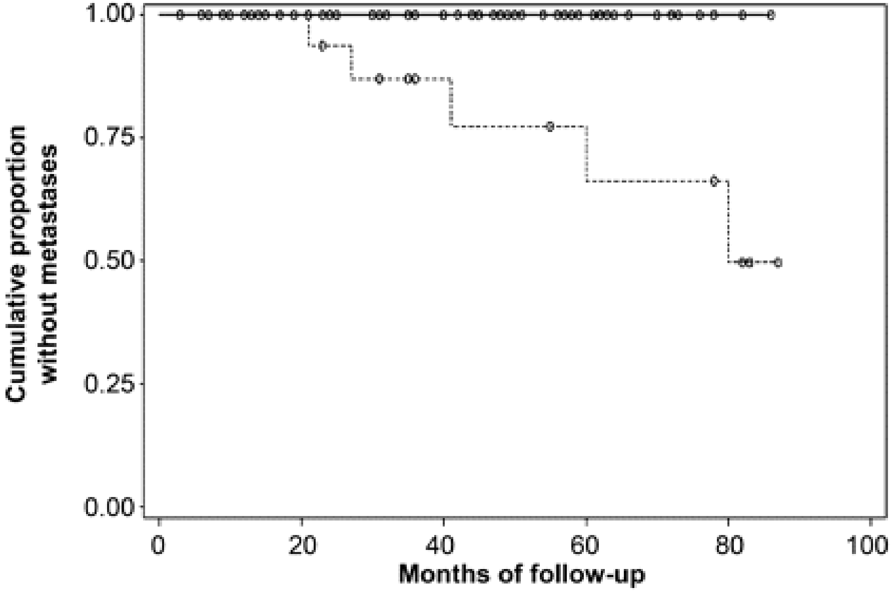

- Nguyen et al. IJROBP 59(2) 2004
- McKenna et al. Radiology 247(1) 2008
- Westphalen et al. Radiology 261(2) 2011

ECE and Brachytherapy

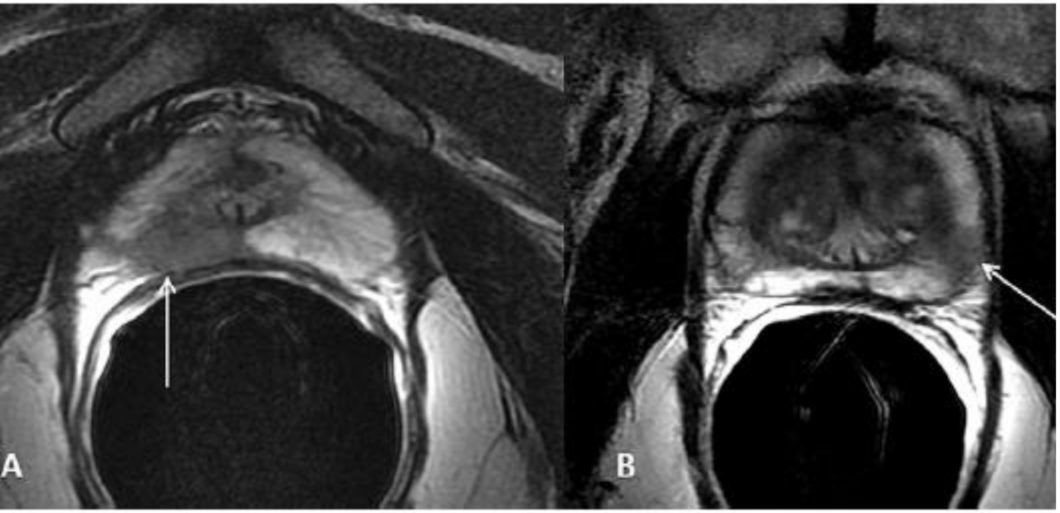

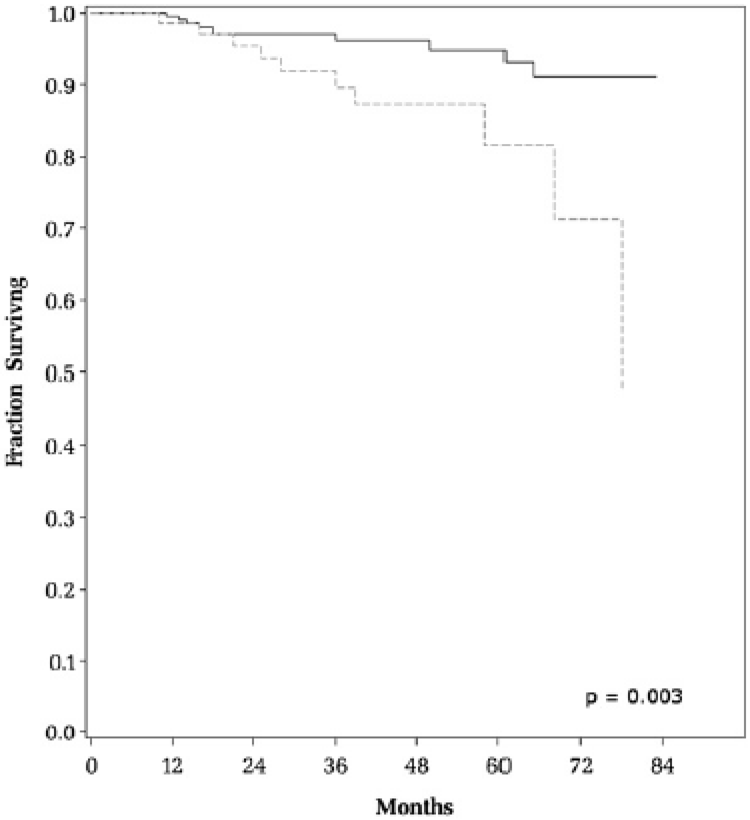

Number at Risk

No ECE	207	173	119	74	55	38	29
ECE	69	55	42	24	13	6	2

📖 Riaz et al, Int J Radiat Oncol Biol Phys 2012

MRI prior to RT - Upstaging

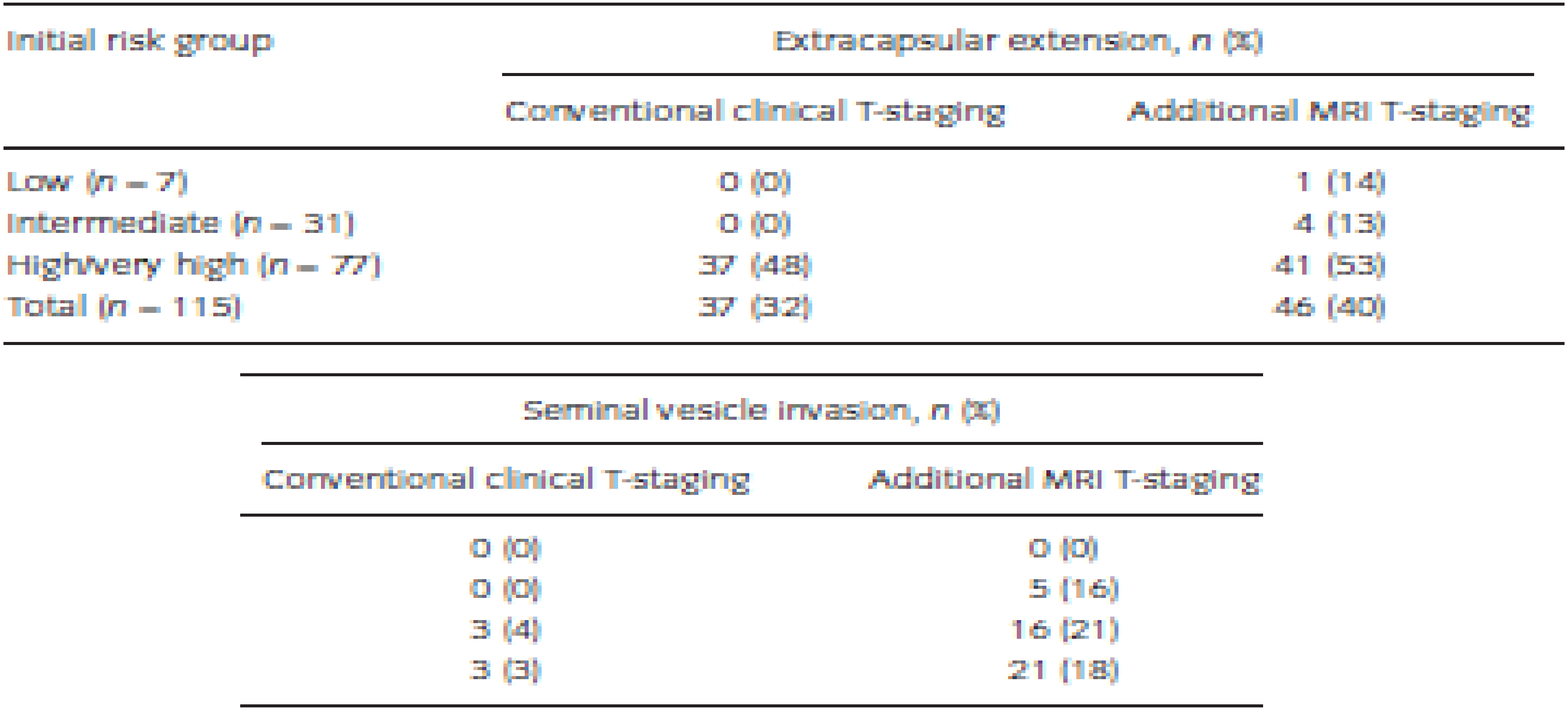

Initial risk group	Extracapsular extension, *n* (%)		Seminal vesicle invasion, *n* (%)	
	Conventional clinical T-staging	Additional MRI T-staging	Conventional clinical T-staging	Additional MRI T-staging
Low (*n* = 7)	0 (0)	1 (14)	0 (0)	0 (0)
Intermediate (*n* = 31)	0 (0)	4 (13)	0 (0)	5 (16)
High/very high (*n* = 77)	37 (48)	41 (53)	3 (4)	16 (21)
Total (*n* = 115)	37 (32)	46 (40)	3 (3)	21 (18)

Chang JMIRO 2014

MRI-Guided Biopsy - Upgrading

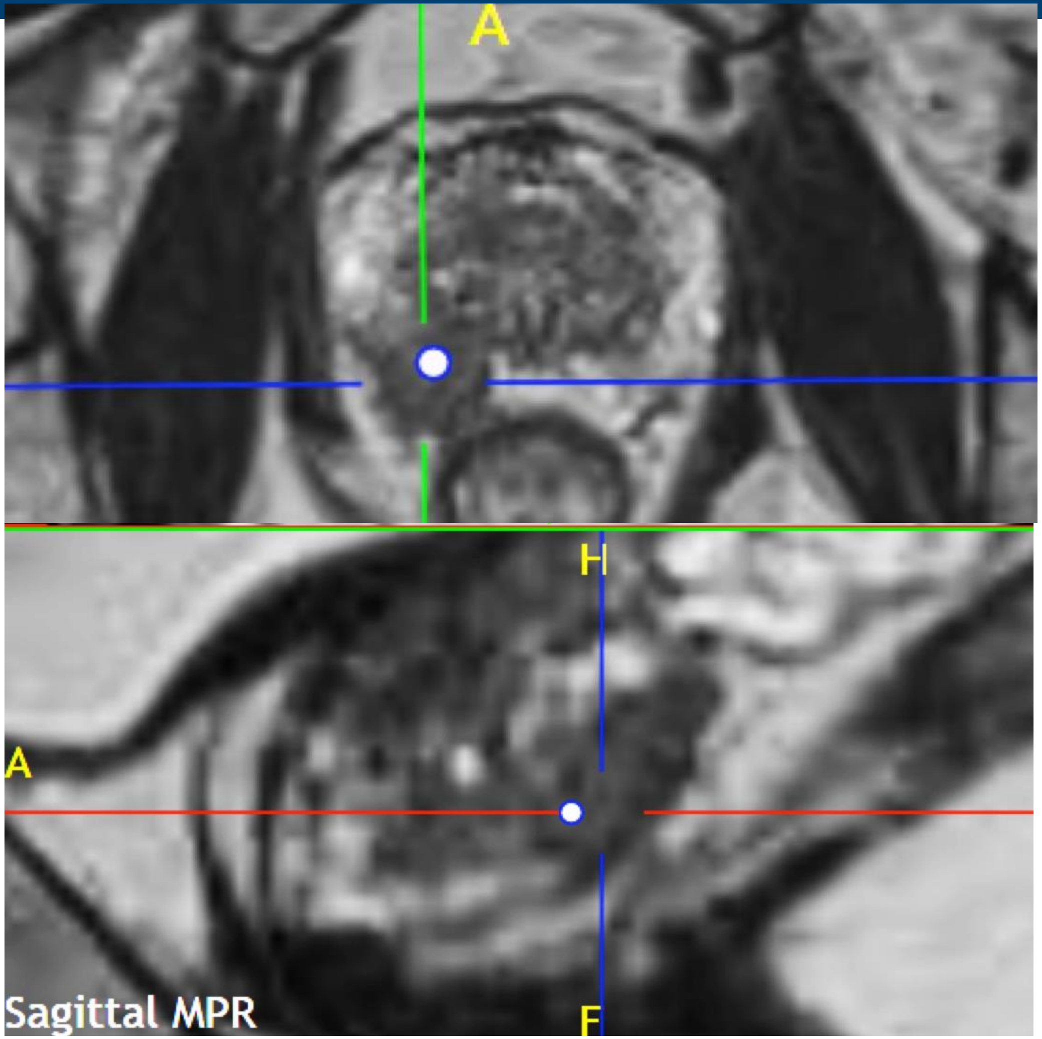
A
H
A
Sagittal MPR
F

📖Ménard et al, Radiol Clin NA, In Press

Volume of Tumor Burden on MRI and Radiotherapy Outcomes

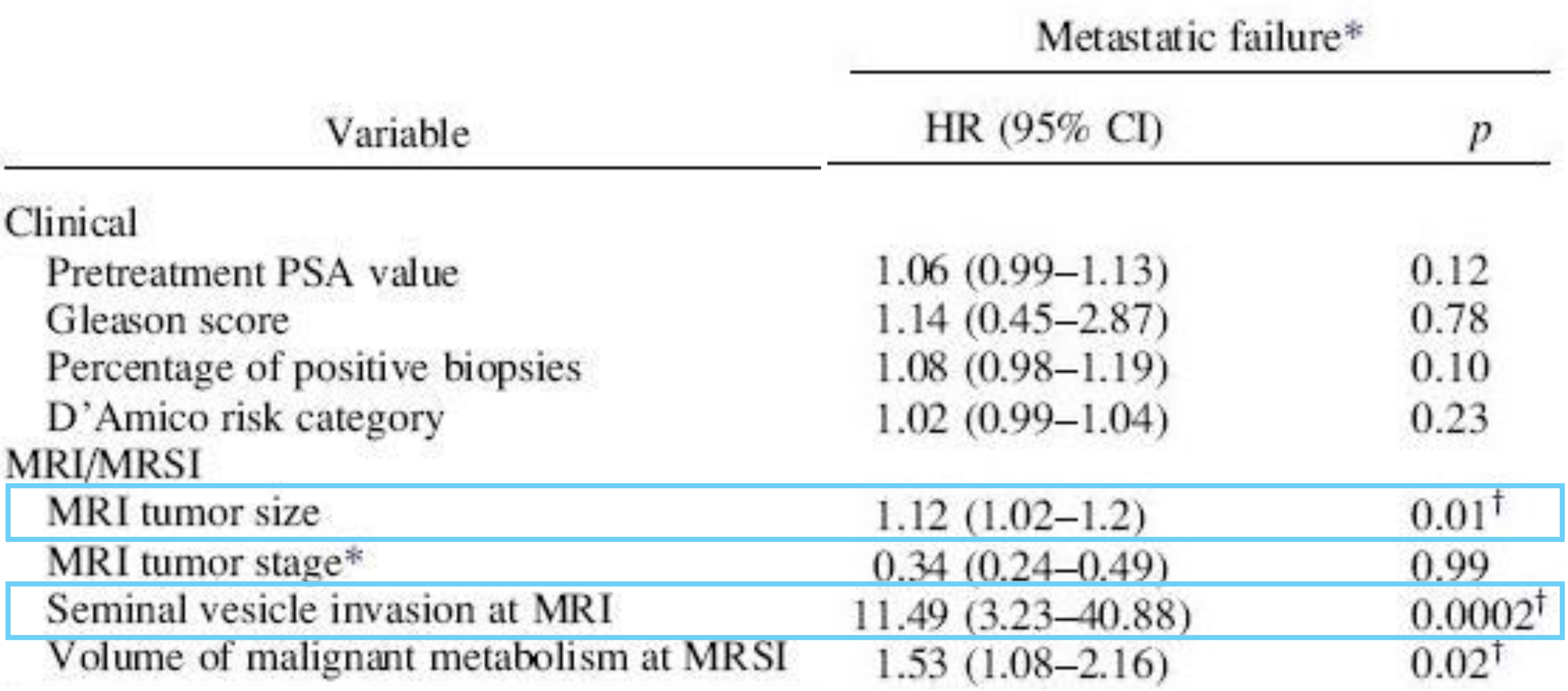

Variable	Metastatic failure*	
	HR (95% CI)	*p*
Clinical		
Pretreatment PSA value	1.06 (0.99–1.13)	0.12
Gleason score	1.14 (0.45–2.87)	0.78
Percentage of positive biopsies	1.08 (0.98–1.19)	0.10
D'Amico risk category	1.02 (0.99–1.04)	0.23
MRI/MRSI		
MRI tumor size	1.12 (1.02–1.2)	0.01†
MRI tumor stage*	0.34 (0.24–0.49)	0.99
Seminal vesicle invasion at MRI	11.49 (3.23–40.88)	0.0002†
Volume of malignant metabolism at MRSI	1.53 (1.08–2.16)	0.02†

📖 Joseph et al. IJROBP 2008

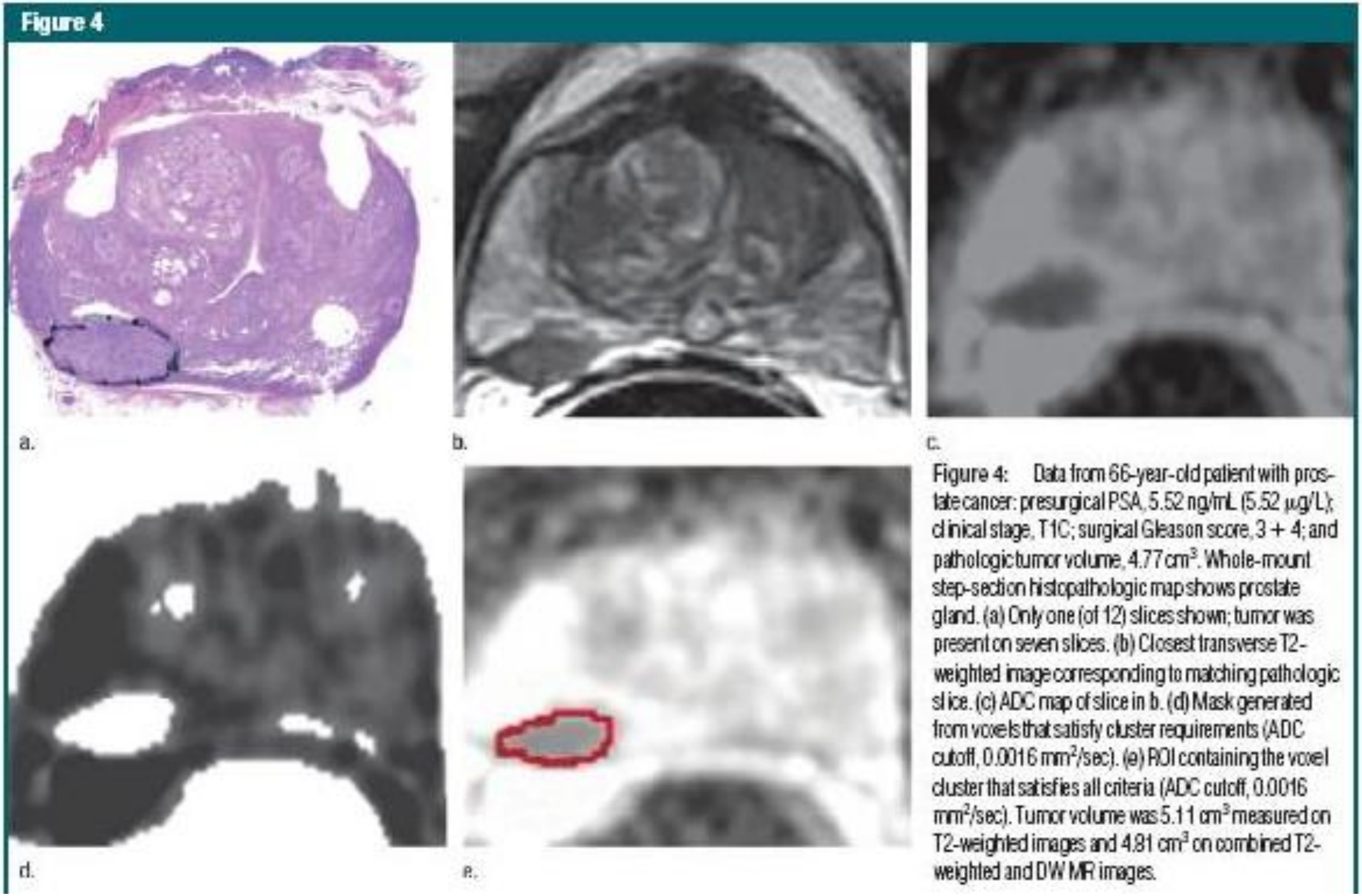

Figure 4: Data from 66-year-old patient with prostate cancer: presurgical PSA, 5.52 ng/mL (5.52 µg/L); clinical stage, T1C; surgical Gleason score, 3 + 4; and pathologic tumor volume, 4.77 cm^3. Whole-mount step-section histopathologic map shows prostate gland. (a) Only one (of 12) slices shown; tumor was present on seven slices. (b) Closest transverse T2-weighted image corresponding to matching pathologic slice. (c) ADC map of slice in b. (d) Mask generated from voxels that satisfy cluster requirements (ADC cutoff, 0.0016 mm^2/sec). (e) ROI containing the voxel cluster that satisfies all criteria (ADC cutoff, 0.0016 mm^2/sec). Tumor volume was 5.11 cm^3 measured on T2-weighted images and 4.81 cm^3 on combined T2-weighted and DW MR images.

📖 Mazaheri Y et al. Radiology 2009;252:449-457

Scatterplots of tumor volume measurements made on basis of MR images (T2-weighted and combined T2-weighted and DW MR images) versus histopathologic measurements

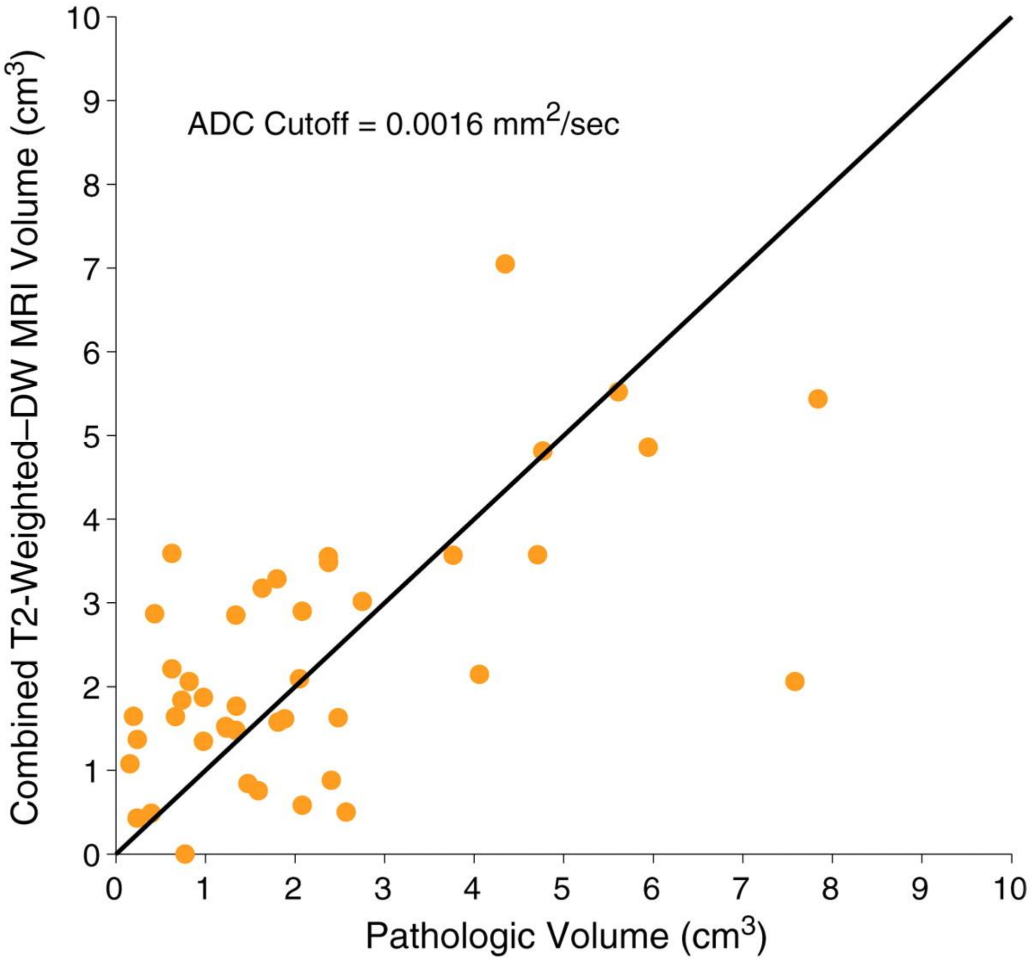

Mazaheri Y et al. Radiology 2009;252:449-457

©2009 by Radiological Society of North America

Box-and-whisker plot of ADCs of tumor lesions for three Gleason grades from 60 cancer lesions in 42 patients

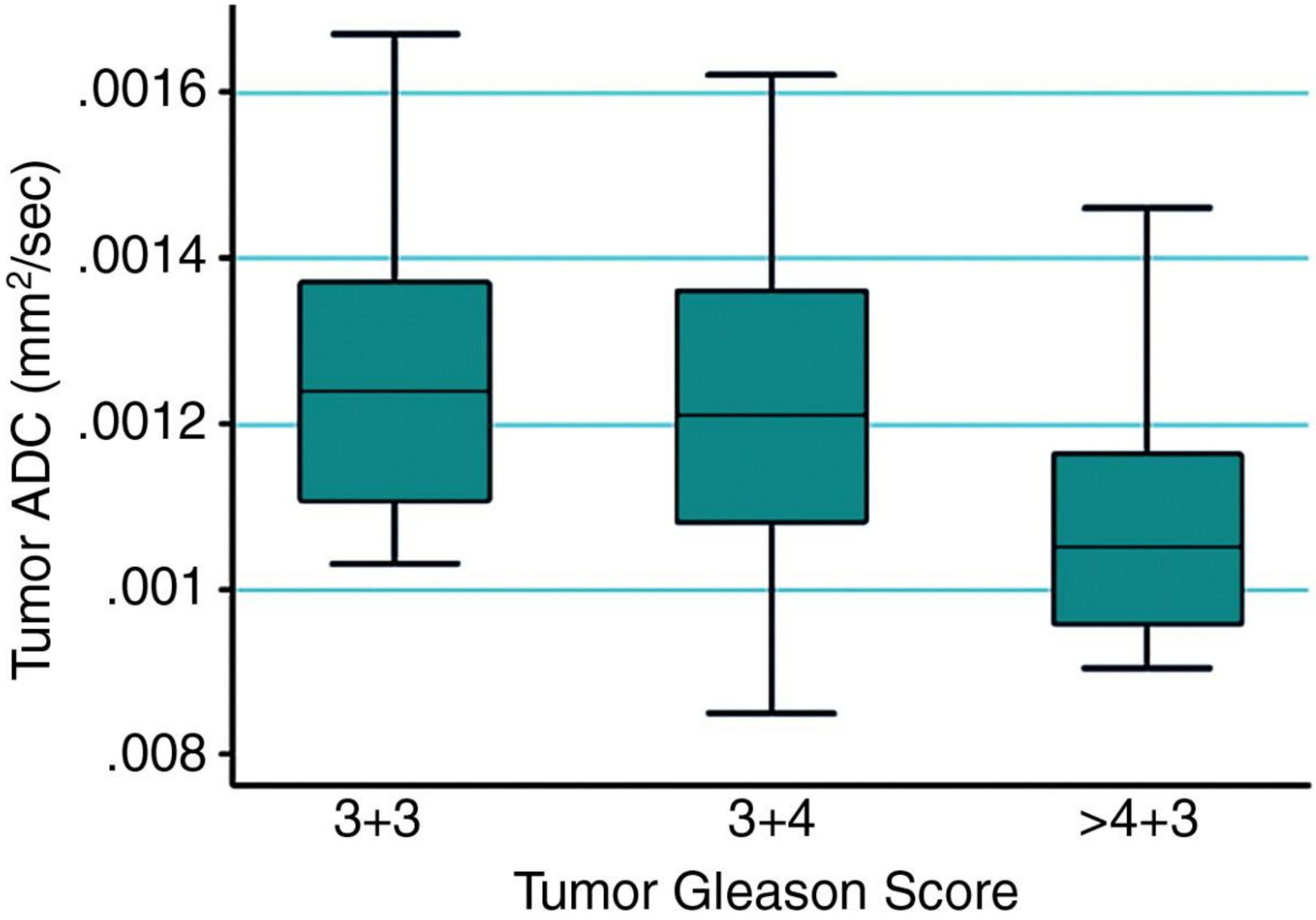

Mazaheri Y et al. Radiology 2009;252:449-457

©2009 by Radiological Society of North America

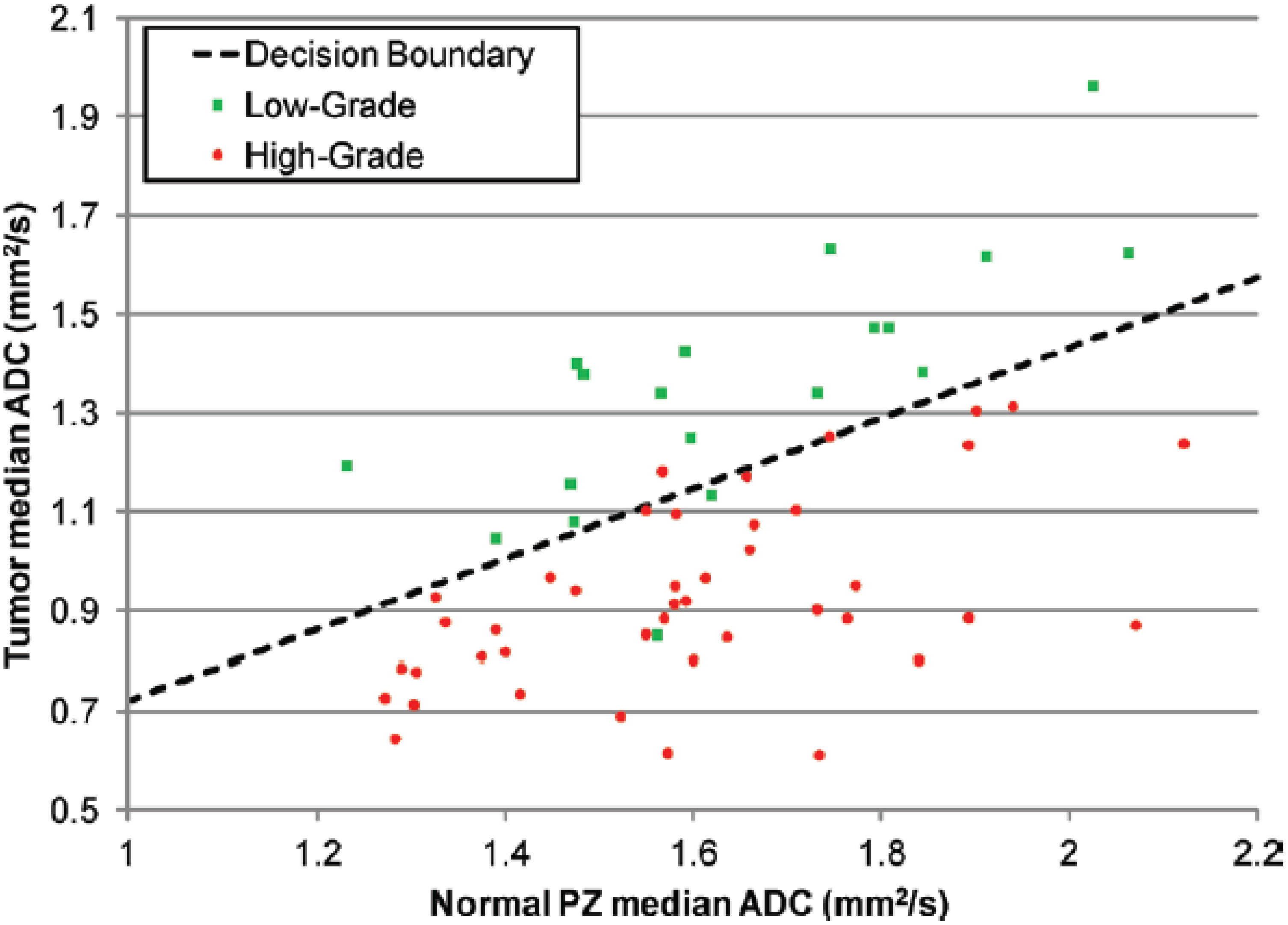

📖 Litjens et al. Radiology 2012

Neo-adjuvant Hormones

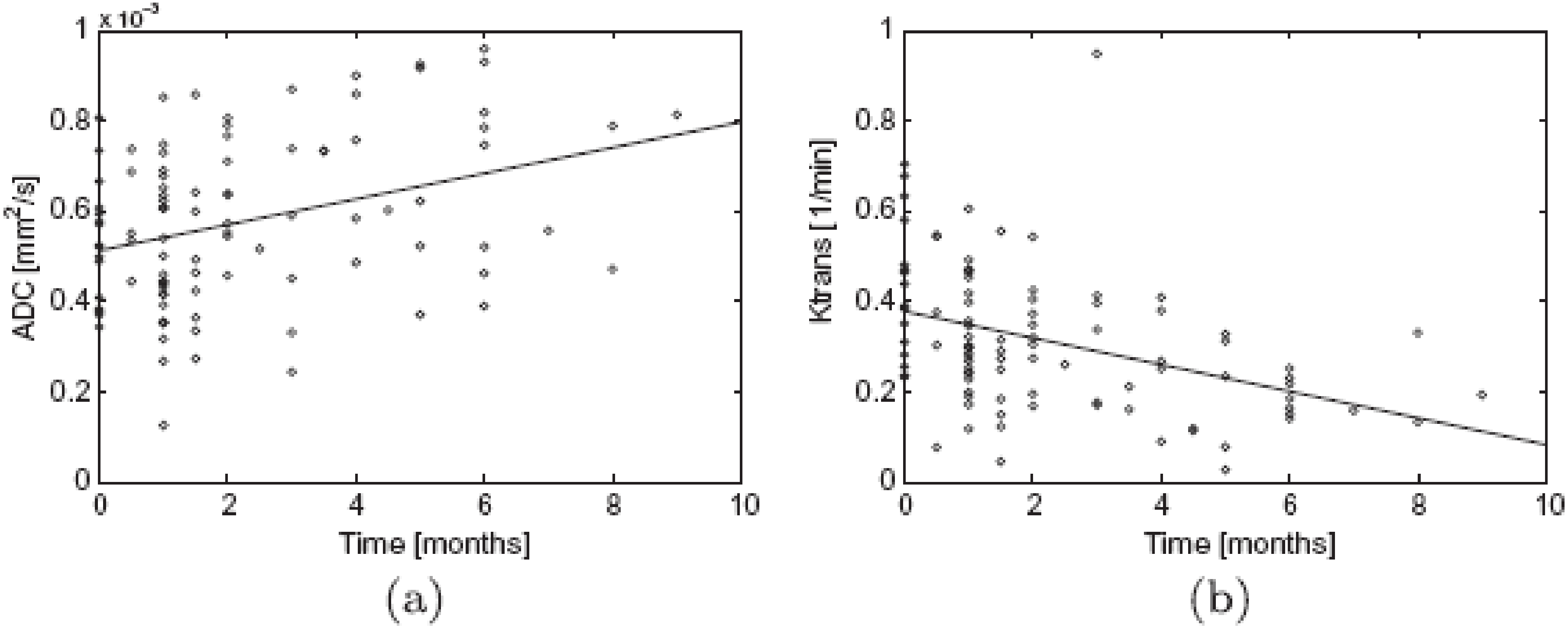

📖 Groenendaal et al., Radiother Oncol 2012

Probability Maps - Radiomics

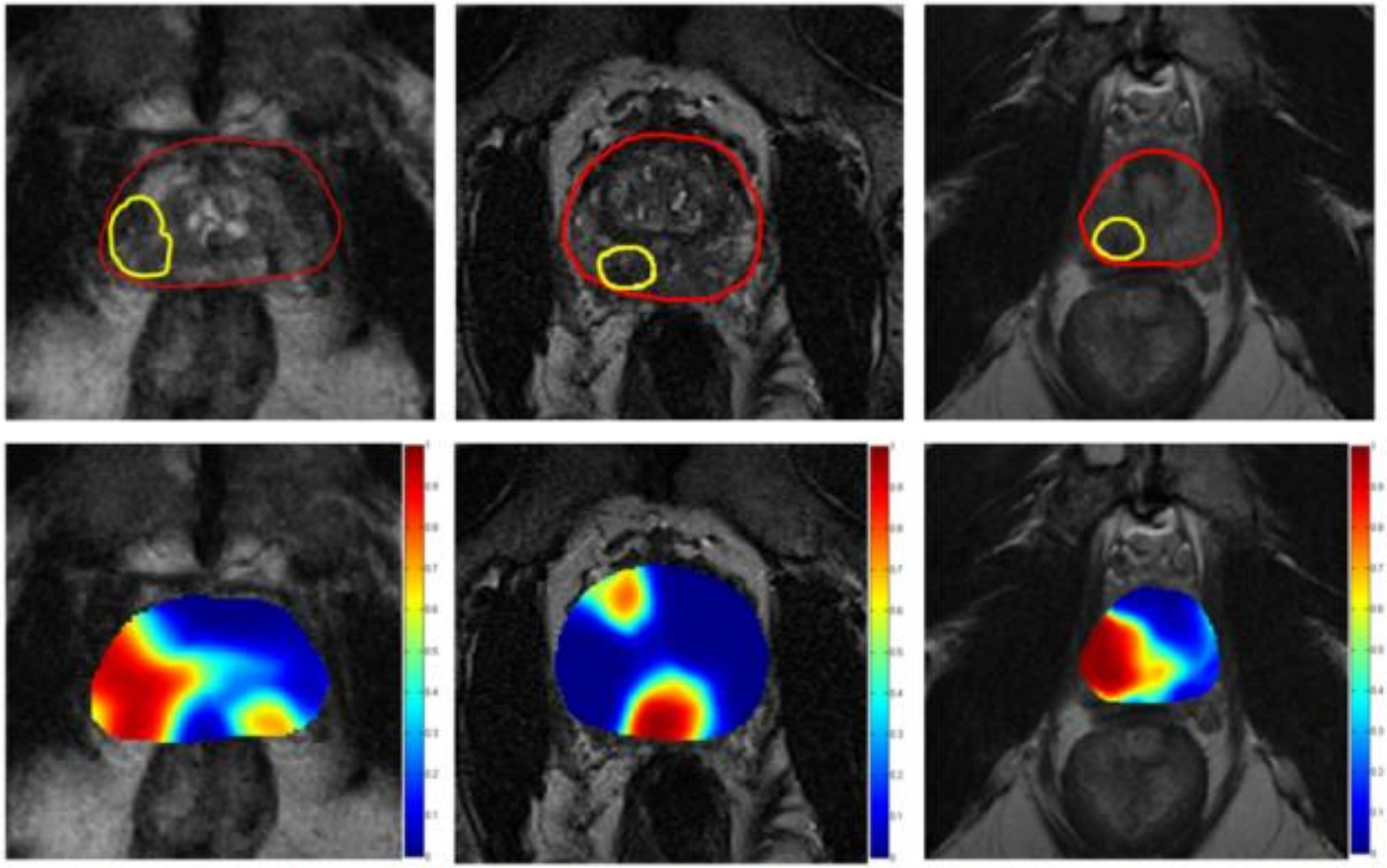

Fig. 4 Classification results for three patients from the test set D_1, obtained from the radiomics based machine learning classifier trained on D_2, shown on a single representative image. The *top row* shows the T2w MRI image with the prostate capsule (*red*) and the ground truth lesion (*yellow*). The *bottom row* shows the probability maps obtained from the classifier overlaid on the image; the colorbar indicates the range of probabilities of cancer presence with *red* being the highest and *blue* being the lowest

📖 Shiradkar et al., Radiat Oncol 2016

MRI + Clinical Features

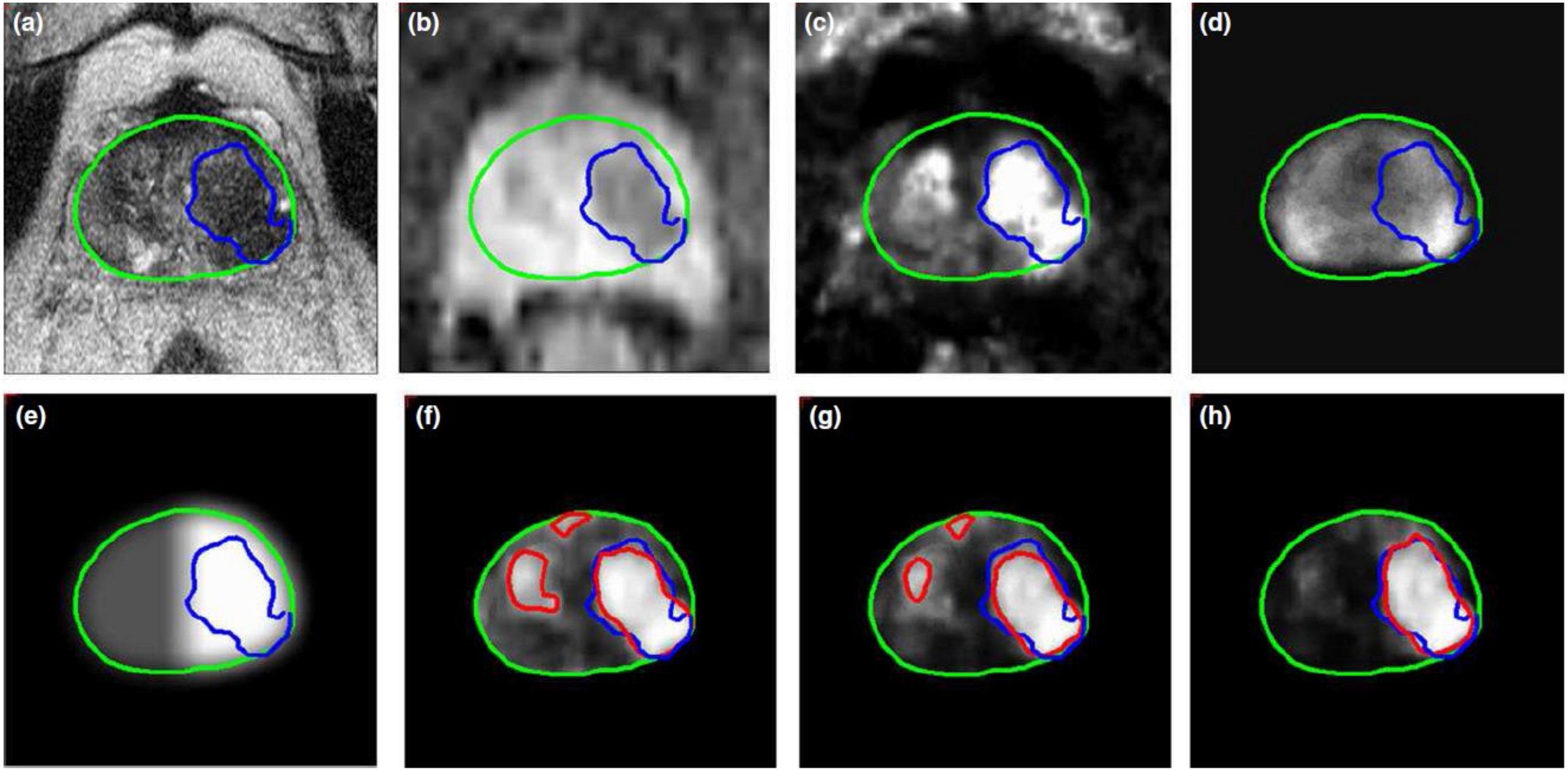

📖 Dinh et al., Med Phys, 2017

MRF → Better Machine Leaning?

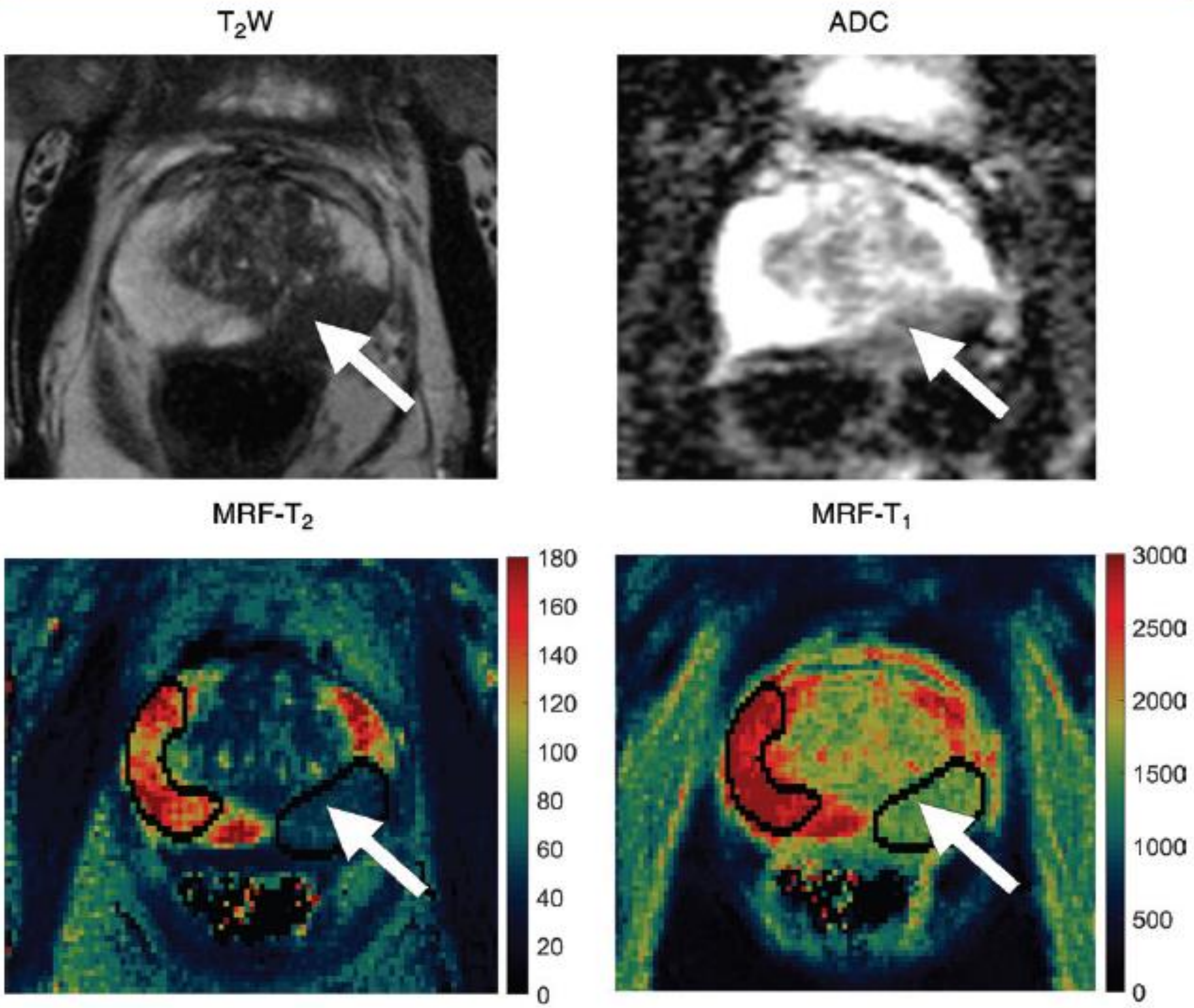
T2W
ADC
MRF-T2
MRF-T1
180
160
140
120
100
80
60
40
20
0
3000
2500
2000
1500
1000
500
0

📖 Siemens: Yu et al., Radiology, 2017

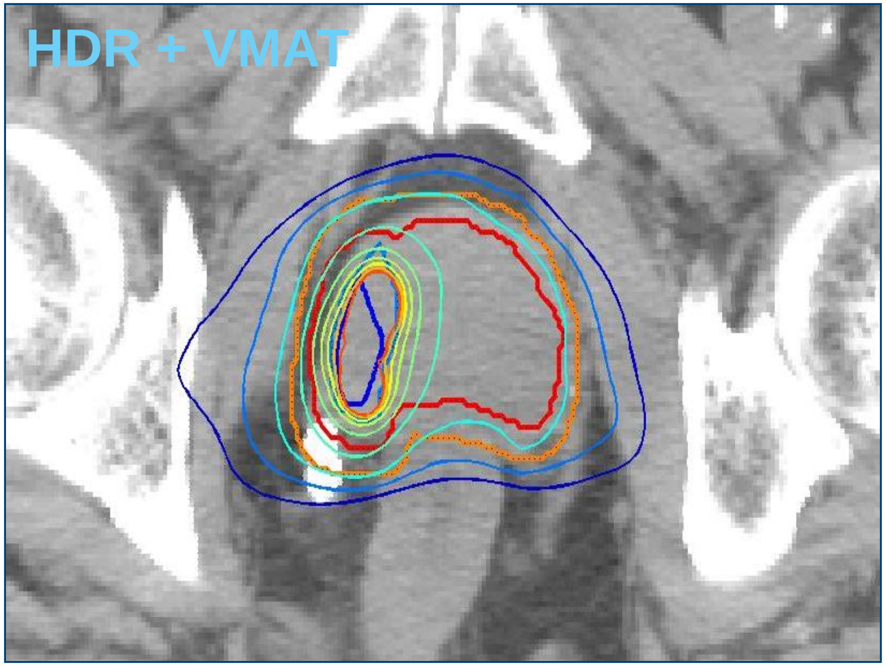

HDR + VMAT

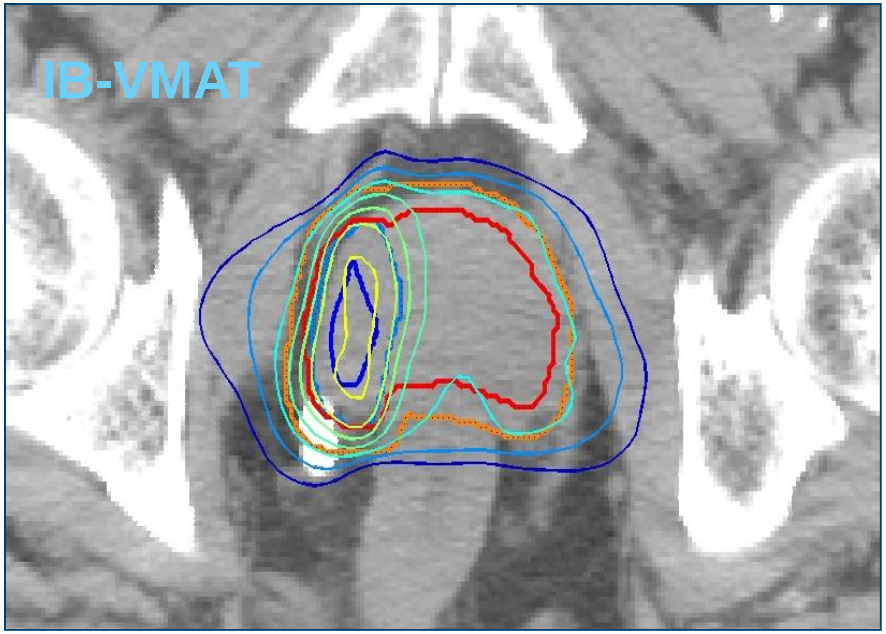

IB-VMAT

Dose (EQD2 [Gy])

50
60
70
80
90
100
110
120
130

Structures

GTV
CTV
PTV(GTV)
PTV(CTV)

Systematic Review – Tumor Boost

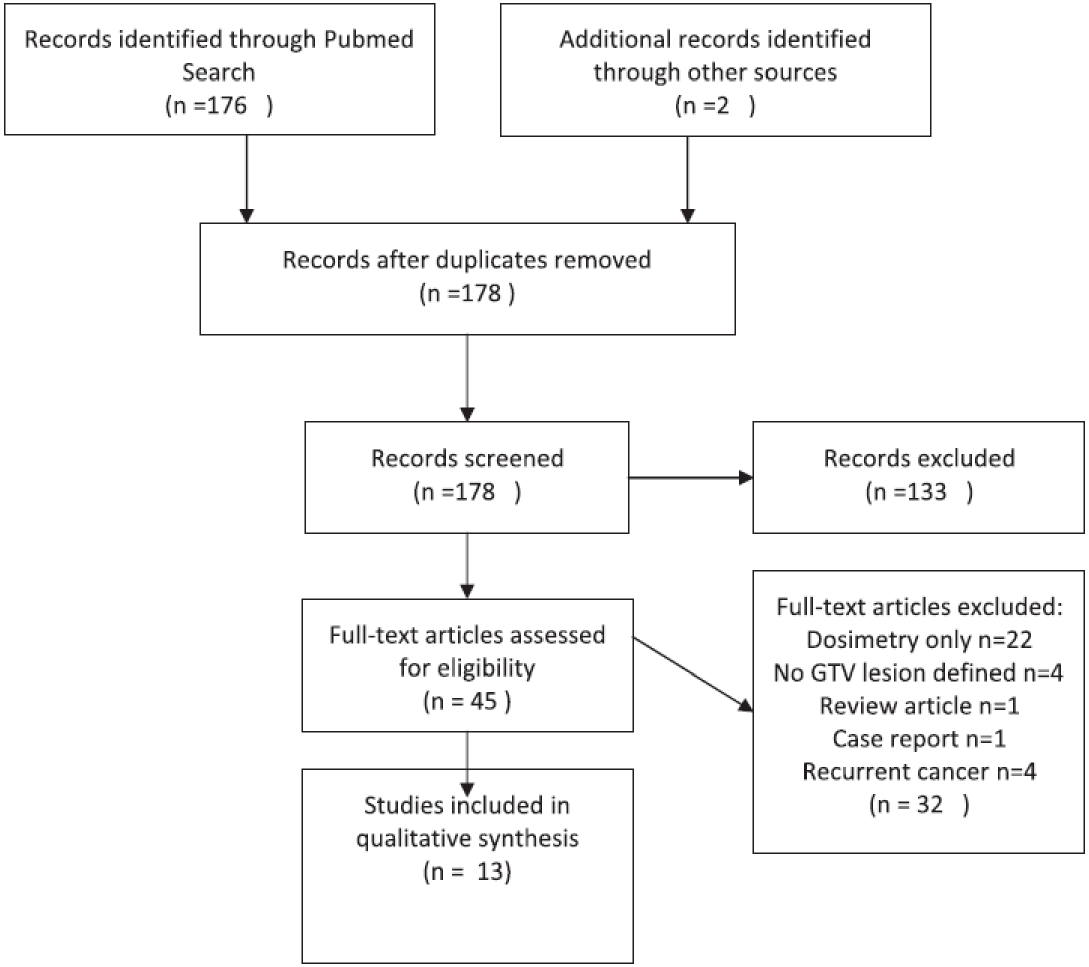

Records identified through Pubmed Search (n =176)

Additional records identified through other sources (n =2)

Records after duplicates removed (n =178)

Records screened (n =178)

Records excluded (n =133)

Full-text articles assessed for eligibility (n = 45)

Full-text articles excluded:
Dosimetry only n=22
No GTV lesion defined n=4
Review article n=1
Case report n=1
Recurrent cancer n=4
(n = 32)

Studies included in qualitative synthesis (n = 13)

📖 Bauman et al., Radiotherapy & Oncology 2013

Systematic Review

- Thirteen papers describing 11 unique patient series and 833 patients in total were identified.

- Methods and details of GTV definition and treatment varied substantially between series.

- GTV boosts were on average 8 Gy (range 3–35 Gy) for external beam, or 150% for brachytherapy (range 130–155%) and GTV volumes were small (<10 ml).

- Reported toxicity rates were low and may reflect the modest boost doses, small volumes and conservative DVH constraints employed in most studies.

📖 Bauman et al., Radiotherapy & Oncology 2013

Caution in De-escalation

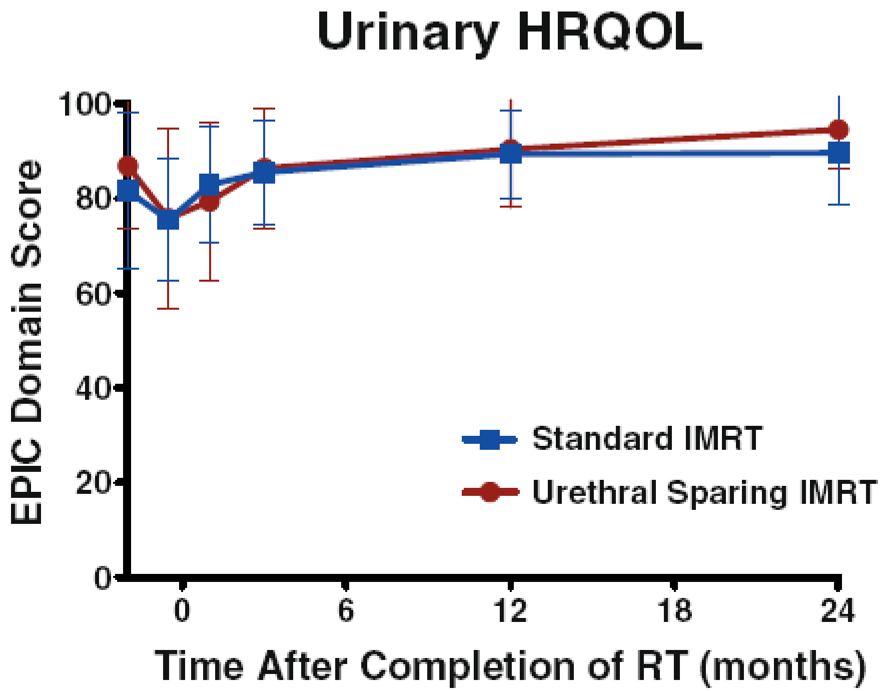

Figure 4 Urinary HRQOL by EPIC Urinary Domain Summary Score after Urethral Sparing IMRT and Standard IMRT.

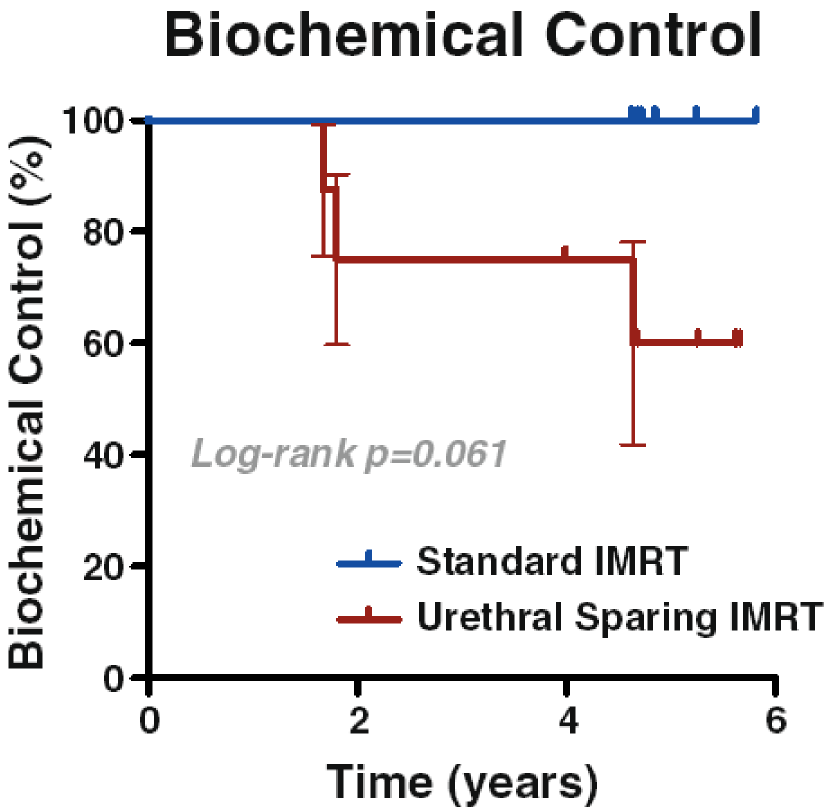

Figure 5 Biochemical Control after Urethral Sparing IMRT and Standard IMRT.

📖 Vainshtein et al., Radiat Oncol 2012

CHUM

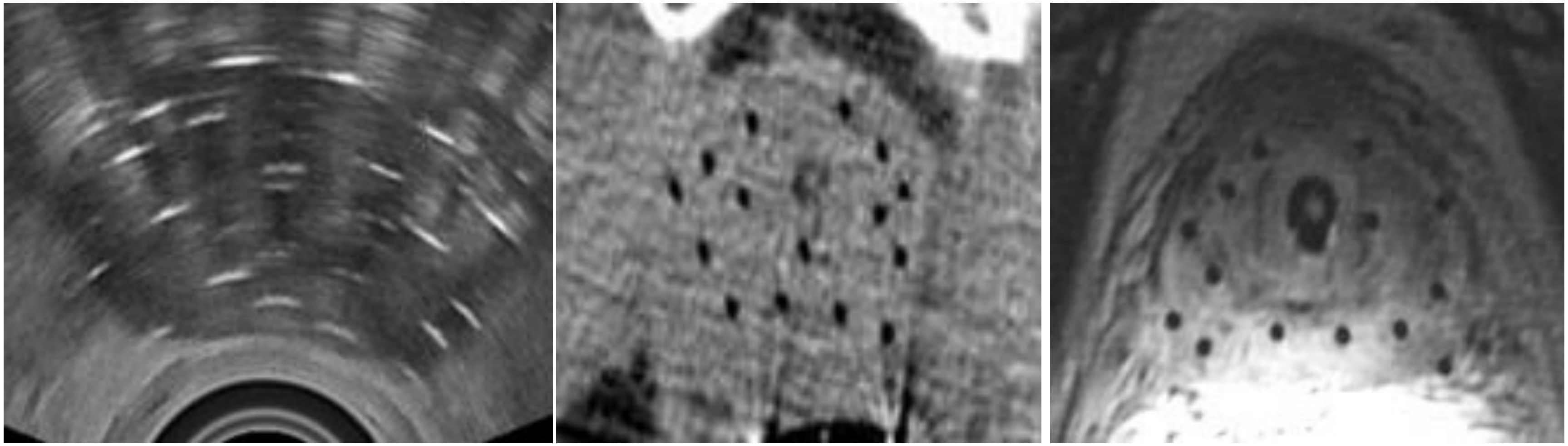

Atalar et al.

Real-Time TRUS-only Workflow

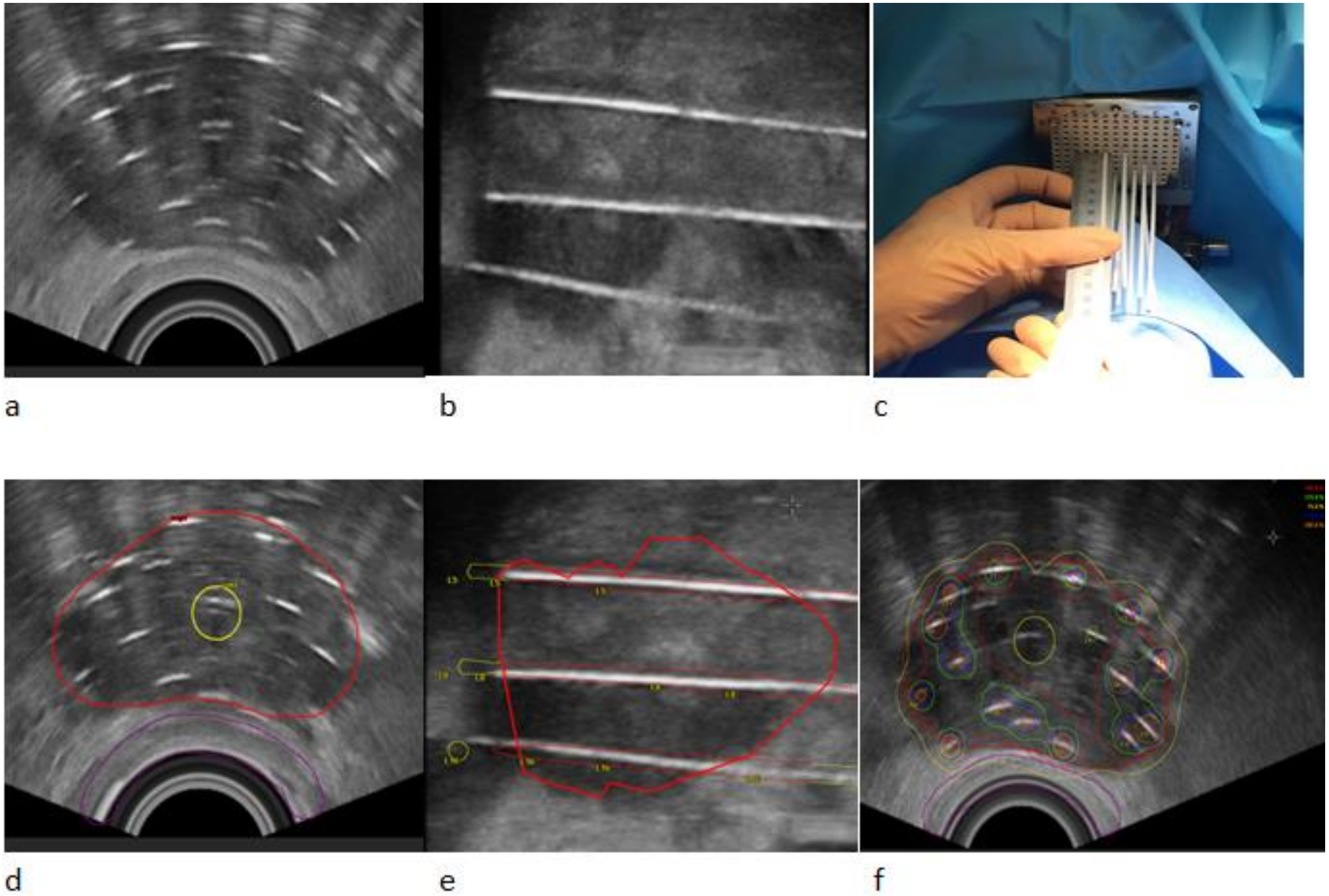

Lauche et al., 2016

First - MRI for LDR Post-Planning - 1997

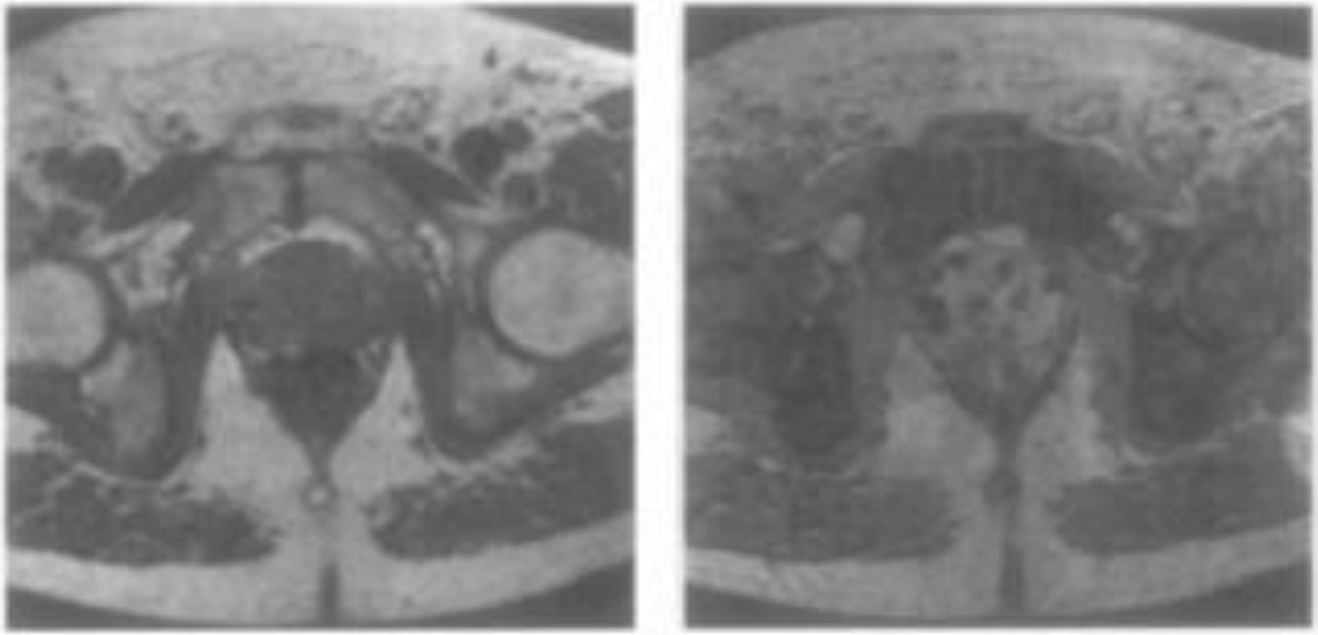

Fig. 1. Transversal spin-echo (left) and gradient-echo (right) image of the prostate. I-125 seeds are depicted as signal voids.

Moerland et al. Int J Radiat Oncol Biol Phys 1997

Prostate Post-Plan

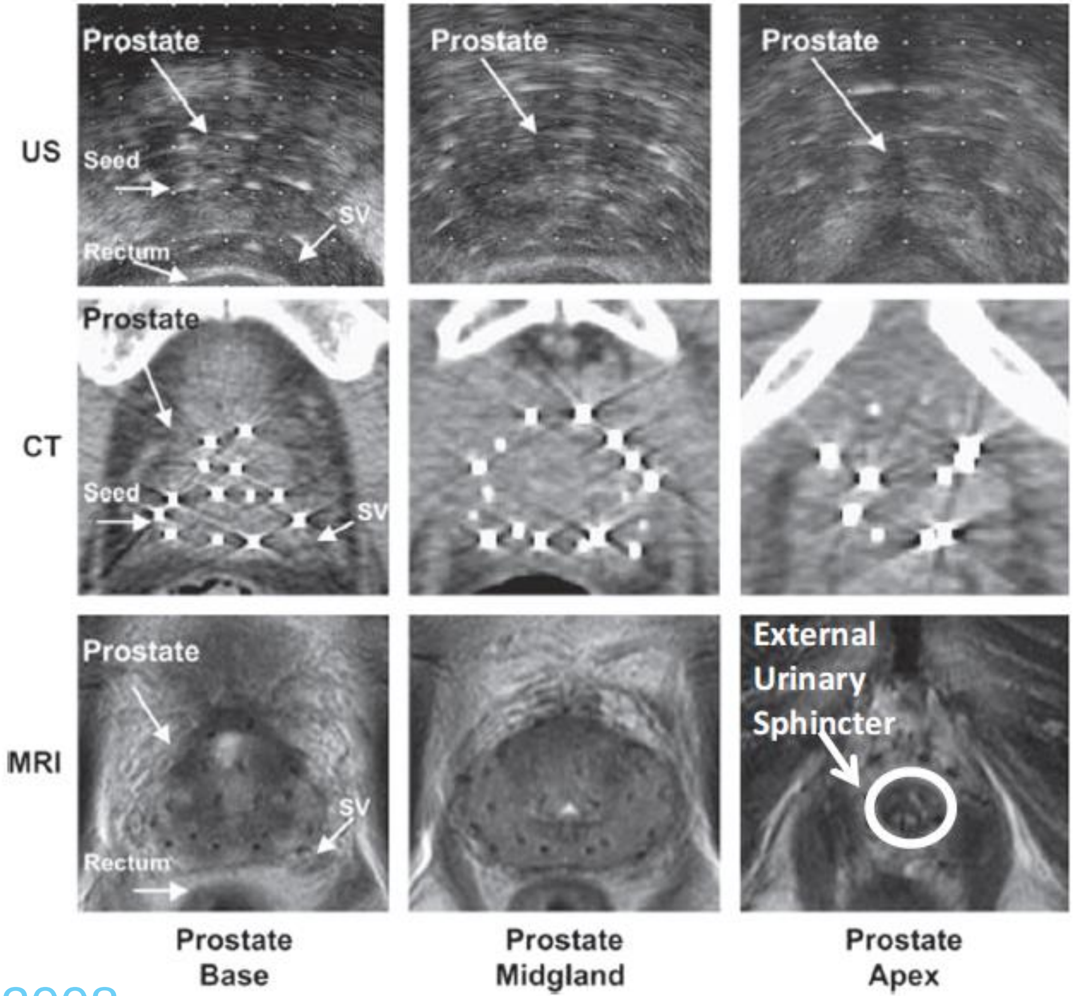
US
CT
MRI
Prostate
Seed
SV
Rectum
Prostate
Prostate
Prostate
Seed
SV
Prostate
SV
Rectum
External Urinary Sphincter
Prostate Base
Prostate Midgland
Prostate Apex

Frank et al., 2008

MRI Post-Plan

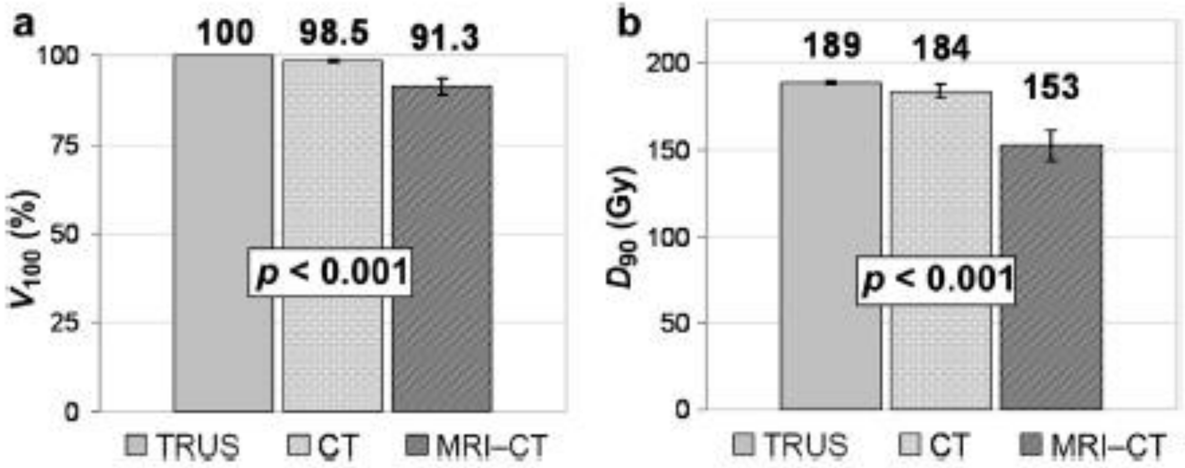

Fig. 2. Mean V_{100} values (a) and D_{90} values (b) for the whole prostate, calculated by using TRUS, postimplant CT alone, and postimplant MRI−CT fusion (MRI−CT). The MRI−CT fusion scan revealed significantly lower mean D_{90} and V_{100} values compared with the TRUS scans obtained before implantation and standard dosimetry based on CT alone ($p < 0.001$). Vertical bars represent 95% confidence intervals. TRUS = transrectal ultrasonography.

📖 Brown et al., Brachytherapy 2013

📖 Dinkla et al., Acta Oncol 2013

Dosimetric Innacuracies - Quality

72

V. Takiar et al. / Brachy

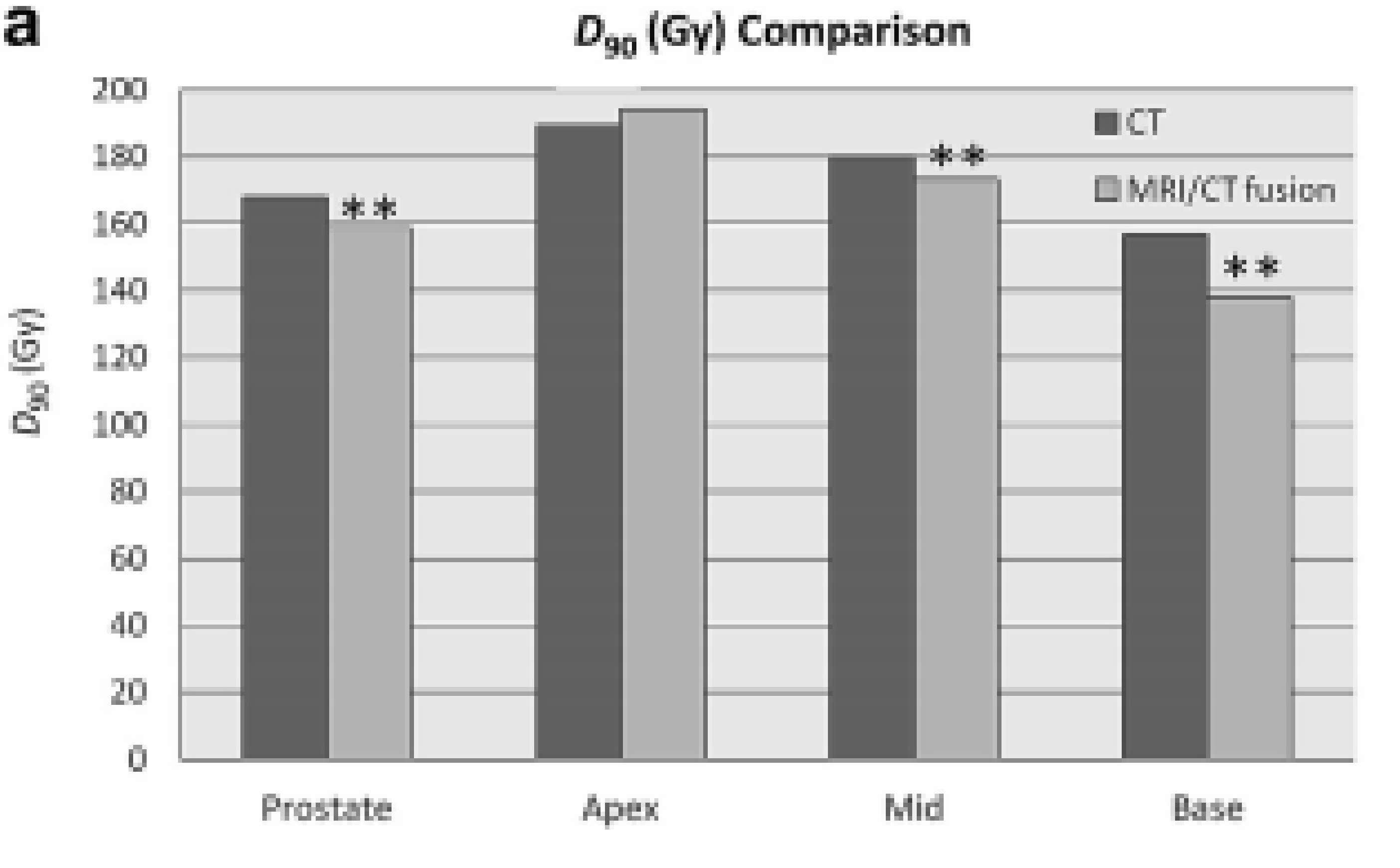

Takiar et al. Brachytherapy 2014

MRI - GEC/ESTRO 2005 → 2013

- T2 weighted MR images will provide optimal anatomical definition *but T1 weighted images will provide more accurate catheter reconstruction*
- CTV + plus any macroscopic extracapsular disease or seminal vesicle involvement identified on diagnostic images expanded by 3 mm to encompass potential microscopic disease
- GTV may be defined, CTV subvolumes may be defined

📖 Hoskin et al. Radiot Oncol 2013

CHUM

Computational Integration of diagnostic MRI to Online TRUS

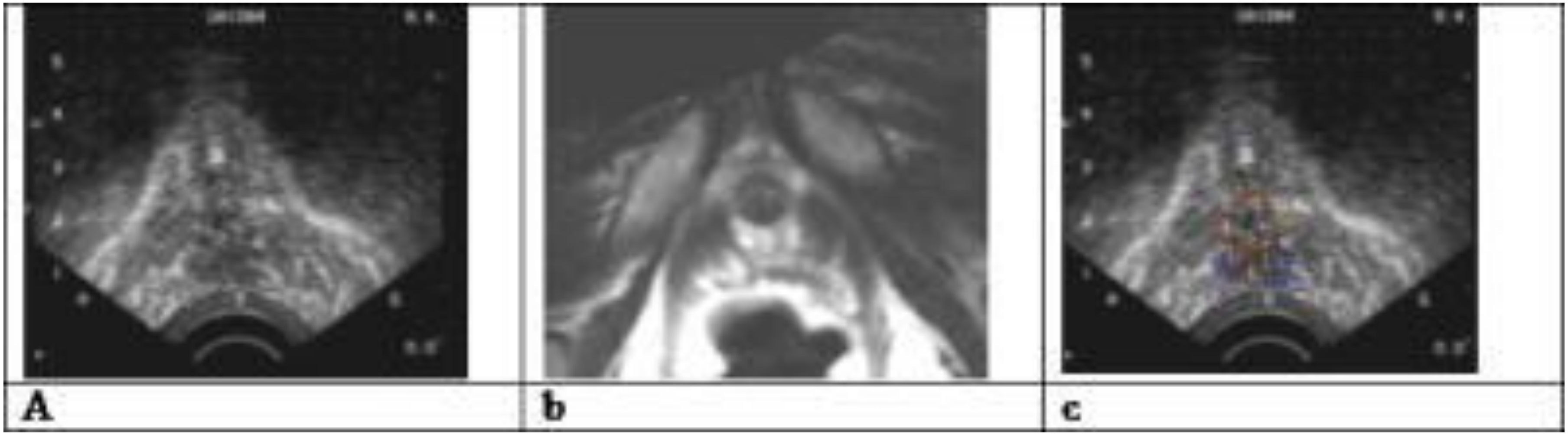

📖 Reynier et al. 2004

CHUM

Registration to TRUS

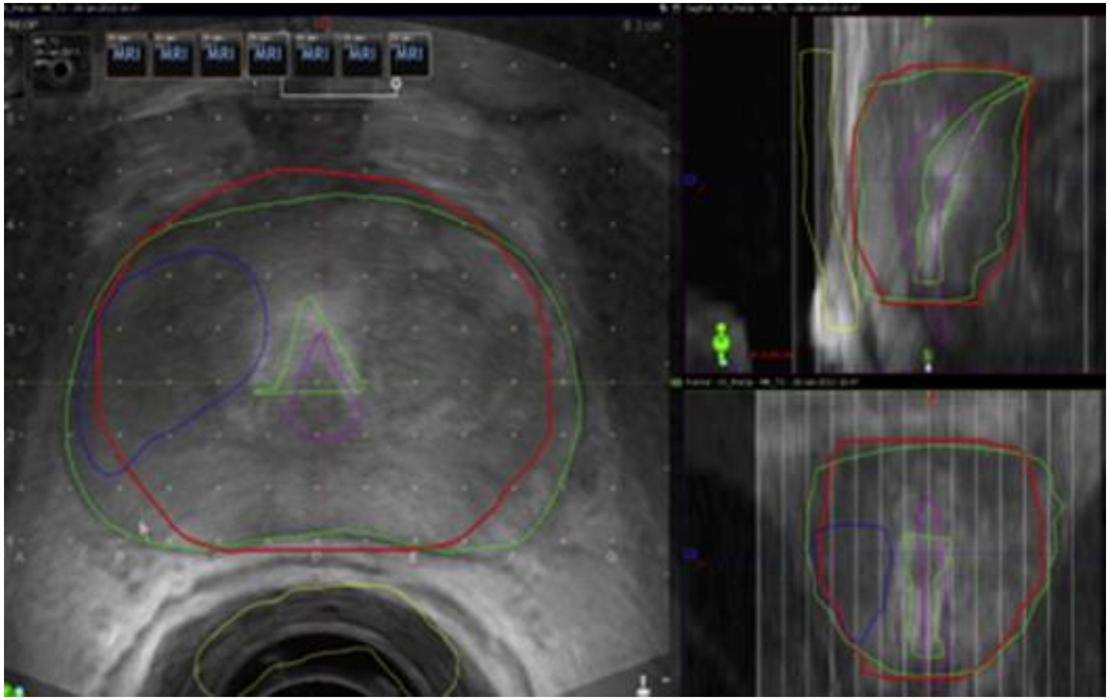

Fig. 2. Three-way fusion of eMRI, intraoperative TRUS, and preoperative TRUS (eMRI prostate, green; TRUS prostate, red; and DIL, blue). Note slight deformation of prostate by endorectal coil. eMRI = endorectal MRI; TRUS = transrectal ultrasound; DIL = dominant...

Juanita Crook, Ana Ots, Miren Gaztañaga, Matt Schmid, Cynthia Araujo, Michelle Hilts, Deidre Batchelar, Brent Parker, François Bachand, Marie-Pierre Milette

Ultrasound-planned high-dose-rate prostate brachytherapy: Dose painting to the dominant intraprostatic lesion

Brachytherapy, Volume 13, Issue 5, 2014, 433–441

SLICER

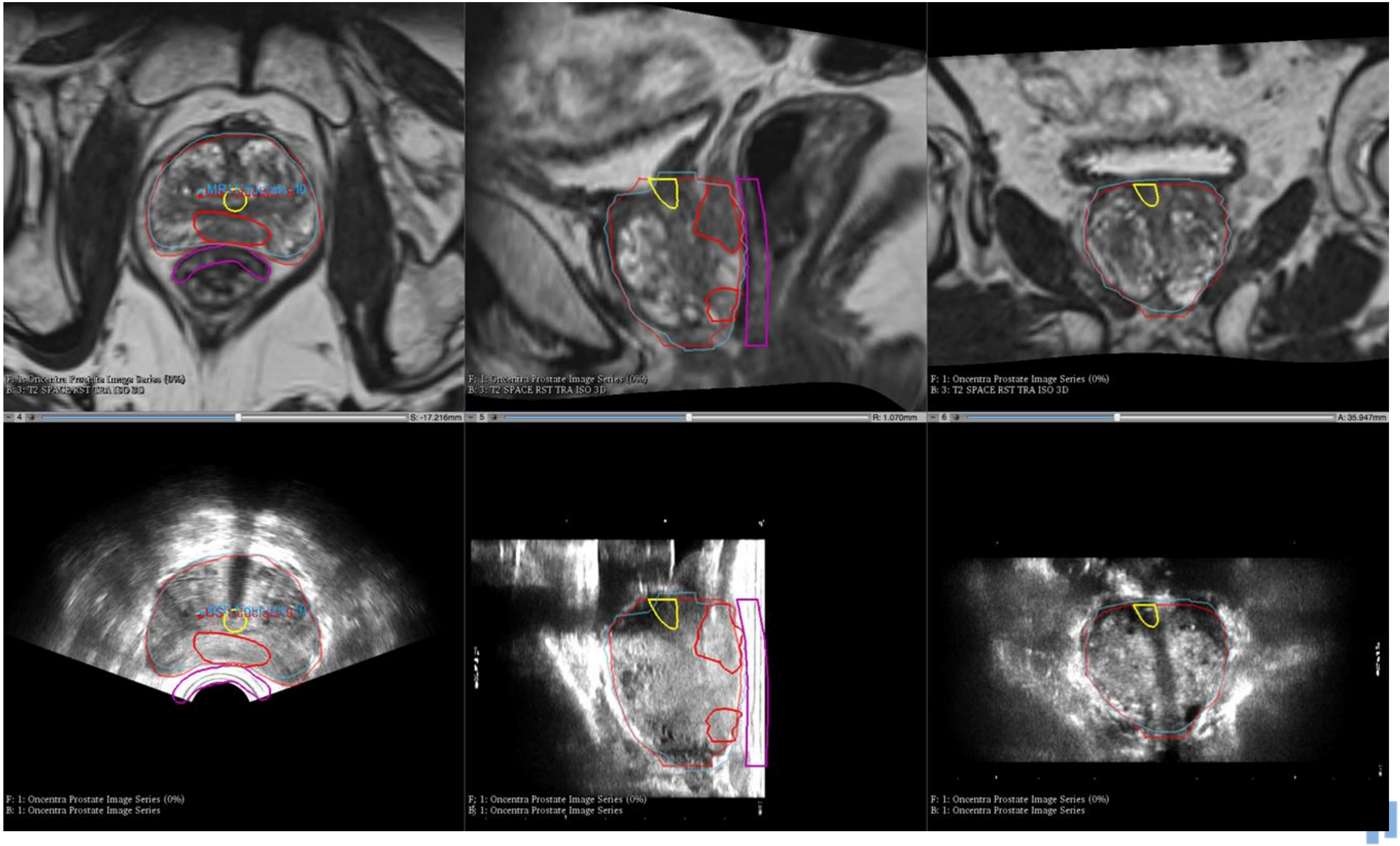
F: 1: Oncentra Prostate Image Series (0%)
B: 3: T2 SPACE RST TRA ISO 3D
S: -17.216mm
F: 1: Oncentra Prostate Image Series (0%)
B: 3: T2 SPACE RST TRA ISO 3D
R: 1.070mm
F: 1: Oncentra Prostate Image Series (0%)
B: 3: T2 SPACE RST TRA ISO 3D
A: 35.947mm
F: 1: Oncentra Prostate Image Series (0%)
B: 1: Oncentra Prostate Image Series
F: 1: Oncentra Prostate Image Series (0%)
B: 1: Oncentra Prostate Image Series
F: 1: Oncentra Prostate Image Series (0%)
B: 1: Oncentra Prostate Image Series

CHUM

High-field MRI-only Workflow (HDR)

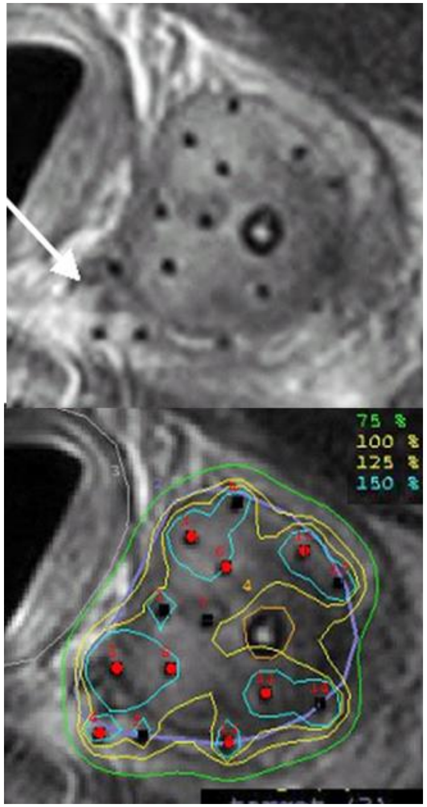

Ménard and Susil et al. 2004

InVivo – Philips – Sentinelle Endocoil Array

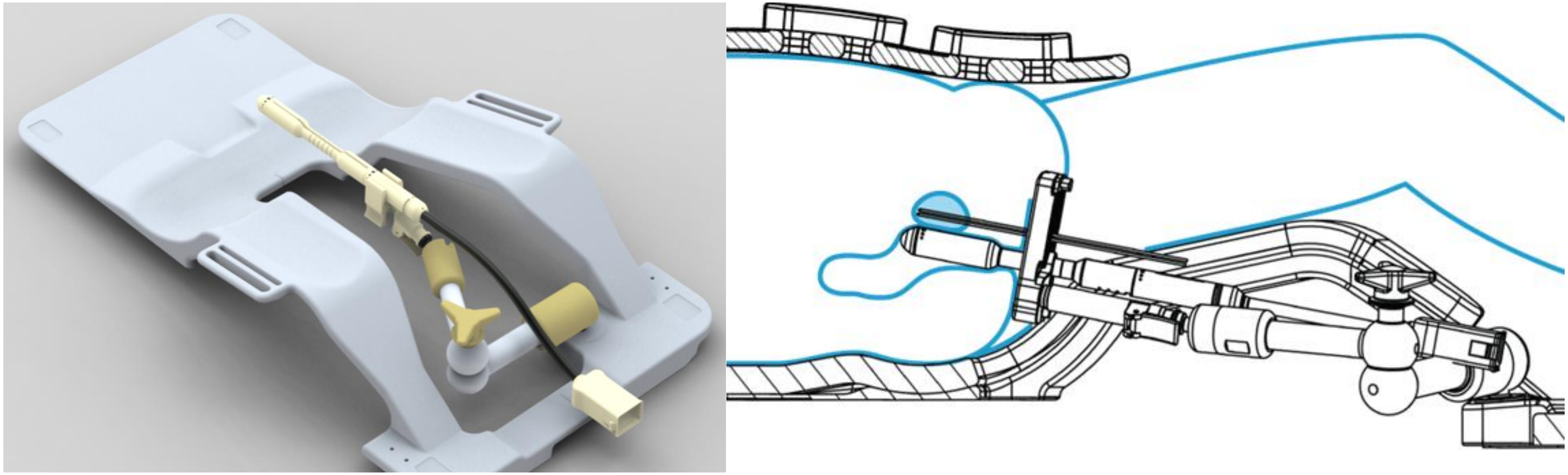

MAGNETOM Verio

- Set-up – median 25 min
- Imaging + catheter insertion – median 100 min
- Overall sedation 4.0 hours (2.1-6.9)

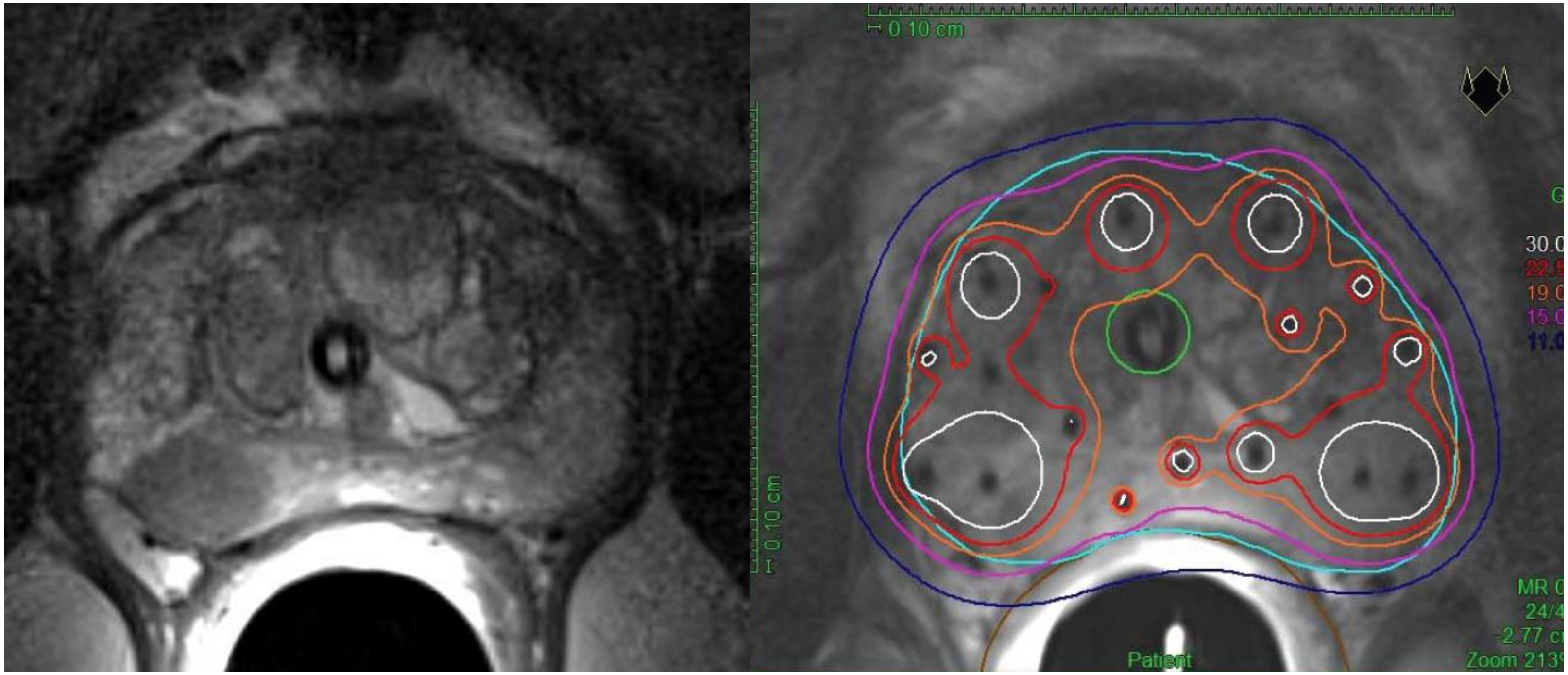
0.10 cm
0.10 cm
G
30.0
22.5
19.0
15.0
11.0
MR 0
24/4
-2.77 c
Zoom 213
Patient

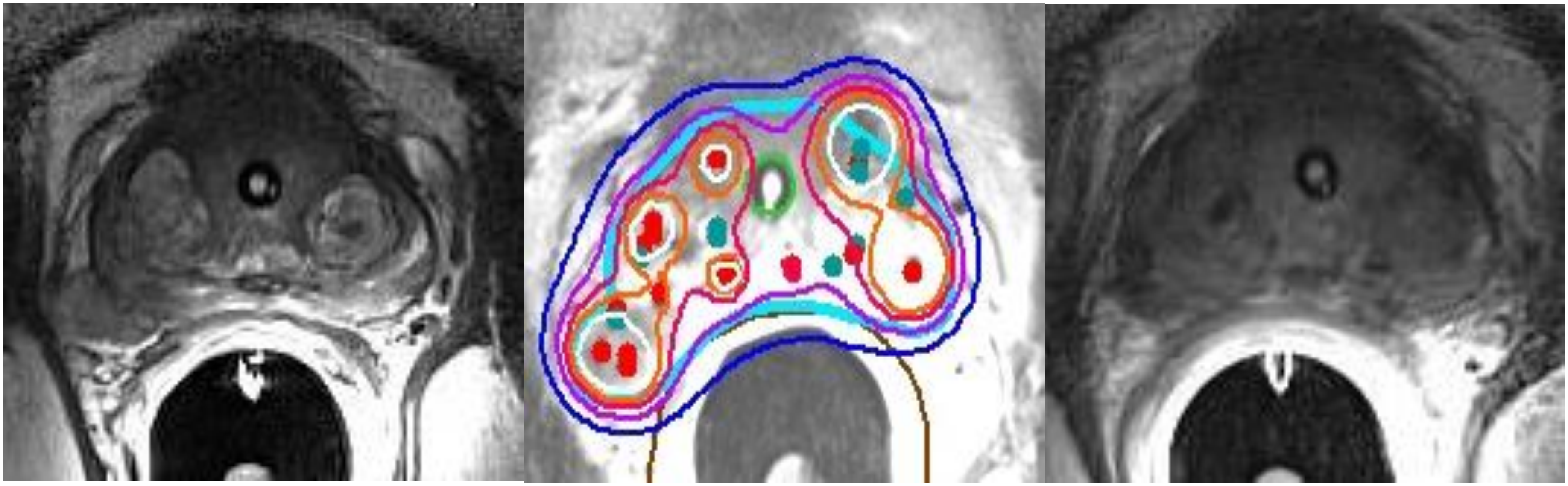

Needle Guidance – Anterior Tumours

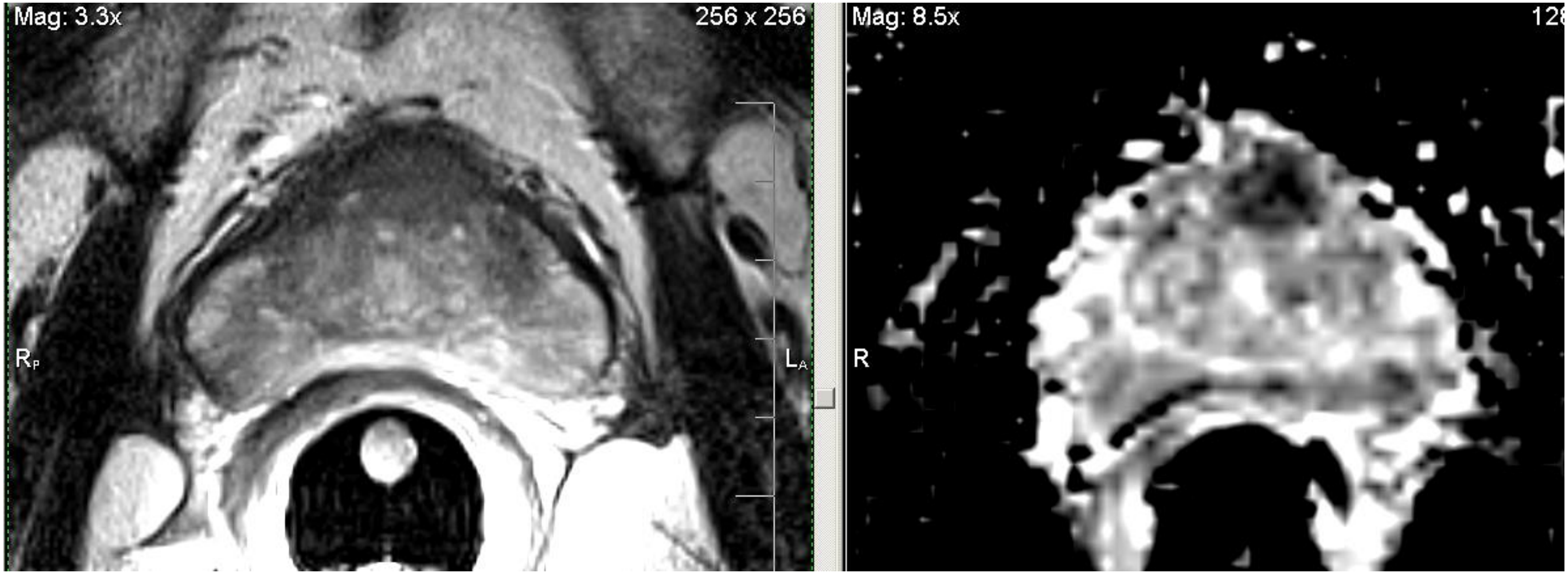
Mag: 3.3x
256 x 256
R_P
L_A
Mag: 8.5x
12
R

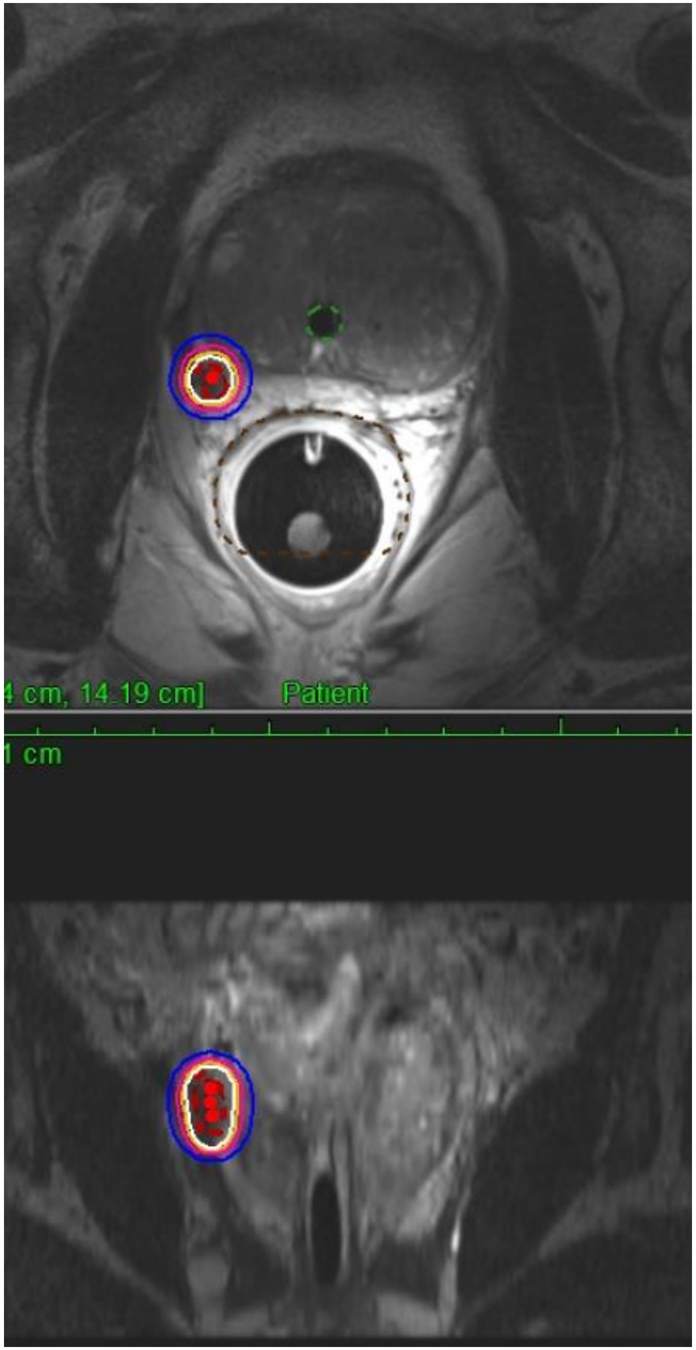
4 cm, 14.19 cm]
Patient
1 cm

Next Generation MRI-TRUS

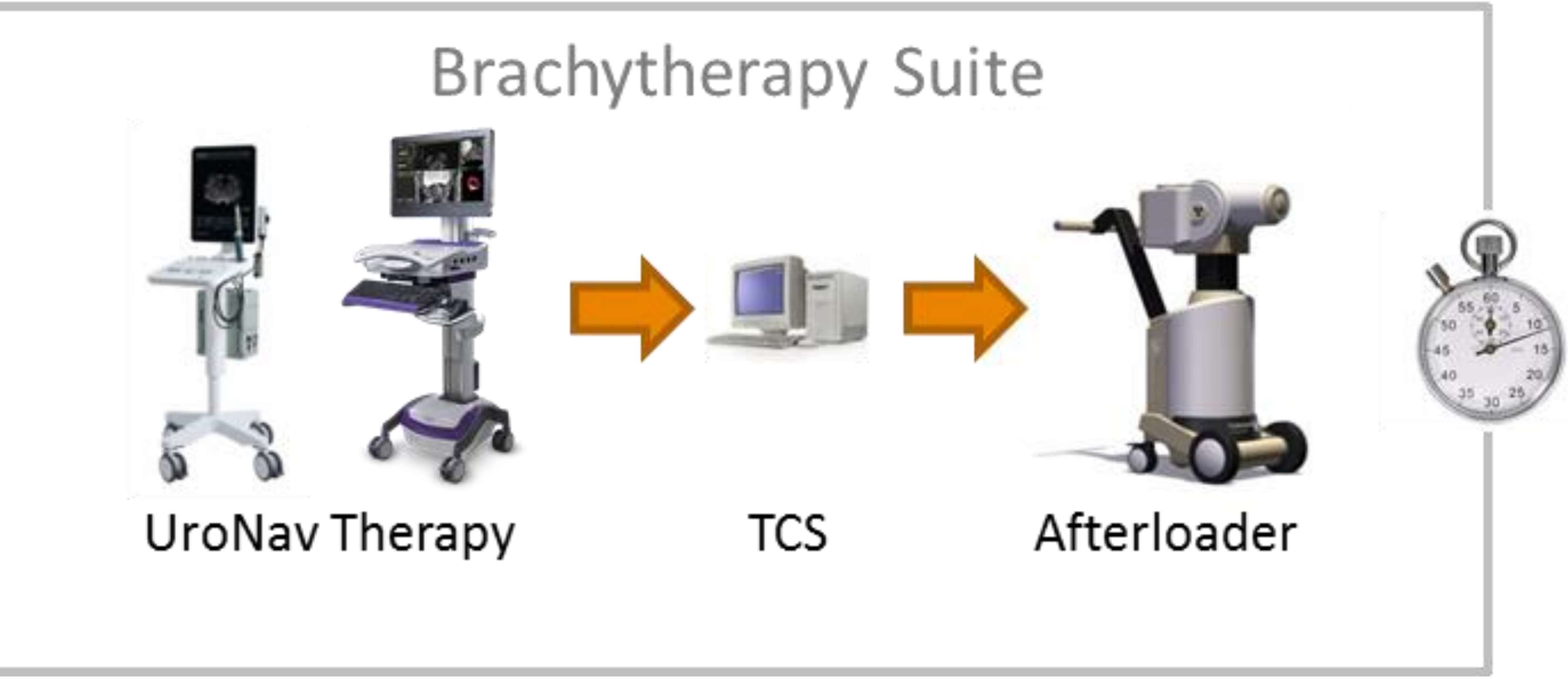
Brachytherapy Suite
UroNav
Therapy
TCS
Afterloader

InVivo, Philips

FT?

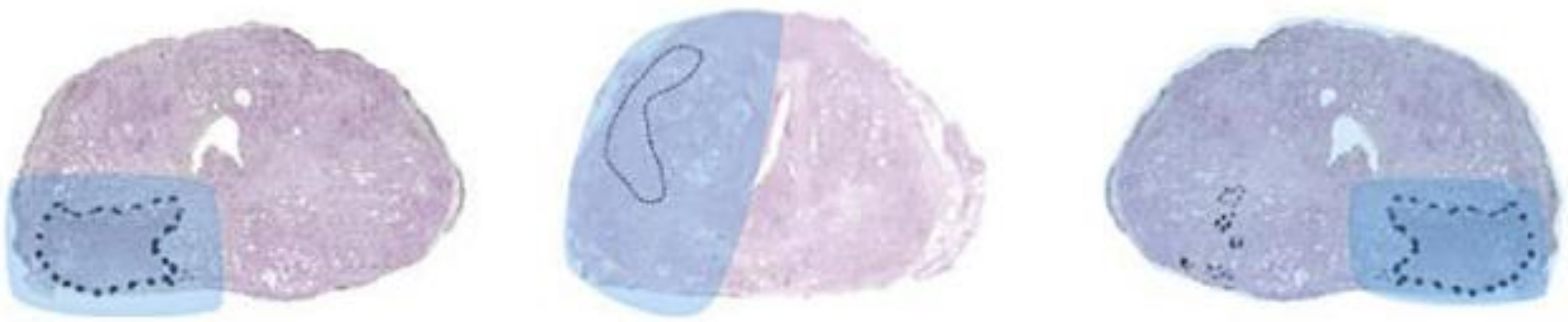

Ultra-Focal Therapy

Focal Therapy

Focused Therapy

📖Kollmeier et al. (Siddiqui et al.)

Modalities for FT

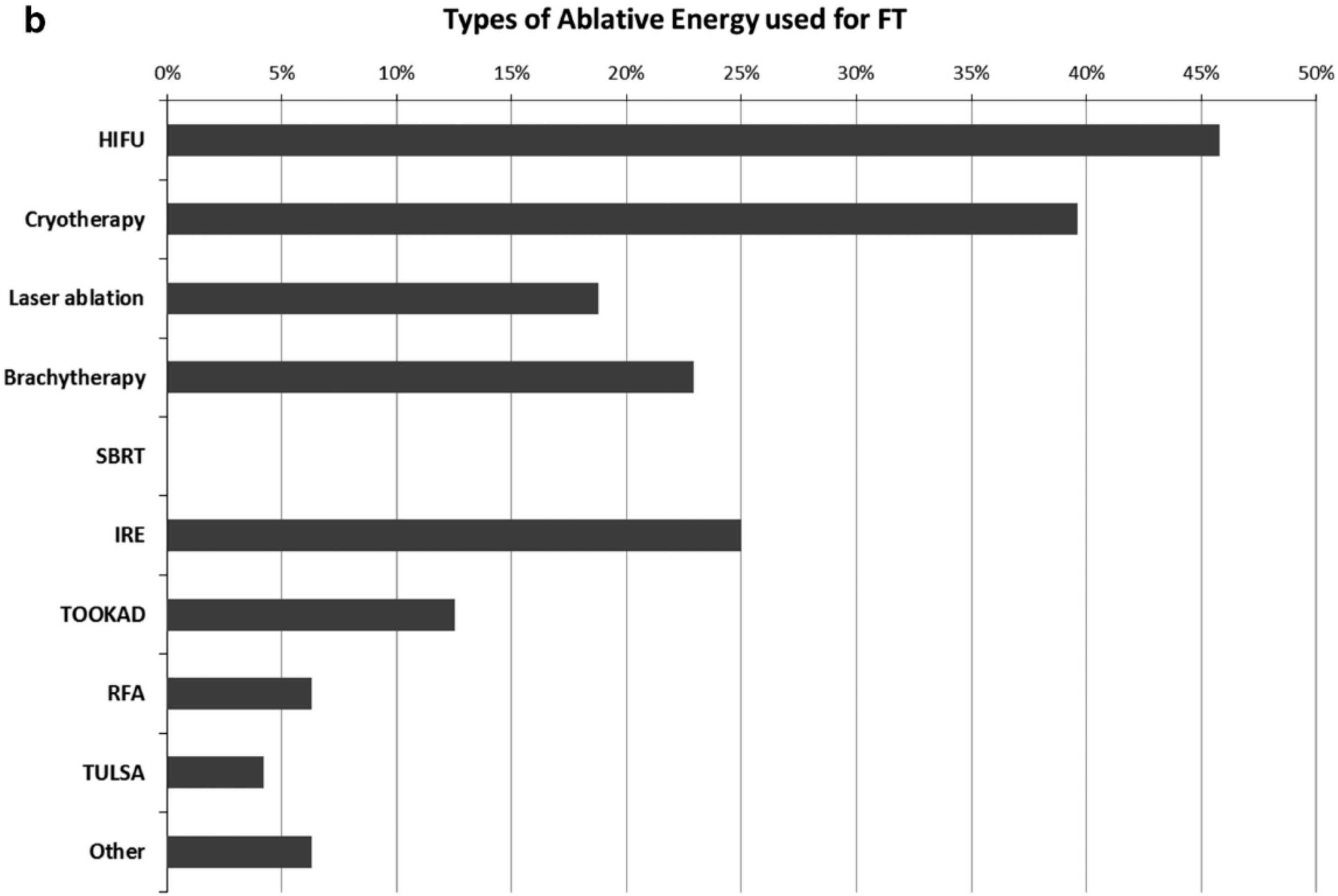

📖 Tay et al.

Goal for FT

Alternative to whole-gland therapy

vs.

Complement to active surveillance

FDA-AUA-SUO workshop 2015

- Criteria for patient selection remain debatable
- Long term cancer control remains to be established in properly designed and well-performed prospective clinical trials
- Concerns
  - excessive, unnecessary use, and
  - inadequate treatment

📖 Jarow et al.

Location and Toxicity

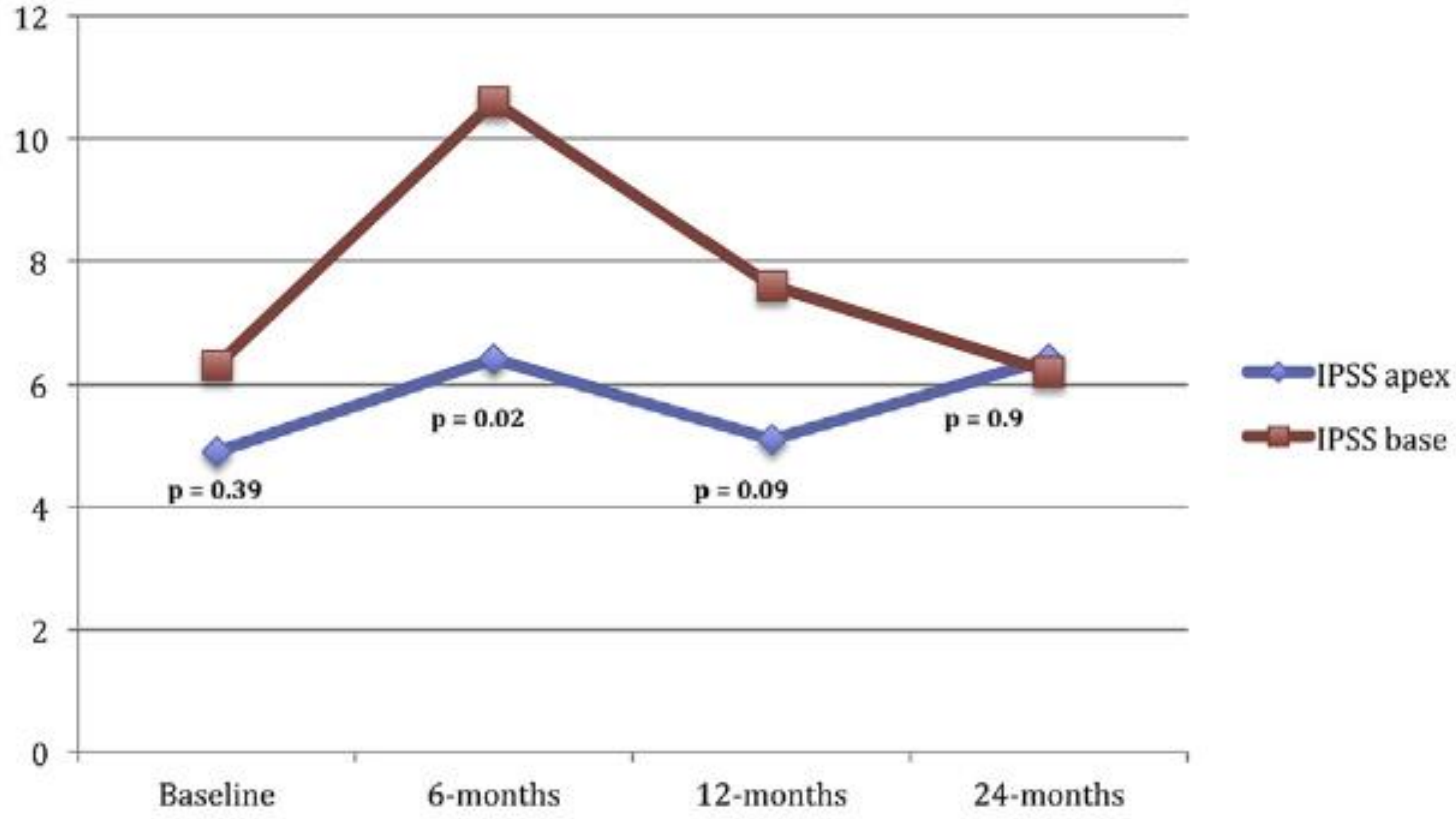

📖 Srougi et al.

Innadequate Treatment ?

- Yes - prostate cancer us usually multifocal
- BUT - Not treating indolent, microscopic, Gleason 6 disease is a legitimate proposal

Consensus - Selection

- mpMRI guided biopsy
- Low+ Int Risk planned for whole-gland therapy
- PSA < 10
- GTV 1.5ml or 20% of gland volume (3ml and 25% if lateralized to one hemigland)
- One core of G6 (<1mm) can be ignored

Tay et al.

CHUM

Back-up Plan in 25%

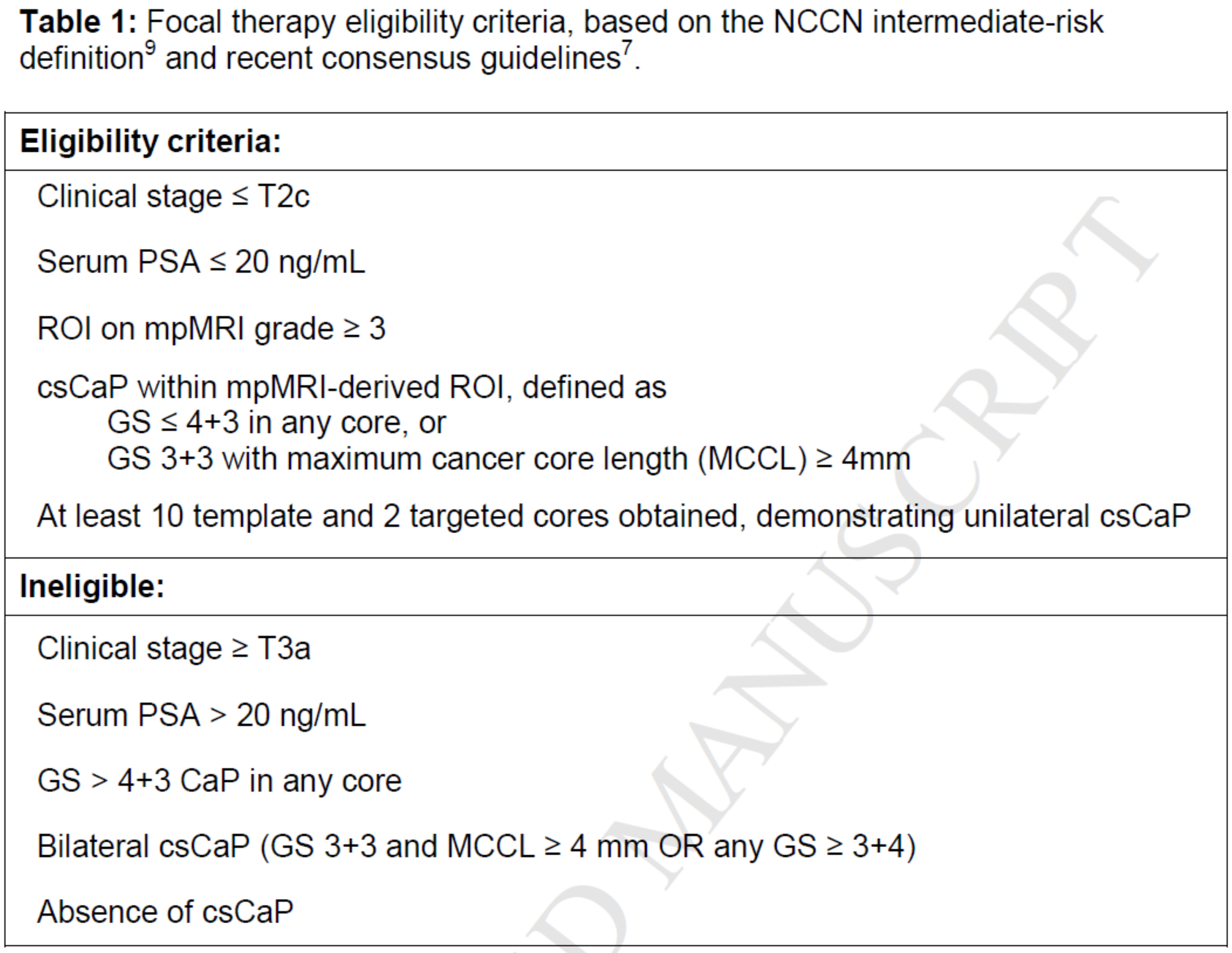

Table 1: Focal therapy eligibility criteria, based on the NCCN intermediate-risk definition[9] and recent consensus guidelines[7].

Eligibility criteria:
Clinical stage ≤ T2c
Serum PSA ≤ 20 ng/mL
ROI on mpMRI grade ≥ 3
csCaP within mpMRI-derived ROI, defined as GS ≤ 4+3 in any core, or GS 3+3 with maximum cancer core length (MCCL) ≥ 4mm
At least 10 template and 2 targeted cores obtained, demonstrating unilateral csCaP
Ineligible:
Clinical stage ≥ T3a
Serum PSA > 20 ng/mL
GS > 4+3 CaP in any core
Bilateral csCaP (GS 3+3 and MCCL ≥ 4 mm OR any GS ≥ 3+4)
Absence of csCaP

D MANUSCRIPT

Nassiri et al.

Salvage FT (brachytherapy)

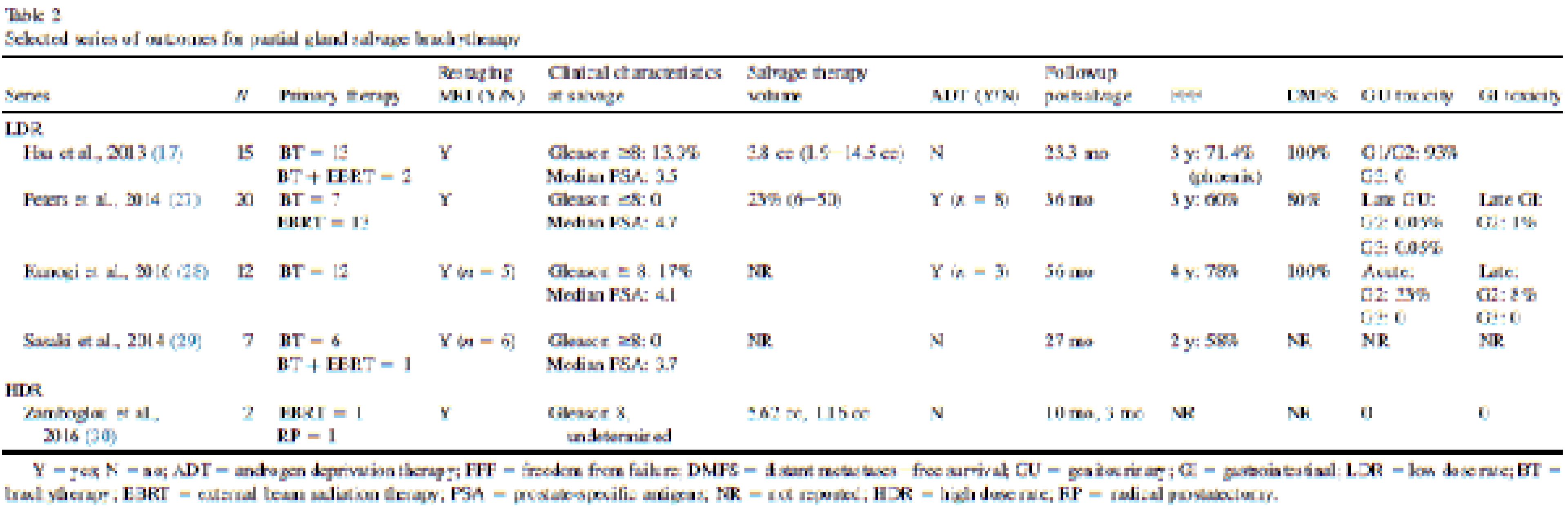

Table 2
Selected series of outcomes for partial gland salvage brachytherapy

Series	*N*	Primary therapy	Restaging MRI (Y/N)	Clinical characteristics at salvage	Salvage therapy volume	ADT (Y/N)	Followup postsalvage	FFF	DMFS	GU toxicity	GI toxicity
LDR											
Hsu et al., 2013 (17)	15	BT = 13 BT + EBRT = 2	Y	Gleason ≥8: 13.3% Median PSA: 3.5	2.8 cc (1.5–14.5 cc)	N	23.3 mo	3 y: 71.4% (phoenix)	100%	G1/G2: 93% G3: 0	
Peters et al., 2014 (27)	20	BT = 7 EBRT = 13	Y	Gleason ≥8: 0 Median PSA: 4.7	23% (6–53)	Y (*n* = 8)	36 mo	3 y: 60%	90%	Late GU: G2: 0.05% G3: 0.05%	Late GI: G2: 1%
Kunogi et al., 2016 (28)	12	BT = 12	Y (*n* = 5)	Gleason ≥ 8: 17% Median PSA: 4.1	NR	Y (*n* = 3)	56 mo	4 y: 78%	100%	Acute: G2: 23% G3: 0	Late: G2: 8% G3: 0
Sasaki et al., 2014 (29)	7	BT = 6 BT + EBRT = 1	Y (*n* = 6)	Gleason ≥8: 0 Median PSA: 3.7	NR	N	27 mo	2 y: 58%	NR	NR	NR
HDR											
Zamboglou et al., 2016 (30)	2	EBRT = 1 RP = 1	Y	Gleason 8, undetermined	5.62 cc, 1.15 cc	N	10 mo, 3 mo	NR	NR	0	0

Y = yes; N = no; ADT = androgen deprivation therapy; FFF = freedom from failure; DMFS = distant metastases–free survival; GU = genitourinary; GI = gastrointestinal; LDR = low dose rate; BT = brachytherapy; EBRT = external beam radiation therapy; PSA = prostate-specific antigen; NR = not reported; HDR = high dose rate; RP = radical prostatectomy.

📖Kollmeier et al.

Focal (only) Salvage

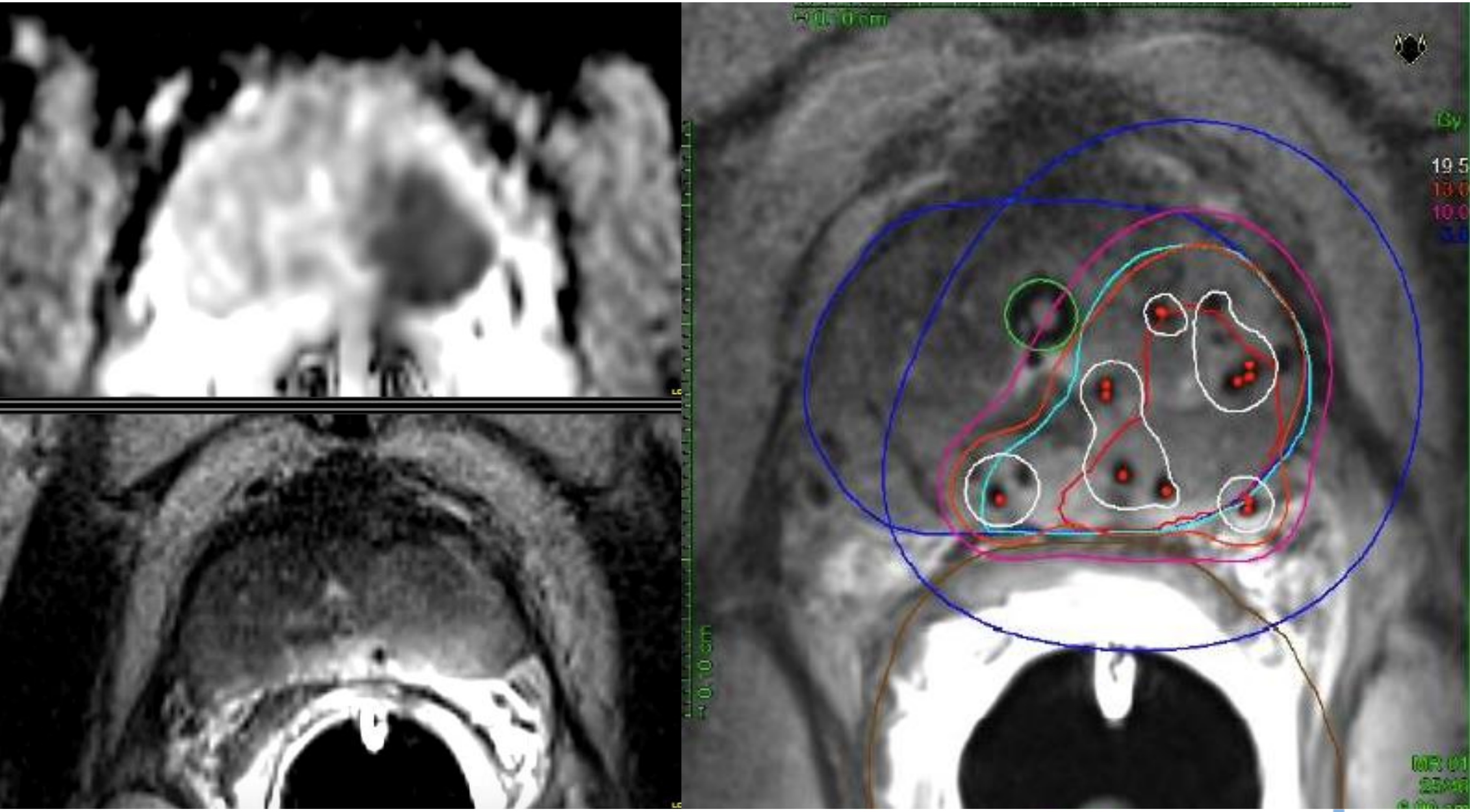
10.0cm
Gy
19.5
10.0 cm

Indications for Prostate MRI Sim

Quality Indicator	**Importance Rating (9,essential)**
When CT image quality is compromised (e.g. prosthetic hip implants) or absent from workflow	7,8
When PTV margins are small (≤5mm).	7
In post-planning for LDR prostate brachytherapy to improve dosimetric accuracy.	7.3
When delineating a distinct GTV (MRI-visible tumor volume) and CTV volumes	9

📖Ménard et al, Radiol Clin NA, In Press

Preparation and Set-Up

Quality Indicator	Importance Rating (9,essential)
Endorectal coil acquisitions should be avoided in the absence of robust deformable image registration tools.	8
Administration of anti-peristaltic agents should be strongly considered to improve image quality, unless contraindicated	7.3
Bladder filling state should be comfortable in order to reduce motion-related artifacts.	7.1
Patient positioning should approximate treatment conditions (bowel prep, bladder prep, +/- immobilization devices), while maximizing SNR (i.e. surface coils should be applied as close as possible to the patient surface).	8

MRI Acquisition

Quality Indicator	**Importance Rating (9,essential)**
MRI acquisition protocols should generally follow PIRADSv2 guidelines (acr.org) in order to facilitate diagnostic reporting.	7,7
Replacing coronal and sagittal T2w images with an isotropic T2w 3D axial acquisition is justified in radiotherapy planning, especially at 1.5T.	6
When implanted fiducial markers (FMs) or brachytherapy seeds must be resolved, strategies to augment the FM signature on above images may suffice (eg. Increase voxel resolution, PD via dual echo acquisition, intermediate TE).	7
A separate image may be acquired to more clearly highlight FMs (e.g. GRE, PD, SSFP, UTE)	7

MRI Acquisition

Quality Indicator	Importance Rating (9,essential)
DWI is recommended to assist in depiction of tumours if needed.	9
DCE is considered optional except for salvage of recurrence.	7
Activation of vendor-provided gradient distortion correction and optimization of bandwidth (fat/water pixel shift <1mm) is recommended to maintain geometric fidelity.	8
DWI should follow the QIBA profile (qibawiki.rsna.org). Distortion can be minimized using i) R-L phase-encode direction, ii) volume shimming over the gland, iii) minimizing effective echo-spacing, and iv) considering segmented or other non-EPI techniques.	8.5
Motion-related artefacts should be mitigated by limiting acquisition time to < 5 minutes when possible. Sequences should be repeated if motion-related artifacts.	7.8

Image Registration

Quality Indicator	**Importance Rating (9,essential)**
MRI registration to CT consists of a prostate-to-prostate local registration. Bone-to-bone registration of the pelvis is discouraged.	8,7
The quality of image registration must be evaluated by a physicist and/or physician prior to treatment planning. Rotations should be carefully scrutinized. Errors in registration translate to systematic errors that propagate through the treatment course, and must be minimized.	7,8
In salvage after prostatectomy, users should use great care to consider and mitigate variation in bladder and bowel filling between CT and MRI, and to reproduce treatment conditions. The potential for registration error is considered large in this setting. Accurate registration at the level of the external urethral sphincter and gross recurrent tumour (if present) is prioritised.	7.7
Inter-sequence motion of the prostate gland during an MRI examination may occur. Such displacements must be evaluated and corrected if present. DWI may require registration to T2w when distortions are observed.	7.2

CHUM Workflow

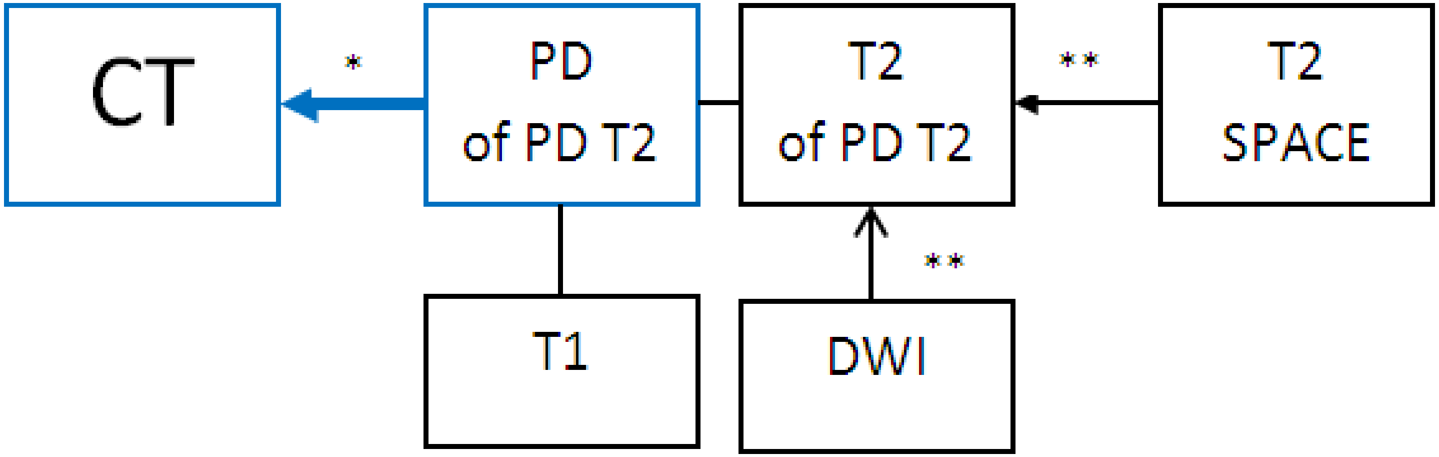

CT

*

PD
of PD T2

T2
of PD T2

**

T2
SPACE

T1

**

DWI

* manual point-based registration (PD to CT) using 4 implanted markers (sup and inf) for a total of 8 points.

** if required (due to motion) anatomic automated registration prostate-to-prostate using mutual information algorithm.

CHUM Example - FM

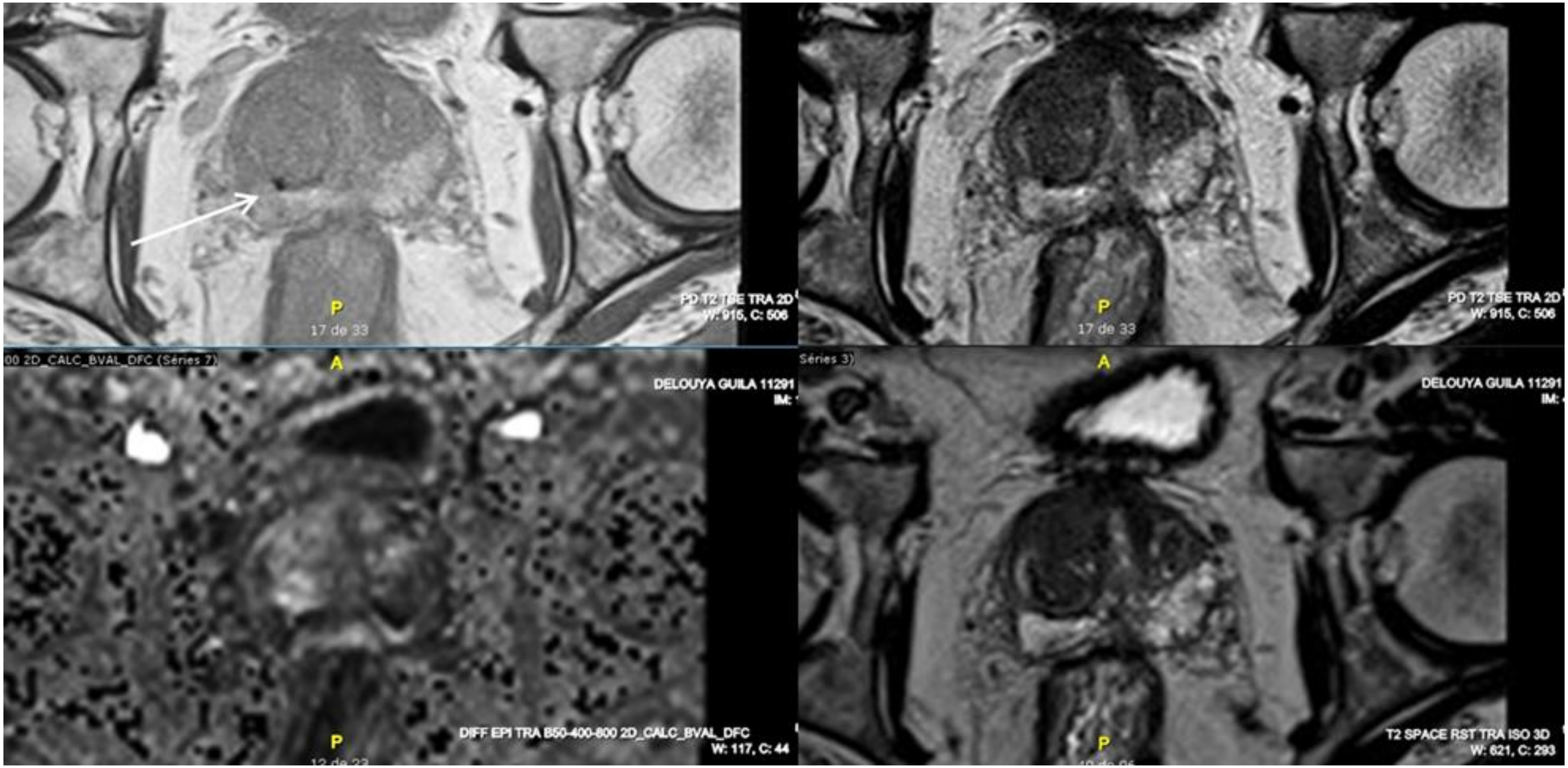
P
17 de 33
PD T2 TSE TRA 2D
W: 915, C: 506
P
17 de 33
PD T2 TSE TRA 2D
W: 915, C: 506
00 2D_CALC_BVAL_DFC (Séries 7)
A
DELOUYA GUILA 11291
IM:
P
DIFF EPI TRA B50-400-800 2D_CALC_BVAL_DFC
W: 117, C: 44
Séries 3)
A
DELOUYA GUILA 11291
IM:
P
T2 SPACE RST TRA ISO 3D
W: 621, C: 293

CHUM Example - Tumor

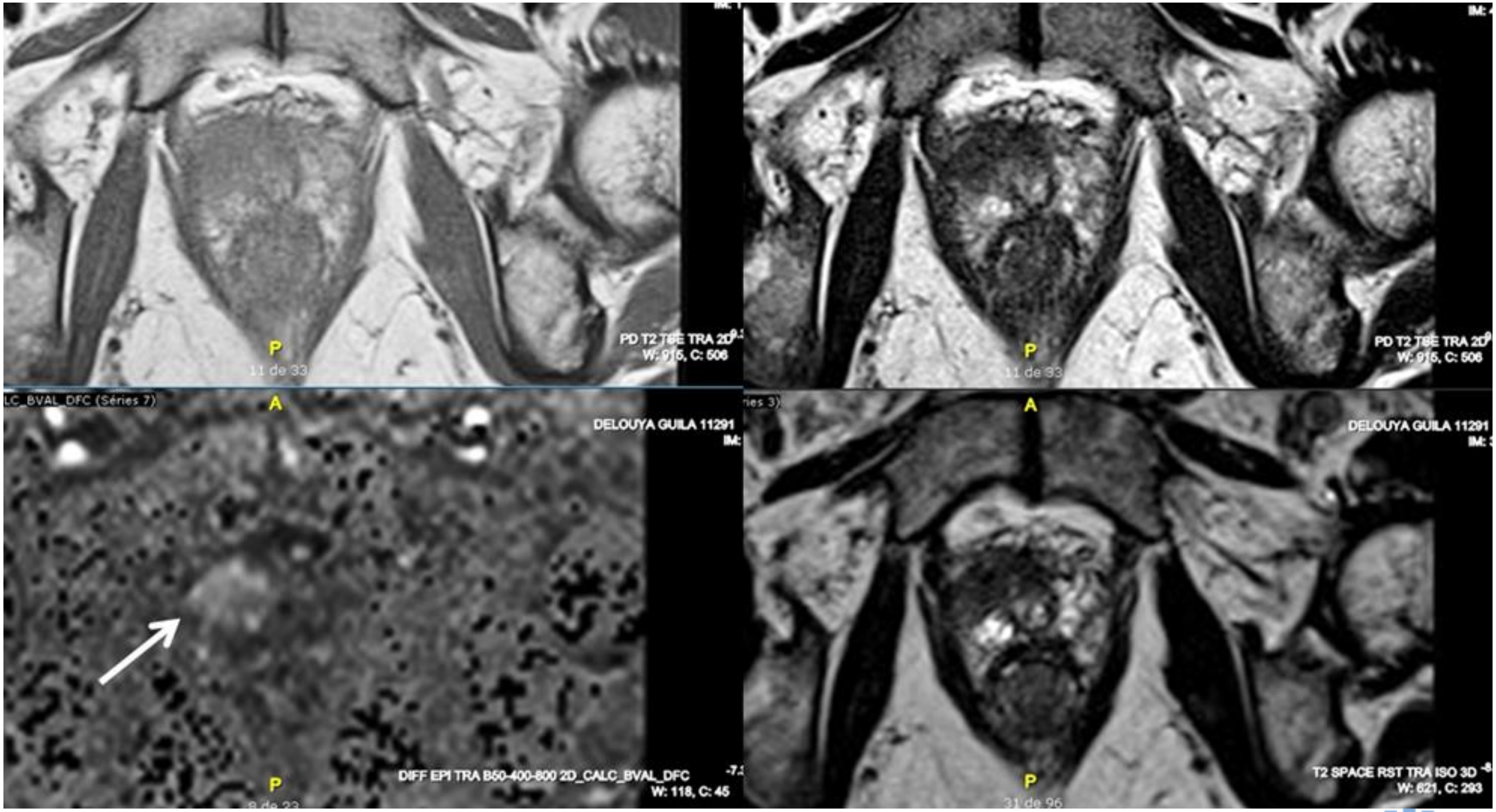
IM: 1
PD T2 TSE TRA 2D
W: 915, C: 506
P
11 de 33
IM: 4
PD T2 TSE TRA 2D
W: 915, C: 506
P
11 de 33
LC_BVAL_DFC (Séries 7)
A
DELOUYA GUILA 11291
IM:
DIFF EPI TRA B50-400-800 2D_CALC_BVAL_DFC
W: 118, C: 45
P
8 de 23
ies 3)
A
DELOUYA GUILA 11291
IM:
T2 SPACE RST TRA ISO 3D
W: 621, C: 293
P
31 de 96

WB-MRI

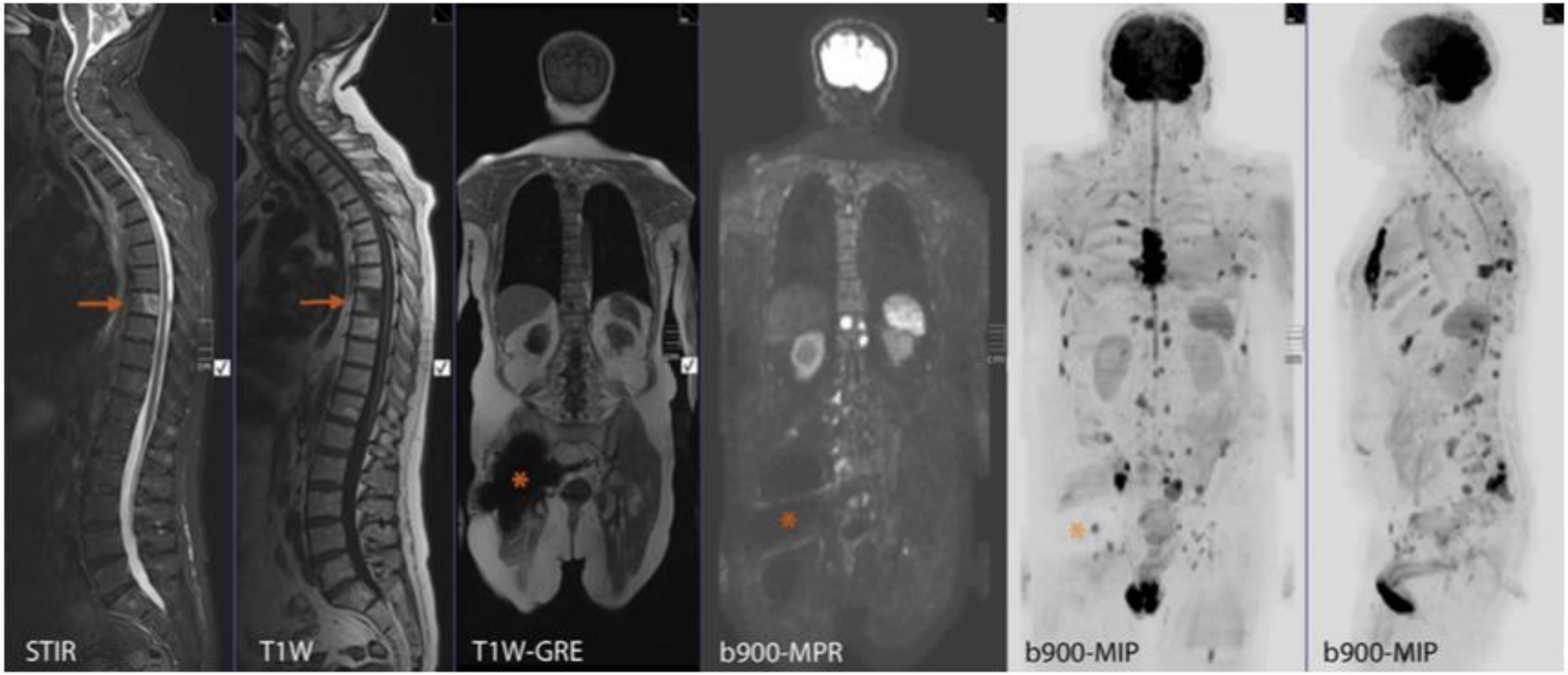
STIR
T1W
T1W-GRE
b900-MPR
b900-MIP
b900-MIP

📖 Padhani et al., Eur Urol 2016

PSMA-PET/MRI

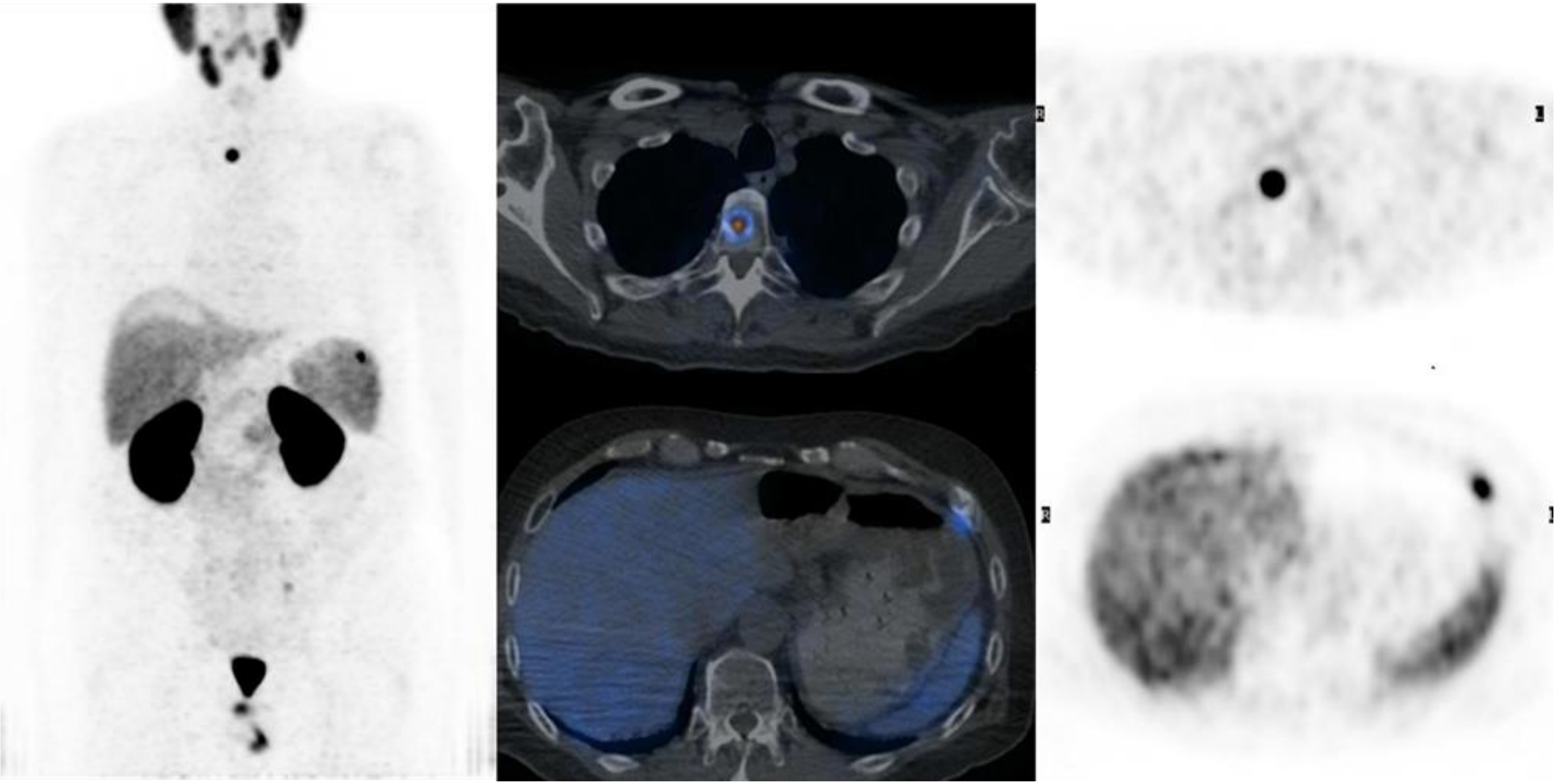

bDFS according to MRI findings

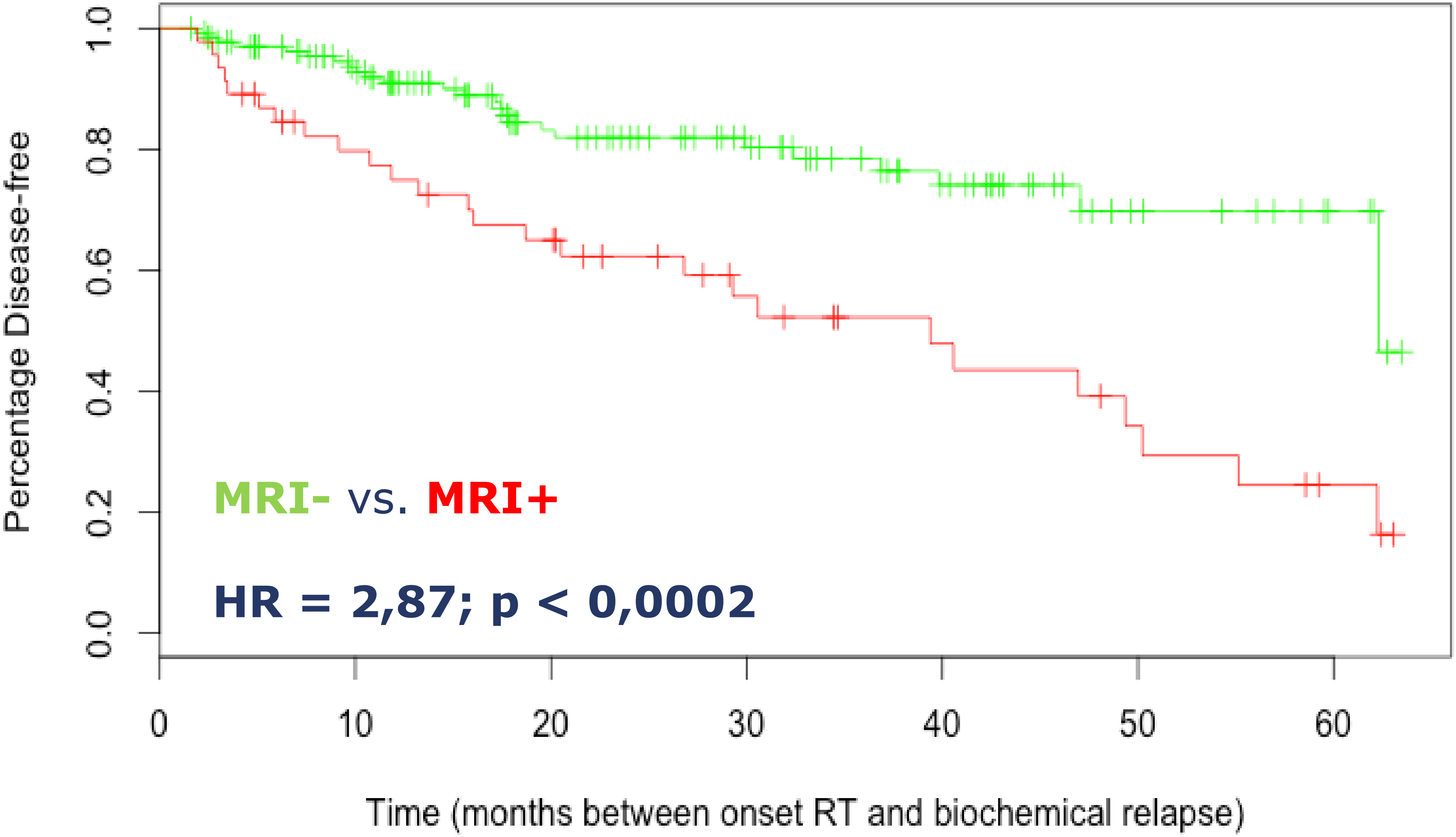

MRI- vs. **MRI+**

HR = 2,87; p < 0,0002

📖 Dirix et al., Acta Oncol 2017

bDFS according to dose to macroscopic disease

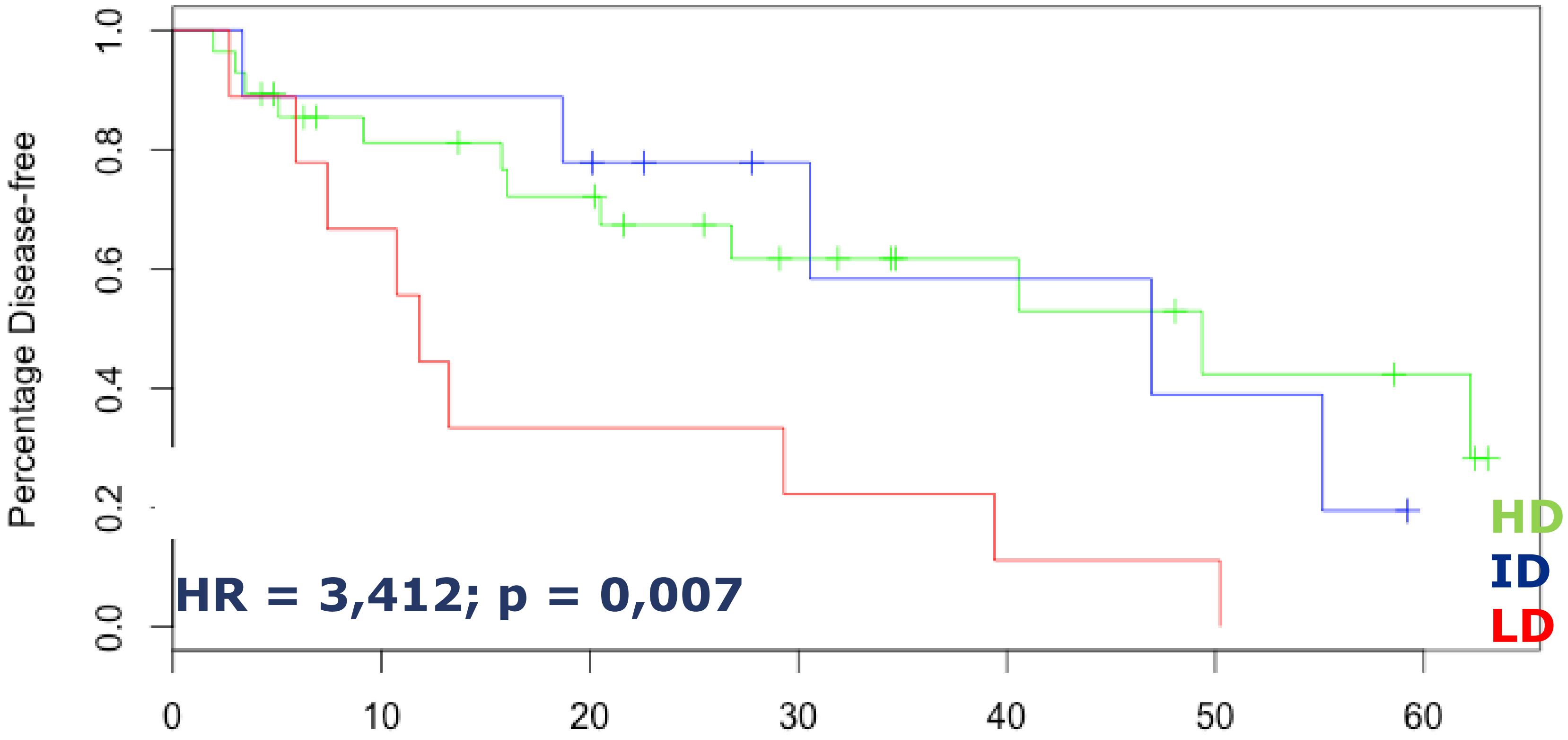

HR = 3,412; p = 0,007

Dirix et al., Acta Oncol 2017

CHUM

Acknowledgements

Uulke van der Heide
Eric Paulson
Tufve Nyholm
Patrick McLaughlan
Piet Dirix
Gary Liney

David Roberge
Philip Wong
Jean DaSilva
Samuel Kadoury
Karim Boudam
Jean-Charles Coté
Mary Gospodarowicz
David Jaffray
Peter Chung
Alejandro Berlin

CHUM

APPLICATIONS:
PET/MRI IN HEAD & NECK

Piet Dirix MD, PhD

Dpt. of Radiation Oncology, Iridium Cancer Network

Associate Professor, University of Antwerp

www.iridiumkankernetwerk.be

PET/MRI in radiotherapy for HNC

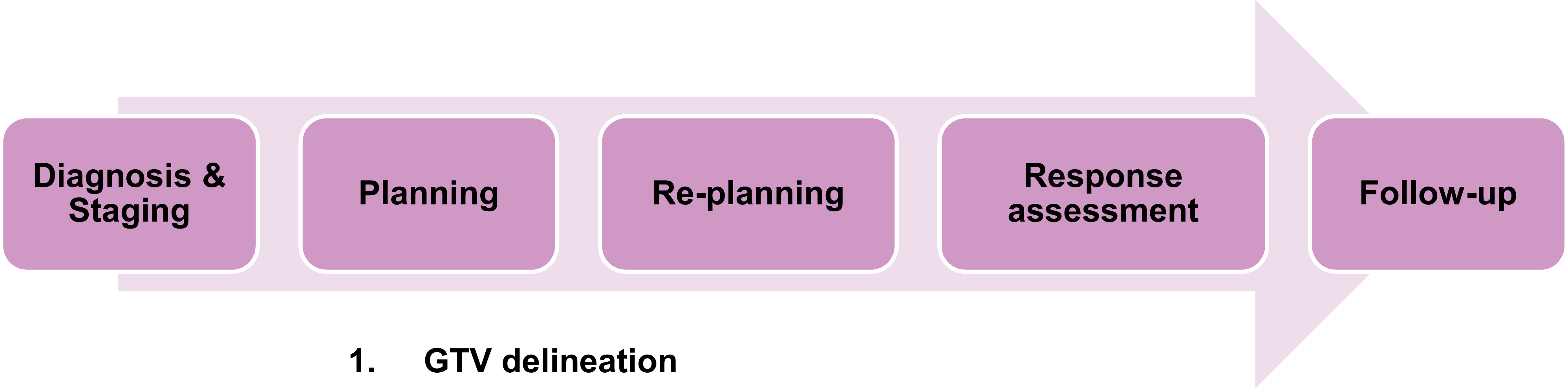
Diagnosis & Staging
Planning
Re-planning
Response assessment
Follow-up

1. **GTV delineation**
2. **CTV selection**
3. **Early response assessment**
4. **Dose-painting on a BTV**
5. **Follow-up**
6. **Organ-sparing**
7. **Pitfalls**

Head and neck cancer (HNC)

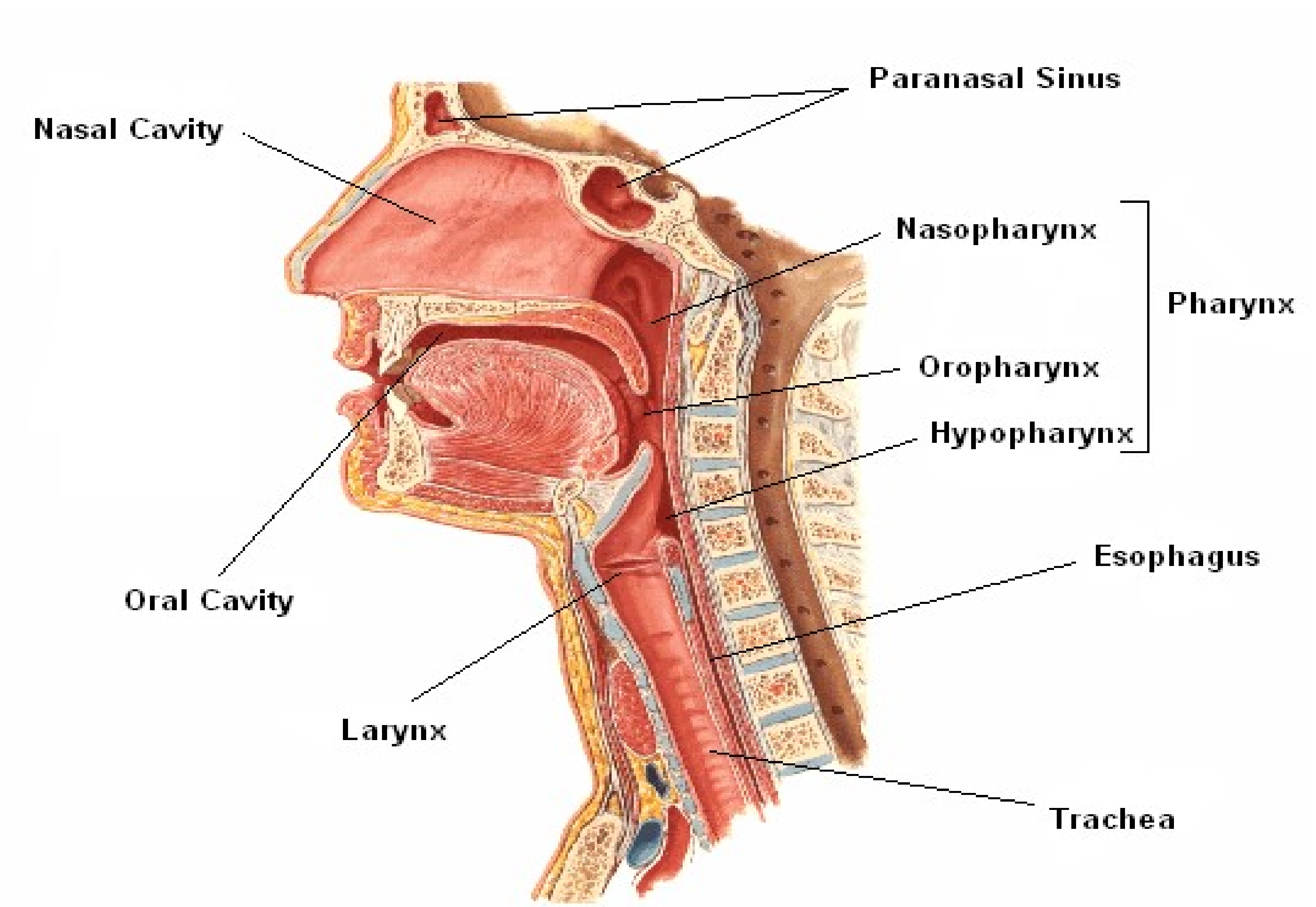
Paranasal Sinus
Nasal Cavity
Nasopharynx
Pharynx
Oropharynx
Hypopharynx
Oral Cavity
Esophagus
Larynx
Trachea

Current standard: concomitant CRT

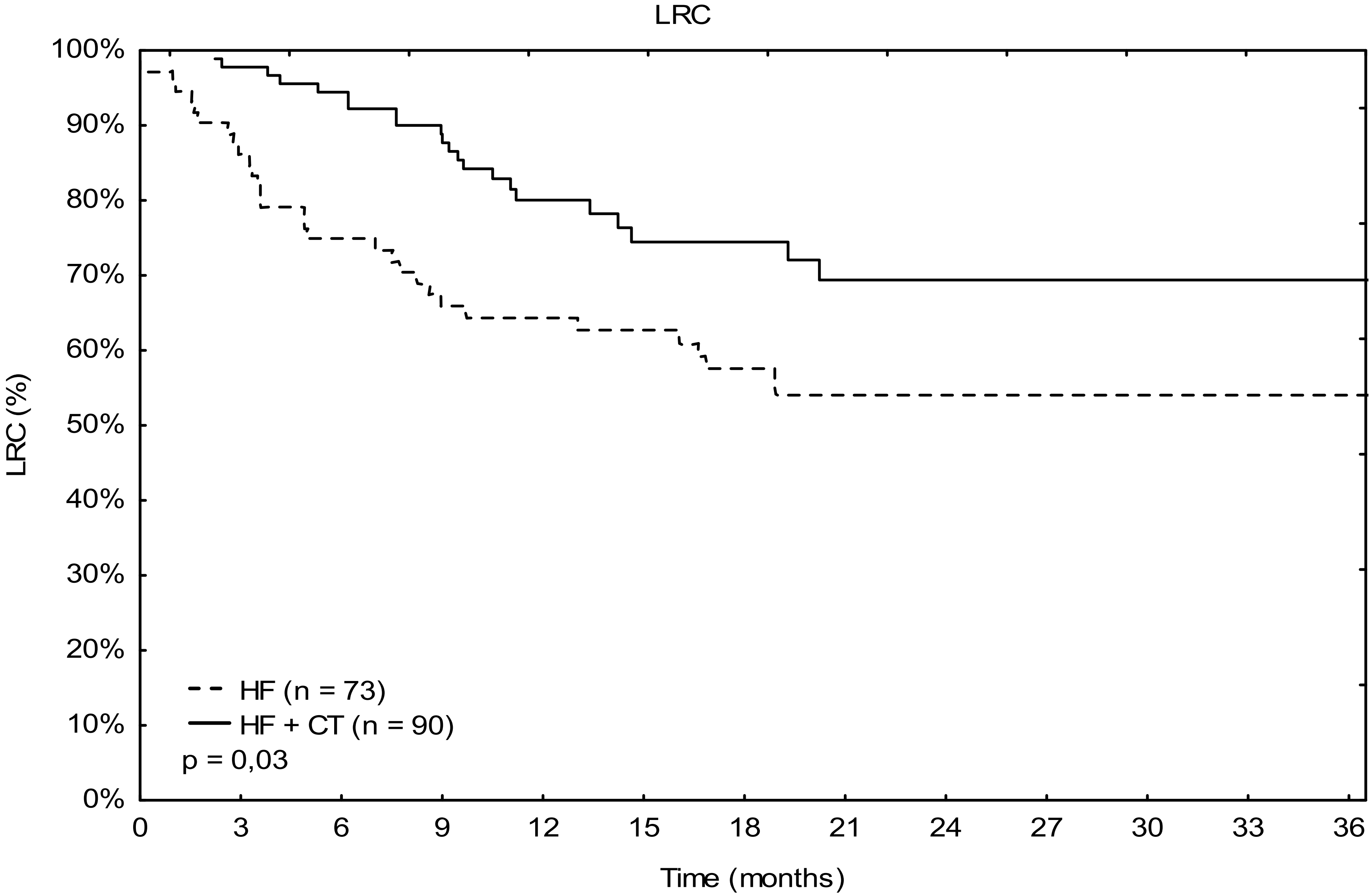

Nuyts S. et al. Int J Radiat Oncol Biol Phys 2009.

Towards a higher conformality

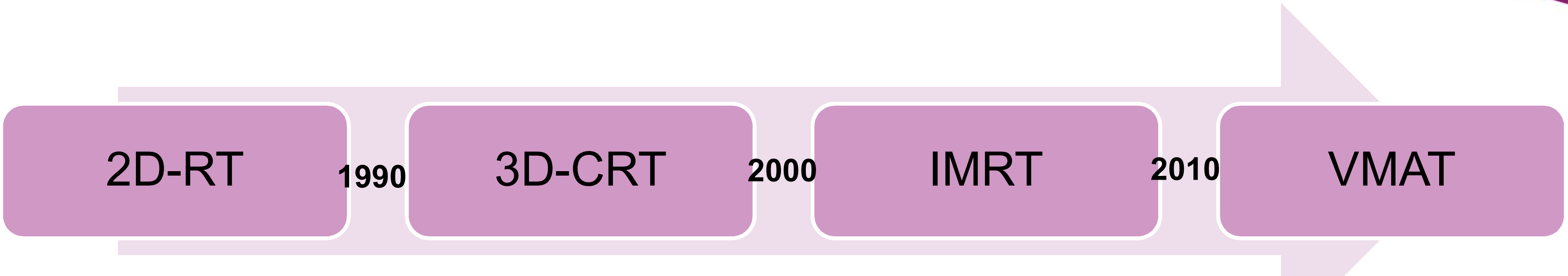

2D-RT

1990

3D-CRT

2000

IMRT

2010

VMAT

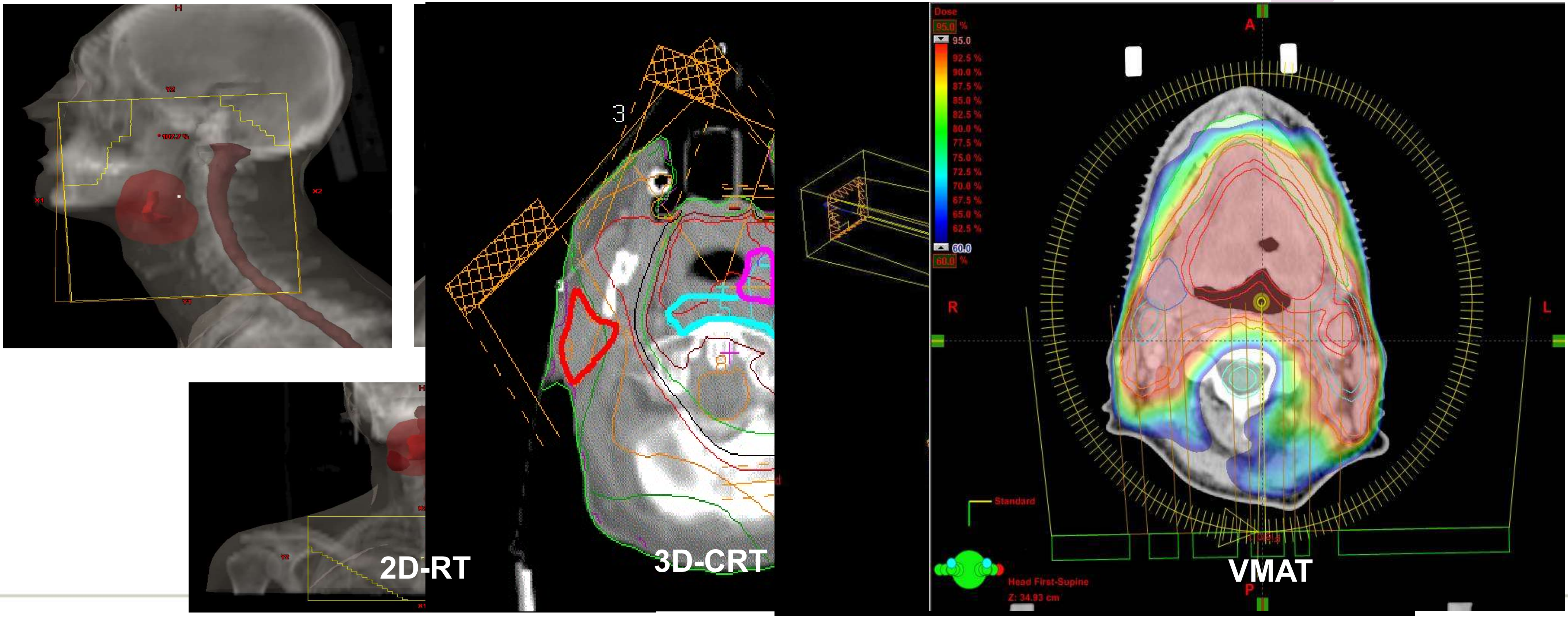
H
Y2
X1
X2
Y1
3
2D-RT
3D-CRT
Dose
95.0 %
95.0
92.5 %
90.0 %
87.5 %
85.0 %
82.5 %
80.0 %
77.5 %
75.0 %
72.5 %
70.0 %
67.5 %
65.0 %
62.5 %
60.0
60.0 %
A
R
L
P
Standard
Head First-Supine
Z: 34.93 cm
VMAT

1. GTV delineation becomes critical

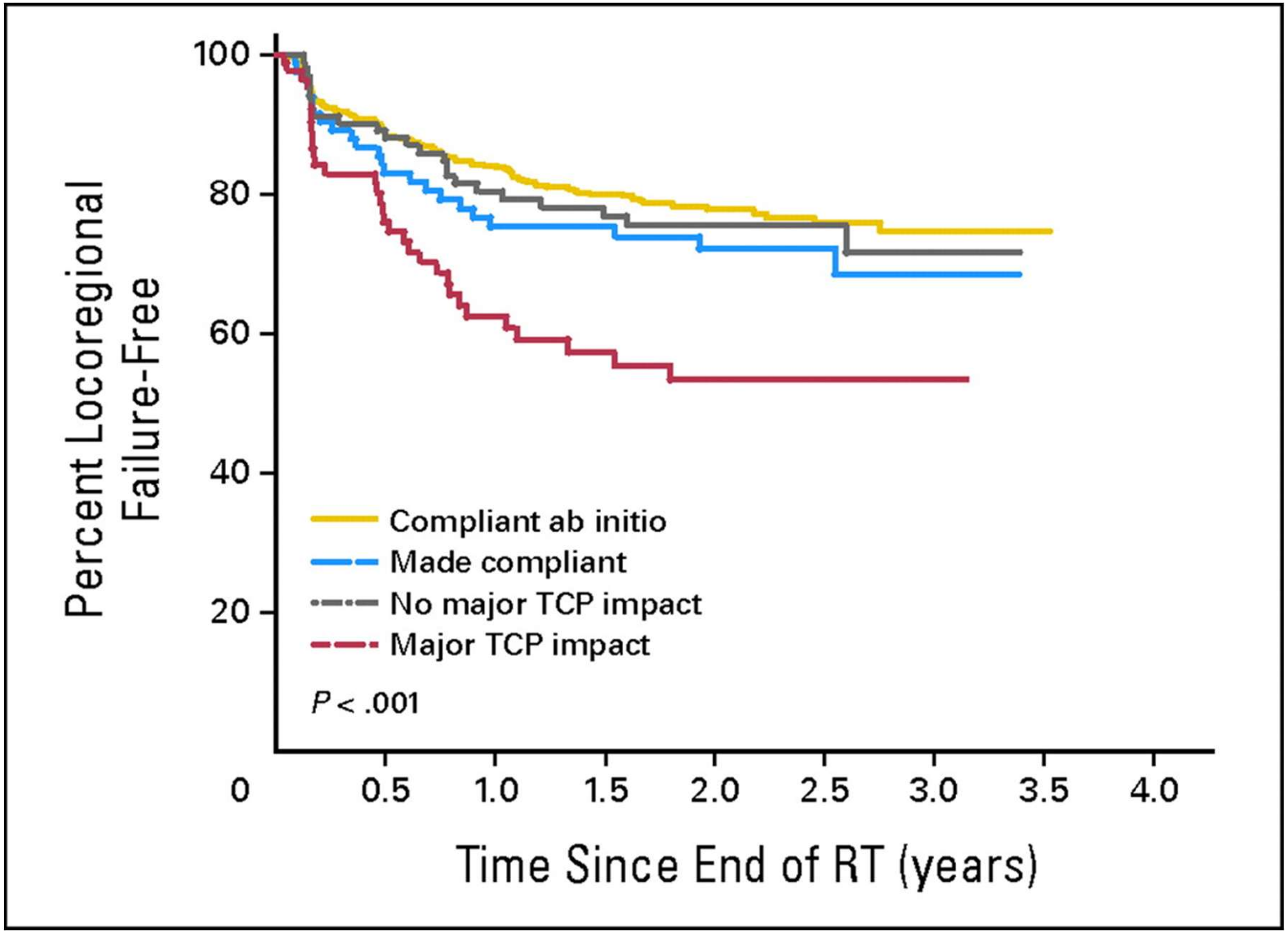

Peters L.J. et al. J Clin Oncol 2010.

Delineation remains crucial, even in HPV+ patients

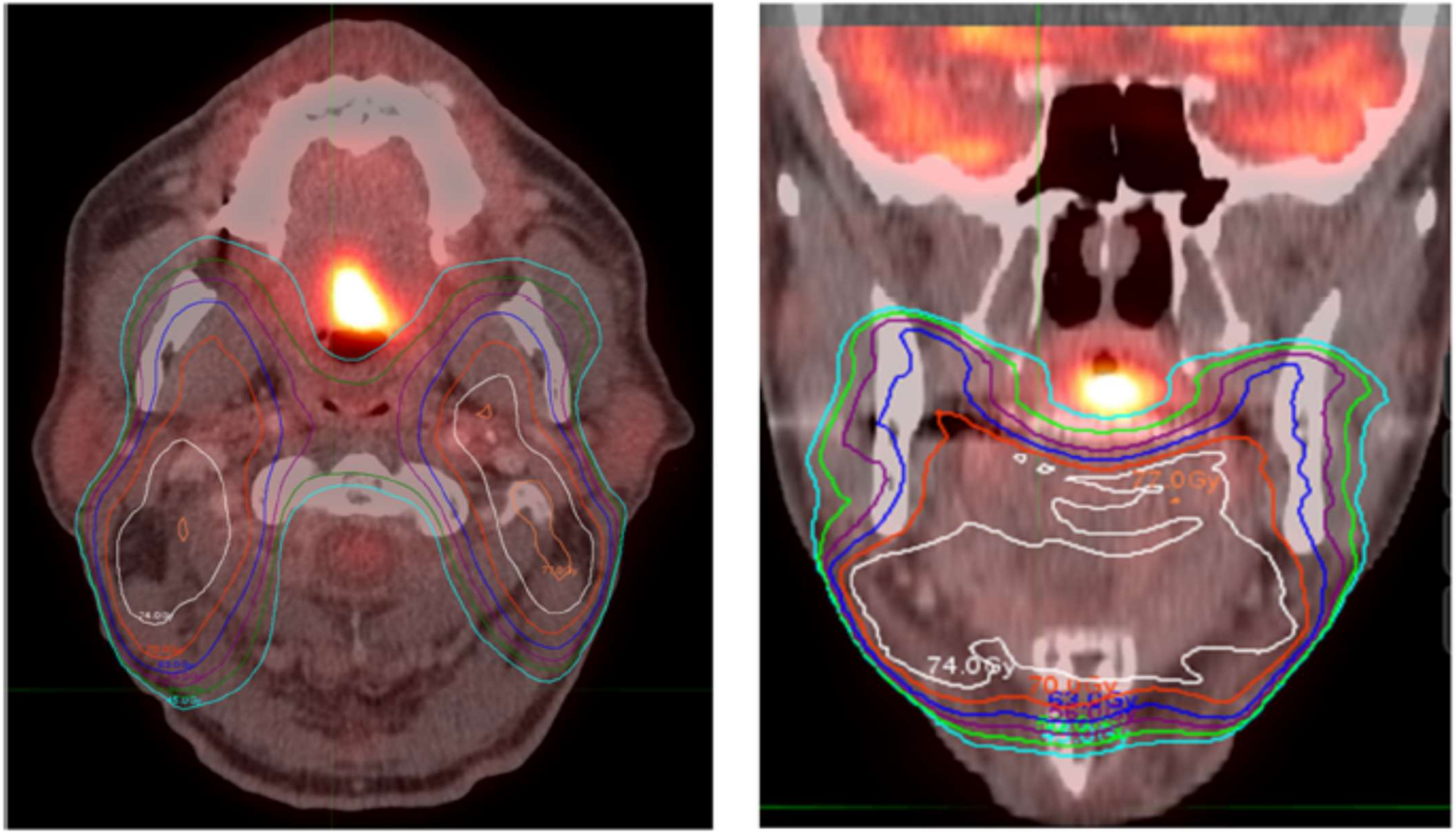
72.0Gy
74.0Gy
70.0Gy
63.0Gy

Chen A.M. et al. Radiother Oncol 2017.

Is imaging reliable?

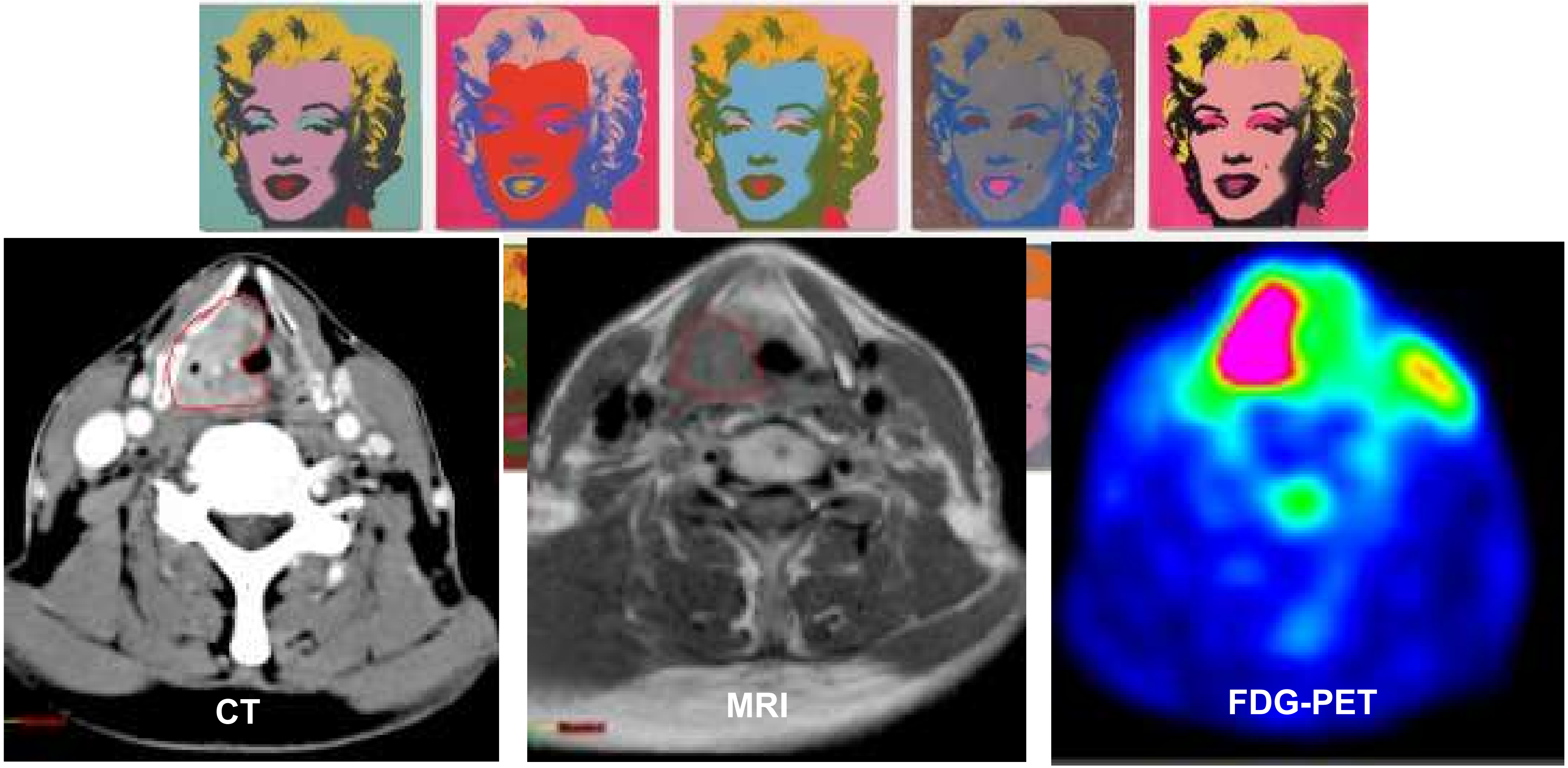
CT
MRI
FDG-PET

Imaging provides several different representations of 1 ground truth (i.e. pathology)…

Radiation oncologists live inside Plato’s cave

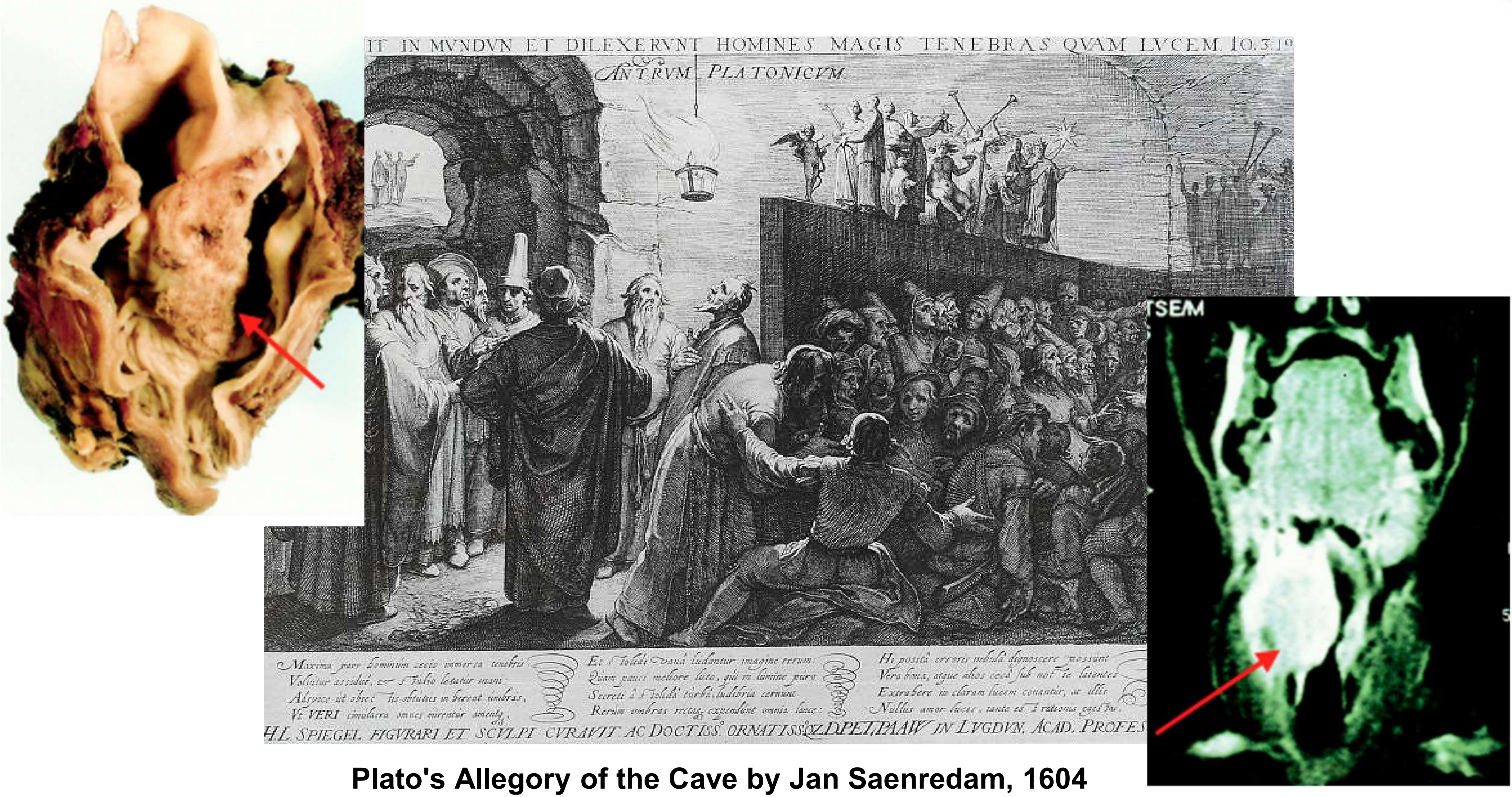
IT IN MVNDVN ET DILEXERVNT HOMINES MAGIS TENEBRAS QVAM LVCEM. IO.3.19
ANTRVM PLATONICVM
HL. SPIEGEL FIGVRARI ET SCVLPI CVRAVIT AC DOCTISS. ORNATISSQ. D. PET. PAAW IN LVGDVN. ACAD. PROFES
TSEM

Plato's Allegory of the Cave by Jan Saenredam, 1604

Large intra/inter-observer variability on CT

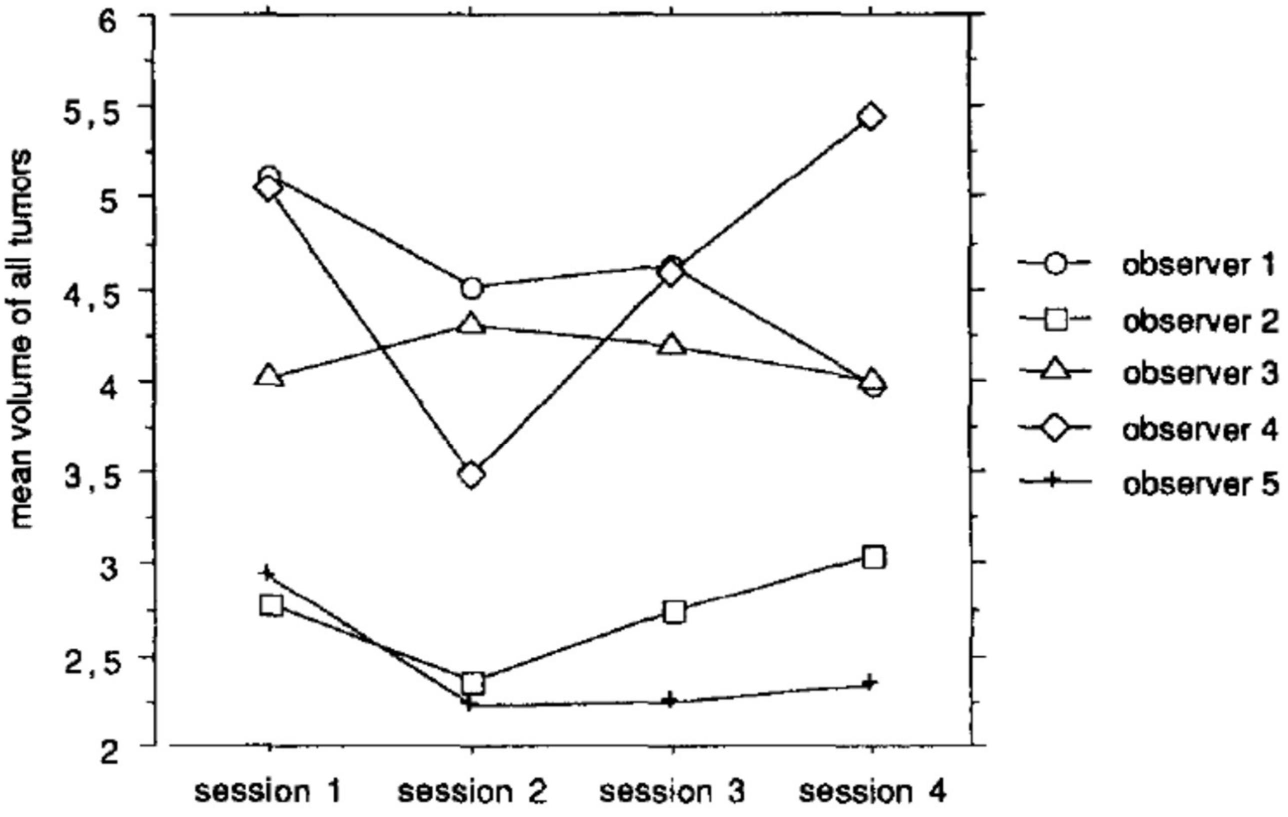

Fig. 1. Graph showing the interaction of the mean volume of all tumors (ml) and the four measurement sessions.

Hermans R. et al. Int J Radiat Oncol Biol Phys 1998.

CT vs. MRI: advantages

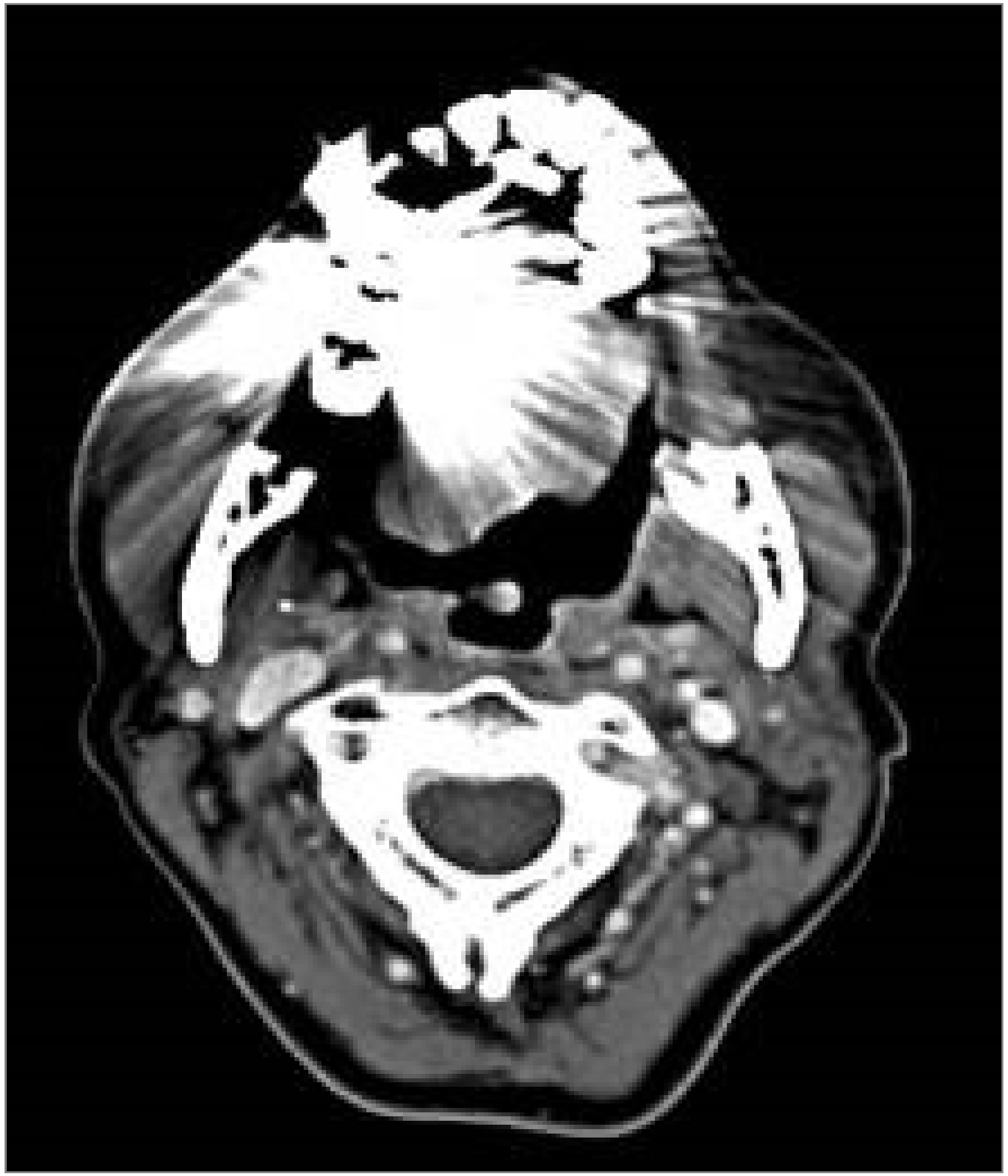

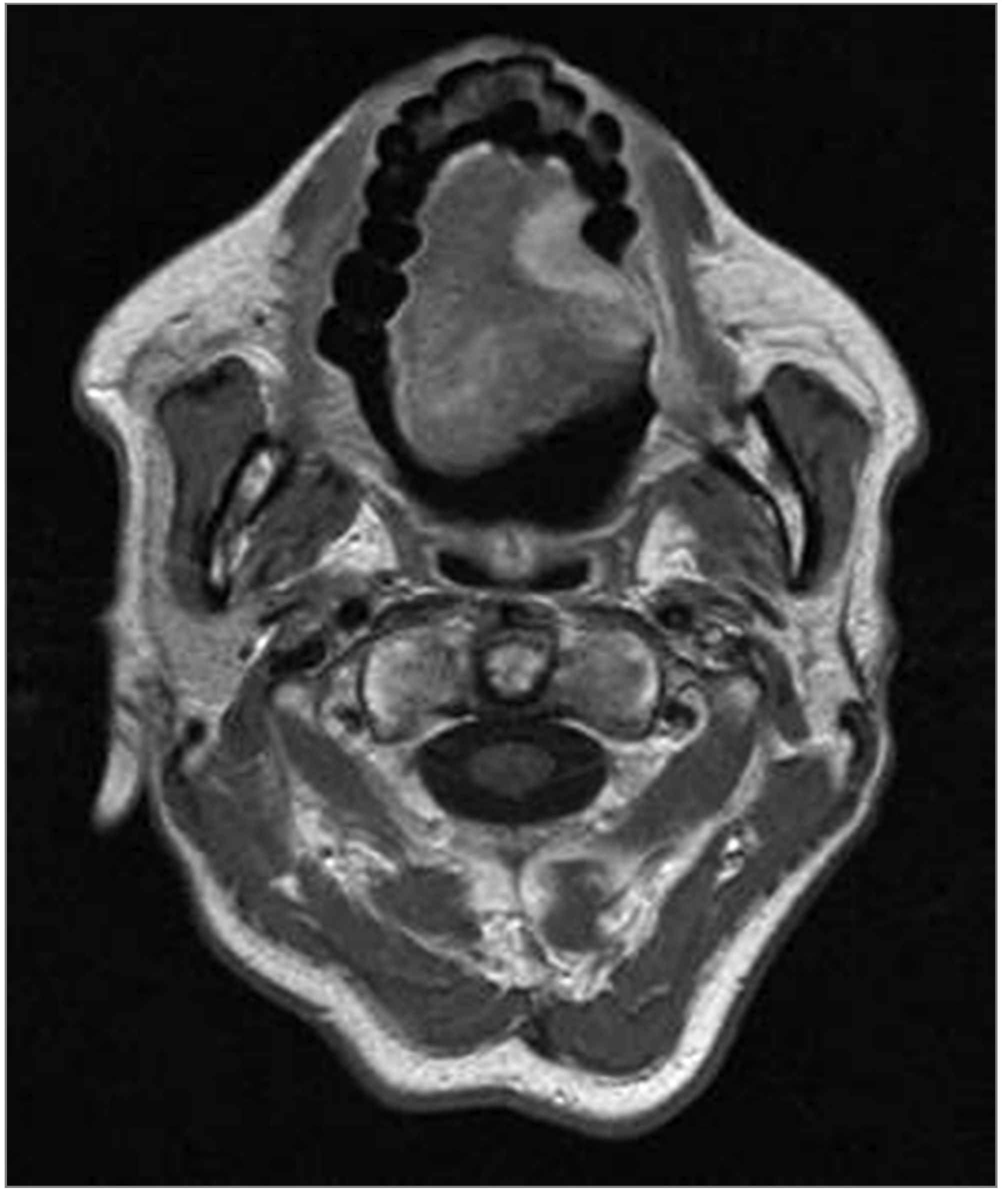

Images courtesy of Prof. R. Hermans.

CT vs. MRI: disadvantages

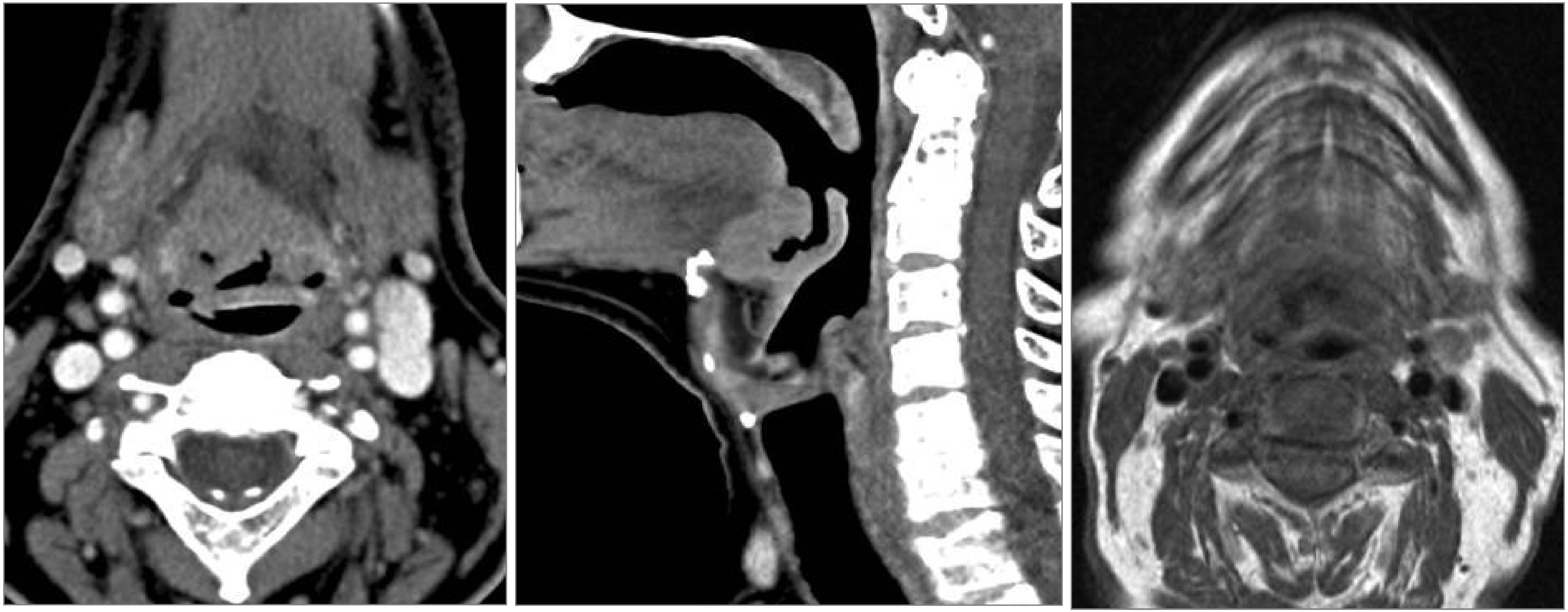

Images courtesy of Prof. R. Hermans.

MRI in treatment position

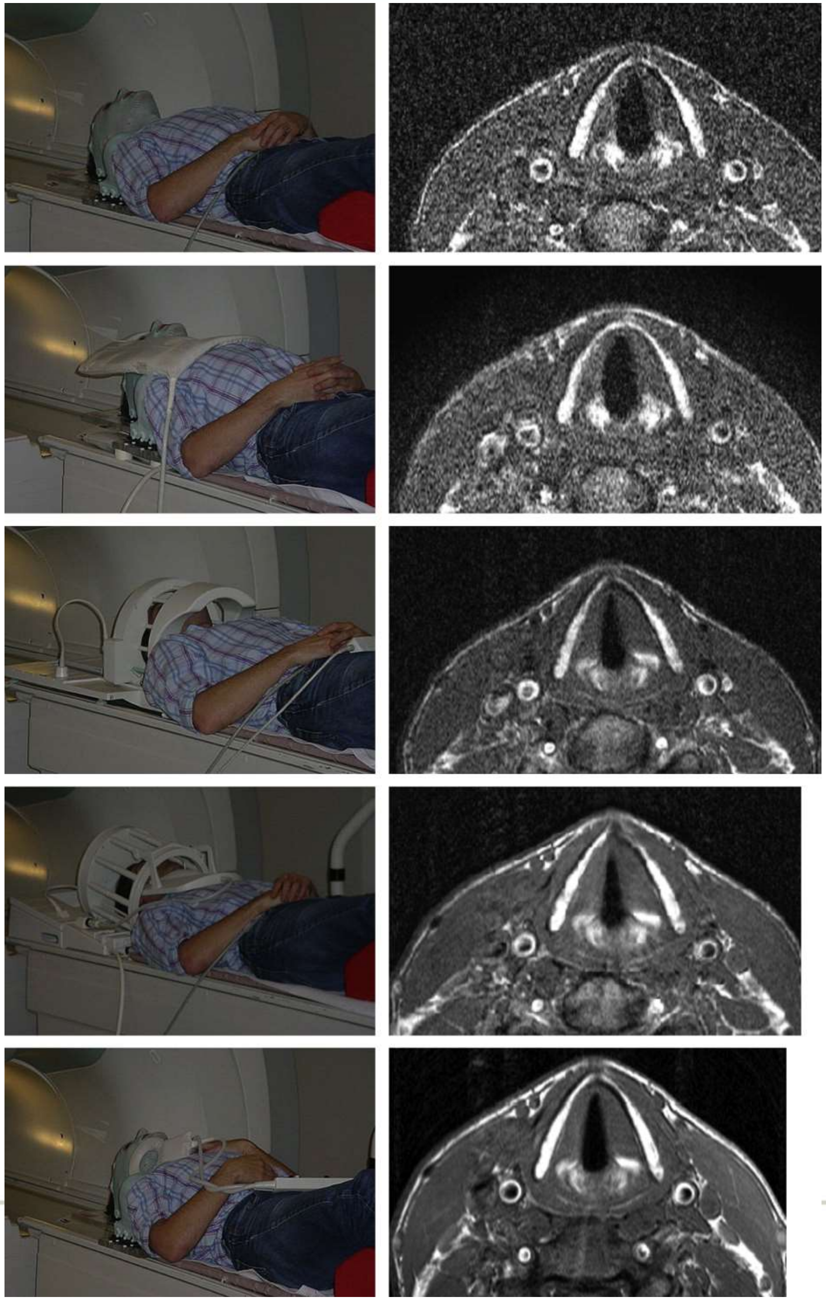

Verduijn G.M. et al. Int J Radiat Oncol Biol Phys 2009.
Webster G.J. et al. Br J Radiol 2009.
Ahmed M. et al. Radiother Oncol 2010.

MRI for nasopharyngeal cancer (NPC)

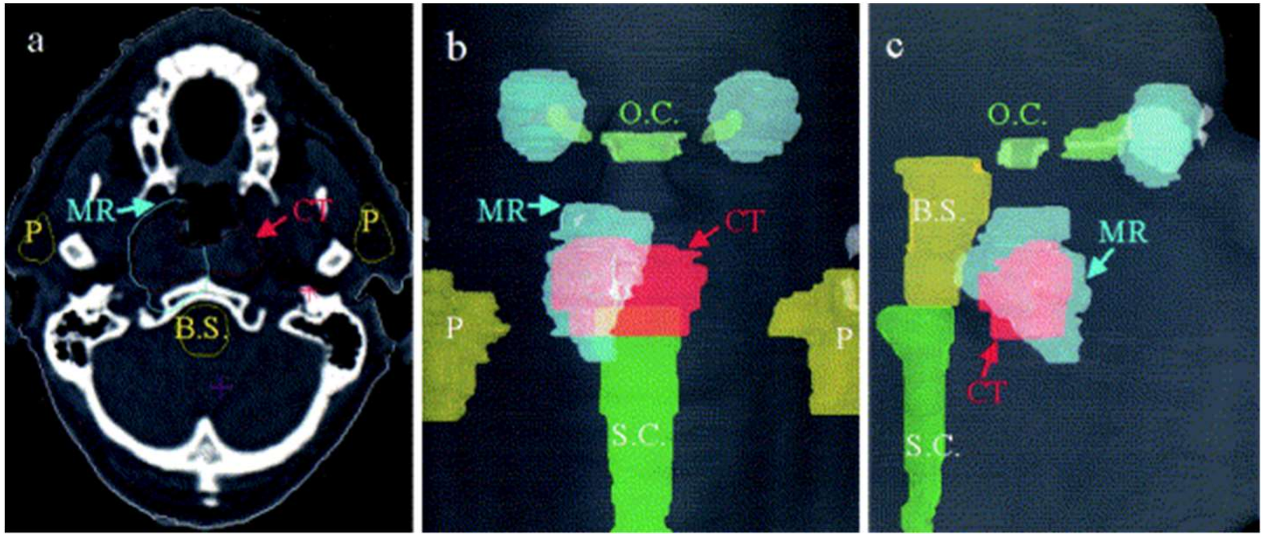
a
MR
CT
P
P
B.S.
b
O.C.
MR
CT
P
P
S.C.
c
O.C.
B.S.
MR
CT
S.C.

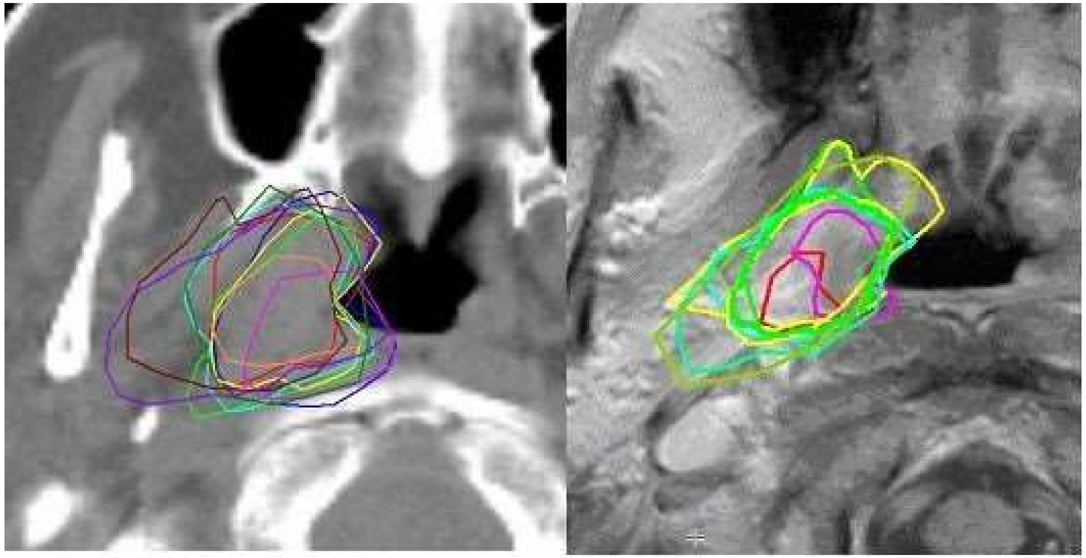

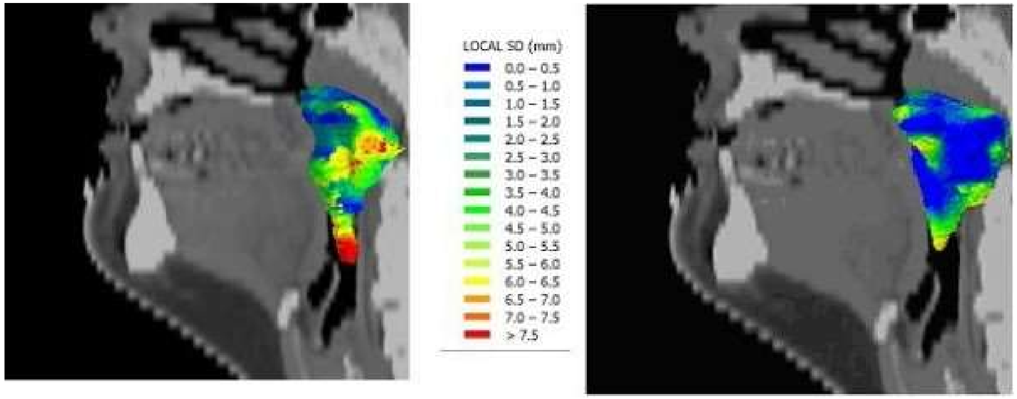
LOCAL SD (mm)
0.0 – 0.5
0.5 – 1.0
1.0 – 1.5
1.5 – 2.0
2.0 – 2.5
2.5 – 3.0
3.0 – 3.5
3.5 – 4.0
4.0 – 4.5
4.5 – 5.0
5.0 – 5.5
5.5 – 6.0
6.0 – 6.5
6.5 – 7.0
7.0 – 7.5
> 7.5

Emami B. et al. Int J Radiat Oncol Biol Phys 2003.
Rasch C. et al. Radiat Oncol 2010.

MRI for sinonasal cancer (SNC)

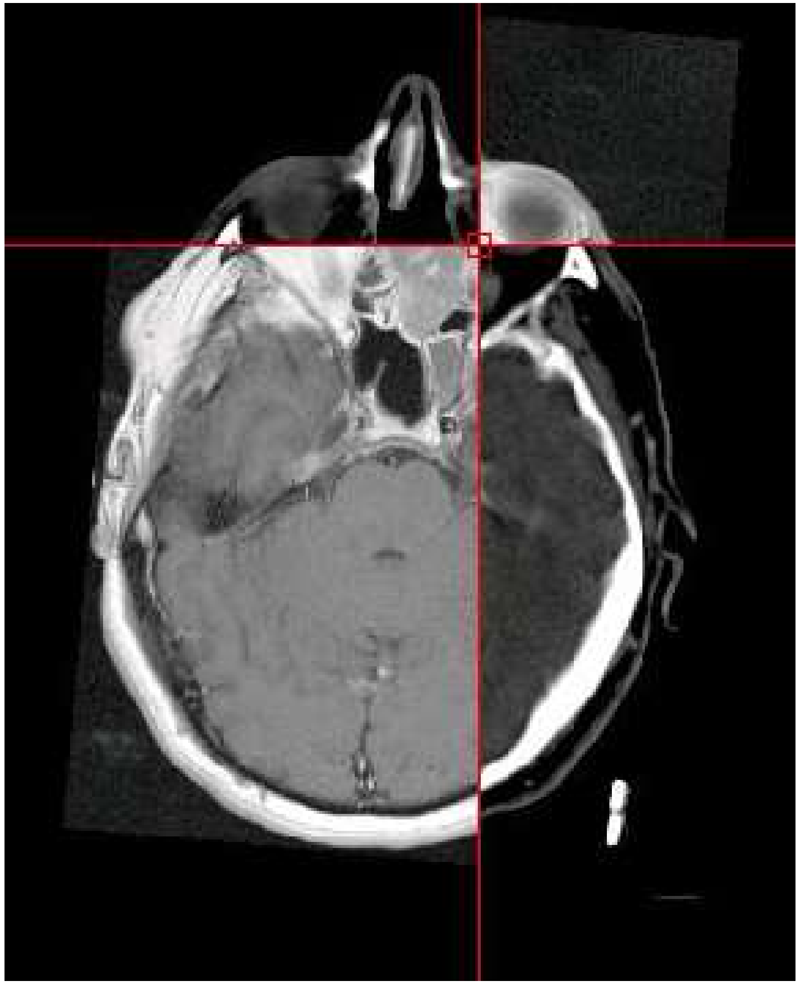

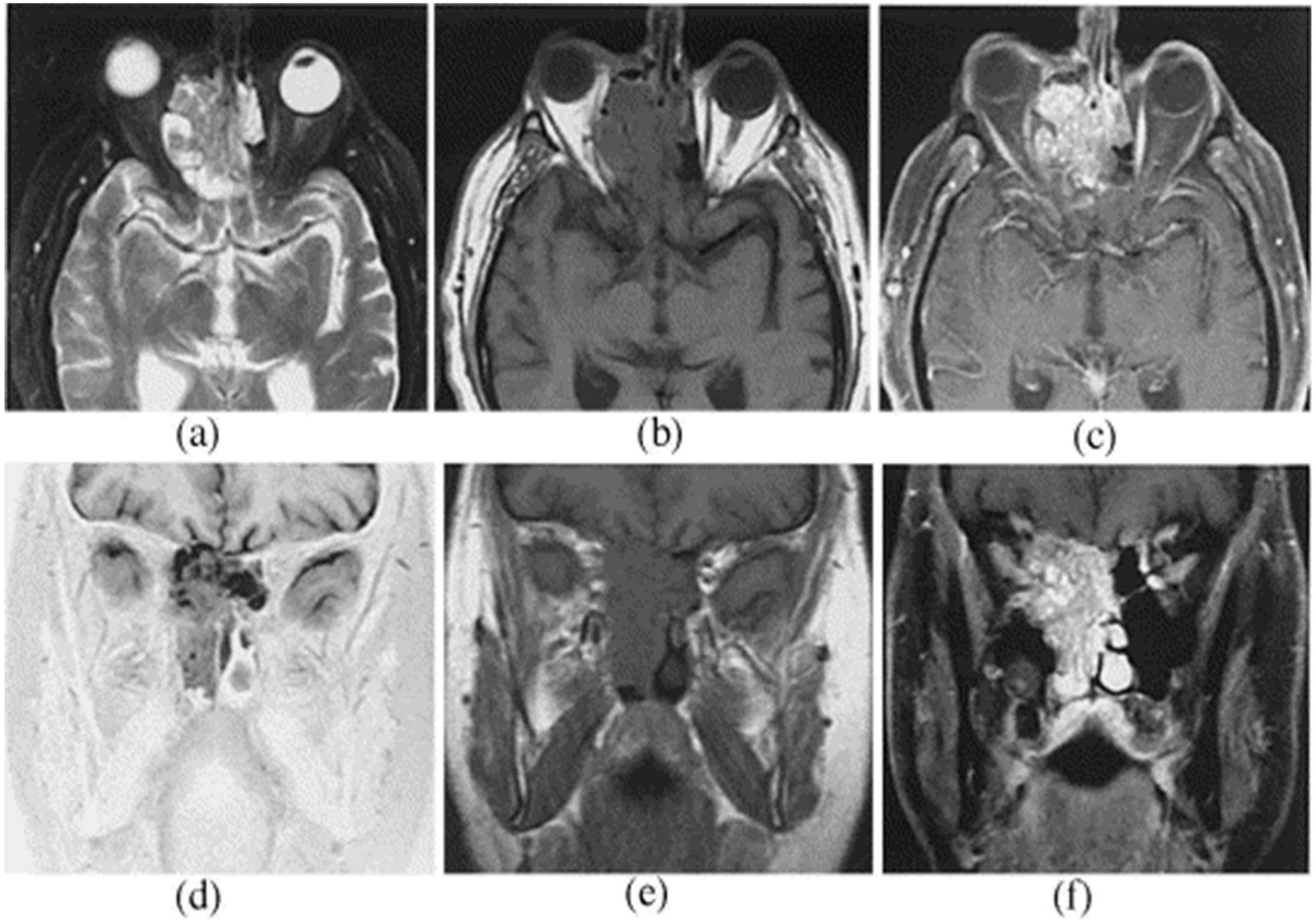

Sievers K. W. et al. Eur J Radiol 2000.
Dirix P. et al. Int J Radiat Oncol Biol Phys 2010.

MRI for all base of skull tumors!

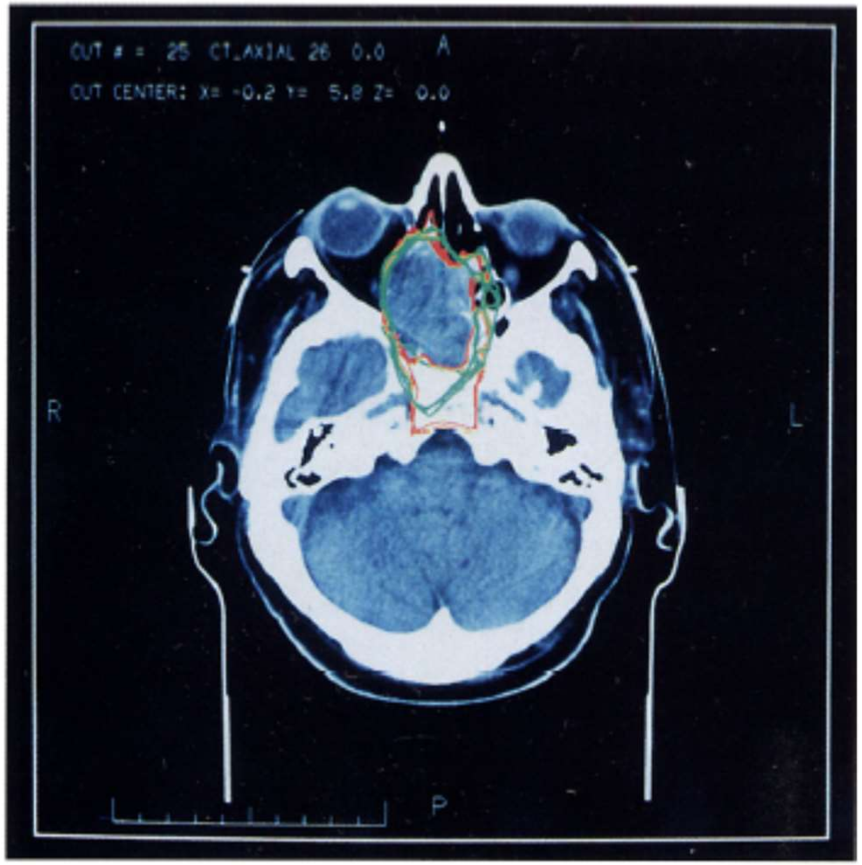
CUT # = 25 CT_AXIAL 26 0.0
A
CUT CENTER: X= -0.2 Y= 5.8 Z= 0.0
R
L
P

Fig. 2. The axial CT scan of patient 1 (ethmoid tumor). In red, the four contours as outlined on this scan by the four observers; in green, the contours outlined on axial MRI. Note the difference in the posterior border; on the CT either the clivus is entirely included in the Gross Tumor Volume or not at all.

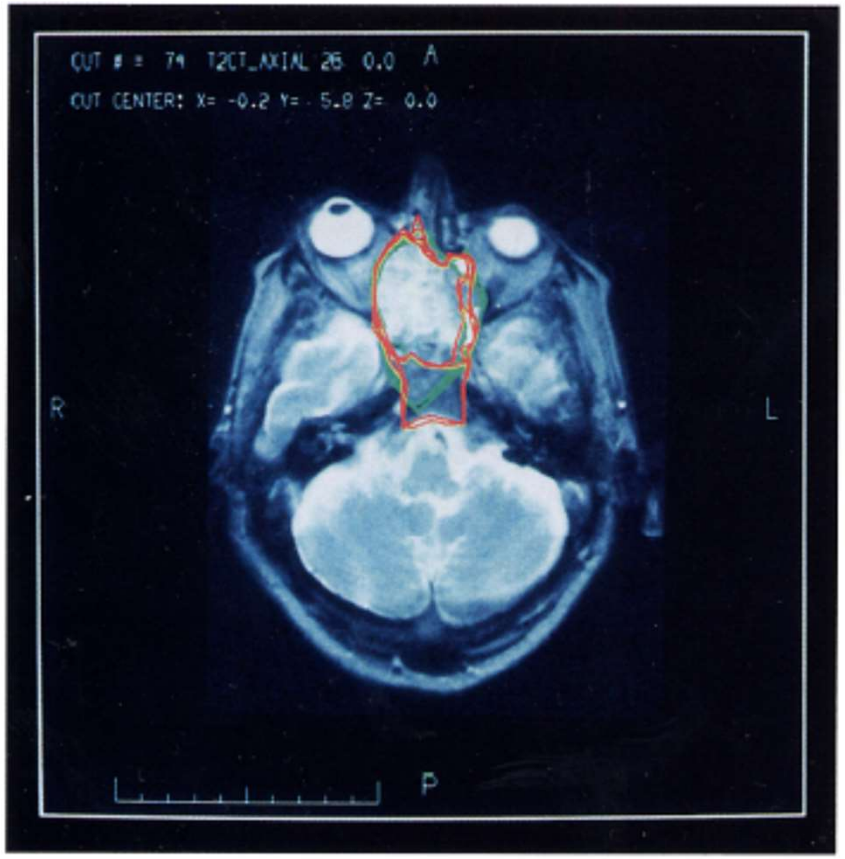
CUT # = 74 T2CT_AXIAL 26 0.0
A
CUT CENTER: X= -0.2 Y= 5.8 Z= 0.0
R
L
P

Fig. 3. The axial MRI scan of patient 1 (ethmoid tumor), resampled to fit the CT scan of Fig. 2. The contours outlined in the CT scan are red; the contours drawn on this axial MRI are green. On the CT scan, the observers outlined either the whole clivus as tumor or did not include the clivus at all in their Gross Tumor Volume. On the MRI, half of the clivus was included in the GTV.

Rasch C. et al. Int J Radiat Oncol Biol Phys 1997.

MRI for oropharyngeal cancer (OPC)

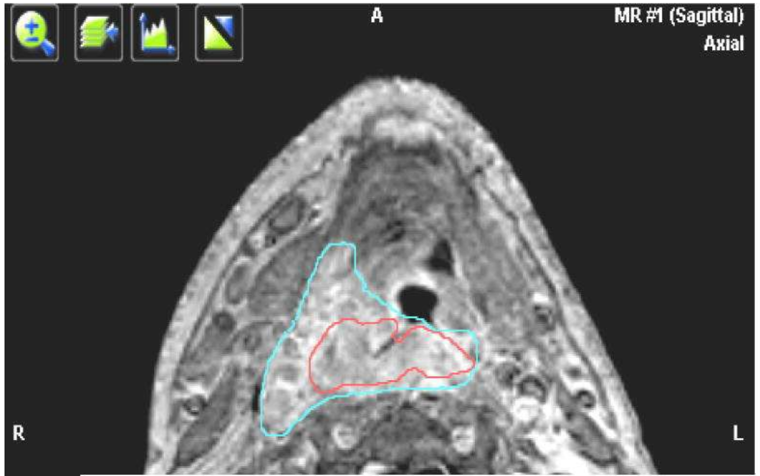

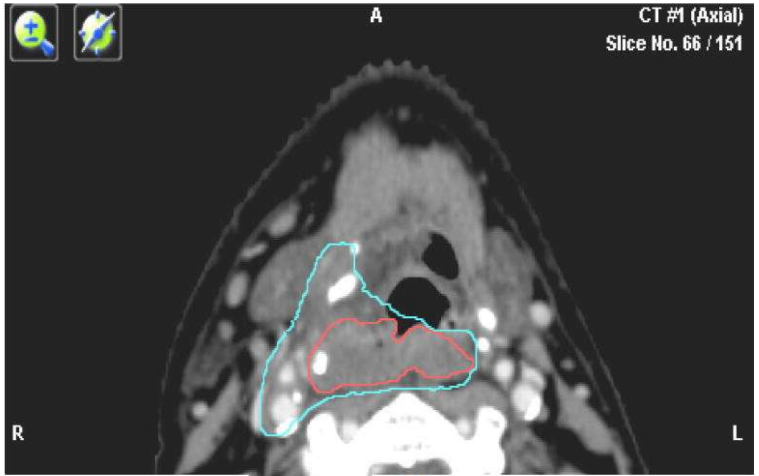

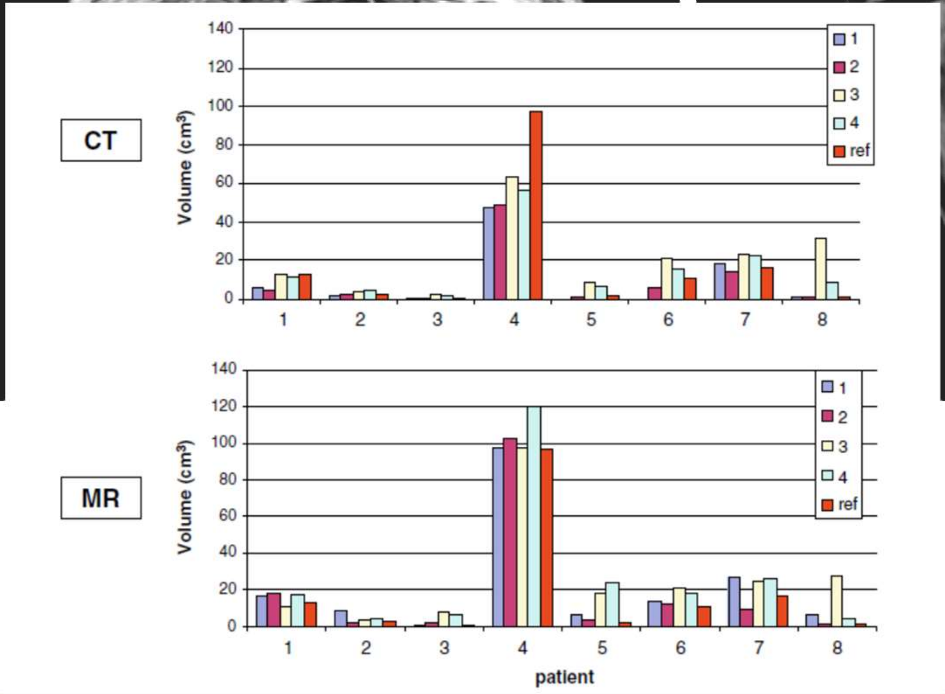

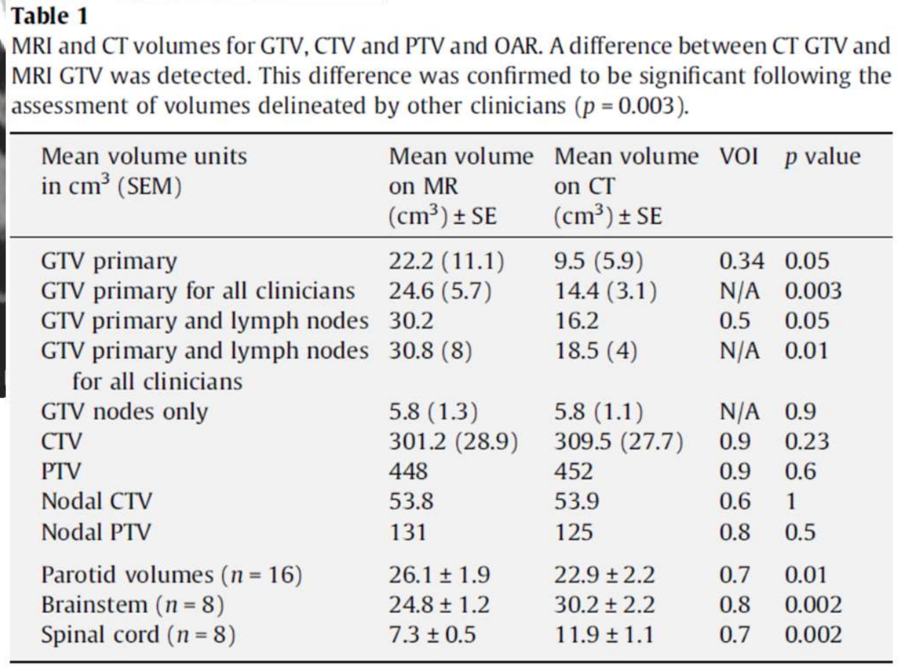

Table 1

MRI and CT volumes for GTV, CTV and PTV and OAR. A difference between CT GTV and MRI GTV was detected. This difference was confirmed to be significant following the assessment of volumes delineated by other clinicians ($p = 0.003$).

Mean volume units in cm^3 (SEM)	Mean volume on MR (cm^3) ± SE	Mean volume on CT (cm^3) ± SE	VOI	p value
GTV primary	22.2 (11.1)	9.5 (5.9)	0.34	0.05
GTV primary for all clinicians	24.6 (5.7)	14.4 (3.1)	N/A	0.003
GTV primary and lymph nodes	30.2	16.2	0.5	0.05
GTV primary and lymph nodes for all clinicians	30.8 (8)	18.5 (4)	N/A	0.01
GTV nodes only	5.8 (1.3)	5.8 (1.1)	N/A	0.9
CTV	301.2 (28.9)	309.5 (27.7)	0.9	0.23
PTV	448	452	0.9	0.6
Nodal CTV	53.8	53.9	0.6	1
Nodal PTV	131	125	0.8	0.5
Parotid volumes ($n = 16$)	26.1 ± 1.9	22.9 ± 2.2	0.7	0.01
Brainstem ($n = 8$)	24.8 ± 1.2	30.2 ± 2.2	0.8	0.002
Spinal cord ($n = 8$)	7.3 ± 0.5	11.9 ± 1.1	0.7	0.002

Ahmed M. et al. Radiother Oncol 2010.

MRI for hypopharyngo-laryngeal cancer (1)

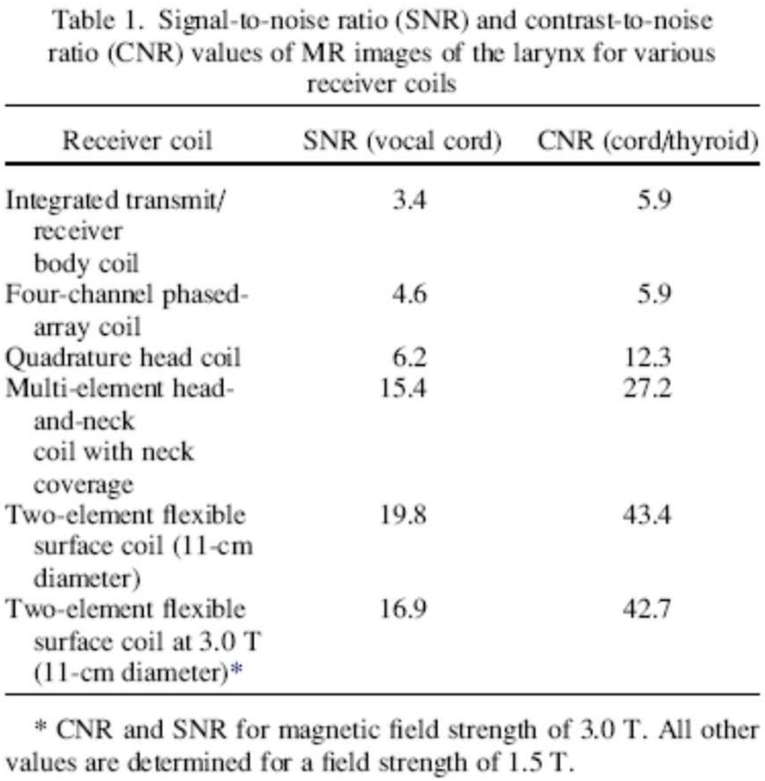

Table 1. Signal-to-noise ratio (SNR) and contrast-to-noise ratio (CNR) values of MR images of the larynx for various receiver coils

Receiver coil	SNR (vocal cord)	CNR (cord/thyroid)
Integrated transmit/ receiver body coil	3.4	5.9
Four-channel phased-array coil	4.6	5.9
Quadrature head coil	6.2	12.3
Multi-element head-and-neck coil with neck coverage	15.4	27.2
Two-element flexible surface coil (11-cm diameter)	19.8	43.4
Two-element flexible surface coil at 3.0 T (11-cm diameter)*	16.9	42.7

* CNR and SNR for magnetic field strength of 3.0 T. All other values are determined for a field strength of 1.5 T.

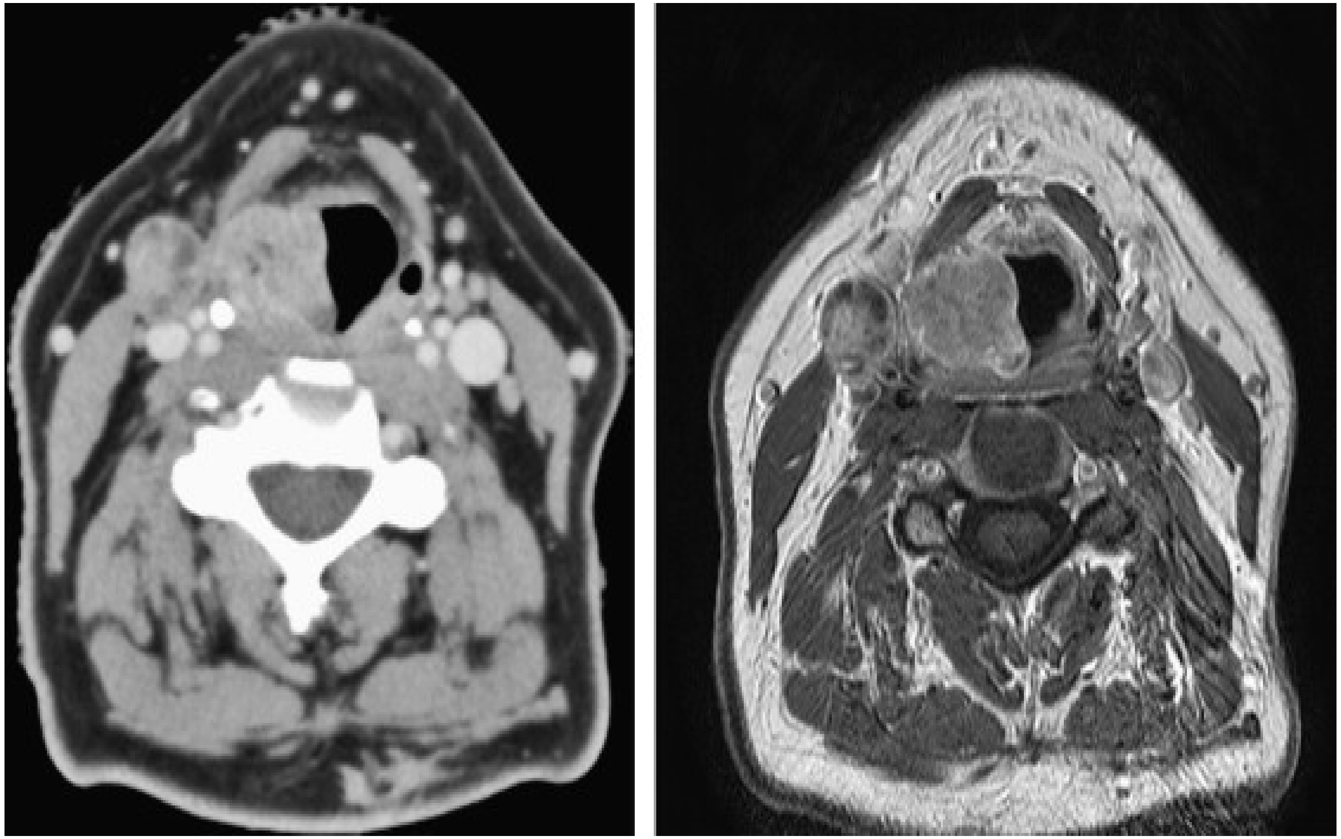

Verduijn G. M. et al. Int J Radiat Oncol Biol Phys 2010.

MRI for hypopharyngo-laryngeal cancer (2)

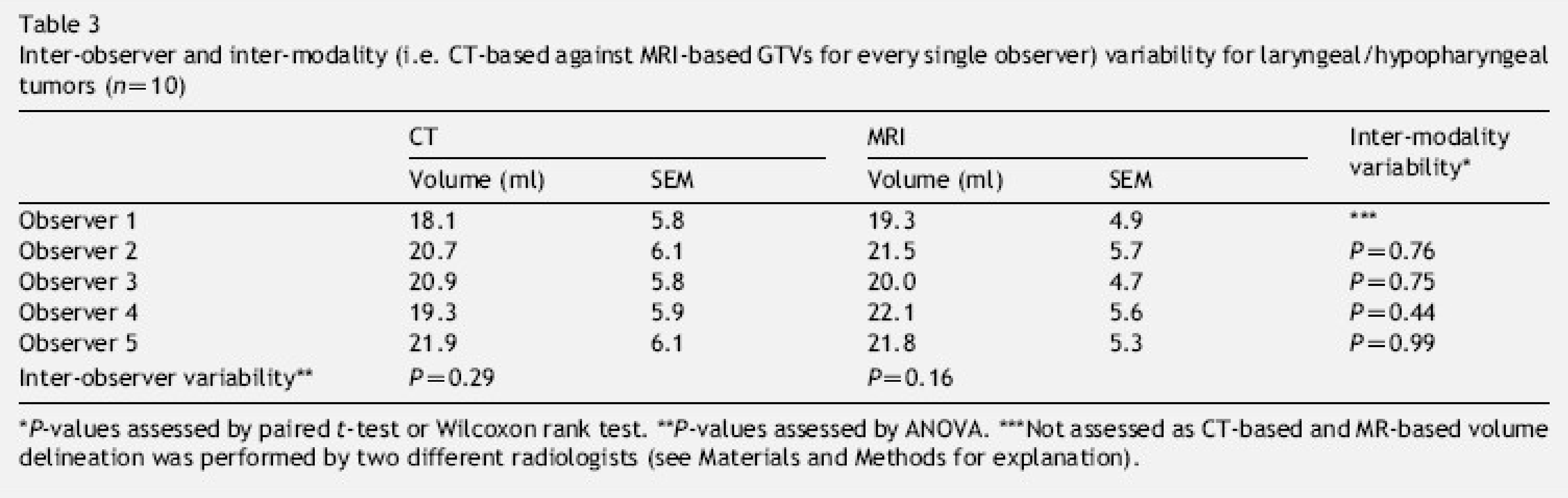

Table 3

Inter-observer and inter-modality (i.e. CT-based against MRI-based GTVs for every single observer) variability for laryngeal/hypopharyngeal tumors ($n=10$)

	CT		MRI		Inter-modality variability*
	Volume (ml)	SEM	Volume (ml)	SEM	
Observer 1	18.1	5.8	19.3	4.9	***
Observer 2	20.7	6.1	21.5	5.7	$P=0.76$
Observer 3	20.9	5.8	20.0	4.7	$P=0.75$
Observer 4	19.3	5.9	22.1	5.6	$P=0.44$
Observer 5	21.9	6.1	21.8	5.3	$P=0.99$
Inter-observer variability**	$P=0.29$		$P=0.16$		

*P-values assessed by paired t-test or Wilcoxon rank test. **P-values assessed by ANOVA. ***Not assessed as CT-based and MR-based volume delineation was performed by two different radiologists (see Materials and Methods for explanation).

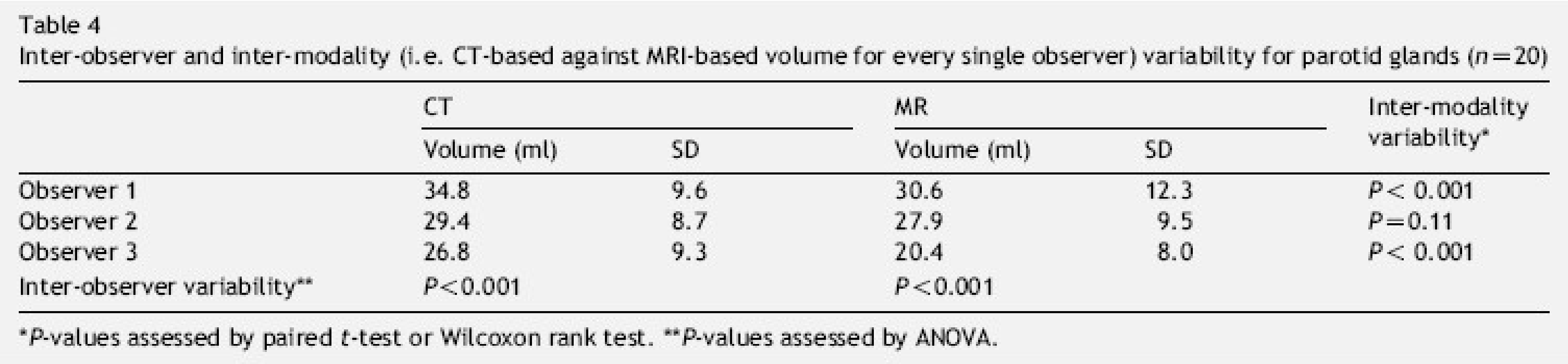

Table 4

Inter-observer and inter-modality (i.e. CT-based against MRI-based volume for every single observer) variability for parotid glands ($n=20$)

	CT		MR		Inter-modality variability*
	Volume (ml)	SD	Volume (ml)	SD	
Observer 1	34.8	9.6	30.6	12.3	$P<0.001$
Observer 2	29.4	8.7	27.9	9.5	$P=0.11$
Observer 3	26.8	9.3	20.4	8.0	$P<0.001$
Inter-observer variability**	$P<0.001$		$P<0.001$		

*P-values assessed by paired t-test or Wilcoxon rank test. **P-values assessed by ANOVA.

Geets X. et al. Radiother Oncol 2005.

Validated for guidelines hypopharyngo-laryngeal cancer

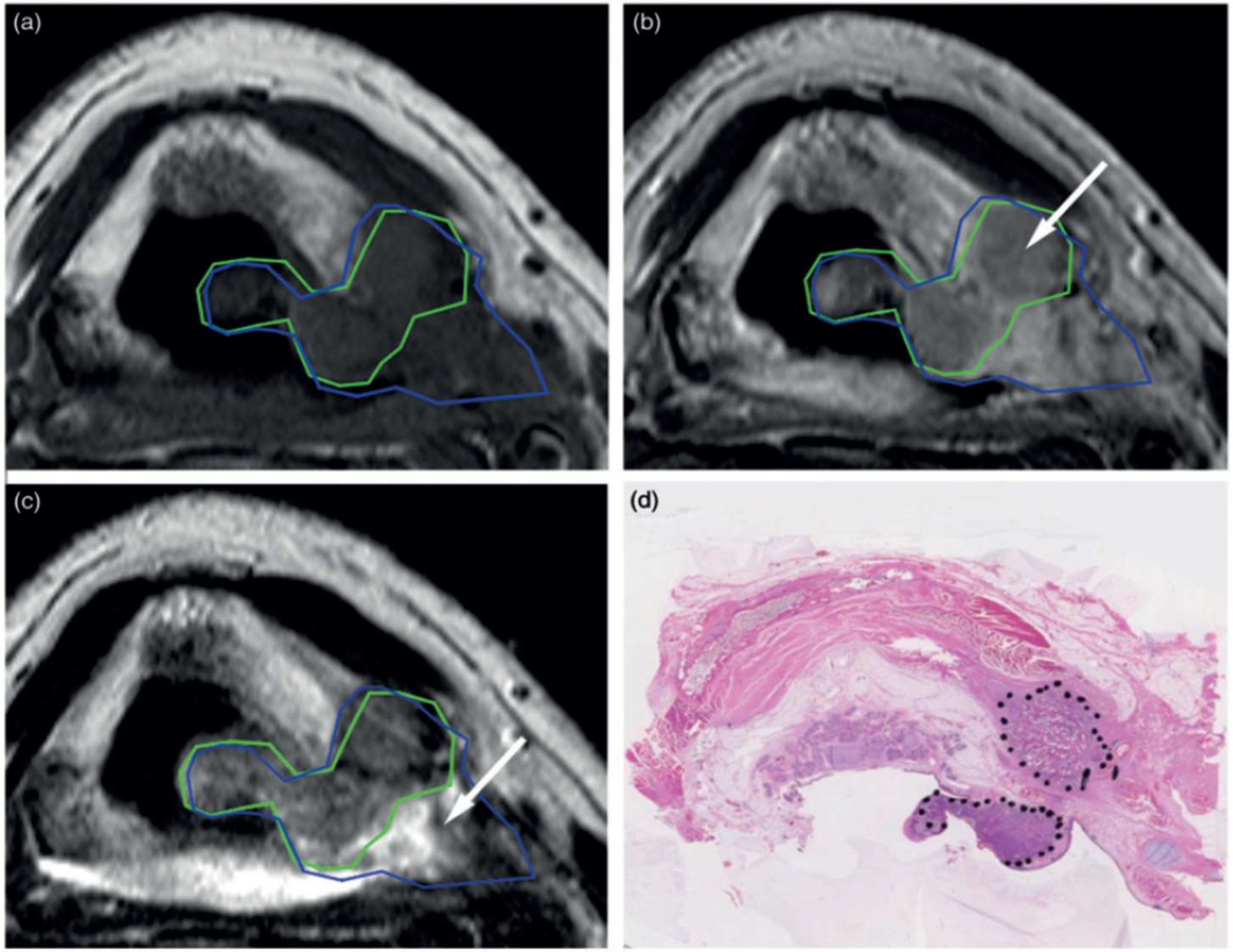

Jager E. et al. Acta Oncol 2016.

MR sequences for RT target delineation

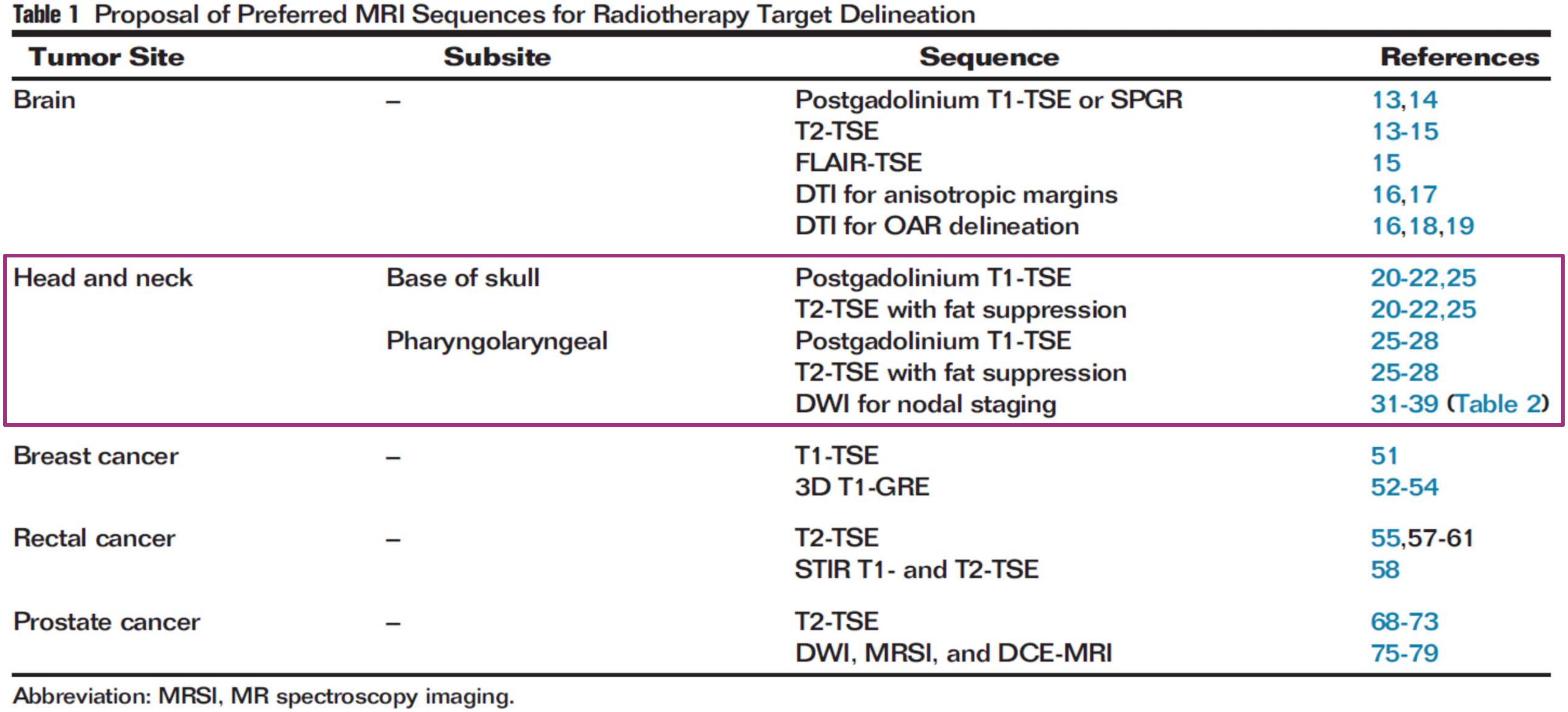

Table 1 Proposal of Preferred MRI Sequences for Radiotherapy Target Delineation

Tumor Site	Subsite	Sequence	References
Brain	–	Postgadolinium T1-TSE or SPGR	13,14
		T2-TSE	13-15
		FLAIR-TSE	15
		DTI for anisotropic margins	16,17
		DTI for OAR delineation	16,18,19
Head and neck	Base of skull	Postgadolinium T1-TSE	20-22,25
		T2-TSE with fat suppression	20-22,25
	Pharyngolaryngeal	Postgadolinium T1-TSE	25-28
		T2-TSE with fat suppression	25-28
		DWI for nodal staging	31-39 (Table 2)
Breast cancer	–	T1-TSE	51
		3D T1-GRE	52-54
Rectal cancer	–	T2-TSE	55,57-61
		STIR T1- and T2-TSE	58
Prostate cancer	–	T2-TSE	68-73
		DWI, MRSI, and DCE-MRI	75-79

Abbreviation: MRSI, MR spectroscopy imaging.

Dirix P. et al. Semin Radiat Oncol 2014.

PET/MRI for hypopharyngo-laryngeal cancer

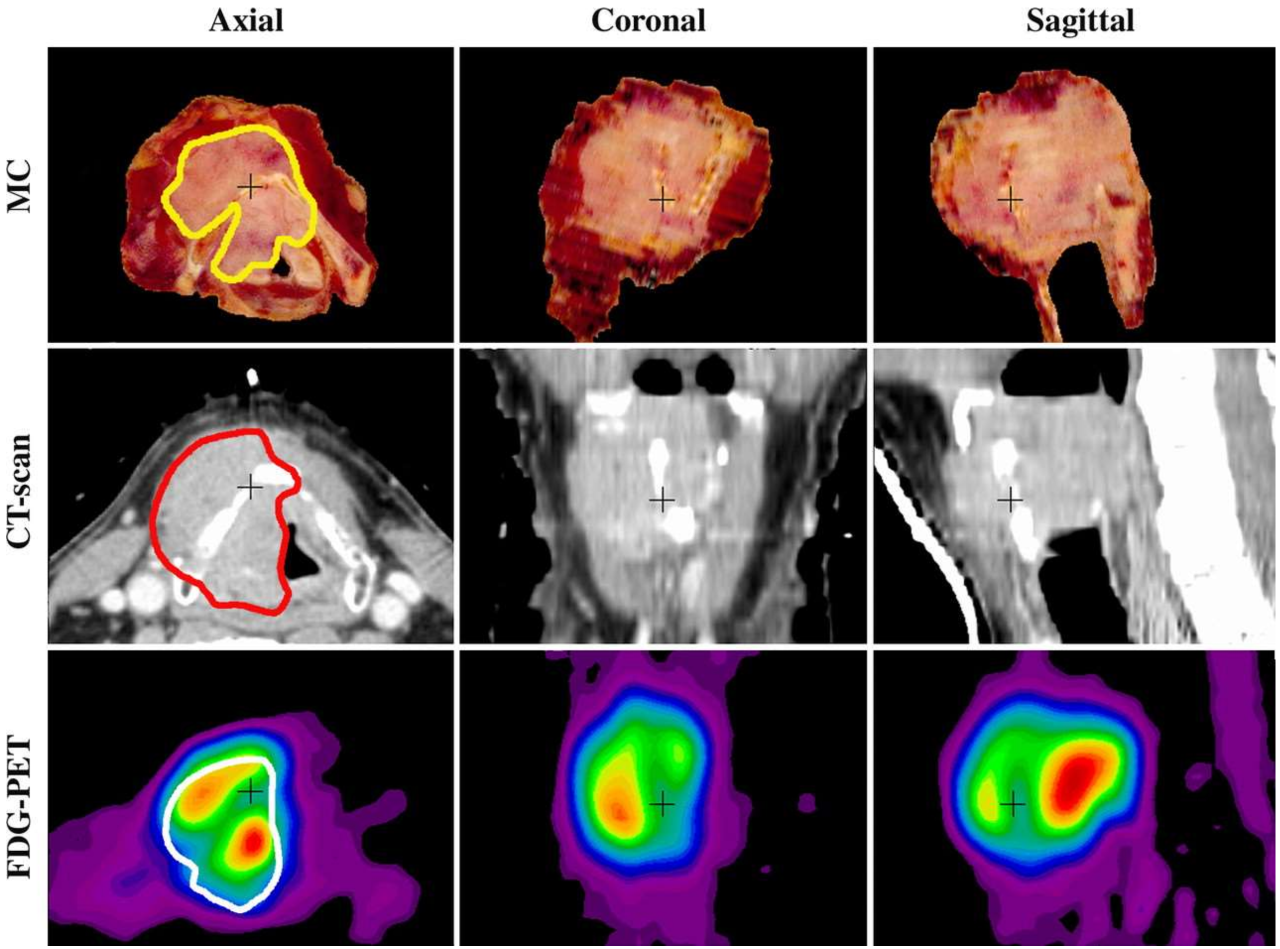
Axial
Coronal
Sagittal
MC
CT-scan
FDG-PET

- In 9 laryngectomy patients: PET was most accurate modality.
- However, no modality depicted superficial tumor extension.

Daisne JF. et al. Radiology 2004.

Caution with FDG-PET for GTV delineation

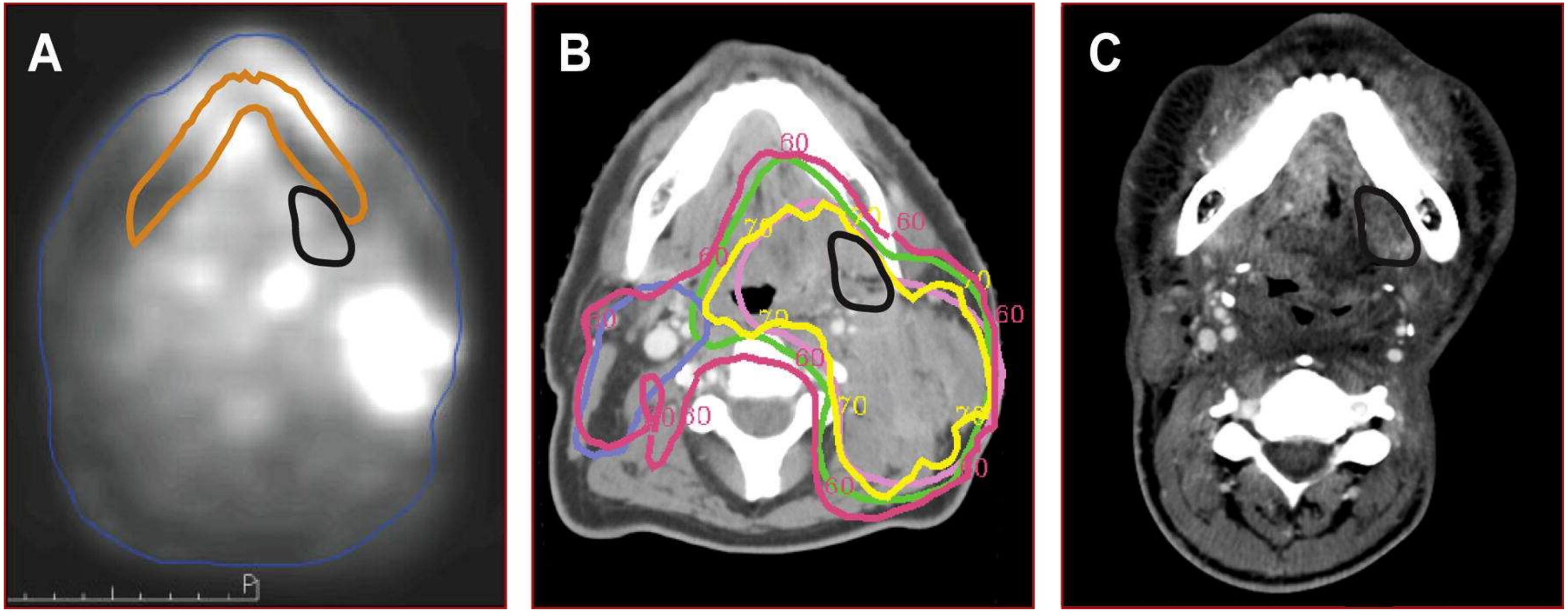

- Local in-field recurrences can occur outside the PET-GTV.
- FDG-PET is not suitable as an exclusive modality for GTV delineation.
- Inherently low spatial resolution functional imaging such as FDG-PET should not be used as a surrogate for anatomical imaging.
- Functional imaging indicates tumor biology (proliferation, hypoxia,…), rather than the exact tumor extension.

Soto D. et al. Radiother Oncol 2008.

Belgian prospective trial on PET delineation

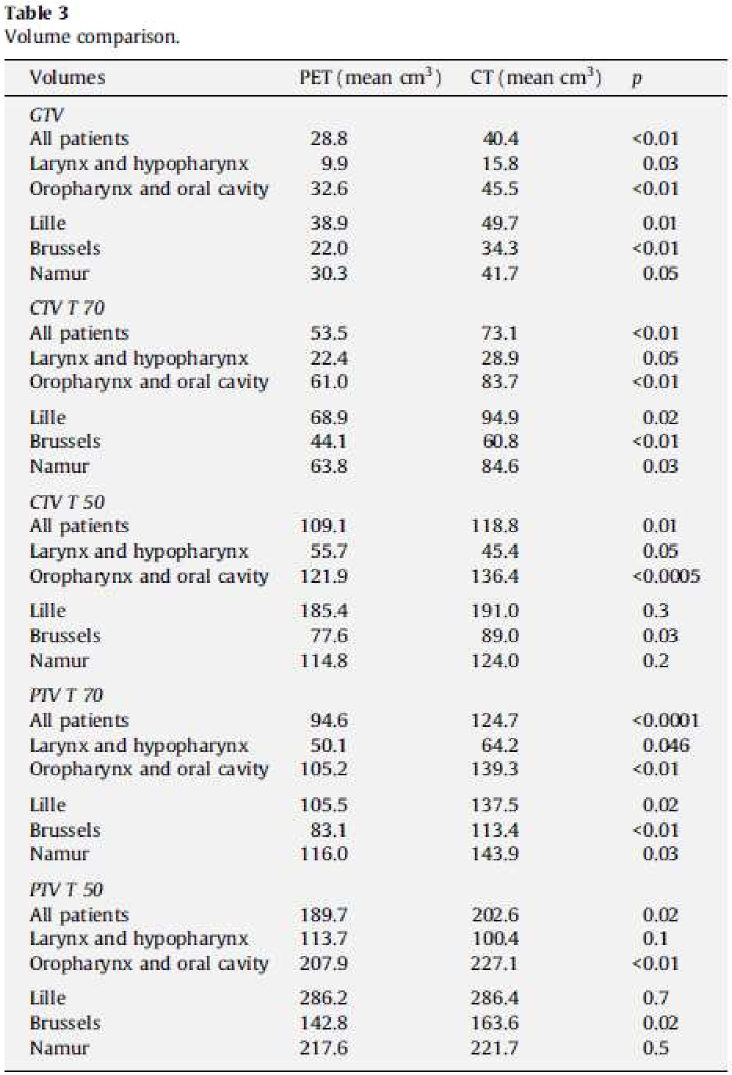

Table 3
Volume comparison.

Volumes	PET (mean cm^3)	CT (mean cm^3)	*p*
GTV			
All patients	28.8	40.4	<0.01
Larynx and hypopharynx	9.9	15.8	0.03
Oropharynx and oral cavity	32.6	45.5	<0.01
Lille	38.9	49.7	0.01
Brussels	22.0	34.3	<0.01
Namur	30.3	41.7	0.05
CTV T 70			
All patients	53.5	73.1	<0.01
Larynx and hypopharynx	22.4	28.9	0.05
Oropharynx and oral cavity	61.0	83.7	<0.01
Lille	68.9	94.9	0.02
Brussels	44.1	60.8	<0.01
Namur	63.8	84.6	0.03
CTV T 50			
All patients	109.1	118.8	0.01
Larynx and hypopharynx	55.7	45.4	0.05
Oropharynx and oral cavity	121.9	136.4	<0.0005
Lille	185.4	191.0	0.3
Brussels	77.6	89.0	0.03
Namur	114.8	124.0	0.2
PTV T 70			
All patients	94.6	124.7	<0.0001
Larynx and hypopharynx	50.1	64.2	0.046
Oropharynx and oral cavity	105.2	139.3	<0.01
Lille	105.5	137.5	0.02
Brussels	83.1	113.4	<0.01
Namur	116.0	143.9	0.03
PTV T 50			
All patients	189.7	202.6	0.02
Larynx and hypopharynx	113.7	100.4	0.1
Oropharynx and oral cavity	207.9	227.1	<0.01
Lille	286.2	286.4	0.7
Brussels	142.8	163.6	0.02
Namur	217.6	221.7	0.5

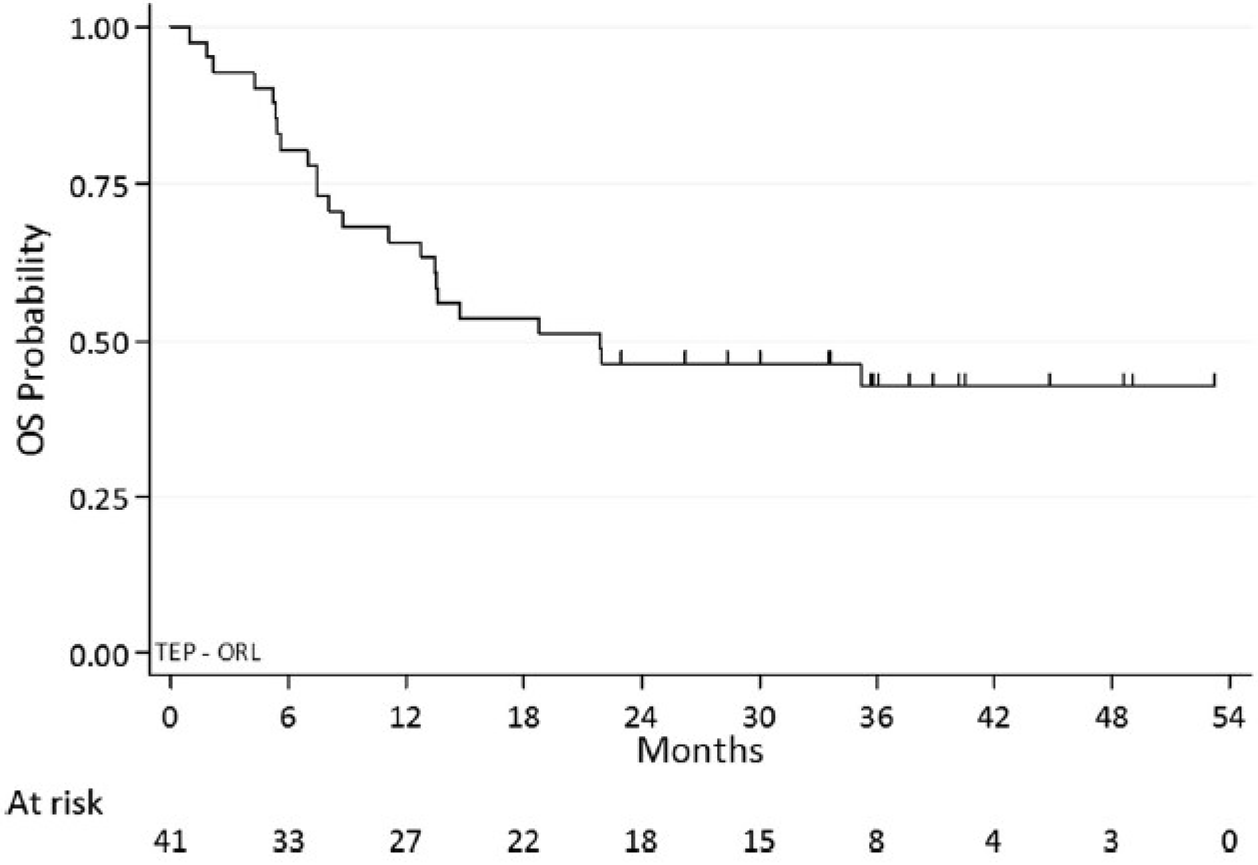

No marginal recurrences (in the CTV-CT but outside the CTV-PET) were observed.

Leclerc M. et al. Radiother Oncol 2015.

2. Highly conformal RT: LN staging is crucial

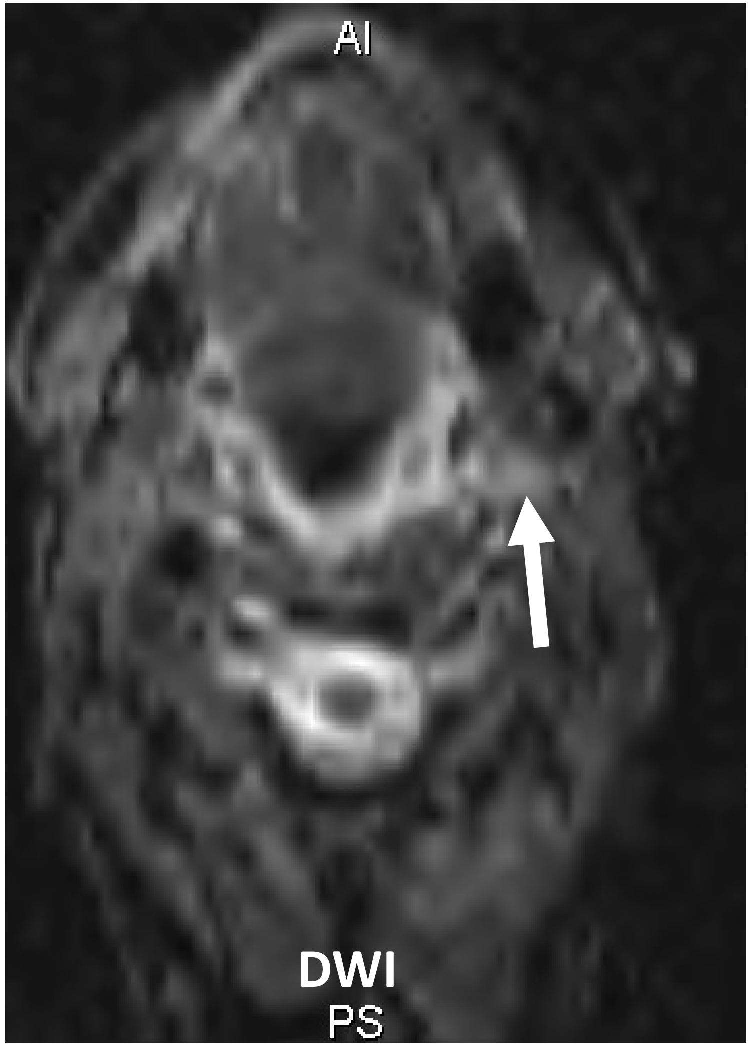

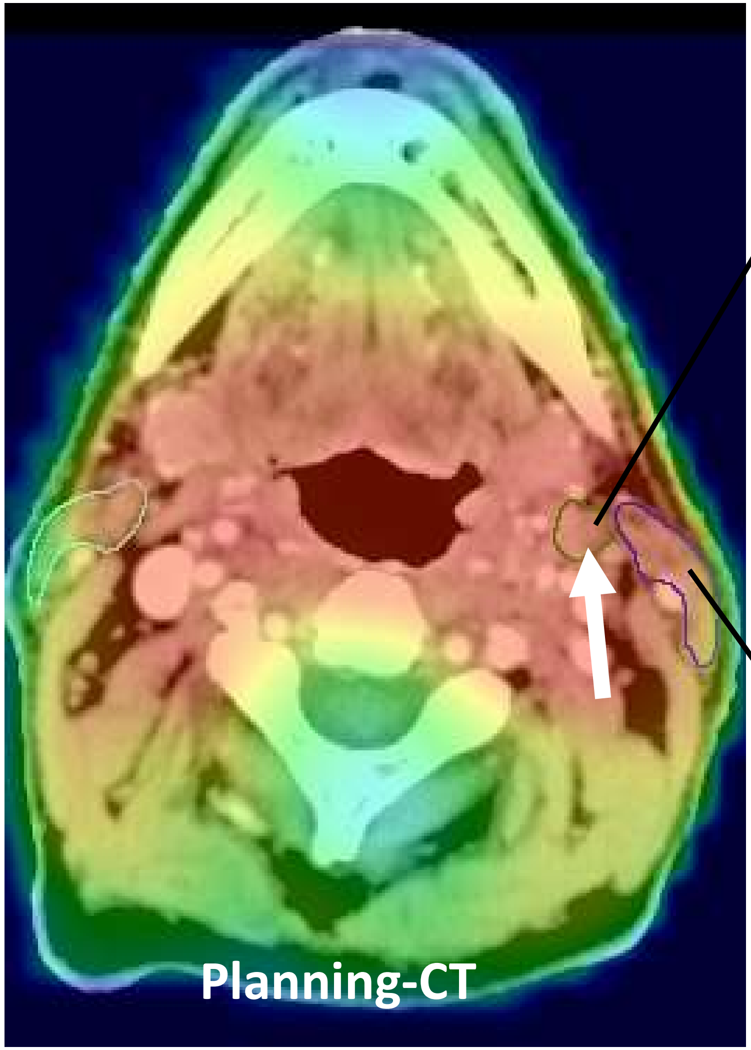
Planning-CT

avoid geographic miss & regional recurrence

optimize organ-sparing e.g. salivary glands, swallowing structures

FDG-PET/CT

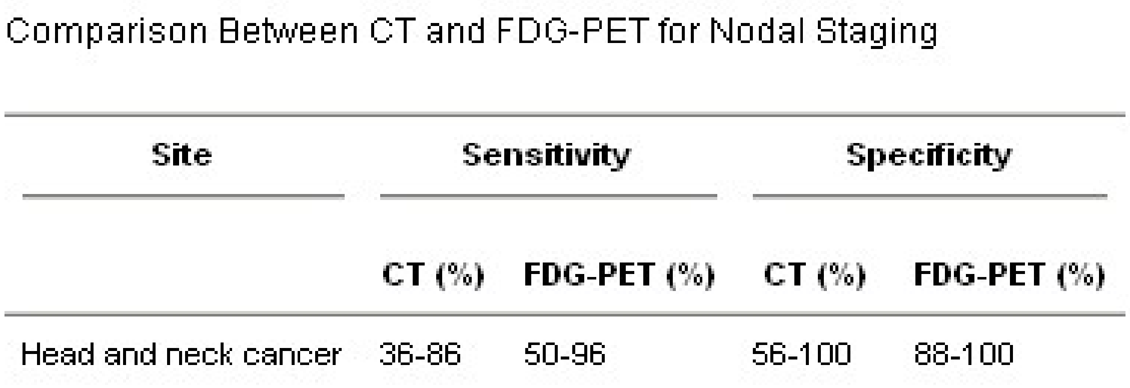

Comparison Between CT and FDG-PET for Nodal Staging

Site	Sensitivity		Specificity	
	CT (%)	FDG-PET (%)	CT (%)	FDG-PET (%)
Head and neck cancer	36-86	50-96	56-100	88-100

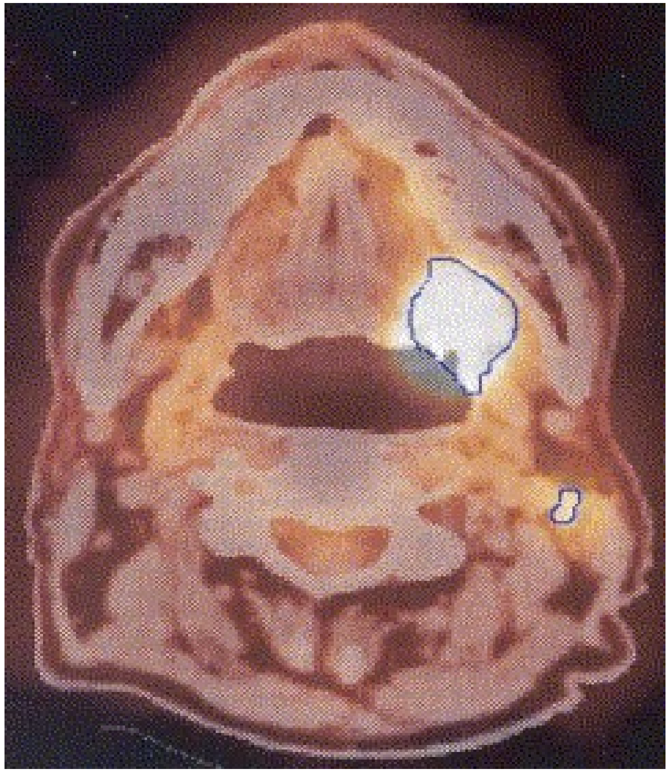

Sensitivity: FN because limited spatial resolution (0.5 cm)

Specificity: FP due to inflammation

Very promising, especially PET/CT, but not yet standard.

Grégoire V. et al. Semin Radiat Oncol 2006.

Materials and Methods

- 33 patients with advanced HNSCC planned for surgery with neck dissection:

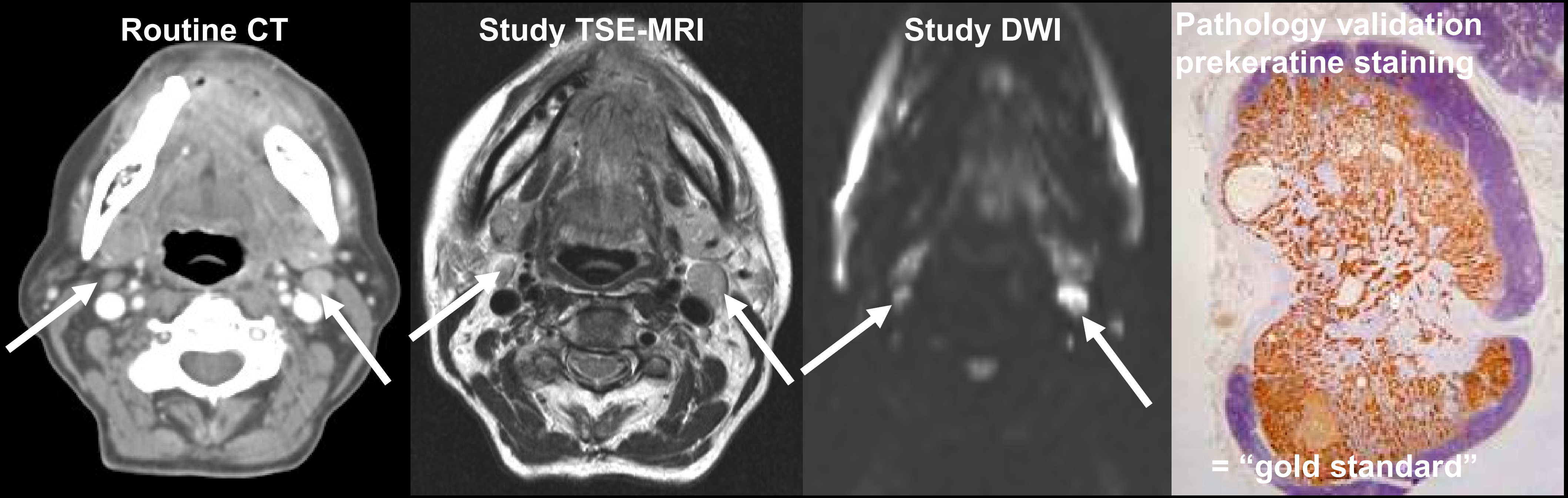

Routine CT

Study TSE-MRI

Study DWI

Pathology validation prekeratine staining

= “gold standard”

- Radiotherapy planning study:

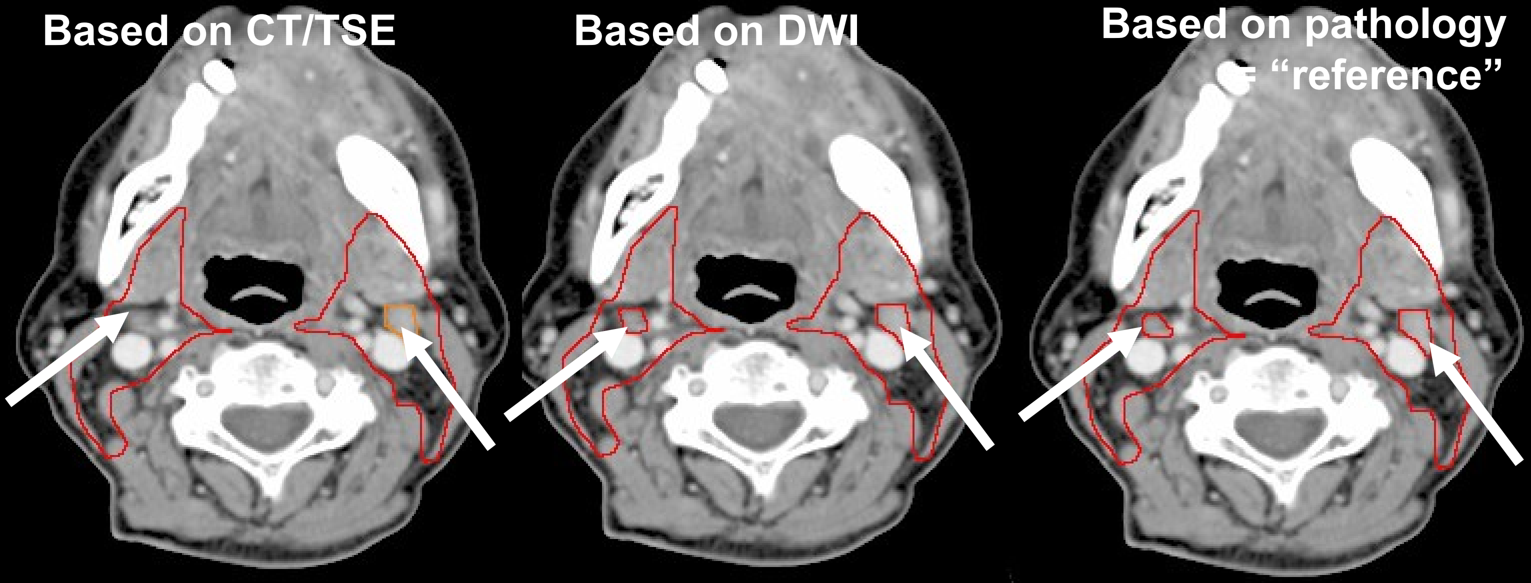

Based on CT/TSE

Based on DWI

Based on pathology = “reference”

Results (1)

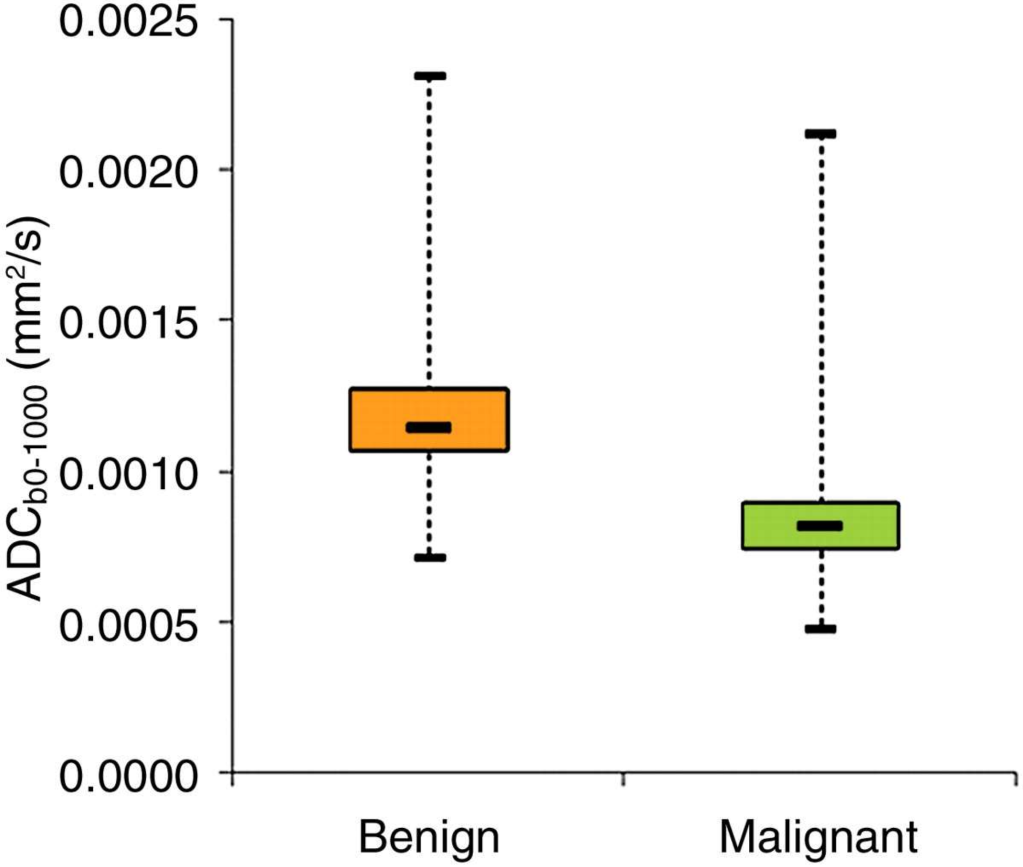

198 LN could be evaluated:

153 benign LN:
ADC = 0.00119 ± 0.00022 mm^2/sec

45 malignant LN:
ADC = 0.00085 ± 0.00027 mm^2/sec

$p < 0.0001$

Cut-off ADC value: 0.00094 mm^2/sec

Vandecaveye V. et al. Radiology 2009.

Results (2)

Nodal staging agreement between imaging results & pathology findings			
Modality	**Kappa**	**95% CI**	**McNemar's test**
CT/TSE	**0.56**	**0.16 - 0.96**	**P = 0.019**
DWI	**0.97**	**0.84 - 1.00**	

Sensitivity of 89% & specificity of 97% per LN.

DWI allows the radiation oncologist to very closely approach the true nodal target volume:

- **Dose-escalation (~ PPV of 91%)?**
- **Organ-sparing (~ NPV of 97%)?**

Preliminary results, require confirmation in a larger group…

Dirix P. et al. Int J Radiat Oncol Biol Phys 2010.

Clinical example of DWI for LN staging

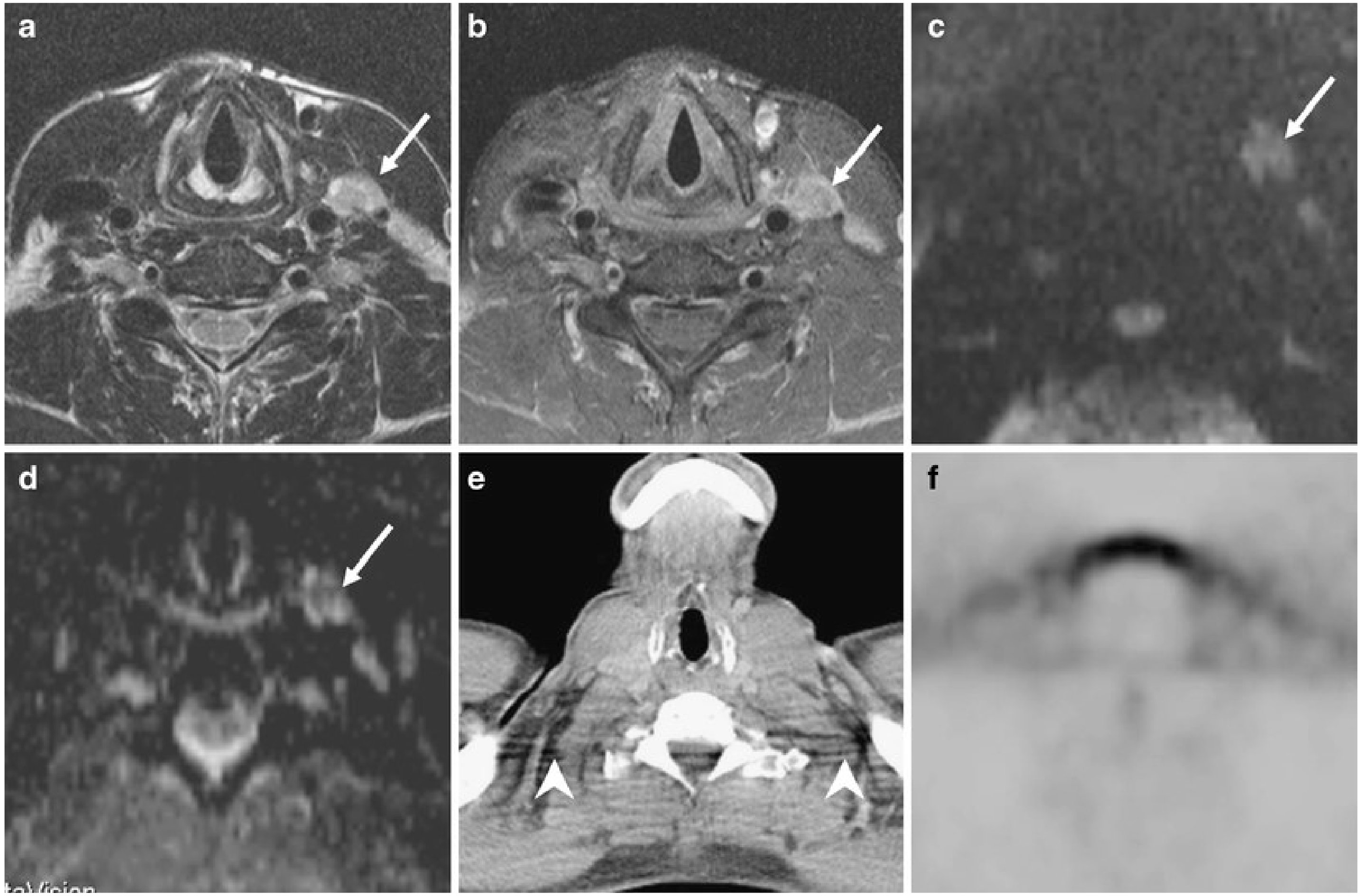

Images courtesy of Dr. V. Vandecaveye.

Similar results at Maastricht University

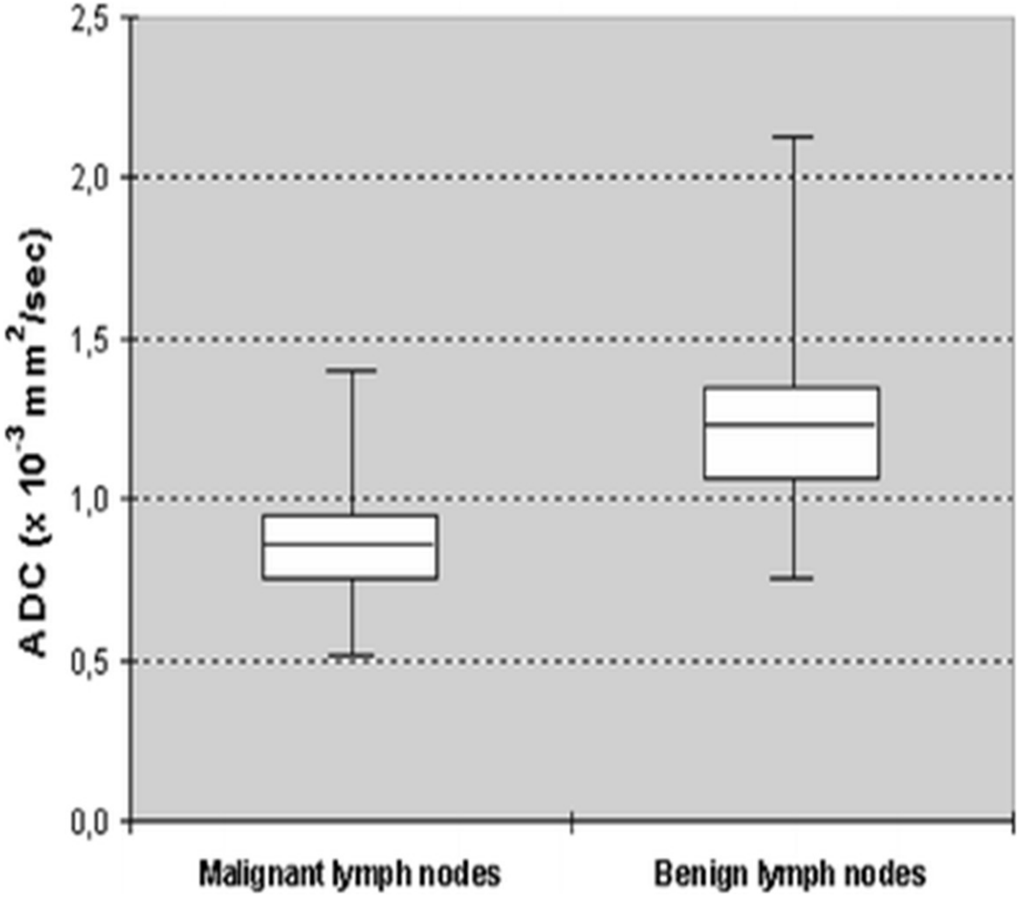

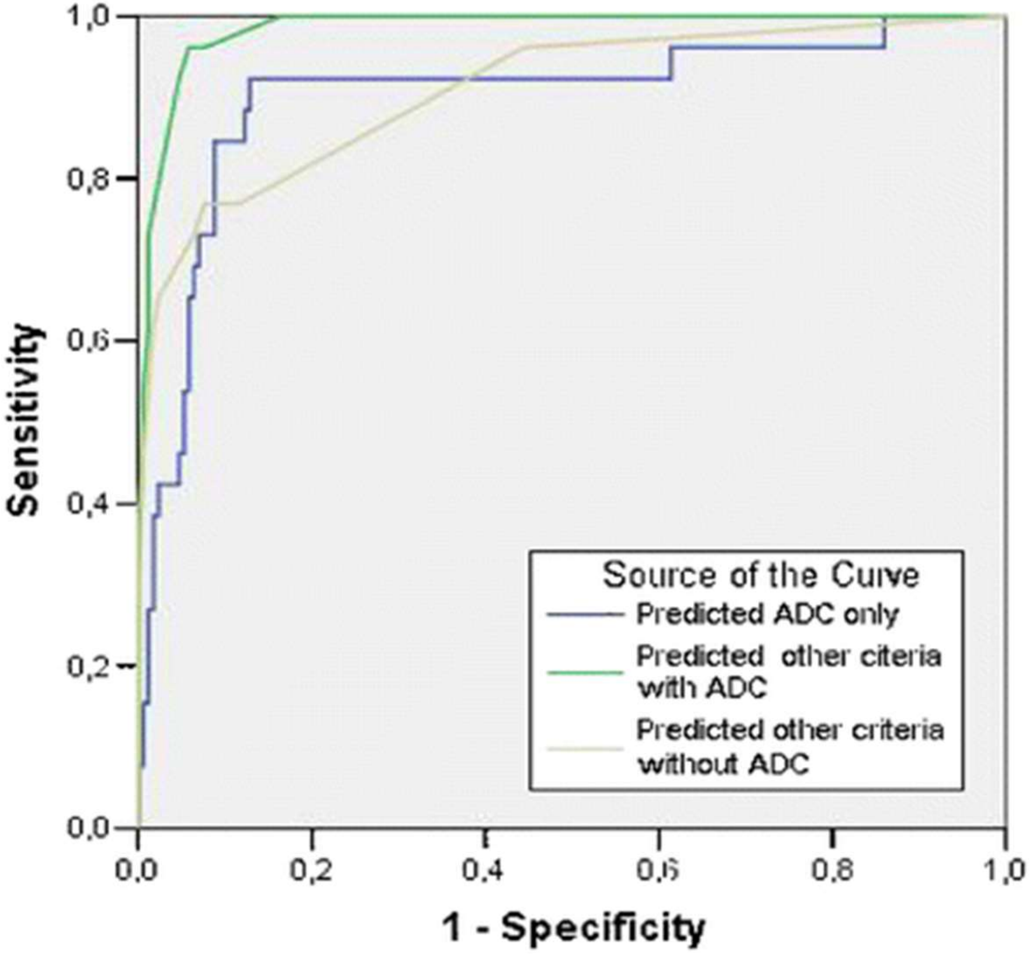

ADC cut-off: 0.0001 mm^2/sec: sensitivity 92% and specificity 84%

de Bondt R.B.J. et al. Neuroradiology 2009.

All reported results for ADC-based nodal staging

Study	Lesion size (cm)	Mean ADC N+ (x 10^{-3} mm^2/sec)	Mean ADC N- (x 10^{-3} mm^2/sec)	p-value	Threshold (x 10^{-3} mm^2/sec)	Sens (%)	Spec (%)
Wang et al. *Radiology 2001*	> 1.0	1.13 ± 0.43	1.56 ± 0.51	0.002	1.22	84	91
Sumi et al. *J Neuroradiol 2003*	> 1.0	0.41 ± 0.11	0.30 ± 0.06	< 0.01	0.4	52	97
Abdel Razek et al. *Eur Radiol 2006*	0.9 – 1.5	1.09 ± 0.11	1.64 ± 0.16	< 0.04	1.38	98	88
Sumi et al. *AJR 2006*	> 1.0	1.17 ± 0.45	0.63 ± 0.10	< 0.001	0.74	86	94
Vandecaveye et al. *Radiology 2009*	0.4 – 1.5	0.85 ± 0.27	1.19 ± 0.22	< 0.0001	0.94	84	94
de Bondt et al. *Neuroradiology 2009*	0.5 – 3.0	0.85 ± 0.19	1.2 ± 0.24	< 0.05	1.0	92	84
Holzapfel et al. *Eur J Radiol 2009*	> 1.0	0.78 ± 0.09	1.24 ± 0.16	< 0.05	1.02	100	87
Perrone et al. *Eur J Radiol 2011*	NA	0.85	1.45	< 0.01	1.03	100	93

Lambrecht M. et al. Expert Rev Anticancer Ther 2010.

Towards dose de-escalation on the elective neck?

200 patients included

Arm A
(NID2Gy 40 Gy)
96 patiens *

Arm B
(NID2Gy 50 Gy)
97 patients *

Study Arm

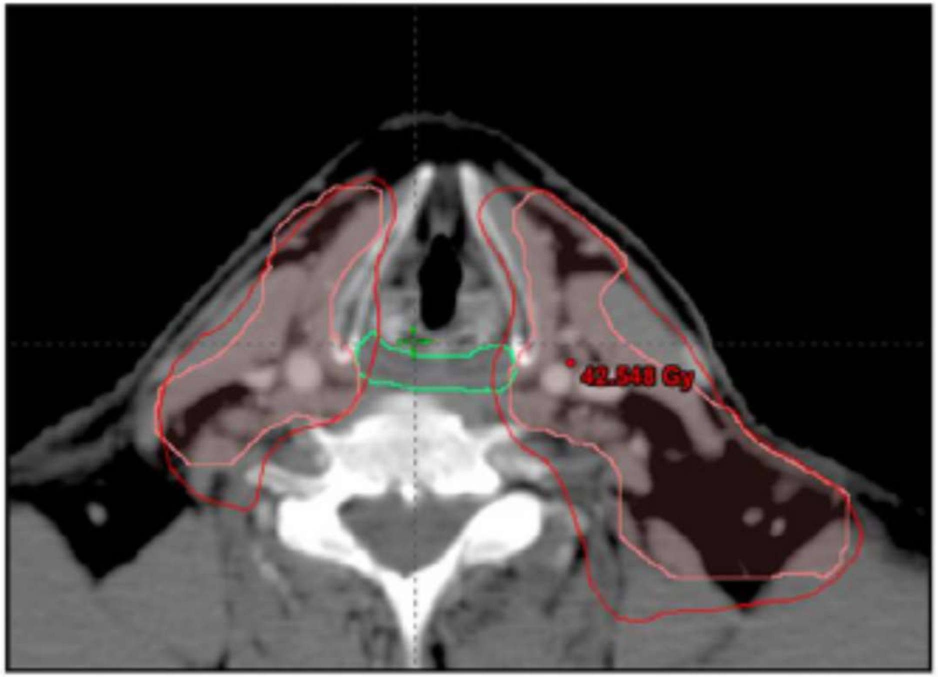

Control Arm

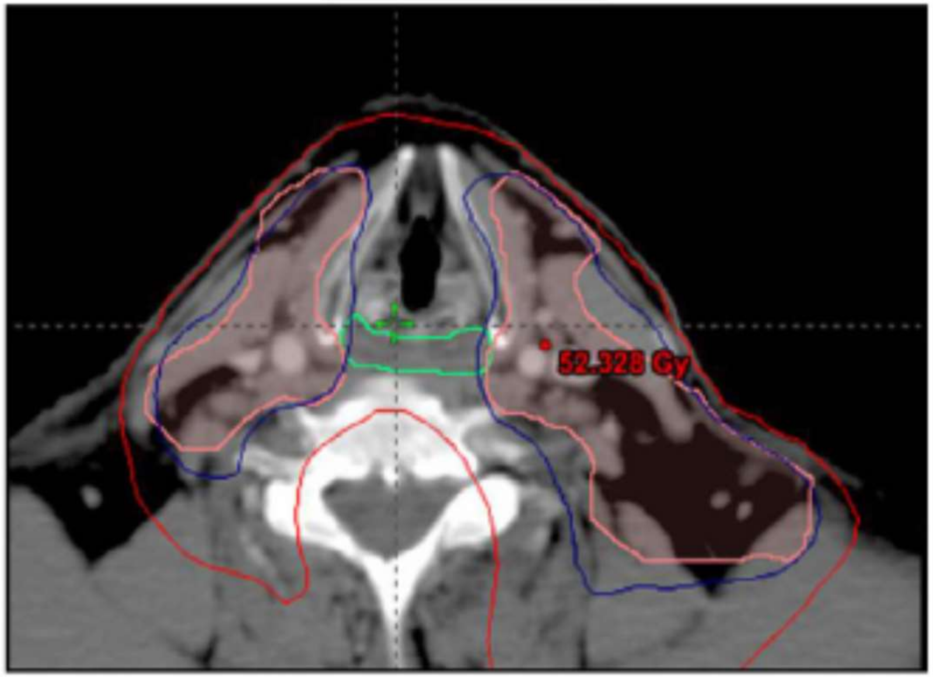

Microscopic tumor burden is probably low in cN0 neck on FDG-PET & DWI, and could be sterilized with lower doses than used to be necessary when only CT was used.

Nuyts S. et al. Radiother Oncol 2013.

Significantly less acute dysphagia

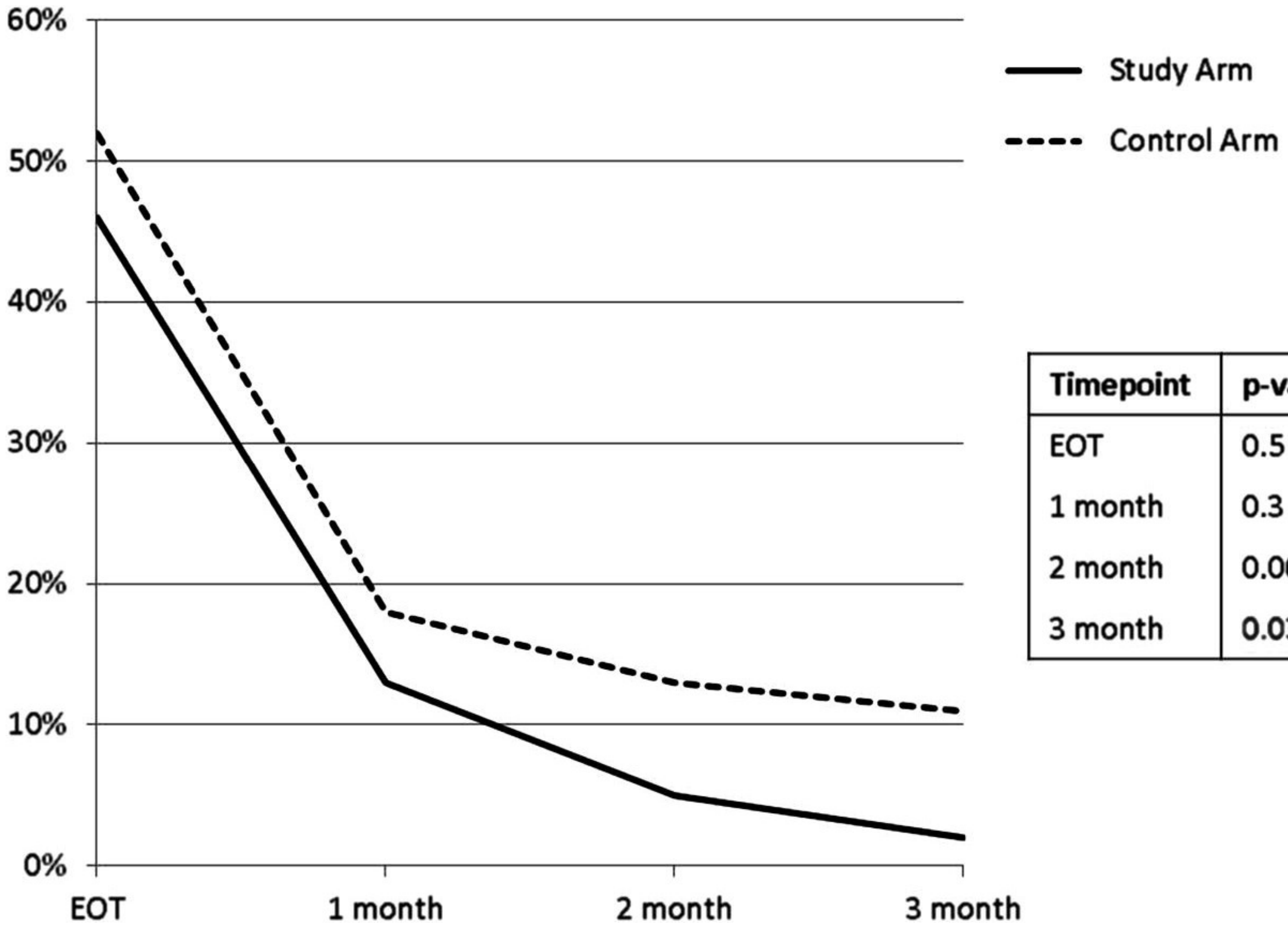

Timepoint	p-value
EOT	0.5
1 month	0.3
2 month	0.06
3 month	0.03

Nuyts S. et al. Radiother Oncol 2013.

Regional recurrences

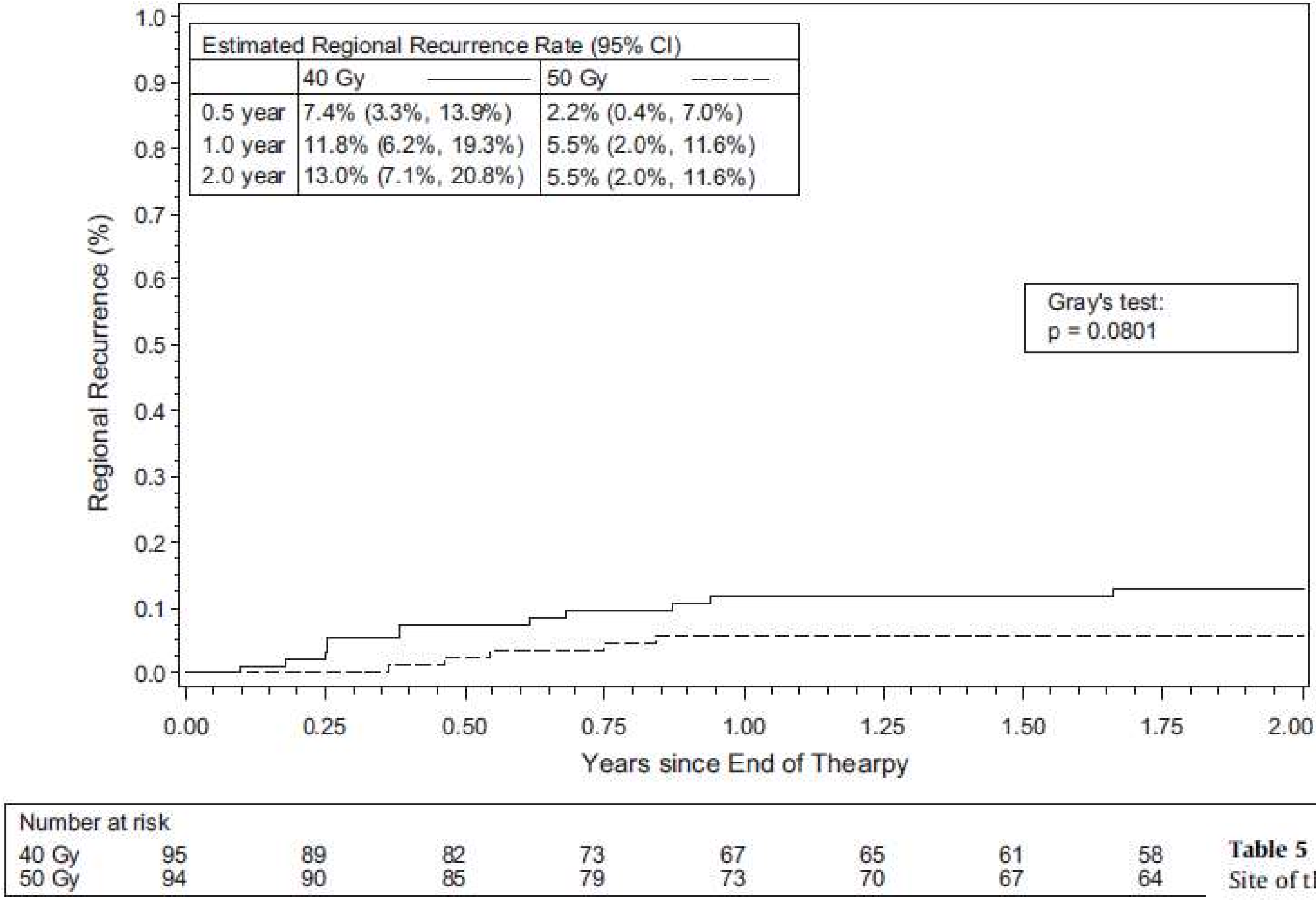

Estimated Regional Recurrence Rate (95% CI)		
	40 Gy ———	50 Gy – – – –
0.5 year	7.4% (3.3%, 13.9%)	2.2% (0.4%, 7.0%)
1.0 year	11.8% (6.2%, 19.3%)	5.5% (2.0%, 11.6%)
2.0 year	13.0% (7.1%, 20.8%)	5.5% (2.0%, 11.6%)

Number at risk								
40 Gy	95	89	82	73	67	65	61	58
50 Gy	94	90	85	79	73	70	67	64

Table 5
Site of the regional recurrences.

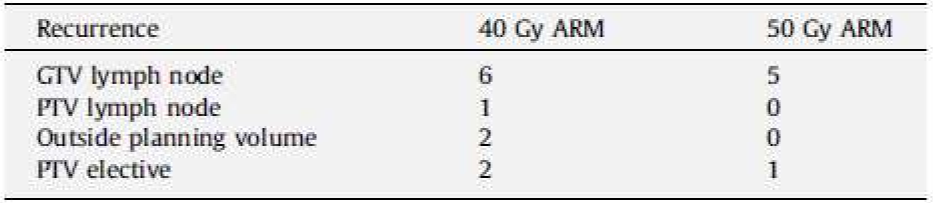

Recurrence	40 Gy ARM	50 Gy ARM
GTV lymph node	6	5
PTV lymph node	1	0
Outside planning volume	2	0
PTV elective	2	1

Nevens D. et al. Radiother Oncol 2016.

3. RT is no longer a “black box”

Fractionated RT

Simulation

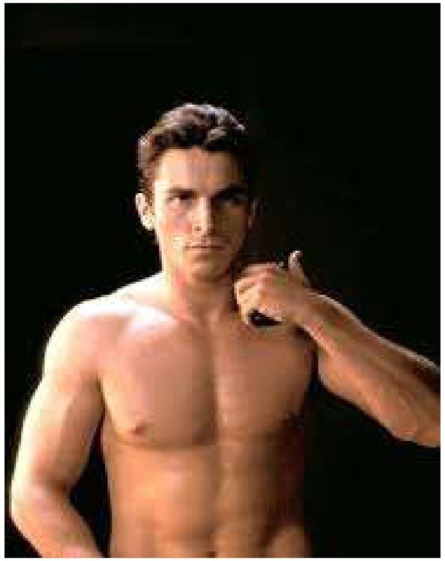

Patient in

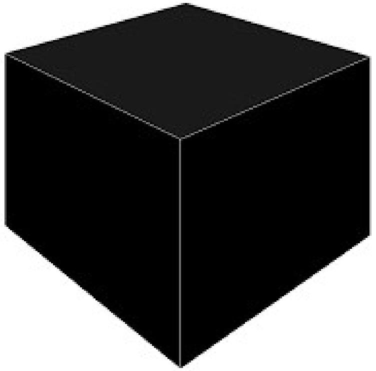

Patient out

Follow-up

Assuming:
- Identical anatomy
- No tumor changes

FDG-PET for early response assessment

FDG-PET at 8 weeks after RT

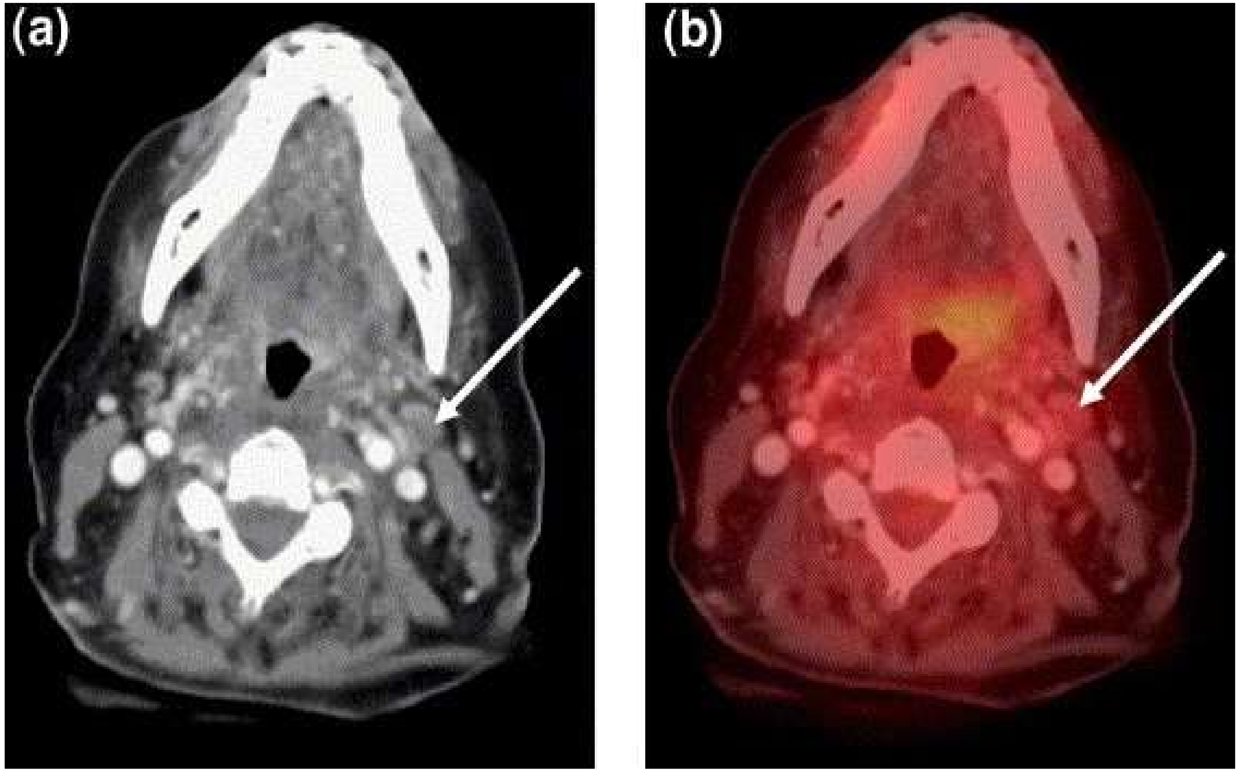

	FDG-PET/CT	CT
Sensitivity (%)	76.9	92.3
Specificity (%)[*]	93.3	46.7
Positive predictive value (%)[†]	90.9	60
Negative predictive value (%)	82.4	87.5
Accuracy (%)	85.7	67.9

Promising, applicability mainly limited by the number of false negatives.

Andrade R. et al. Int J Radiat Oncol Biol Phys 2006.

DWI as a response biomarker (1)

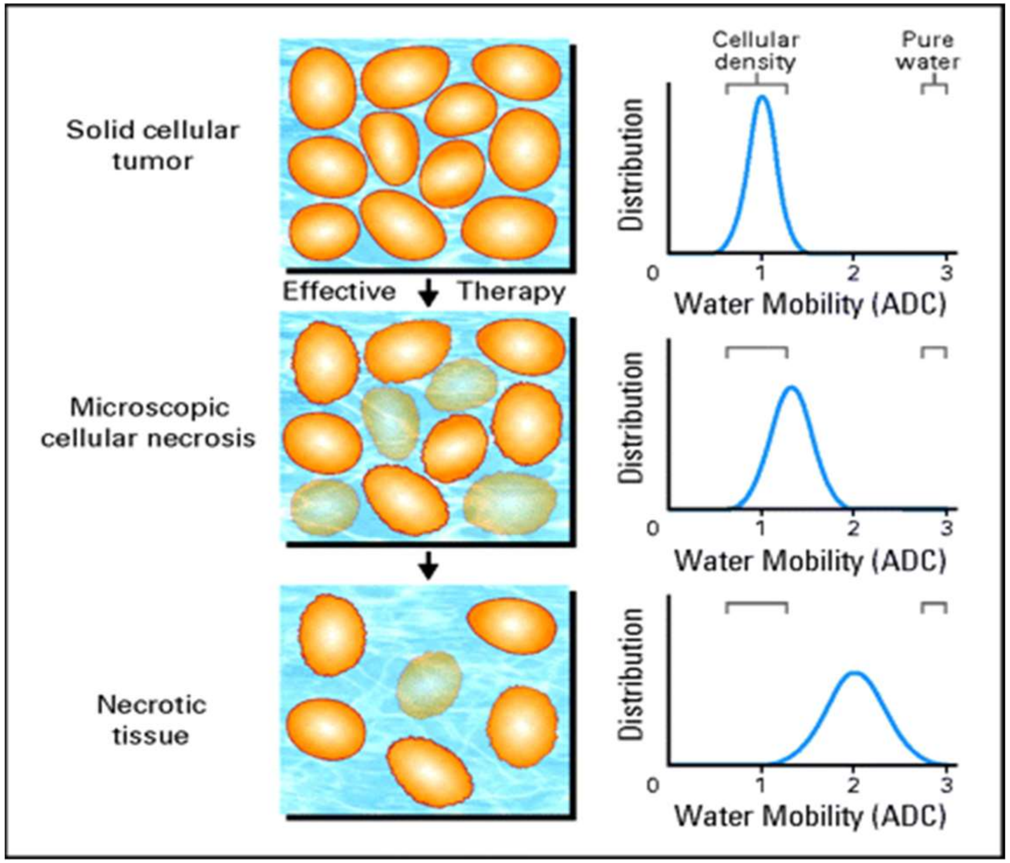
Solid cellular tumor
Effective Therapy
Microscopic cellular necrosis
Necrotic tissue
Cellular density
Pure water
Distribution
0
1
2
3
Water Mobility (ADC)

Hamstra D.A. et al. J Clin Oncol 2007.

DWI as a response biomarker (2)

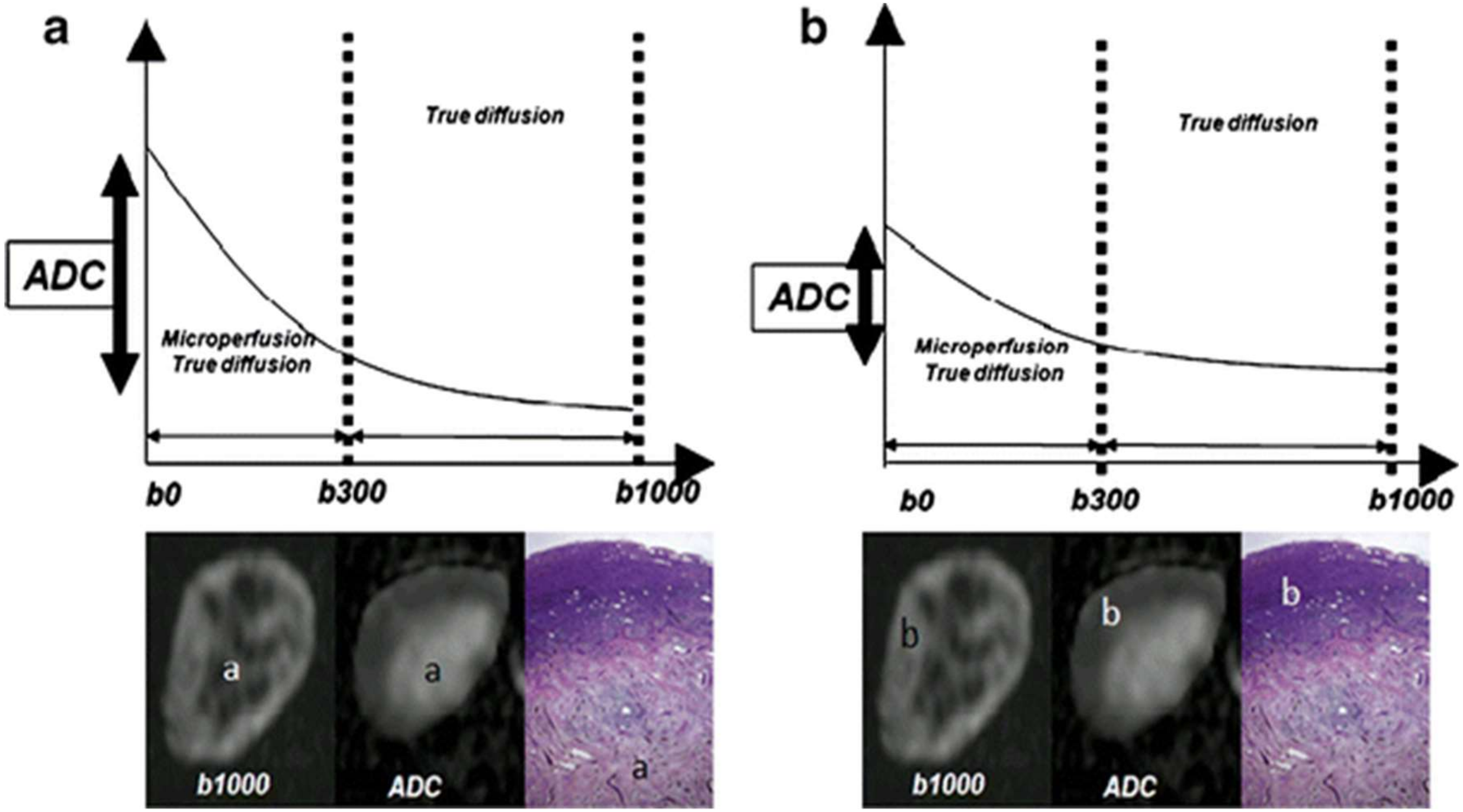
a
ADC
True diffusion
Microperfusion
True diffusion
b0
b300
b1000
a
b1000
a
ADC
a
b
ADC
True diffusion
Microperfusion
True diffusion
b0
b300
b1000
b
b1000
b
ADC
b

Vandecaveye V. et al. Neuroradiology 2010.

Materials and Methods

TSE

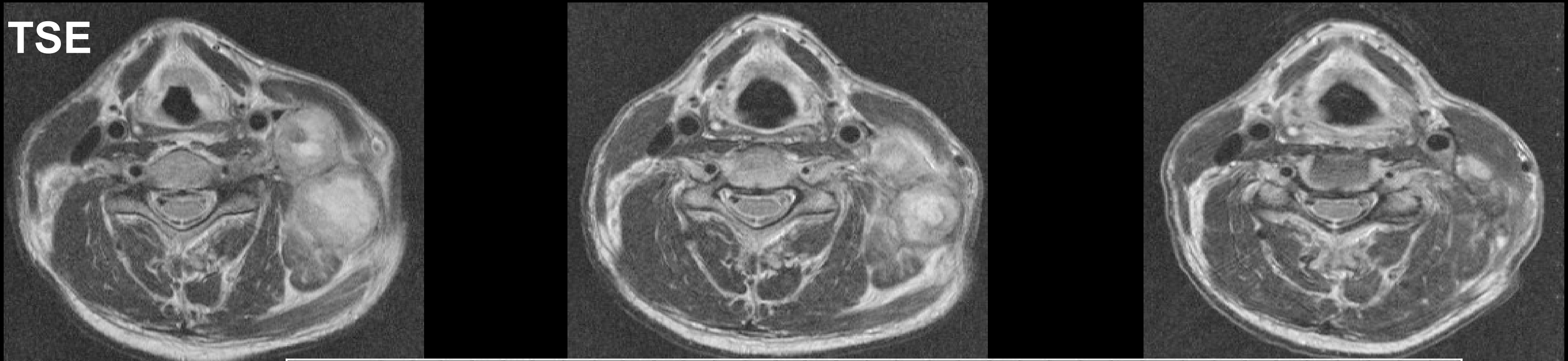

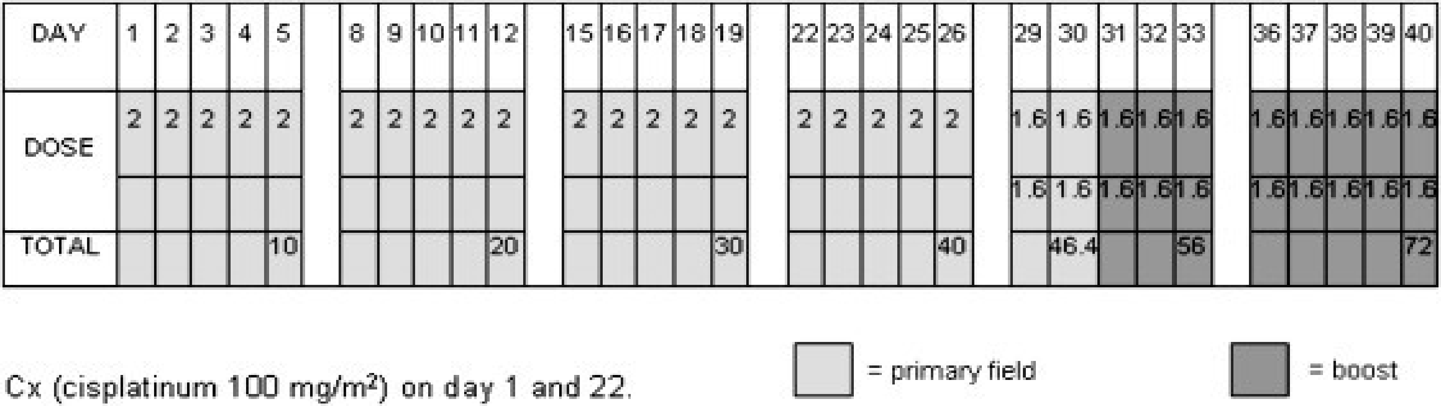

DAY	1	2	3	4	5	8	9	10	11	12	15	16	17	18	19	22	23	24	25	26	29	30	31	32	33	36	37	38	39	40
DOSE	2	2	2	2	2	2	2	2	2	2	2	2	2	2	2	2	2	2	2	2	1.6	1.6	1.6	1.6	1.6	1.6	1.6	1.6	1.6	1.6
																					1.6	1.6	1.6	1.6	1.6	1.6	1.6	1.6	1.6	1.6
TOTAL					10					20					30					40		46.4			56					72

Cx (cisplatinum 100 mg/m²) on day 1 and 22.

░ = primary field

▓ = boost

DWI

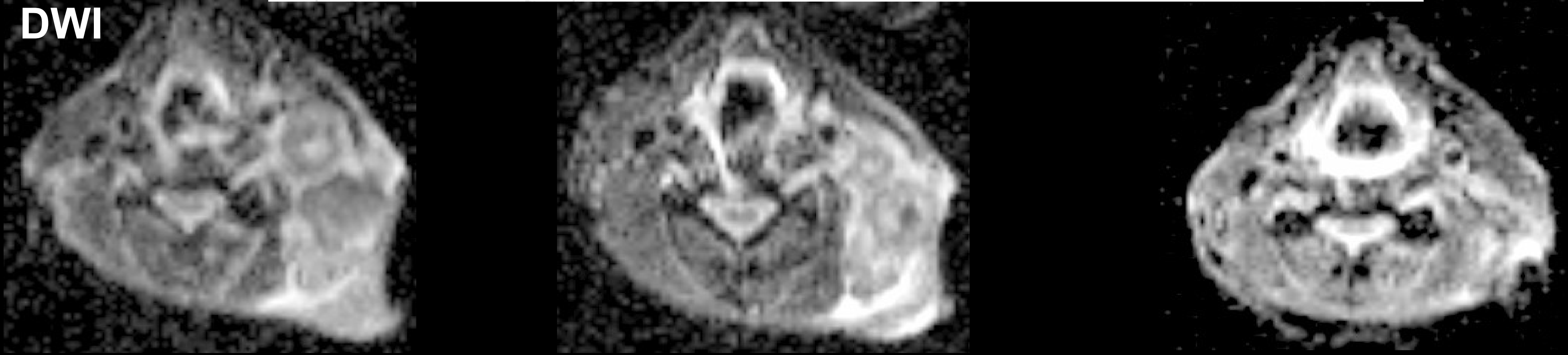

before RT

days 10 and 24

3 weeks after RT

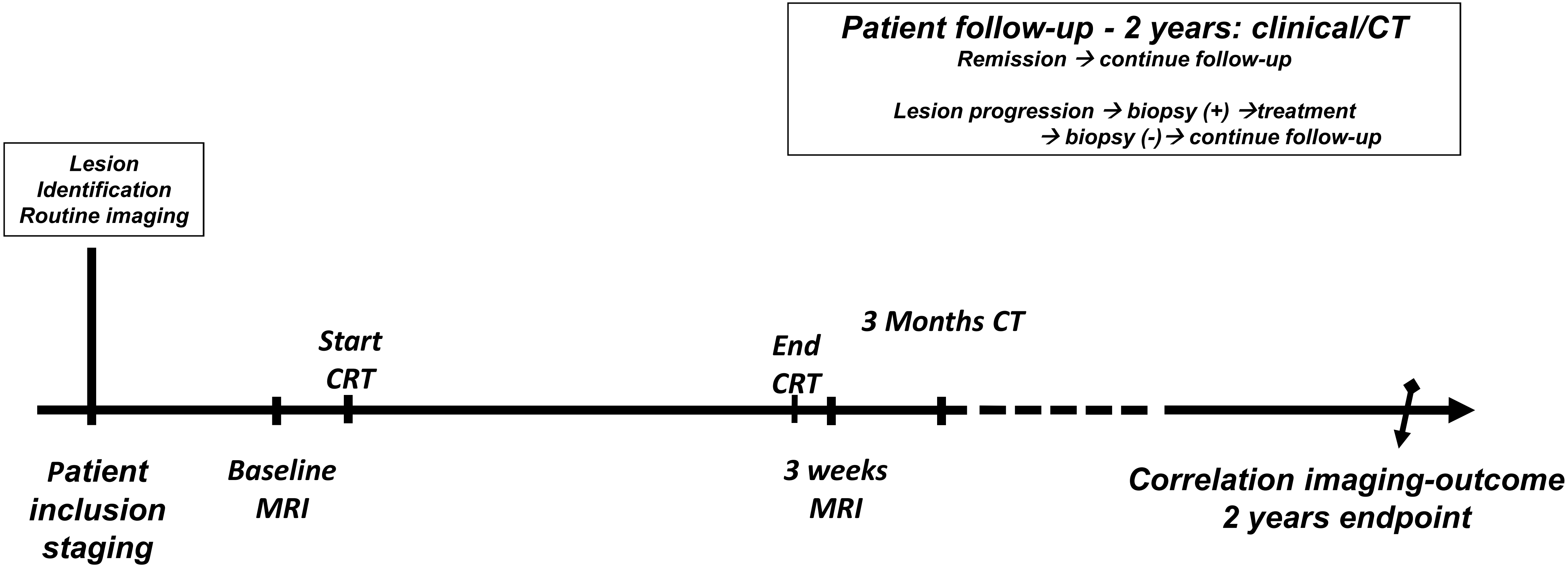

Patient follow-up - 2 years: clinical/CT

Remission → continue follow-up

Lesion progression → biopsy (+) →treatment
→ biopsy (-)→ continue follow-up

Lesion Identification Routine imaging

Patient inclusion staging

Baseline MRI

Start CRT

End CRT

3 weeks MRI

3 Months CT

Correlation imaging-outcome
2 years endpoint

Results (1): DWI during CRT

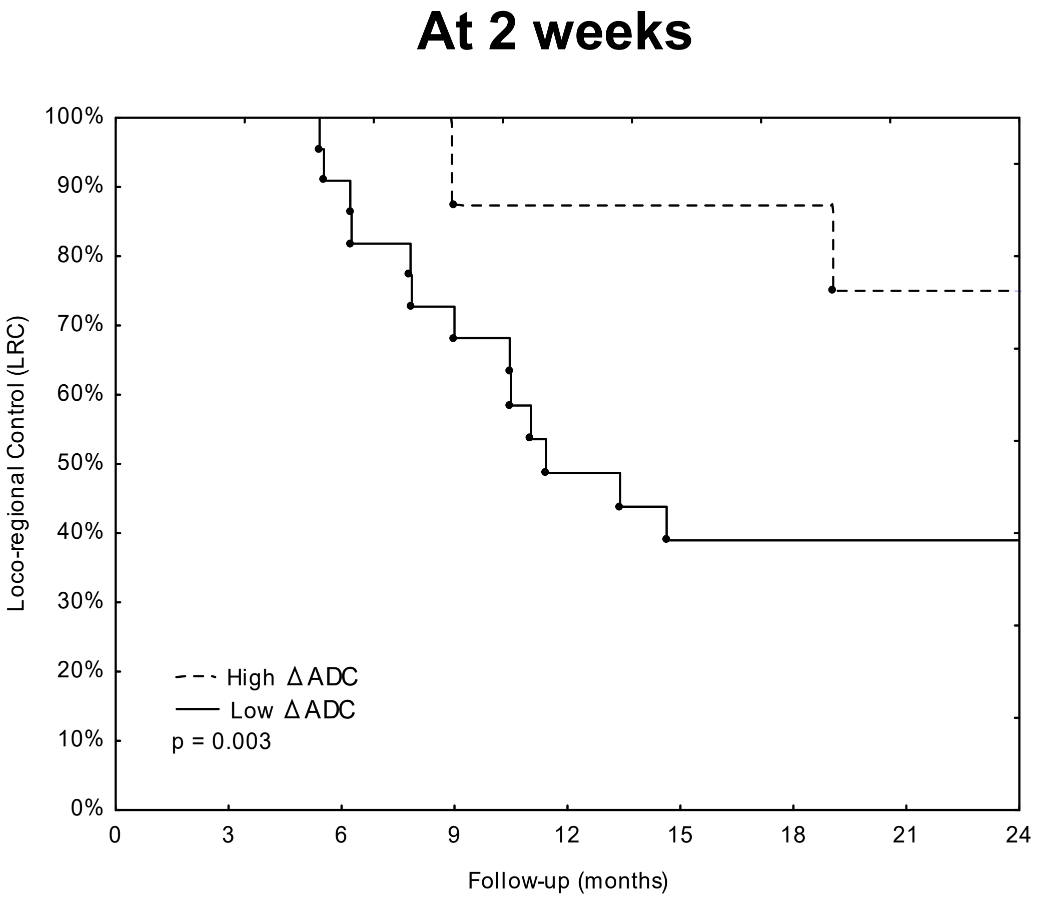

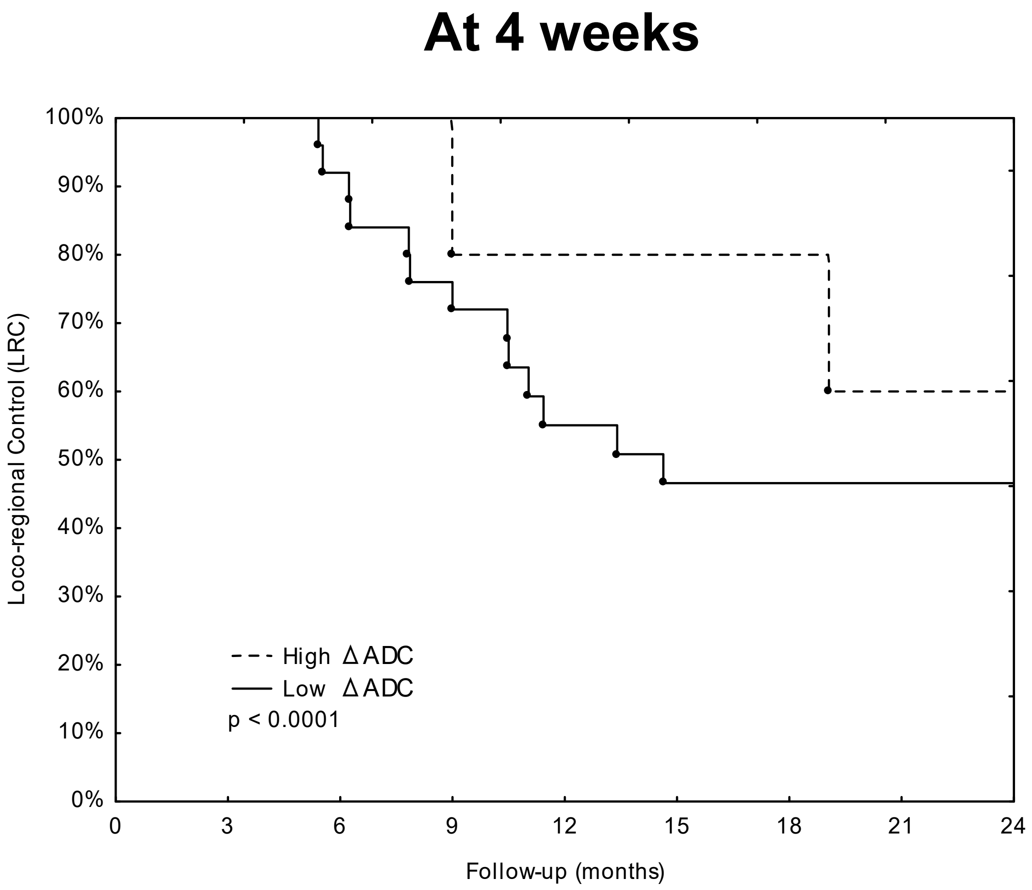

$\%\Delta ADC = (ADC\ 2w - ADC\ base) / ADC\ base$

$\%\Delta ADC = (ADC\ 4w - ADC\ base) / ADC\ base$

Dirix P. et al. J Nucl Med 2009.
Vandecaveye V. et al. Eur Radiol 2010.

Results (2): DWI at 3 weeks after CRT

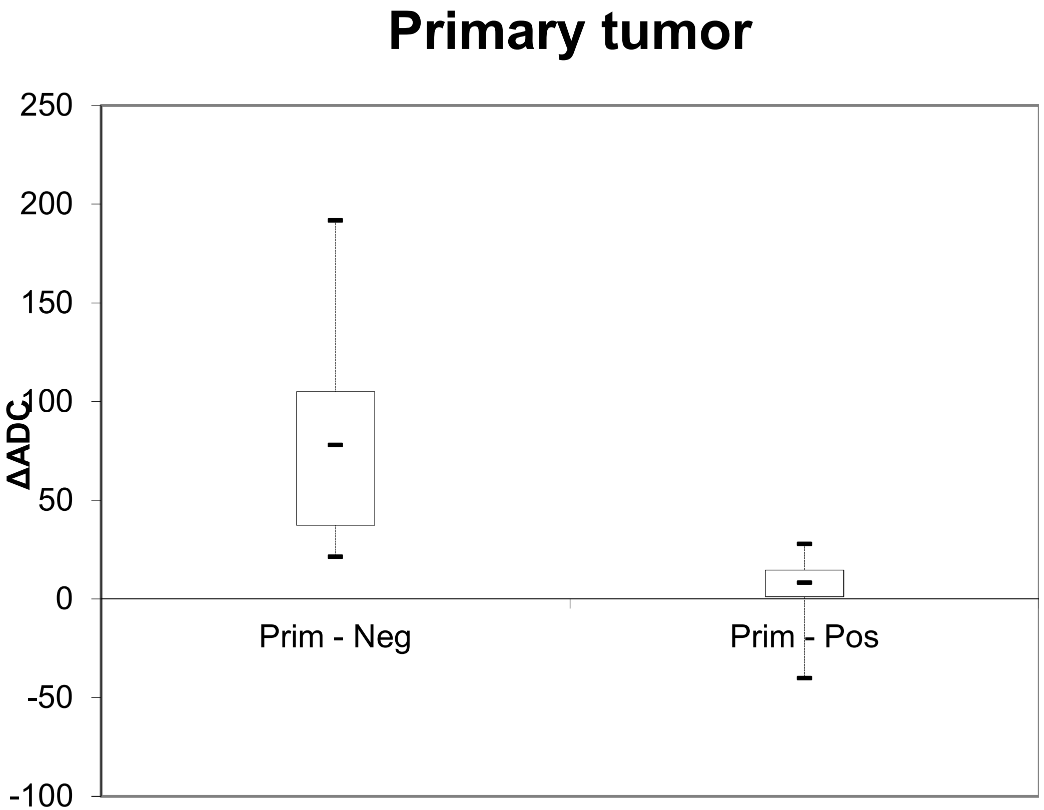

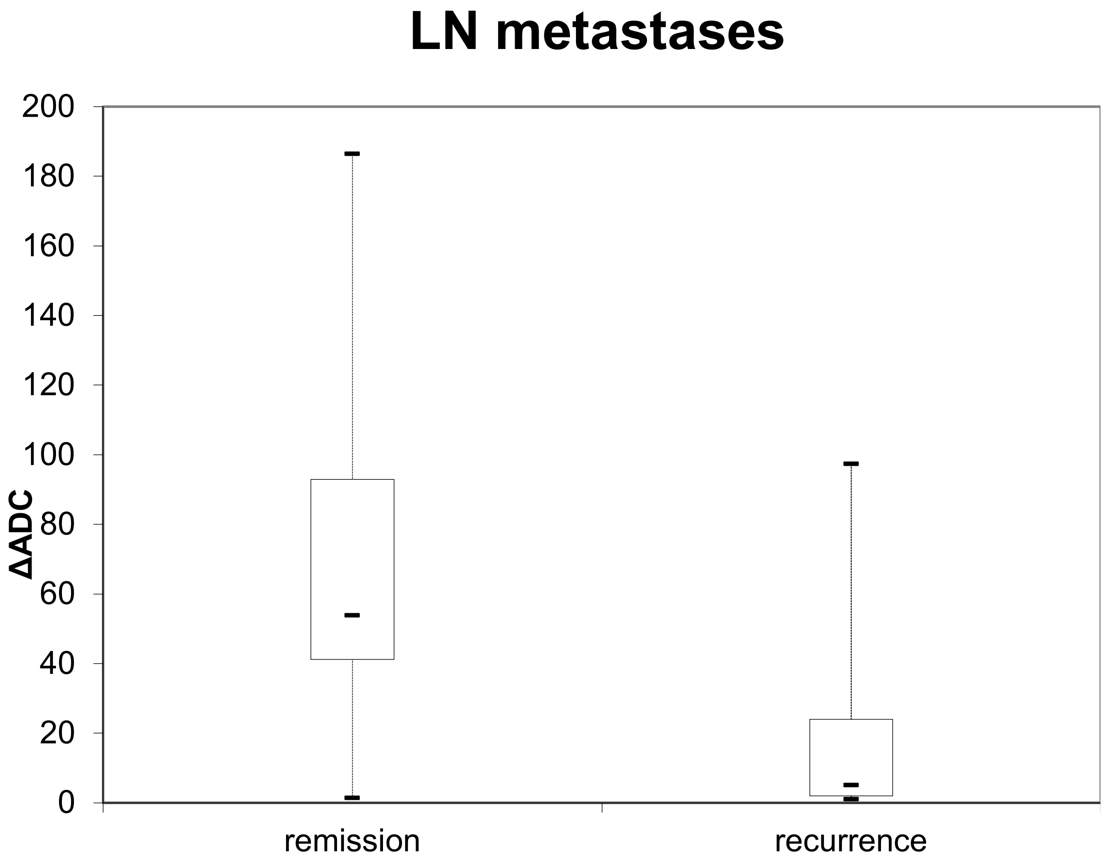

%ΔADC = (ADC 9w – ADC base) / ADC base

Vandecaveye V. et al. Int J Radiat Oncol Biol Phys 2012.

Visual representation of ∆ADC within the tumor

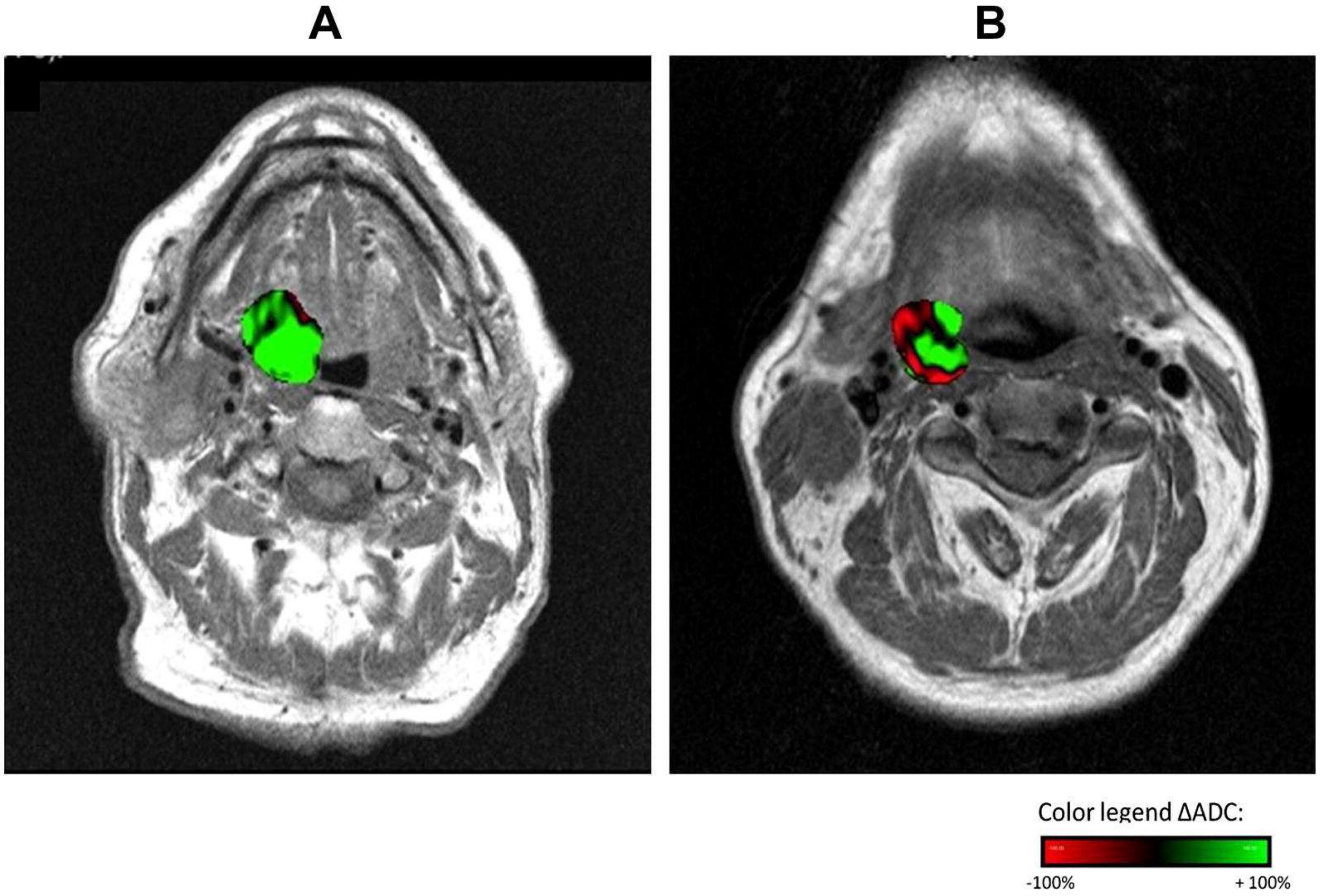
A
B
Color legend ΔADC:
-100%
+ 100%

$$\%\Delta \mathrm{ADC} = (\mathrm{ADC\ 2w} - \mathrm{ADC\ base}) / \mathrm{ADC\ base}$$

Lambrecht M. et al. Radiother Oncol 2014.

Clinical example of DWI for response assessment (1)

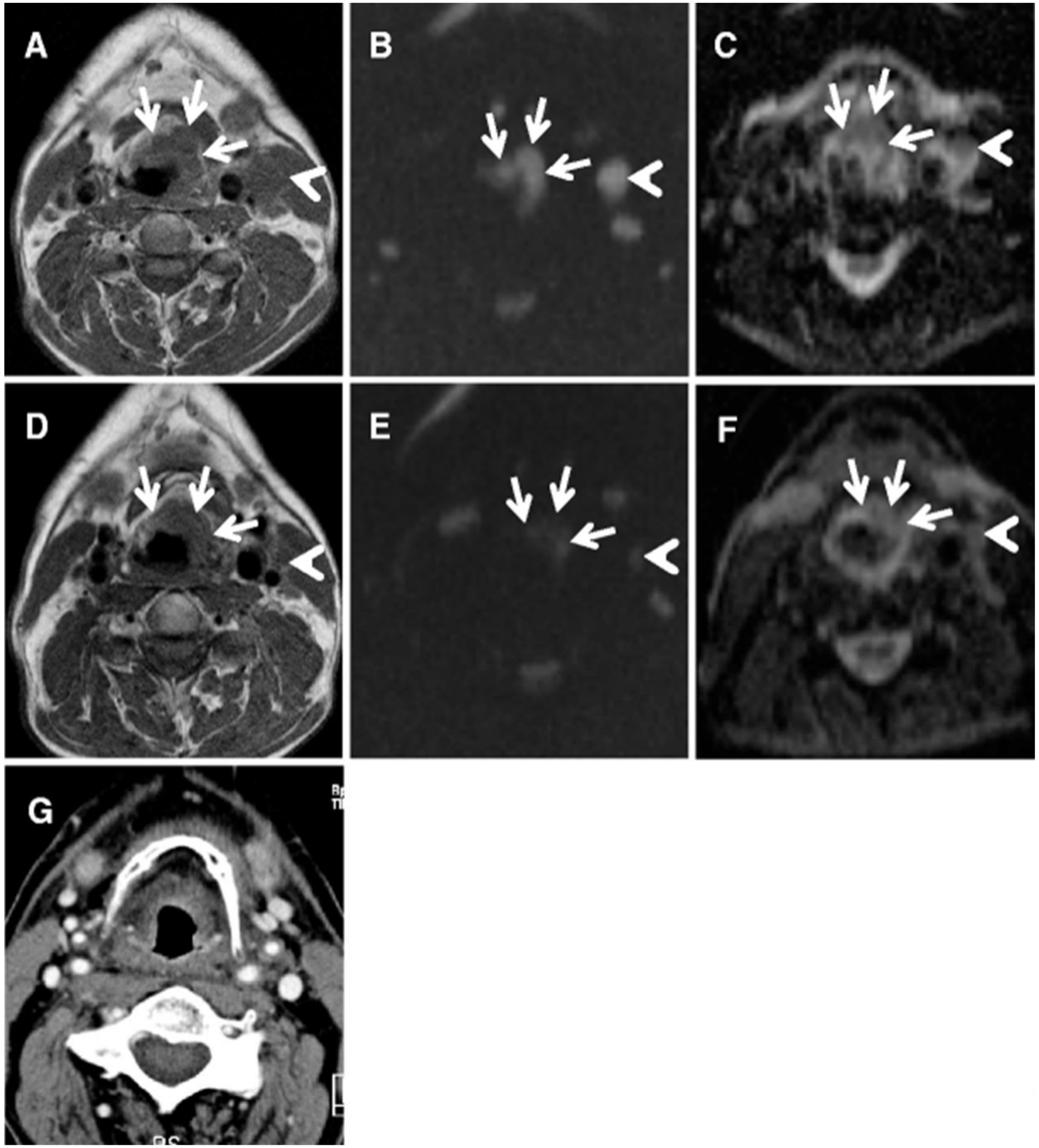

Images courtesy of Prof. V. Vandecaveye.

Clinical example of DWI for response assessment (2)

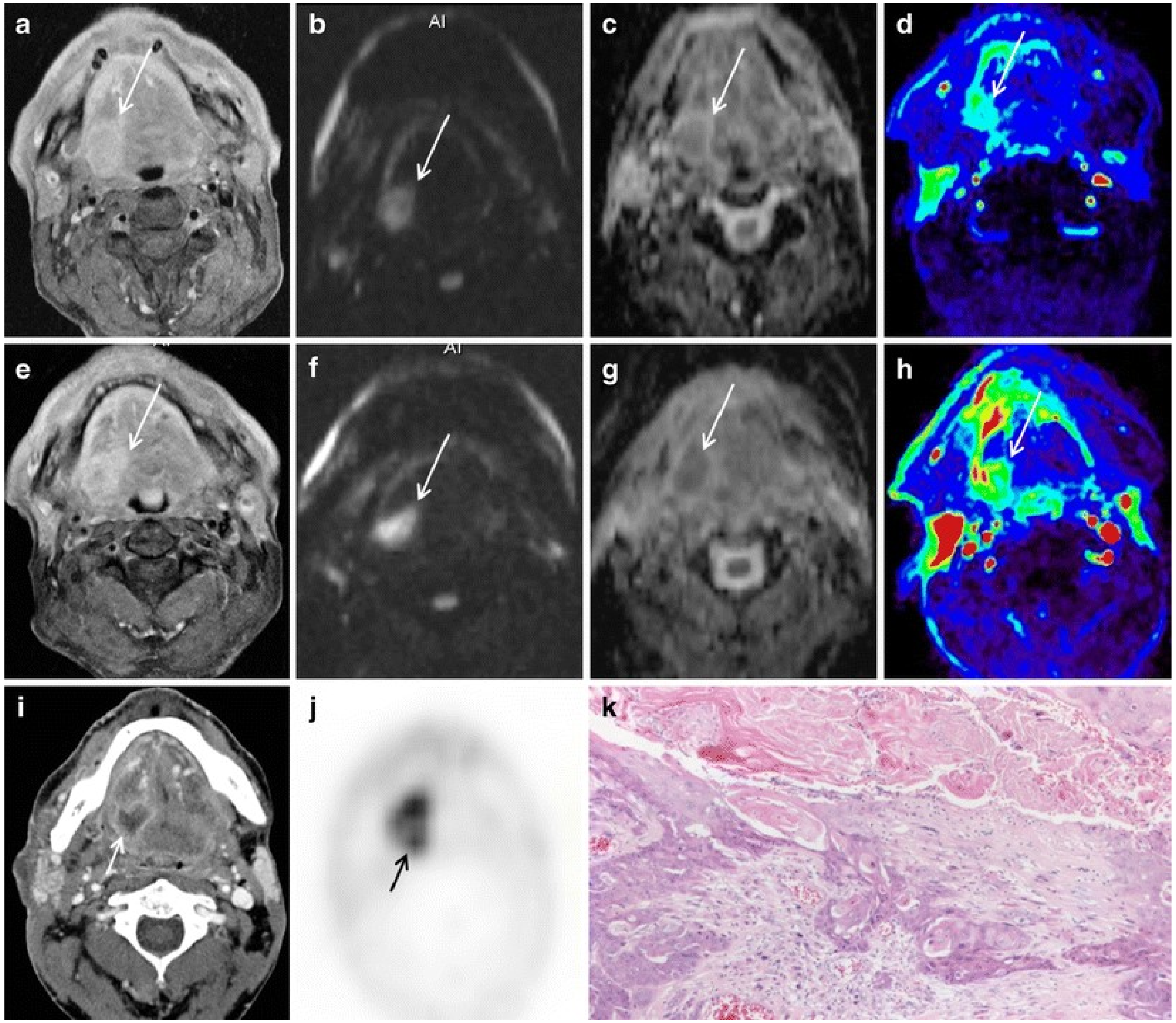
a
b
AI
c
d
e
f
AI
g
h
i
j
k

Images courtesy of Prof. V. Vandecaveye.

Clinical example of DWI for response assessment (3)

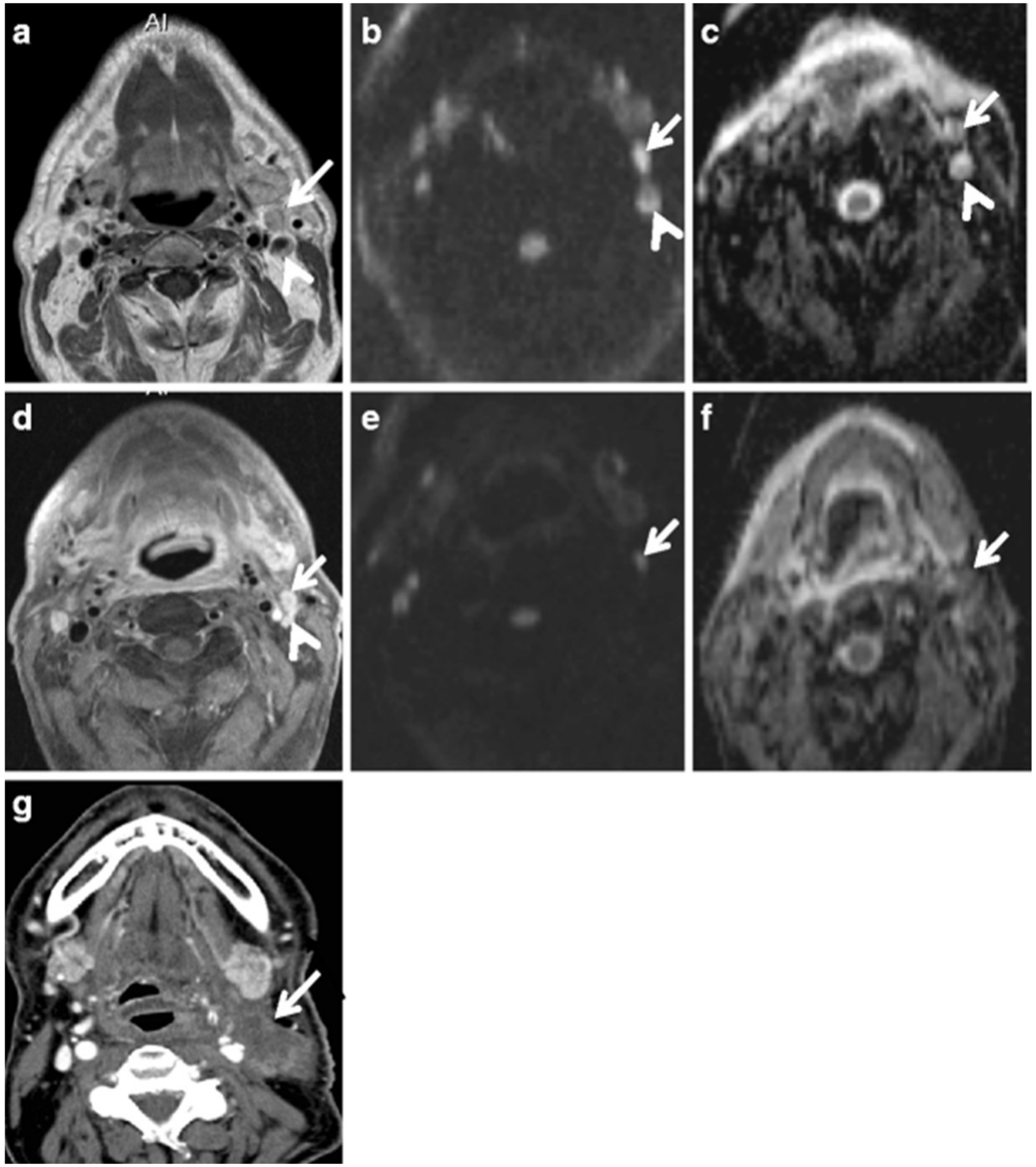

Images courtesy of Prof. V. Vandecaveye.

Similar results at the University of Pennsylvania

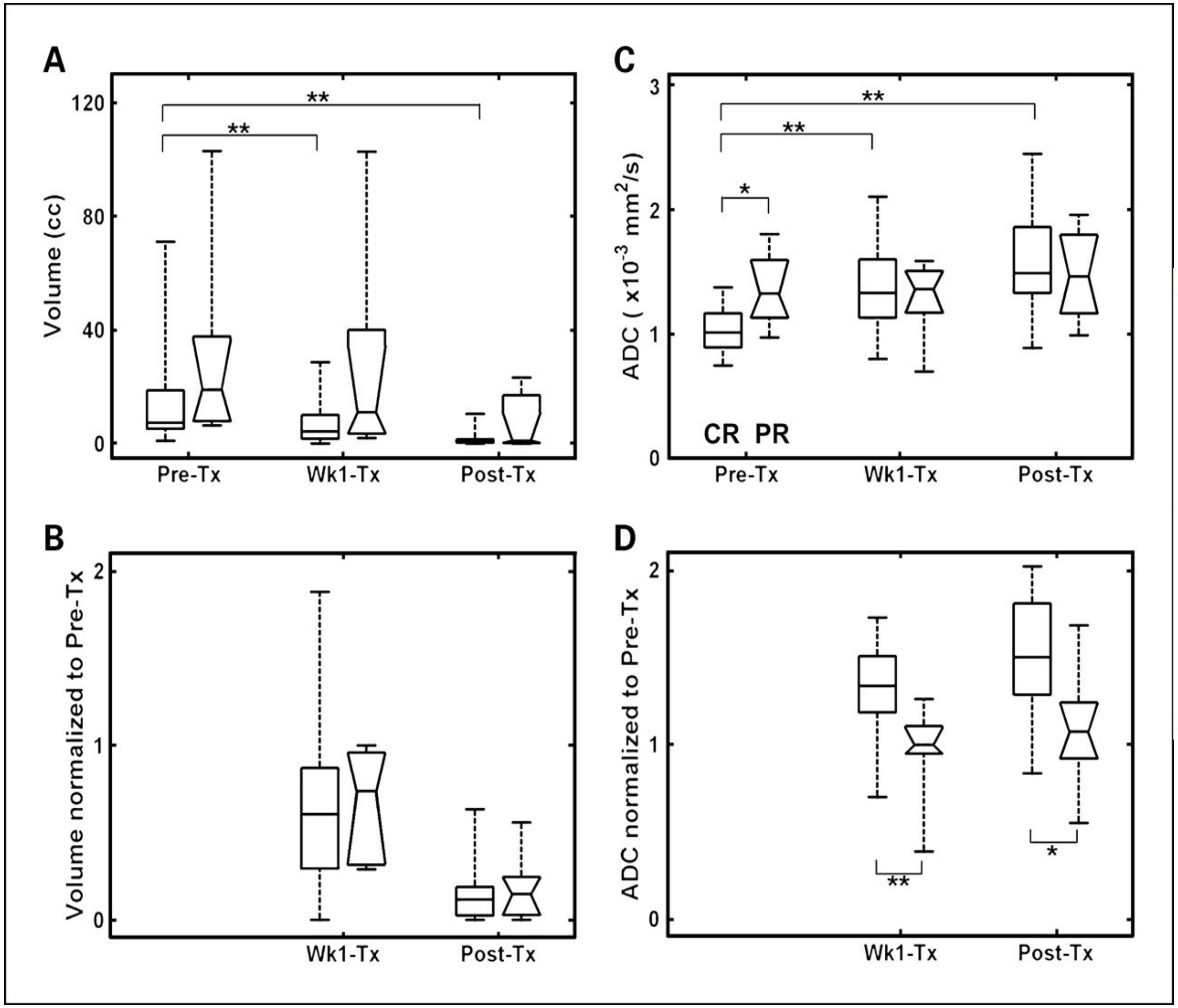

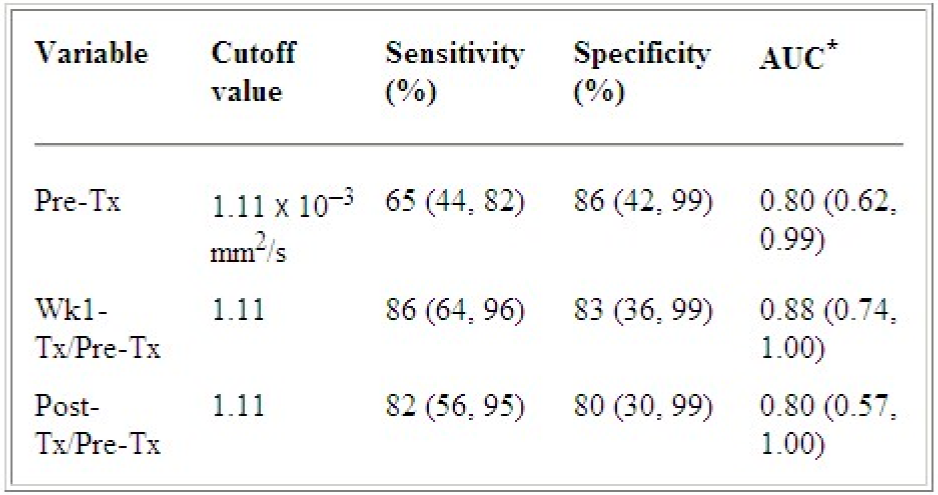

Variable	Cutoff value	Sensitivity (%)	Specificity (%)	AUC*
Pre-Tx	1.11 x 10^{-3} mm^2/s	65 (44, 82)	86 (42, 99)	0.80 (0.62, 0.99)
Wk1-Tx/Pre-Tx	1.11	86 (64, 96)	83 (36, 99)	0.88 (0.74, 1.00)
Post-Tx/Pre-Tx	1.11	82 (56, 95)	80 (30, 99)	0.80 (0.57, 1.00)

Kim S. et al. Clin Cancer Res 2009.

Similar results at the University of Michigan

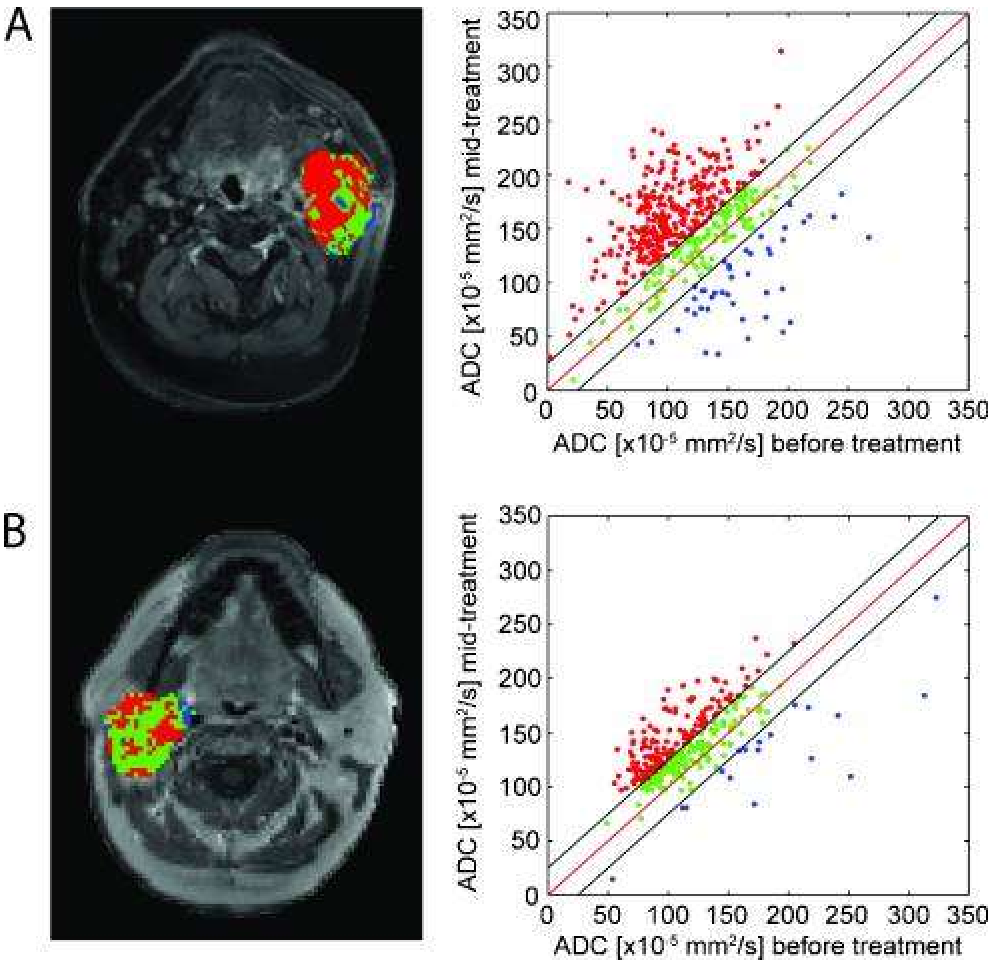
A
B
ADC [x10⁻⁵ mm²/s] mid-treatment
ADC [x10⁻⁵ mm²/s] before treatment
0
50
100
150
200
250
300
350

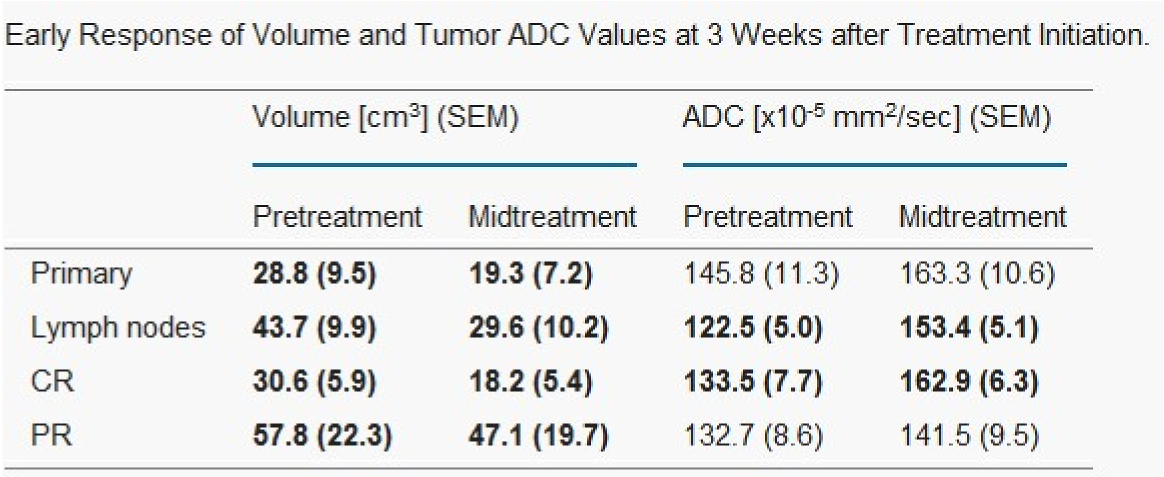

Early Response of Volume and Tumor ADC Values at 3 Weeks after Treatment Initiation.

	Volume [cm^3] (SEM)		ADC [x10^{-5} mm^2/sec] (SEM)	
	Pretreatment	Midtreatment	Pretreatment	Midtreatment
Primary	**28.8 (9.5)**	**19.3 (7.2)**	145.8 (11.3)	163.3 (10.6)
Lymph nodes	**43.7 (9.9)**	**29.6 (10.2)**	**122.5 (5.0)**	**153.4 (5.1)**
CR	**30.6 (5.9)**	**18.2 (5.4)**	**133.5 (7.7)**	**162.9 (6.3)**
PR	**57.8 (22.3)**	**47.1 (19.7)**	132.7 (8.6)	141.5 (9.5)

Galbán C.J. et al. Transl Oncol 2009.

Similar results at the Prince of Wales Hospital (Hong Kong)

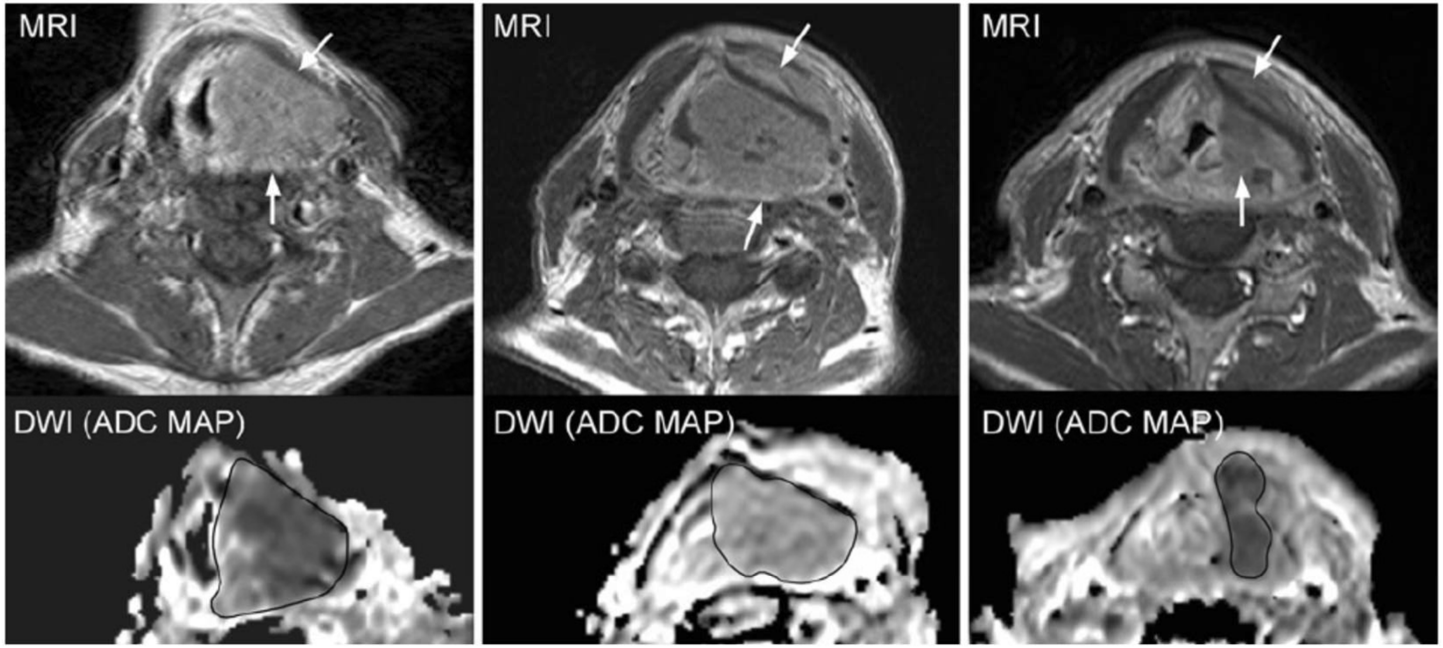

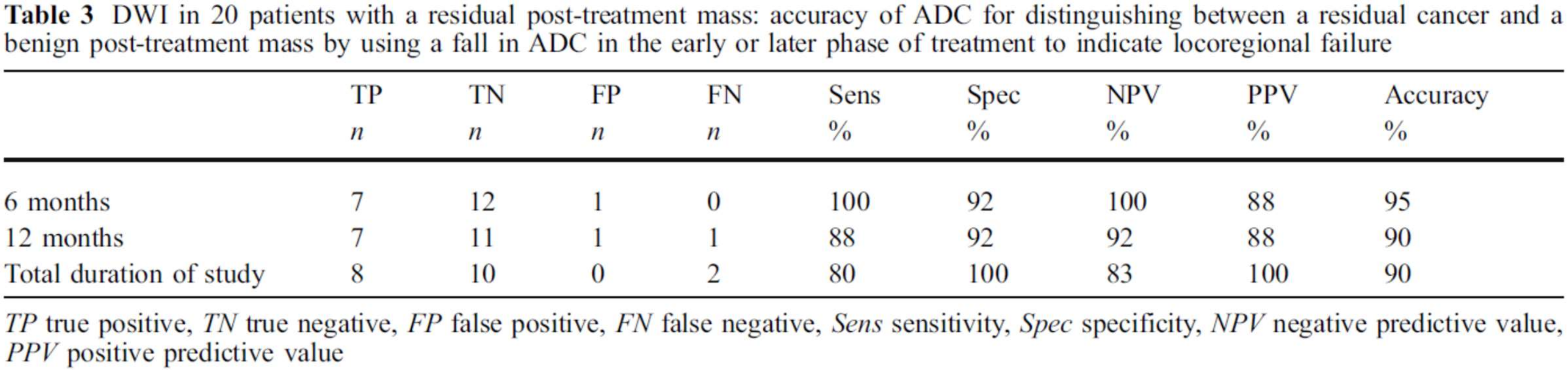

Table 3 DWI in 20 patients with a residual post-treatment mass: accuracy of ADC for distinguishing between a residual cancer and a benign post-treatment mass by using a fall in ADC in the early or later phase of treatment to indicate locoregional failure

	TP *n*	TN *n*	FP *n*	FN *n*	Sens %	Spec %	NPV %	PPV %	Accuracy %
6 months	7	12	1	0	100	92	100	88	95
12 months	7	11	1	1	88	92	92	88	90
Total duration of study	8	10	0	2	80	100	83	100	90

TP true positive, *TN* true negative, *FP* false positive, *FN* false negative, *Sens* sensitivity, *Spec* specificity, *NPV* negative predictive value, *PPV* positive predictive value

King A. D. et al. Transl Oncol 2009.

DCE-MRI for early response assessment

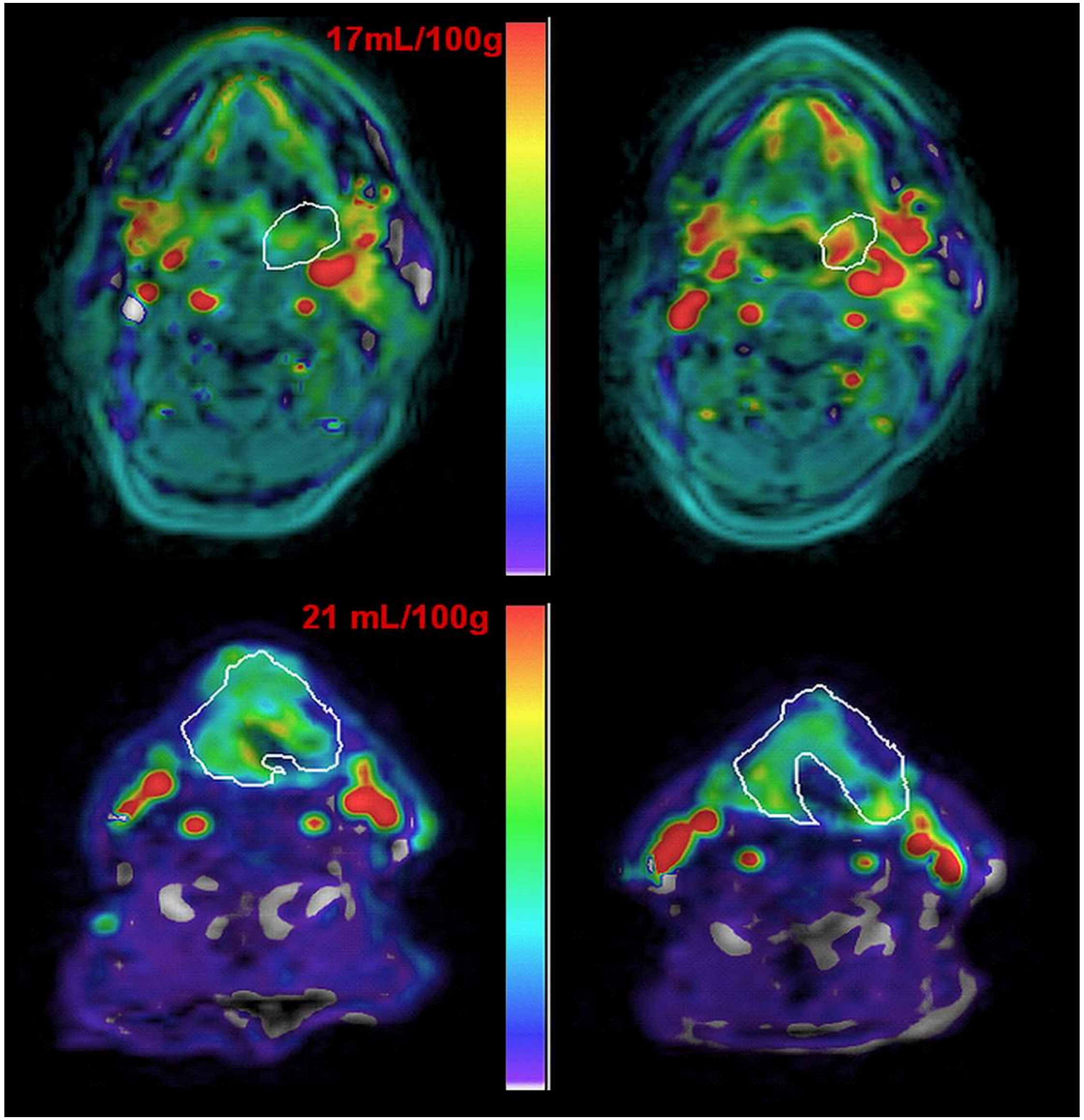
17mL/100g
21 mL/100g

Cao Y. et al. Int J Radiat Oncol Biol Phys 2008.

4. Towards a biological target volume (BTV)?

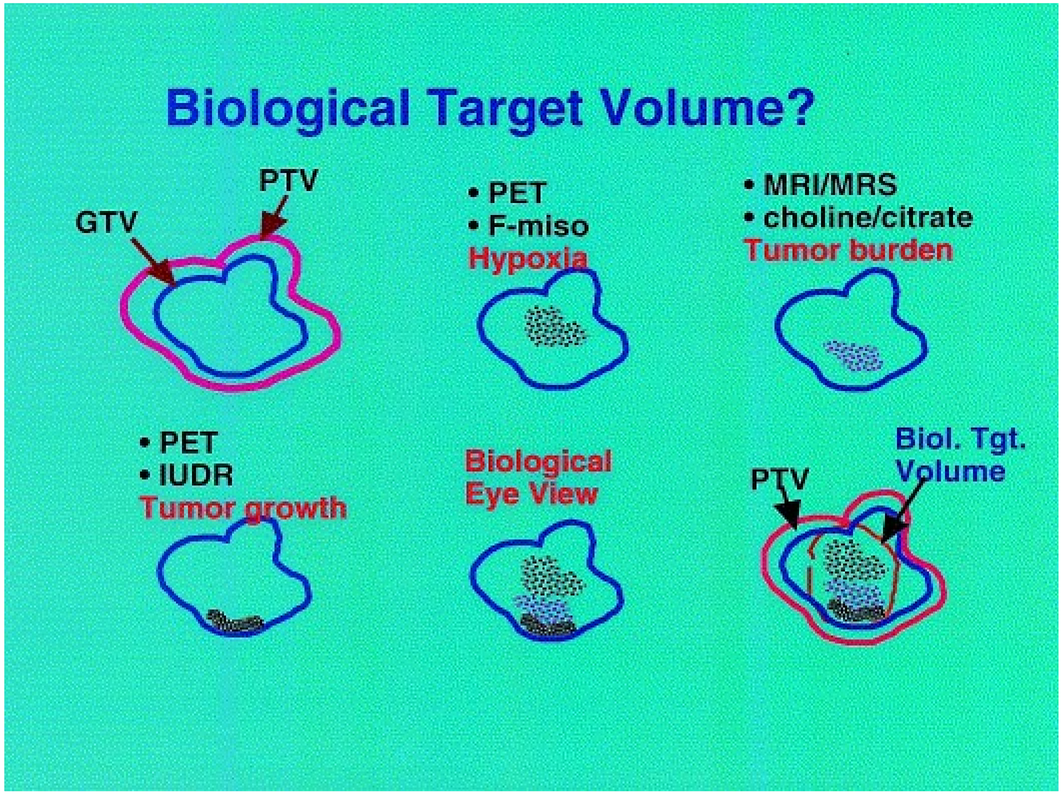
Biological Target Volume?
PTV
GTV
• PET
• F-miso
Hypoxia
• MRI/MRS
• choline/citrate
Tumor burden
• PET
• IUDR
Tumor growth
Biological
Eye View
Biol. Tgt.
Volume
PTV

- BTV derived from functional/biological imaging guides customized dose delivery to various parts of the treatment volume.
- = “dose-painting” or “dose-sculpting”.

Ling C. et al. Int J Radiat Oncol Biol Phys 2000.

FDG-PET

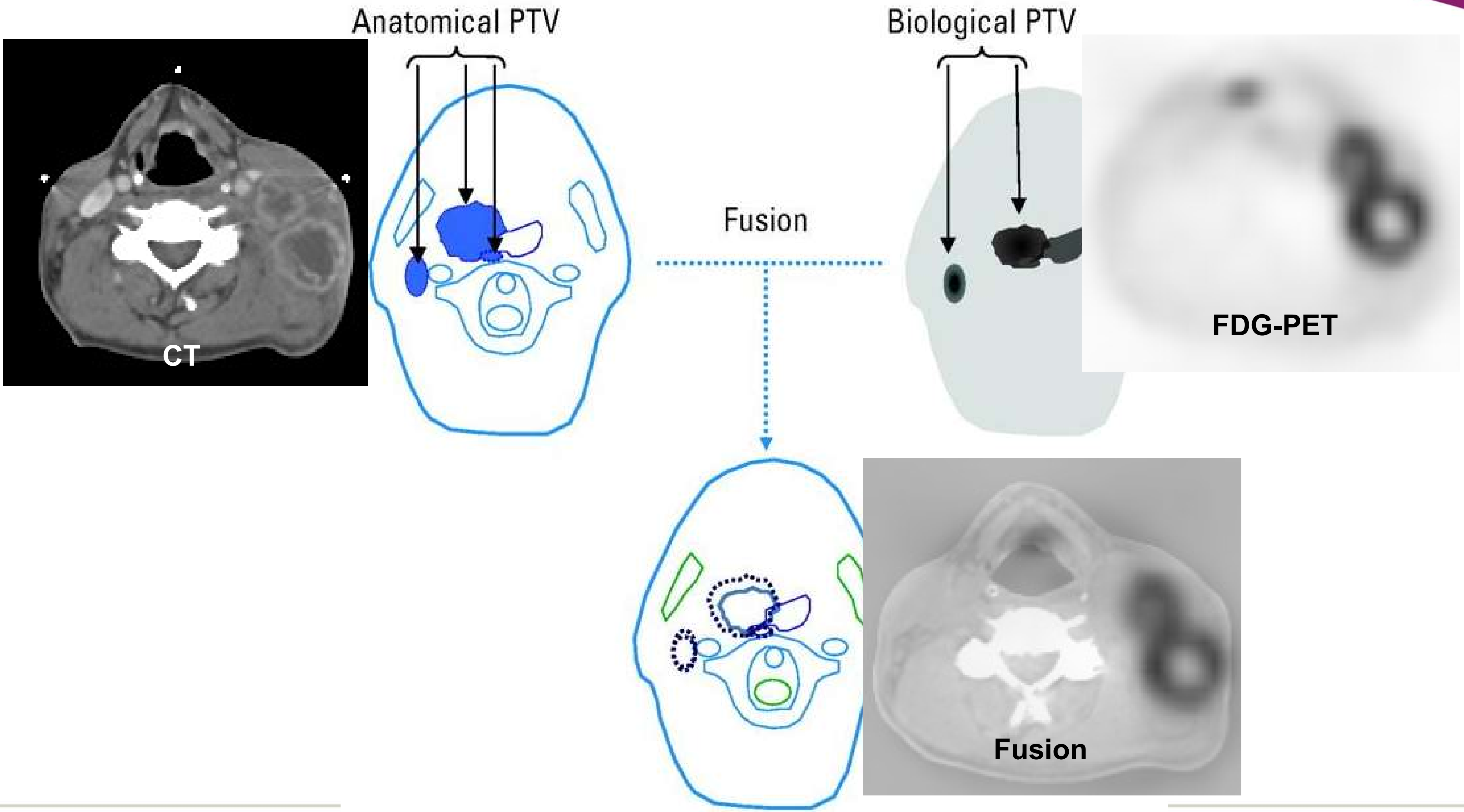
Anatomical PTV
Biological PTV
CT
FDG-PET
Fusion
Fusion

Galvin J. & De Neve W. J Clin Oncol 2007.

UZ Gent Phase I trial

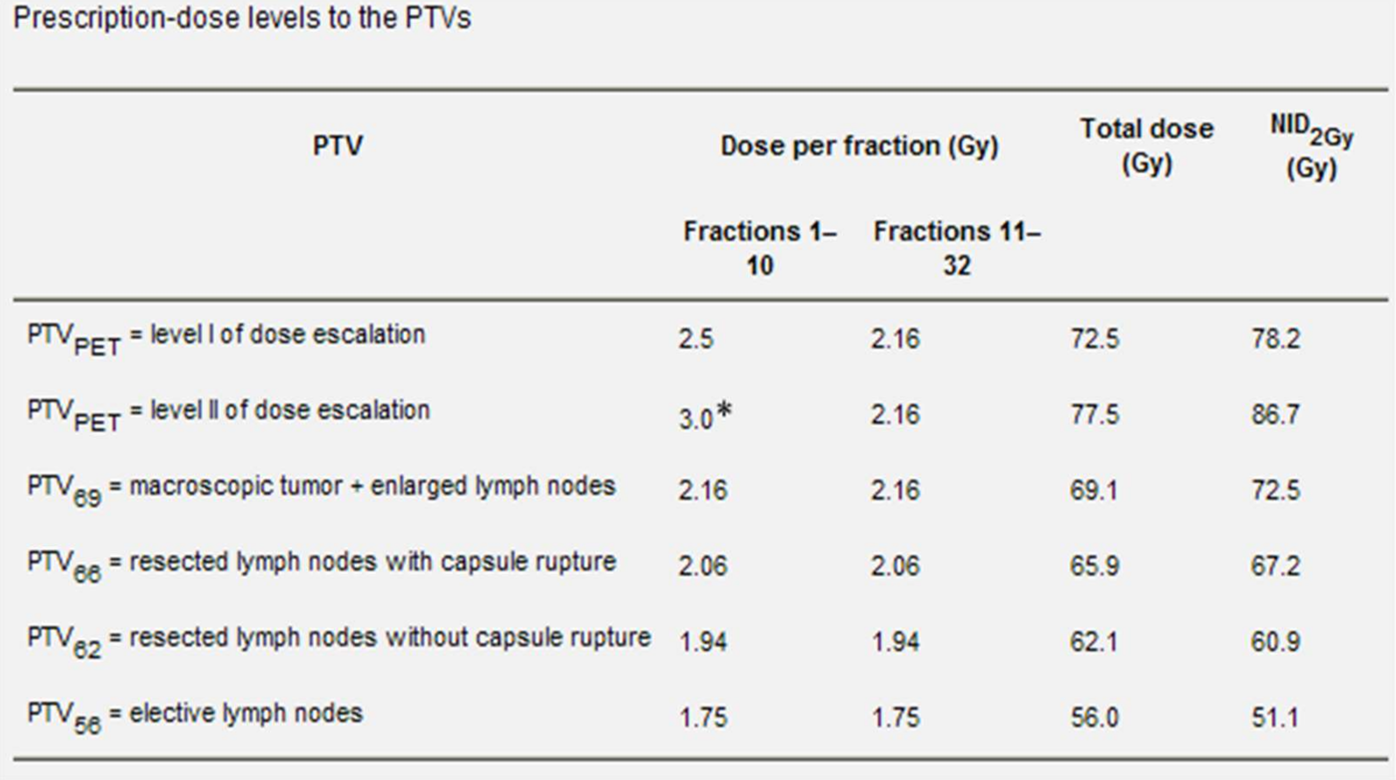

Prescription-dose levels to the PTVs

PTV	Dose per fraction (Gy)		Total dose (Gy)	NID_{2Gy} (Gy)
	Fractions 1–10	Fractions 11–32		
PTV_{PET} = level I of dose escalation	2.5	2.16	72.5	78.2
PTV_{PET} = level II of dose escalation	3.0*	2.16	77.5	86.7
PTV_{69} = macroscopic tumor + enlarged lymph nodes	2.16	2.16	69.1	72.5
PTV_{66} = resected lymph nodes with capsule rupture	2.06	2.06	65.9	67.2
PTV_{62} = resected lymph nodes without capsule rupture	1.94	1.94	62.1	60.9
PTV_{56} = elective lymph nodes	1.75	1.75	56.0	51.1

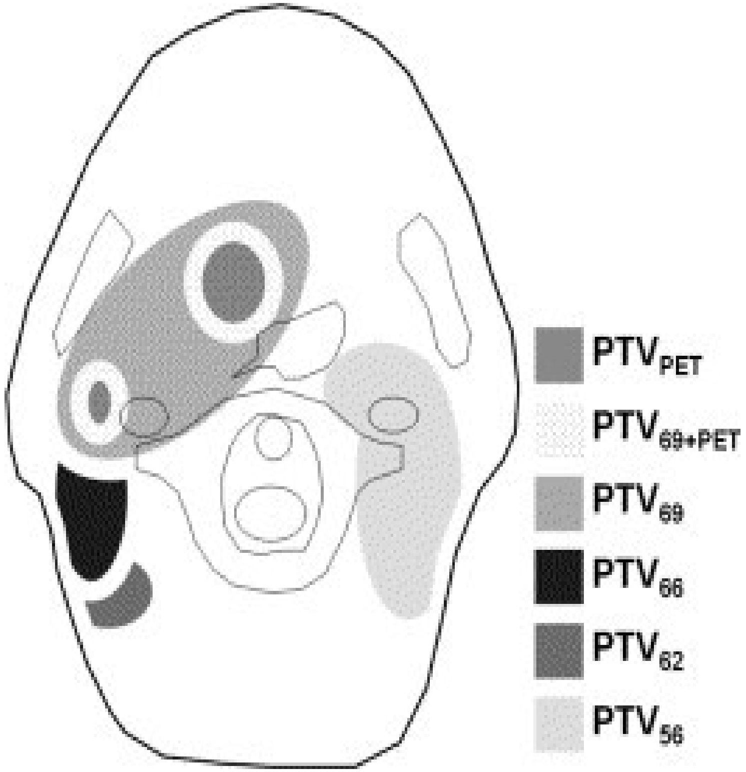

- 23 pts dose level I (5.7 Gy), 18 pts dose level II (14.2 Gy) in first 10 fractions.
- 2 cases of DLT at dose level I (grade 4 dermitis & dysphagia).
- 1 toxic death at dose level II (not RT-related?).
- In 4 of 9 relapsed patients, the site of relapse was in the PTV-PET.
- PET-guided dose escalation appears to be well-tolerated?

Madani I. et al. Int J Radiat Oncol Biol Phys 2007.
Duprez F. et al. Int J Radiat Oncol Biol Phys 2011.

Pretreatment ADC of the primary lesion

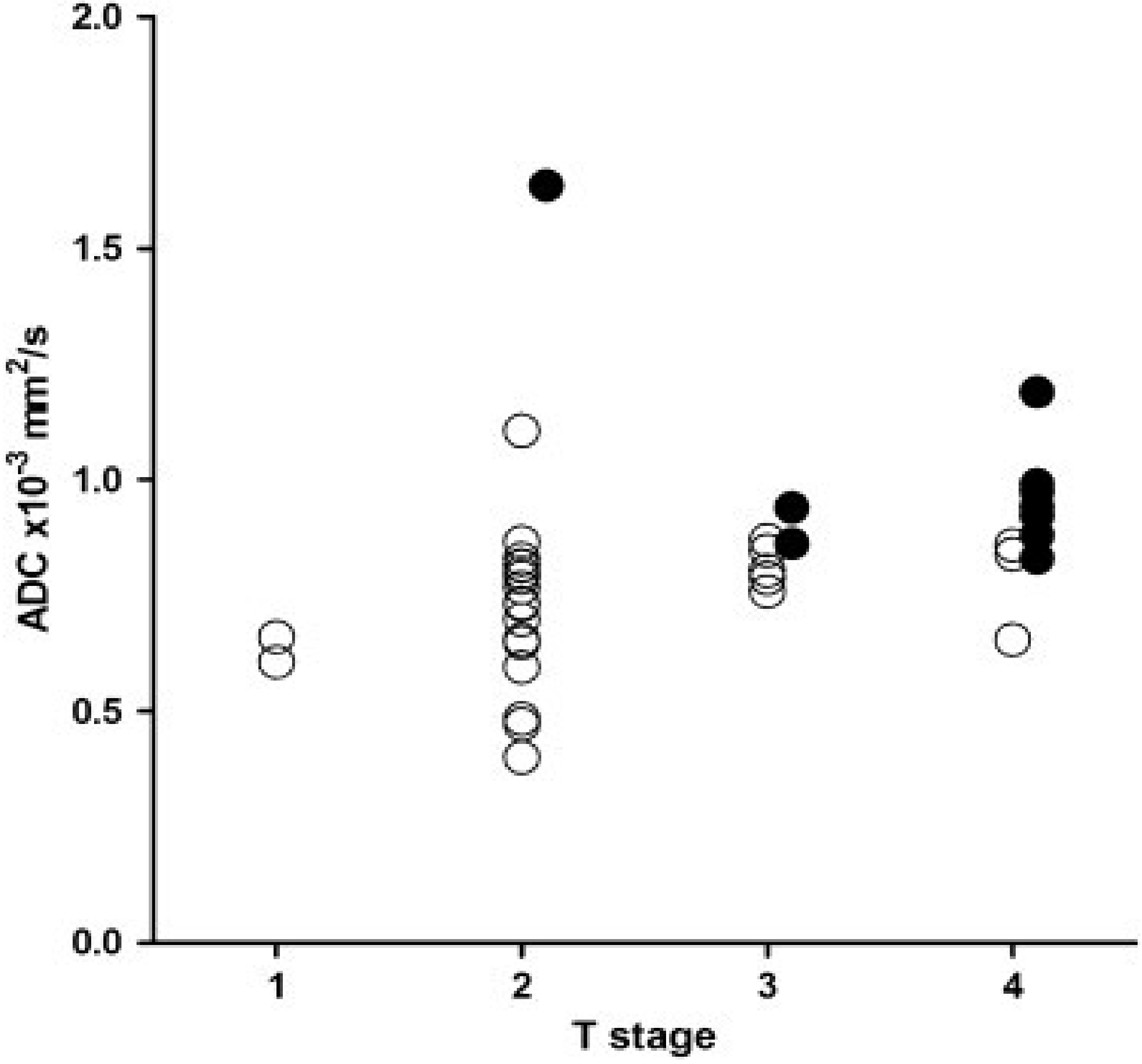

Hatakenaka M. et al. Int J Radiat Oncol Biol Phys 2011.

Pre-treatment ADC correlates with outcome?

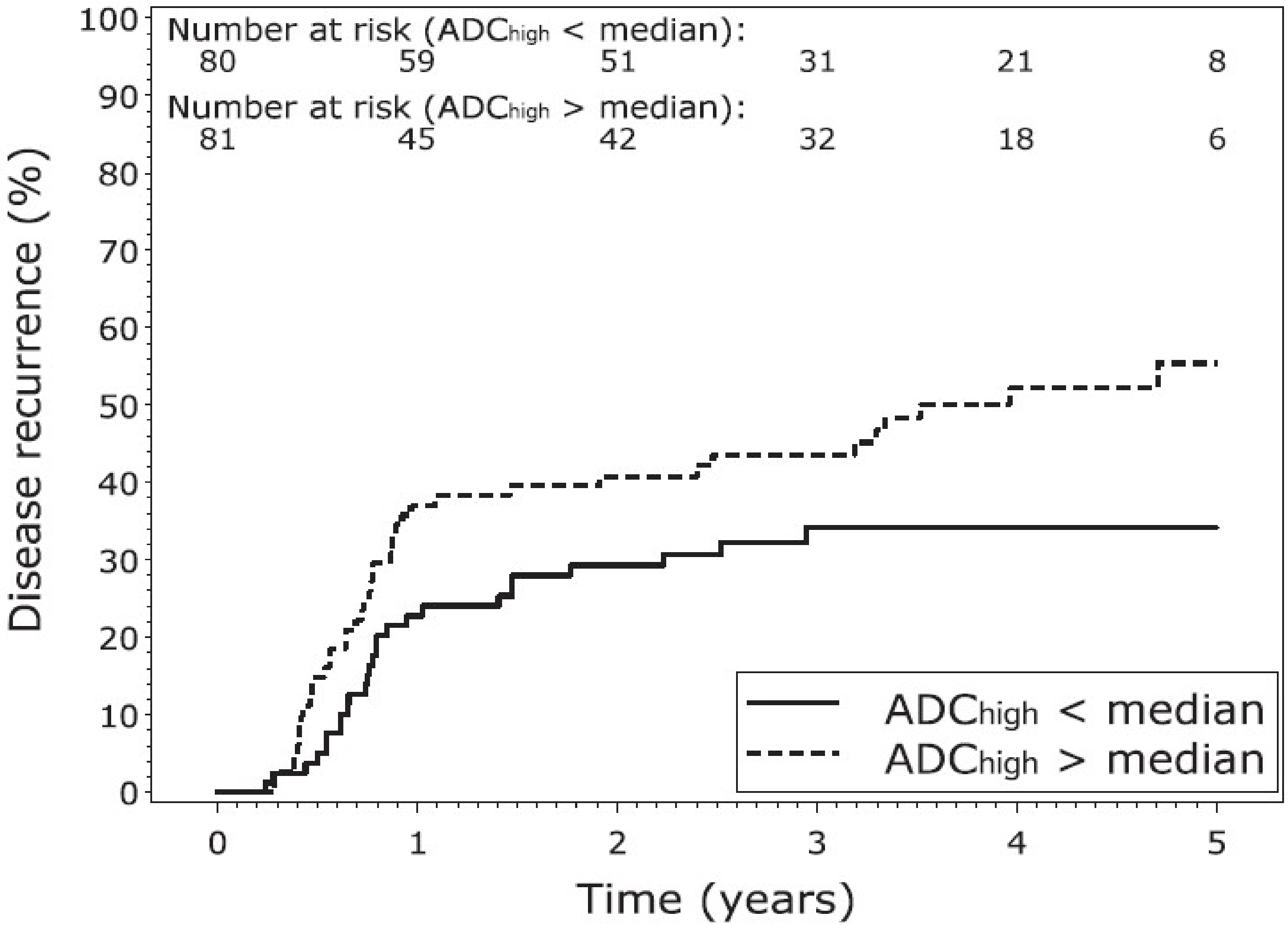

Five studies failed to distinguish patients with unfavourable disease based on pretreatment ADC.

Six studies found high pre-treatment tumour ADC to be predictive of poor outcome following CRT.

The pre-treatment ADC thresholds appear to be fairly concordant with primary ADC < 0.79–0.88 x 10^{-3} mm^2/s and nodal ADC < 1.11–1.14 x 10^{-3} mm^2/s to be predictive of favourable outcome.

Lambrecht M. et al. Radiother Oncol 2014.

In preparation.

Multivariable prognostic model

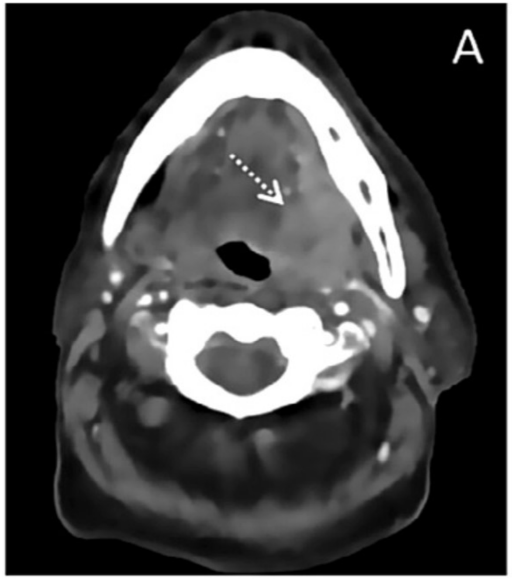

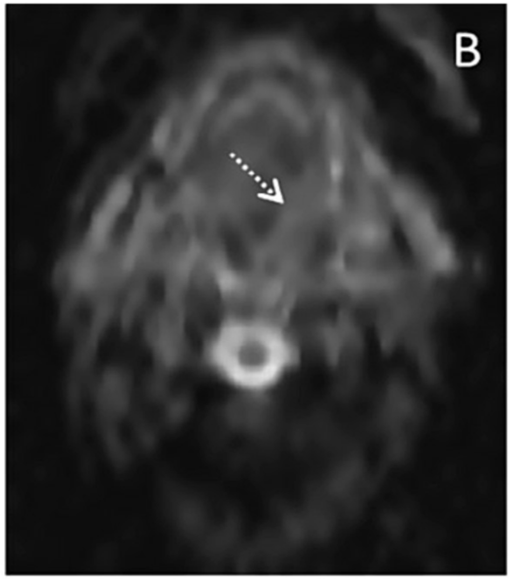

C

Age :	56
Location	Oropharynx
Tumour Volume	0,3 dl:
Nodal Volume	0,05 dl:
ADC_{high} value	11 x10^{-4} mm²/s:
Recurrence probability:	**42%**

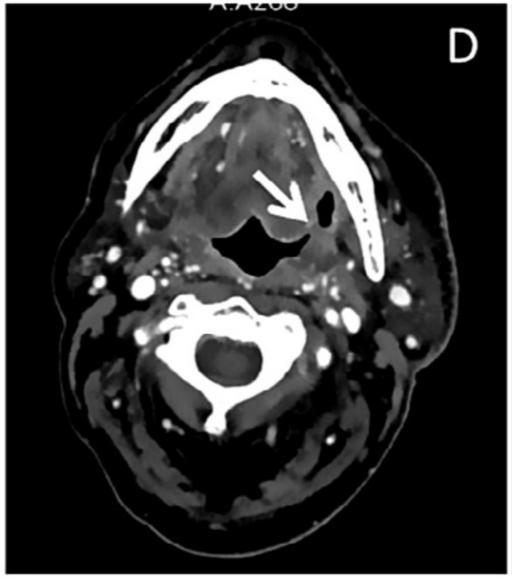

Lambrecht M. et al. Radiother Oncol 2014.

FDG-PET & DWI contain different info

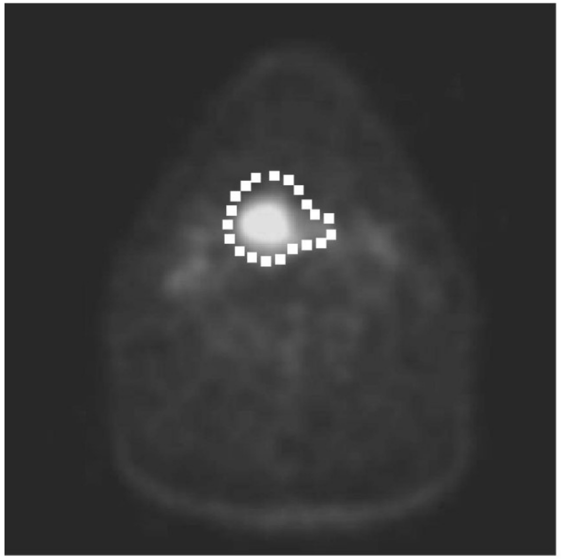

(a)

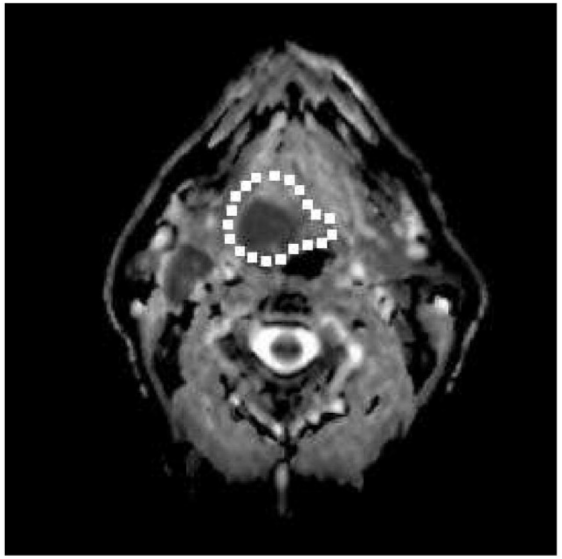

(b)

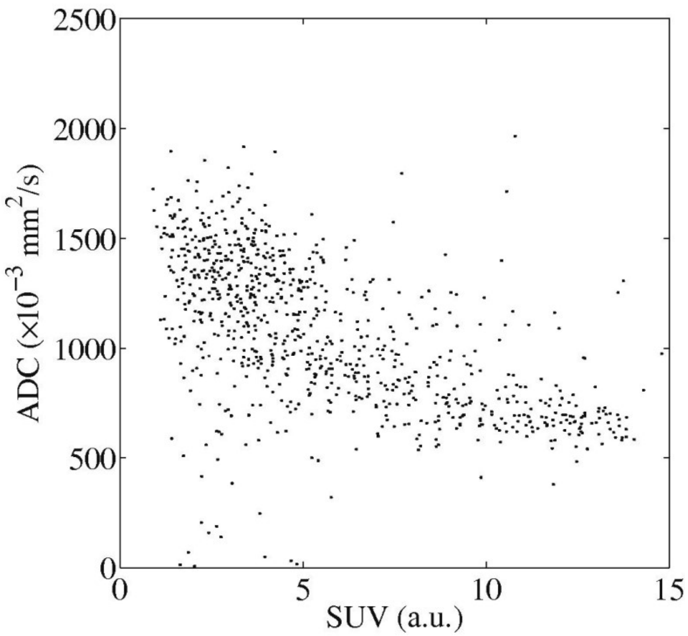

(c)

Table 2

Overlap of the different targets with the SUV$_{50\%max}$-target.

	Volume (ml)		Overlap (%)	
	Average	Range	Average	Range
SUV$_{50\%max}$	7.7	1.3–30.6	–	–
SUV$_{60\%max}$	5.1	0.9–22.5	100	100– 100
SUV$_{40\%max}$	11.2	2.1–38.3	67.9	51.1–80.2
ADC$_{<mean}$	18.4	2.7–61.2	30.2	8.0–68.1
ADC$_{<mean-SD}$	4.6	0.9–12.4	27.0	3.9–72.5
ADC$_{>mean}$	16.3	3.0–57.5	18.6	0.7–56.3

Houweling A.C. et al. Radiother Oncol 2013.

Combination of both can be valuable

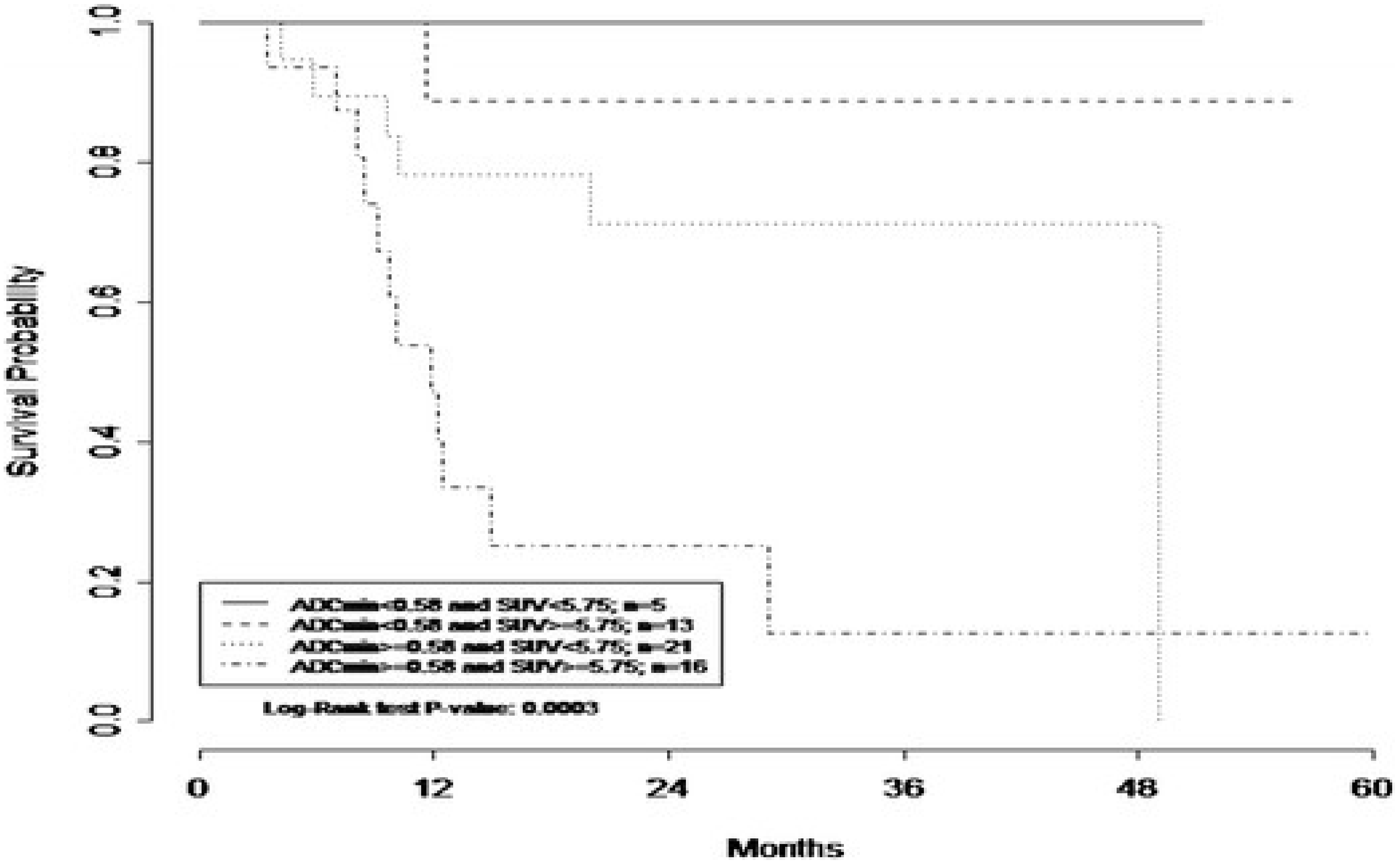

Preda L. et al. Eur Radiol 2016.

Pathology validation study

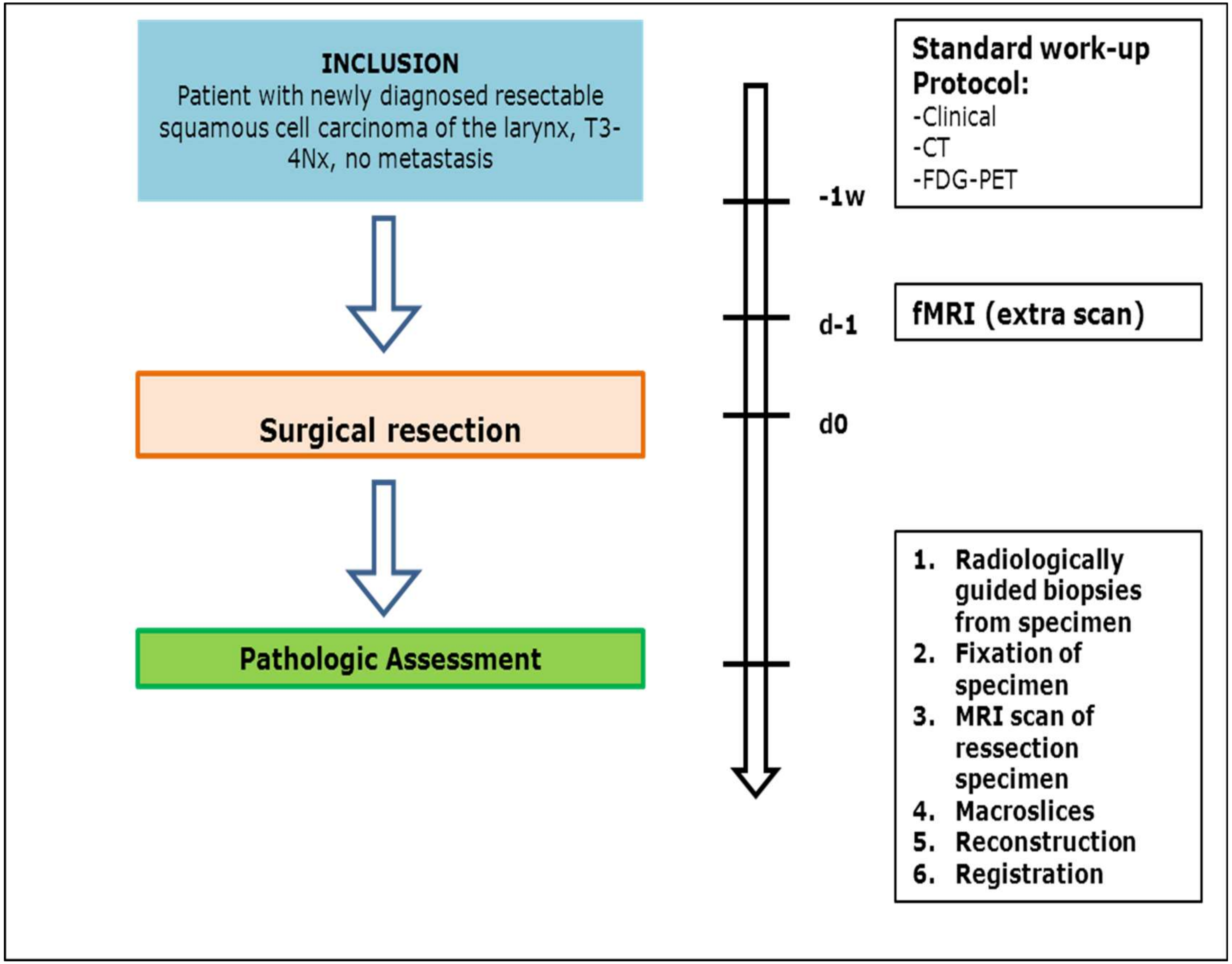

INCLUSION
Patient with newly diagnosed resectable squamous cell carcinoma of the larynx, T3-4Nx, no metastasis

Surgical resection

Pathologic Assessment

Standard work-up Protocol:
-Clinical
-CT
-FDG-PET

fMRI (extra scan)

1. **Radiologically guided biopsies from specimen**
2. **Fixation of specimen**
3. **MRI scan of ressection specimen**
4. **Macroslices**
5. **Reconstruction**
6. **Registration**

Slide courtesy of Dr. D. Nevens

Pathology validation study

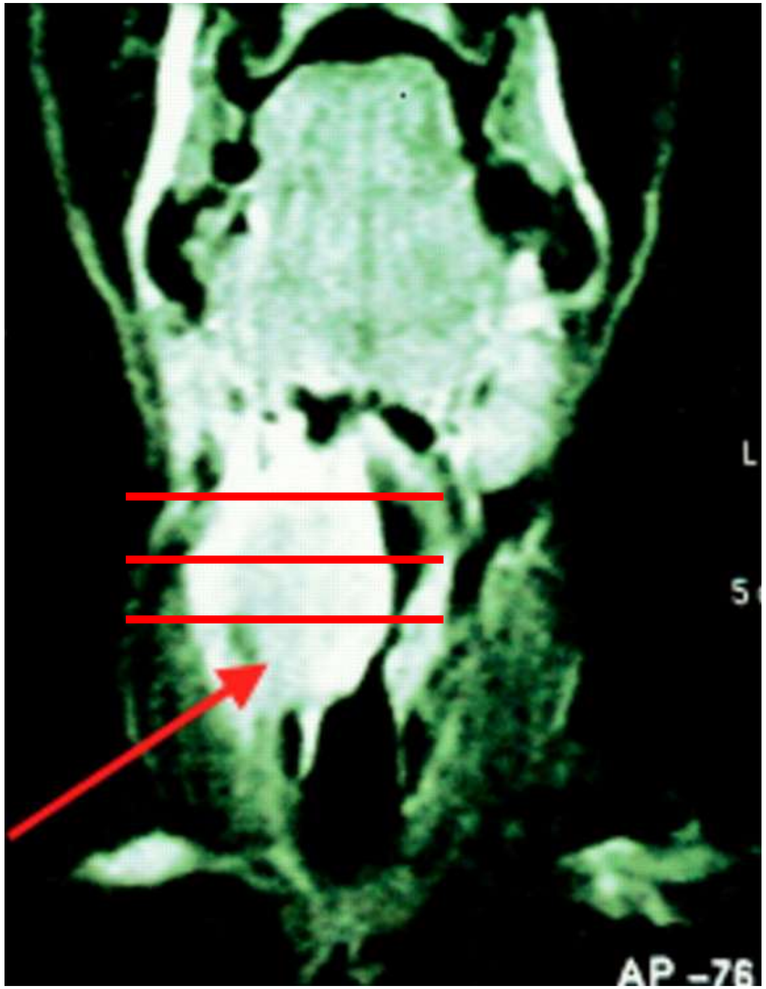

± 5mm

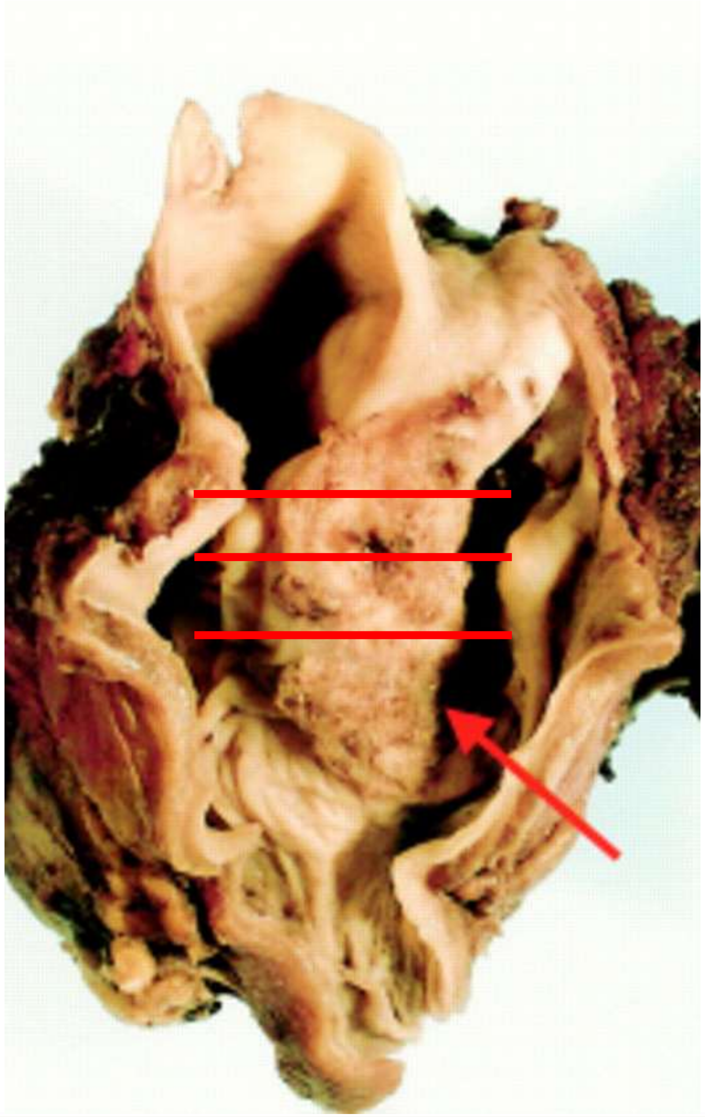

Slide courtesy of Dr. D. Nevens

Pathology validation study

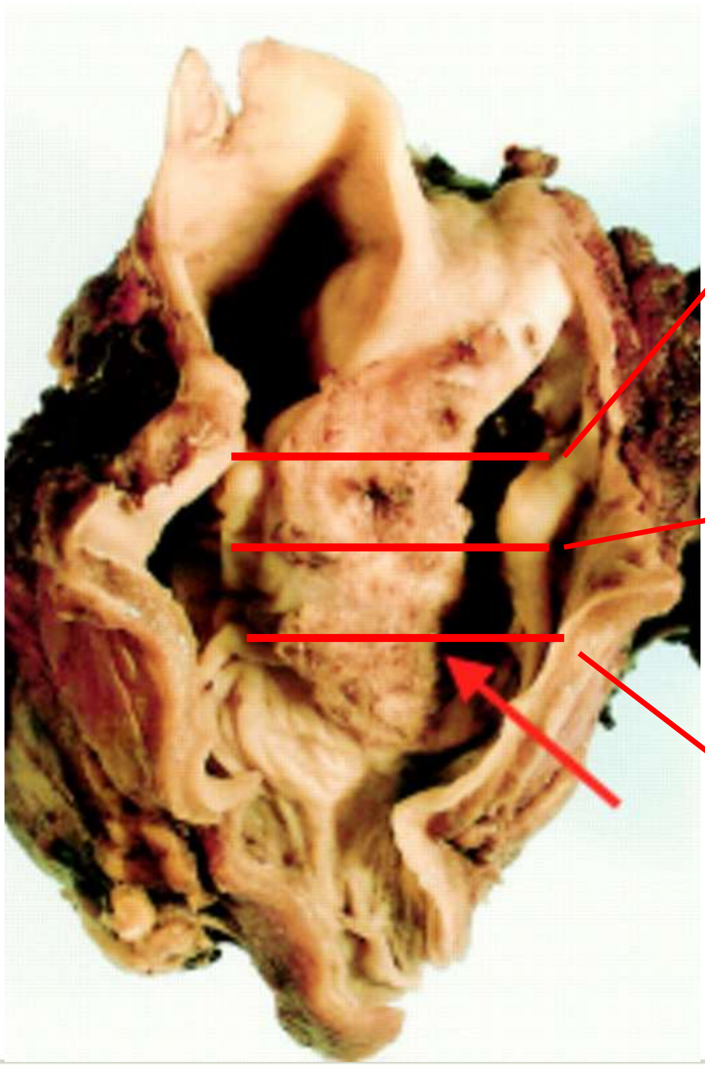

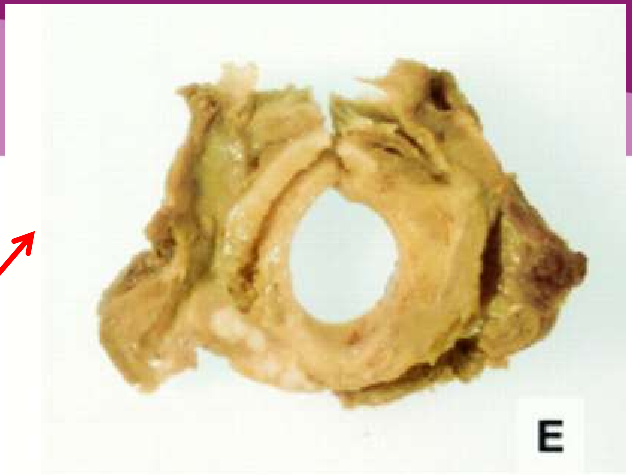

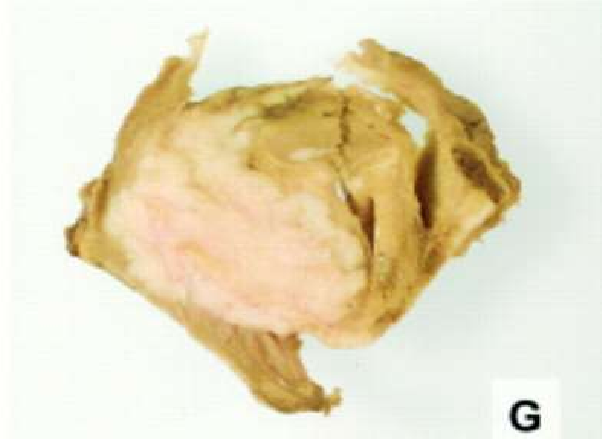

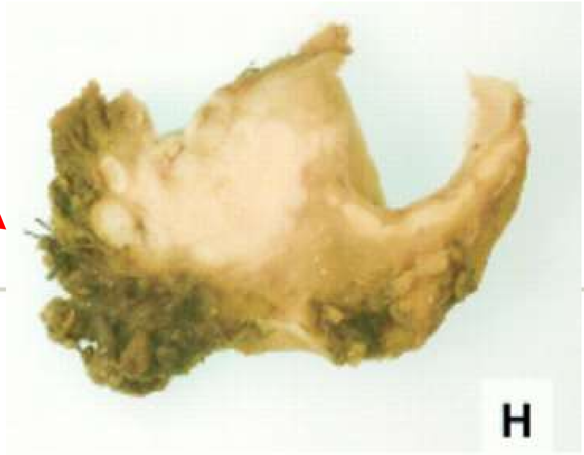

Slide courtesy of Dr. D. Nevens

Association between ADC and pathology (1)

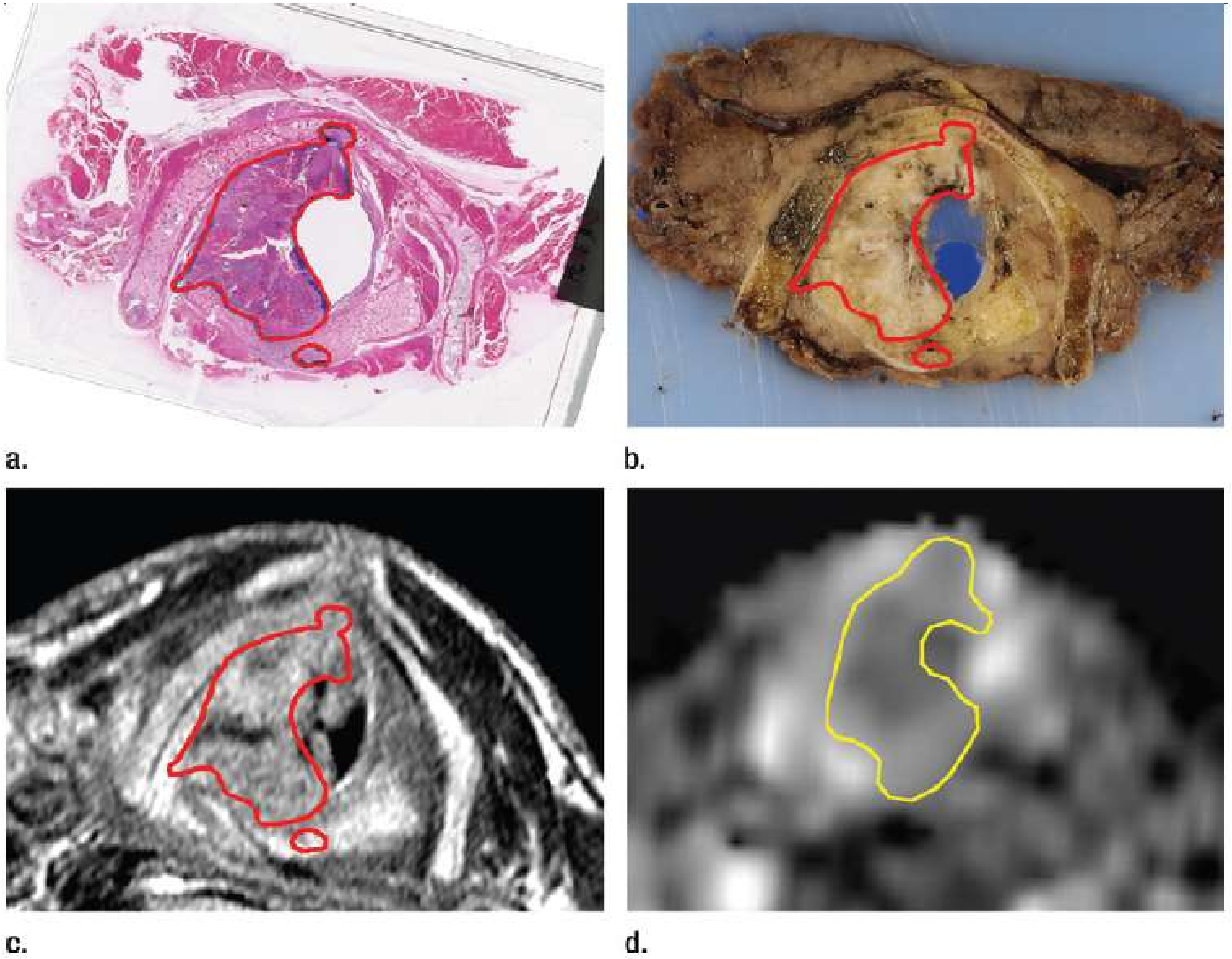

Driessen J.P. et al. Radiology 2015.

Association between ADC and pathology (2)

Figure 5

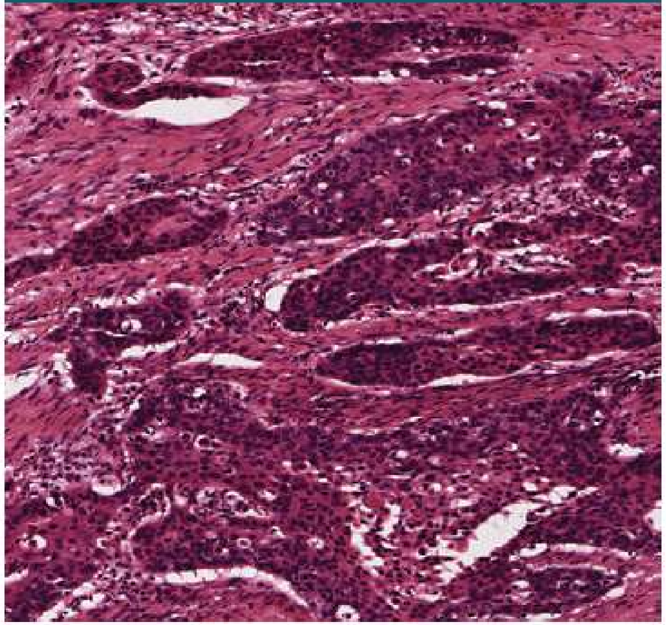

Figure 5: Digitized whole-mount H-E section (original magnification, ×10) of a T3 hypopharyngeal carcinoma. The tumor shows an intermediate CD of 6188 cells per square millimeter, 38% nuclear area, 38% stromal area, NC ratio of 1.59, and intermediate ADC of 1.19×10^{-3} mm^2/sec.

Figure 6

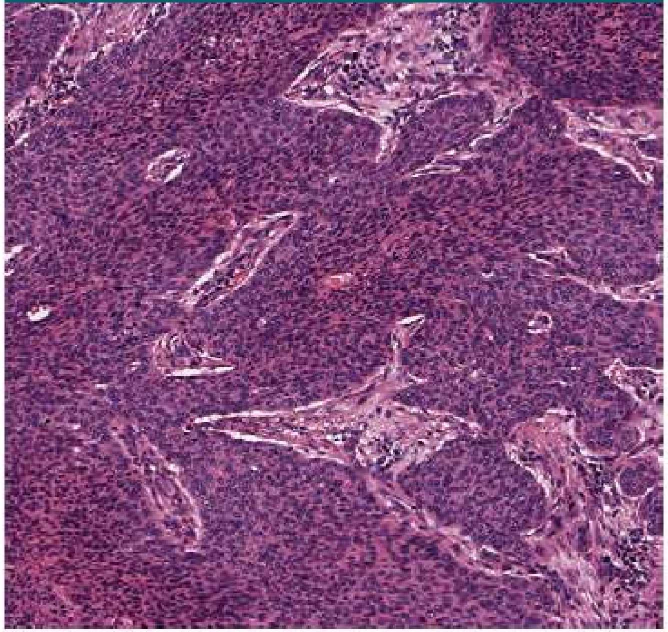

Figure 6: Digitized whole-mount H-E section (original magnification, ×10) of a T4a laryngeal carcinoma. The tumor shows a high CD of 8050 cells per square millimeter, 65% nuclear area, 18% stromal area, NC ratio of 4.14, and low ADC of 0.96 $\times 10^{-3}$ mm^2/sec.

Driessen J.P. et al. Radiology 2015.

All reported results for DWI & response assessment

Study	n	During CRT	After CRT	Correlation	Results
Kim et al. *Clin Cancer Res 2009*	33	1w	2w	Response after CRT	Baseline ADC of responders was significantly lower. A significant increase in ADC was observed in responders within 1 week of CRT which remained until after CRT.
Galban et al. *Transl Oncol 2009*	15	3w	-	6-month LC	Significant differences in ADC were observed between patients with different outcomes.
Vandecaveye et al. *Eur Radiol 2010*	30	2w & 4w	-	2-year LRC	The ΔADC 2 and 4 weeks after the start of CRT was significantly lower in lesions with recurrence.
King et al. *Eur Radiol 2010*	50	2w	6w	2-year LRC	A significant correlation was found between local failure and post-treatment ADC but not pre- or intra-treatment ADC.
Hatakenaka et al. *IJROBP 2011*	38	-	-	2-year LC	Baseline ADC of responders was significantly lower.
Vandecaveye et al. *IJROBP 2012*	29	-	3w	2-year LRC	The ΔADC of lesions with later recurrence was significantly lower.
Srinivasan et al. *JCAT 2012*	17	-	-	2-year outcome	Baseline ADC of responders was significantly lower.
King et al. *Radiology 2013*	30	2w	-	2-year LC	Baseline ADC showed no correlation with local failure. During treatment, primary tumors showed a significantly lower ΔADC for local failure.

Dirix P. et al. Seminars in Radiation Oncology 2014.

Initial K^{trans} predicts outcome

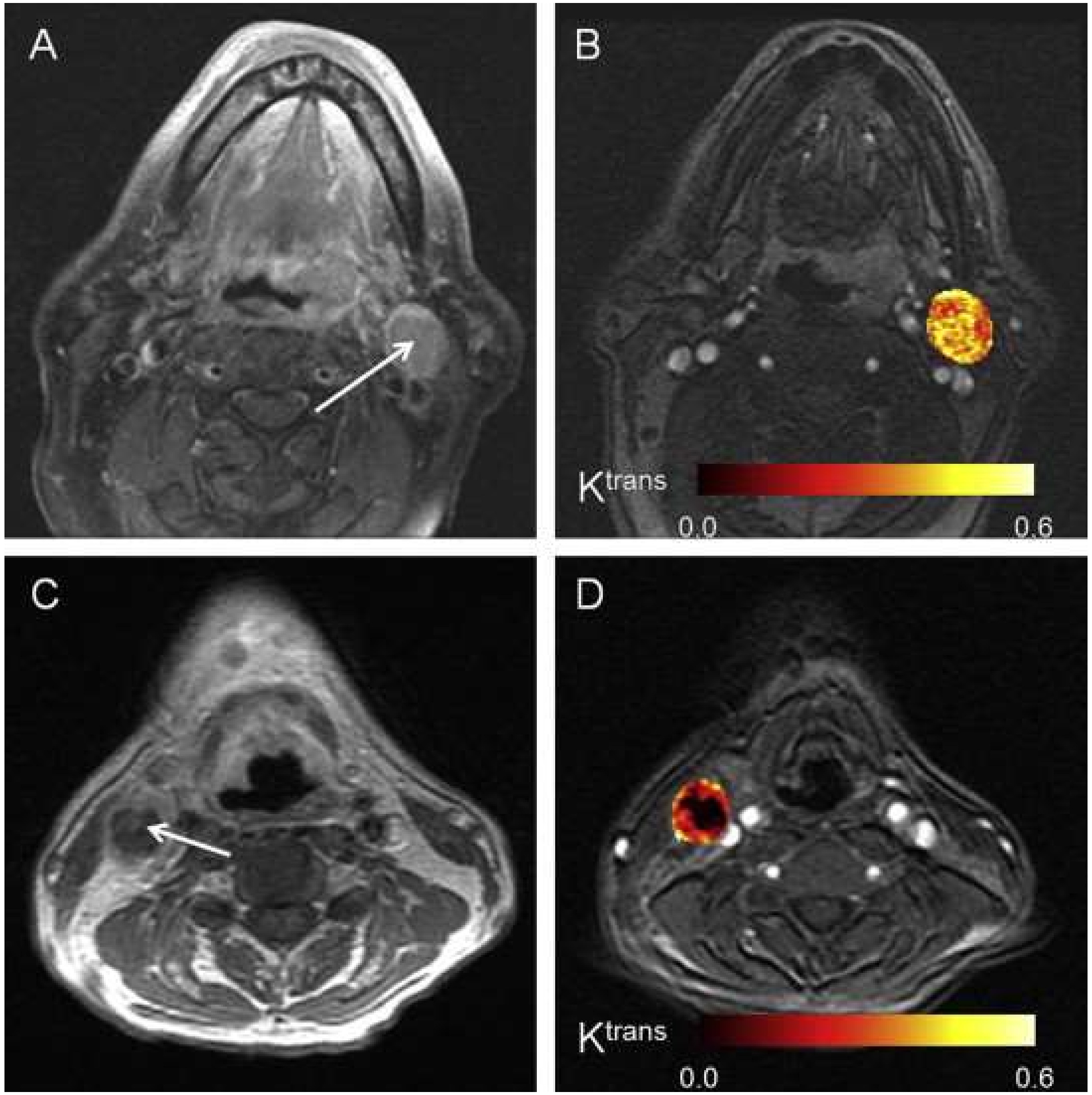
A
B
C
D
Ktrans
0.0
0.6
Ktrans
0.0
0.6

Shukla-Dave A. et al. Int J Radiat Oncol Biol Phys 2012.

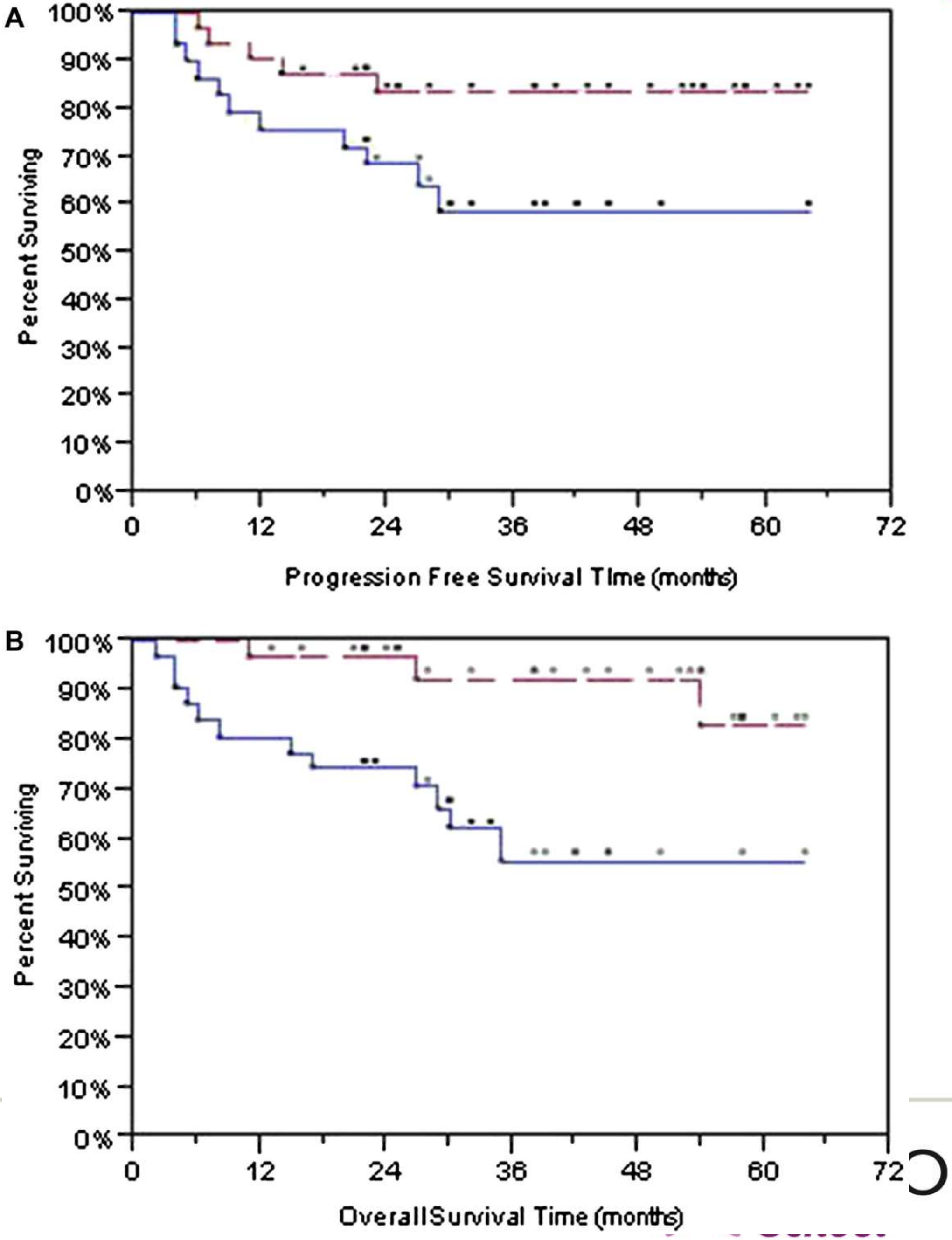

Repeated imaging during RT

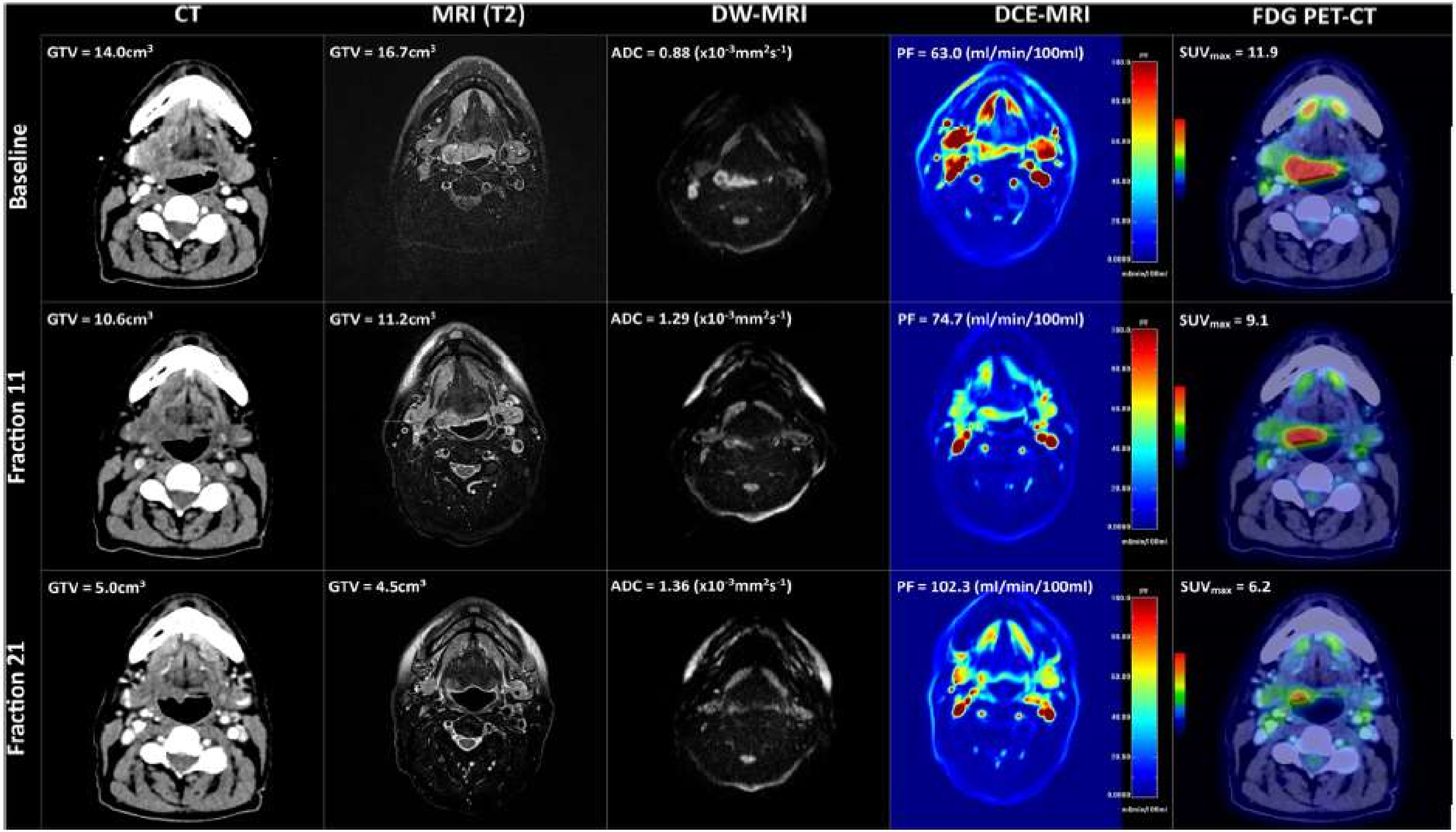
CT
MRI (T2)
DW-MRI
DCE-MRI
FDG PET-CT
Baseline
GTV = 14.0cm³
GTV = 16.7cm³
ADC = 0.88 (x10⁻³mm²s⁻¹)
PF = 63.0 (ml/min/100ml)
SUVmax = 11.9
Fraction 11
GTV = 10.6cm³
GTV = 11.2cm³
ADC = 1.29 (x10⁻³mm²s⁻¹)
PF = 74.7 (ml/min/100ml)
SUVmax = 9.1
Fraction 21
GTV = 5.0cm³
GTV = 4.5cm³
ADC = 1.36 (x10⁻³mm²s⁻¹)
PF = 102.3 (ml/min/100ml)
SUVmax = 6.2

Subesinghe M. et al. BMC cancer 2015.

First results confirm good prognosis of HPV+

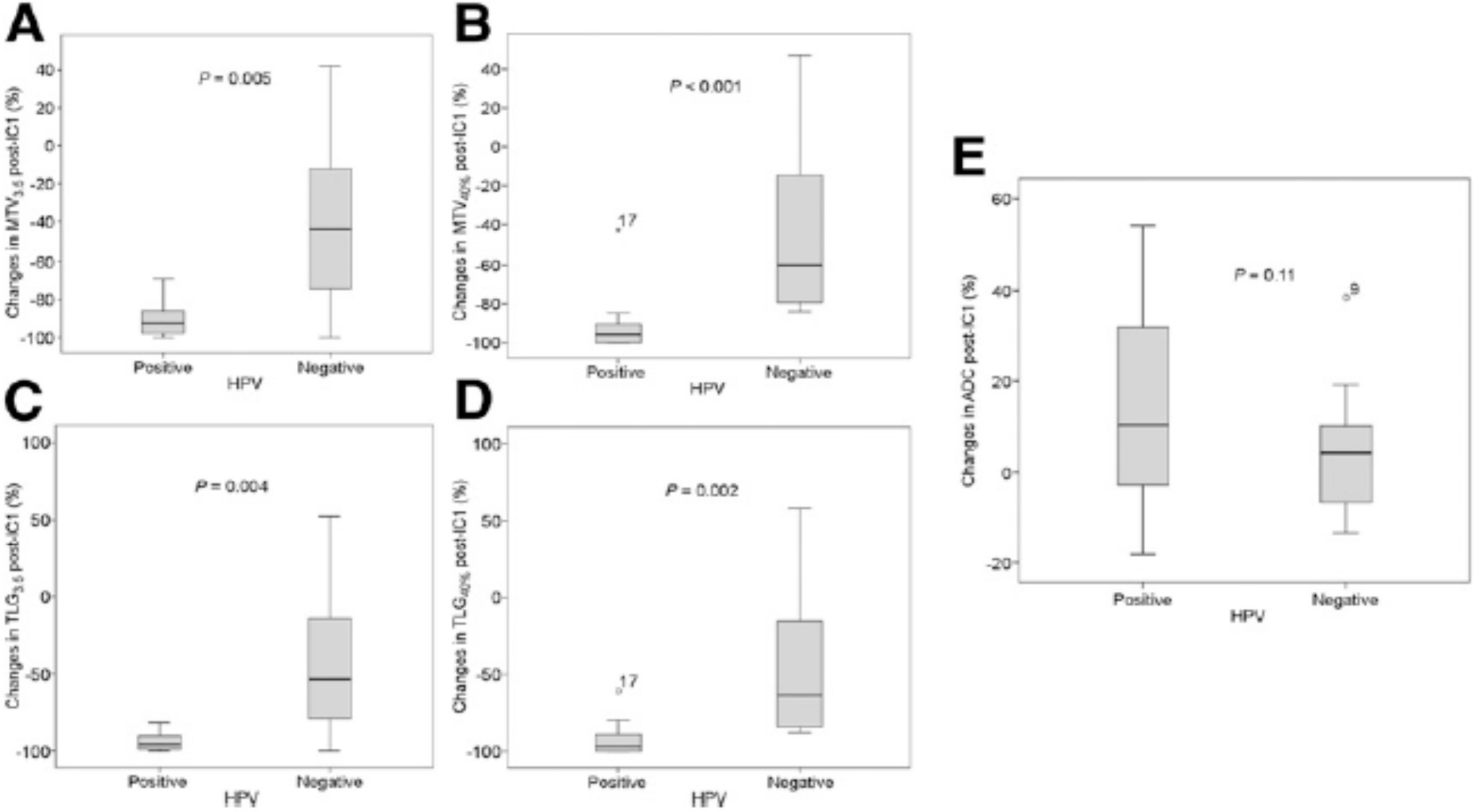

Wong K.H. et al. J Nucl Med 2016.

18F-FDG MTV or TLG as early predictors of response

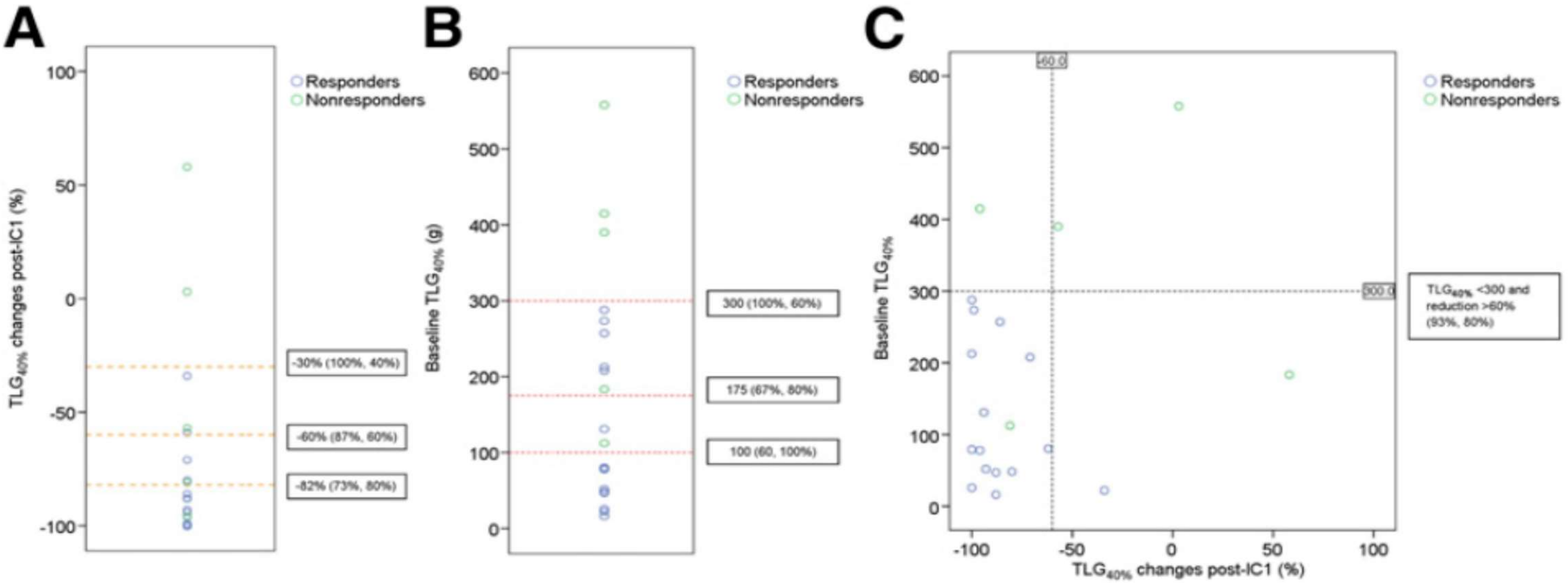

Wong K.H. et al. J Nucl Med 2016.

Large variations in pre-CT ADT due to HPV+ patients

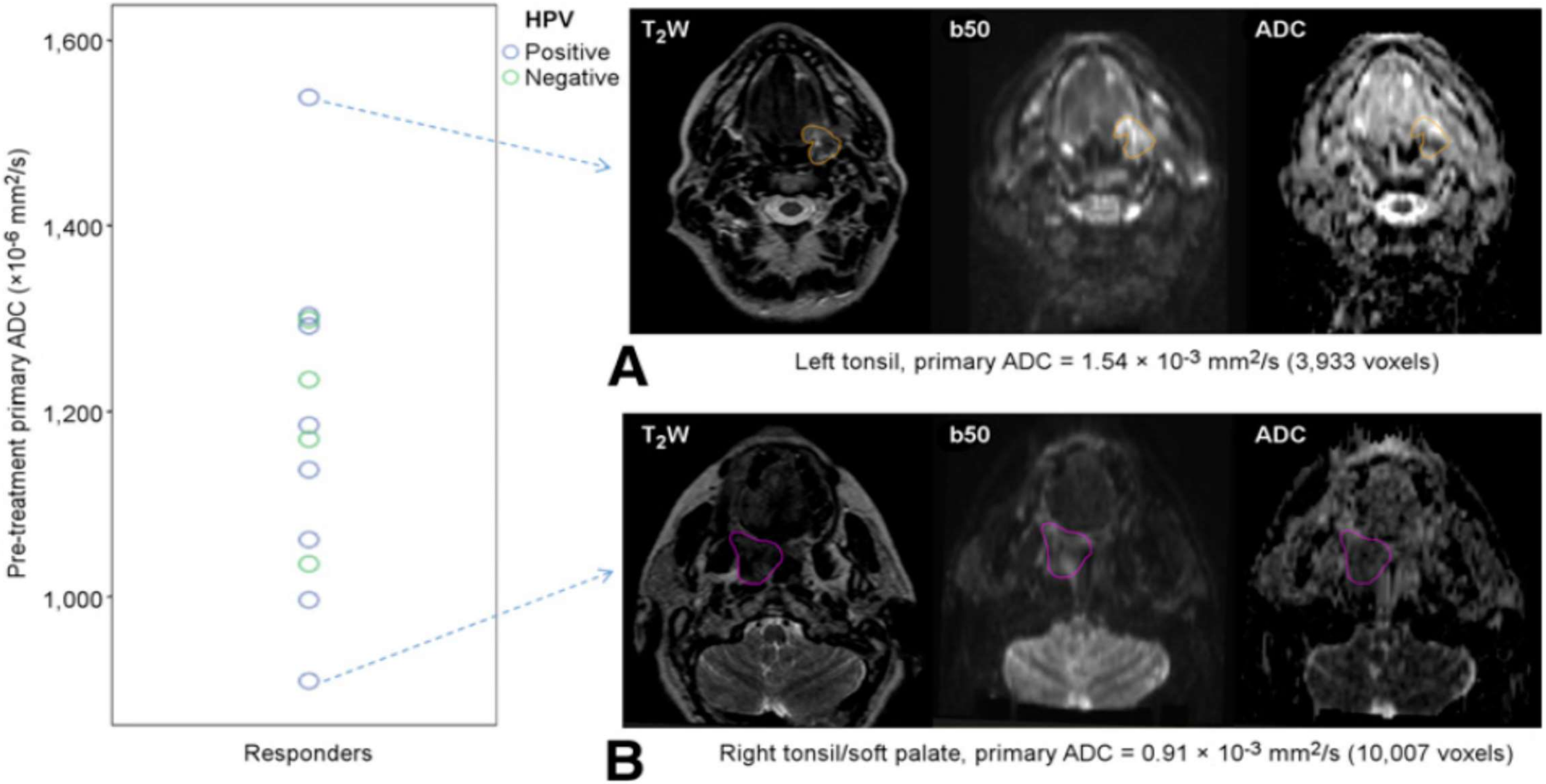
HPV
○ Positive
○ Negative
1,600
1,400
1,200
1,000
Pre-treatment primary ADC (×10⁻⁶ mm²/s)
Responders
T₂W
b50
ADC
A
B

A Left tonsil, primary ADC = 1.54 × 10^{-3} mm^2/s (3,933 voxels)

B Right tonsil/soft palate, primary ADC = 0.91 × 10^{-3} mm^2/s (10,007 voxels)

Wong K.H. et al. J Nucl Med 2016.

Ideally on an MRI-RT machine?

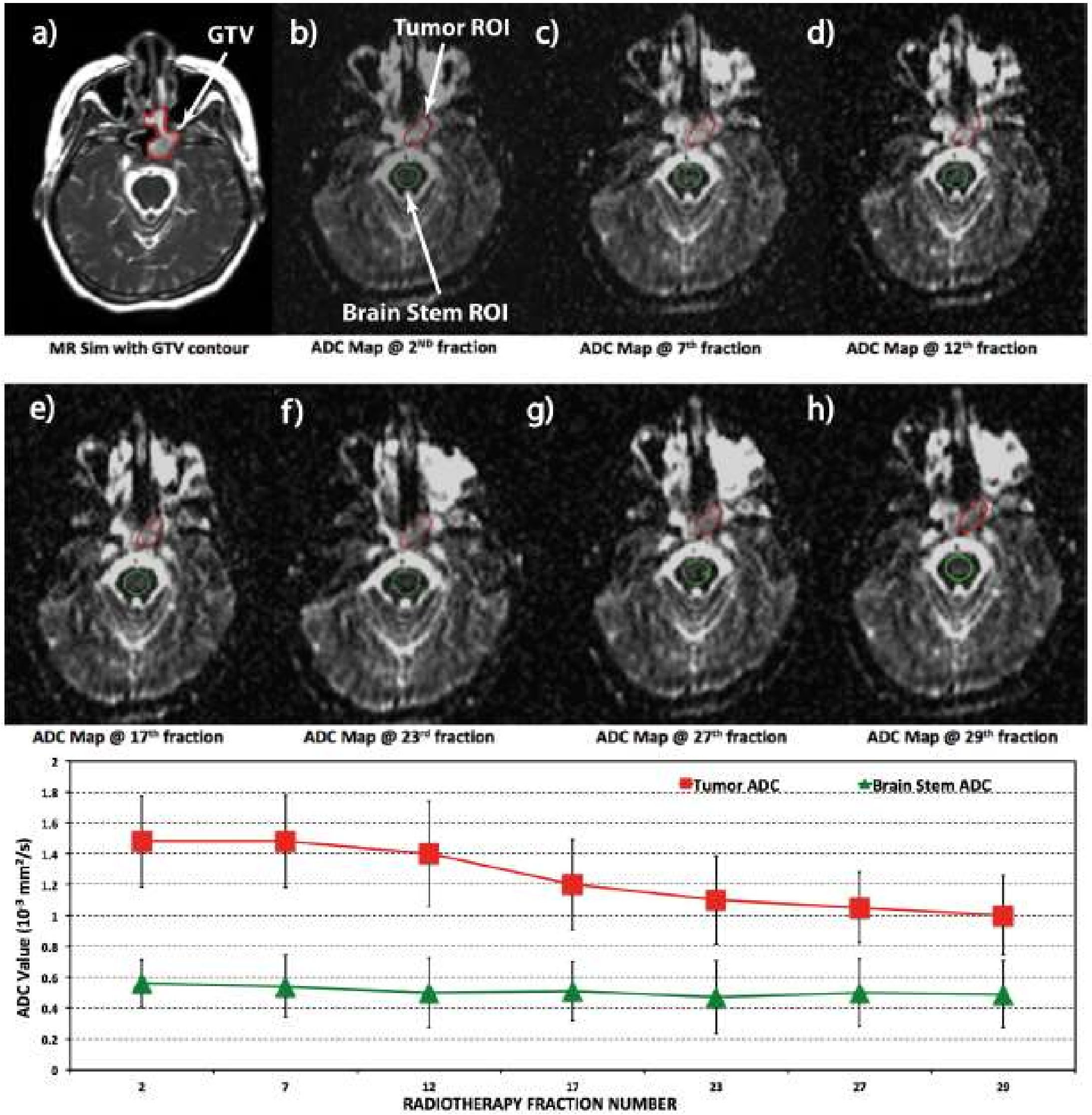
a)
GTV
b)
Tumor ROI
c)
d)
Brain Stem ROI
MR Sim with GTV contour
ADC Map @ 2ND fraction
ADC Map @ 7th fraction
ADC Map @ 12th fraction
e)
f)
g)
h)
ADC Map @ 17th fraction
ADC Map @ 23rd fraction
ADC Map @ 27th fraction
ADC Map @ 29th fraction
Tumor ADC
Brain Stem ADC
ADC Value (10⁻³ mm²/s)
2
1.8
1.6
1.4
1.2
1
0.8
0.6
0.4
0.2
0
2
7
12
17
23
27
29
RADIOTHERAPY FRACTION NUMBER

Yang Y. et al. Med Phys 2016.

5. DWI during follow-up

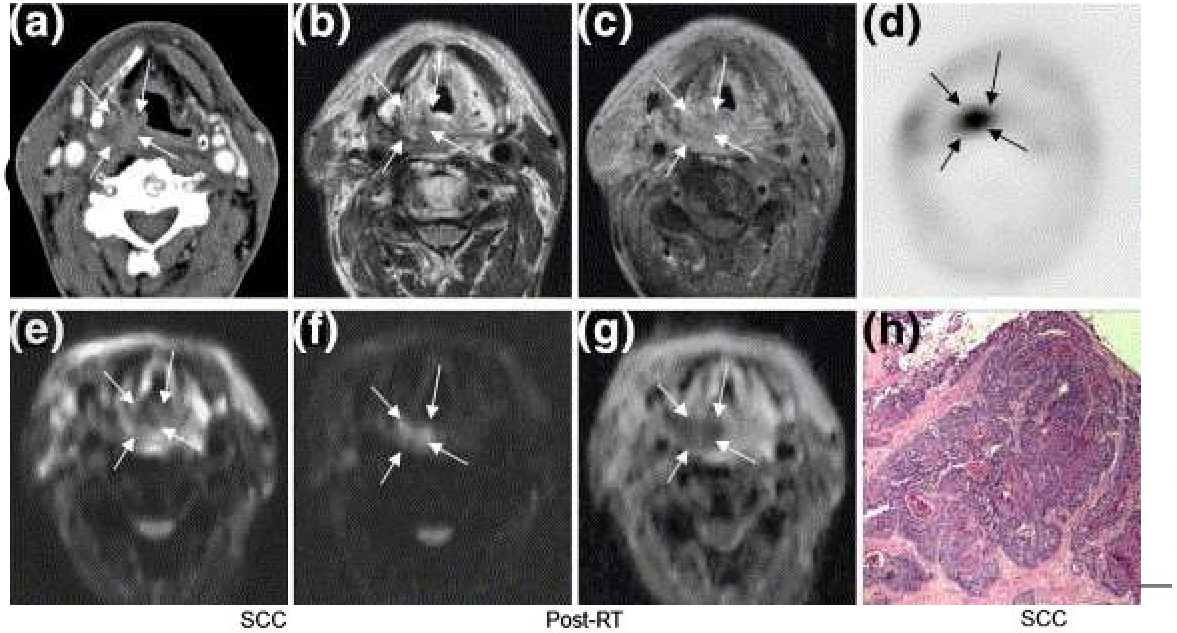

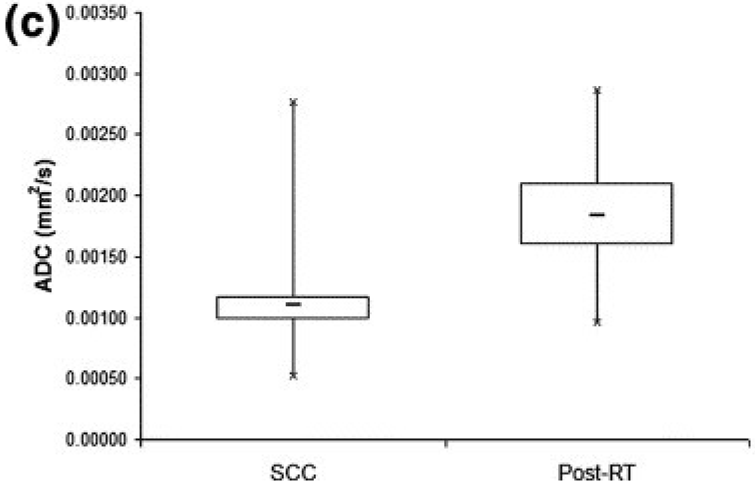

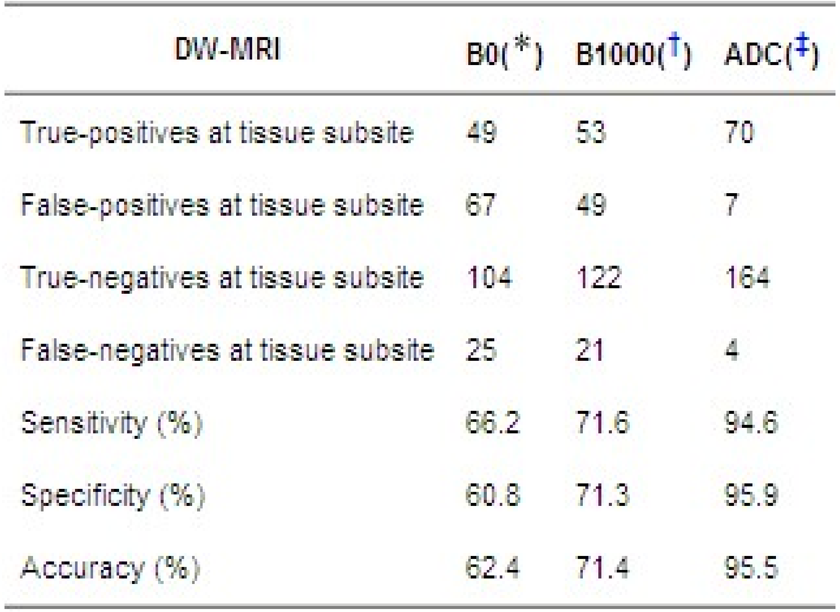

DW-MRI	B0(*)	B1000(†)	ADC(‡)
True-positives at tissue subsite	49	53	70
False-positives at tissue subsite	67	49	7
True-negatives at tissue subsite	104	122	164
False-negatives at tissue subsite	25	21	4
Sensitivity (%)	66.2	71.6	94.6
Specificity (%)	60.8	71.3	95.9
Accuracy (%)	62.4	71.4	95.5

Vandecaveye V. et al. Int J Radiat Oncol Biol Phys 2007.

Clinical example of DWI during follow-up

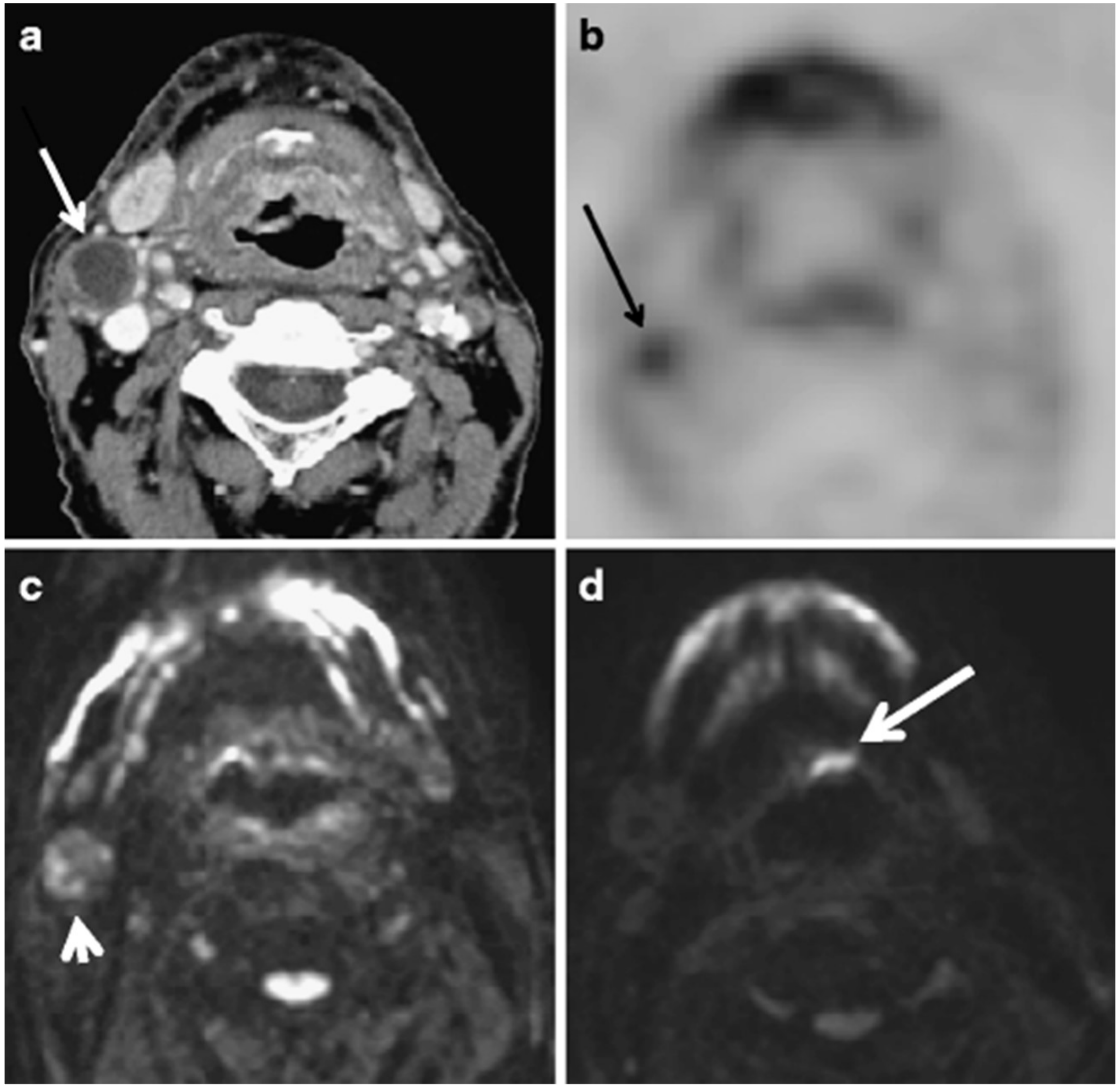

Images courtesy of Prof. V. Vandecaveye

Similar results at Mansoura University (Egypt)

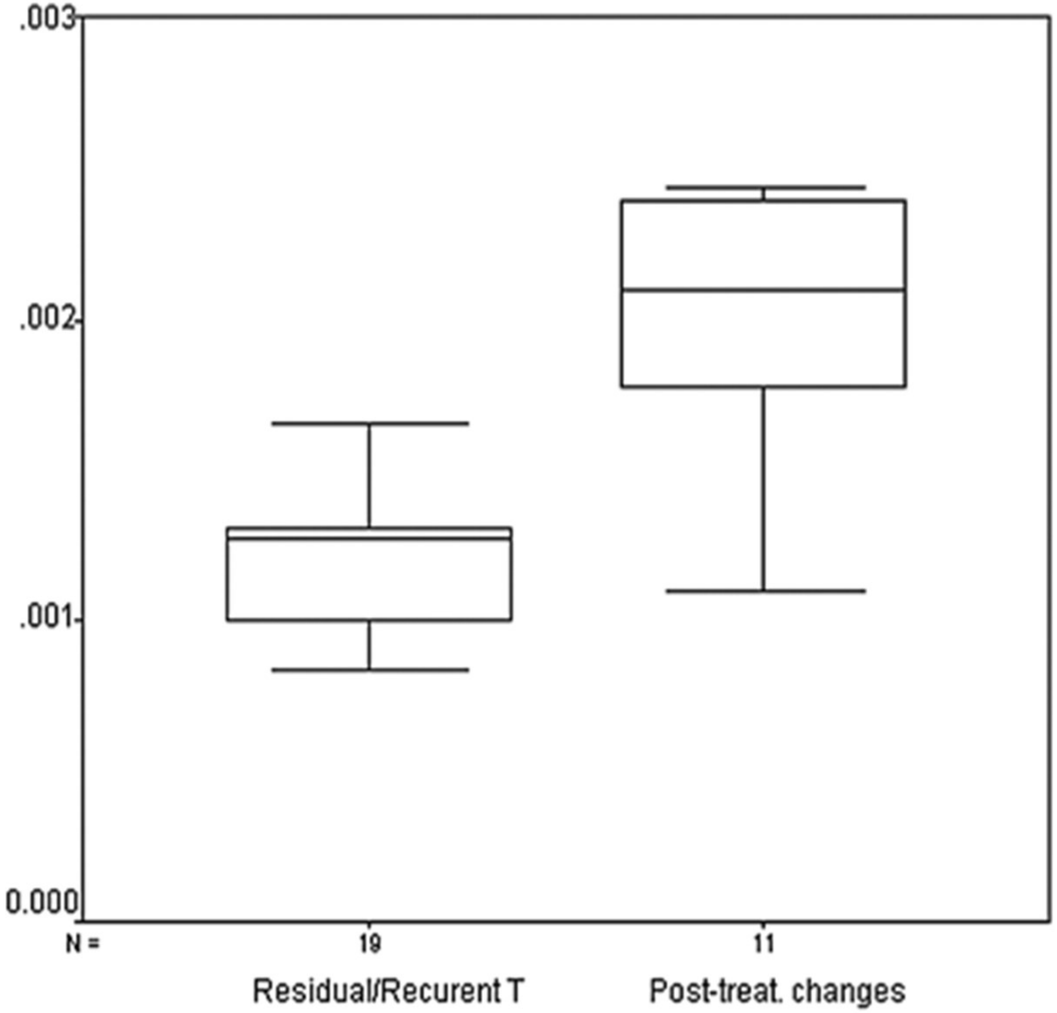

Variable	Range of ADC Value	Mean ADC Value
Residual or recurrent tumor	(0.83–1.65) x 10^{-3} mm^2/s	1.17 ± 0.33 x 10^{-3} mm^2/s
Posttreatment changes	(1.10–2.44) x 10^{-3} mm^2/s	2.07 ± 0.25 x 10^{-3} mm^2/s

Threshold of ADC Value (x10^{-3} mm^2/s)	Sensitivity % (*n*/*N*)	Specificity % (*n*/*N*)	Accuracy %	Positive Predictive Value % (*n*/*N*)	Negative Predictive Value % (*n*/*N*
≤1.00	37 (7/19)	100 (11/11)	60	100 (7/7)	47 (11/23)
≤1.30	84 (16/19)	90 (10/11)	87	94 (16/17)	76 (10/13)
≤1.50	89 (16/19)	73 (9/11)	83	85 (17/20)	80 (8/10)
≤2.00	100 (19/19)	45 (5/11)	80	76 (19/25)	100 (5/5)
≤2.40	100 (19/19)	9 (1/11)	66	65 (19/29)	100 (1/1)

Abdel Razek A. A. et al. AJNR Am J Neuroradiol 2007.

DCE during follow-up

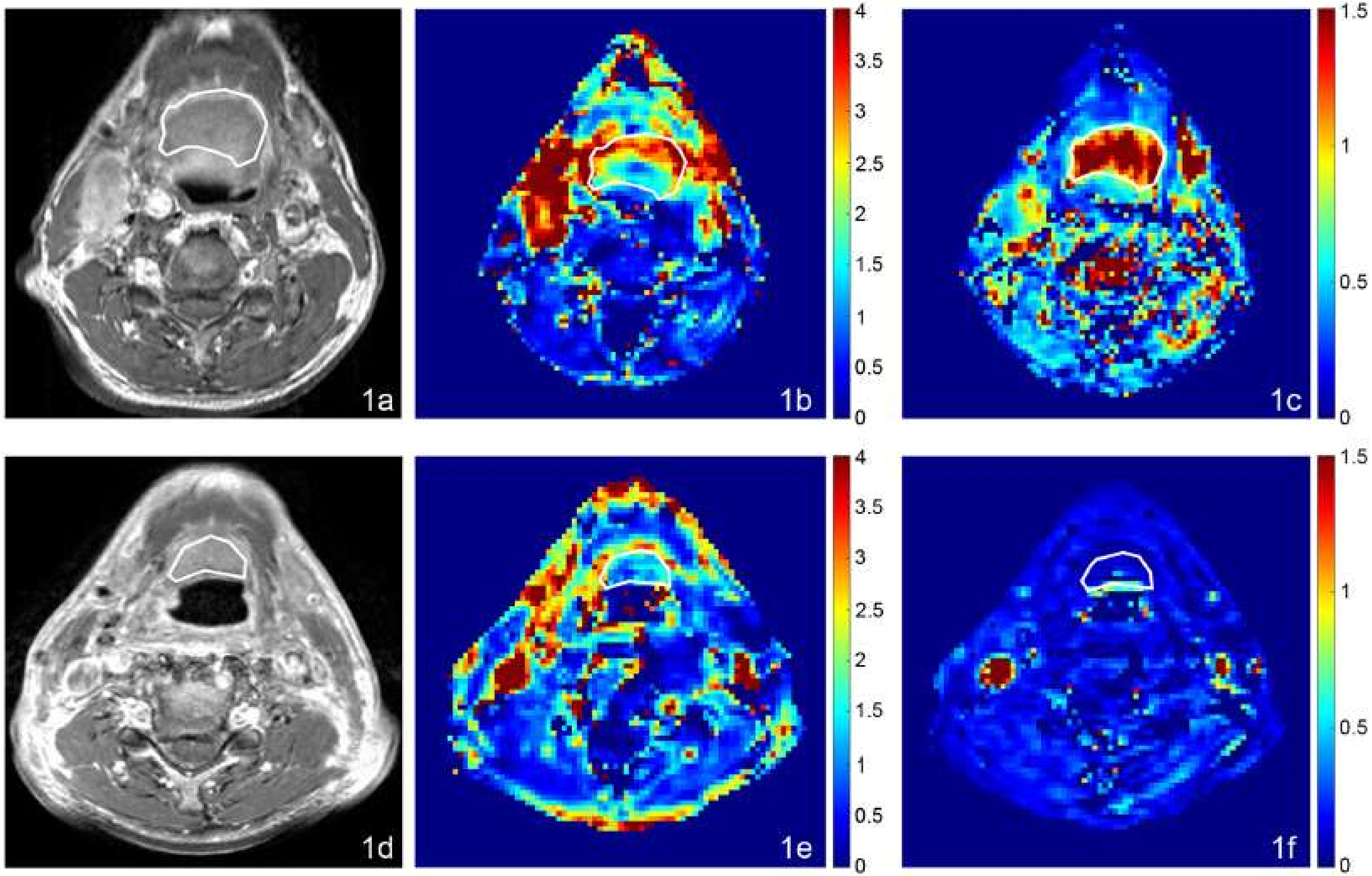

1a
1b
4
3.5
3
2.5
2
1.5
1
0.5
0
1c
1.5
1
0.5
0
1d
1e
4
3.5
3
2.5
2
1.5
1
0.5
0
1f
1.5
1
0.5
0

Pre-treatment DCE-MRI did not predict which SCC sites would fail treatment, but post-treatment DCE-MRI showed potential for identifying residual masses that had failed treatment.

King A. et al. Plos One 2016.

6. Organ-sparing

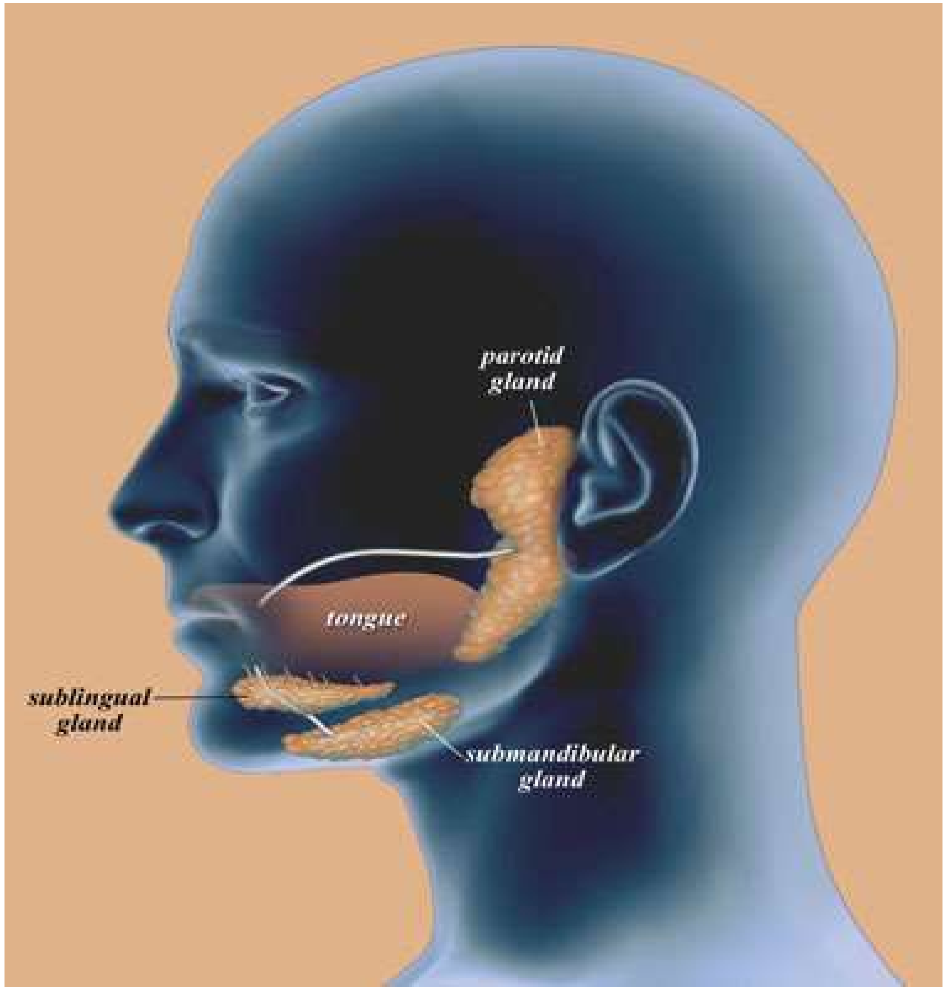
parotid gland
tongue
sublingual gland
submandibular gland

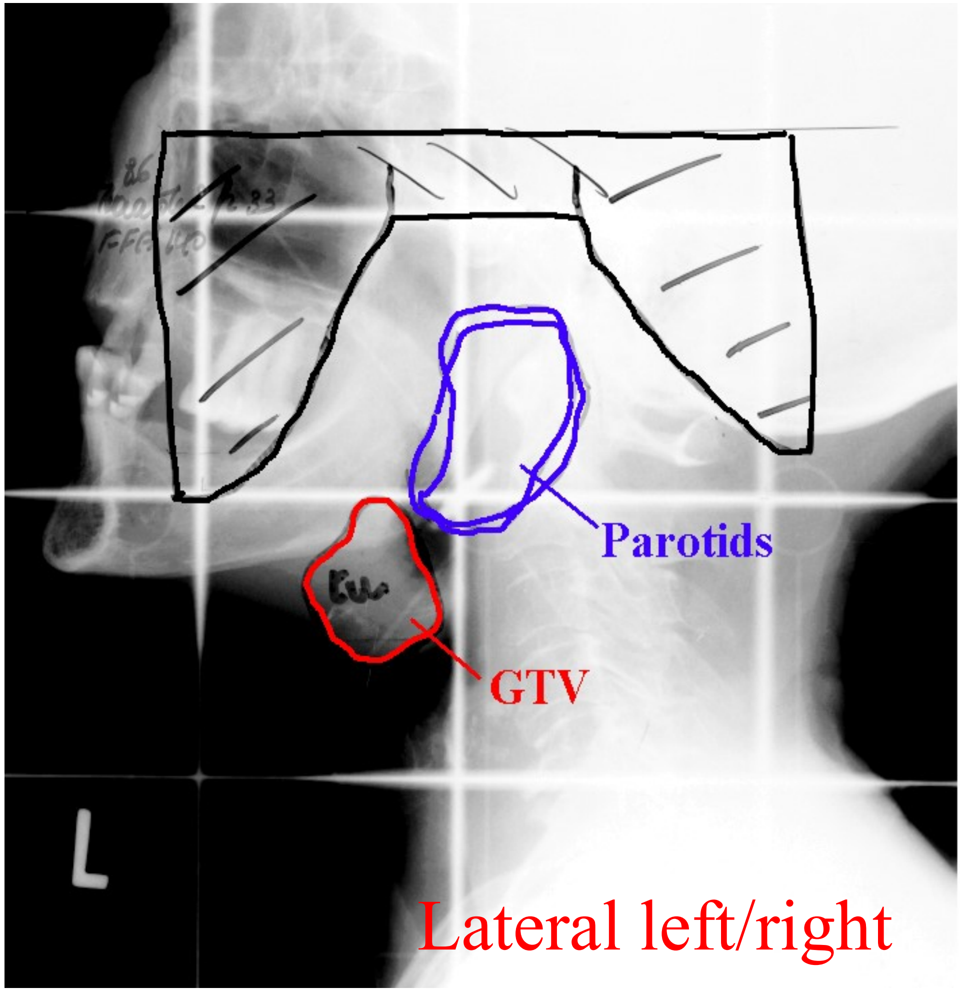
Parotids
GTV
L
Lateral left/right

Xerostomia is one of the most common complications of RT for HNC.

Dirix P. et al. Cancer 2006.
Dirix P. et al. Lancet Oncol 2010.

PARSPORT trial

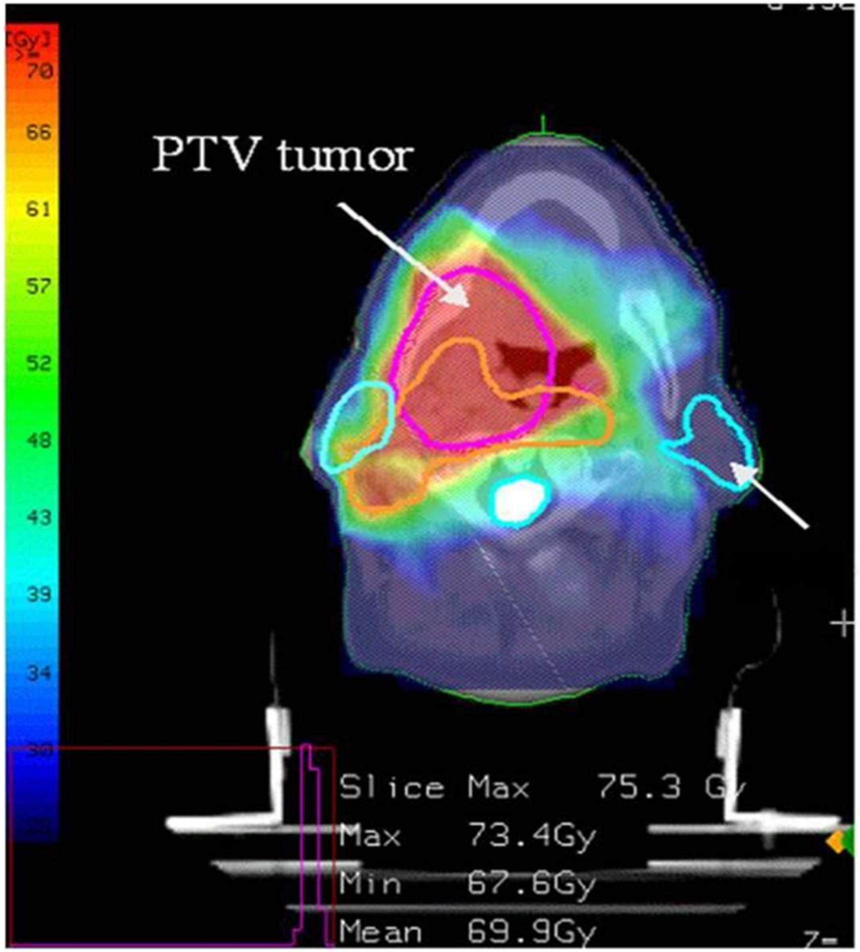
[Gy]
>=
70
66
61
57
52
48
43
39
34
PTV tumor
Slice Max 75.3 Gy
Max 73.4Gy
Min 67.6Gy
Mean 69.9Gy

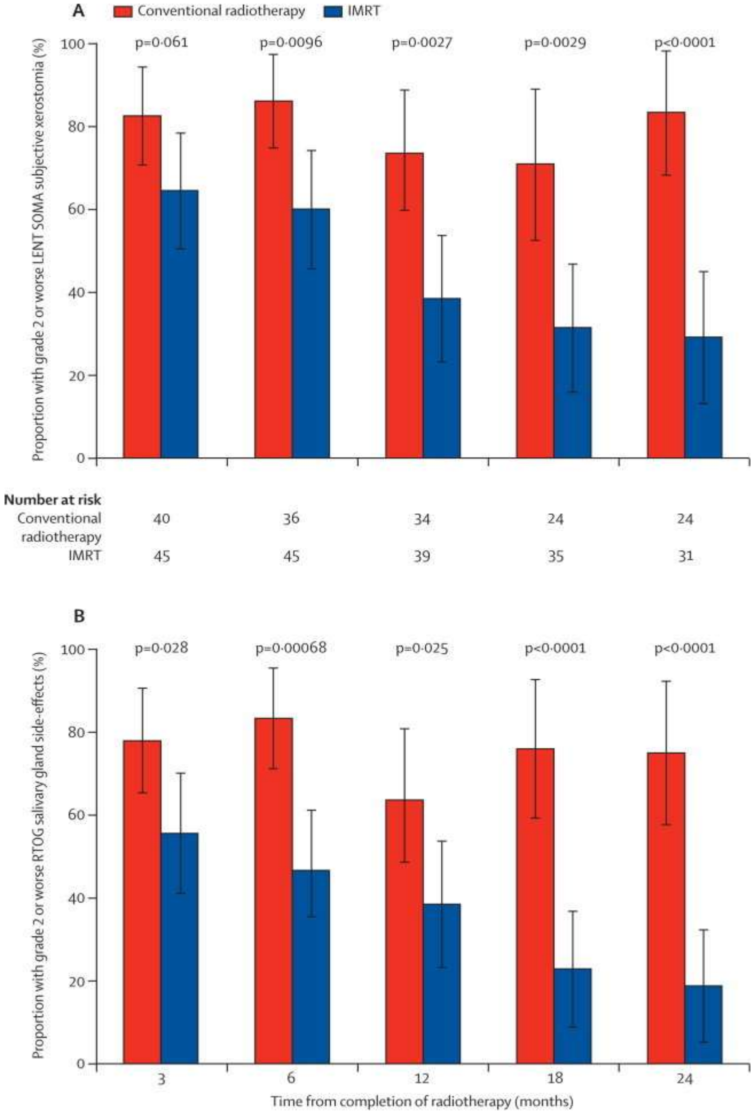

A

Number at risk					
Conventional radiotherapy	40	36	34	24	24
IMRT	45	45	39	35	31

B

Number at risk					
Conventional radiotherapy	41	36	34	25	24
IMRT	45	45	39	35	32

Nutting C.M. et al. Lancet Oncol 2011.

DWI: non-invasive evaluation of salivary gland function

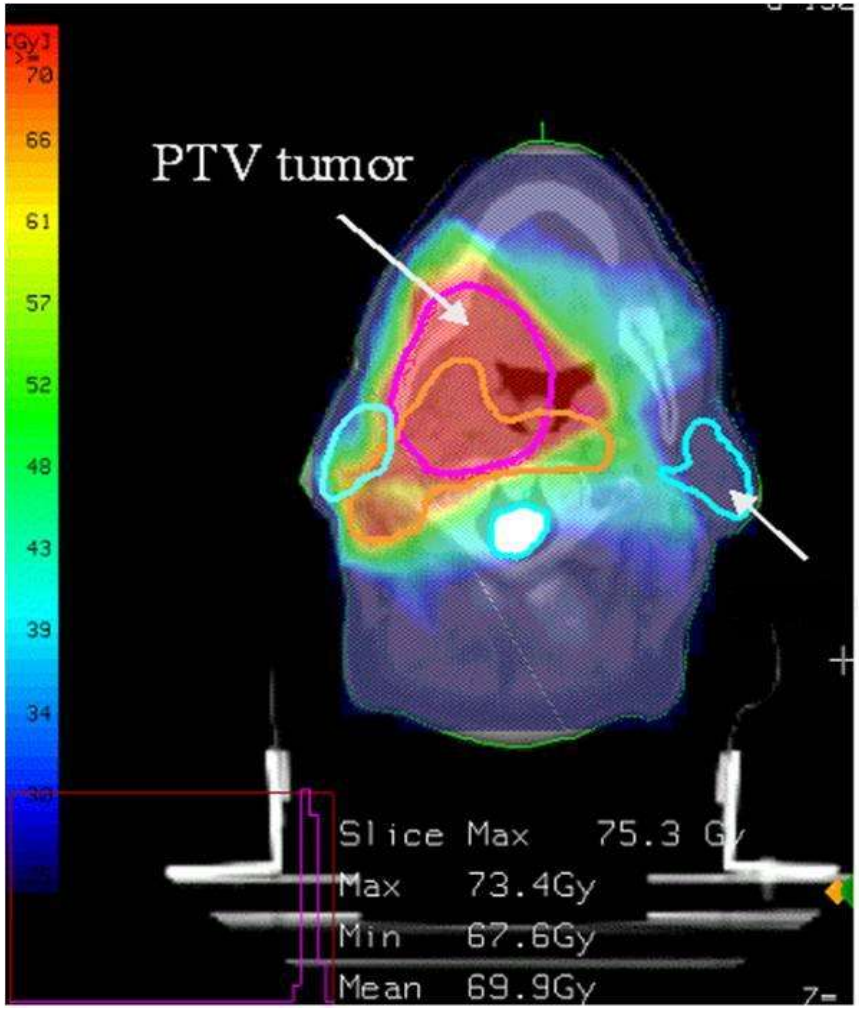
[Gy] >=
70
66
61
57
52
48
43
39
34
PTV tumor
Slice Max 75.3 Gy
Max 73.4Gy
Min 67.6Gy
Mean 69.9Gy

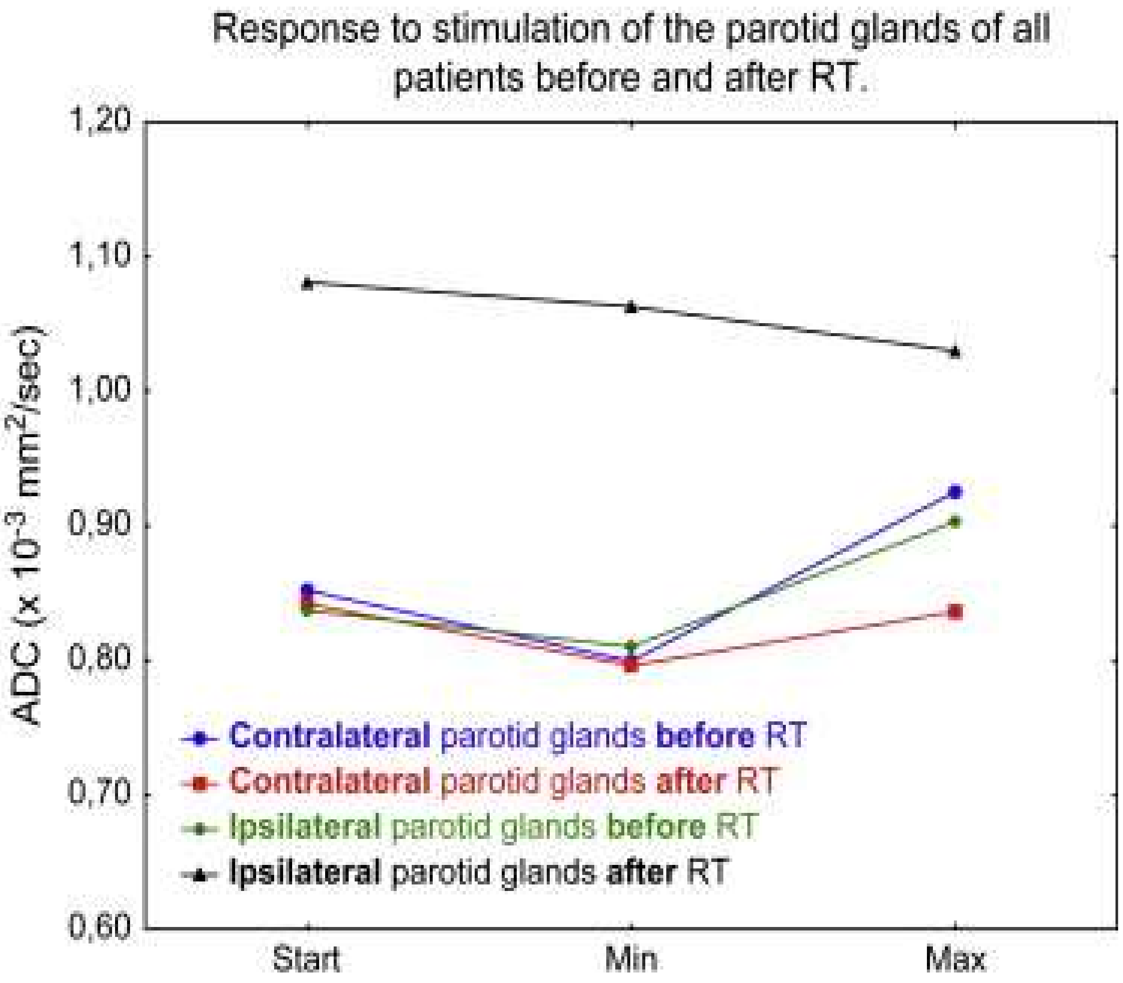

Dirix P. et al. Int J Radiat Oncol Biol Phys 2007.

DWI: non-invasive evaluation of salivary gland function

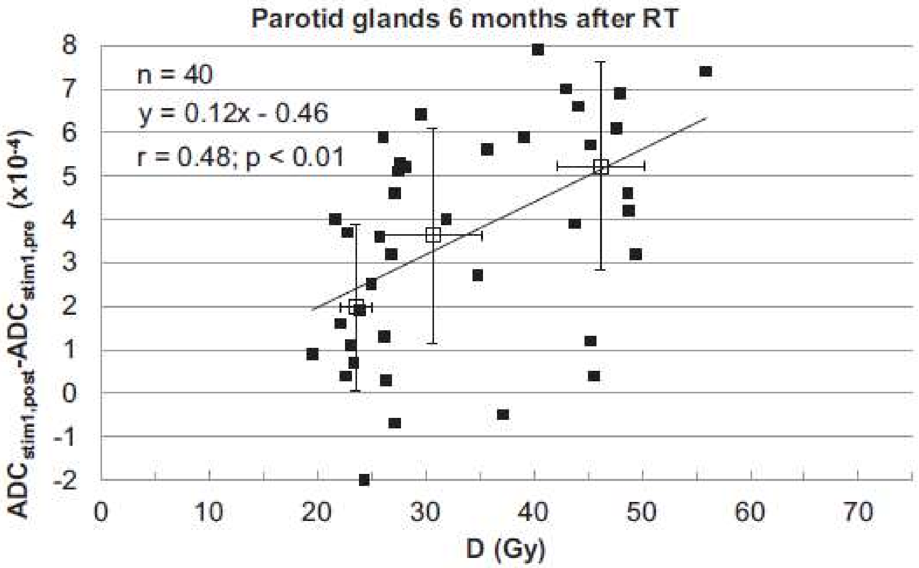
Parotid glands 6 months after RT

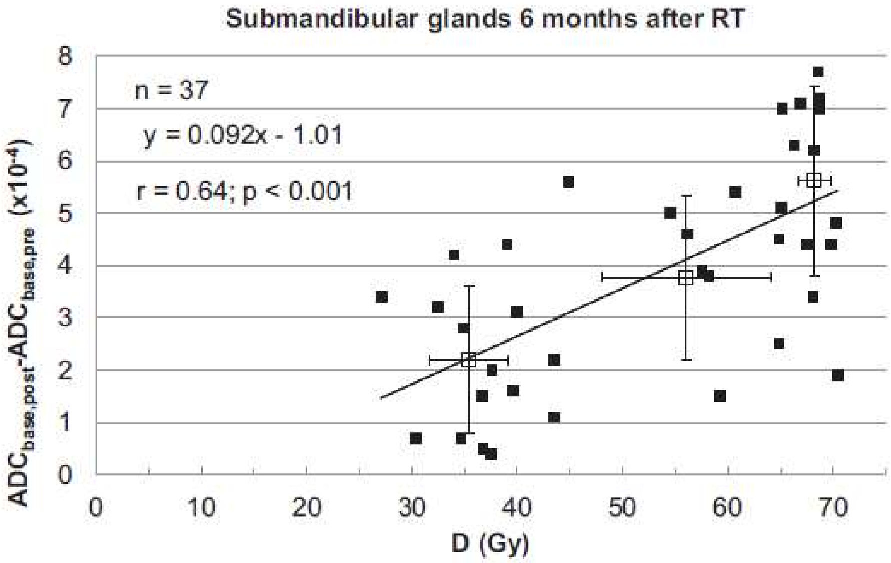
Submandibular glands 6 months after RT

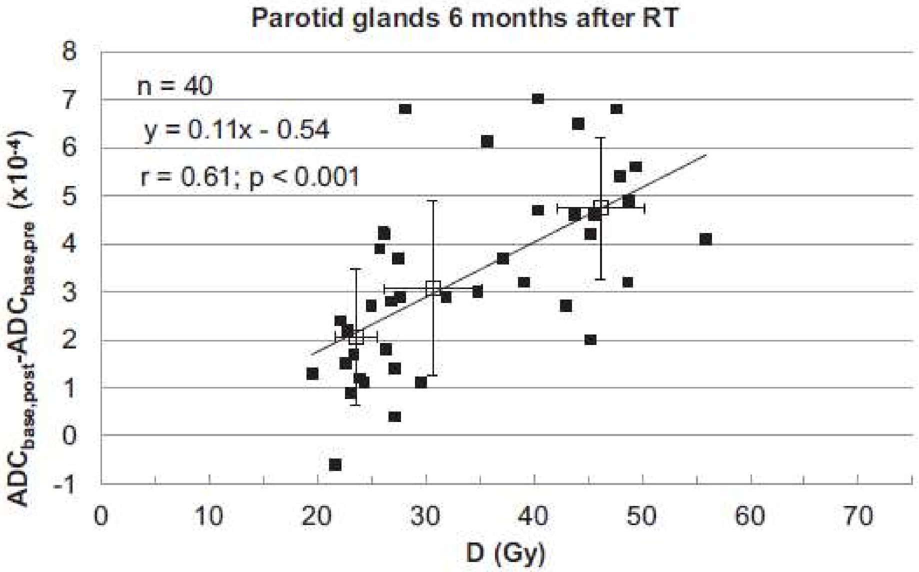
Parotid glands 6 months after RT

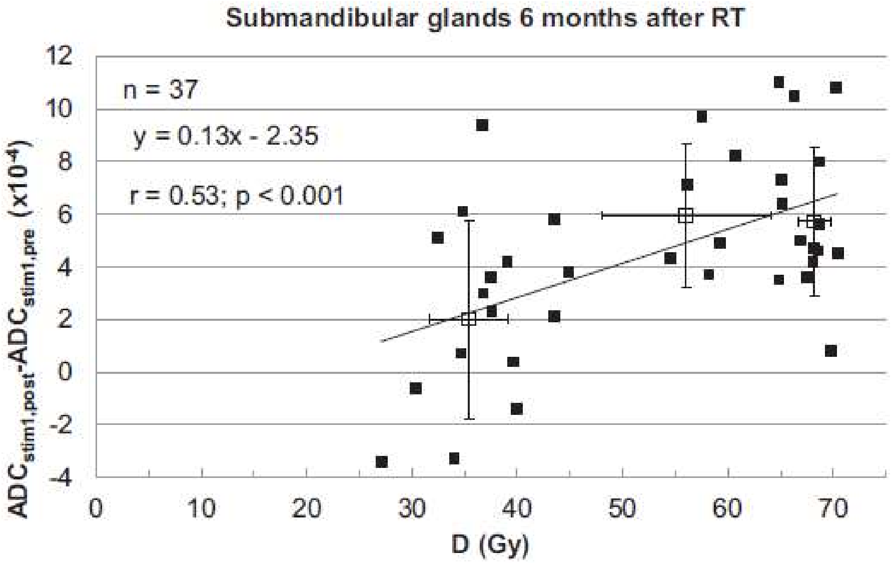
Submandibular glands 6 months after RT

Loimu V. et al. Radiother Oncol 2016.

7. Pitfalls of DWI

Rapid evolution of body imaging protocols

Divergence among and between vendors on data measurements/analysis and lack of transparency on how measurements are made

No accepted standards for measurements and analysis

Multiple data acquisition protocols depending on body part and usage of data

Qualitative to quantitative assessments

Lack of understanding of DW-MRI at a microscopic level

Multiexponential decay components which affect the calculated ADC values

Incomplete validation and documentation of reproducibility

Divergent nomenclature and symbols

Lack of multicenter working methodologies, accepted quality assurance (QA) standards, and physiologically realistic phantoms

Padhani A.R. et al. Neoplasia 2009.

Registration (1)

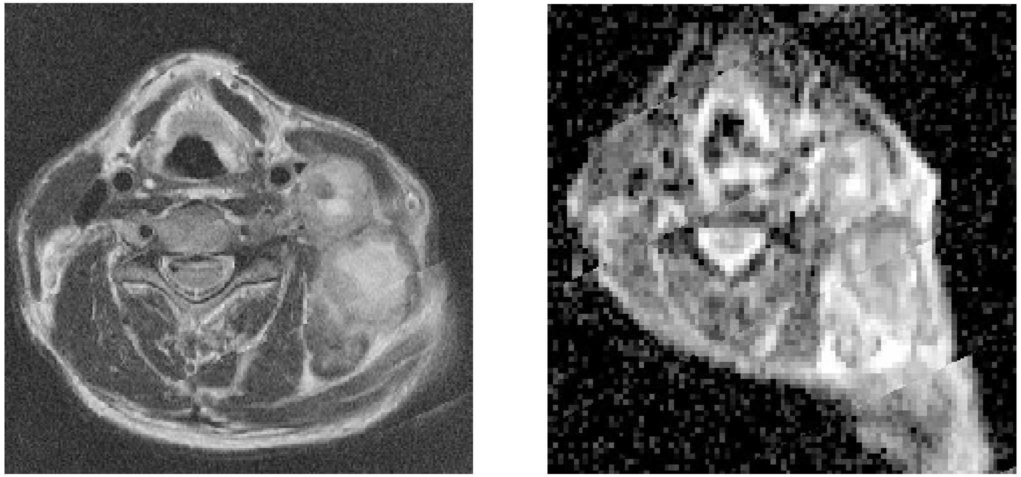

Non-rigid registration needed for distortion

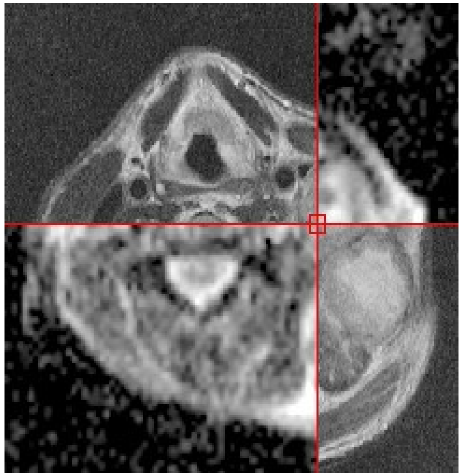

Registration (2)

	Mean error	SD	Median error	Maximal error
Original SSD	7.78 mm	4.15 mm	7.10 mm	20.26 mm
Final SSD	2.10 mm	1.39 mm	1.83 mm	6.53 mm

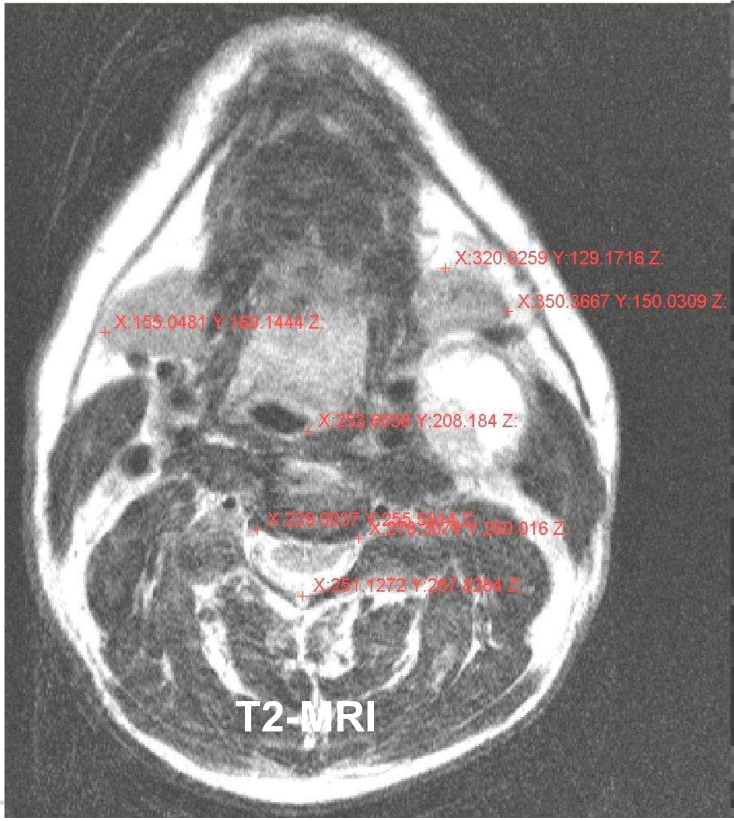
X:320.0259 Y:129.1716 Z:
X:350.3667 Y:150.0309 Z:
X:155.0481 Y:160.1444 Z:
X:253.6556 Y:208.184 Z:
X:229.0037 Y:255.3614 Z:
X:278.3074 Y:290.016 Z:
X:251.1272 Y:287.8284 Z:
T2-MRI

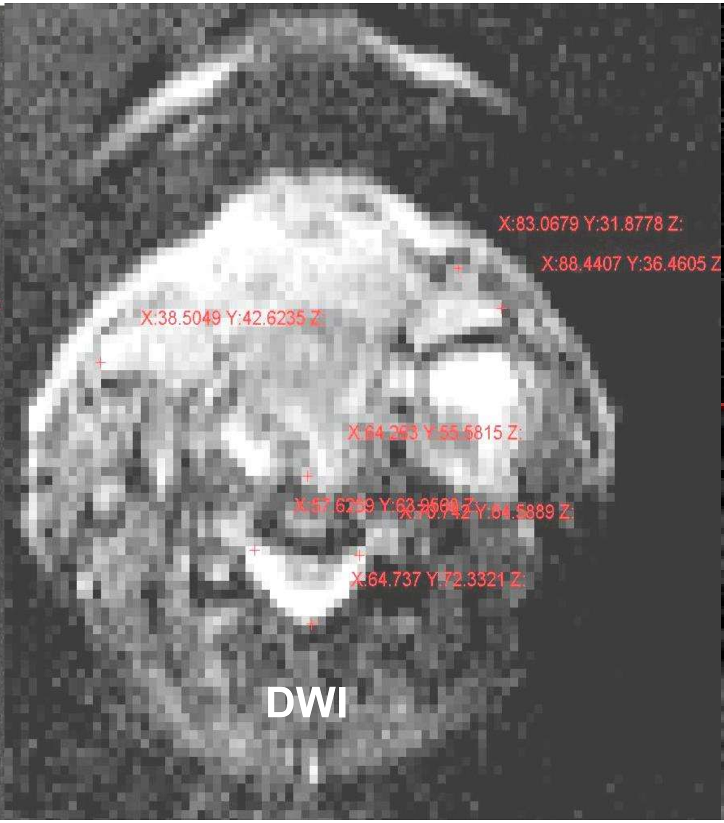
X:83.0679 Y:31.8778 Z:
X:88.4407 Y:36.4605 Z
X:38.5049 Y:42.6235 Z:
X:64.263 Y:55.5815 Z:
X:57.6259 Y:63.9560 Z:
X:70.742 Y:64.5889 Z:
X:64.737 Y:72.3321 Z:
DWI

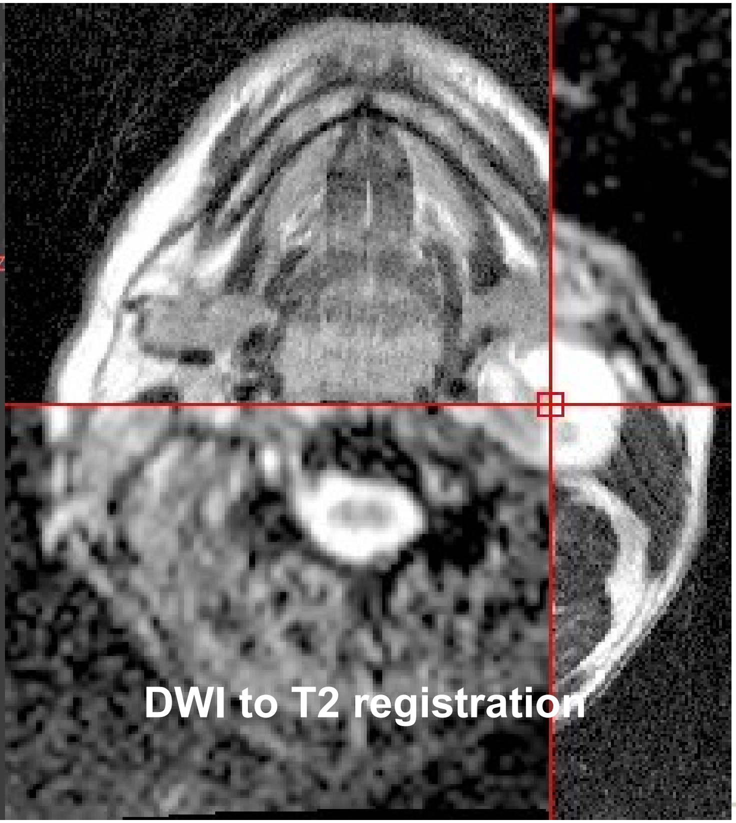
DWI to T2 registration

Registration (3)

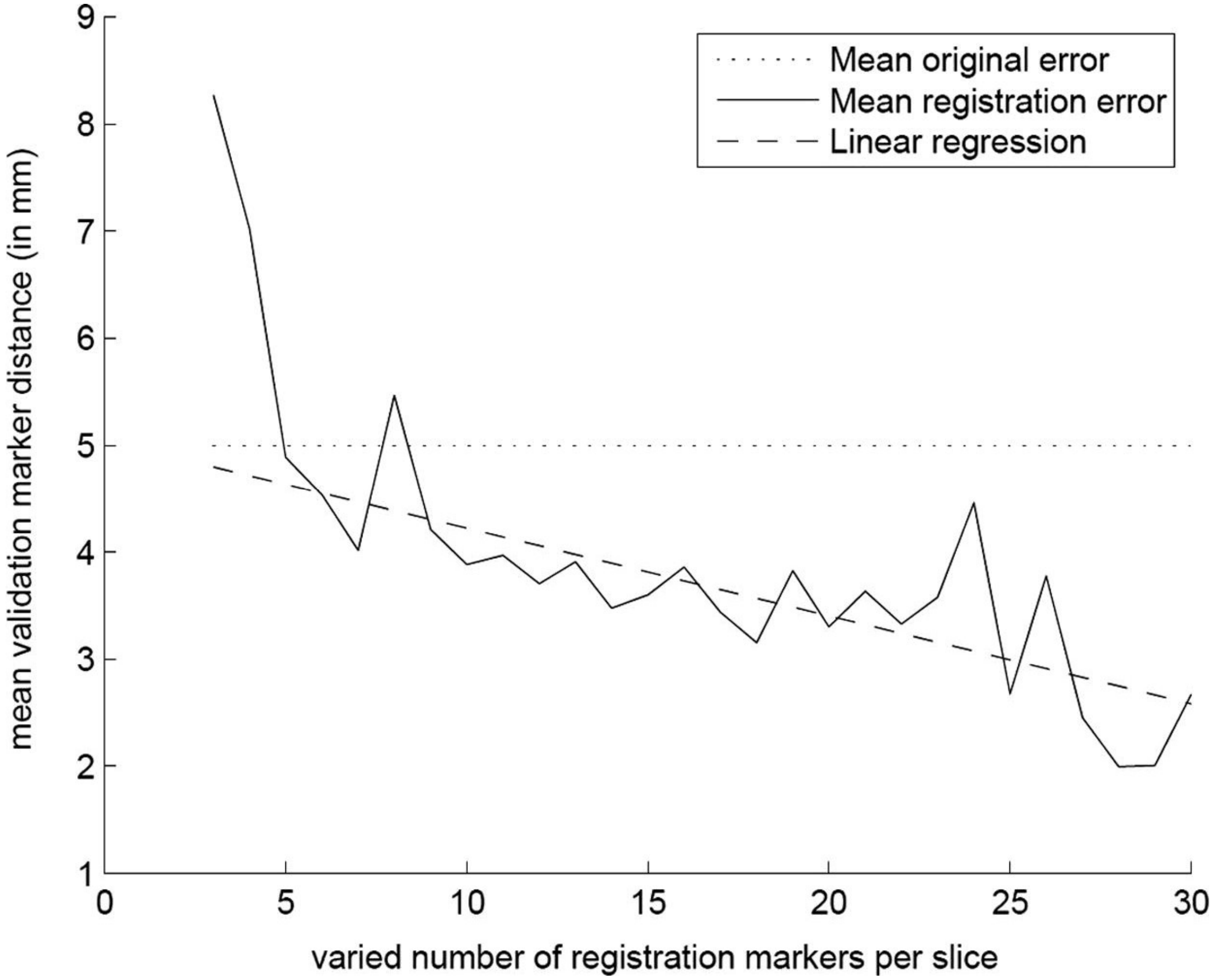

Lambrecht M. et al. Radiother Oncol 2014.

Conclusions

- **Important role for anatomical MRI, especially in base of skull and oropharyngeal cancer.**
- **DWI and DCE-MRI could guide dose-painting and early response assessment.**
- **Standardisation of technique (b-values), interpretation, and registration.**

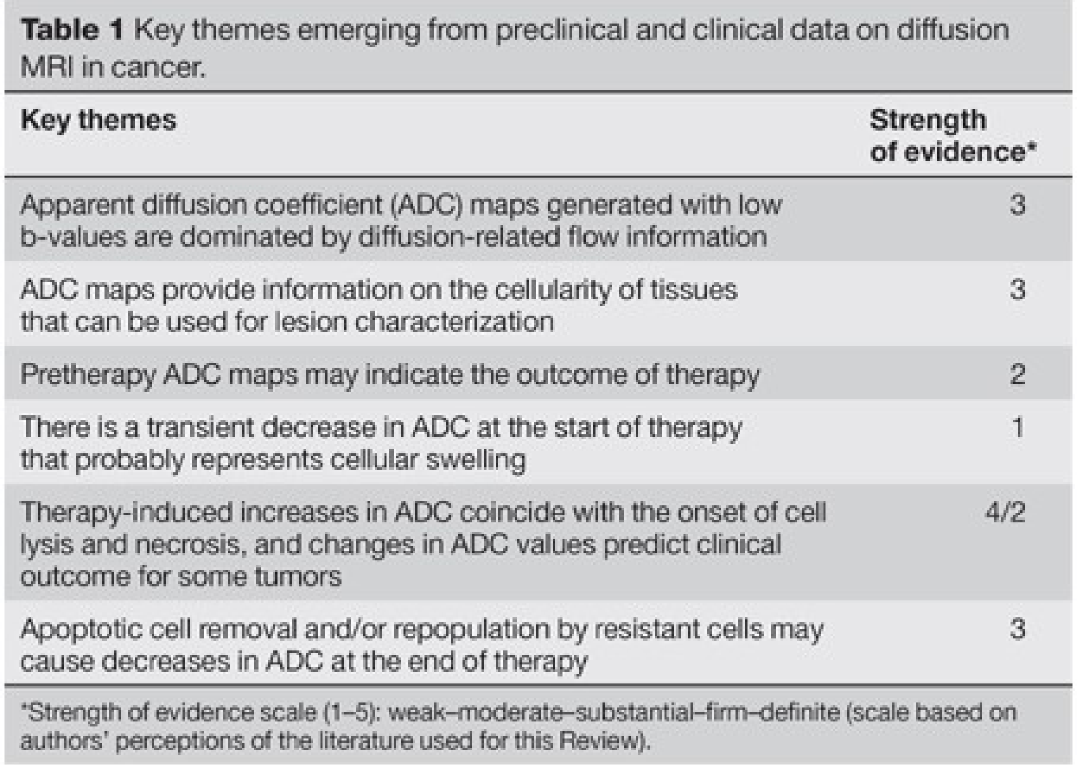

Table 1 Key themes emerging from preclinical and clinical data on diffusion MRI in cancer.

Key themes	Strength of evidence*
Apparent diffusion coefficient (ADC) maps generated with low b-values are dominated by diffusion-related flow information	3
ADC maps provide information on the cellularity of tissues that can be used for lesion characterization	3
Pretherapy ADC maps may indicate the outcome of therapy	2
There is a transient decrease in ADC at the start of therapy that probably represents cellular swelling	1
Therapy-induced increases in ADC coincide with the onset of cell lysis and necrosis, and changes in ADC values predict clinical outcome for some tumors	4/2
Apoptotic cell removal and/or repopulation by resistant cells may cause decreases in ADC at the end of therapy	3

*Strength of evidence scale (1–5): weak–moderate–substantial–firm–definite (scale based on authors' perceptions of the literature used for this Review).

Patterson D.M. et al. Nat Clin Pract Oncol 2008.

Personalized precision radiotherapy for HNC

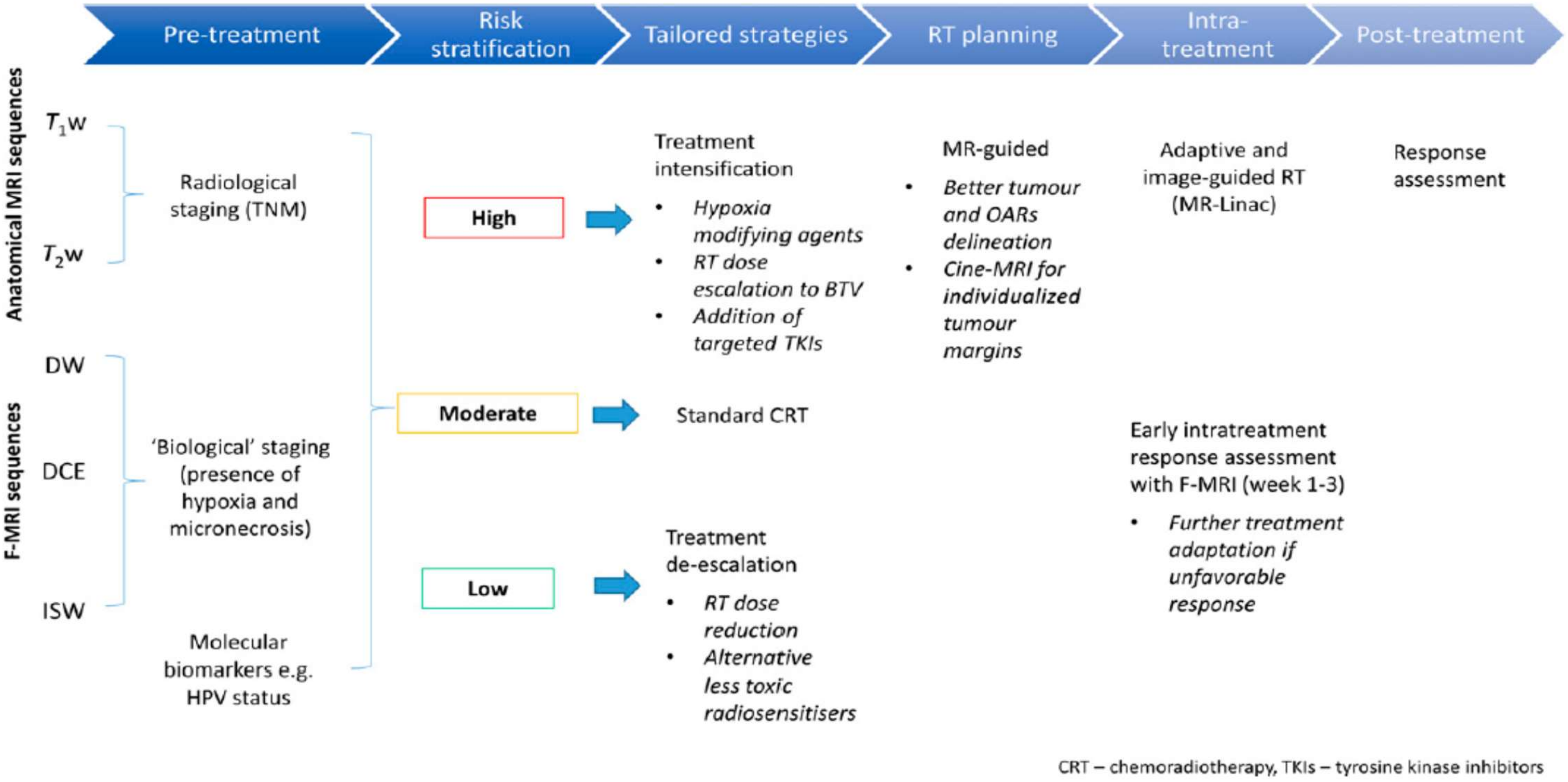

Pre-treatment

Risk stratification

Tailored strategies

RT planning

Intra-treatment

Post-treatment

Anatomical MRI sequences

T_1w

T_2w

Radiological staging (TNM)

F-MRI sequences

DW

DCE

ISW

'Biological' staging (presence of hypoxia and micronecrosis)

Molecular biomarkers e.g. HPV status

High

Treatment intensification

- *Hypoxia modifying agents*
- *RT dose escalation to BTV*
- *Addition of targeted TKIs*

Moderate

Standard CRT

Low

Treatment de-escalation

- *RT dose reduction*
- *Alternative less toxic radiosensitisers*

MR-guided

- *Better tumour and OARs delineation*
- *Cine-MRI for individualized tumour margins*

Adaptive and image-guided RT (MR-Linac)

Early intratreatment response assessment with F-MRI (week 1-3)

- *Further treatment adaptation if unfavorable response*

Response assessment

CRT – chemoradiotherapy, TKIs – tyrosine kinase inhibitors

Wong K.H. et al. Br J Radiol 2017.

Introduction to Computed Tomography

Francesco Pisana

German Cancer Research Center (DKFZ), Heidelberg, Germany

Index of Contents

- **Introduction:**
  - Overview and components
  - History
- **Physics:**
  - X-ray generation
  - X-ray attenuation
  - X-ray detection
- **Image reconstruction:**
  - Filtered back-projection
  - Algebraic reconstructions
- **Noise and artifacts:**
  - Noise
  - Motion artifacts
  - Beam hardening artifacts
- **Dose and image quality:**
  - mAs modulation
  - kV selection

Overview and Components

Computed tomography shows the spatial distribution of X-ray attenuation in our body.

SIEMENS
SOMATOM Force

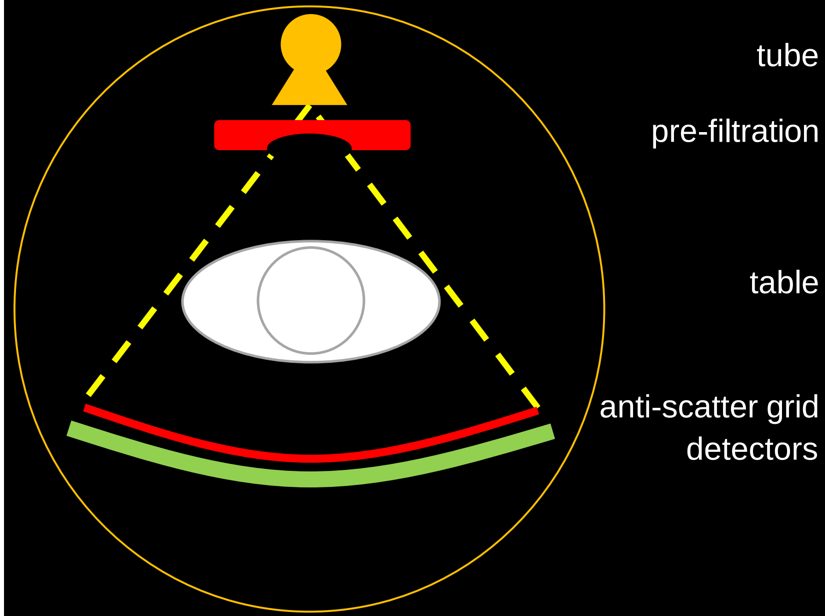
tube
pre-filtration
table
anti-scatter grid
detectors

Overview and Components

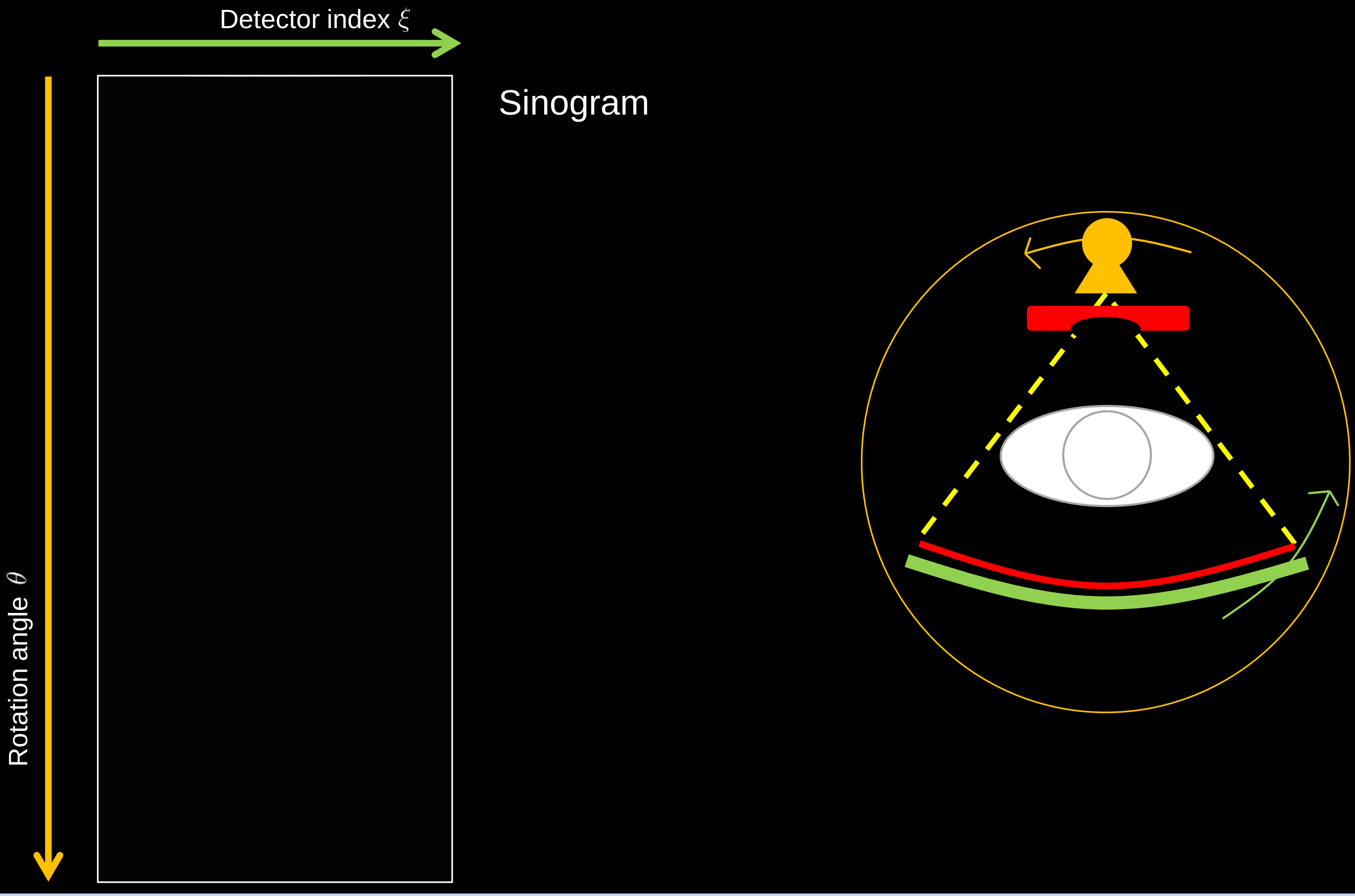
Detector index ξ
Sinogram
Rotation angle θ

History

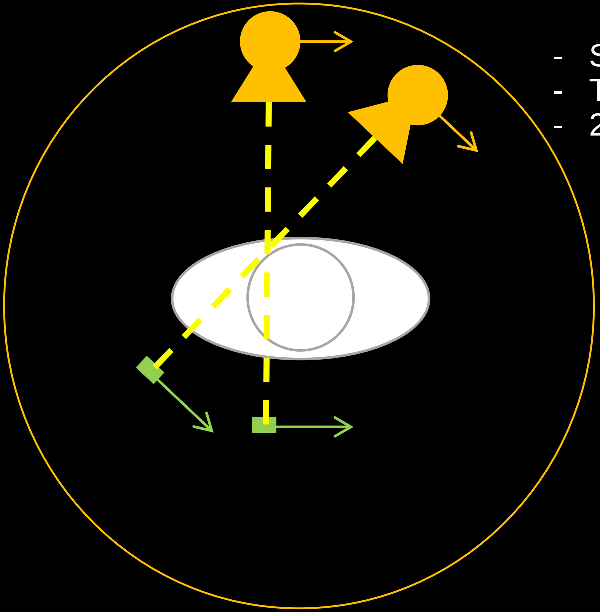

- Single detector
- Translation + rotation
- 20-30 min

- Multi-detector
- Translation + rotation
- 2 min

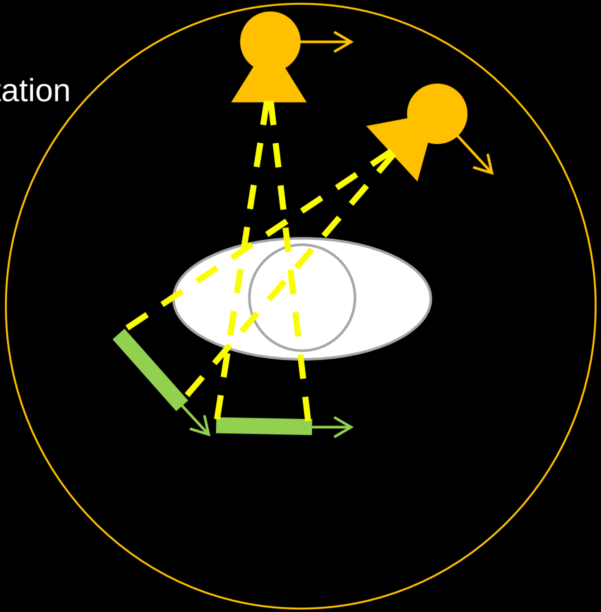

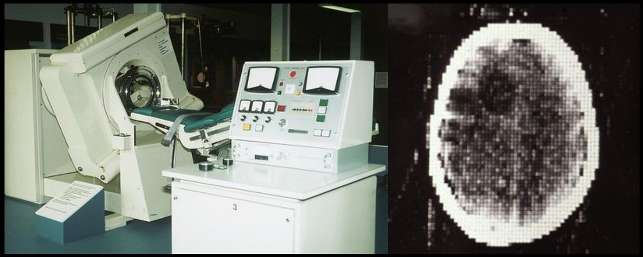

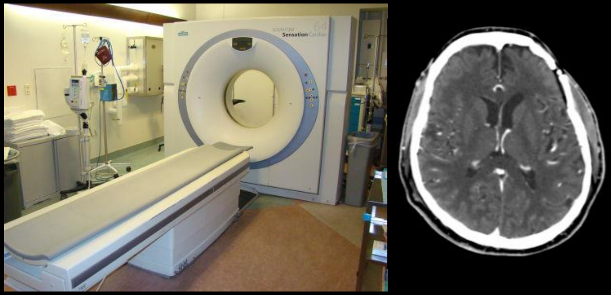

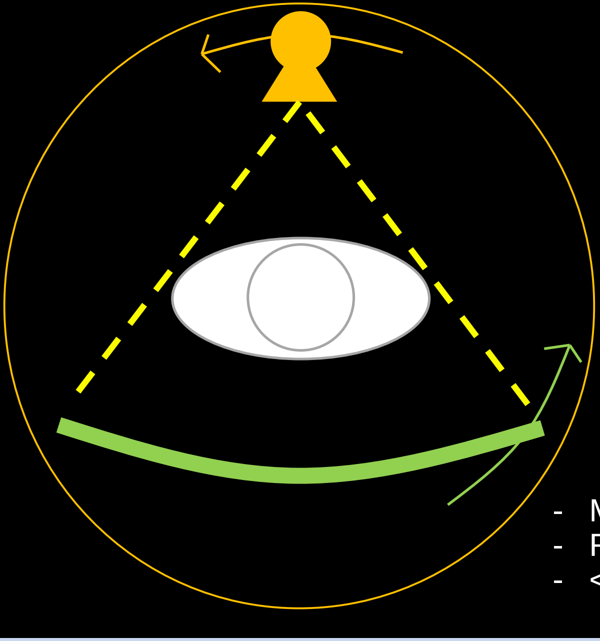

- Multi-detector
- Rotation
- < 1 s

- Full multi-detector ring stationary
- Tube rotation
- < 1 s

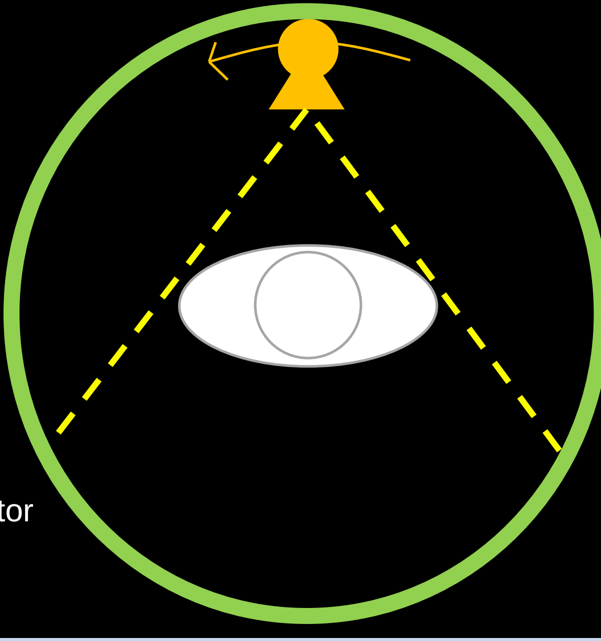

Nowadays CT

Procedure:
Transcatheter aortic valve implantation (TAVI)

Patient age: 80 years

Tube voltage: 80 kV
Current: 340 ref mAs/rot

Rotation time: 0.25 s
Pitch: 3.2
Slice thickness: 0.75 mm
Scan length: 557 mm
Scan time: 0.76 s
Scan speed: 737 mm/s

Kernel : B40
Recon: ADMIRE 3

CTDIvol: 2.7 mGy
DLP: 162 mGy·cm
Effective dose: 2.3 mSv

Case information

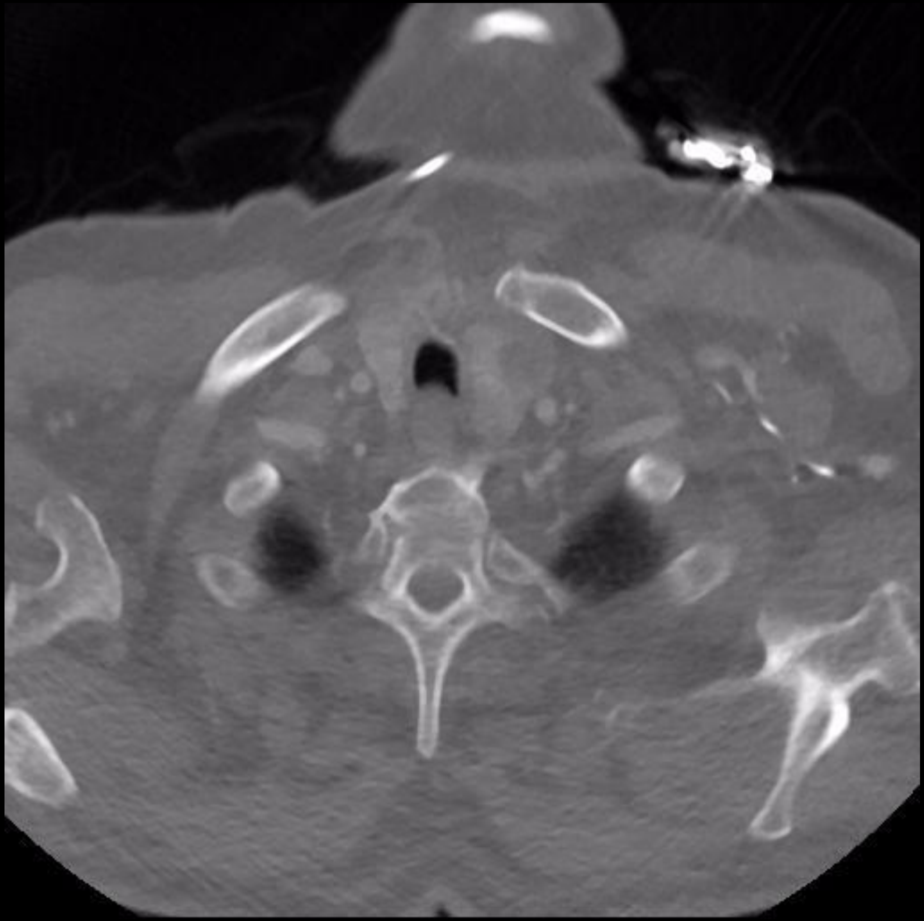

Axial slices, *C* = 0 HU, *W* = 1500 HU

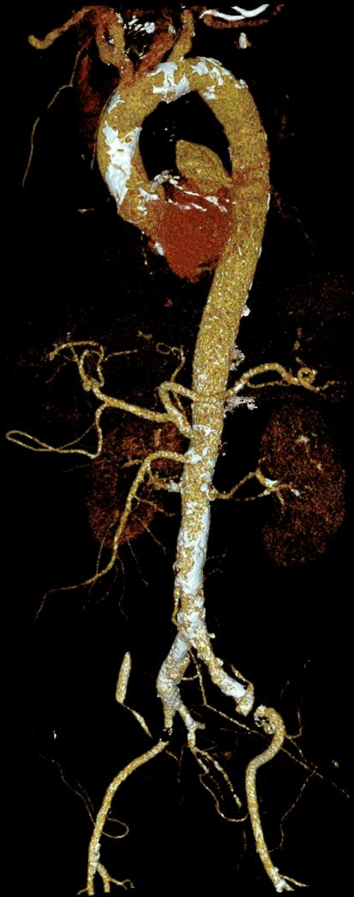

Volume Rendering

Detector Coverage Along z-axis

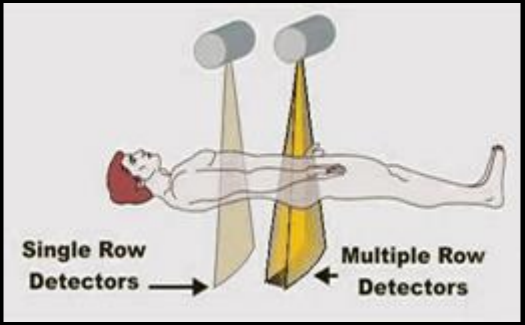
Single Row
Detectors
Multiple Row
Detectors

Pitch value:

$$\text{pitch} = \frac{\text{Table movement in one rotation}}{\text{Coverage}}$$

Index of Contents

- **Introduction:**
  - **Overview and components**
  - **History**
- **Physics:**
  - **X-ray generation**
  - **X-ray attenuation**
  - **X-ray detection**
- **Image reconstruction:**
  - **Filtered back-projection**
  - **Algebraic reconstructions**
- **Noise and artifacts:**
  - **Noise**
  - **Motion artifacts**
  - **Beam hardening artifacts**
- **Dose and image quality:**
  - **mAs modulation**
  - **kV selection**

X-ray Spectrum Generation

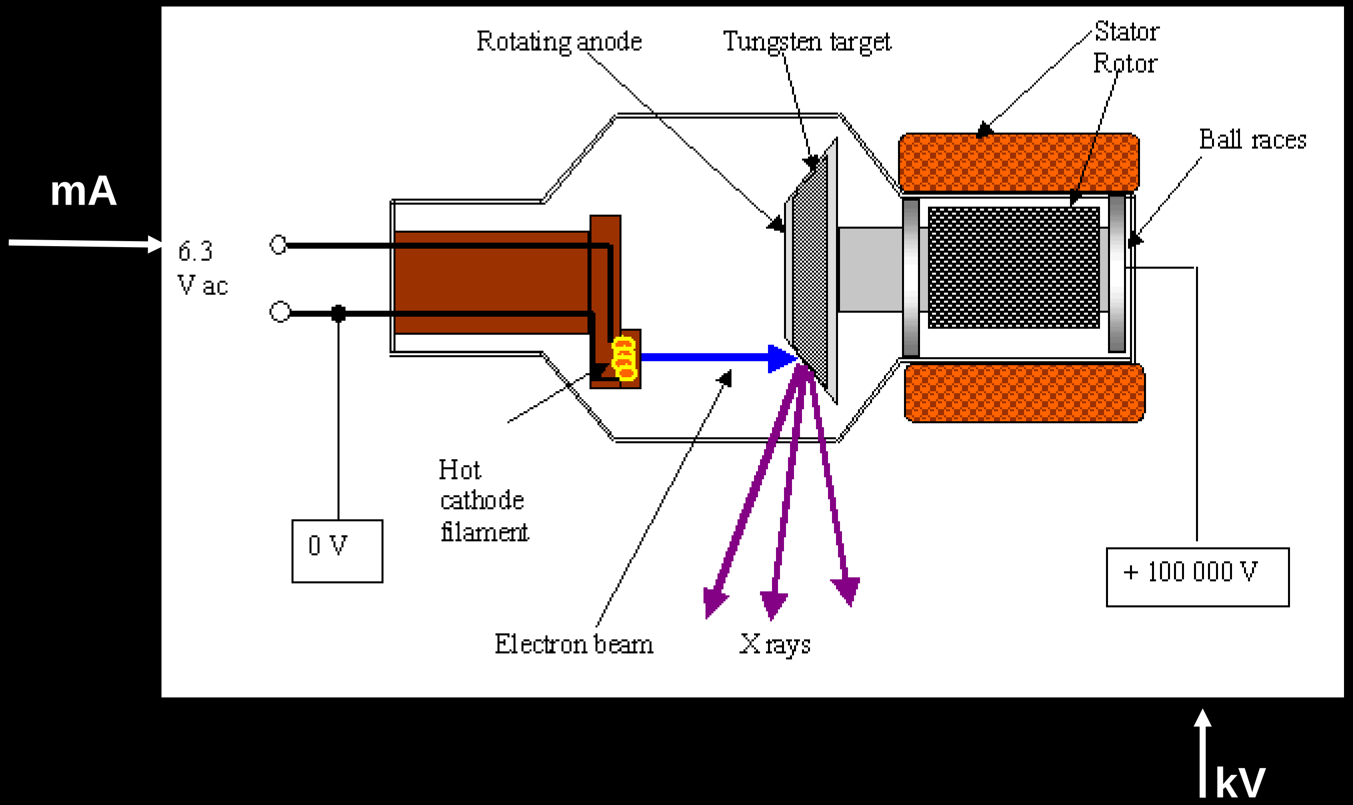
Rotating anode
Tungsten target
Stator
Rotor
Ball races
6.3
V ac
0 V
Hot
cathode
filament
Electron beam
X rays
+ 100 000 V

mA

kV

X-ray Spectrum Generation

Bremmstrahlung

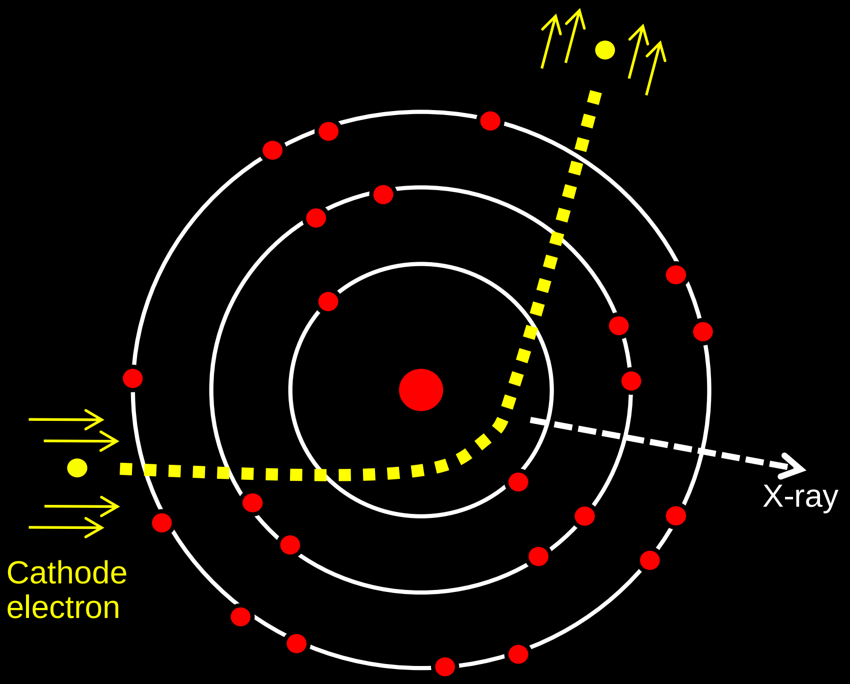
X-ray
Cathode electron

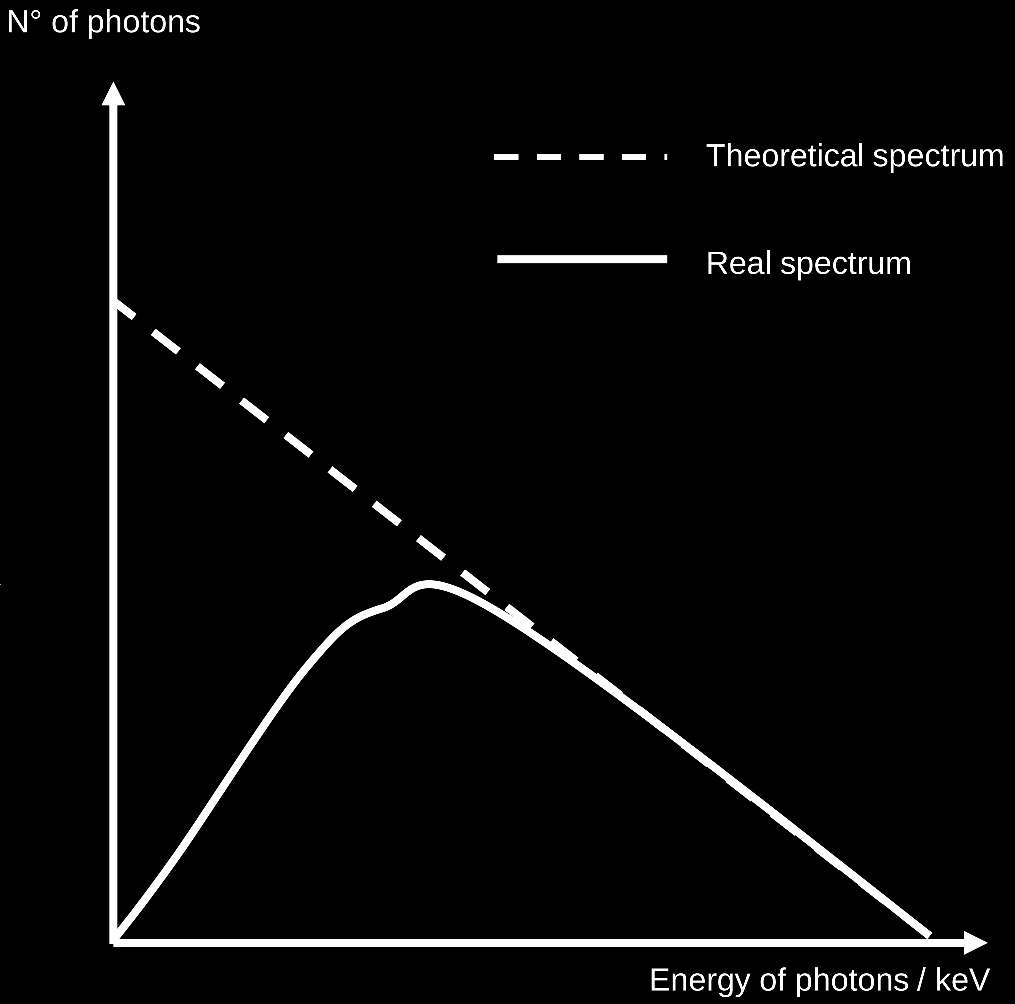

Energy of photons eV =

electron charge (e) · Voltage (V)

X-ray Spectrum Generation

Characteristic radiation

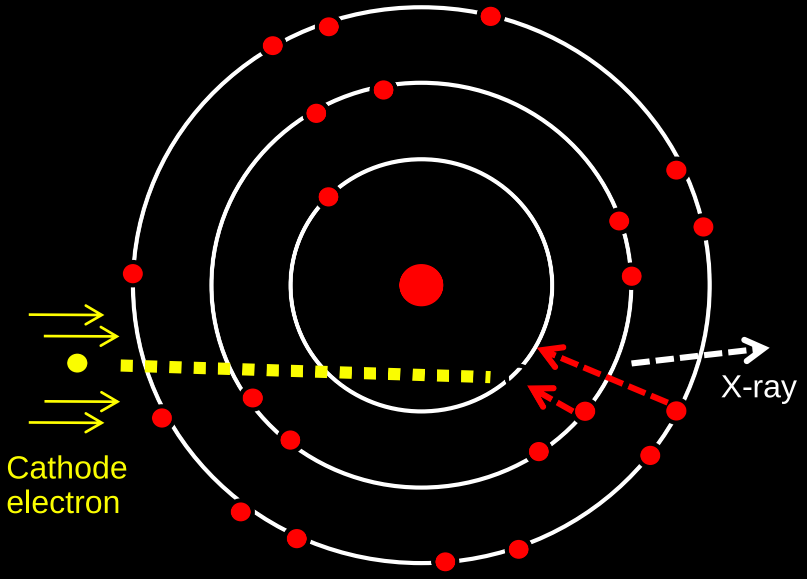
X-ray
Cathode electron

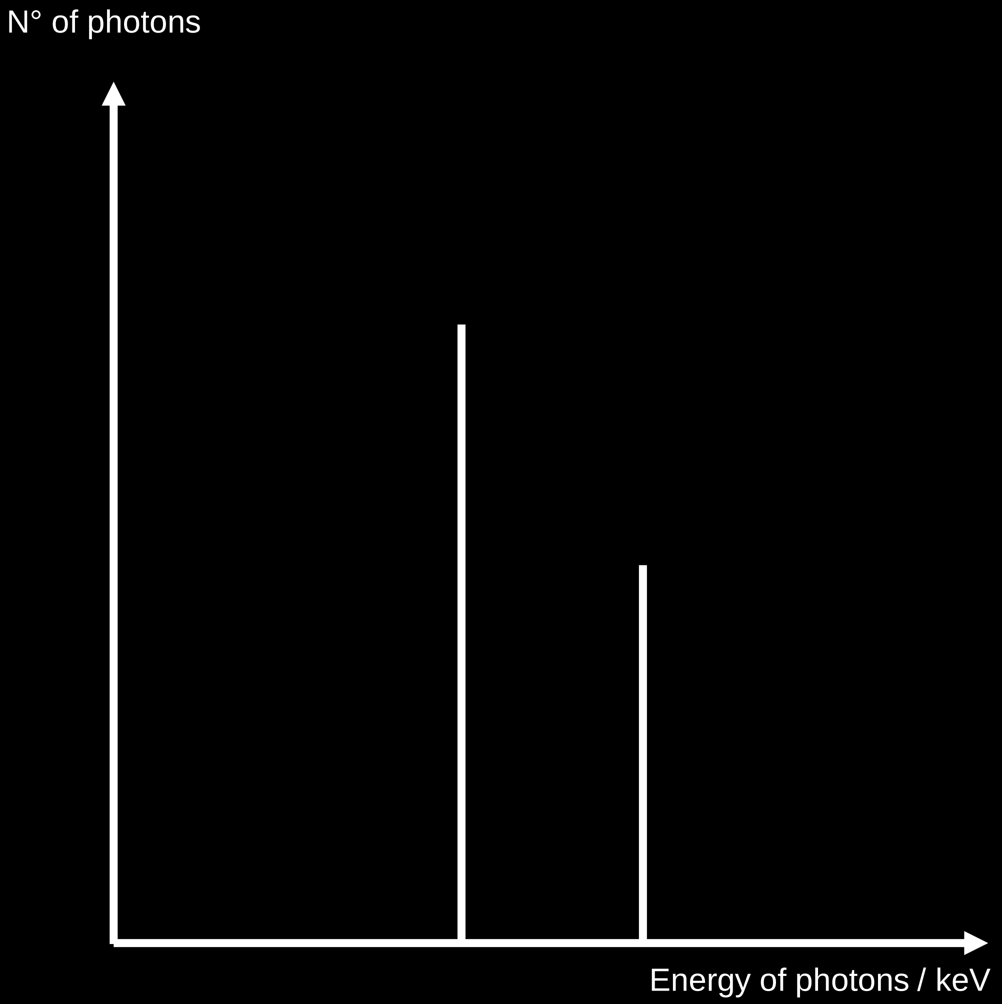

X-ray Spectrum Generation

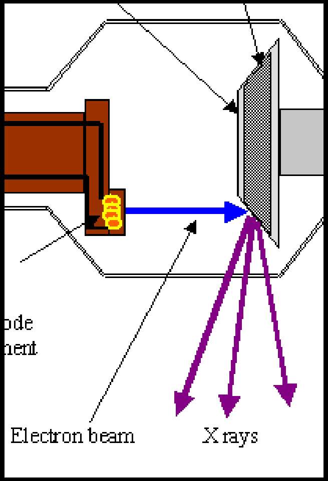
ode
nent
Electron beam
X rays

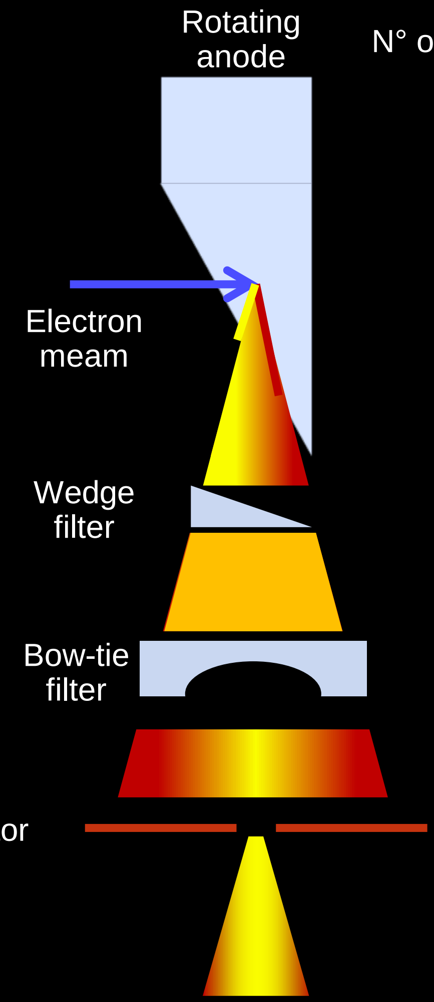
Rotating anode
Electron meam
Wedge filter
Bow-tie filter
Beam collimator

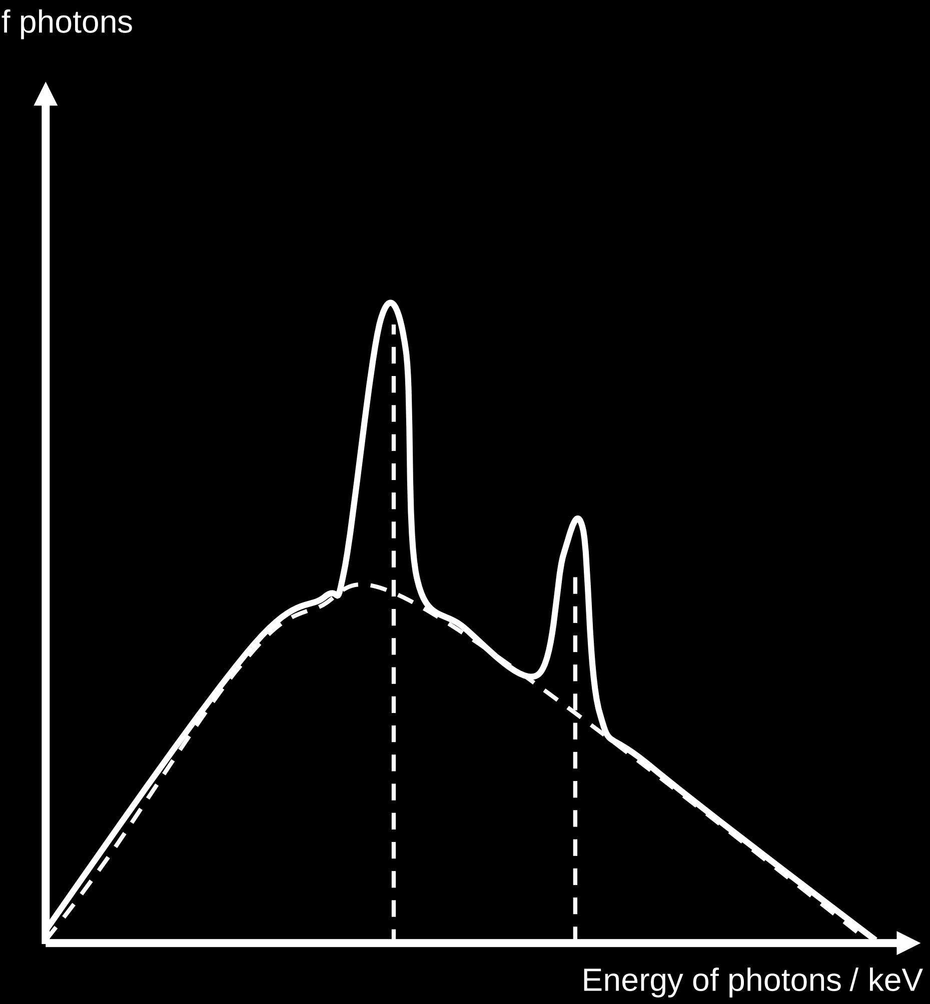

X-ray Spectrum Generation

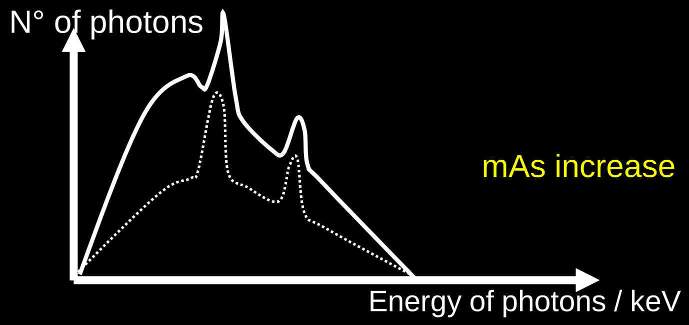
N° of photons
mAs increase
Energy of photons / keV

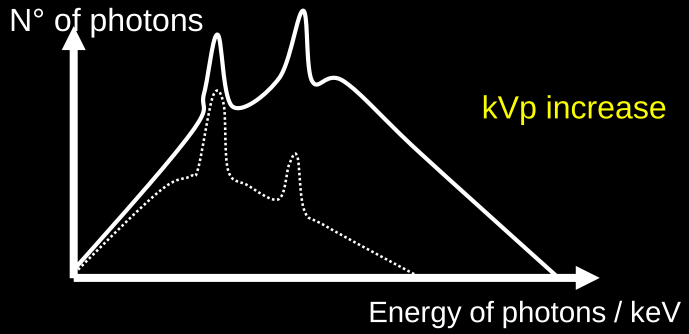
N° of photons
kVp increase
Energy of photons / keV

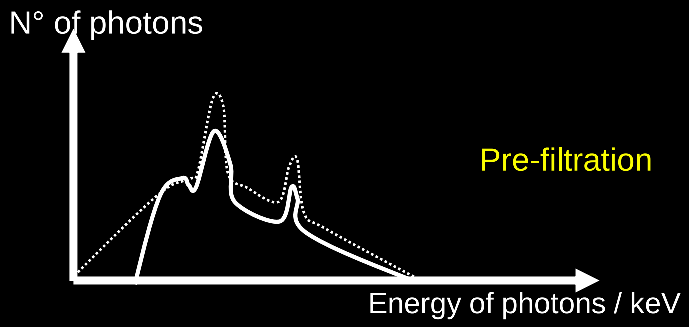
N° of photons
Pre-filtration
Energy of photons / keV

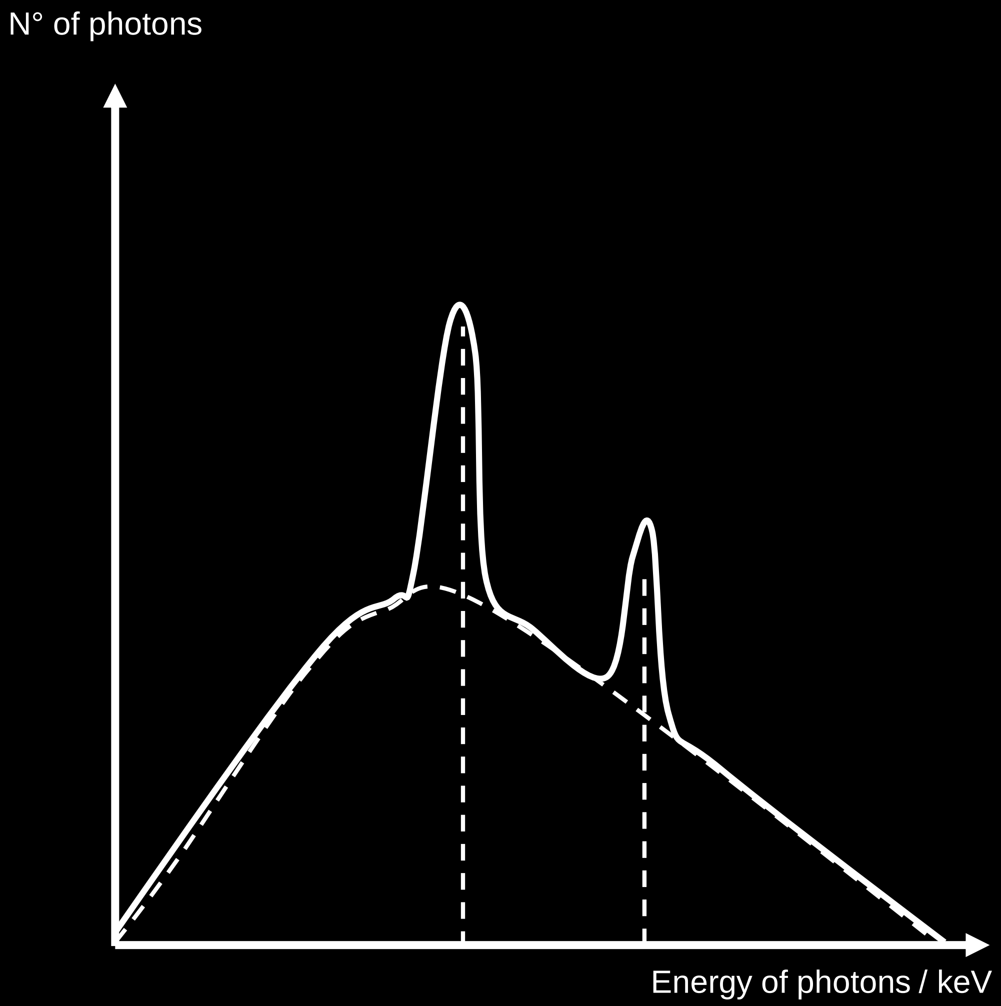
N° of photons
Energy of photons / keV

X-ray Attenuation

- Beer’s law:

$$I = I_0\, e^{-\int_0^{\mathrm{keVp}} \int_0^L \mu(x,\mathrm{E}) dx\, dE}$$

Used for filtered back-projection: $I = I_0\, e^{-\int_0^L \mu(x) dx}$

- Attenuation coefficient:

$$\mu_x(E) = \xcancel{x_\mathrm{R}\, f_\mathrm{R}}(E) + x_\mathrm{P}\, f_\mathrm{P}(E) + x_\mathrm{C}\, f_\mathrm{C}(E) + \xcancel{x_\mathrm{PP}\, f_\mathrm{PP}}(E)$$

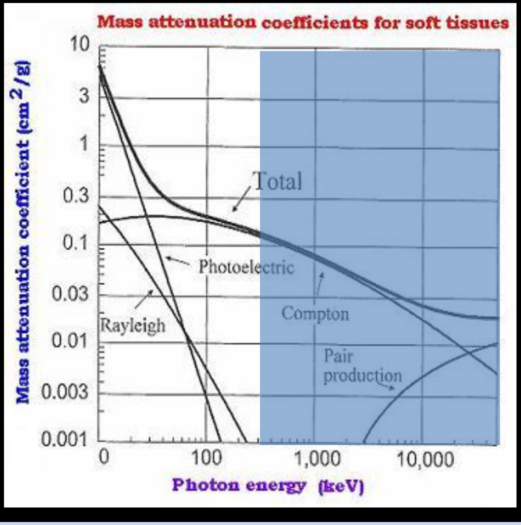

X-ray Detection

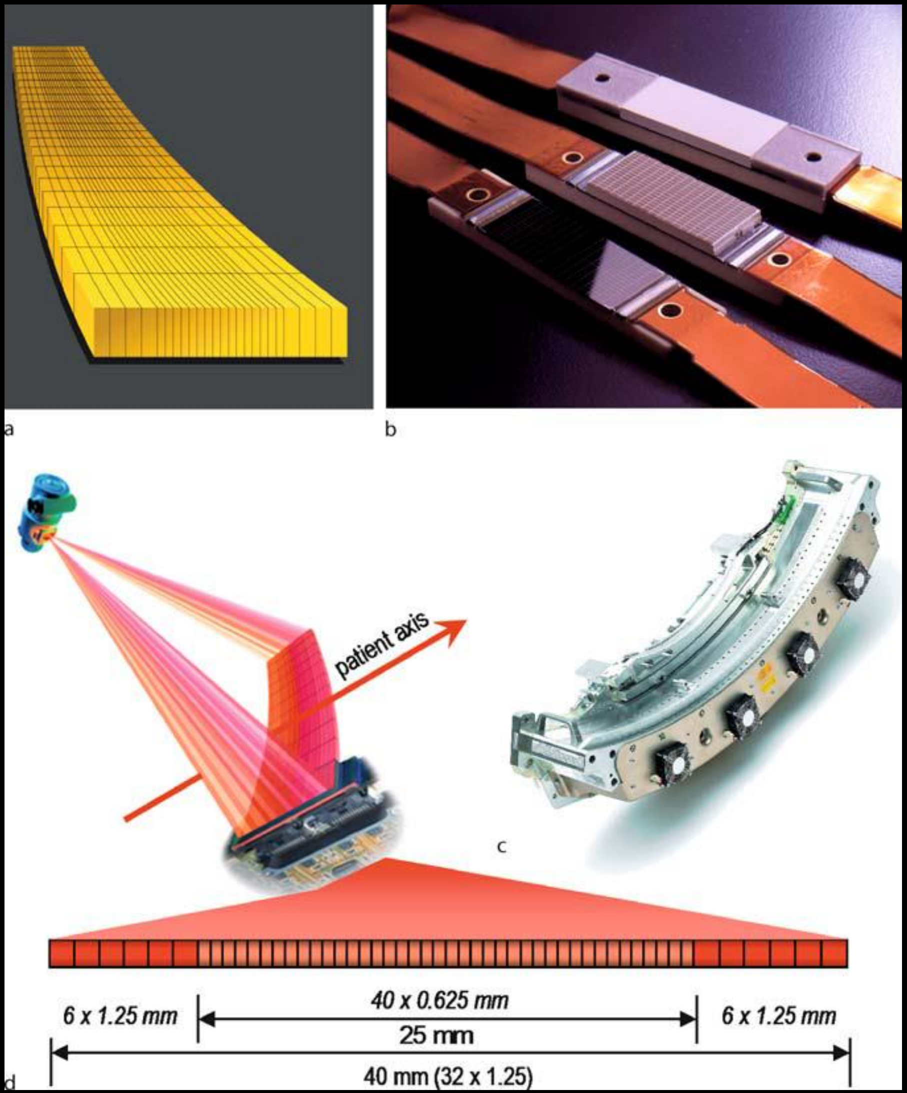
a
b
patient axis
c
6 x 1.25 mm
40 x 0.625 mm
25 mm
6 x 1.25 mm
40 mm (32 x 1.25)
d

X-ray Detection

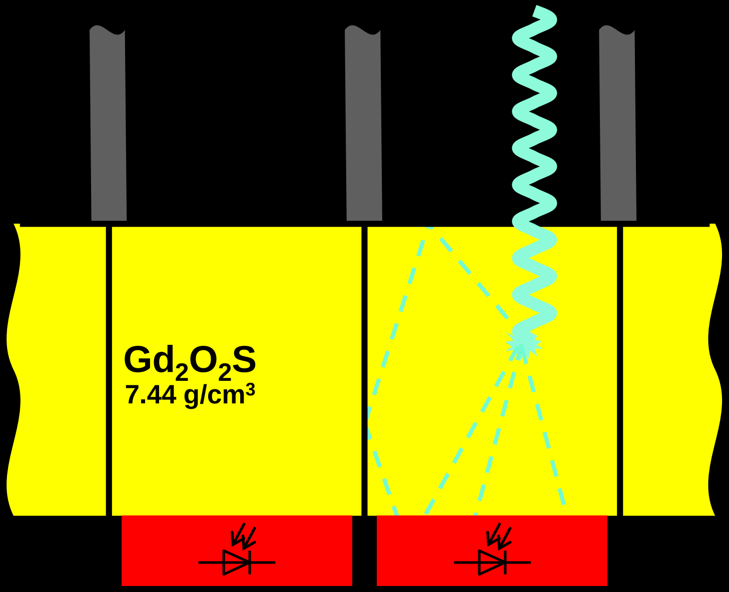

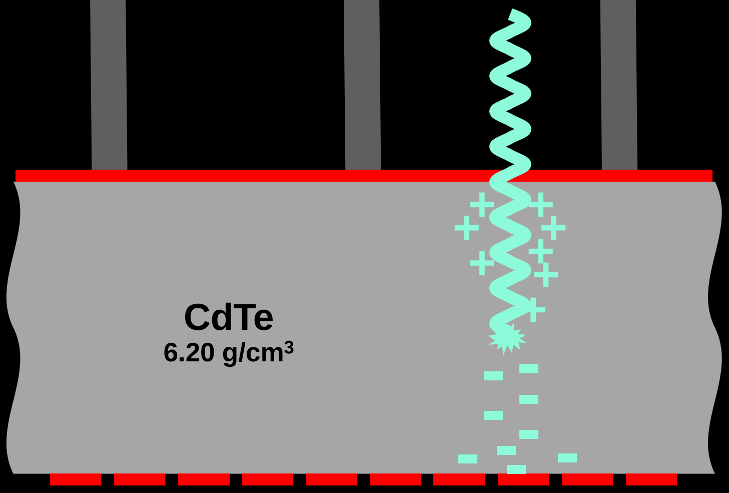

Scintillator-based detector:

- Detector divided up into small blocks (pixelated)
- Conversion of the x-ray photon into the visible light
- Isotropic emission of the light collected by reflection at the septa and then detected by the photodiode

Semiconductor-based detector:

- Continuous crystal with a pixelated anode
- Conversion of the x-ray photons into free charge carriers
- Drift of the charge cloud towards the pixelated anode by a bias voltage

X-ray Detection

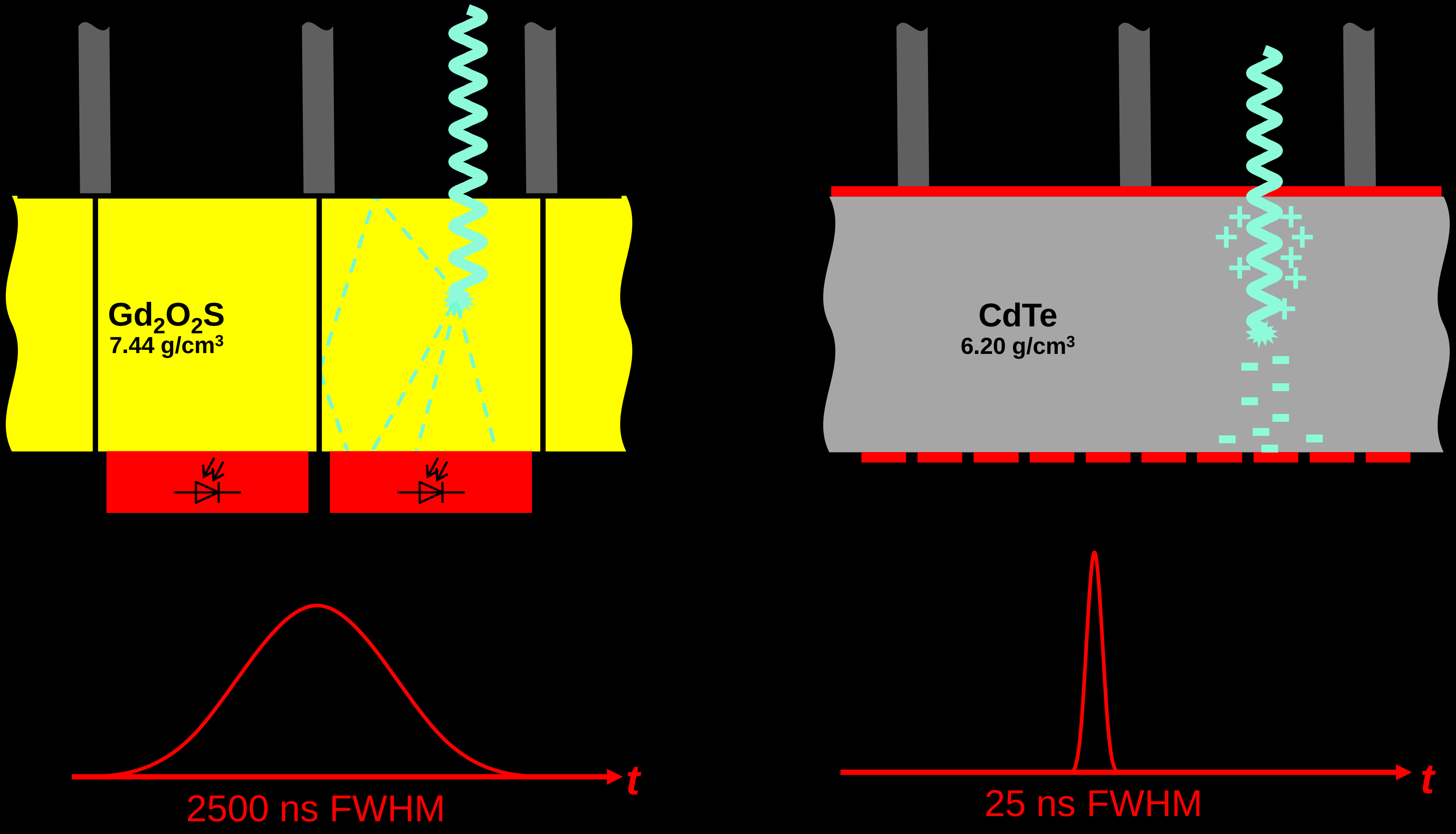

Gd_2O_2S
7.44 g/cm³
CdTe
6.20 g/cm³
t
2500 ns FWHM
t
25 ns FWHM

X-ray Detection

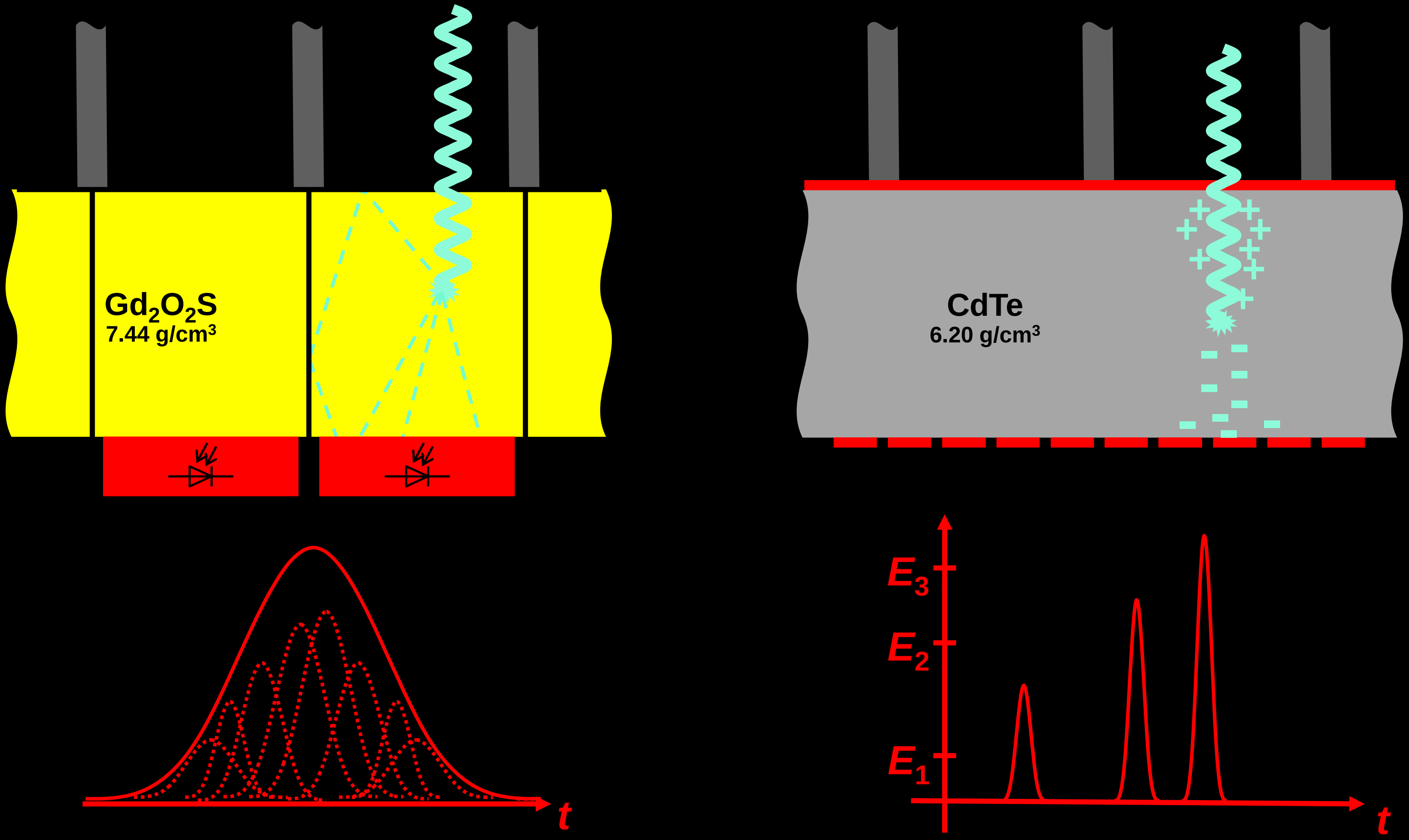
Gd_2O_2S
7.44 g/cm³
t
CdTe
6.20 g/cm³
E_3
E_2
E_1
t

X-ray Detection

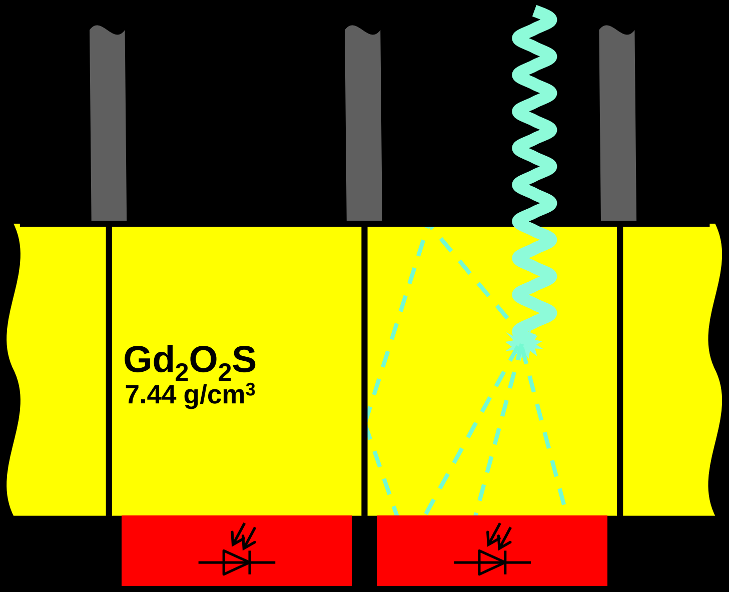
Gd_2O_2S
7.44 g/cm³

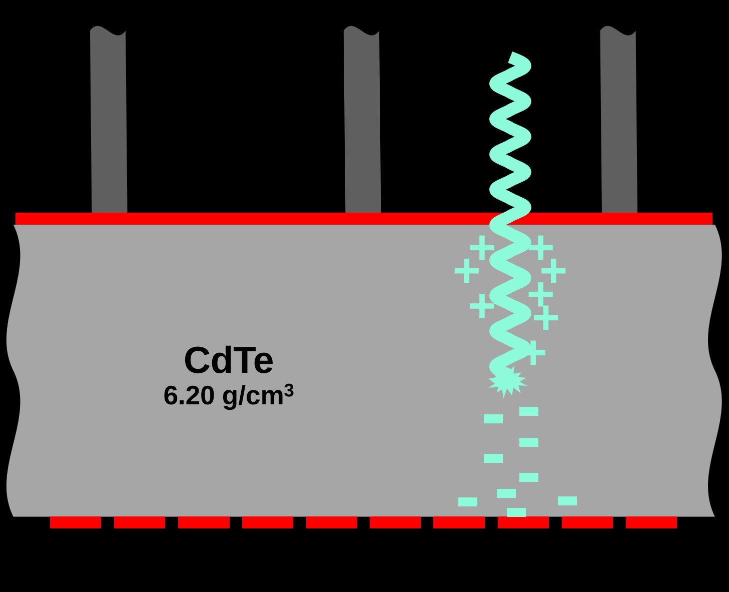
CdTe
6.20 g/cm³

- Indirect conversion
- Pulse overlap (only pile-up)
- Energy integrating (EI)

- Direct conversion
- Photon counting (PC)
- Energy-selective

Index of Contents

- Introduction:
  - Overview and components
  - History
- Physics:
  - X-ray generation
  - X-ray attenuation
  - X-ray detection
- Image reconstruction:
  - Filtered back-projection
  - Algebraic reconstructions
- Noise and artifacts:
  - Noise
  - Motion artifacts
  - Beam hardening artifacts
- Dose and image quality:
  - mAs modulation
  - kV selection

Sinogram Creation

Rebinning:

All projections from different angles are re-sorted in such a way to be parallel.

This means only the central projection is considered for each view angle theta, while all the others are parallel to it and comes from different rotation steps.

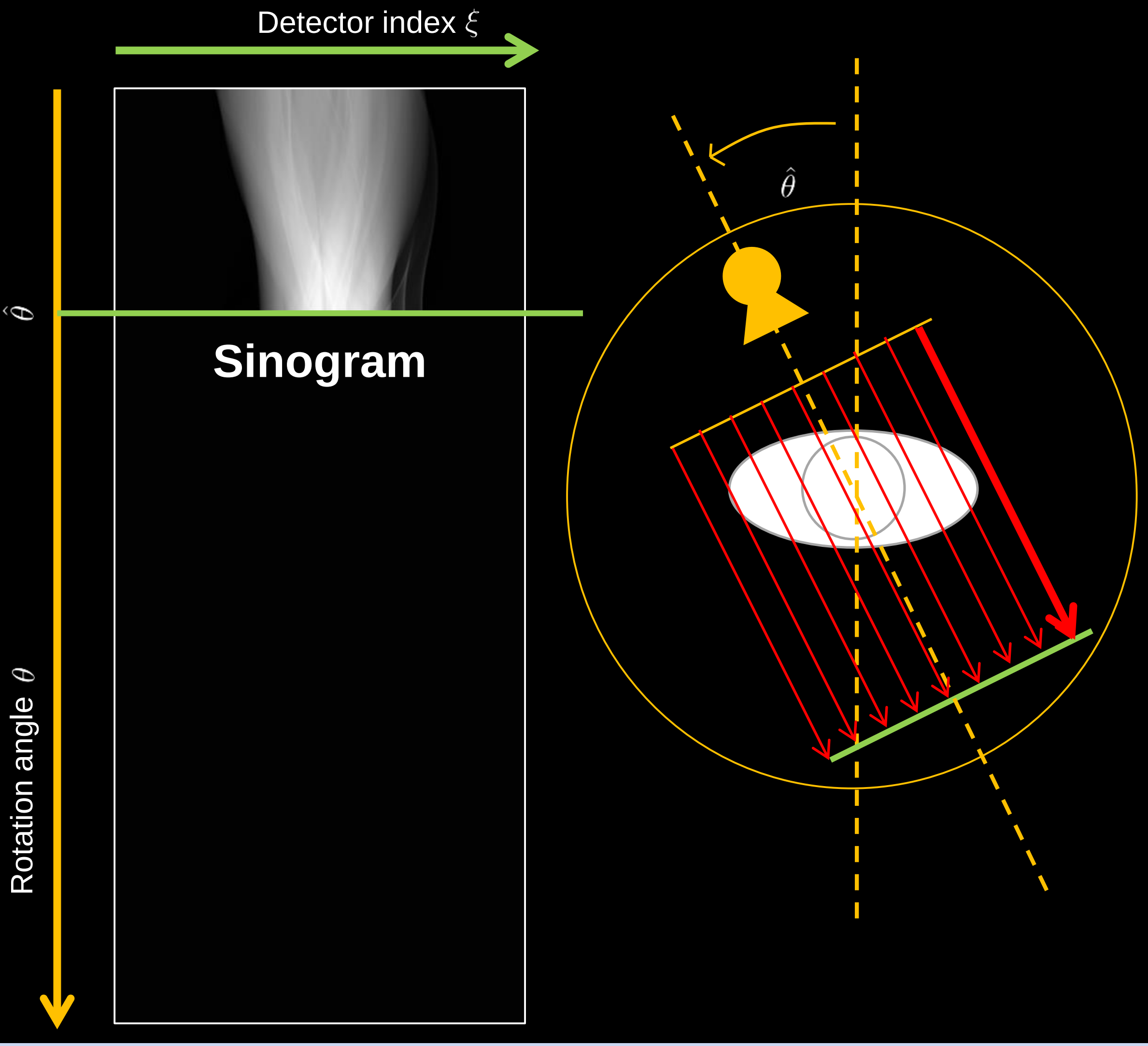

Detector index ξ
$\hat{\theta}$
Sinogram
Rotation angle θ
$\hat{\theta}$

Sinogram Creation

Rebinning:

All projections from different angles are re-sorted in such a way to be parallel.

This means only the central projection is considered for each view angle theta, while all the others are parallel to it and comes from different rotation steps.

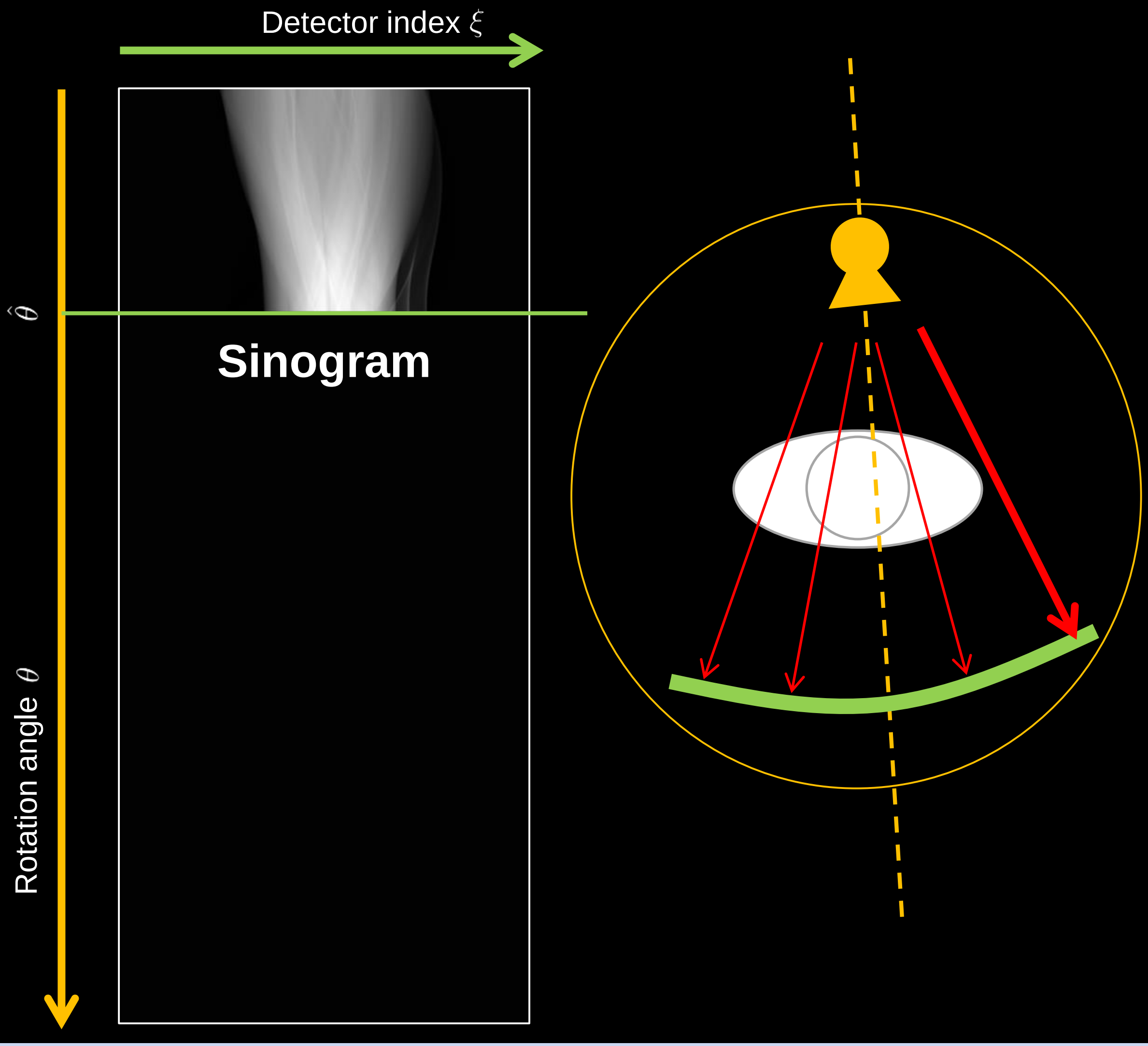
Detector index ξ
$\hat{\theta}$
Sinogram
Rotation angle θ

Sinogram Creation

- Lambert-Beer law is considered with some semplifications:
  - No dependancy on the energy.
  - No detector response is modeled.
  - Focal spot is assumed dimensionless.
  - No scatter or other artifacts are considered.
- Each detector ξ measures the attenuated intensity along the direction θ .
- The attenuation follows a negative exponential behavior and depends on the line integral of the attenuation coefficients met along that way.

$$I(\theta,\xi) = I_0(\theta,\xi)\, e^{-\int_0^L \mu(\xi,\eta)d\eta}$$

- Since for each angle and detector only the structures along that path are responsible for the attenuation, the coordinates x and y can be expressed as:

$$\xi = x\cos(\theta) + y\sin(\theta)$$

$$\eta = -x\sin(\theta) + y\cos(\theta)$$

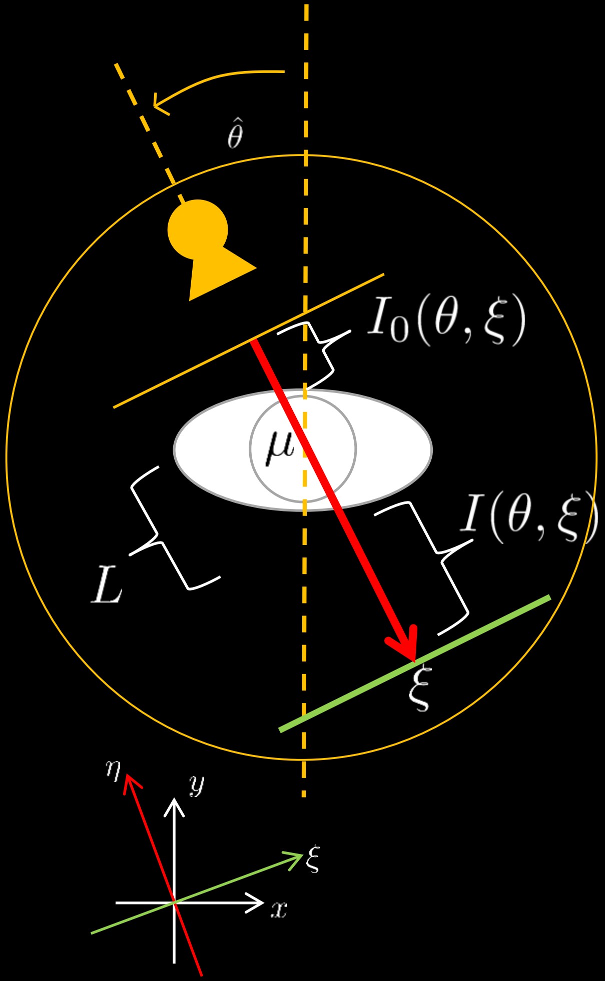

Sinogram Creation

From the intensity domain, it is convenient to move to projections domain, via division and negative log operation:

$$I(\theta,\xi) = I_0(\theta,\xi)\, e^{-\int_0^L \mu(\xi,\eta)d\eta}$$

$$\frac{I(\theta,\xi)}{I_0(\theta,\xi)} = e^{-\int_0^L \mu(\xi,\eta)d\eta}$$

$$-\ln\left(\frac{I(\theta,\xi)}{I_0(\theta,\xi)}\right) = \int\limits_0^L \mu(\xi,\eta)d\eta = p(\theta,\xi) = p_\theta(\xi)$$

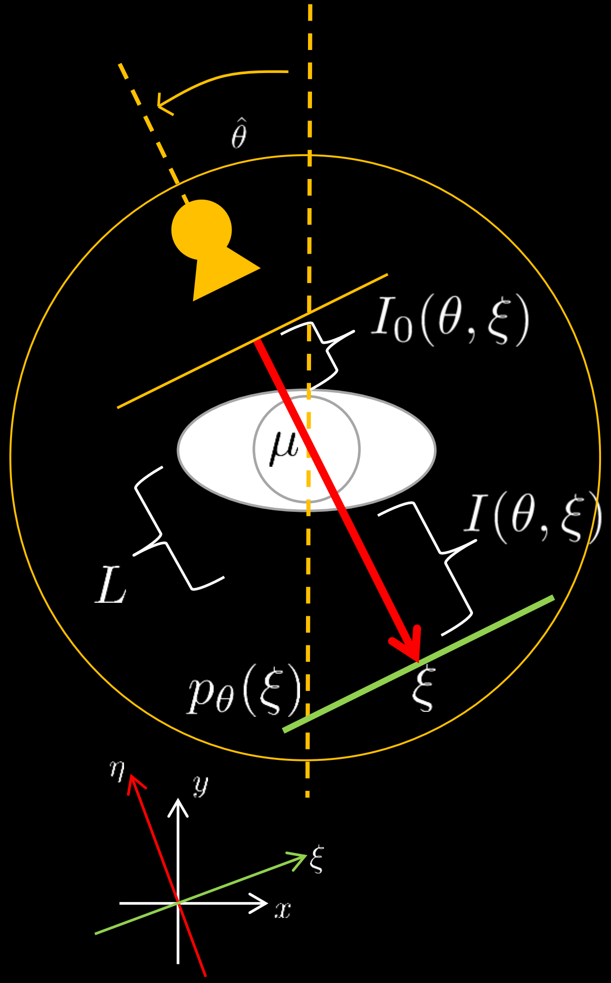
$\hat{\theta}$
$I_0(\theta,\xi)$
μ
$I(\theta,\xi)$
L
$p_\theta(\xi)$
ξ
η
y
ξ
x

Sinogram Creation

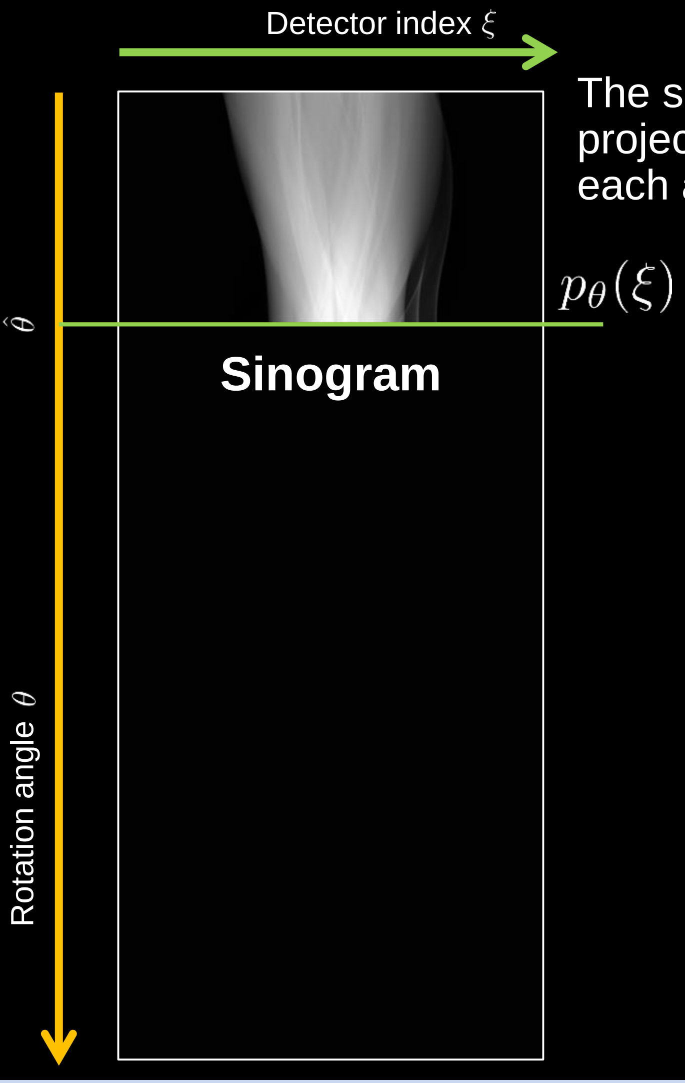
Detector index ξ
$\hat{\theta}$
$p_\theta(\xi)$
Sinogram
Rotation angle θ

The sinogram is the collection of projections for each detector, for each angle (from 0 to π).

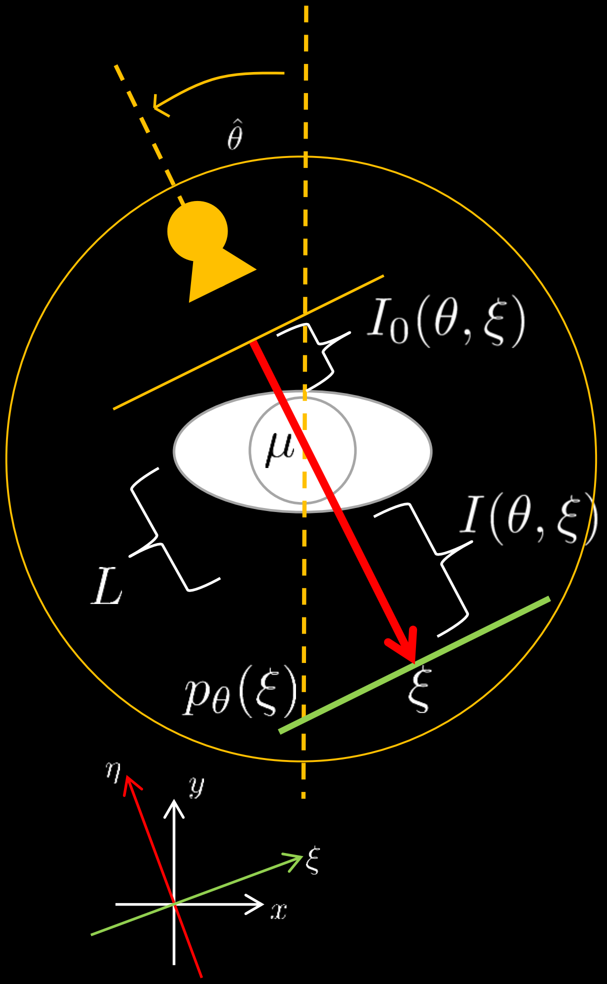
$\hat{\theta}$
$I_0(\theta, \xi)$
μ
L
$I(\theta, \xi)$
$p_\theta(\xi)$
ξ
η
y
ξ
x

Sinogram Creation

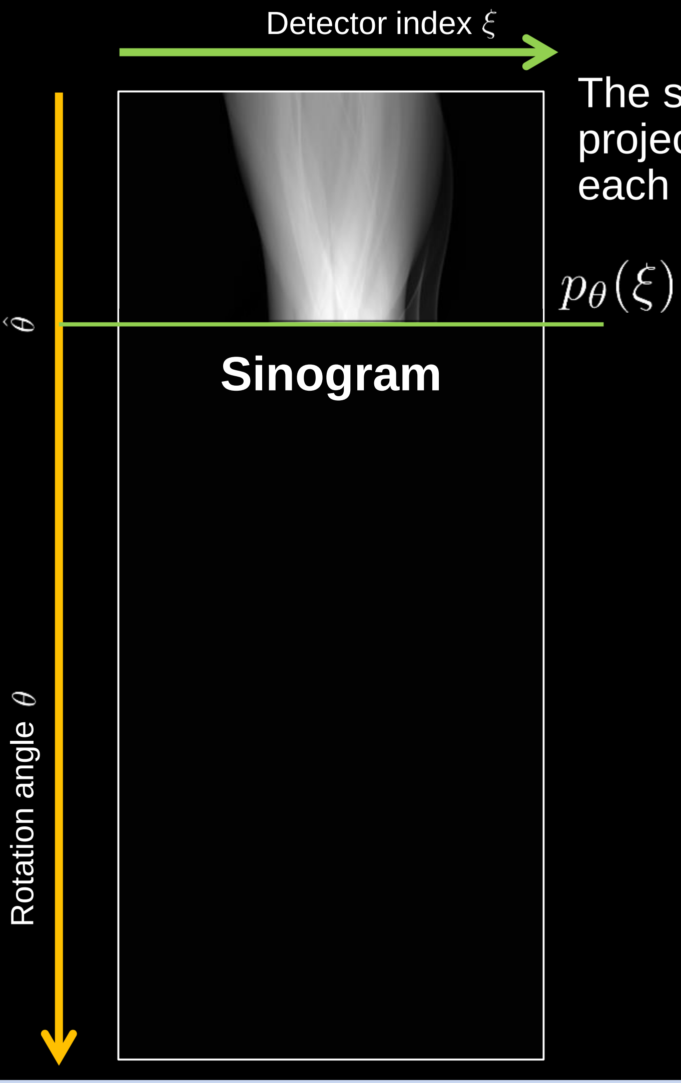
Detector index ξ
$\hat{\theta}$
$p_{\theta}(\xi)$
Sinogram
Rotation angle θ

The sinogram is the collection of projections for each detector, for each angle (from 0 to π).

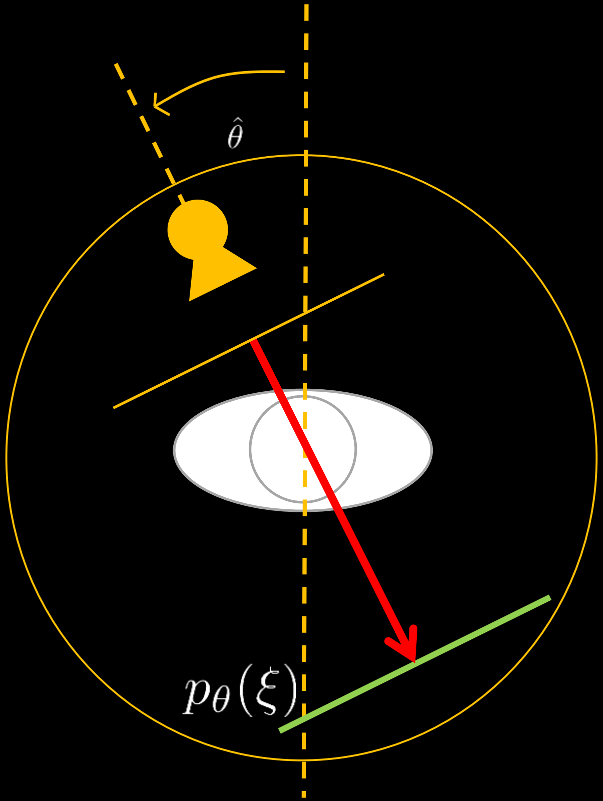
$\hat{\theta}$
$p_{\theta}(\xi)$

Sinogram Creation

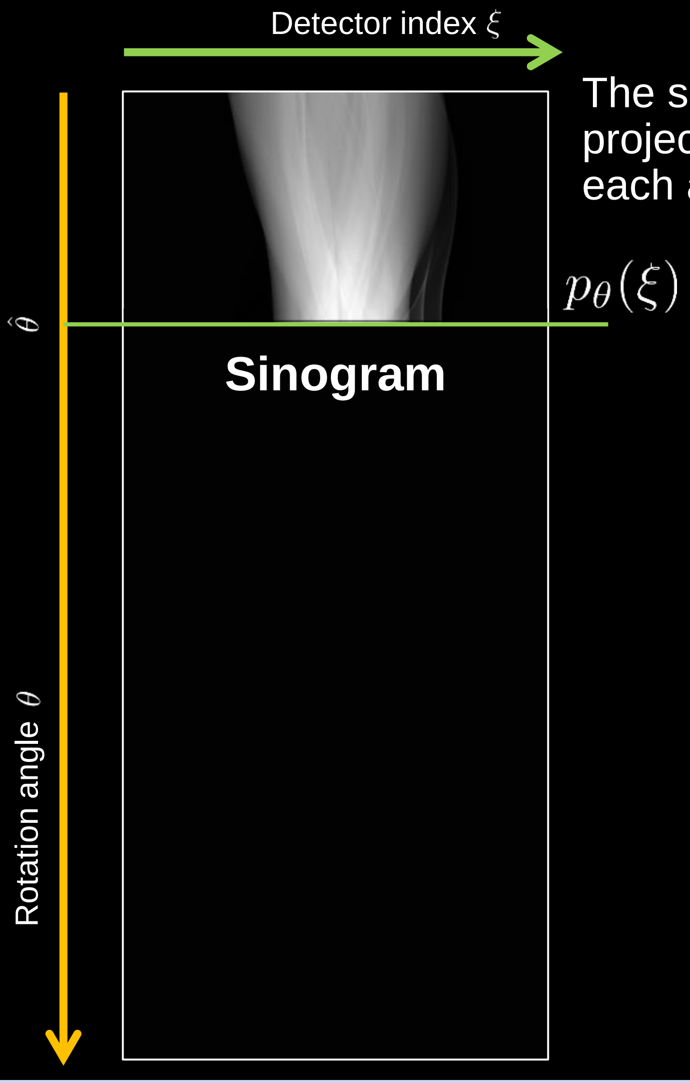
Detector index ξ
$\hat{\theta}$
Rotation angle θ
$p_\theta(\xi)$
Sinogram

The sinogram is the collection of projections for each detector, for each angle (from 0 to π).

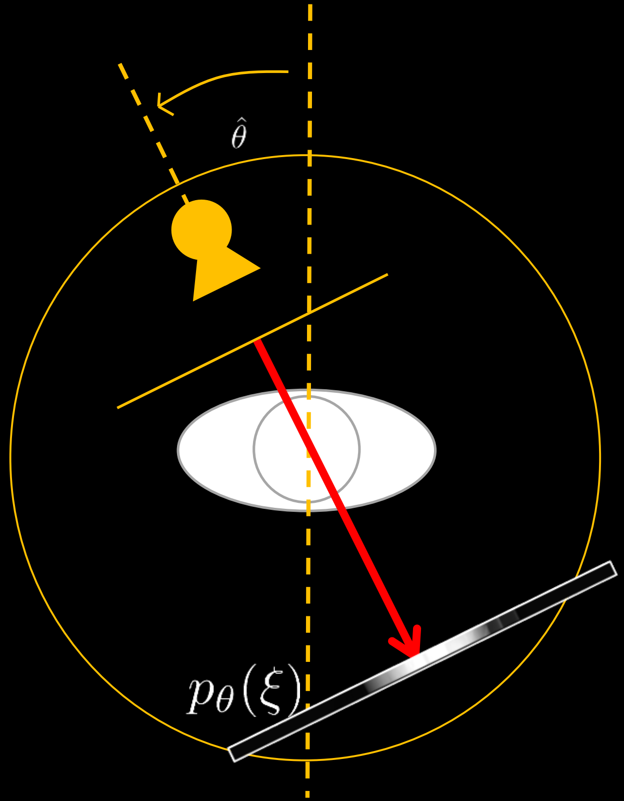
$\hat{\theta}$
$p_\theta(\xi)$

Slice Theorem

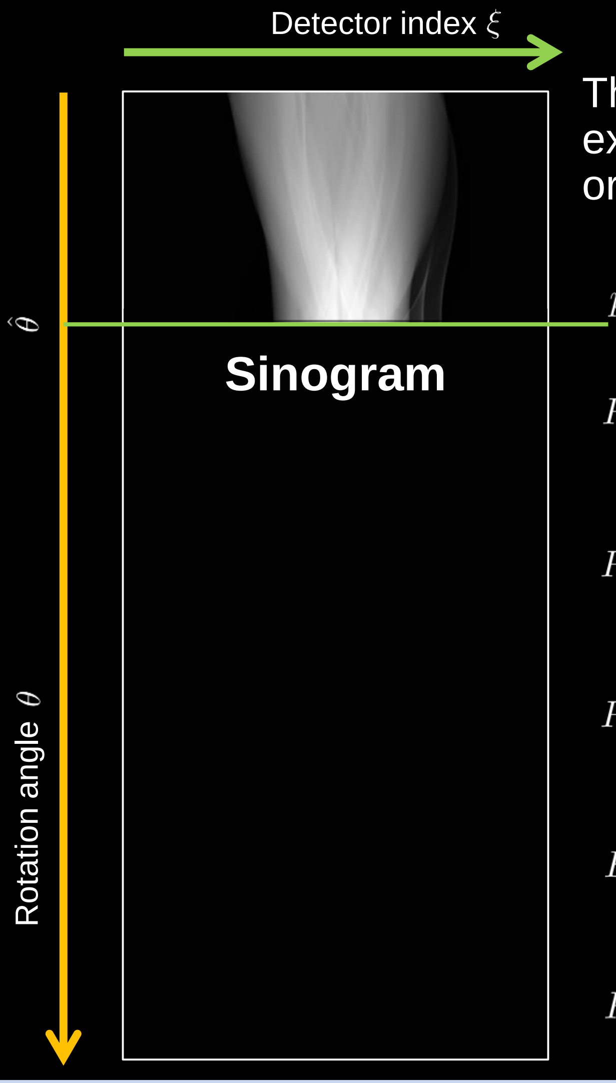

The 1D Fourier transform of a sinogram line, is equal to the the extrapolation of the 1D line from the 2D Fourier transform of the original image along the respective angle:

$$p_\theta(\xi) = \int_0^L \mu(\xi,\eta)\,d\eta$$

$$P_\theta(q) = \mathcal{F}(p_\theta(\xi)) = \int_{-\infty}^{\infty} \left(\int_0^L \mu(\xi,\eta)\,d\eta \right) e^{-2\pi i q \xi}\,d\xi$$

$$P_\theta(q) = \mathcal{F}(p_\theta(\xi)) = \int_{-\infty}^{\infty} \int_{-\infty}^{\infty} \mu\big(\xi(x,y),\eta(x,y)\big) e^{-2\pi i q (x\cos(\theta) + y\sin(\theta))}\,dx\,dy$$

$$P_\theta(q) = \mathcal{F}(p_\theta(\xi)) = \int_{-\infty}^{\infty} \int_{-\infty}^{\infty} f(x,y) e^{-2\pi i (xq\cos(\theta) + yq\sin(\theta))}\,dx\,dy$$

$$F(u,v) = \int_{-\infty}^{\infty} \int_{-\infty}^{\infty} f(x,y) e^{-2\pi i (xu + yv)}\,dx\,dy$$

$$P_\theta(q) = F(u,v) \qquad \text{for } u = q\cos(\theta),\ v = q\sin(\theta)$$

Slice Theorem

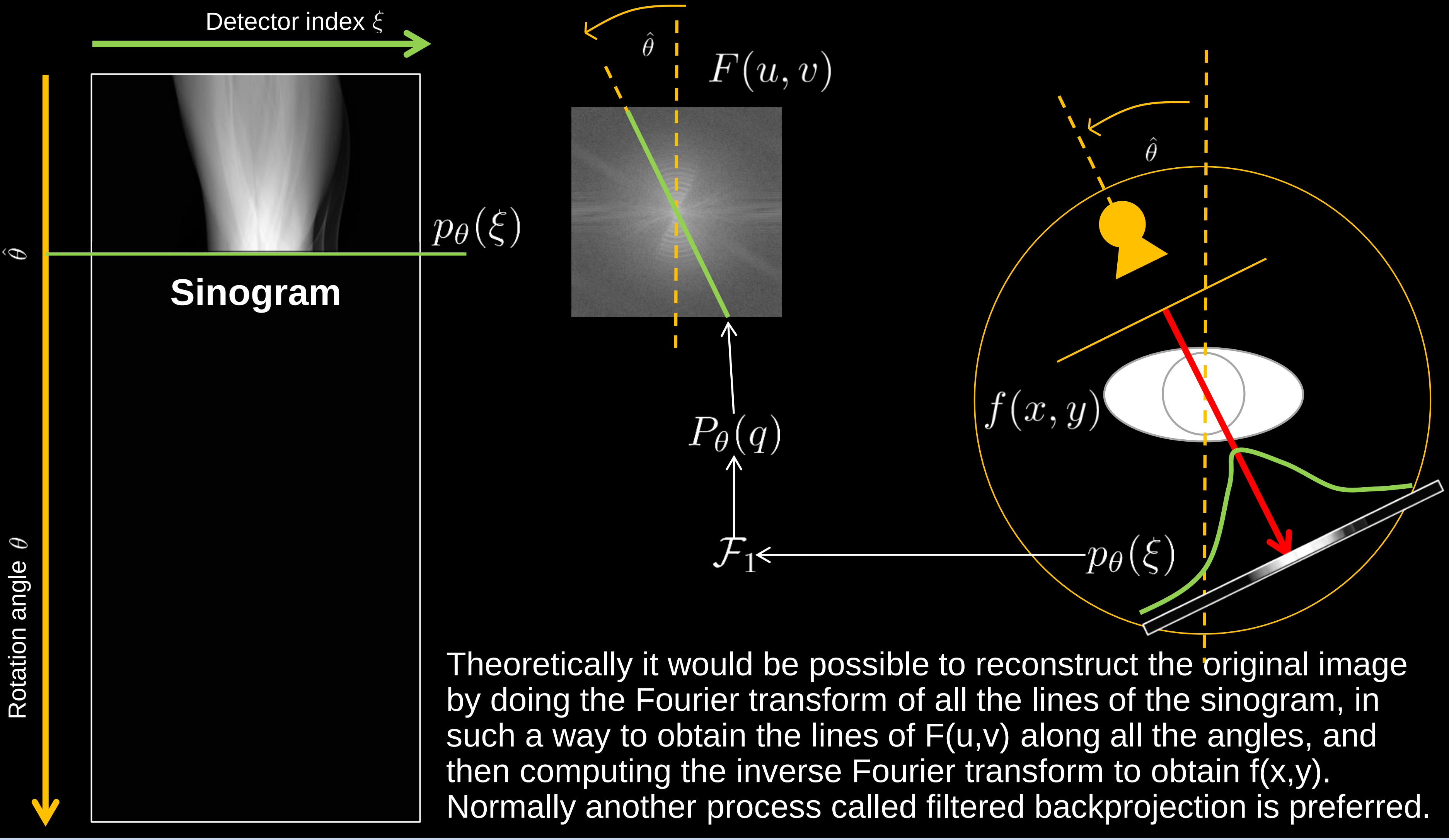
Detector index ξ
$\hat{\theta}$
Rotation angle θ
$p_\theta(\xi)$
Sinogram
$\hat{\theta}$
$F(u,v)$
$P_\theta(q)$
$\mathcal{F}_1$
$p_\theta(\xi)$
$\hat{\theta}$
$f(x,y)$

Theoretically it would be possible to reconstruct the original image by doing the Fourier transform of all the lines of the sinogram, in such a way to obtain the lines of F(u,v) along all the angles, and then computing the inverse Fourier transform to obtain f(x,y). Normally another process called filtered backprojection is preferred.

Backprojection

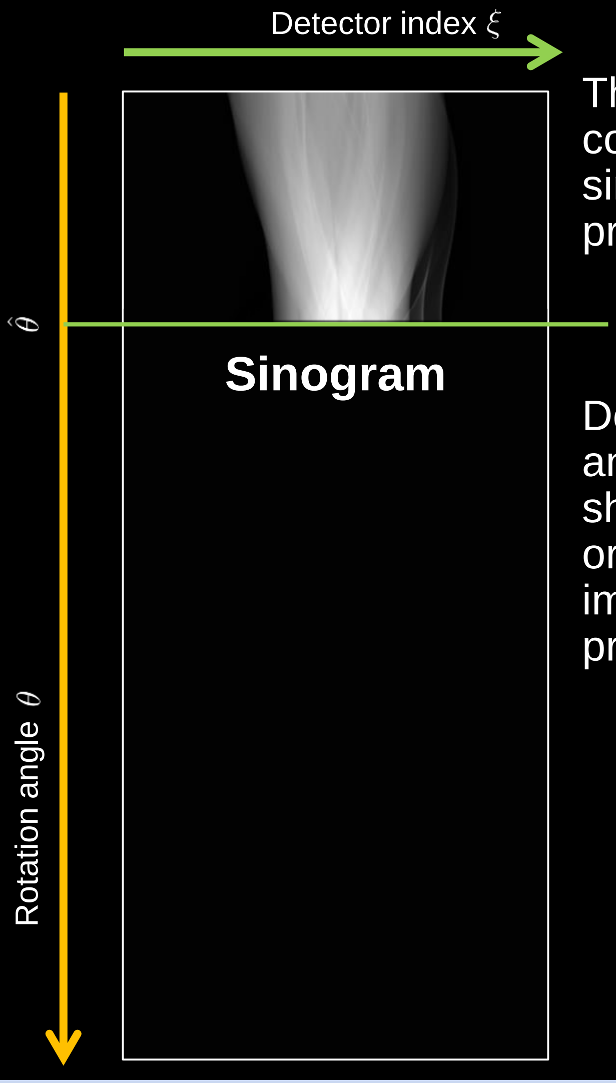
Detector index ξ
$\hat{\theta}$
Sinogram
Rotation angle θ

The back-projection operation consists in smearing back each sinogram line along the projection angle.

Doing this operation for each angle, for at least 180 degrees, should allow to obtain again the original image, via super imposition of all the projections profiles.

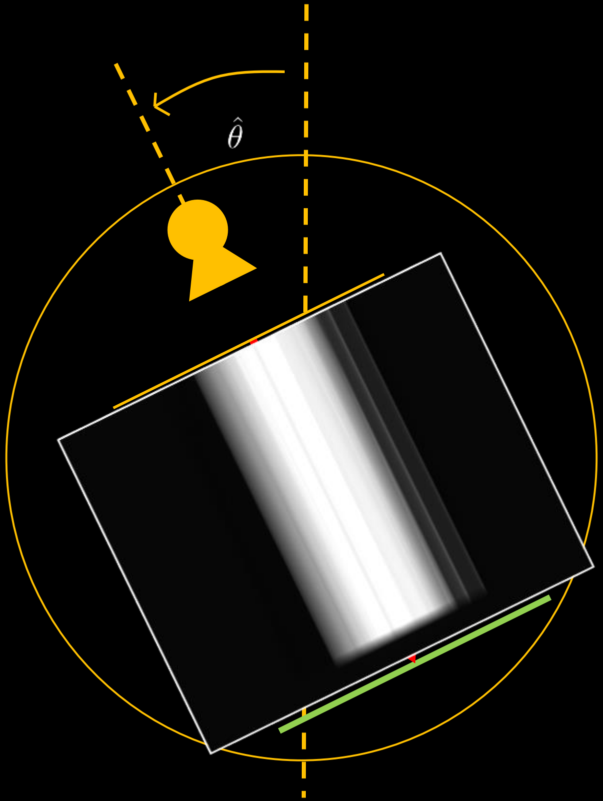

Backprojection

Developing the mathematics behind, one can see that via simple back-projection a different image is obtained, which does not correspond to the inital one (for example positive values are assigned also to pixels outside of the object).

It turns out that a simple back-projection results in:

$$g(x,y) = f(x,y) * h(x,y)$$

which means the original image is convolved with a point spread function h(x,y).

Backprojection

Simple backprojection

Filtered Backprojection

For inverse Fourier transform we have:

$$f(x,y) = \int_{-\infty}^{\infty}\int_{-\infty}^{\infty} F(u,v)e^{2\pi i(xu+yv)}dudv$$

We saw from slice theorem, that for $u = q\cos(\theta)$ and $v = q\sin(\theta)$, we have that F(u,v) equals $P_\vartheta(q)$.

We can move to polar coordinates and re-write

$$f(x,y) = \int_{0}^{2\pi}\int_{-\infty}^{\infty} F(q\cos(\theta), q\sin(\theta))e^{2\pi i(xq\cos(\theta)+yq\sin(\theta))}q\,dq\,d\theta$$

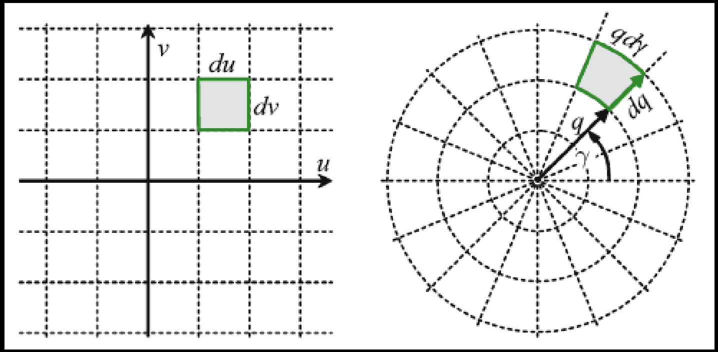

which can be re-written after some passages as:

$$f(x,y) = \int_{0}^{pi}\int_{-\infty}^{\infty} P_\theta(q)e^{2\pi i q\xi}|q|\,dq\,d\theta$$

Filtered Backprojection

$$f(x,y) = \int_{0}^{pi} \int_{-\infty}^{\infty} P_\theta(q) e^{2\pi i q \xi} |q| \, dq \, d\theta = f(x,y) = \int_{0}^{pi} \int_{-\infty}^{\infty} P_\theta(q) e^{2\pi i q \xi} |q| \, dq \;\; d\theta$$

We can recognize that the integral in dq (marked in yellow) is nothing but the sinogram high-pass filtered in Fourier domain, where the filter is |q|.

With some approximation, the inverse Fourier transform of the filter is a sync function, which means that, to obtain the original image, we have to convolve the sinogram with a „edge enhancing“ filter.

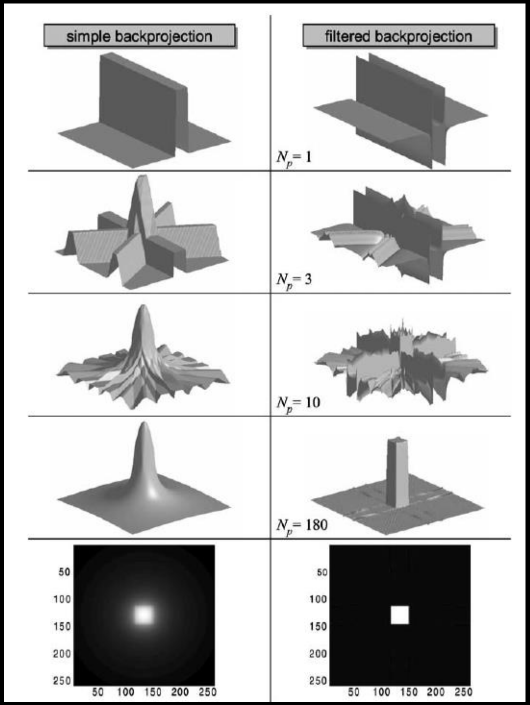

Filtered Backprojection

Simple backprojection

Filtered backprojection

Filtered Backprojection

With FBP, not so much can be optimized, except for the reconstruction kernel, which can be chosen to control the Modulation Transfer Function (i.e. the spatial frequency response of the algorithm).

Smooth kernels reduce noise and spatial frequency.

Sharp kernels allow to see more fine structures, but introduce more noise in the image.

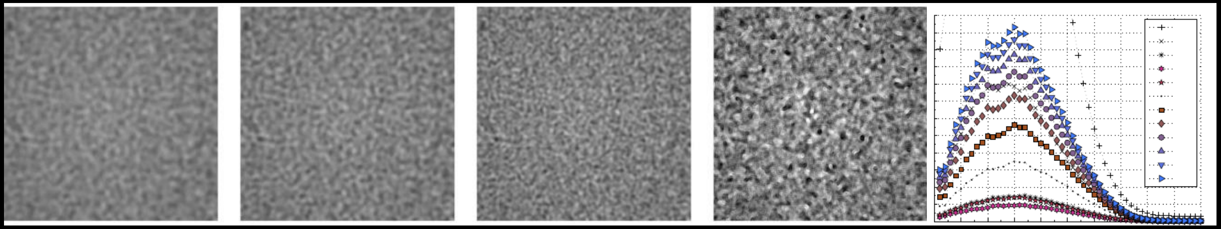

MTFs

Furthermore:

- all approximation done to solve the inverse problem might generate artifacts,
- to reconstruct an image, the rotation must be at least 180° plus fan angle.

Algebraic Reconstructions

Algebraic reconstructions are much more flexible, but significantly slower.
They approach the problem as a set of linear equations to be solved.

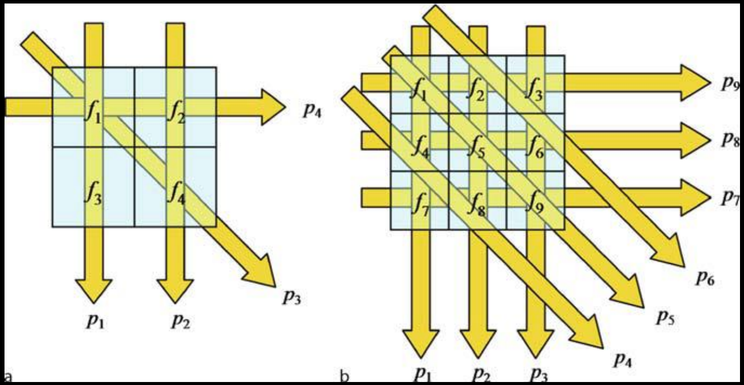

a
f_1
f_2
f_3
f_4
p_1
p_2
p_3
p_4
b
f_1
f_2
f_3
f_4
f_5
f_6
f_7
f_8
f_9
p_1
p_2
p_3
p_4
p_5
p_6
p_7
p_8
p_9

$$\begin{cases} w_{1,1}f(1) + w_{1,2}f(2) + \cdots + w_{1,N}f(N) = p_1 \\ \vdots \\ w_{M,1}f(1) + w_{M,2}f(2) + \cdots + w_{M,N}f(N) = p_M \end{cases}$$

Where:

- $f(i)$ are the unknowns, i.e. the values of the image for each voxel $1 \leq i \leq N$
- $w(i,j)$ are the coefficients which are known and derived from system‘s geometry. They indicate how much each voxel i „falls“ into the path of that specific projection$1 \leq j \leq M$
- p_j are the measured projections.

Algebraic Reconstructions

$$\begin{cases} w_{1,1}f(1) + w_{1,2}f(2) + \cdots + w_{1,N}f(N) = p_1 \\ \vdots \\ w_{M,1}f(1) + w_{M,2}f(2) + \cdots + w_{M,N}f(N) = p_M \end{cases}$$

In a matrix form we can write:

$$\boldsymbol{A} \cdot \boldsymbol{f} = \boldsymbol{p}$$

Where $$\boldsymbol{A} = \begin{pmatrix} w(1,1) & \cdots & w(N,1) \\ \vdots & \vdots & \vdots \\ w(1,M) & \cdots & w(N,M) \end{pmatrix} \quad \boldsymbol{f} = \begin{pmatrix} f(1) \\ \vdots \\ f(N) \end{pmatrix} \quad \boldsymbol{p} = \begin{pmatrix} p_1 \\ \vdots \\ p_M \end{pmatrix}$$

The system cannot be exactly solved because of the presence of noise and artifacts, and also because the system matrix A is difficult to invert, since it is very sparse and big.

Normally the pseudo-solution is found as:

$$\boldsymbol{f}^* = \arg\min_{\boldsymbol{f}} \|\boldsymbol{A} \cdot \boldsymbol{f} - \boldsymbol{p}\|_2^2$$

Algebraic Reconstructions

The algorithm is very flexible and allows, for example, to weight each projection according to how reliable it is, remembering that when very few photons are measured, the signal to noise ratio of the projection decreases.

This variation of the algorithm is known as penalized weighted least suqare error (PWLS):

$$\boldsymbol{f}^* = \arg\min_{\boldsymbol{f}} \left((\boldsymbol{A} \cdot \boldsymbol{f} - \boldsymbol{p})^T \boldsymbol{W}^{-1} (\boldsymbol{A} \cdot \boldsymbol{f} - \boldsymbol{p}) \right)$$

Where the matrix W is a diagonal matrix containing the weights for each projection.

Algebraic Reconstructions

Normally, a so-called „regularizer“ function is added to the cost function to be minimized, in such a way to incorporate noise and/or artifacts reduction and create an algebraic reconstruction algorithm optimized for a specific problem or scenario.

Here few examples:

- Total variation:

$$\boldsymbol{f}^* = \arg\min_{\boldsymbol{f}} \|\boldsymbol{A}\cdot\boldsymbol{f} - \boldsymbol{p}\|_2^2 + \lambda\|\boldsymbol{\nabla}\boldsymbol{f}\|_1$$

- Nuclear norm (for correlated images):

$$\boldsymbol{f}^* = \arg\min_{\boldsymbol{f}} \|\boldsymbol{A}\cdot\boldsymbol{f} - \boldsymbol{p}\|_2^2 + \lambda\|\boldsymbol{f}\|_*$$

- Prior-induce similarity:

$$\boldsymbol{f}^* = \arg\min_{\boldsymbol{f}} \|\boldsymbol{A}\cdot\boldsymbol{f} - \boldsymbol{p}\|_2^2 + \lambda\|R(\boldsymbol{f} - \boldsymbol{g})\|_2$$

- Dicitionary based:

$$\boldsymbol{f}^* = \arg\min_{\boldsymbol{f}} \|\boldsymbol{A}\cdot\boldsymbol{f} - \boldsymbol{p}\|_2^2 + \lambda\|\boldsymbol{f} - \boldsymbol{D}\boldsymbol{c}\|_2^2$$

Index of Contents

- Introduction:
  - Overview and components
  - History
- Physics:
  - X-ray generation
  - X-ray attenuation
  - X-ray detection
- Image reconstruction:
  - Filtered back-projection
  - Algebraic reconstructions
- Noise and artifacts:
  - Noise
  - Motion artifacts
  - Beam hardening artifacts
- Dose and image quality:
  - mAs modulation
  - kV selection

Noise

Theoretically, the number of photons that reach the detectors can be described as a cascade of Bernoulli distribution, describing the probability that a photon is emitted or not, absorbed from the patient or not, detected or not etc. This cascade can be approximated with a Poisson distribution and hence we can write:

$$n \sim \mathcal{P}(N, N)$$

Meaning that the variance of the distribution is equivalent to the expected number of photons. This means that for a high number of photons also the noise is increasing, but the SNR will overall decrease since

$$\mathrm{SNR} = \frac{N}{\sqrt{N}} = \sqrt{N}$$

The noise is theoretically uncorrelated, but the cross-talk between adjacent detectors, the logarithmic operation to obtain the sinogram, and especially the filtering of the sinogram and backprojection operations make such that the noise is spatially correlated in image domain.

Motion Artifacts

While noise has a stochastic nature, artifacts arises for specific reasons, and sometimes can be corrected or reduced.

All artifacts are due to some inconsistencies in the projections. For example motion artifacts are generated when an object moves during the acquisition.

Since the object is moving, only some projections are passing through it, while other that should have intersected the object do not intersect it anymore, and the other way around.

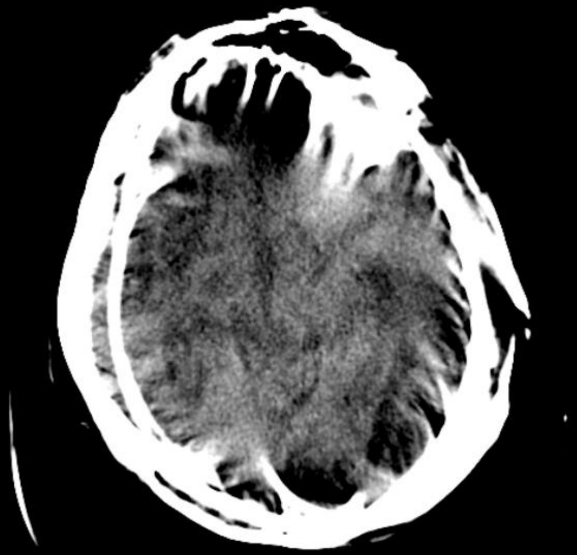

Some of the possible ways to solve this issue are:

- Improving scan speed
- Instructing the patient
- Acquiring data with less than 180° of rotation. This would generate other types of artifacts (namely truncation artifacts) since the data are incomplete, but these new artifacts might be easier to correct for.
- Reduce entropy in selected regions of the image

Beam Hardening Artifacts

Another type of inconsistency is the fact that the Beer Lambert law is simplified without taking into account the energy dependency.

$$I = I_0\, e^{-\int_0^{\mathrm{keVp}} \int_0^L \mu(x,\mathrm{E})dx\, dE} \longrightarrow I = I_0\, e^{-\int_0^L \mu(x)dx}$$

In particular lower energy photons are attenuated more respect to higher energy ones. But the formula used for the reconstruction assumes that the only reasons for different attenuations are the attenuation coefficients and the intersection lenghts.

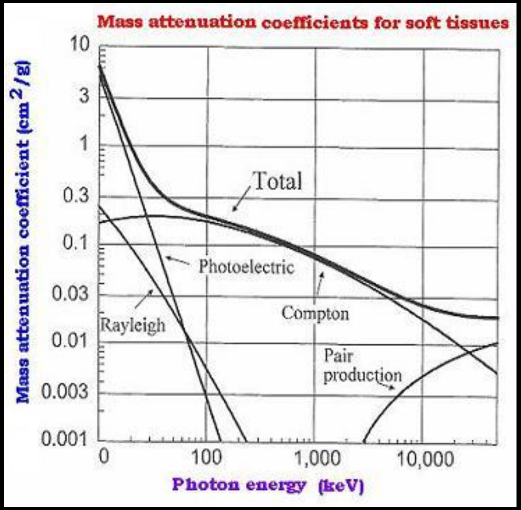

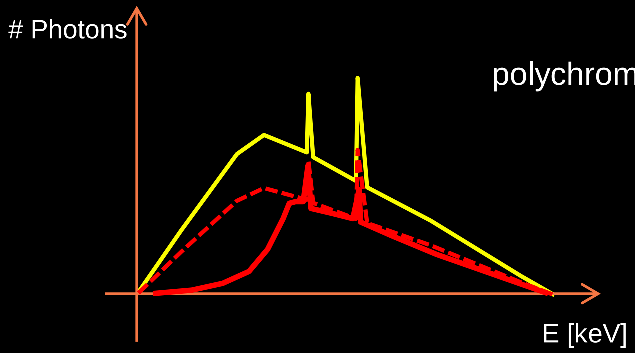

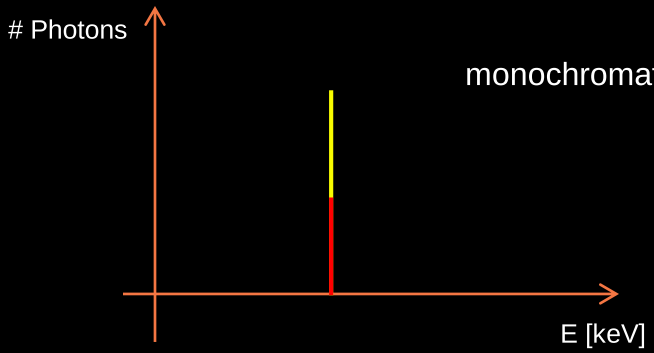

Beam Hardening Artifacts

Common ways to correct for these artifacts consist in:

- Segmenting the metal or high attenuating objects in the image (which are the main responsible of the artifacts, since the inhomogeneity in the absorption due to the energy is maximum when highly attenuating objects are met).
- Identifying all the affected projections, i.e. those projections that have passed throught these objects.
- Replacing the affected projection with some sort of interpolation of the non-affected adjacent ones.

These types of algorithms are normally iterative: small improvements are done in each iteration, until a cost function is minimized.

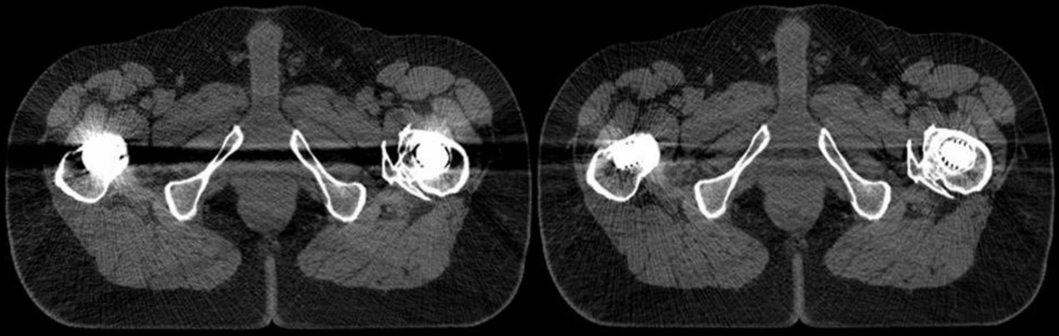

original corrected

Index of Contents

- Introduction:
  - Overview and components
  - History
- Physics:
  - X-ray generation
  - X-ray attenuation
  - X-ray detection
- Image reconstruction:
  - Filtered back-projection
  - Algebraic reconstructions
- Noise and artifacts:
  - Noise
  - Motion artifacts
  - Beam hardening artifacts
- Dose and image quality:
  - mAs modulation
  - kV selection
  - Dose measurements

CTDI

CTDI measures the dose absorbed by the phantom in one tube rotation, without any table movement.

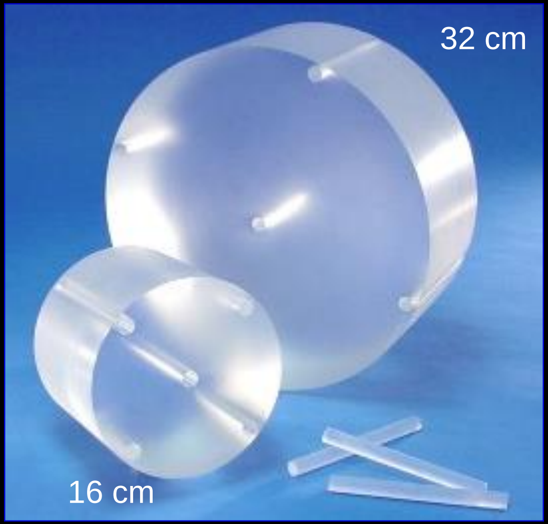

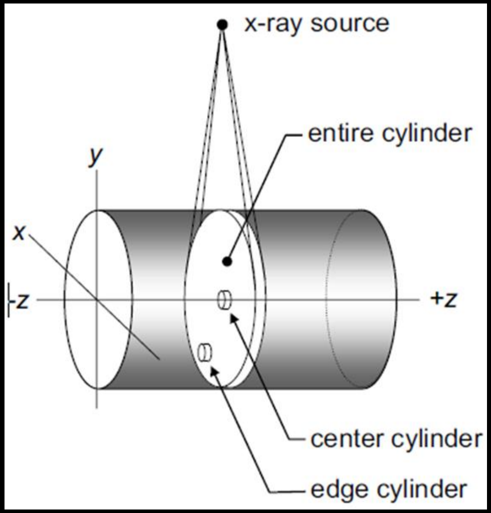
x-ray source
entire cylinder
y
x
-z
+z
center cylinder
edge cylinder

CTDI

Absorbed dose:

1 Gy = 1 J/Kg

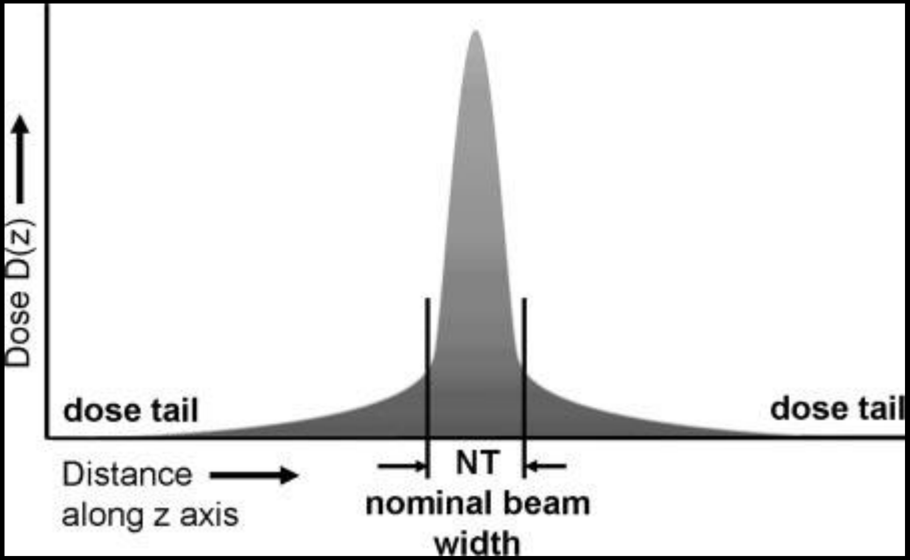

CTDI

CTDI definiton:

$$\mathrm{CTDI} = \frac{1}{NT} \int_{-\infty}^{\infty} D(z)dz$$

CTDI measures the entire dose along z-axis (integral along z), accumulated in the phantom in one tube rotation, without any table movement. The result is normalized by the beam nominal width, (i.e. detectors coverage: NT)

N = number of detectros

T = single detector´s width

CTDI

CTDI measurement:

We cannot measure an integral from -∞ to +∞.

Plus, we need a reference standardized value.

10 cm sensors are used.

So the dose accumulated in the phantom in a distance from -50 mm to +50 mm from the center is measured

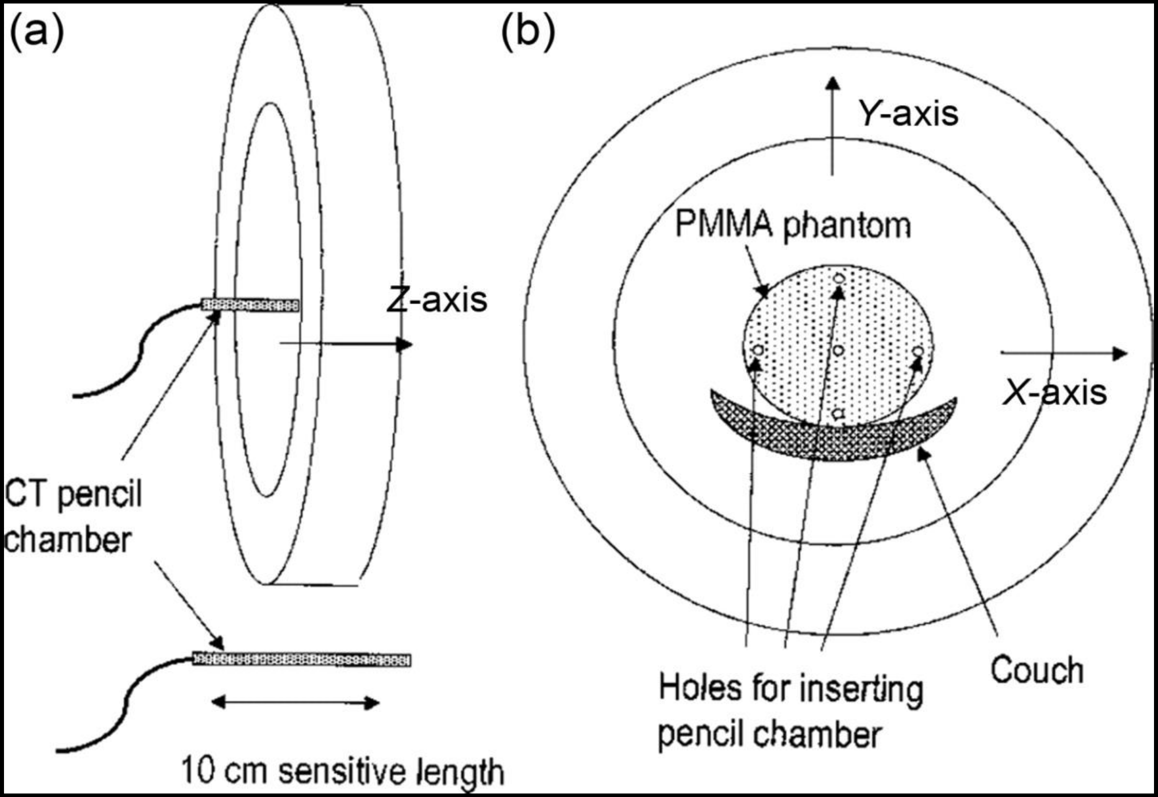
(a)
(b)
Y-axis
PMMA phantom
Z-axis
X-axis
CT pencil chamber
Couch
Holes for inserting pencil chamber
10 cm sensitive length

CTDI

CTDI$_{100}$

Unsing sensors of 100 mm, we define CTDI$_{100}$ like:

$$\mathrm{CTDI}_{100} = \frac{1}{NT} \int_{-50}^{50} D(z)dz$$

CTDI

CTDI_w

The dose accumulated will be different in the center and in the periphery of the phantom.

Sensors are positioned both in the center and in the periphery.

The absorbed dose, will be calculated as a weighted average of central and peripheral measured values:

$$\mathrm{CTDI}_w = \frac{1}{3}\mathrm{CTDI}_{100}^{\mathrm{central}} + \frac{2}{3}\mathrm{CTDI}_{100}^{\mathrm{peripheral}}$$

CTDI

CTDI$_{vol}$

Now we have to take into account the fact that the table (for spiral examinations) is actually moving. We define CTDI$_{vol}$ as:

$$\mathrm{CTDI}_{\mathrm{vol}} = \frac{\mathrm{CTDI}_w}{\mathrm{pitch}}$$

CTDI$_{vol}$ reflects the dose that a 32 cm or 16 cm water phantom would absorb with the specific scan settings.

Patient size plays an important role in estimating the effectively absorbed dose and should be taken into account.

One way of doing it is to calculate the effective diameter of the patient and estimate the aborbed dose via a proportion with the diameter of the phantom.

Effective dose is calculated as DLP*w, where the weight w depends on the body region and the DLP is the CTDI multiplied by the scan lenght.

Form DLP to Effective Dose

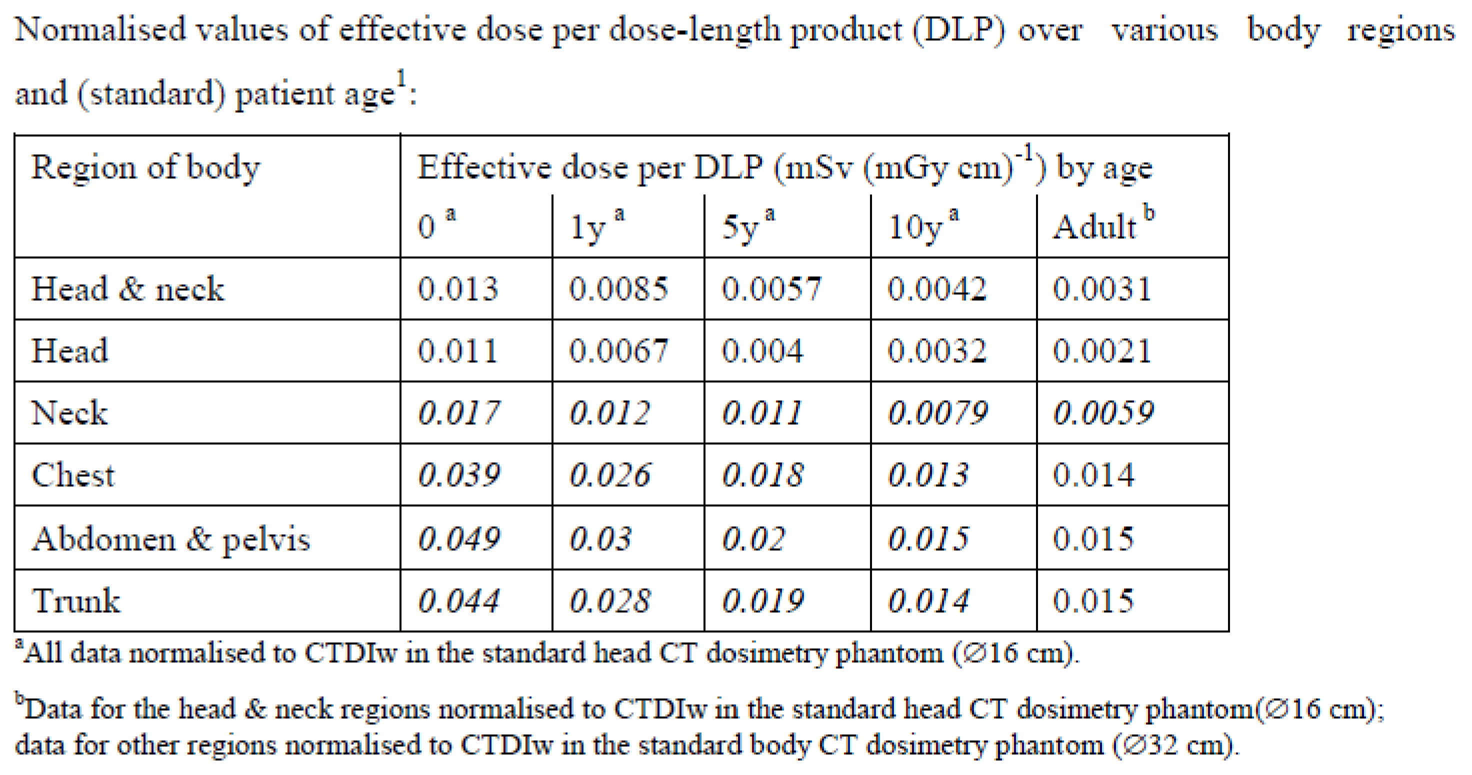

Normalised values of effective dose per dose-length product (DLP) over various body regions and (standard) patient age[1]:

Region of body	Effective dose per DLP (mSv (mGy cm)$^{-1}$) by age				
	0 [a]	1y [a]	5y [a]	10y [a]	Adult [b]
Head & neck	0.013	0.0085	0.0057	0.0042	0.0031
Head	0.011	0.0067	0.004	0.0032	0.0021
Neck	*0.017*	*0.012*	*0.011*	*0.0079*	*0.0059*
Chest	*0.039*	*0.026*	*0.018*	*0.013*	0.014
Abdomen & pelvis	*0.049*	*0.03*	*0.02*	*0.015*	0.015
Trunk	*0.044*	*0.028*	*0.019*	*0.014*	0.015

[a] All data normalised to CTDIw in the standard head CT dosimetry phantom (∅16 cm).

[b] Data for the head & neck regions normalised to CTDIw in the standard head CT dosimetry phantom(∅16 cm); data for other regions normalised to CTDIw in the standard body CT dosimetry phantom (∅32 cm).

mAs Modulation

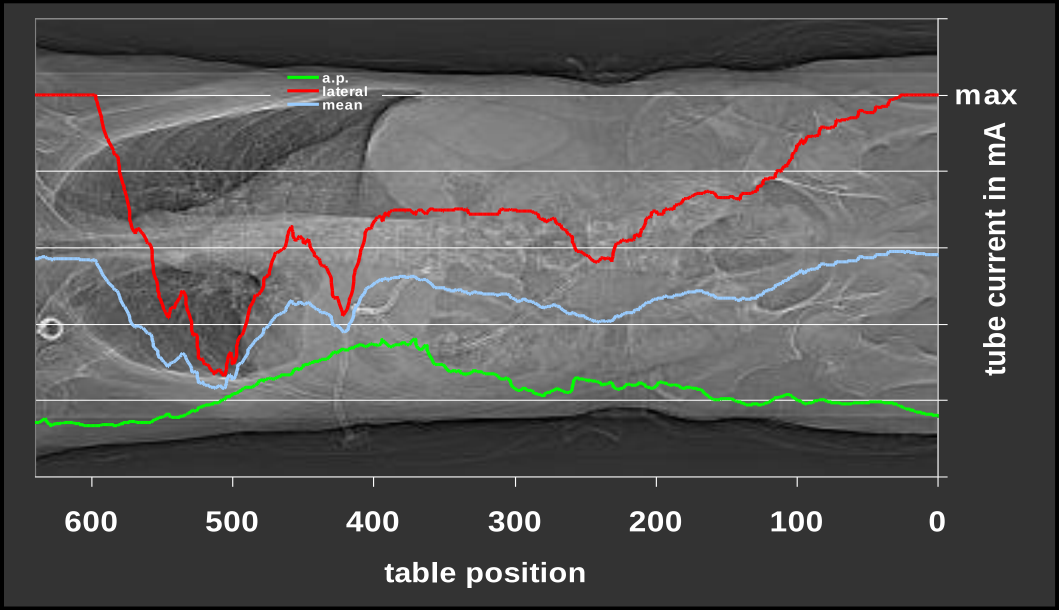

kVp Automatic Selection

Reference kV = 120kV
Reference mAs = 210 mAs

Slider position = Tissue with contrast (TOI)

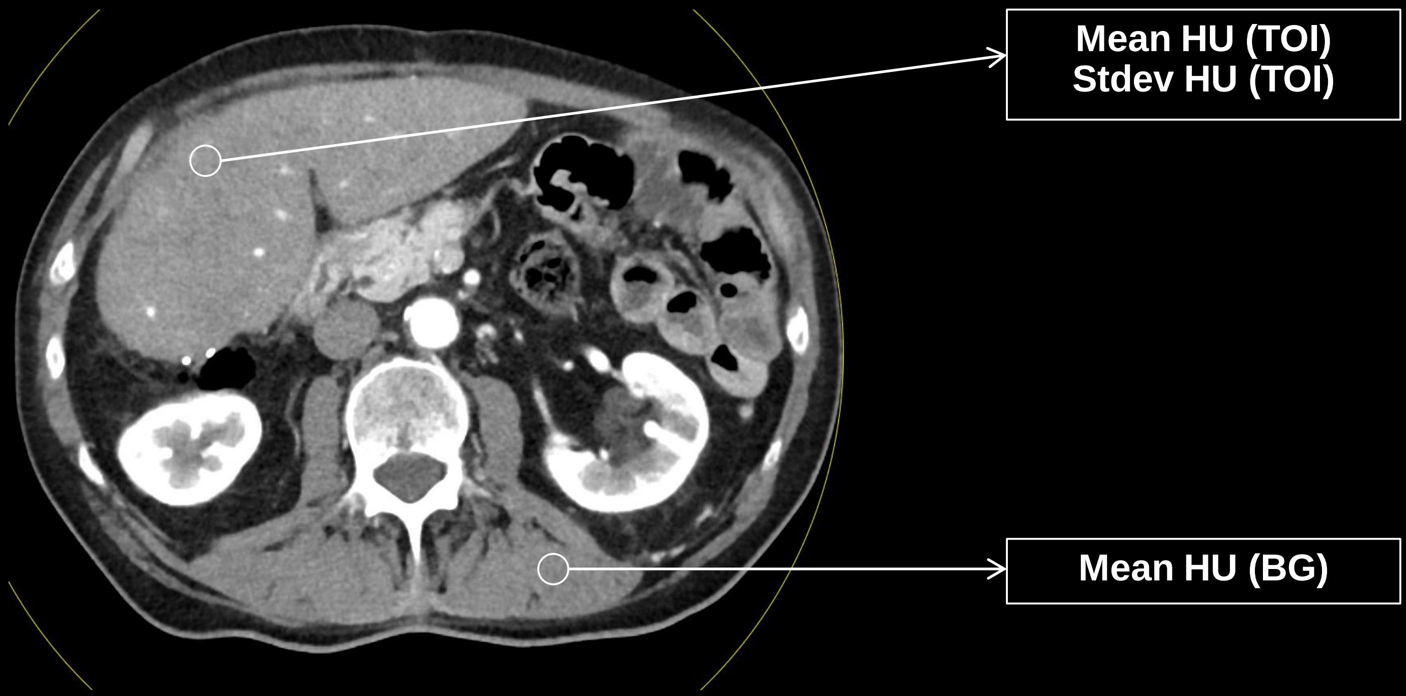

Mean HU (TOI)
Stdev HU (TOI)

Mean HU (BG)

kVp Automatic Selection

$$\mathrm{CNR} = \frac{|\hat{\mu}_1 - \hat{\mu}_2|}{\sqrt{\sigma_1^2 + \sigma_2^2}}$$

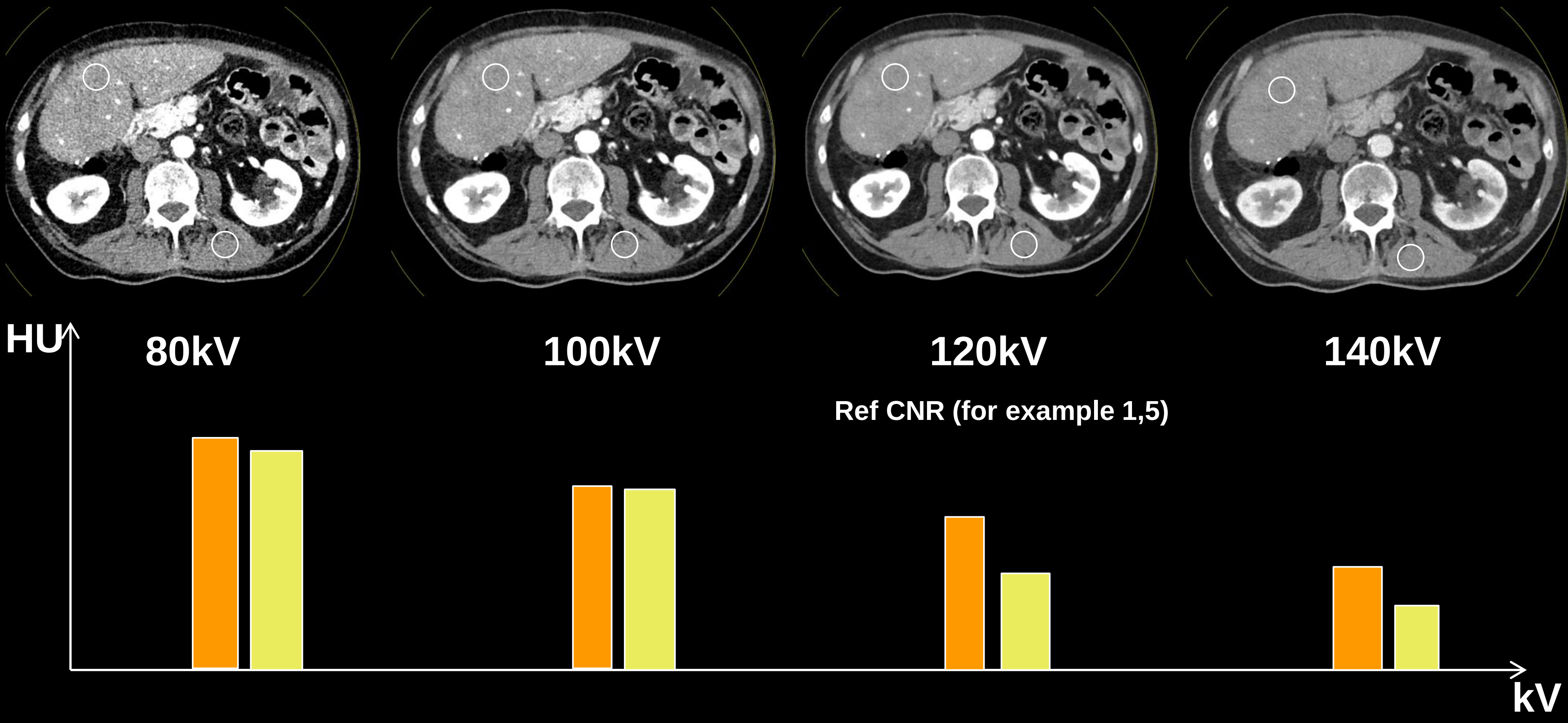
HU
80kV
100kV
120kV
140kV
kV

Ref CNR (for example 1,5)

kVp Automatic Selection

mAs adaptation

$$\mathrm{CNR} = \frac{|\hat{\mu}_1 - \hat{\mu}_2|}{\sqrt{\sigma_1^2 + \sigma_2^2}}$$

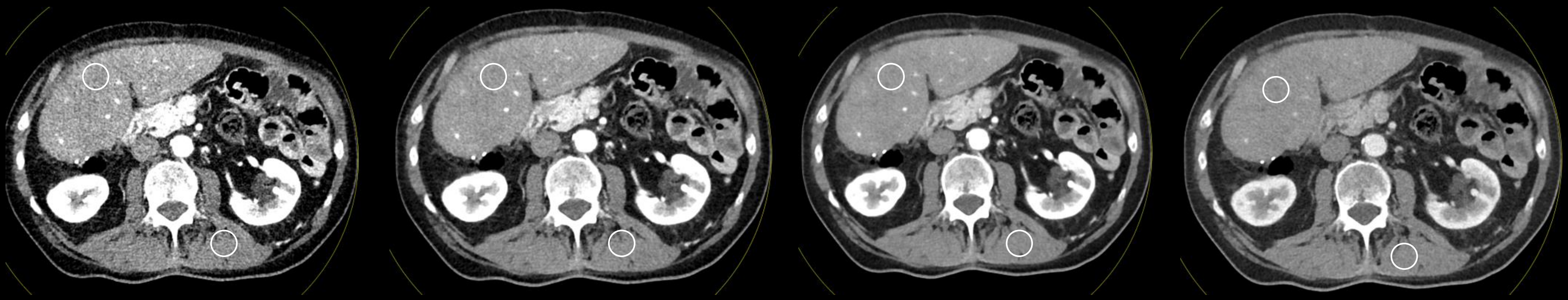

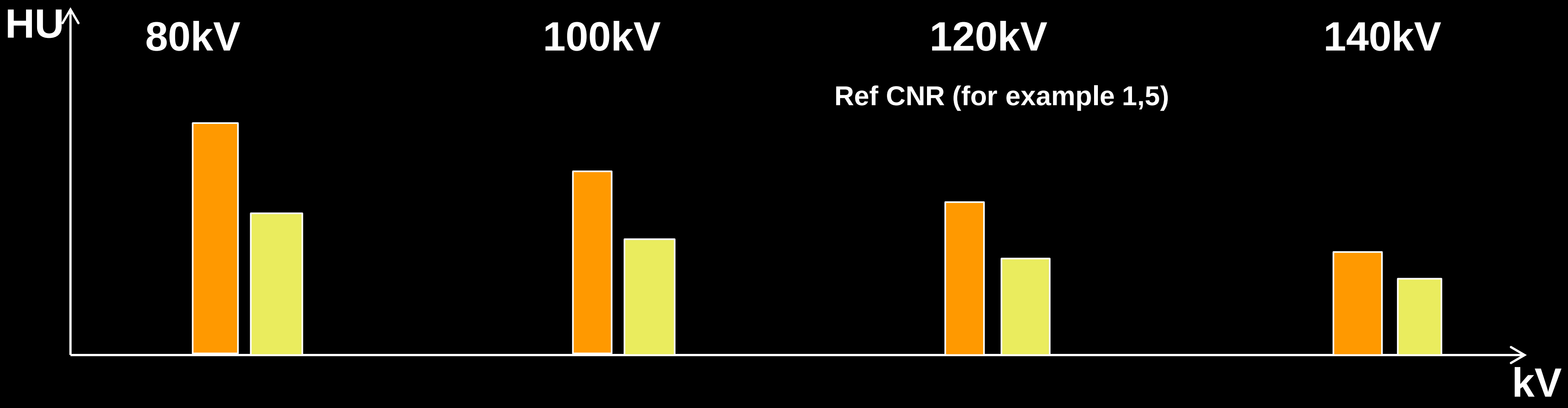

Ref CNR (for example 1,5)

kVp Automatic Selection

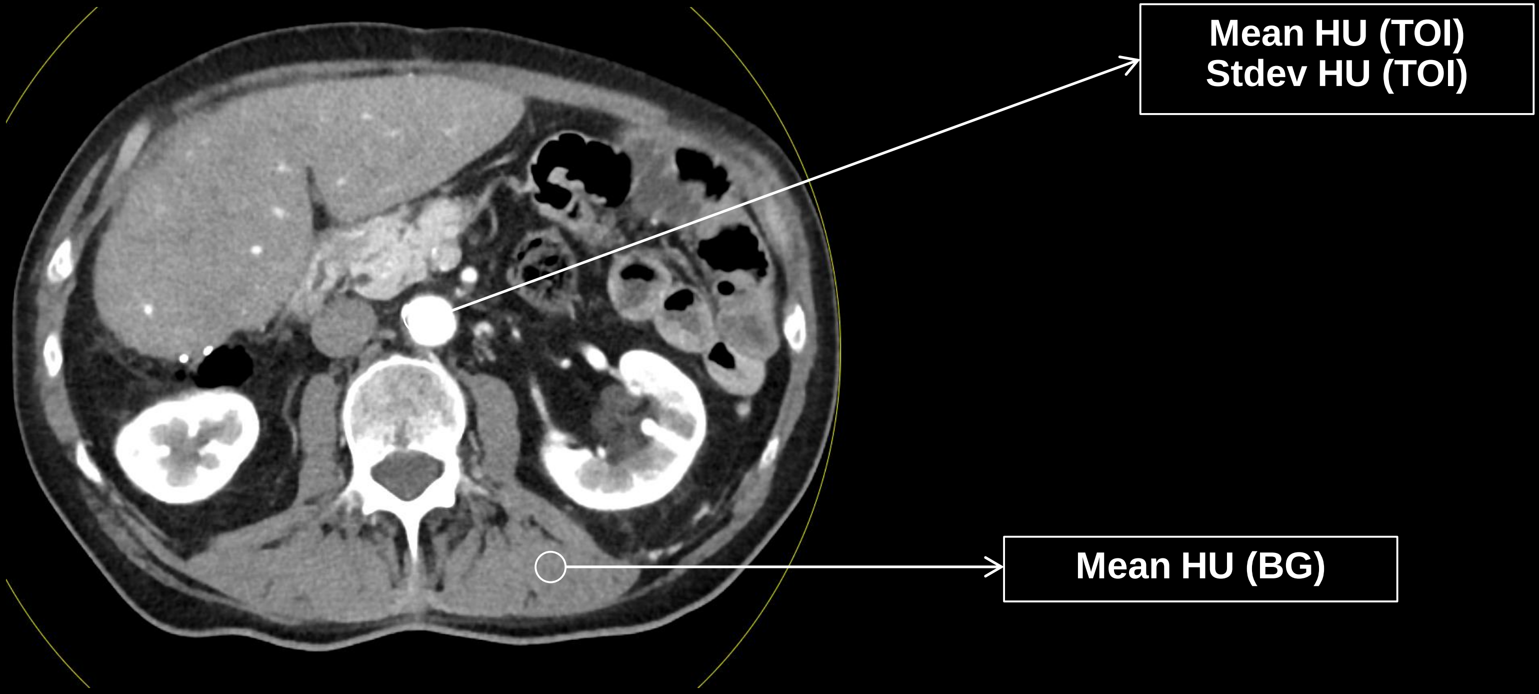
Mean HU (TOI)
Stdev HU (TOI)
Mean HU (BG)

kVp Automatic Selection

$$\mathrm{CNR} = \frac{|\hat{\mu}_1 - \hat{\mu}_2|}{\sqrt{\sigma_1^2 + \sigma_2^2}}$$

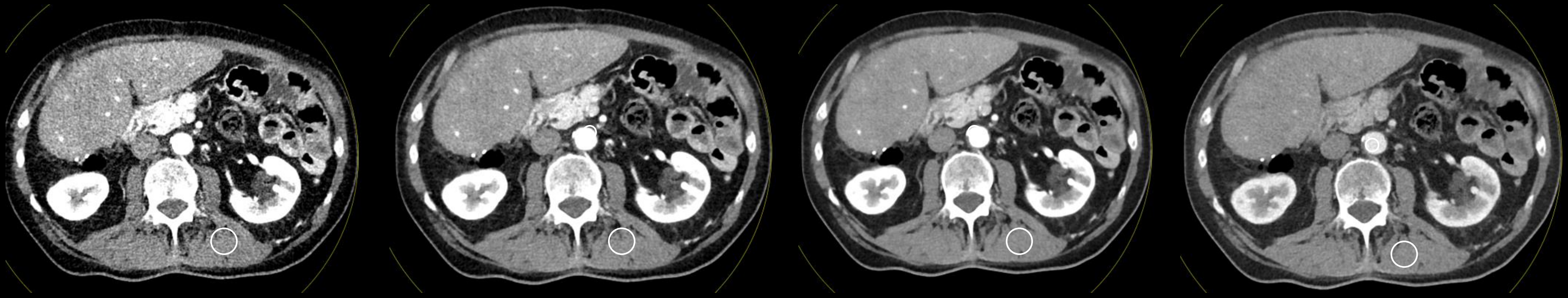

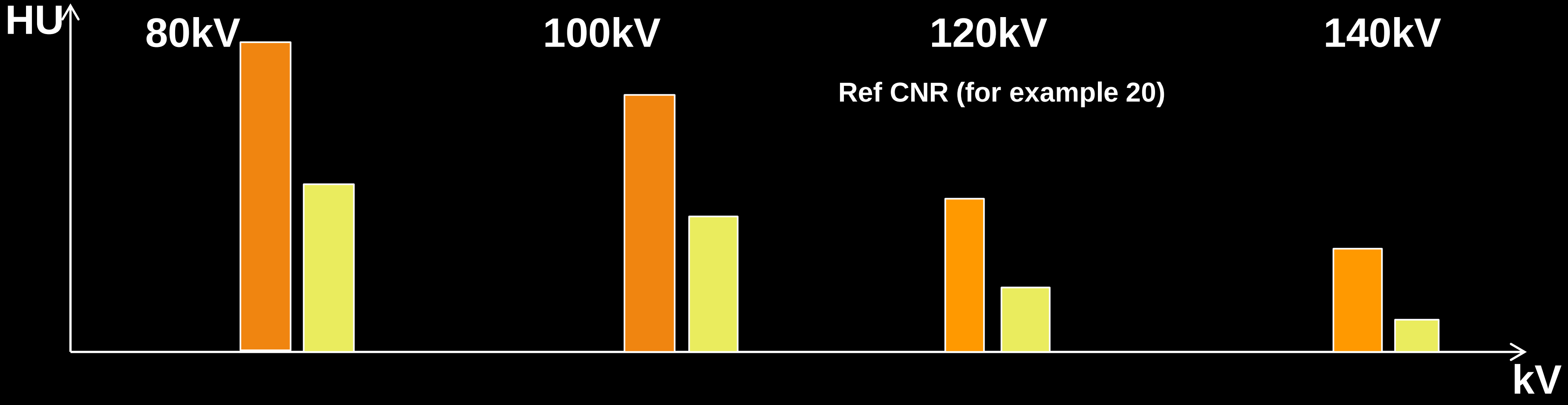

kVp Automatic Selection

mAs adaptation

$$\mathrm{CNR} = \frac{|\hat{\mu}_1 - \hat{\mu}_2|}{\sqrt{\sigma_1^2 + \sigma_2^2}}$$

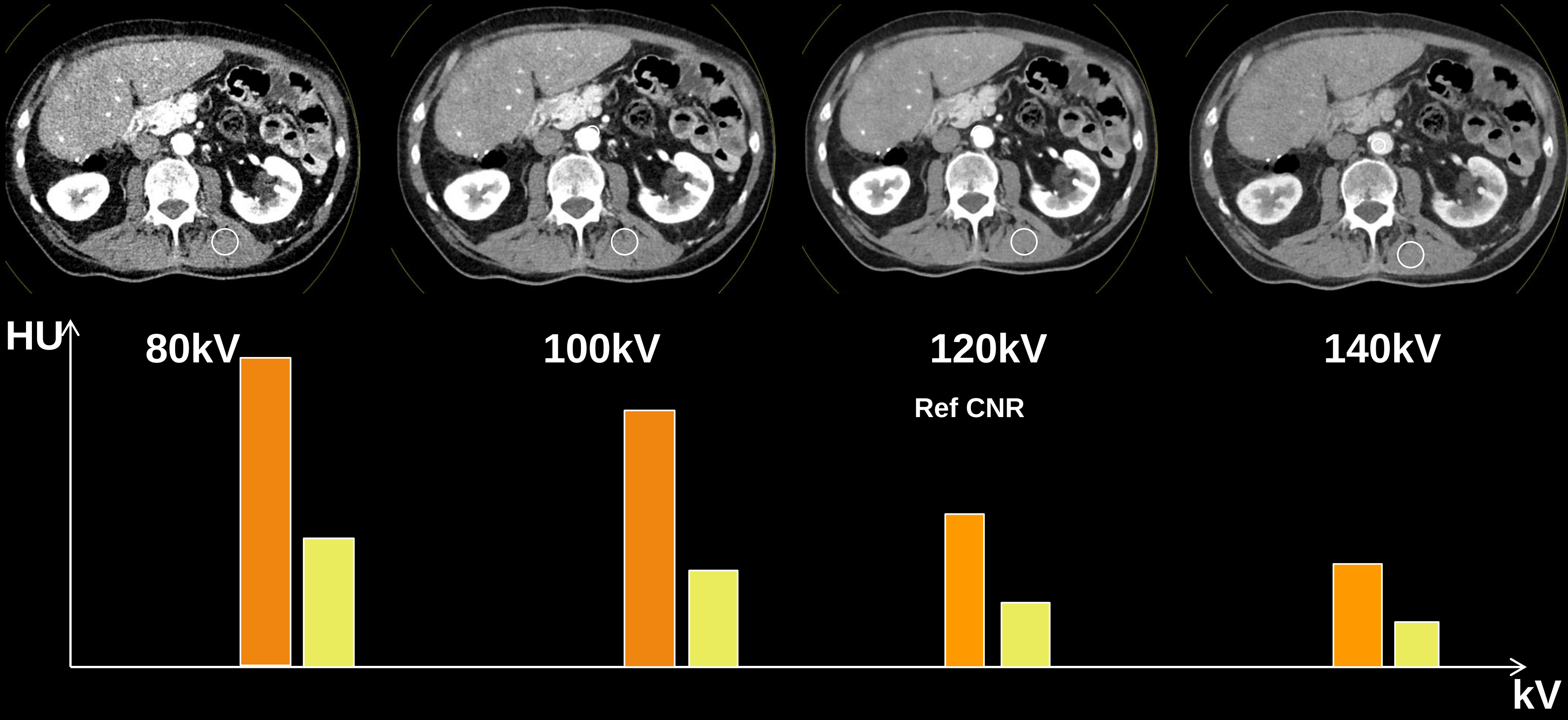
HU
80kV
100kV
120kV
140kV
Ref CNR
kV

Advanced CT Applications

DE CT, Metal Artifact Reduction

Francesco Pisana

German Cancer Research Center (DKFZ), Heidelberg, Germany

DEUTSCHES
KREBSFORSCHUNGSZENTRUM
IN DER HELMHOLTZ-GEMEINSCHAFT

Dual Energy CT

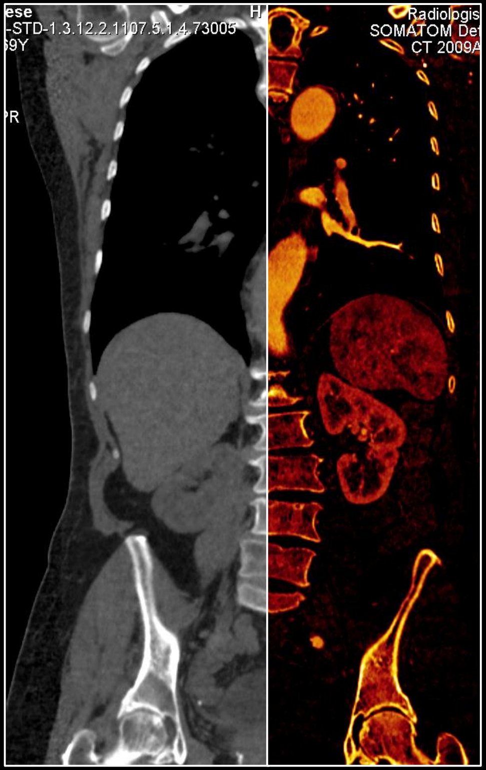
ese
-STD-1.3.12.2.1107.5.1.4.73005
;9Y
H
R
Radiologis
SOMATOM Def
CT 2009A

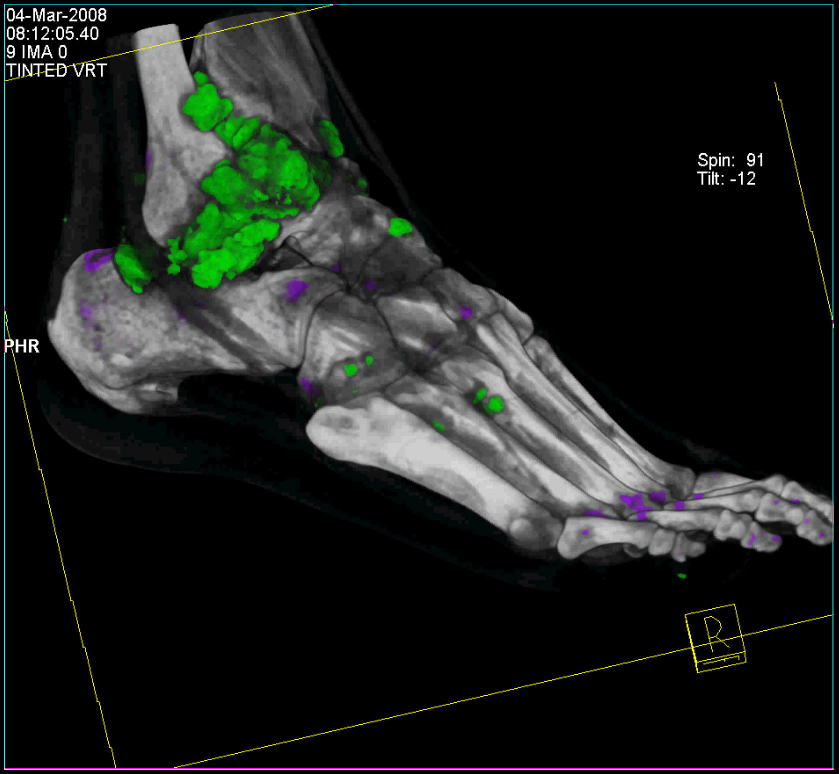
04-Mar-2008
08:12:05.40
9 IMA 0
TINTED VRT
Spin: 91
Tilt: -12
PHR
R

Index of Contents

- Introduction:
  - X-ray attenuation
  - DE principles and technical solutions
- Clinical applications and protocol optimization:
  - Material classification
  - Material quantification (decomposition)
  - Pseudo-monoenergetic images
  - Electron density and effective atomic number images

Index of Contents

- **Introduction:**
  - X-ray attenuation
  - DE principles and technical solutions
- **Clinical applications and protocol optimization:**
  - Material classification
  - Material quantification (decomposition)
  - Pseudo-monoenergetic images
  - Electron density and effective atomic number images

X-ray Attenuation

- Beer’s law:

$$I = I_0\, e^{-\int_0^{\mathrm{keVp}} \int_0^L \mu(s,\mathrm{E})ds\, dE}$$

- Attenuation coefficient of a material *x*:

$$\mu_x(E) = \cancel{x_{\mathrm{R}}\, f_{\mathrm{R}}}(E) + x_{\mathrm{P}}\, f_{\mathrm{P}}(E) + x_{\mathrm{C}}\, f_{\mathrm{C}}(E) + \cancel{x_{\mathrm{PP}}\, f_{\mathrm{PP}}}(E)$$

$$\mu_x(E) \sim \rho_x \frac{\mathrm{N_A}}{A_x} Z_x^4 f_{\mathrm{P}}(E) + \rho_x \frac{\mathrm{N_A}}{A_x} Z_x f_{\mathrm{C}}(E)$$

$$\mu_x(E) \sim \rho_x \frac{\mathrm{N_A}}{A_x} Z_x \left(Z_x^3 \frac{1}{E^3} + f_{\mathrm{KN}}(E) \right)$$

Where f_{KN} is the Klein-Nishina function

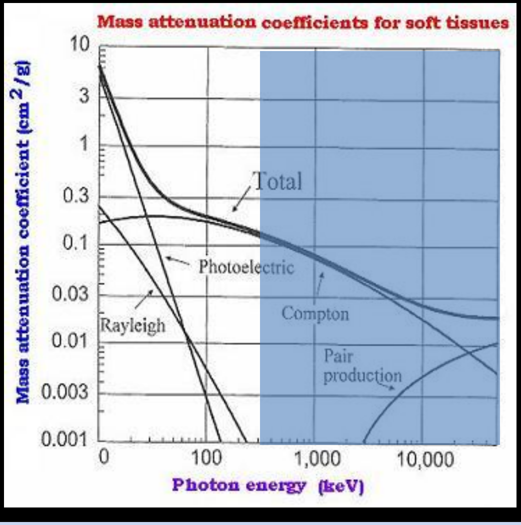

X-ray Attenuation

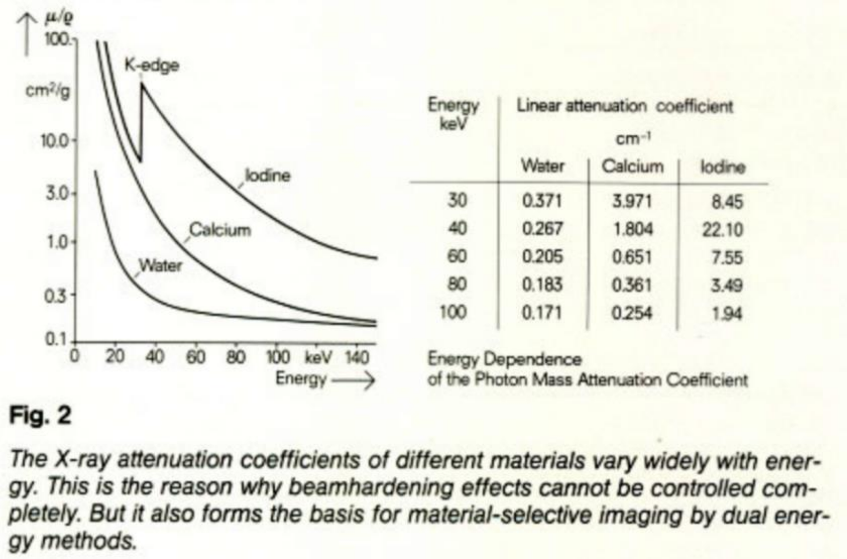

Energy keV	Linear attenuation coefficient cm⁻¹		
	Water	Calcium	Iodine
30	0.371	3.971	8.45
40	0.267	1.804	22.10
60	0.205	0.651	7.55
80	0.183	0.361	3.49
100	0.171	0.254	1.94

Energy Dependence
of the Photon Mass Attenuation Coefficient

Fig. 2

The X-ray attenuation coefficients of different materials vary widely with energy. This is the reason why beamhardening effects cannot be controlled completely. But it also forms the basis for material-selective imaging by dual energy methods.

Kalender WA et al. Radiology 164:419-423, 1987

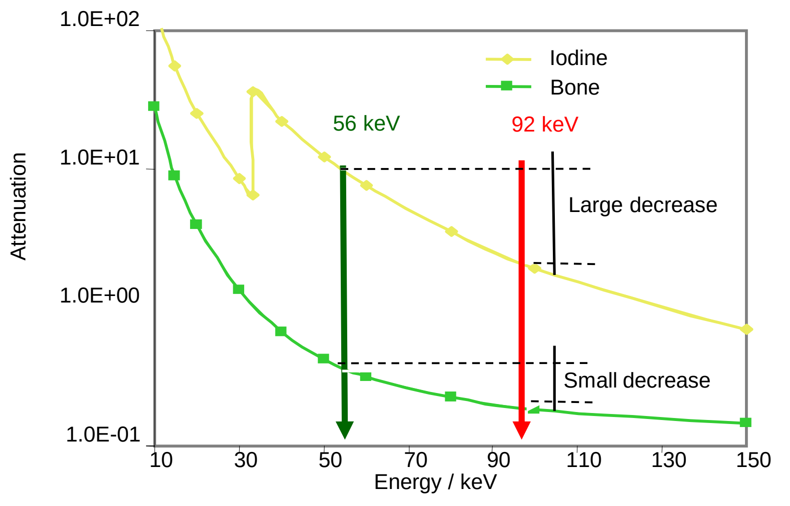

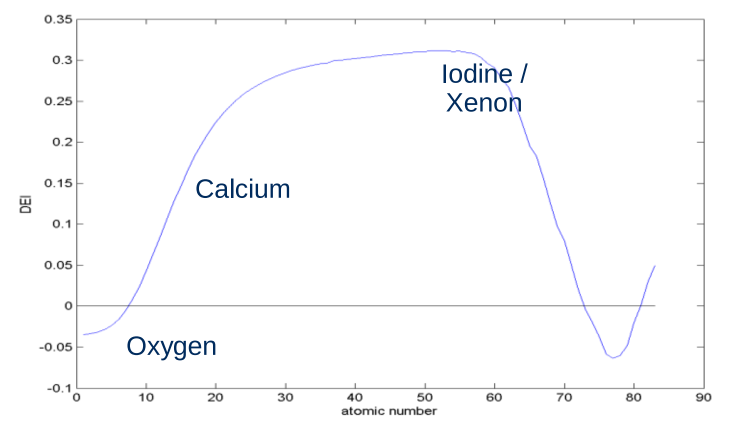

$$\mathrm{D.E.I.}_x = \frac{\mu_x(E_1) - \mu_x(E_2)}{\mu_x(E_1) + \mu_x(E_2)}$$

Index of Contents

- **Introduction:**
  - X-ray attenuation
  - DE principles and technical solutions
- **Clinical applications and protocol optimization:**
  - Material classification
  - Material quantification (decomposition)
  - Pseudo-monoenergetic images
  - Electron density and effective atomic number images

DE Principles

- Basic assumptions.
  - Noise
  - Motion
  - Artifacts
- K-edge.
- Materials with “DE properties”.

DE Principles

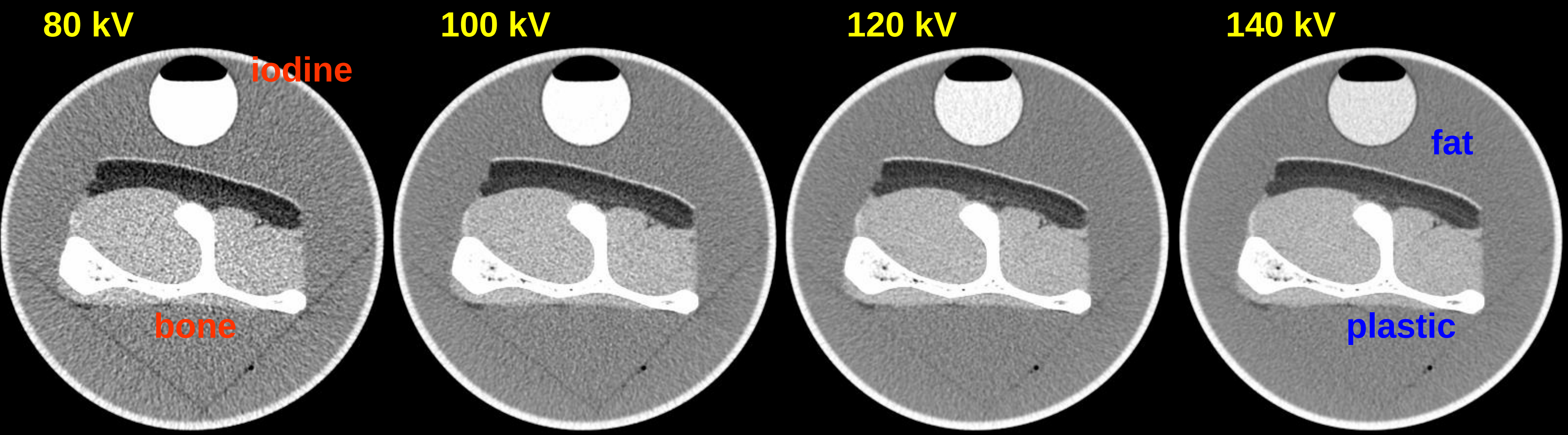
80 kV
iodine
bone
100 kV
120 kV
140 kV
fat
plastic

Technical Implementation

• In the clinic:	
– Multiple scans at different spectra	mid-range
– Dual source CT (DSCT), generations 2, and 3	high-end
– Fast tube voltage switching	high-end
– Dual layer sandwich detectors	high-end
– Split filter	mid-range
• First prototypes:	
– Photon counting detectors (two or more energy bins)	high-end?

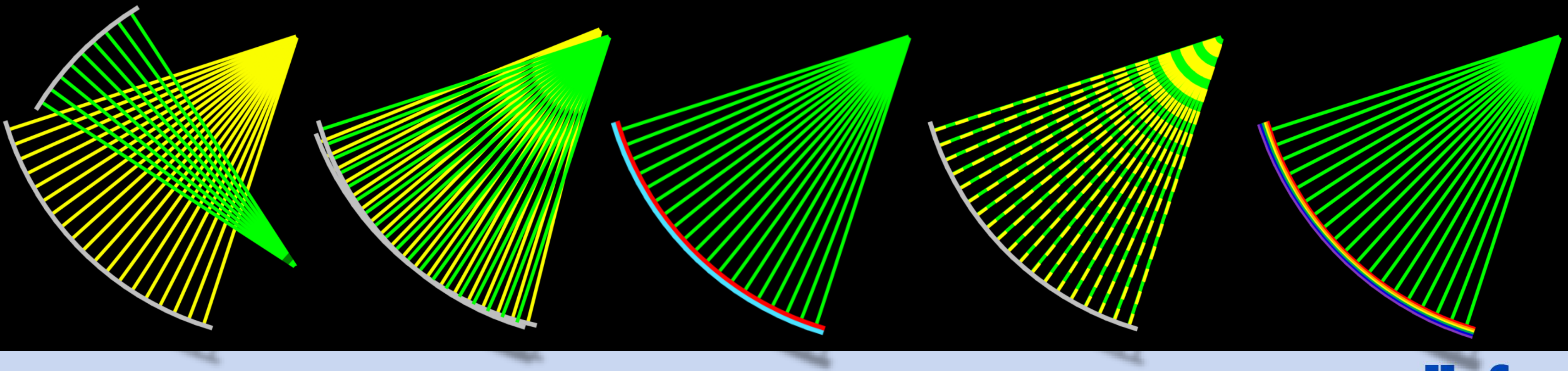

Technical Implementation

- DECT approaches in the clinic:
  - Dual source DECT (Siemens)

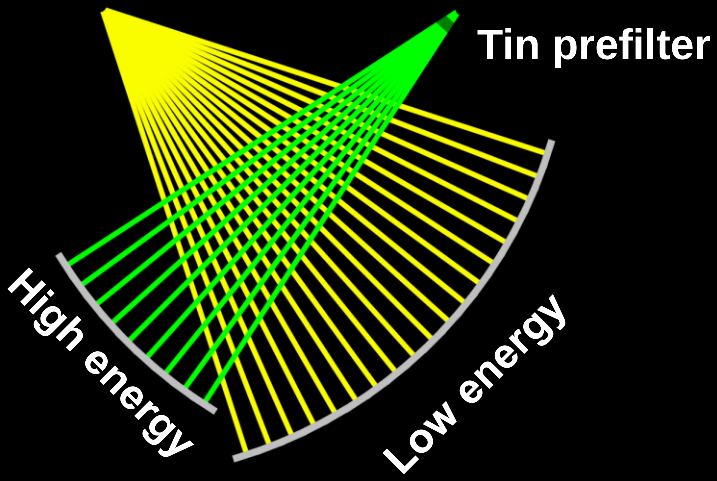
Tin prefilter
High energy
Low energy

SIEMENS
SOMATOM Force

Siemens Somatom Force

Technical Implementation

- DECT approaches in the clinic:
  - Dual source DECT (Siemens)
  - Fast tube voltage switching (GE)

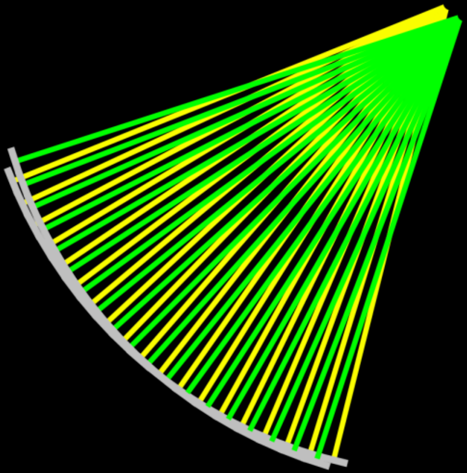

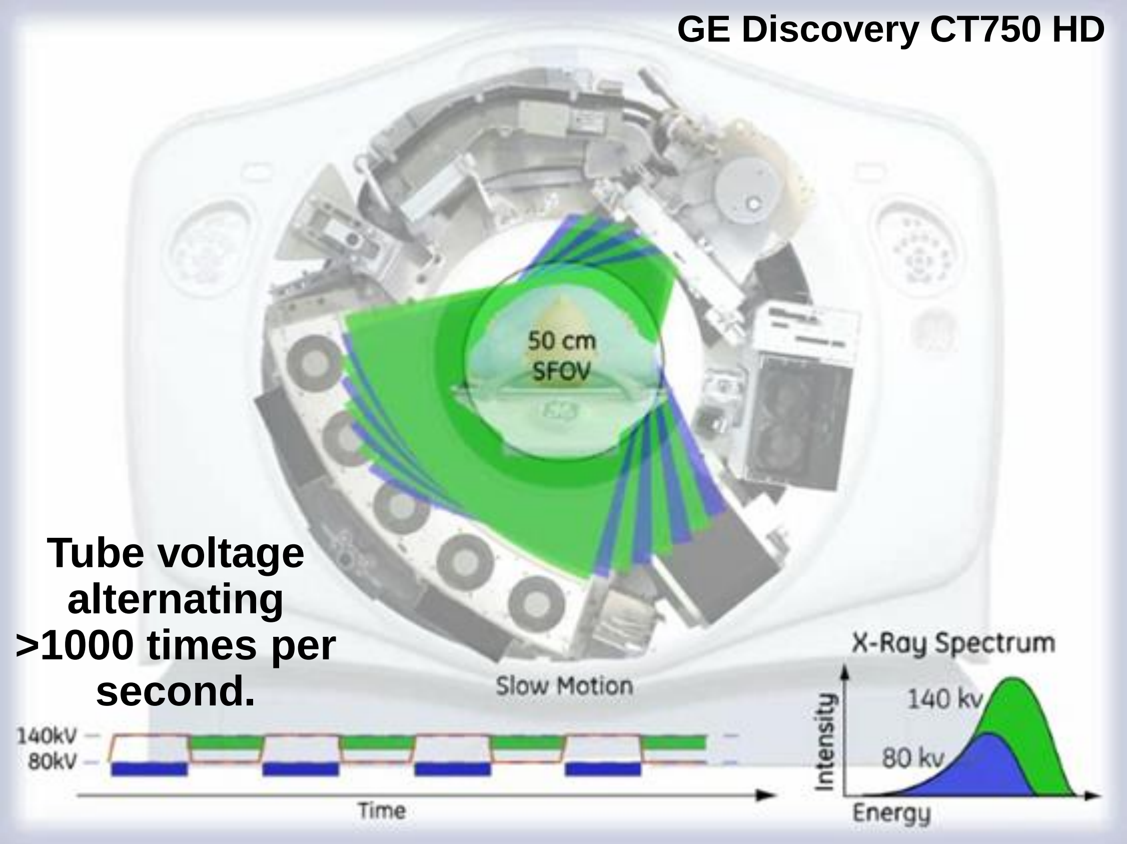

GE Discovery CT750 HD

Tube voltage alternating >1000 times per second.

50 cm
SFOV
Slow Motion
140kV
80kV
Time
X-Ray Spectrum
140 kv
80 kv
Intensity
Energy

Technical Implementation

- DECT approaches in the clinic:
  - Dual source DECT (Siemens)
  - Fast tube voltage switching (GE)

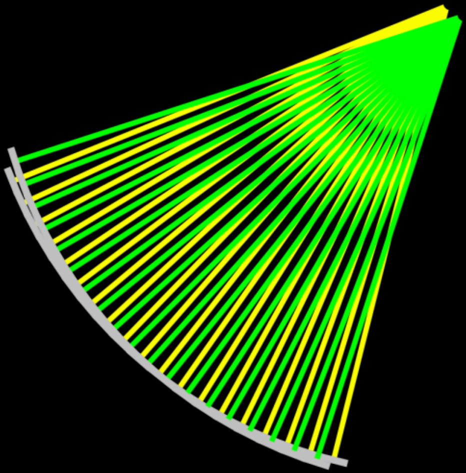

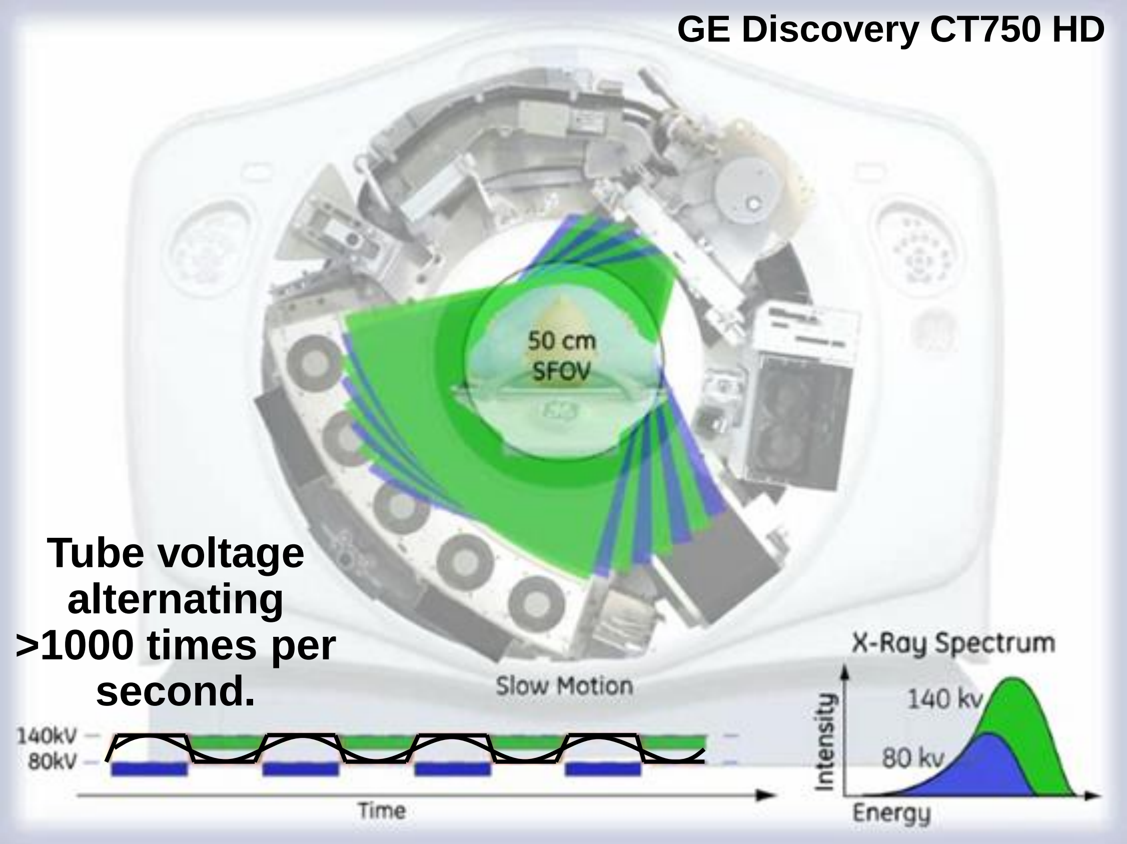
GE Discovery CT750 HD

Tube voltage alternating >1000 times per second.

50 cm
SFOV
Slow Motion
140kV
80kV
Time
X-Ray Spectrum
Intensity
140 kv
80 kv
Energy

Technical Implementation

- DECT approaches in the clinic:
  - Dual source DECT (Siemens)
  - Fast tube voltage switching (GE)
  - Dual layer (sandwich) detector (Philips)

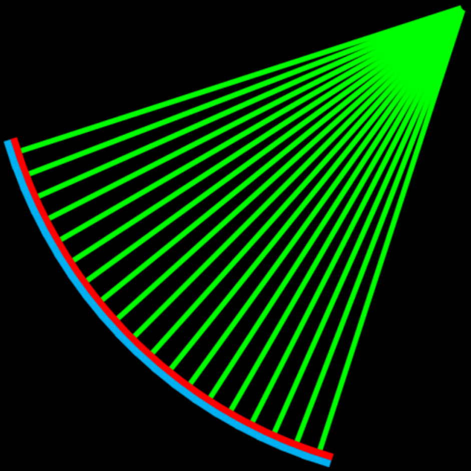

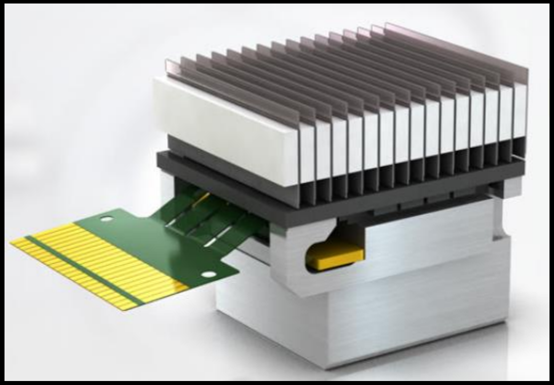

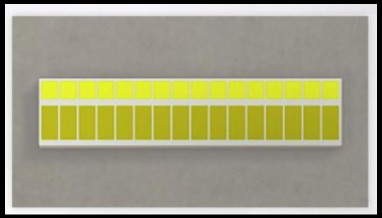

Philips IQon

Technical Implementation

- DECT approaches in the clinic:
  - Dual source DECT (Siemens)
  - Fast tube voltage switching (GE)
  - Dual layer (sandwich) detector (Philips)
  - Split filter (Siemens)

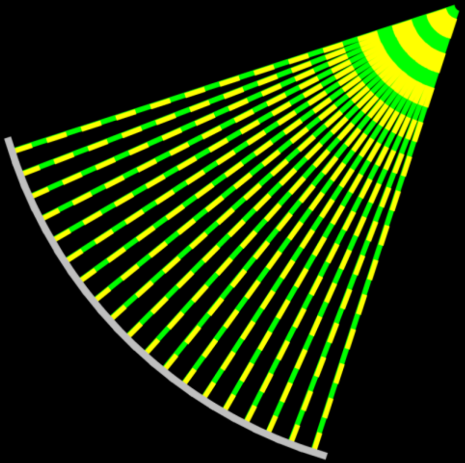

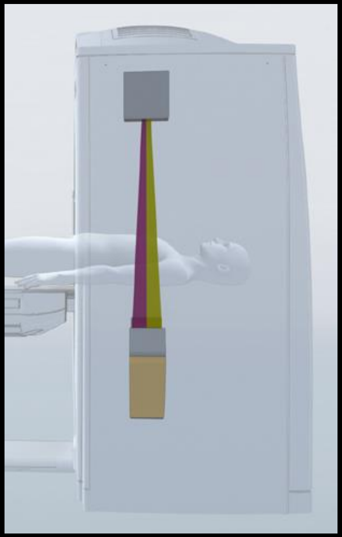

SIEMENS
SOMATOM
Definition Edge

Siemens Definition Edge TwinBeam

Technical Implementation

- DECT approaches in the clinic:
  - Dual source DECT (Siemens)
  - Fast tube voltage switching (GE)
  - Dual layer (sandwich) detector (Philips)
  - Split filter (Siemens)
- First prototype systems
  - Photon counting detector, multiple energy bins

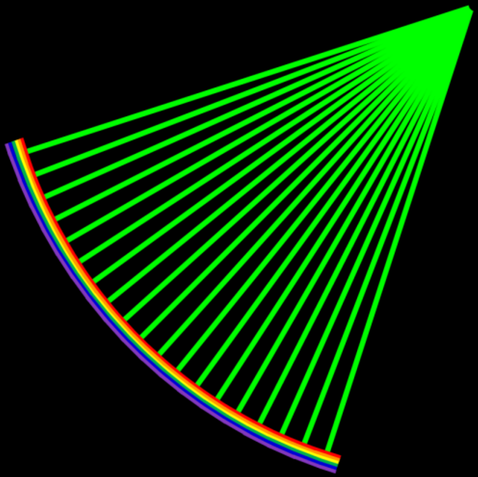

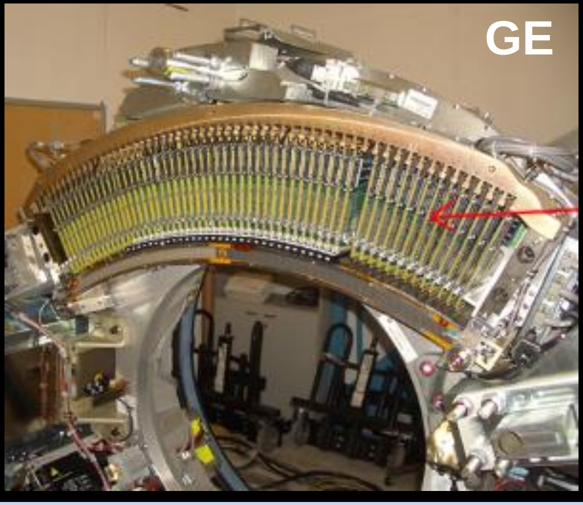

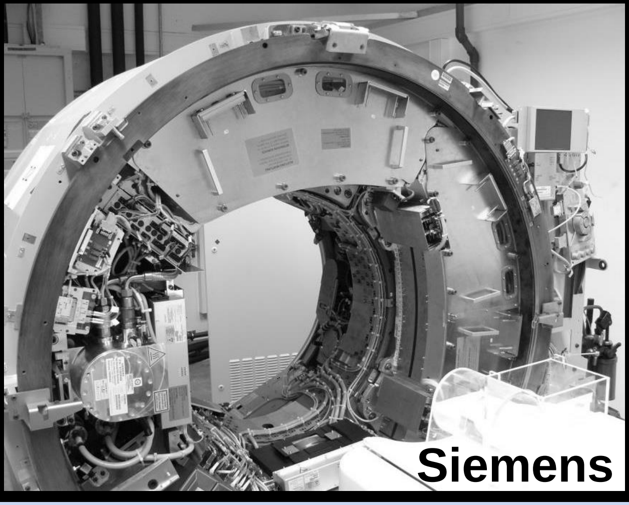

Spectral Separation

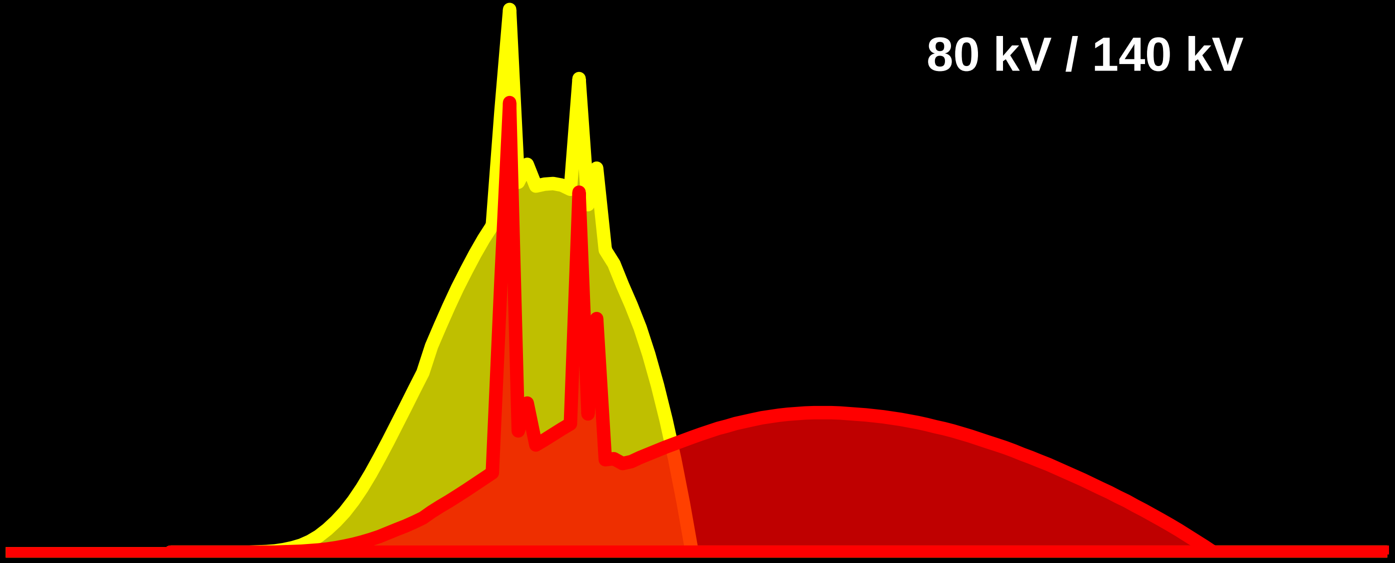

Used in
- Siemens‘ 1st generation DSCT

80 kV / 140 kV

Spectra as seen after having passed a 32 cm water layer.

Faby S and Kachelrieß M.: “Performance of today’s dual energy CT and future multi energy CT in virtual non-contrast imaging and in iodine quantification: A simulation study”, *Med Phys* **42**, 4349 (2015);

Spectral Separation

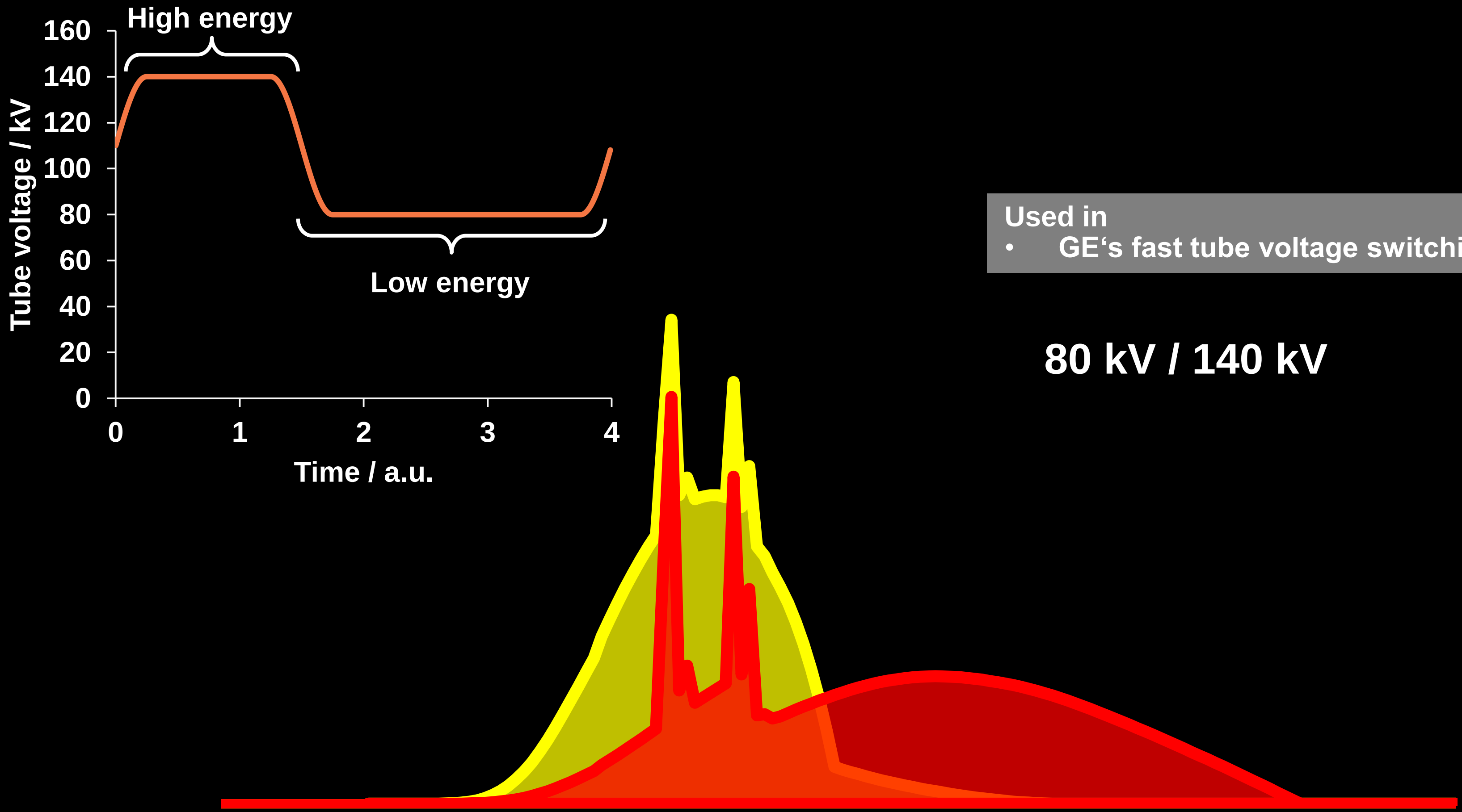

Used in
- GE‘s fast tube voltage switching CT

80 kV / 140 kV

Spectra as seen after having passed a 32 cm water layer.

Faby S and Kachelrieß M.: “Performance of today’s dual energy CT and future multi energy CT in virtual non-contrast imaging and in iodine quantification: A simulation study”, *Med Phys* **42**, 4349 (2015);

Spectral Separation

Used in

- Siemens‘ 2^{nd} generation DSCT

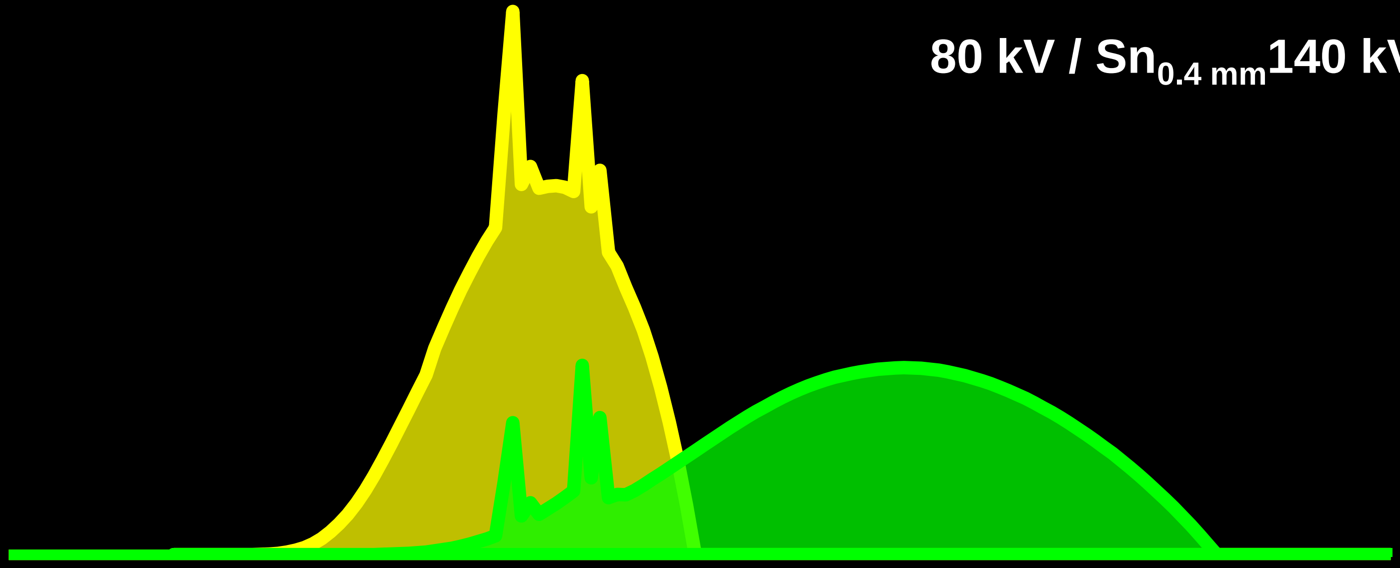

80 kV / $Sn_{0.4\ mm}$140 kV

Spectra as seen after having passed a 32 cm water layer.

Faby S and Kachelrieß M.: “Performance of today’s dual energy CT and future multi energy CT in virtual non-contrast imaging and in iodine quantification: A simulation study”, *Med Phys* **42**, 4349 (2015);

Spectral Separation

Used in
- Siemens‘ 3rd generation DSCT

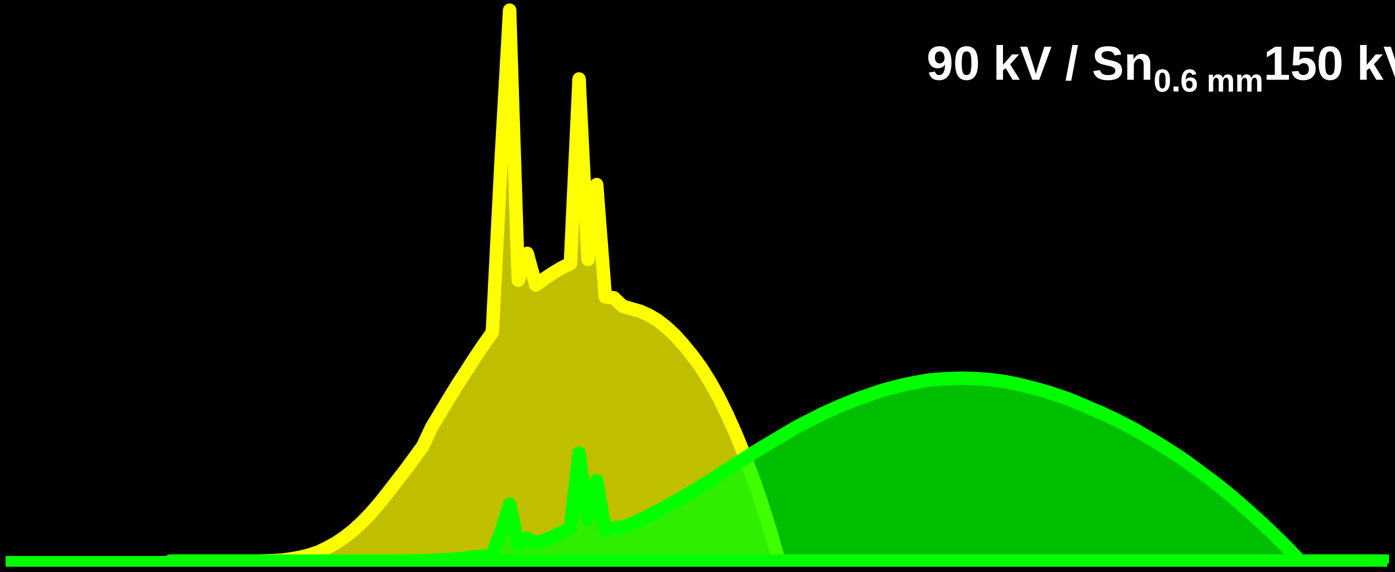

90 kV / Sn$_{0.6\ mm}$150 kV

Spectra as seen after having passed a 32 cm water layer.

Faby S and Kachelrieß M.: “Performance of today’s dual energy CT and future multi energy CT in virtual non-contrast imaging and in iodine quantification: A simulation study”, *Med Phys* **42**, 4349 (2015);

Spectral Separation

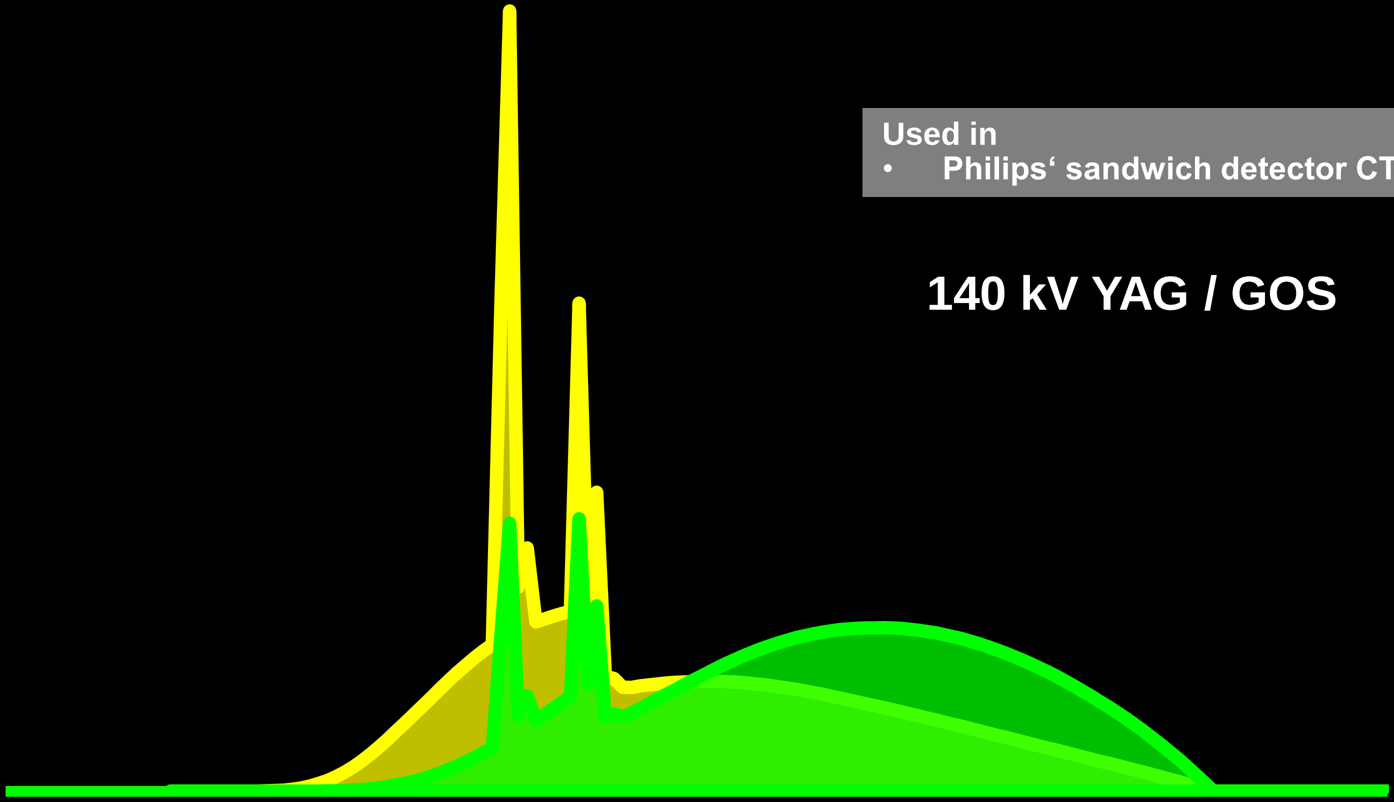

Used in
- Philips‘ sandwich detector CT

140 kV YAG / GOS

Spectra as seen after having passed a 32 cm water layer.

Faby S and Kachelrieß M.: “Performance of today’s dual energy CT and future multi energy CT in virtual non-contrast imaging and in iodine quantification: A simulation study”, *Med Phys* **42**, 4349 (2015);

Spectral Separation

Used in
- Siemens‘ split filter DSCT

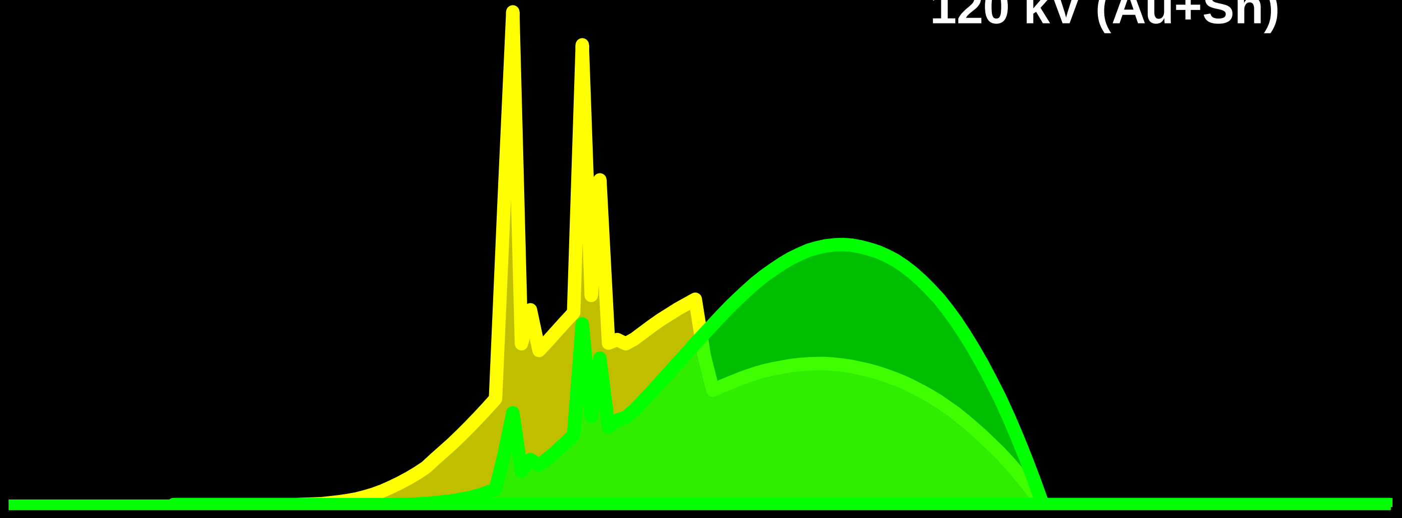

Spectra as seen after having passed a 32 cm water layer.

Faby S and Kachelrieß M.: “Performance of today’s dual energy CT and future multi energy CT in virtual non-contrast imaging and in iodine quantification: A simulation study”, *Med Phys* **42**, 4349 (2015);

Spectral Separation

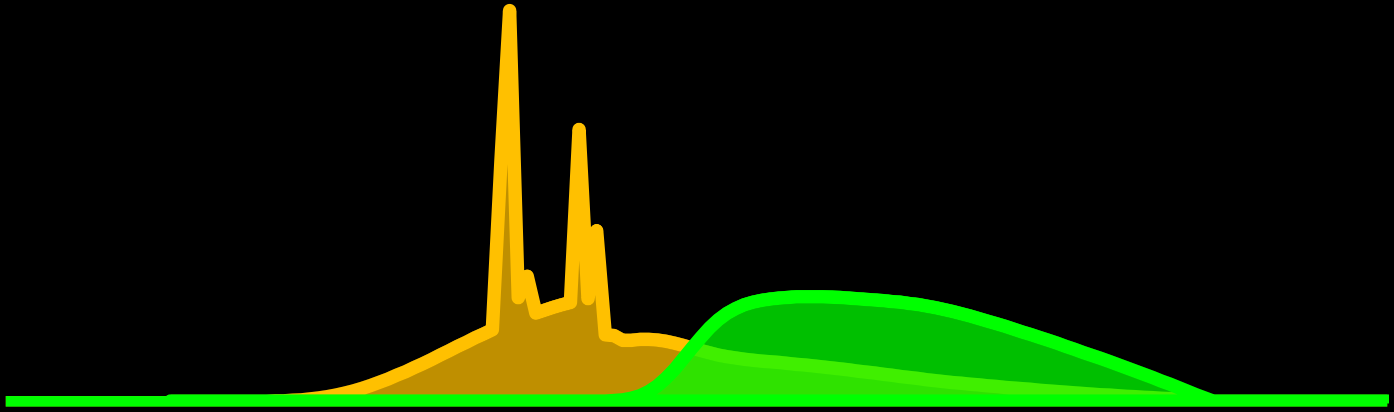

PC 140 kV (2 Bins)

Spectra as seen after having passed a 32 cm water layer.

Faby S and Kachelrieß M.: “Performance of today’s dual energy CT and future multi energy CT in virtual non-contrast imaging and in iodine quantification: A simulation study”, *Med Phys* **42**, 4349 (2015);

Index of Contents

- **Introduction:**
  - **X-ray attenuation**
  - **DE principles and technical solutions**
- **Clinical applications and protocol optimization:**
  - **Material classification**
  - **Material quantification (decomposition)**
  - **Pseudo-monoenergetic images**
  - **Electron density and effective atomic number images**

Material Classification

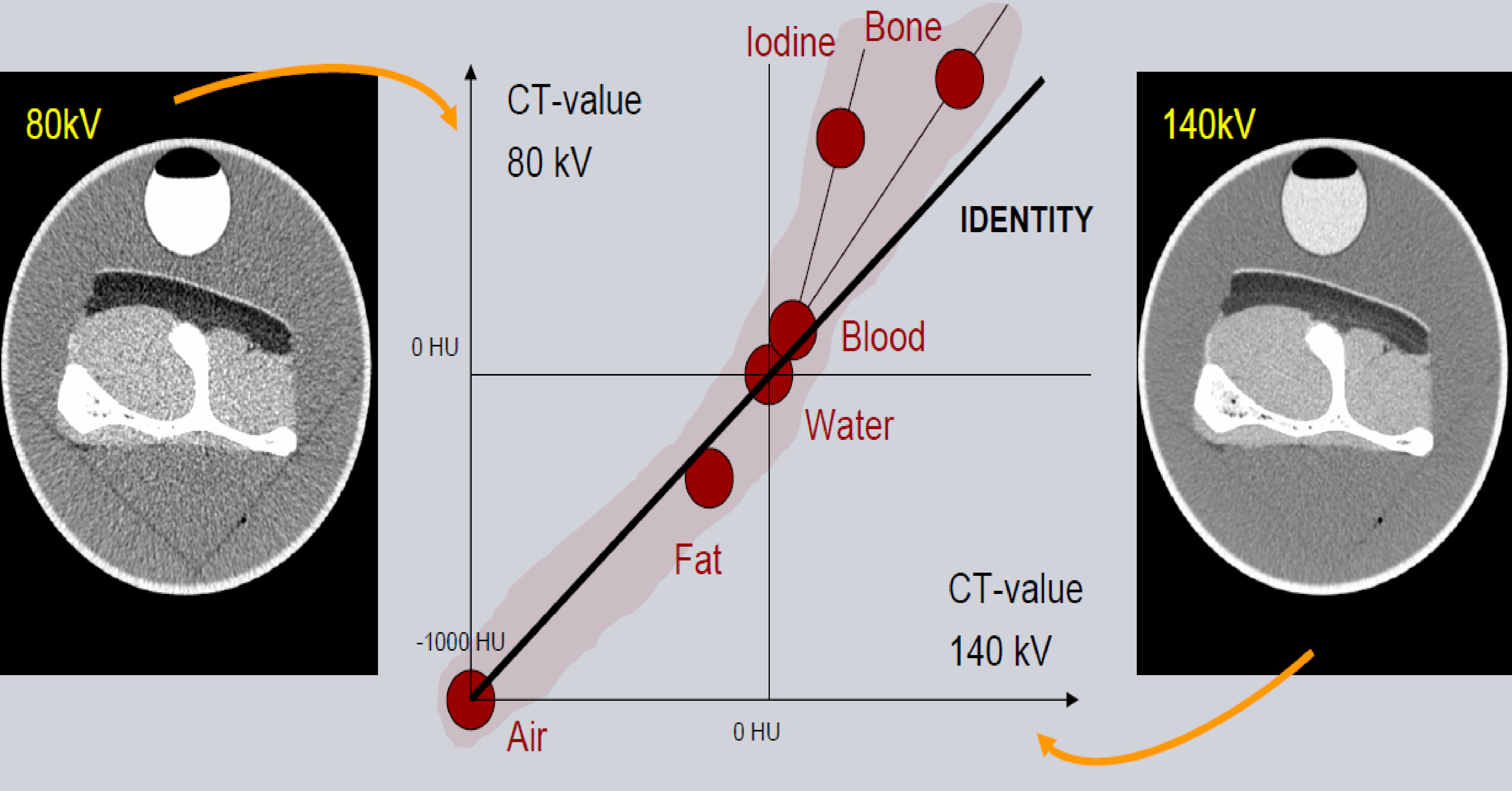
80kV
CT-value
80 kV
0 HU
-1000 HU
Iodine
Bone
IDENTITY
Blood
Water
Fat
Air
0 HU
CT-value
140 kV
140kV

Slides courtesy of Siemens Healthcare GmbH

Material Classification

Bone Removal

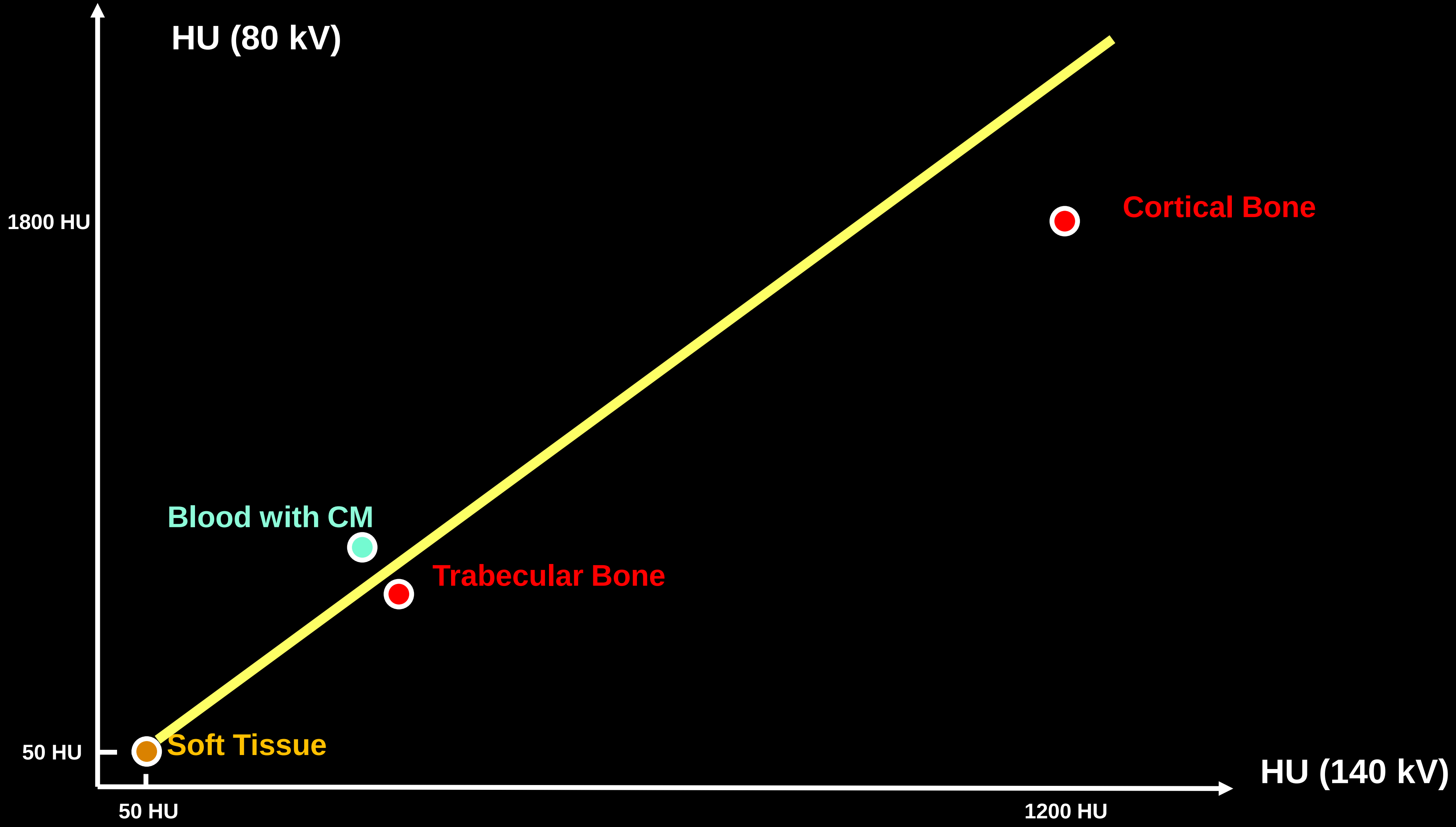

Material Classification

Bone Removal

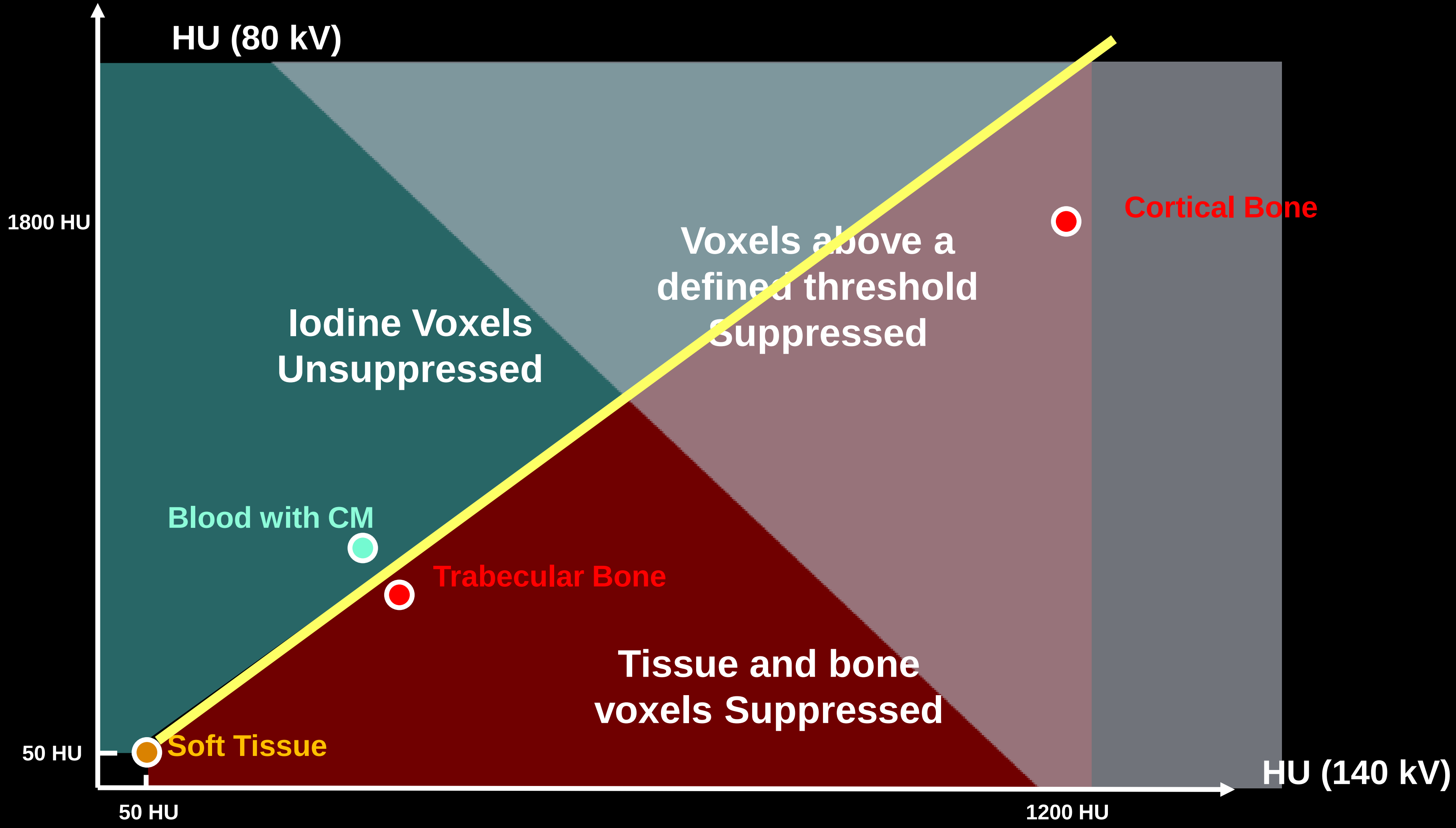
HU (80 kV)
1800 HU
50 HU
50 HU
1200 HU
HU (140 kV)
Iodine Voxels Unsuppressed
Voxels above a defined threshold Suppressed
Tissue and bone voxels Suppressed
Cortical Bone
Blood with CM
Trabecular Bone
Soft Tissue

Material Classification

Bone Removal

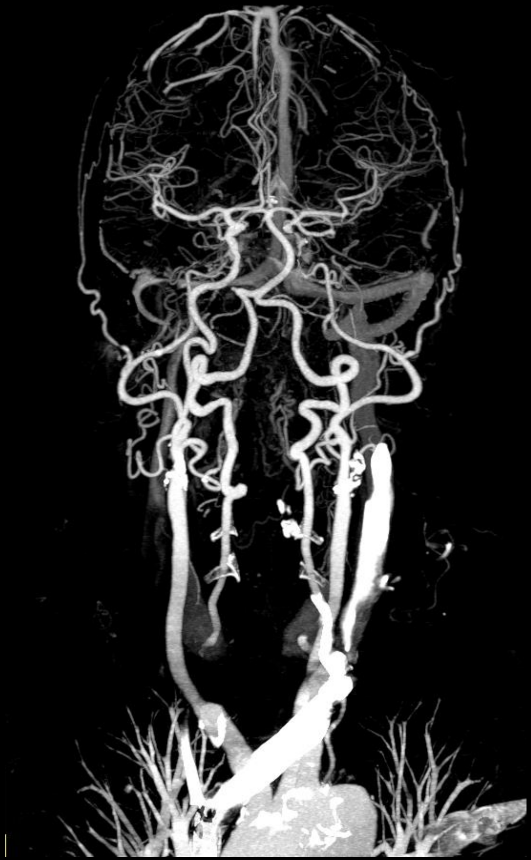

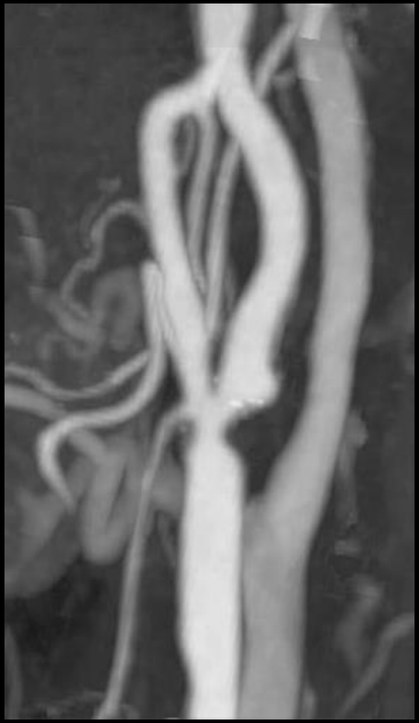

Dual energy CT
plaque-removal

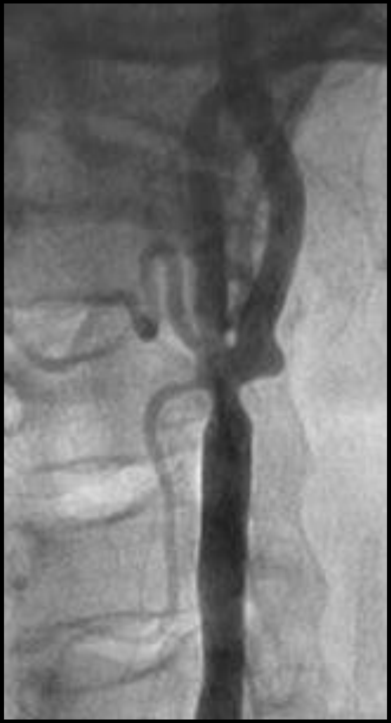

Digital subtraction
angiography

Courtesy of University Hospital Krakau, Polen and PUMC, Beijing, China

Slides courtesy of Siemens Healthcare GmbH

Material Classification

Kidney Stones

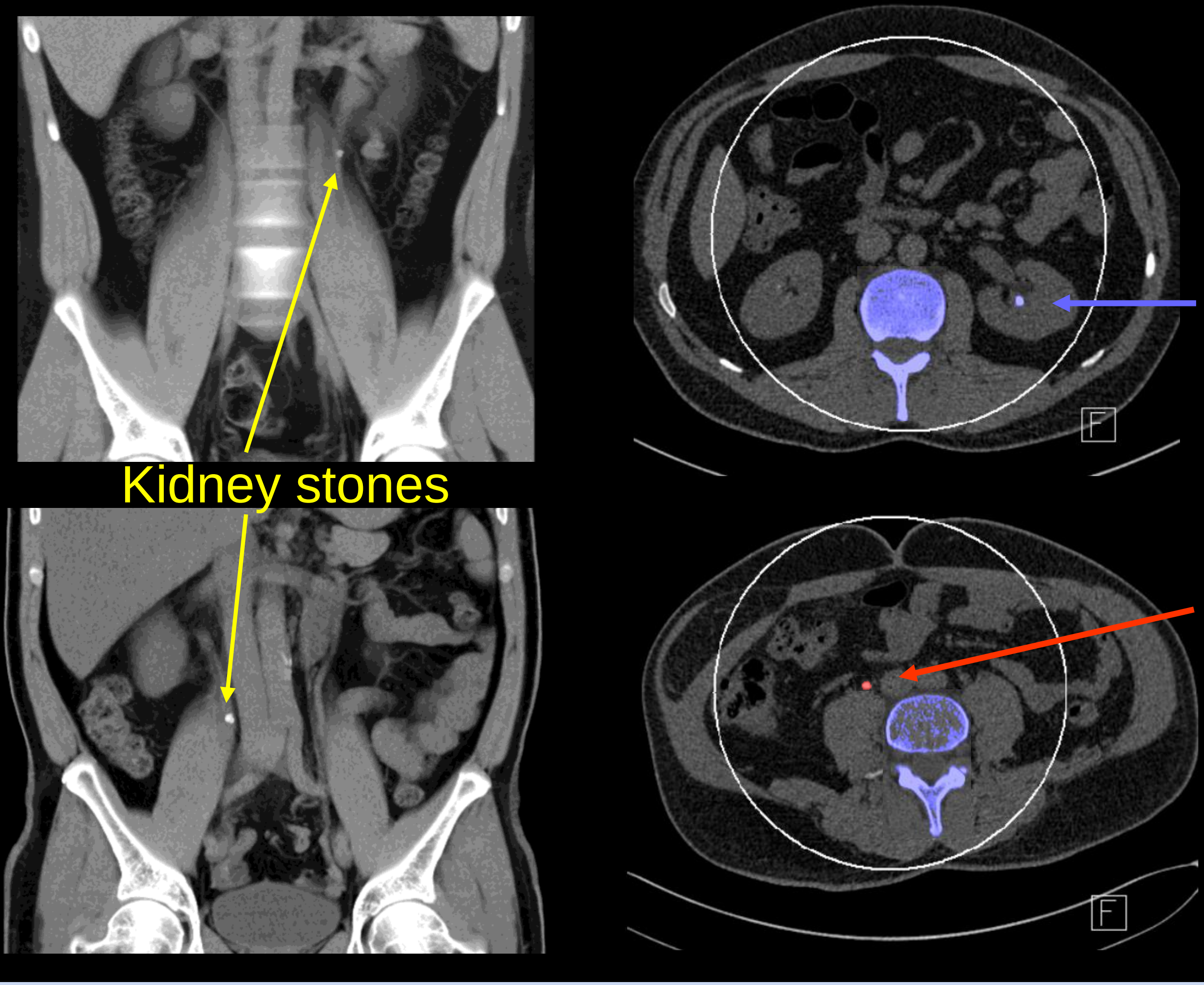

Kidney stones

Calcium-oxalate-stone

Uric acid-stone

Different
therapy options!

Courtesy of Klinikum Großhadern, LMU München

Slides courtesy of Siemens Healthcare GmbH

Material Classification

Gout

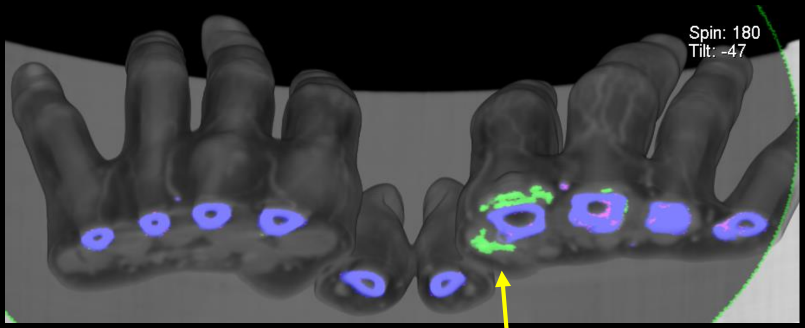
Spin: 180
Tilt: -47

Uric acid-crystals

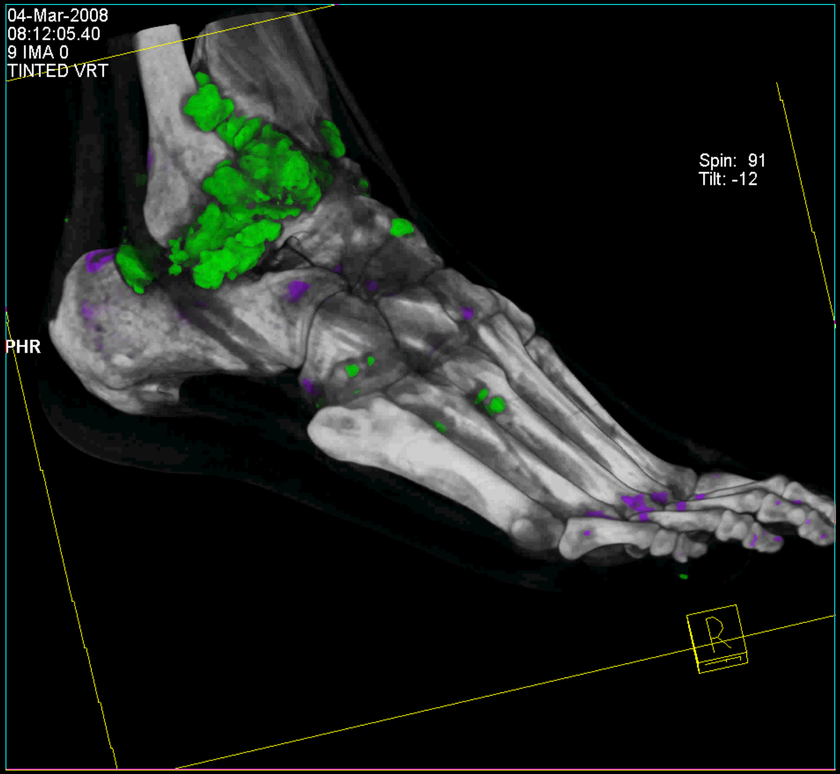
04-Mar-2008
08:12:05.40
9 IMA 0
TINTED VRT
Spin: 91
Tilt: -12
PHR
R

→ Differential diagnosis of gout

Courtesy of Klinikum Großhadern, LMU München, and
CIC, Mayo Clinic Rochester, MN, USA

Slides courtesy of Siemens Healthcare GmbH

Index of Contents

- **Introduction:**
  - X-ray attenuation
  - DE principles and technical solutions
- **Clinical applications and protocol optimization:**
  - Material classification
  - Material quantification (decomposition)
  - Pseudo-monoenergetic images
  - Electron density and effective atomic number images

Material Quantification

Liver VNC

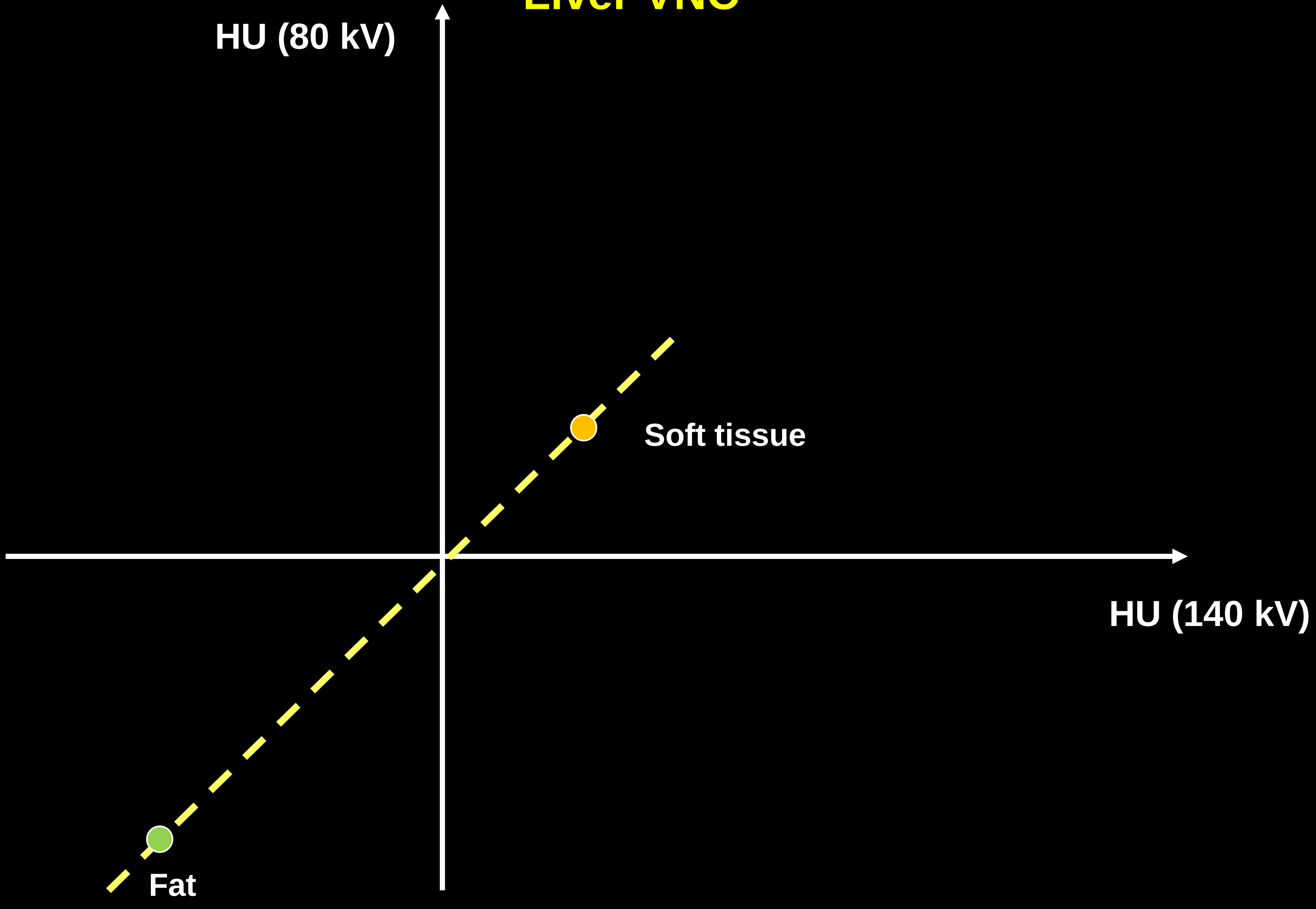
HU (80 kV)
Soft tissue
HU (140 kV)
Fat

Material Quantification

Liver VNC

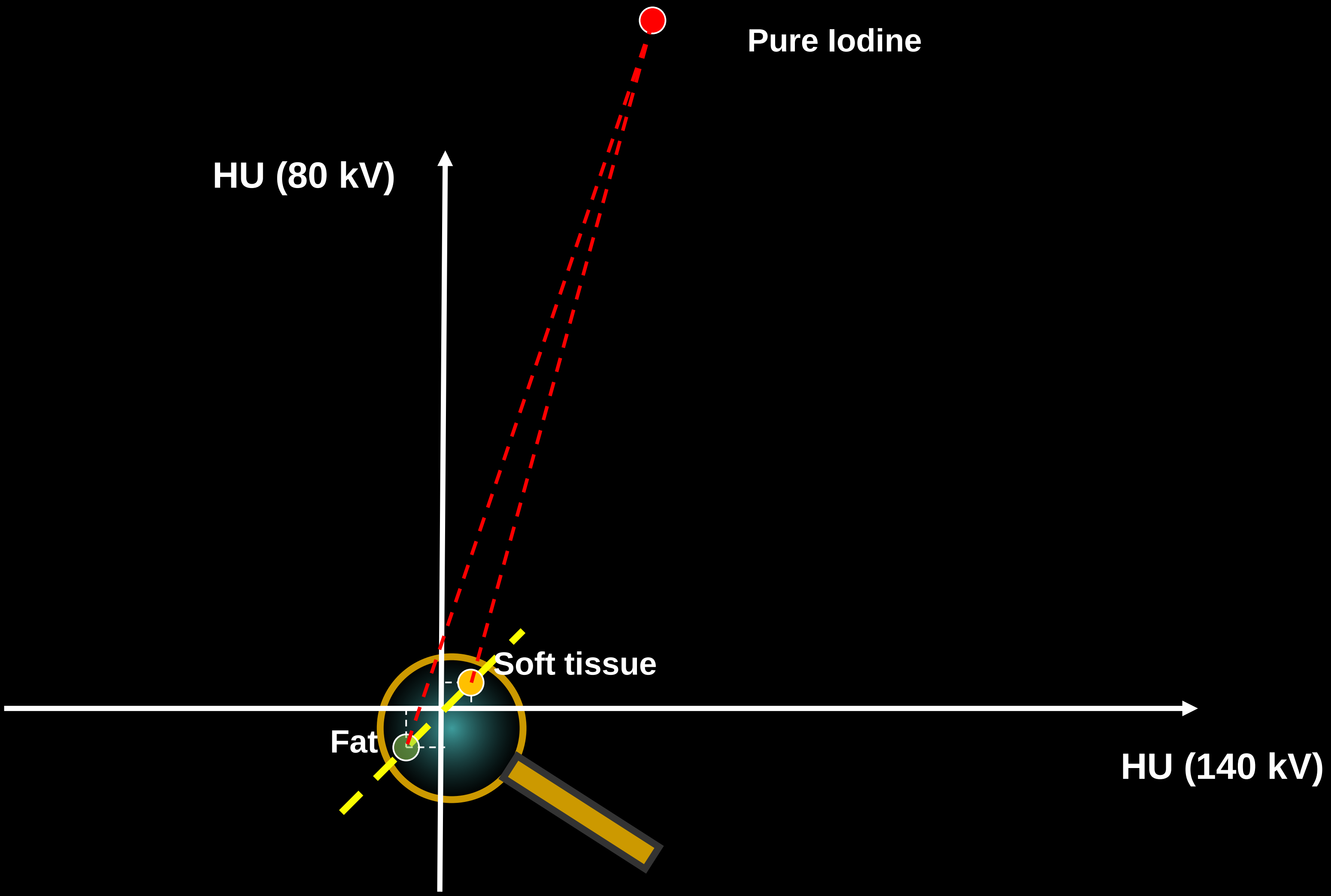
Pure Iodine
HU (80 kV)
Soft tissue
Fat
HU (140 kV)

Material Quantification

Liver VNC

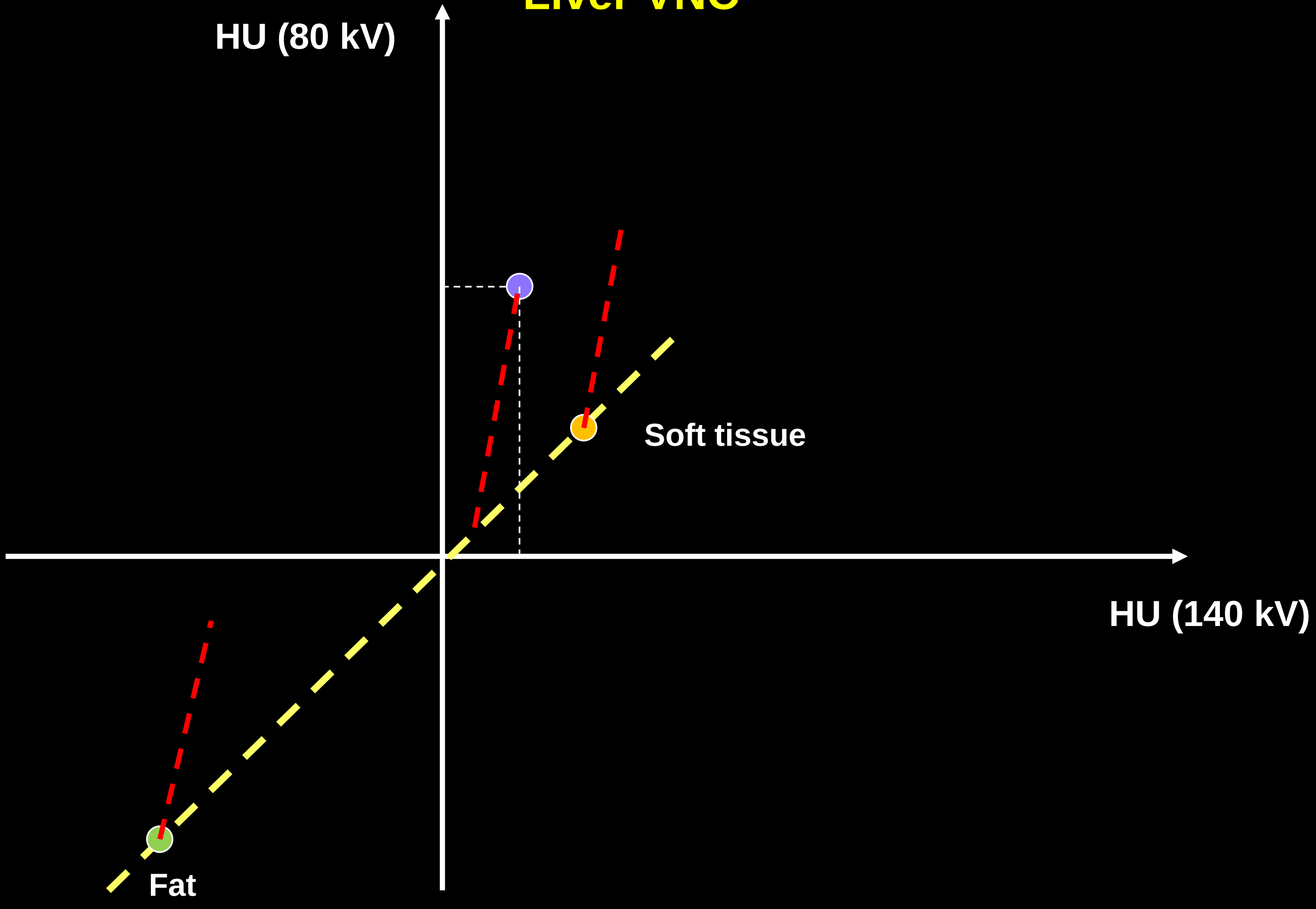
HU (80 kV)
Soft tissue
HU (140 kV)
Fat

Material Quantification

Liver VNC

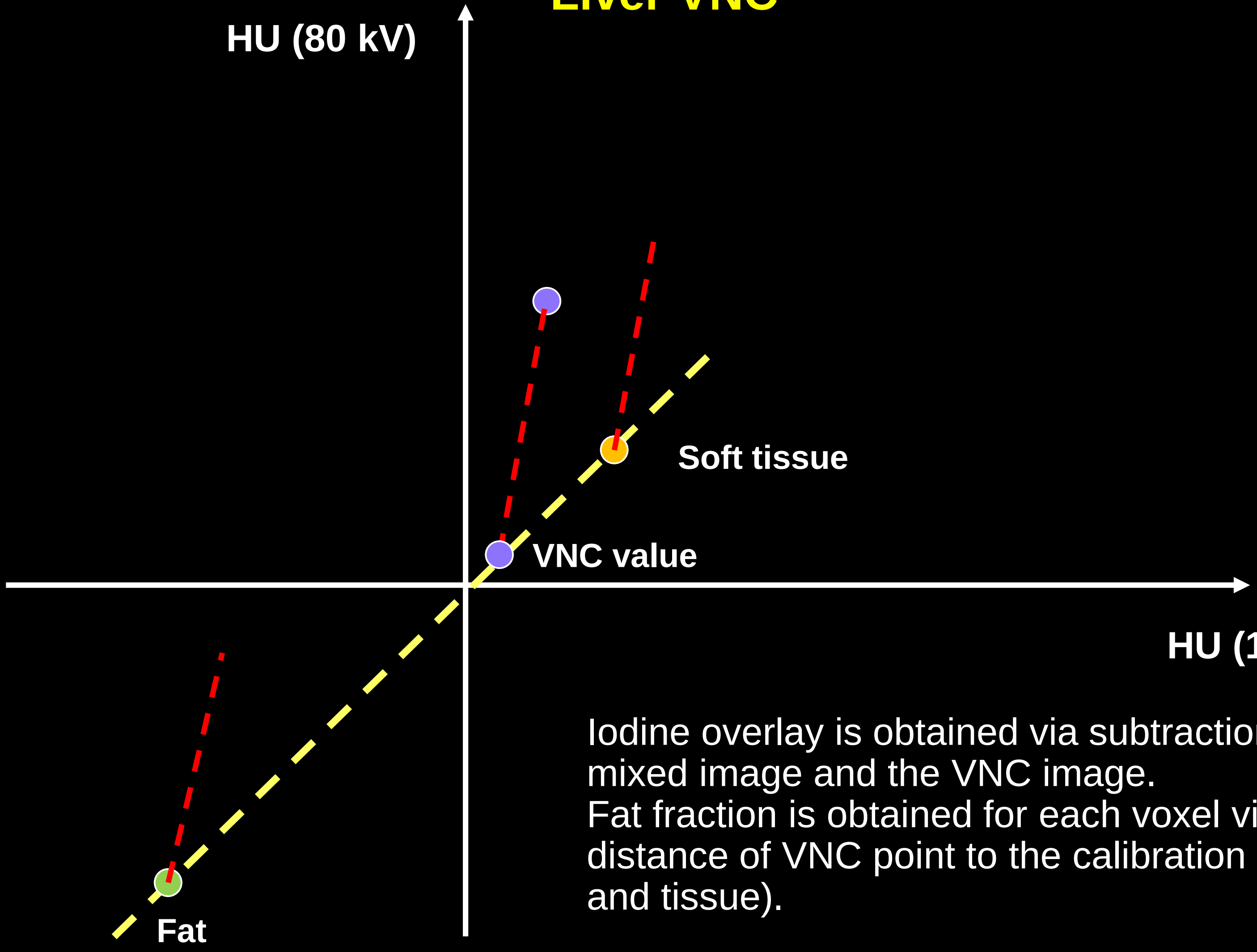
HU (80 kV)
Soft tissue
VNC value
HU (140 kV)
Fat

Iodine overlay is obtained via subtraction of the mixed image and the VNC image.
Fat fraction is obtained for each voxel via relative distance of VNC point to the calibration points (fat and tissue).

Material Quantification

Problem in Presence of a 4th Material (i.e. Calcium)

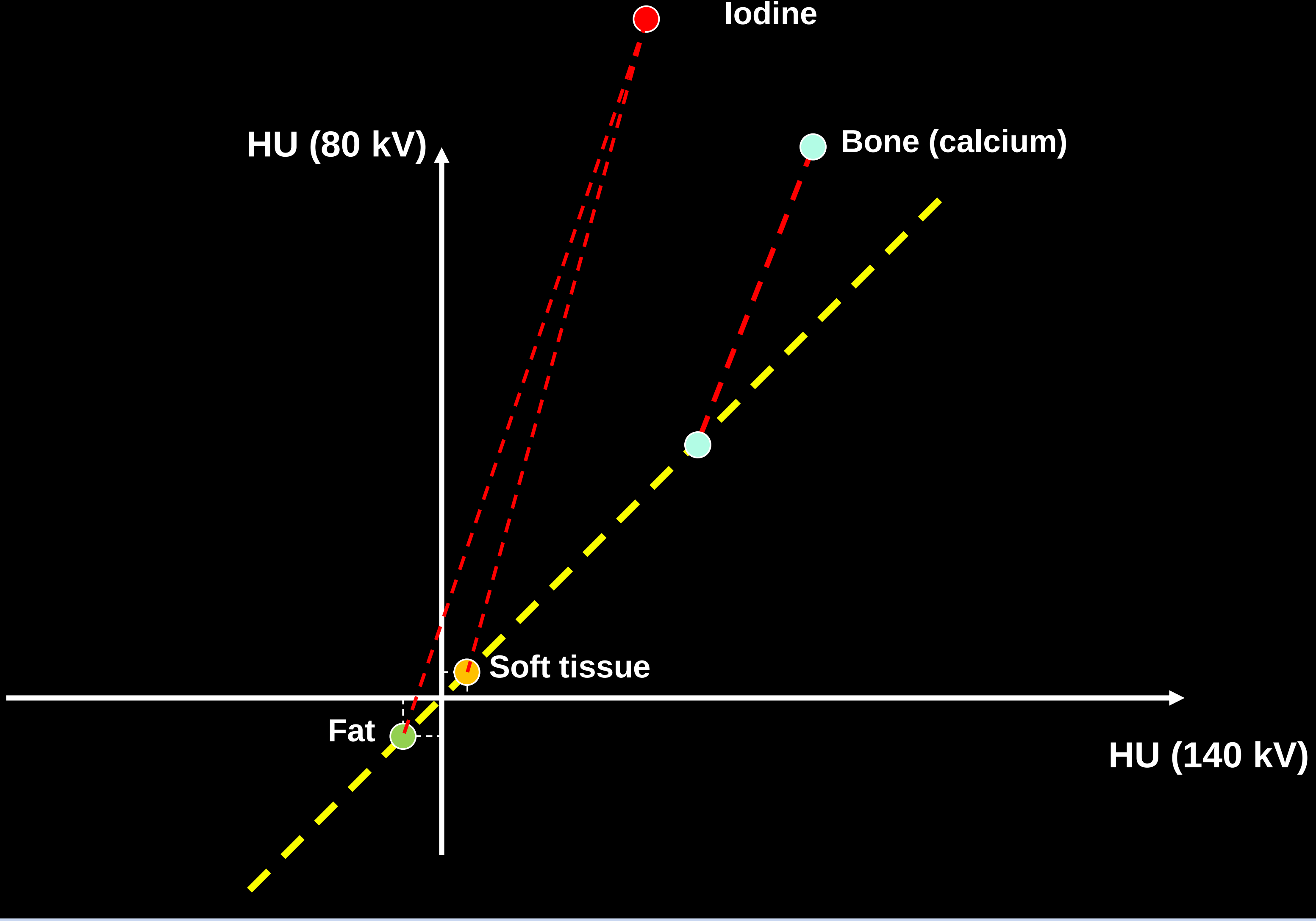

Material Quantification

Liver VNC

Other quantification application are possible changing:

- Calibration materials (for example air and soft tissue for lung iodine enhancement)
- Material to be quantified (for example calcium instead of iodine, VNCa)

Single DECT Scan

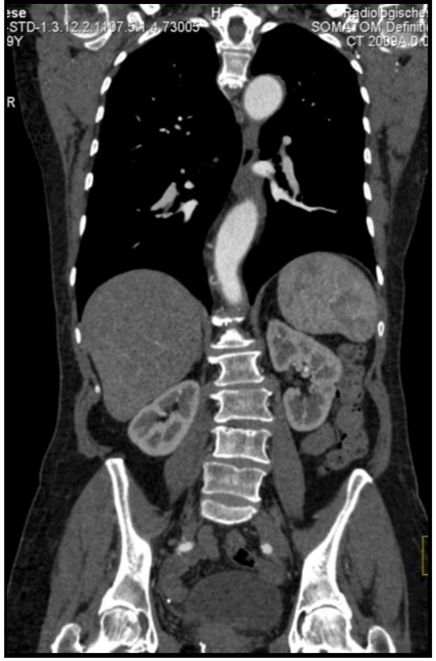

Mixed image

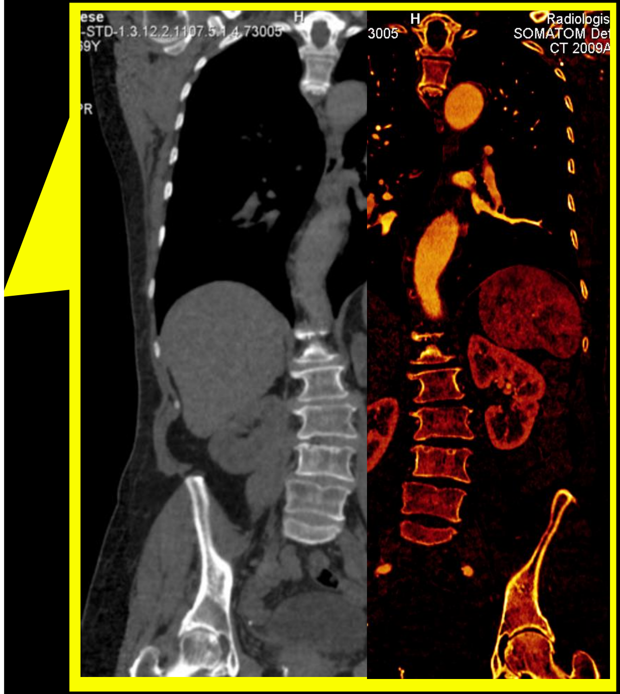

Virtual non-contrast and iodine image

Courtesy of Friedrich-Alexander University Erlangen-Nürnberg

Slides courtesy of Siemens Healthcare GmbH

Material Quantification

Other Applications

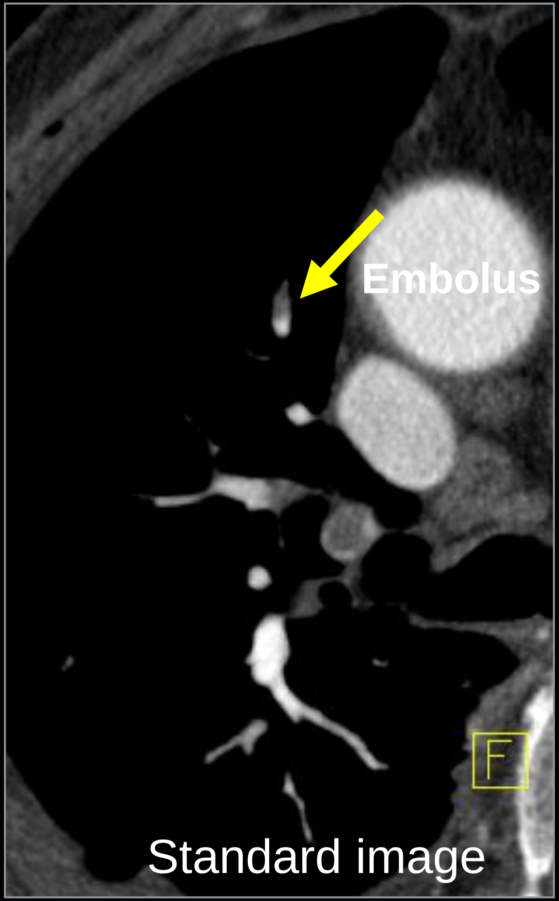

Standard image

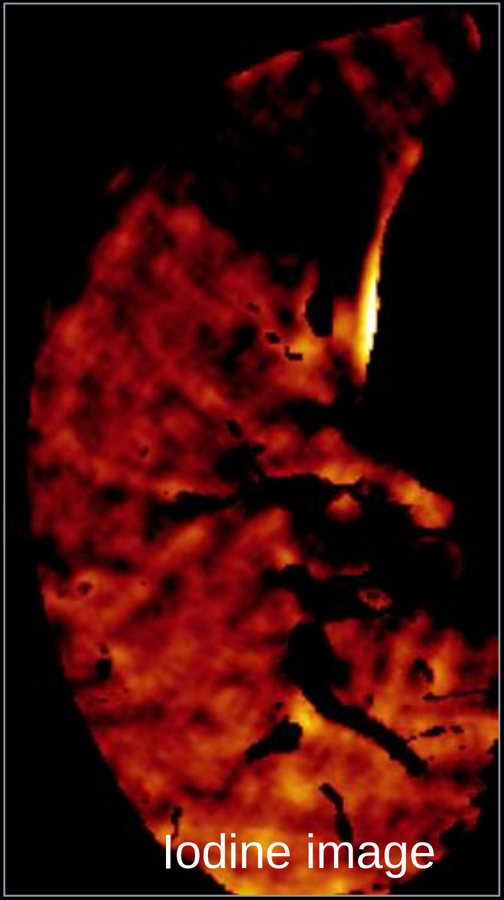

Iodine image

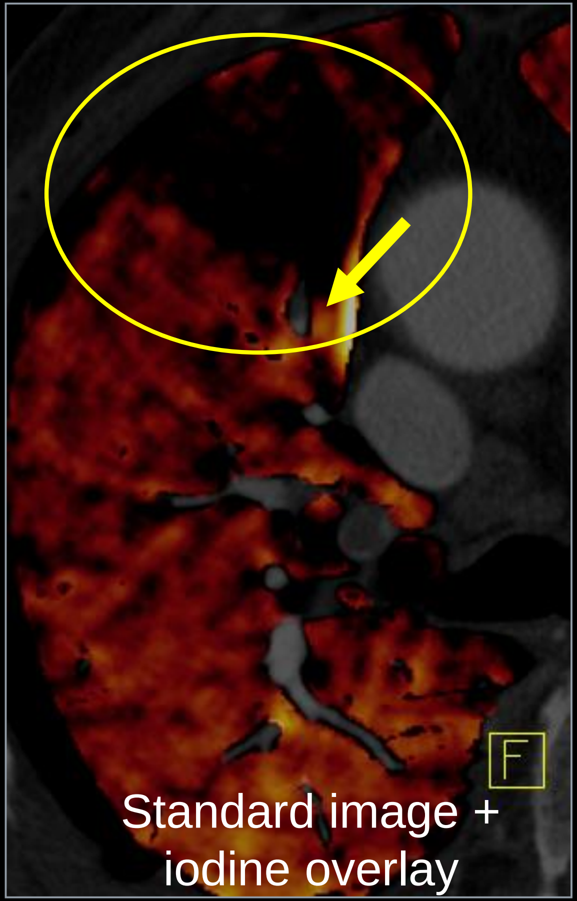

Standard image + iodine overlay

Courtesy of Hopital Calmette, Lille, France

Material Quantification

Other Applications

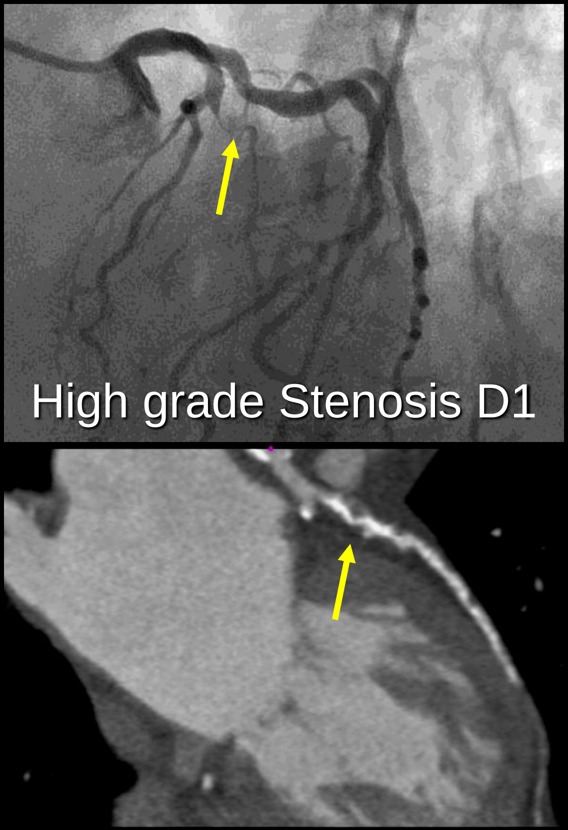
High grade Stenosis D1

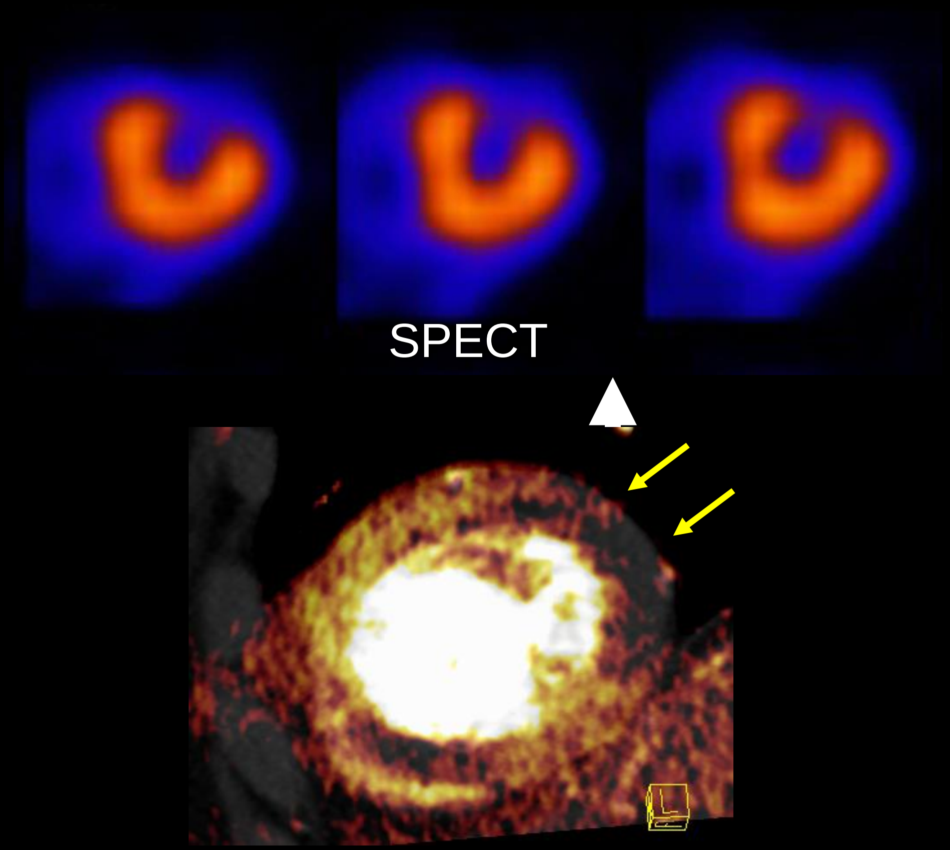

Courtesy of MUSC, Charleston, USA

Slides courtesy of Siemens Healthcare GmbH

Material Quantification

Other Applications

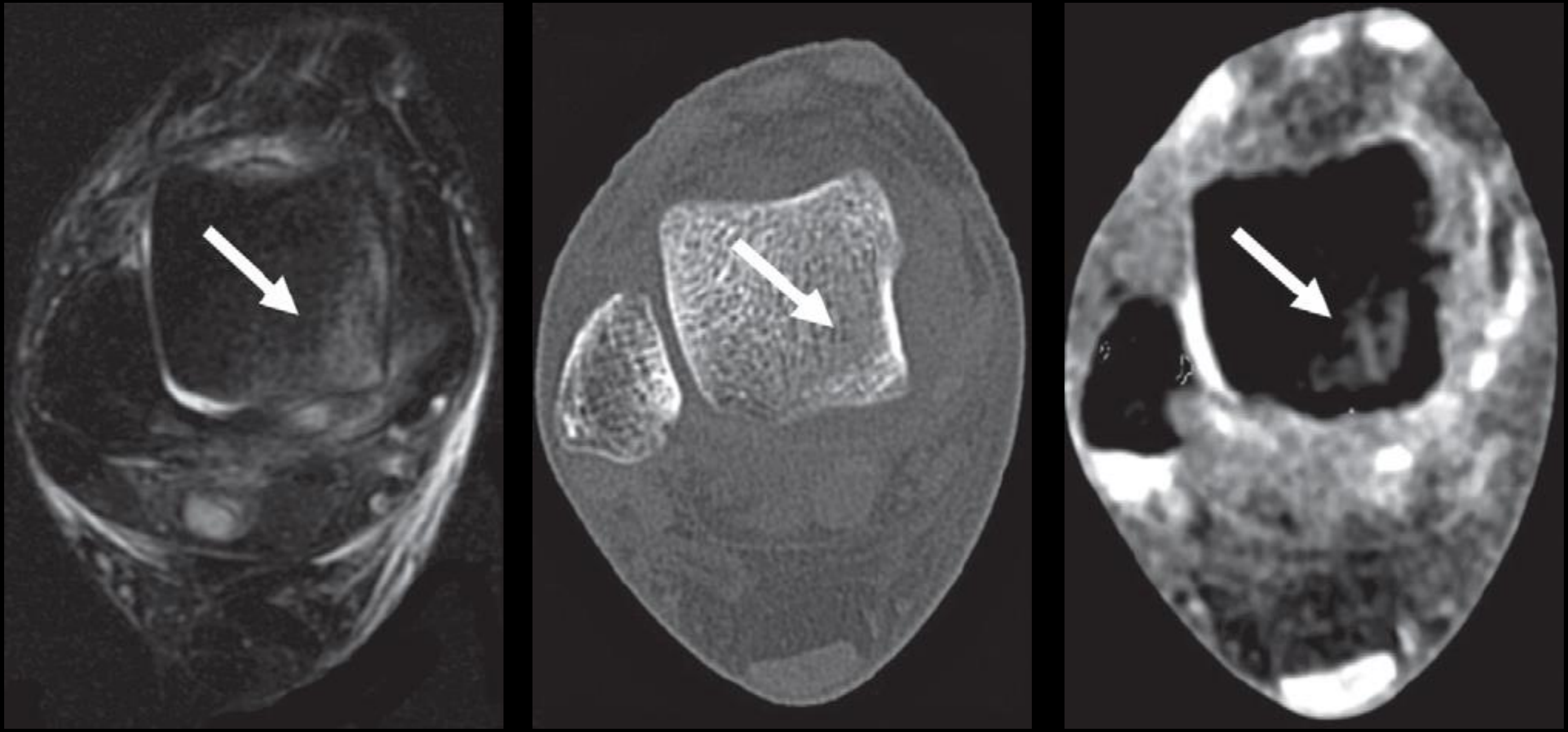

MR

DE mixed CT
(equivalent to SE 120 kV)

VNCa

Calcium has weak DE properties. VNCa works fine for small body regions.

R. Guggemberger et al.: “Diagnostic Performance of Dual-Energy CT for the Detection of Traumatic Bone Marrow Lesions in the Ankle: Comparison with MR Imaging”. *Radiology* **264**, (2012)

Material Quantification

Spectral Separation

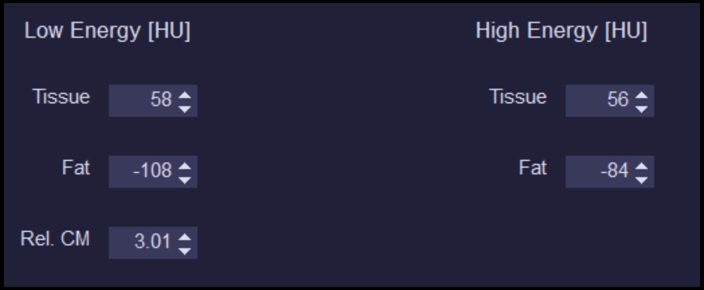

Low Energy [HU]
Tissue 58
Fat -108
Rel. CM 3.01

High Energy [HU]
Tissue 56
Fat -84

90 kV / Sn 150 kV

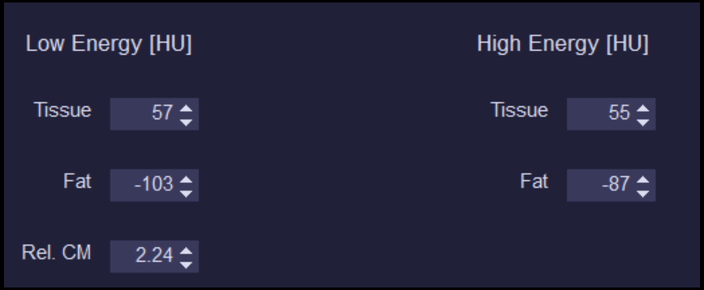

Low Energy [HU]
Tissue 57
Fat -103
Rel. CM 2.24

High Energy [HU]
Tissue 55
Fat -87

100 kV / Sn 140 kV

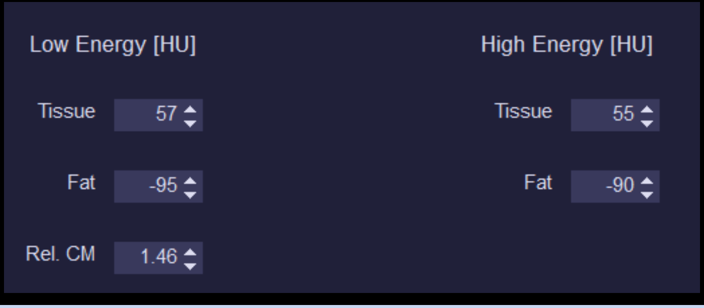

Low Energy [HU]
Tissue 57
Fat -95
Rel. CM 1.46

High Energy [HU]
Tissue 55
Fat -90

120 kV (Split Filter Au+Sn)

Material Quantification

Protocols Considerations

- Post-processing:
  - Do not change calibration parameters.
- Dedicated kernels.
- Pitch should be low (<1).
- Slow rotation time (0.5 s)
- If possible, narrow collimation should be employed (e.g. to minimize scatter), at the expenses of examination time.
- Reconstructed slice thickness S_{eff}.
- Noise and false iodine overlay values.
- The main assumption fails in presence of:
  - Noise
  - Physical artifacts (beam hardening)
  - Motion
  - Contrast media flow

Photon Counting Principle

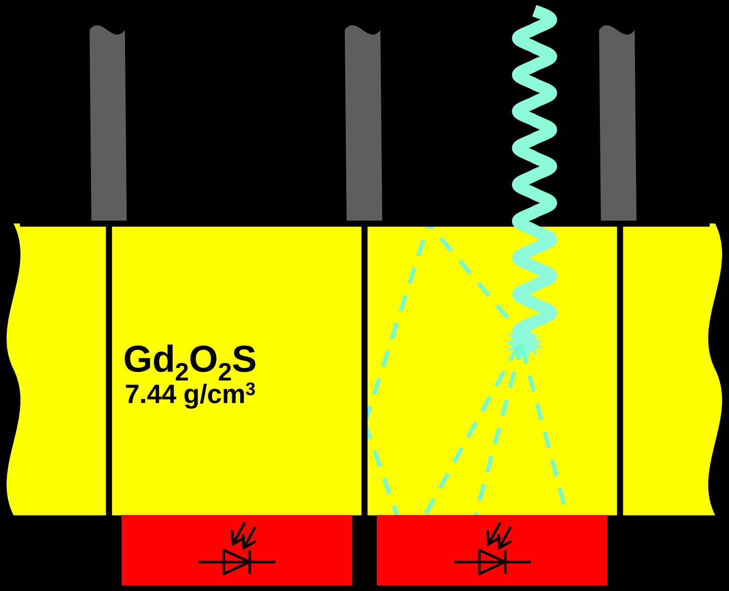

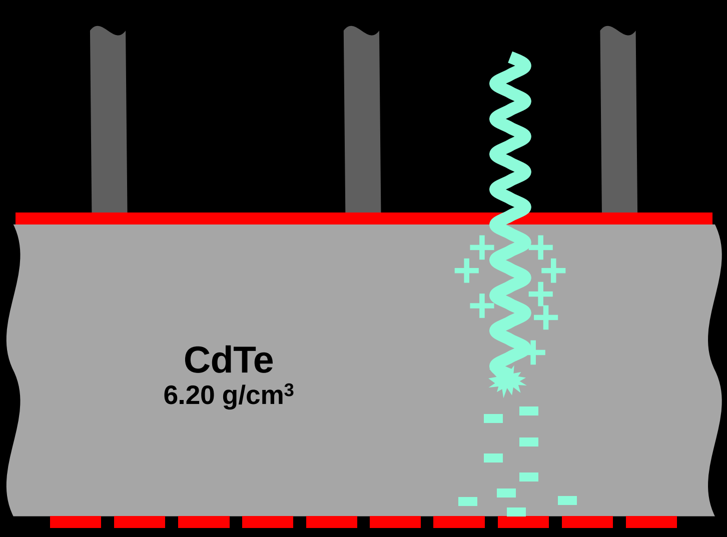

Scintillator-based detector:

- Detector divided up into small blocks (pixelated)
- Conversion of the x-ray photon into the visible light
- Isotropic emission of the light collected by reflection at the septa and then detected by the photodiode

Semiconductor-based detector:

- Continuous crystal with a pixelated anode
- Conversion of the x-ray photons into free charge carriers
- Drift of the charge cloud towards the pixelated anode by a bias voltage

Photon Counting Principle

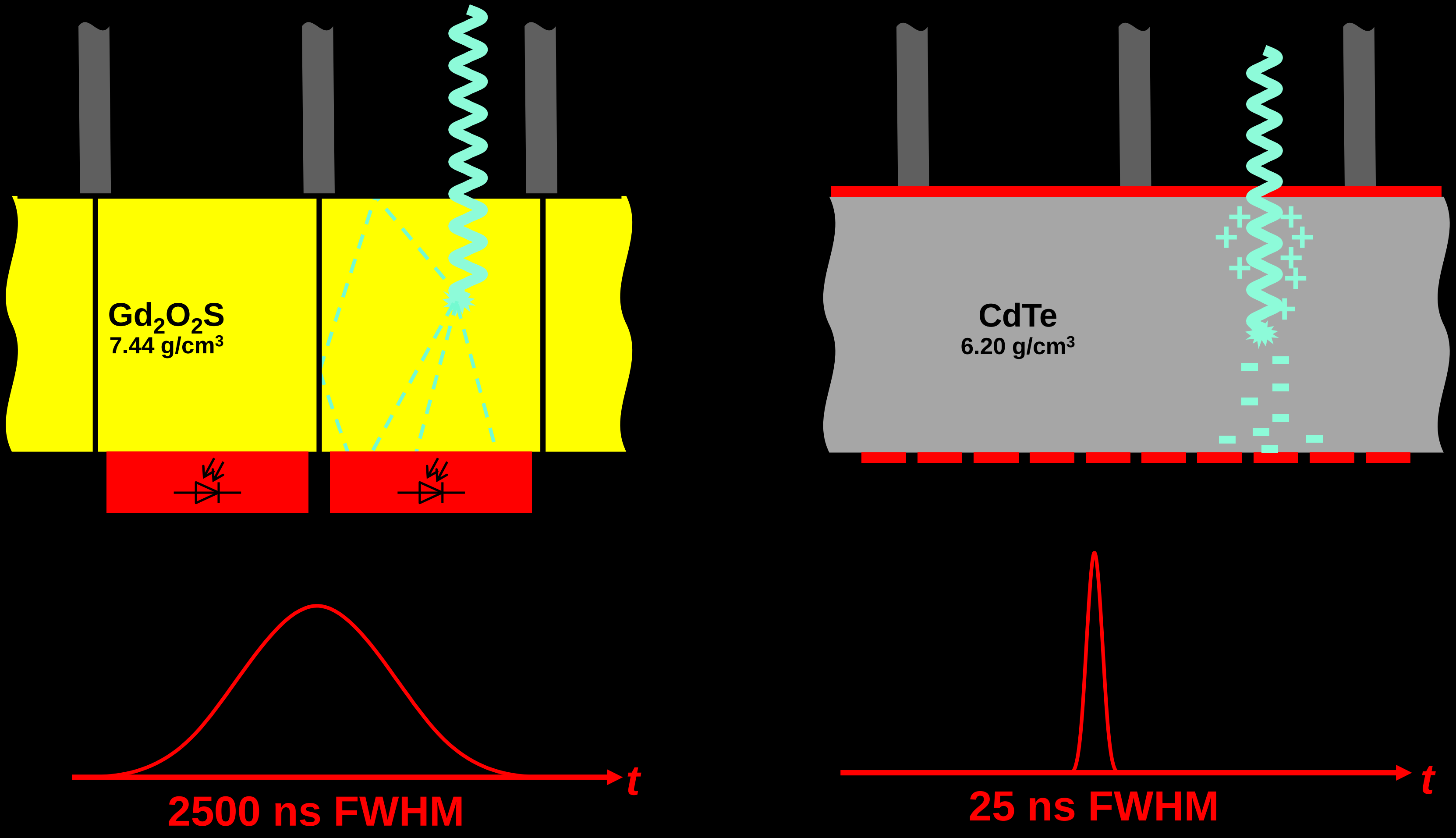

Gd_2O_2S
7.44 g/cm³
CdTe
6.20 g/cm³
t
2500 ns FWHM
t
25 ns FWHM

Photon Counting Benefits

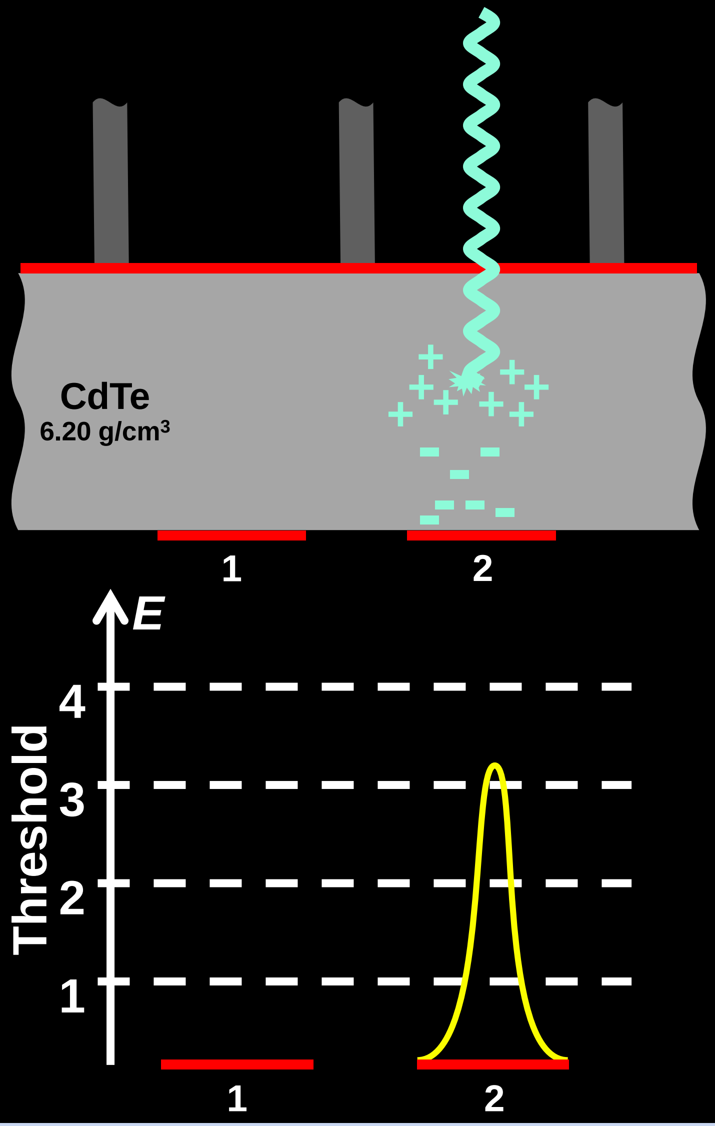
CdTe
6.20 g/cm³
1
2
E
Threshold
4
3
2
1
1
2

Up to 4 energy bins images.
- Multiple contrast material
- Separation of calcium and Iodine

Better spatial resolution.
- Lung structures
- Inner ear, bones

No electronic noise.

Photon Counting Limitations

charge-sharing and plie-up

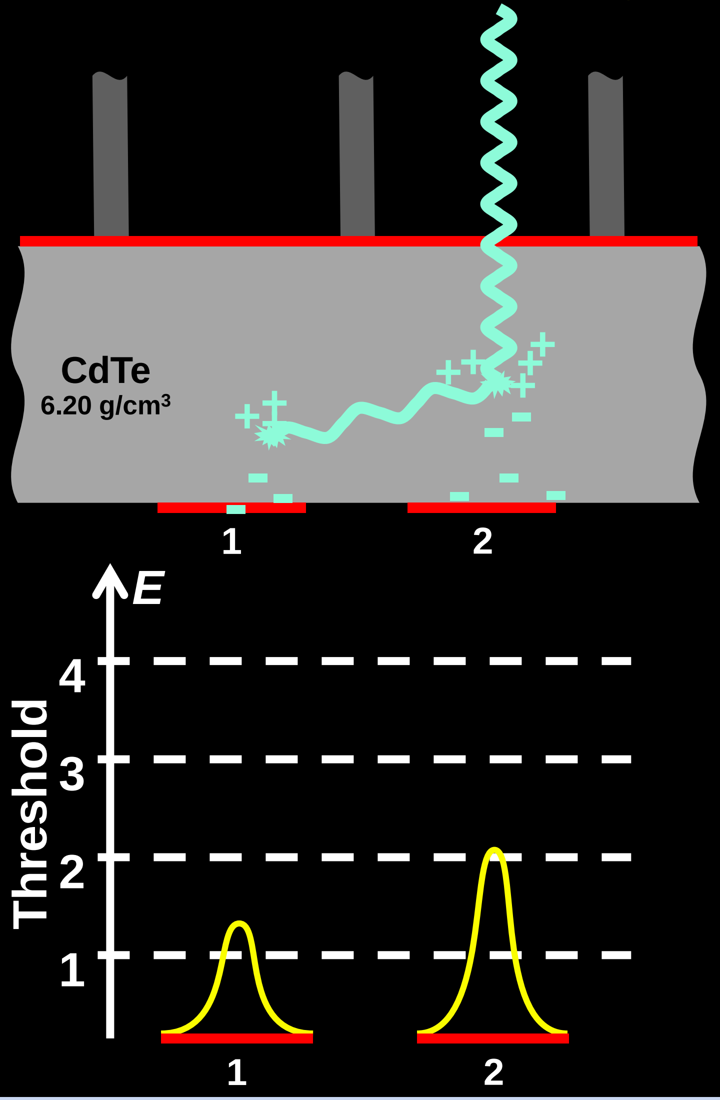
CdTe
6.20 g/cm³
1
2
E
Threshold
4
3
2
1
1
2

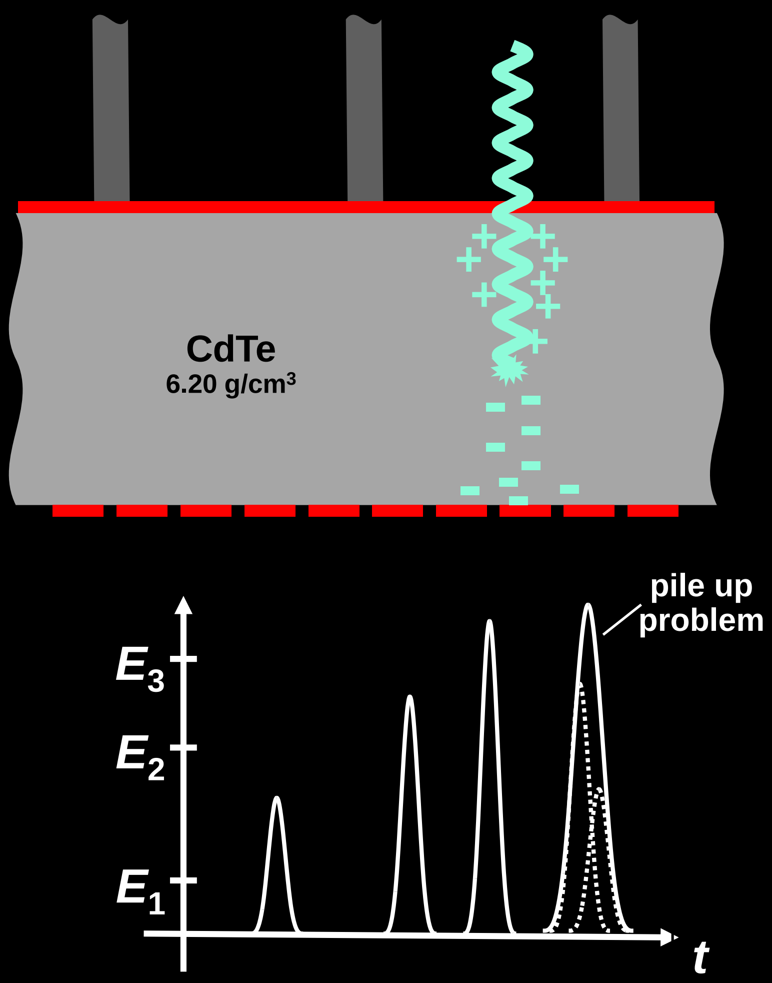
CdTe
6.20 g/cm³
pile up
problem
E3
E2
E1
t

Charge-sharing

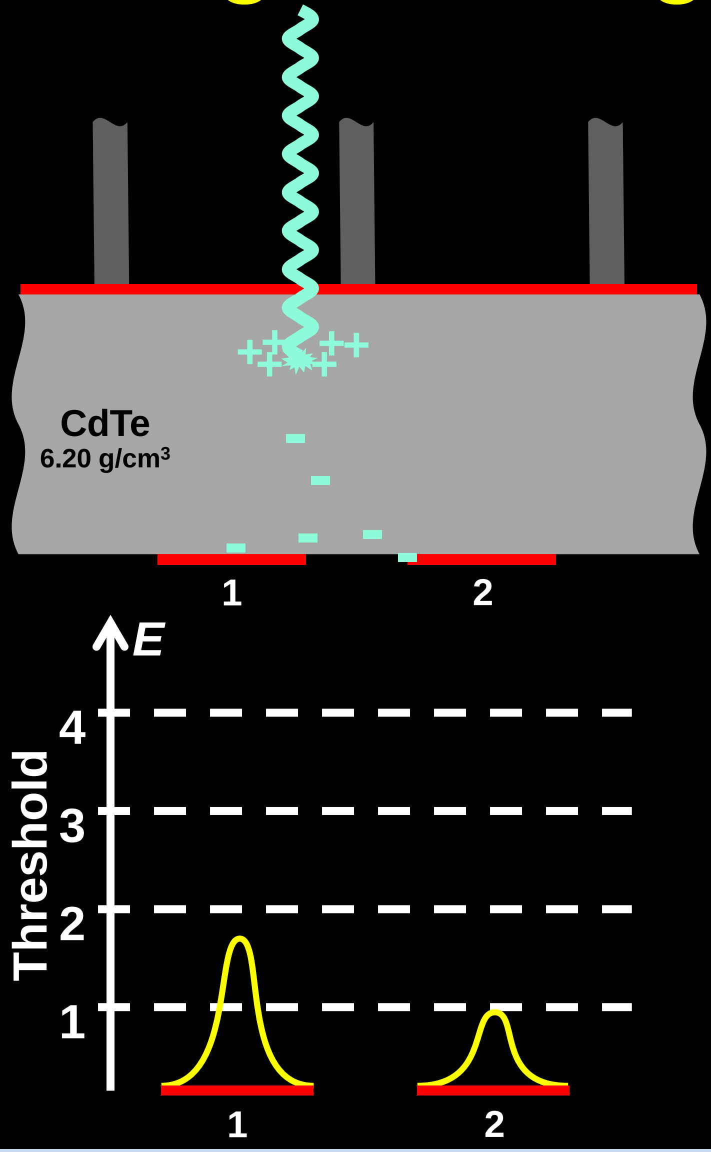
CdTe
6.20 g/cm³
1
2
E
Threshold
4
3
2
1
1
2

Ideal case

Low energy bin

High energy bin

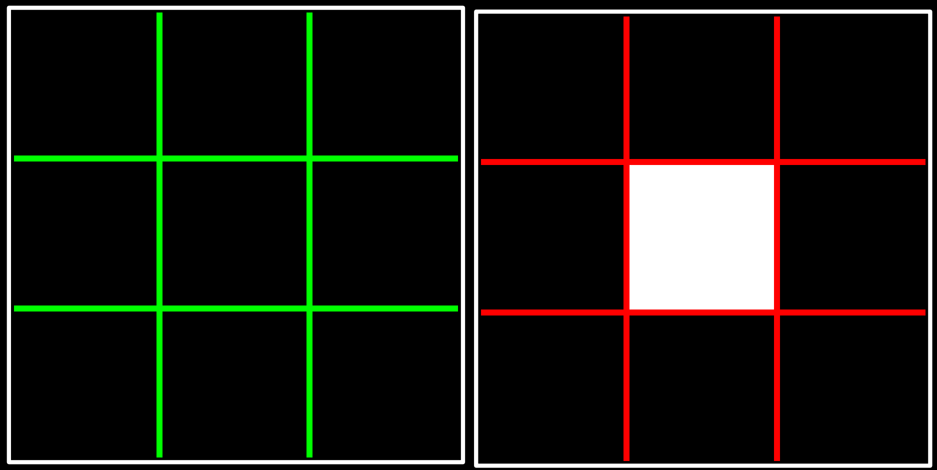

Realistic case

Low energy bin

High energy bin

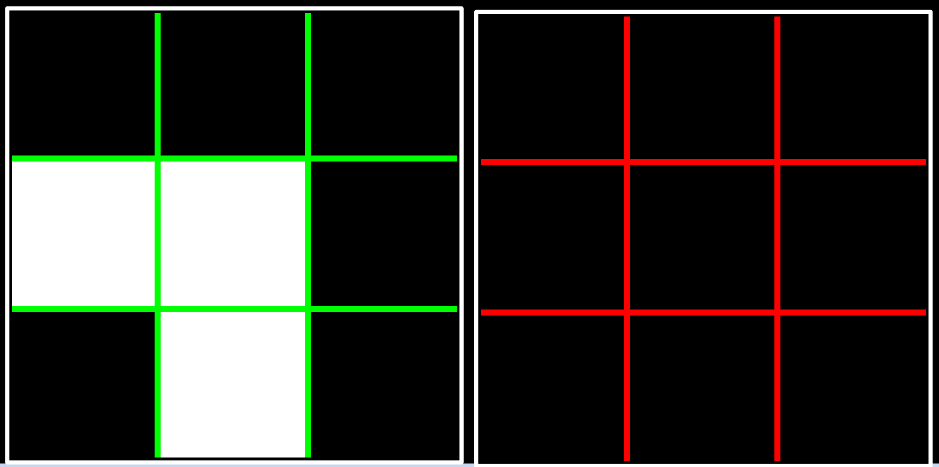

Index of Contents

- **Introduction:**
  - X-ray attenuation
  - DE principles and technical solutions
- **Clinical applications and protocol optimization:**
  - Material classification
  - Material quantification (decomposition)
  - Pseudo-monoenergetic images
  - Electron density and effective atomic number images

Pseudo-Monoenergetic Images

Attenuation coefficient for a material x:

$$\mu_x(E) = x_{\mathrm{P}}\, f_{\mathrm{P}}(E) + x_{\mathrm{C}}\, f_{\mathrm{C}}(E)$$

Attenuation coefficient for materials y and z:

$$\mu_y(E) = y_{\mathrm{P}}\, f_{\mathrm{P}}(E) + y_{\mathrm{C}}\, f_{\mathrm{C}}(E)$$

y and z are called “basis material”. They have to be chosen in such a way that their photoelectric and Compton cross-sections (y_P, z_P and y_C, z_C respectively) are known.

$$\mu_z(E) = z_{\mathrm{P}}\, f_{\mathrm{P}}(E) + z_{\mathrm{C}}\, f_{\mathrm{C}}(E)$$

Pseudo-Monoenergetic Images

Direct Method

$$\mu_x(E) = x_\mathrm{P}\, f_\mathrm{P}(E) + x_\mathrm{C}\, f_\mathrm{C}(E)$$

$$\begin{cases} \mu_x(E_\mathrm{low}) = x_\mathrm{P}\, f_\mathrm{P}(E_\mathrm{low}) + x_\mathrm{C}\, f_\mathrm{C}(E_\mathrm{low}) \\ \\ \mu_x(E_\mathrm{high}) = x_\mathrm{P}\, f_\mathrm{P}(E_\mathrm{high}) + x_\mathrm{C}\, f_\mathrm{C}(E_\mathrm{high}) \end{cases}$$

Unknown: x_P, x_C

Known: $f_P(E), f_C(E) \quad \forall E$

Measured: $\mu_x(E_\mathrm{low}), \mu_x(E_\mathrm{high})$

Pseudo-Monoenergetic Images

Material Basis Method (more robust)

$$\mu_x(E) = x_\mathrm{P}\, f_\mathrm{P}(E) + x_\mathrm{C}\, f_\mathrm{C}(E)$$

$$\begin{cases} \mu_y(E) = y_\mathrm{P}\, f_\mathrm{P}(E) + y_\mathrm{C}\, f_\mathrm{C}(E) \\ \\ \mu_z(E) = z_\mathrm{P}\, f_\mathrm{P}(E) + z_\mathrm{C}\, f_\mathrm{C}(E) \end{cases} \rightarrow \begin{aligned} f_P(E) &= g_1(\mu_y(E), \mu_z(E)) \\ f_C(E) &= g_2(\mu_y(E), \mu_z(E)) \end{aligned}$$

Pseudo-Monoenergetic Images

Material Basis Method (more robust)

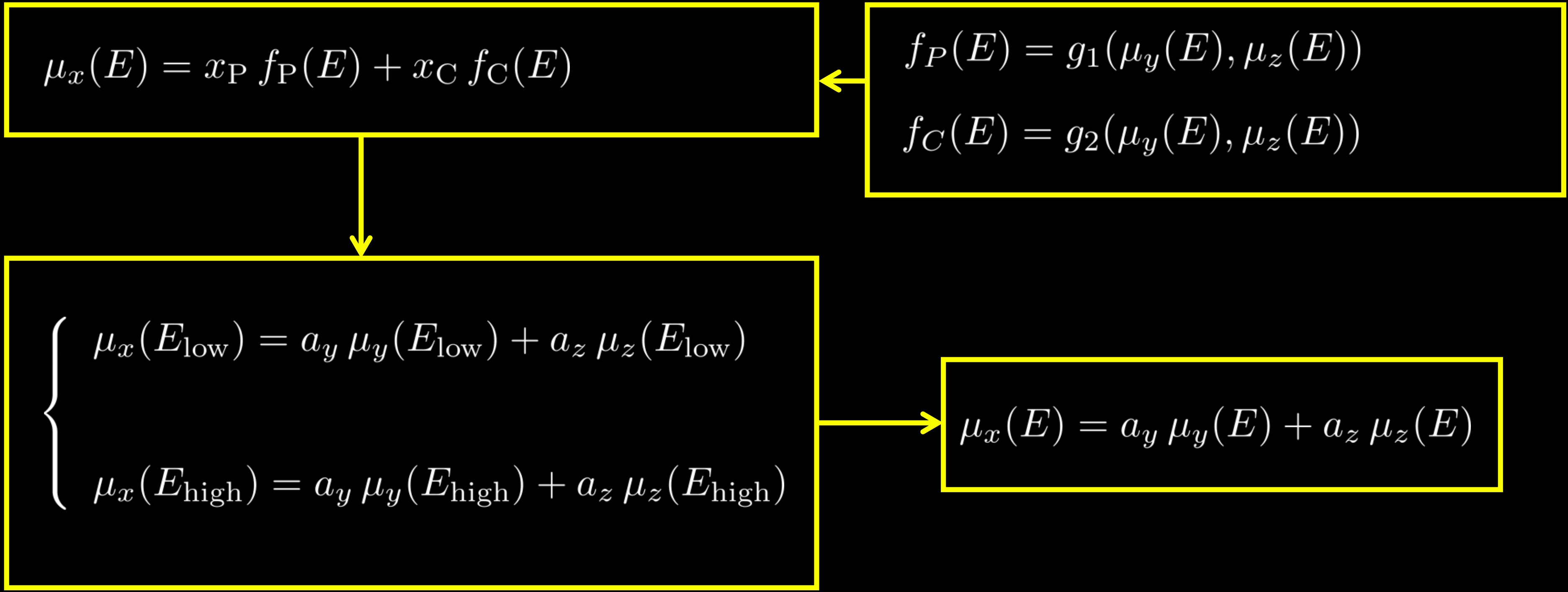

$$\mu_x(E) = x_\mathrm{P}\, f_\mathrm{P}(E) + x_\mathrm{C}\, f_\mathrm{C}(E)$$

$$f_P(E) = g_1(\mu_y(E), \mu_z(E))$$

$$f_C(E) = g_2(\mu_y(E), \mu_z(E))$$

$$\begin{cases} \mu_x(E_\mathrm{low}) = a_y\, \mu_y(E_\mathrm{low}) + a_z\, \mu_z(E_\mathrm{low}) \\ \mu_x(E_\mathrm{high}) = a_y\, \mu_y(E_\mathrm{high}) + a_z\, \mu_z(E_\mathrm{high}) \end{cases}$$

$$\mu_x(E) = a_y\, \mu_y(E) + a_z\, \mu_z(E)$$

Pseudo-Monoenergetic Images

Solving the system and expressing everything in CT values, if one of the two basis material is water, we obtain:

$$\mathrm{HU}_x(E) = (1-\alpha(E))\,\mathrm{HU}_x(E_\mathrm{low}) + \alpha(E)\,\mathrm{HU}_x(E_\mathrm{high})$$

Pseudo-Monoenergetic Images

E / keV

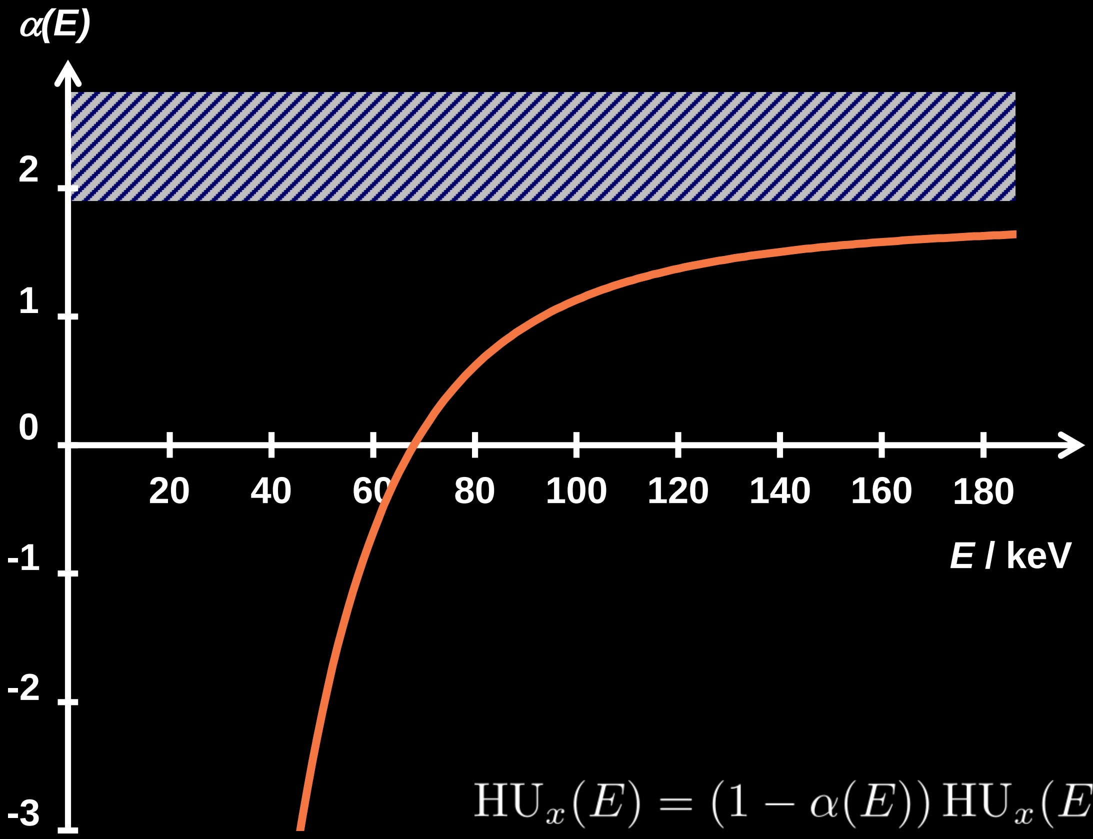

$$\mathrm{HU}_x(E) = (1-\alpha(E))\,\mathrm{HU}_x(E_{\mathrm{low}}) + \alpha(E)\,\mathrm{HU}_x(E_{\mathrm{high}})$$

Pseudo-Monoenergetic Images

Considerations

- The two basis materials are iodine and water. All calibration values are stored and cannot be changed.
- The acquisition protocol is straight forward. In vendors' softwares, pseudo-monoenergetic images can be calculated in rawdata domain directly.
- Pseudo-monoenergetic can be used for spectroscopic analysis, plotting CT values of an ROI for different energies.
- It can be used also to optimize CNR.
- Again, spectral separation and low noise would lead to better and more robust results.

Index of Contents

- **Introduction:**
  - X-ray attenuation
  - DE principles and technical solutions
- **Clinical applications and protocol optimization:**
  - Material classification
  - Material quantification (decomposition)
  - Pseudo-monoenergetic images
  - Electron density and effective atomic number images

Electron Density and Effective Atomic Number Images

Direct Method

$$\mu_x(E) \sim \rho_x \frac{\mathrm{N_A}}{A_x} Z_x \left(Z_x^3 \frac{1}{E^3} + f_{\mathrm{KN}}(E) \right)$$

- ρ_x, density of the element $\left[\frac{g}{m^3}\right]$ → unknown
- N_A, Avogadro number: number of atoms needed to have A grams of an element of atomic mass A → known
- A_x, atomic mass of the element $[\mathrm{a.m.u.}](\sim g)$ → unknown
- Z_x, average atomic number of the voxel (i.e. number of electrons of the element) → unknown

Electron Density and Effective Atomic Number Images

Direct Method

Electron density is defined as the number of electrons in one unit of volume:

$$\rho_e = \frac{n}{m^3} = \frac{g}{m^3}\frac{n}{g} = \frac{g}{m^3}\left(n_e\frac{n_a}{g}\right) = \rho Z\frac{N_A}{A}$$

↓

$$\mu_x(E) \sim \rho_x\frac{\mathrm{N_A}}{A_x}Z_x\left(Z_x^3\frac{1}{E^3} + f_{\mathrm{KN}}(E)\right)$$

$$\mu_x(E) \sim \rho_{e_x}\left(Z_x^3\frac{1}{E^3} + f_{\mathrm{KN}}(E)\right)$$

Electron Density and Effective Atomic Number Images

Material Basis Method (more robust)

Same principles and derivation employed for pseudo-monoenergetic images.

Once the contribution of each basis material are calculated for one voxel, a weighted average of their electron densities (instead of the attenuation values) is performed.

$$\mu_x(E) = a_y\,\mu_y(E) + a_z\,\mu_z(E)$$

Pseudo-monoenergetic formula

$$\rho_{e_x} = a_y\,\rho_{e_y} + a_z\,\rho_{e_z}$$

Electron density formula (does not depend on energy)

Electron Density and Effective Atomic Number Images

Material Basis Method (more robust)

Since electron density is usually normalized by the electron density of water, if water is also one of the basis materials (y=water and z=iodine, for example), then the formula becomes:

$$\hat{\rho}_{e_x} = \frac{\rho_{e_x}}{\rho_{e_w}} = a_w \frac{\rho_{e_w}}{\rho_{e_w}} + a_i \frac{\rho_{e_i}}{\rho_{e_w}} = a_w + a_i\,\hat{\rho}_{e_i}$$

The effective atomic number is a weighted average of the atomic numbers of basis materials:

$$Z_x = \left[\left(\frac{a_w}{a_w + a_i\,\hat{\rho}_{e_i}} Z_w \right)^n + \left(\frac{a_i\,\hat{\rho}_{e_i}}{a_w + a_i\,\hat{\rho}_{e_i}} Z_i \right)^n \right]^{\frac{1}{n}}$$

Electron Density and Effective Atomic Number Images

Considerations

Since the principles are so similar to pseudo-monoenergetic applications, the same considerations hold.

Clinical application is different: electron density is useful for radiotherapy treatment planning, since it is linear with stopping power, while CT values are not.

Metal Artifacts Reduction

Metal artifacts generation:

- Beam harding
- Photon starvation
- Scattering

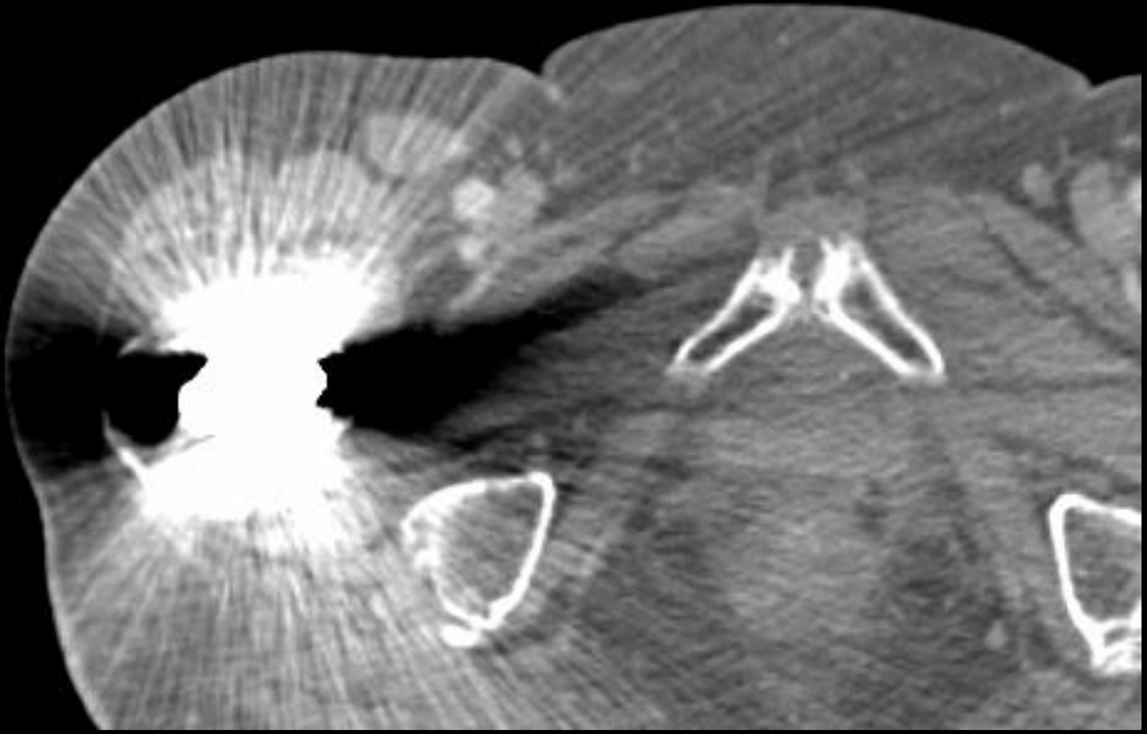

Metal Artifact Reduction
DE MAR

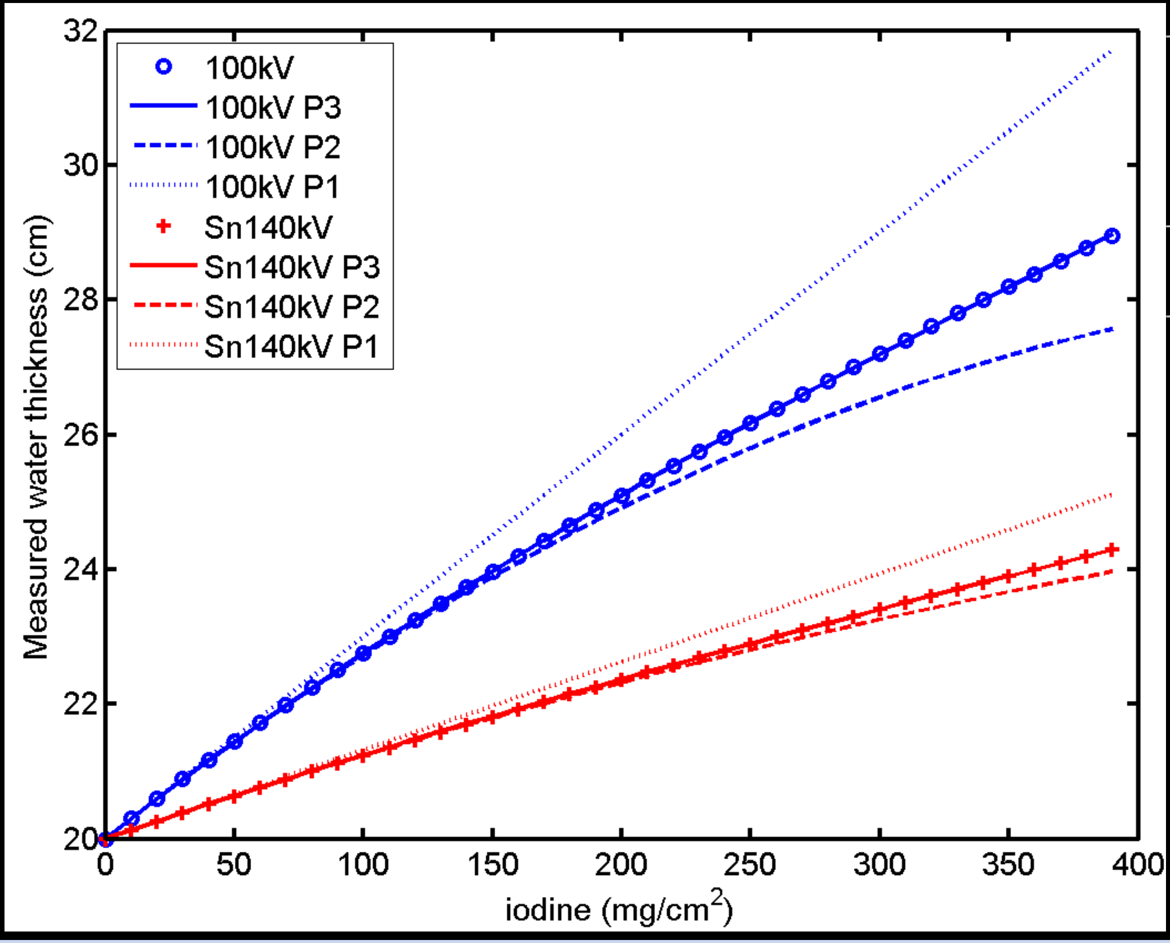

$$D = W + \alpha_1 \delta$$

$$D = W + \alpha_1 \delta + \alpha_2 \delta^2 + \alpha_3 \delta^3$$

$$D = W + \alpha_1 \delta + \alpha_2 \delta^2$$

Metal Artifact Reduction
DE MAR

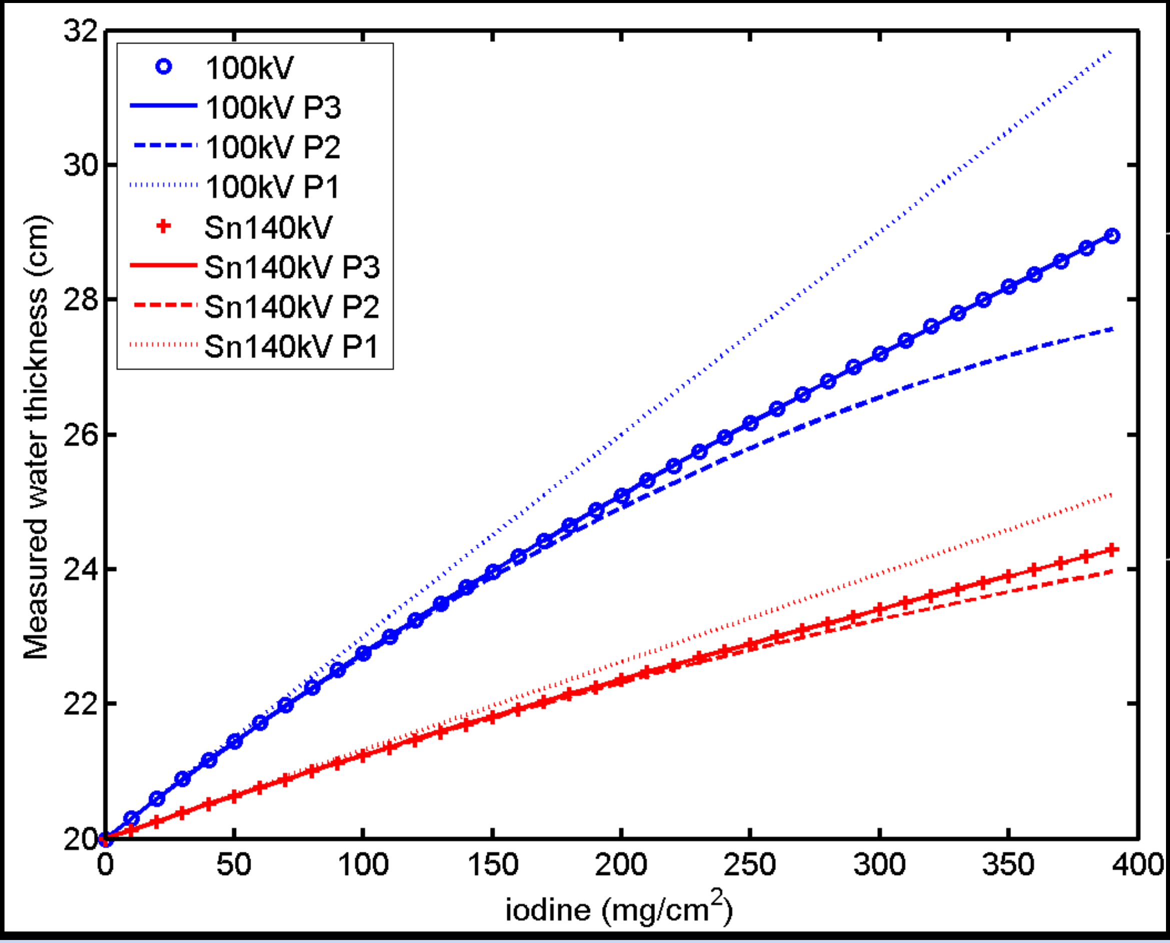

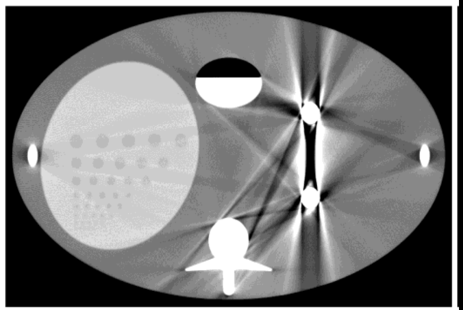

$$D^L = W + \alpha_1^L\delta + \alpha_2^L\delta^2 + \alpha_3^L\delta^3$$

$$D^H = W + \alpha_1^H\delta + \alpha_2^H\delta^2 + \alpha_3^H\delta^3$$

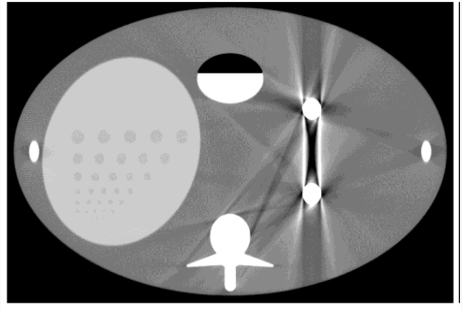

Metal Artifact Reduction
DE MAR

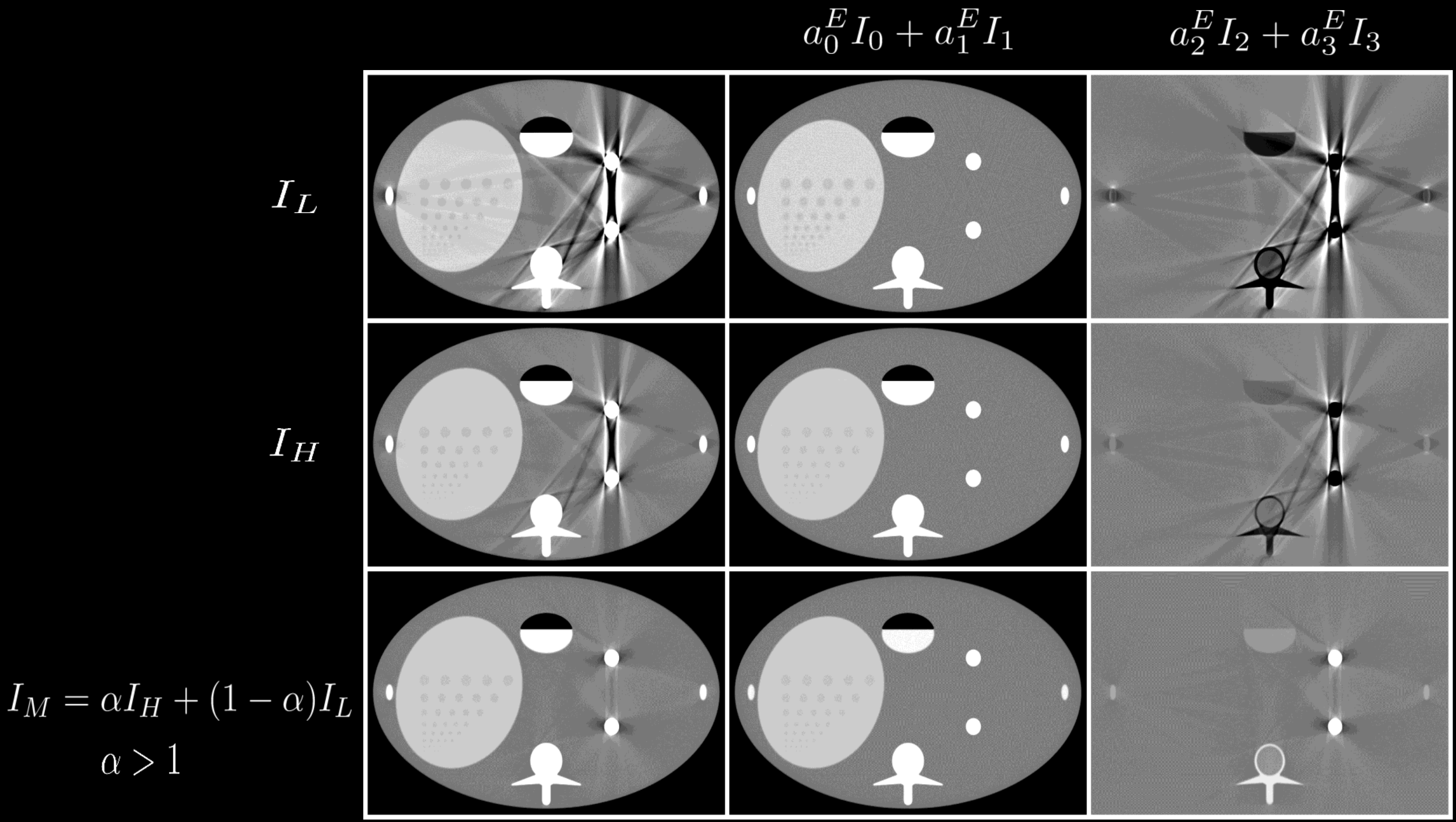
$a_0^E I_0 + a_1^E I_1$
$a_2^E I_2 + a_3^E I_3$
I_L
I_H
$I_M = \alpha I_H + (1 - \alpha) I_L$
$\alpha > 1$

Kuckenbecker et al.: „Dual energy CT: How well can pseudo-monochromatic imaging reduce metal artifacts?”, *Med. Phys.*, 42 **(2)**, 2015.

Metal Artifact Reduction
DE MAR

Limitations:

- Loss of quantitative HU information
- Loss of contrast

Improvement:

Frequency split approach (Mono+):

- Low spatial frequencies from a positive combination of I_L and I_H
- High spatial frequencies from the negative combination of I_L and I_H

Metal Artifact Reduction
IMAR

General impainting methods

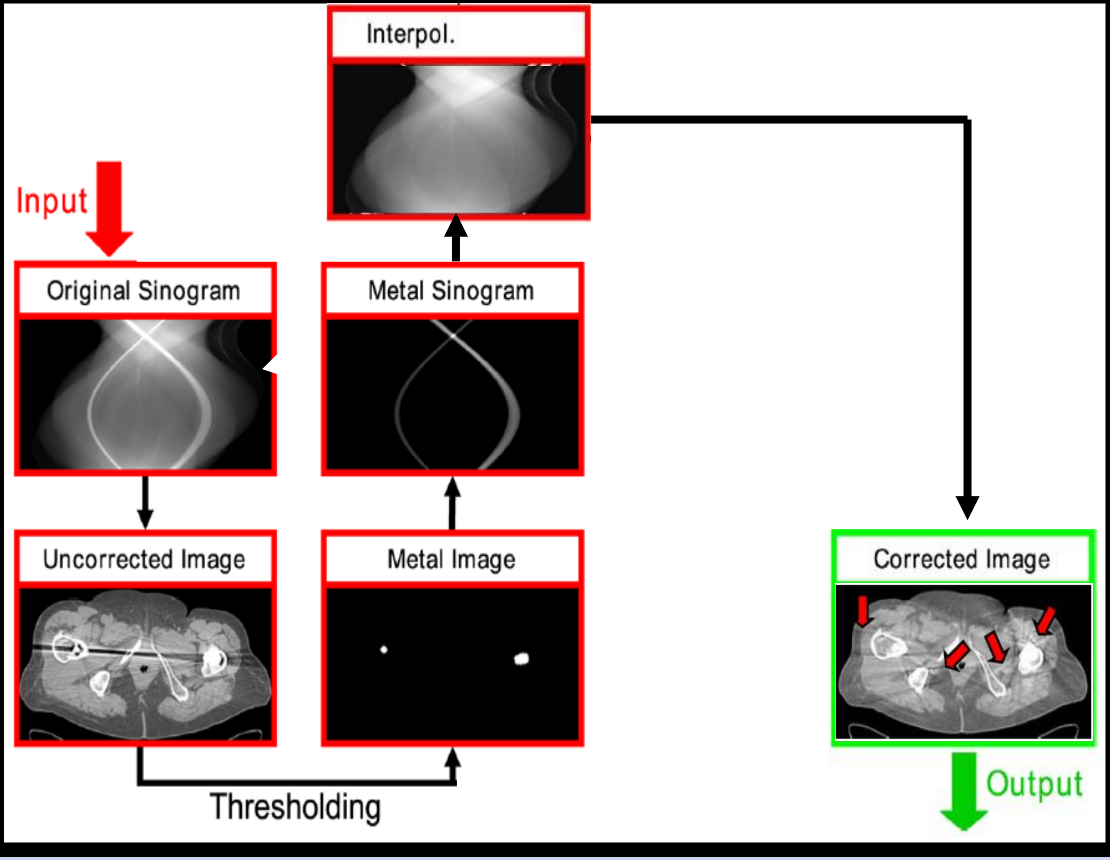
Interpol.
Input
Original Sinogram
Metal Sinogram
Uncorrected Image
Metal Image
Corrected Image
Output
Thresholding

Metal Artifact Reduction
IMAR

Normalized metal artifact reduction (NMAR)

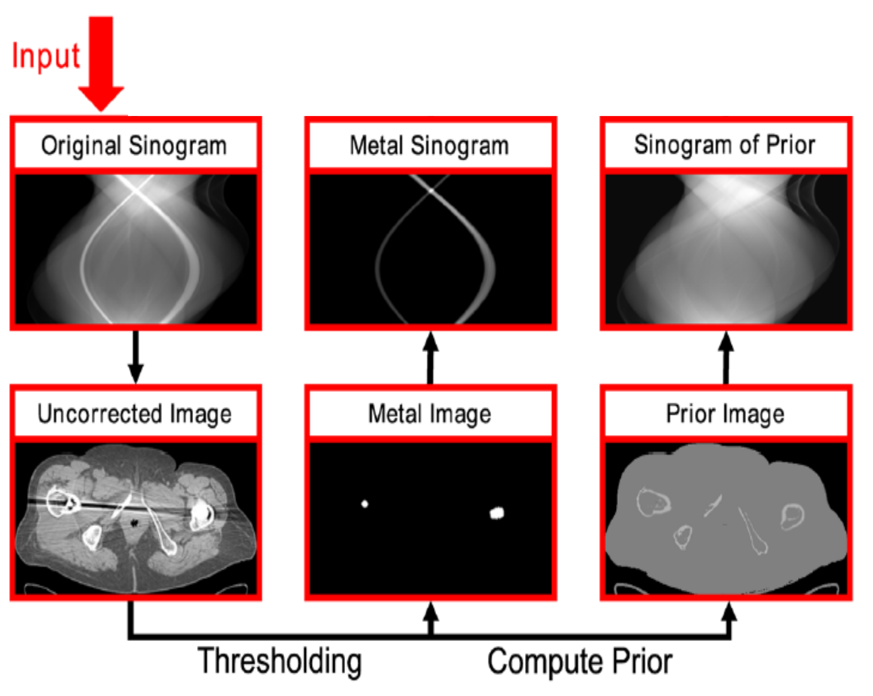
Input
Original Sinogram
Metal Sinogram
Sinogram of Prior
Uncorrected Image
Metal Image
Prior Image
Thresholding
Compute Prior

Meyer et a. : „Normalized metal artifact reduction (NMAR) in computed tomography", *Med. Phys*. 37 **(10)**, 2010

Metal Artifact Reduction
IMAR

Normalized metal artifact reduction (NMAR)

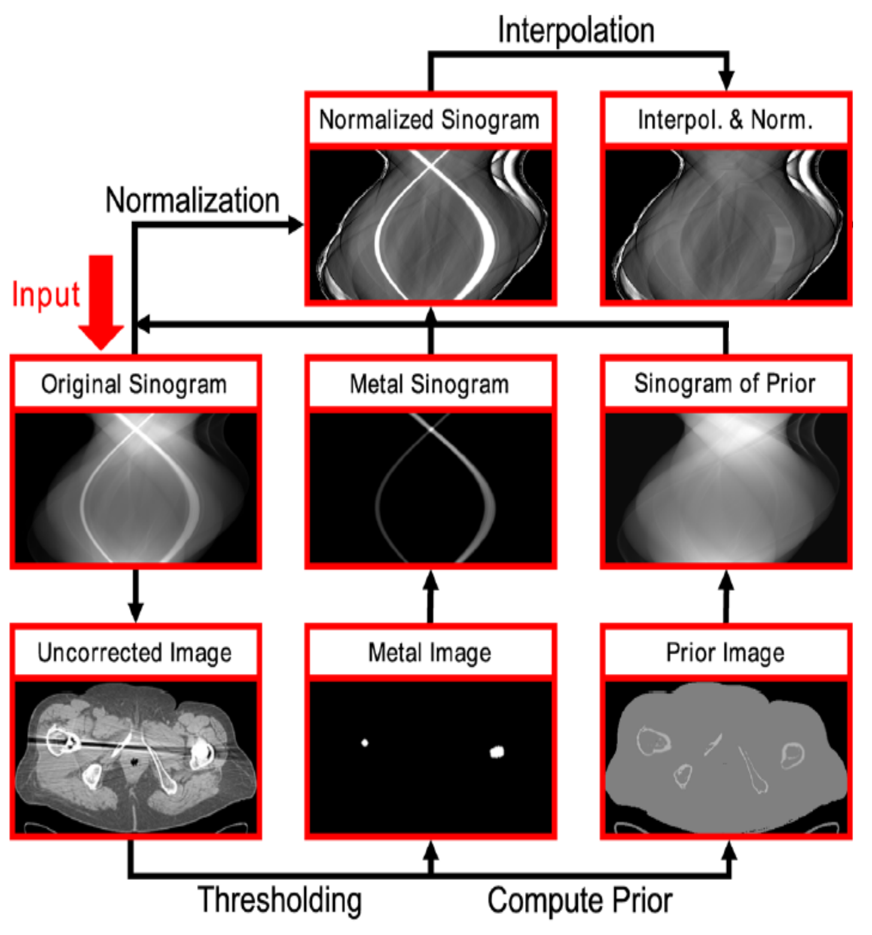
Interpolation
Normalized Sinogram
Interpol. & Norm.
Normalization
Input
Original Sinogram
Metal Sinogram
Sinogram of Prior
Uncorrected Image
Metal Image
Prior Image
Thresholding
Compute Prior

Meyer et a. : „Normalized metal artifact reduction (NMAR) in computed tomography”, *Med. Phys*. 37 **(10)**, 2010

Metal Artifact Reduction
IMAR

Normalized metal artifact reduction (NMAR)

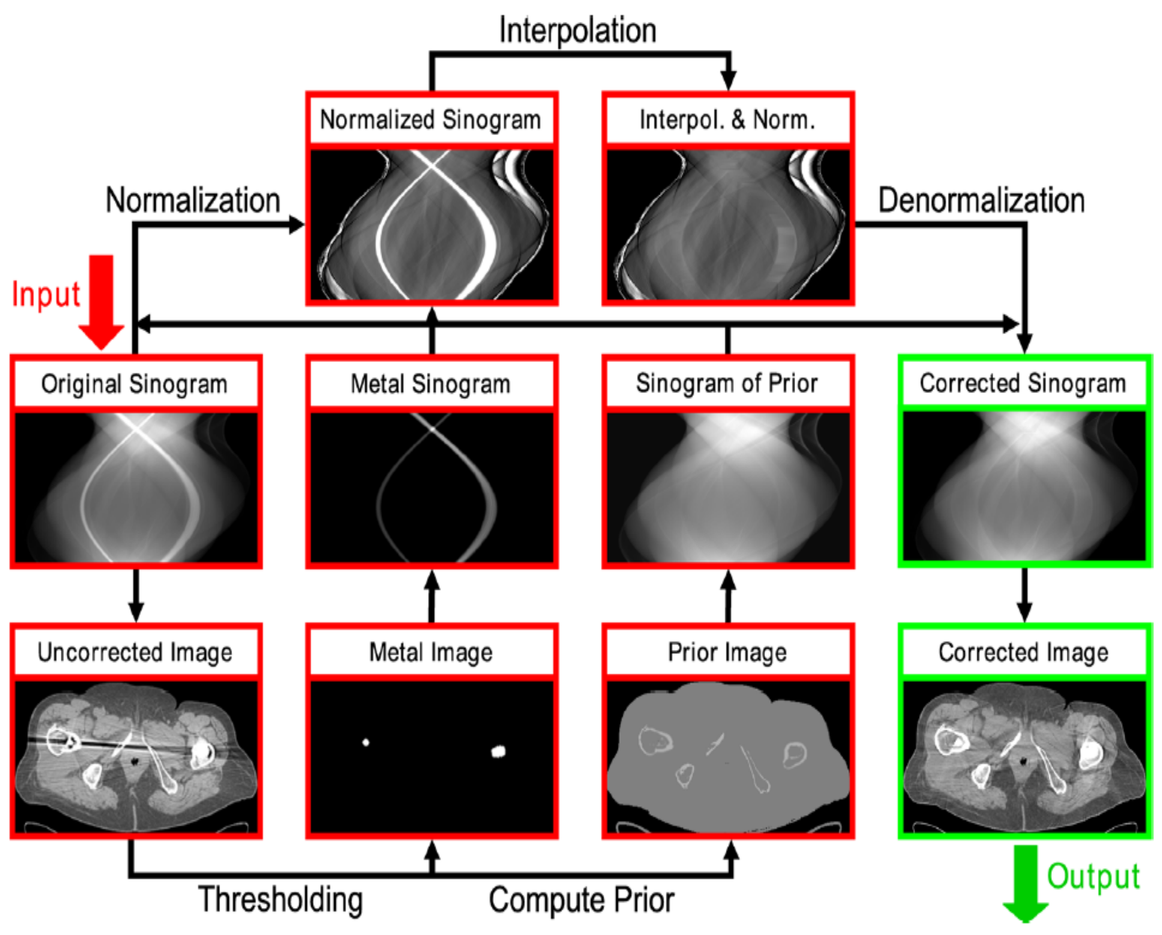
Interpolation
Normalized Sinogram
Interpol. & Norm.
Normalization
Denormalization
Input
Original Sinogram
Metal Sinogram
Sinogram of Prior
Corrected Sinogram
Uncorrected Image
Metal Image
Prior Image
Corrected Image
Output
Thresholding
Compute Prior

Meyer et a. : „Normalized metal artifact reduction (NMAR) in computed tomography", *Med. Phys*. 37 **(10)**, 2010

Metal Artifact Reduction
IMAR

Frequency split metal artifact reduction (FSMAR)

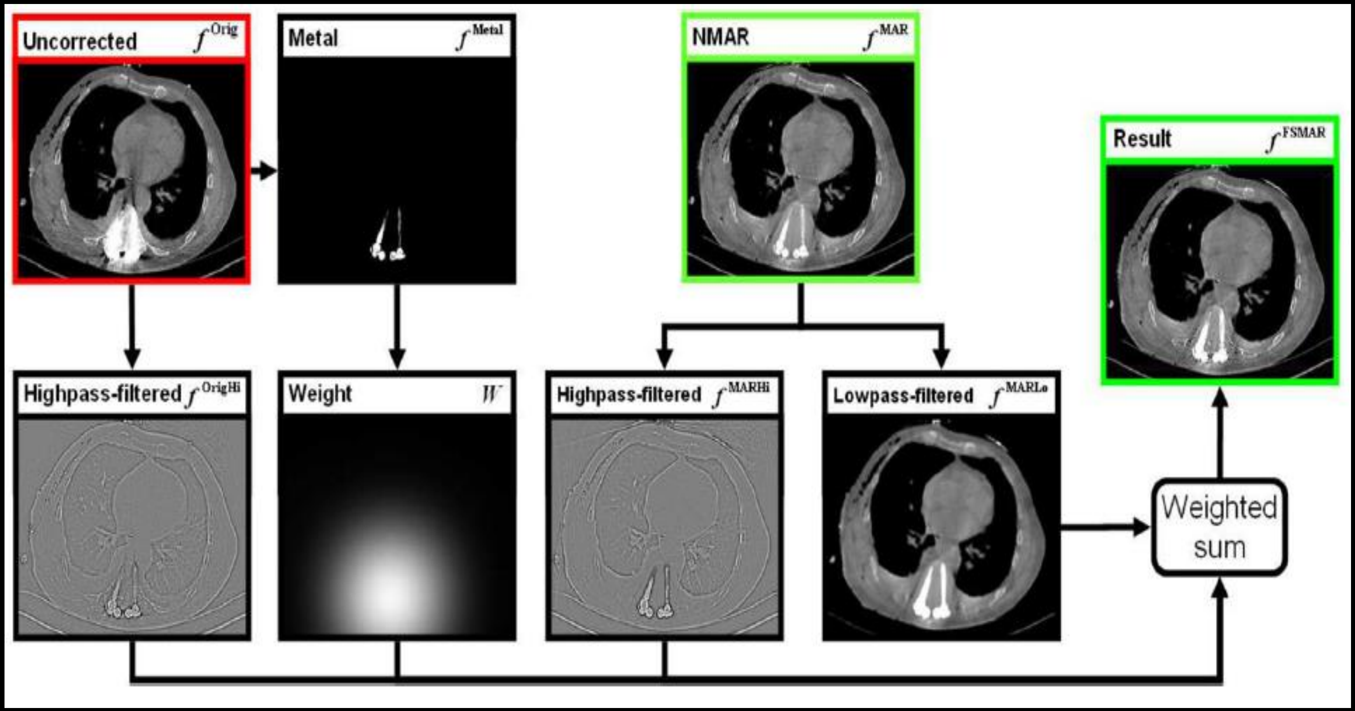
Uncorrected f^{Orig}
Metal f^{Metal}
NMAR f^{MAR}
Result f^{FSMAR}
Highpass-filtered f^{OrigHi}
Weight W
Highpass-filtered f^{MARHi}
Lowpass-filtered f^{MARLo}
Weighted sum

Meyer et a. : „Frequency split metal artifact reduction (FSMAR) in computed tomography", *Med. Phys*. 39 **(4)**, 2012

Metal Artifact Reduction
IMAR

Iterative combination of NMAR and FSMAR.

Hard-coded set of parameters for different types of implants:

- threshold value
- cut-off frequency
- weights
- number of iterations

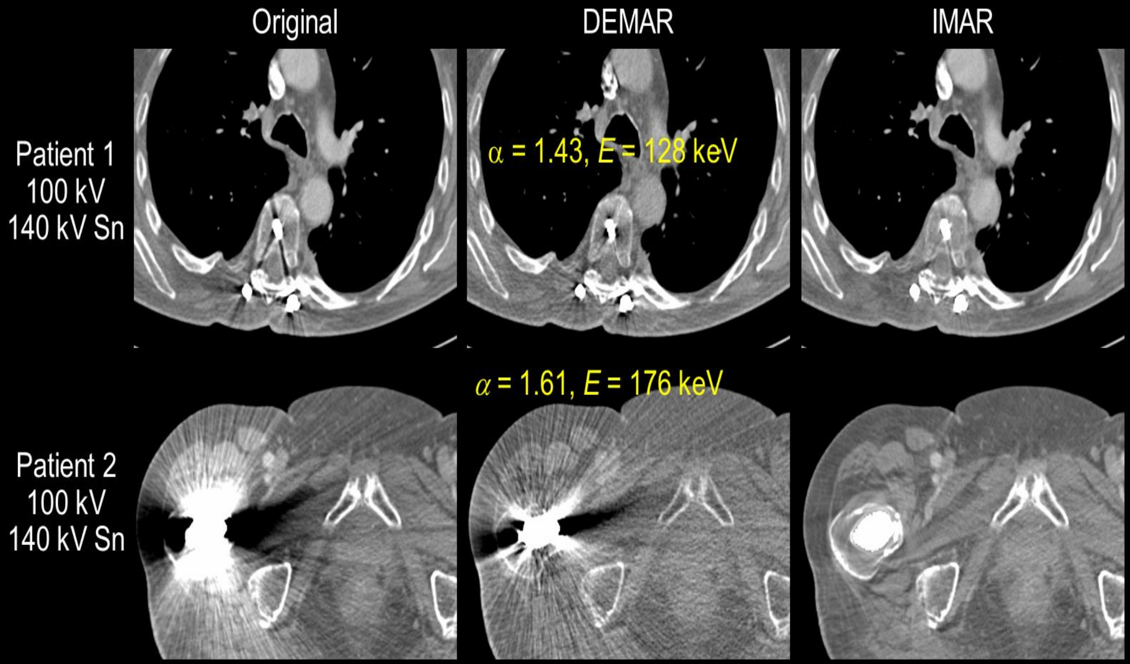
Original
DEMAR
IMAR
Patient 1
100 kV
140 kV Sn
α = 1.43, E = 128 keV
α = 1.61, E = 176 keV
Patient 2
100 kV
140 kV Sn

Courtesy of Prof. Michael Lell, Friedrich-Alexander University Erlangen-Nürnberg

UiO : Department of Physics
University of Oslo

Oslo
University Hospital

PET tracers and applications

Eirik Malinen

Why PET

- Cancer has upregulated cellular pathways that can be exploited in molecular imaging
- Localize and define the tumor and nodes
- Assess disease aggressiveness
- Evaluate treatment

Uptake reflects cellular processes

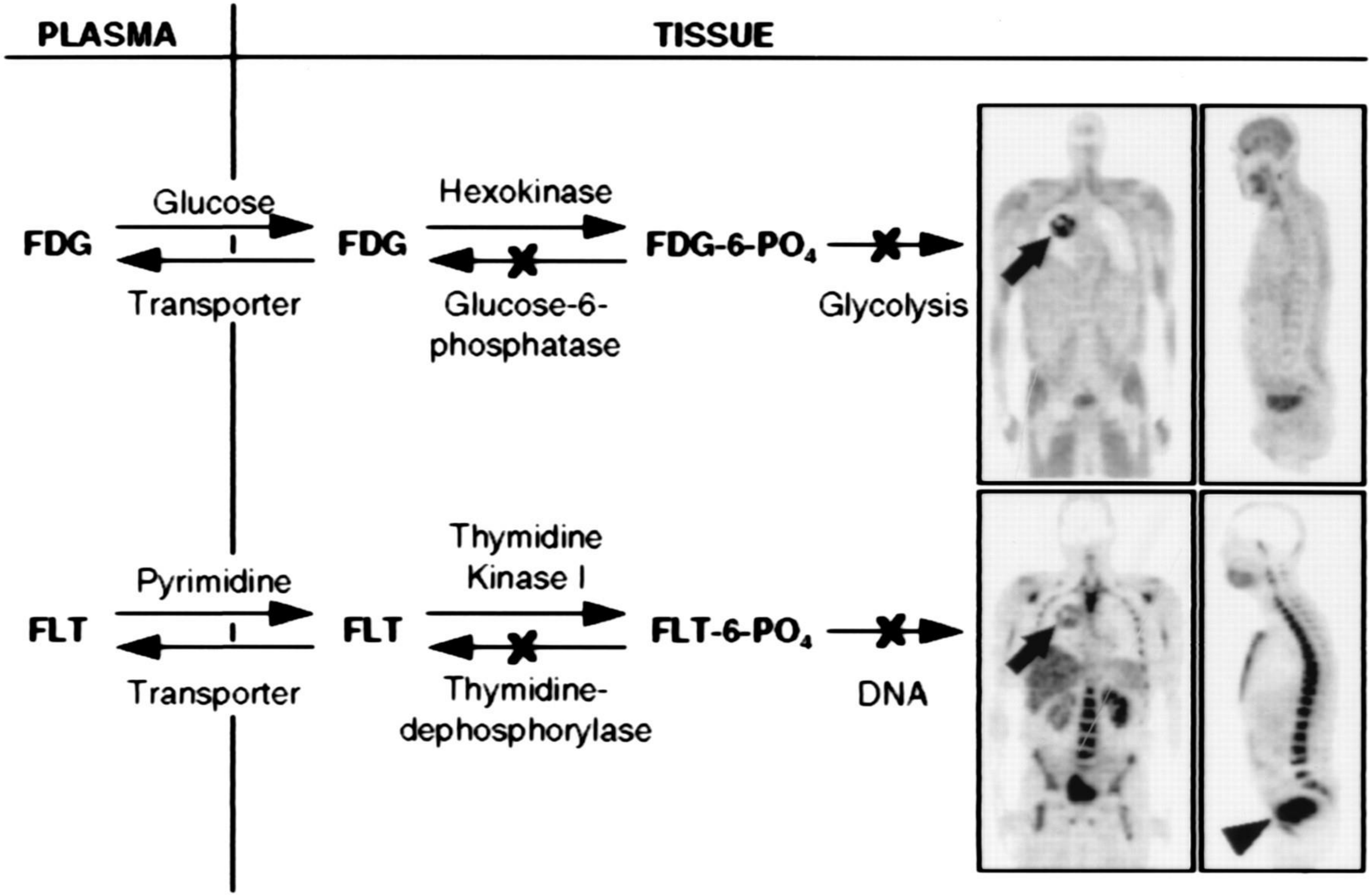
PLASMA
TISSUE
Glucose
FDG
FDG
Transporter
Hexokinase
FDG-6-PO$_4$
Glucose-6-phosphatase
Glycolysis
Pyrimidine
FLT
FLT
Transporter
Thymidine Kinase I
FLT-6-PO$_4$
Thymidine-dephosphorylase
DNA

PNAS 97; 9226–9233 (2000)

Tracer production - cyclotron

- Cyclotron provides e.g. accelerated protons
- Target undergoes nuclear reactions

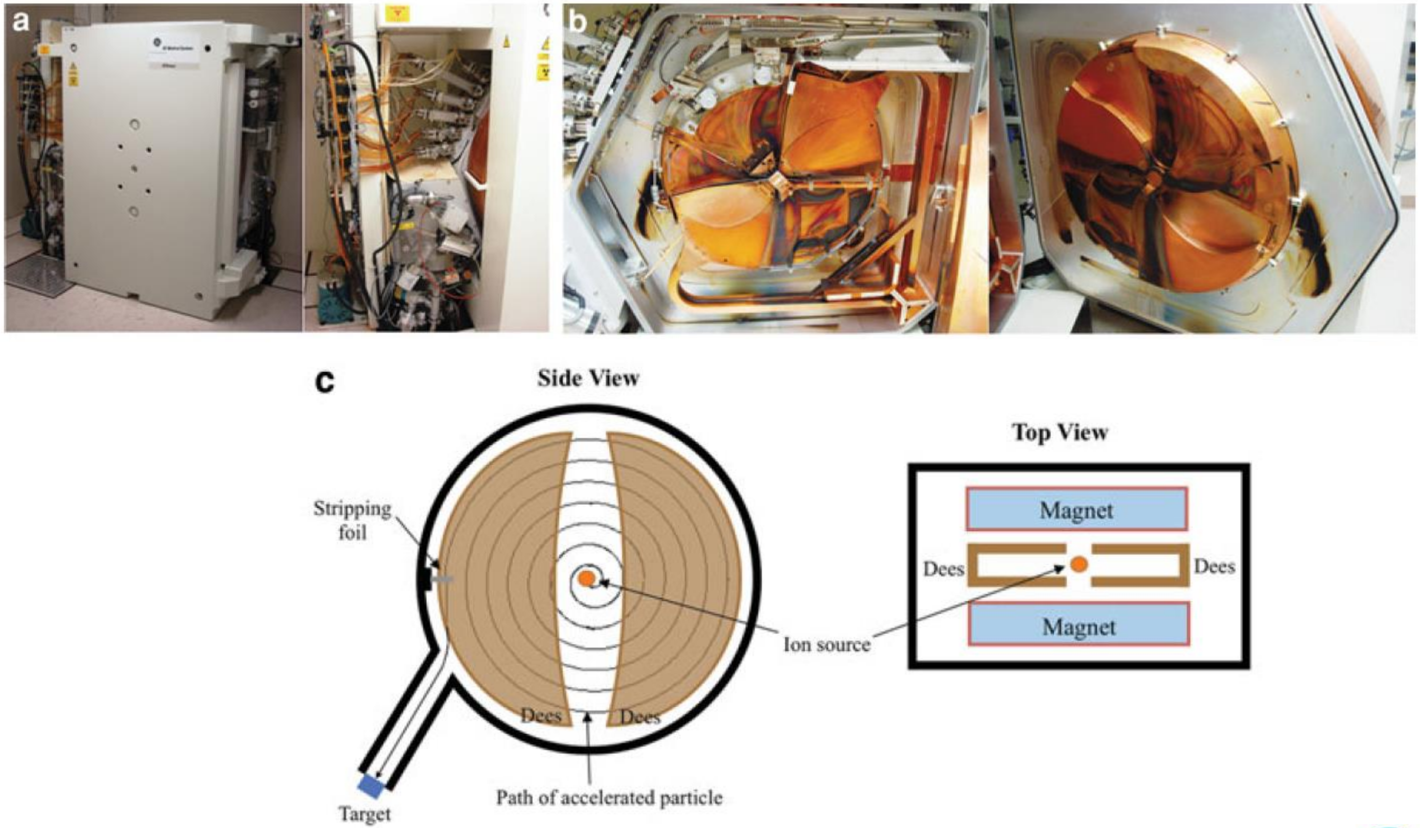
a
b
c
Side View
Top View
Stripping foil
Magnet
Dees
Dees
Magnet
Ion source
Dees
Dees
Target
Path of accelerated particle

DOI: 10.1007/174_2012_703

Tracer production - generator

- Long lived parent nuclei decays to short-lived positron emitting daughter, e.g. $^{68}Ge \rightarrow ^{68}Ga$

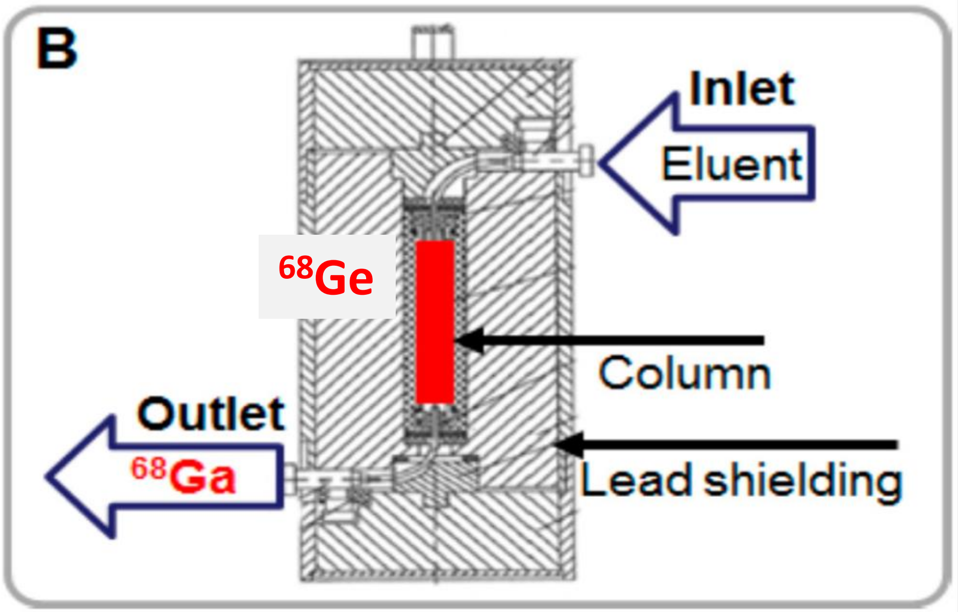
B
Inlet
Eluent
^{68}Ge
Column
Outlet
^{68}Ga
Lead shielding

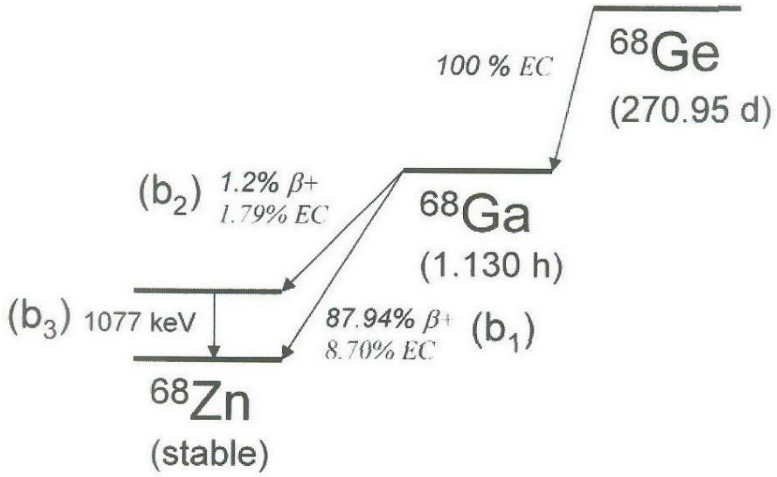
^{68}Ge
(270.95 d)
100 % EC
^{68}Ga
(1.130 h)
(b$_2$) 1.2% β+
1.79% EC
(b$_3$) 1077 keV
87.94% β+
8.70% EC
(b$_1$)
^{68}Zn
(stable)

- No need for cyclotron onsite

Molecules 2015, 20(7), 12913-12943

Isotopes and disintegration

Radionuclide	*Half-life*	*E_{max}(Mev)*	*β^+ Branching Fraction*
^{11}C	20.4 min	0.96	1.00
^{13}N	9.97 min	1.20	1.00
^{15}O	122 s	1.73	1.00
^{18}F	109.8 min	0.63	0.97
^{22}Na	2.60 y	0.55	0.90
^{62}Cu	9.74 min	2.93	0.97
^{64}Cu	12.7 h	0.65	0.29
^{68}Ga	67.6 min	1.89	0.89
^{76}Br	16.2 h	Various	0.56
^{82}Rb	1.27 min	2.60, 3.38	0.96
^{124}I	4.17 d	1.53, 2.14	0.23

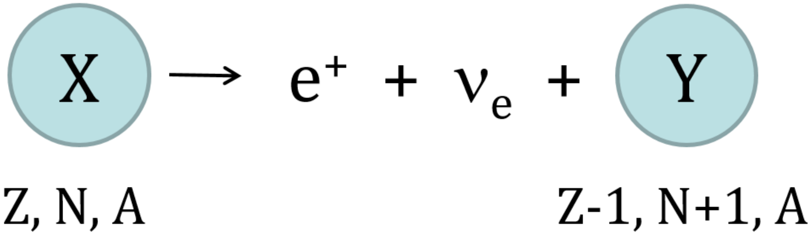

$$X \rightarrow e^+ + \nu_e + Y$$

Z, N, A

Z-1, N+1, A

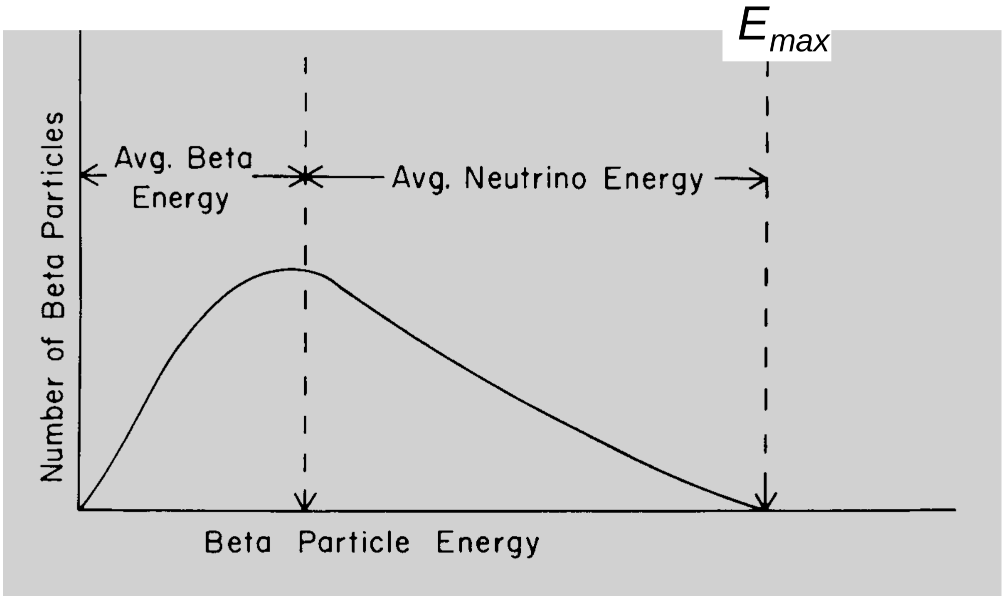

Tracer production – ^{18}F-FDG

- ^{18}O irradiated with protons

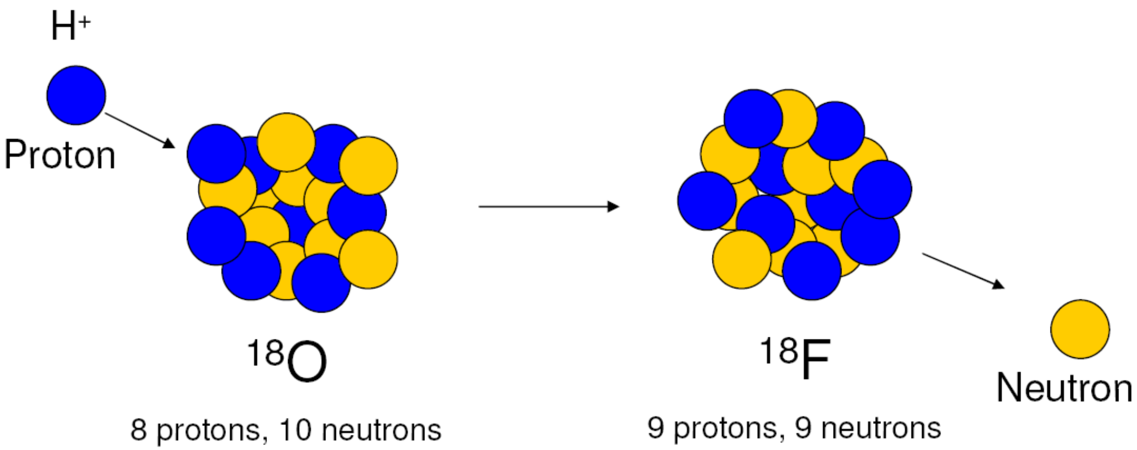
H+
Proton
^{18}O
8 protons, 10 neutrons
^{18}F
9 protons, 9 neutrons
Neutron

- 18F added to mannose triflate→

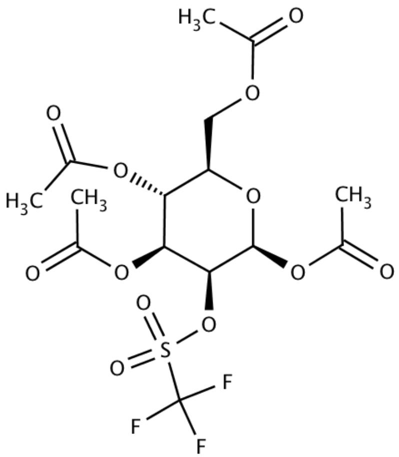
H$_3$C
O
O
O
O
H$_3$C
CH$_3$
O
CH$_3$
O
O
O
O
O
O
O
S
F
F
F

- Several steps involving labelling, purification and hydrolysis

^{18}F-FDG

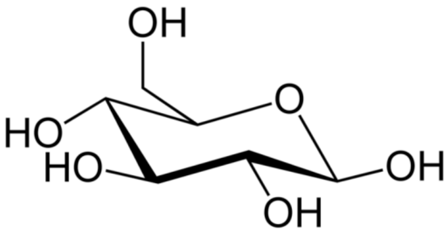

Glucose

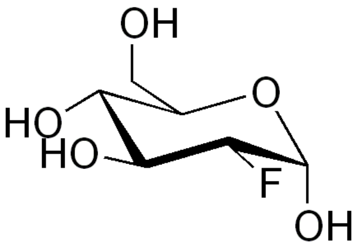

Flourodeoxyglucose

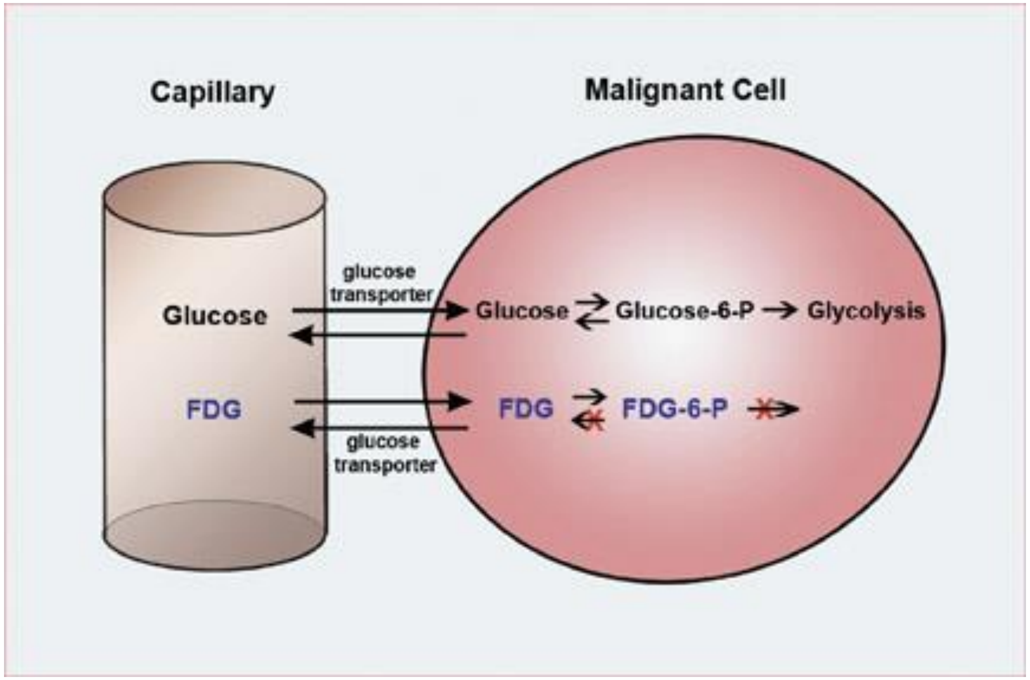
Capillary
Malignant Cell
Glucose
FDG
glucose transporter
glucose transporter
Glucose
Glucose-6-P
Glycolysis
FDG
FDG-6-P

PET workflow

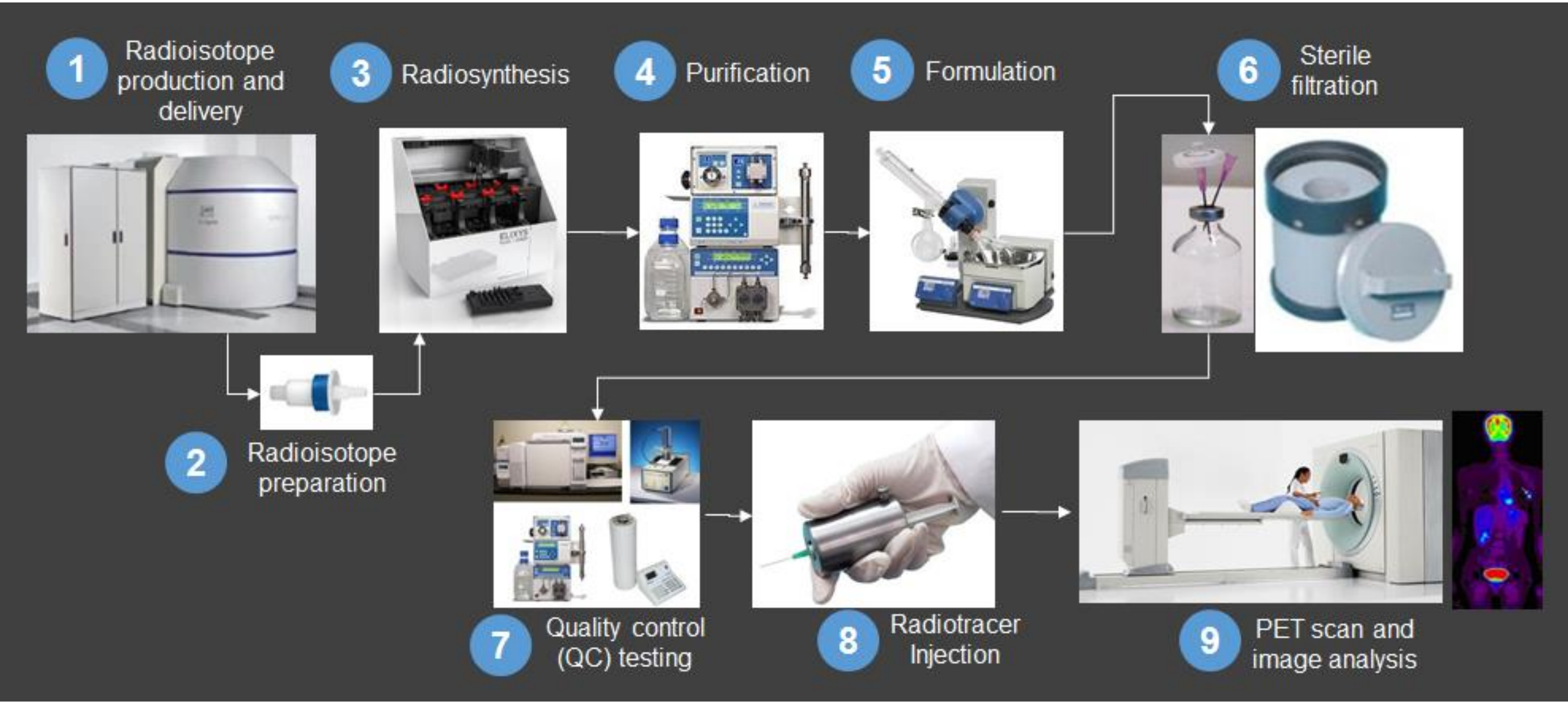
1 Radioisotope production and delivery
3 Radiosynthesis
4 Purification
5 Formulation
6 Sterile filtration
2 Radioisotope preparation
7 Quality control (QC) testing
8 Radiotracer Injection
9 PET scan and image analysis

http://www.vandamlab.org/research

^{18}F-FDG – a biomarker

Extract maximum uptake

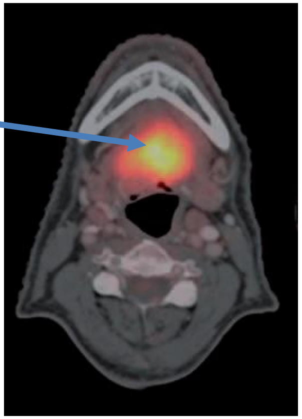

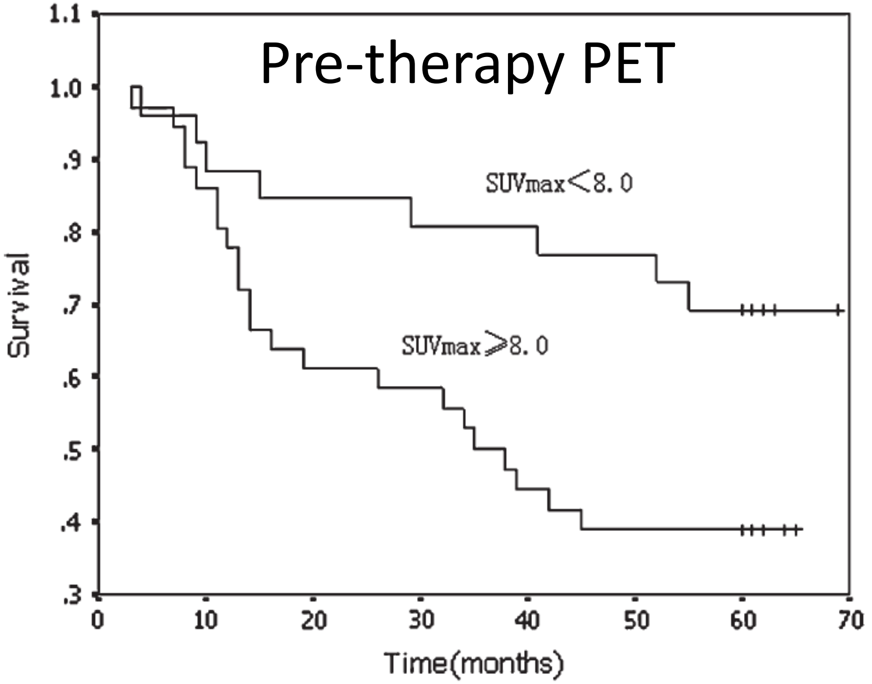
Pre-therapy PET

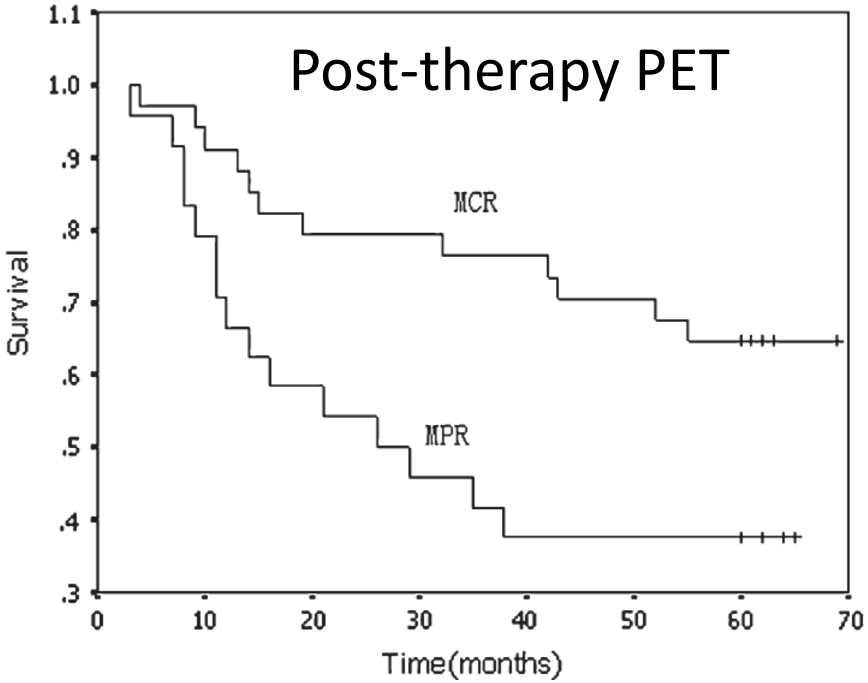
Post-therapy PET

Annals of Oncology 21, 1078–1082

Conventional *vs* dynamic PET

Conventional PET:

- Patient rests for 1 hour after injection
- Produces a ”static” PET image series (3D)

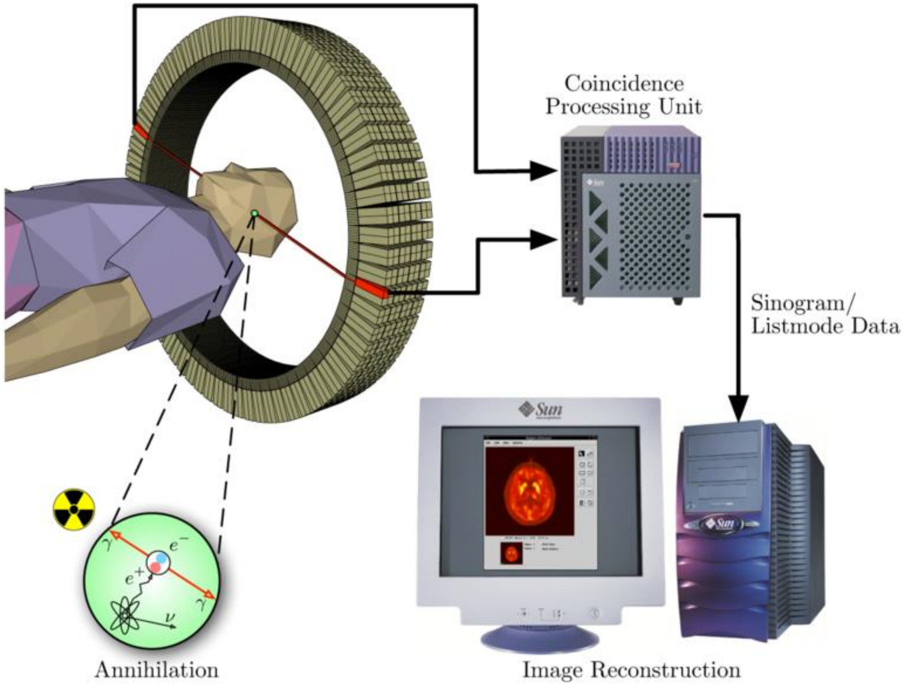
Coincidence Processing Unit
Sinogram/ Listmode Data
Annihilation
Image Reconstruction

Dynamic PET

- PET-acquisition starts at the time of injection
- May give a dynamic image series (4D)

Dynamic FDG-PET

- Time stamp for each coincidence in the listmode file → reconstruct in time intervals

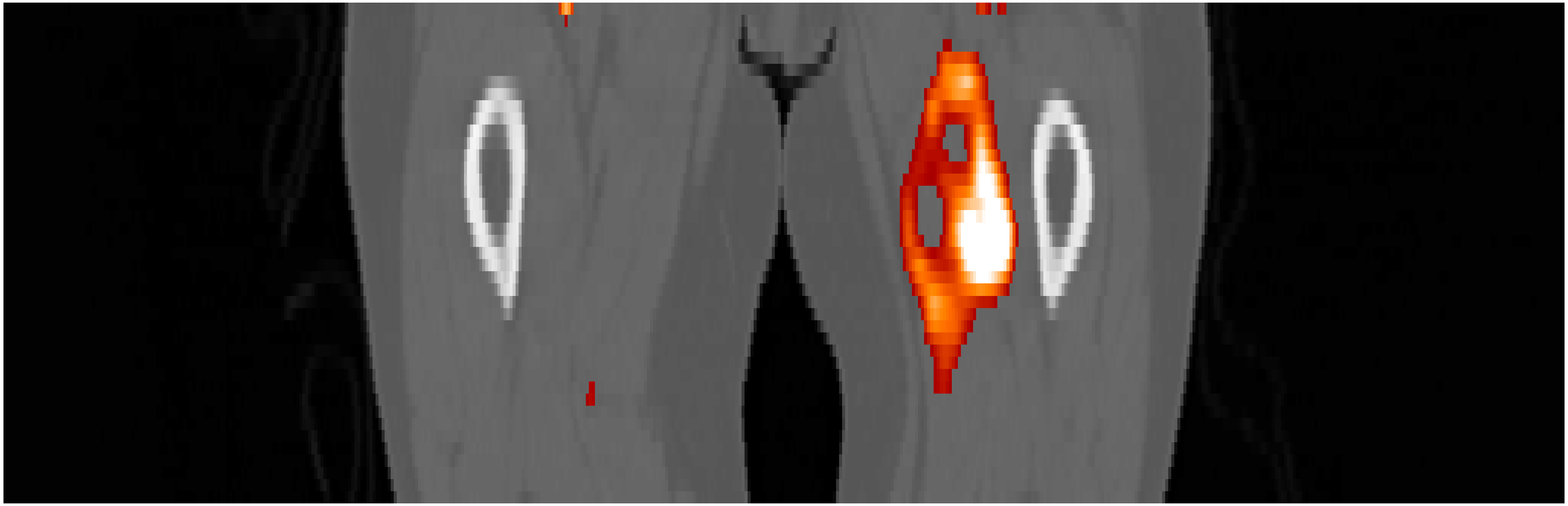

Dynamic FDG-PET

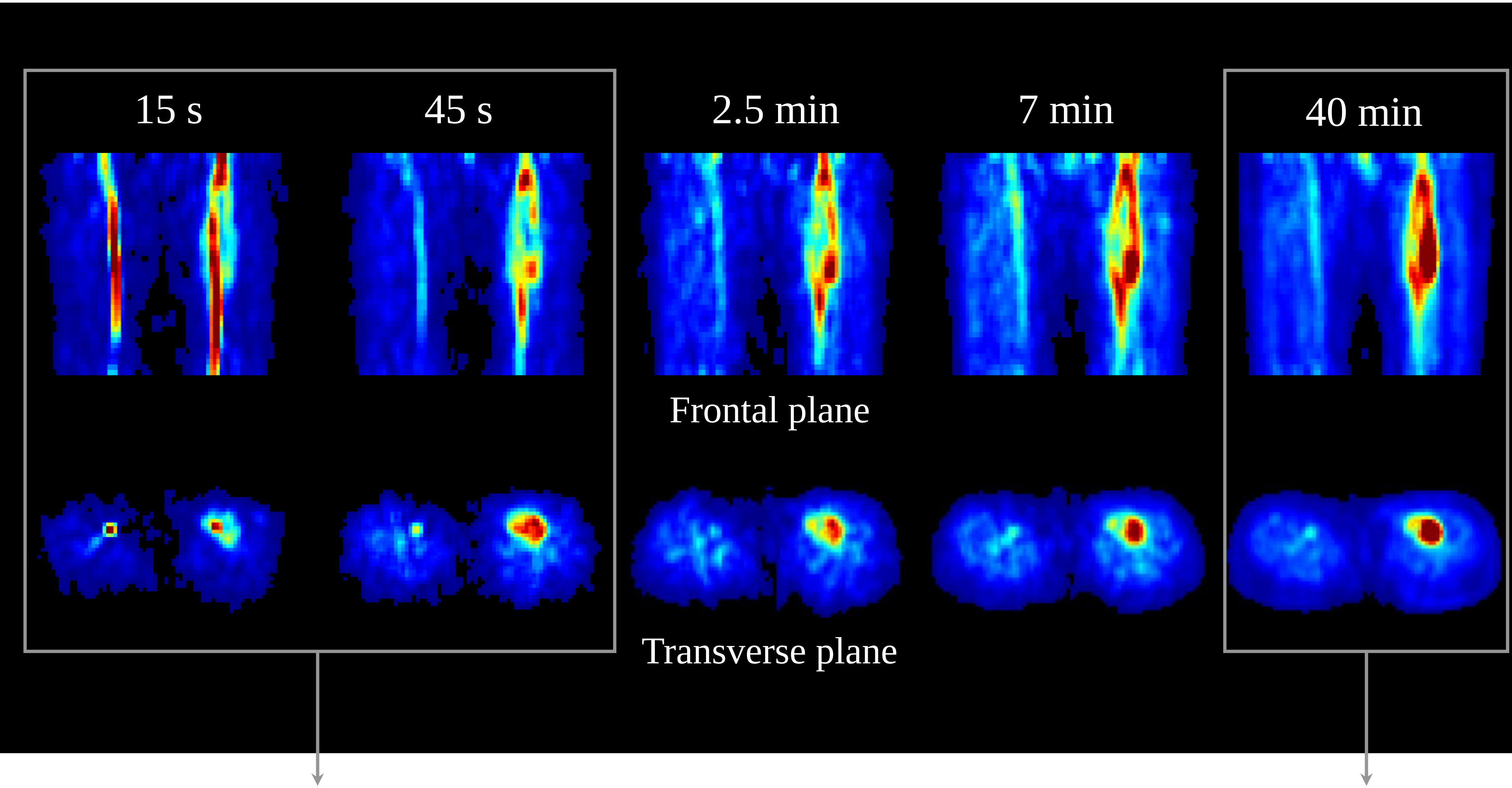
15 s
45 s
2.5 min
7 min
40 min
Frontal plane
Transverse plane

Vascular

Metabolic

Kinetic modelling

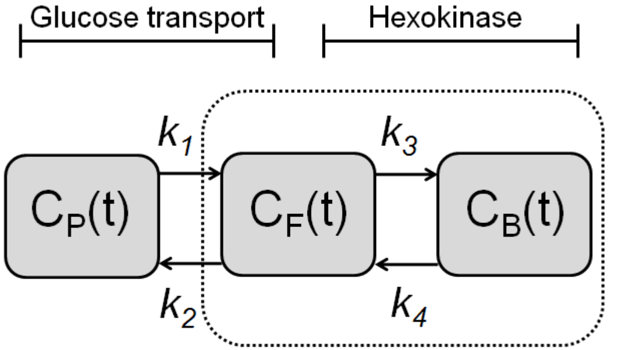
Glucose transport
Hexokinase
k_1
k_3
$C_P(t)$
$C_F(t)$
$C_B(t)$
k_2
k_4

$$C_T(t) = C_F(t) + C_B(t)$$

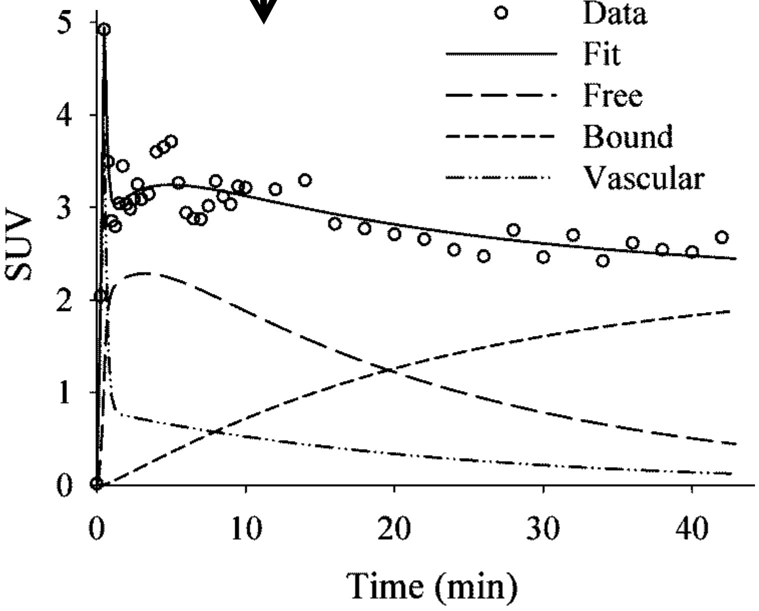

$K_1 = 0.20$
$k_2 = 0.40$
$k_3 = 0.037$
$\nu_p = 0.16$
$MR_{FDG} = 0.016$
$r^2 = 0.89$

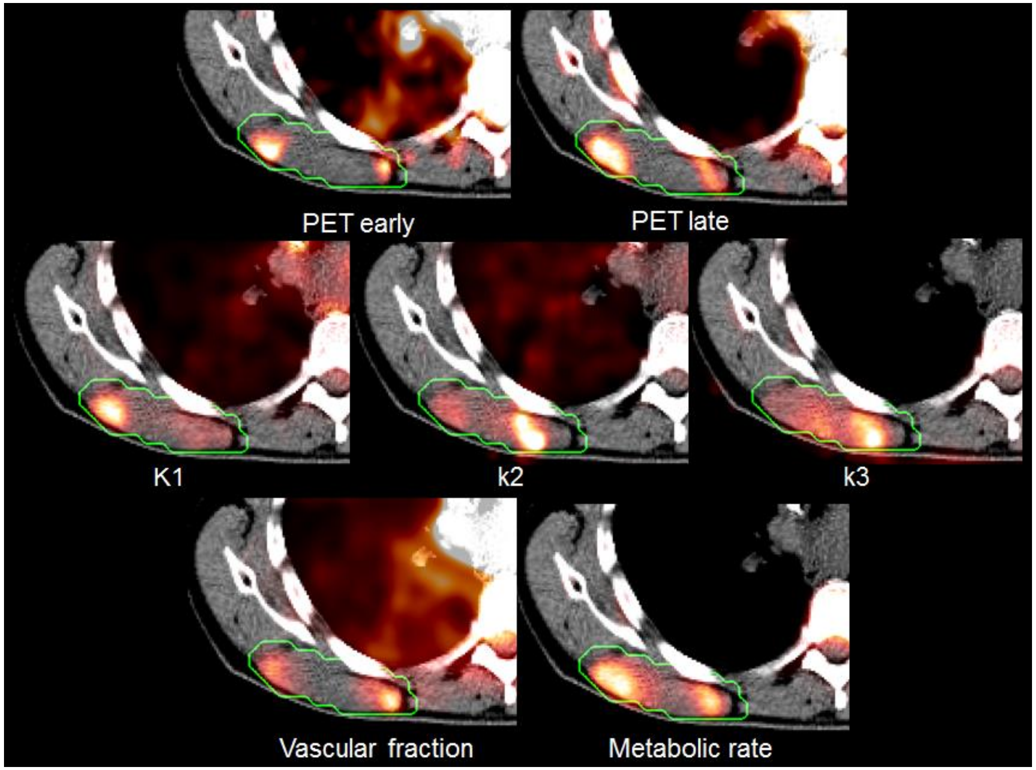
PET early
PET late
K1
k2
k3
Vascular fraction
Metabolic rate

Acta Oncol. 2013 Aug;52(6):1160-7

Parametric imaging

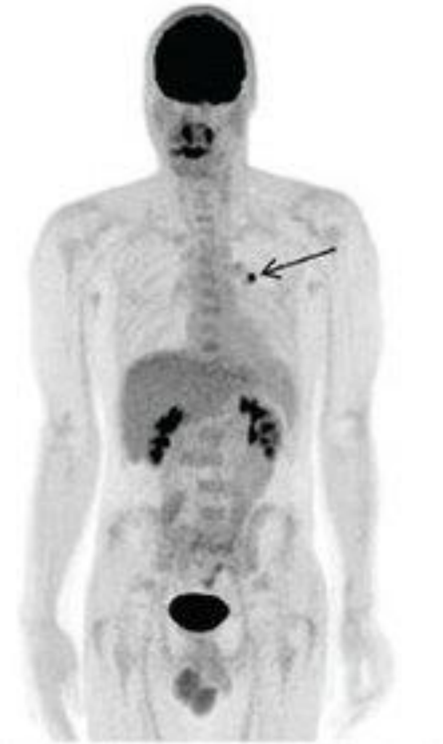

Mean image
60-90 min p.i.

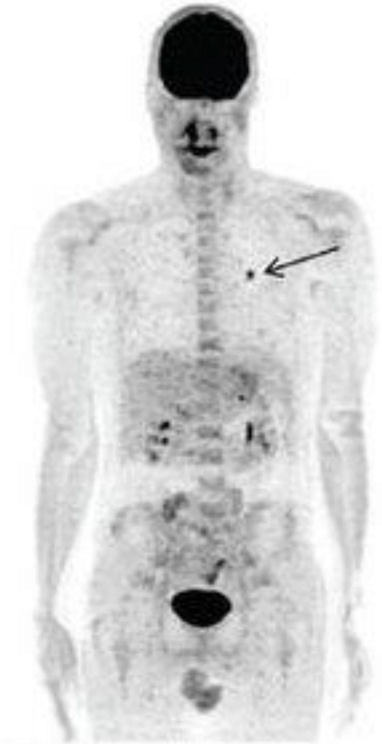

Patlak slope image

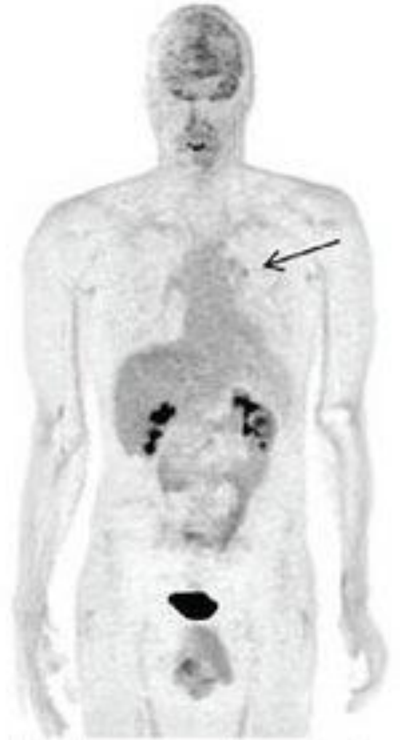

Patlak intercept image

Yale University, New Haven, Connecticut, USA

PET tracers

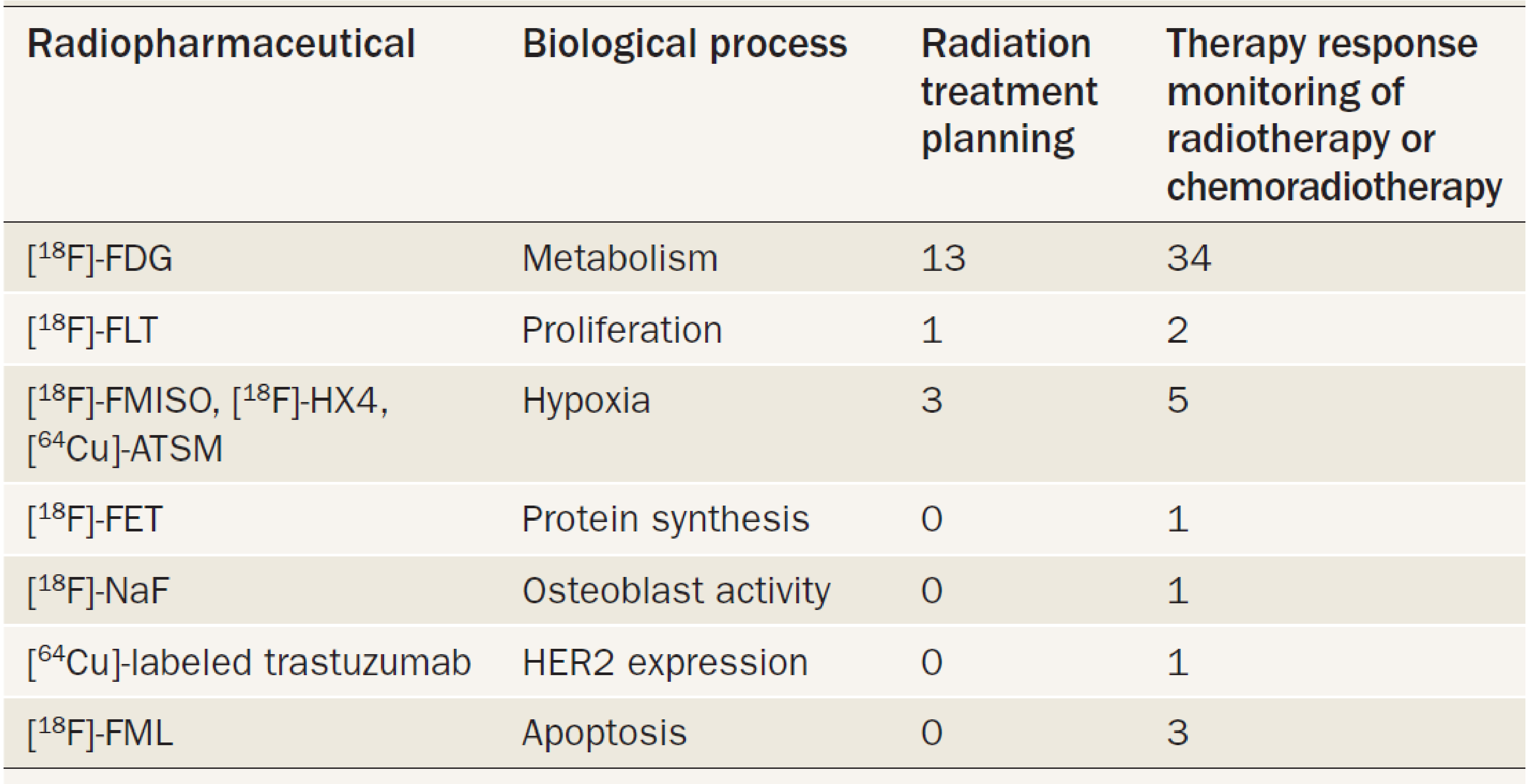

Radiopharmaceutical	Biological process	Radiation treatment planning	Therapy response monitoring of radiotherapy or chemoradiotherapy
[^{18}F]-FDG	Metabolism	13	34
[^{18}F]-FLT	Proliferation	1	2
[^{18}F]-FMISO, [^{18}F]-HX4, [^{64}Cu]-ATSM	Hypoxia	3	5
[^{18}F]-FET	Protein synthesis	0	1
[^{18}F]-NaF	Osteoblast activity	0	1
[^{64}Cu]-labeled trastuzumab	HER2 expression	0	1
[^{18}F]-FML	Apoptosis	0	3

NATURE REVIEWS | CLINICAL ONCOLOGY 8 2011, 233-

Hypoxia tracers

- Fluorine labeled nitroimidazoles and copper labeled dithiosemicarbazones
- Slow clearance, low tumor to background

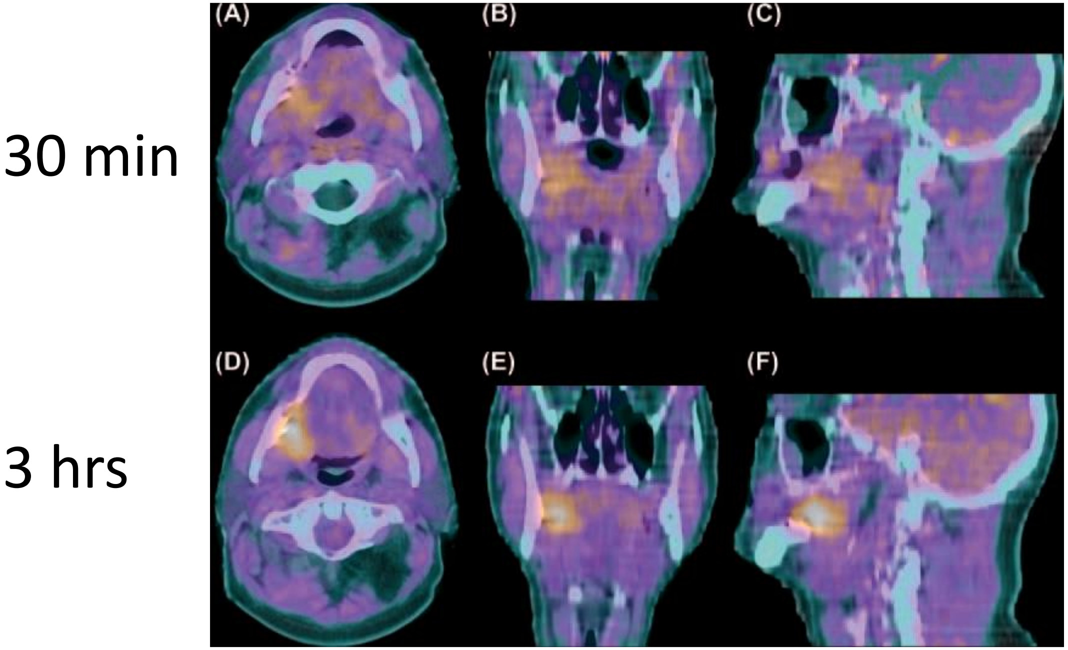

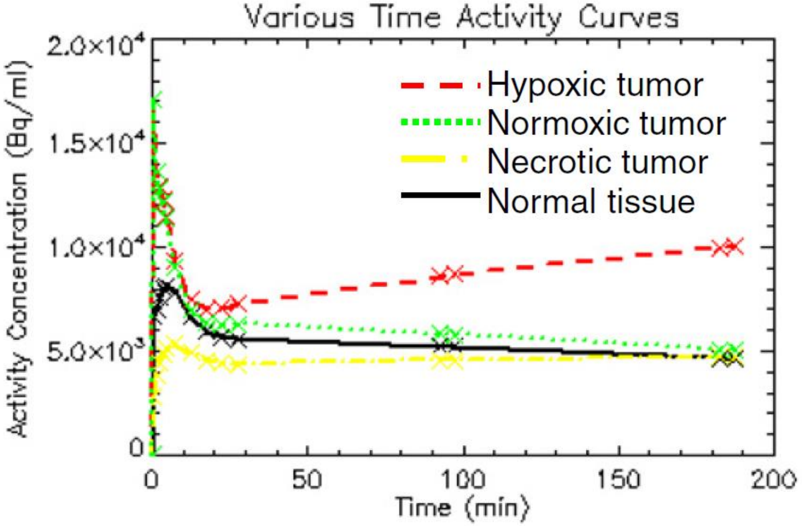

Acta Oncologica, 2013; 52: 1257–1271

18F-MISO PET

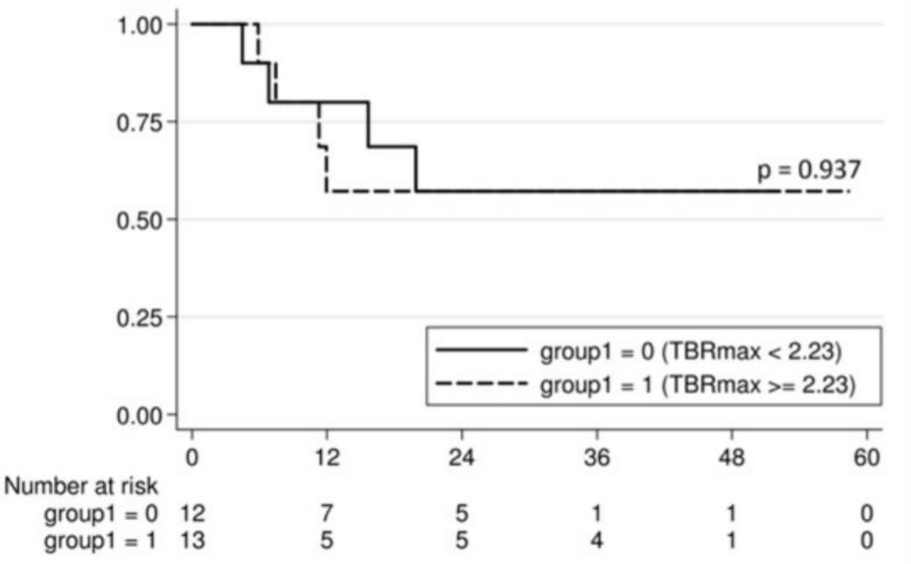

Pre-treatment

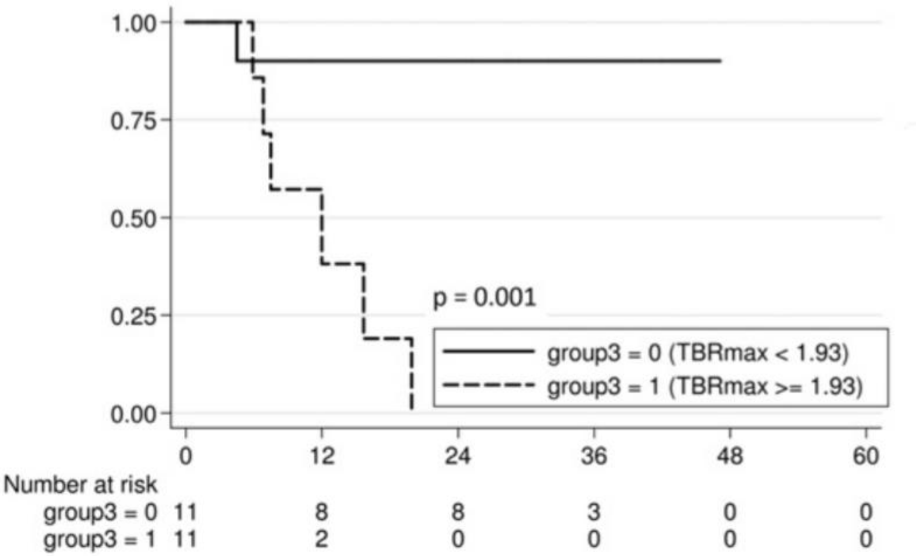

18-20 Gy

- Early hypoxia imaging may be useful for selection to hypoxia modification

HX4-PET vs FDG-PET

HX4 FDG

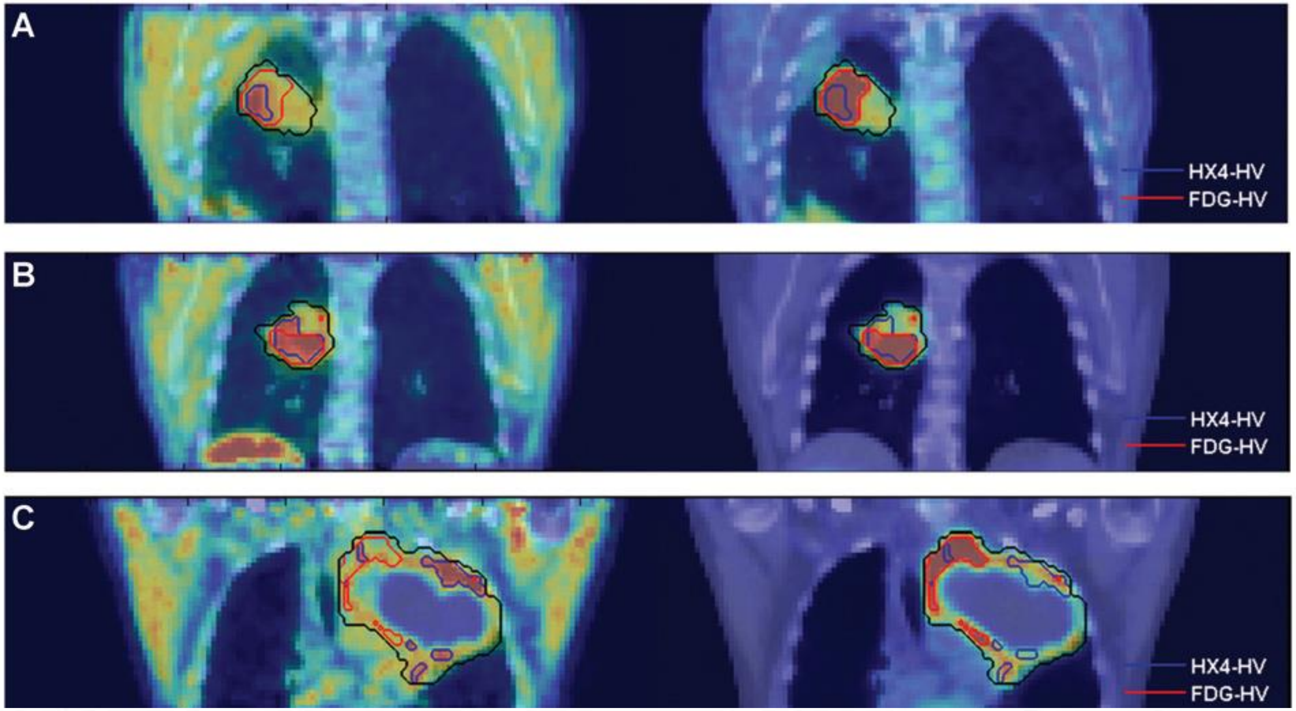
A
HX4-HV
FDG-HV
B
HX4-HV
FDG-HV
C
HX4-HV
FDG-HV

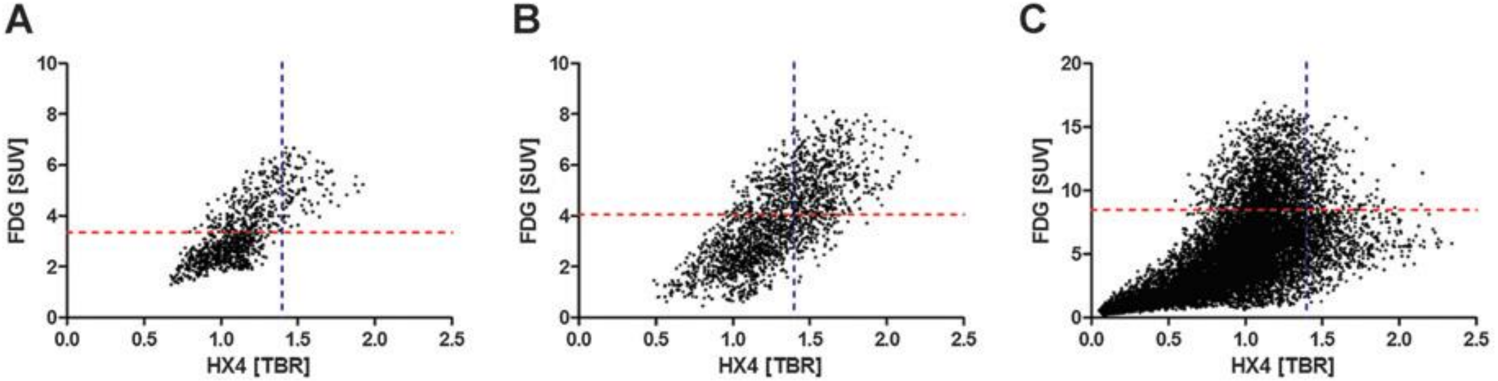

Clin Cancer Res; 20(24) ,2014

PET/CT in RT

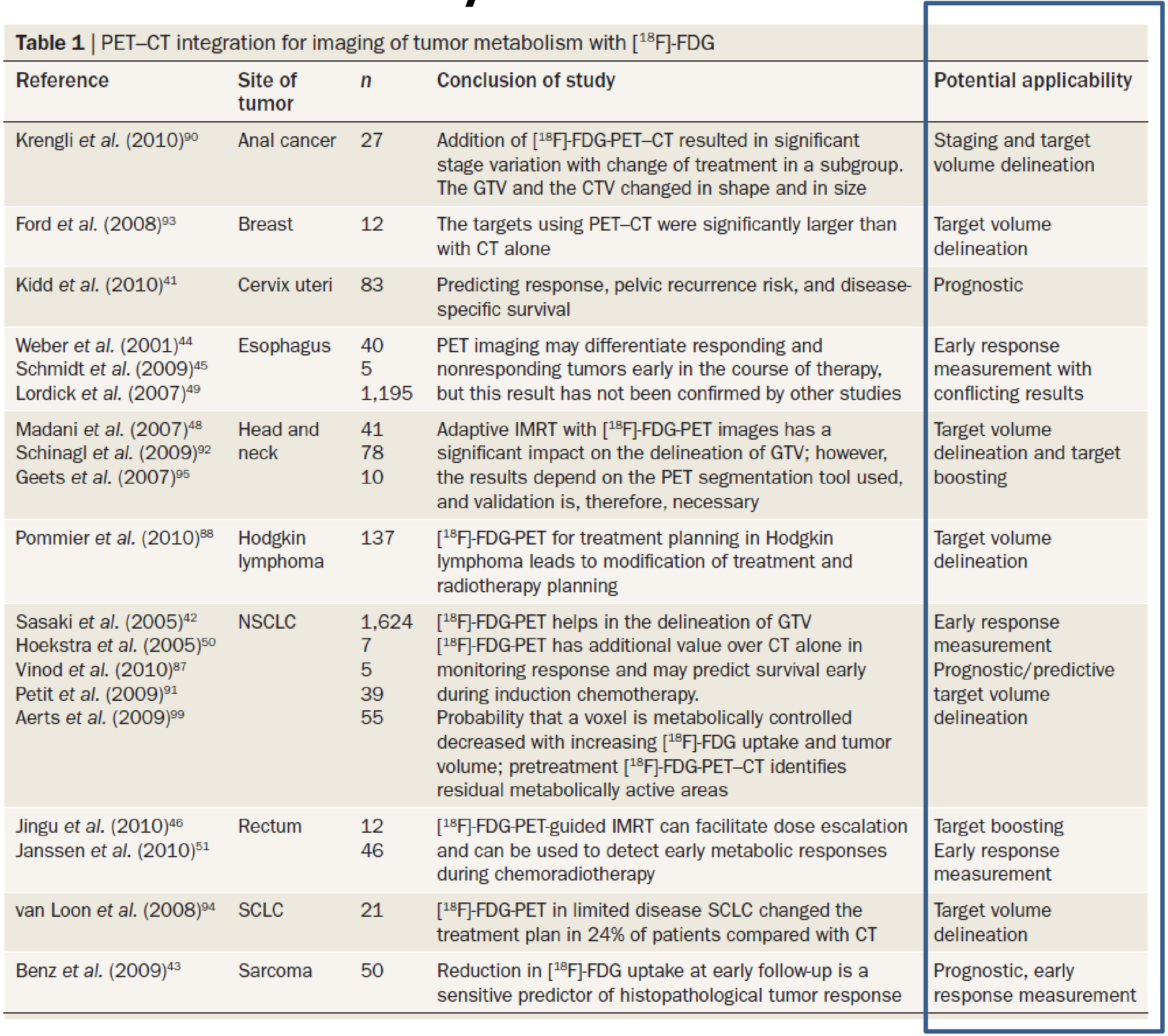

Table 1 | PET–CT integration for imaging of tumor metabolism with [^{18}F]-FDG

Reference	Site of tumor	*n*	Conclusion of study	Potential applicability
Krengli *et al.* (2010)[90]	Anal cancer	27	Addition of [^{18}F]-FDG-PET–CT resulted in significant stage variation with change of treatment in a subgroup. The GTV and the CTV changed in shape and in size	Staging and target volume delineation
Ford *et al.* (2008)[93]	Breast	12	The targets using PET–CT were significantly larger than with CT alone	Target volume delineation
Kidd *et al.* (2010)[41]	Cervix uteri	83	Predicting response, pelvic recurrence risk, and disease-specific survival	Prognostic
Weber *et al.* (2001)[44] Schmidt *et al.* (2009)[45] Lordick *et al.* (2007)[49]	Esophagus	40 5 1,195	PET imaging may differentiate responding and nonresponding tumors early in the course of therapy, but this result has not been confirmed by other studies	Early response measurement with conflicting results
Madani *et al.* (2007)[48] Schinagl *et al.* (2009)[92] Geets *et al.* (2007)[95]	Head and neck	41 78 10	Adaptive IMRT with [^{18}F]-FDG-PET images has a significant impact on the delineation of GTV; however, the results depend on the PET segmentation tool used, and validation is, therefore, necessary	Target volume delineation and target boosting
Pommier *et al.* (2010)[88]	Hodgkin lymphoma	137	[^{18}F]-FDG-PET for treatment planning in Hodgkin lymphoma leads to modification of treatment and radiotherapy planning	Target volume delineation
Sasaki *et al.* (2005)[42] Hoekstra *et al.* (2005)[50] Vinod *et al.* (2010)[87] Petit *et al.* (2009)[91] Aerts *et al.* (2009)[99]	NSCLC	1,624 7 5 39 55	[^{18}F]-FDG-PET helps in the delineation of GTV [^{18}F]-FDG-PET has additional value over CT alone in monitoring response and may predict survival early during induction chemotherapy. Probability that a voxel is metabolically controlled decreased with increasing [^{18}F]-FDG uptake and tumor volume; pretreatment [^{18}F]-FDG-PET–CT identifies residual metabolically active areas	Early response measurement Prognostic/predictive target volume delineation
Jingu *et al.* (2010)[46] Janssen *et al.* (2010)[51]	Rectum	12 46	[^{18}F]-FDG-PET-guided IMRT can facilitate dose escalation and can be used to detect early metabolic responses during chemoradiotherapy	Target boosting Early response measurement
van Loon *et al.* (2008)[94]	SCLC	21	[^{18}F]-FDG-PET in limited disease SCLC changed the treatment plan in 24% of patients compared with CT	Target volume delineation
Benz *et al.* (2009)[43]	Sarcoma	50	Reduction in [^{18}F]-FDG uptake at early follow-up is a sensitive predictor of histopathological tumor response	Prognostic, early response measurement

NATURE REVIEWS | CLINICAL ONCOLOGY 8 2011, 233-

Tumor delineation

- Where is the tumor tissue in a blurred image?

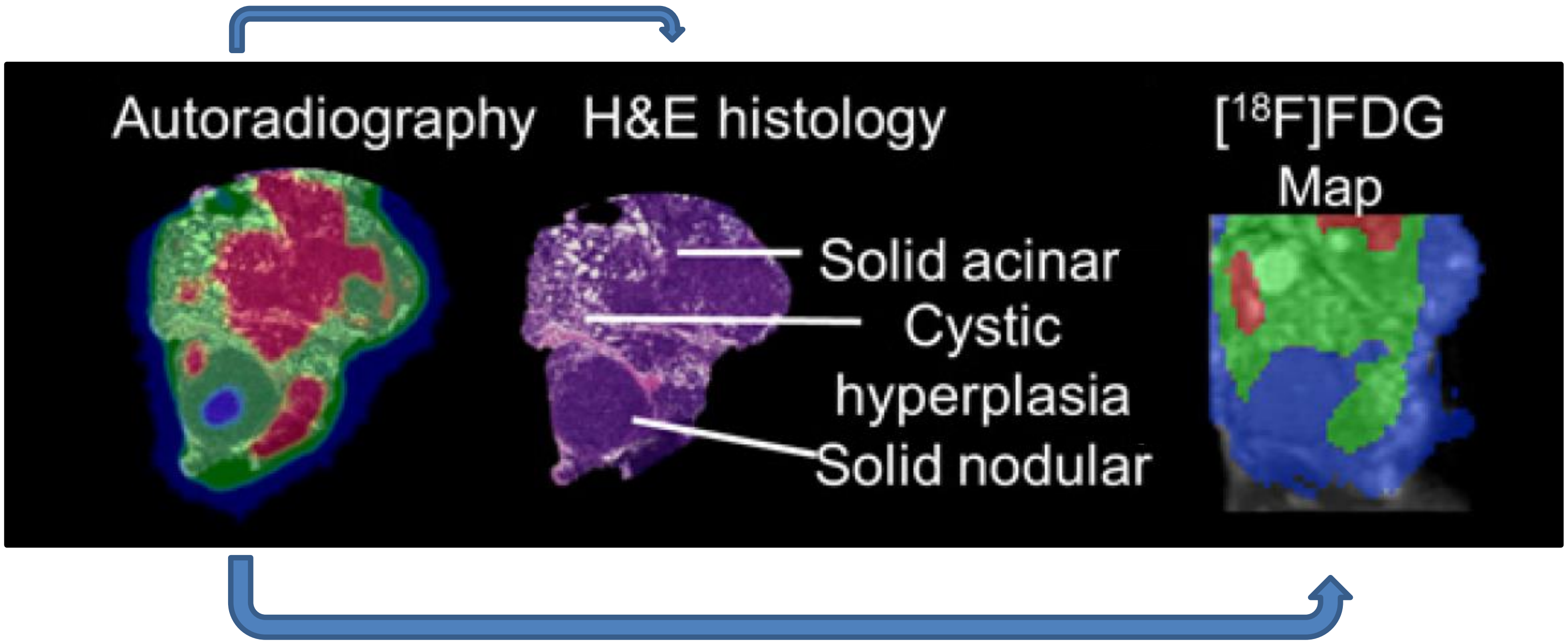
Autoradiography
H&E histology
[18F]FDG Map
Solid acinar
Cystic hyperplasia
Solid nodular

Not perfect correspondence

Blurring due to PET limitations

- One specific tracer reflect one tumor property

Cancer Res; 76(18), 2016

Tumor delineation

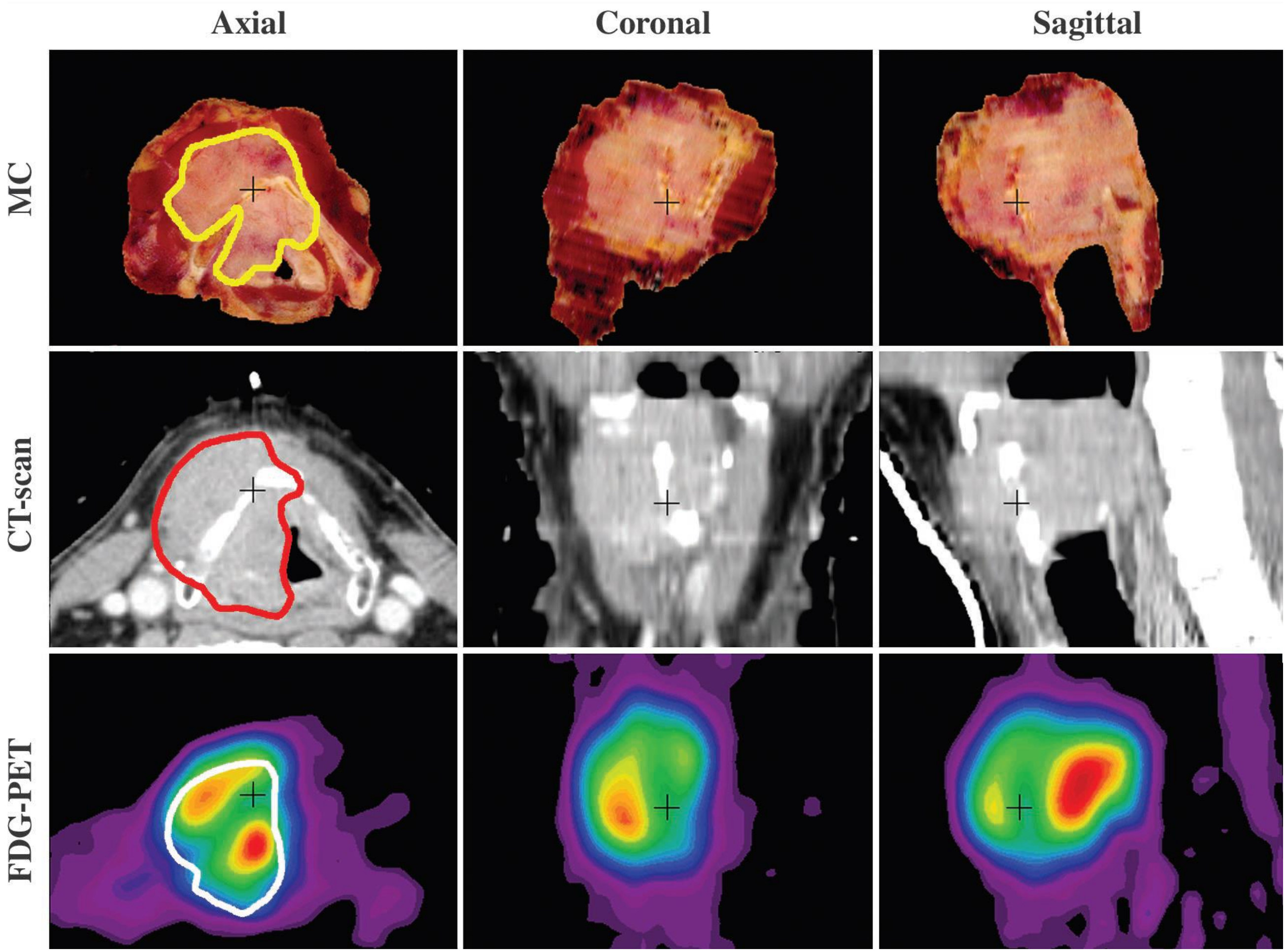
Axial
Coronal
Sagittal
MC
CT-scan
FDG-PET

Radiology 233 (2004)

PET was most accurate. No modality (PET/MRI/CT) managed to depict superficial tumor extension.

Tumor delineation

PET/CT

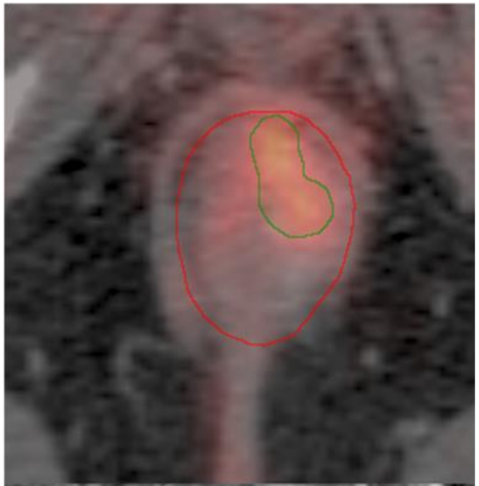

MRI

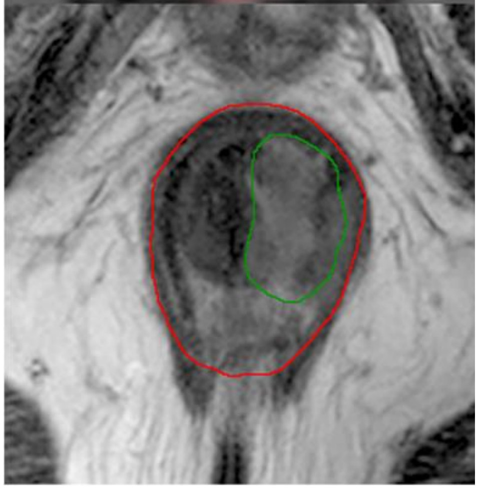

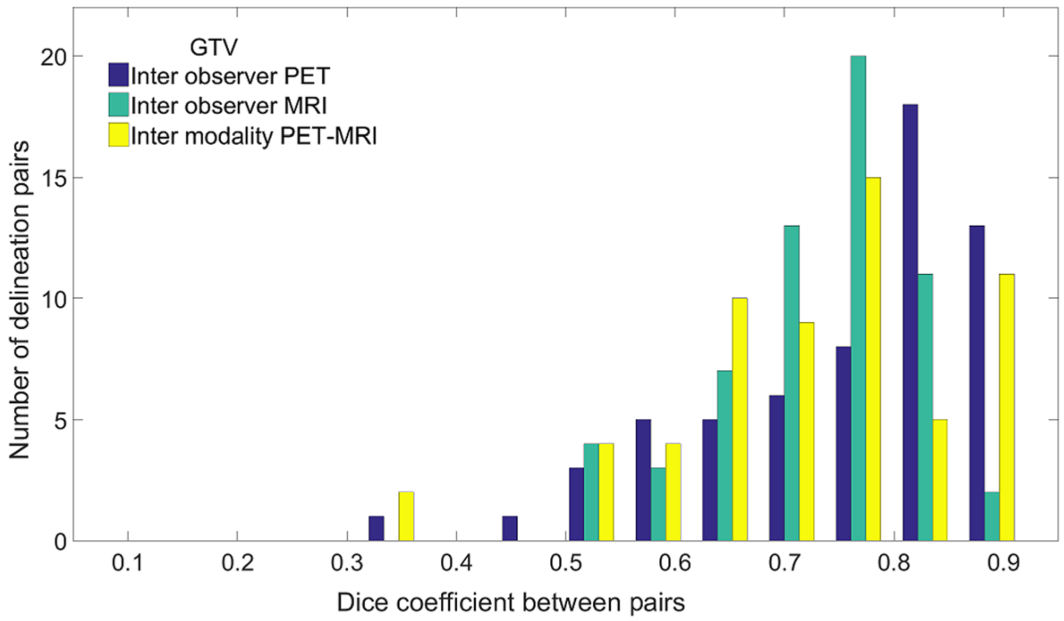

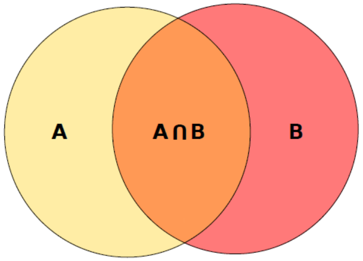

$$\mathrm{DSC} = \frac{A \cap B}{\frac{1}{2} \cdot (|A| + |B|)}$$

Interobserver $\mathrm{DICE}_{\mathrm{PET}}$ 0.8

Interobserver $\mathrm{DICE}_{\mathrm{MR}}$ 0.74

Inter-modality DICE 0.75

Radiation Oncology (2017) 12:147

Tumor and lymph node delineation

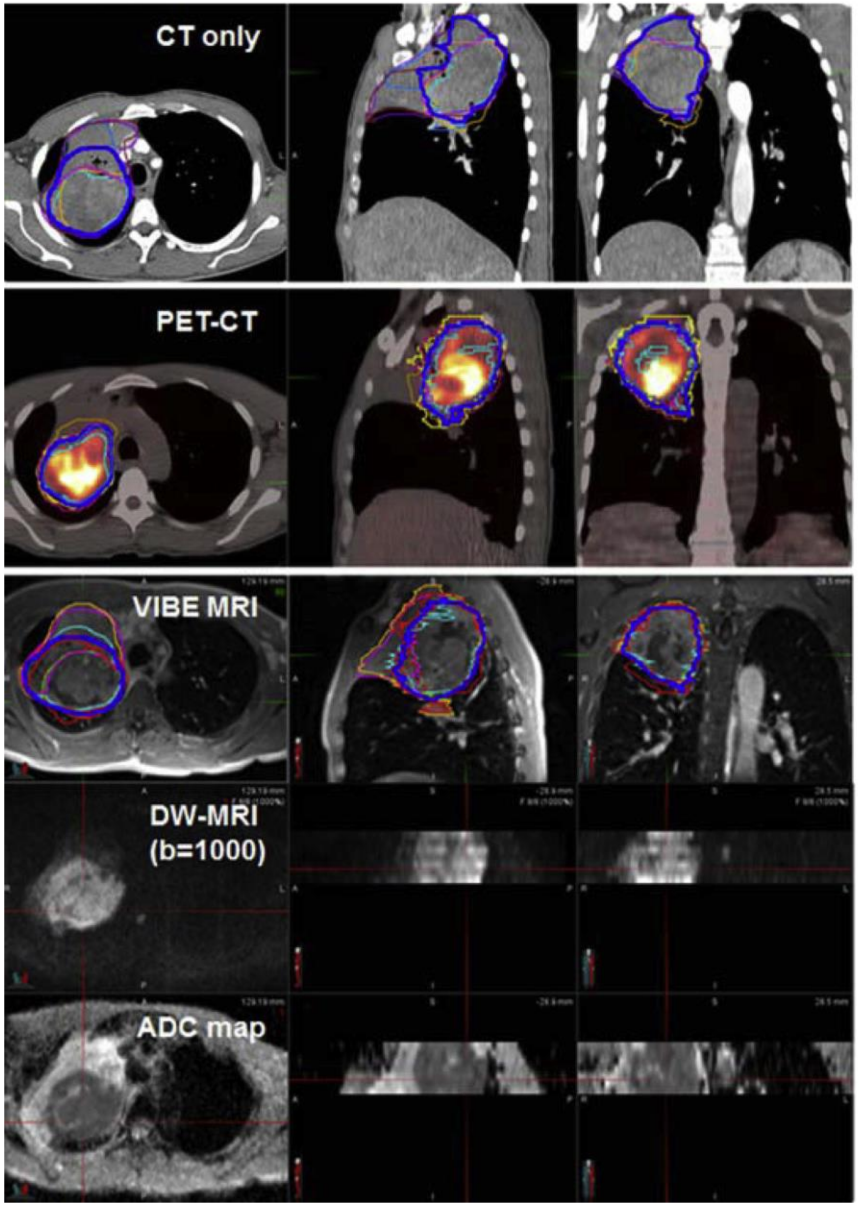
CT only
PET-CT
VIBE MRI
DW-MRI
(b=1000)
ADC map

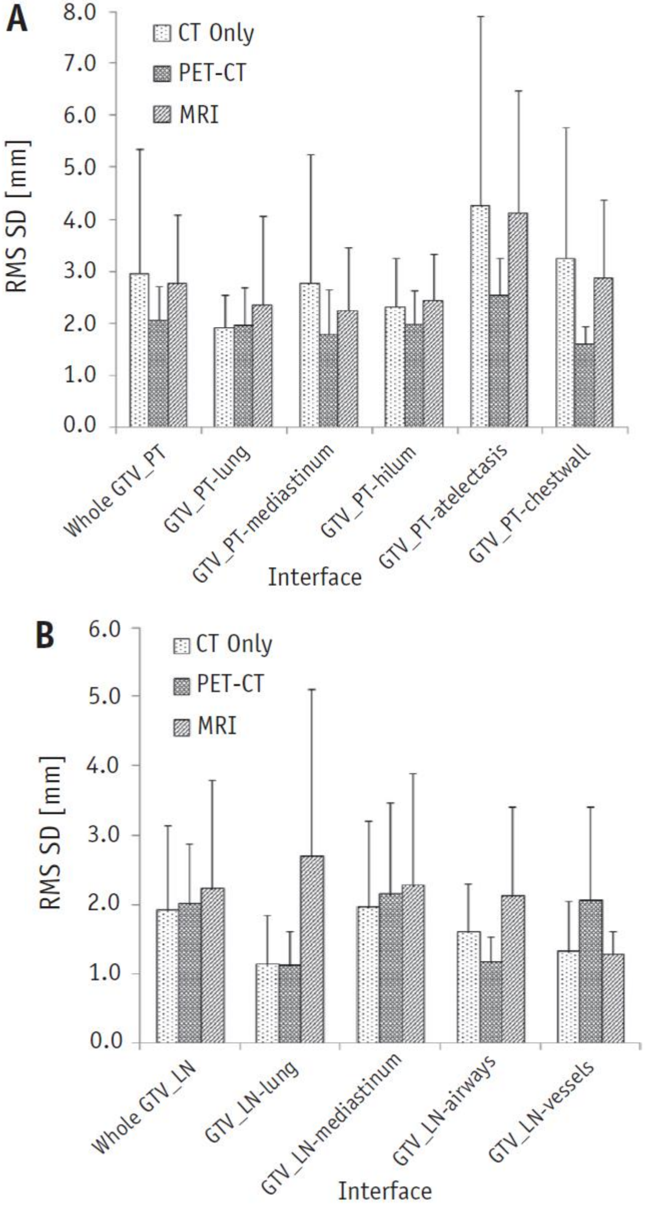

IJROBP. 99, 80e89, 2017

^{18}F-FDG PET with IMRT

3D-CRT
w/o PET

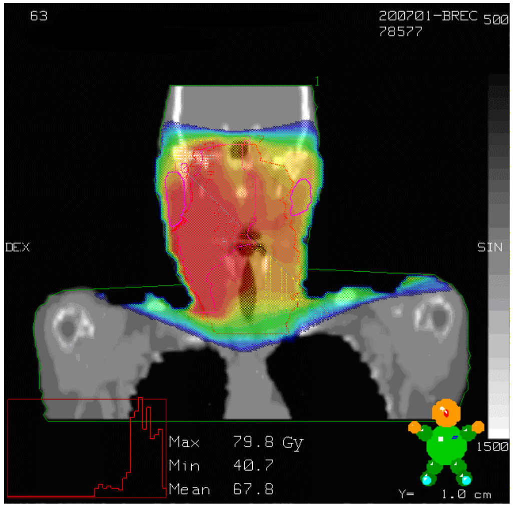
63
200701-BREC 500
78577
DEX
SIN
Max 79.8 Gy
Min 40.7
Mean 67.8
1500
Y= 1.0 cm

IMRT
w/ PET

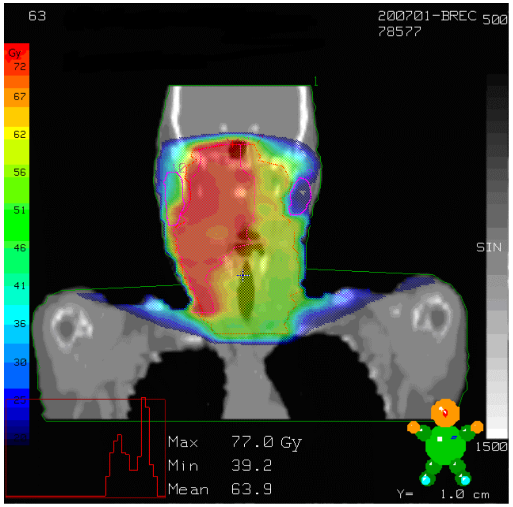
63
200701-BREC 500
78577
Gy
72
67
62
56
51
46
41
36
30
SIN
Max 77.0 Gy
Min 39.2
Mean 63.9
1500
Y= 1.0 cm

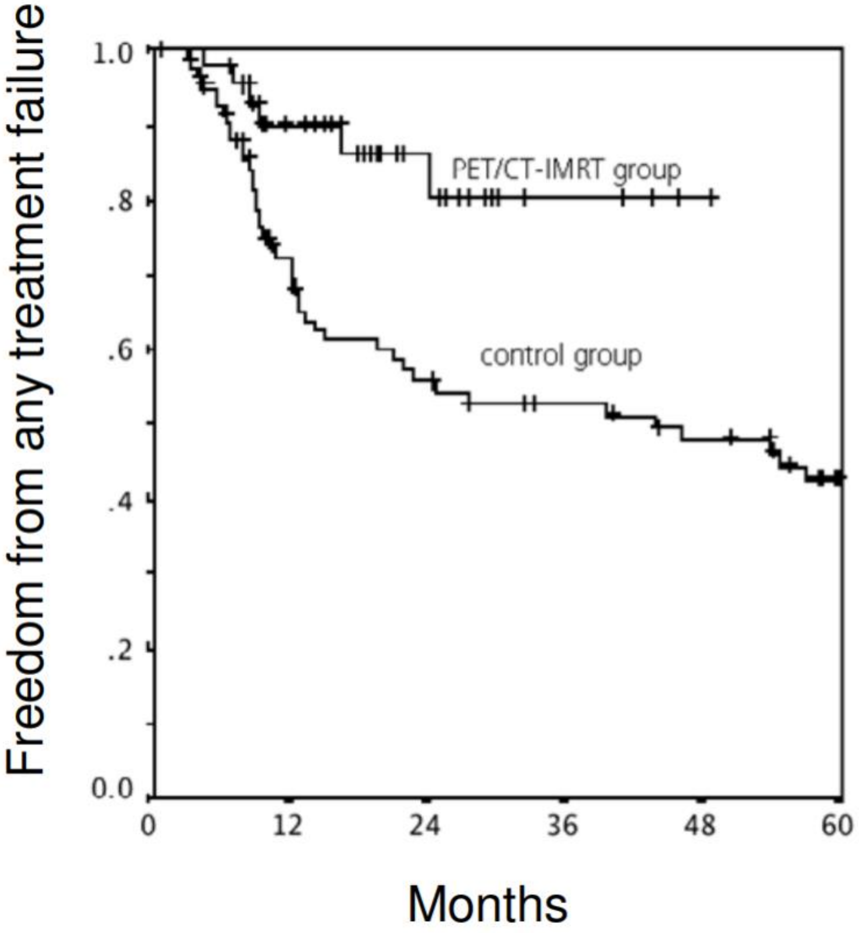

Radiation Oncology 2007, 2:22

68Ga-PSMA

- RT of prostate bed + elective region + node

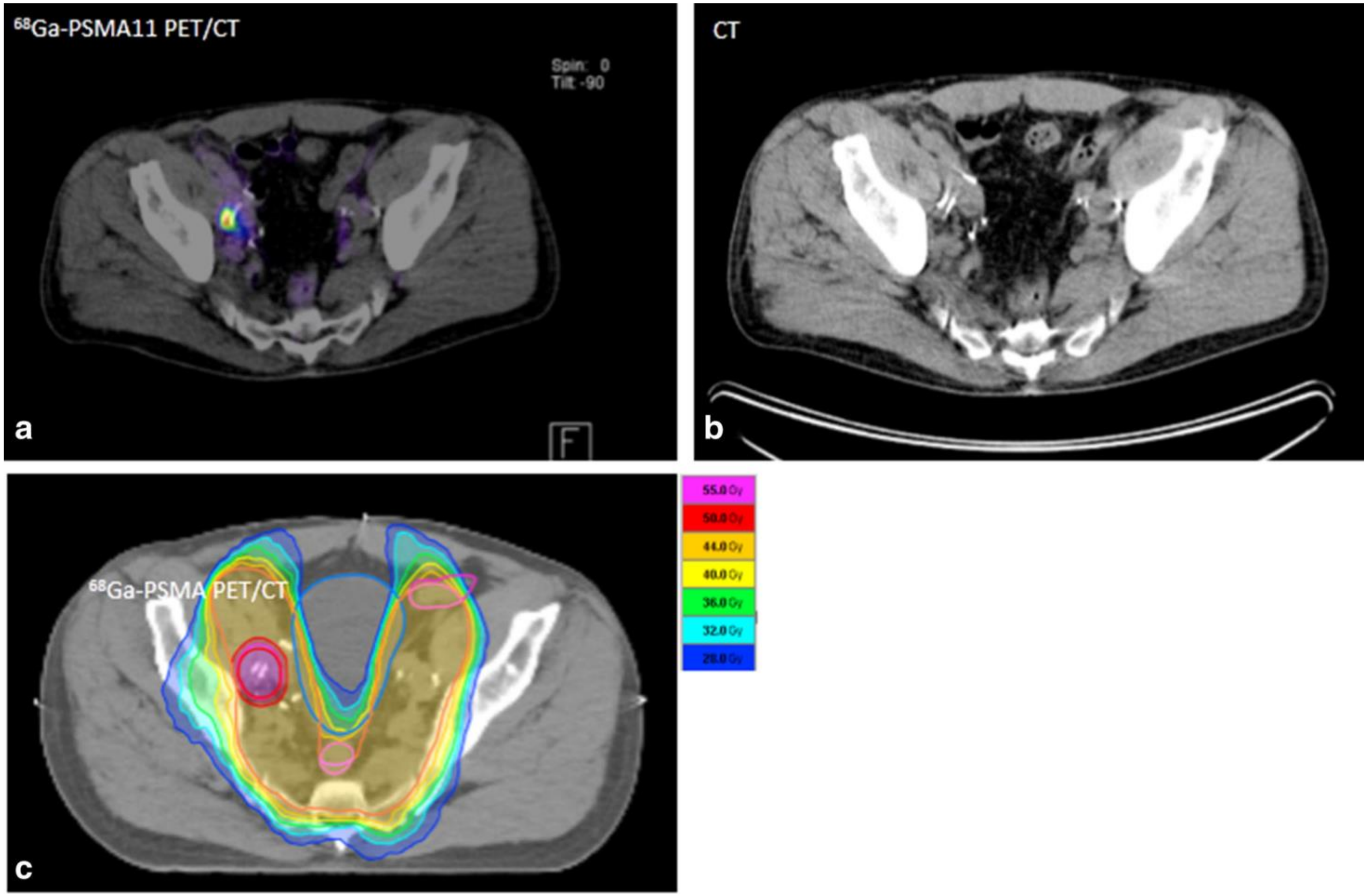
^{68}Ga-PSMA11 PET/CT
Spin: 0
Tilt -90
a
CT
b
^{68}Ga-PSMA PET/CT
c
55.0 Gy
50.0 Gy
44.0 Gy
40.0 Gy
36.0 Gy
32.0 Gy
28.0 Gy

Eur J Nucl Med Mol Imaging (2016) 43:34–41

Analyzing recurrence patterns

- Where do recurrences appear? Are these reflected in uptake patterns in the primary?

CT scan of recurrent tumor

Centroid on original 18F-FDG-PET scan

Recurrence locations

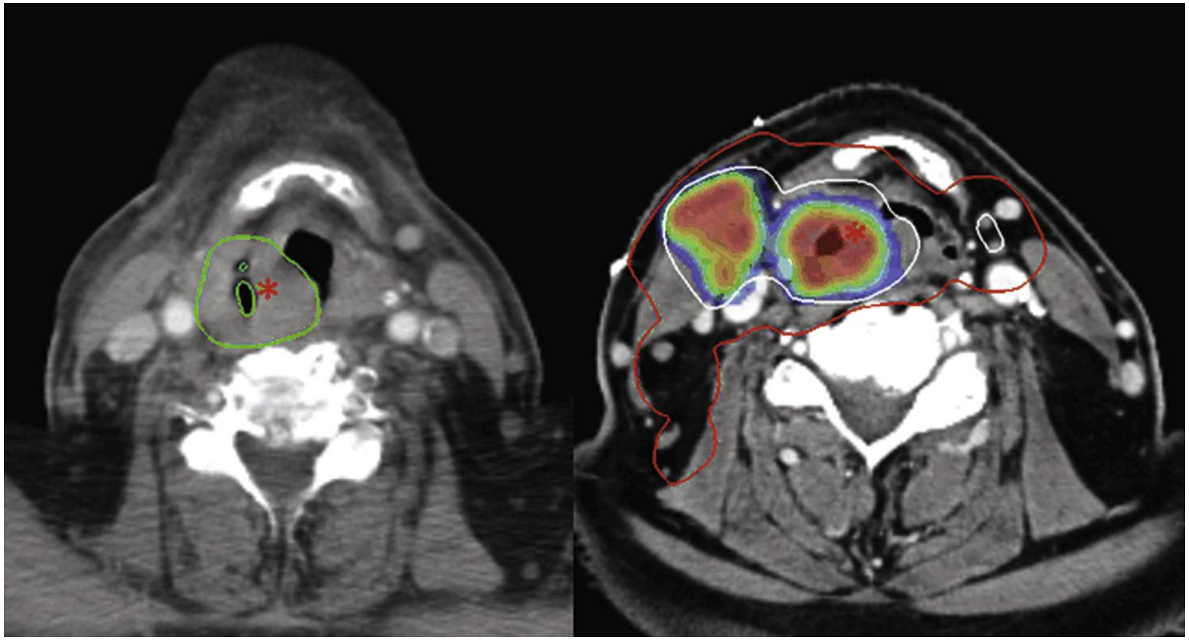

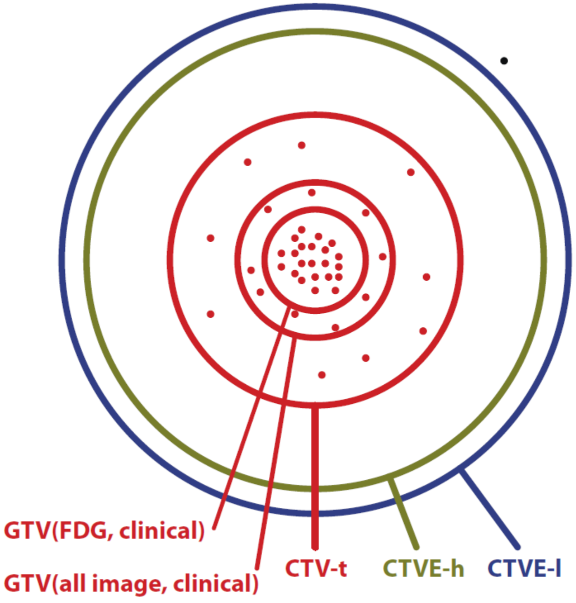
GTV(FDG, clinical)
GTV(all image, clinical)
CTV-t
CTVE-h
CTVE-l

Radiotherapy and Oncology 111 (2014) 360–365

Dose painting

- Deliver dose where dose is needed

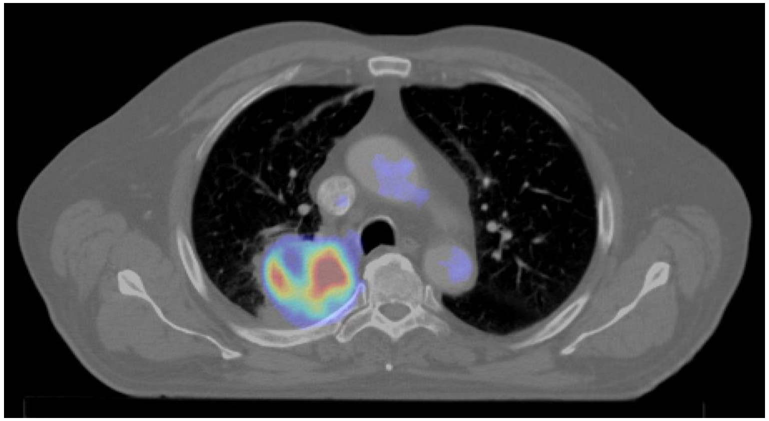

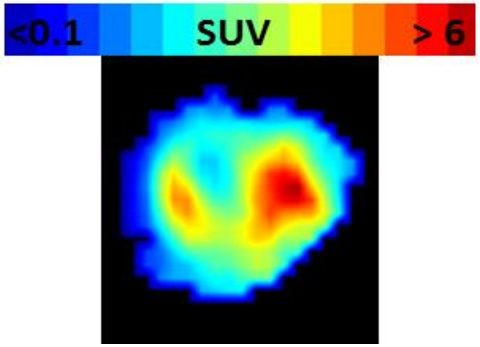

PET intensity map

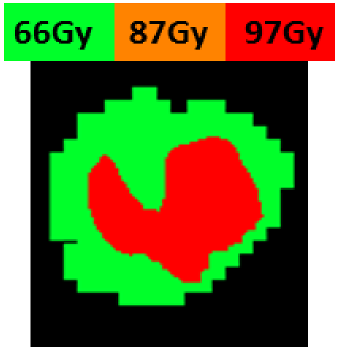
66Gy
87Gy
97Gy

DPBC –
Dose painting
by contours

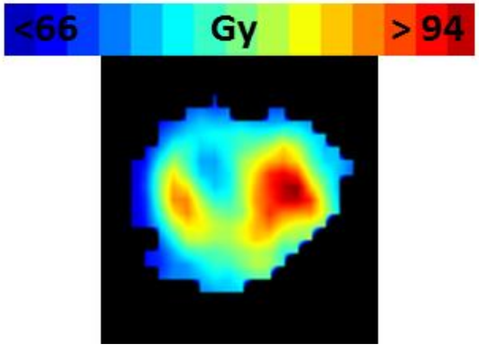

DPBN –
Dose painting
by numbers

Radiotherapy and Oncology 113 (2014) 210–214

Hypoxia dose painting

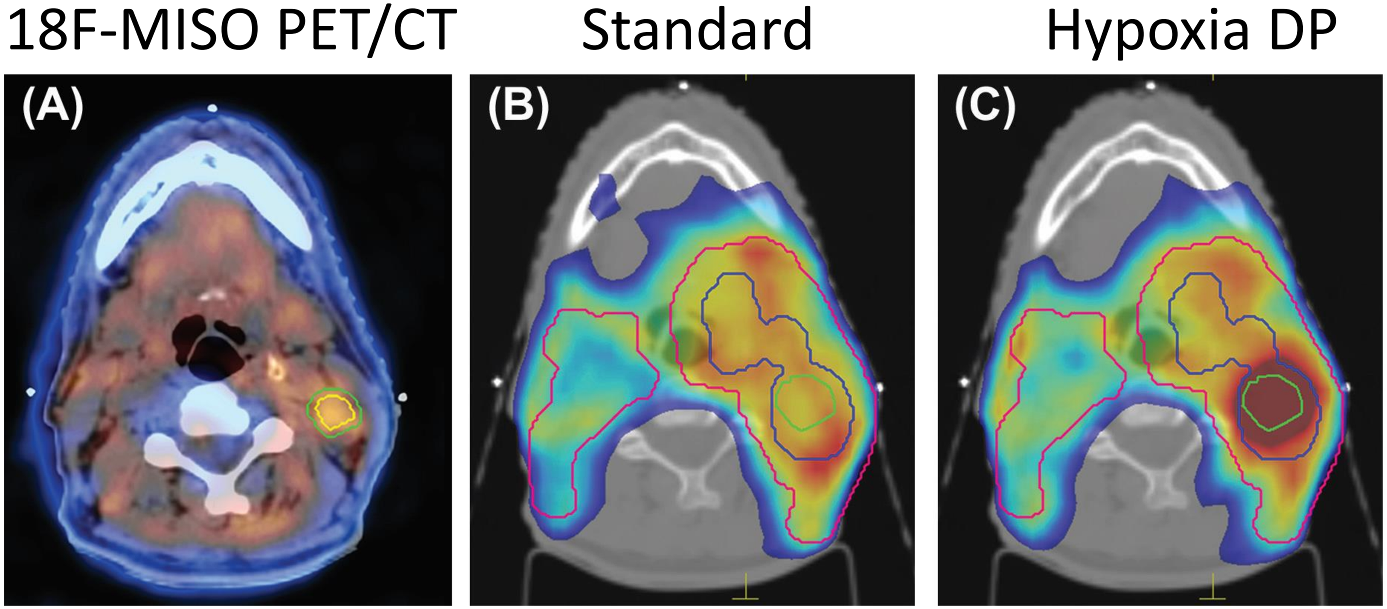

18F-MISO PET/CT

Standard

Hypoxia DP

$$TCP = \sum_i g_i(\sigma_\alpha) \cdot TCP(\alpha_i, \beta_i)$$

	TCP (%)	
Patient	STD	HDP
1	71	93
2	70	92
3	70	92
4	75	93
5	72	94
6	74	95
7	71	91
8	83	94
Mean ± SD	73 ± 4	93 ± 1

Acta Oncol. 2013;52(8):1723-9

Treatment monitoring

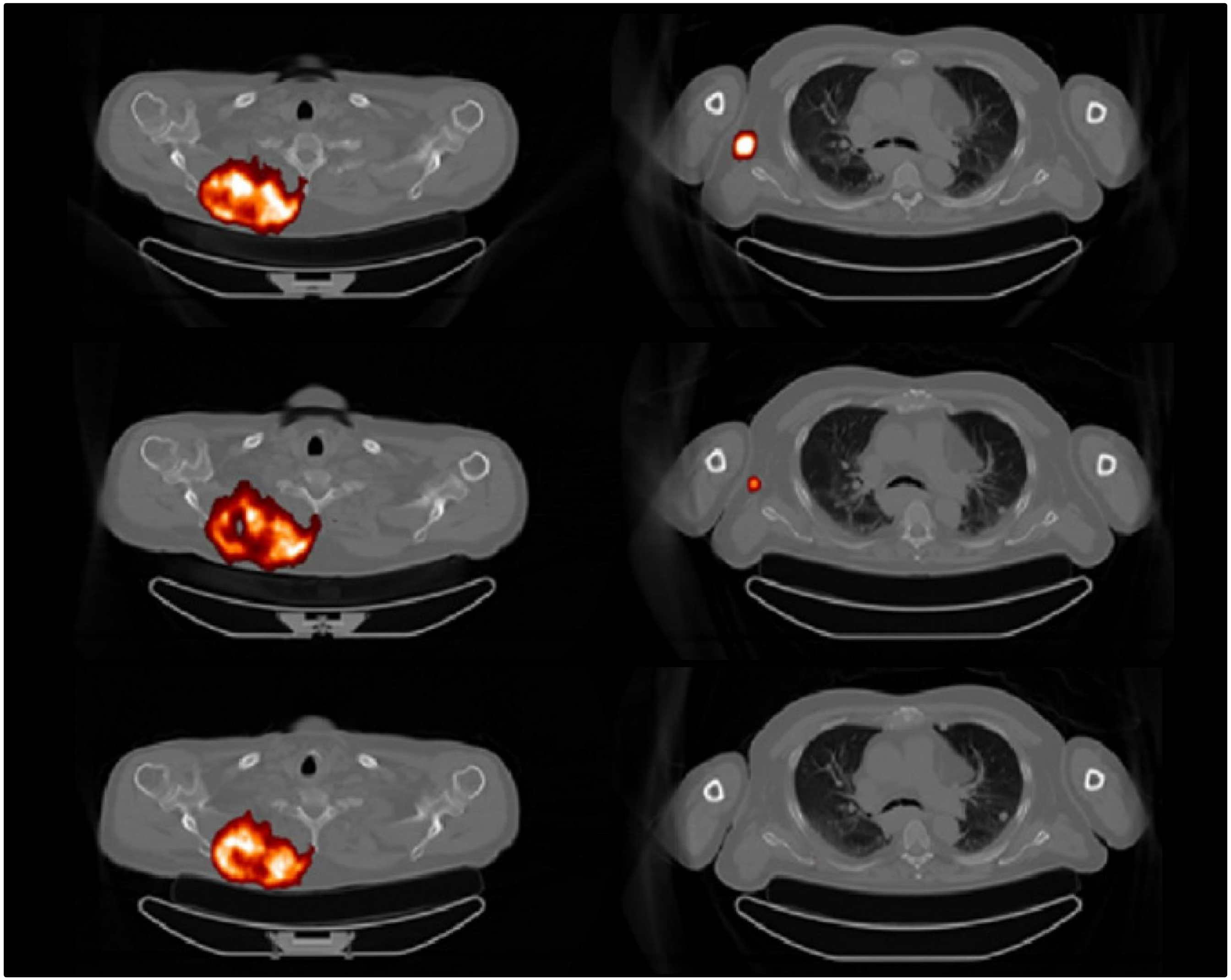
Resistant sarcoma
Sensitive lymphoma
Pre
8 Gy
40 Gy

Semin Radiat Oncol 20:138-146

Treatment monitoring

- Repeated imaging to assess changes in disease
- RECIST - Response Evaluation Criteria In Solid Tumors

Tumor shrinkage in different cervical tumors

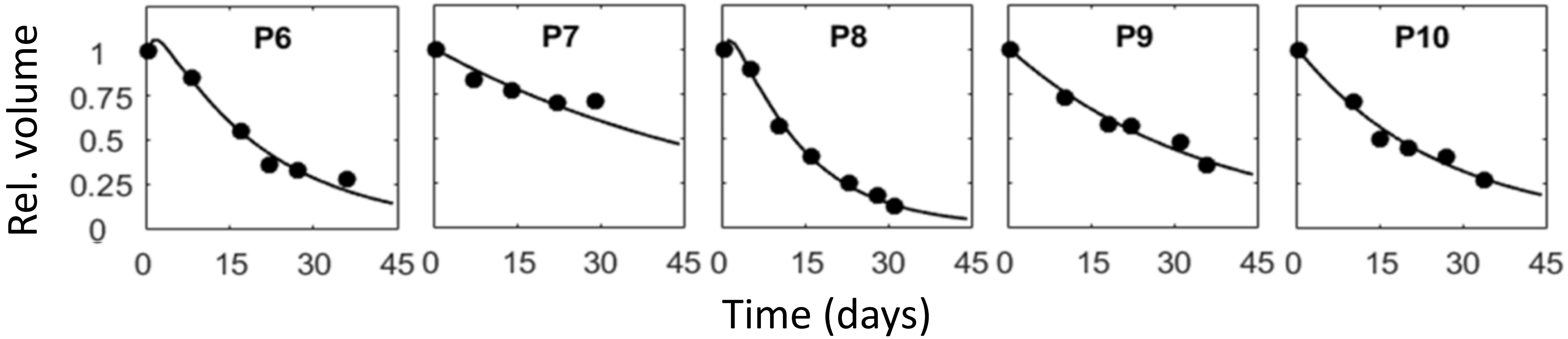

- Tumor volume may not reflect clonogens
- Shrinkage depends on cell kill, inter-fraction proliferation *and* cell clearance

Phys. Med. Biol. 62 N107

PET quantification issues

- Intra-patient variation

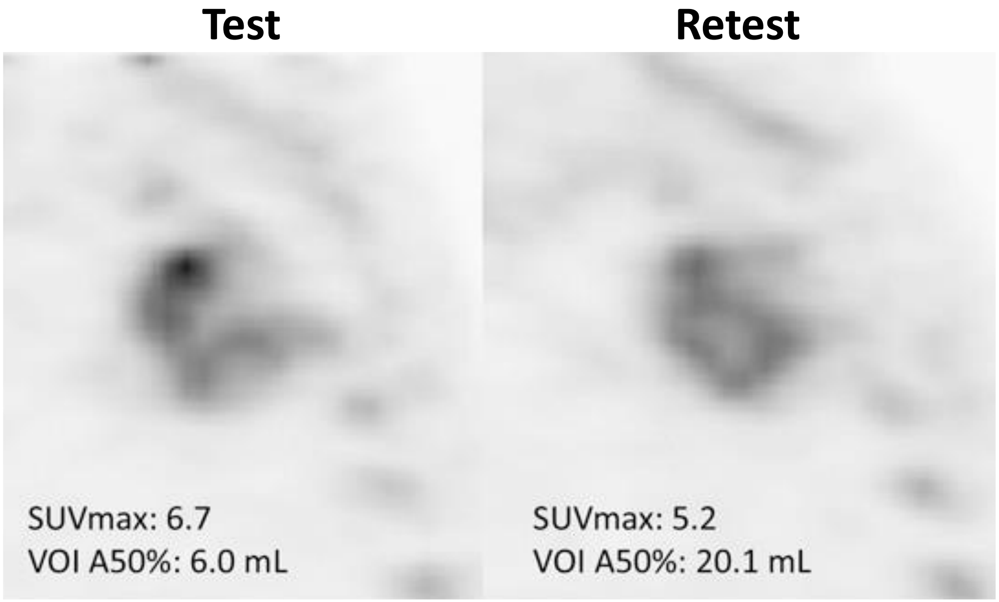
Test
Retest
SUVmax: 6.7
VOI A50%: 6.0 mL
SUVmax: 5.2
VOI A50%: 20.1 mL

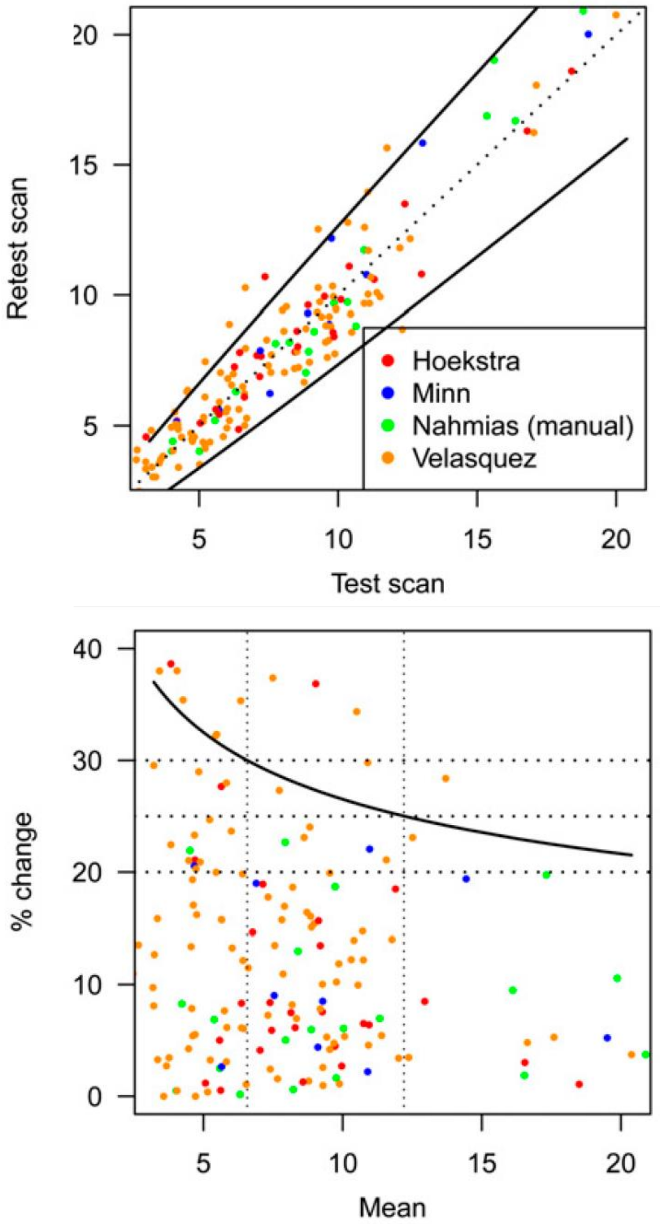

- SUV is 'semi-quantitative'

J Nucl Med 2012; 53:701–708

Treatment monitoring

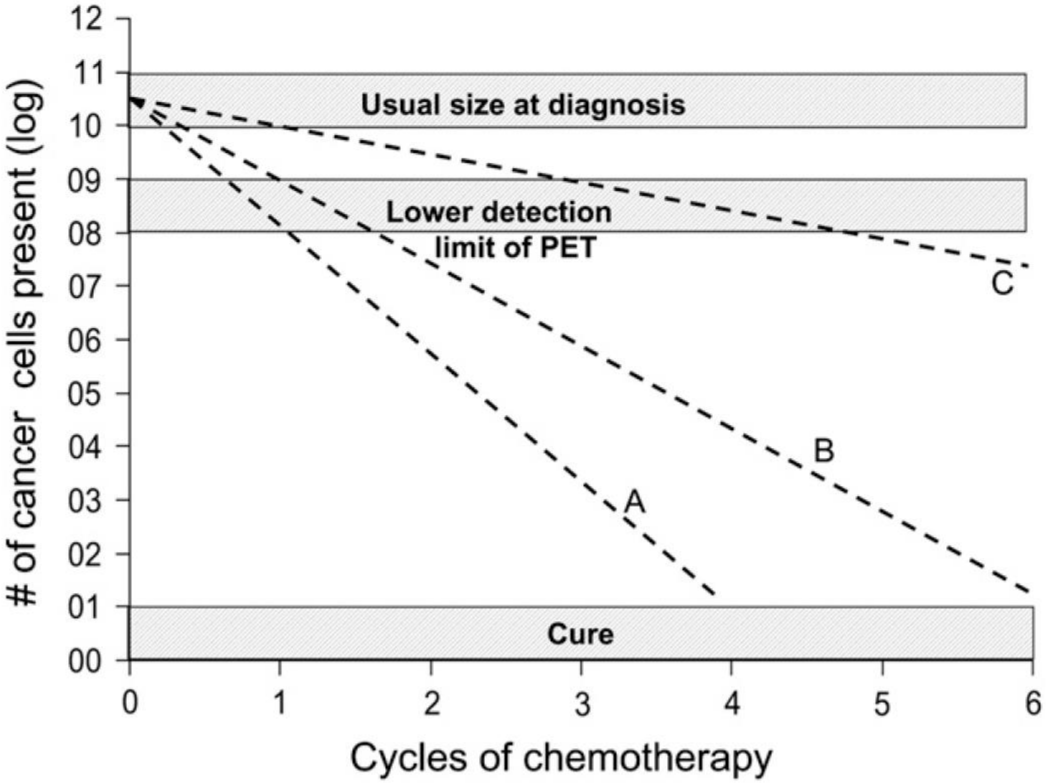

- Early decline better than evaluation later (?)
- When to image?

THE JOURNAL OF NUCLEAR MEDICINE 50(5); 2009

PERCIST

- 18F-FDG PET response criteria
- Complete metabolic response; disappearance of signal
- Partial metabolic response; > 30 % reduction in uptake
- Progressive metabolic disease; > 30 % increase
- Liver normalization recommended to minimize variability
- Still, few applications in RT

THE JOURNAL OF NUCLEAR MEDICINE 50(5); 2009

Response evalution

- 18F-FDG PET of liver mets after stereotactic RT

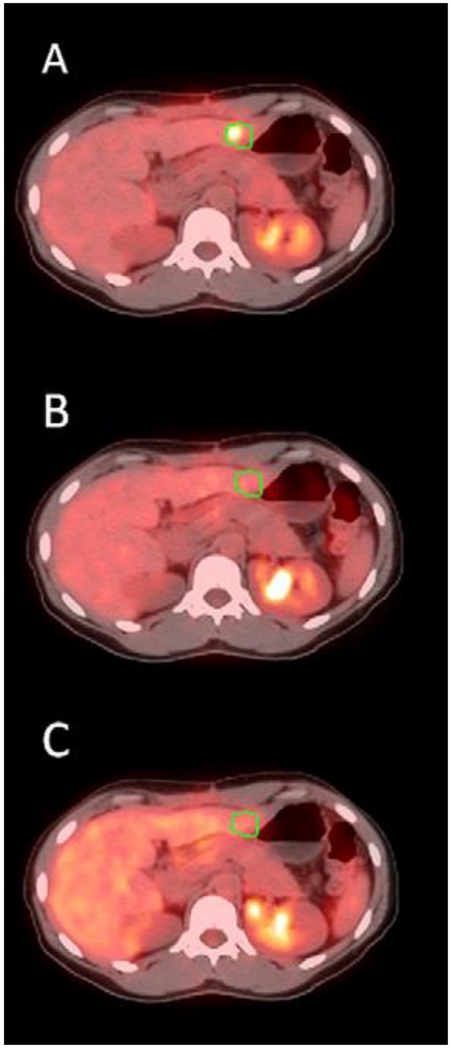

Pre

5 months

9 months

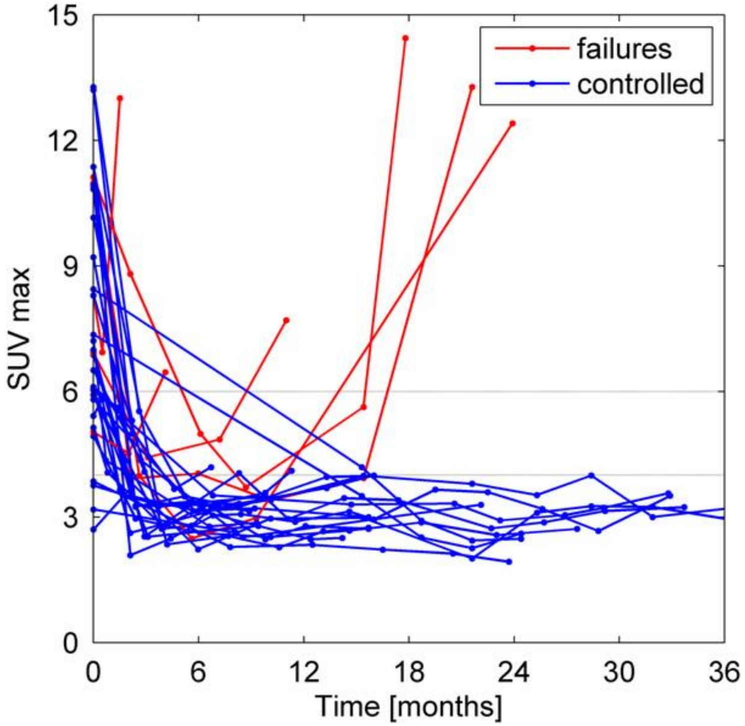

IJROBP, Vol. 83, No. 5, pp. e613ee618, 2012

Radiobiological interpretation

- Use images to estimate tumor radioresistance

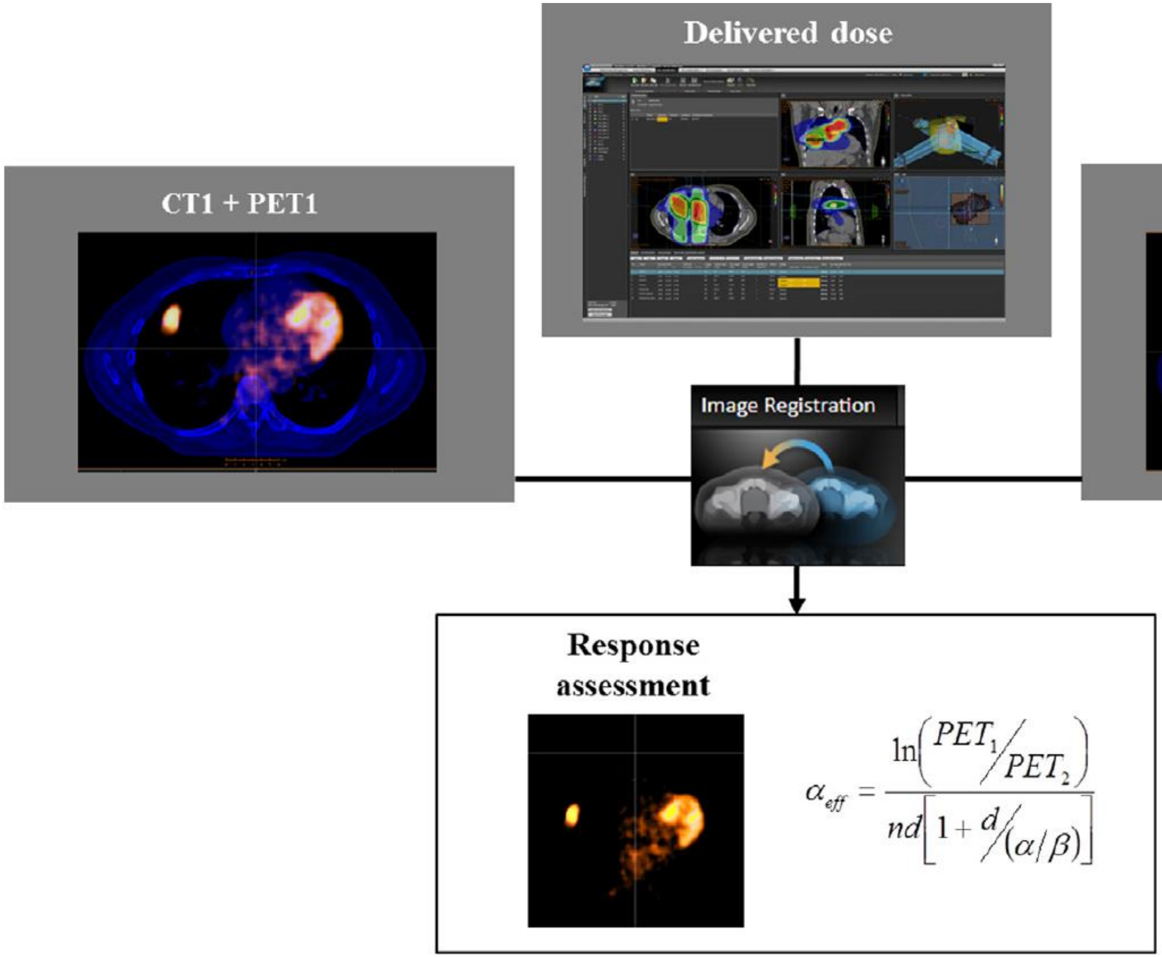
Delivered dose
CT1 + PET1
CT2 + PET2
Image Registration
Response assessment

$$\alpha_{eff} = \frac{\ln\left(\frac{PET_1}{PET_2}\right)}{nd\left[1 + \frac{d}{(\alpha/\beta)}\right]}$$

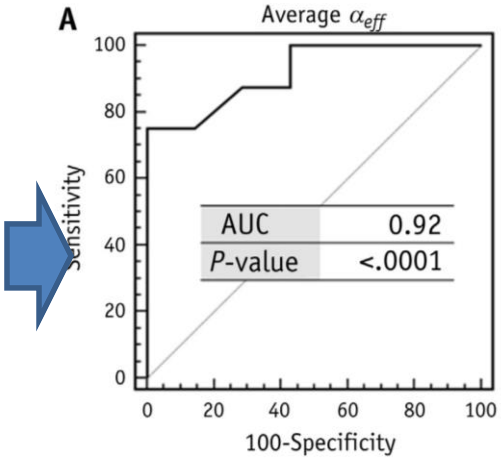

IJROBP 91, 376–384 (2015)

Multi-tracer assessment

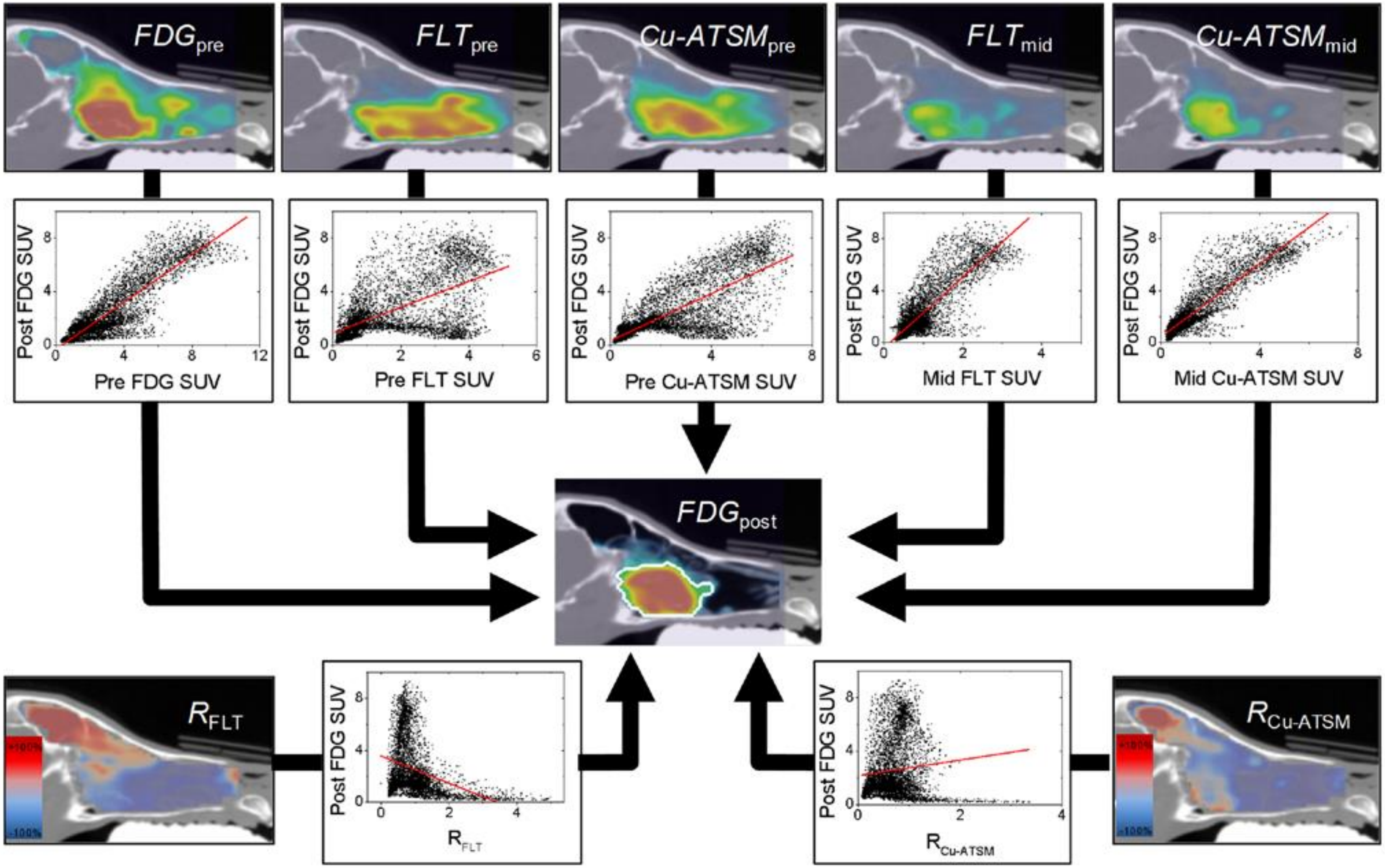

Phys. Med. Biol. 60 (2015) 5211–5224

Monitoring normal tissues

- Parotid gland function as measured by 11C-methionine-PET

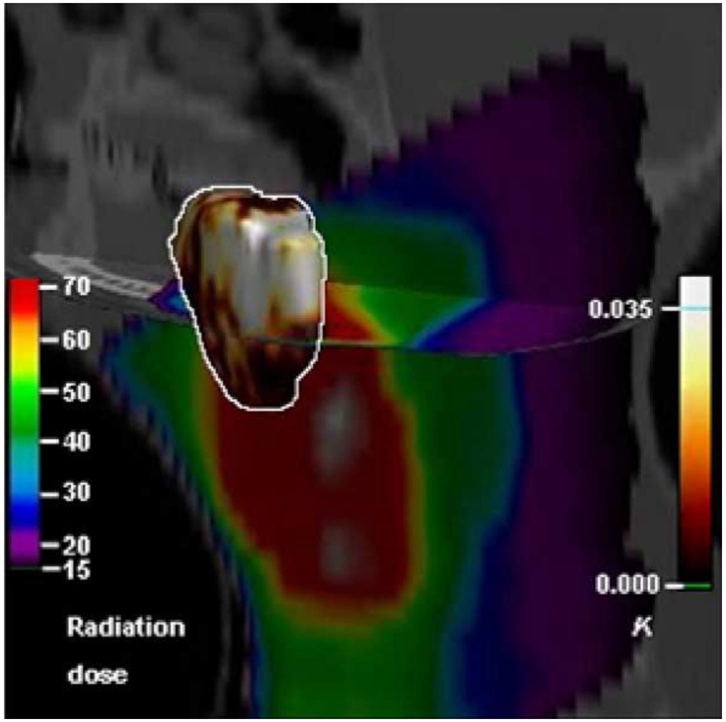

70
60
50
40
30
20
15
Radiation dose
0.035
0.000
K

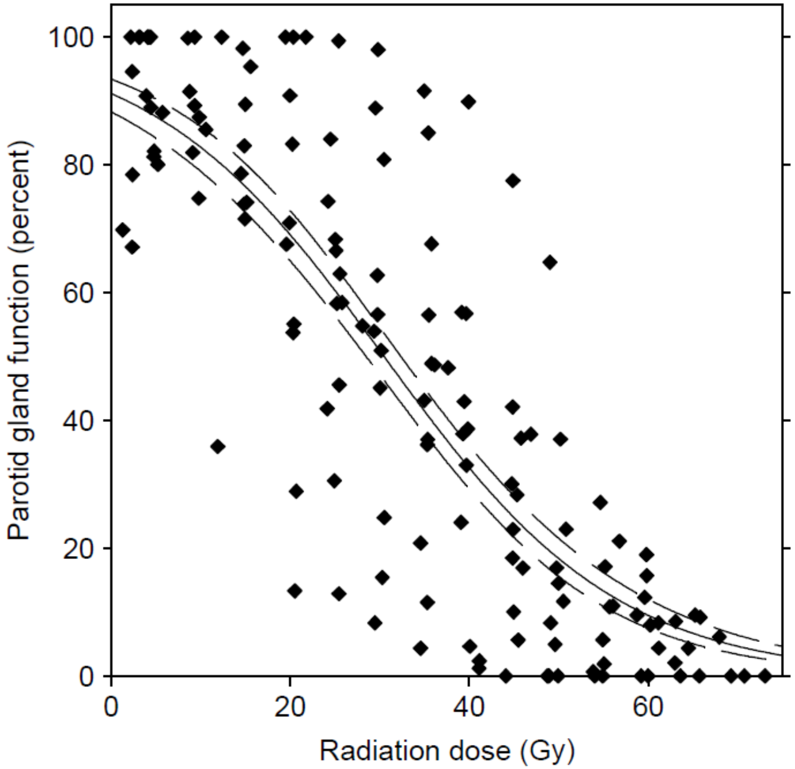

Radiotherapy and Oncology 78 (2006) 262–269

Problem

Patient 1

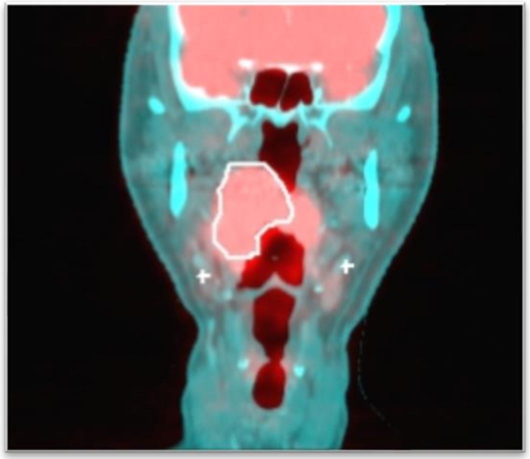

Same max. image value!

Patient 2

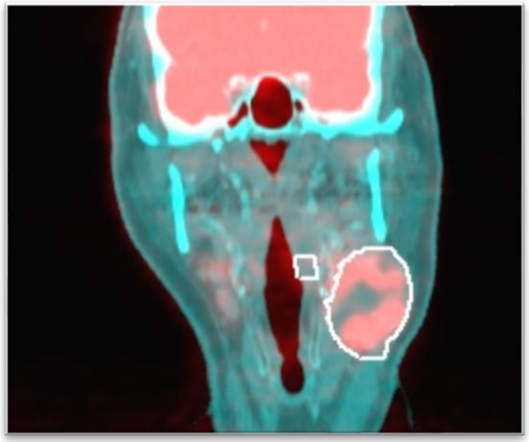

How to *quantify* differences in tumor appearance?

→ look for e.g. *texture* in images

Radiomics

- Extracting more information from medical images

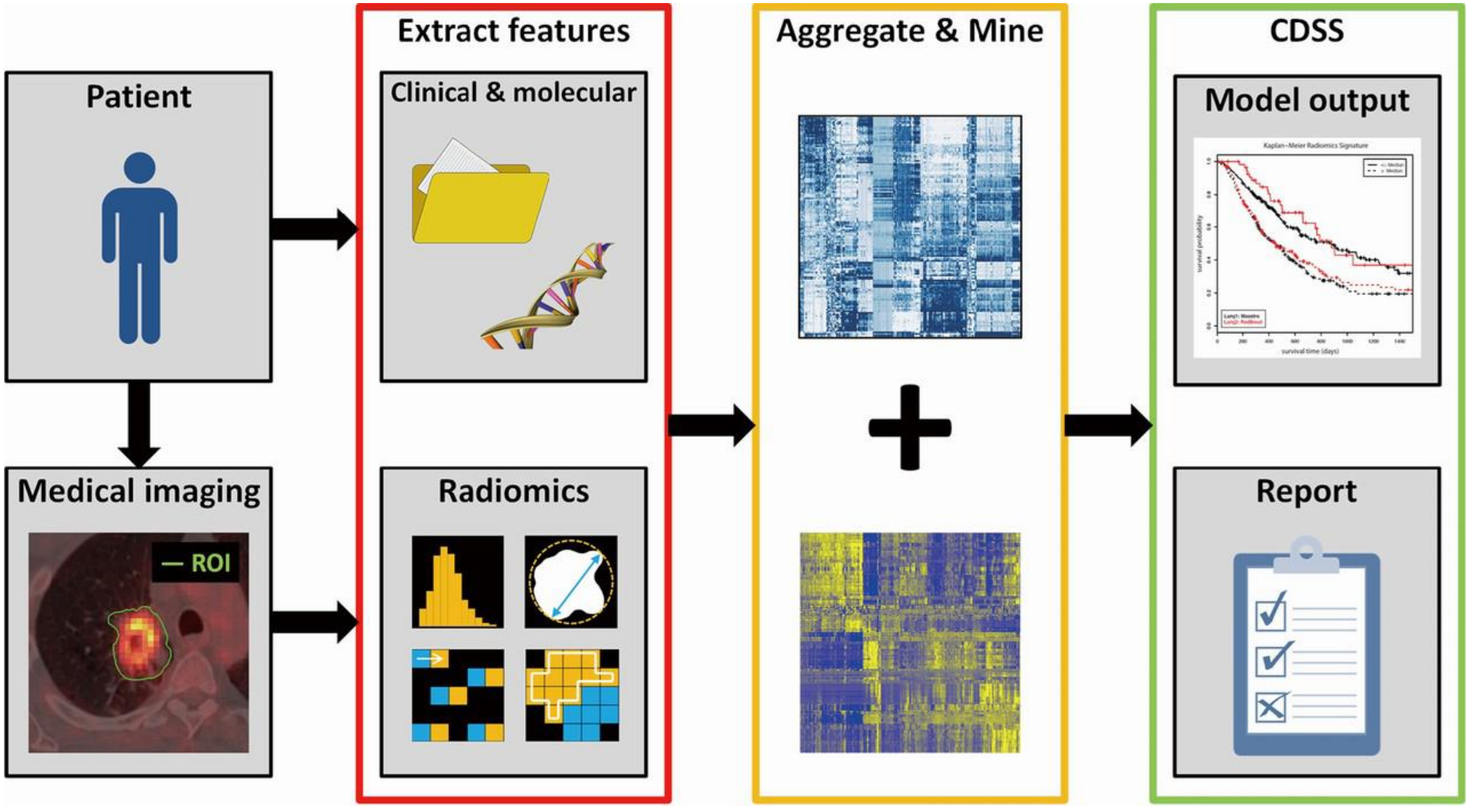
Patient
Medical imaging
— ROI
Extract features
Clinical & molecular
Radiomics
Aggregate & Mine
CDSS
Model output
Report

Transl Cancer Res 5, 398-409 (2016)

UiO : Department of Physics
University of Oslo

Oslo University Hospital

Suggestions for use of PET in radiotherapy

Eirik Malinen

Tumor delineation

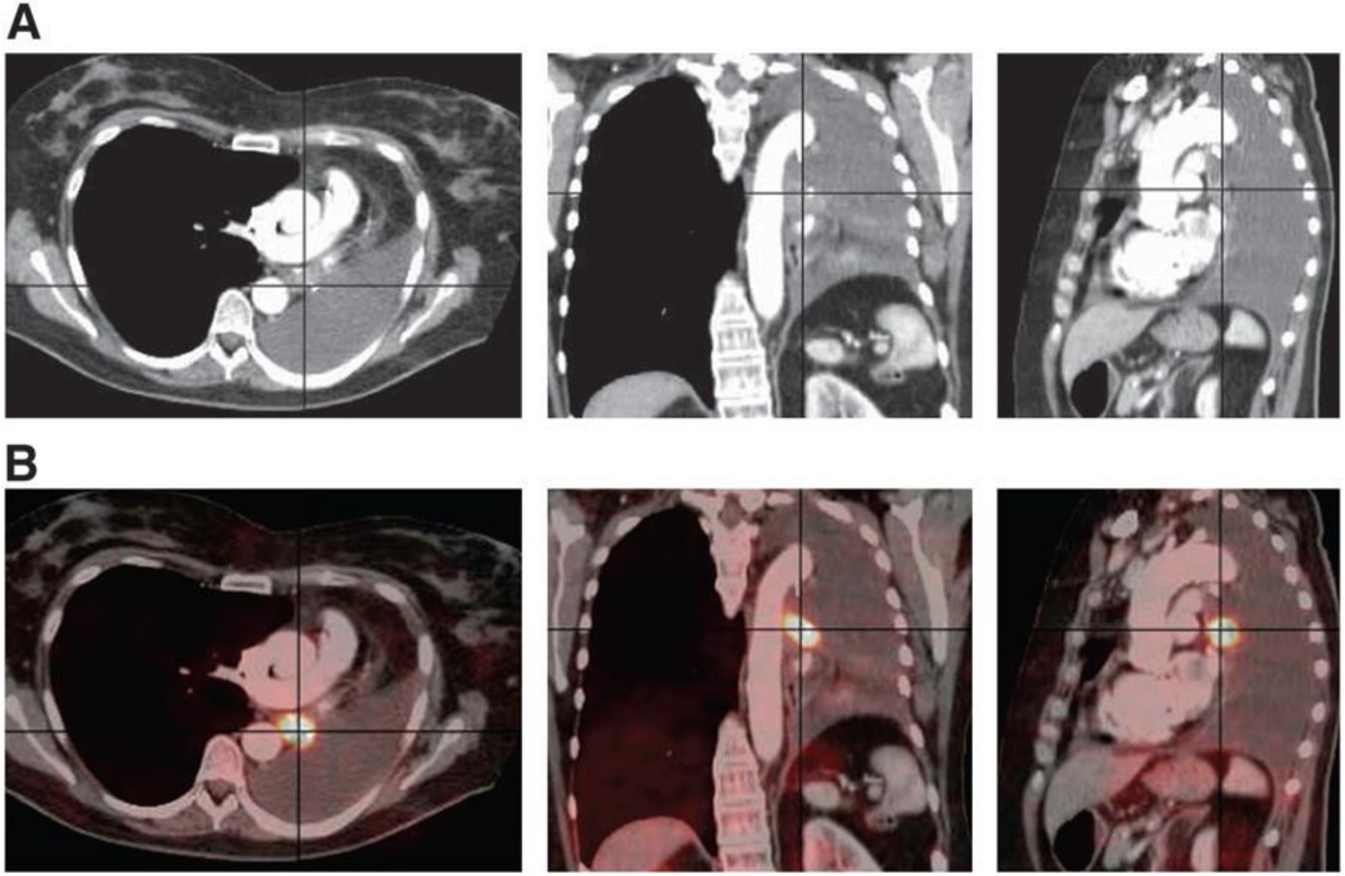

CT

PET/CT

J Nucl Med 2007; 48:68S–77S

Lymph node definition

- Presence of positive lymph nodes affects treatment

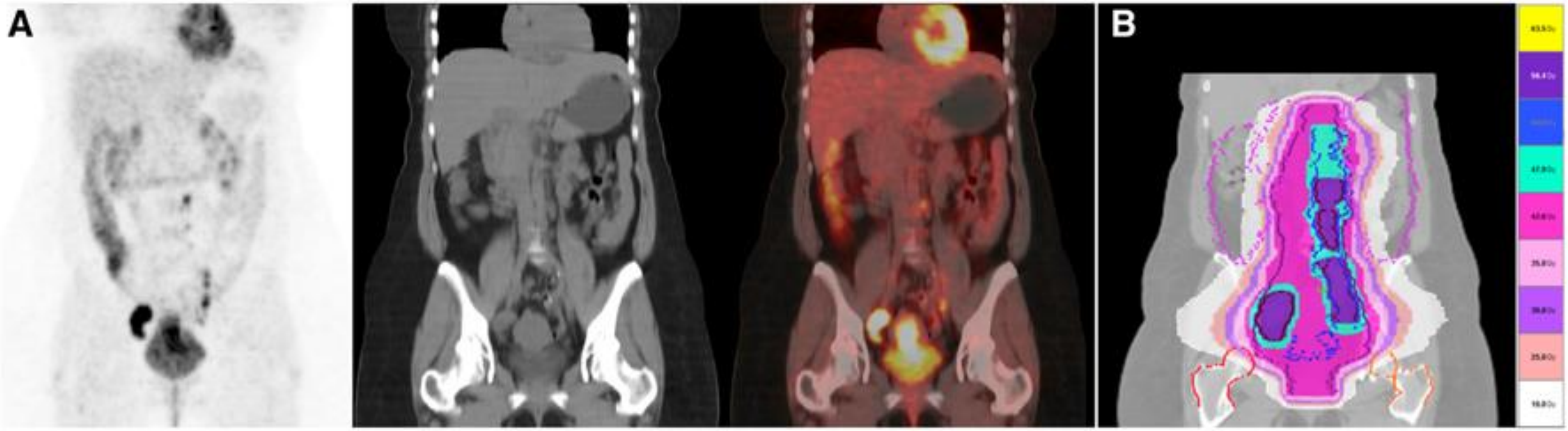

Front. Oncol Volume 3 | Article 34 |

Dose painting

PET/ CT

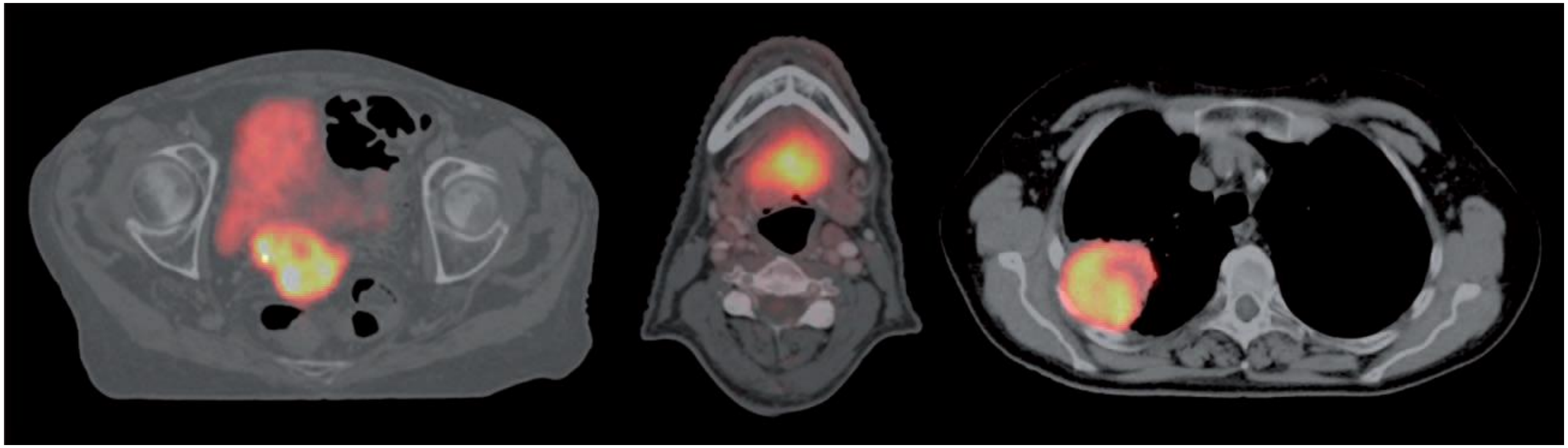

Dose maps

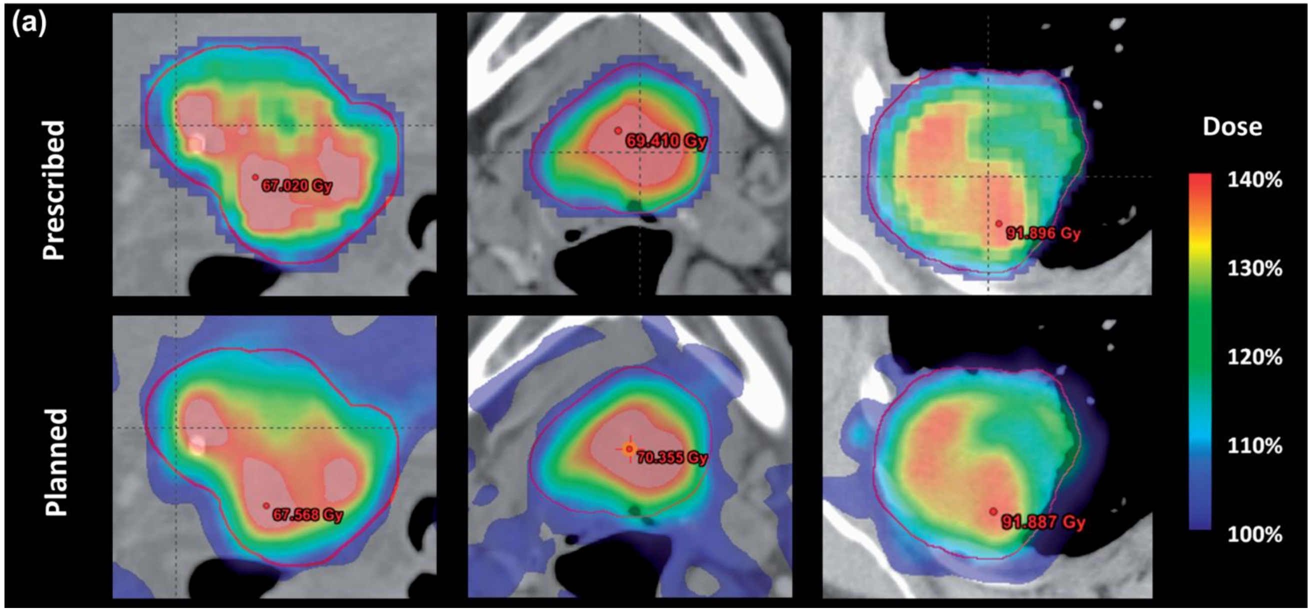
(a)
Prescribed
Planned
67.020 Gy
69.410 Gy
91.896 Gy
67.568 Gy
70.355 Gy
91.887 Gy
Dose
140%
130%
120%
110%
100%

Acta Oncol. 2015;54(9):1607-13

Response assessment

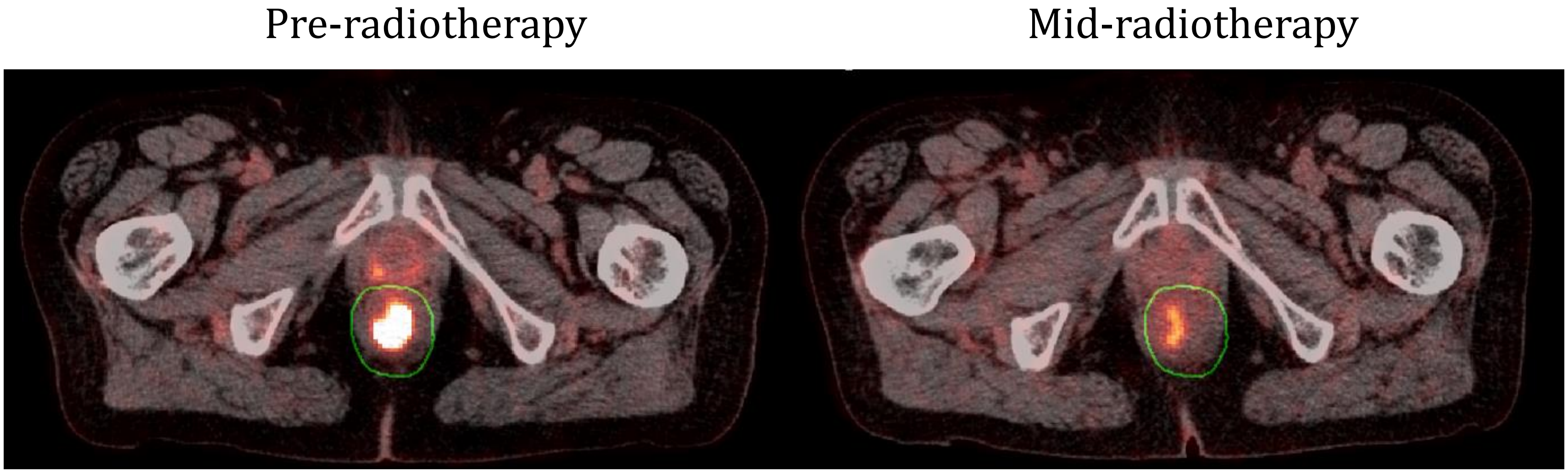
Pre-radiotherapy

Mid-radiotherapy

Simplified PET/CT process

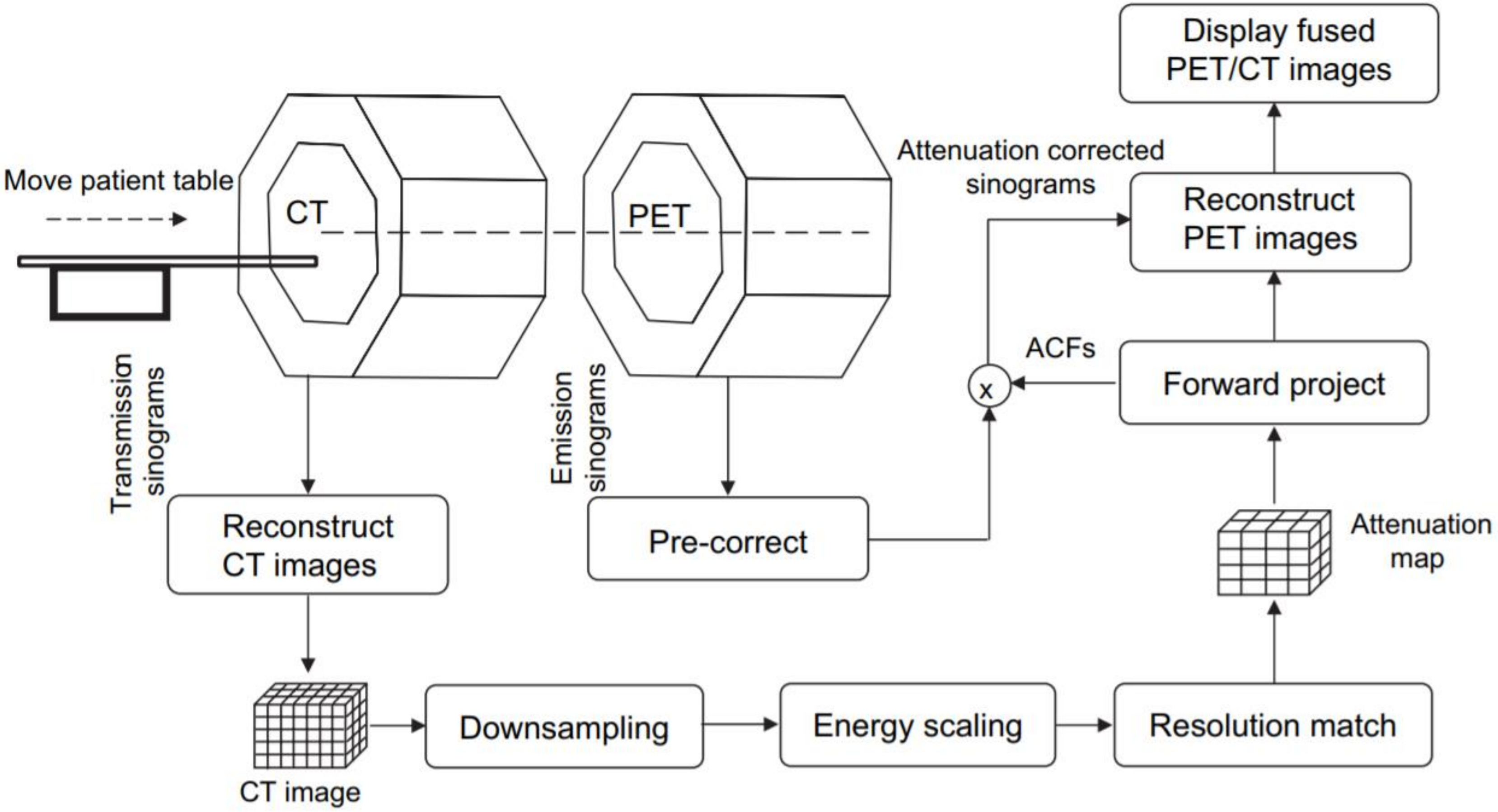
Display fused PET/CT images
Attenuation corrected sinograms
Reconstruct PET images
Move patient table
CT
PET
ACFs
x
Forward project
Transmission sinograms
Emission sinograms
Reconstruct CT images
Pre-correct
Attenuation map
CT image
Downsampling
Energy scaling
Resolution match

PET Clin 2 (2007) 109–123

Quality control – imaging devices

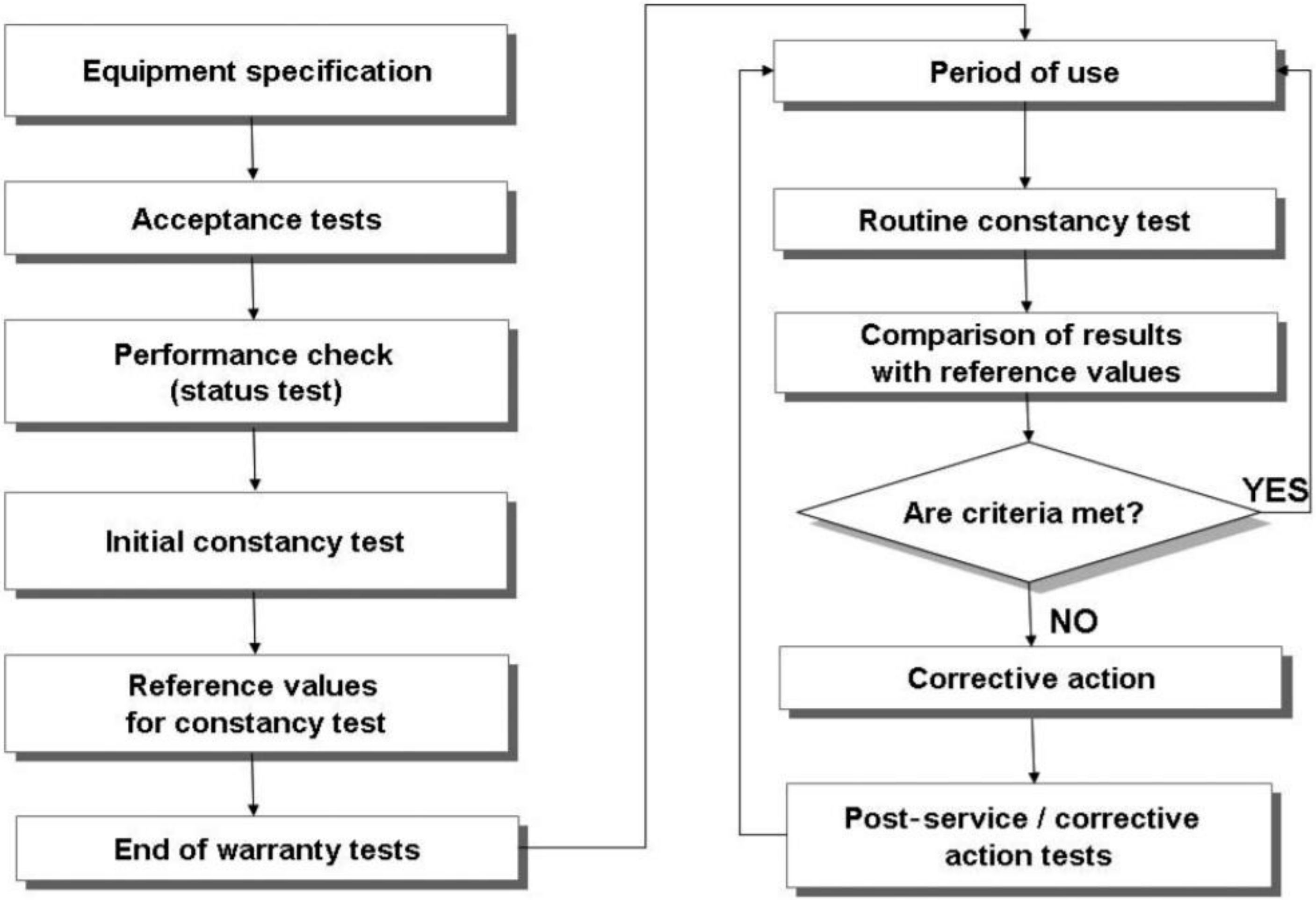
Equipment specification

Acceptance tests

Performance check
(status test)

Initial constancy test

Reference values
for constancy test

End of warranty tests

Period of use

Routine constancy test

Comparison of results
with reference values

Are criteria met?

YES

NO

Corrective action

Post-service / corrective
action tests

From PET scanner to RT

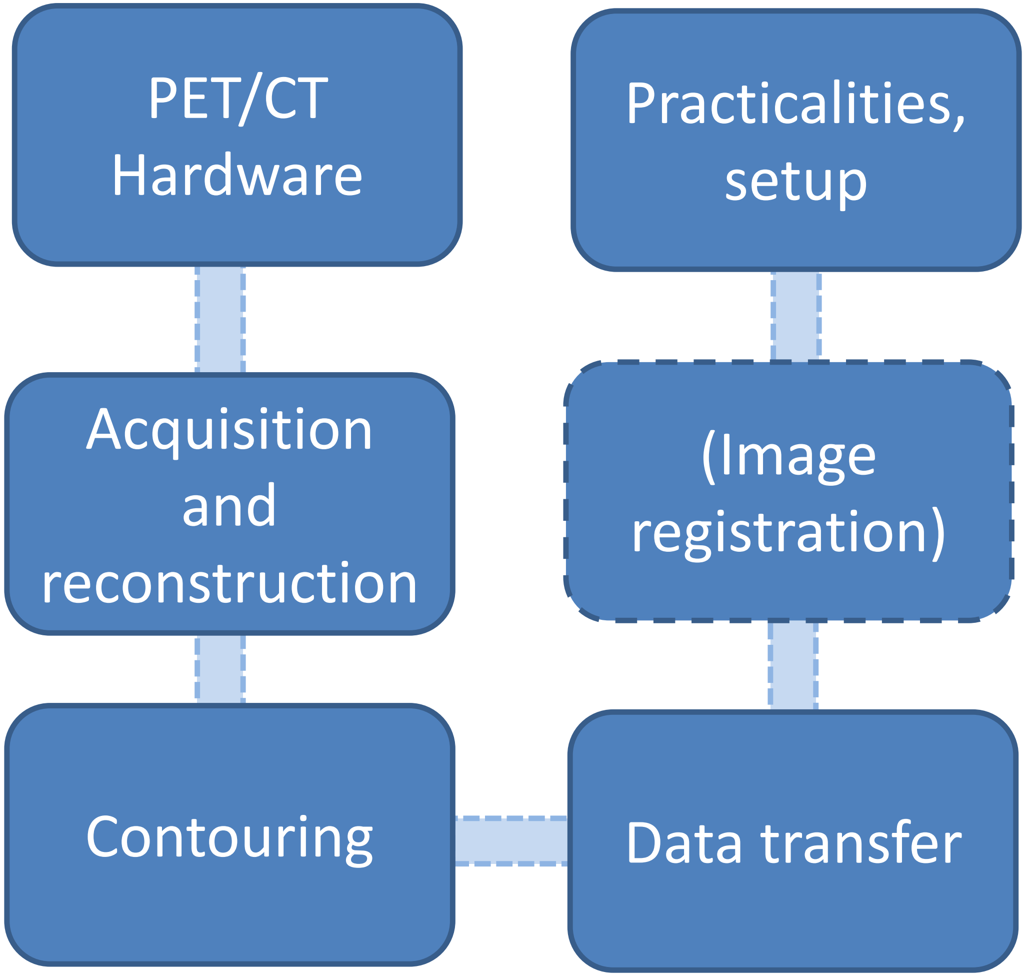

PET/CT Hardware

Acquisition and reconstruction

Contouring

Data transfer

(Image registration)

Practicalities, setup

PET/CT hardware

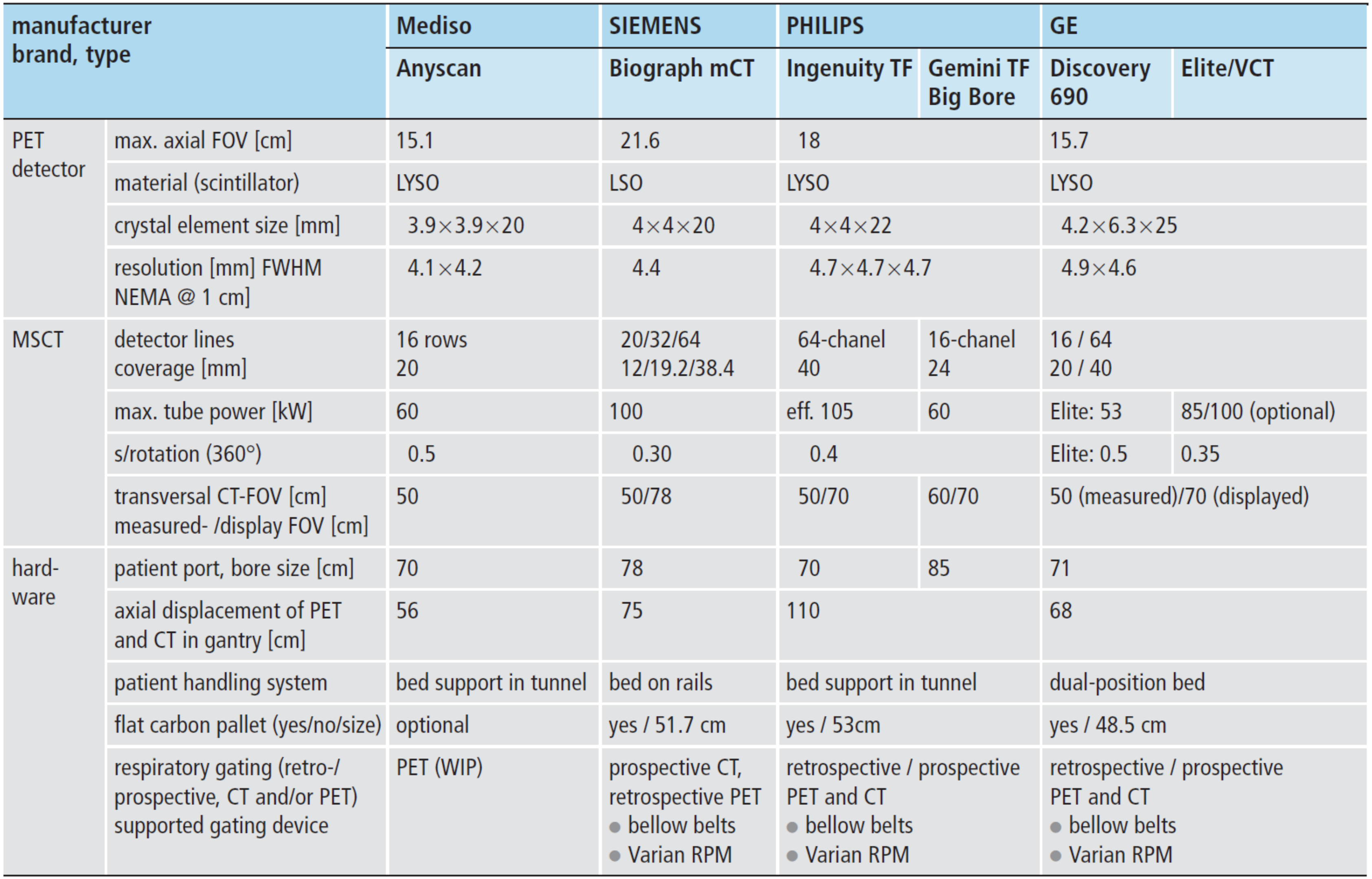

manufacturer brand, type		Mediso	SIEMENS	PHILIPS		GE	
		Anyscan	Biograph mCT	Ingenuity TF	Gemini TF Big Bore	Discovery 690	Elite/VCT
PET detector	max. axial FOV [cm]	15.1	21.6	18		15.7	
	material (scintillator)	LYSO	LSO	LYSO		LYSO	
	crystal element size [mm]	3.9×3.9×20	4×4×20	4×4×22		4.2×6.3×25	
	resolution [mm] FWHM NEMA @ 1 cm]	4.1×4.2	4.4	4.7×4.7×4.7		4.9×4.6	
MSCT	detector lines coverage [mm]	16 rows 20	20/32/64 12/19.2/38.4	64-chanel 40	16-chanel 24	16 / 64 20 / 40	
	max. tube power [kW]	60	100	eff. 105	60	Elite: 53	85/100 (optional)
	s/rotation (360°)	0.5	0.30	0.4		Elite: 0.5	0.35
	transversal CT-FOV [cm] measured- /display FOV [cm]	50	50/78	50/70	60/70	50 (measured)/70 (displayed)	
hard-ware	patient port, bore size [cm]	70	78	70	85	71	
	axial displacement of PET and CT in gantry [cm]	56	75	110		68	
	patient handling system	bed support in tunnel	bed on rails	bed support in tunnel		dual-position bed	
	flat carbon pallet (yes/no/size)	optional	yes / 51.7 cm	yes / 53cm		yes / 48.5 cm	
	respiratory gating (retro-/prospective, CT and/or PET) supported gating device	PET (WIP)	prospective CT, retrospective PET ● bellow belts ● Varian RPM	retrospective / prospective PET and CT ● bellow belts ● Varian RPM		retrospective / prospective PET and CT ● bellow belts ● Varian RPM	

PET/CT hardware for RT

- Laser bridge
- Flat table top
- Positioning aids
- Fixation devices

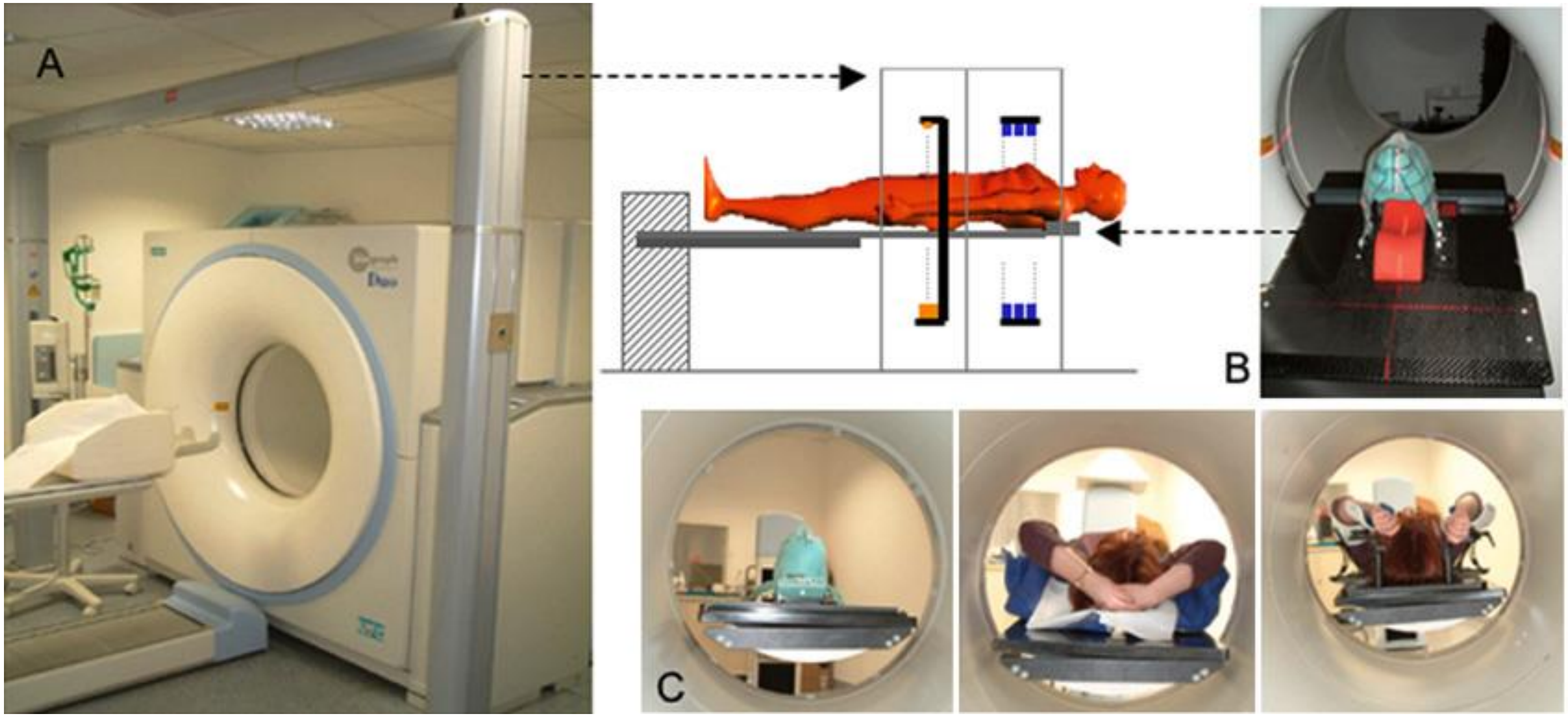

Quality control – RT components

- As with regular CT simulators:
  - Check for table motion constancy, also with varying load
  - Immobilization devices; check e.g. landmarks relative to table top
  - Assess laser geometry and accuracy by alignment tools

Med Phys 2003; 30: 2762–2792

Quality control – CT scanner

- CT numbers (HU)
- Noise, uniformity
- Slice thickness
- Spatial resolution
- Table accuracy

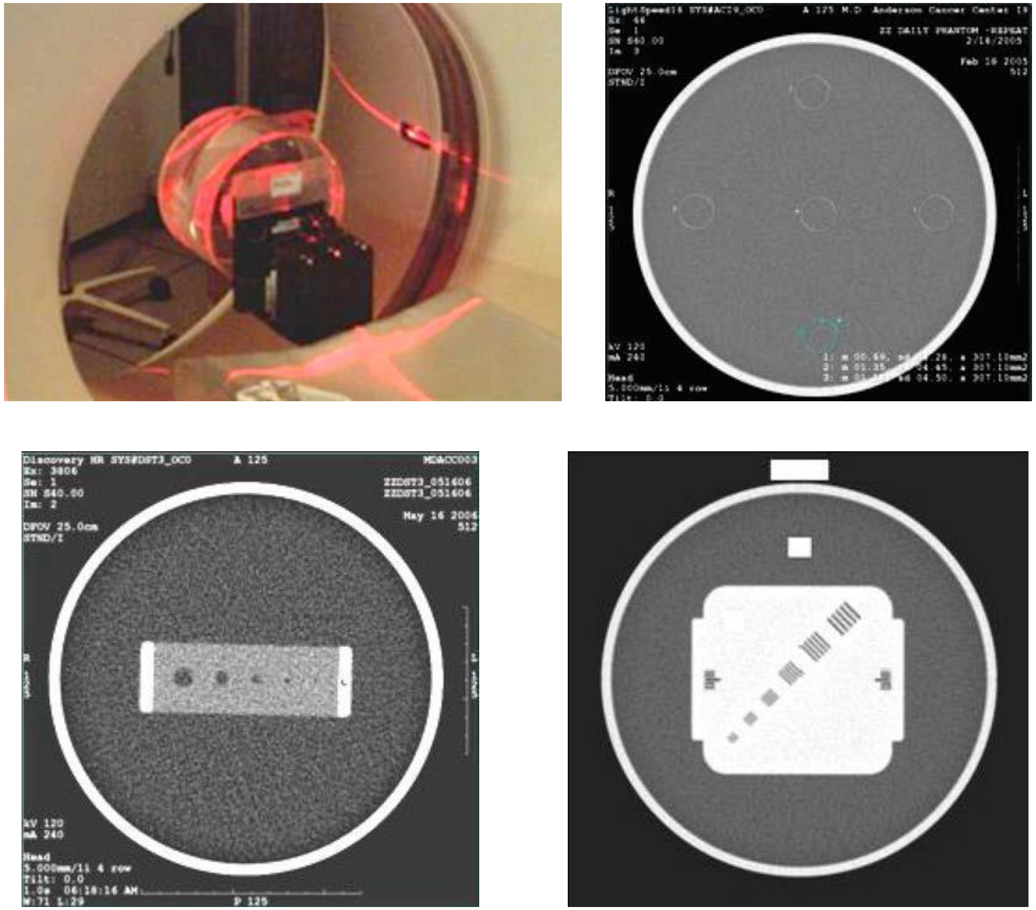

Eur J Nucl Med Mol Imaging (2010) 37:662–671
Med Phys 2003; 30: 2762–2792
IAEA HUMAN HEALTH SERIES 27

Quality control – PET scanner

- Uniformity, coincid. sensitivity
- Activity calibr., normalization
- Correctional measures
  - randoms, scatter, atten.

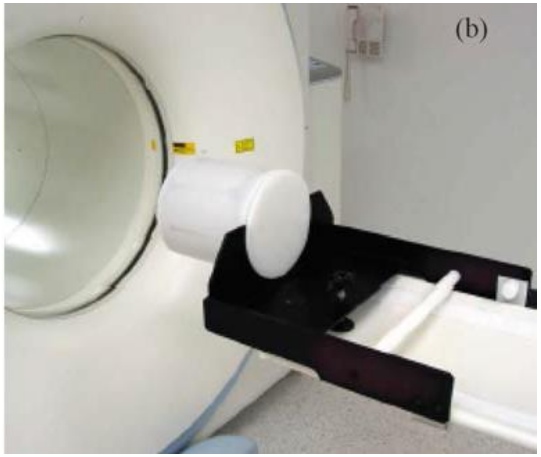

Cylindrical ^{68}Ge phantom

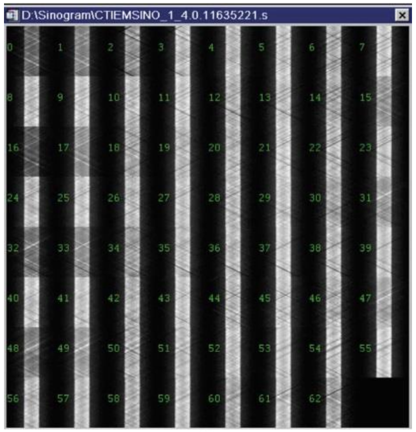
D:\Sinogram\CTIEMSINO_1_4.0.11635221.s
0 1 2 3 4 5 6 7
8 9 10 11 12 13 14 15
16 17 18 19 20 21 22 23
24 25 26 27 28 29 30 31
32 33 34 35 36 37 38 39
40 41 42 43 44 45 46 47
48 49 50 51 52 53 54 55
56 57 58 59 60 61 62

QC sinogram

Image quality tests - PET

NEMA phantom

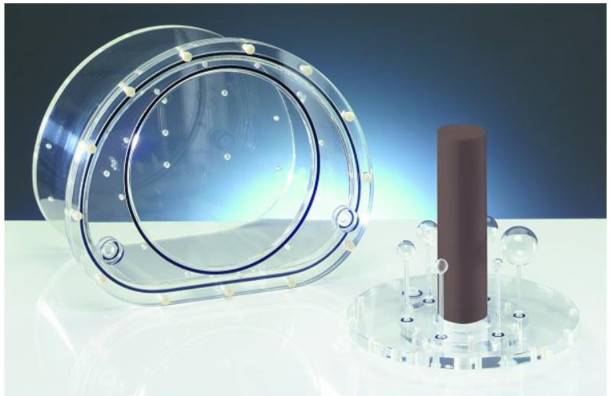

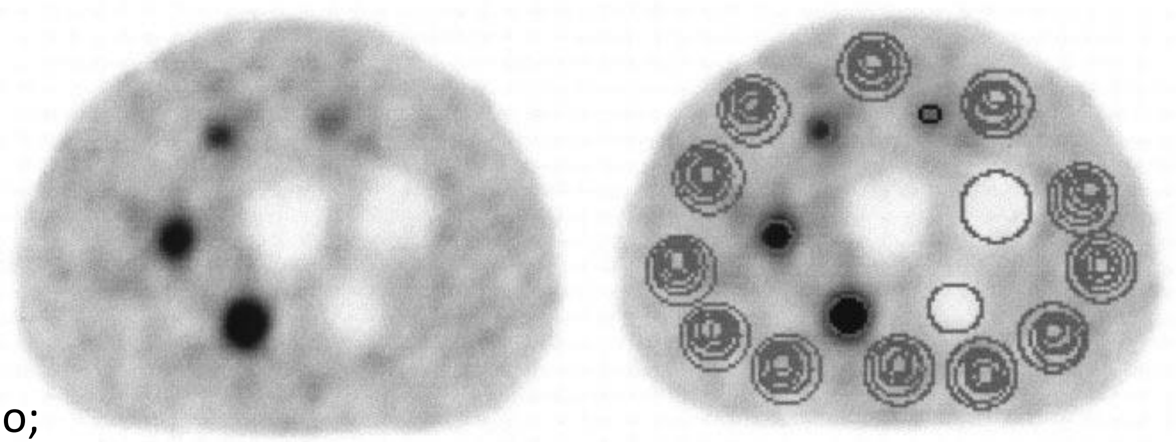

6-min scan (8:1 ratio;
sphere-to-background)

THE JOURNAL OF NUCLEAR MEDICINE 43 10 2002

PET/CT alignment

- Offset between PET and CT image measured during acceptance
- Maintenance/upgrades/repairs may change offset

PET image reconstruction

- Affects detection and delineation
- Standardized protocols and procedures are required

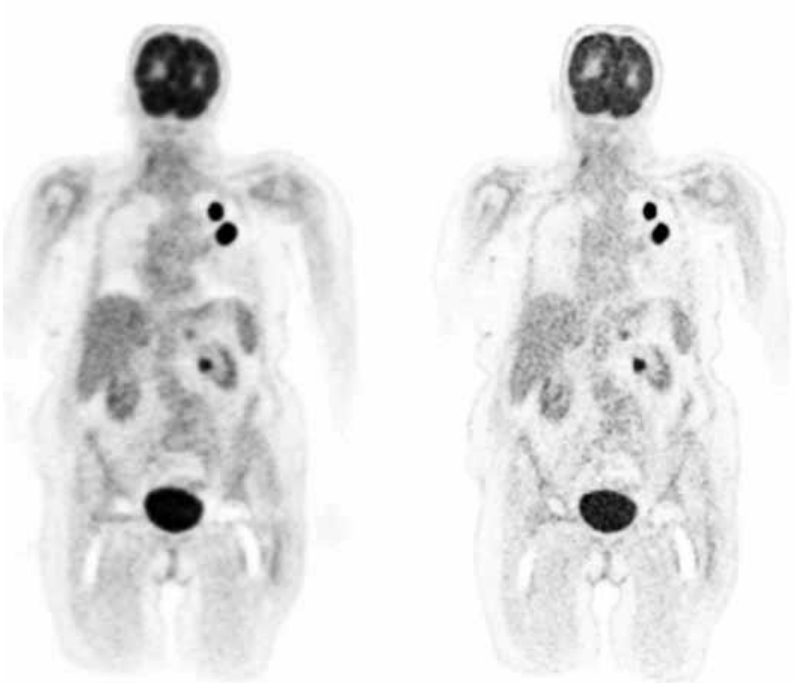

Regular iterative reconstruction

TOF+PSF reconstruction

PET image reconstruction

- Iterative methods are standard, and characterized by
  - Number of iterations and subsets
  - Matrix and voxel size
  - Smoothing kernel
- Number of iterations × subsets > 40
- Full 3D reconstruction *without* acceleration (e.g. Fourier rebinning)
- PET image reconstruction with and without attenuation correction

PET reconstruction and quantification

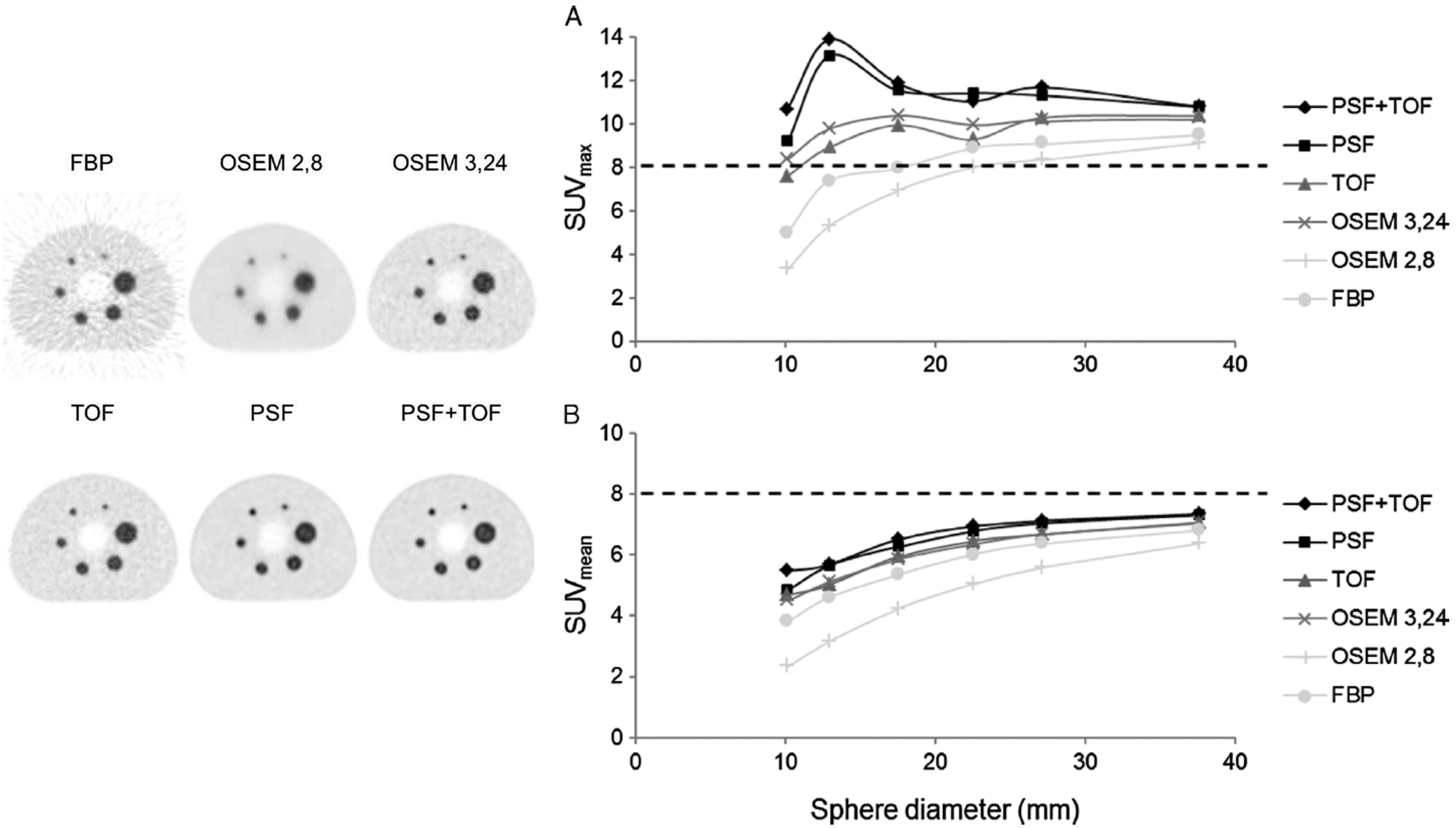

Clinical Nuclear Medicine 38, 2013

PET reconstruction and quantification

- Affects e.g. SUVs and autosegmented volumes

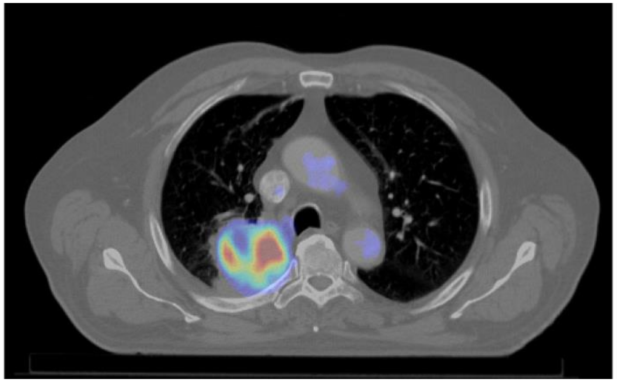

OSEM2i image

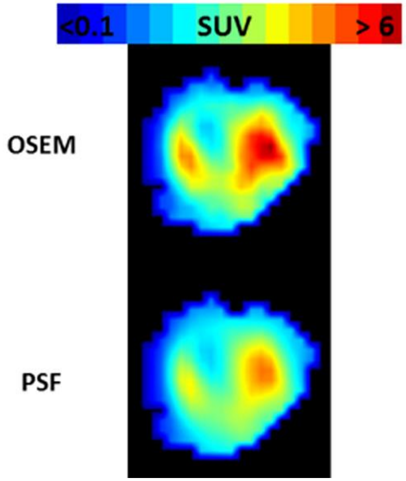

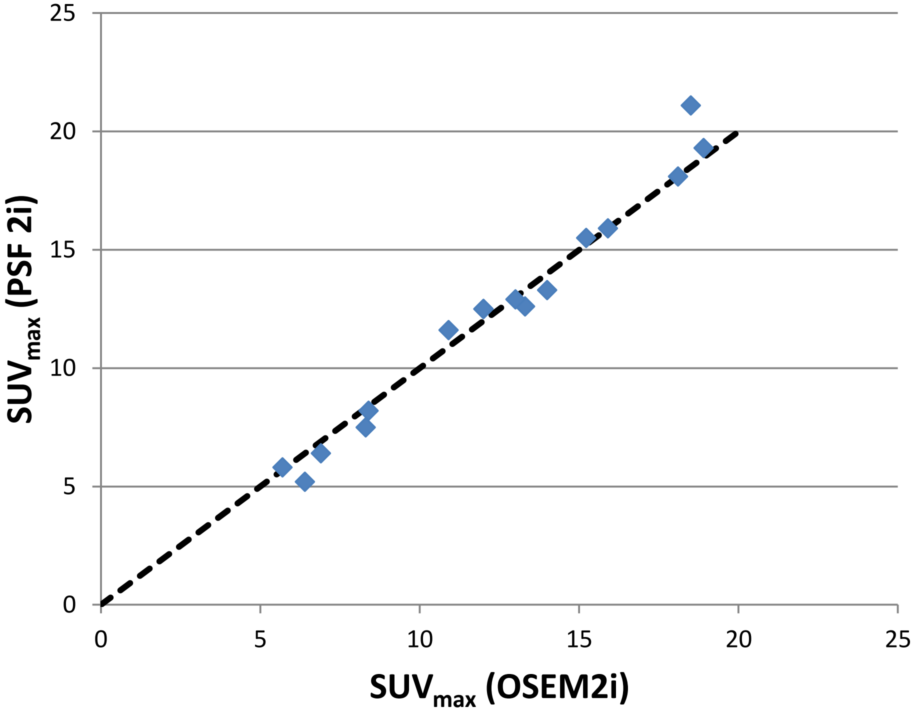

~15% difference in thresholded TVs

Radiotherapy and Oncology 113 (2014) 210–214

Example PET protocol

NARLAL-trial: Heterogeneous FDG-guided dose escalation (with concomitant Navelbine®)

- $\mathrm{SUV}_{\mathrm{peak}}$ more robust than $\mathrm{SUV}_{\mathrm{max}}$
- NEMA phantom at participating centers:

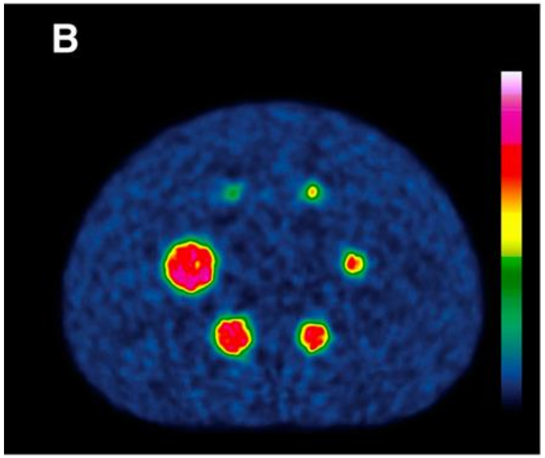

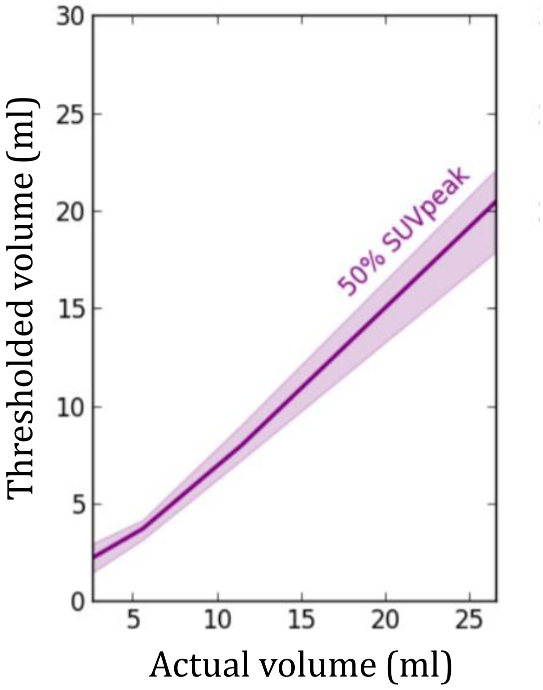

Clinical trials: NCT02354274

Contouring

- Different automated approaches such as thresholding and gradient-based methods

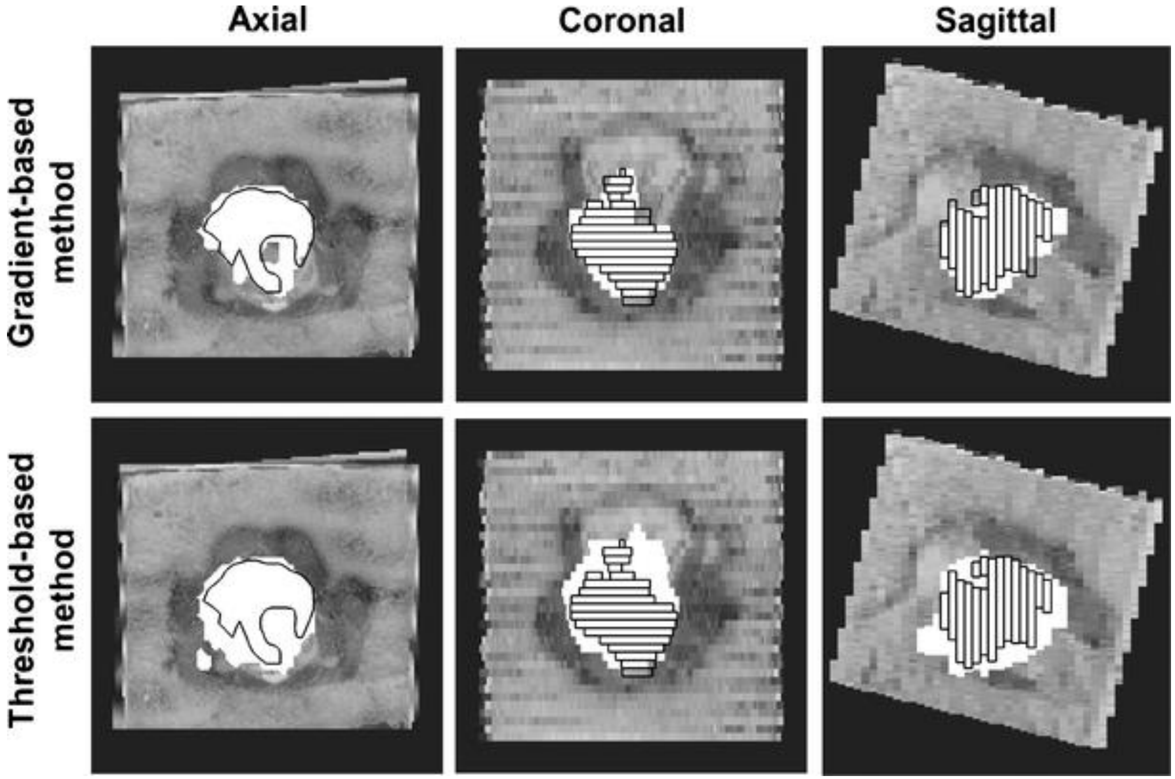
Axial
Coronal
Sagittal
Gradient-based method
Threshold-based method

TVs on macroscopic specimen (black) and FDG-PET (white)

UiO : Department of Physics
University of Oslo

Eur J Nucl Med Mol Imaging (2007) 34:1427–1438

Oslo University Hospital

Contouring

3 observers' delineations

Thresholded volume

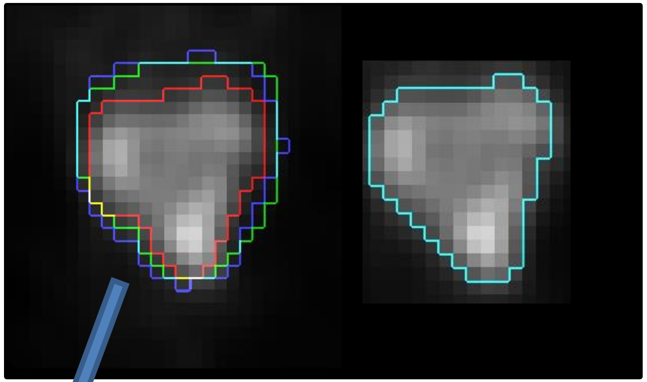

Median inter-observer DICE: 0.68

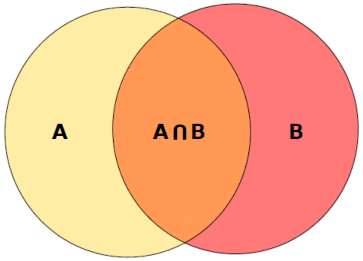

$$\mathrm{DSC} = \frac{A \cap B}{\frac{1}{2} \cdot (|A| + |B|)}$$

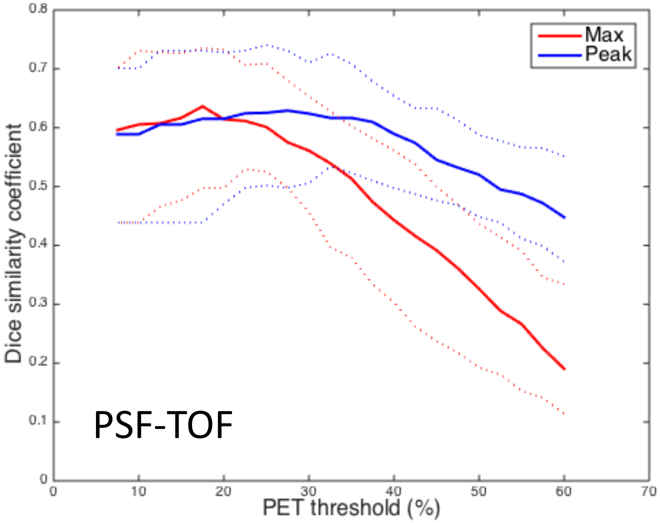

PSF-TOF

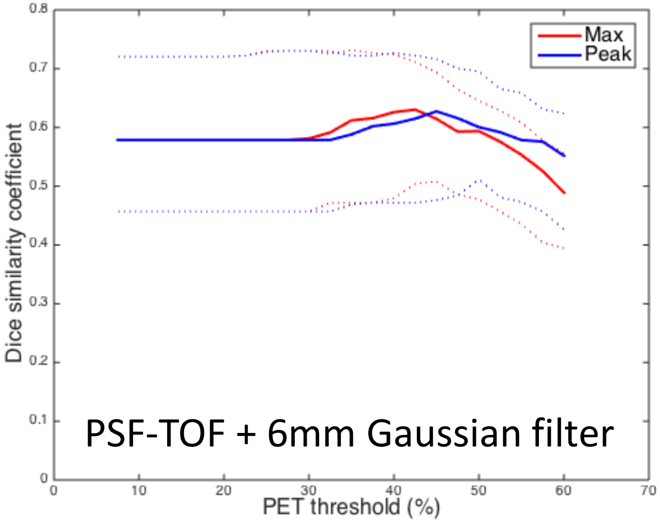

PSF-TOF + 6mm Gaussian filter

Radiation Oncology (2017) 12:147
Work in progress

Contouring

- Segmentation may not result in useful tumor definitions because of
  - Noise
  - Tracer uptake inhomogeneities (tumour+ backgr.)
  - Sometimes low tumour-to-background ratios
- This also causes inter-method variability
- Segmented VOIs must be checked visually

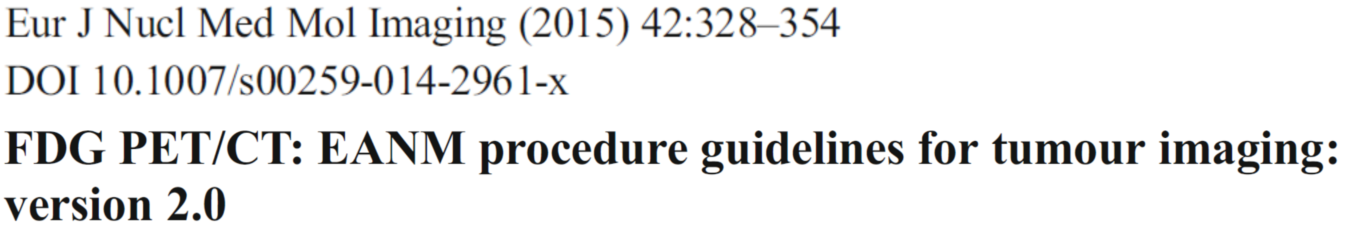

Eur J Nucl Med Mol Imaging (2015) 42:328–354
DOI 10.1007/s00259-014-2961-x

FDG PET/CT: EANM procedure guidelines for tumour imaging: version 2.0

+ Eur J Nucl Med Mol Imaging. 2011;38(12):2136–44

Image registration

- Misregistration in PET/CT can occur:

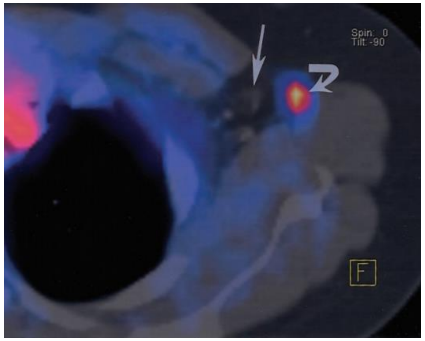

Axial fused FDG PET–CT image of axilla incl. lymph node

- CT-series of PET/CT represents reference frame
- Image registration may be required:
  - In multimodal delineation applications (e.g. +MRI)
  - If PET/CT is not acquired in RT setting (then coreg. with planning CT)
  - For IGRT with e.g. CBCT

Image registration

- Linear, rigid methods
  - Landmark – based
  - Mutual information
- Non-linear ‘deformable’ methods
  - Volume / feature-based algorithms
  - Optical flow methods
  - Demons algorithm
- Deformable methods difficult to validate

DICOM transfer

- Comply with DICOM (RT) standard

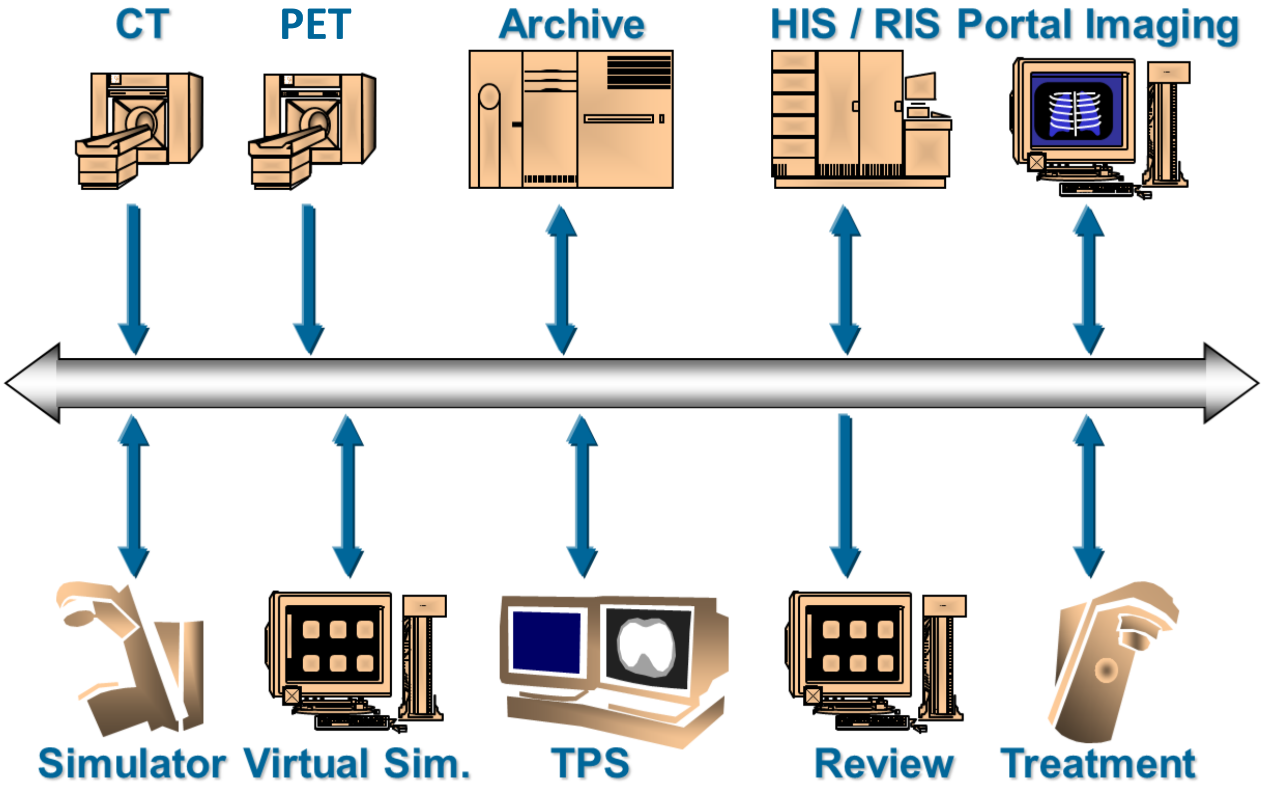
CT
PET
Archive
HIS / RIS
Portal Imaging
Simulator
Virtual Sim.
TPS
Review
Treatment

- RT planning system is not NM viewer

Respiratory motion

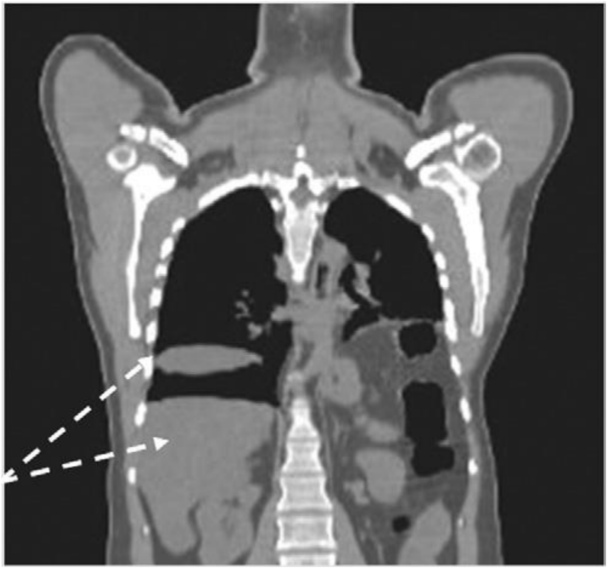

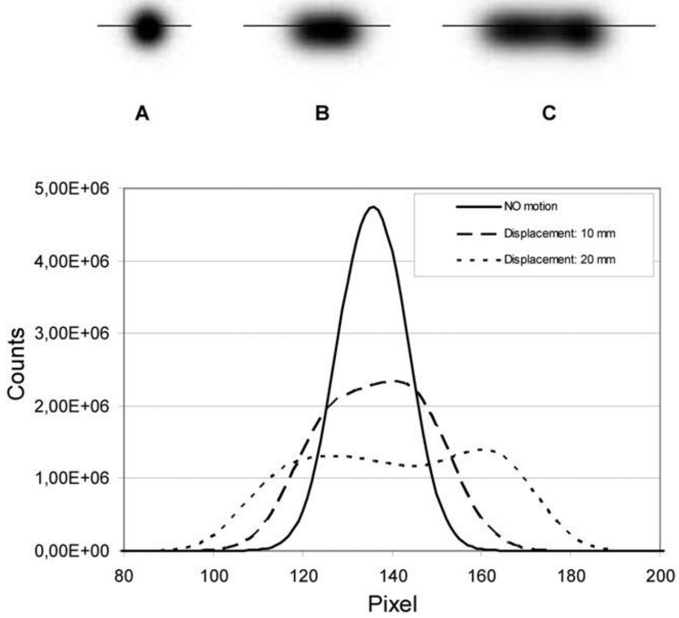

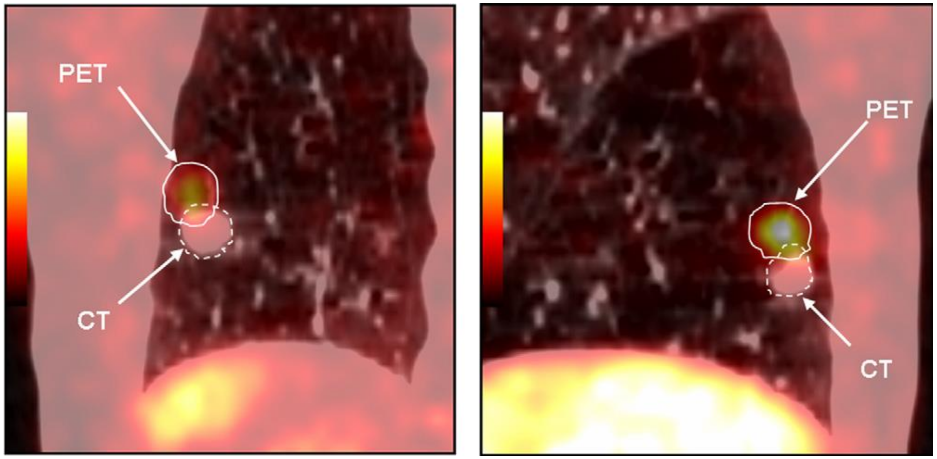

Semin Nucl Med 42:289-307 (2012)

Motion management

- Respiratory gating
  - synchronization of the acquisition systems (CT and PET) to the patient’s respiration
- Breath-hold techniques
  - patient is asked to hold his/her breath
- Tidal breathing
  - patient instructed to breathe shallowly
- Slow CT scan
  - Both PET and CT image motion blurred

Semin Nucl Med 42:289-307 (2012)

Breath hold vs free breathing

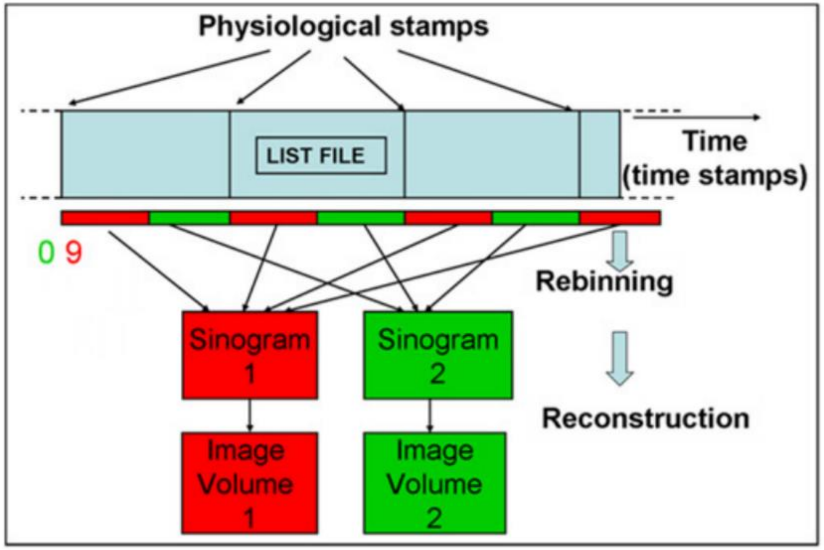

Physiological stamps

LIST FILE

Time
(time stamps)

0 9

Rebinning

Sinogram 1

Sinogram 2

Reconstruction

Image Volume 1

Image Volume 2

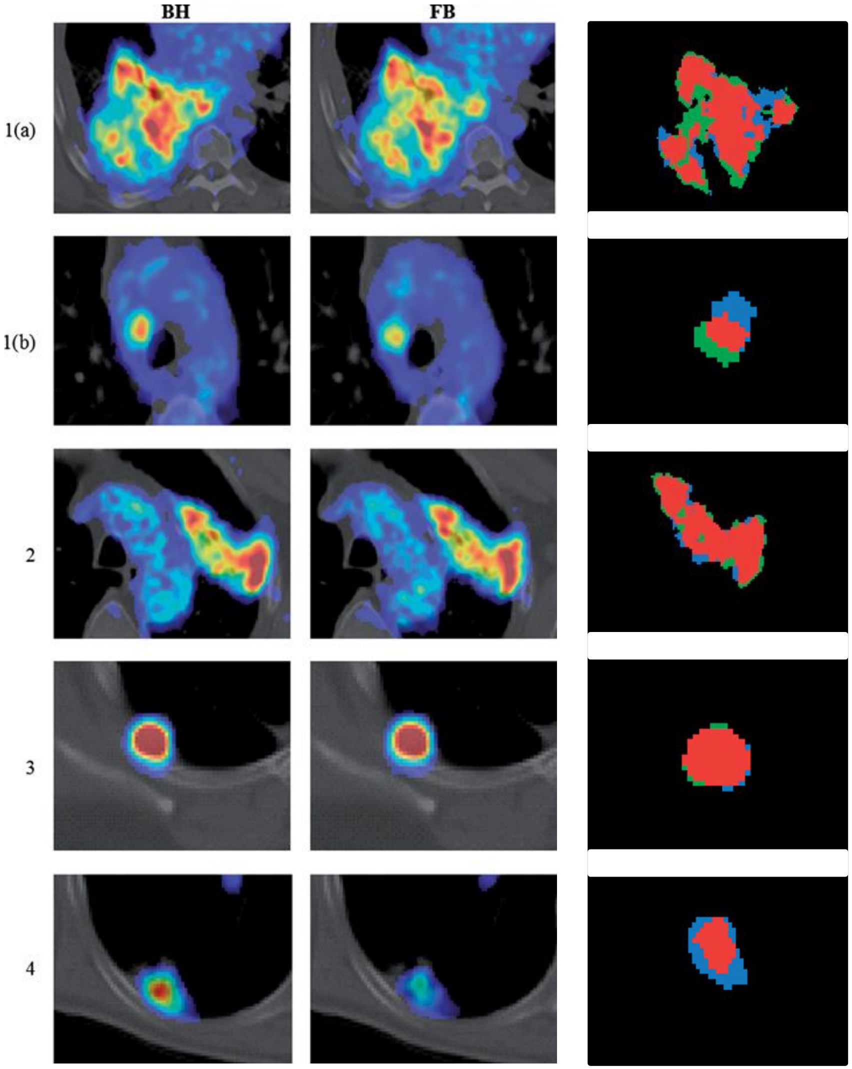

Acta Oncologica, 2011; 50: 889–896
Acta Radiologica 2013; 54: 672–675

Respiratory gated 4D PET/CT

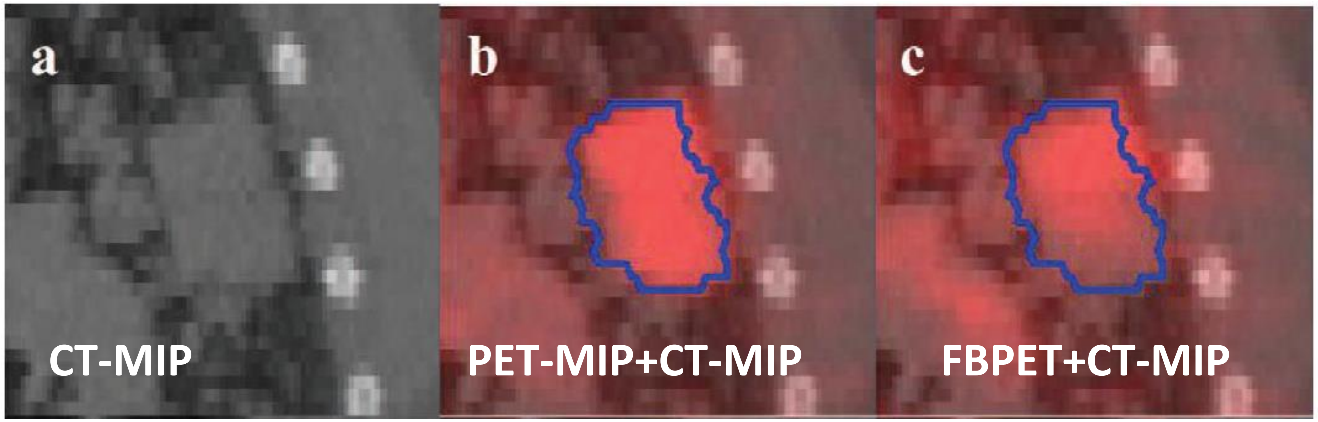
a
CT-MIP
b
PET-MIP+CT-MIP
c
FBPET+CT-MIP

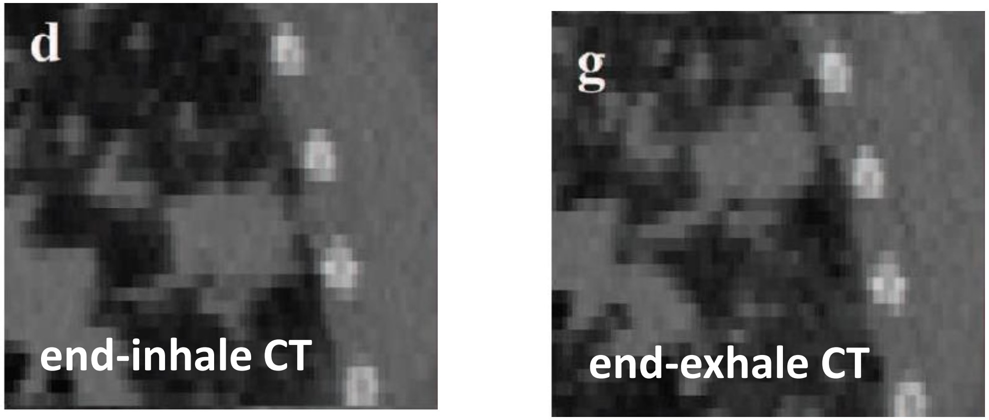
d
end-inhale CT
g
end-exhale CT

Blue contour:
ITV from CT-MIP

Med. Phys. 38 (10), 2011

Staff training

- Adequate training is important
- Include personnel from nuclear medicine and radiotherapy
- Patient instructions pivotal

"Whoa! *That* was a good one! Try it, Hobbs—just poke his brain right where my finger is!"

PET/CT use

- TVs should be delineated by an oncologist together with an experienced nuclear medicine physician
- Automated delineation techniques may be appropriate, subject to manual editing and visual confirmation
- Registration algorithms used should be validated; non-rigid algorithms should be used with caution.
- Ensure that there is an common understanding of QC requirements
- Transfer of DICOM data to TPS should be validated

Br J Radiol. 2012; 85(1016): e544–e548

PET/CT suggestions

- Design for use in RT at the department
- Set up team of nuclear medicine physician, oncologist, PET physicist, RT physicist, RTT
- Determine protocols (may vary with cancer diagnosis), e.g. use of CE-CT
- PET/CT-only (‘direct’) or PET-supplemented (‘indirect’) workflow
- If PET/CT at external department, more crosstalk and bilateral decisions

PET/CT suggestions

- Torso scan for staging
  - ‘Low-dose’ CT possible
- Limited longitudinal scan for TV delination
  - Particular attention to CE-CT / ‘high-dose’ CT, fixation
- Standardize set of image acquisition parameters and injected activity

PET/MR for RT

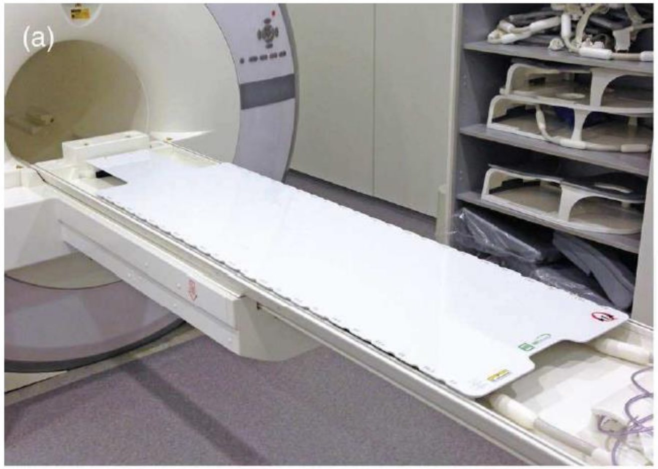

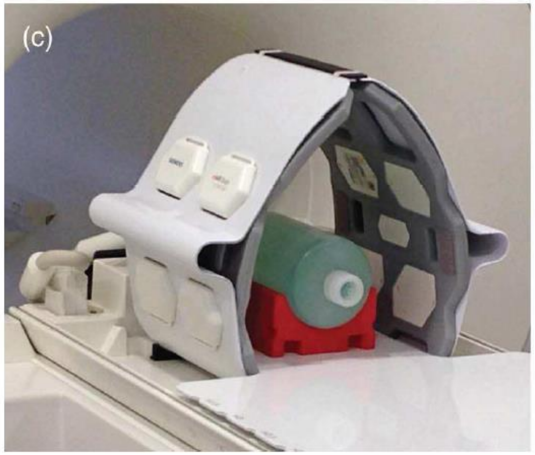

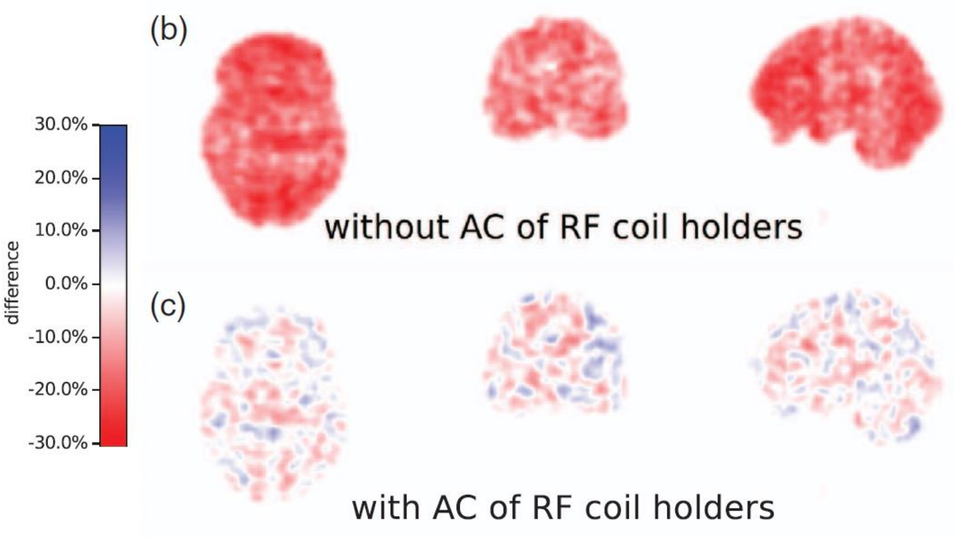
(b)
without AC of RF coil holders
(c)
with AC of RF coil holders
30.0%
20.0%
10.0%
0.0%
-10.0%
-20.0%
-30.0%
difference

Med. Phys. 41 (7), 2014

Acknowledgements

Daniela Thorwarth

Ingerid Skjei Knudtsen

Espen Rusten

MRI for Treatment Planning, Registrations

A/Prof Gary Liney

8th November 2017

ESTRO Imaging for Physicists

MRI for RT Planning Workflow

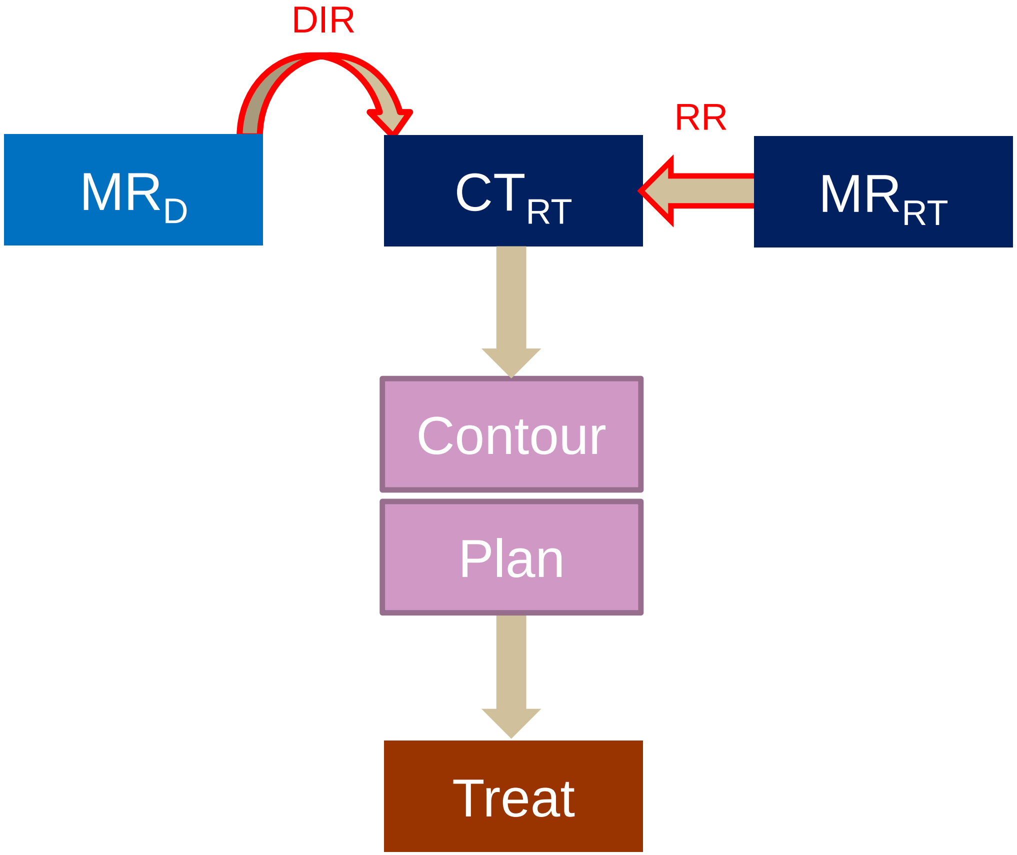
DIR
RR
MR$_D$
CT$_{RT}$
MR$_{RT}$
Contour
Plan
Treat

MR-CT RT

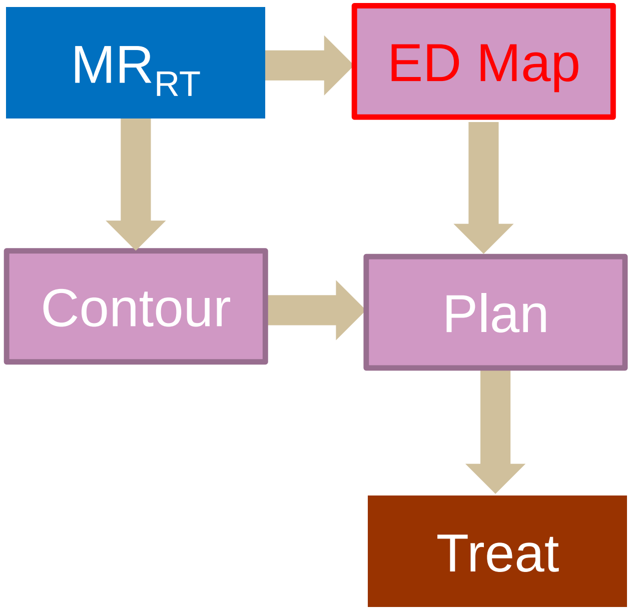
MR$_{RT}$
ED Map
Contour
Plan
Treat

MR-Only RT

Diagnostic vs Treatment Set-up

MRI_D

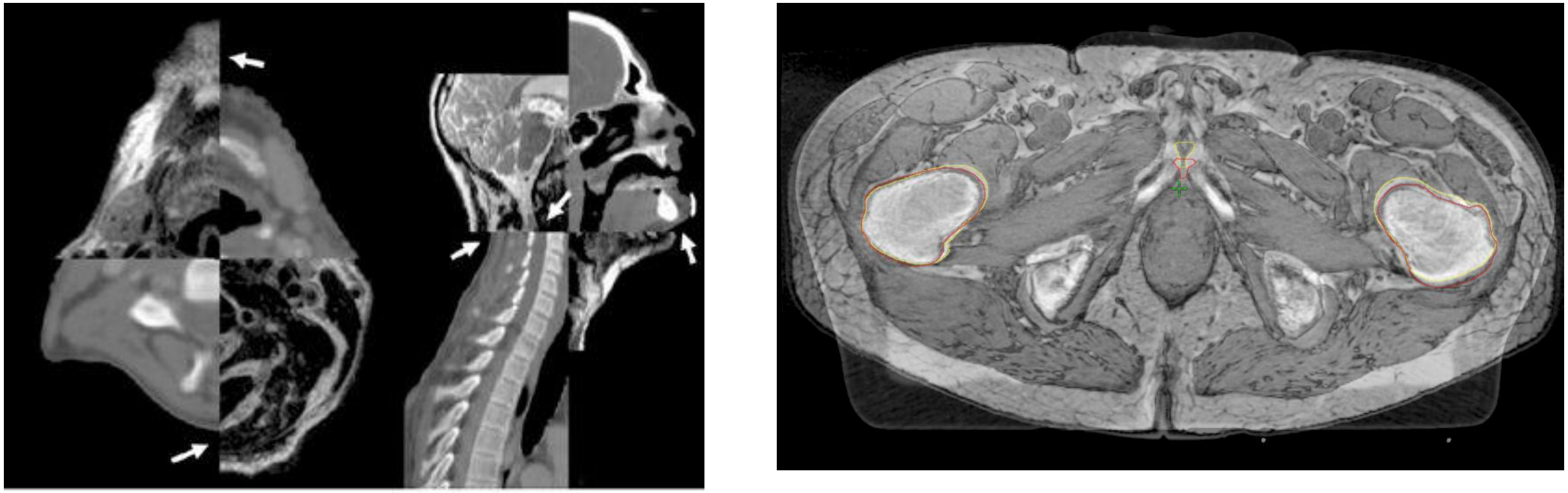

MRI_{RT}

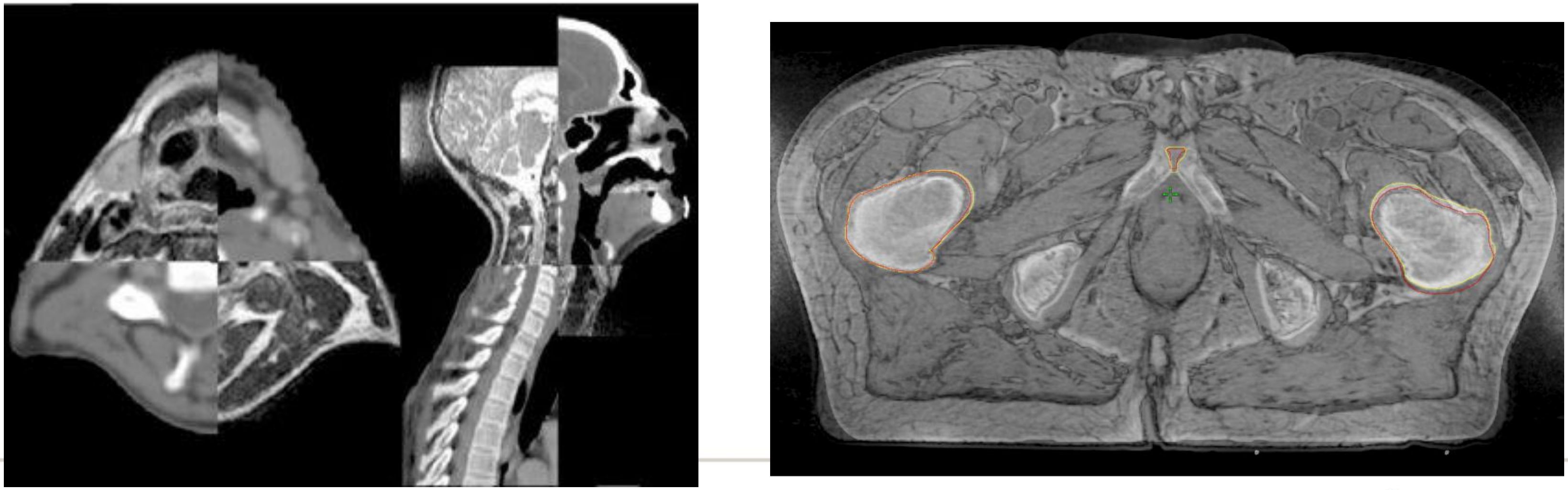

Courtesy of Scott Hanvey

Deformable Image Registration (DIR)

- DIR still not in clinical use
- Small study in 5 H&N patients (Speight et al, Leeds, UK)
- Using MIRADA RTx (Oxford, UK) software
- Propagation of spheres & points to quantify plus visual assessment
- Qualitative evaluation sufficient following quantitative commissioning of DIR tool
- Inaccuracy in spine, register ROI in that region

- DIR improves use of diagnostic MRI

Diagnostic MRI in RT

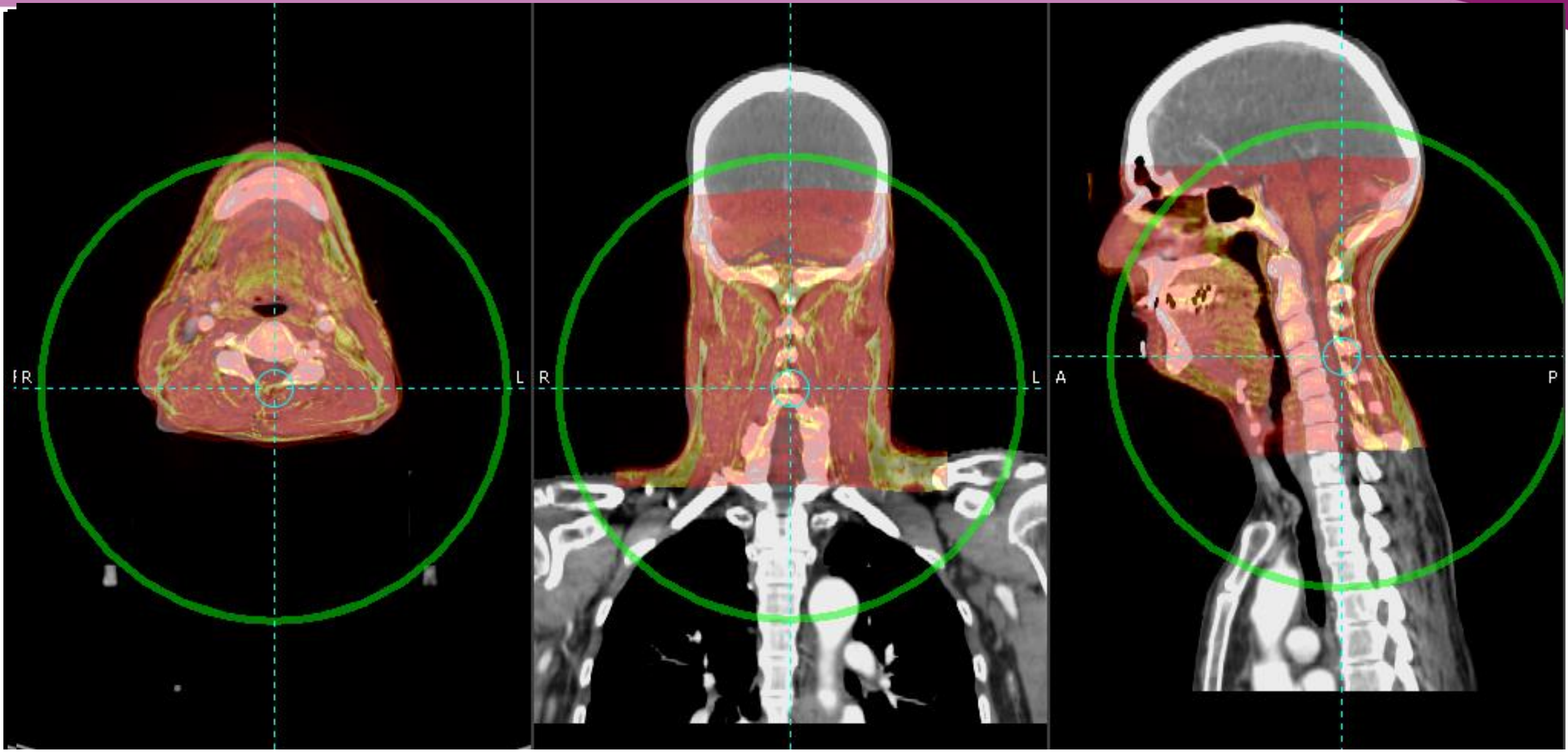

2 stage process: Rigid & Deformable

Deformable Image Registration (DIR)

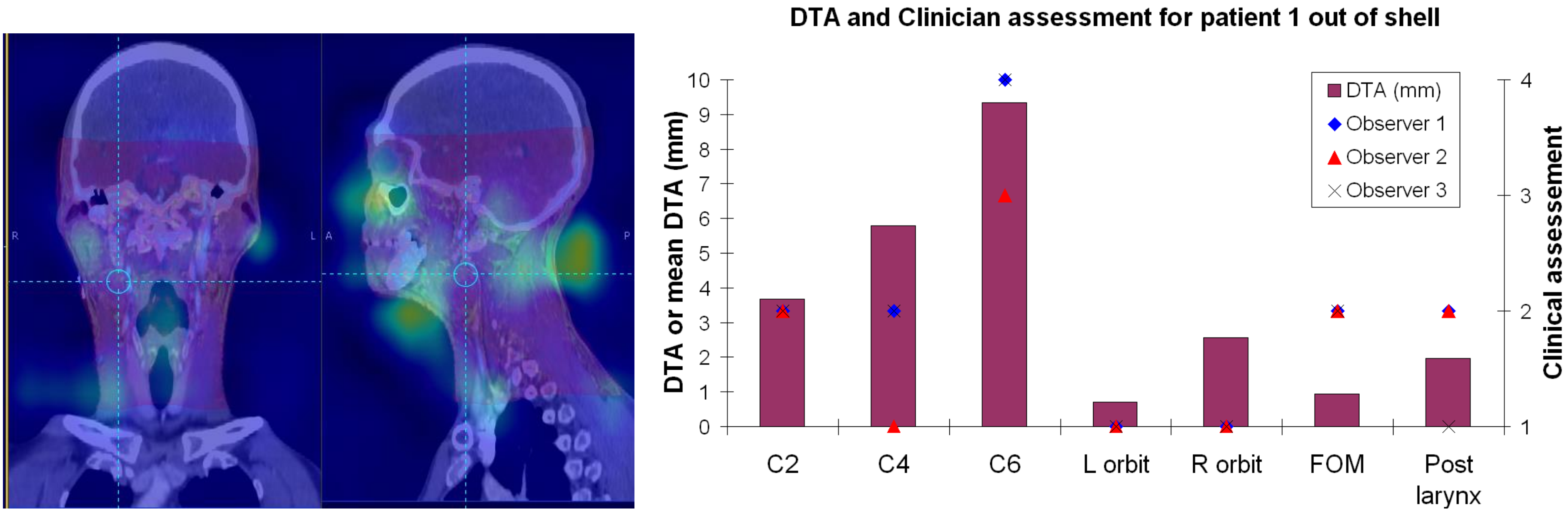

(left) Visual assessment of ‘plausibility’
(right) results in one patient

Dedicated MR-Simulator

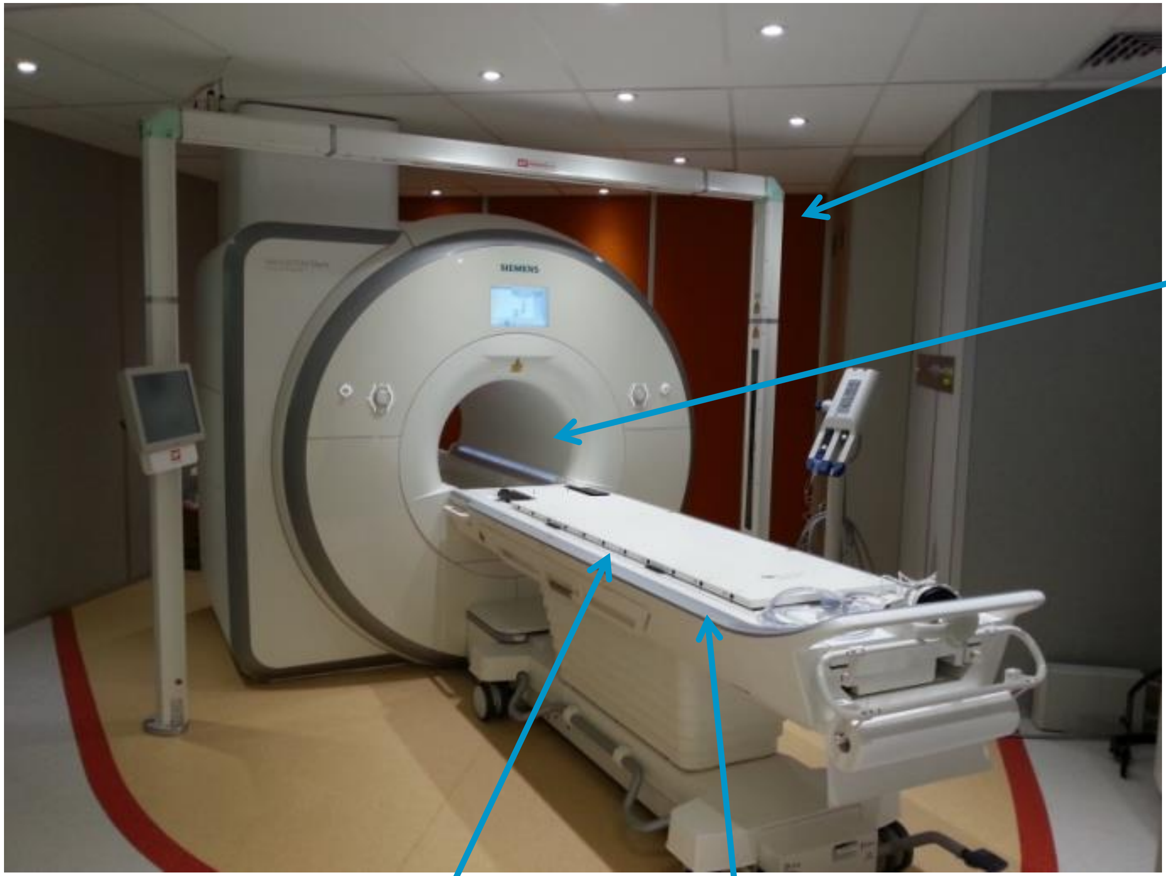

Positioning lasers

Wide bore

Flat table top

32 ch RF coil in bed

- 3.0 Tesla
- 45 mT/m, 200 T/m/s gradients
- Digital RF
- Dual transmitters
- 64 channel system
- Full suite of functional imaging

MR-Simulator

Requirement	Recommendation/Comment
System	1.5 T or 3.0 T wide bore (70 cm) scanner
Set-up	Flat table & immobilisation; utilise high channel RF coil arrays & intensity correction
Distortion	3D gradient correction; measure residual. High BW; Optimise shim where needed; B0 mapping still not widely available
Protocol	2D TSE & DIXON (±C) primary planning sequences; 3D important in specific cases (e.g. T2 MR-only, T1 SRS) Functional & motion assessment not standard
Resolution/ coverage	maximum 1mm or 1 pixel fat-water shift 2-3/0 mm slices (2D) standard; 4 mm functional (e.g. DWI) Single concatenation 3D isotropic as required 30 cm scan coverage

MRI in RT Position: H&N

SIEMENS
INSIGHT
Large 4

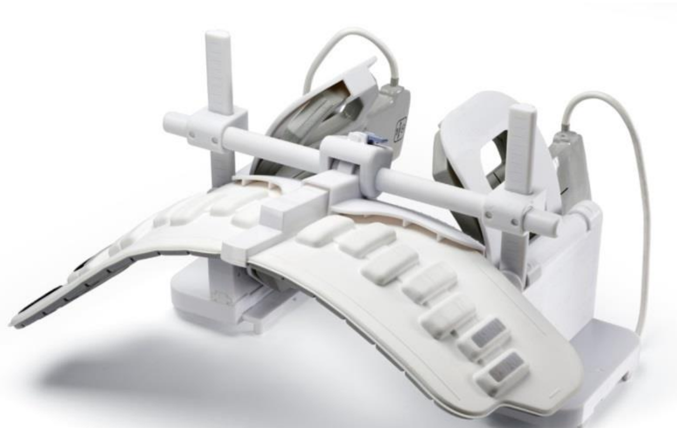

Courtesy GE Healthcare Research

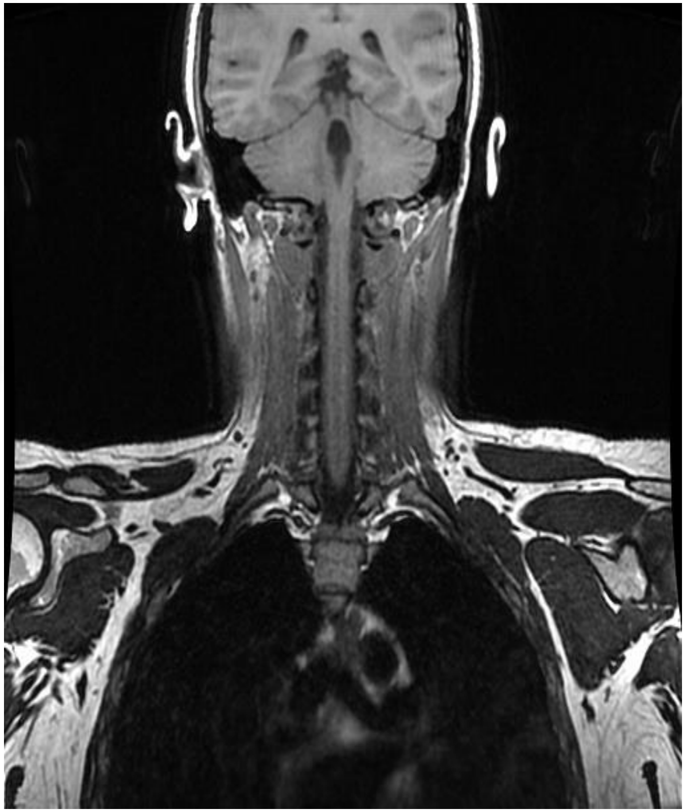

Extended SI coverage

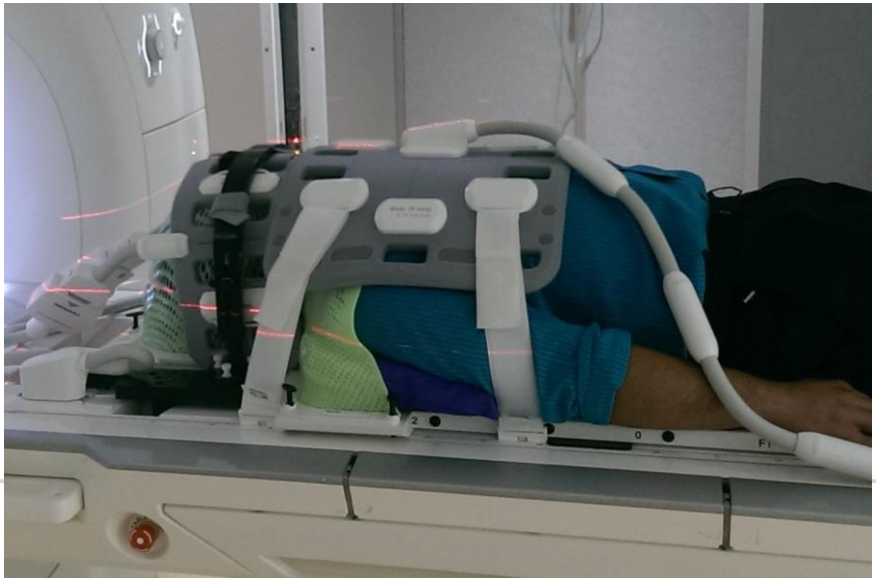

- Combination of head, anterior and posterior (table) coils

MRI in RT Position: Body

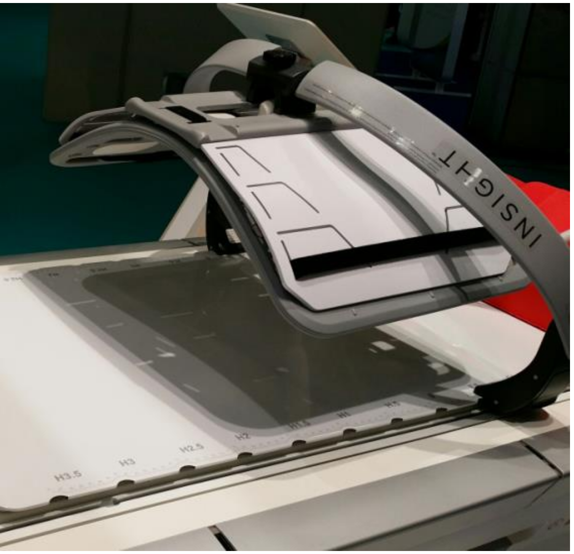

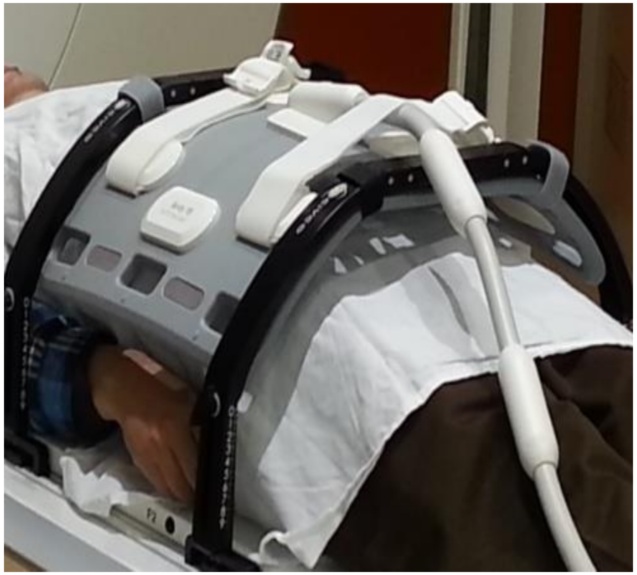

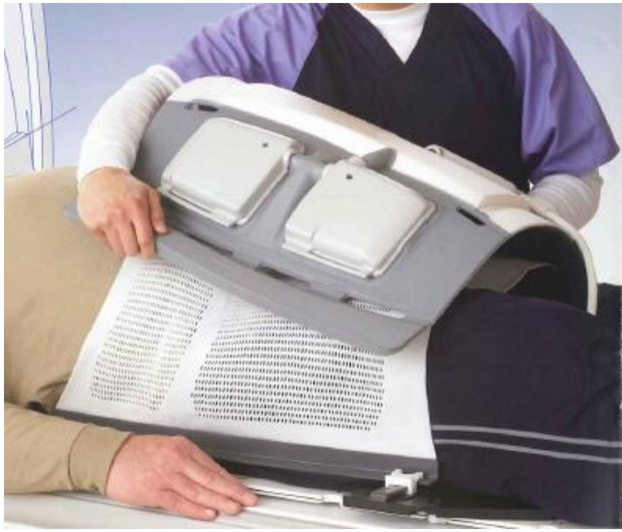

Coil support vs compression

Preservation of skin contour vs maximise SNR

PET-MR (right)-rigid set-up permits attenuation correction

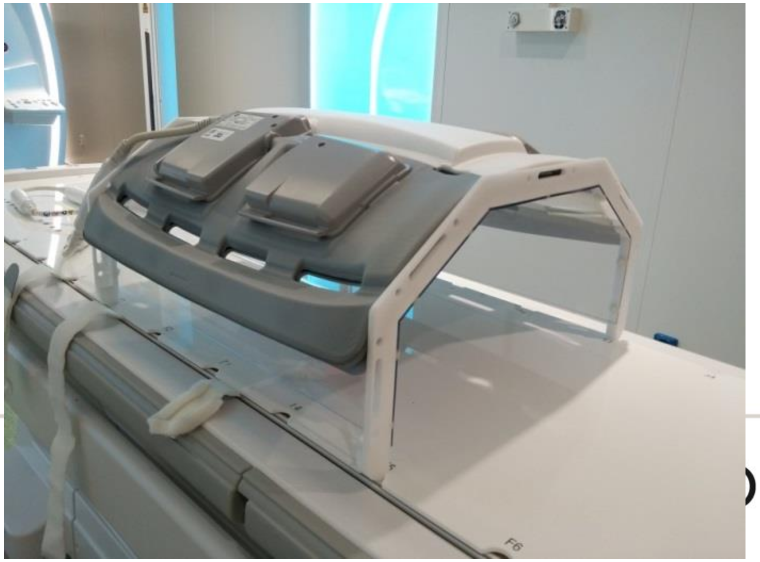

Rigid Registration

- Registration based on bones/markers/soft-tissue?
- Variability between scans/anatomy
- Variability between fusion

- Errors of 2-5 mm reported

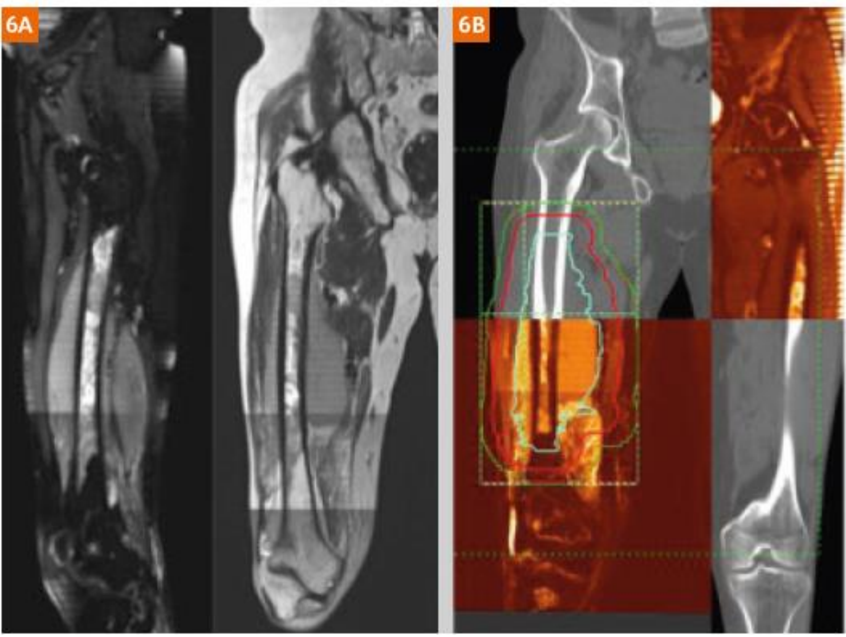

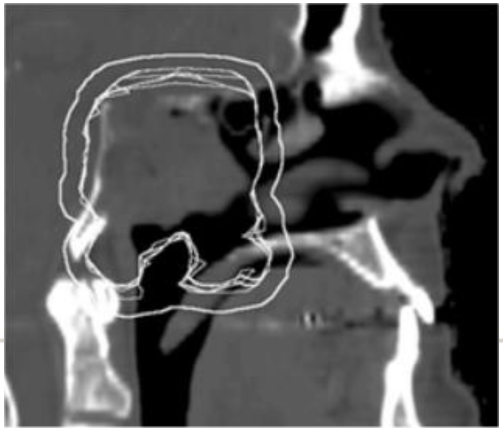

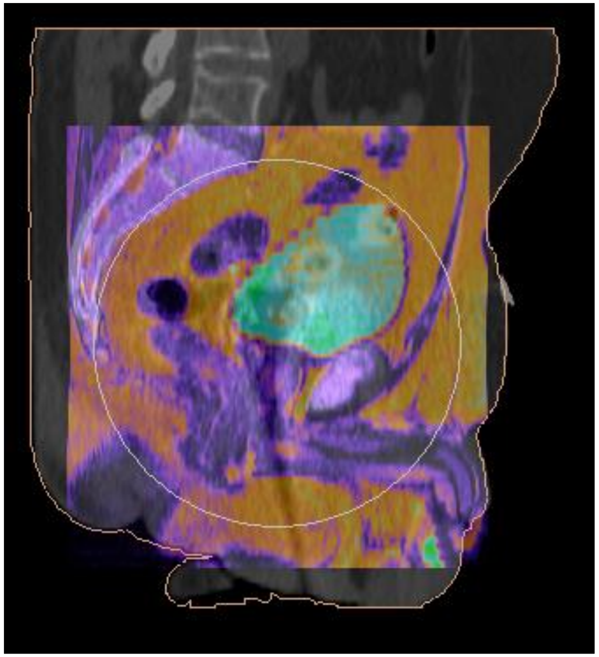

Interest in MR-Only

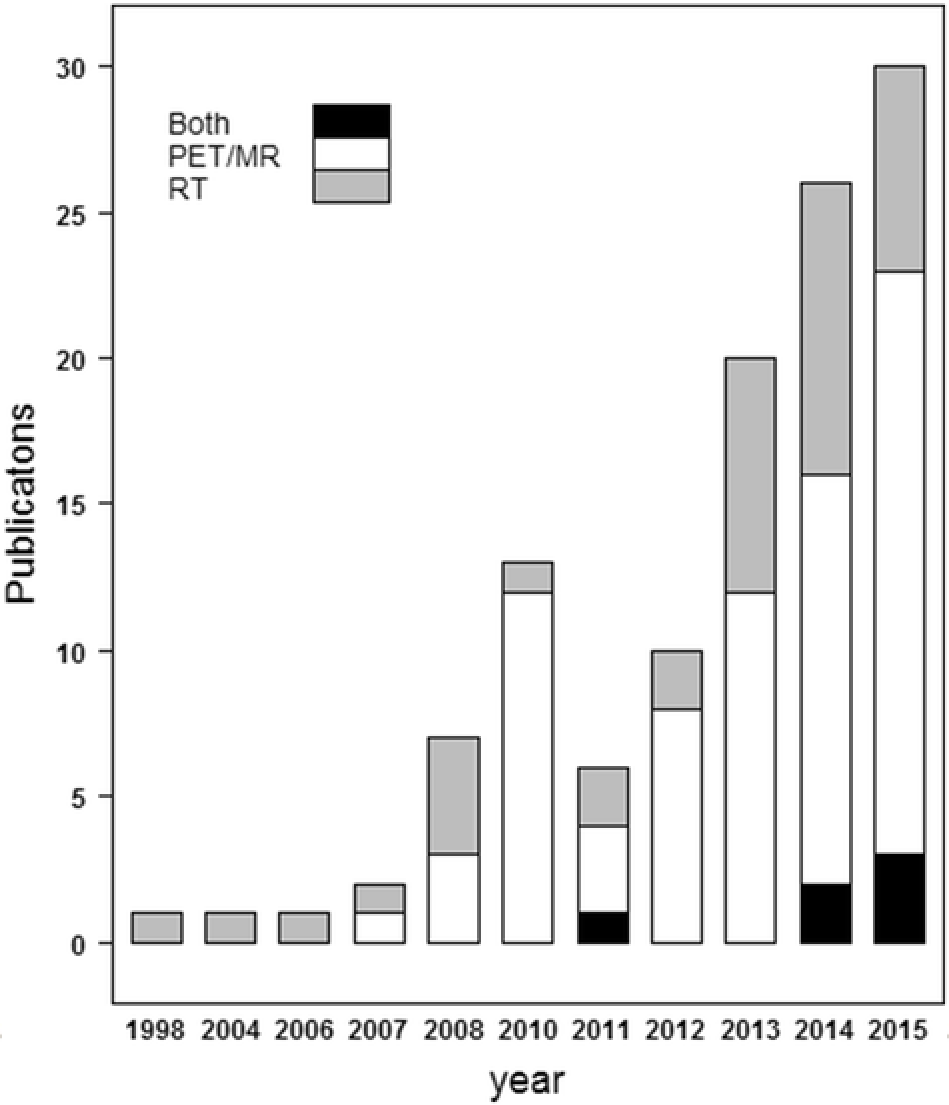

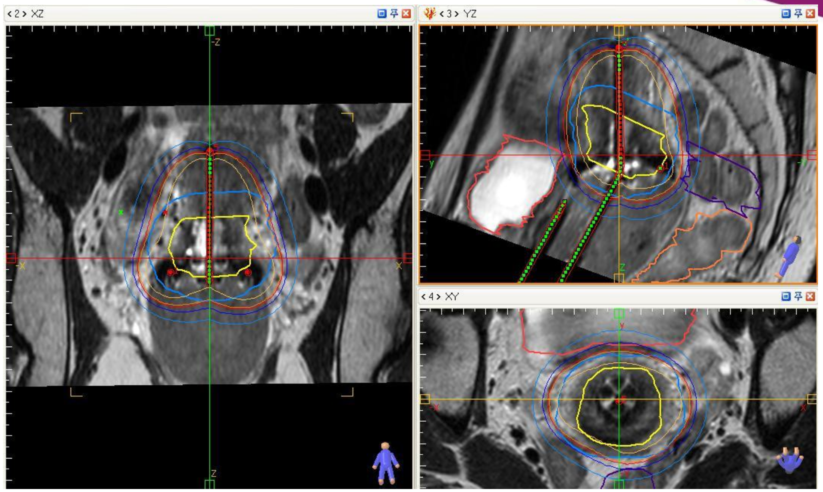

Increase due to MR-PET (from 2010) and MRg (from 2013)

Edmund, J. M., & Nyholm, T. (2017). A review of substitute CT generation for MRI-only radiation therapy. *Radiation Oncology*, 12(1), 28.

Can we get rid of CT? ED Accuracy

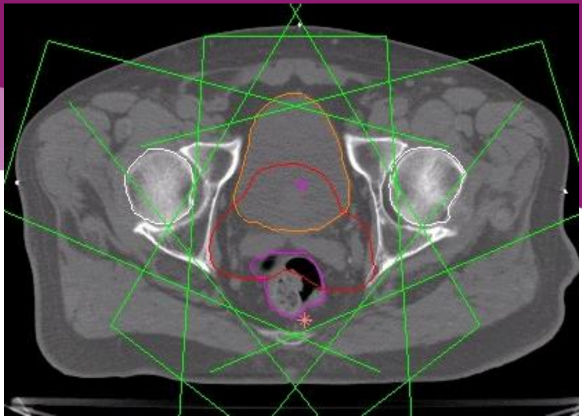

2010 Jonsson

- Adequate bulk density sufficient <1.6% accuracy

  looked at prostate head & even in lung with air cavity
- Large (15%) change in assigned density ⇒ modest 1-2% dose change

2016 Juha

- Dual bulk (water, bone) *vs* homogenous *vs* full conversion for brain & prostate
- Homogenous unacceptable errors in certain cases; bone and soft tissue essential; further heterogeneity improves accuracy
- Dual <2% ; heterogeneous model <0.5%

MR-Only

- Reduce errors associated with MR-CT
- Simplify workflow & cost
- Remove CT scan- synthetic or substitute CT (**s**CT)
- Move towards MRg delivery systems and MR-PET
- Three main methods:
  - Bulk density (tissue class/segmentation)
  - Voxel based (‘model learning’)
  - Atlas based
- Hybrid approaches also exist
- Commericial solutions now available from several vendors

Typical MR-only Sequences

Generic name	Use/Comment
T2/T1	Conventional image contrasts. Has been used extensively in prostate Atlas methods.
DIXON	Images at specific echo times to generate 4 contrasts (in, out-phase, fat & water) in one scan.
UTE	With TE < 0.1 ms to generate positive signal in bone. Separates air & bone. Sometimes used as dual echo sequence.
TOF	Angiography scan to generate high blood signal. Distinguish vessels from bone in certain cases

2D or 3D?

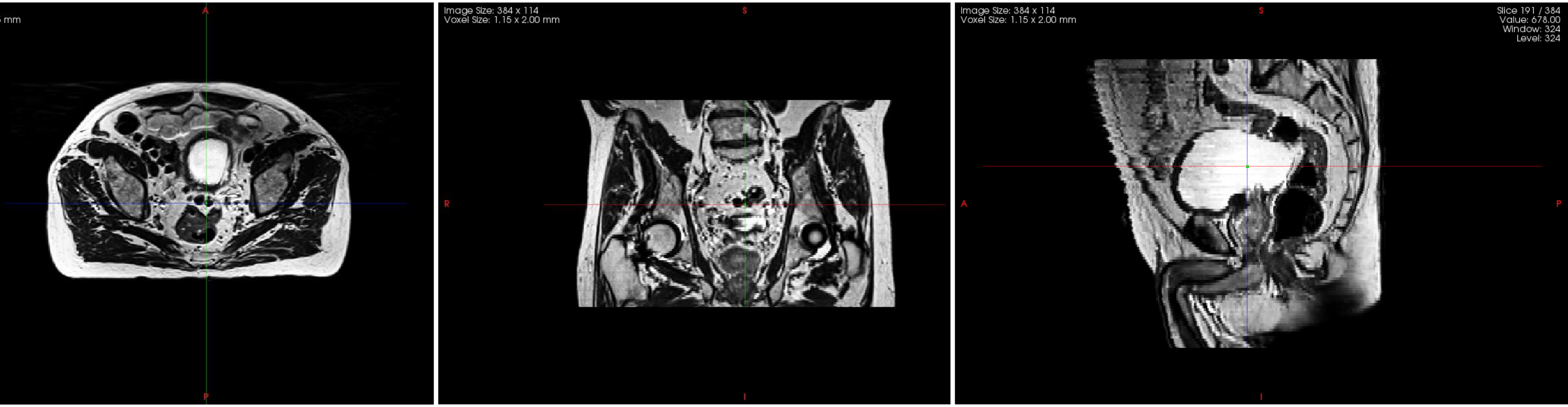
mm
A
P
Image Size: 384 x 114
Voxel Size: 1.15 x 2.00 mm
S
R
I
Image Size: 384 x 114
Voxel Size: 1.15 x 2.00 mm
S
Slice 191 / 384
Value: 678.00
Window: 324
Level: 324
A
P
I

Contiguous thin 2D T2-w FSE showing good contrast for RT planning

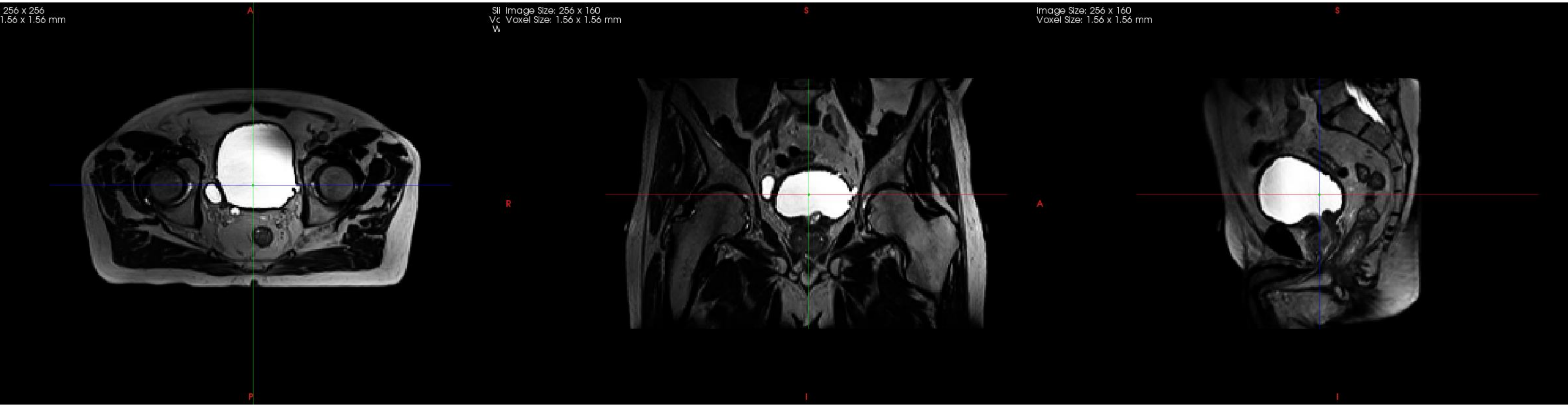
256 x 256
1.56 x 1.56 mm
A
P
Image Size: 256 x 160
Voxel Size: 1.56 x 1.56 mm
S
R
I
Image Size: 256 x 160
Voxel Size: 1.56 x 1.56 mm
S
A
I

3D T2-w FSE showing better resolution and no motion issue

ESTRO School

1. Bulk Density

Assign bulk density to tissue class(es)

- Advantages

No registration

Robust wrt abnormal anatomy

- Disadvantages

Accuracy depends on increasing classes

Manual contouring required

sDRR not realistic

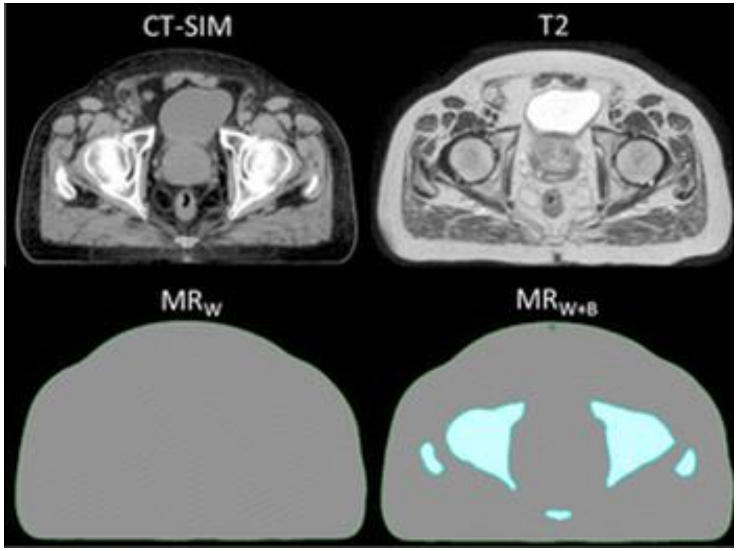

Kim J, Garbarino K,, et al. . Radiat Oncol (2015)

2. Voxel Based

Use a model or statistical learning to identify tissue components.

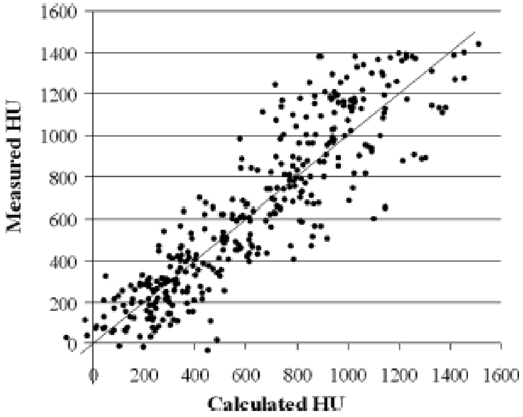

Kapanen M. et al (2013)

- Advantages

Fast, robust

- Disadvantages

Multiple sequences (or echoes) required

Generalisability

May require manual bone contours

Johansson et al Med Phys (2011)

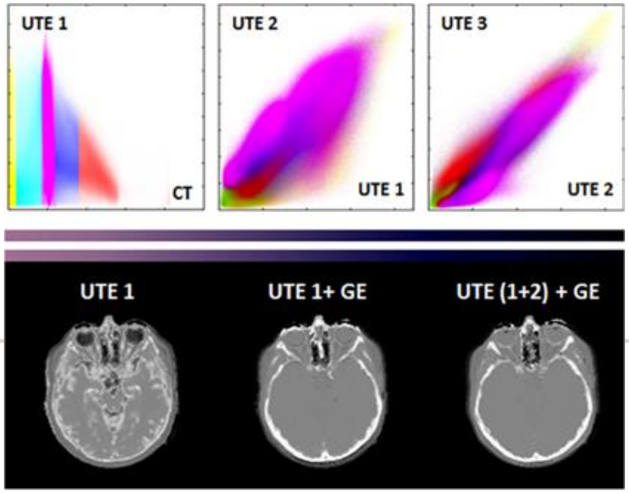
UTE 1
CT
UTE 2
UTE 1
UTE 3
UTE 2
UTE 1
UTE 1+ GE
UTE (1+2) + GE

Example: Dual calibration model (prostate)

Korhonen et al. 2014

- 1.5 T wide bore GE scanner
- MRI signal from Dixon in-phase MRI scan mapped to HU value
- Requires separate mapping models for bone and soft tissue regions (requires bone contouring)
- Method has been used clinically on prostate patients for MRI-only workflow
- n=200; 16 (8%) requiring additional CT

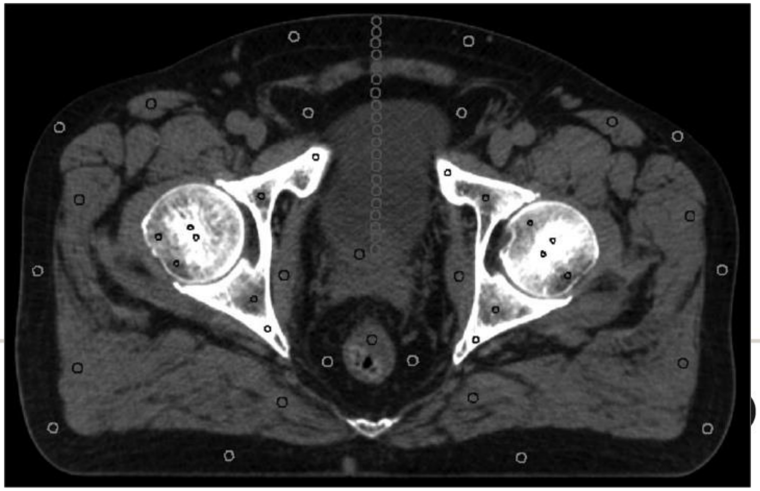

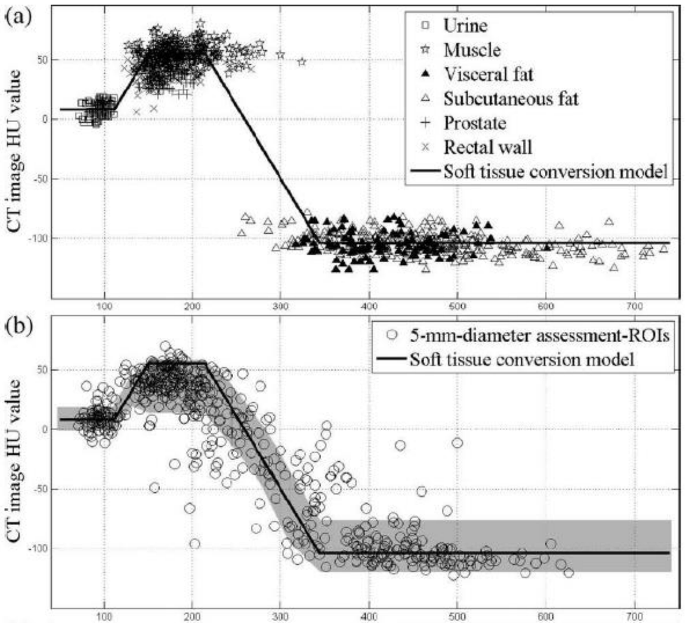

Korhonen, et al. 2014. Med Phys 41(1)

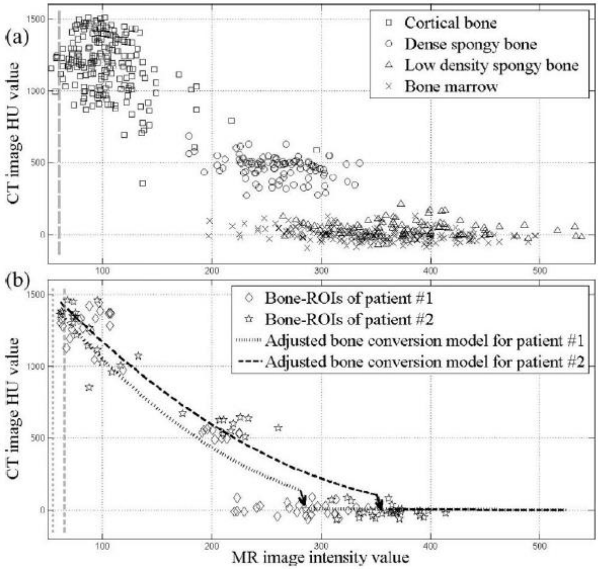

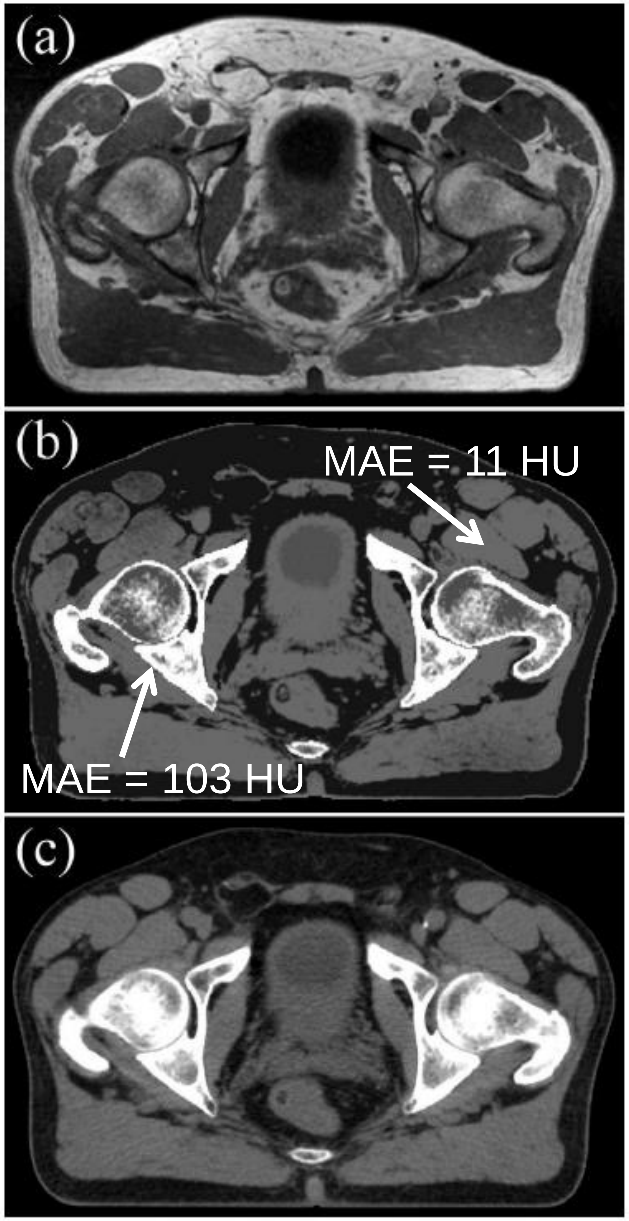

MAE = 11 HU

MAE = 103 HU

Probabilistic Modelling

Dynamic class assignment

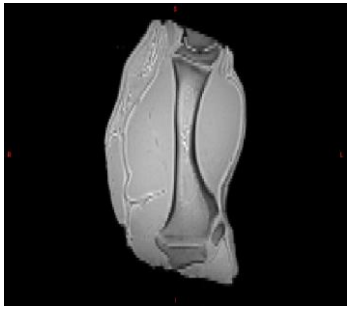

Test Image

Clustering

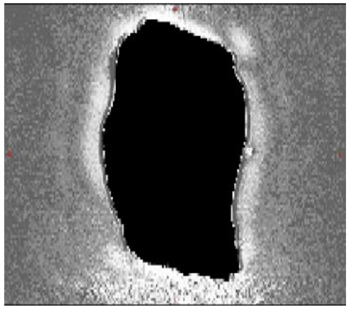

Air

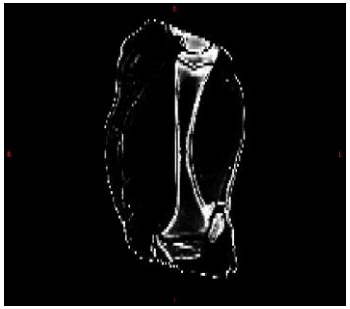

Bone

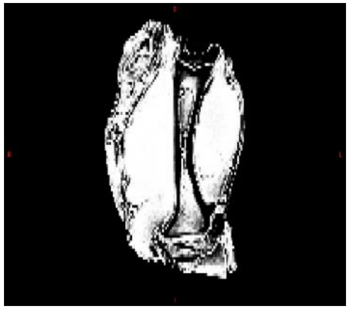

Soft Tissue

Air Class assigned -1000

Bone Class regression

Soft Tissue Class regression

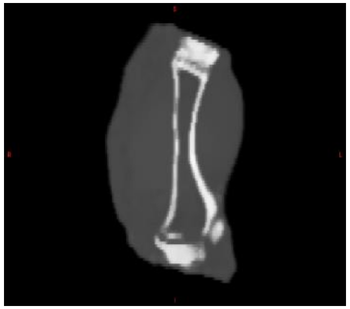

Synthetic CT

HU model based on class probability

Ghose et al PMB, 2017

Results

Measure	Sequence(s)	Mask Air	Result
Bone Surface Distance between CT and sCT	PETRA	N/A	1.34 mm
	UTE (4ms & 40µs)	N/A	1.89 mm
Mean HU error between CT and sCT	PETRA	Not Masked	-0.01 ± 22.84
	UTE (4ms & 40µs)		1.52 ± 39.13
	T2 and PETRA		-0.26 ± 18.86
	PETRA	Masked	15.59 ± 180.71
	UTE (4ms & 40µs)		102.35 ± 332.48
	T2 and PETRA		-12.63 ± 101.77

HU generation from a single 3-class sequence (bone, air, soft-tissue) versus 4-class (bone, air, fat, muscle)

3. Atlas Based

Use image registration to map previous MR-CT scans to a new MRI

- Advantages

Robust to image variation

Can be used to generate autocontours

- Disadvantages

Can be slow

Anatomy specific & abnormalities cause problems

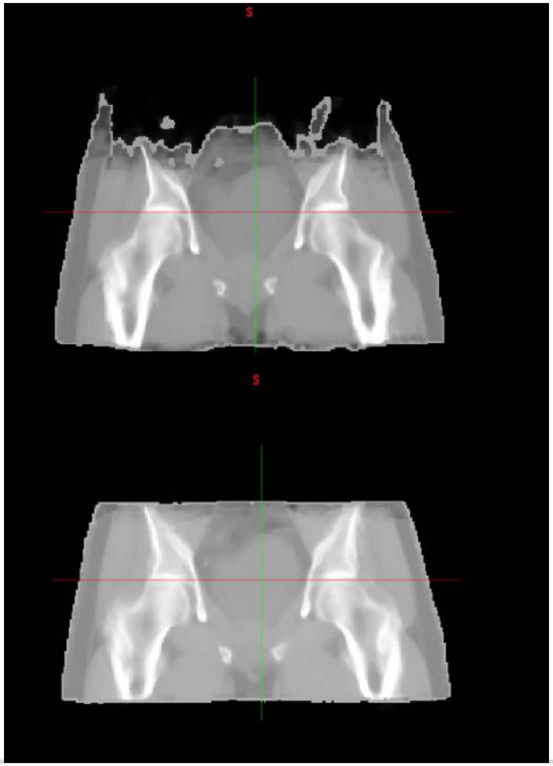

sCT: Multi-Patient Atlas approach

Construct offline database

Rigid and structure guided NR MR-CT database

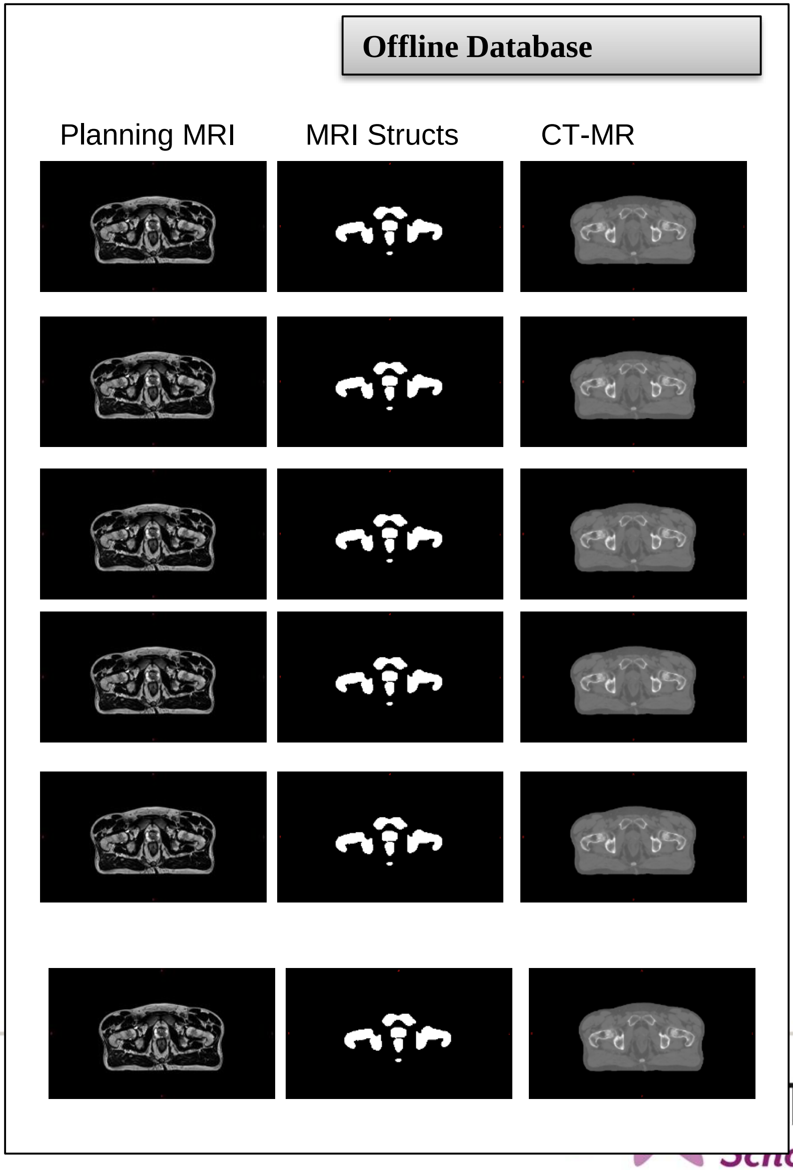

Offline Database

Planning MRI

MRI Structs

CT-MR

sCT: Multi-Patient Atlas approach

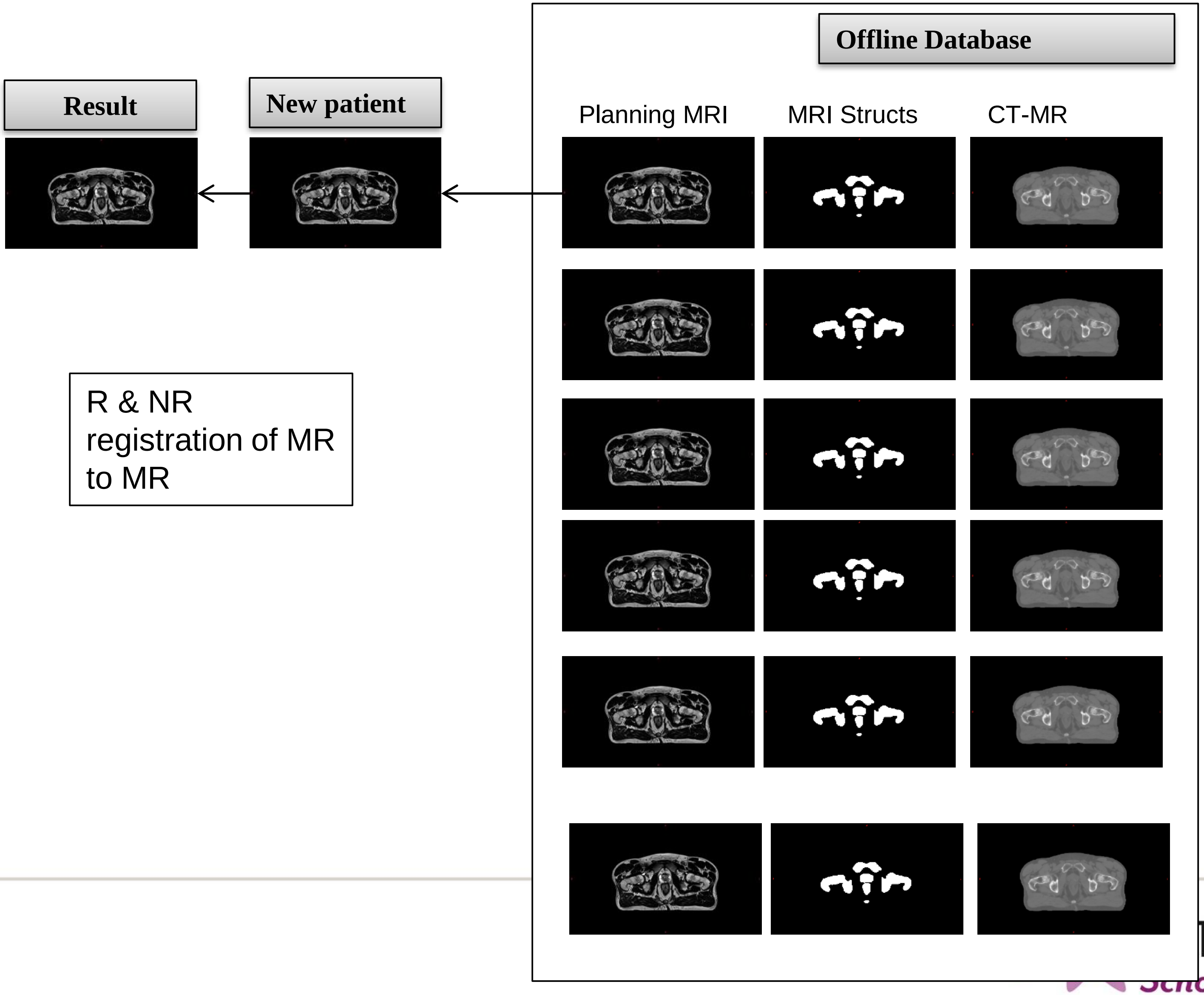
Result
New patient
Offline Database
Planning MRI
MRI Structs
CT-MR

R & NR registration of MR to MR

sCT: Multi-Patient Atlas approach

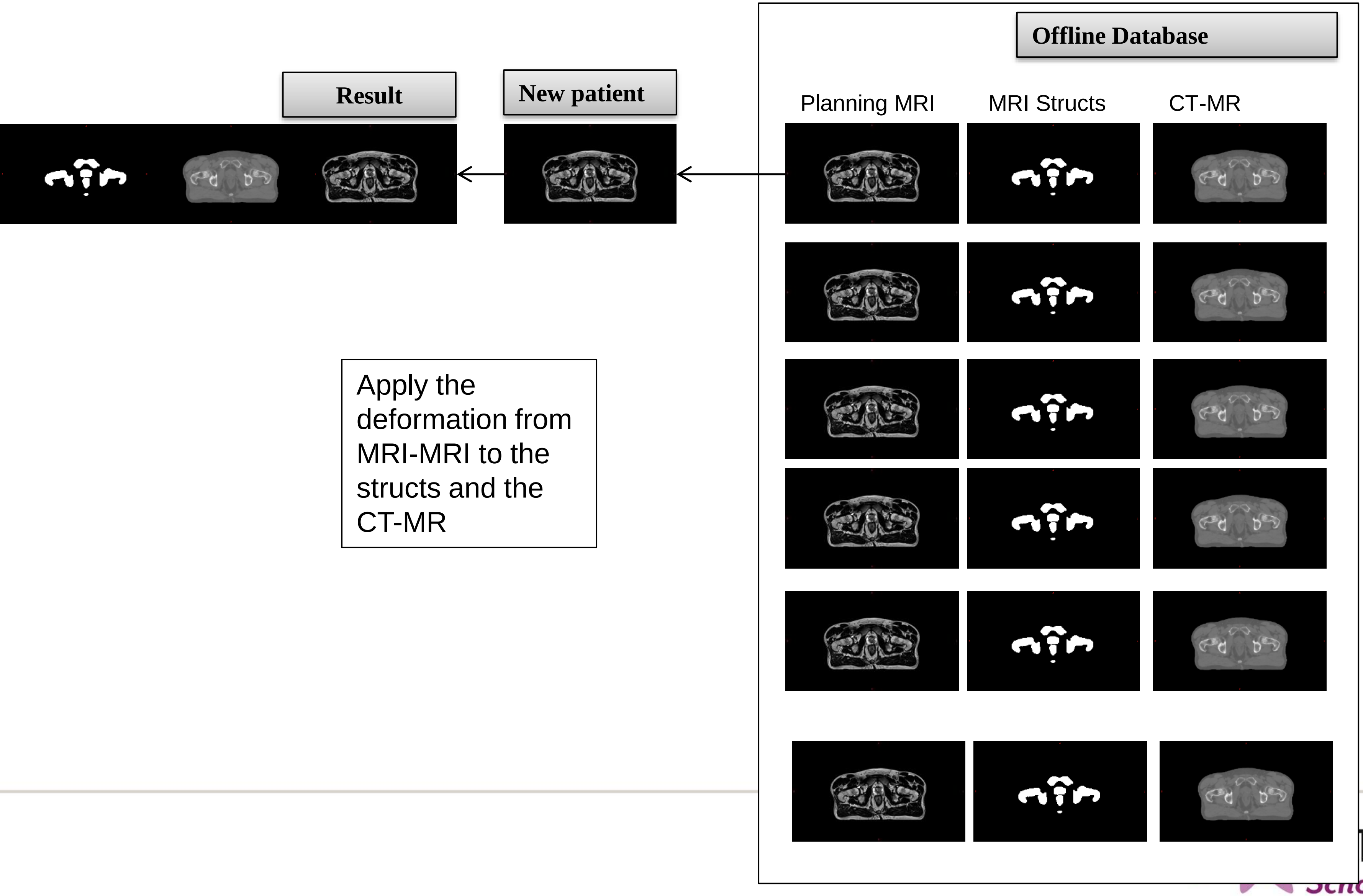

Offline Database

Planning MRI

MRI Structs

CT-MR

New patient

Result

Apply the deformation from MRI-MRI to the structs and the CT-MR

sCT: Multi-Patient Atlas approach

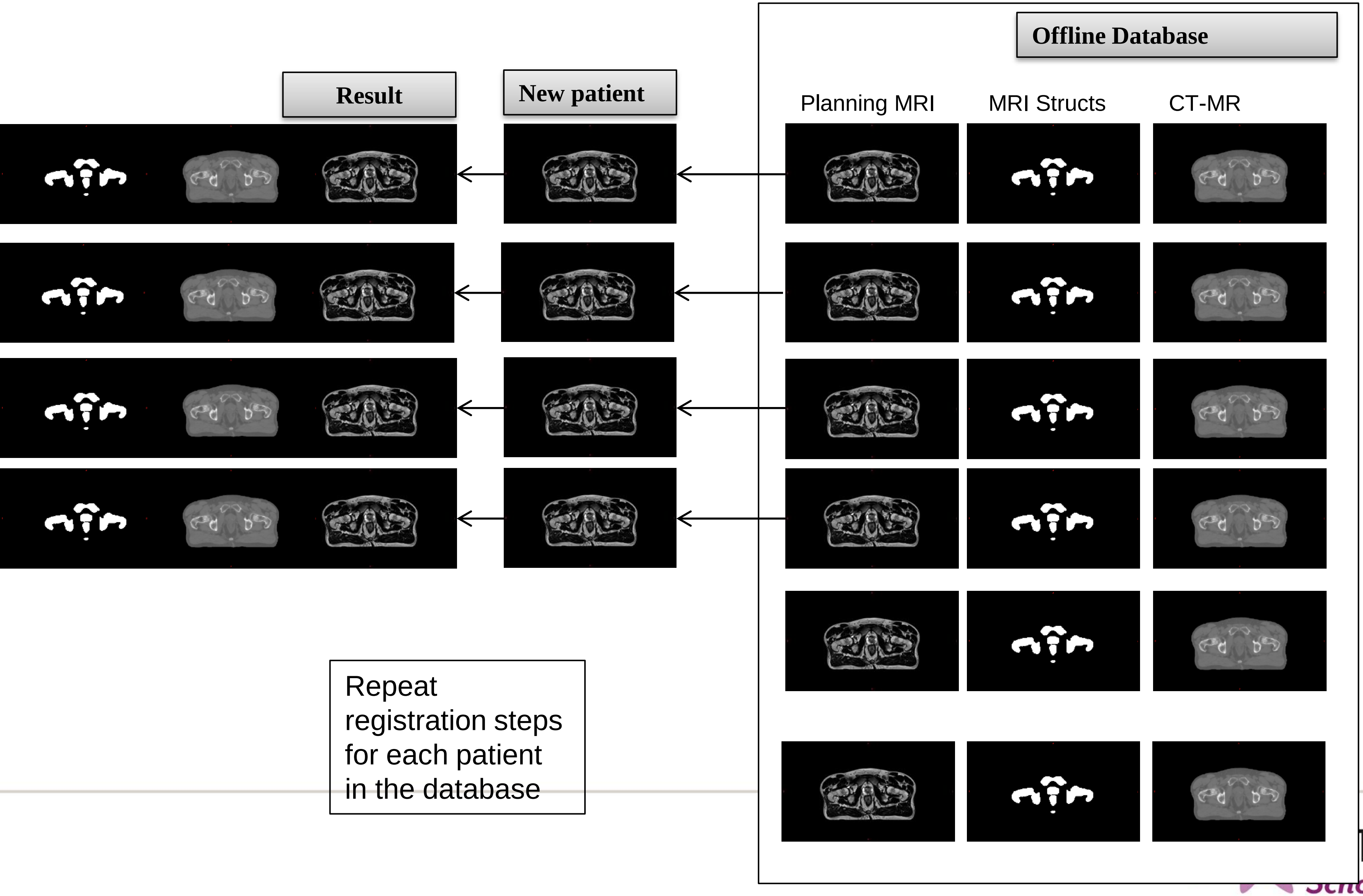

Offline Database

Result

New patient

Planning MRI

MRI Structs

CT-MR

Repeat registration steps for each patient in the database

sCT: Multi-Patient Atlas approach

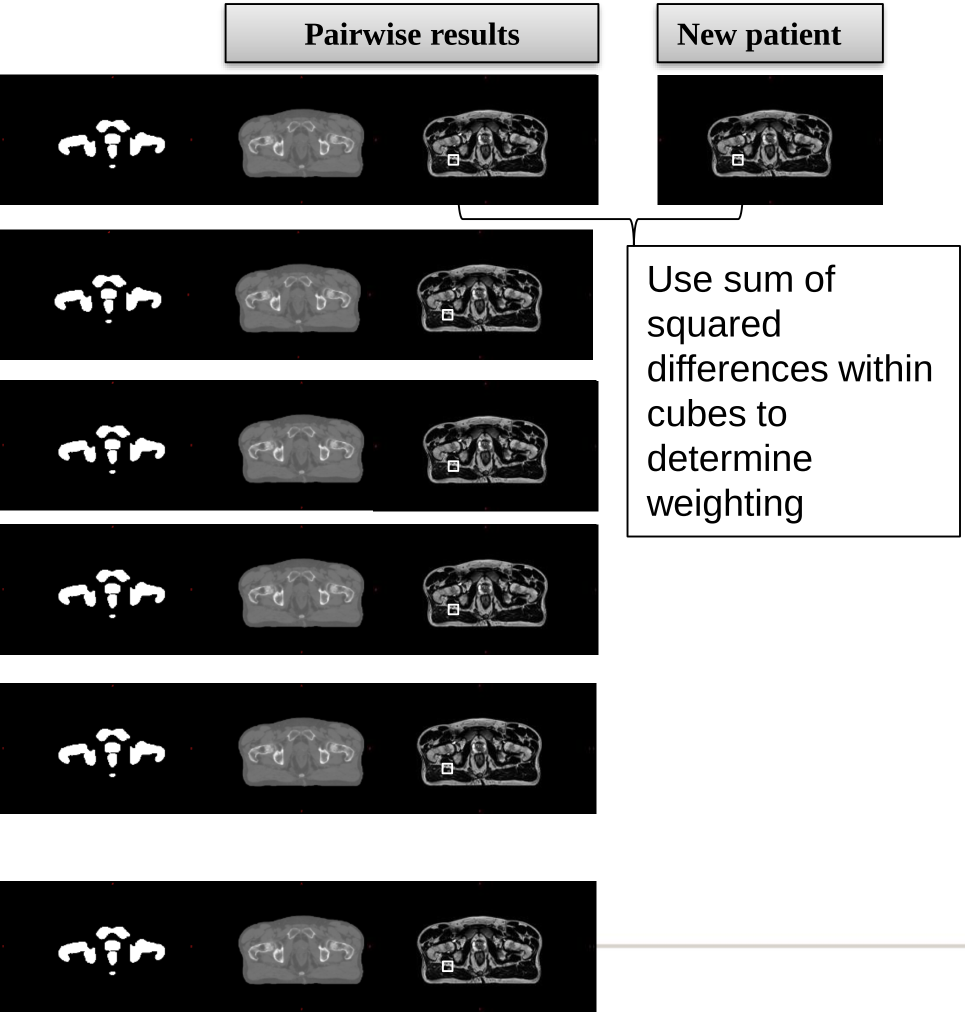

Pairwise results

New patient

Use sum of squared differences within cubes to determine weighting

The CT images are then combined to generate a sCT for the current patient

Robustness

sequence →

sCT ↓

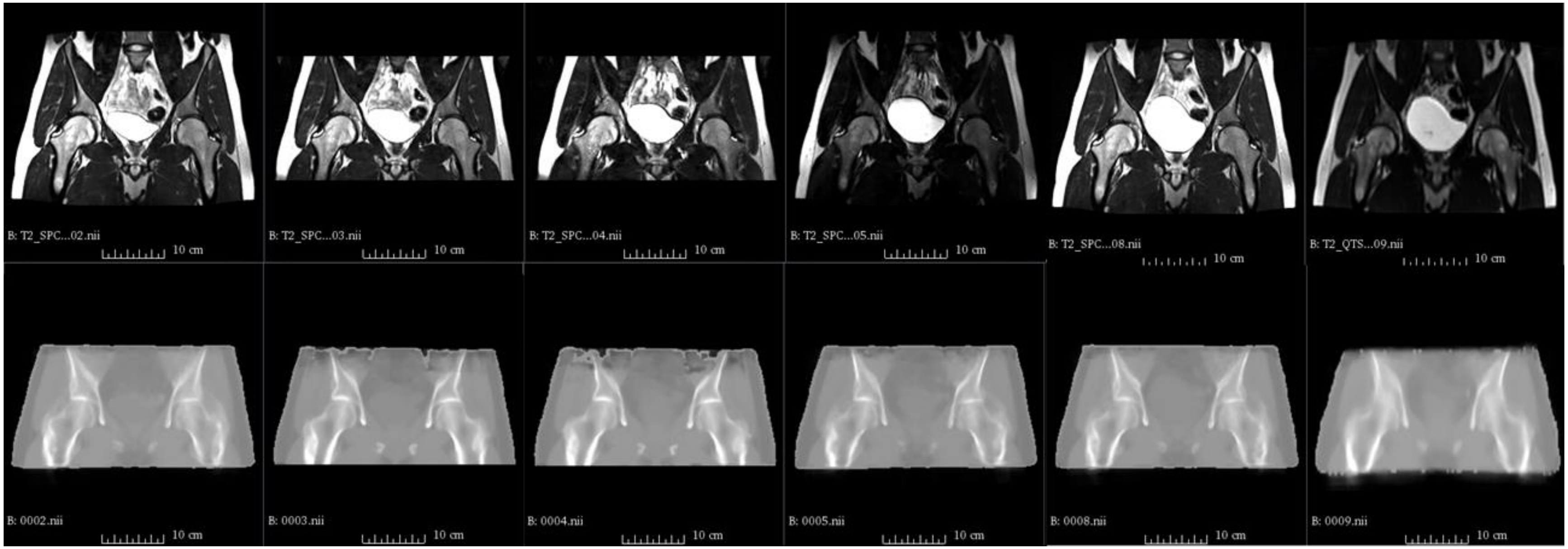
B: T2_SPC...02.nii
10 cm
B: T2_SPC...03.nii
10 cm
B: T2_SPC...04.nii
10 cm
B: T2_SPC...05.nii
10 cm
B: T2_SPC...08.nii
10 cm
B: T2_QTS...09.nii
10 cm
B: 0002.nii
10 cm
B: 0003.nii
10 cm
B: 0004.nii
10 cm
B: 0005.nii
10 cm
B: 0008.nii
10 cm
B: 0009.nii
10 cm

Variations in MRI protocol did not produce significant dosimetric changes in sCT.

Commercial Solutions (I)

MRCAT (Philips)

- Prostate
- Uses DIXON in-phase SI and bone atlas for bone shape/HU
- Uses DIXON (water and fat) to assign HU to soft-tissues

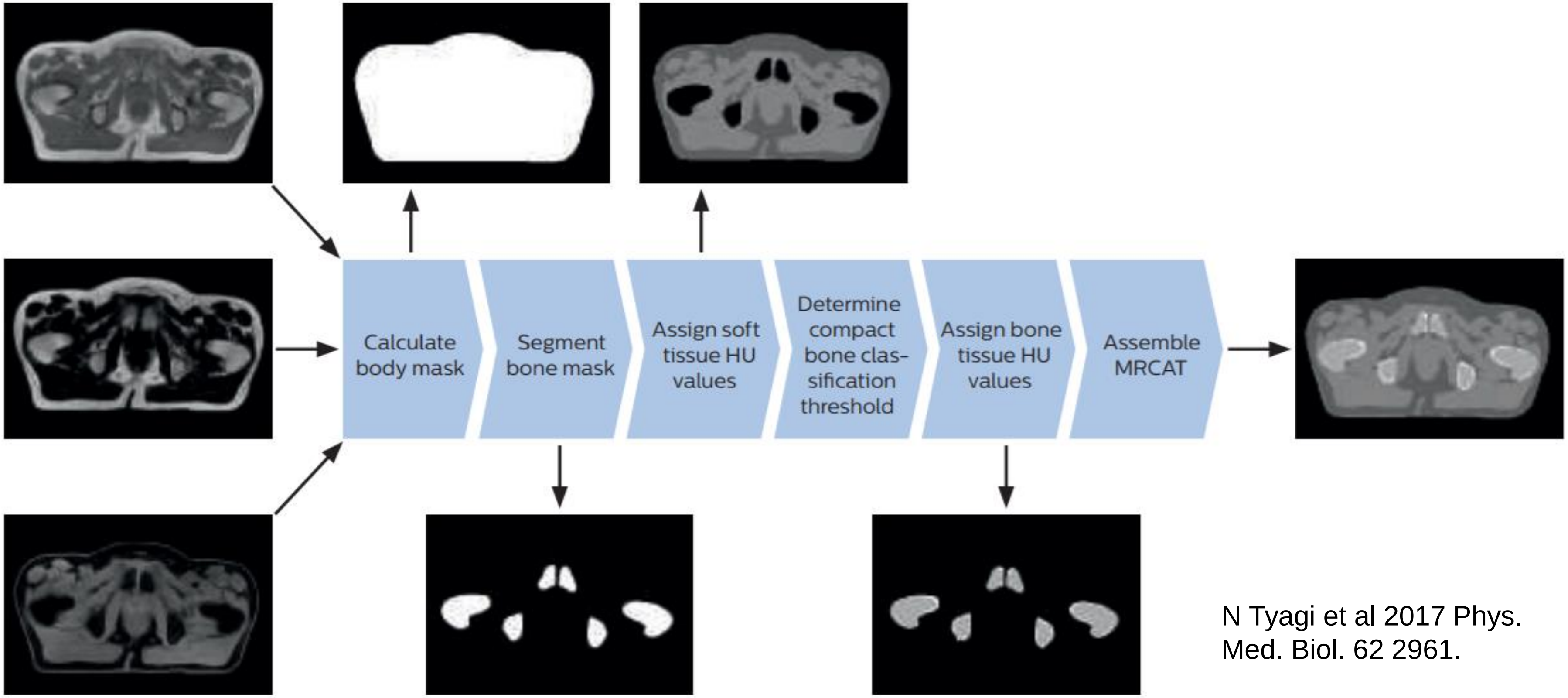
Calculate body mask
Segment bone mask
Assign soft tissue HU values
Determine compact bone classification threshold
Assign bone tissue HU values
Assemble MRCAT

N Tyagi et al 2017 Phys. Med. Biol. 62 2961.

Commercial Solutions (II)

MRIPlanner (Spectronic Medical, Sweden)

- See *Siversson et al Med. Phys 2015*
- Prostate
- Uses Statistical Decomposition Algorithm along with template Atlas
- Atlas of 15 patients
- T2-w SPACE or multislice 2D FSE was used similar results
- Possible slight worse with 3T (patient distortion lower BW)
- Speight at al showed similar results in other male pelvic sites

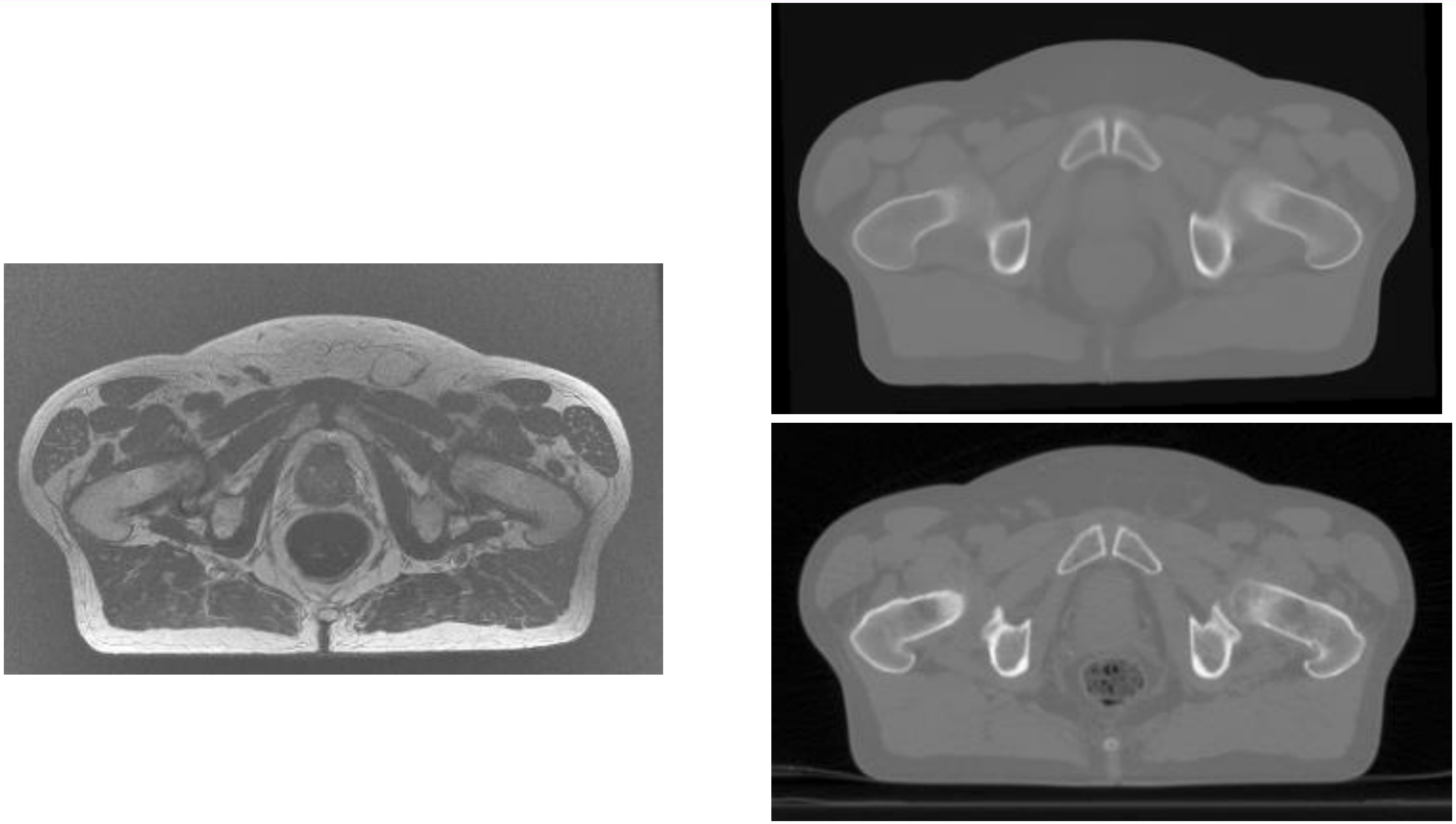

T_2-w MRI to the left, sCT generated using MRIPlanner (top right) & original CT (bottom right)

Commercial Solutions (III)

Siemens Healthcare (WIP)

- See *Hsu et al Phys Med Biol 2013*
- Brain
- Probabilistic approach using fuzzy c-means clustering with spatial constraint
- Requires input of 5 separate image series (6 contrasts)
- UTE & TOF used as masks

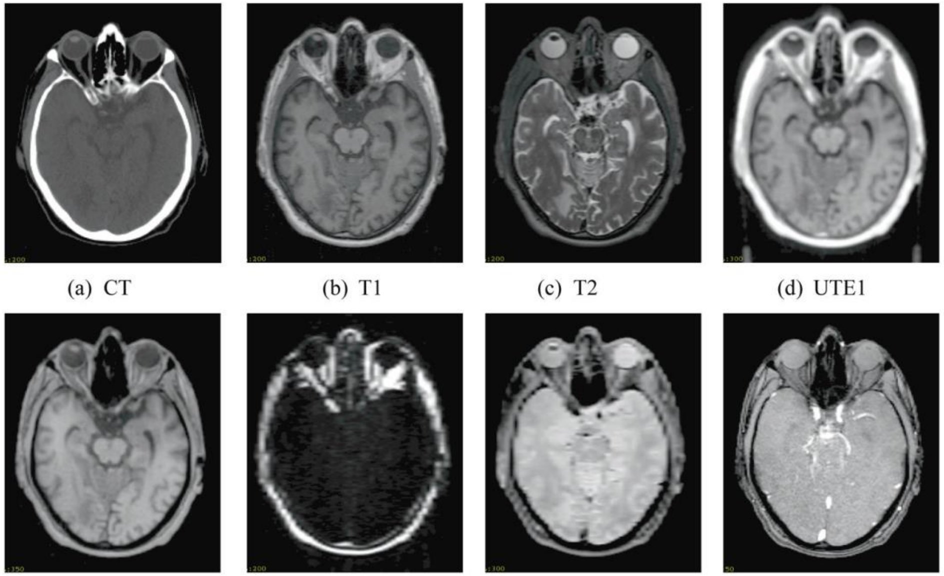
(a) CT (b) T1 (c) T2 (d) UTE1

(e) UTE2 (f) Fat (g) Water (h) Vessel

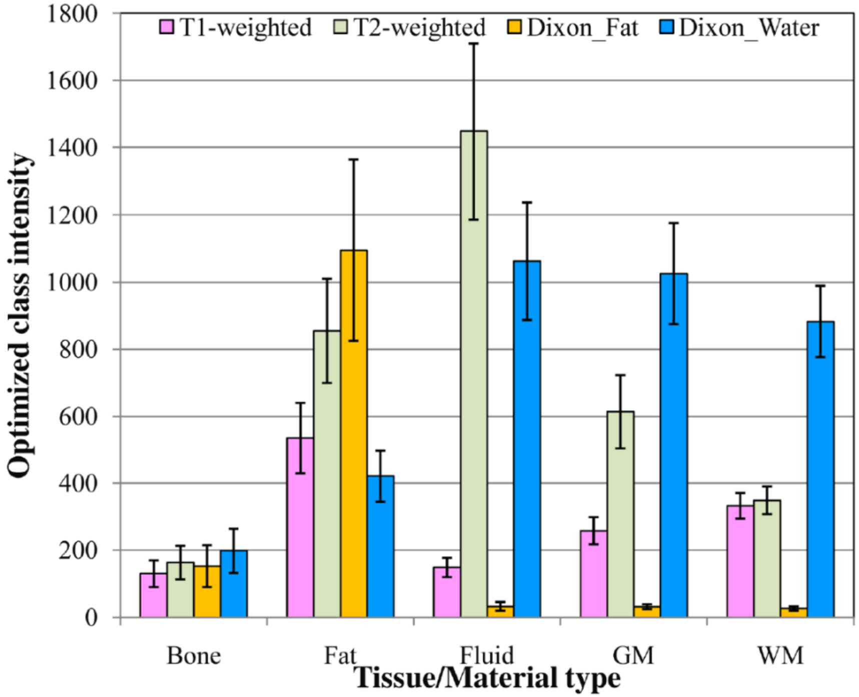

T_1, T_2, Dixon used in soft-tissue classifiers

UTE1 & TOF used as pre-processing masks

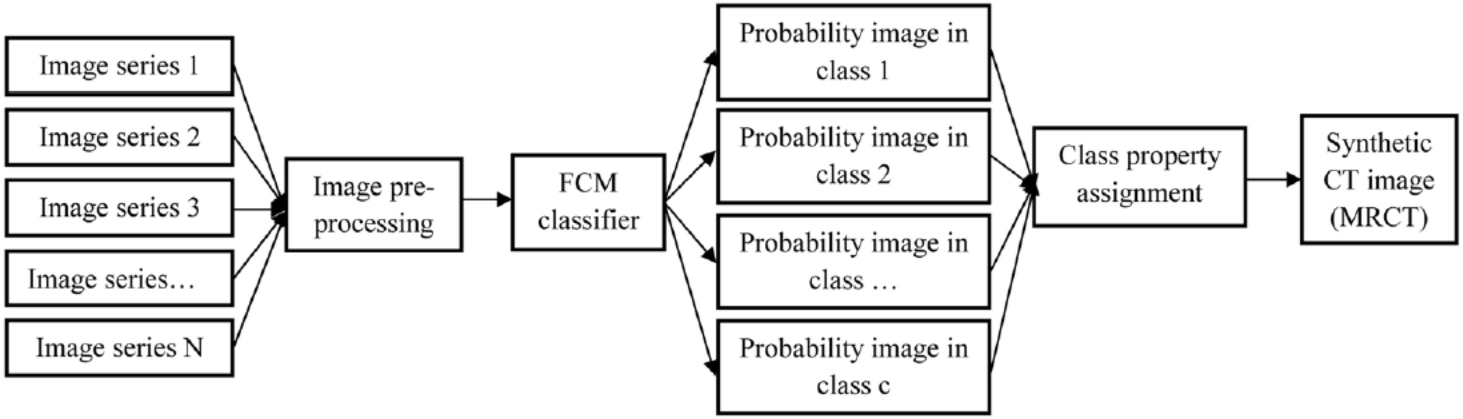

Image series 1

Image series 2

Image series 3

Image series…

Image series N

Image pre-processing

FCM classifier

Probability image in class 1

Probability image in class 2

Probability image in class …

Probability image in class c

Class property assignment

Synthetic CT image (MRCT)

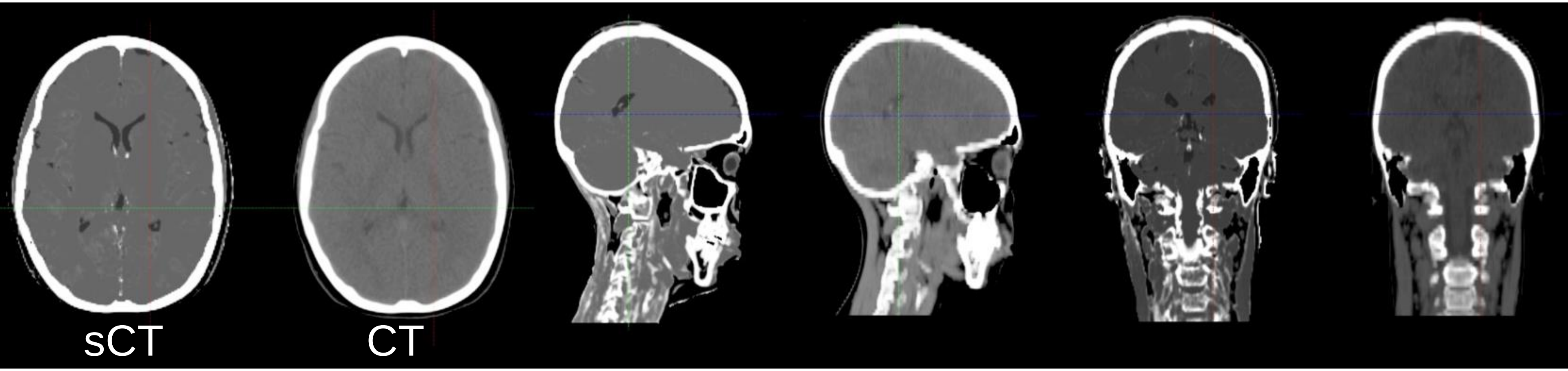

Multi-Centre Trials

MR-Only Prostate External RAdiotherpay (OPERA) trial

Persson et al 2017

4 Centres different scanners/field strength

170 prostates patients; whole FOV T2-w scan high BW

Commercial software (Spectronic Medical)

Dose 0.3%, gamma 99.97% PTV 2/2

Slight contour differences between CT & MR- density correction improves this (air/water etc)

HIgh precision Prostate Substitute CT External beam Radiotherapy (HIPSTER)

2 Australian Centres (Newcastle & Liverpool)

Phase I roll-out & QA stage

3D SPACE sequence & in-house (Atlas based) software

Trial currently in progress

Validation of sCT

A number of performance metrics are used:

Dose difference

- Percentage difference at prescription points, isocentre or DVH points

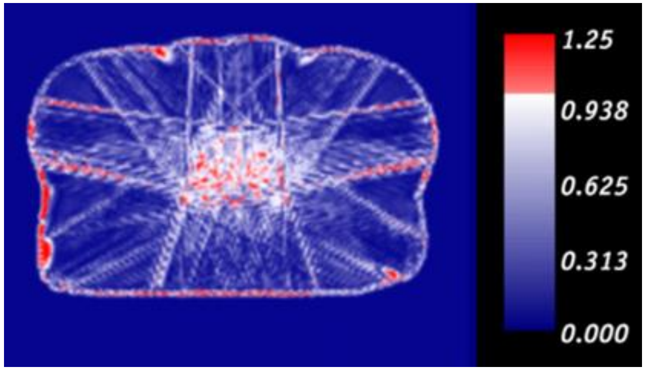
1.25
0.938
0.625
0.313
0.000

MAE

- Voxel-wise mean difference in HU; Values sensitive to inclusion of more soft-tissue or air

Overlap (DSC or MASD) in bone

- Dice similarity coefficient or Mean Hausendorf Distance

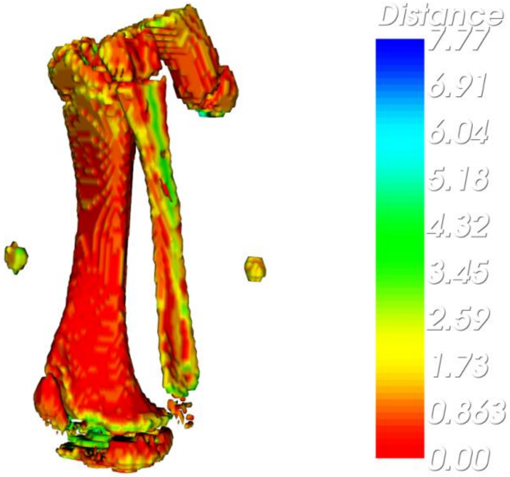
Distance
7.77
6.91
6.04
5.18
4.32
3.45
2.59
1.73
0.863
0.00

Gamma index

- Displayed as a map; combined distance to agreement and dose difference

Validation of sCT

*Typical values observed.

Dose difference

- Percentage difference at prescription points, isocentre or DVH points

0.3-2.5%

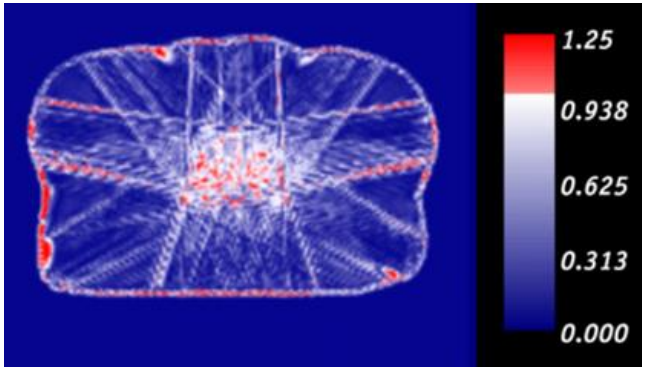
1.25
0.938
0.625
0.313
0.000

MAE

- Voxel-wise mean difference in HU; Values sensitive to inclusion of more soft-tissue or air

80-200 HU (brain) & 40 HU (prostate)

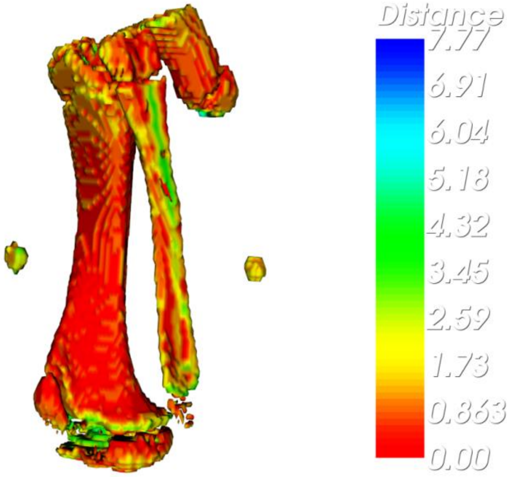
Distance
7.77
6.91
6.04
5.18
4.32
3.45
2.59
1.73
0.863
0.00

Overlap (DSC or MASD) in bone

- Dice similarity coefficient or Mean Hausendorf Distance

0.5 < DSC > 0.95

Gamma index

- Displayed as a map; combined distance to agreement and dose difference

2% & 2mm > 98%

*Edmund, J. M., & Nyholm, T. (2017).

MRg-RT: Current Status

System	Radiation type	Field strength	Magnet type	Orientation	1st Patient Tx
Elekta Unity	6 MV	1.5 T	Closed supercon	Perpendicular	May 2017
Australian	4 & 6 MV	1.0 T	Split supercon	Inline (and perp.)	Early 2018
Alberta	6 MV	0.5 T	High temp supercon with steel yoke	Inline	Not known
Viewray	^{60}Co or 6 MV	0.35 T	Split resistive	Perpendicular	July 2017 (Linac) February 2014 (Co)

MRg-RT

- 0.35 T MRI integrated with 3 Co-60 heads
- Integrated planning system Monte Carlo dose calculation
- Still use CT initially
- Use of manual bulk density override
- Whole exam typical 1 hour

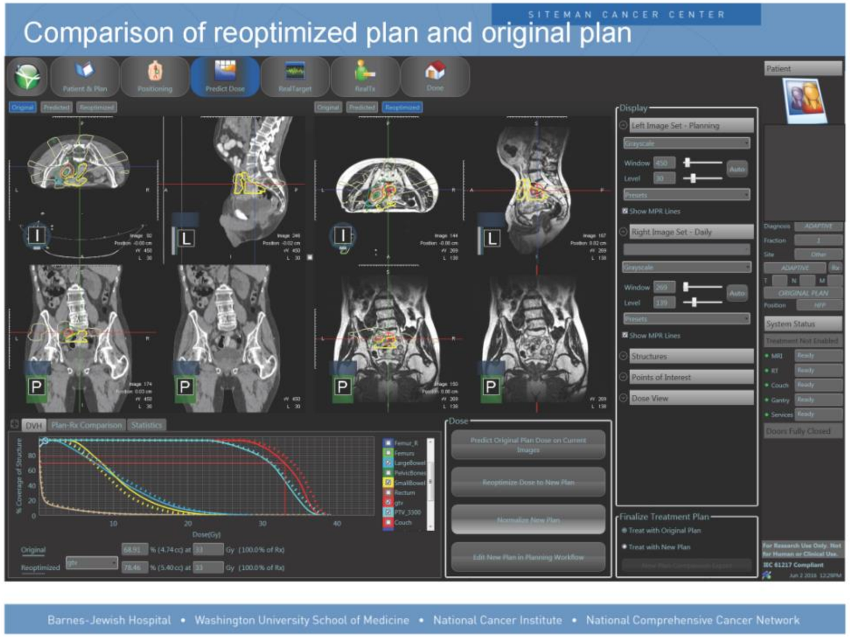

SITEMAN CANCER CENTER

Comparison of reoptimized plan and original plan

Barnes-Jewish Hospital • Washington University School of Medicine • National Cancer Institute • National Comprehensive Cancer Network

Summary

- MR-CT planning requires treatment position scans
- Diagnostic MRI possible with DIR
- Three main methods for sCT: tissue class, learning and atlas with some overlap
    - Most sCT papers focus on brain with MAE ~130 HU
    - Prostate MAE ~40 HU
- Commercial solutions for prostate include: MRCAT (Phillips), MRIPlanner (Spectronic) & research prototype (Siemens)
- Need for standardisation in approach, validation & implementation
- Further clinical trials

Acknowledgements

Thanks to following people for slides:

James Balter

Jason Dowling

Scott Hanvey

Juha Korhonen

Tufve Nyholm

Mike Roach

Richard Speight

CT Perfusion

Physical Principles, Clinical Application, Protocol Optimization

Francesco Pisana

German Cancer Research Center (DKFZ), Heidelberg, Germany

Index of Contents

- **Introduction:**
  - What is CT perfusion
  - Derived parameters
  - Different techniques
- **Models:**
  - Perfusion models introduction
  - One compartment models – maximum slope
  - Two compartments models – deconvolution, Toft, Patlak
- **Clinical applications and optimization:**
  - Oncology: liver, lung, other organs
  - Neurology: brain perfusion for stroke
  - Myocardial perfusion

Index of Contents

- **Introduction:**
  - What is CT perfusion
  - Derived parameters
  - Different techniques
- **Models:**
  - Perfusion models introduction
  - One compartment models – maximum slope
  - Two compartments models – deconvolution, Toft, Patlak
- **Clinical applications and optimization:**
  - Oncology: liver, lung, other organs
  - Neurology: brain perfusion for stroke
  - Myocardial perfusion

What is CT Perfusion (CTP)

- Dynamic scan.
- Normally c.ca 30 volumes are acquired over a time of c.ca 1 minute.
- Functional information.

General Workflow

- Topogram.
- Planning.
- Test bolus. For example: 10 mL contrast @ 5 or 6 mL/s + 50 mL saline @ same flow.
- Set perfusion scan parameters. For example: 45 mL contrast @ 5 or 6 mL/s + 50 mL saline @ same flow
- Set delay of perfusion scan.
- Set injection parameters.

Klotz et al: “Technical prerequisites and imaging protocols for CT perfusionimaging in oncology”, *Eur J Radiol* **84**, (2015)

What is CT Perfusion (CTP)

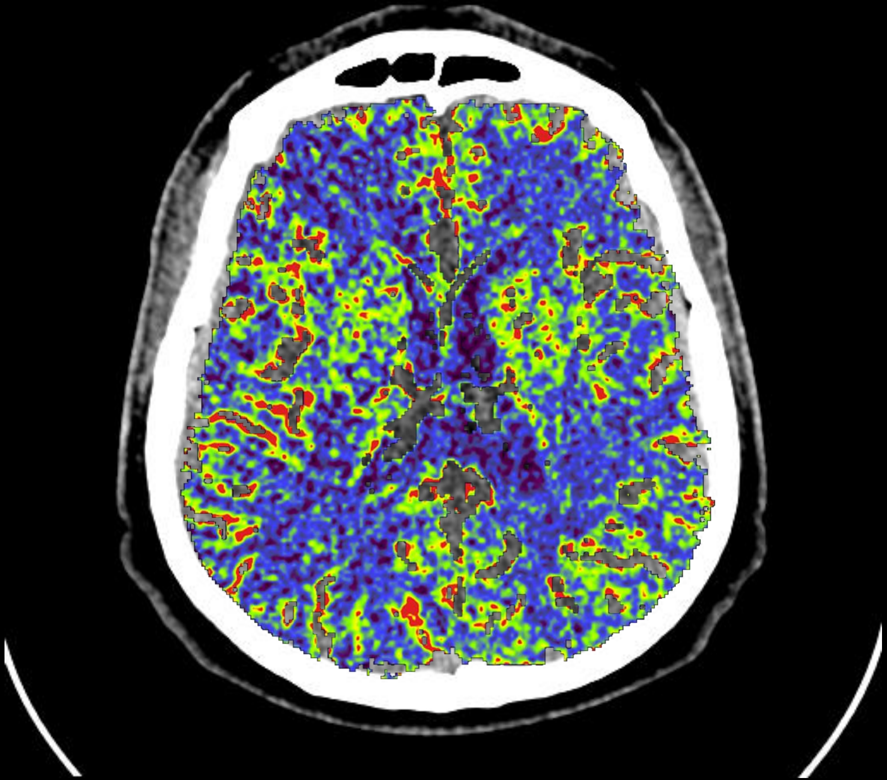

C = 80 HU, W = 200 HU

What is CT Perfusion (CTP)

- Time-attenuation curves (TACs).
- Baseline to be acquired.
- Motion to be avoided.

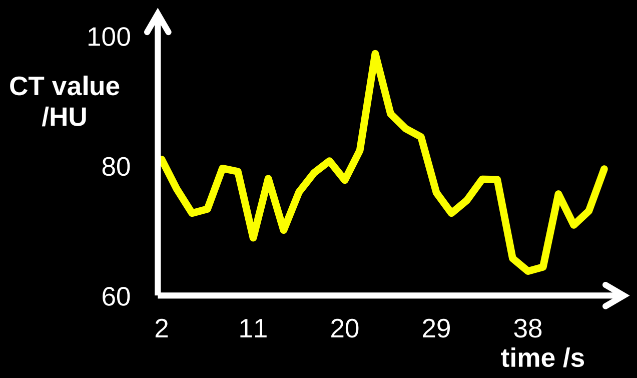

What is CT Perfusion (CTP)

In reality TACs SNR is very poor.

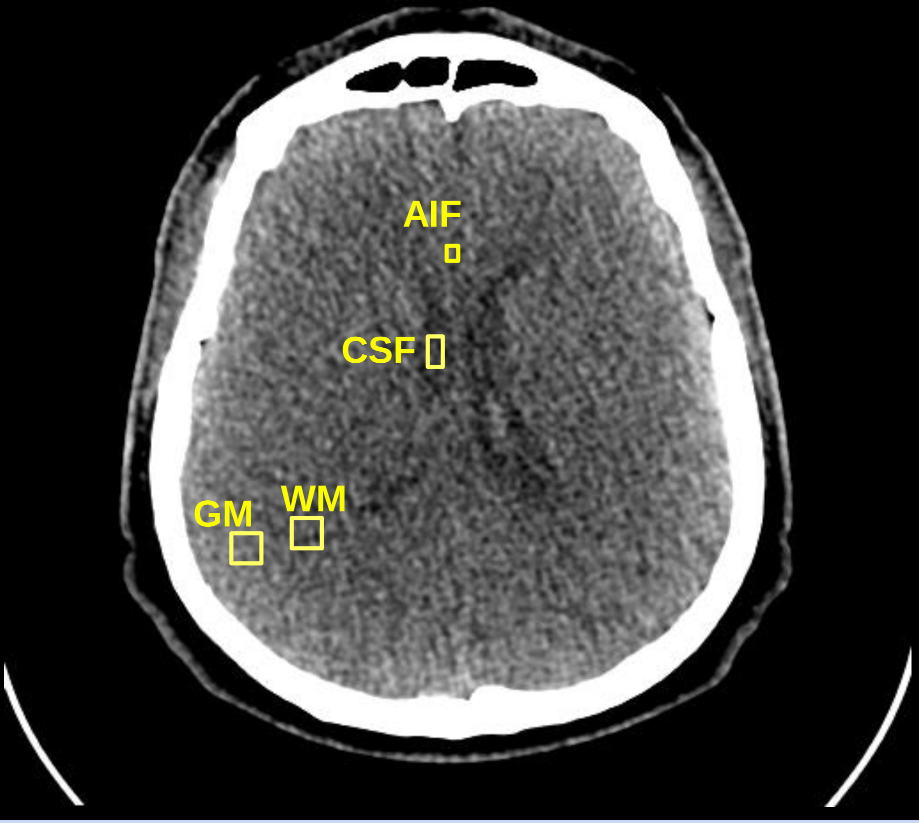
AIF
CSF
GM
WM

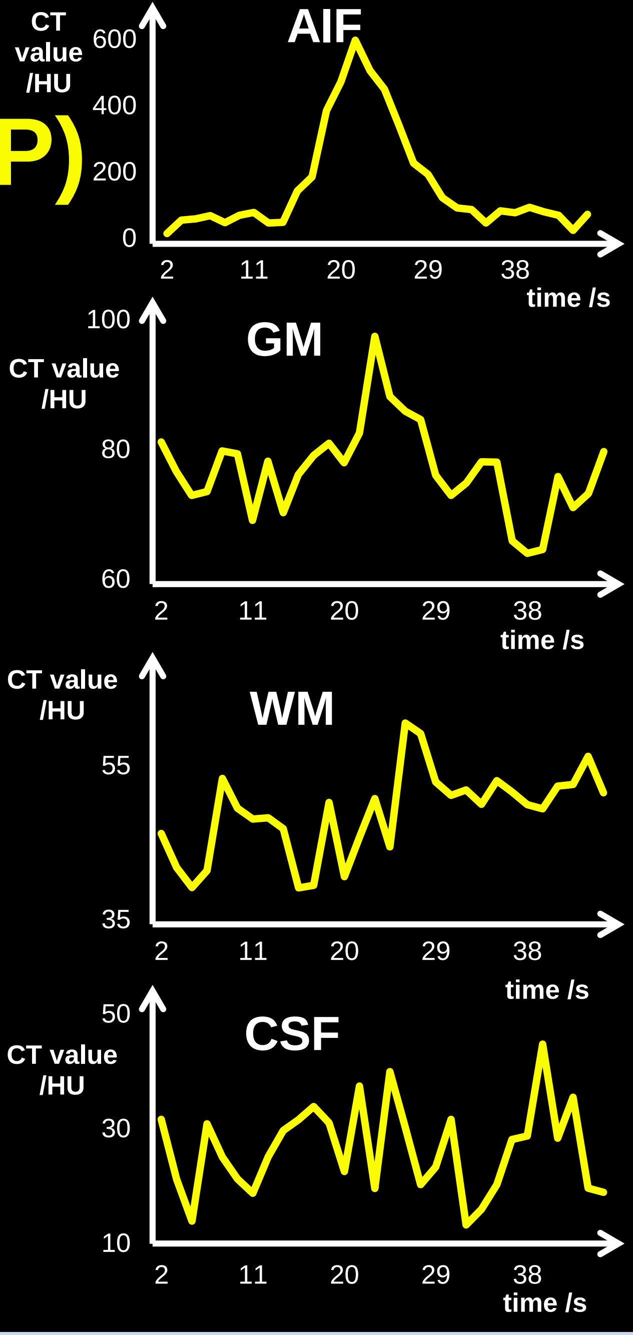

C = 80 HU, W = 200 HU

What is CT Perfusion (CTP)

Taking one single voxel:

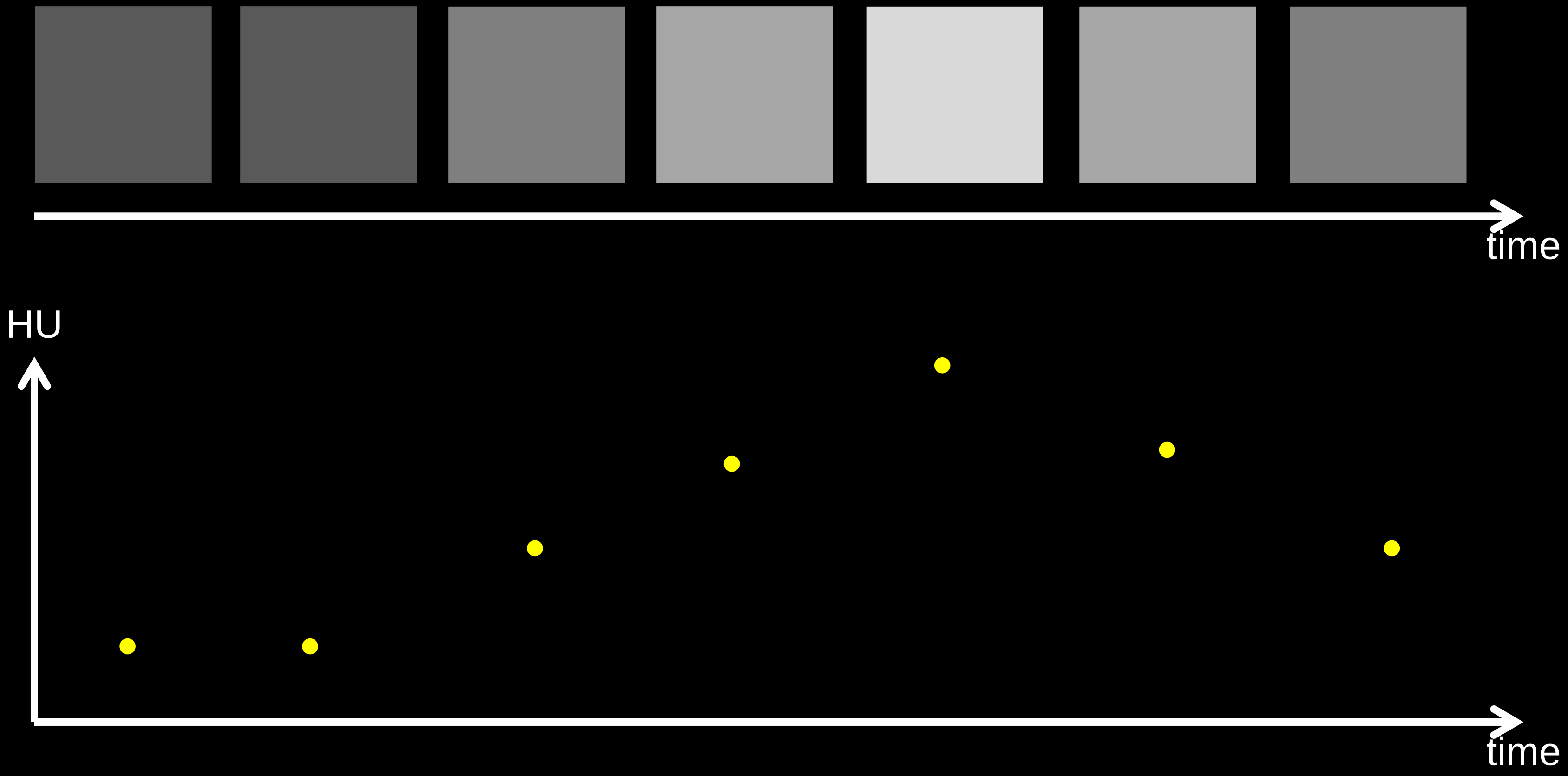
time
HU
time

What is CT Perfusion (CTP)

If we could look inside one single voxel:

- What we see:

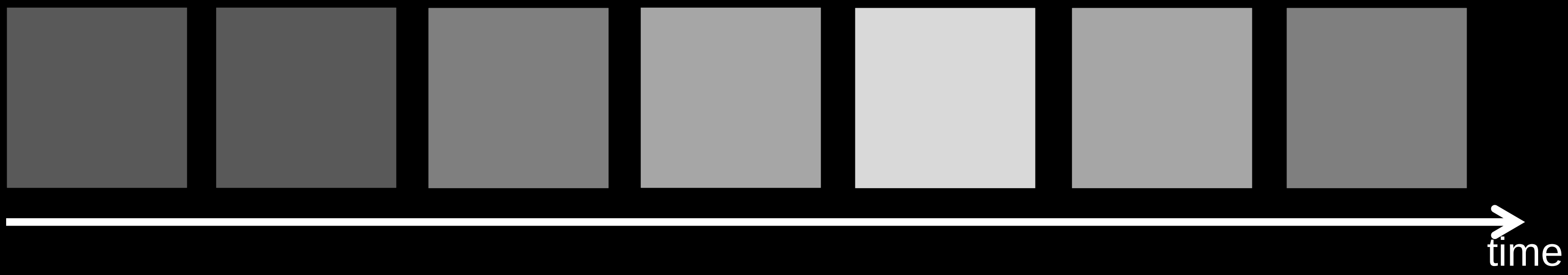

- What happens really (capillaries):

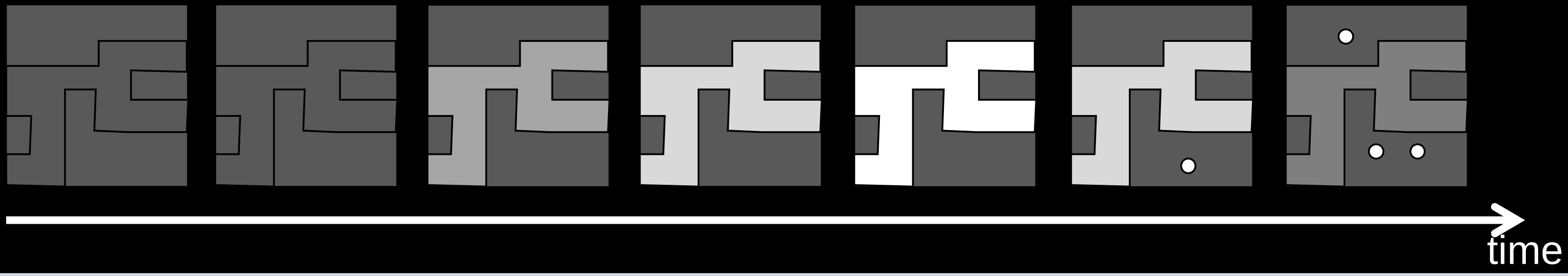

Index of Contents

- Introduction:
  - What is CT perfusion
  - Derived parameters
  - Different techniques
- Models:
  - Perfusion models introduction
  - One compartment models – maximum slope
  - Two compartments models – deconvolution, Toft, Patlak
- Clinical applications and optimization:
  - Oncology: liver, lung, other organs
  - Neurology: brain perfusion for stroke
  - Myocardial perfusion

Derived Parameters

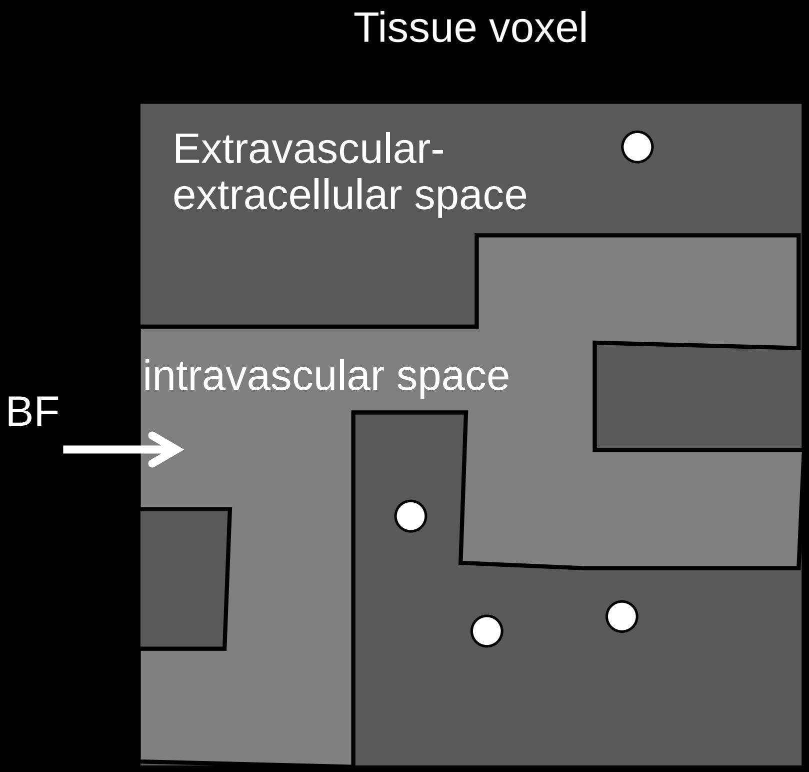
Tissue voxel
Extravascular-
extracellular space
intravascular space
BF

Blood flow (BF): volume of contrast media entering the voxel in one unit of time (in mL/min), normalized by one unit of volume (typically 100 mL). The unit of measure is

$$\frac{\mathrm{mL}}{\mathrm{min} \cdot 100\,\mathrm{mL}}$$

Tofts: "Modeling Tracer Kinetick in Dynamic Gd-DTPA MR Imaging" *JMRI* 7(1), 92-101 (1997)

Derived Parameters

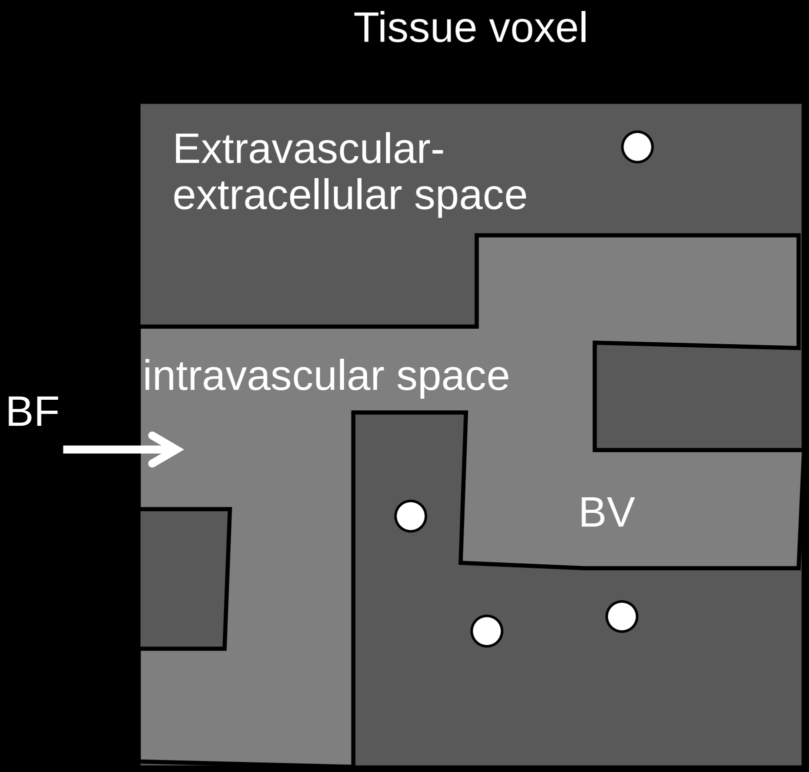
Tissue voxel
Extravascular-
extracellular space
intravascular space
BF
BV

Blood volume (BV): volume of contrast media allowable in the voxel (mL), normalized by one unit of volume (typically 100 mL).
Unit of measure: $\frac{\text{mL}}{100\,\text{mL}}$

Tofts: “Modeling Tracer Kinetick in Dynamic Gd-DTPA MR Imaging” *JMRI* **7(1)**, 92-101 (1997)

Derived Parameters

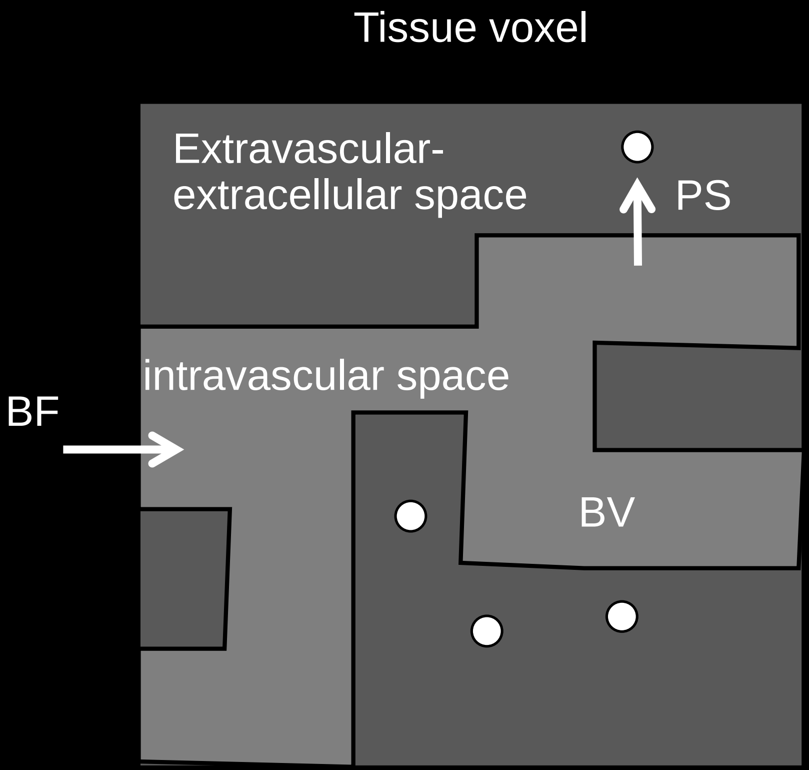
Tissue voxel
Extravascular-
extracellular space
PS
intravascular space
BF
BV

Permeability-surface area product (PS): volume of contrast media exiting the intravascular space and entering the extravascular-extracellular space (EES) in one unit of time, normalized by one unit of volume.

Unit of measure:

$$\frac{\mathrm{mL}}{\mathrm{min} \cdot 100\,\mathrm{mL}}$$

Tofts: “Modeling Tracer Kinetick in Dynamic Gd-DTPA MR Imaging” *JMRI* **7(1)**, 92-101 (1997)

Derived Parameters

Other parameters:

- Extraction fraction (*E*): average volume of contrast media allowable in the extravascular-extracellualr space (EES):

$$E = 1 - e^{-\frac{\mathrm{PS}}{\mathrm{BF}}}$$

if BF>>PS (like for tumors) we can write:

$$E \simeq \frac{\mathrm{PS}}{\mathrm{BF}}$$

, dimensionless.

- k^{trans}: constant of transfer from intravascular space to EES. It is closely related to PS, and often given instead of it, under the assumption BF>>PS.

$$k^{\mathrm{trans}} = E \cdot \mathrm{BF} \simeq \mathrm{PS}$$

Unit of measure $$\frac{\mathrm{mL}}{\mathrm{min} \cdot 100\,\mathrm{mL}}$$

Tofts: “Modeling Tracer Kinetick in Dynamic Gd-DTPA MR Imaging” *JMRI* **7(1)**, 92-101 (1997)

Derived Parameters

- Mean transit time (MTT): average time needed from one single molecule of contrast media to transit through the voxel.
- Time to peak (TTP): time of maximum concentration in the voxel.
- Time to start (TTS): time of contrast media arrival.

Tofts: “Modeling Tracer Kinetick in Dynamic Gd-DTPA MR Imaging” *JMRI* **7(1)**, 92-101 (1997)

Index of Contents

- Introduction:
  - What is CT perfusion
  - Derived parameters
  - Different techniques
- Models:
  - Perfusion models introduction
  - One compartment models – maximum slope
  - Two compartments models – deconvolution, Toft, Patlak
- Clinical applications and optimization:
  - Oncology: liver, lung, other organs
  - Neurology: brain perfusion for stroke
  - Myocardial perfusion

GE Revolution CT

Philips IQon Spectral CT

Siemens Somatom Force

SIEMENS
SOMATOM Force

Toshiba Aquilion ONE Vision

Different Techniques

Coverage increase:

- Heterogeneous tumors.
- Absence of a-priori knowledge.
- Motion compensation.

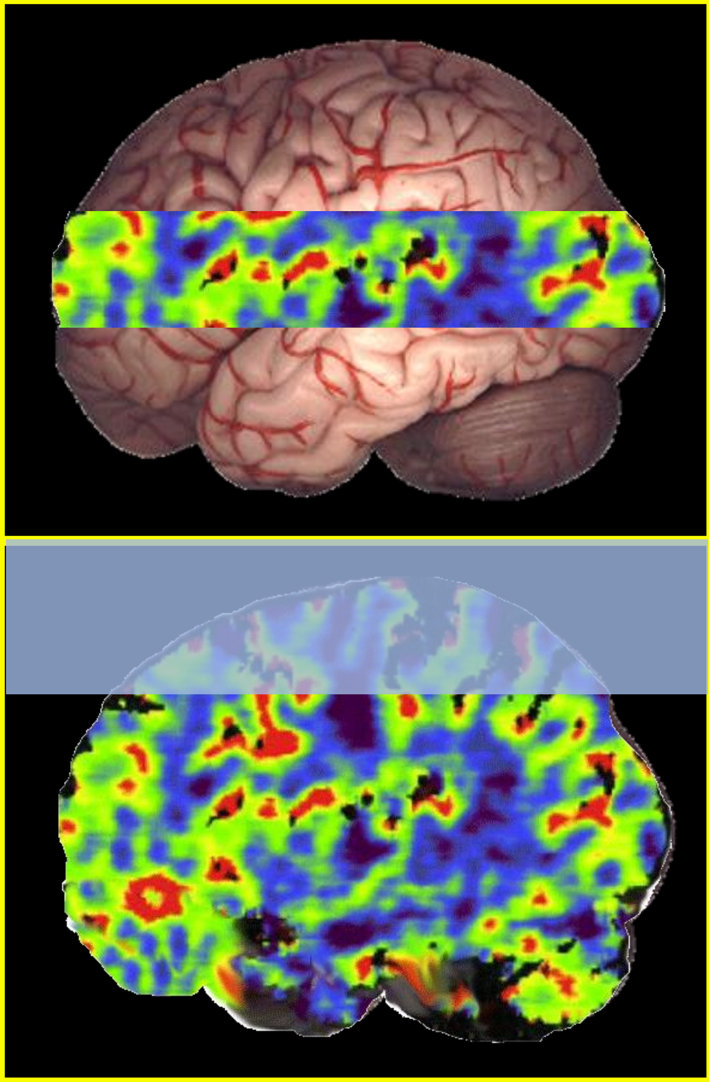

Different Techniques

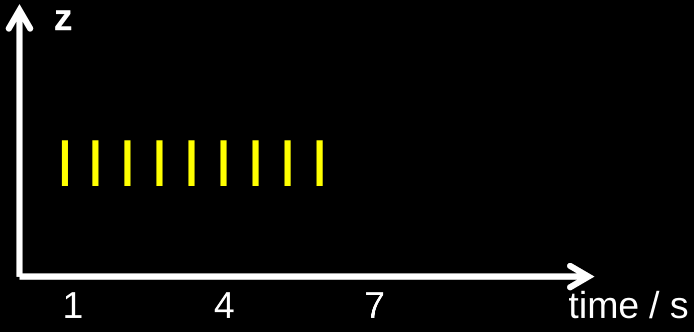

CTP. The coverage is limited to detector coverage, which is normally ~ 40 mm.

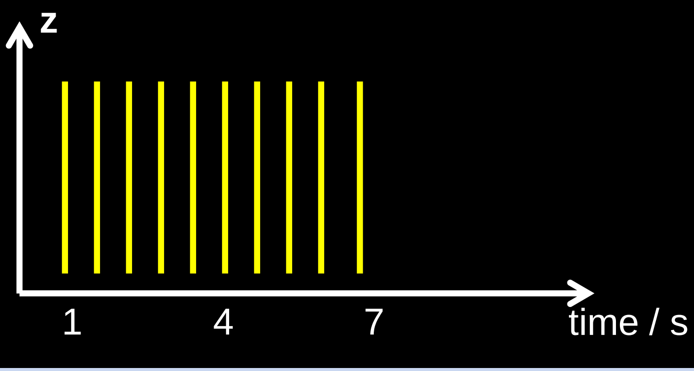

CTP high detector coverage.
Coverage is ~ 160 mm.

Different Techniques

Shuttle mode.

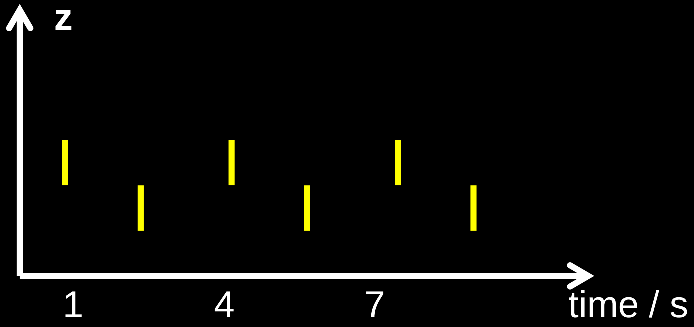

Adaptive spiral mode.

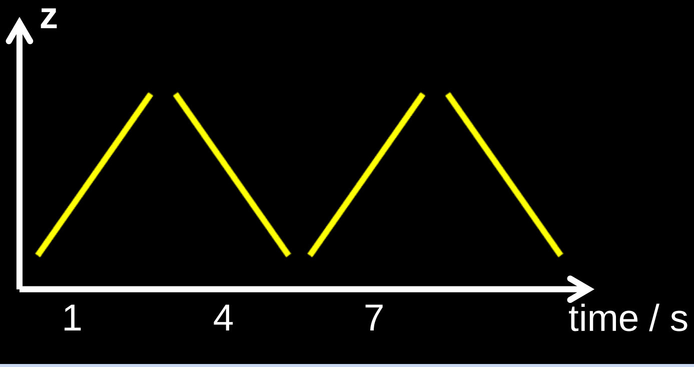

Index of Contents

- Introduction:
  - What is CT perfusion
  - Derived parameters
  - Different techniques
- Models:
  - Perfusion models introduction
  - One compartment models – maximum slope
  - Two compartments models – deconvolution, Toft, Patlak
- Clinical applications and optimization:
  - Oncology: liver, lung, other organs
  - Neurology: brain perfusion for stroke
  - Myocardial perfusion

Perfusion Models Introduction

At the basis of each model there is a simple and intuitive formulation made by Fick:

$$c_{\mathrm{t}}(t) = \mathrm{BF}_{\mathrm{in}} \int_0^t c_{\mathrm{a}}(t)\,dt - \mathrm{BF}_{\mathrm{out}} \int_0^t c_{\mathrm{v}}(t)\,dt$$

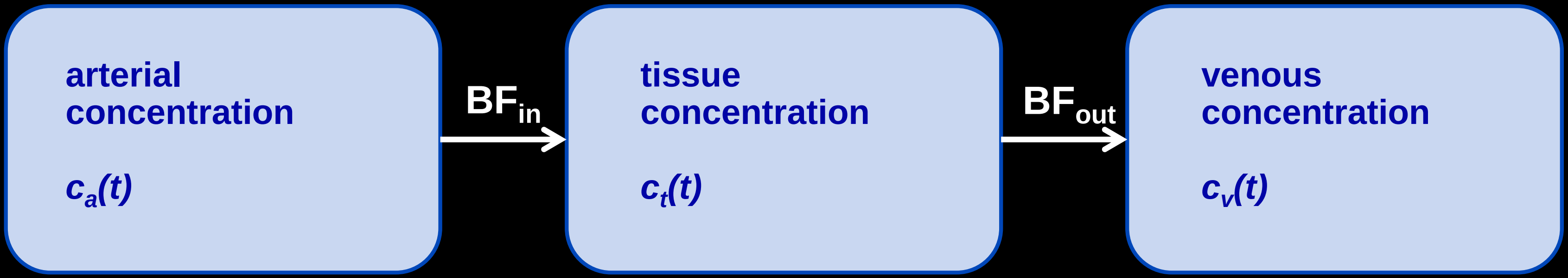
arterial concentration

$c_a(t)$

BF_{in}

tissue concentration

$c_t(t)$

BF_{out}

venous concentration

$c_v(t)$

Since the outflow from tissue to the venous system is of less clinical interest, it is normally not investigated. It is relatively safe to assume $BF_{in} = BF_{out} = BF$

Perfusion Models Introduction

Fick´s principle becomes:

$$c_{\mathrm{t}}(t) = \mathrm{BF} \int_0^t \big(c_{\mathrm{a}}(t) - c_{\mathrm{v}}(t)\big)dt$$

- Same AIF for each voxel.
- Different assumptions on vein.

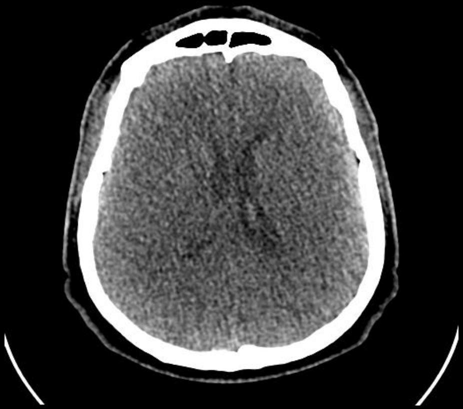

Index of Contents

- **Introduction:**
  - What is CT perfusion
  - Derived parameters
  - Different techniques
- **Models:**
  - Perfusion models introduction
  - One compartment models – maximum slope
  - Two compartments models – deconvolution, Toft, Patlak
- **Clinical applications and optimization:**
  - Oncology: liver, lung, other organs
  - Neurology: brain perfusion for stroke
  - Myocardial perfusion

One Compartment Models
Maximum Slope

$$c_\mathrm{t}(t) = \mathrm{BF} \int_0^t \big(c_\mathrm{a}(t) - c_\mathrm{v}(t)\big)\, dt$$

Maximum slope model simply assumes $c_v(t) = 0$

$$c_\mathrm{t}(t) = \mathrm{BF} \int_0^t c_\mathrm{a}(t)\, dt \quad \Rightarrow \quad \frac{d}{dt} c_\mathrm{t}(t) = \mathrm{BF}\, c_\mathrm{a}(t) \quad \Rightarrow \quad \frac{d}{dt} c_\mathrm{t}(t)\Big|_\mathrm{max} = \mathrm{BF}\, c_\mathrm{a}(t)\Big|_\mathrm{max}$$

According to this model, the maximum slope of tissue TAC occur at the same time of arterial peak, and their ratio gives the blood flow.

$$\mathrm{BF} = \frac{\frac{d}{dt} c_\mathrm{t}(t)\Big|_\mathrm{max}}{c_\mathrm{a}(t)\Big|_\mathrm{max}}$$

One Compartment Models
Maximum Slope

Correct acquisition

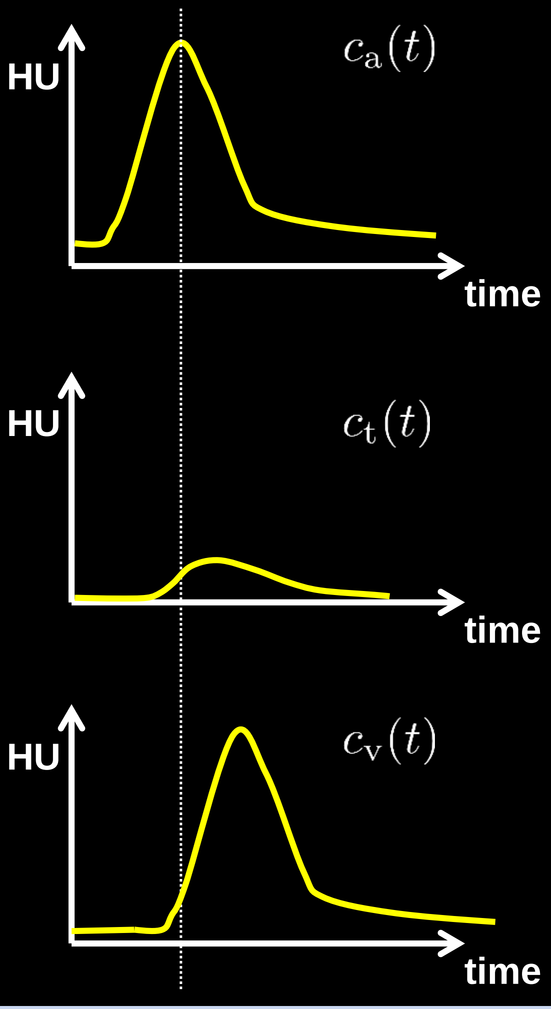

- Few points used.
- Empty vein assumption.
- Robust to noise and artifacts.
- Short times.
- High sampling time.
- Not all parameters are calculated.

One Compartment Models
Maximum Slope

Incorrect acquisition

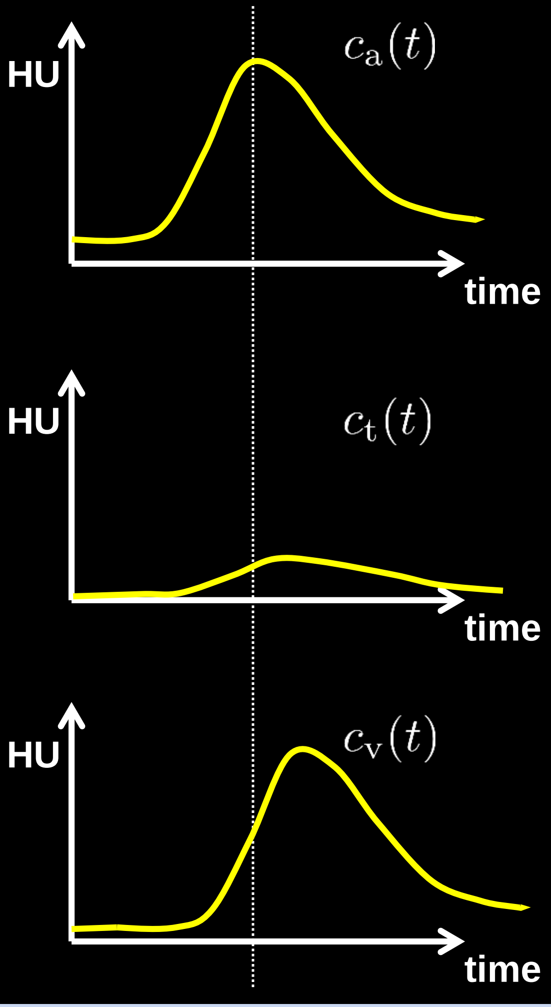

- Few points used.
- Empty vein assumption.
- Robust to noise and artifacts.
- Short times.
- High sampling time.
- Not all parameters are calculated.

Index of Contents

- Introduction:
  - What is CT perfusion
  - Derived parameters
  - Different techniques
- Models:
  - Perfusion models introduction
  - One compartment models – maximum slope
  - Two compartments models – deconvolution, Toft, Patlak
- Clinical applications and optimization:
  - Oncology: liver, lung, other organs
  - Neurology: brain perfusion for stroke
  - Myocardial perfusion

Two Compartments Models
Deconvolution

$$c_{\mathrm{t}}(t) = \mathrm{BF} \int_0^t \big(c_{\mathrm{a}}(t) - c_{\mathrm{v}}(t)\big)\, dt$$

The deconvolution model assumes $c_{\mathrm{v}}(t) = p(t) * c_{\mathrm{a}}(t)$ where

$p(t)$ is the probability that a molecule of contrast takes time *t* to transit through the tissue voxel.
Now we can write:

$$c_{\mathrm{t}}(t) = \mathrm{BF} \int_0^t \big(c_{\mathrm{a}}(t) - c_{\mathrm{v}}(t)\big) dt \;=\; \mathrm{BF} \int_0^t \big(c_{\mathrm{a}}(t) - p(t) * c_{\mathrm{a}}(t)\big) dt = \mathrm{BF}\; c_{\mathrm{a}}(t) * \left(1 - \int_0^t p(t) dt\right)$$

$\int_0^t p(t)\, dt$ is the probability that a molecule of contrast is already in the vein at time *t*.

$1 - \int_0^t p(t)\, dt$ is the probability that a molecule of contrast is still in the tissue voxel at time *t*. This quantity is also called IRF (impulse response function).

Fieselman et al: “Deconvolution-Based CT and MR Brain Perfusion Measurement: Theoretical Model Revisited and Practical Implementation Details”, *International Journal of Biomedical Images* (2011).

Two Compartments Models
Deconvolution

$$p(t)$$

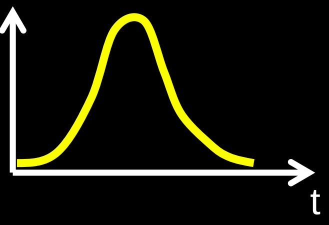

$$\int_0^t p(t)\,dt$$

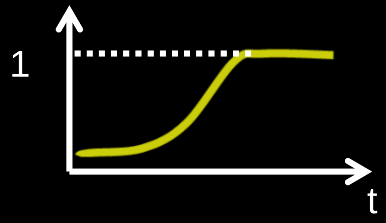

$$1 - \int_0^t p(t)\,dt = \mathrm{IRF}(t)$$

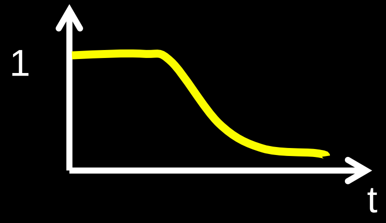

$$c_{\mathrm{t}}(t) = \mathrm{BF}\int_0^t \big(c_{\mathrm{a}}(t) - c_{\mathrm{v}}(t)\big)dt = \mathrm{BF}\, c_{\mathrm{a}}(t) * \mathrm{IRF}(t)$$

Fieselman et al: “Deconvolution-Based CT and MR Brain Perfusion Measurement: Theoretical Model Revisited and Practical Implementation Details”, *International Journal of Biomedical Images* (2011).

Two Compartments Models Deconvolution

$$c_{\mathrm{t}}(t) = \mathrm{BF}\int_{0}^{t}\big(c_{\mathrm{a}}(t) - c_{\mathrm{v}}(t)\big)dt = \mathrm{BF}\, c_{\mathrm{a}}(t) * \mathrm{IRF}(t)$$

Deconcolving the tissue TAC with the arterial input function, would result in a BF-scaled IRF:

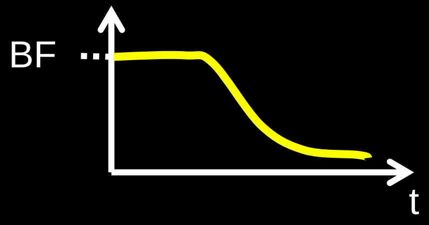

There are different ways to perform the deconvolution step, and different assumptions that can be made to model the obtained IRF and to calculate different parameters.

Fieselman et al: “Deconvolution-Based CT and MR Brain Perfusion Measurement: Theoretical Model Revisited and Practical Implementation Details”, *International Journal of Biomedical Images* (2011).

Two Compartments Models Deconvolution

In matrix form, we can write:

$$\begin{pmatrix} c_v(t_1) \\ c_v(t_2) \\ \vdots \\ c_v(t_T) \end{pmatrix} = \mathrm{BF} \cdot \begin{pmatrix} c_a(t_1) & 0 & 0 & 0 \\ c_a(t_2) & c_a(t_1) & \cdots & 0 \\ \vdots & \vdots & \ddots & 0 \\ c_a(t_T) & c_a(t_{T-1}) & \cdots & c_a(t_1) \end{pmatrix} \cdot \begin{pmatrix} \mathrm{IRF}(t_1) \\ \mathrm{IRF}(t_2) \\ \vdots \\ \mathrm{IRF}(T) \end{pmatrix}$$

The matrix of the AIF must be inverted to calculate the BF-scaled IRF. Normally, deconvolution is performed via singular values decomposition (SVD).

Fieselman et al: “Deconvolution-Based CT and MR Brain Perfusion Measurement: Theoretical Model Revisited and Practical Implementation Details”, *International Journal of Biomedical Images* (2011).

Two Compartments Models Deconvolution

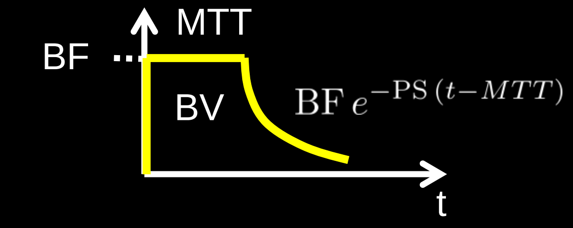
MTT
BF
BV
$\mathrm{BF}\, e^{-\mathrm{PS}\,(t-MTT)}$
t

- Different assumptions on IRF shape.

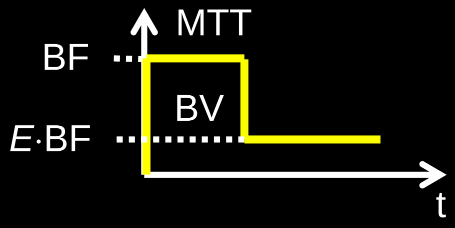
MTT
BF
BV
E·BF
t

- Parametric deconvolution.
- scan times are too long, *E* is not constant.

Abels et al: “Perfusion CT in Acute Ischemic Stroke: A Qualitative and Quantitative Comparison of Deconvolution and Maximum Slope Approach”, *AJNR* (2010).

Two Compartments Models Deconvolution

Important considerations on the deconvolution model:

- More robust to suboptimal injection.
- Different assumptions and different guidelines for each vendor.
- High sampling time.
- Dose, coverage, sampling time tradeoff.
- Entire TAC is used for each voxel.
- Dose reduction strategies.
- All the most important parameters are calculated.

Maximum Slope vs. Deconvolution

Fick principle:

$$c_\mathrm{t}(t) = \mathrm{BF} \int_0^t \big(c_\mathrm{a}(t) - c_\mathrm{v}(t)\big)\, dt$$

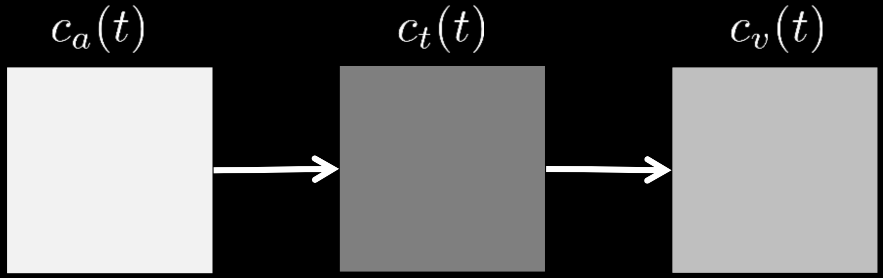

Maximum slope model:

$$c_\mathrm{t}(t) = \mathrm{BF} \int_0^t c_\mathrm{a}(t)\, dt$$

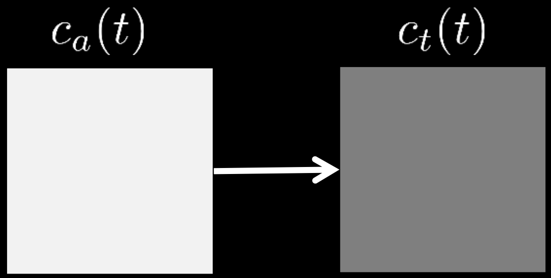

Deconvolution model:

$$c_\mathrm{t}(t) = \mathrm{BF}\, c_\mathrm{a}(t) * \mathrm{IRF}$$

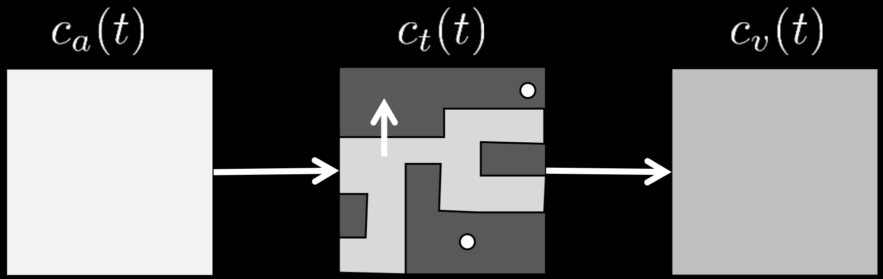

Two Compartments Models

Tofts model.

Patlak model.

Two Compartments Models
Tofts Model

Capillaries concentration is assumed to be equal to artery concentration, which means we are in an equilibrium phase. For these models late data are used, and the exchange of contrast from arteries to capillaries (BF) cannot be calculated.

Deconvolution model:

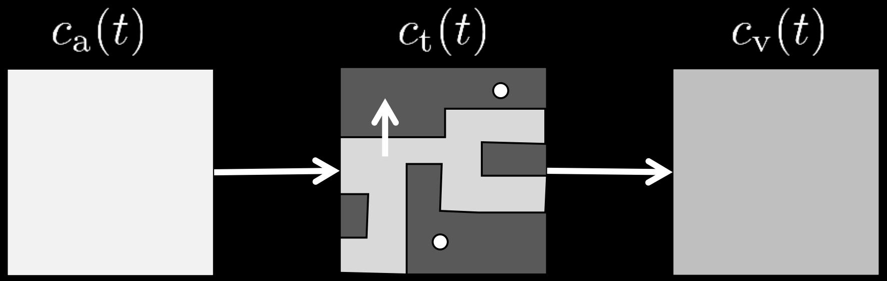
$c_{\mathrm{a}}(t)$
$c_{\mathrm{t}}(t)$
$c_{\mathrm{v}}(t)$

Tofts model:

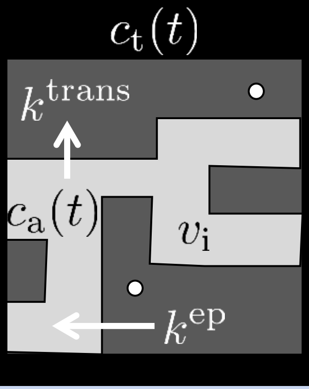
$c_{\mathrm{t}}(t)$
k^{trans}
$c_{\mathrm{a}}(t)$
v_{i}
k^{ep}

Two Compartments Models
Tofts Model

$$c_\mathrm{t}(t) = v_\mathrm{i}\, c_\mathrm{a}(t) + k^\mathrm{trans} \int_0^t c_\mathrm{a}(t)\, e^{-k^\mathrm{ep}\,(t-t_0)}\, dt$$

The Tofts model considers the concentration in one voxel as a weighted sum of the intravascular component and the extravascular-extracellular component. The three open parameters are:

- $v_\mathrm{e}, v_\mathrm{i}$ Extra- and intravascular volume
- k^trans Transfer function from capillaries to EES
- k^ep Transfer function from EES to capillaries

Where it holds

$$k^\mathrm{ep} = \frac{k^\mathrm{trans}}{v_\mathrm{e}}$$

Two Compartments Models
Patlak Model

Patlak model is a simplification of Tofts model.

It assumes no backflow is occurring:

$$c_{\mathrm{t}}(t) = v_{\mathrm{i}}\, c_{\mathrm{a}}(t) + k^{\mathrm{trans}} \int\limits_0^t c_{\mathrm{a}}(t)\, dt$$

If we normalize by the arterial input function:

$$\frac{c_{\mathrm{t}}(t)}{c_{\mathrm{a}}(t)} = v_{\mathrm{i}} + k^{\mathrm{trans}} \frac{\int_0^t c_{\mathrm{a}}(t)\, dt}{c_{\mathrm{a}}(t)}$$

it becomes a linear fitting, the slope being k^{trans} and the intercept v_i .

Two Compartments Models
Patlak Model

Some considerations on the Patlak model:

- Late data.
- Few data.
- Limits of the “no-backflow” assumption.
- Sometimes used in combination with other models.

Index of Contents

- **Introduction:**
  - What is CT perfusion
  - Derived parameters
  - Different techniques
- **Models:**
  - Perfusion models introduction
  - One compartment models – maximum slope
  - Two compartments models – deconvolution, Toft, Patlak
- **Clinical applications and optimization:**
  - Oncology: liver, lung, other organs
  - Neurology: brain perfusion for stroke
  - Myocardial perfusion

General Workflow

- Topogram.
- Planning.
- Test bolus. For example: 10 mL contrast @ 5 or 6 mL/s + 50 mL saline @ same flow.
- Set perfusion scan parameters. For example: 45 mL contrast @ 5 or 6 mL/s + 50 mL saline @ same flow
- Set delay of perfusion scan.
- Set injection parameters.

Oncology: Liver

Liver model:

dual maximum lope model.

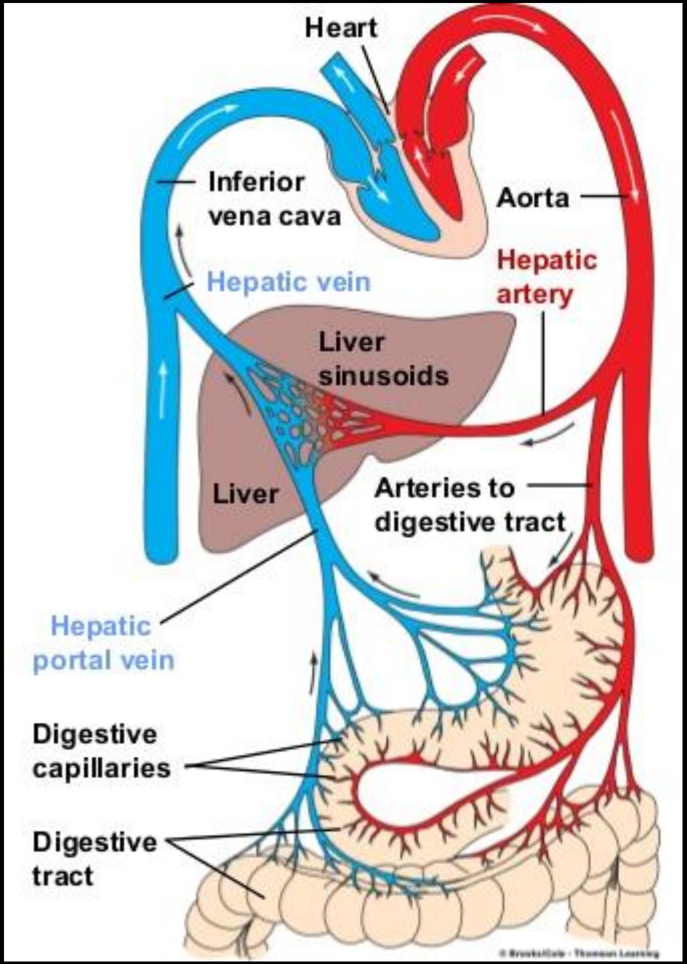
Heart
Inferior vena cava
Aorta
Hepatic vein
Hepatic artery
Liver sinusoids
Liver
Arteries to digestive tract
Hepatic portal vein
Digestive capillaries
Digestive tract
© Brooks/Cole - Thomson Learning

Liver – Example

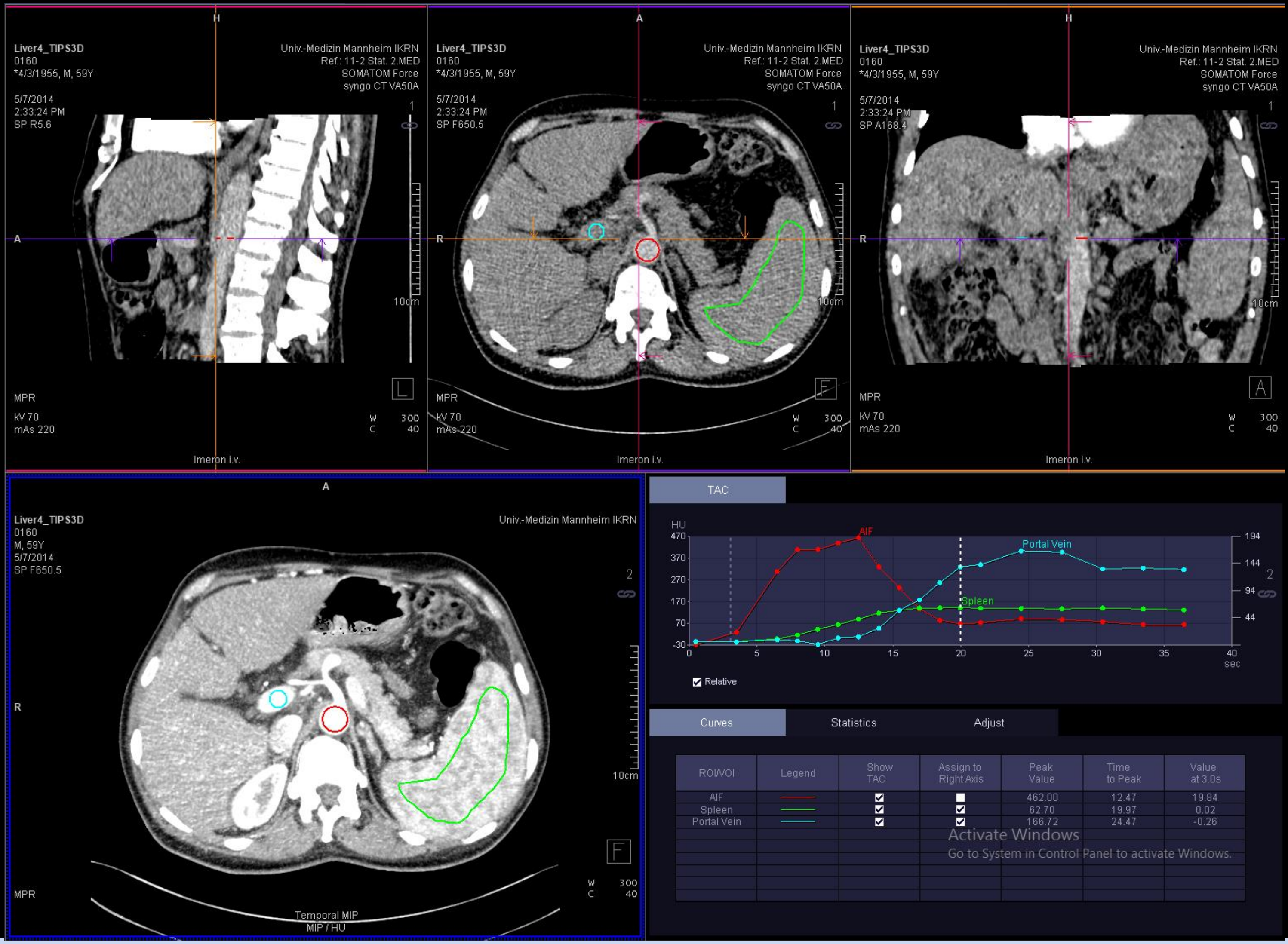
H
A
H
Liver4_TIPS3D
0160
*4/3/1955, M, 59Y
5/7/2014
2:33:24 PM
SP R5.6
SP F650.5
SP A168.4
Univ.-Medizin Mannheim IKRN
Ref.: 11-2 Stat. 2.MED
SOMATOM Force
syngo CT VA50A
A
R
R
10cm
MPR
kV 70
mAs 220
W 300
C 40
Imeron i.v.
L
F
A
M, 59Y
2
Temporal MIP
MIP / HU
TAC
HU
470
370
270
170
70
-30
0
5
10
15
20
25
30
35
40
sec
194
144
94
44
AIF
Portal Vein
Spleen
☑ Relative
Curves
Statistics
Adjust

ROI/VOI	Legend	Show TAC	Assign to Right Axis	Peak Value	Time to Peak	Value at 3.0s
AIF	🟥	☑	☐	462.00	12.47	19.84
Spleen	🟩	☑	☑	62.70	19.97	0.02
Portal Vein	🟦	☑	☑	166.72	24.47	-0.26

Activate Windows
Go to System in Control Panel to activate Windows.

Oncology:
Liver

Some useful parameters that can be obtained are:

- ALP (arterial liver perfusion): arterial BF
- PLP (portal liver perfusion): portal BF
- HPI (hepatic index) = ALP/(ALP+PLP)

So far no dual input deconvolution models have been included in vendors solution.

Liver – Example (Unfiltered)

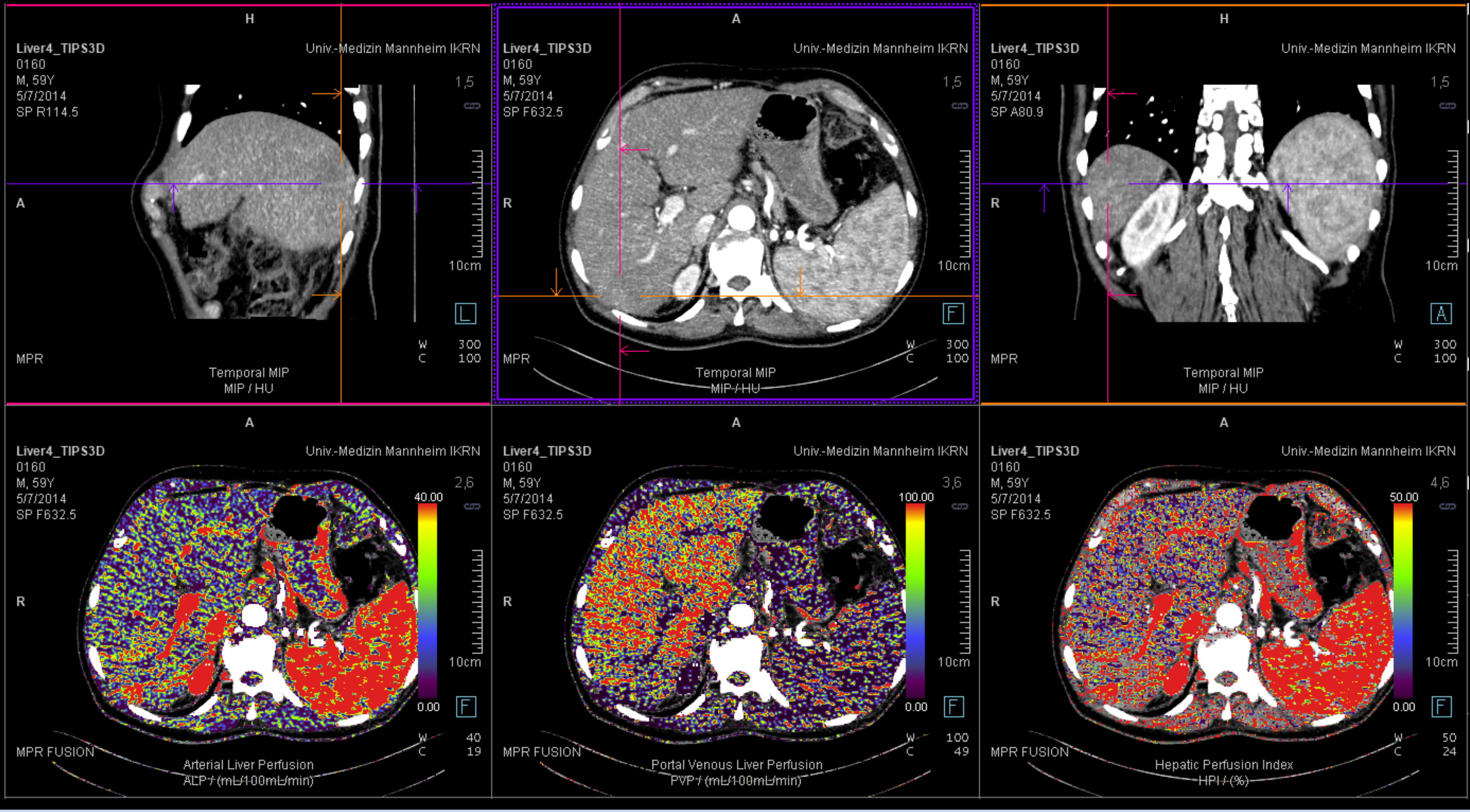
H
Liver4_TIPS3D
0160
M, 59Y
5/7/2014
SP R114.5
Univ.-Medizin Mannheim IKRN
1,5
A
10cm
L
W 300
C 100
MPR
Temporal MIP
MIP / HU
A
Liver4_TIPS3D
0160
M, 59Y
5/7/2014
SP F632.5
Univ.-Medizin Mannheim IKRN
1,5
R
10cm
F
W 300
C 100
MPR
Temporal MIP
MIP / HU
H
Liver4_TIPS3D
0160
M, 59Y
5/7/2014
SP A80.9
Univ.-Medizin Mannheim IKRN
1,5
R
10cm
A
W 300
C 100
MPR
Temporal MIP
MIP / HU
A
Liver4_TIPS3D
0160
M, 59Y
5/7/2014
SP F632.5
Univ.-Medizin Mannheim IKRN
2,6
40.00
0.00
R
10cm
F
W 40
C 19
MPR FUSION
Arterial Liver Perfusion
ALP / (mL/100mL/min)
A
Liver4_TIPS3D
0160
M, 59Y
5/7/2014
SP F632.5
Univ.-Medizin Mannheim IKRN
3,6
100.00
0.00
R
10cm
F
W 100
C 49
MPR FUSION
Portal Venous Liver Perfusion
PVP / (mL/100mL/min)
A
Liver4_TIPS3D
0160
M, 59Y
5/7/2014
SP F632.5
Univ.-Medizin Mannheim IKRN
4,6
50.00
0.00
R
10cm
F
W 50
C 24
MPR FUSION
Hepatic Perfusion Index
HPI / (%)

Liver – Example (Filtered)

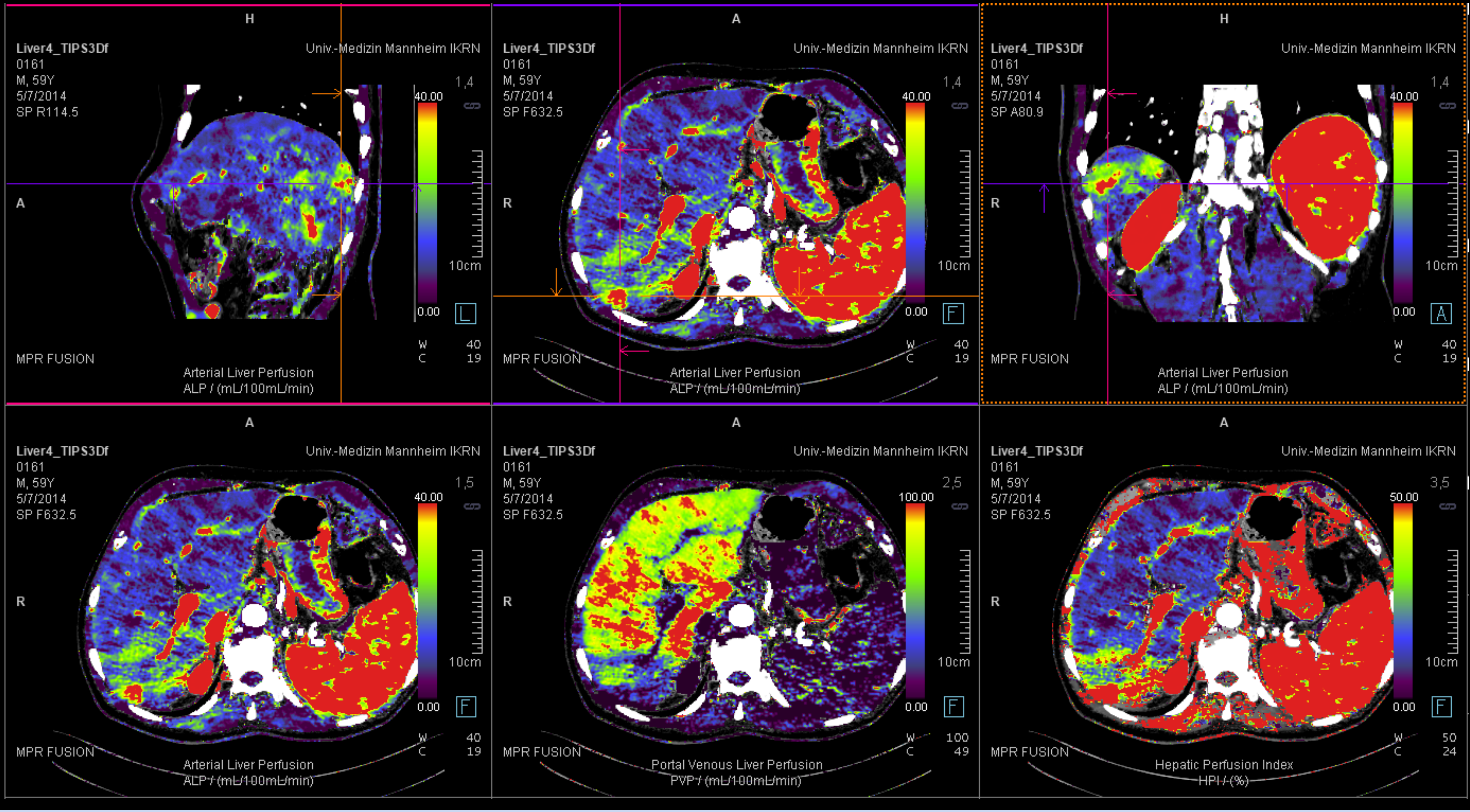
H
Liver4_TIPS3Df
0161
M, 59Y
5/7/2014
SP R114.5
Univ.-Medizin Mannheim IKRN
1,4
40.00
A
10cm
0.00
L
W 40
C 19
MPR FUSION
Arterial Liver Perfusion
ALP / (mL/100mL/min)
A
Liver4_TIPS3Df
0161
M, 59Y
5/7/2014
SP F632.5
Univ.-Medizin Mannheim IKRN
1,4
40.00
R
10cm
0.00
F
W 40
C 19
MPR FUSION
Arterial Liver Perfusion
ALP / (mL/100mL/min)
H
Liver4_TIPS3Df
0161
M, 59Y
5/7/2014
SP A80.9
Univ.-Medizin Mannheim IKRN
1,4
40.00
R
10cm
0.00
A
W 40
C 19
MPR FUSION
Arterial Liver Perfusion
ALP / (mL/100mL/min)
A
Liver4_TIPS3Df
0161
M, 59Y
5/7/2014
SP F632.5
Univ.-Medizin Mannheim IKRN
1,5
40.00
R
10cm
0.00
F
W 40
C 19
MPR FUSION
Arterial Liver Perfusion
ALP / (mL/100mL/min)
A
Liver4_TIPS3Df
0161
M, 59Y
5/7/2014
SP F632.5
Univ.-Medizin Mannheim IKRN
2,5
100.00
R
10cm
0.00
F
W 100
C 49
MPR FUSION
Portal Venous Liver Perfusion
PVP / (mL/100mL/min)
A
Liver4_TIPS3Df
0161
M, 59Y
5/7/2014
SP F632.5
Univ.-Medizin Mannheim IKRN
3,5
50.00
R
10cm
0.00
F
W 50
C 24
MPR FUSION
Hepatic Perfusion Index
HPI / (%)

Oncology:
Liver

Practical important considerations:

- Breath hold.
- High flow injection, short injection time.
- Pre-warm contrast media.
- Spleen or kidney scanned (if hepatic index is needed).

Oncology: Liver

- One example on Siemens machine (Somatom Force):

  80 kV
  110 mAs
  176 mm coverage
  20×1.5 s + 5×3 s
  Injection 50 mL contrast @ 5 mL/s + 40 mL saline @ 5 mL/s

  54.62 mGy
  1031.4 mGy·cm
  15.4 mSv

Oncology:
Lung

- Two inputs. Decide upfront.
- Limit motion.

Index of Contents

- **Introduction:**
  - **What is CT perfusion**
  - **Derived parameters**
  - **Different techniques**
- **Models:**
  - **Perfusion models introduction**
  - **One compartment models – maximum slope**
  - **Two compartments models – deconvolution, Toft, Patlak**
- **Clinical applications and optimization:**
  - **Oncology: liver, lung, other organs**
  - **Neurology: brain perfusion for stroke**
  - **Myocardial perfusion**

Neurology:
Brain Perfusion for Stroke

- Small signal enhancement.
- Small and rigid motion.
- High sampling time.
- Injection time should be not longer than 8 s.
- Patlak model does not really apply in this case (unless there is a tumor) for two main reasons:
  - The presence of blood-brain barrier prevents the blood from going to the EES.
  - Permeability is BF-limited.

Brain – Example (Unfiltered)

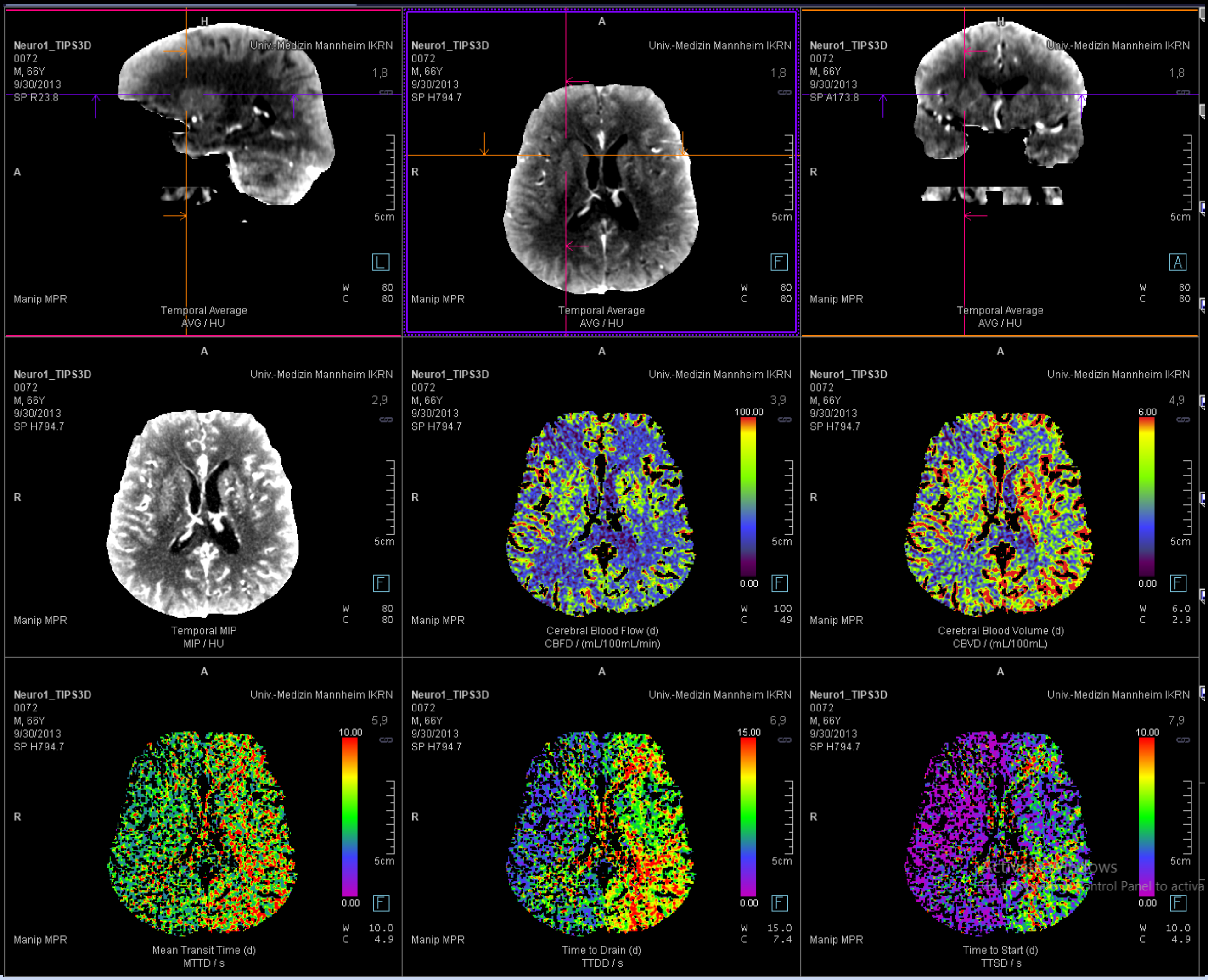
Neuro1_TIPS3D
0072
M, 66Y
9/30/2013
SP R23.8
Univ.-Medizin Mannheim IKRN
H
A
1,8
5cm
L
Manip MPR
W 80
C 80
Temporal Average
AVG / HU
SP H794.7
R
F
SP A173.8
Temporal MIP
MIP / HU
2,9
100.00
0.00
3,9
W 100
C 49
Cerebral Blood Flow (d)
CBFD / (mL/100mL/min)
6.00
4,9
W 6.0
C 2.9
Cerebral Blood Volume (d)
CBVD / (mL/100mL)
10.00
5,9
W 10.0
C 4.9
Mean Transit Time (d)
MTTD / s
15.00
6,9
W 15.0
C 7.4
Time to Drain (d)
TTDD / s
7,9
Time to Start (d)
TTSD / s

Brain – Example (Filtered)

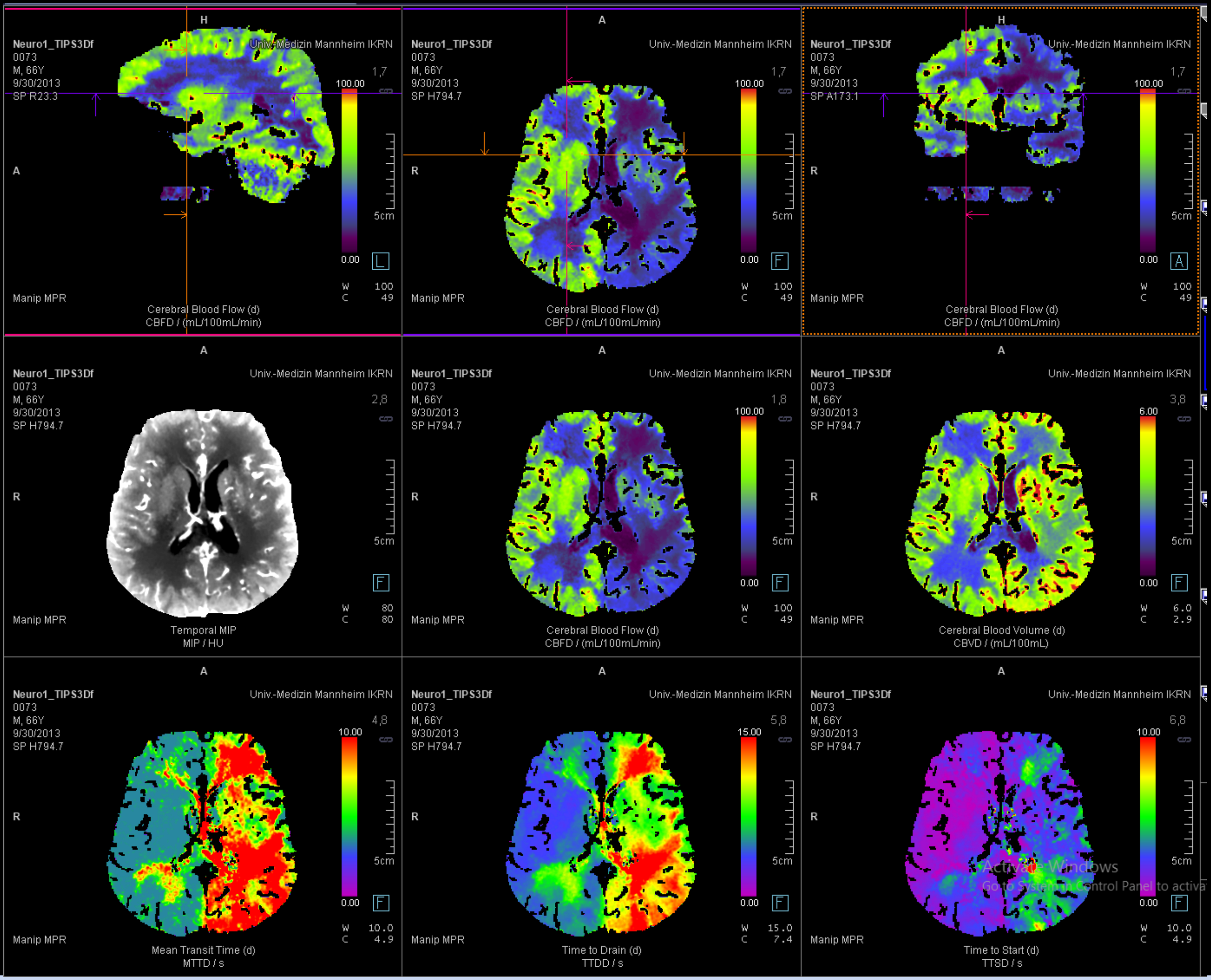
Neuro1_TIPS3Df
0073
M, 66Y
9/30/2013
SP R23.3
Univ.-Medizin Mannheim IKRN
H
A
1,7
100.00
0.00
5cm
L
W 100
C 49
Manip MPR
Cerebral Blood Flow (d)
CBFD / (mL/100mL/min)
Neuro1_TIPS3Df
0073
M, 66Y
9/30/2013
SP H794.7
Univ.-Medizin Mannheim IKRN
A
R
1,7
100.00
0.00
5cm
F
W 100
C 49
Manip MPR
Cerebral Blood Flow (d)
CBFD / (mL/100mL/min)
Neuro1_TIPS3Df
0073
M, 66Y
9/30/2013
SP A173.1
Univ.-Medizin Mannheim IKRN
H
R
1,7
100.00
0.00
5cm
A
W 100
C 49
Manip MPR
Cerebral Blood Flow (d)
CBFD / (mL/100mL/min)
Neuro1_TIPS3Df
0073
M, 66Y
9/30/2013
SP H794.7
Univ.-Medizin Mannheim IKRN
A
R
2,8
5cm
F
W 80
C 80
Manip MPR
Temporal MIP
MIP / HU
Neuro1_TIPS3Df
0073
M, 66Y
9/30/2013
SP H794.7
Univ.-Medizin Mannheim IKRN
A
R
1,8
100.00
0.00
5cm
F
W 100
C 49
Manip MPR
Cerebral Blood Flow (d)
CBFD / (mL/100mL/min)
Neuro1_TIPS3Df
0073
M, 66Y
9/30/2013
SP H794.7
Univ.-Medizin Mannheim IKRN
A
R
3,8
6.00
0.00
5cm
F
W 6.0
C 2.9
Manip MPR
Cerebral Blood Volume (d)
CBVD / (mL/100mL)
Neuro1_TIPS3Df
0073
M, 66Y
9/30/2013
SP H794.7
Univ.-Medizin Mannheim IKRN
A
R
4,8
10.00
0.00
5cm
F
W 10.0
C 4.9
Manip MPR
Mean Transit Time (d)
MTTD / s
Neuro1_TIPS3Df
0073
M, 66Y
9/30/2013
SP H794.7
Univ.-Medizin Mannheim IKRN
A
R
5,8
15.00
0.00
5cm
F
W 15.0
C 7.4
Manip MPR
Time to Drain (d)
TTDD / s
Neuro1_TIPS3Df
0073
M, 66Y
9/30/2013
SP H794.7
Univ.-Medizin Mannheim IKRN
A
R
6,8
10.00
0.00
5cm
F
W 10.0
C 4.9
Manip MPR
Time to Start (d)
TTSD / s

Index of Contents

- **Introduction:**
  - What is CT perfusion
  - Derived parameters
  - Different techniques
- **Models:**
  - Perfusion models introduction
  - One compartment models – maximum slope
  - Two compartments models – deconvolution, Toft, Patlak
- **Clinical applications and optimization:**
  - Oncology: liver, lung, other organs
  - Neurology: brain perfusion for stroke
  - Myocardial perfusion

Myocardial Perfusion

- Many limitations:
  - Motion. Synchronization with ECG. Breath-hold.
  - Must be done in stress conditions. High HR. Increase of motion. need to increase acquisition time. Systolic phase.
  - Synchronization with ECG seriously limits sampling time.
  - If a big coverage (16 cm) is not available, the shuttle mode must be used: sampling time further reduced by half.
  - BF is really fast in the myocardium (~ 300 mL / min·100 mL). Normally such values cannot easily be obtained with such low temporal sampling (~3 to 4 s), thus some models derived from Tofts are normally employed to calculate PS and backflow, capillaries volume etc. BF is then calculated with MS models.
  - Backflow occurs very quickly, so models assuming no backflow (like Patlak) are not suitable to this application.
  - Beam hardening artifacts in myocardium (limitation on how low the kV can be set).

General Principle

Both in DE and CTP, the software will provide numbers. There is no way to know if these numbers are correct or not, the only possible thing to do is knowing upfront what to do in order to have reliable results, by combining:

- Clinical knowledge of physiological principles.
- Background knowledge of algorithms assumptions.
- Physical knowledge of CT and of the algorithms.
- Experience.

Imaging For Physicists

Artifacts 2

Uulke van der Heide

Many reasons for artifacts

Erroneous sampling of k-space

- Aliasing
- Ringing

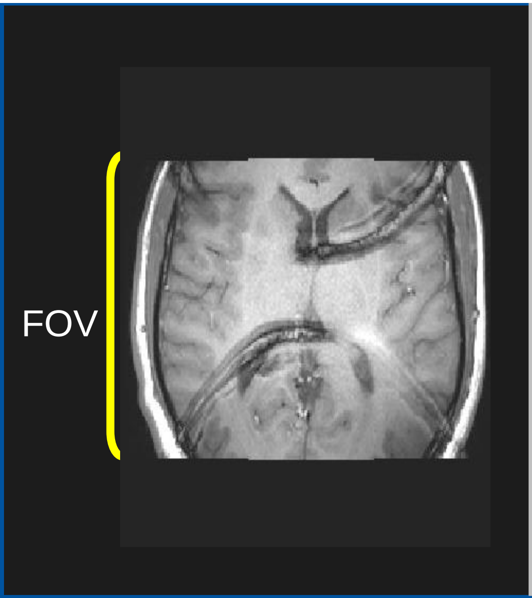

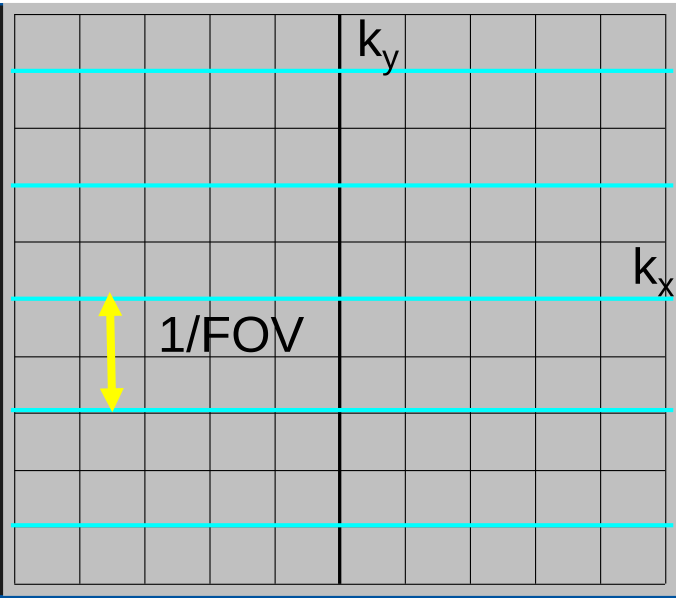

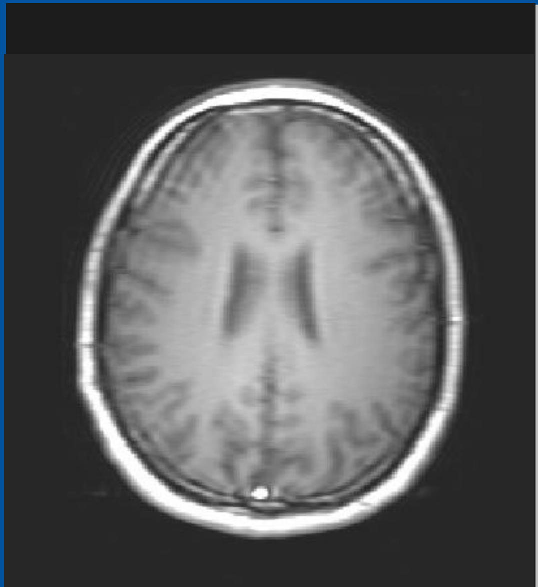

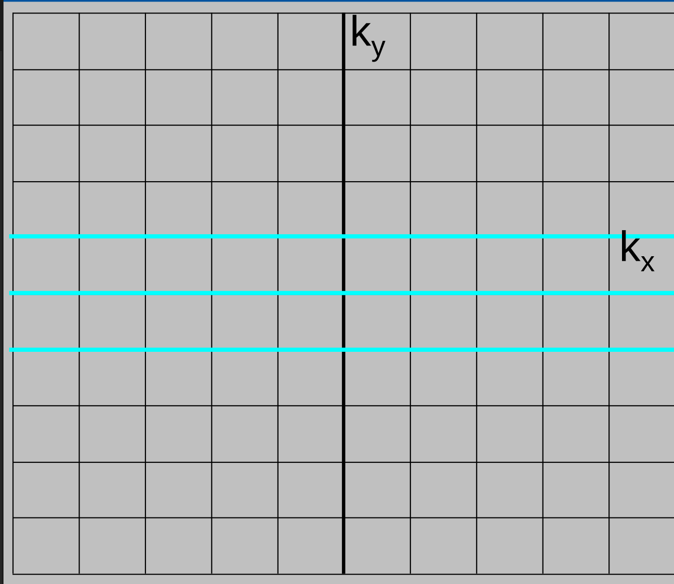

Many reasons for artifacts

- Magnetic field errors
  - Gradient artifacts
  - Susceptibility artifacts
  - Water-fat shift

- Geometrical artifacts show up in a particular direction

$$x_1 = x + \frac{\Delta B_0(x,y,z)}{G_x} + \frac{\Delta B_{G_x}(x,y,z)}{G_x}$$

$$y_1 = y + \frac{\Delta B_{G_y}}{G_y}$$

Many reasons for artifacts

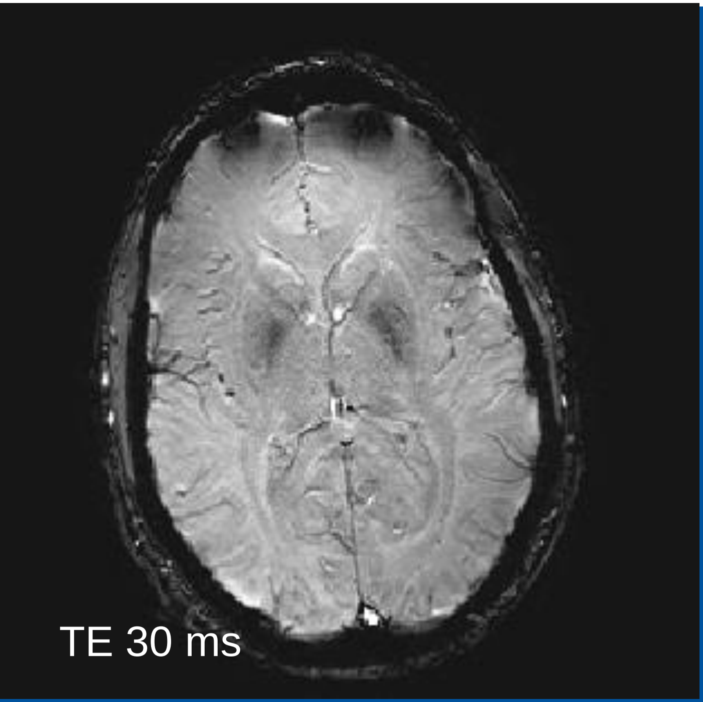

TE 30 ms

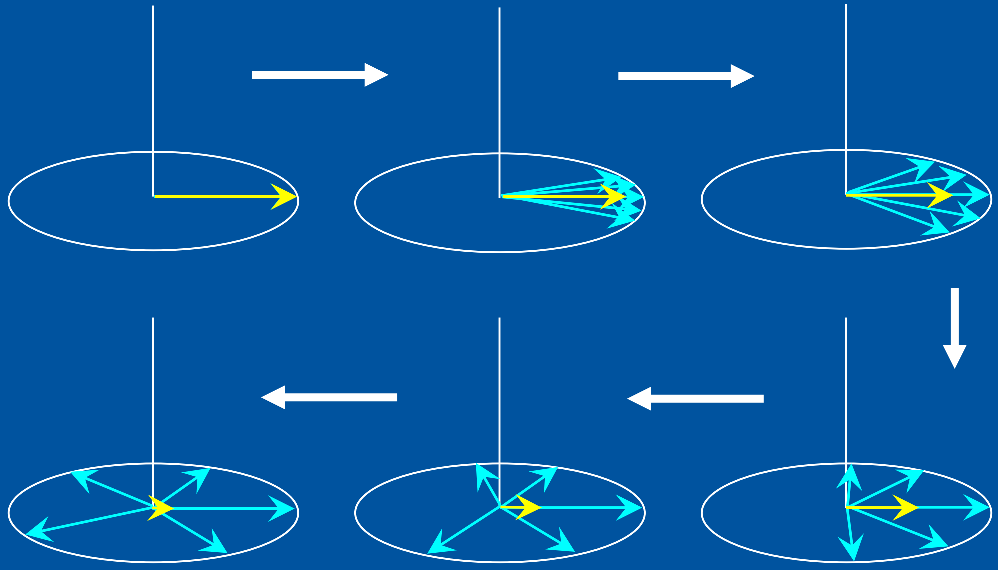

- Field distortions lead to signal loss in gradient echo sequences due to dephasing
- Dephasing is proportional to echo time

Outline lecture 2

- Measurements for characterizing geometrical accuracy
  - Phantom design
  - Characterizing gradient errors
- Examples
- Practical consequences
- Summary

Homogeneity of the main magnetic field

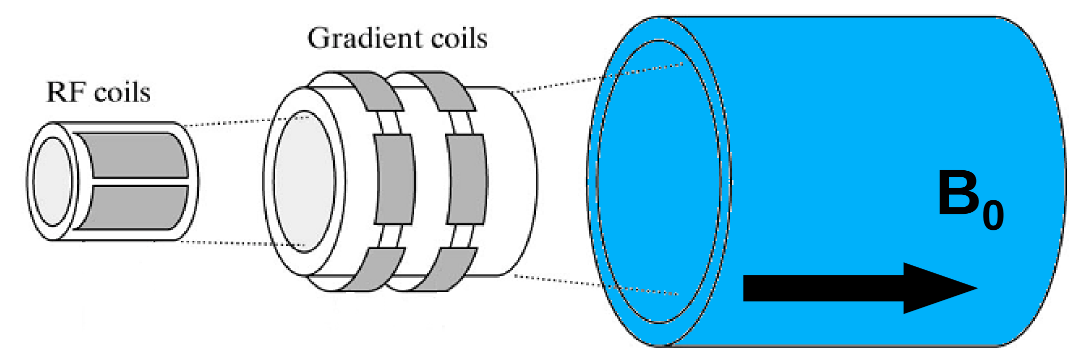
Gradient coils
RF coils
B_0

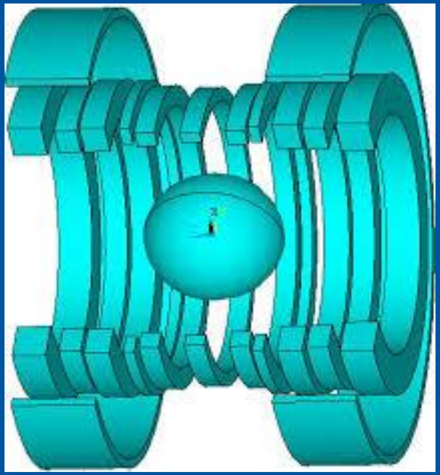

e.g. uniformity in diameter of spherical volume DSV_{40cm} = 0.2 ppm

(at 1.5 T):
0.2 x 63.87 MHz = 12.8 Hz

- Magnet is shimmed at installation- additional (dynamic) shimming may be required

Gradient fields

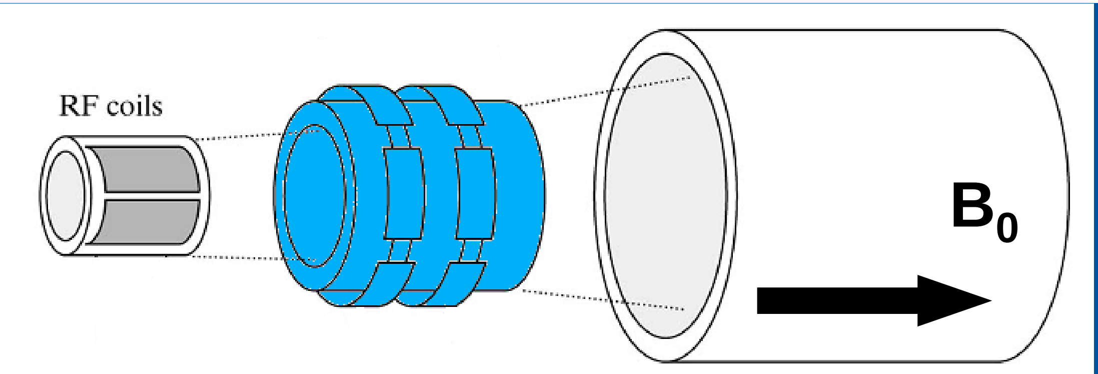

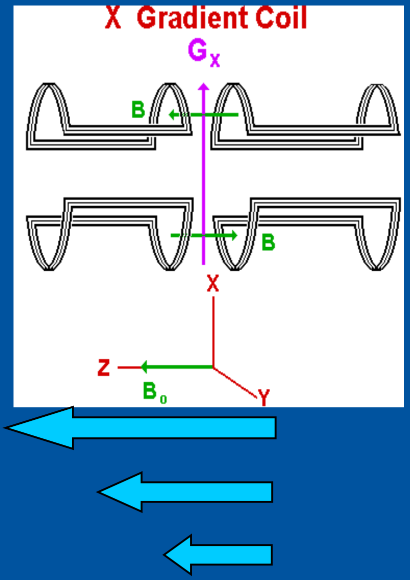
X Gradient Coil
Gx
B
B
X
Z
B0
Y

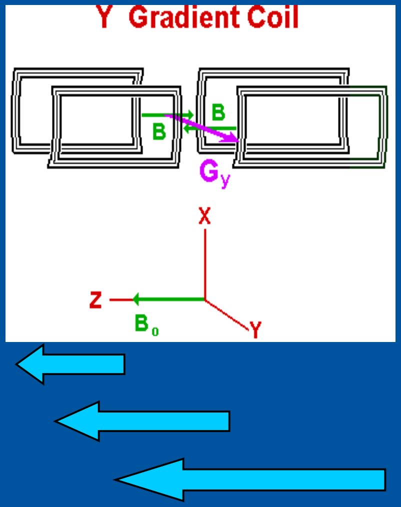
Y Gradient Coil
B
B
Gy
X
Z
B0
Y

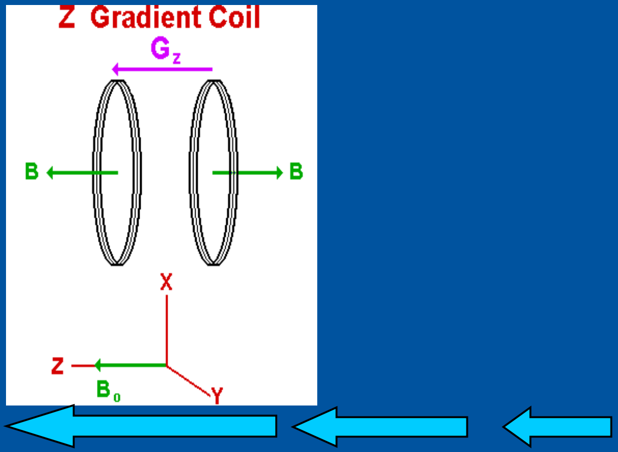
Z Gradient Coil
Gz
B
B
X
Z
B0
Y

Linear changes in B_0 in each orthogonal direction

Correction of imperfect B_0 and gradient fields

Image distortion and correction on a 0.23 T open MRI scanner

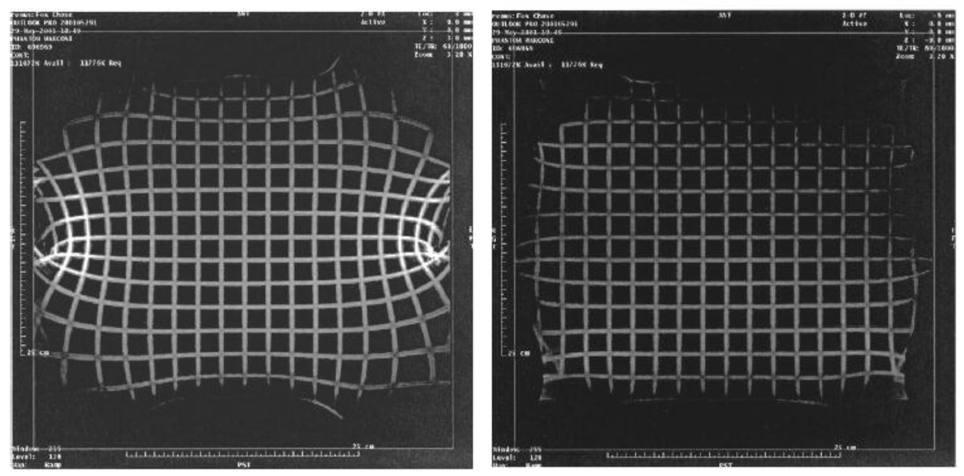

Mah et al. 2002 Int. J. Radiat. Oncol. Biol. Phys. 53 (3), 757-765

Phantoms

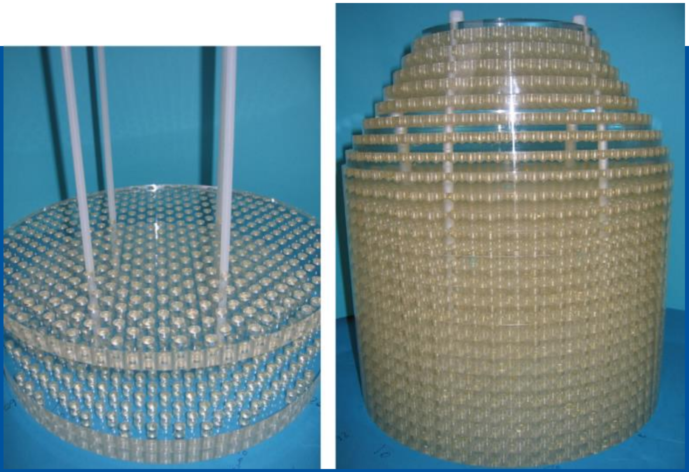

Vermandel 2014

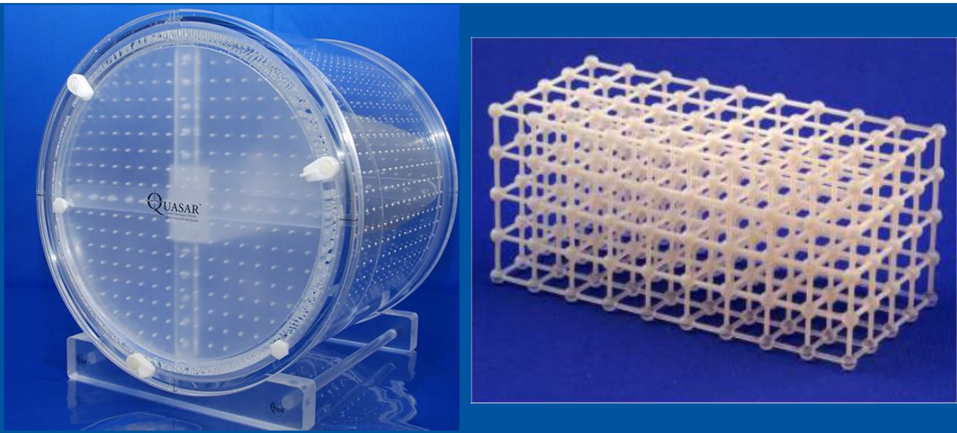

Commercial: Quasar, Modus

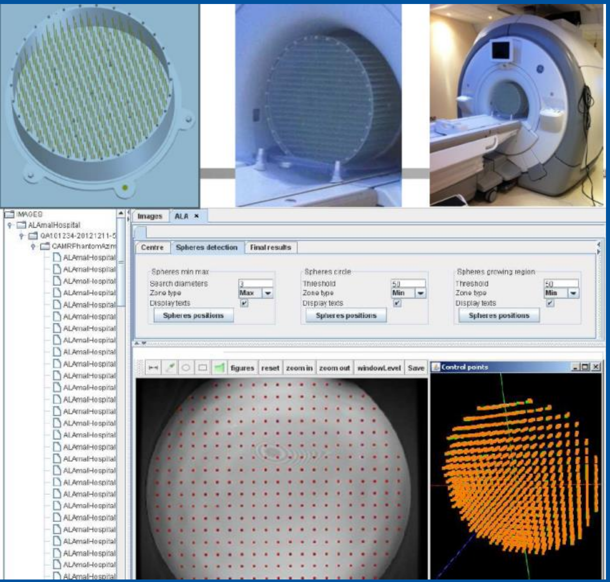
IMAGES
ALAmalHospital
Images
ALA
Centre
Spheres detection
Final results
Spheres positions
figures
reset
zoom in
zoom out
windowLevel
Save
Control points

Spheres min max
Search diameters 3
Zone type Max
Display texts ☑

Spheres circle
Threshold 50
Zone type Min
Display texts ☑

Spheres growing region
Threshold 50
Zone type Min
Display texts ☑

Torfeh 2015

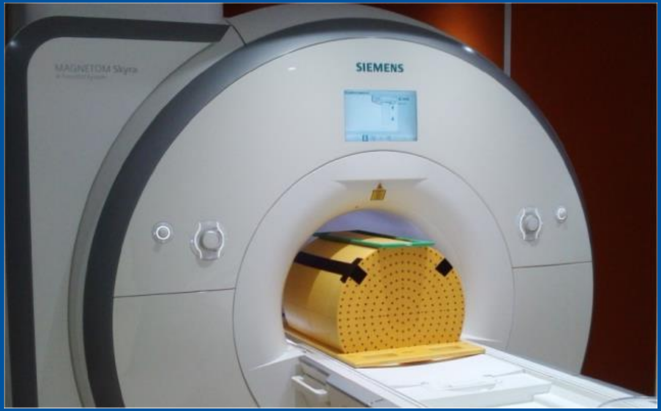
SIEMENS
MAGNETOM Skyra

Walker 2015

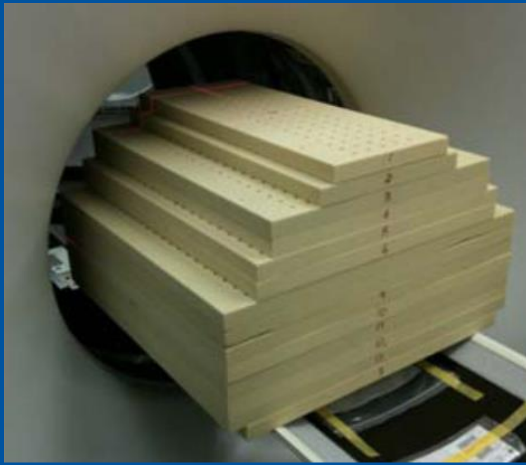

Vendor: GE

Design of a phantom for field-error measurements

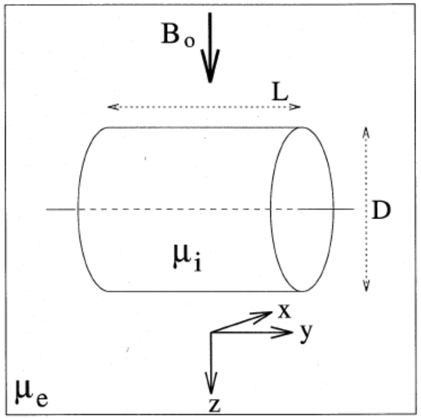

A schematic overview of the cylinder with respect to $\boldsymbol{B}_0$ (D is the diameter and L the length).

- Use tubes that are long relative to their diameter

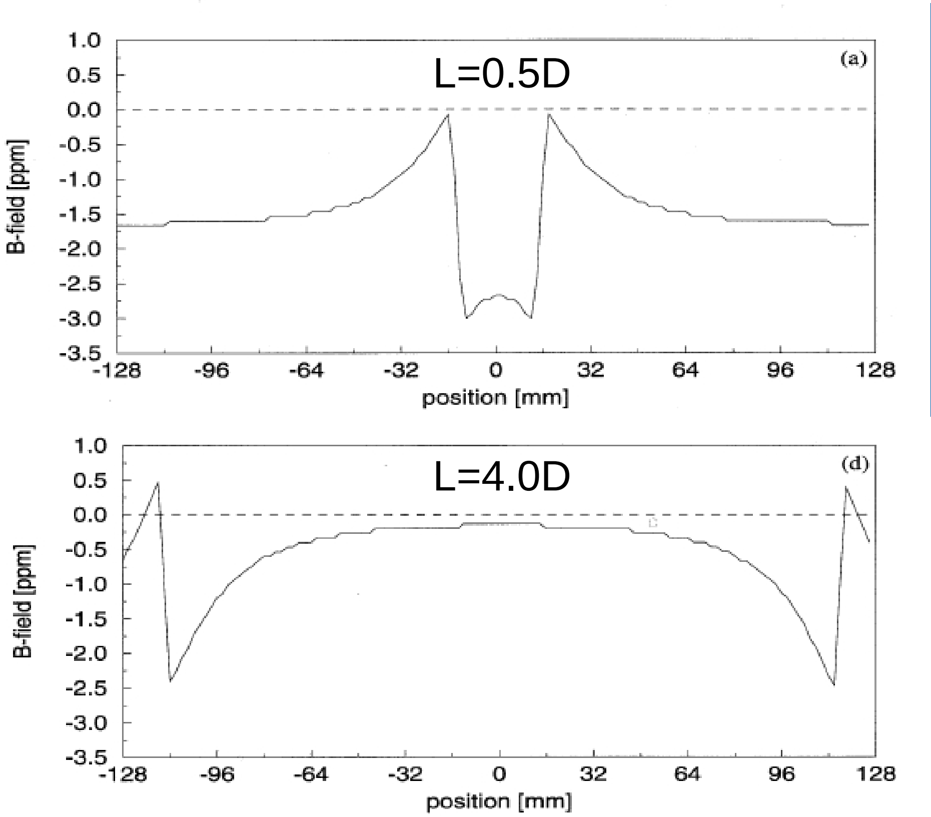

Cross-section of calculated B-field in ppm along the cylinder axis

Baghwandien et al. 1994 Magn. Res. Imag. 12:101-107

Setup of experiments to characterize magnetic field inhomogeneity and gradient non-linearity

Experiment 1:

- phase encoding along y
- Frequency encoding along x

$$x_1 = x + \frac{\Delta B_0(x,y,z)}{G_x} + \frac{\Delta B_{G_x}(x,y,z)}{G_x}$$

$$y_1 = y + \frac{\Delta B_{G_y}}{G_y}$$

Experiment 2:

- phase encoding along x
- Frequency encoding along y

$$x_2 = x + \frac{\Delta B_{G_x}}{G_x}$$

$$y_2 = y + \frac{\Delta B_0(x,y,z)}{G_y} + \frac{\Delta B_{G_y}(x,y,z)}{G_y}$$

Distortion mapping

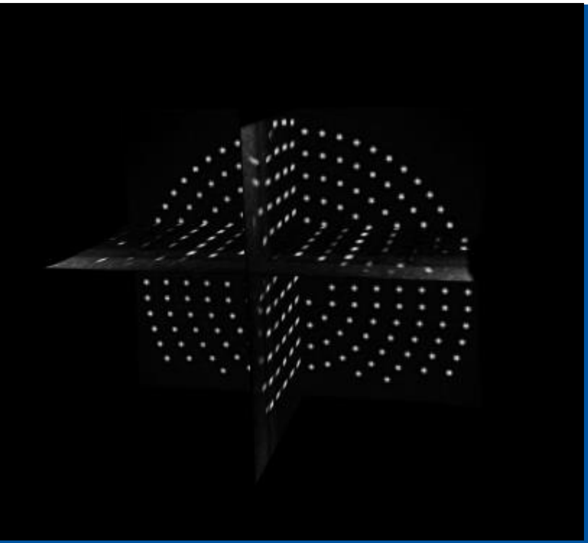

Frequency encoding:

$$x' = x + \frac{\Delta B_0}{G_x} + \frac{\Delta B_{G_x}}{G_x}$$

Phase encoding:

$$y' = y + \frac{\Delta B_{G_y}}{G_y}$$

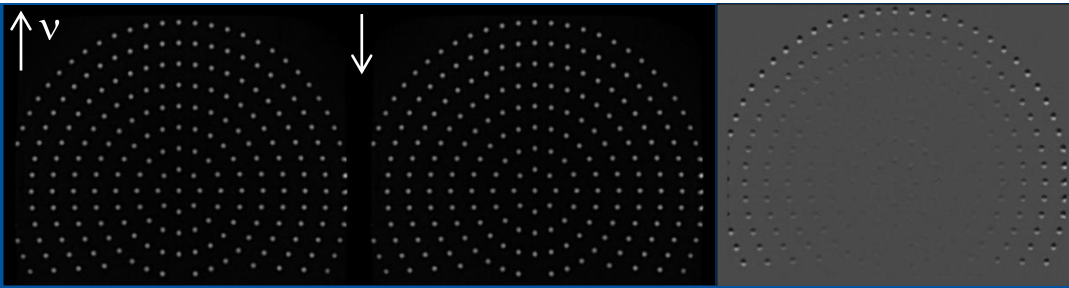

Gradient reversal and subtraction

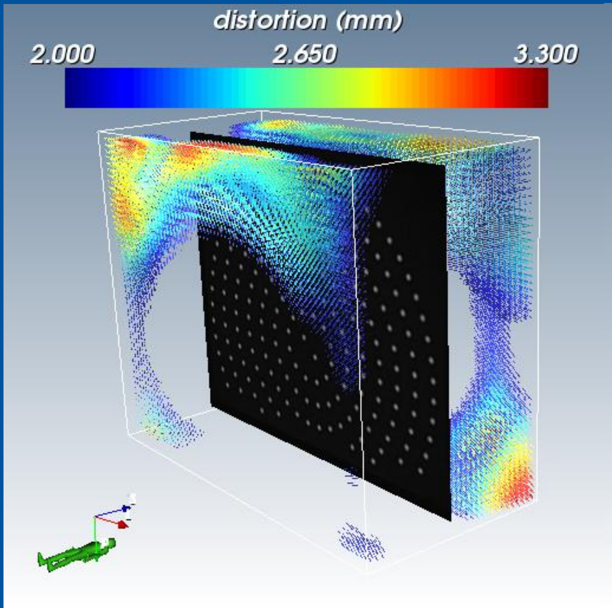
distortion (mm)
2.000
2.650
3.300

Residual gradient

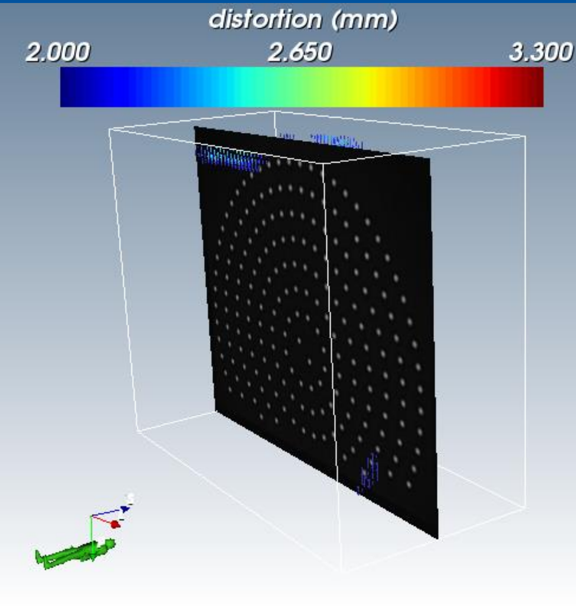
distortion (mm)
2.000
2.650
3.300

B_0 component

Continuous or stepped table measurement

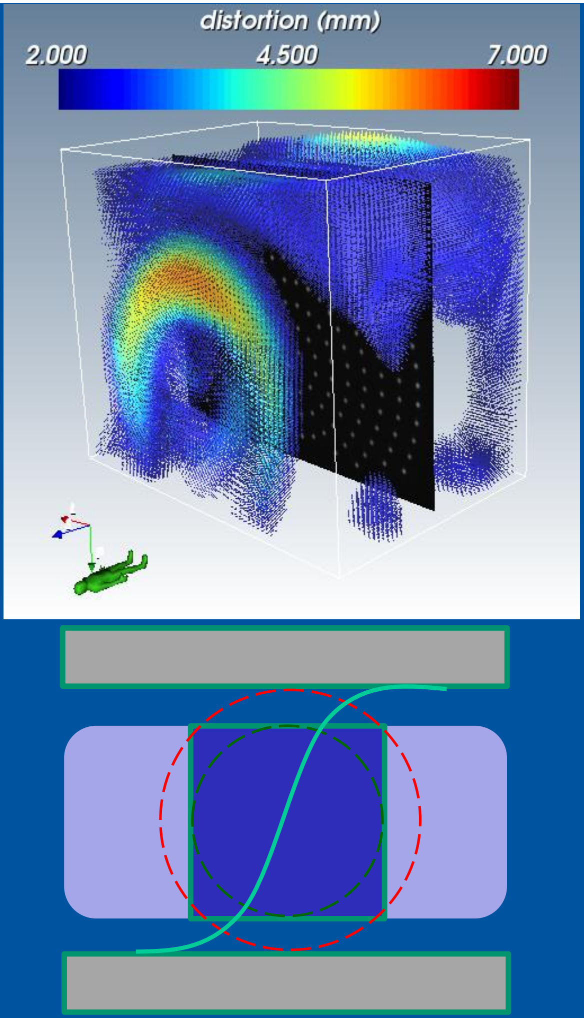
distortion (mm)
2.000
4.500
7.000

Restrict volume

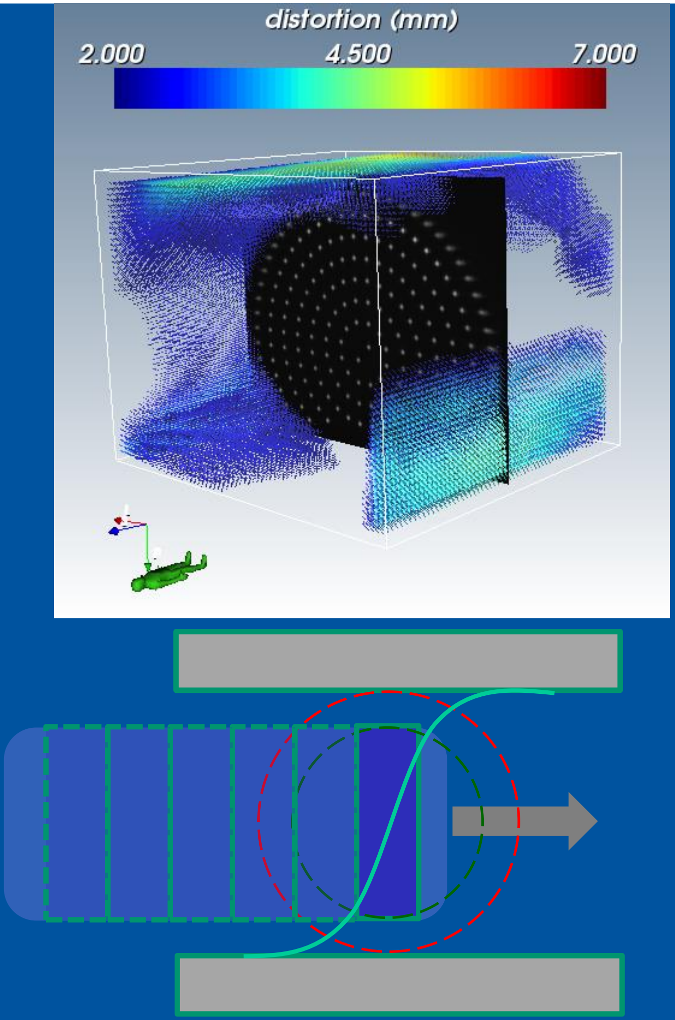
distortion (mm)
2.000
4.500
7.000

Move table through isocentre

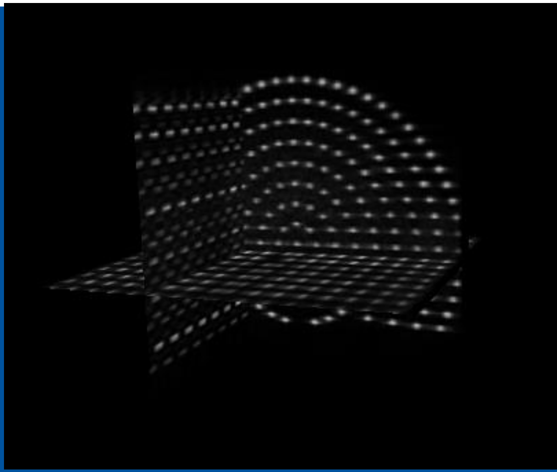

A Walker et al. Med. Phys. 2015; 42:1982-1991

Gradient corrections

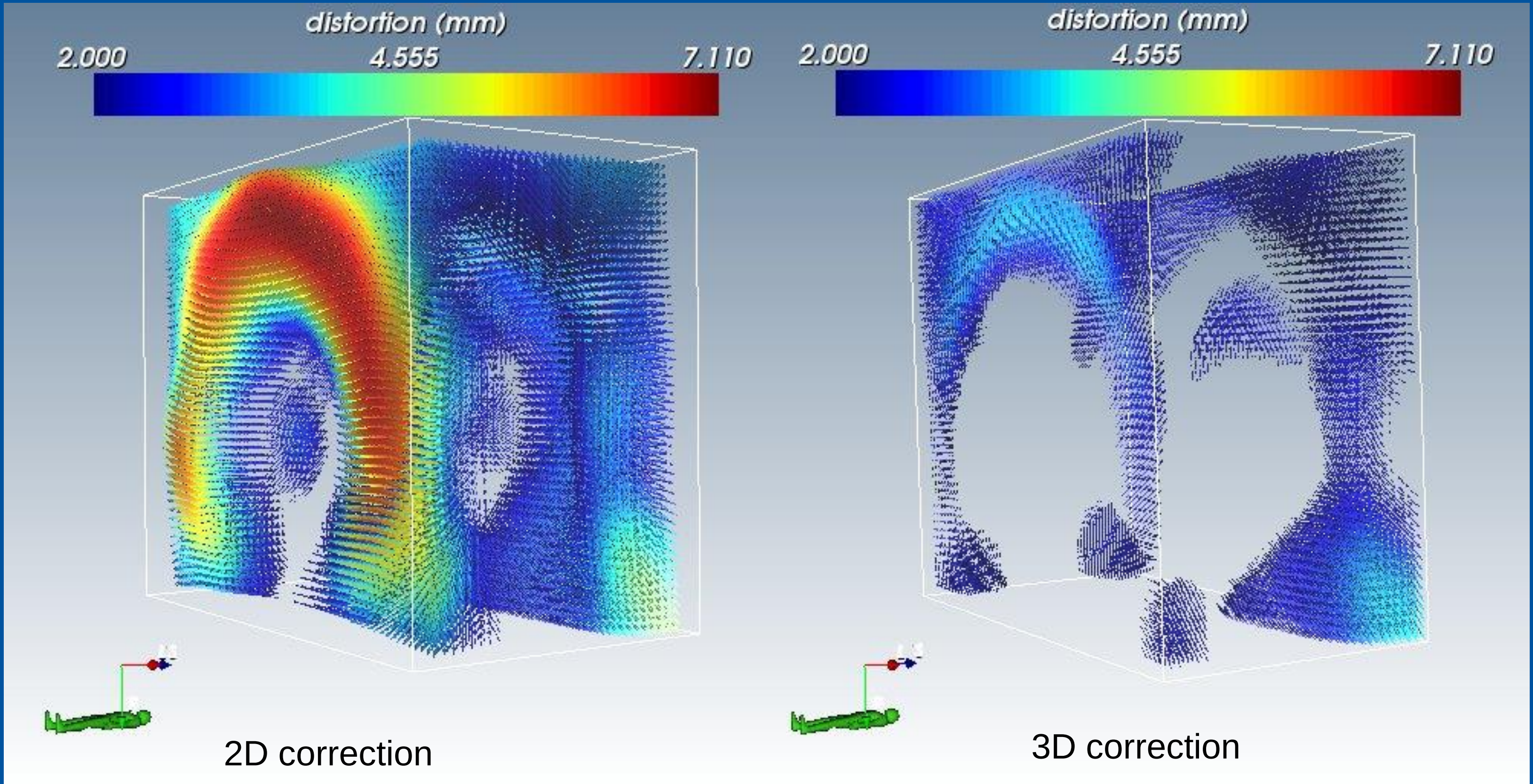
distortion (mm)
2.000
4.555
7.110
distortion (mm)
2.000
4.555
7.110

2D correction

3D correction

- 3D correction introduced circa 2006 and adopted by vendors

System measurements

Paper	Year	Phantom size	System	Error
Vermandel	2014	(Head) 24 cm	Various 3.0T & 1.5T	Mean 1 mm uncorrected, 0.5 mm corrected
Glide-Hurst	2014	2500 points, 40 x 40 x 40 cm	1.0T Panorama	24% > 3mm at 150-200 mm radius
Balter	2014	4689 points, 46 x 35 x17 cm	3.0T Skyra	<1 mm at 17 cm radius (60 mm z)
Walker	2015	5830 points, 50 x 38 x 51 cm	3.0T Skyra	250 mm radial, 200 mm z 29-87% of phantom <2mm
Torfeh	2015	357 rods, 40 x 40 x 19 cm	1.5T GE 450w	95% <1mm at 200 mm radial

Characterizing geometrical distortions

- Currently no standard phantom/QA
- Good resolution of points
- Large coverage (x,y,z)
- Flexible design (weight)
- CT compatible
- Rods v points (susceptibility)
- Positive/negative signal material
- Semi-automated measurements

Magnetic susceptibility

Paramagnetic
$\chi > 0$

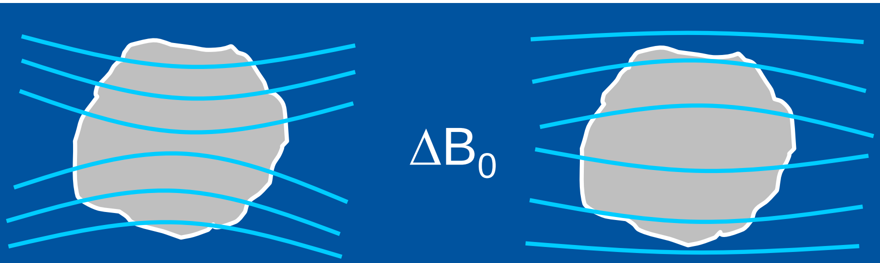

Diamagnetic
$\chi < 0$

Local field variation ΔB_0 superimposes linear gradient

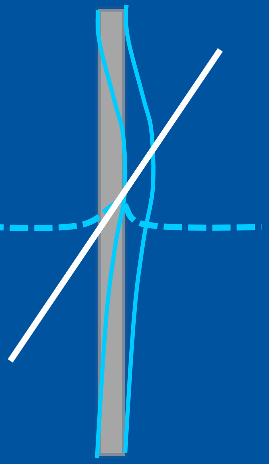

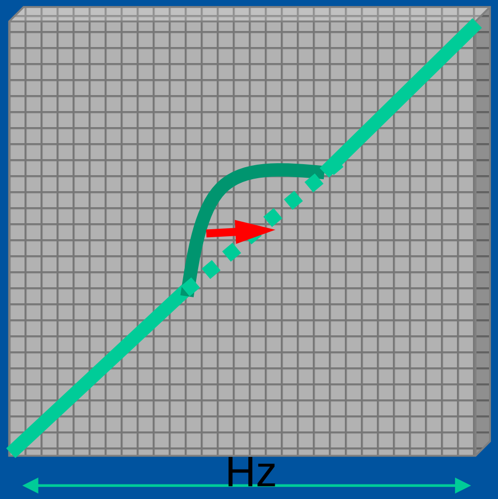

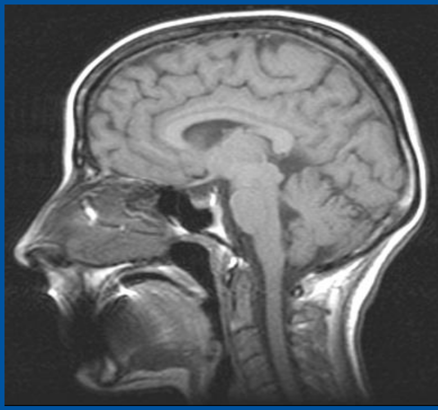

- Off-resonance effects: distortion and signal variations (voids & hyperintensity)
- Ferromagnetic material (χ>>0) has severe effect

Susceptibility artifacts

- Markers around head

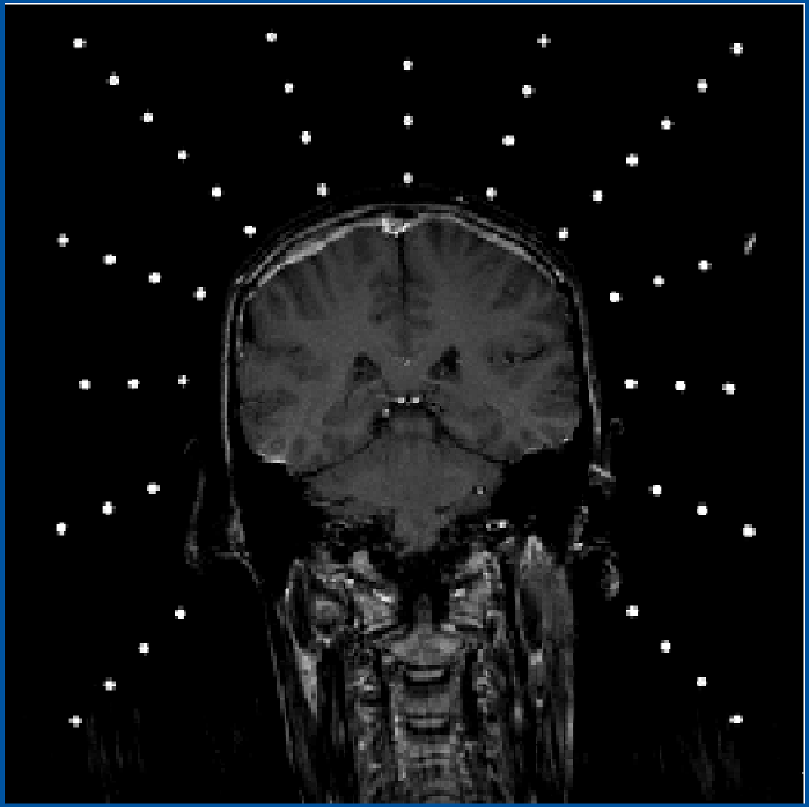

Moerland, PhD thesis 1996

Susceptibility artifacts

- Markers without head

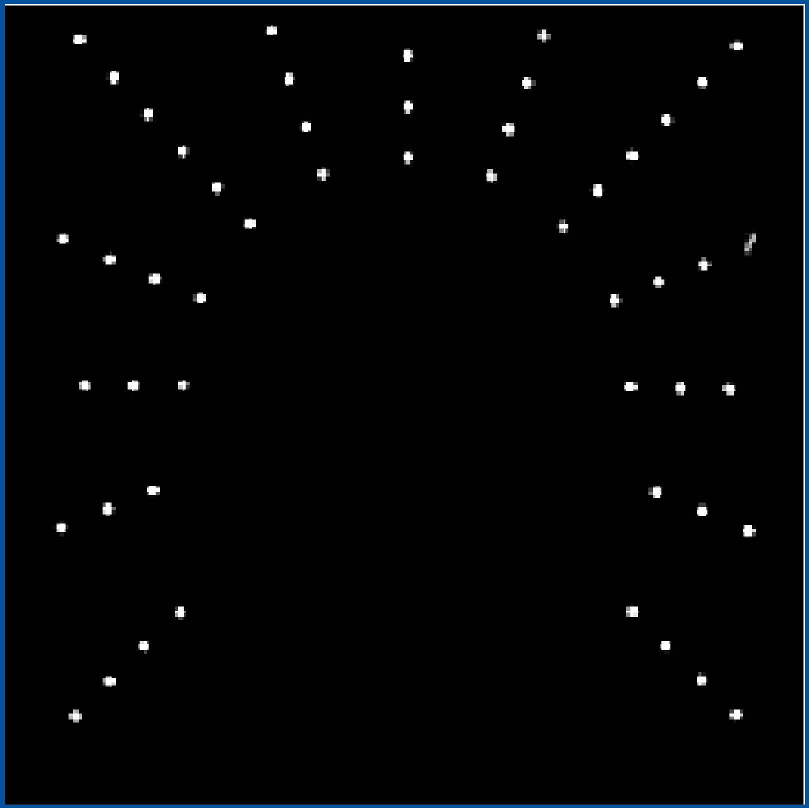

Moerland, PhD thesis 1996

Susceptibility artifacts

- Overlay of images

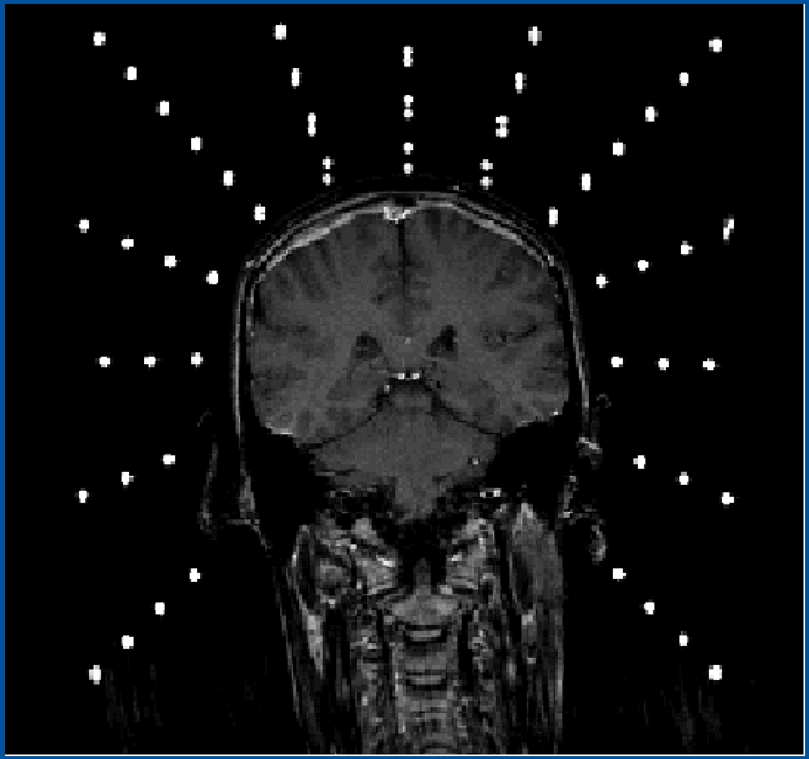

Moerland, PhD thesis 1996

Calculation of field distortions

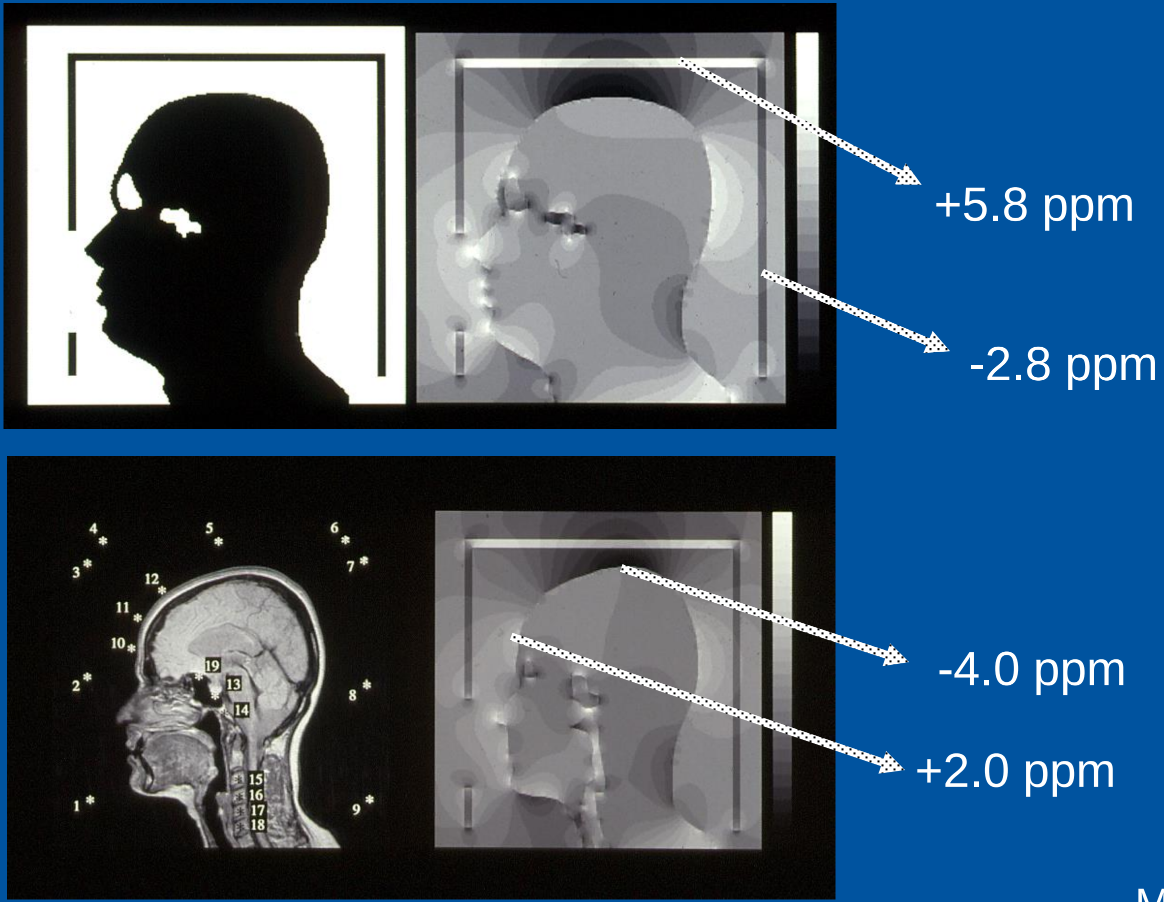
1
2
3
4
5
6
7
8
9
10
11
12
13
14
15
16
17
18
19

+5.8 ppm

-2.8 ppm

-4.0 ppm

+2.0 ppm

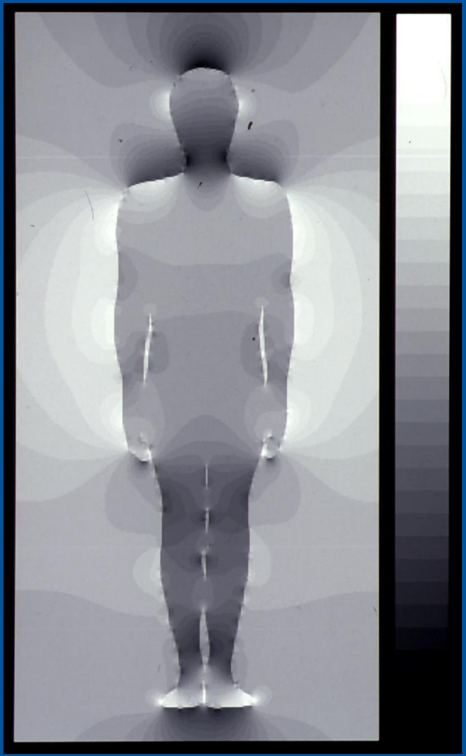

Moerland et al. 1996; Phys. Med. Biol. 40:1651-1664

Susceptibility artifact in read-out direction

$$x_1 = x + \frac{\Delta B_0(x,y,z)}{G_x} + \frac{\Delta B_{G_x}(x,y,z)}{G_x}$$

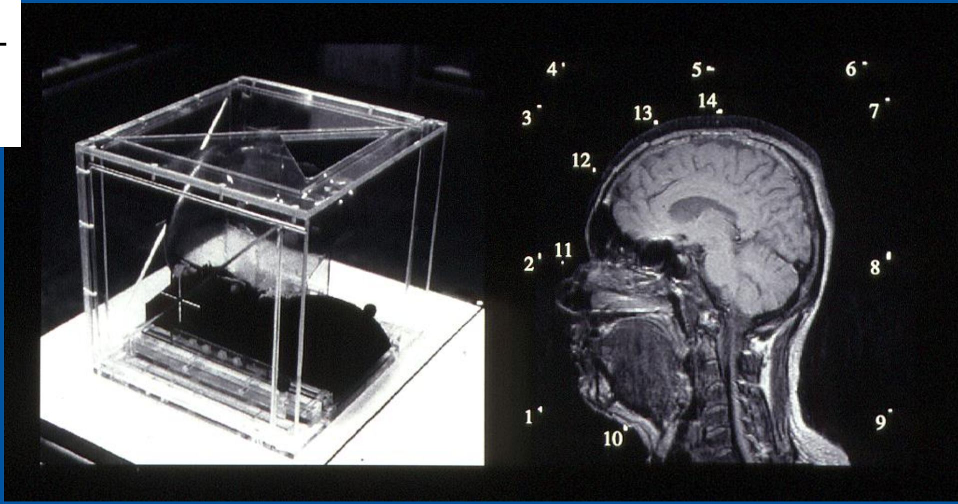
4
5
6
3
13
14
7
12
2
11
8
1
10
9

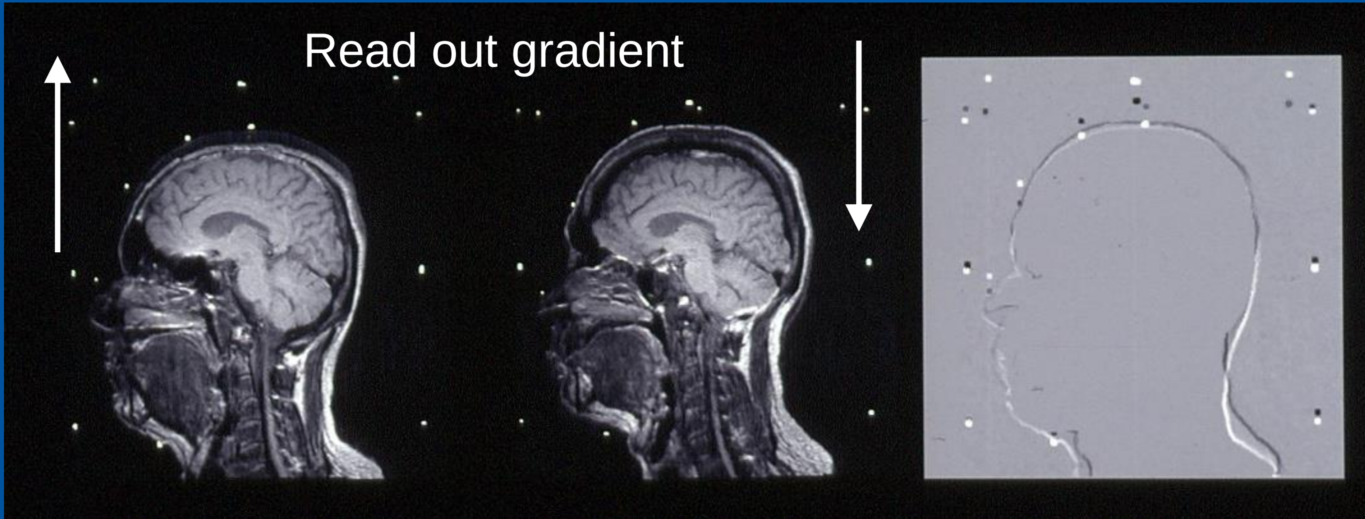
Read out gradient

Moerland et al. 1996;
Phys. Med. Biol. 40:1651-

Shimming

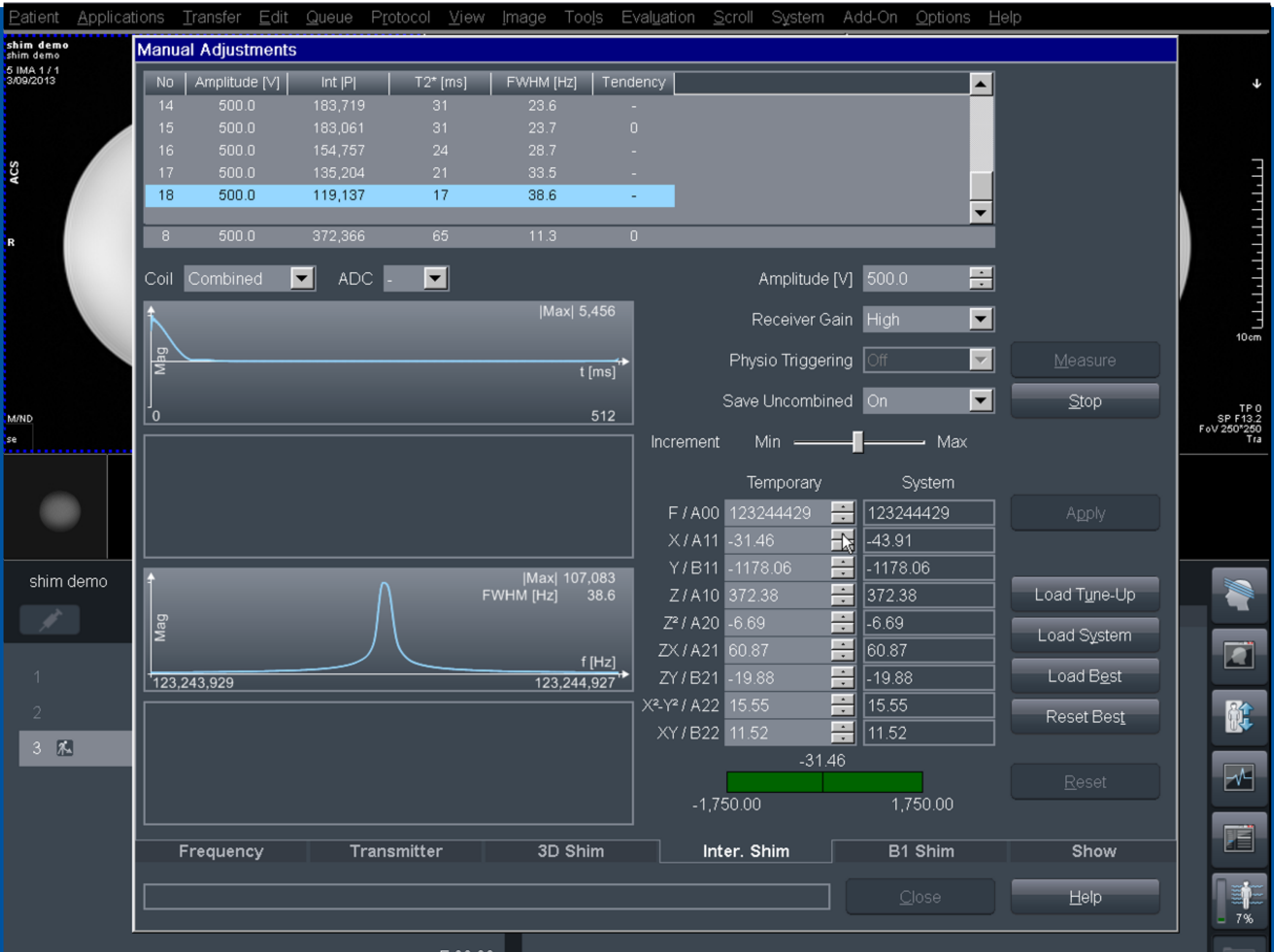

Patient Applications Transfer Edit Queue Protocol View Image Tools Evaluation Scroll System Add-On Options Help
shim demo
shim demo
5 IMA 1 / 1
3/09/2013
ACS
R
M/ND
se
10cm
TP 0
SP F13.2
FoV 250*250
Tra
shim demo
1
2
3
7%
Measure
Stop
Apply
Load Tune-Up
Load System
Load Best
Reset Best
Reset
Frequency
Transmitter
3D Shim
Inter. Shim
B1 Shim
Show
Close
Help
|Max| 5,456
Mag
t [ms]
0
512
|Max| 107,083
FWHM [Hz] 38.6
f [Hz]
123,243,929
123,244,927

Manual Adjustments

No	Amplitude [V]	Int |P|	T2* [ms]	FWHM [Hz]	Tendency
14	500.0	183,719	31	23.6	-
15	500.0	183,061	31	23.7	0
16	500.0	154,757	24	28.7	-
17	500.0	135,204	21	33.5	-
18	500.0	119,137	17	38.6	-
8	500.0	372,366	65	11.3	0

Coil: Combined
ADC: -
Amplitude [V]: 500.0
Receiver Gain: High
Physio Triggering: Off
Save Uncombined: On
Increment: Min – Max

	Temporary	System
F / A00	123244429	123244429
X / A11	-31.46	-43.91
Y / B11	-1178.06	-1178.06
Z / A10	372.38	372.38
Z² / A20	-6.69	-6.69
ZX / A21	60.87	60.87
ZY / B21	-19.88	-19.88
X²-Y² / A22	15.55	15.55
XY / B22	11.52	11.52

-31.46
-1,750.00 … 1,750.00

B0 mapping

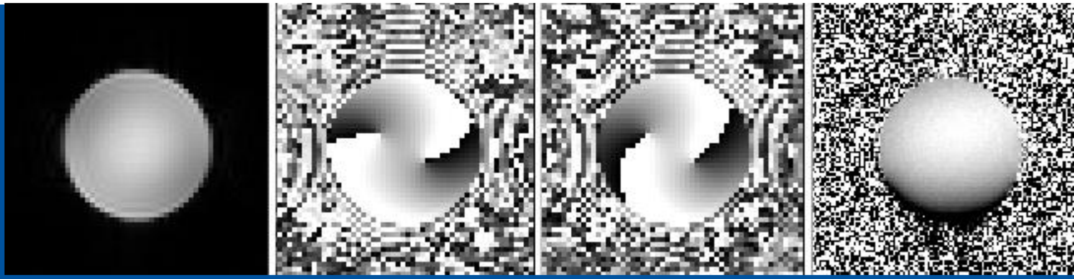
Magnitude Phase (TE1) Phase (TE2) Difference

- Air/tissue interfaces problematic
- Dynamic & HO shimming
- May be measured/corrected:
  - Image at two different TEs
  - Reconstruct phase difference
- Bhagwandien measured -5 to +6ppm i.e. nearly twice WFS

$$\Delta B_0 = \frac{\Delta\varphi}{\gamma \Delta TE}$$

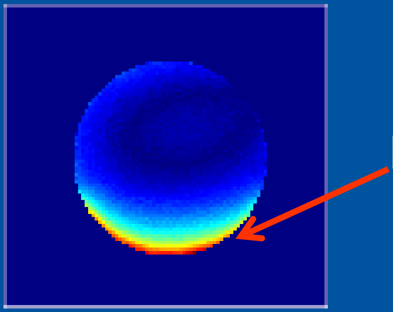
Maximum 34 Hz (0.3 ppm)

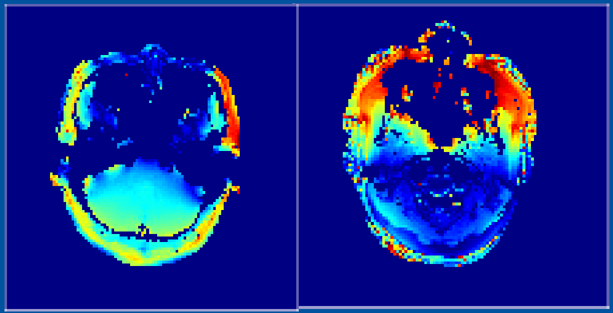
Maximum 203 Hz (1.6 ppm @ 3T)

B0 mapping

Male volunteer. Notice B_0 variations near the rectum due to susceptibility effects of rectal gas

Such a map can be used to calculate the distortion of the image, and in some cases correct for it

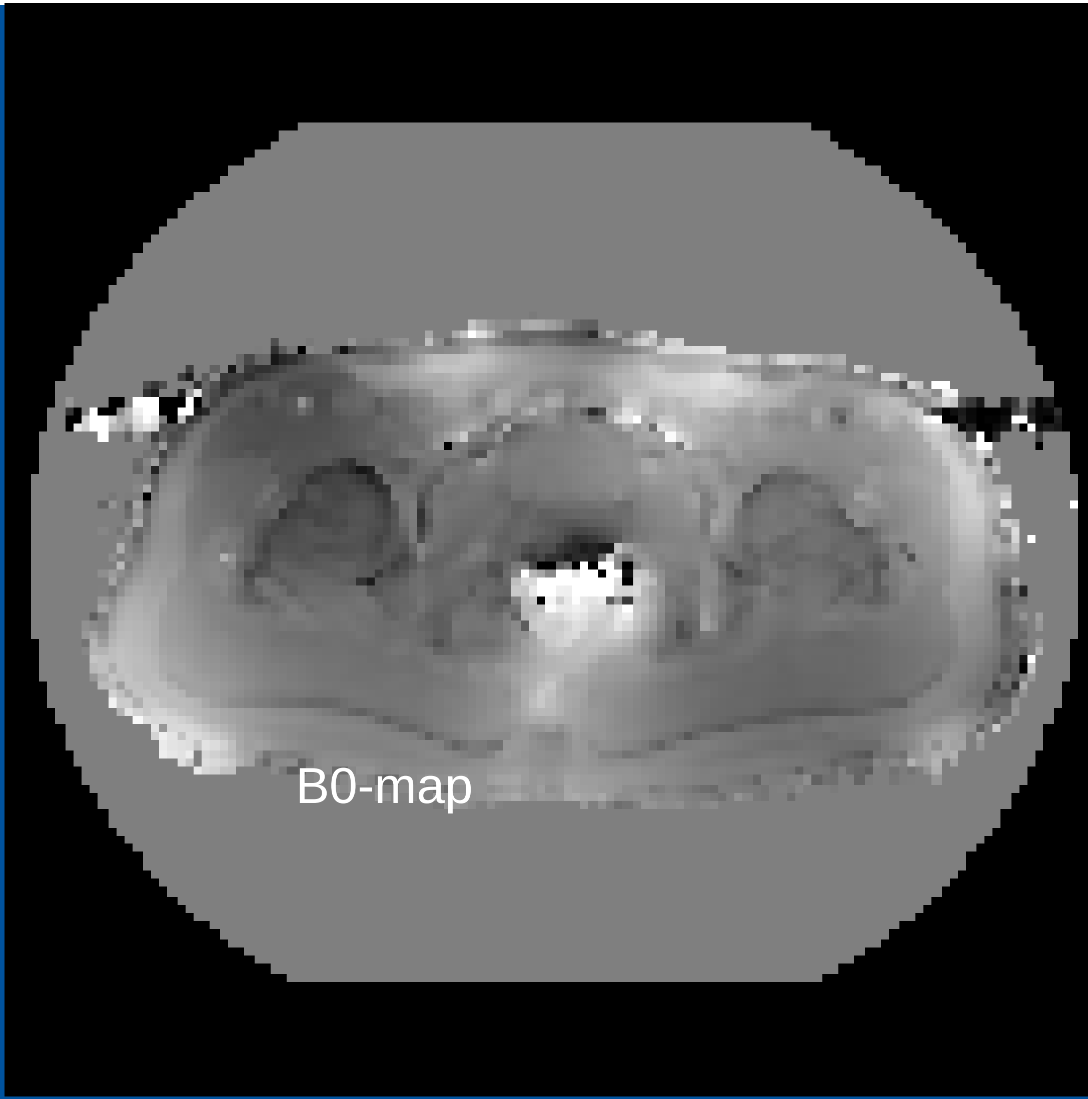

Examples of artifacts

- Susceptibility artifacts
- Water-fat shift
- Motion
- bSSFP artifacts (bTFE, bFFE, trueFISP)
- EPI artifacts

Example from clinical practice.
What is wrong?

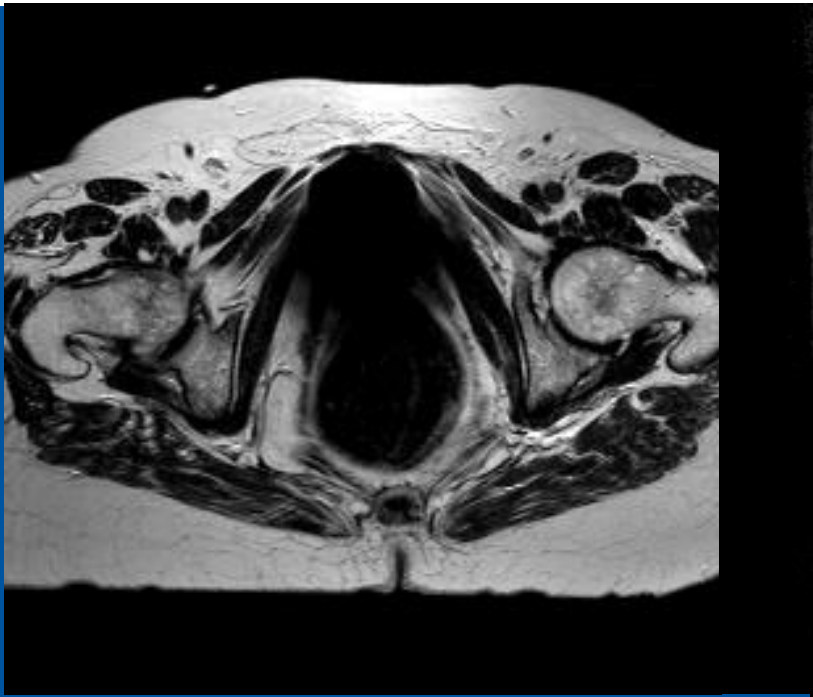

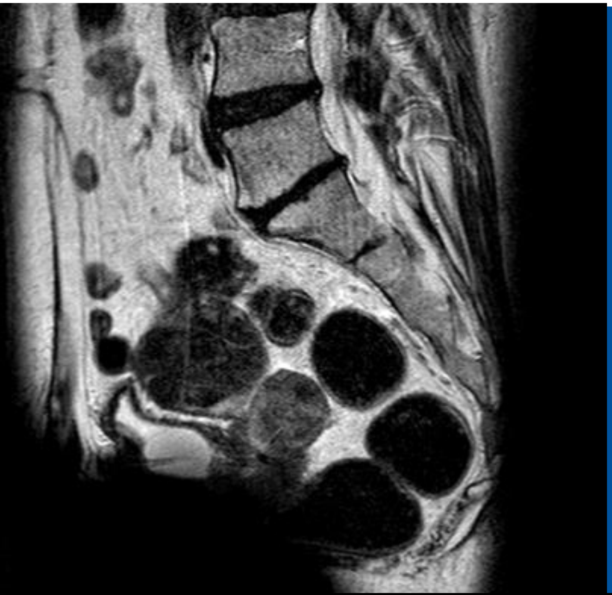

- MRI exam of patient with cervical cancer
- T2-SE sequences shows large area with signal loss
- T1w-THRIVE sequence shows dark ring

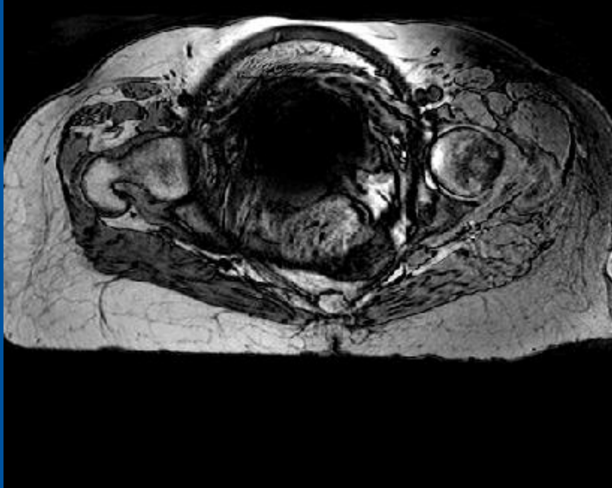

CT scan of same patient

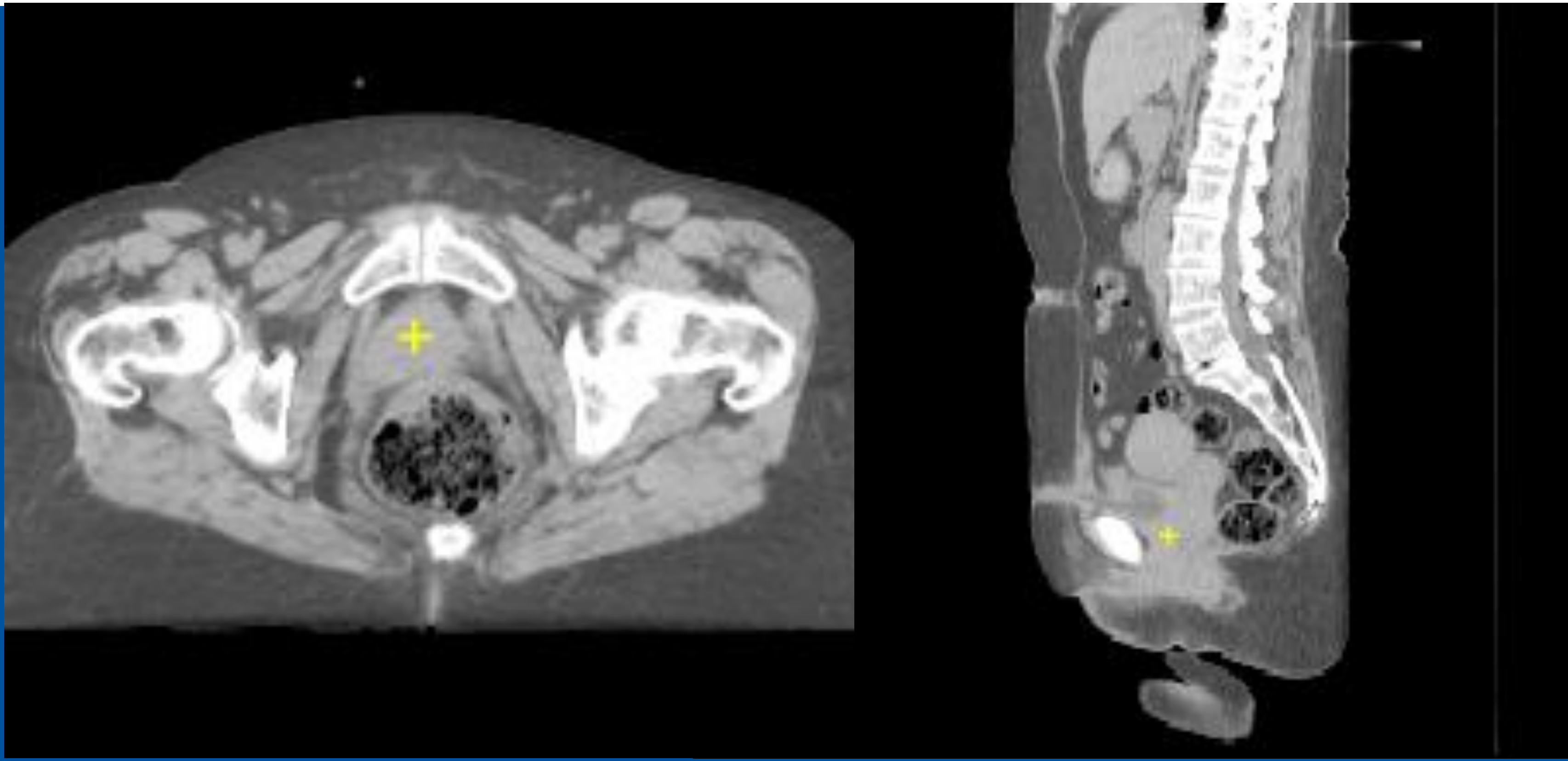

- No obvious metal
- However: a small ferro-magnetic button in her clothes
- Solution: remove metal

Patient with hip prosthesis

- A metal hip prosthesis (titanium)
- Verified that it is safe for the patient
- Big artifact on bSSFP sequence

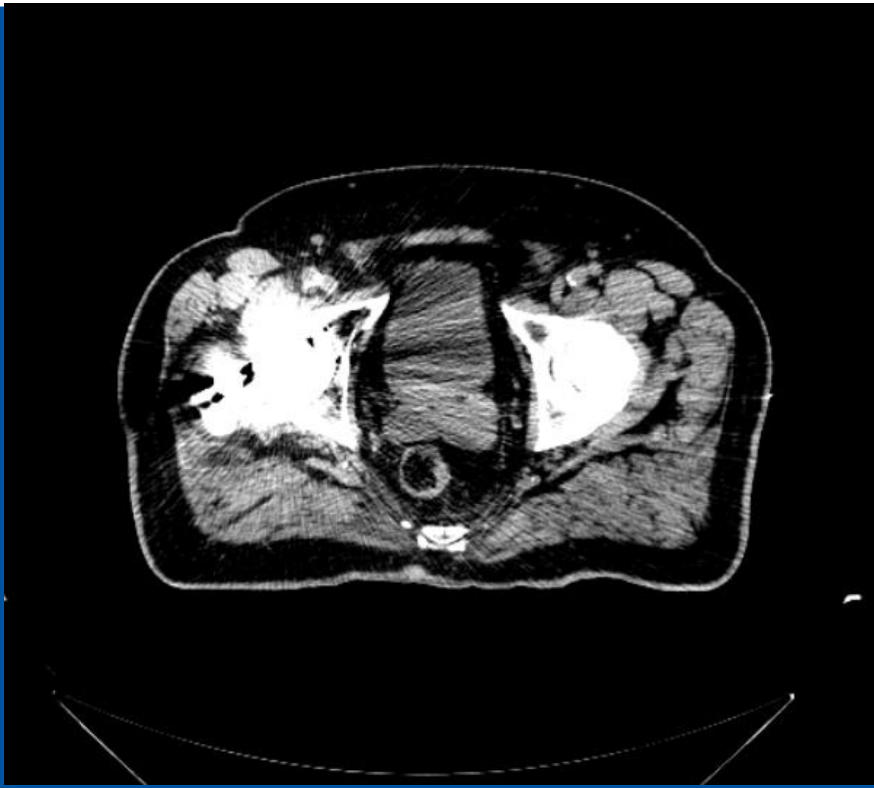

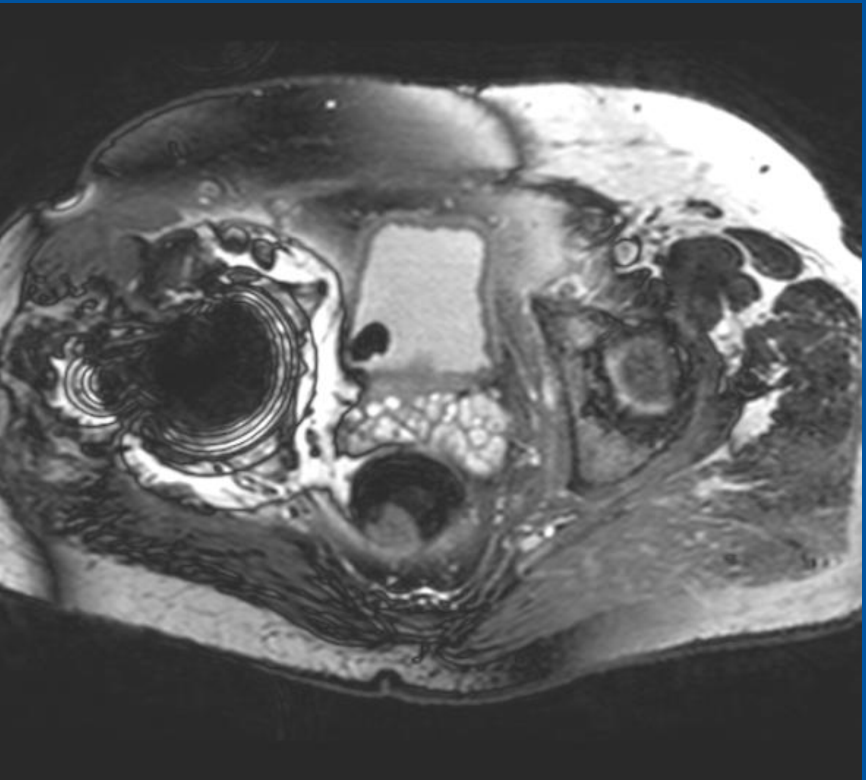

Patient with hip prosthesis

- The T_1-SE sequence and T_2-TSE sequence show a void a the location of the hip, but minimal distortions

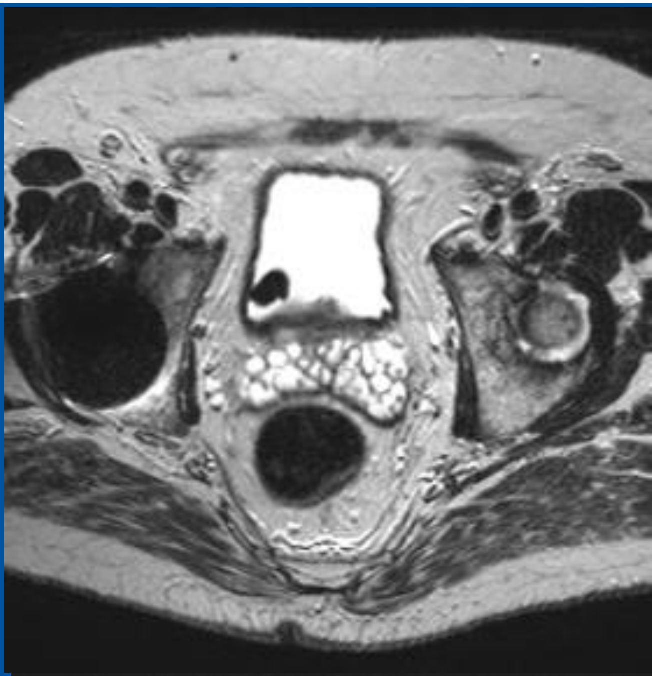

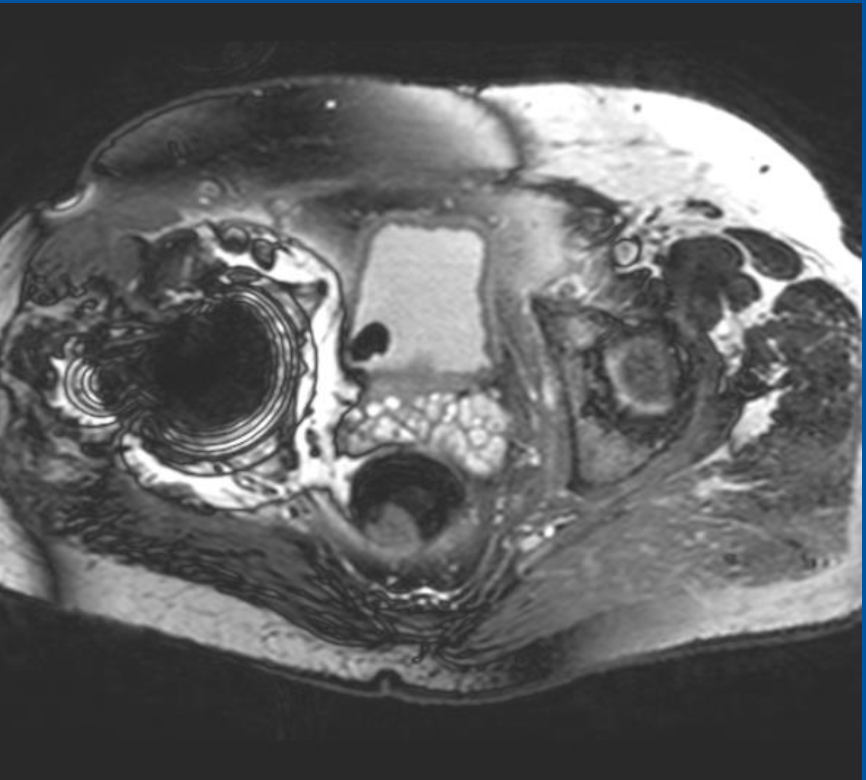

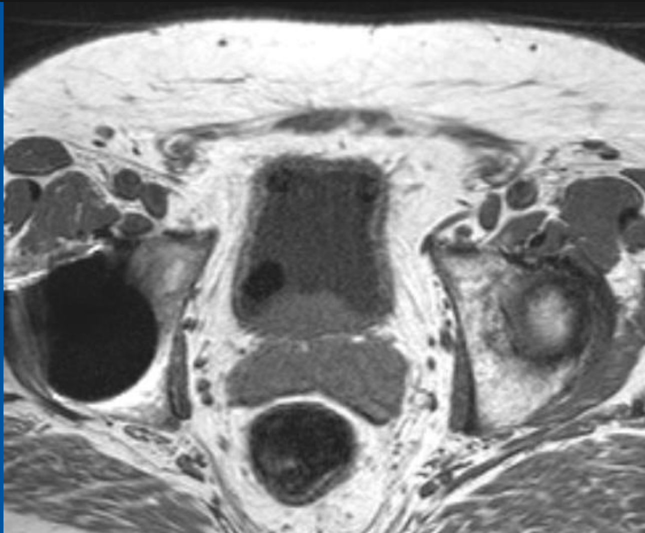

Susceptibility artifact

Artifact:

- Geometrical distortions
- Signal loss

What to do about it:

- Avoid metal, as much as you can
- Minimize pockets of air if possible
- maximize band-width (maximize gradient strength)
- Avoid GE sequences, use SE
- Use short echo times

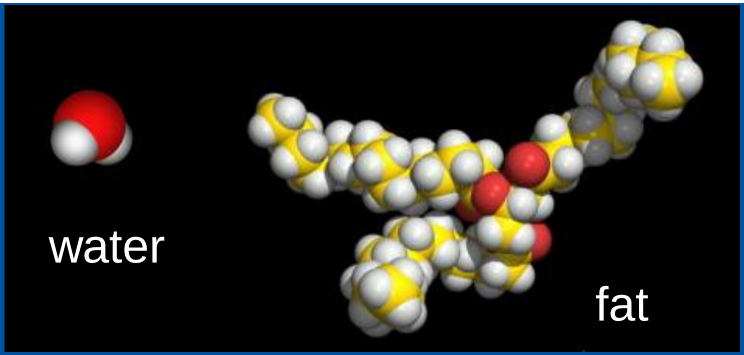

Electron shielding different between molecules

$$B' = B \times (1 - \sigma)$$

Water-fat shift (WFS) = 220 Hz at 1.5 T

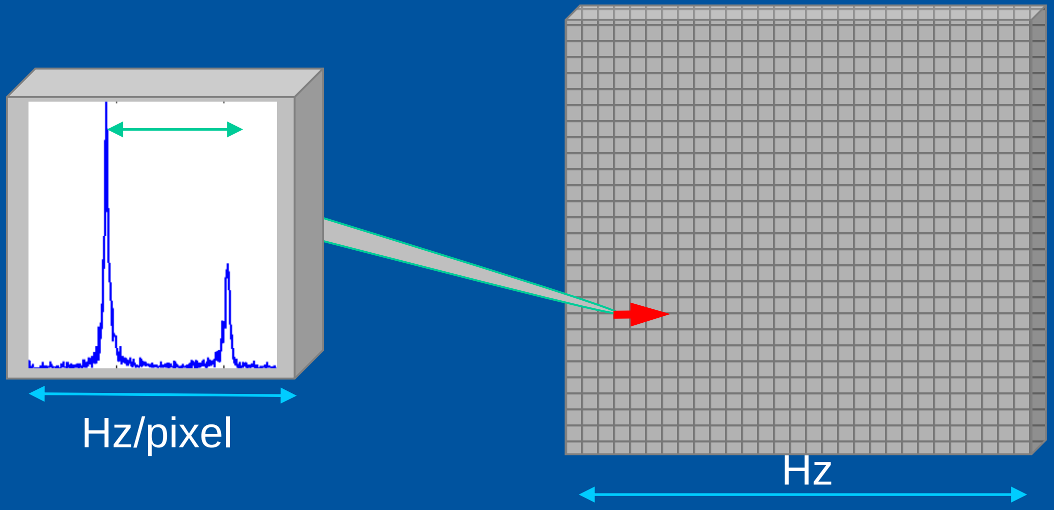

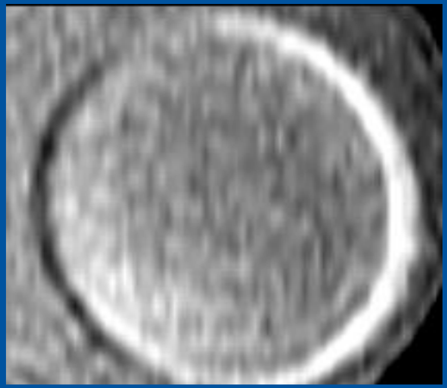

- Produces characteristic signal misregistration
- Assign enough ‘Hz’ across each pixel..increase BW

Water-fat shift

Magnetic field at the nucleus depends on magnetic shielding of surrounding electron clouds, depends on molecular environment

example:
resonant frequencies of protons in fat and water differ by 220 Hz

220 Hz = 3.4 ppm at 1.5 T

$3.4\ 10^{-6} \cdot 1.5\text{T} = 5.1\ \mu\text{T}$ at 1.5 T

$= 5.1\ \mu\text{T} / 3\ \text{mT/m} = 1.7\ \text{mm}$ at 1.5 T and read out gradient 3 mT/m

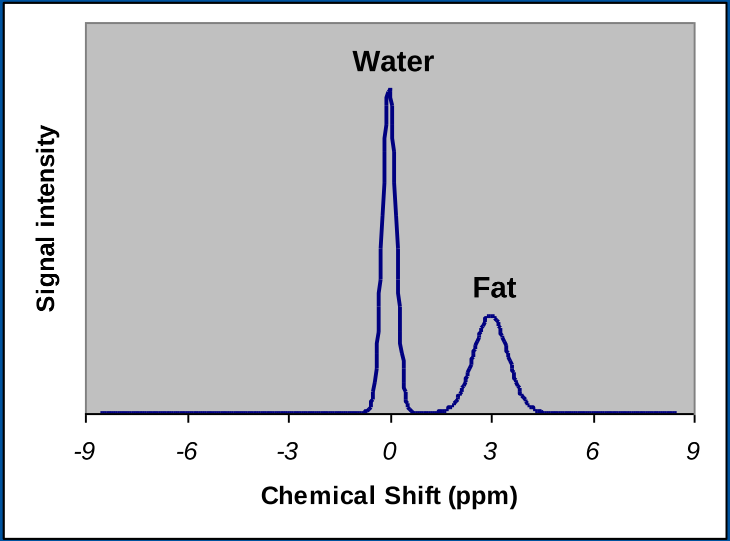

- artifact
  - increases with B_0
  - decreases with gradient strength

Impact of band width in read-out direction (water-fat shift)

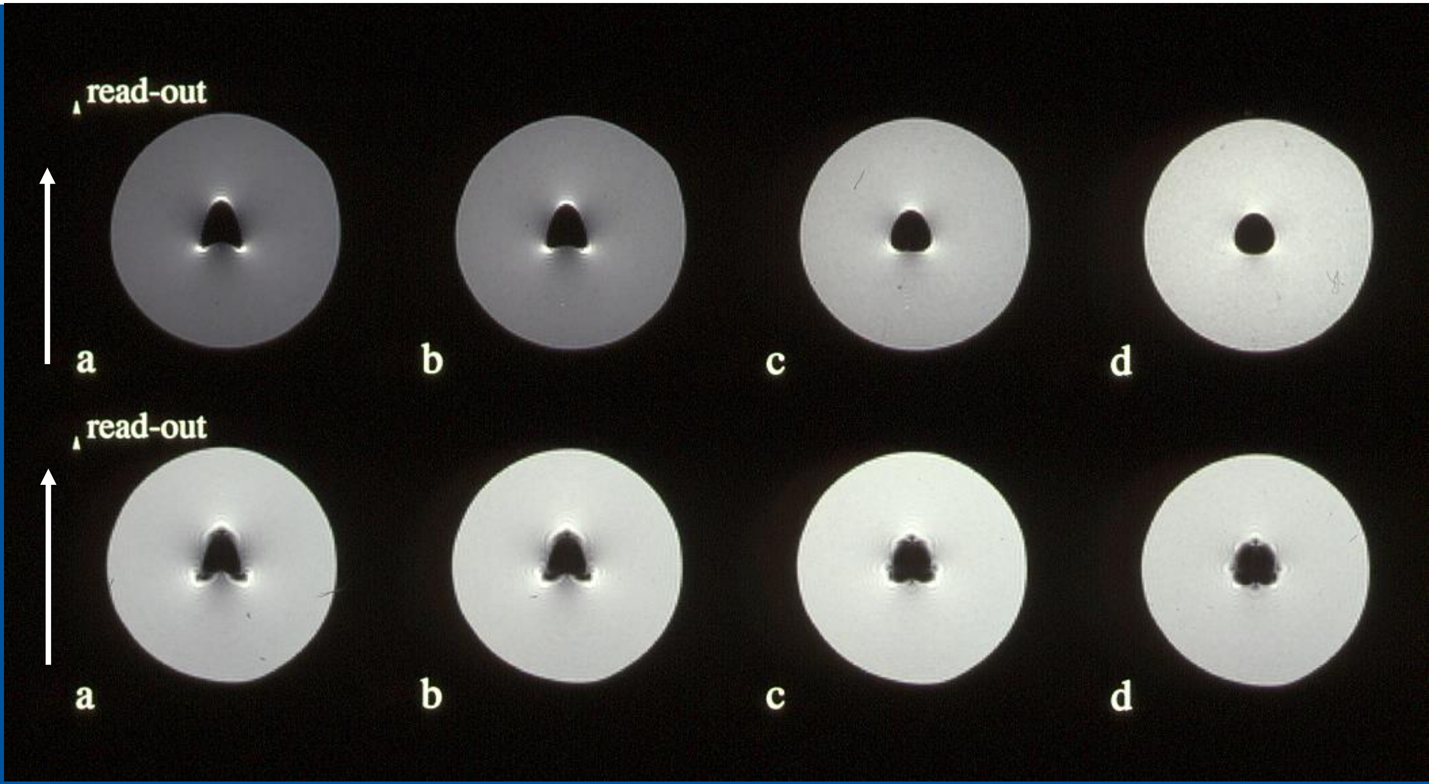
read-out
a
b
c
d
read-out
a
b
c
d

Spin echo

Gradient echo

Water-fat shift: 5 pixels 4 pixels 2 pixel 1 pixel

- Susceptibility artifact occurs in read-out direction
- Gradient echo shows additional dephasing

Water-fat shift

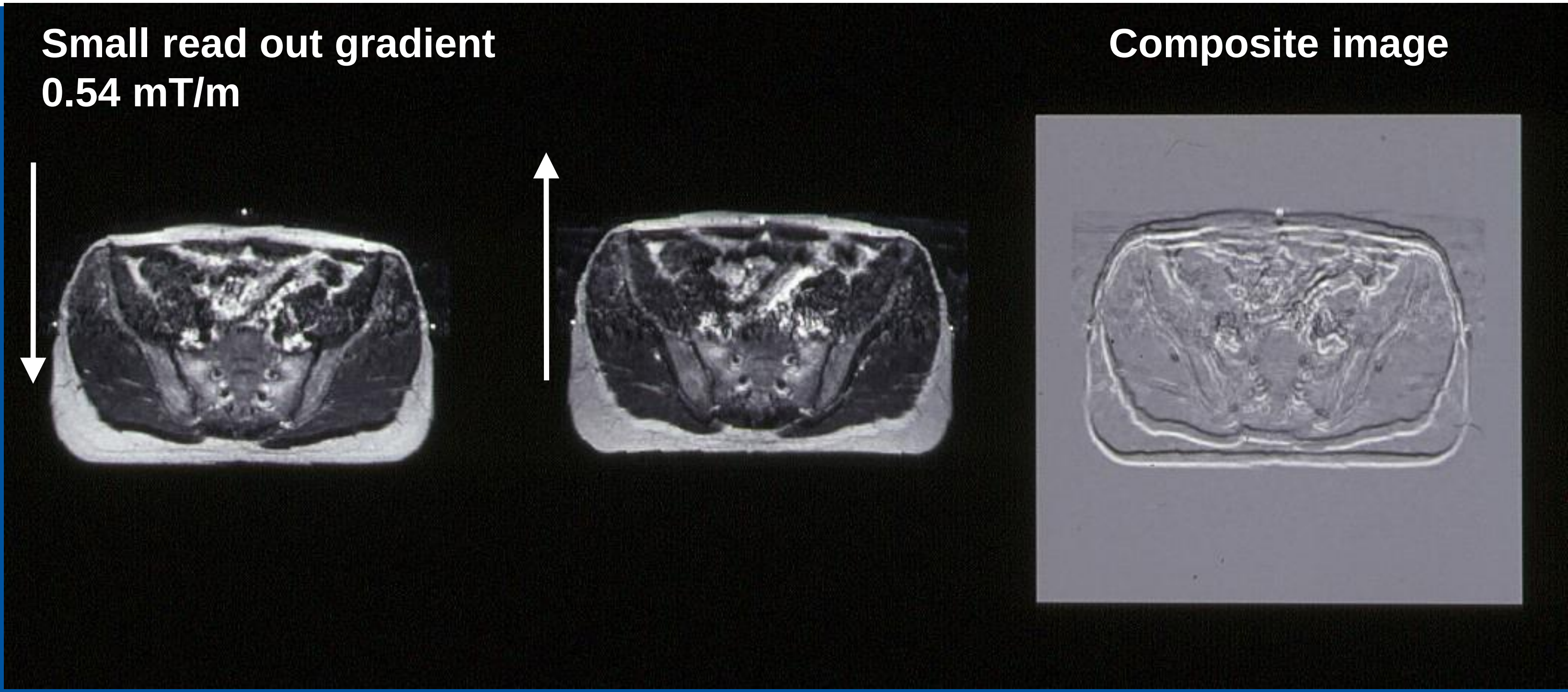
Small read out gradient
0.54 mT/m
Composite image

Water-fat shift $\approx$ 9 mm
Contour distortions
marker position error

Distortions due to ΔB_0 (water fat shift, susceptibility) can be reduced to < 1mm by increasing gradient strength, However: gradient errors remain!

Water-fat shift

Artifact:

- Geometrical distortions
- Signal loss

What to do about it:

- Maximize band-width (maximize gradient strength)
- Fat suppression

Question: motion artifacts

- Motion of a patient in the MRI scanner results in an artifact. What is the appearance of this artifact?

1. Blurring of the image in each slice
2. Ghost images in each slice, overlaying the ‘true’ image
3. Shifts between the slices

Motion of a patient in the MRI scanner results in an artifact. What is the appearance of this artifact?

1. Blurring of the image in each slice
2. ★ Ghost images in each slice, overlaying the ‘true’ image
3. Shifts between the slices

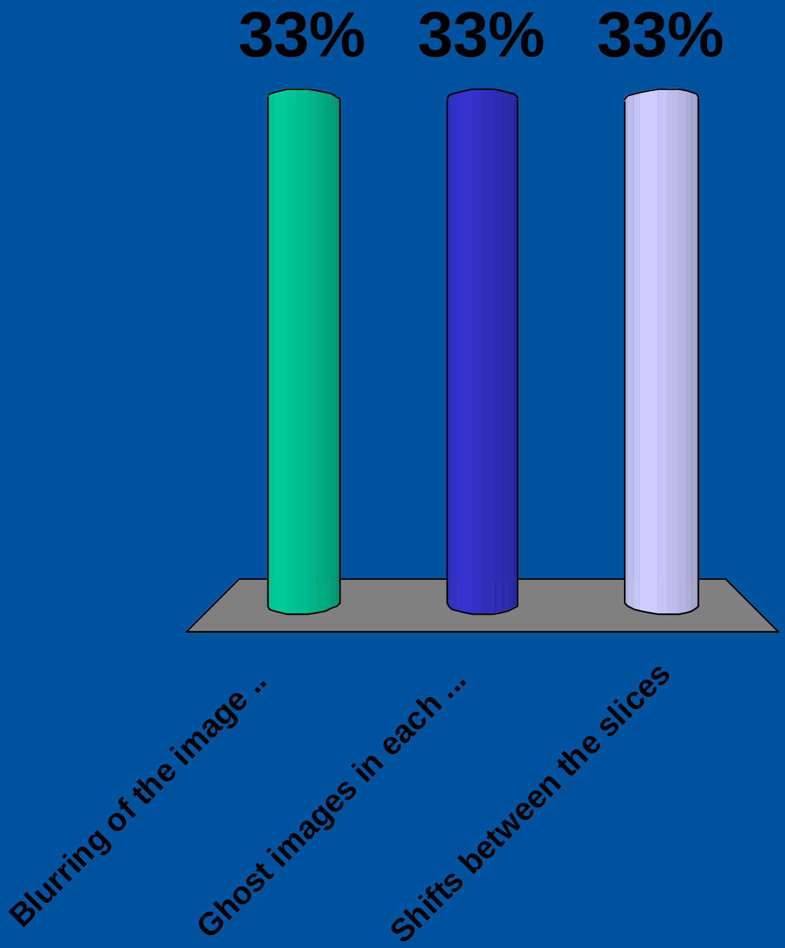

Motion artifacts

Ghost images

- Interference at periodical intervals along phase encoding axis
- A small motion may result in large offsets

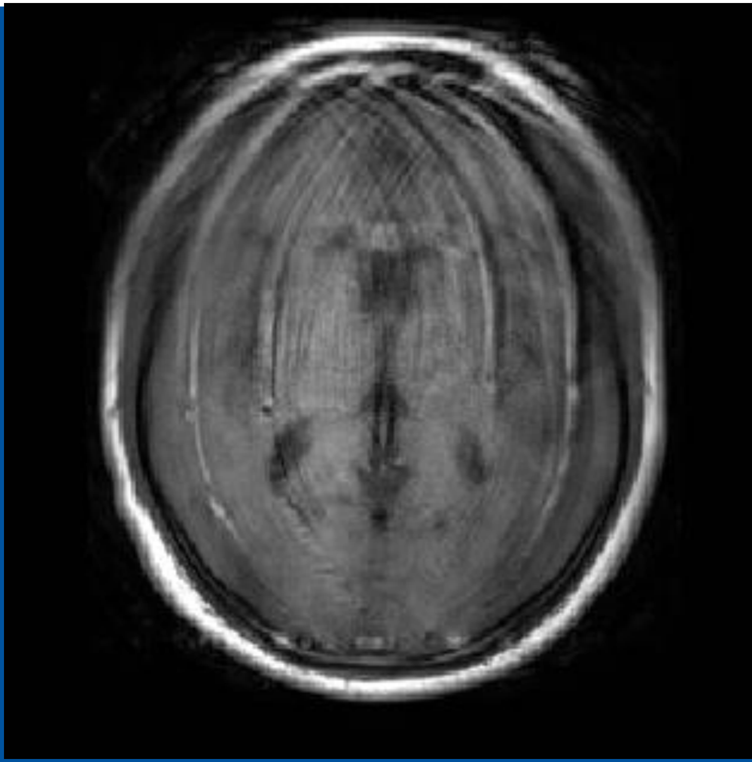

Motion artifacts

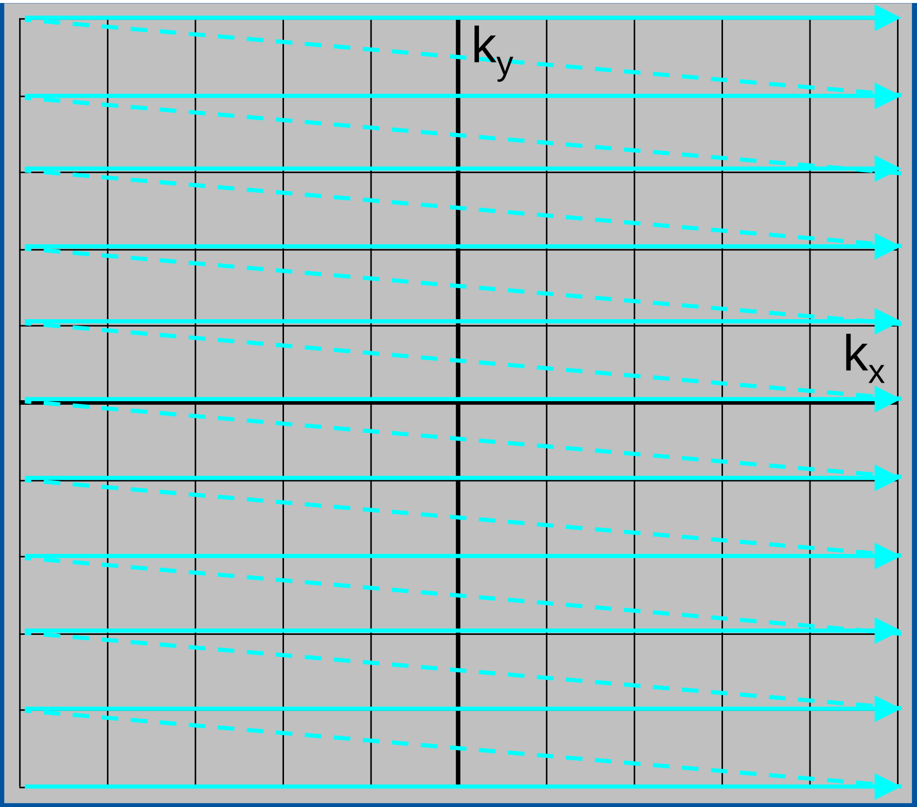

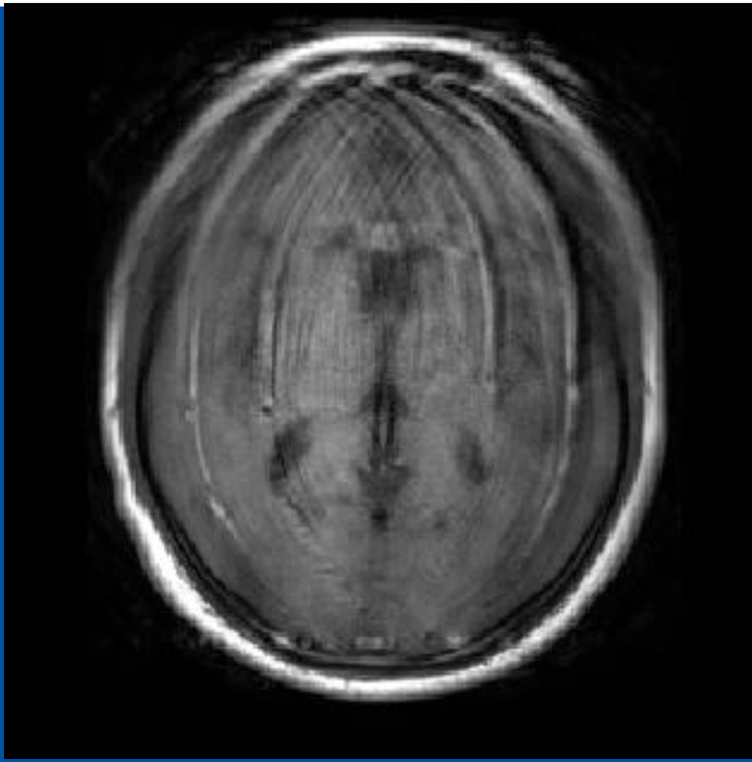

- Motion artifacts propagate mainly in the phase-encoding direction. Motion between phase encoding steps will corrupt the phase-encoding, resulting in ghosts
- Signal sampling in the read-out direction is usually faster than physiological motion and may produce only some spatial blurring

What to do about it?

- Fixation
  - Breath hold
- Fast imaging, cine MRI
- Respiratory gating, cardiac gating etc.
- Navigators, Propeller/MultiVane

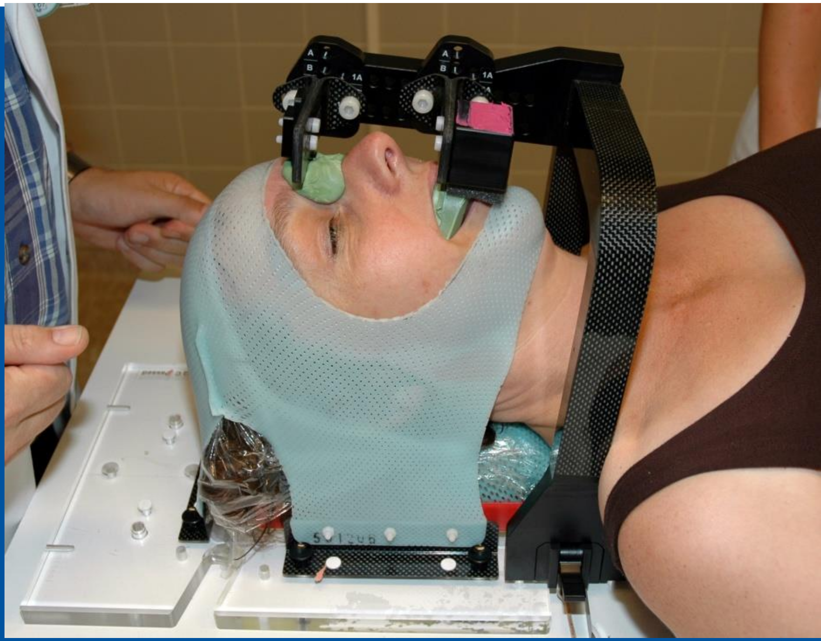

Motion correction with a Propeller sequence

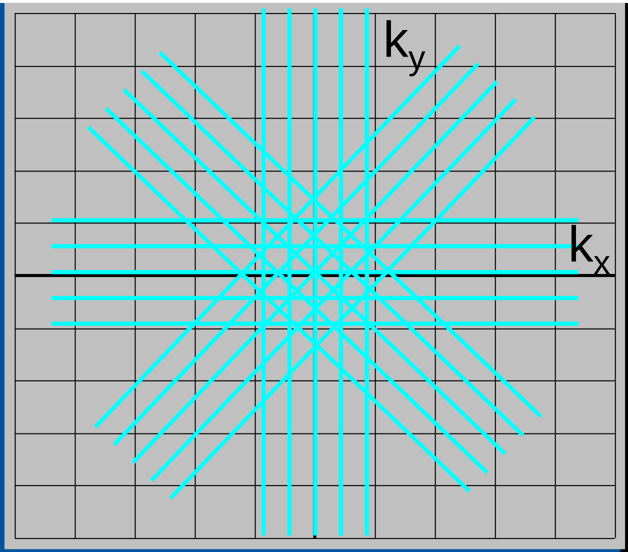

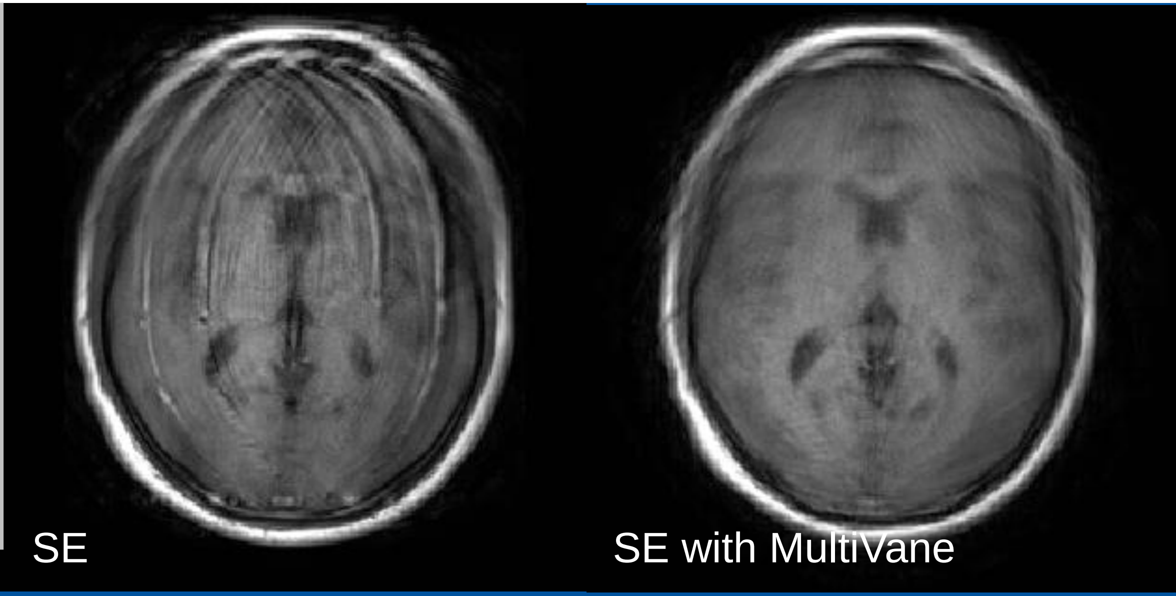

- Sample a set of lines in k-space repeatedly at a different orientation
  - The central part is sampled each time, allowing for a phase correction of the signal
  - The outer part of k-space is sampled only by one of the vanes

Propeller sequence: Eye movement

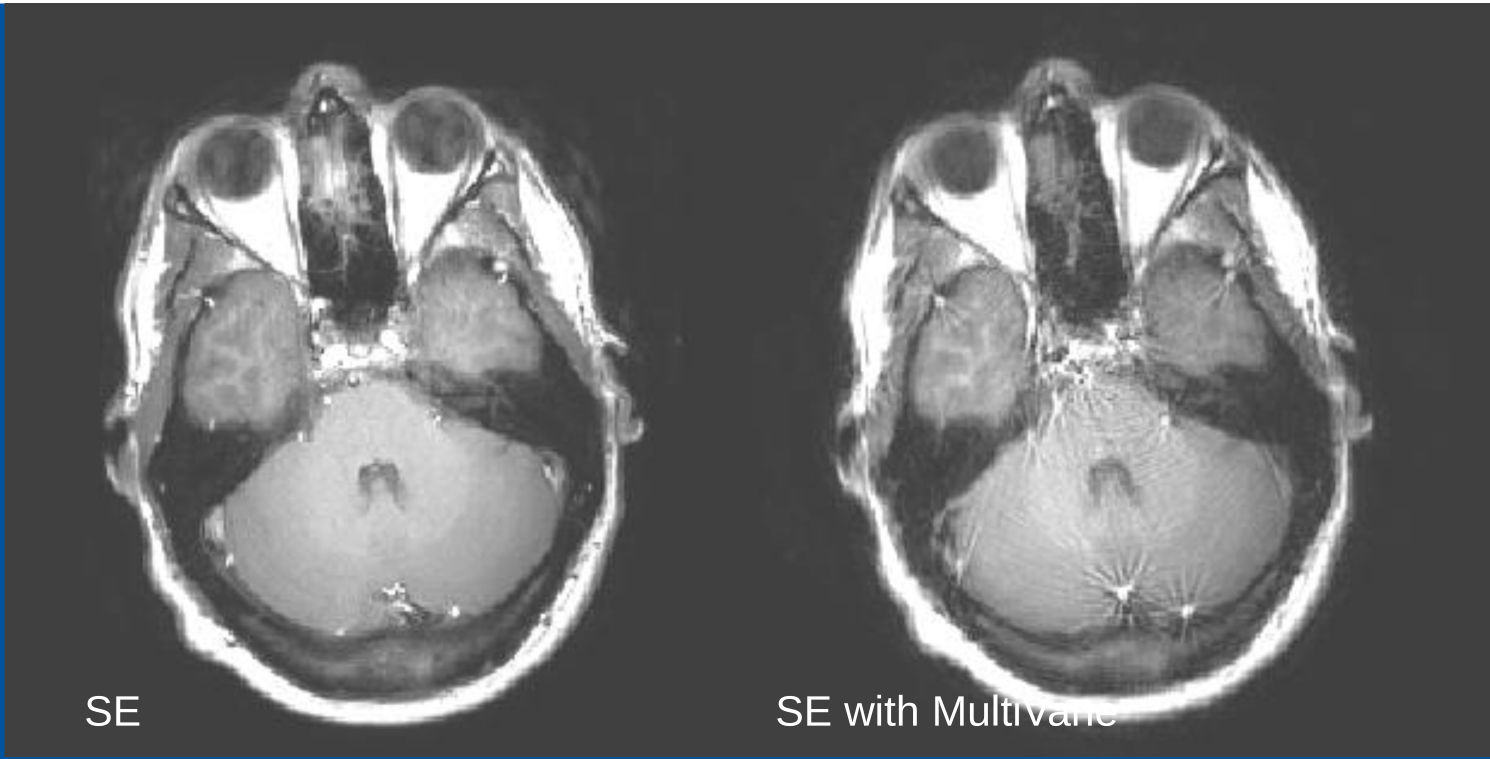

- The MultiVane sequence in a Philips 3T achieva scanner reduces the ghosting artifact around the eyes
- Near blood vessels ‘streak’ artifacts show up, due to undersampling of the outer part of k-space

bSSFP artifact

- Balanced Steady State Free Precession

  also known as:

  - bTFE, bFFE (Philips)
  - trueFISP (Siemens)
  - FIESTA (GE)

- Steady state depends on T_1 and T_2
- Spins from many excitations create a steady state of precessing spins
- B0 distortions (susceptibility) result in spins that are off-resonance and don’t see the RF pulses. Thus they don’t produce a signal

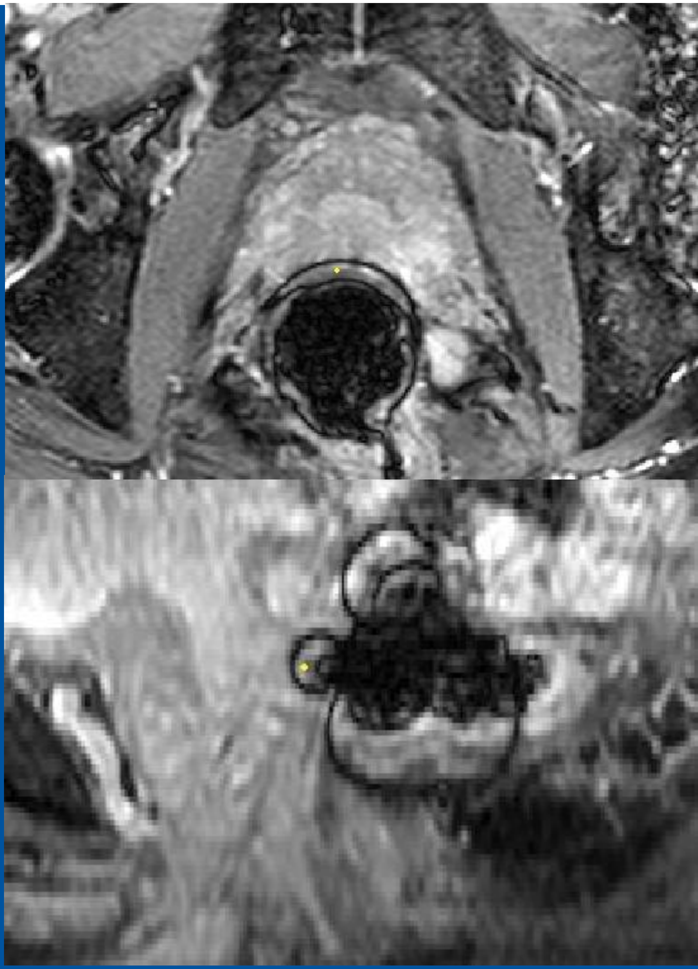

bSSFP artifacts at rectum prostate interface

bSSFP artifact

Artifact:

- A periodic pattern of dark bands in the image

What to do about it:

- Avoid metal, as much as you can
- Minimize pockets of air if possible
- Optimize shimming
- Change the center frequency f_0 (multiple series with shifted f_0)

EPI artifacts

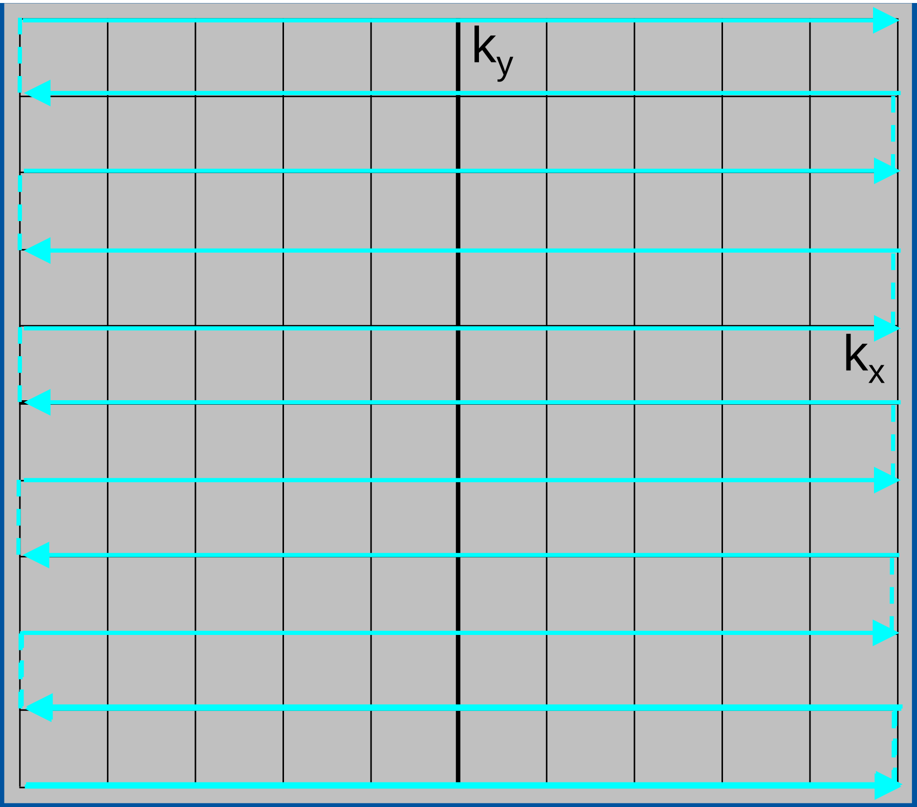

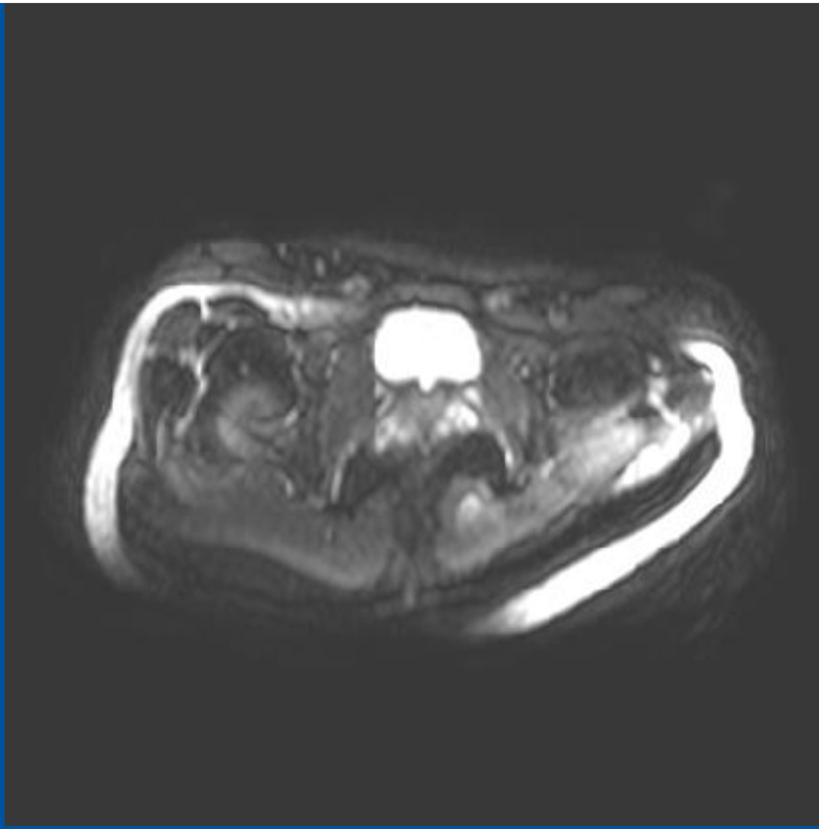

- Very fast switching of gradients because all phase-encoding is done within one read-out
- A very narrow band width is used to collect the data rapidly (example BW = 42 Hz per pixel)
- Therefore very sensitive to B_0 distortions

EPI artifact

Artifact:

- Geometrical distortion

What to do about it:

- Optimize shimming
- Use multi-shot EPI, rather than single shot

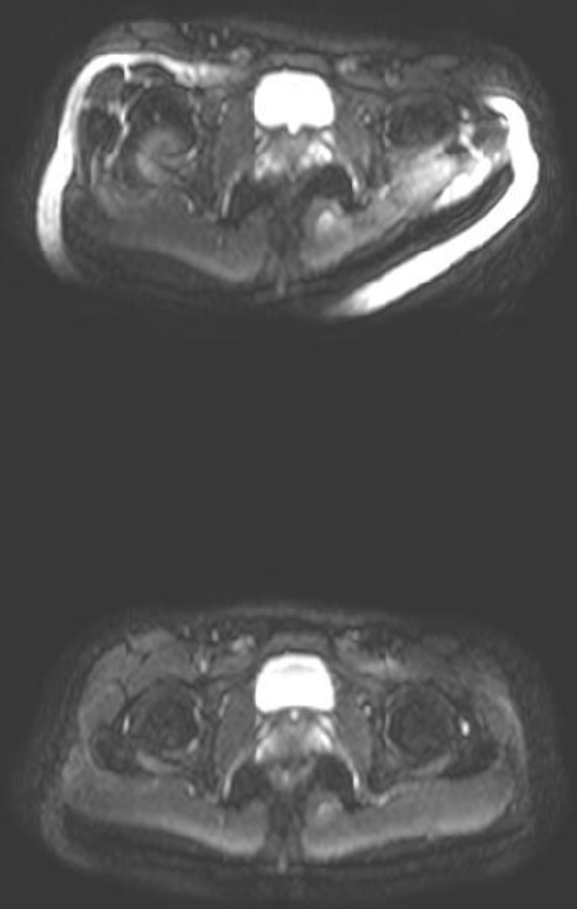

Geometrical artifacts

Artifact	axis	remedy
Fold-over (aliasing)	phase encoding	increase FOV
Ringing (truncation)	both	reduce voxel size
Susceptibility	read-out	increase BW
Water-fat shift	read-out	increase BW
Motion (ghosting)	phase encoding	reduce motion gating fast scanning

Practical consequences

- The geometrical accuracy of MR images tends to be worse towards the edges of the field of view
- Field distortions due to susceptibility differences are larges near interfaces (body contour, air pockets)
- Devices used during interventions (brachytherapy) make cause artifacts

Pracitical consequences

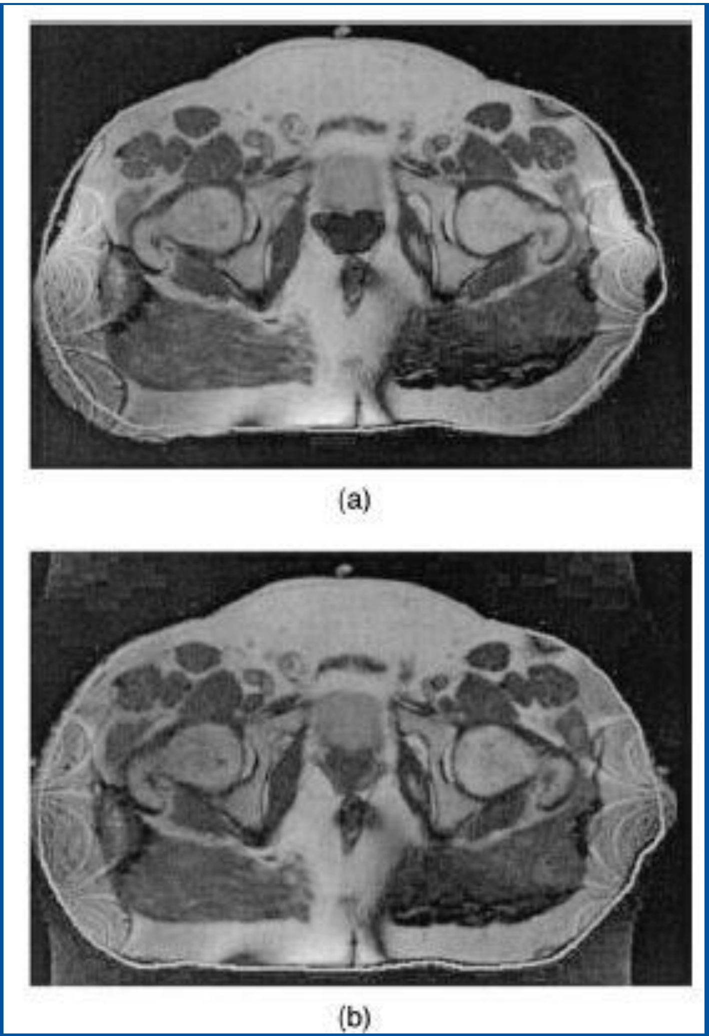
(a)

(b)

Mah et al. 2002 Int. J. Radiat. Oncol. Biol. Phys. 53 (3), 757-765

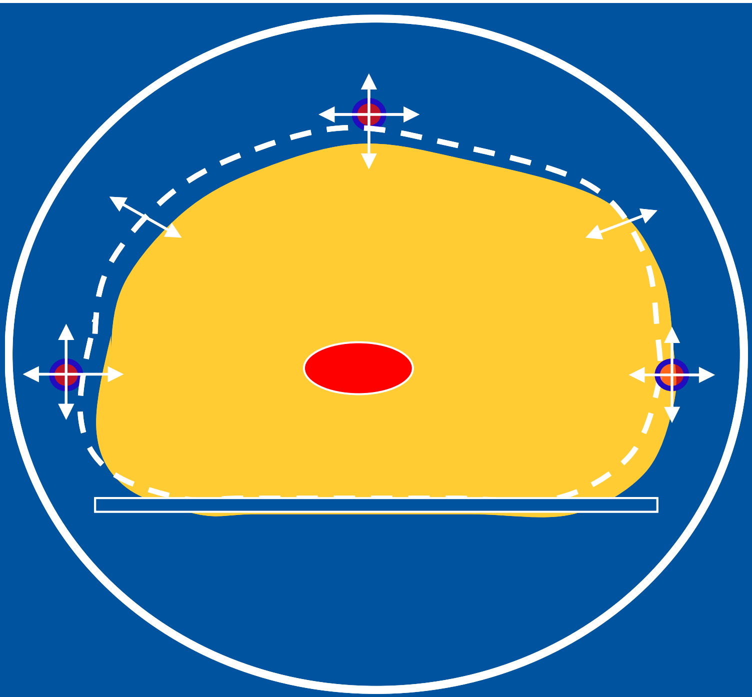

Largest distortions at the edges of the MR bore

Markers on the skin not reliable as reference for beam setup

▯ Registration of planning CT and MRI

MRI-guided interventions: needles

Spin echo images of needles (18G/1.3 mm) in a 1.5 T B0 field

0 degrees with respect to Bo field

40 degrees

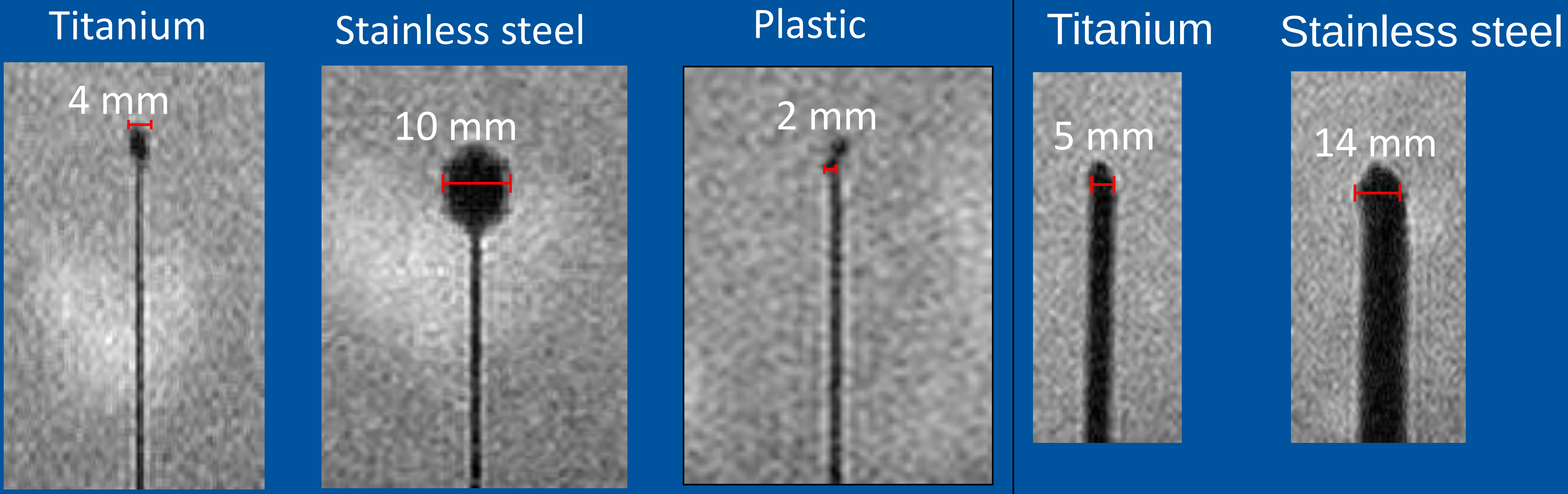
Titanium
Stainless steel
Plastic
Titanium
Stainless steel
4 mm
10 mm
2 mm
5 mm
14 mm

Distortions depend on material, shape and orientation

Summary 1

- Many reasons exists for artifacts in images
  - Erroneous sampling of k-space
    - Aliasing
    - Ringing
  - Magnetic field errors
    - Gradient artifacts
    - Susceptibility artifacts
    - Water-fat shift

- Geometrical artifacts show up in a particular direction
  - Phase encoding direction: aliasing
  - Read-out direction: susceptibility, water-fat shift

- Dephasing results in signal loss in gradient echo sequences

Summary 2

- Characterizing geometrical distortions can be done with a phantom
  - Avoid inducing additional susceptibility artifacts
  - Distortions depend on specific sequence

- Geometrical accuracy tends to deteriorate towards the body contour and tends to be good in the center of the body
  - Localization of external markers may be inaccurate

- Many possibilities exist to avoid artifacts or to minimize their impact. It is important to be aware of possible artifacts

‘Elk nadeel heb z’n voordeel’

‘Every drawback has a benefit’

Artifacts are often exploited to create new contrast mechanisms

Artifact	MRI technique
Susceptibility	Dynamic Susceptibility Contrast MRI
	Blood Oxygen Level Dependent (BOLD) MRI
Water-fat shift	DIXON (separation of water and fat imaging)
	MRI spectroscopy
In-flow artifacts	MR angiography
….	

Acknowledgments

Thanks for many slides and help in preparing these lectures:

- Gary Liney
- Rien Moerland
- Alexis Kotte
- Marielle Phillipens

VÄSTERBOTTENS
LÄNS LANDSTING

Functional MRI and Cone-beam CT

Tufve Nyholm

UMEÅ UNIVERSITET

Contents

- **Cone beam CT**
  - Conceptual differences to fan beam CT
  - Technical problems and solutions
  - A few words on QA and references

- **Functional MRI**
  - Short rational why it is important
  - Dynamic contrast enhanced MRI (DCE-MRI)
  - Spectroscopy

Cone beam CT in RT

- Positioning of the patient
- Monitor changes in anatomy
- (Re-planning)

Image quality

Quantification (HU)

Fan beam vs Cone beam

Fan beam CT (traditional CT)

- Just a slice of the sample is irradiated (2D)
- Detector row (1D)

Fan beam CT (traditional CT)

- A larger 3D volume is irradiated
- Planar detector (2D)

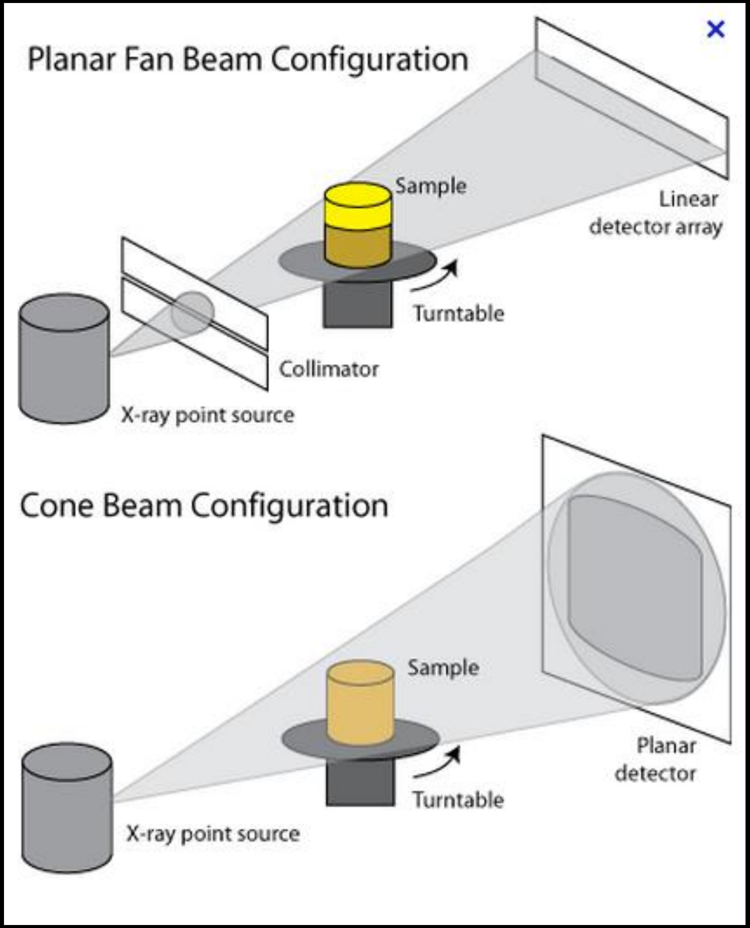
×
Planar Fan Beam Configuration
Sample
Linear detector array
Turntable
Collimator
X-ray point source
Cone Beam Configuration
Sample
Turntable
Planar detector
X-ray point source

Richard Ketcham, University of Texas at Austin

Cone beam CT

For 4-slice CT scanners an ideal fan beam geometry can be assumed during the reconstruction. For cone angles above around 2-4 degrees reconstruction adapted to the cone beam should be used (Feldkamp algorithm, 1984).

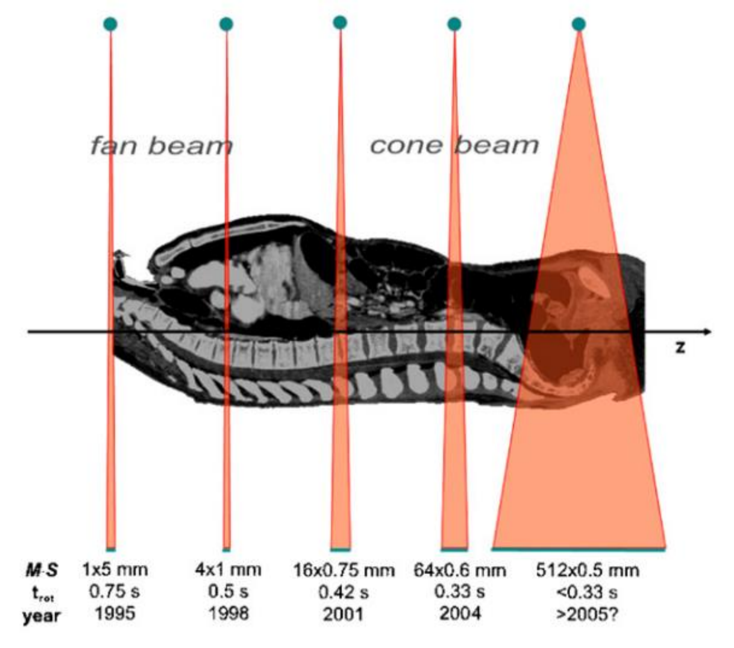
fan beam
cone beam
z
M-S
t_rot
year
1x5 mm
0.75 s
1995
4x1 mm
0.5 s
1998
16x0.75 mm
0.42 s
2001
64x0.6 mm
0.33 s
2004
512x0.5 mm
<0.33 s
>2005?

Flat-detector computed tomography (FD-CT)
Kalender et al. Eur Radiol (2007)

Cone beam CT

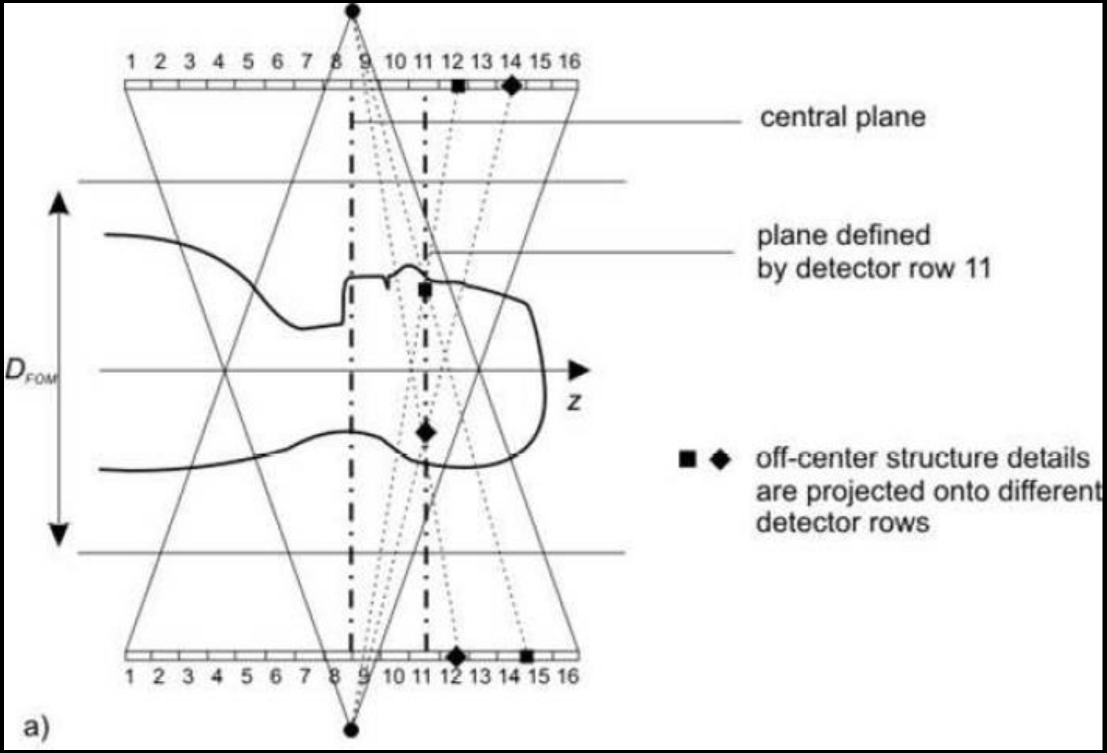
1 2 3 4 5 6 7 8 9 10 11 12 13 14 15 16
central plane
plane defined by detector row 11
D_{FOM}
z
■ ◆ off-center structure details are projected onto different detector rows
1 2 3 4 5 6 7 8 9 10 11 12 13 14 15 16
a)

The cone-beam problem in CT: a single off-center detector row does not yield data representing details of solely one object slice. The larger the cone beam angle, the greater are potential inconsistencies in the data.

W.A. Kalender, Computed Tomography, 2005

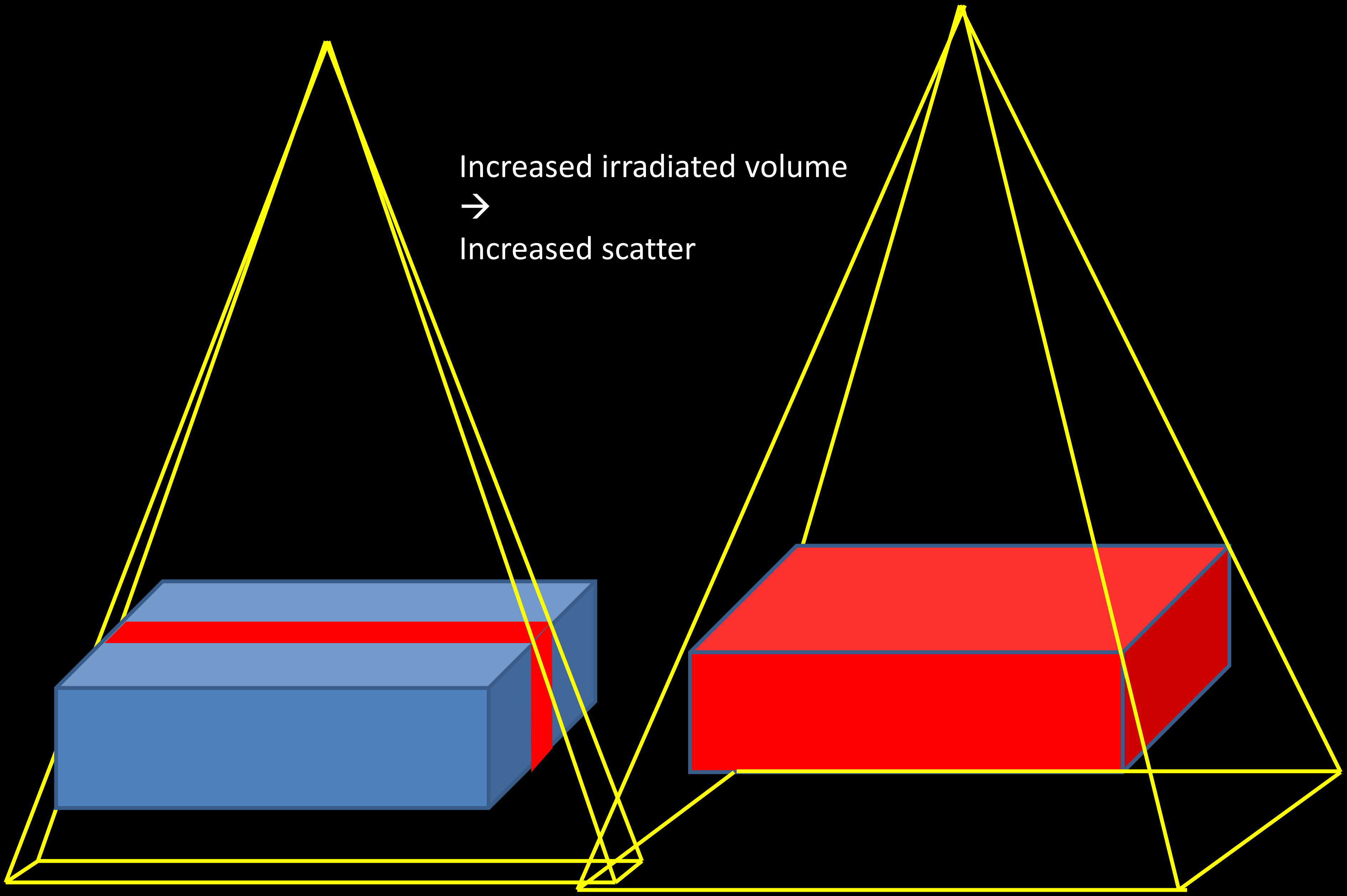

Increased irradiated volume

→

Increased scatter

Scattered photons

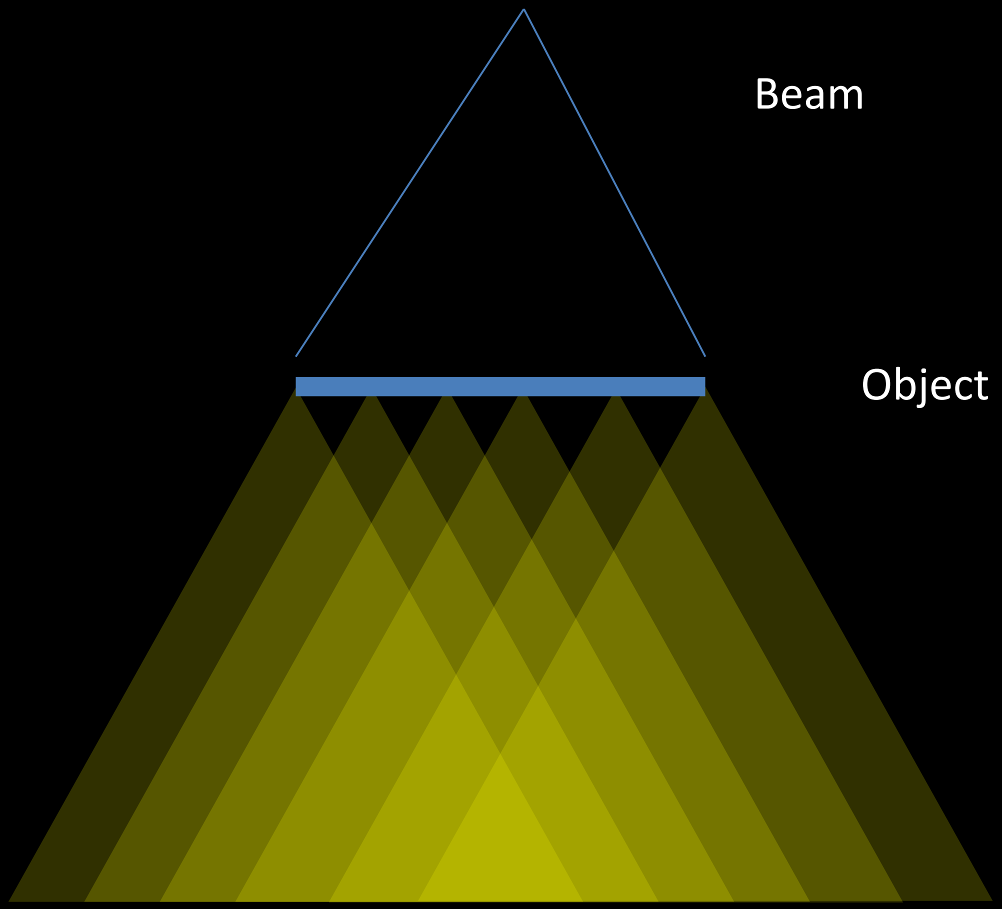

Beam

Object

Scattered Photons

Scatter artifacts in CBCT

- Reduction of image contrast
- Increased image noise
- Non-uniformity artifacts (Cupping)

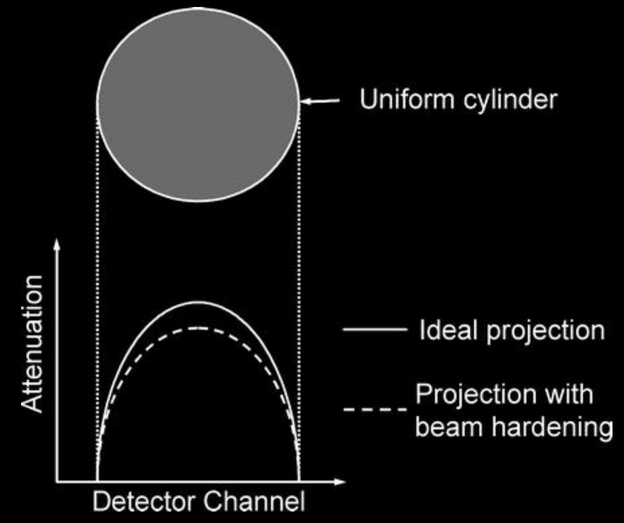
Uniform cylinder
Attenuation
Ideal projection
Projection with beam hardening
Detector Channel

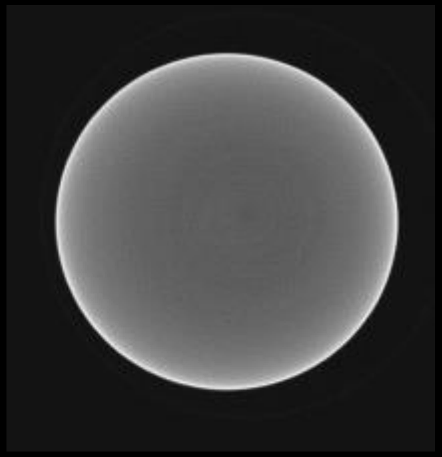

Corrected

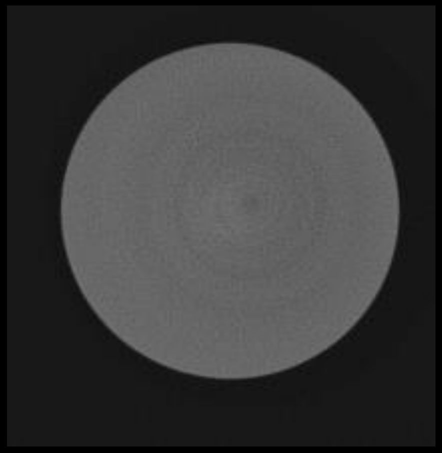

Barrett J F , Keat N Radiographics 2004;24:1679-1691

Dealing with scatter

- Avoidance
  - Limit the field of view
  - Grids
  - Distance between patient and detector
- Correction

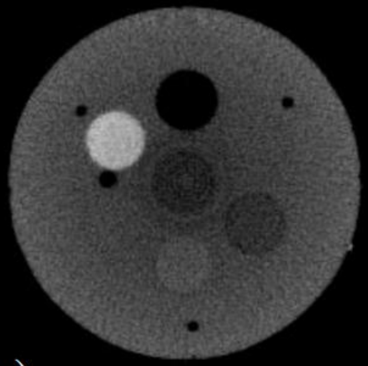

Not corrected for scatter
Corrected for beam hardning

(a)

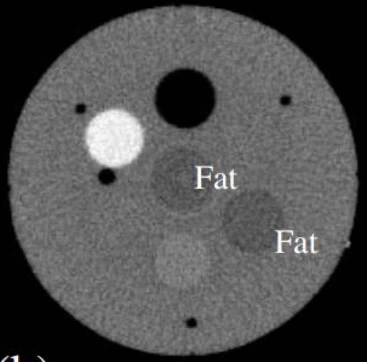

Corrected for scatter
and beam hardning

(b)

Correction of scatter in megavoltage cone-beam CT
Spies et al. Phys. Med. Biol 2001

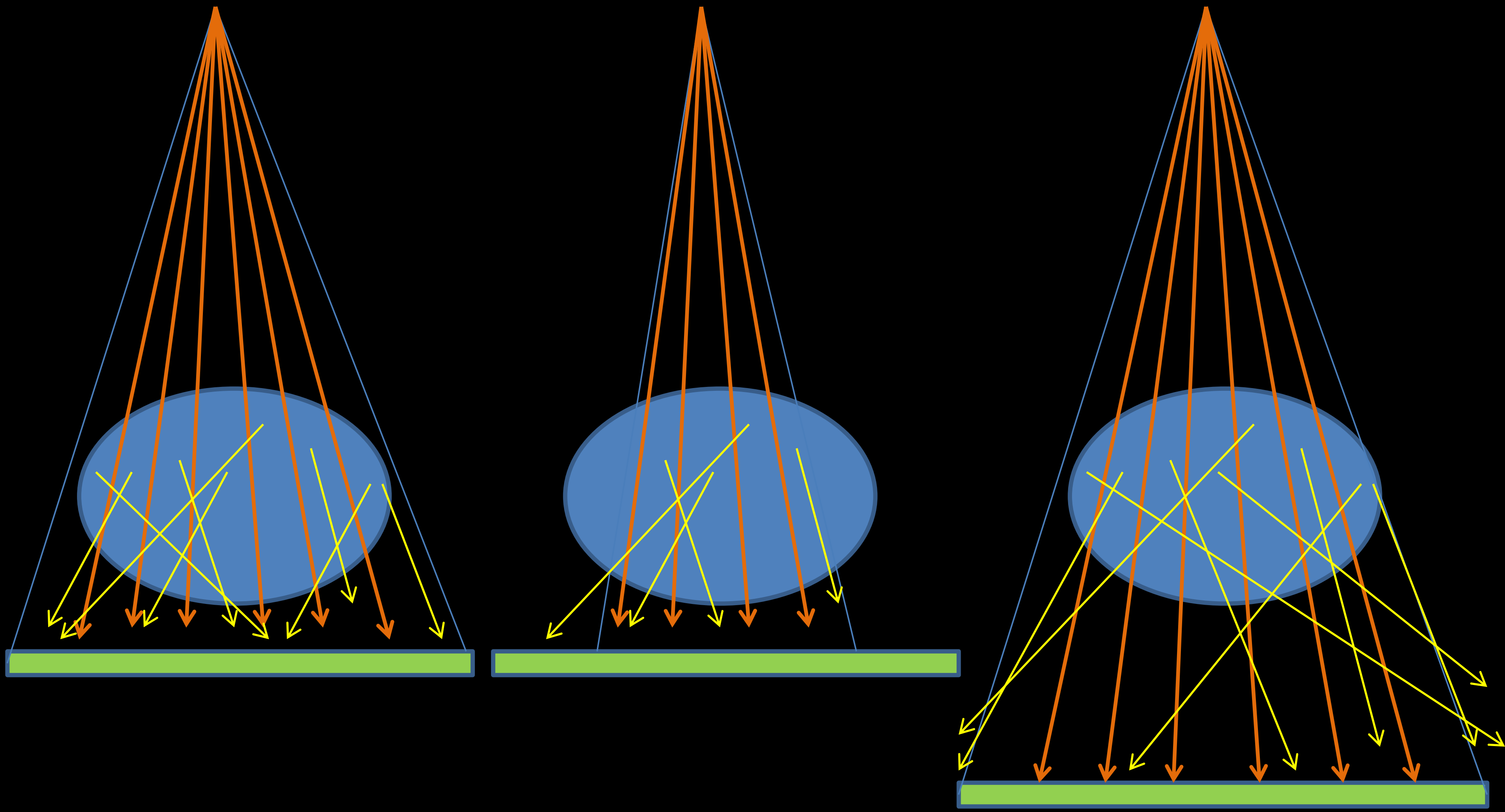

Decreased volume

Increased distance

Correction

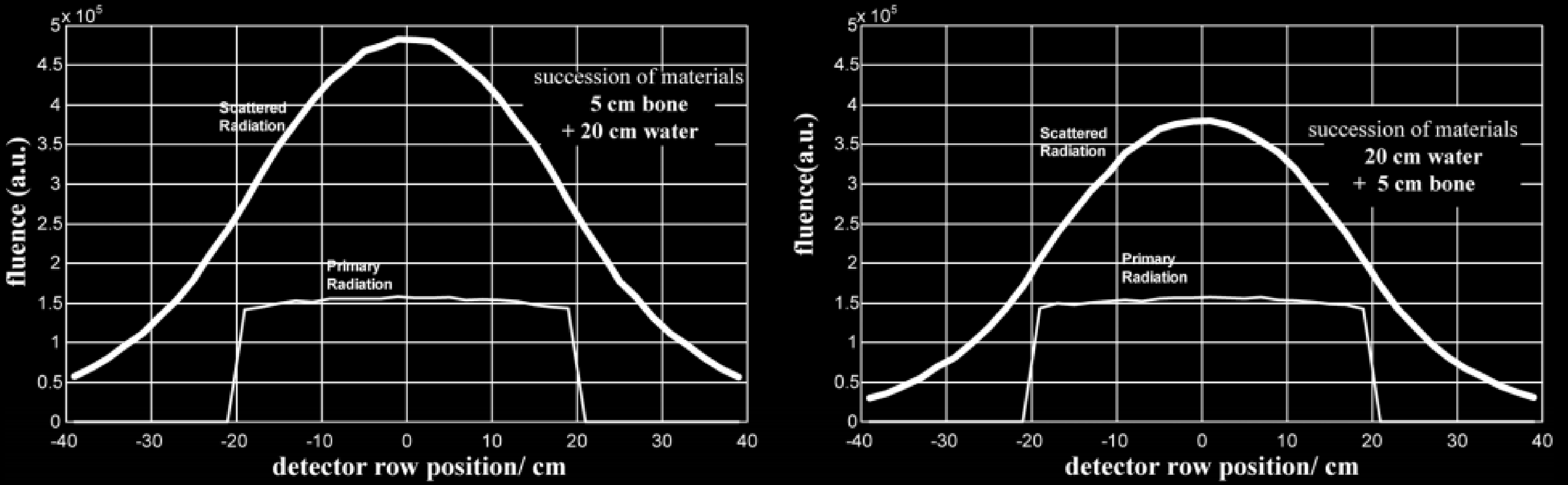

(a) bone-water succession

(b) water-bone succession

FIG. 4. Scatter dependency on material succession along the ray. Monte Carlo simulation. Phantom: two slabs, 5 cm bone and 20 cm water. Acquisition: X-ray spectrum at 70 kV, field-size 40 × 30 cm^2, no antiscatter grid. Plots show scatter and primary fluence in central line at the detector. (a) *SPR* in center is 25% higher than in (b).

Ruhrnschopf et al. , Med Phys 2011

Scatter reduction with grid

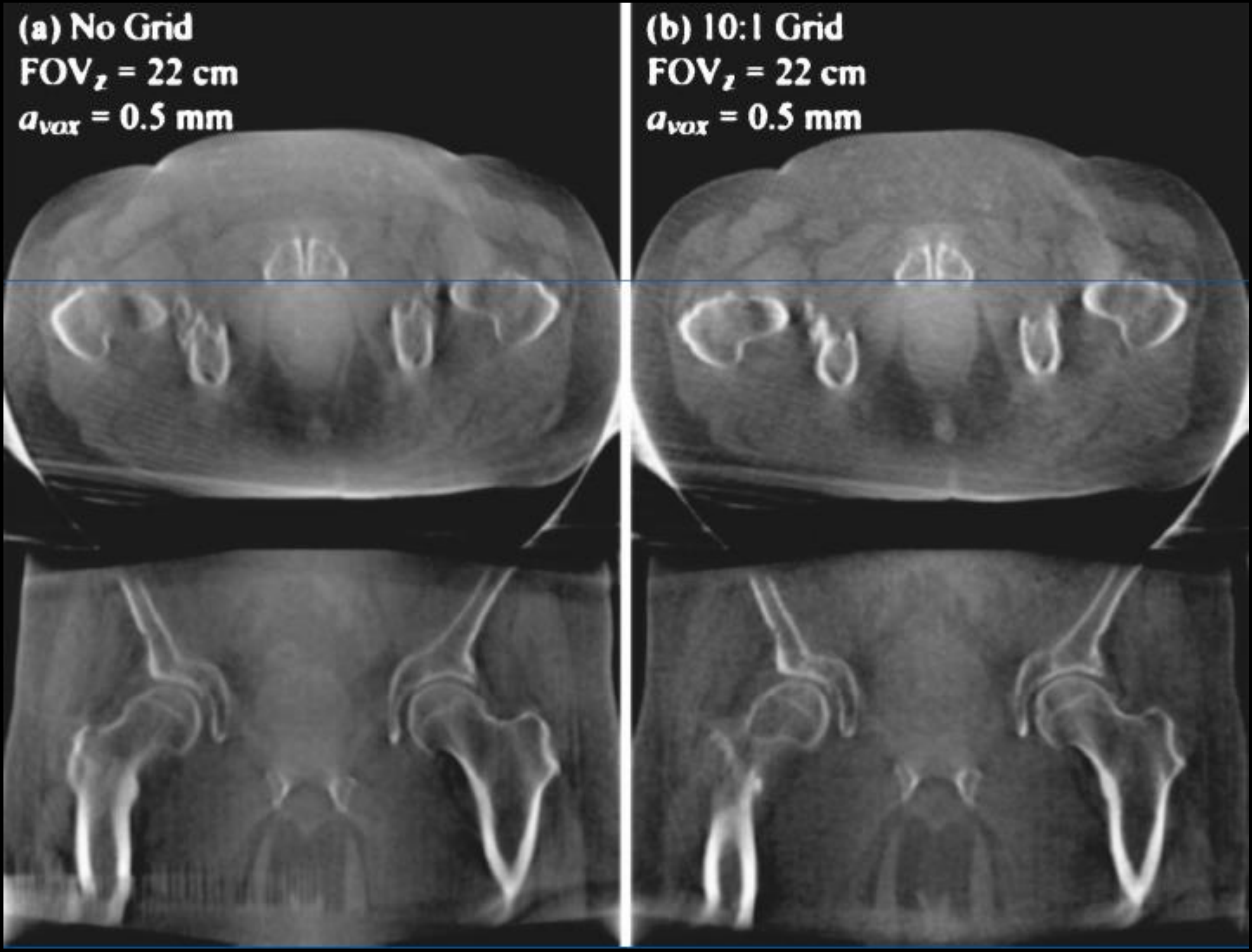
(a) No Grid
FOV$_z$ = 22 cm
a_{vox} = 0.5 mm
(b) 10:1 Grid
FOV$_z$ = 22 cm
a_{vox} = 0.5 mm

Siewerdsen et al. 2004. Med. Phys. 31:3506-3520

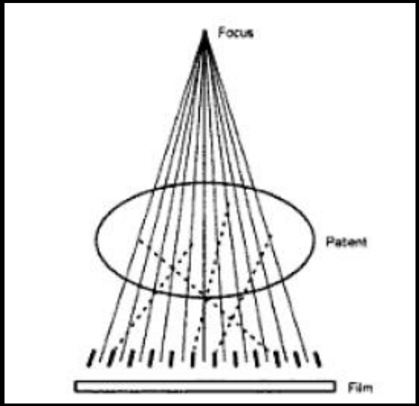
Focus
Patient
Film

Encyclopaedia of Medical Imaging; Petterson ed.

Other artifacts

- Ghosting – Detector after-glow from previous exposure
- Aliasing – Undersamplig of voxels far from the source due to the cone shape of the beam
  - Cause the commonly seen lines from the center to the peripheral part of the image
- Patient motion
- Non-ideal gantry rotation
  - Variation in gantry rotation speed
  - Sag of detector and/or X-ray source

Schulze et al. 2011

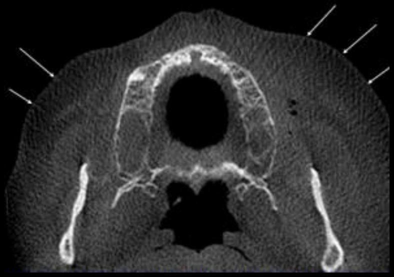

Not corrected

Corrected

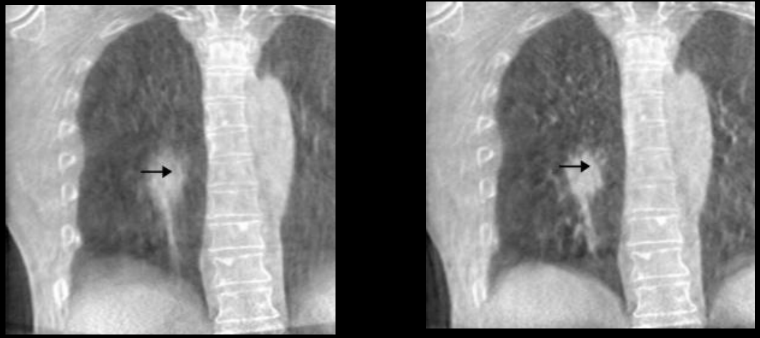

Rit et al. 2008

QA of CBCT

- Alignment of kV and MV lines
  - verify isocenter 3D agreement
  - verify registration and alignment process
- Image quality
  - monitor image quality parameters
  - watch for degradation
- Patient dose
  - measure base value (surrogates: air dose, HVL)
  - monitor changes

Recommended reading:
Commissioning experience with cone beam computed tomography for image-guided radiation therapy
Lehmann et al. Journal of applied clinical physics 2007

Clinical use of electronic portal imaging: Report of AAPM Radiation Therapy Committee Task Group 58

AAPM Medical Physics Practice Guideline 2.a: Commissioning and quality assurance of X-ray–based image-guided radiotherapy systems

Penta Guide

Catphan

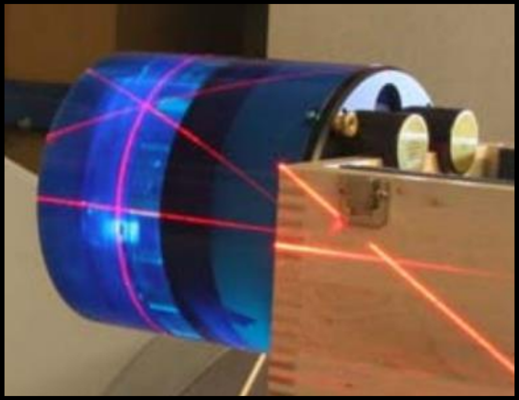

New QA recommendations

Quality control in cone-beam computed tomography (CBCT)

EFOMP-ESTRO-IAEA protocol

E
F
M
P

EFOMP

European Federation of Organisations for Medical Physics

ESTRO

European Society for RADIOTHERAPY & ONCOLOGY

IAEA

International Atomic Energy Agency

Quality control in cone-beam computed tomography (CBCT)

EFOMP-ESTRO-IAEA protocol

EFOMP

Final version 2nd of June 2017

Dynamic contrast enhanced MRI
DCE-MRI

- Measurement of perfusion and capillary exchange
  June 21-23, 2017
  Bremen/DE
  Course is confirmed!

Tumor angiogenesis

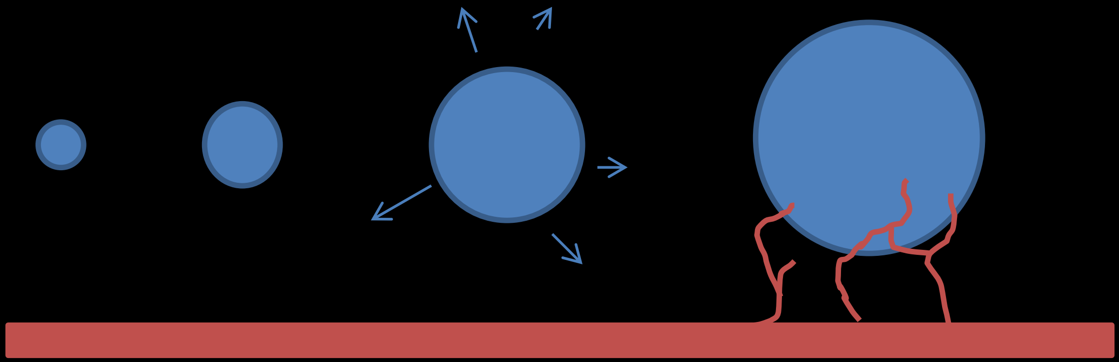

VEGF – Vascular endothelial growth factor
FGF – Fibroblast growth factors
Etc

Unbalanced growth factor
And inhibiting factors

↓

Poor vessle structure and quality

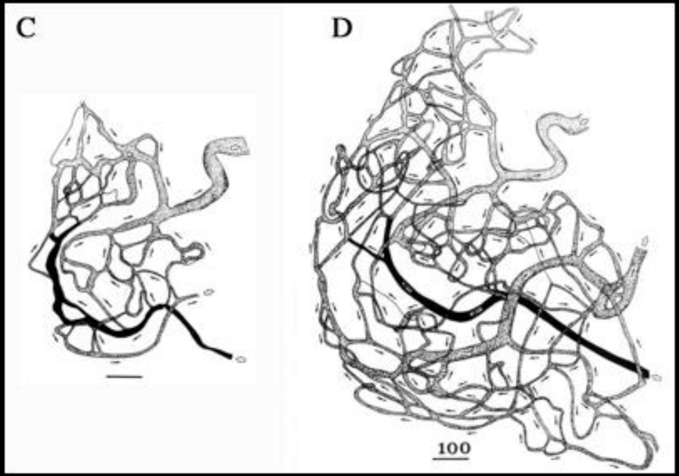

Cancer therapy by means of irreversible tumor blood flow stasis:
Starvation tactics against solid tumors
Katsuyoshi Hori
Gene Ther Mol Biol Vol 9, 203-216, 2005

Heterogeneity

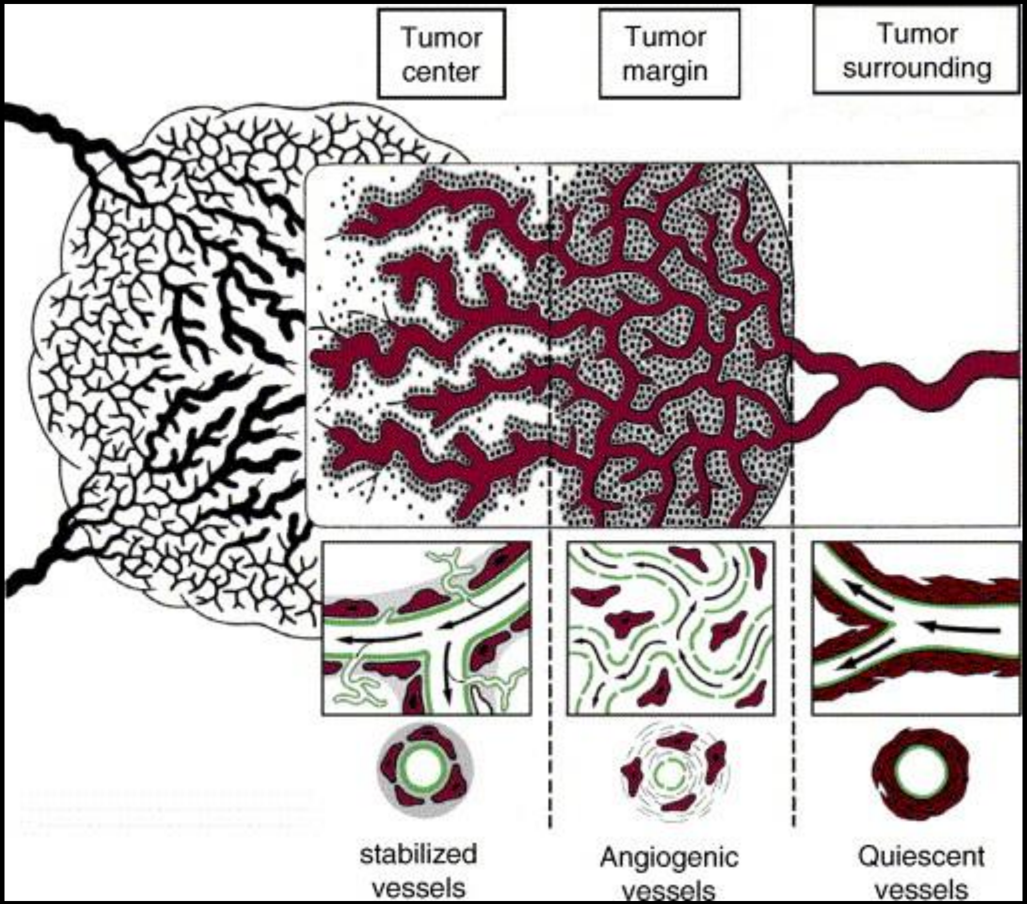
Tumor center
Tumor margin
Tumor surrounding
stabilized vessels
Angiogenic vessels
Quiescent vessels

Significance of vascular stabilization for tumor growth and metastasis
Suleyman Ergun et al.
Cancer Letters
Volume 238, Issue 2, 18 July 2006, Pages 180–187

Why do we want to image this?

1. To characterize the tumor – decide upon treatment strategy – outcome prediction
2. To monitor treatment responce – can changes in vessle quality or structure be surrugate marker for treatment responce?
3. To identify volumes for local therapy or boosting

U. Heide et al 2011

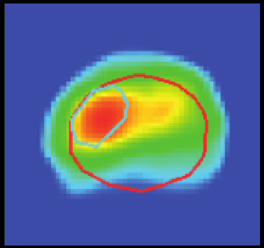
DCE
K-trans

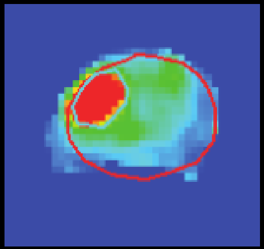
Dose
dist.

Contrast media

- Gd3+ paramagnetic ion
- Reduce both T1 and T2 relaxation
- Gadolinium chelated to diethylenetriamine pentaacetic acid to reduce toxicity – Magnevist
- Some concern re: Nephrogenic Systemic Fibrosis

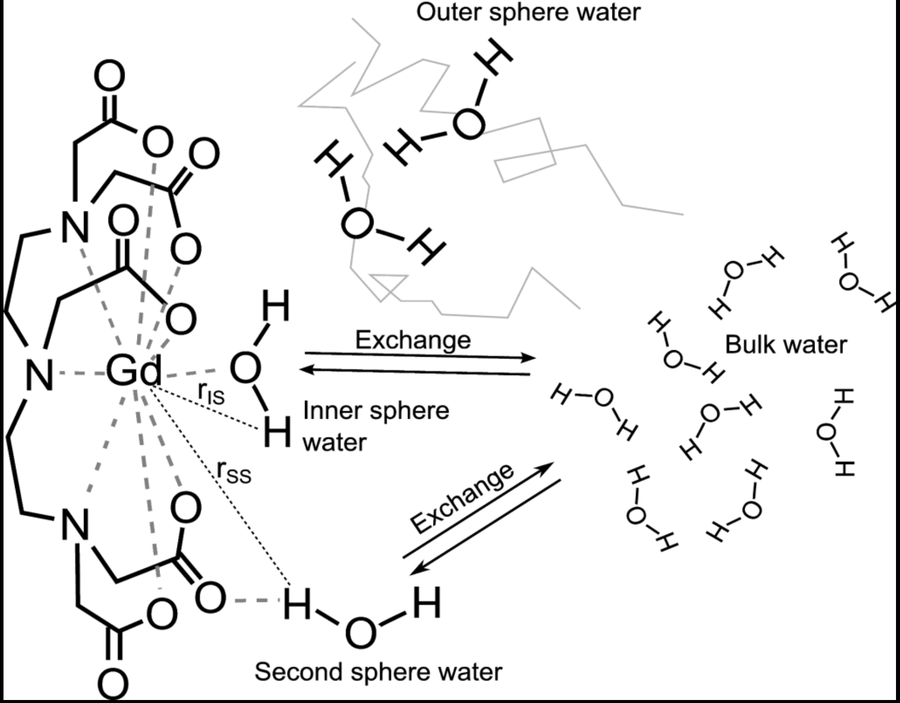
Outer sphere water
Exchange
Bulk water
Inner sphere water
r_{IS}
r_{SS}
Exchange
Second sphere water
Gd
N
O
H

Courtesy Anders Garpebring, Umeå

T1 contrast

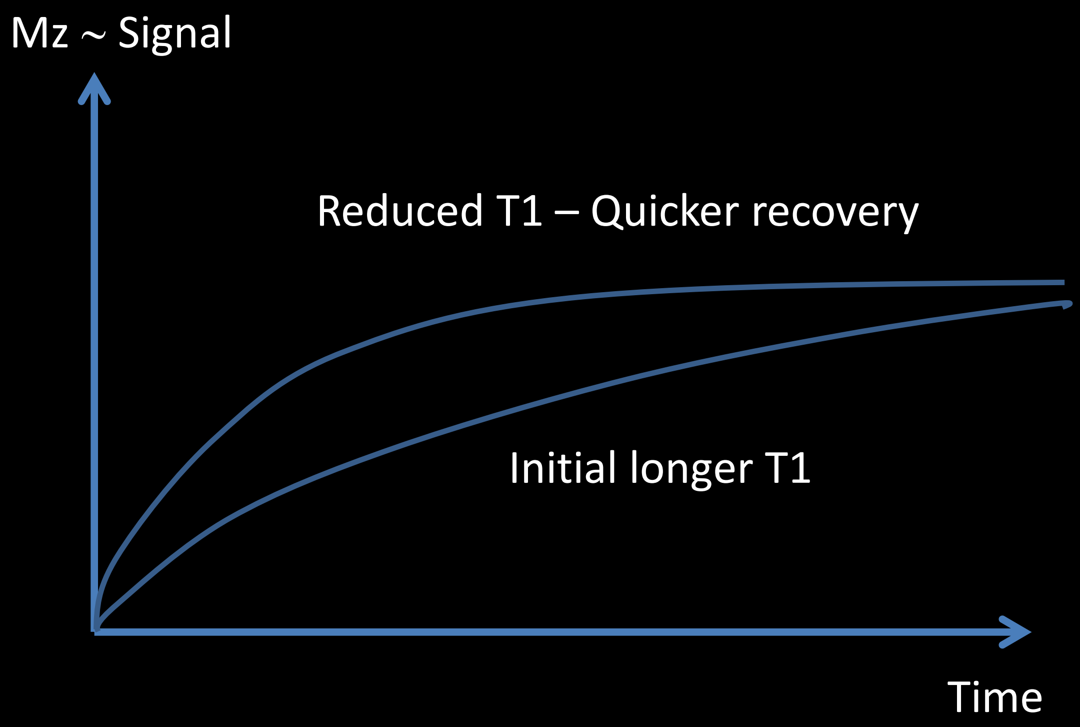
Mz ~ Signal
Reduced T1 – Quicker recovery
Initial longer T1
Time

Before and after administration of contrast agent

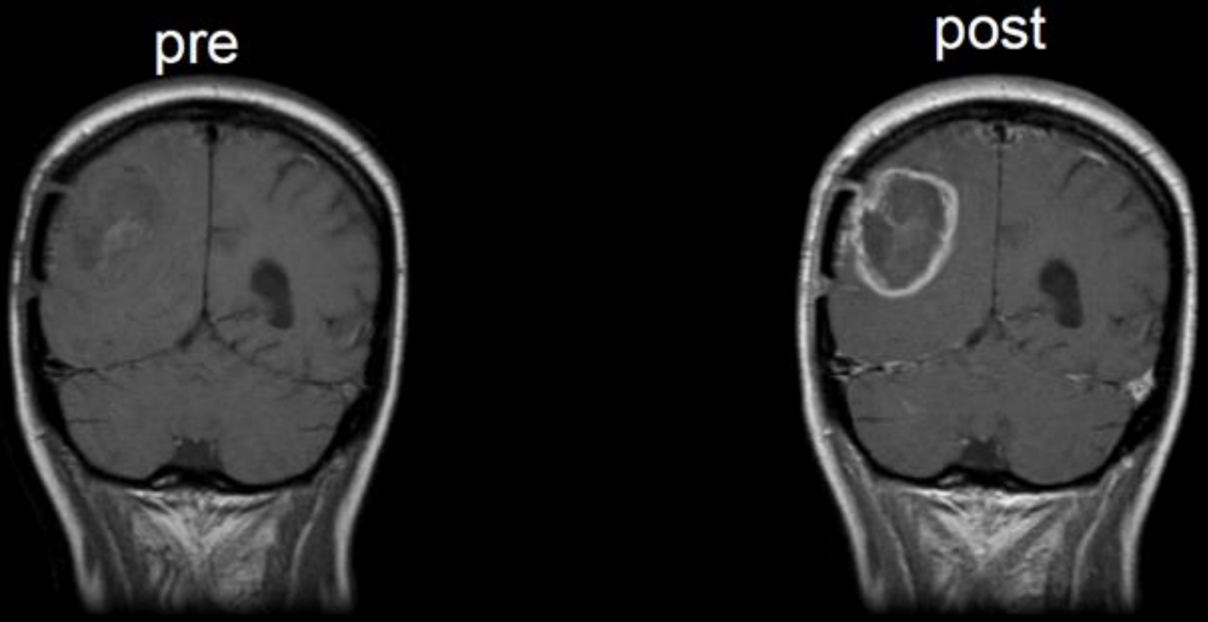

The DCE-MRI experiment

Dynamic series

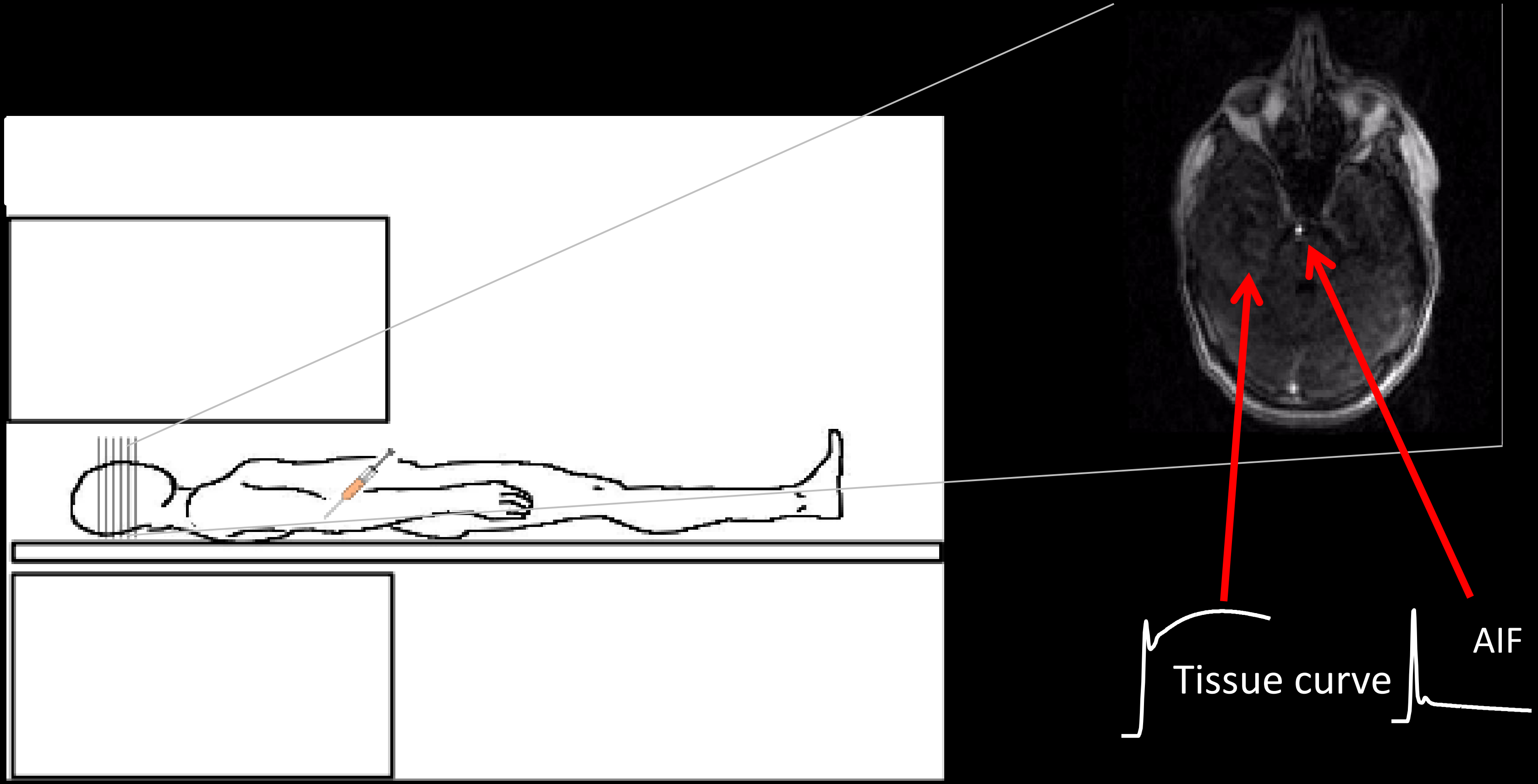
Tissue curve
AIF

Courtesy Anders Garpebring, Umeå

Registration

Following uptake in individual voxel over a time period is challenging

Original

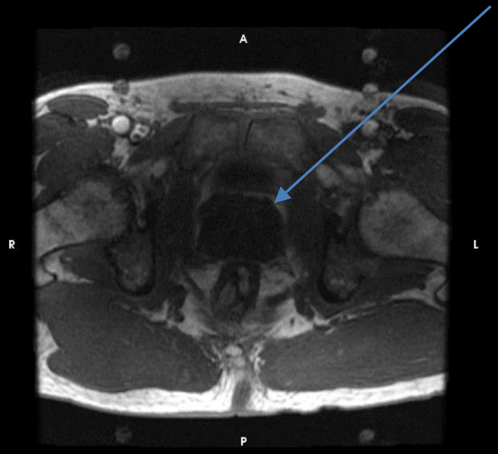

Registered

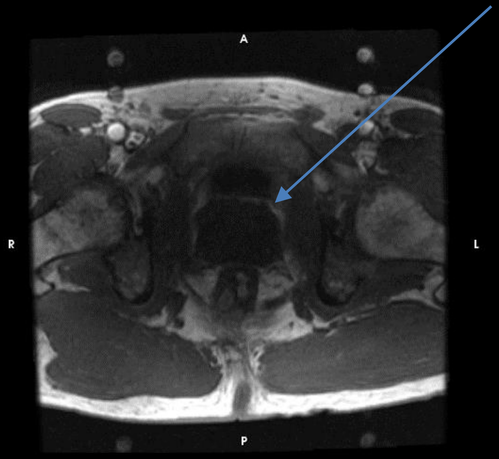

Breast

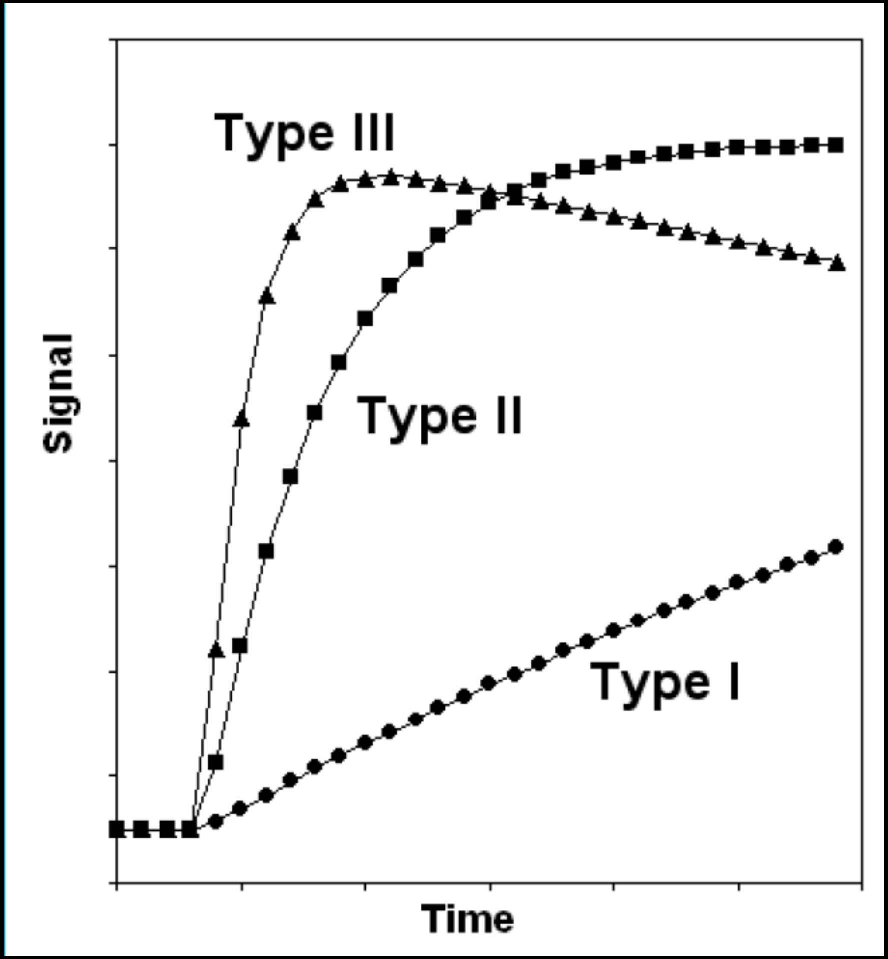

- Type 1
  - – generally benign lesions
  - – parenchyma
- Type 2
  - – equivocal
  - – some benign lesions
  - – many tumours
- Type 3
  - – mostly malignant lesions
  - – some fibroadenomas

Courtasy Gary Liney

Prostate

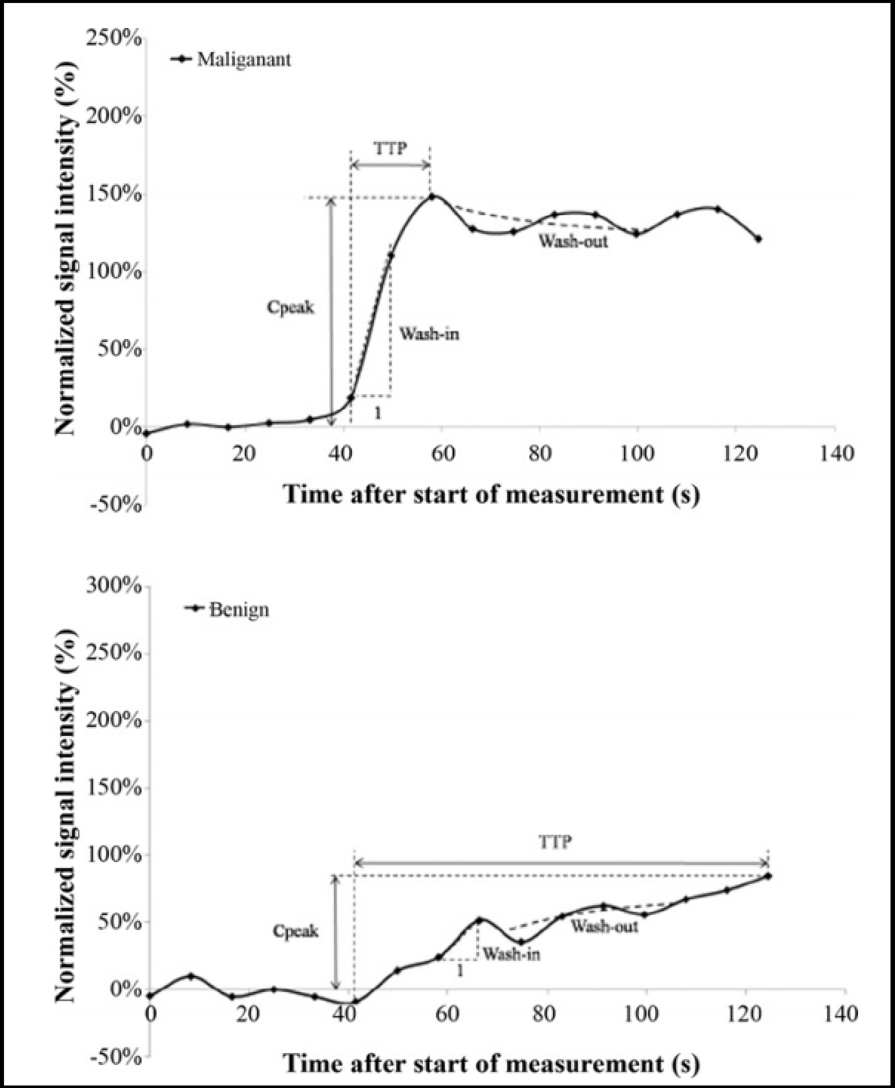

Evaluation of semi-quantitative dynamic contrast-enhanced MRI parameters for prostate cancer in correlation to whole-mount histopathology
Sofie Isebaert et al.
European Journal of Radiology 2012

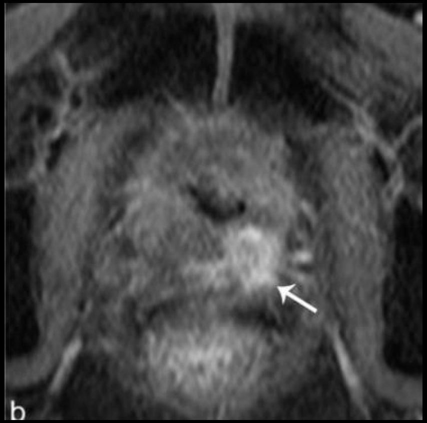

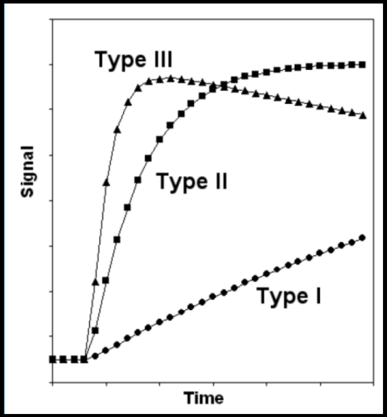

Qualitative methods

Quantitative methods

Courtesy Anders Garpebring, Umeå

Qualitative methods

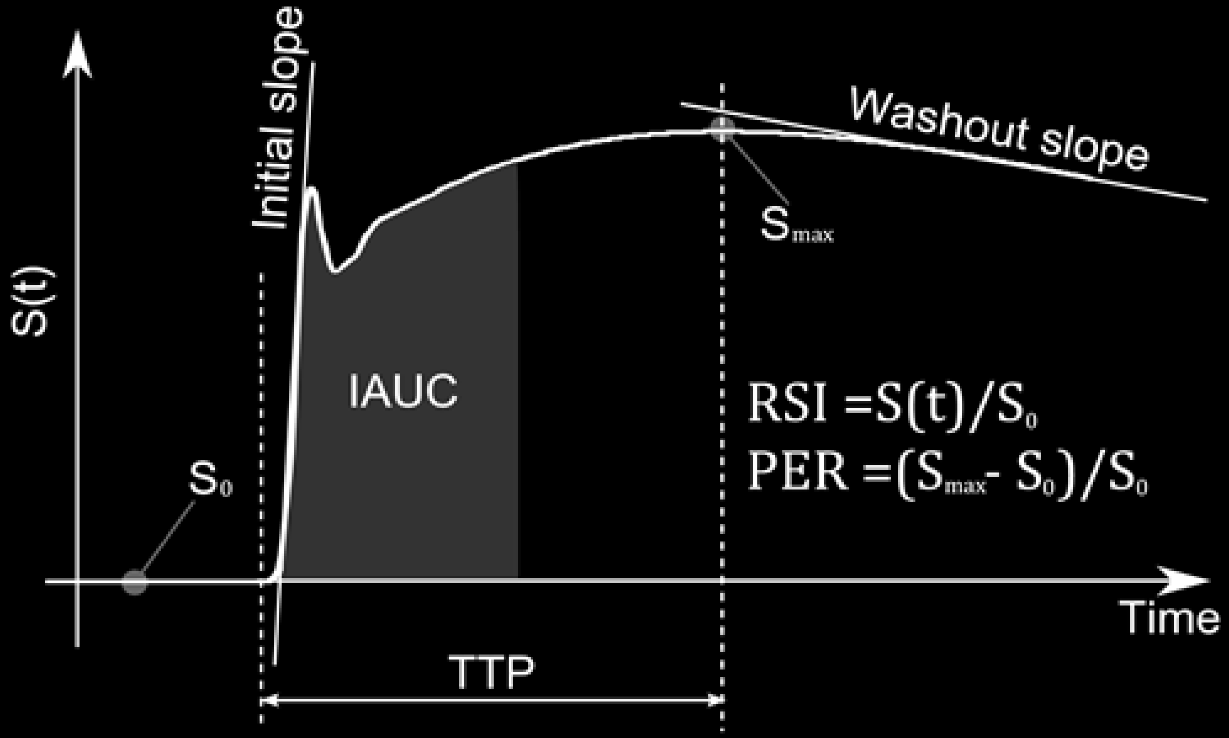

$RSI = S(t)/S_0$

$PER = (S_{max} - S_0)/S_0$

The initial area under curve (IAUC) is one of the most frequently used parameters
But time to peak (TTP), maximum signal (S_{max}), initial and washout slope relative signal enhancement (RSI), and peak enhancement ratio (PER) are also popular.

Prostate

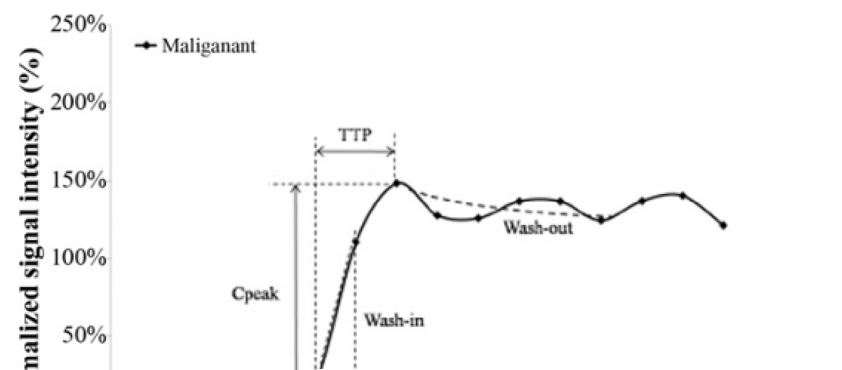

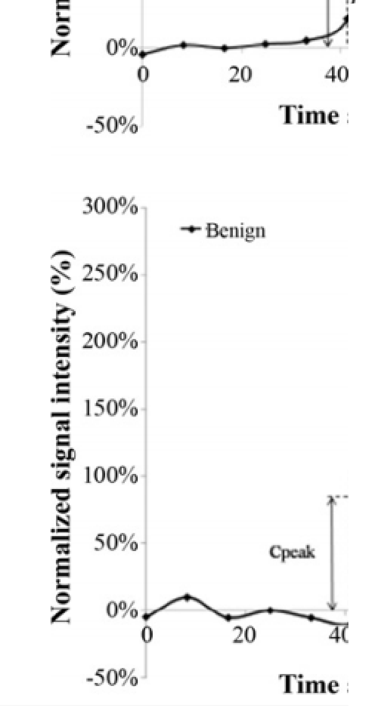

Evaluation of semi-quantitative dynamic contrast-enhanced MRI parameters for prostate cancer in correlation to whole-mount histopathology
Sofie Isebaert et al.
European Journal of Radiology 2012

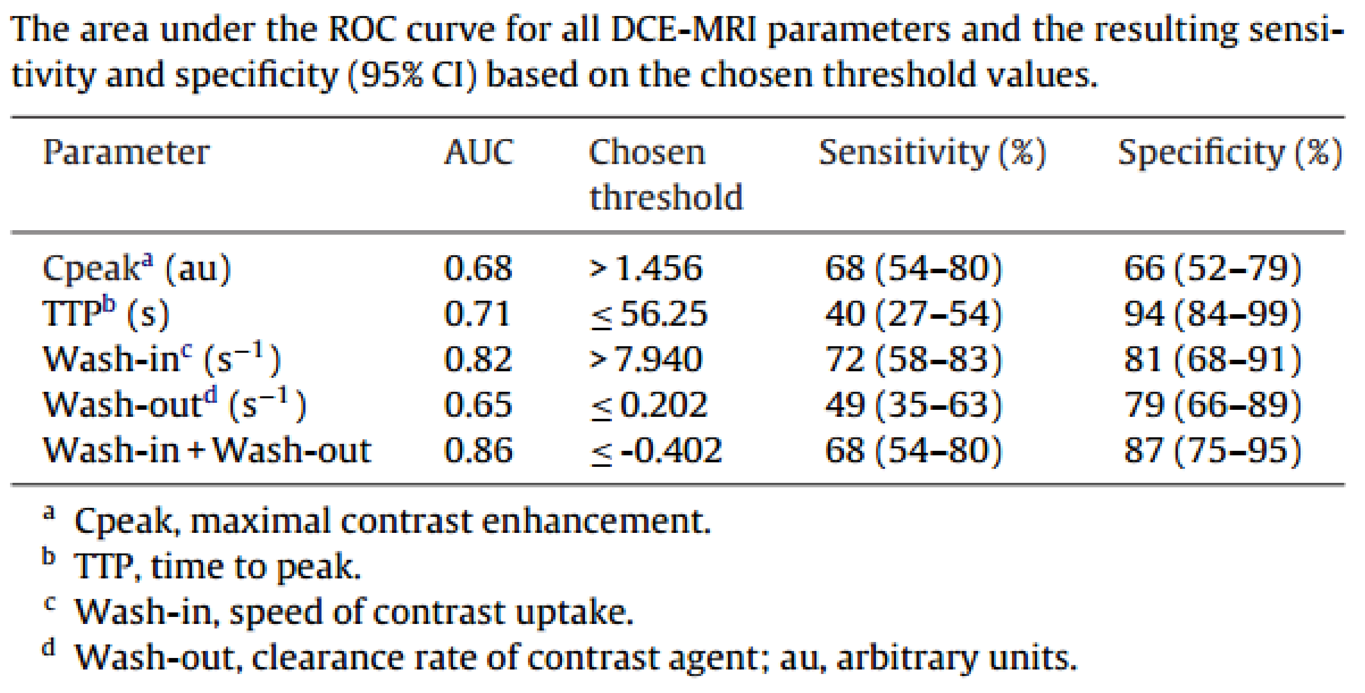

The area under the ROC curve for all DCE-MRI parameters and the resulting sensitivity and specificity (95% CI) based on the chosen threshold values.

Parameter	AUC	Chosen threshold	Sensitivity (%)	Specificity (%)
Cpeak[a] (au)	0.68	> 1.456	68 (54–80)	66 (52–79)
TTP[b] (s)	0.71	≤ 56.25	40 (27–54)	94 (84–99)
Wash-in[c] (s^{-1})	0.82	> 7.940	72 (58–83)	81 (68–91)
Wash-out[d] (s^{-1})	0.65	≤ 0.202	49 (35–63)	79 (66–89)
Wash-in + Wash-out	0.86	≤ -0.402	68 (54–80)	87 (75–95)

[a] Cpeak, maximal contrast enhancement.
[b] TTP, time to peak.
[c] Wash-in, speed of contrast uptake.
[d] Wash-out, clearance rate of contrast agent; au, arbitrary units.

Dynamic contrast-enhanced MRI as a predictor of tumour response to radiotherapy
Dr Mark A Zahra et al.
Lancet Oncology 2007

Qualitative methods

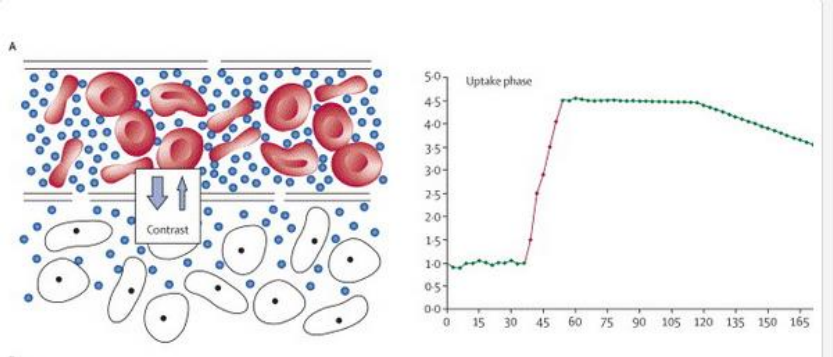

Slope dependent on blood flow, permability, and propetries of surrounding tissue

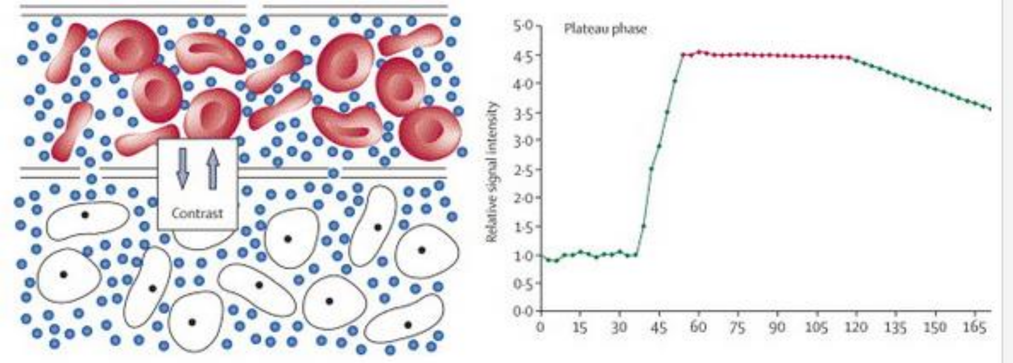

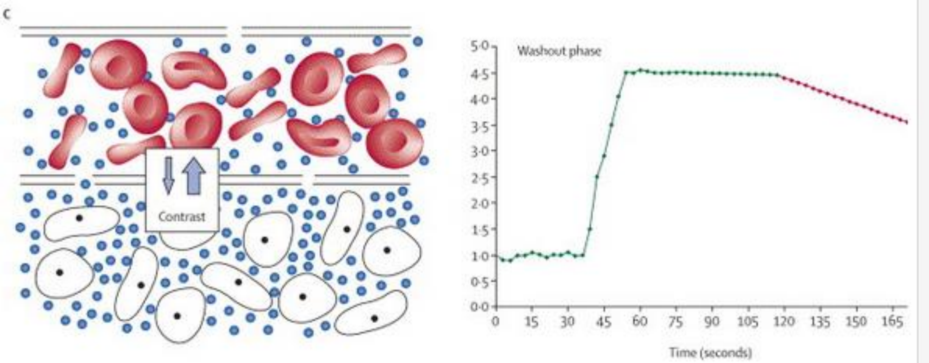

Slope dependent on blood flow, permability, and propetries of surrounding tissue

Courtesy Anders Garpebring, Umeå

The DCE-MRI experiment

$$\frac{1}{T_i} = \frac{1}{T_{i,0}} + r_i C$$

T_i – *Relaxation time* with contrast agent
$T_{i,0}$ – *Relaxation time without contrast agent*
R_i – *proportionality constant*
C – *concentration of contrast agent*

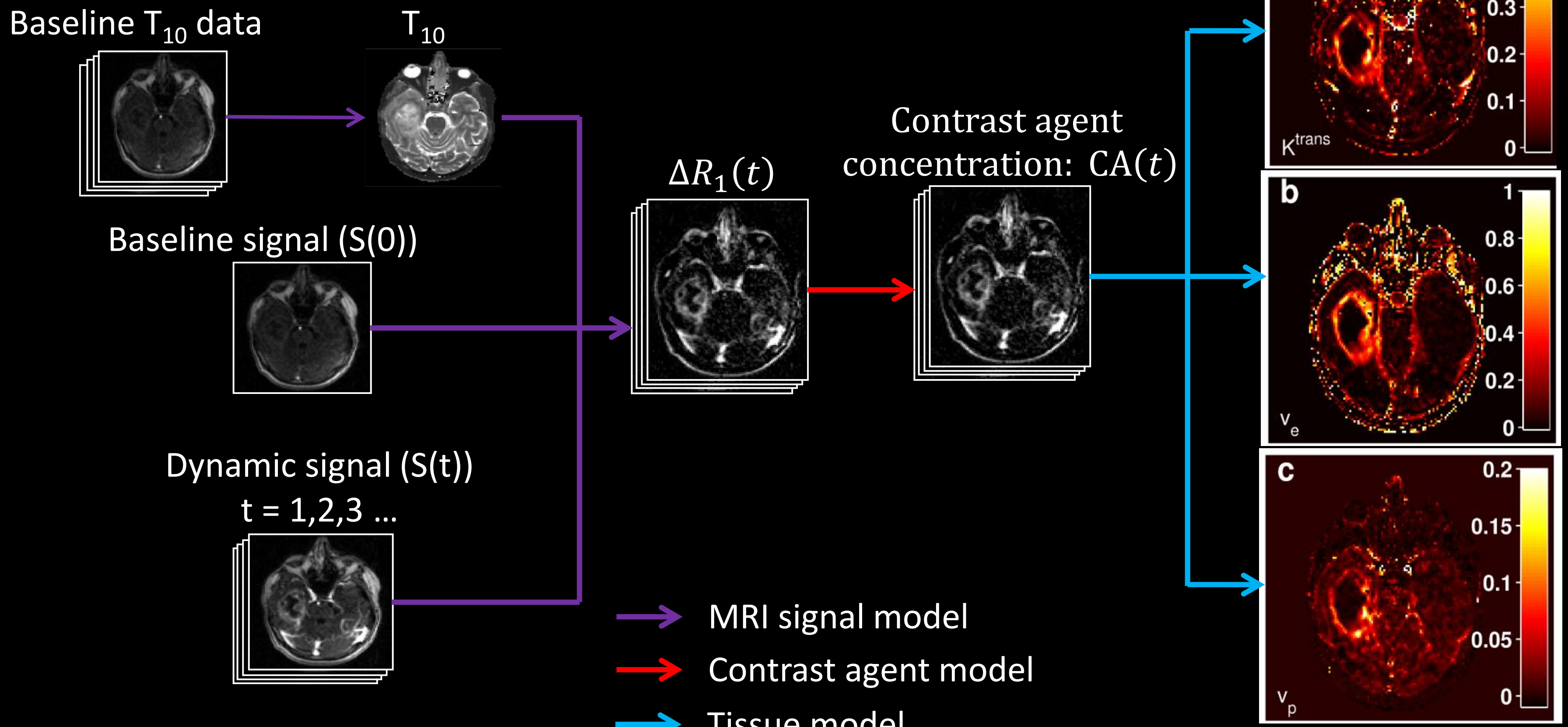

Baseline T_{10} data

T_{10}

Baseline signal (S(0))

Dynamic signal (S(t))
t = 1,2,3 …

$\Delta R_1(t)$

Contrast agent concentration: $\mathrm{CA}(t)$

a
0.5
0.4
0.3
0.2
0.1
0
K^{trans}
b
1
0.8
0.6
0.4
0.2
0
v_e
c
0.2
0.15
0.1
0.05
0
v_p

→ MRI signal model
→ Contrast agent model
→ Tissue model
(Pharmacokinetic model)

The DCE-MRI experiment

Sequence

3D - Spoiled Gradent Echo

- Short TE → small effect from T2*
- Short TR → fast sequence

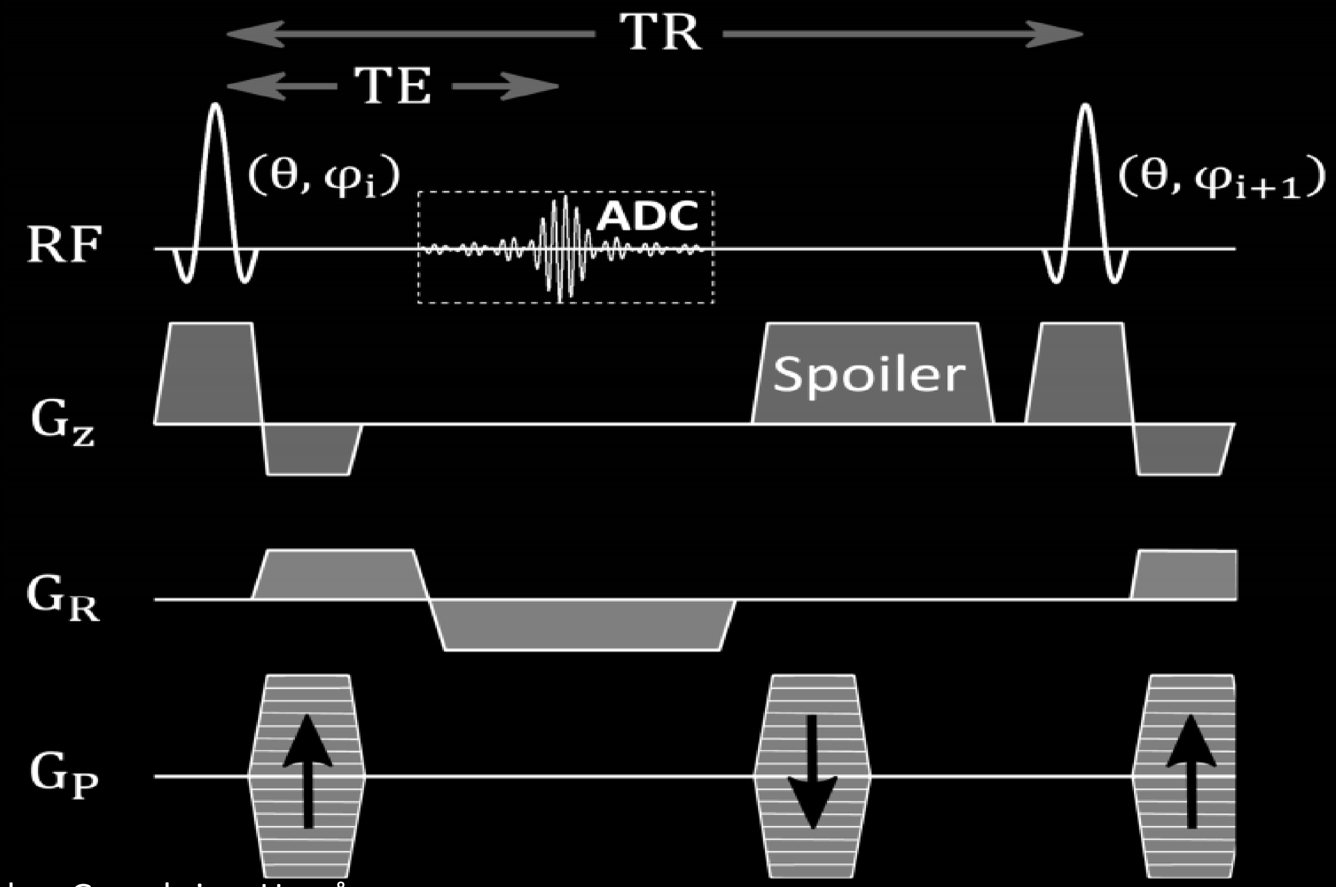
TR
TE
RF
(θ, φ_i)
ADC
(θ, φ_{i+1})
G_z
Spoiler
G_R
G_P

Courtesy Anders Garpebring, Umeå

The DCE-MRI experiment

Initial T1 relaxation

$$\frac{1}{T_1} = \frac{1}{T_{1,0}} + r_1 C$$

T_1 – *Relaxation time* with contrast agent
$T_{1,0}$ – *Relaxation time without contrast agent*
R_1 – *proportionality constant* (Relaxivity)
C – *concentration of contrast agent*

Signal dependence on flip angle and T1

$$S \propto M_0 \sin(\theta) e^{-TE/T_2^*} \left(\frac{1 - e^{-TR/T_1}}{1 - \cos(\theta) e^{-TR/T_1}} \right).$$

Make repeated measurements with different flip angles

Fit the equation and determine T1

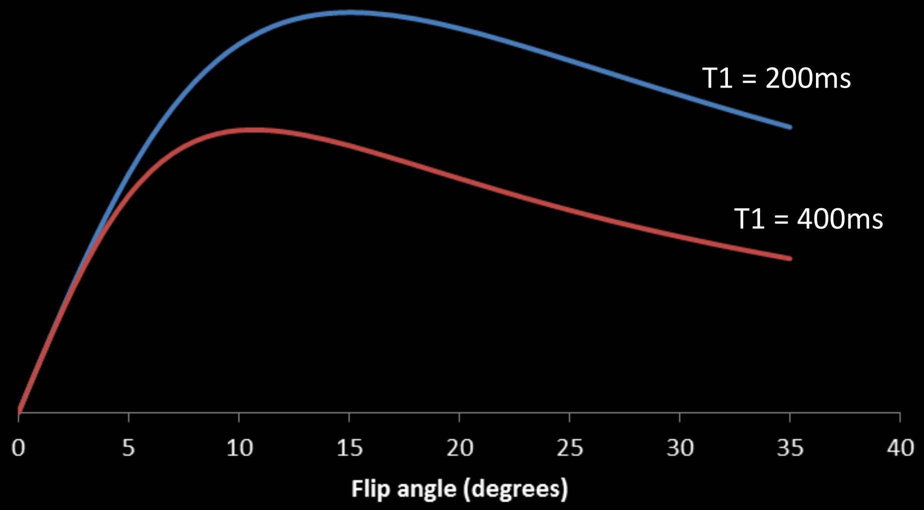

The DCE-MRI experiment

Signal equation

Combining

$$\frac{1}{T_1} = \frac{1}{T_{1,0}} + r_1 C$$

With

$$S \propto M_0 \sin(\theta) e^{-TE/T_2^*} \left(\frac{1-e^{-TR/T_1}}{1-\cos(\theta) e^{-TR/T_1}} \right).$$

We get

$$\Delta(t) = \frac{S(t)}{S_0} = \frac{\left(1-\cos(\theta)e^{-TR\cdot T_{10}^{-1}}\right)\left(1-e^{-TR\left(T_{10}^{-1}+r_1C(t)\right)}\right)}{\left(1-e^{-TR\cdot T_{10}^{-1}}\right)\left(1-\cos(\theta)e^{-TR\left(T_{10}^{-1}+r_1C(t)\right)}\right)}$$

For low concentrations:

$$C(t) = \left(r_1 T_{10}\right)^{-1}\left(\Delta(t)-1\right).$$

Summary so far

Dynamic series gives clinically relevant information

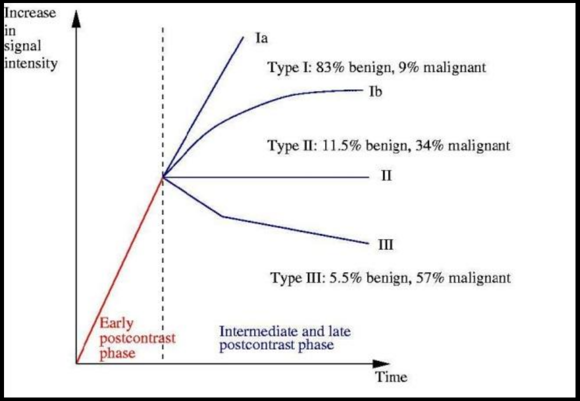

Problem: without quantitative methods the results will be:

1. Dependent on scanner
2. Dependent on sequence
3. Dependent on coils
4. Etc.

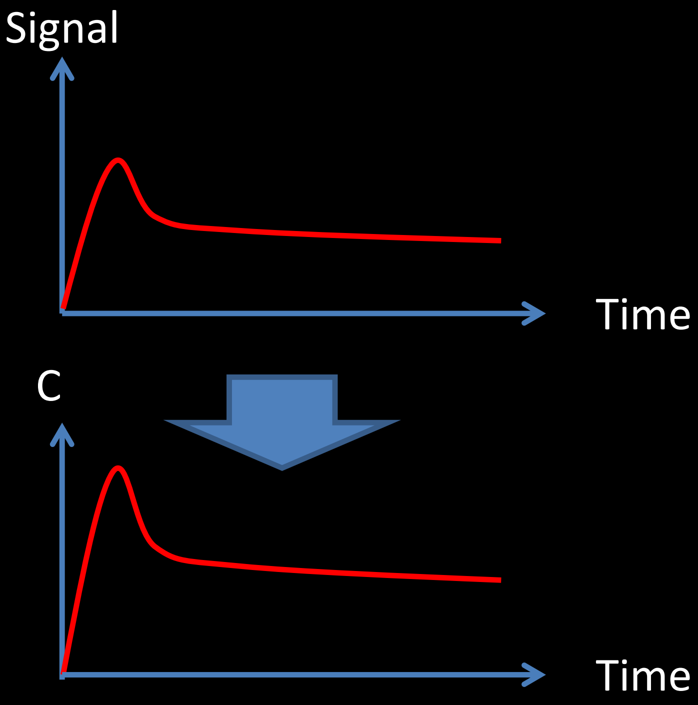

Quantitative methods rely on determination of the contrast agent concentration

Problem: This is not easy to determine

1. Unknown relaxivity
2. Complicated relation between concentration and signal
3. Inflow effects
4. Water exchange
5. Spoiling
6. Etc.

Next step

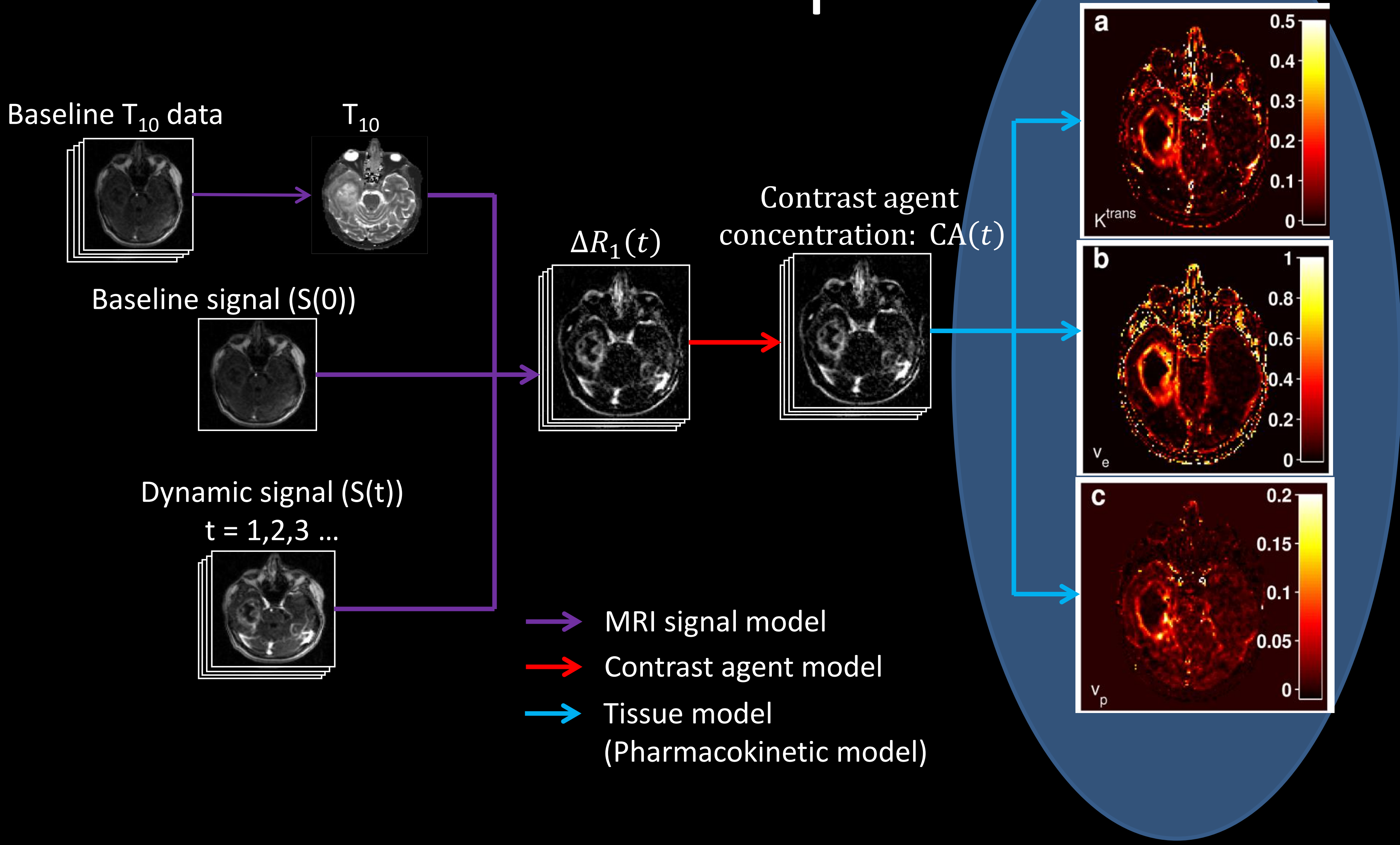

Baseline T_{10} data

T_{10}

Baseline signal (S(0))

Dynamic signal (S(t))
t = 1,2,3 …

$\Delta R_1(t)$

Contrast agent concentration: $\mathrm{CA}(t)$

a
0.5
0.4
0.3
0.2
0.1
0
K^{trans}
b
1
0.8
0.6
0.4
0.2
0
v_e
c
0.2
0.15
0.1
0.05
0
v_p

→ MRI signal model

→ Contrast agent model

→ Tissue model
(Pharmacokinetic model)

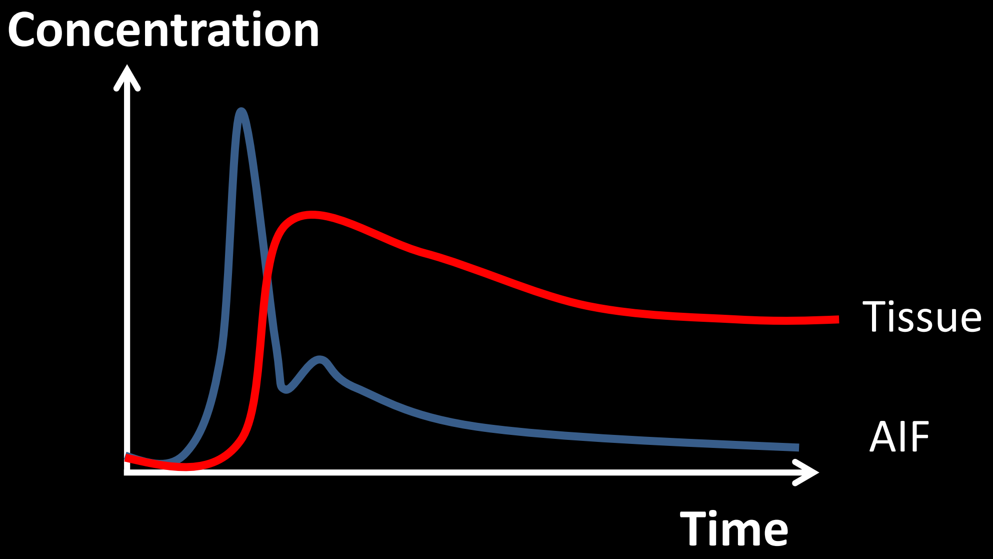

Kinetic modelling

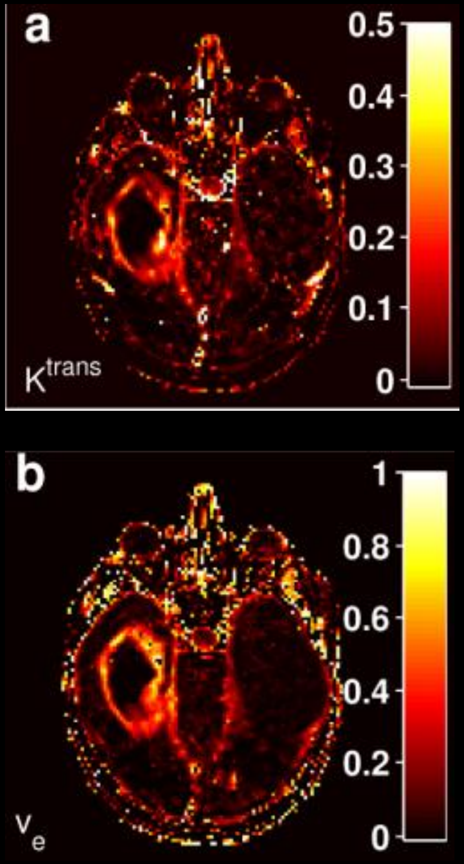
a
0.5
0.4
0.3
0.2
0.1
0
K^{trans}
b
1
0.8
0.6
0.4
0.2
0
v_e

Parametic tissue models

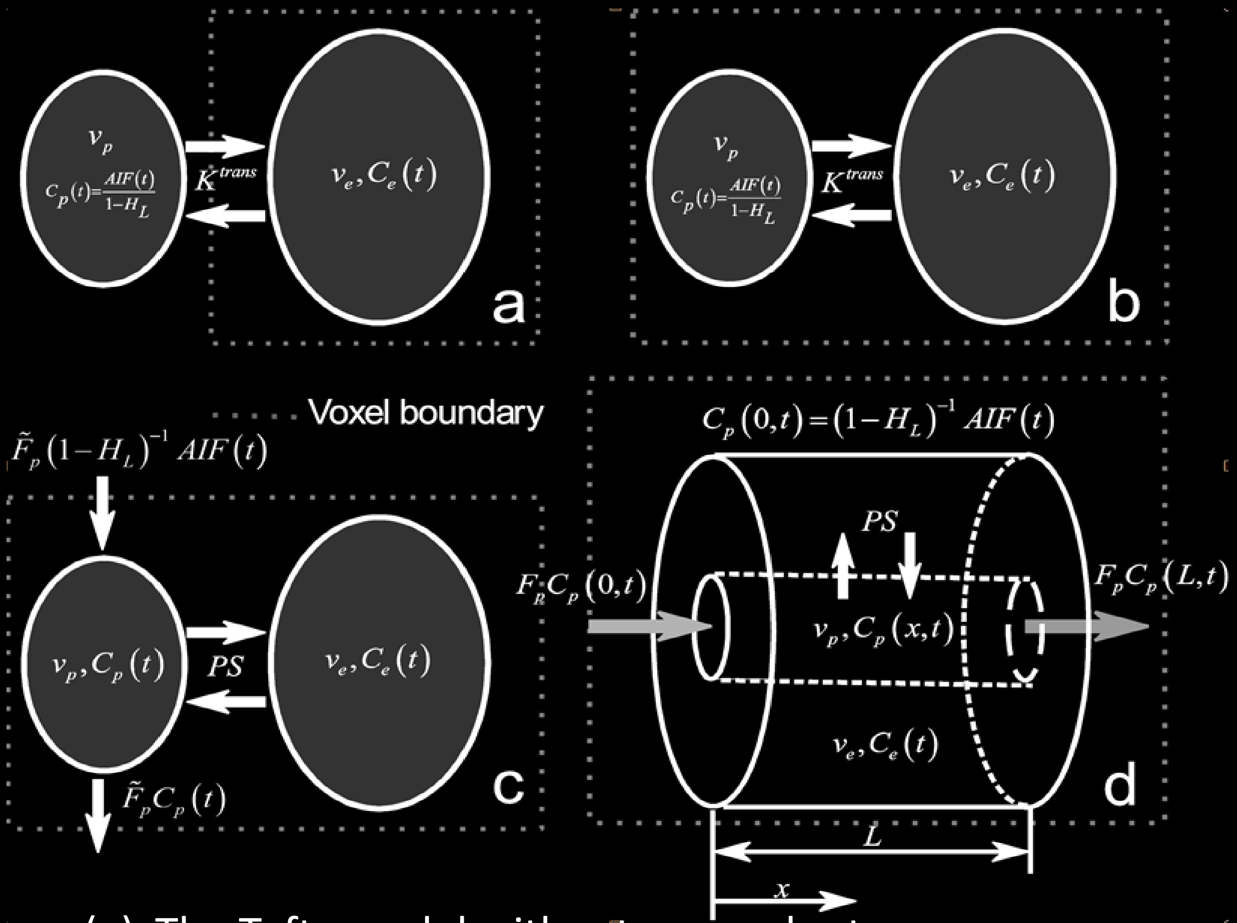
v_p
$C_p(t)=\frac{AIF(t)}{1-H_L}$
K^{trans}
$v_e, C_e(t)$
a
v_p
$C_p(t)=\frac{AIF(t)}{1-H_L}$
K^{trans}
$v_e, C_e(t)$
b
Voxel boundary
$\tilde{F}_p(1-H_L)^{-1}\,AIF(t)$
$v_p, C_p(t)$
PS
$v_e, C_e(t)$
$\tilde{F}_p C_p(t)$
c
$C_p(0,t)=(1-H_L)^{-1}\,AIF(t)$
PS
$F_p C_p(0,t)$
$v_p, C_p(x,t)$
$F_p C_p(L,t)$
$v_e, C_e(t)$
d
L
x

(a) The Tofts model without a vascular term

(b) The Tofts model with a vascular term.

(c) The Brix model.

(d) The tissue homogeneity model.

Injection of contrast agent

- Intravenous administration followed by saline flush
- Infusion or bolus (preferred)
- Manual injection or power injector
- Tight reproducible bolus
- Delivered in ~10 s to reduce errors in modeling
- Image before, during and after

Image aqusition

Imaging Procedure

- **Localizer**
- **Anatomic sequences T1, T2 weighted imaging**
- **Variable Flip angle (VFA) T1 weighted imaging (T1 fitting) (a)**
- **3D Gradient echo volumetric imaging (dynamic imaging) (b)**

(a) A variable flip angle series, for pre-contrast agent native tissue $T_{1,0}$ *mapping.*

- *Ensure TR and TE values stay constant for all flip angles,*
- *Flip angles: The range of # of flip angles supported in the literature varies from 2-7.*
- *Number of signal averages (NSA or NEX) > 2.*

(b). DCE-MRI Protocol: Pulse Sequence:

- ***Pulse Sequence:*** 3D fast spoiled gradient recalled echo or equivalent
- ***Coils:*** Transmit: Body coil; Receive: Body coil or phased array receive coil

No parallel imaging options??????
No magnetization preparation schemes

http://www.rsna.org/QIBA_.aspx

Quantitative
Imaging
Biomarkers
Alliance
RSNA

Dynamic series

Parameter	Compliance Levels
TE	
Acceptable	2.0-2.5ms
Target	1.5-2.0ms
Ideal	<1.5ms

Parameter	Compliance Levels
TR	
Acceptable	5-7ms
Target	3-5ms
Ideal	< 3ms

Temporal resolution: The temporal resolution should be less than 10 sec.
Flip angles: Smaller flip angles will lead to potential saturation of the signal intensity vs. gadolinium concentration, particularly in vessels. Note should be made that SAR limits may affect the maximum allowable flip angle. Operators should use the maximal allowed flip angle when SAR limitations occur. Flip angles ranging from 25-35 degrees are recommended in order to minimize saturation effects and to avoid specific absorption rate (SAR) problems.
Receiver Bandwidth: Greater or equal to ±31.25 kHz (or ~250 Hz/pixel)
Field of View (FOV) and Partial Fourier ("fractional echo" and/or reduced phase-encoding FOV) as needed to meet temporal resolution requirements
Number of Slices: Acceptable: ≥10 prior to zero fill. Ideal: as many as possible while maintaining ideal temporal resolution.
Slice thickness: *Ideal*: <5 mm, *Target*: 5.1-6 mm, *Acceptable*: 6.1-8 mm
Matrix: 256 x 160 (before applying rectangular FOV) – in order to meet 1-2mm in-plane spatial resolution
Number of acquisitions (phases): Sufficient to allow acquisition of at least 5 minutes of post injection data plus at least 5 phases acquired before contrast agent injection (baseline images).
Digitized bit depth: The maximum dynamic range should be utilized, e.g., "extended dynamic range" or equivalent.
Temporal resolution < 10sec.

http://www.rsna.org/QIBA_.aspx

Quantitative Imaging Biomarkers Alliance RSNA

Further reading

Overviews
Contributions to quantitative dynamic contrast-enhanced MRI, Phd theises Anders Garpebring
http://umu.diva-portal.org/smash/get/diva2:457450/FULLTEXT01

Modelling
Tracer kinetic modelling in MRI: estimating perfusion and capillary permeability.
Sourbron, S P and Buckley, D L
Physics in medicine and biology 2011

Fundamentals of Tracer Kinetics for Dynamic Contrast-Enhanced MRI
Tong San Koh, Sotirios Bisdas, Dow Mu Koh, Choon Hua Thng
Journal of magnetic resonance imaging 2011

Image aqusition
http://www.rsna.org/QIBA_.aspx

Summary

- Potential
  - Provides information about physiological properties of the tissue on a voxel by voxel level
    - Selection of treatment modality
    - Design of radiotherapy
    - Follow-up and adoption of therapy
- Problems
  - Not fully quantitative
    - Depends on models
  - Standardization

Magnetic resonance spectroscopy (MRS)

- With strong magnetic field
  - Nuclei spins are oriented and rotate with a well defined frequency

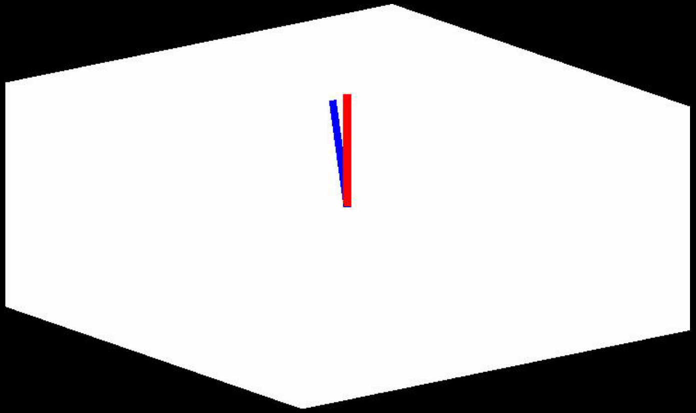

Larmor frequency

$$\omega = -\gamma B$$

42.576 MHz/T

Magnetic field

Shielding

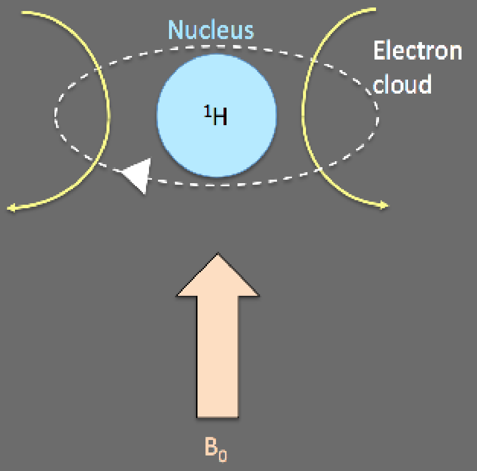
Nucleus
Electron cloud
^{1}H
B_0

$$B_{local} = -\sigma B_0$$

$$\omega = \gamma B_0(1-\sigma)$$

σ = chemical shift shielding constant

$$\sigma_A < \sigma_B < \sigma_C$$

$$\omega_A > \omega_B > \omega_C$$

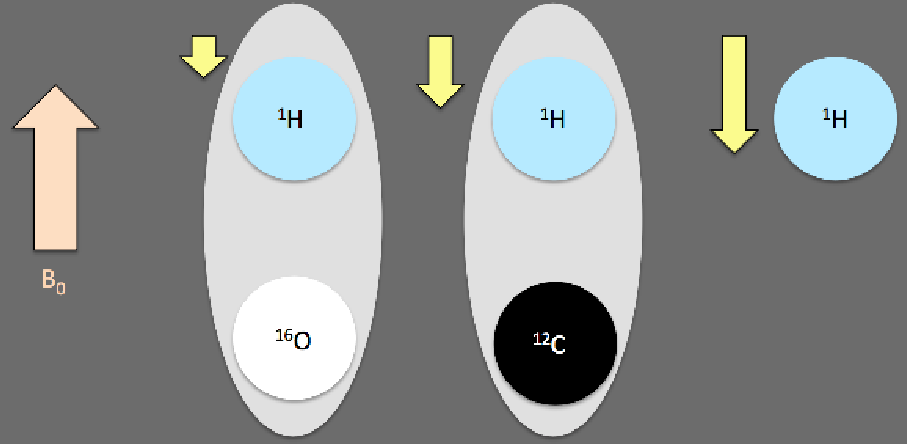
^{1}H
^{1}H
^{1}H
^{16}O
^{12}C
B_0

MRI vs MRS

- Magnetic resonance imaging (MRI) is almost always based on measurement of water signal
  - A lot of signal
- Magnetic resonance spectroscopy (MRS) measures protons in other molecules
  - Low concentrations → Low SNR → Many averages, large voxels, limited FOV

Spectra

Example Lactate

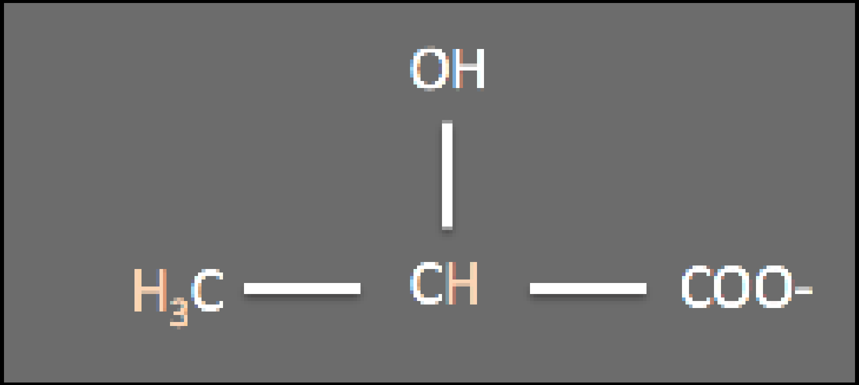

$H_3C-CH(OH)-COO^-$

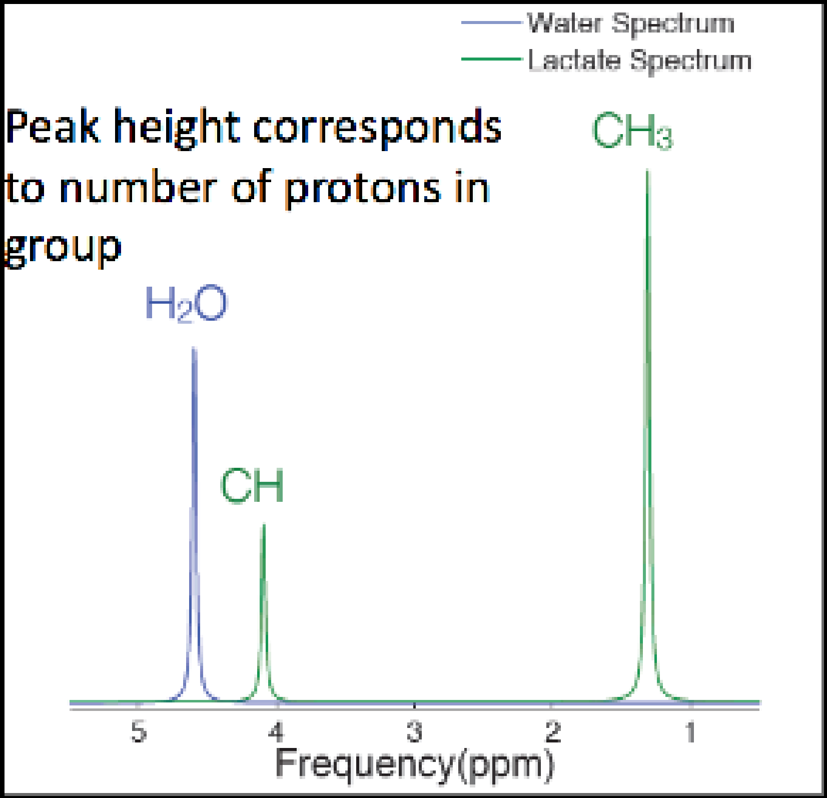

Peak height corresponds to number of protons in group

Commonly reported metabolites (Brain)

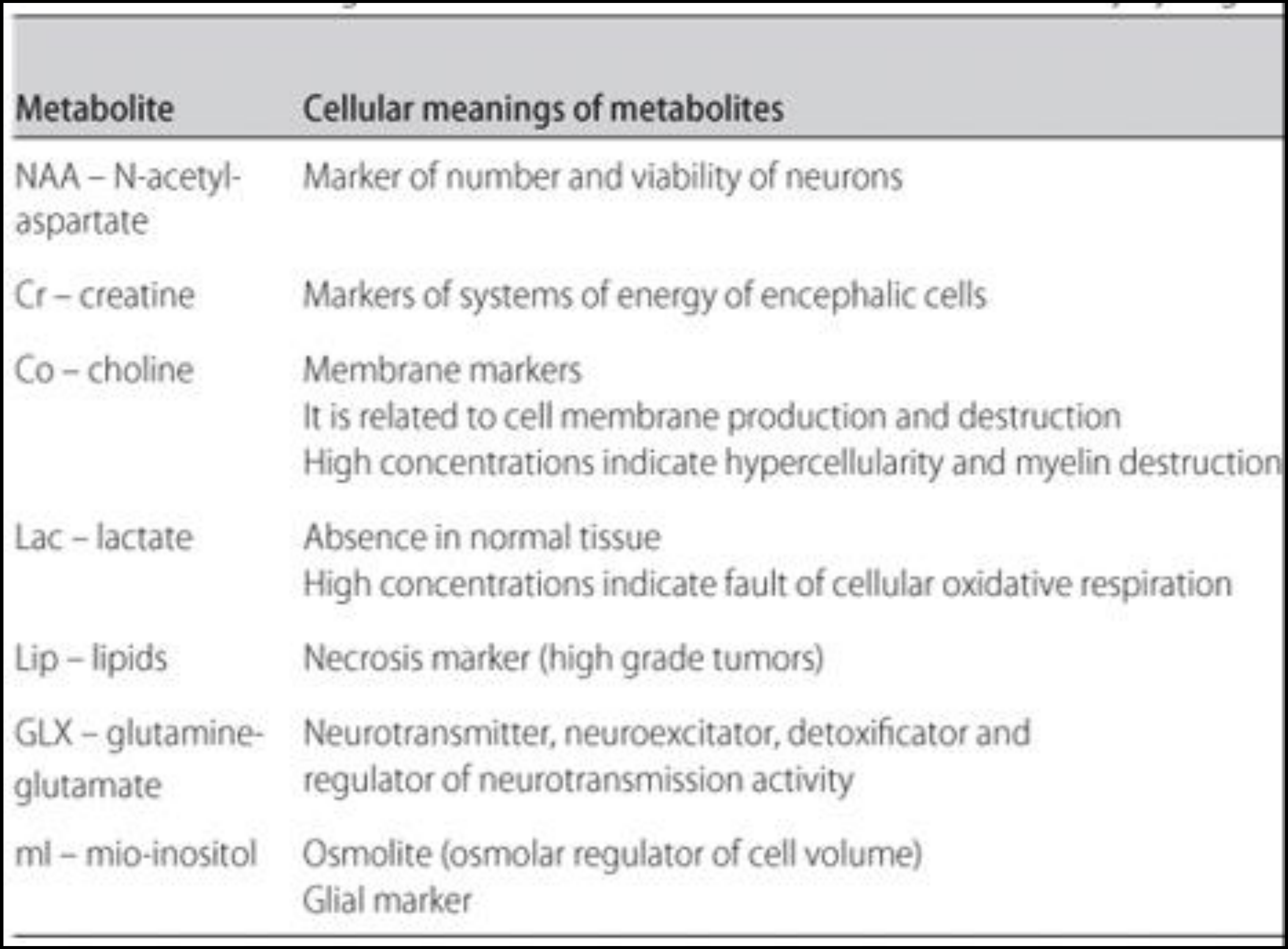

Metabolite	Cellular meanings of metabolites
NAA – N-acetyl-aspartate	Marker of number and viability of neurons
Cr – creatine	Markers of systems of energy of encephalic cells
Co – choline	Membrane markers It is related to cell membrane production and destruction High concentrations indicate hypercellularity and myelin destruction
Lac – lactate	Absence in normal tissue High concentrations indicate fault of cellular oxidative respiration
Lip – lipids	Necrosis marker (high grade tumors)
GLX – glutamine-glutamate	Neurotransmitter, neuroexcitator, detoxificator and regulator of neurotransmission activity
mI – mio-inositol	Osmolite (osmolar regulator of cell volume) Glial marker

Ricardo André Amorim Leite et al. Arq. Neuro-Psiquiatr. vol.68 no.1 São Paulo Feb. 2010

Spectra

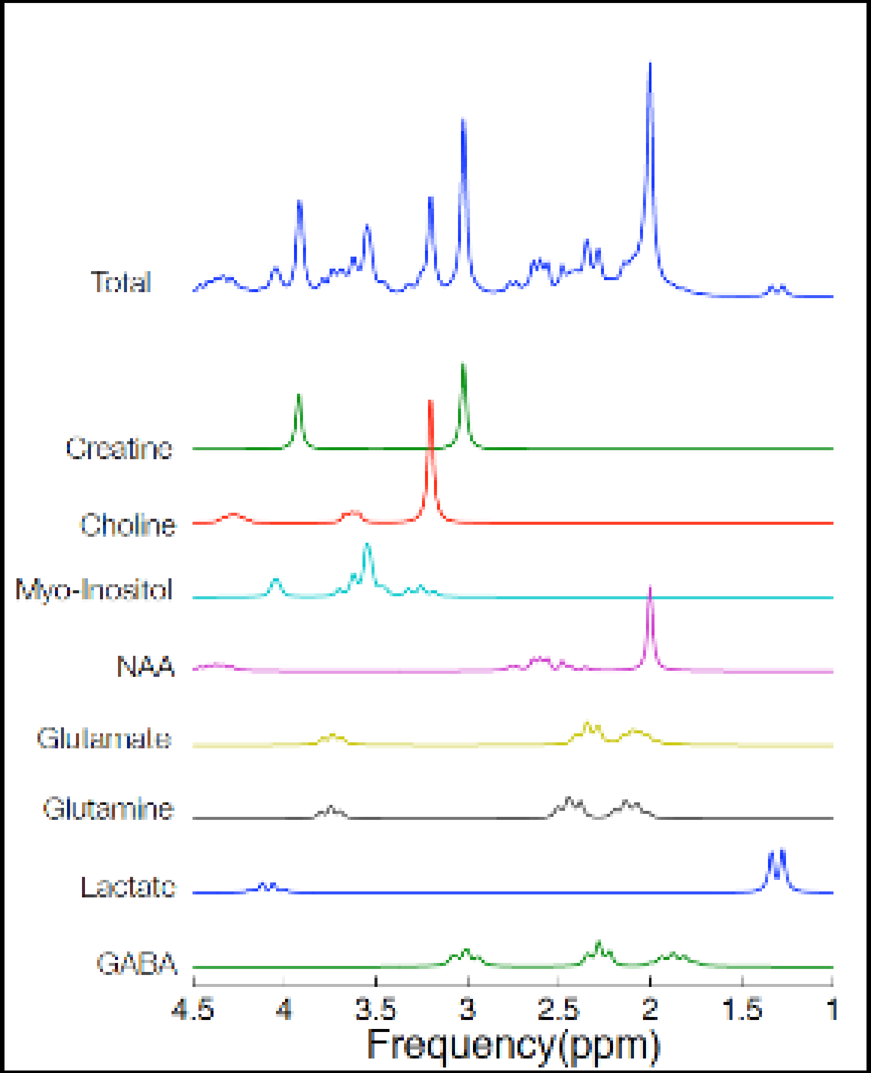
Total
Creatine
Choline
Myo-Inositol
NAA
Glutamate
Glutamine
Lactate
GABA
4.5
4
3.5
3
2.5
2
1.5
1
Frequency(ppm)

Example brain

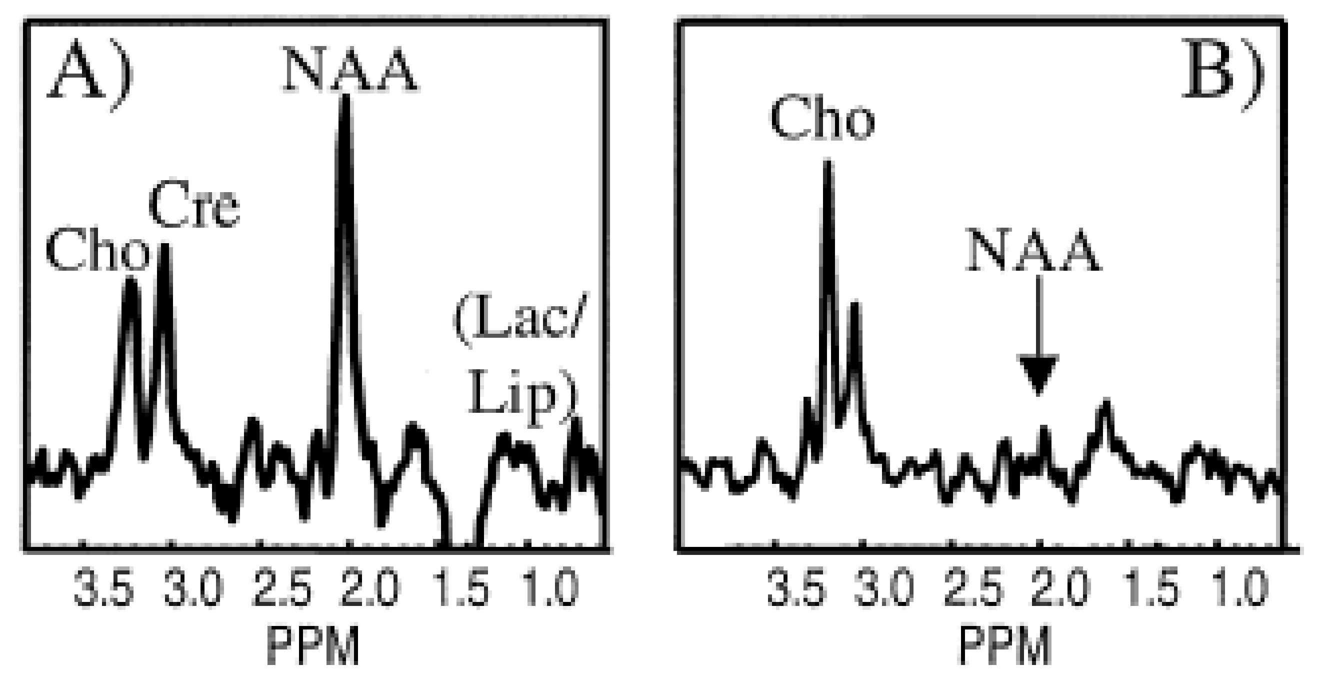

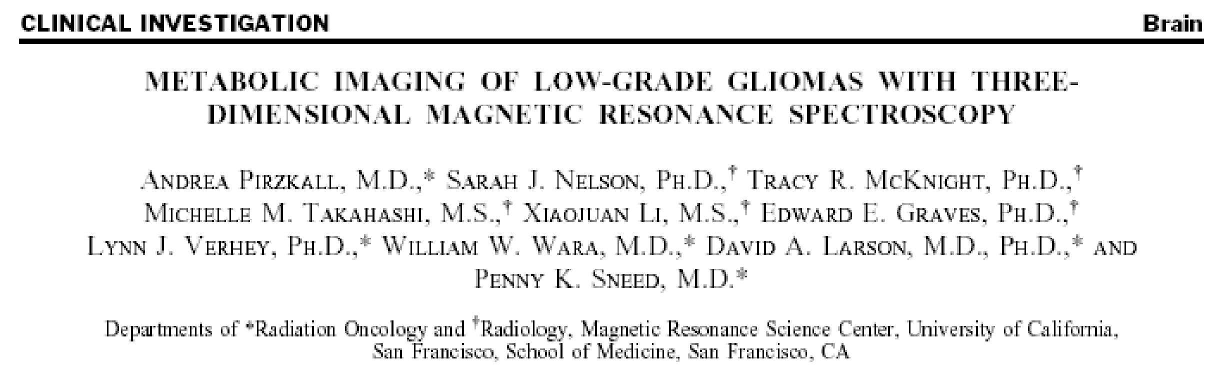
CLINICAL INVESTIGATION **Brain**

METABOLIC IMAGING OF LOW-GRADE GLIOMAS WITH THREE-DIMENSIONAL MAGNETIC RESONANCE SPECTROSCOPY

Andrea Pirzkall, M.D.,* Sarah J. Nelson, Ph.D.,† Tracy R. McKnight, Ph.D.,†
Michelle M. Takahashi, M.S.,† Xiaojuan Li, M.S.,† Edward E. Graves, Ph.D.,†
Lynn J. Verhey, Ph.D.,* William W. Wara, M.D.,* David A. Larson, M.D., Ph.D.,* and
Penny K. Sneed, M.D.*

Departments of *Radiation Oncology and †Radiology, Magnetic Resonance Science Center, University of California,
San Francisco, School of Medicine, San Francisco, CA

Example (prostate)

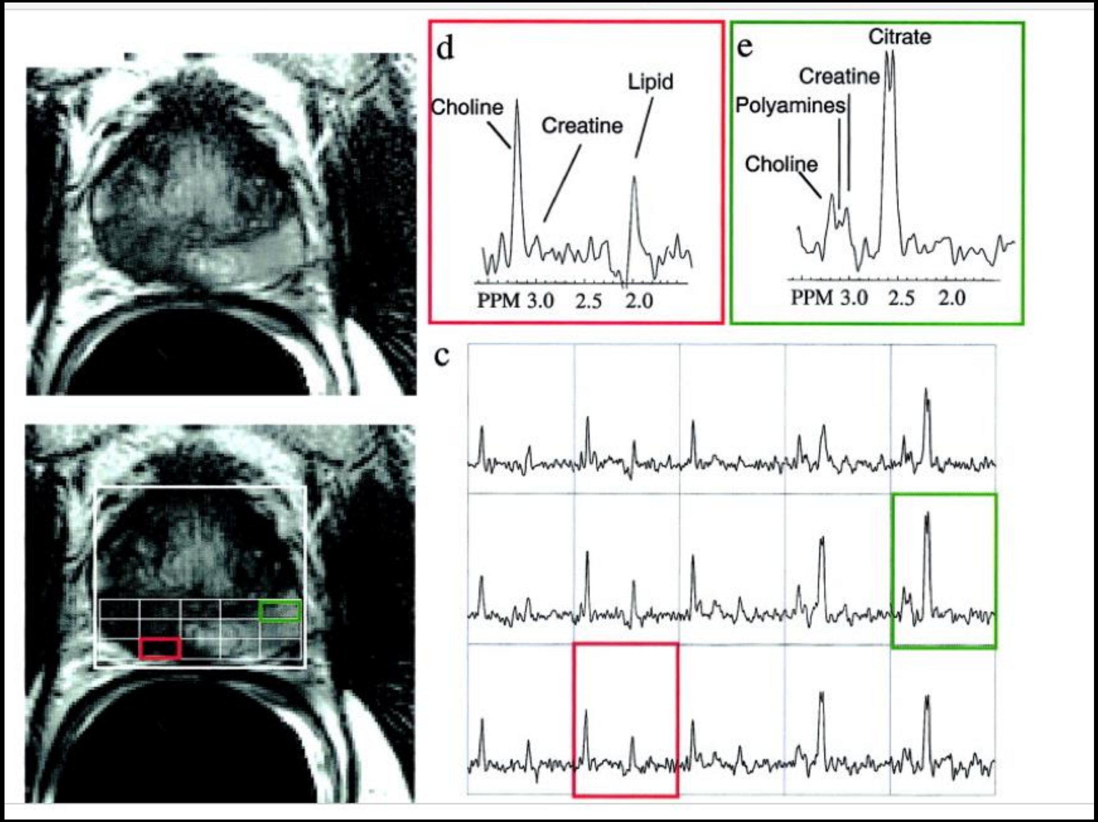
d
Choline
Creatine
Lipid
PPM 3.0 2.5 2.0
e
Citrate
Creatine
Polyamines
Choline
PPM 3.0 2.5 2.0
c

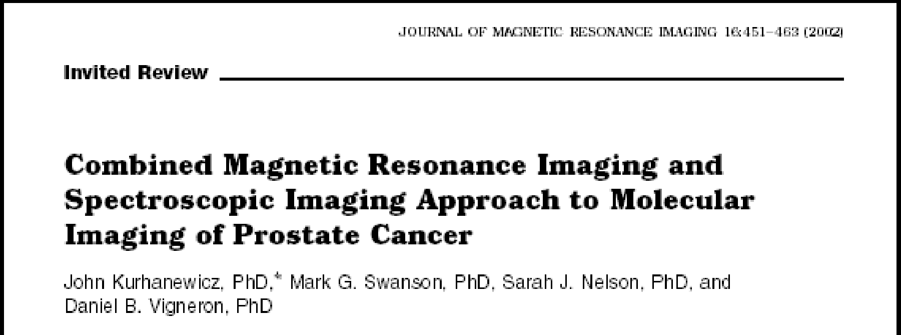
JOURNAL OF MAGNETIC RESONANCE IMAGING 16:451–463 (2002)

Invited Review

Combined Magnetic Resonance Imaging and Spectroscopic Imaging Approach to Molecular Imaging of Prostate Cancer

John Kurhanewicz, PhD,* Mark G. Swanson, PhD, Sarah J. Nelson, PhD, and
Daniel B. Vigneron, PhD

Technical issues in MRS

- Water suppression
  - Water concentration is approx 1000 times higher than metabolites
- Shimming
  - Underlying B0 needs to very well defined in volume
- Outer volume suppression
  - Signal from outside the volume (typically lipids) disturb the measurement

Water suppression

- Apply frequency selective pulse (for water: 4.7 ppm) prior to excitation pulse
- This tips only water spins into transverse plane (all others left along z)
- Apply crusher gradient to dephase water spins, then begin MRS acquisition

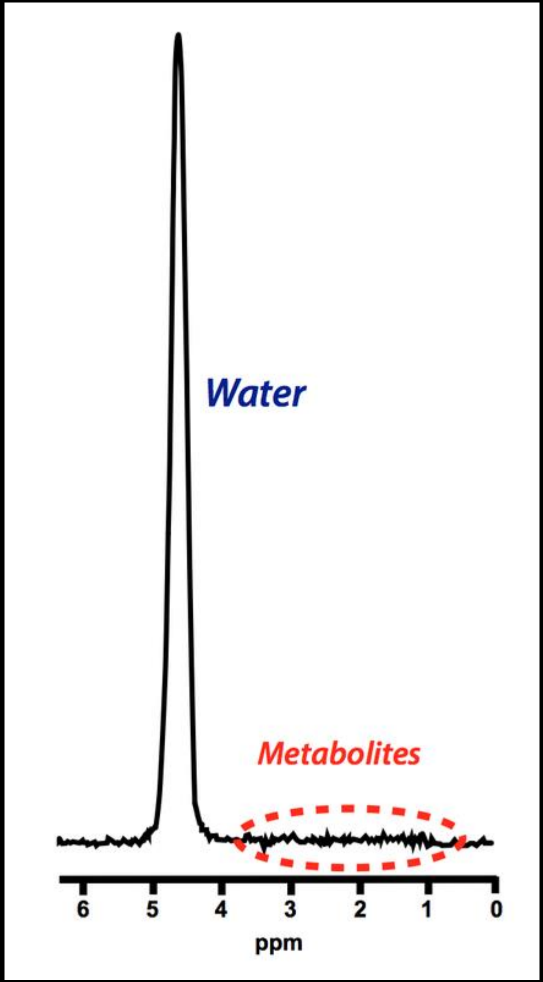

Shimming

Poor Shim

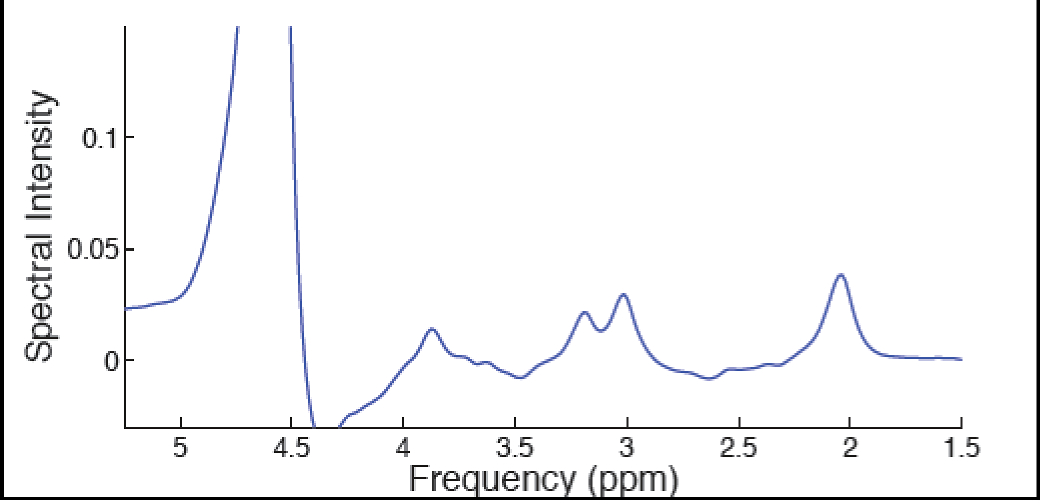

Better Shim

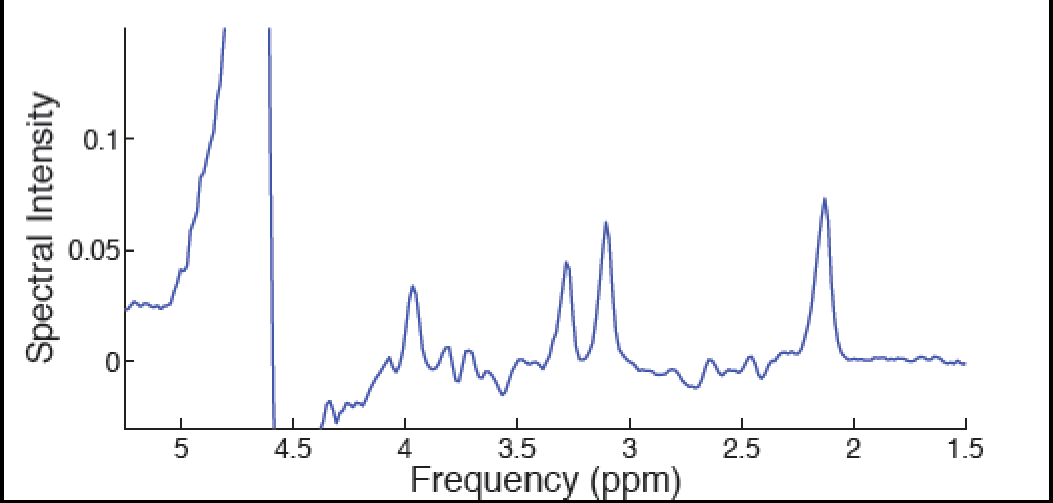

Lipid suppression

- Lipids are found throughout body:
    - – Extracranial lipids
    - – Periprostatic lipids
    - – Breast
    - – Axilla
    - – etc.
- Lipids can distort baseline of spectra so that metabolites cannot be detected
- Lipids resonate at 1.3 ppm
- Lipids can be suppressed using outer volume suppression techniques

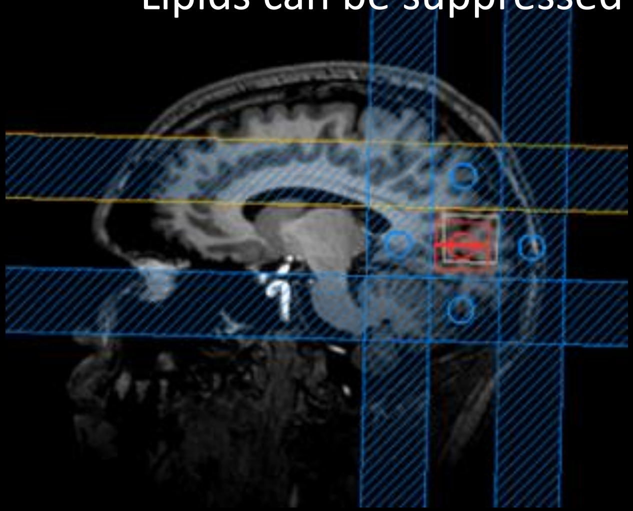

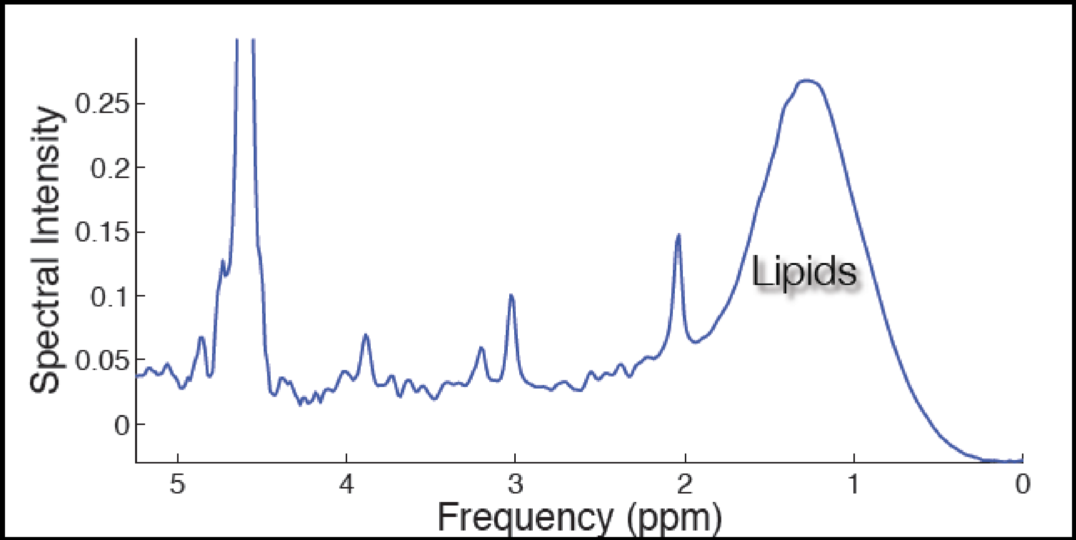

Lipid suppression

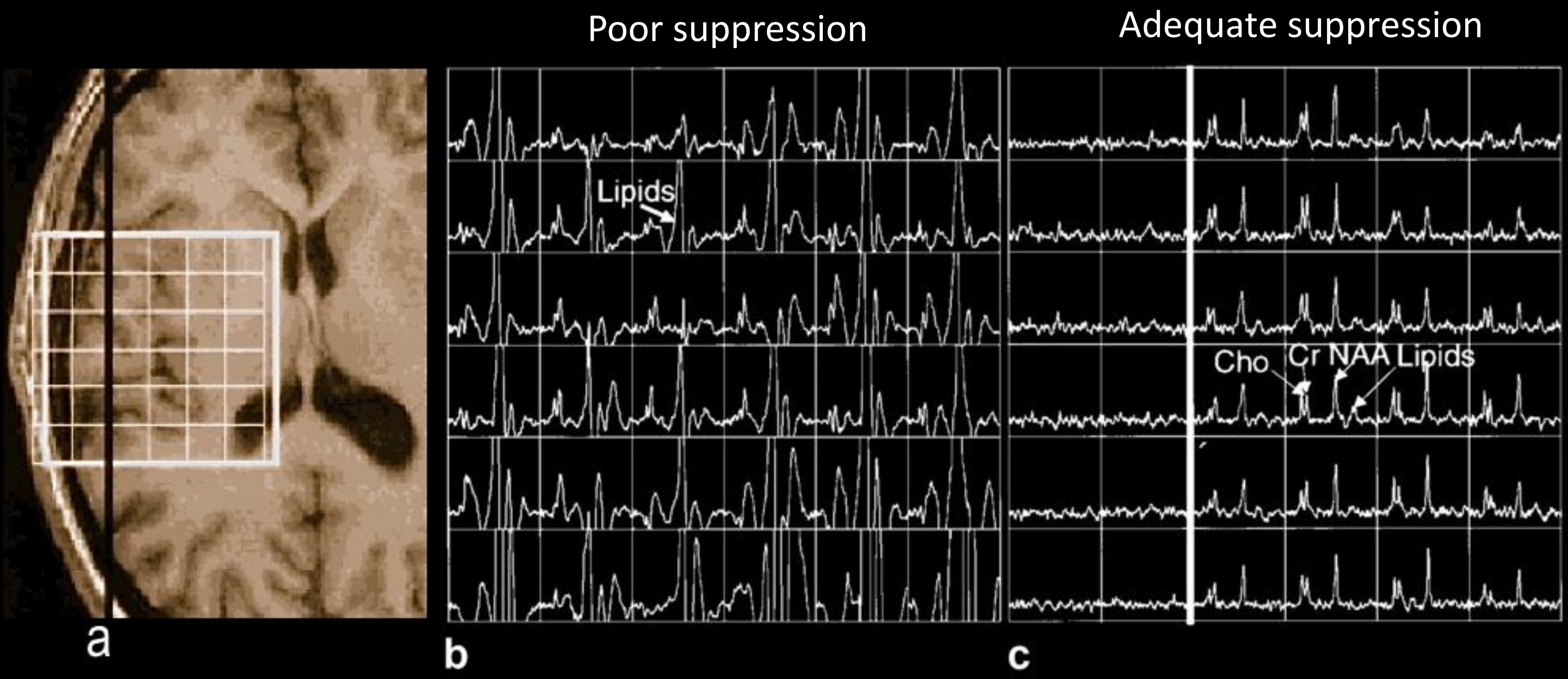
Poor suppression
Adequate suppression
Lipids
Cho
Cr
NAA
Lipids
a
b
c

http://limpeter-mriblog.blogspot.se/2009/09/magnetic-resonance-spectroscopy-iii.html

Summary Spectroscopy

- “MRS is a clinical technique of the future and always will be...”

- The potential is large
- Difficulties with reproducibility and quantification

Thank you!

Acknowledgments

Gary Liney, Anders Garpebring, Uulke v.d. Heide

http://www.mc.vanderbilt.edu/documents/fmri/files/2013_Phys352A_MRS(1).pdf

UMC Utrecht

MR-Guided treatment

Rob Tijssen, Dphil
Dept. of Radiotherapy
University Medical Center Utrecht

UMC Utrecht

MR-Linac

Rob Tijssen, Dphil
Dept. of Radiotherapy
University Medical Center Utrecht

Outline

- Why online MRI guided RT?
- Hardware & technical developments
- Commissioning & QA
- Clinical results
- Towards real-time adaptive radiotherapy

More than just swapping out image modality

Radiotherapy is: dealing with uncertainties

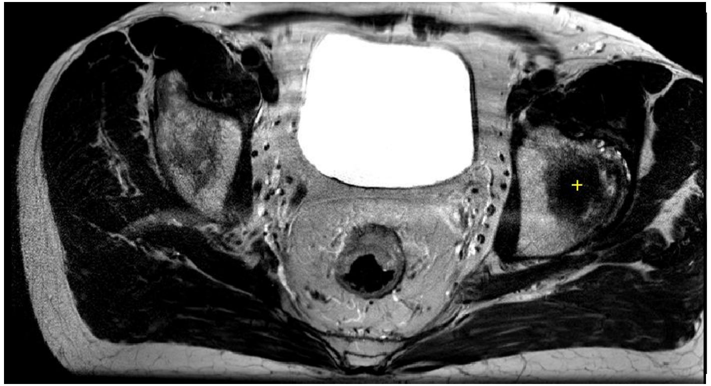

ICRU-50

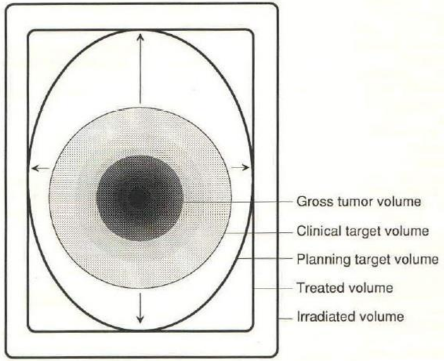
Gross tumor volume
Clinical target volume
Planning target volume
Treated volume
Irradiated volume

Uncertainty requires a homogeneous dose over a large volume

‘invisibility’ of the target limits dose escalation

Reducing Margins

- Better visualization of target (here: lymph nodes) using MRI
- Reduce motion margins by MLC tracking

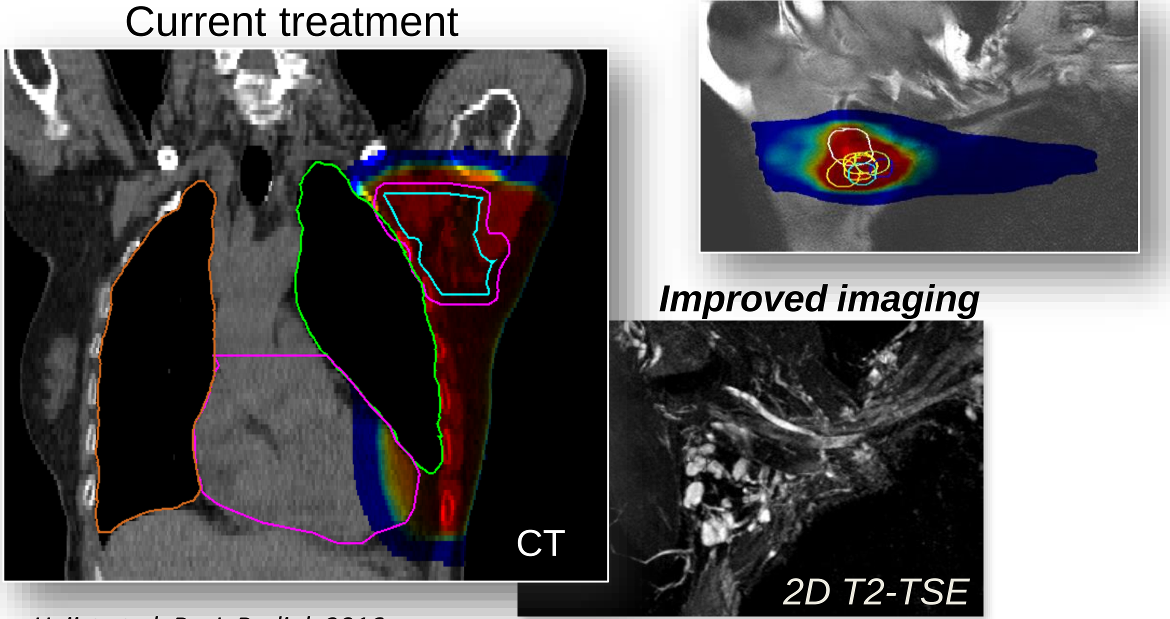
Current treatment

Target ind. lymph nodes

Improved imaging

van Heijst et al. Br. J. Radiol, 2016

Real-time tracking of liver

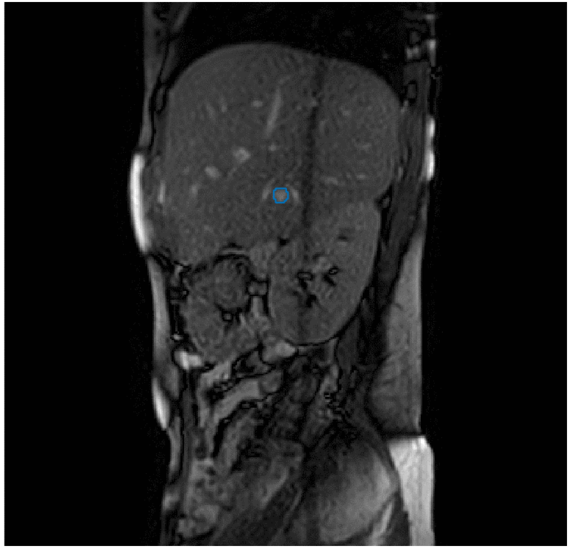

Bourque et al., IJROBP, 2017

Adaptive treatments

Rectal tumor boost

  - 50 Gy to the rectum
  - **+ 10 Gy extra to the tumor**

- 5x daily on MR-Linac

This will allow:

- adapt to local changes in anatomy
- spare surrounding healthy tissue..
- increase dose to tumor..
- reduce number of boost fractions..

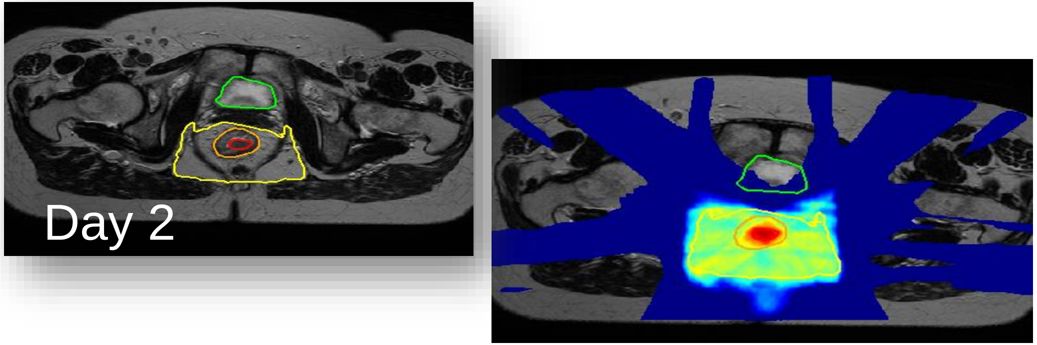

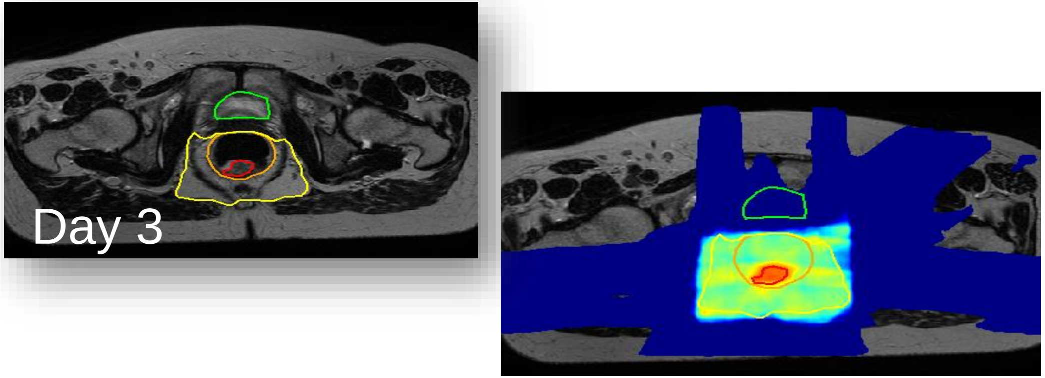

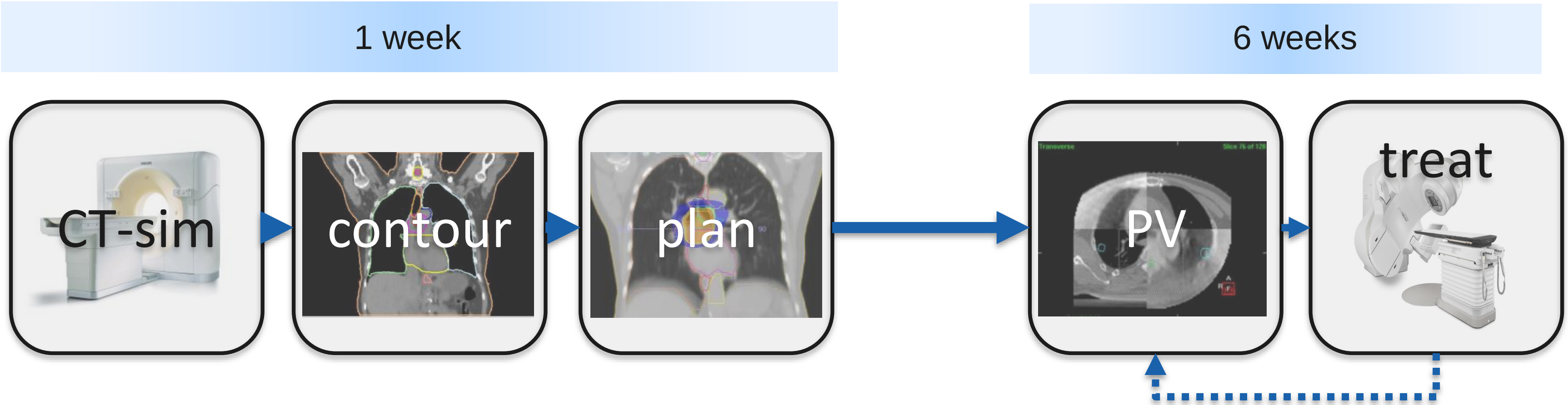

1 week

6 weeks

CT-sim

contour

plan

PV

treat

Conventional treatment process

Conventional Linac

move patient
to suit treatment plan

MRI Linac

adjust treatment plan
to suit the patient

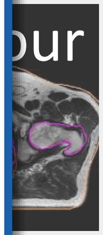

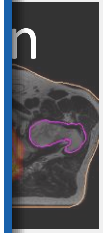

Hardware & technical developments

Overview of the various systems

Design parameters

- radiation window
- image quality aspects

The effects on dose delivery (ERE & EFE)

Various groups working on different solutions

- Viewray, Cleveland, USA
  - 0.35 T MRI, 3 Co sources

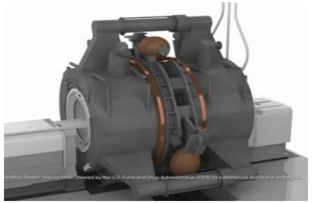
ViewRay System has not been cleared by the U.S. Food and Drug Administration (FDA) for commercial distribution in the U.S.

- Utrecht, The Netherlands
  - 1.5 T MRI, 7 MV linac

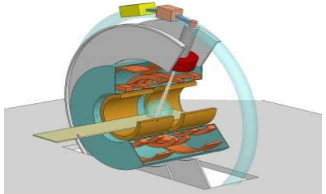

- Edmonton, Canada
  - 0.5 T MRI, 6 MV linac

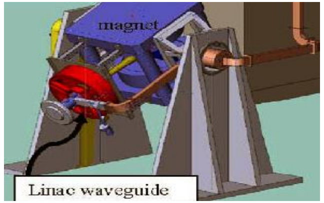

- Australia
  - 1.0 T MRI, 4 & 6 MV linac

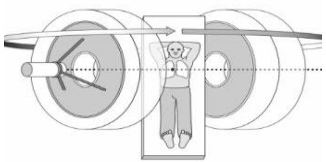

The difference: Magnet Designs

Esaota G-scan 0.25T

Philips Panorama 1.0T

Philips Ingenia 1.5T

Viewray

www.viewray.com
3 Cobalt-60 sources
0.35 T superconducting MRI
Siemens MRI back-end

Treated first patient in February 2014

February 2017: FDA clearance for Linac

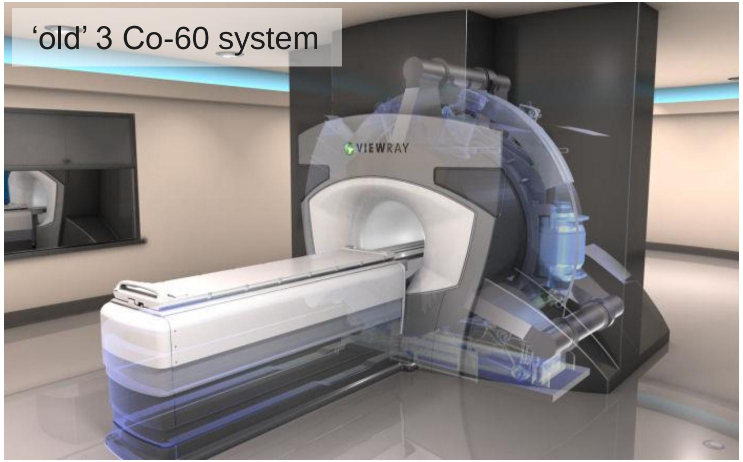
‘old’ 3 Co-60 system

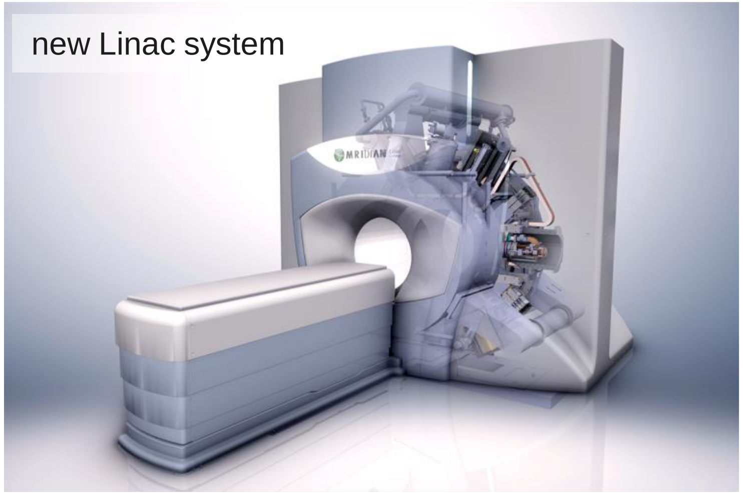
new Linac system

UMC Utrecht

1.5 Tesla wide-bore MRI

+

7 MV Elekta linac

=>

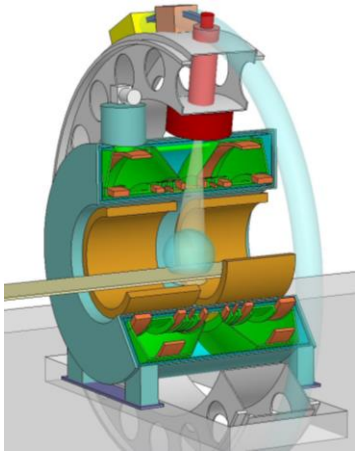

1999

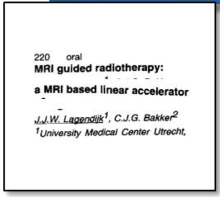

220 oral
MRI guided radiotherapy:
a MRI based linear accelerator
J.J.W. Lagendijk[1], C.J.G. Bakker[2]
[1]University Medical Center Utrecht,

invention

2004

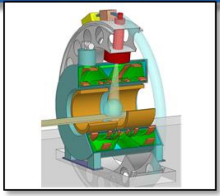

design

2005

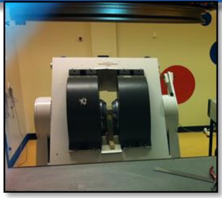

Initial exp.

2009

1st prototype

2012

2nd prototype

2014

3rd prototype

2015

(pre)Clinical

2017

First patient

Lagendijk and Bakker, MRI guided radiotherapy - A MRI based linear accelerator
Radiotherapy and Oncology Volume 56, Supplement 1, September 2000, 220

Cross Cancer Institute, Edmonton

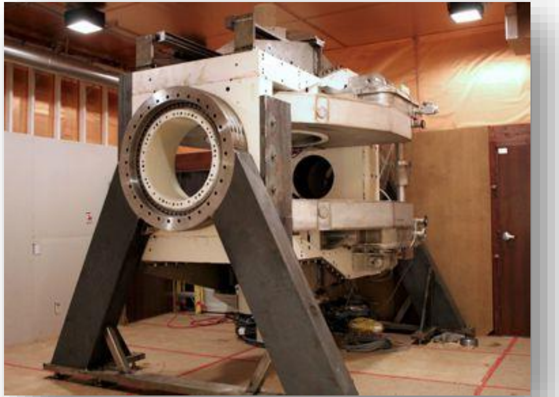

Inline MRI-Linac configuration

Magnet rotates around the patient @ 1 rpm
Larmor Freq. changes with gantry angle due to Earth's magnetic field effects

Gino Fallone and co-workers

- 0.5T Bi-planar MRI
- 6 MV linac in parallel configuration
- Installation began 2013, first images July 2014

From www.linac-mr.ca / www.Magnettx.com

60 cm (H) x 110 cm (W)

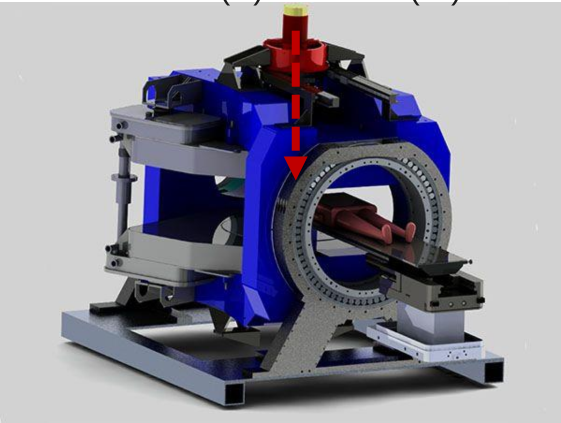

Aurora RT™

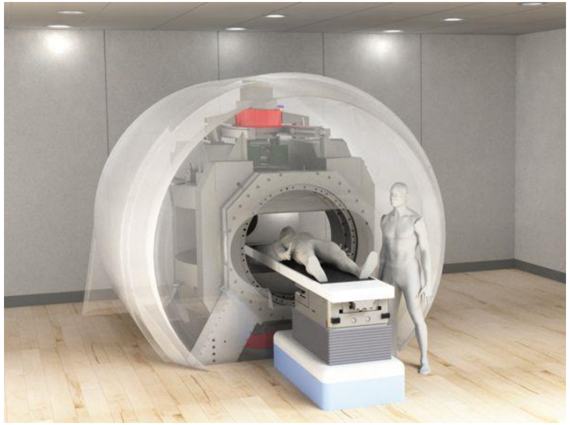

Australian MR-Linac

Gary Liney, Paul Keall & co-workers

- 1T inline system (Siemens)
- 4 & 6 MV, Varian 120 Leaf MLC
- integrated RF and gradient modules to maintain space
- no additional coil on patient.

First patient: expected mid 2018

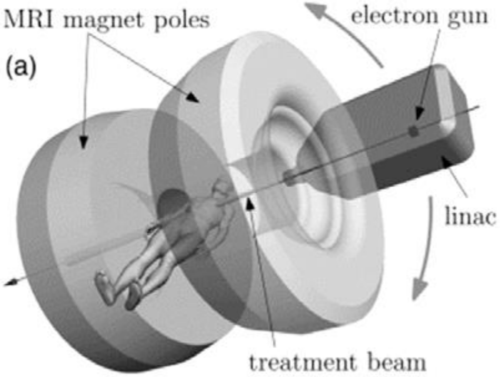
MRI magnet poles
(a)
electron gun
linac
treatment beam

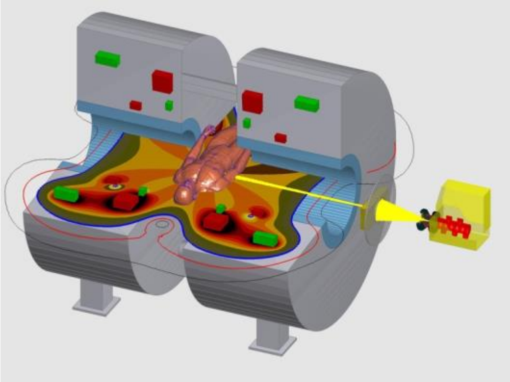

vertical open bore

50cm gap

Agilent Technologies

60cm bore diameter

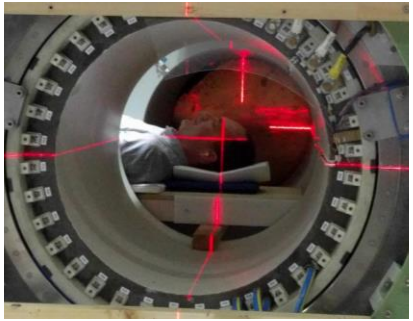

first image: April '17

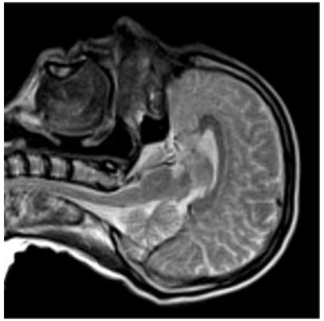

Phys. Med. Biol. **59** (2014) R349–R369

Images courtesy of Gary Liney

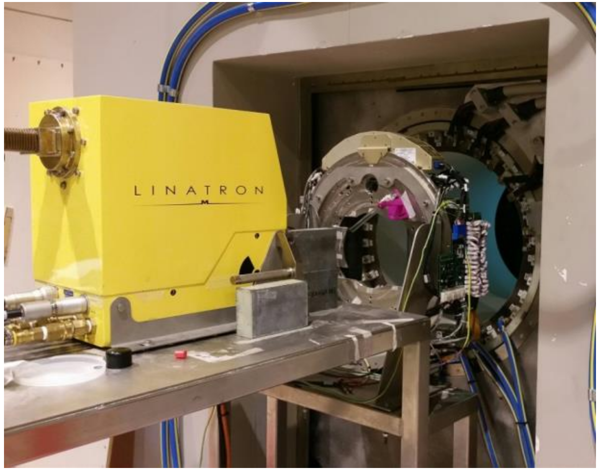

Moveable Treatment head on rail system to change SID (cage panel removed).

Progress to date:
Shielded xray head;
Imaging system
MLC tracking at 3 frames/s;

Agilent Technologies

www.sydney.edu.au

Images courtesy of Gary Liney

Magnet design parameters

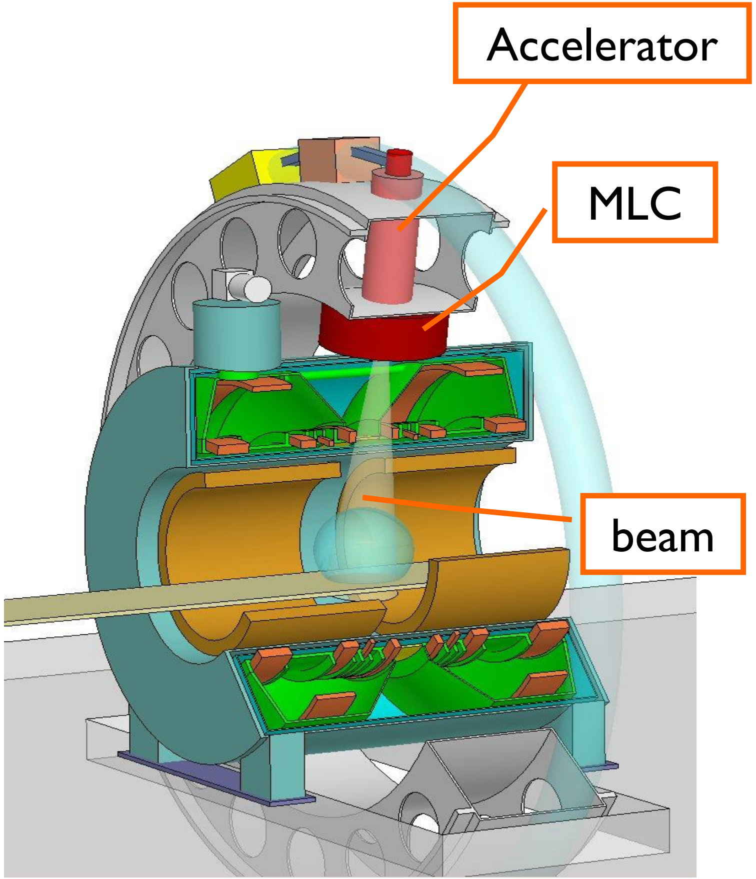
Accelerator
MLC
beam

- **Field strength**
- Openness (bore length & diameter)
- Linac compatibility
- Helium boil off
- Energy consumption
- Homogeniety
- FOV
- Stability

The Effect of Field strength

[1] Hoult DI, JMRI 2000; 12:46-67
[2] Pohman, MRM 2016; 75:801-809

Goal: Spin polarization

Higher B_0 = more polarization
=> higher signal to work with

SNR ~ B_0 [1]

More recently:
SNR ~ $B_0^{1.65}$ [2]

Based on Hanson, Concepts in Magn Res, 2006; 32A:329-240

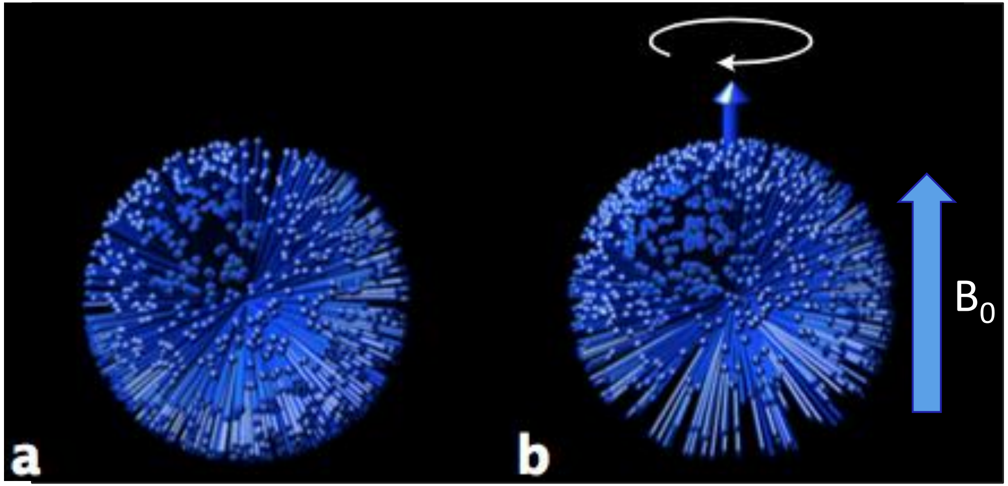

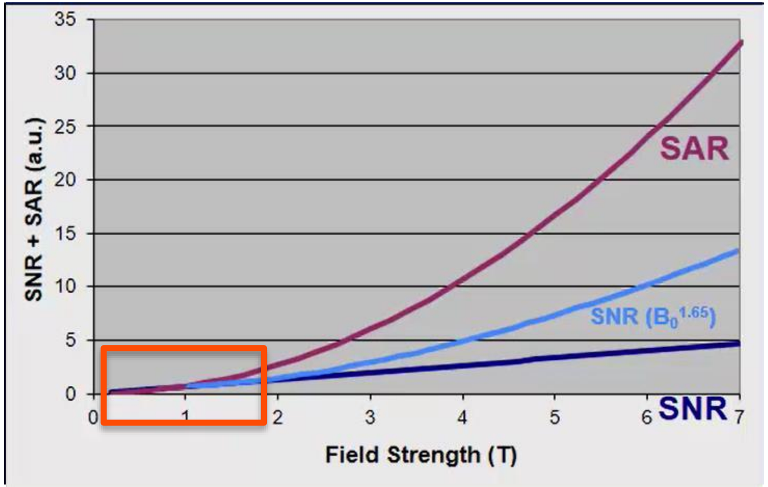

The Effect of Field strength

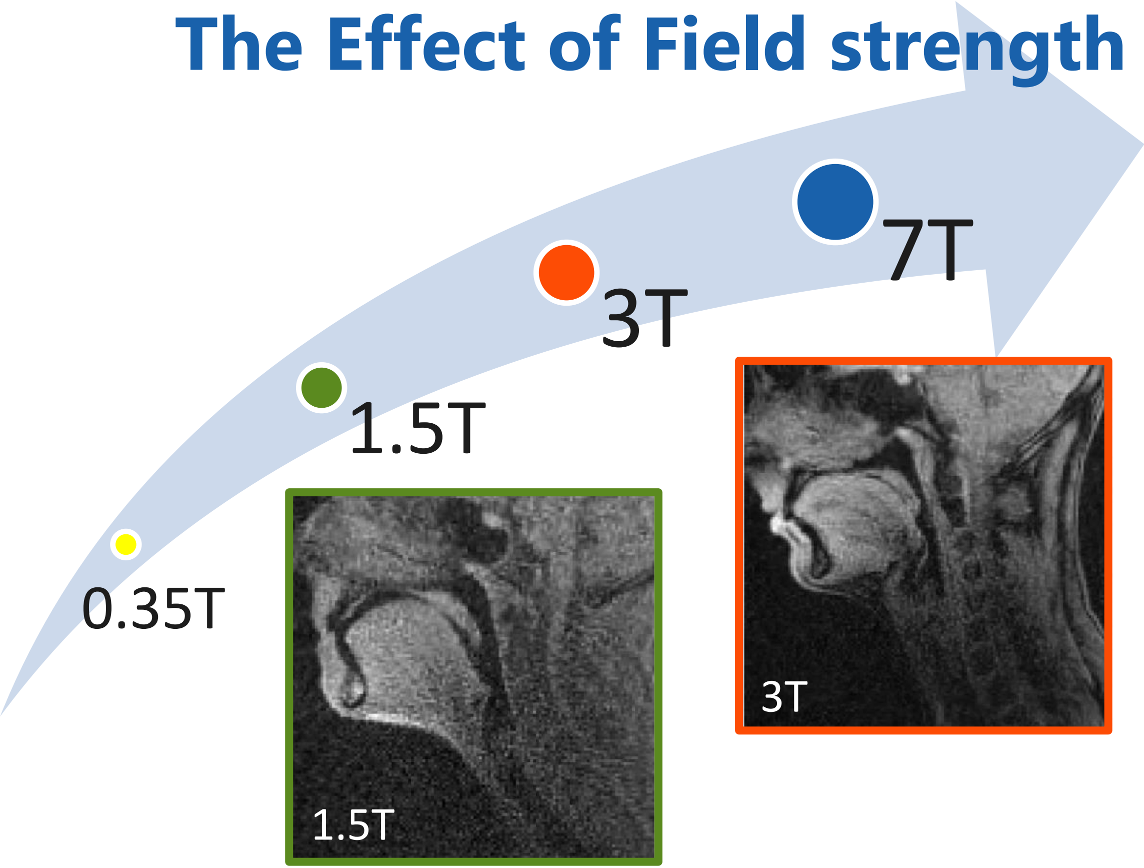

SNR scales with

- field strength
- voxel size
- 1/receiver bandwidth (=speed)

Higher field strength also gives:

- better functional contrast (BOLD, DWI, DCE)

but also,

- Longer T_1 relaxation rates
- higher SAR
- higher susceptibility effects
- different ERE/EFE effects

Magnet design parameters

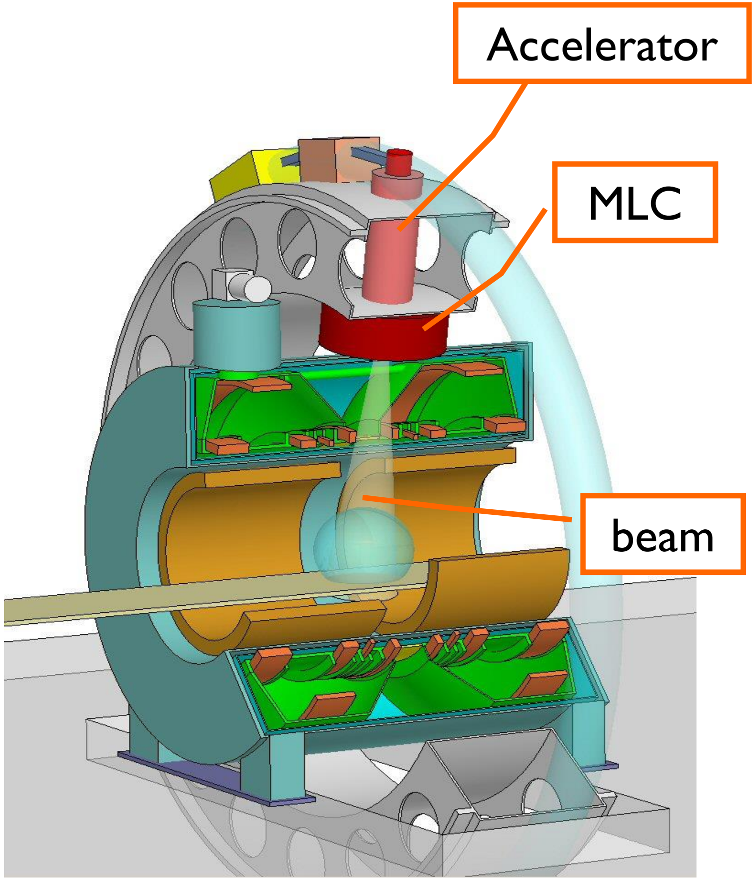
Accelerator
MLC
beam

- Field strength
- Openness (bore length & diameter)
- **Linac compatibility**
- Helium boil off
- Energy consumption
- Homogeniety
- FOV
- Stability

Transmission through the cryostat

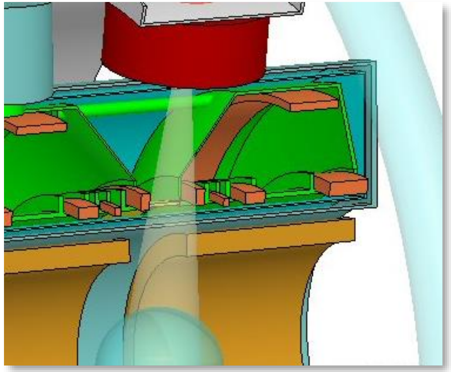

Gap between central coils increased to ~ 150 mm

Cryostat with reduced and uniform gamma attenuation

Possible without loss of field homogeniety

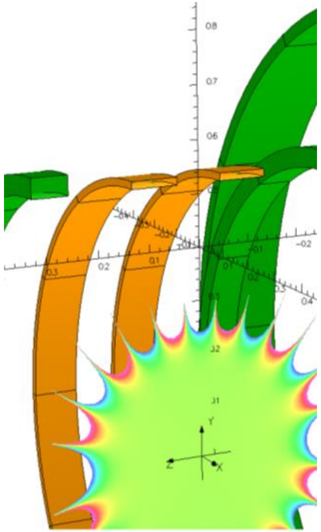

"Standard"

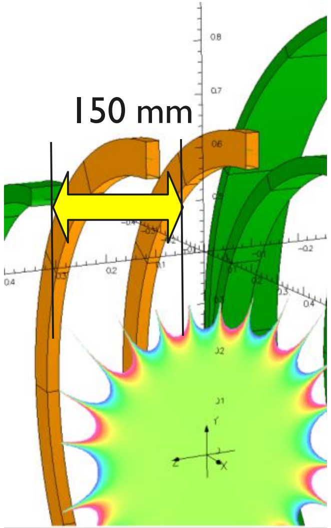

MR/RT design

Johan Overweg, Philips

Active shielding modified to decouple MRI & Linac

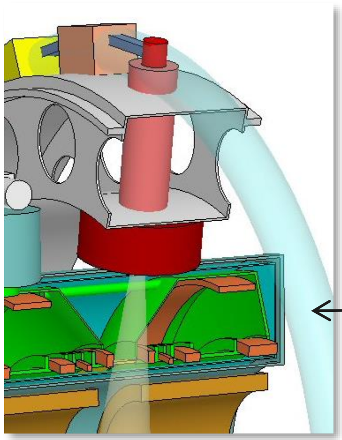

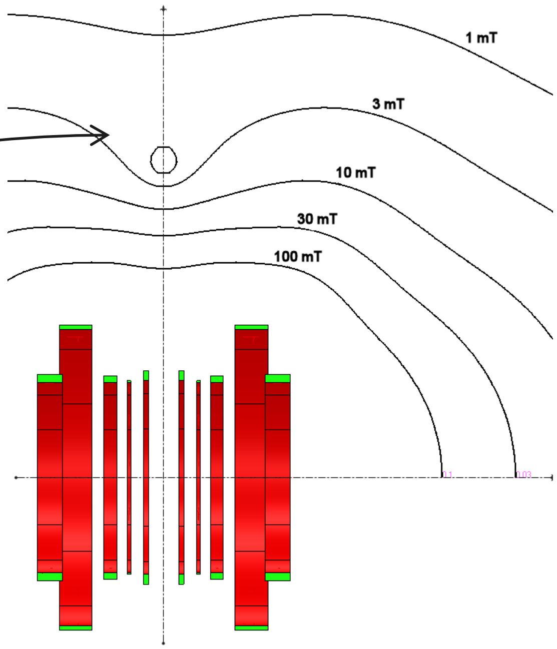
1 mT
3 mT
10 mT
30 mT
100 mT

Zero-field zone on outside of magnet (position of Linac gun)

Achieved by shift and change in #turns of shielding coils

Johan Overweg, Philips

Principle of active shielding

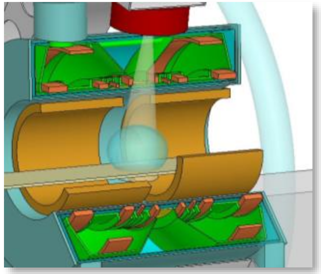

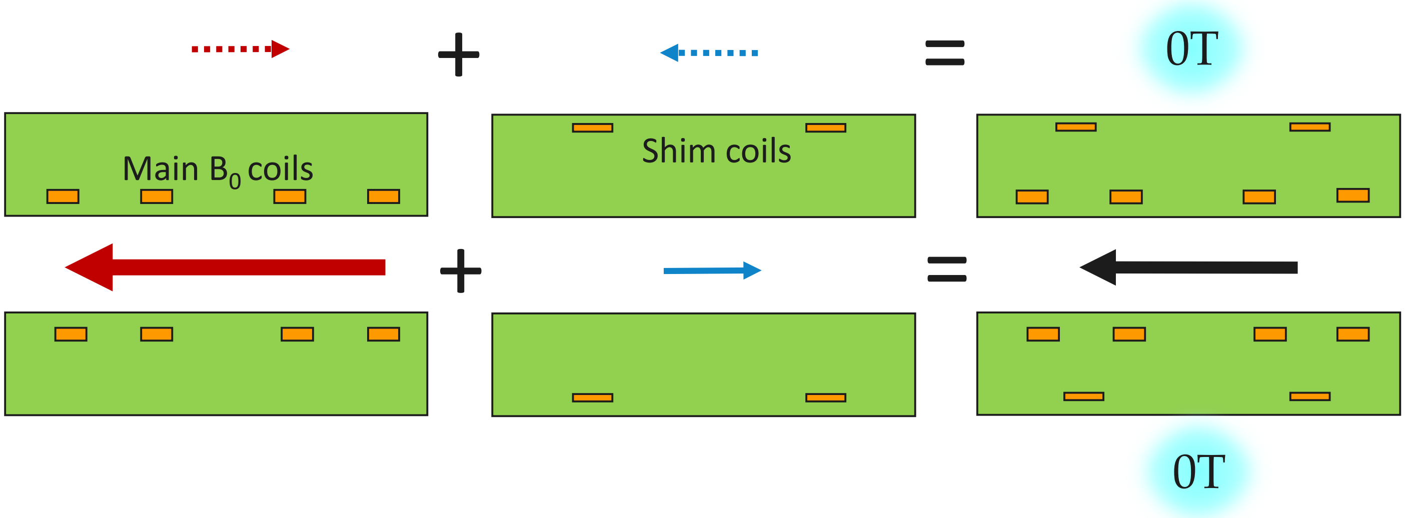

+
=
0T
Main B_0 coils
Shim coils
+
=
0T

Gradient coil design: diagnostic scanners

- Gradient coils in x and y ‘touch’ in the middle (physically and electronically)
- Optimal design based on numerical algorithms

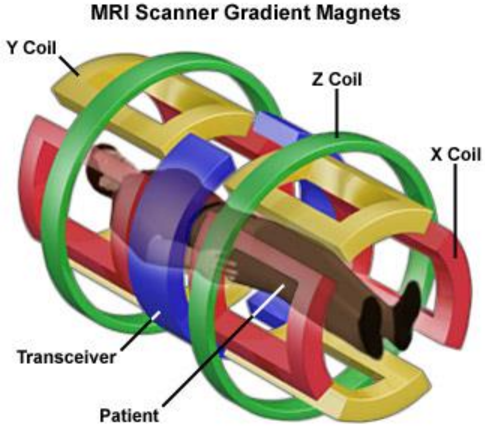
MRI Scanner Gradient Magnets
Y Coil
Z Coil
X Coil
Transceiver
Patient

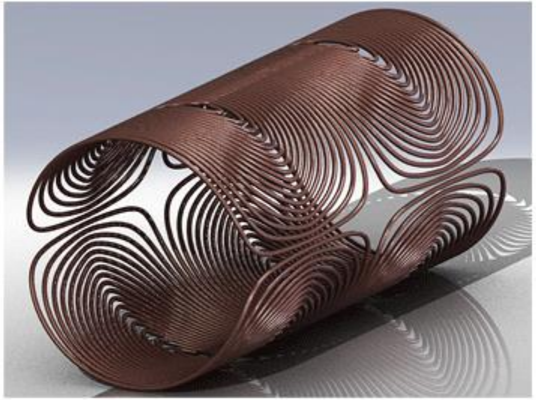

Split gradient coil

Design requirements

Radiotransparant in the centre. As linear as possible for large FOV

Solution:

Central gap width 200 mm

Coil halves joined by 7 mm fiberglass cylinder on the outside

No electrical or cooling interconnections between halves

gradient specs: max (clinical)

Strength: 34 (15) $\mathrm{mTm^{-1}}$

Slew rate: 120 (65) $\mathrm{mTm^{-1}ms^{-1}}$

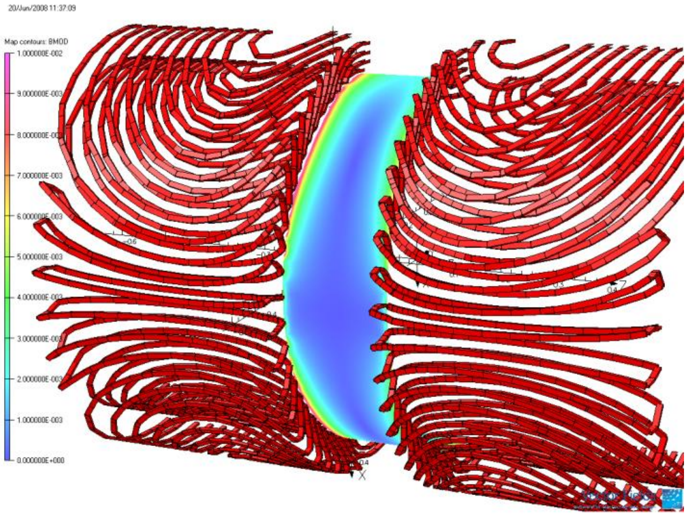
20/Jun/2008 11:37:09
Map contours: BMOD
1.000000E-002
9.000000E-003
8.000000E-003
7.000000E-003
6.000000E-003
5.000000E-003
4.000000E-003
3.000000E-003
2.000000E-003
1.000000E-003
0.000000E+000

Prototype gradient coil (Futura, Heerhugowaard, NL)

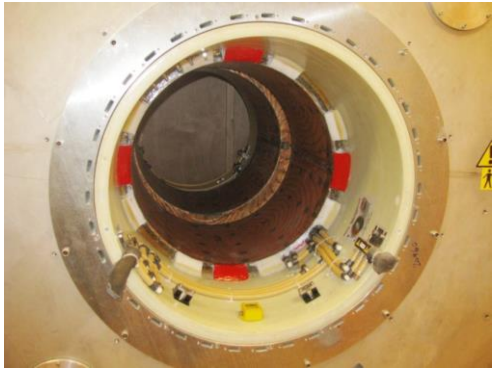

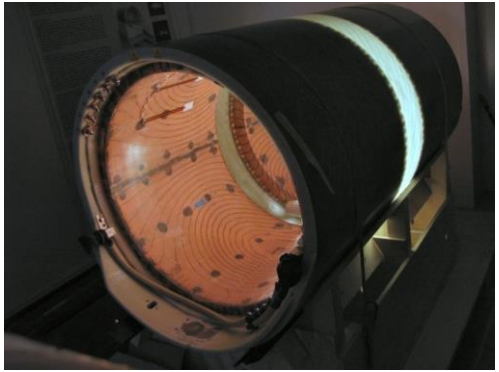

B_0 field exerts a Lorentz force on e^-

$$F = q\vec{v} \times B$$

The resulting effect depends on the orientation of B_0 with respect to the incident beam

- Perpendicular
- Electron Return Effect (ERE)

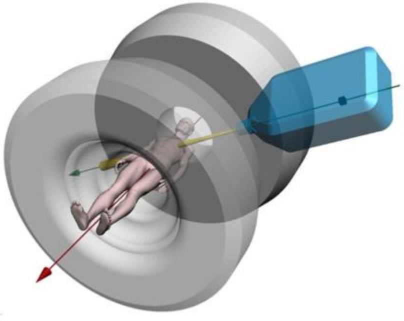

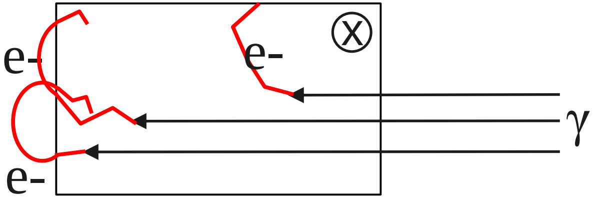

Raaijmakers et al., PMB 2005

- Inline
- Electron Focus Effect (EFE)

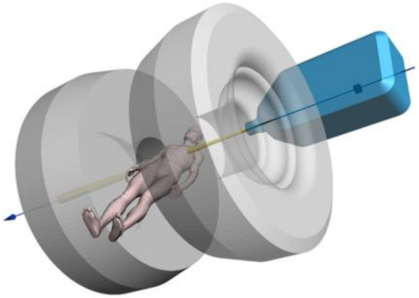

sydney.edu.au

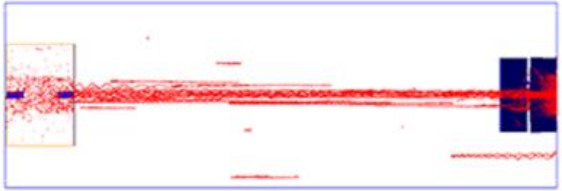

Oborn et al., Med Phys 2010

Dose deposition in a magnetic field: ERE

Electron Return Effect (exiting electrons return to the object)

- 6 MV phton beam
- B_0 = 1.5T
- Radii dependent on energy e^- and B_0

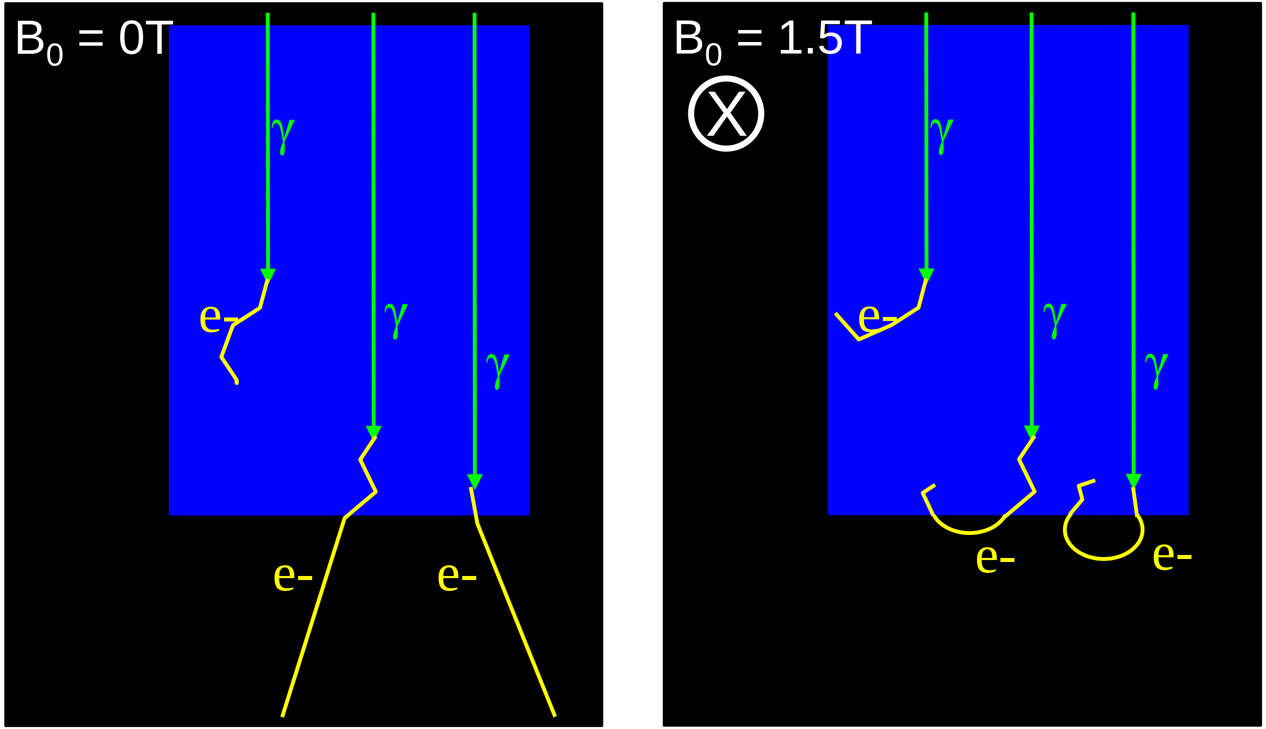
B_0 = 0T
γ
γ
γ
e-
e-
e-
B_0 = 1.5T
⊗
γ
γ
γ
e-
e-
e-

Raaijmakers et al. *Phys. Med. Biol.* **50** (2005) p. 1363-76

ERE (Electron Return Effect)
Dose increase at all tissue-air boundaries

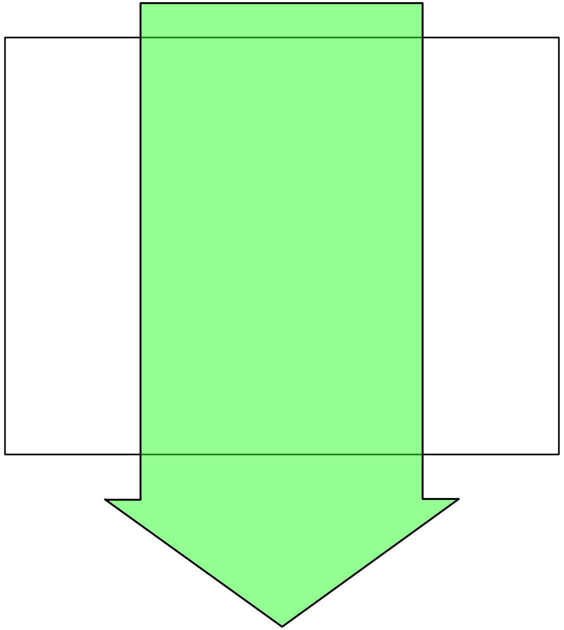

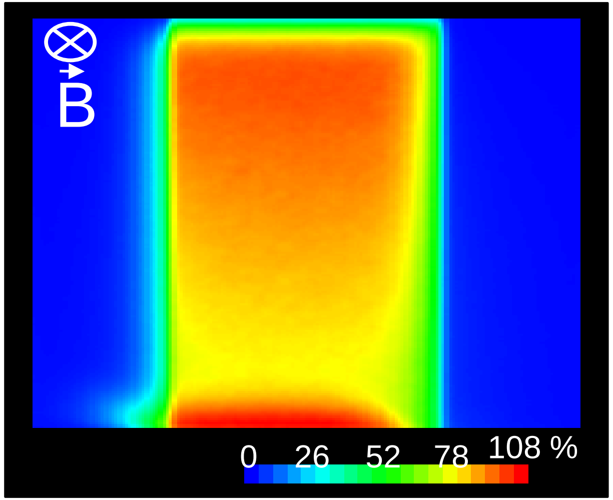

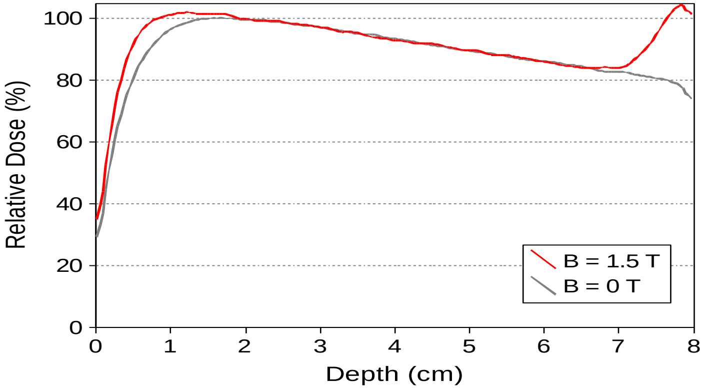

Raaijmakers et al. *Phys. Med. Biol.* **50** (2005) p. 1363-76

ERE (Electron Return Effect)
First order compensation via opposing beams

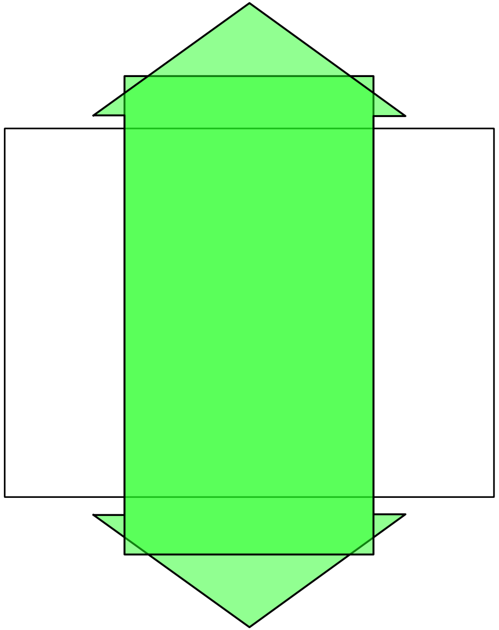

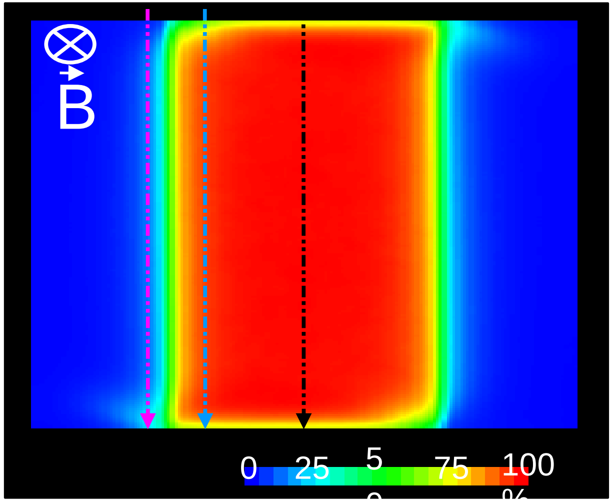

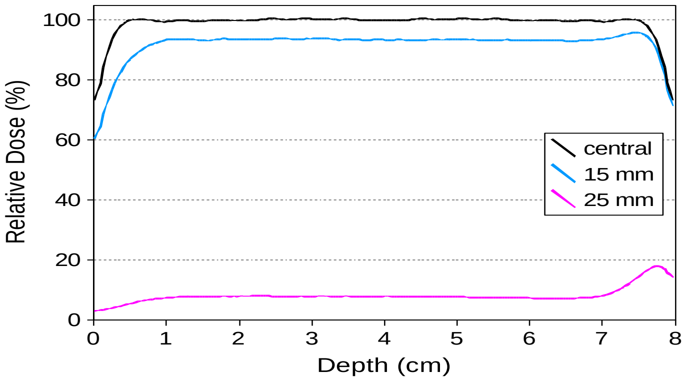

Raaijmakers et al. *Phys. Med. Biol.* **50** (2005) p. 1363-76

IMRT for the MRL: Monaco

- GPUMCD integrated in Monaco
- Clinical work flow (incl sequencing)

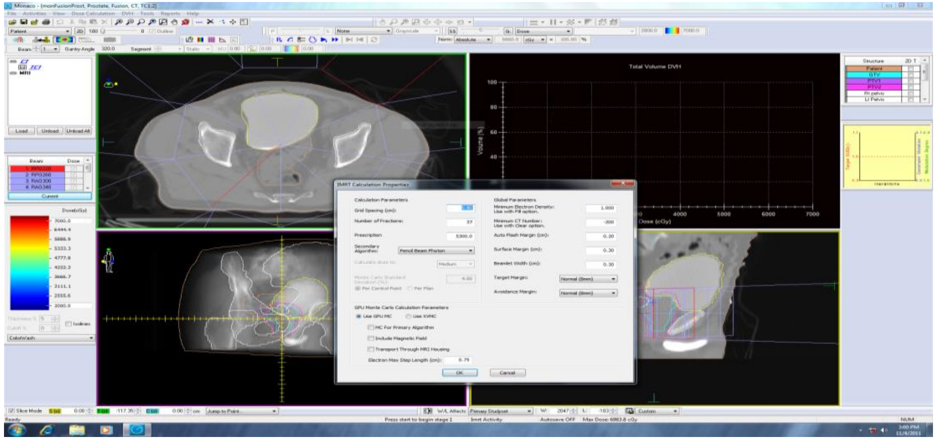

IMRT Calculation Properties

Calculation Parameters

Grid Spacing (cm): [illegible]

Number of Fractions: 37

Prescription: 5300.0

Secondary Algorithm: Pencil Beam Photon

Calculate dose to: Medium

Monte Carlo Standard Deviation (%): 4.00

● Per Control Point ○ Per Plan

Global Parameters

Minimum Electron Density: Use with Fill option. 1.000

Minimum CT Number: Use with Clear option. -200

Auto Flash Margin (cm): 0.20

Surface Margin (cm): 0.30

Beamlet Width (cm): 0.30

Target Margin: Normal (8mm)

Avoidance Margin: Normal (8mm)

GPU Monte Carlo Calculation Parameters

● Use GPU MC ○ Use XVMC

☐ MC For Primary Algorithm

☐ Include Magnetic Field

☐ Transport Through MRI Housing

Electron Max Step Length (cm): 0.75

OK
Cancel
Total Volume DVH
Volume (%)
Dose (cGy)
W/L Affects: Primary Studyset
Press start to begin stage 1
Imrt Activity
Autosave OFF
Max Dose: 6963.8 cGy

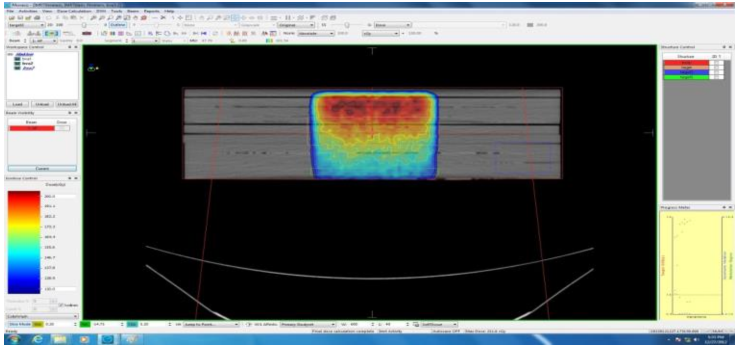

0 T

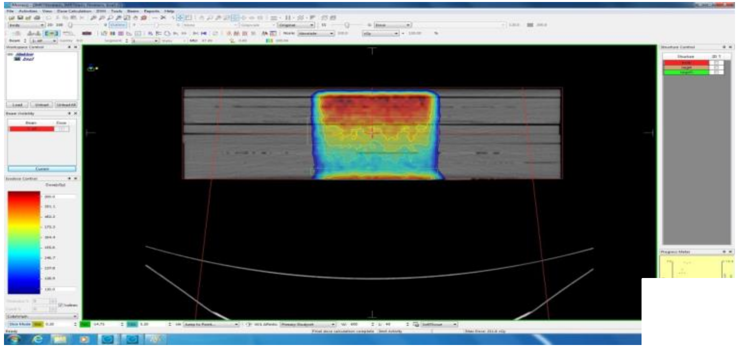

1.5 T

DVH for optimized dose distribution oropharynx

Comparison between B = 0 T and B = 1.5 T

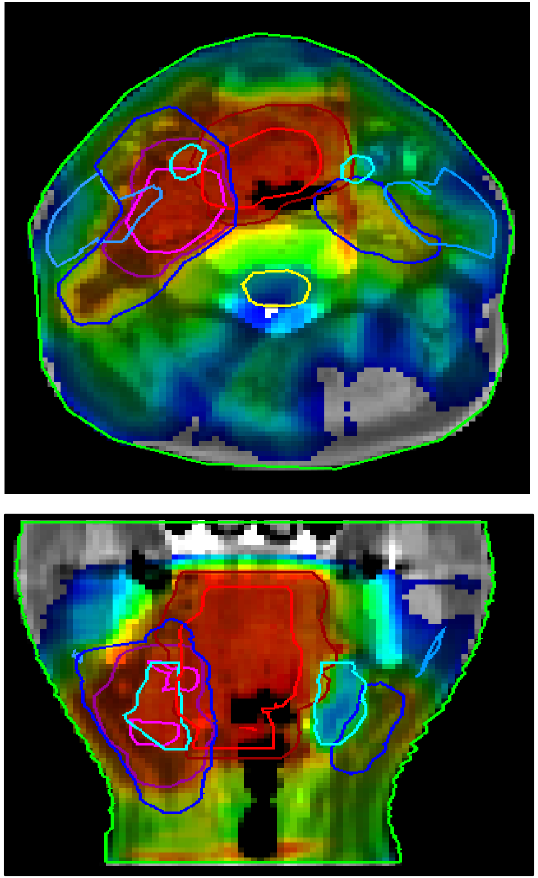

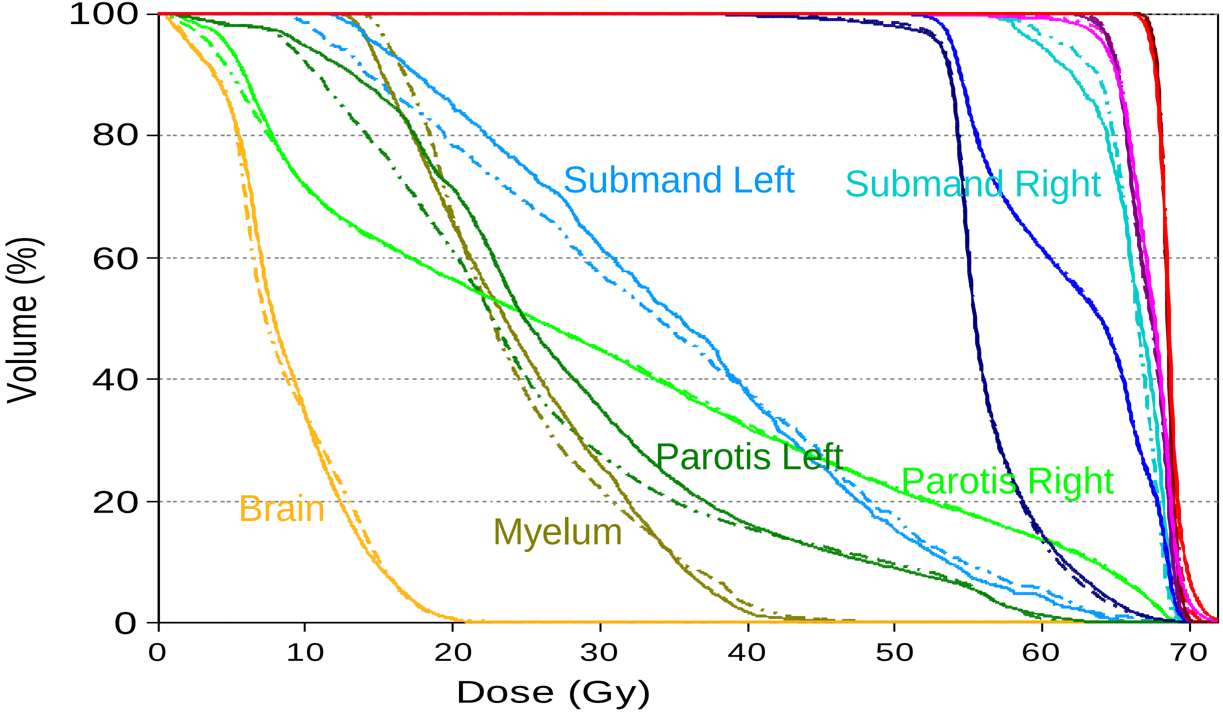

Hardware: Summary

Differences & Modifications

Linac

- Cryostat
- Fixed table
- ERE / EFE
- Receiver coils
- ..

MRI

- Split gradient coil
- Ferromagnetic Gantry
- Receiver coils
- Radiation..

Elekta

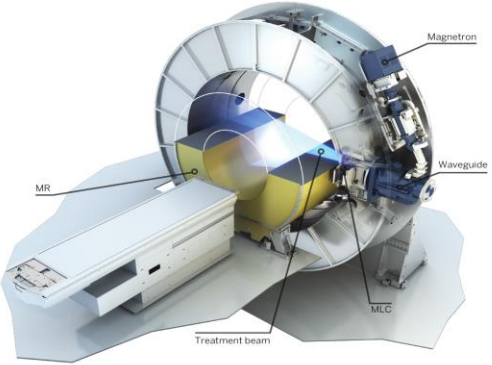
Magnetron
Waveguide
MR
MLC
Treatment beam

Australia

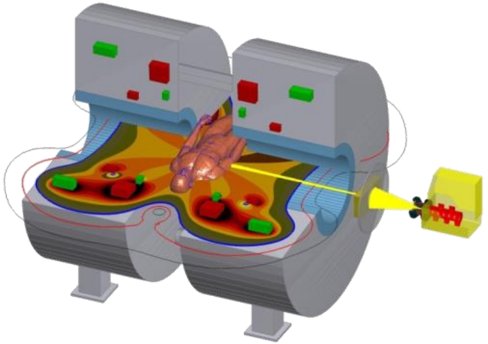

Alberta

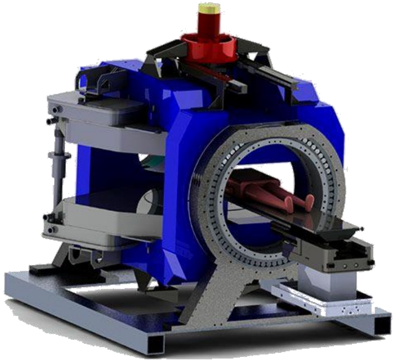

Viewray

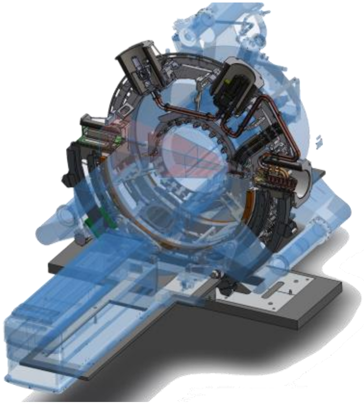

Commissioning & QA

The effects of MRI on Linac

The effects of Linac on MRI

MR-linac clinical introduction

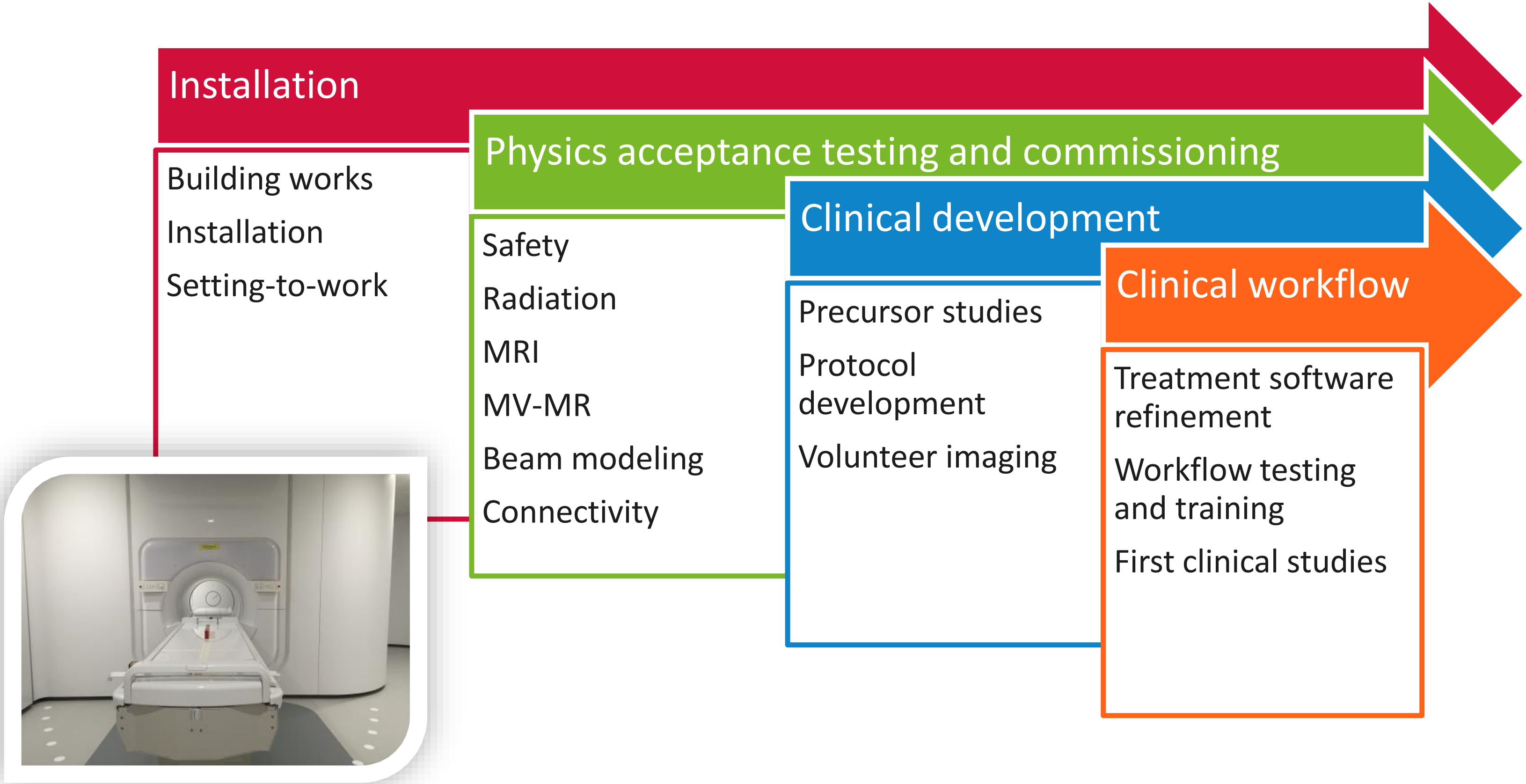

Installation

- Building works
- Installation
- Setting-to-work

Physics acceptance testing and commissioning

- Safety
- Radiation
- MRI
- MV-MR
- Beam modeling
- Connectivity

Clinical development

- Precursor studies
- Protocol development
- Volunteer imaging

Clinical workflow

- Treatment software refinement
- Workflow testing and training
- First clinical studies

Physics acceptance testing and commissioning

Safety
Radiation
Beam modeling
MRI
MV-MR
Connectivity

- Radiation safety
  - Displaced isoc (1.4m)
  - Higher dose rate
  - Vault modifications
- Machine/electrical safety
- MR Safety

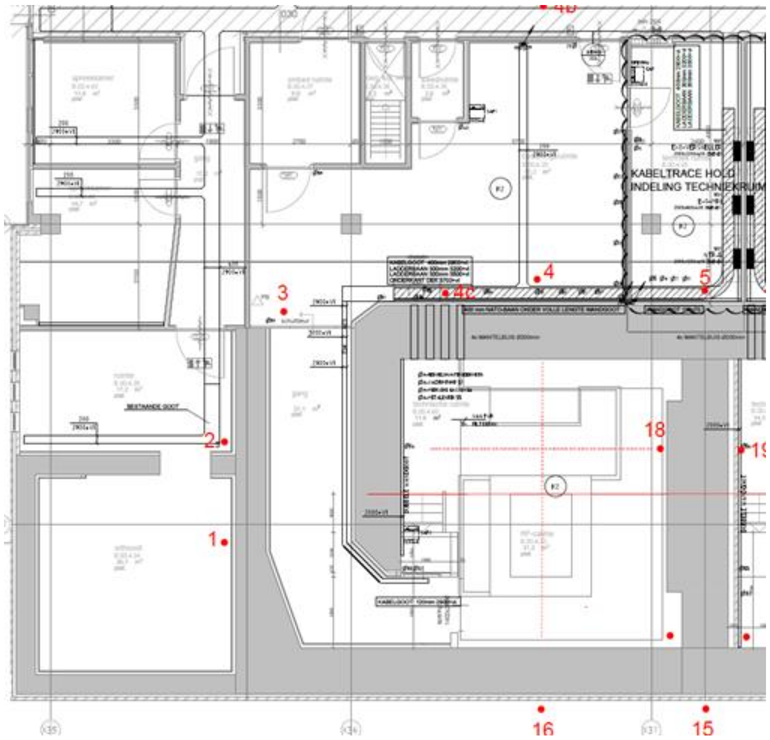
KABELTRACE HOLD
INDELING TECHNIEKRUIM
1
2
3
4
4c
5
18
19
16
15

Linac QA: star shot

“Removal” of impact B field on electrons

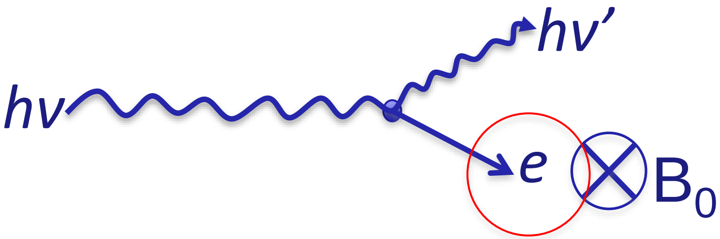
$h\nu'$
$h\nu$
e
$\otimes B_0$

Dose deposition

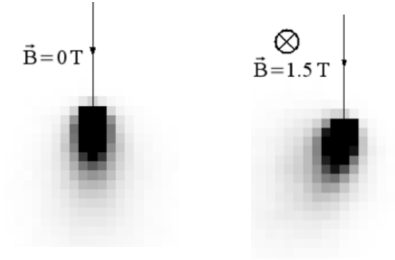

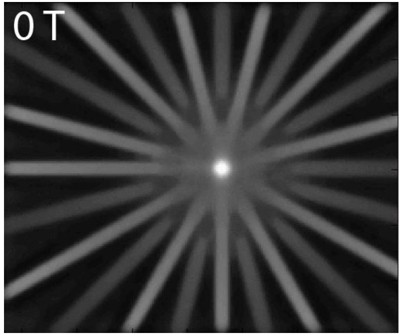

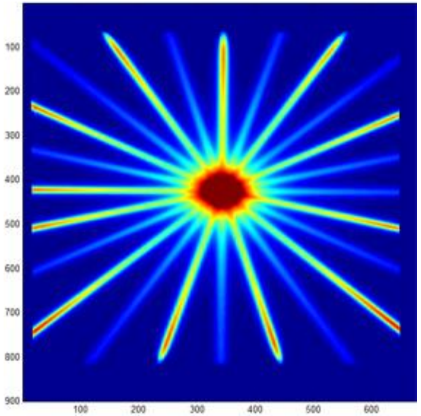

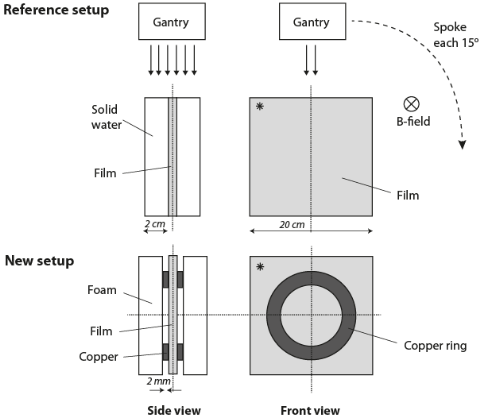
Reference setup
Gantry
Gantry
Spoke each 15°
Solid water
B-field
Film
Film
2 cm
20 cm
New setup
Foam
Film
Copper
Copper ring
2 mm
Side view
Front view

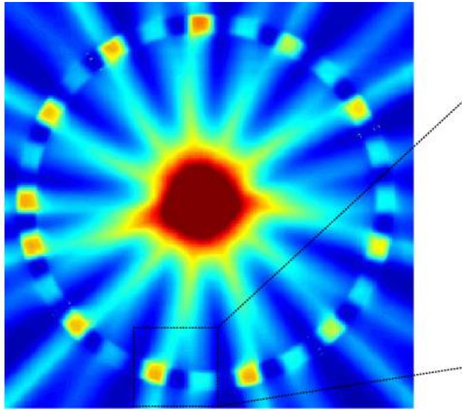

Dose deposition - Alexander Raaijmakers - Thesis 2008, spoke film images – Loes van Zijp – 2015

MRI QA: Gradient non-linearity characterization

Normal gradient coil

MRL gradient coil

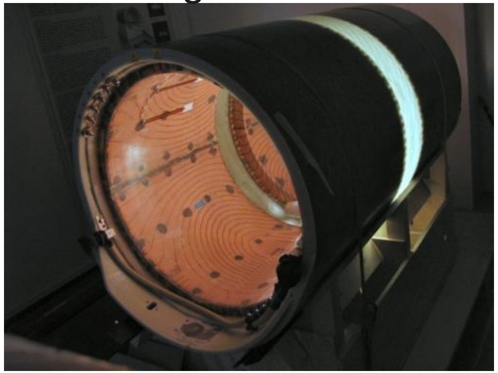

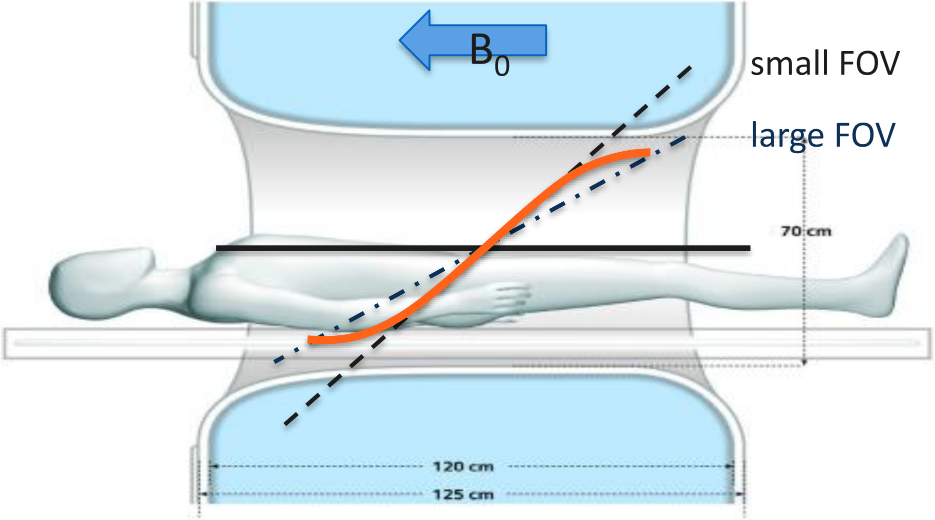
B_0
small FOV
large FOV
70 cm
120 cm
125 cm

- Imaging gradient are non-linear to prevent PNS
- Geometric correction done by vendor software
- MRL has different gradient design (split)
- Careful characterisation needed

Geometric fidelity on the MRL (@umcu)

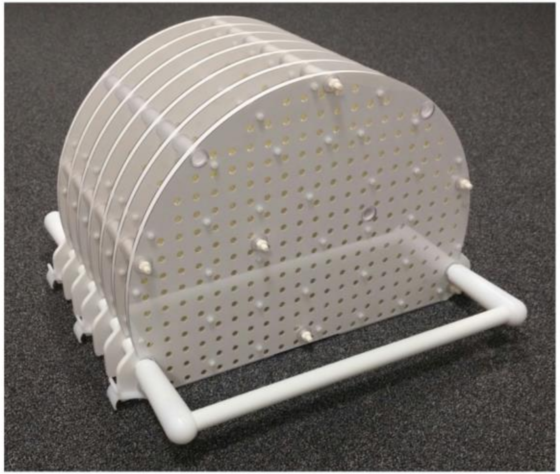

3D Geometric QA
for research use

3D FFE sequence
Geometric correction turned ON

Right column shows total distortion

vector sum of x y and z distortions

DSV (mm)	Maximum error
300	0.9 mm
350	1.8 mm
400	2.3 mm

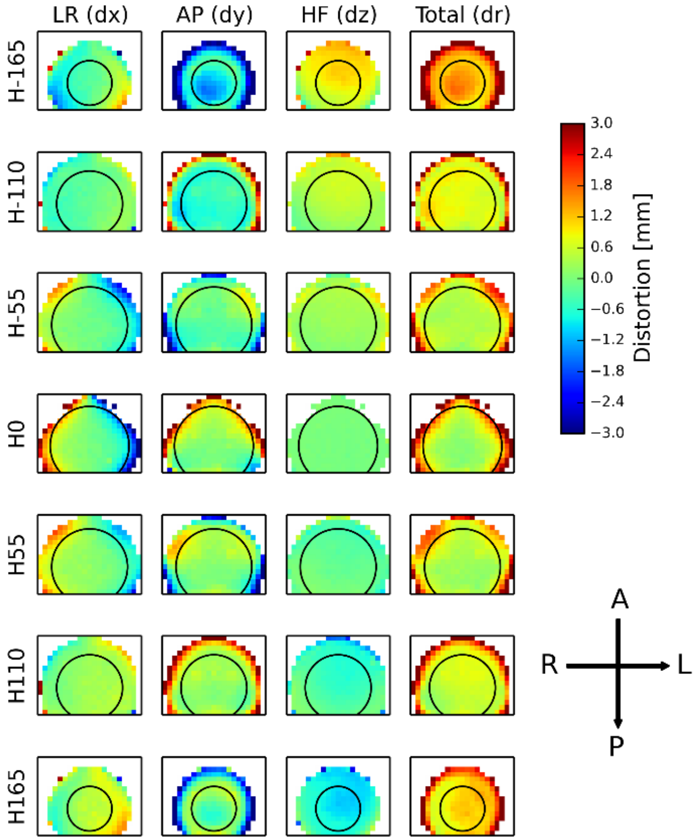

The circles describe a 400 mm DSV.

Tijssen et al., ESTRO 2017

Distortion increases with distance to isoc

- Important to characterize distortions for MRI-only planning and MR-guided systems
- Size of the distortions spatially varying and varies per tumor site!

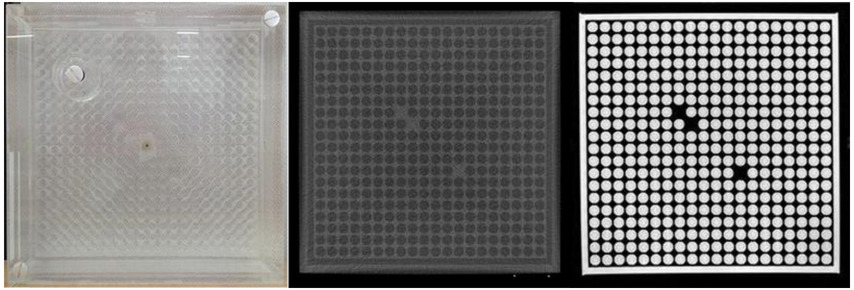

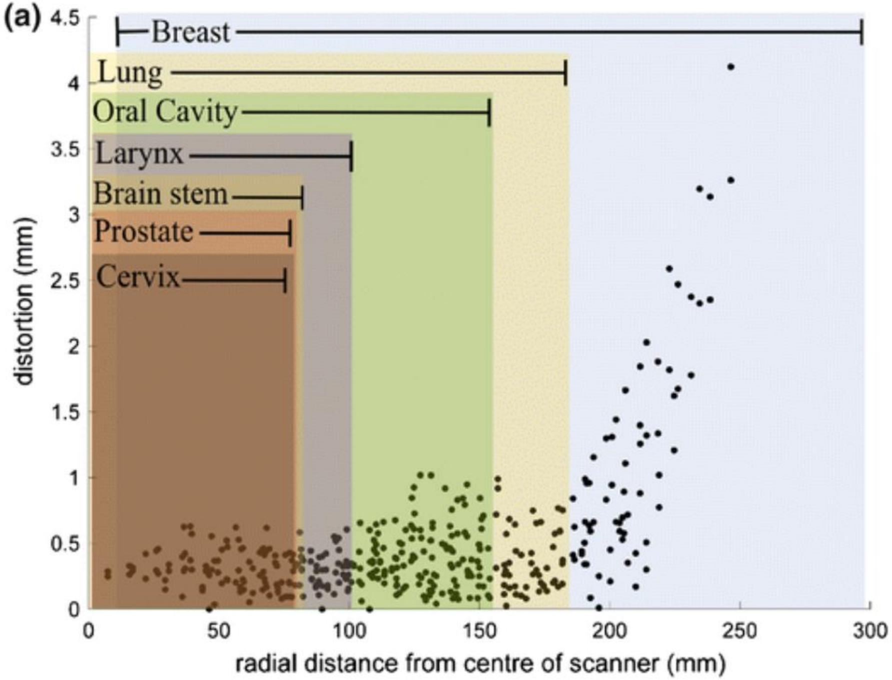

Walker et al., Austr phys & Eng, 2014

The Effect of Radiation

Medical Physics
The International Journal of Medical Physics Research and Practice

Radiation induced current in the RF coils of integrated linac-MR systems: The effect of buildup and magnetic field

Ben Burke, Andrei Ghila, B. G. Fallone, and Satyapal Rathee

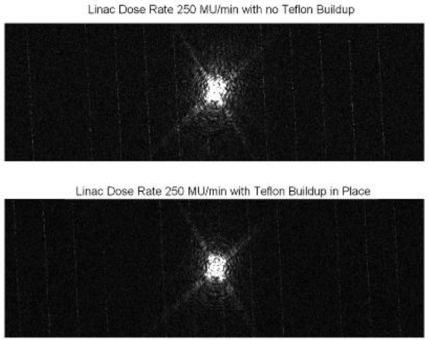
Linac Dose Rate 250 MU/min with no Teflon Buildup
Linac Dose Rate 250 MU/min with Teflon Buildup in Place

FIG. 13. K-space data for images acquired with the linac producing radiation at 250 MU/min and incident upon the coil with no buildup (top image) and with teflon buildup in place (bottom image). The same window and level was used to display each image.

"Radiation induced currents in the coil"

VI. CONCLUSIONS

This investigation demonstrates that the RIC can be reduced with the appropriate combination of coil conductor and buildup. Our results indicate that about 1 cm of teflon wrapped around an aluminum RF coil would essentially eliminate radiation induced currents in the coil. This method of RIC removal can effectively be applied to practical RF coil geometries and the presence of magnetic fields. In cylindrical coil geometries, the air gap is more important than the presence of the magnetic field. In planar geometries, the amount of buildup material required to achieve adequate RIC reduction is similar to that required with no field present. The RIC simulation is a useful tool for practical coil design where radiation effects must be considered. Preliminary experiment using nonideal buildup around the solenoid demonstrated the reduction in SNR lost due to RIC.

Alberta group

Burke et al., PMB 33 (3), 2010
Burke et al., Med Phys 39 (8), 2012
Liney et al., MR in RT Symposium 2016

Aust

Im

Utrecht group

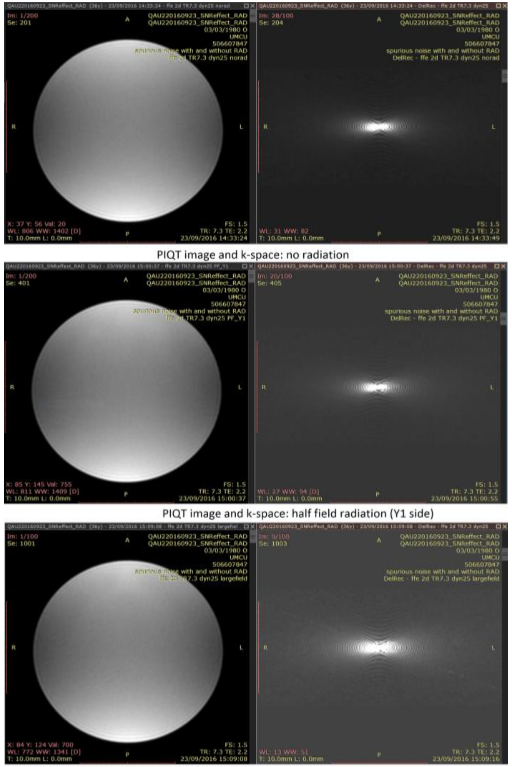

PIQT image and k-space: no radiation

PIQT image and k-space: half field radiation (Y1 side)

PIQT image and k-space: full field (22 cm x 56 cm) radiation

Tijssen et al., ESTRO 2017

Gary Liney

Clinical introduction

Elekta results (First in Man)

Viewray results (pancreas SBRT study)

Clinical results Viewray: Pancreas SBRT

Washington University, St Louis

2011	machine installation
1/2012	patient imaging study
1/2014	First MRIgRT patient treatment
9/2014	First online adaptive treatment
1/2015	First online adaptive SBRT
2/2015	First online adaptive CBRT w/ gating

"Direct visualization allows safe dose escalation"

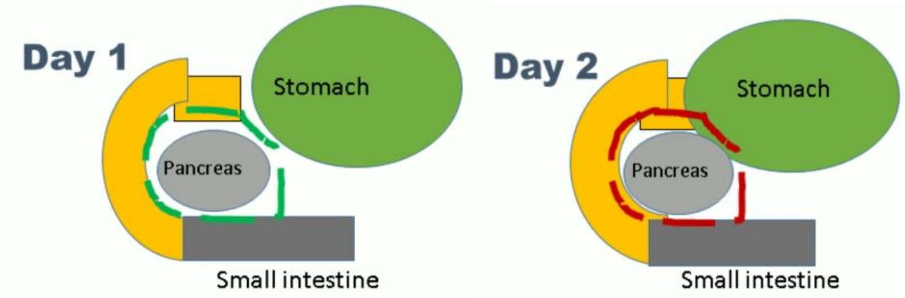
Day 1
Stomach
Pancreas
Small intestine
Day 2
Stomach
Pancreas
Small intestine

"Adaptation mainly on AORs"

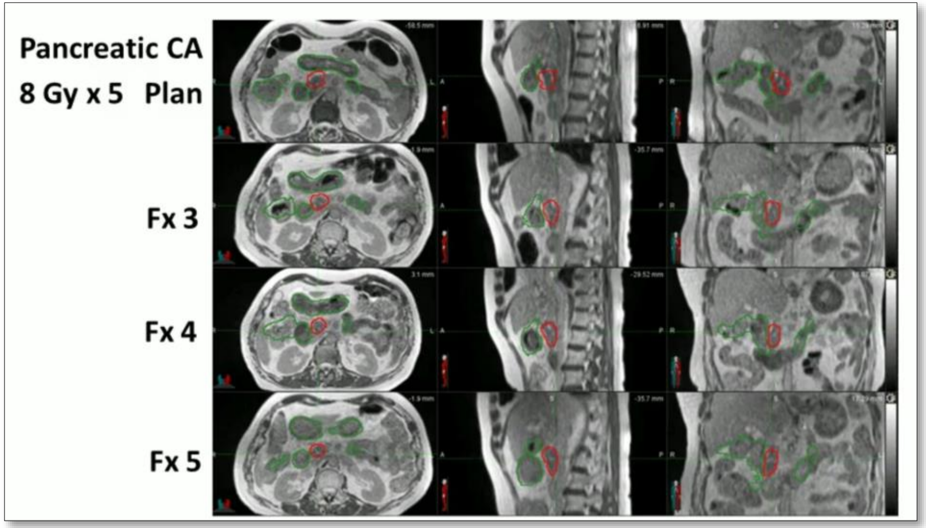
Pancreatic CA
8 Gy x 5 Plan
Fx 3
Fx 4
Fx 5

Percy Lee, UCLA
Parag Parikh, Washington University

Clinical results Viewray: Pancreas SBRT

- Retrospective review of 42 patients, 4 institutions
- Overall survival (OS) and local control (LC)
- Stratified by maxBED_{10} using max point dose in PTV
- Median OS was 27.8 months vs. 14.8 months!

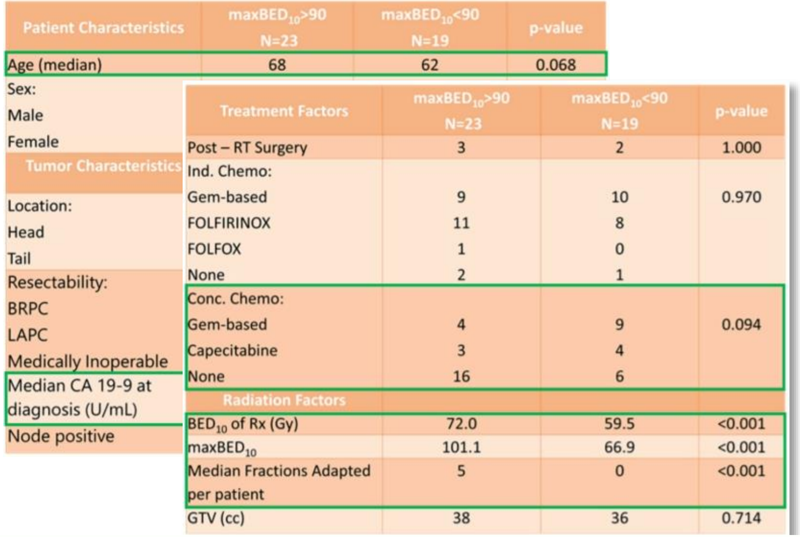

Patient Characteristics	$\text{maxBED}_{10}>90$ N=23	$\text{maxBED}_{10}<90$ N=19	p-value
Age (median)	68	62	0.068
Sex:			
Male			
Female			
Tumor Characteristics			
Location:			
Head			
Tail			
Resectability:			
BRPC			
LAPC			
Medically Inoperable			
Median CA 19-9 at diagnosis (U/mL)			
Node positive			

Treatment Factors	$\text{maxBED}_{10}>90$ N=23	$\text{maxBED}_{10}<90$ N=19	p-value
Post – RT Surgery	3	2	1.000
Ind. Chemo:			
Gem-based	9	10	0.970
FOLFIRINOX	11	8	
FOLFOX	1	0	
None	2	1	
Conc. Chemo:			
Gem-based	4	9	0.094
Capecitabine	3	4	
None	16	6	
Radiation Factors			
BED_{10} of Rx (Gy)	72.0	59.5	<0.001
maxBED_{10}	101.1	66.9	<0.001
Median Fractions Adapted per patient	5	0	<0.001
GTV (cc)	38	36	0.714

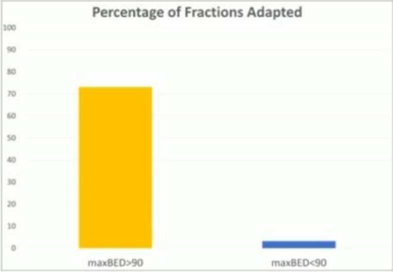

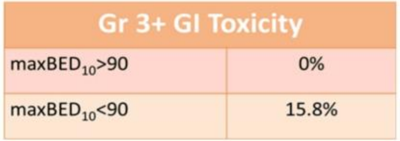

Gr 3+ GI Toxicity	
$\text{maxBED}_{10}>90$	0%
$\text{maxBED}_{10}<90$	15.8%

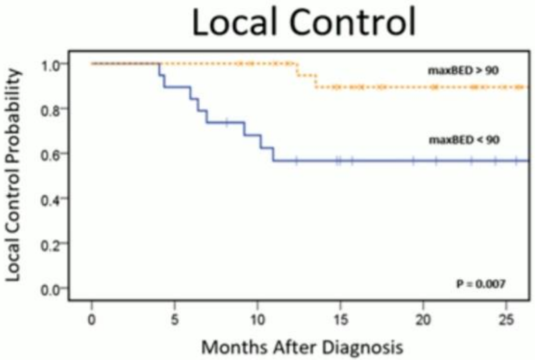

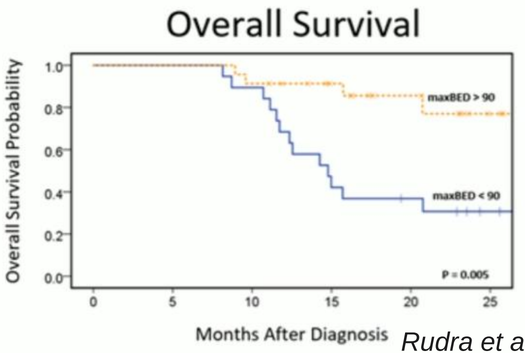

Rudra et al., ASTRO 2017

Clinical Introduction

The Atlantic Consortium

-MCW (Milwaukee)
-Sunnybrook (Toronto)
-MD Anderson (Houston)

Staged clinical introduction

Product development

1ATL: volunteer imaging	2016
2ATL: first treatments	2017
3,4,..ATL: more functionality	2018

Study design: R-ideal

Stage 0: predicate studies	2017
Stage 1&2: technical studies (FIM)	***now***
Stage 3&4: clinical studies	2018

UMCU

MD Anderson ~~Cancer~~ Center

Froedtert &

THE ROYAL MARSDEN ICR The Institute of Cancer Research

Sunnybrook HEALTH SCIENCES CENTRE

The Netherlands Cancer Institute Antoni van Leeuwenhoek Hospital

CHRISTIE'S

PHILIPS sense and simplicity

Clinical results Elekta: First in Man

- Patient population
  - Patients with bone metastases treated with palliative intention
- Treatment

  8 Gy in a single fraction

  3 or 5 field IMRT
- Goal:

  Demonstrate technical accuracy and safety in the clinical setting

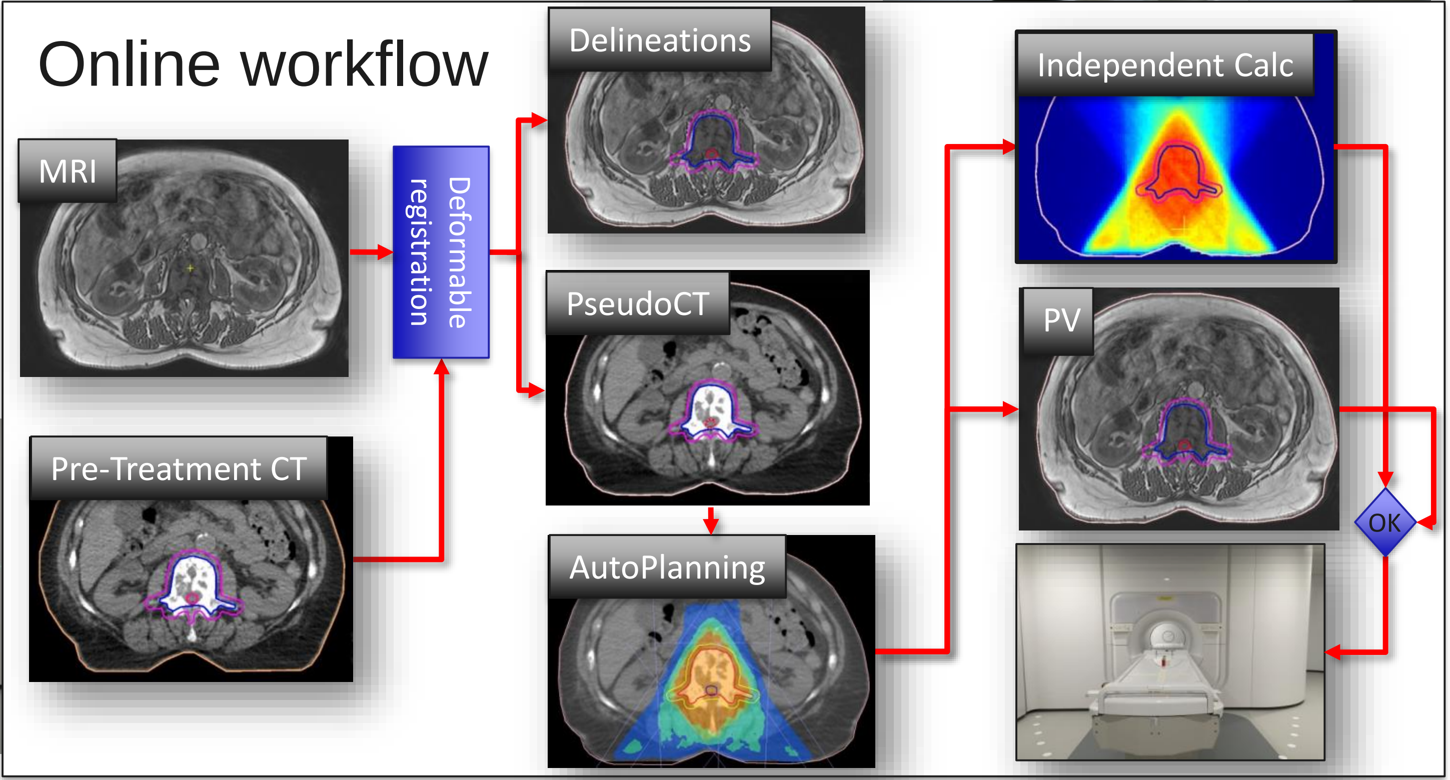
Online workflow
MRI
Deformable registration
Pre-Treatment CT
Delineations
PseudoCT
AutoPlanning
Independent Calc
PV
OK

Raaymakers et al., PMB, accepted

Clinical results Elekta: First in Man

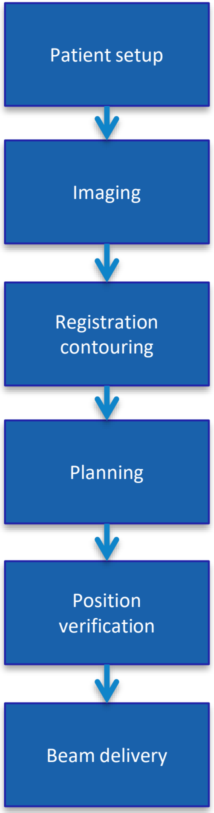
Patient setup

Imaging

Registration contouring

Planning

Position verification

Beam delivery

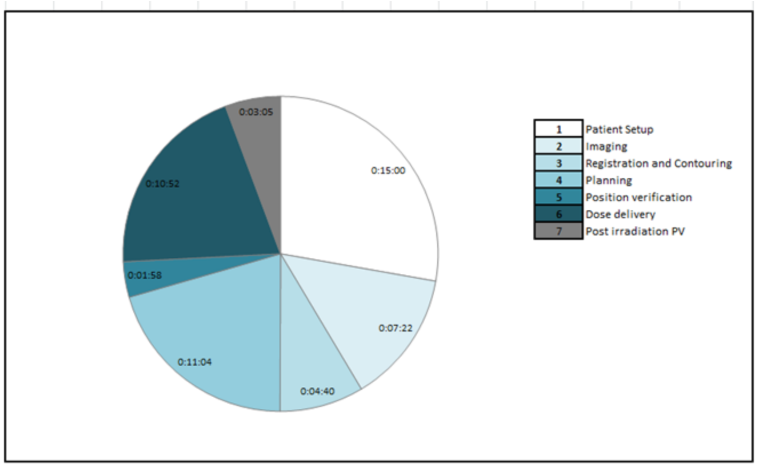

Total time 54 minutes for entire procedure

15 min patient set-up

7 min preparation MRI

4 min registration and contour validation

11 min planning

10 min dose delivery and beam-on MRI

Avg gamma pass:
98.8% ± 3.7%

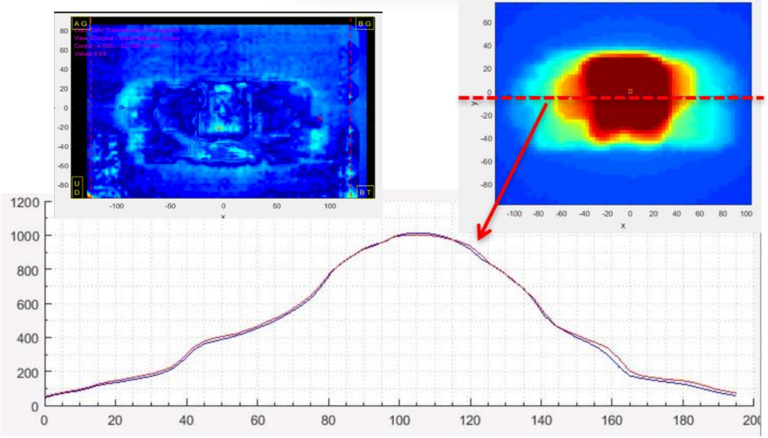

Future Perspectives

UMC Utrecht

Real-time tracking

Abdominal Organ Tracking on a Hybrid MR-Linac System Using a Particle Filter Based Algorithm

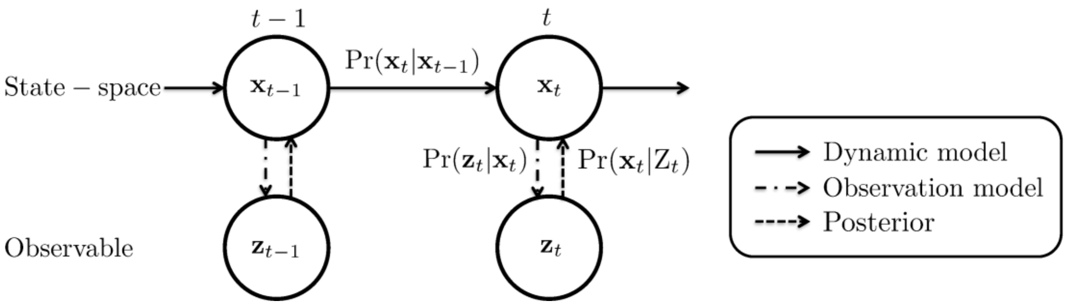
$t-1$
t
State – space
$\mathbf{x}_{t-1}$
$\Pr(\mathbf{x}_t|\mathbf{x}_{t-1})$
$\mathbf{x}_t$
$\Pr(\mathbf{z}_t|\mathbf{x}_t)$
$\Pr(\mathbf{x}_t|Z_t)$
Observable
$\mathbf{z}_{t-1}$
$\mathbf{z}_t$
Dynamic model
Observation model
Posterior

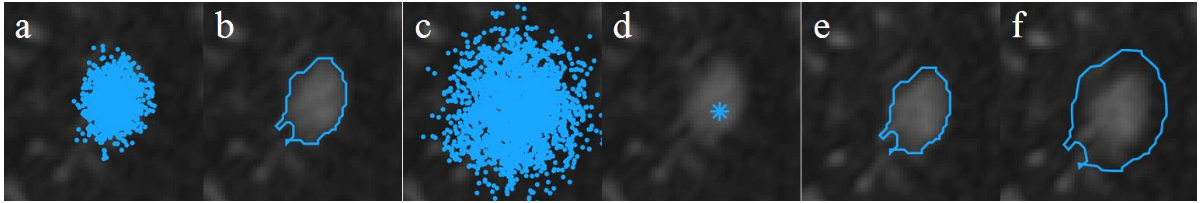

Bourque et al. Med Phys, 2016. Bourque et al., IJROBP 2017

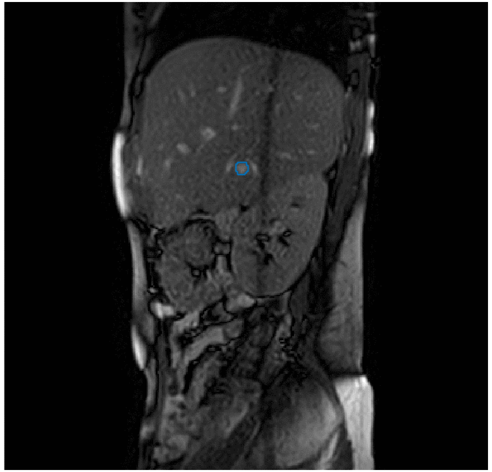

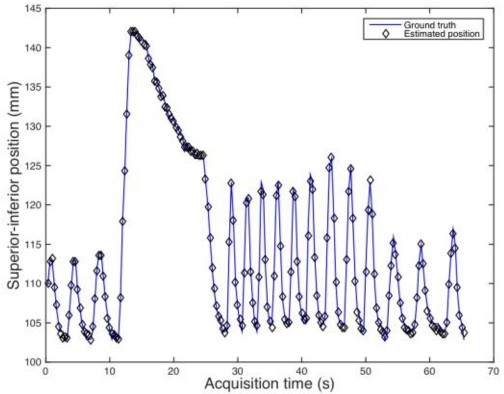

Current status: Interleaved Multi-Stack SMS

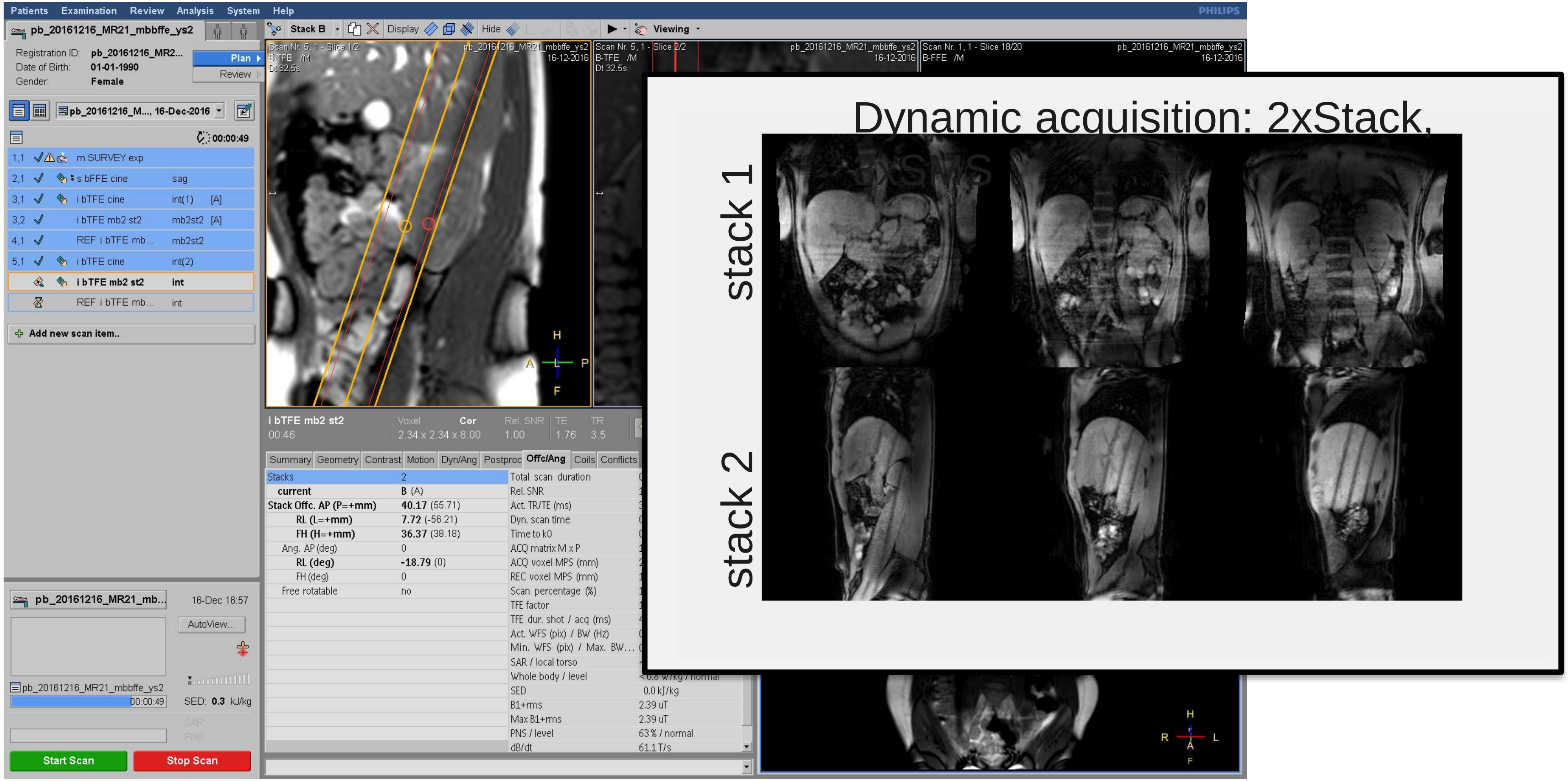

Dynamic acquisition: 2xStack, 2xSMS

stack 1
stack 2

Patients
Examination
Review
Analysis
System
Help
PHILIPS
Stack B
Display
Hide
Viewing
Plan
Review
Add new scan item..
AutoView...
Start Scan
Stop Scan
Summary
Geometry
Contrast
Motion
Dyn/Ang
Postproc
Offc/Ang
Coils
Conflicts
H
A
P
F
L
R

pb_20161216_MR21_mbbffe_ys2

Registration ID: pb_20161216_MR2...
Date of Birth: 01-01-1990
Gender: Female

pb_20161216_M..., 16-Dec-2016

00:00:49

1,1	m SURVEY exp		
2,1	s bFFE cine	sag	
3,1	i bTFE cine	int(1)	[A]
3,2	i bTFE mb2 st2	mb2st2	[A]
4,1	REF i bTFE mb...	mb2st2	
5,1	i bTFE cine	int(2)	
	i bTFE mb2 st2	**int**	
	REF i bTFE mb...	int	

Scan Nr. 5, 1 - Slice 1/2
B-TFE /M
Dt 32.5s
pb_20161216_MR21_mbbffe_ys2
16-12-2016

Scan Nr. 5, 1 - Slice 2/2
B-TFE /M
Dt 32.5s
pb_20161216_MR21_mbbffe_ys2
16-12-2016

Scan Nr. 1, 1 - Slice 18/20
B-FFE /M
pb_20161216_MR21_mbbffe_ys2
16-12-2016

i bTFE mb2 st2 00:46
Voxel **Cor** 2.34 x 2.34 x 8.00
Rel. SNR 1.00
TE 1.76
TR 3.5

Stacks	2
current	**B** (A)
Stack Offc. AP (P=+mm)	**40.17** (55.71)
RL (L=+mm)	**7.72** (-56.21)
FH (H=+mm)	**36.37** (38.18)
Ang. AP (deg)	0
RL (deg)	**-18.79** (0)
FH (deg)	0
Free rotatable	no

Total scan duration
Rel. SNR
Act. TR/TE (ms)
Dyn. scan time
Time to k0
ACQ matrix M x P
ACQ voxel MPS (mm)
REC voxel MPS (mm)
Scan percentage (%)
TFE factor
TFE dur. shot / acq (ms)
Act. WFS (pix) / BW (Hz)
Min. WFS (pix) / Max. BW...
SAR / local torso
Whole body / level < 0.8 W/kg / normal
SED 0.0 kJ/kg
B1+rms 2.39 uT
Max B1+rms 2.39 uT
PNS / level 63 % / normal
dB/dt 61.1 T/s

pb_20161216_MR21_mb... 16-Dec 16:57

pb_20161216_MR21_mbbffe_ys2 00:00:49

SED: 0.3 kJ/kg
SAR:
PNS:

Courtesy of Pim Borman, UMCU

Model based 3D motion estimation

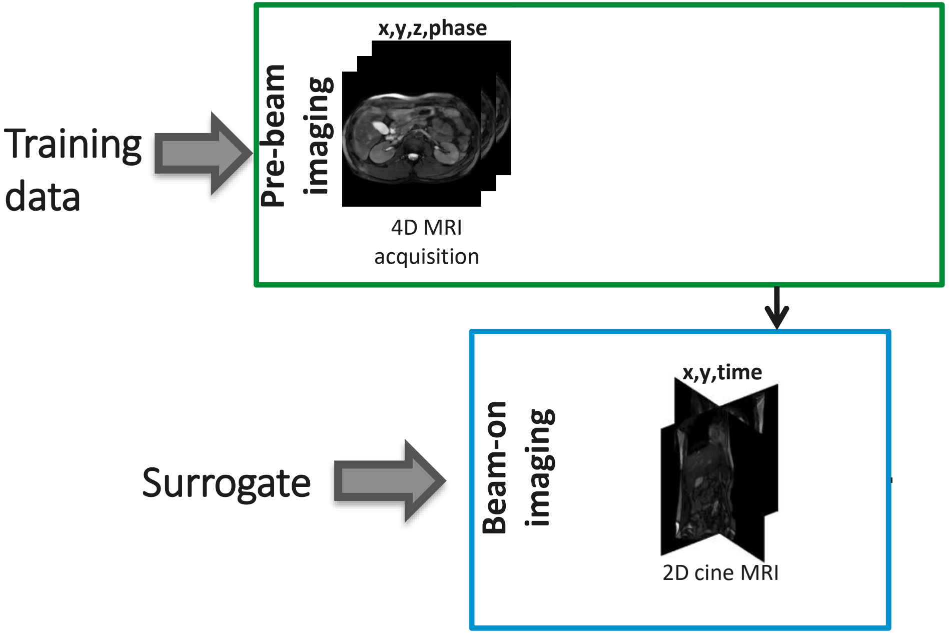

Training data

Pre-beam imaging

x,y,z,phase

4D MRI acquisition

Surrogate

Beam-on imaging

x,y,time

2D cine MRI

Stemkens et al. *PMB*, 2016

The goal we are working towards to..

Patient-ID: 00900 name: F. Ictitious real-time MR-Linac tracking tumor-site: kidney

Tracking is ON

Beam is ON

Real-time imaging

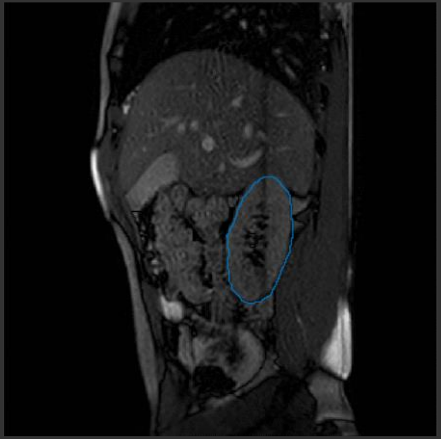

Motion history

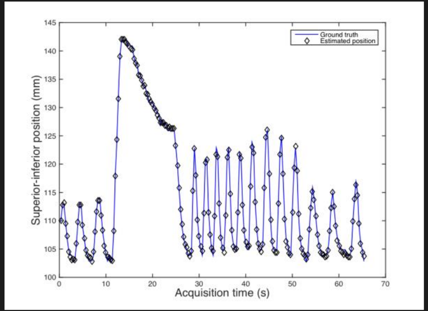

Accumulated Dose

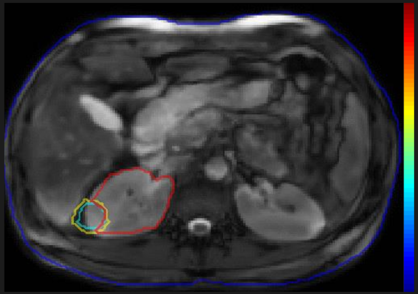

Beam's eye view

offsets

FH: 1.0mm

RL: 0.5mm

AP: 0.2mm

resp:3.2mm

Conclusion

- MRI for IGRT enables **seeing what you treat**
- Given the specific imaging/reconstruction constraints, we have to **adopt MRI techniques** from radiology to the regime of MR-guided radiotherapy
- New MR imaging methods will enable fast, on-line, and real-time **motion characterization**
- Response monitoring by quantitative functional MRI *may* even allow us to adapt our treatment before anatomical change is visible

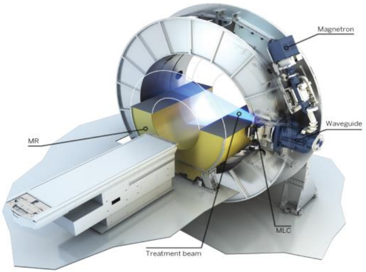

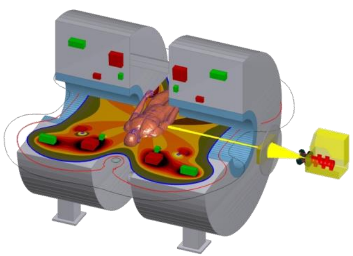

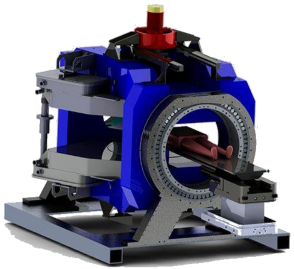

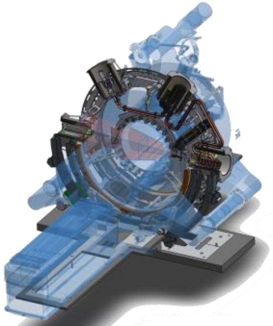

Acknowledgements

Slides & material

- Bram van Asselen
- Alexandra Bourque
- Pim Borman
- Markus Glitzner
- Gary Liney
- Charis Kontaxis
- Ina Schulz

- Bjorn Stemkens
- Jochem Wolthaus
- Simon Woodings
- Loes van Zijp

- Bas Raaymakers
- Jan Lagendijk

Questions?

Advanced Imaging for Physicists

Application of CT and PET for radiotherapy of lung cancer

Uulke van der Heide

NKI-AVL
Het Nederlands Kanker Instituut
Antoni van Leeuwenhoek Ziekenhuis

Imaging for radiotherapy of lung cancer

- Staging and target definition
- Imaging for treatment monitoring and follow-up
- Imaging during treatment

CT imaging for radiotherapy of lung cancer

- Many imaging modalities are possible for lung cancer
- CT is the basic imaging modality in radiotherapy of lung
- Soft tissue contrast is good in lung, densities for RT are important

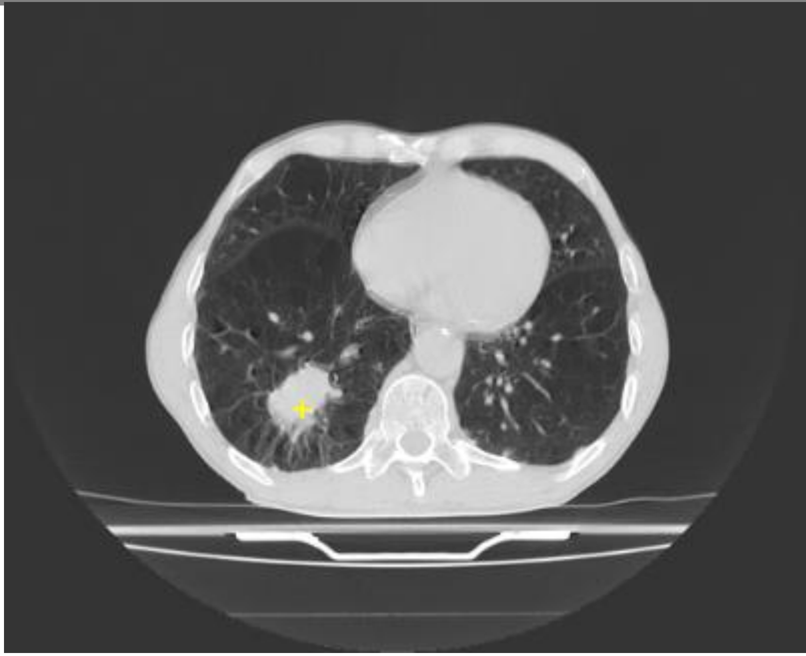

CT imaging for radiotherapy of lung cancer

- Many imaging modalities are possible for lung cancer
- CT is the basic imaging modality in radiotherapy of lung
- Soft tissue contrast is good in lung, densities for RT are important
- A 3D CT scan shows substantial breathing artifacts

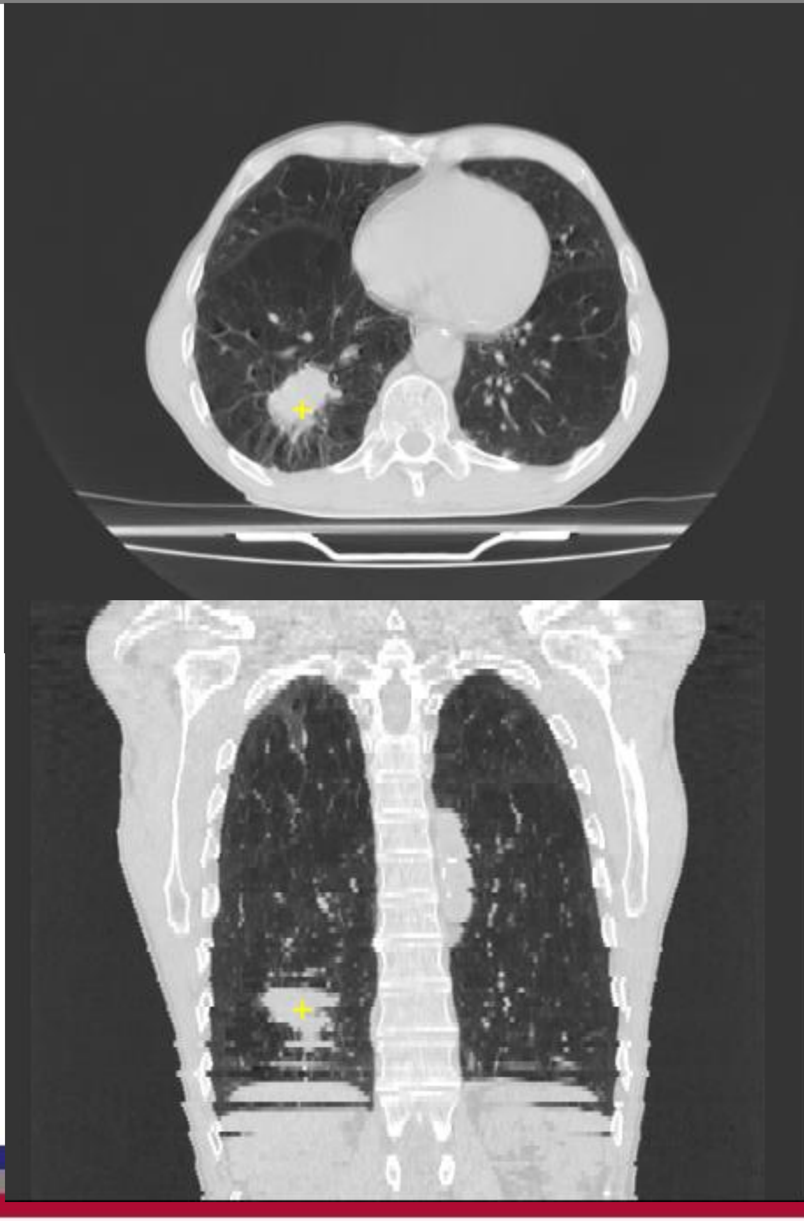

CT imaging for radiotherapy of lung cancer

- Many imaging modalities are possible for lung cancer
- CT is the basic imaging modality in radiotherapy of lung
- Soft tissue contrast is good in lung, densities for RT are important
- A 3D CT scan shows substantial breathing artifacts
- A ‘slow scan’ reveals the extent of the motion, but shows a blurred image
- A 4D CT scan is preferable

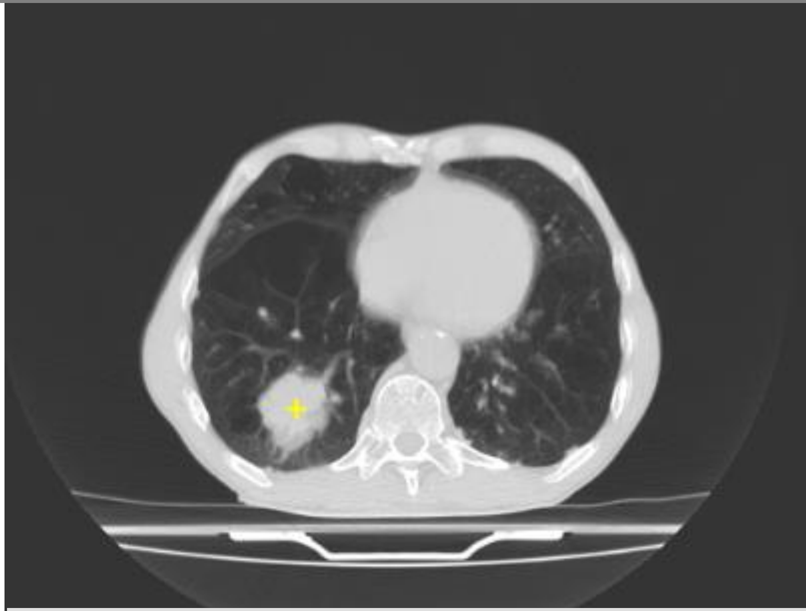

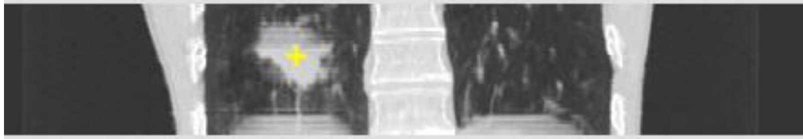

PET and SPECT for radiotherapy of lung cancer

- FDG-PET is commonly used for staging
- Ventilation/Perfusion SPECT shows functional lung tissue

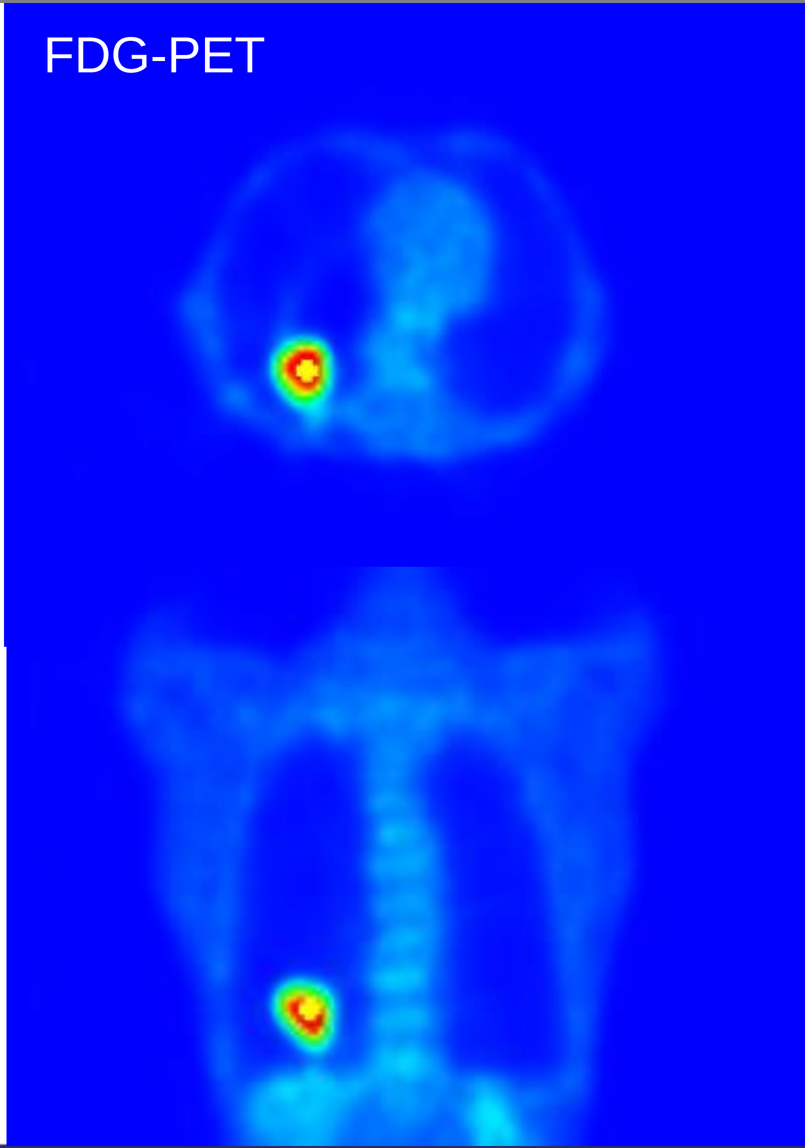
FDG-PET

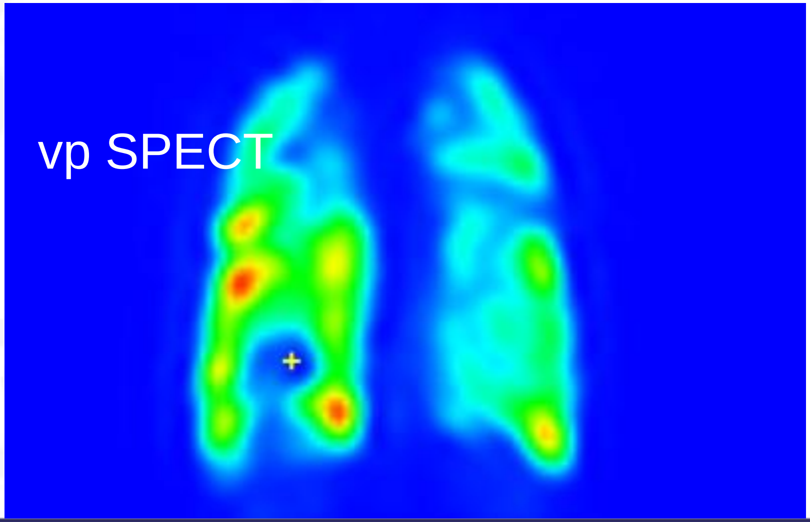
vp SPECT

MRI is not commonly used for lung cancer

- The soft-tissue contrast of MRI is not an advantage in lung cancer, compared to CT
- Susceptibility differences between lung and surrounding tissue may compromise geometrical accuracy
- Is useful to monitor unusual breathing patterns

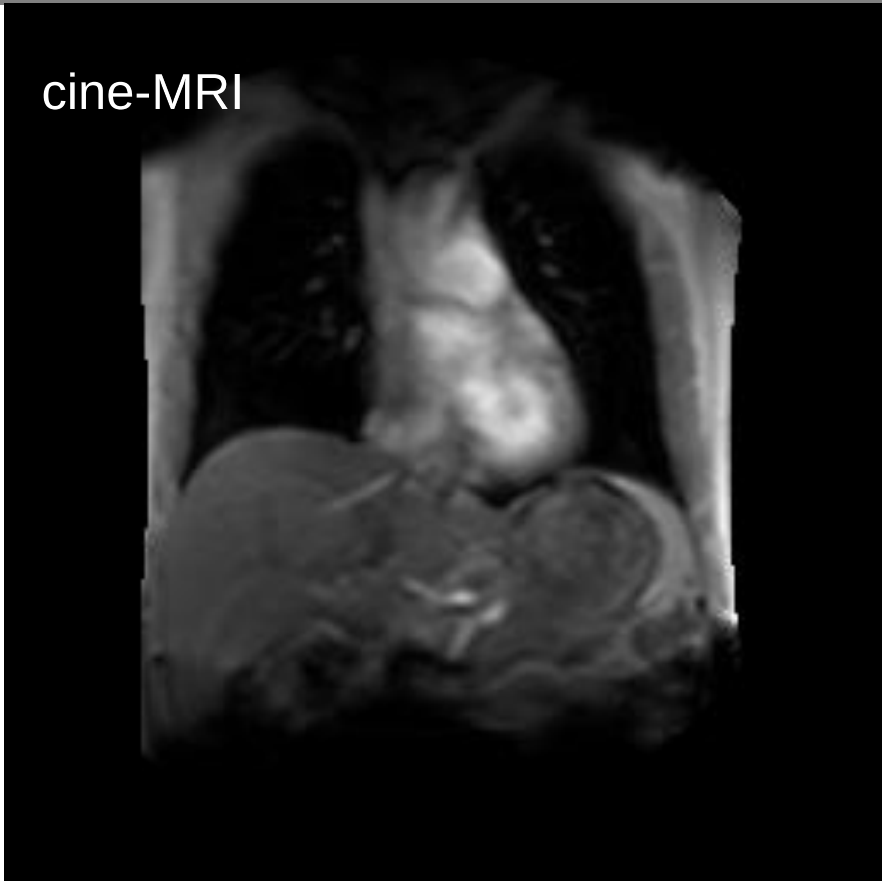
cine-MRI

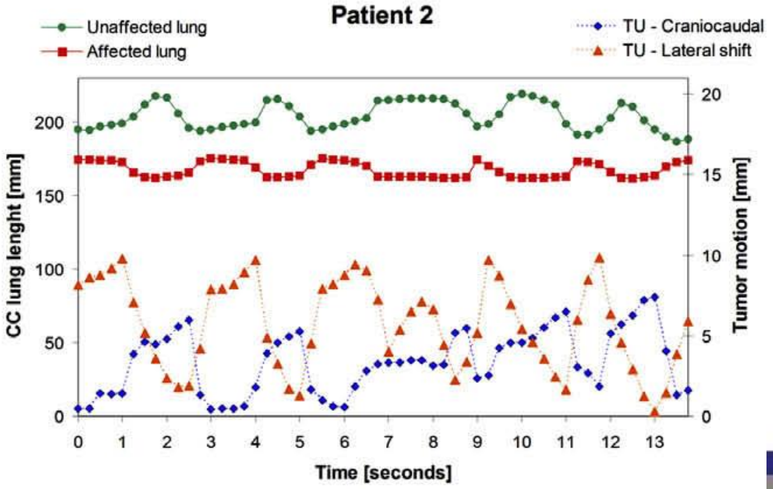

Dinkel et al. 2009; Int. J. Radiat. Oncol. Biol. Phys. 91:449-454

FDG-PET improves accuracy of staging in non-small cell lung cancer

- Addition of PET changes the TNM clinical stage of patients with non-small-cell lung cancer

- patient with diagnosis of T1N0M0 stage I adenocarcinoma.
- PET shows a pre-tracheal lymph node.
- Stage changes to T1N2M0

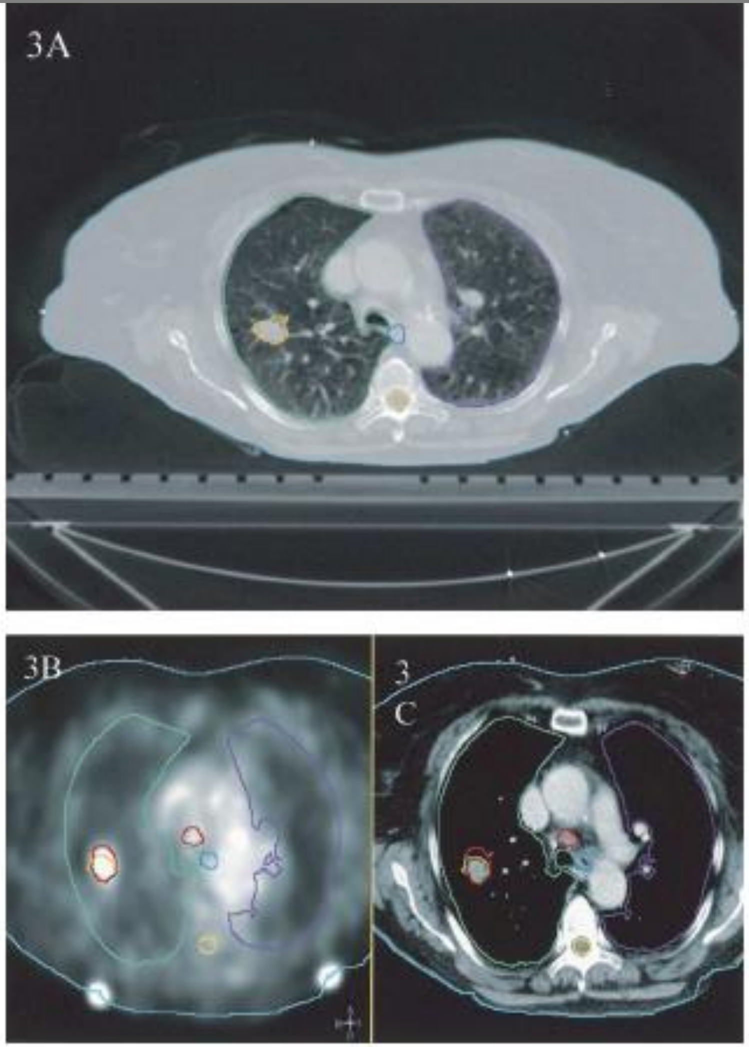

Fig. 3. This patient was enrolled in the study with a diagnosis of a T1N0M0, Stage I adenocarcinoma of the lung. The positron emission tomography (PET) scan demonstrated an FDG-avid pretracheal lymph node, changing the clinical stage to T1N2M0, IIIA disease. One can see the fiducial markers containing FDG on the posterior aspect of the patient's contour.

Bradley et al. 2004; Int. J. Radiat. Oncol. Biol. Phys. 59:78-86

FDG-PET improves accuracy of staging in non-small cell lung cancer

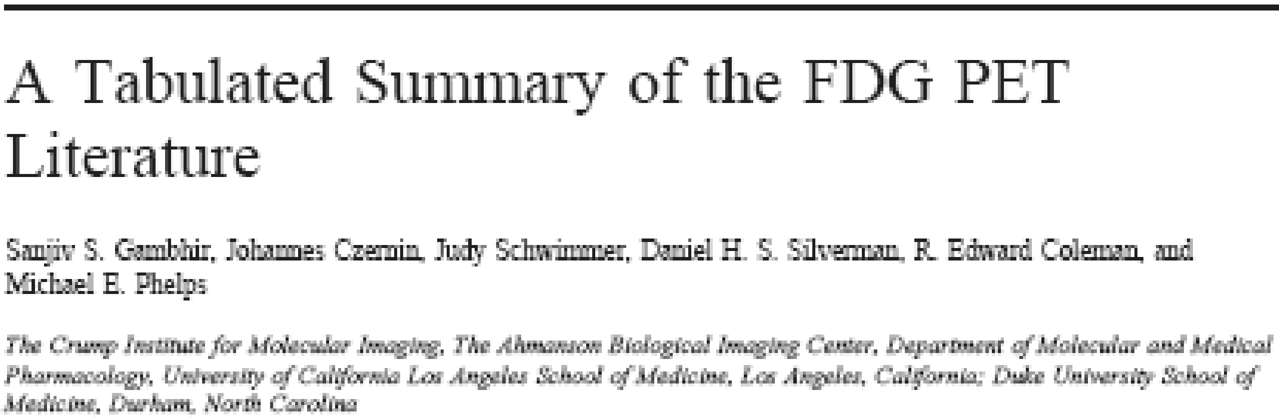

A Tabulated Summary of the FDG PET Literature

Sanjiv S. Gambhir, Johannes Czernin, Judy Schwimmer, Daniel H. S. Silverman, R. Edward Coleman, and Michael E. Phelps

The Crump Institute for Molecular Imaging, The Ahmanson Biological Imaging Center, Department of Molecular and Medical Pharmacology, University of California Los Angeles School of Medicine, Los Angeles, California; Duke University School of Medicine, Durham, North Carolina

- The sensitivity and specificity of staging reported in studies with pathological confirmation:
  - CT alone:
    - sens. 64%
    - spec. 74%
  - PET + CT:
    - sens. 83%
    - spec. 91%

(Gambhir et al. 2001; J. Nucl. Med. 42:1S-93S)

Sensitivity and specificity of mediastinal lymph node staging

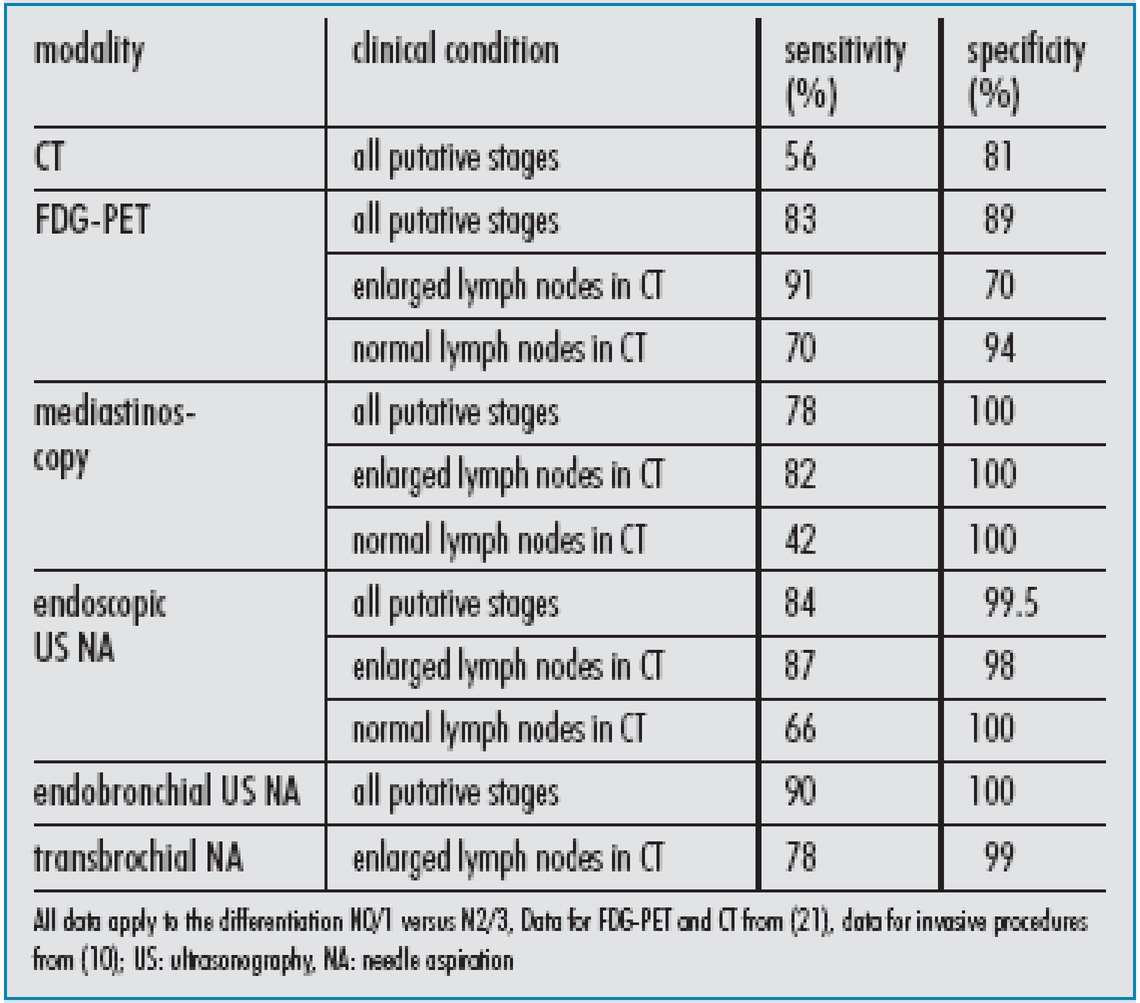

modality	clinical condition	sensitivity (%)	specificity (%)
CT	all putative stages	56	81
FDG-PET	all putative stages	83	89
	enlarged lymph nodes in CT	91	70
	normal lymph nodes in CT	70	94
mediastinoscopy	all putative stages	78	100
	enlarged lymph nodes in CT	82	100
	normal lymph nodes in CT	42	100
endoscopic US NA	all putative stages	84	99.5
	enlarged lymph nodes in CT	87	98
	normal lymph nodes in CT	66	100
endobronchial US NA	all putative stages	90	100
transbrochial NA	enlarged lymph nodes in CT	78	99

All data apply to the differentiation N0/1 versus N2/3, Data for FDG-PET and CT from (21), data for invasive procedures from (10); US: ultrasonography, NA: needle aspiration

Tab. 5
Diagnostic test parameters of different modalities for mediastinal lymph node staging

Hellwig et al. 2009; Nuklearmedizin 48:59-69

PET has a high (>90%) negative predictive value in mediastinal lymph node staging

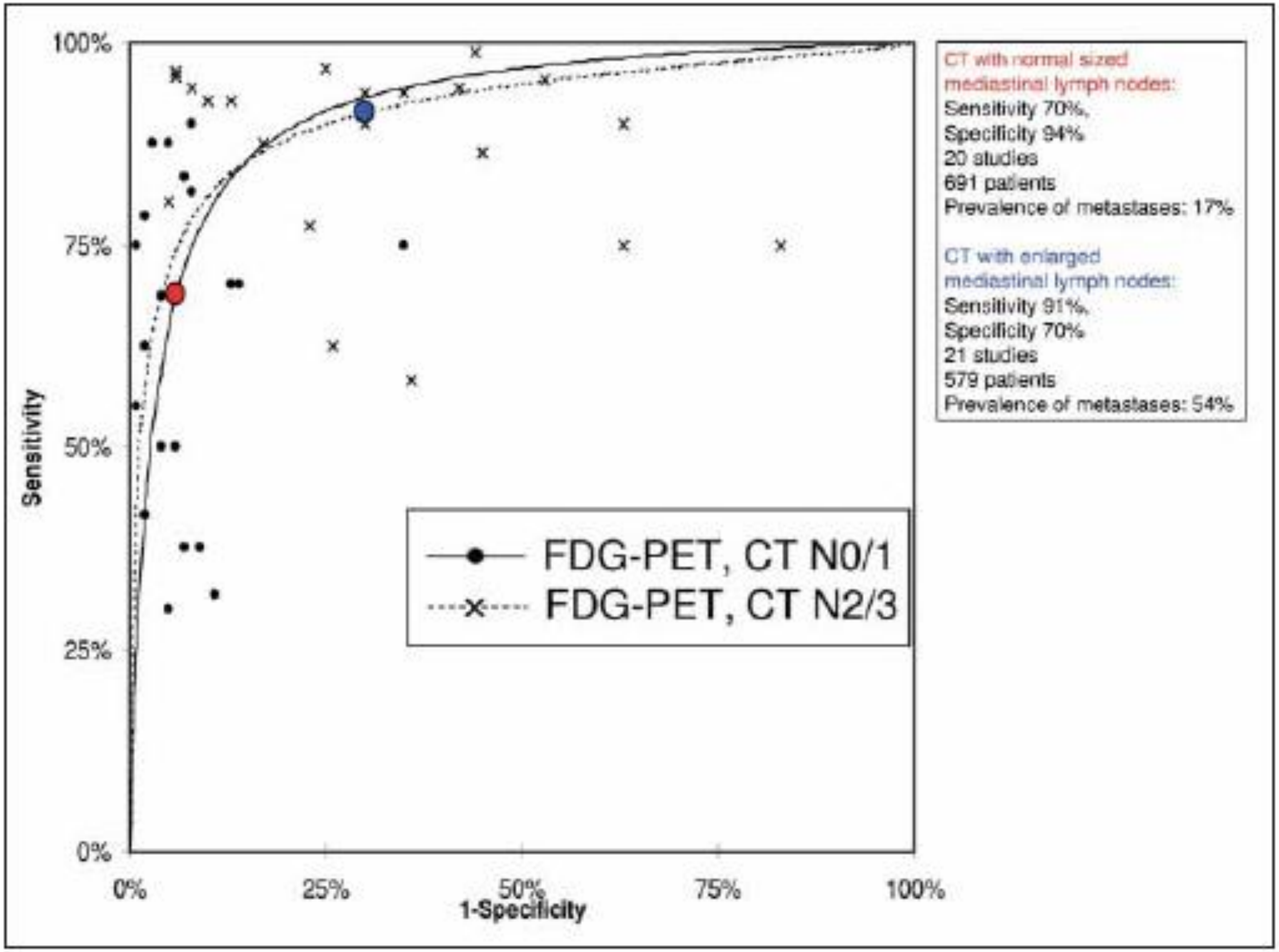

CT with normal sized mediastinal lymph nodes:
Sensitivity 70%,
Specificity 94%
20 studies
691 patients
Prevalence of metastases: 17%

CT with enlarged mediastinal lymph nodes:
Sensitivity 91%,
Specificity 70%
21 studies
579 patients
Prevalence of metastases: 54%

Hellwig et al. 2009; Nuklearmedizin 48:59-69

PET staging in small-cell lung cancer

- Similar findings about the benefit of PET in staging of small-cell lung cancer:

  - Correct upstaging from limited to extensive disease in 2 out of 24 patients (false positive in 1 out of 24)

  (Bradley et al. 2004; J. Clin. Oncol. 22:3248-3254)

  - Correct staging between LD and ED in 11 out of 15 patients

  (Blum et al. 2004; Am. J. Clin. Oncol. 27:164-171)

FDG-PET has impact on treatment strategy

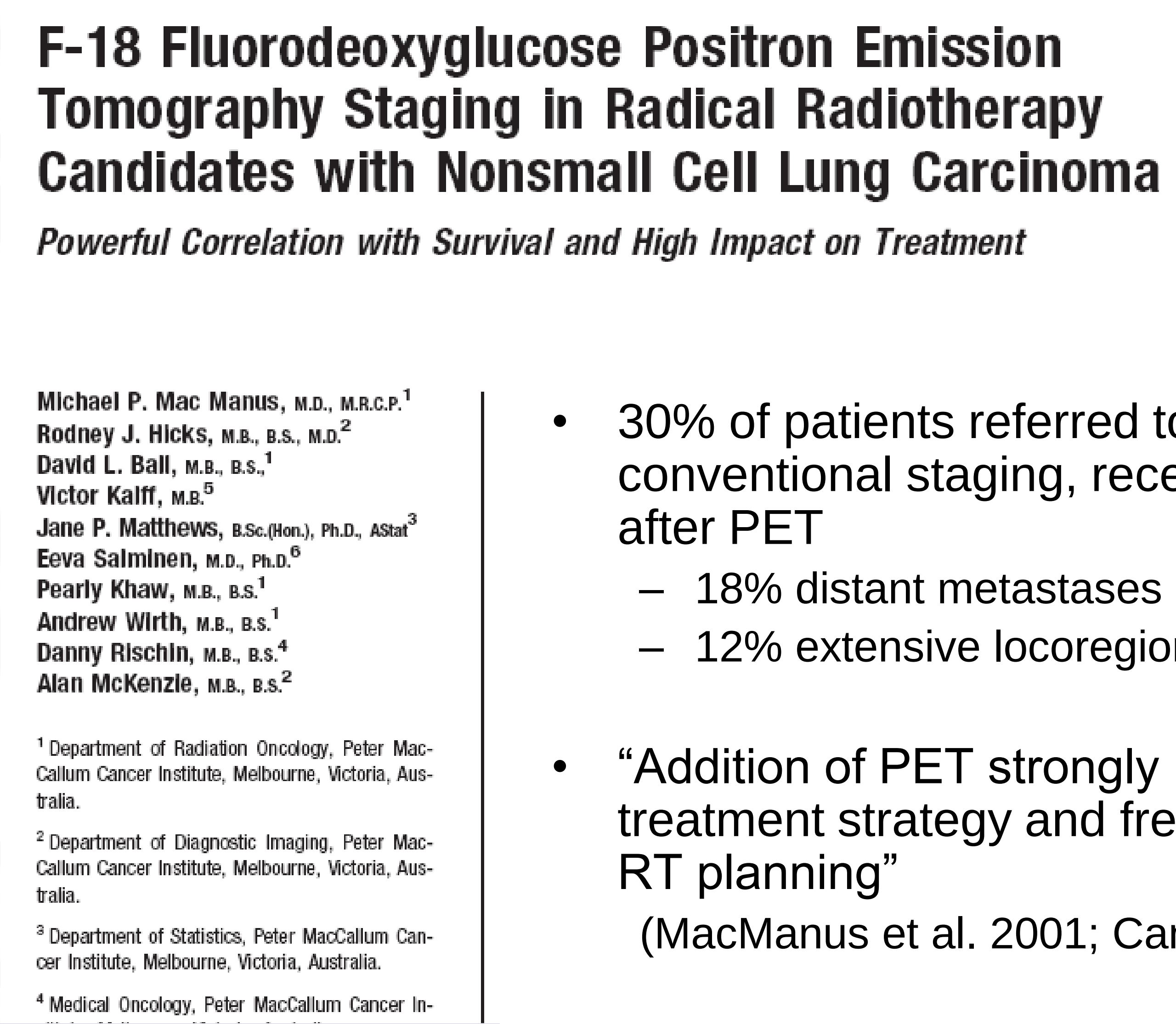

F-18 Fluorodeoxyglucose Positron Emission Tomography Staging in Radical Radiotherapy Candidates with Nonsmall Cell Lung Carcinoma

Powerful Correlation with Survival and High Impact on Treatment

Michael P. Mac Manus, M.D., M.R.C.P.[1]
Rodney J. Hicks, M.B., B.S., M.D.[2]
David L. Ball, M.B., B.S.,[1]
Victor Kalff, M.B.[5]
Jane P. Matthews, B.Sc.(Hon.), Ph.D., AStat[3]
Eeva Salminen, M.D., Ph.D.[6]
Pearly Khaw, M.B., B.S.[1]
Andrew Wirth, M.B., B.S.[1]
Danny Rischin, M.B., B.S.[4]
Alan McKenzie, M.B., B.S.[2]

[1] Department of Radiation Oncology, Peter MacCallum Cancer Institute, Melbourne, Victoria, Australia.

[2] Department of Diagnostic Imaging, Peter MacCallum Cancer Institute, Melbourne, Victoria, Australia.

[3] Department of Statistics, Peter MacCallum Cancer Institute, Melbourne, Victoria, Australia.

[4] Medical Oncology, Peter MacCallum Cancer In-

- 30% of patients referred to RT based on conventional staging, received palliative RT after PET
  - 18% distant metastases
  - 12% extensive locoregional disease

- “Addition of PET strongly influences treatment strategy and frequently impacts RT planning”

  (MacManus et al. 2001; Cancer 92:886-895)

Selective mediastinal irradiation

- The high negative predictive value of PET for mediastinal lymph nodes, can be exploited by irradiating only PET-positive areas
- Selective mediastinal node irradiation results in low isolated nodal failure rates

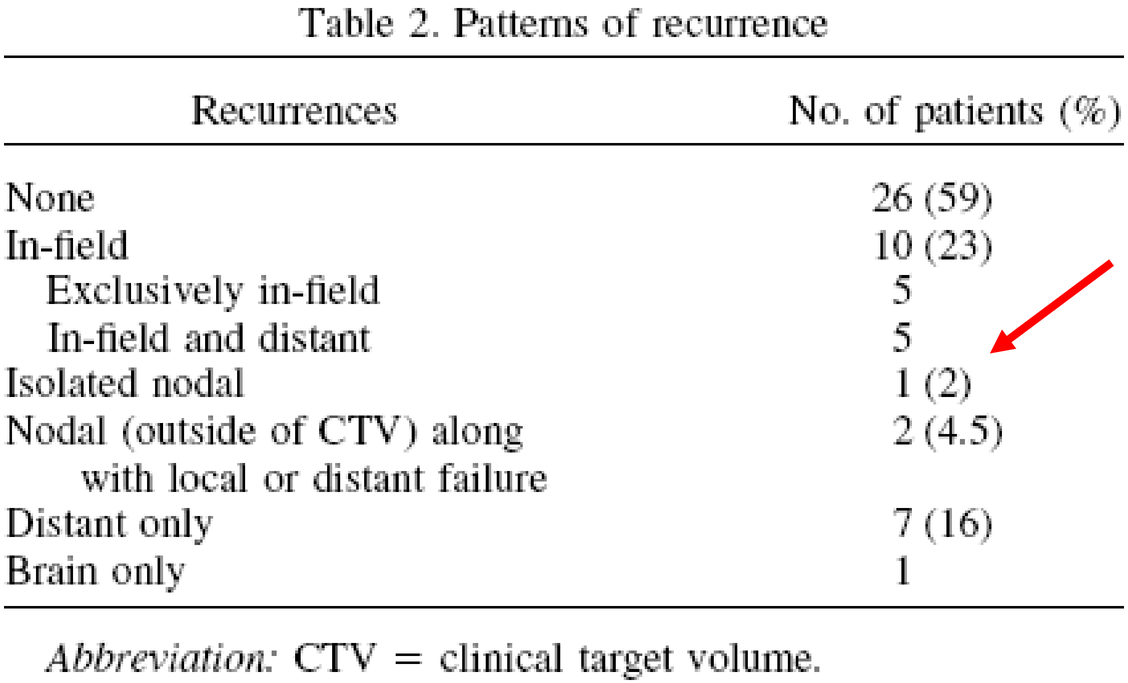

Table 2. Patterns of recurrence

Recurrences	No. of patients (%)
None	26 (59)
In-field	10 (23)
Exclusively in-field	5
In-field and distant	5
Isolated nodal	1 (2)
Nodal (outside of CTV) along with local or distant failure	2 (4.5)
Distant only	7 (16)
Brain only	1

Abbreviation: CTV = clinical target volume.

De Ruysscher et al. 2005; Int. J. Radiat. Oncol. Biol. Phys. 62:998-994

Monitoring volume changes during treatment

- Analyze volume changes during treatment with daily MVCT
- Mean volume decrease is 73 +/-18% in 42 days
- Non-responders show slower regression

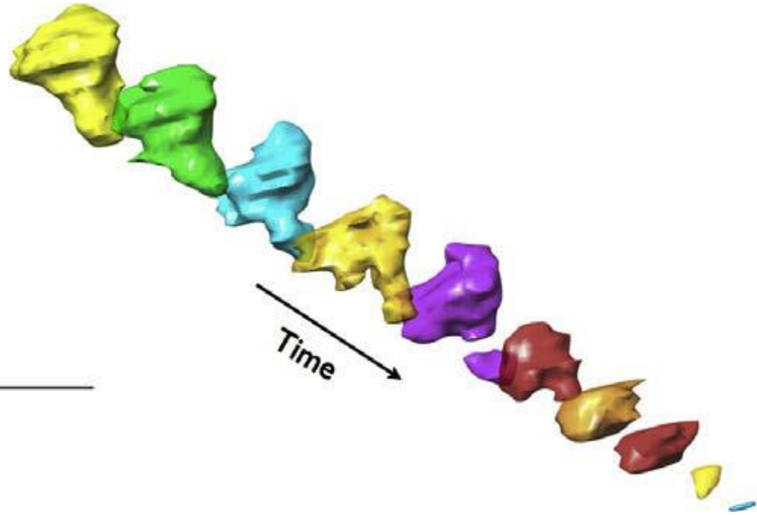

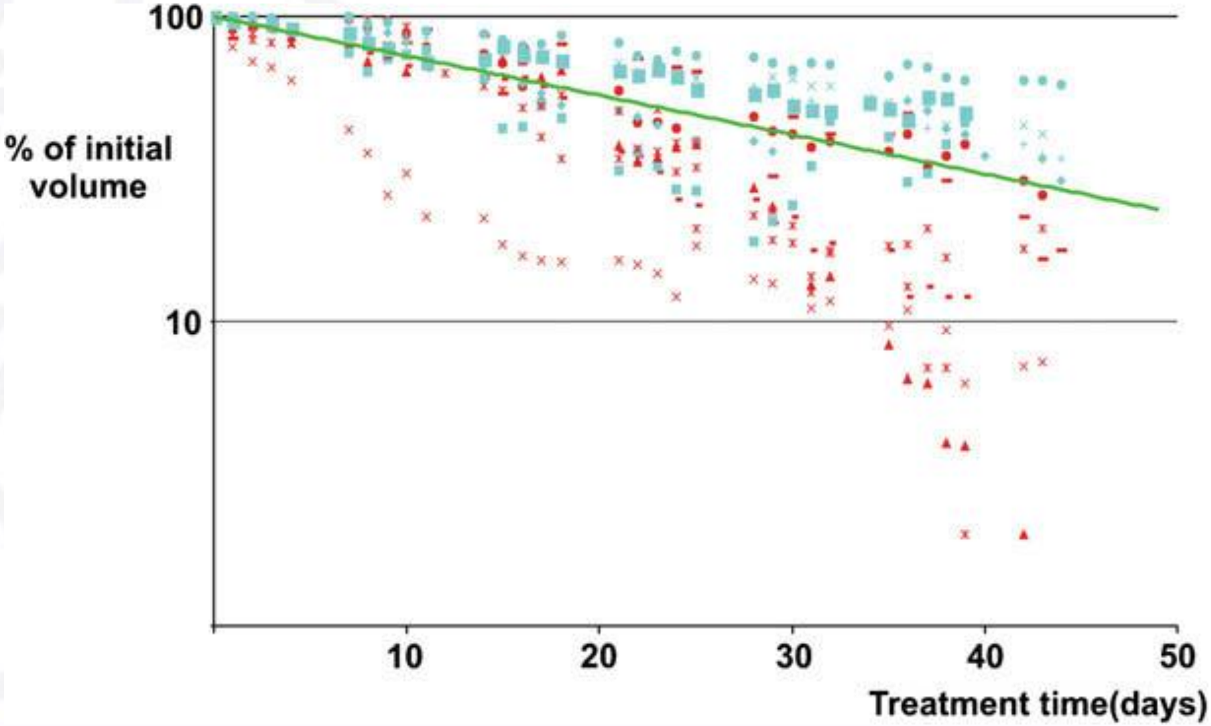

Bral et al. 2009; Int. J. Radiat. Oncol. Biol. Phys. 91:438-442

Imaging of recurrences, follow-up

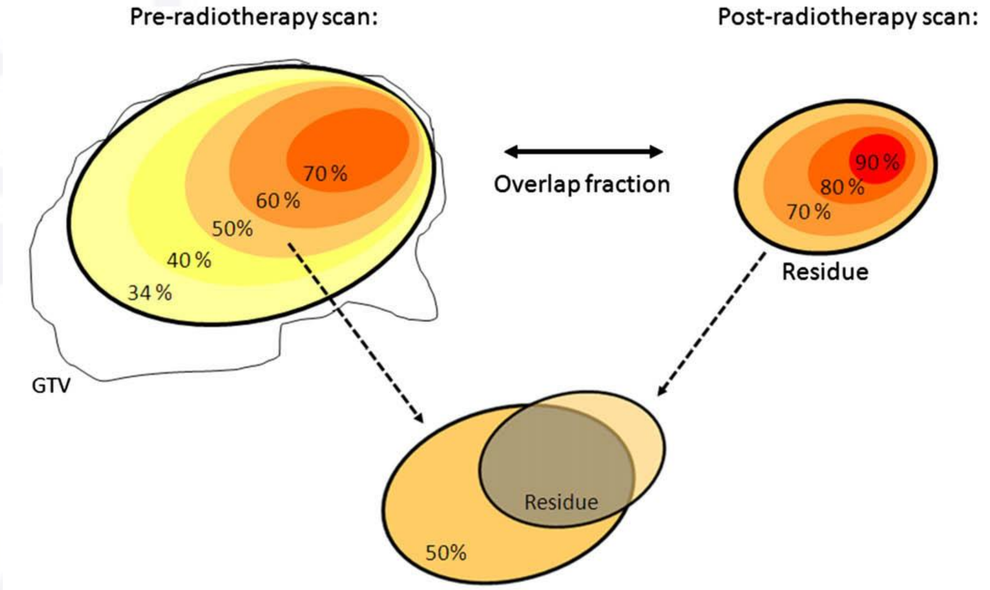
Pre-radiotherapy scan:
Post-radiotherapy scan:
70 %
60 %
50%
40 %
34 %
GTV
Overlap fraction
90 %
80 %
70 %
Residue
Residue
50%

$$\text{overlap fraction (OF)} = \frac{\text{overlapping area}}{\text{smallest volume}}$$

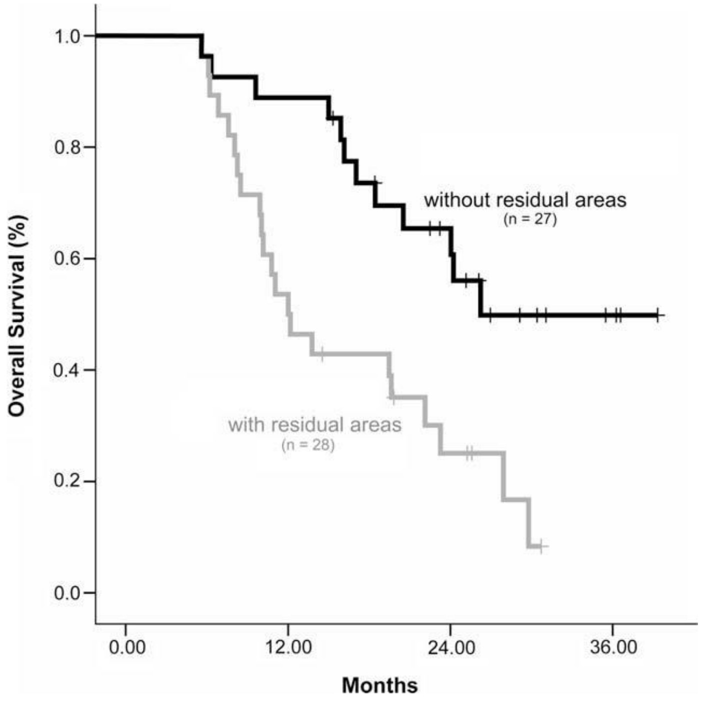

Aerts et al. 2009. Radiother Oncol. 91:386-392

- Compare FDG uptake pre-radiotherapy with post-radiotherapy (49-184 days after end of treatment)
- Residual FDG uptake is associated with worse overall survival after treatment

Imaging of recurrences, follow-up

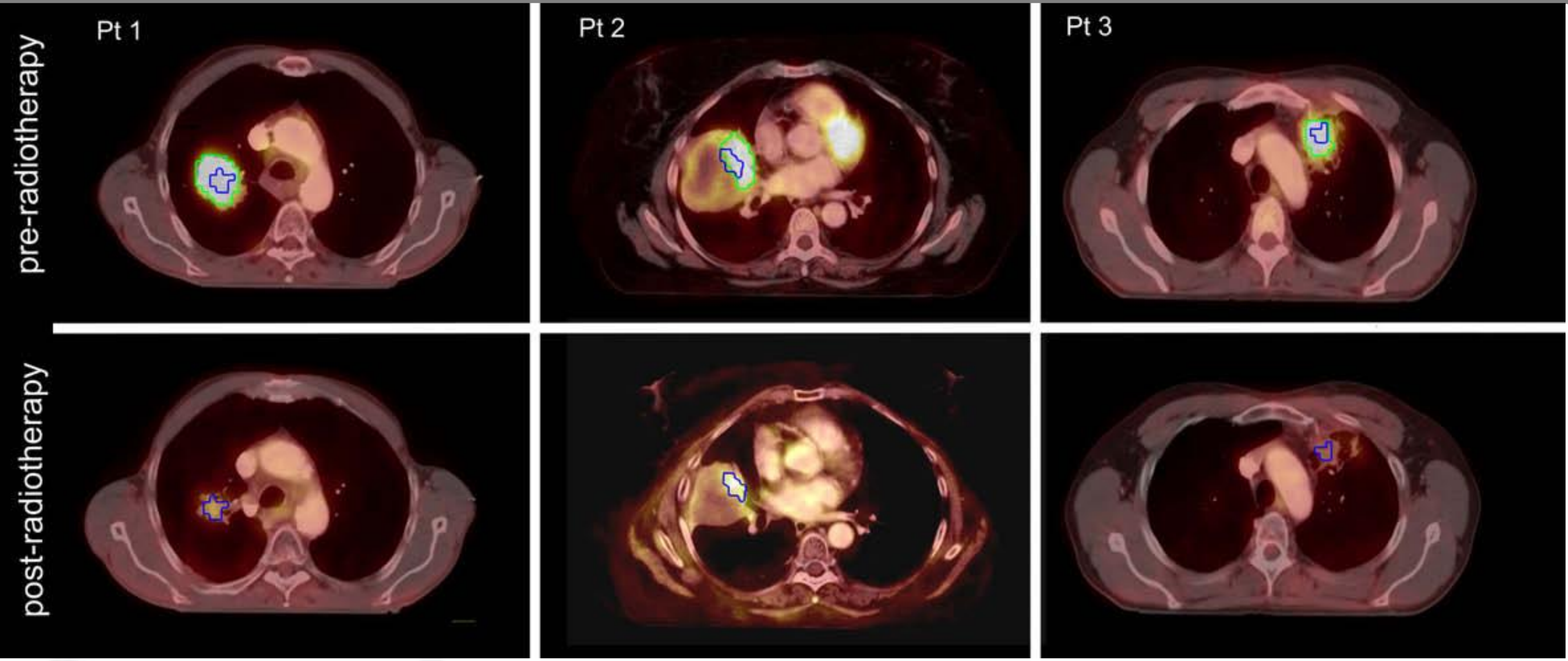
Pt 1
Pt 2
Pt 3
pre-radiotherapy
post-radiotherapy

- Residual FDG uptake correlated with location of high uptake pre-radiotherapy

Aerts et al. 2009. Radiother Oncol. 91:386-392

Limitations of PET for staging of lung cancer

- uptake of FDG in inflamatory sites
- false negative PET after chemotherapy
- small lesions (< 1 cm3) may not be seen
- Respiratory motion causes blurring of image in 3D PET

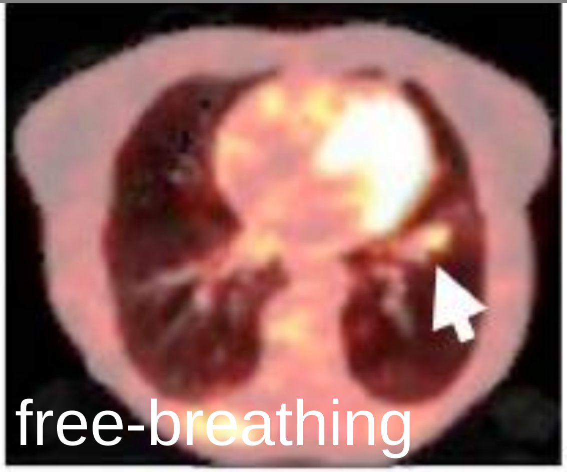

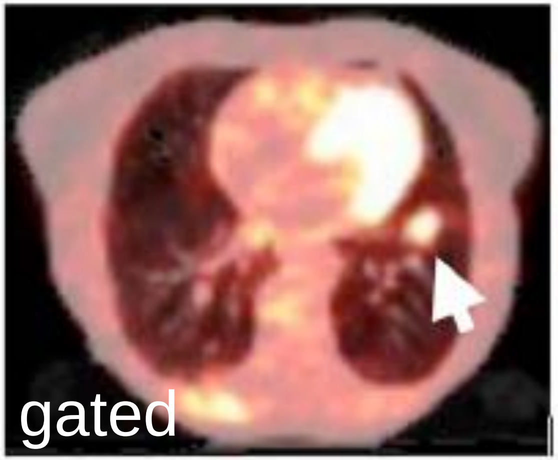

Nehmeh et al. 2004; Med. Phys. 31:3179-3186

PET(-CT) for staging of lung cancer

- PET improves accuracy of staging
  - High negative predictive value of PET for mediastinal lymph nodes
- Improved staging has impact on treatment strategy
  - Selective irradiation of mediastinum based on PET results in low rates of nodal failure
- Residual FDG uptake after treatment correlates with location of high uptake pre-treatment and is associated with worse outcome
- What is the impact of PET on delineation?

Improved consistency of GTV delineation

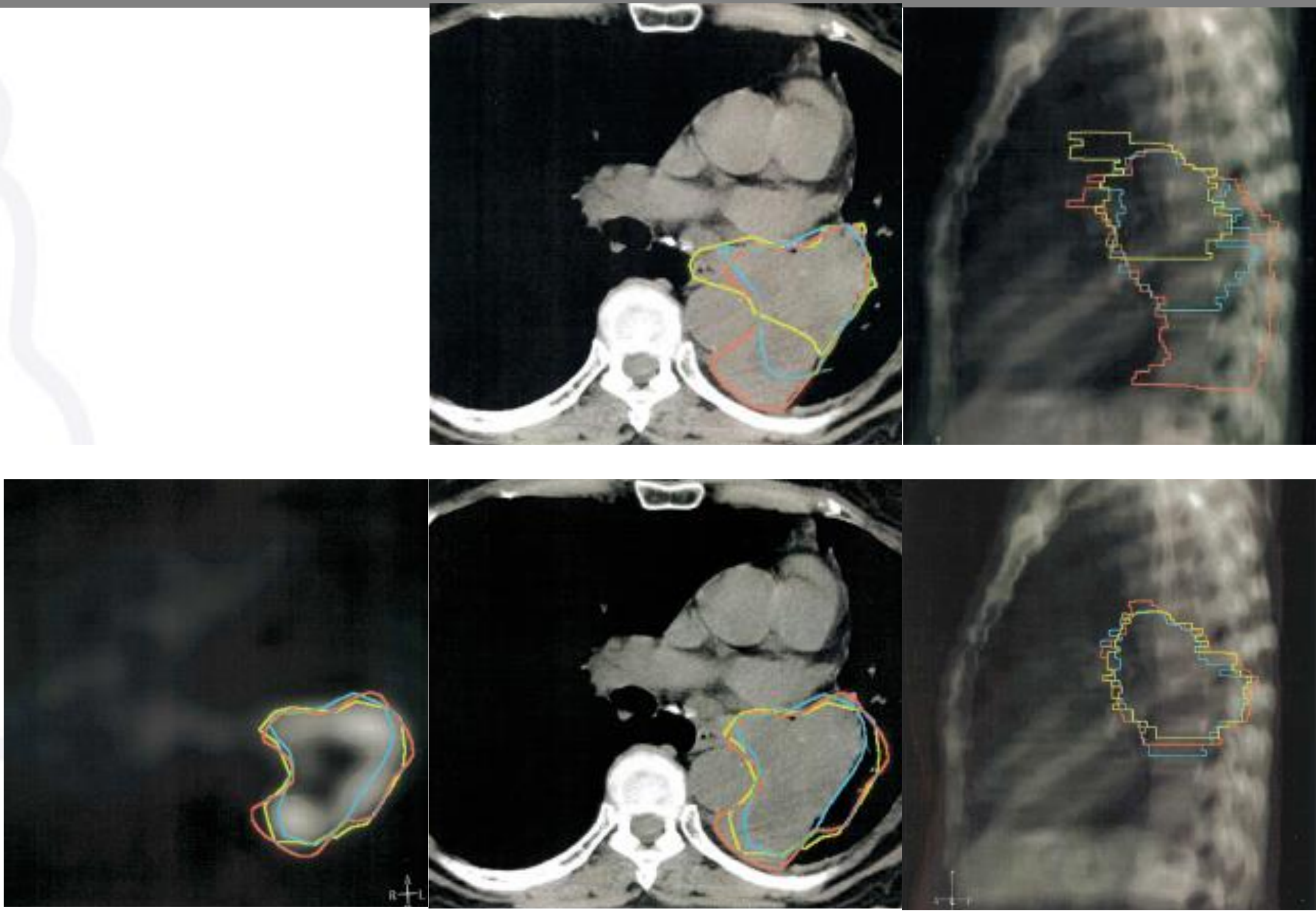

Caldwell et al. 2001; Int. J. Radiat. Oncol. Biol. Phys. 51:923-931

Improved consistency of GTV delineation

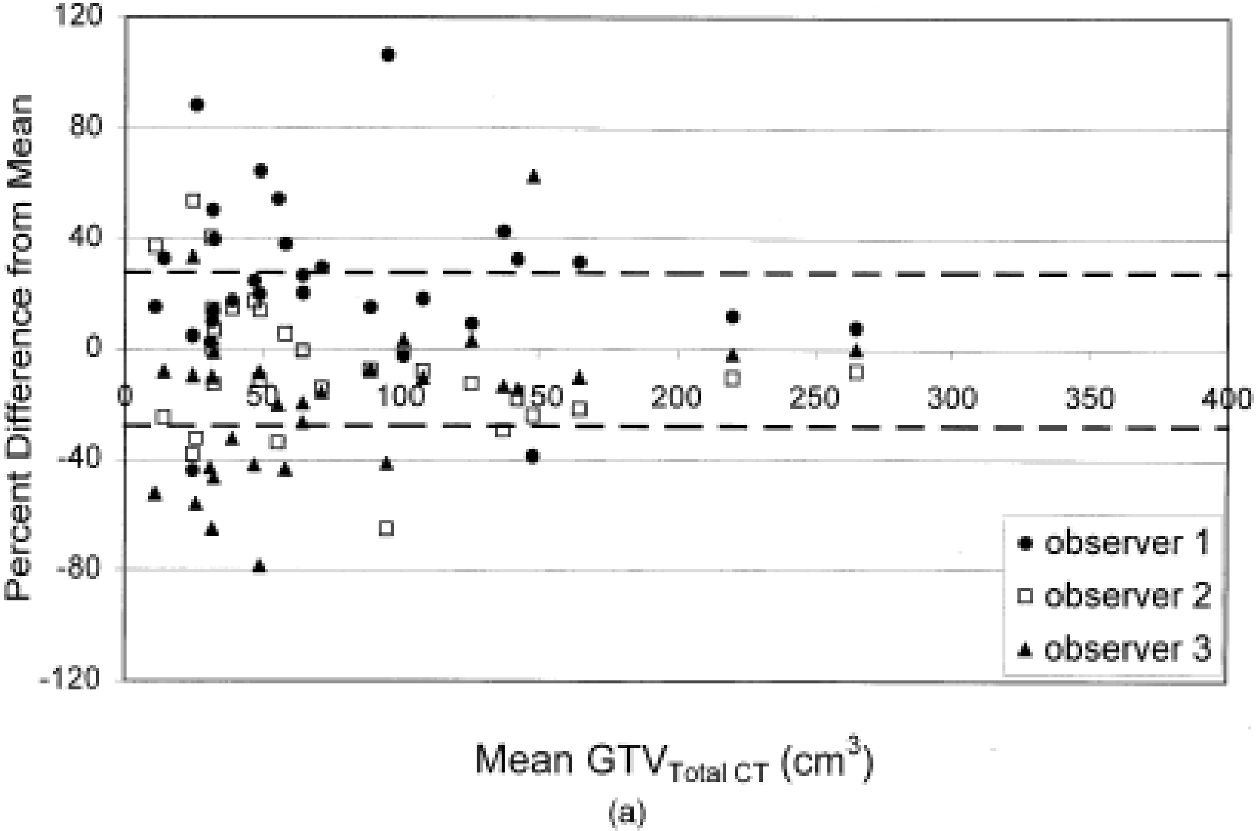

- With CT-only, in 12 of 30 patients, all 3 observers’ volumes lie within 28% (the standard deviation of the variation in the group)

Caldwell et al. 2001; Int. J. Radiat. Oncol. Biol. Phys. 51:923-931

Improved consistency of GTV delineation

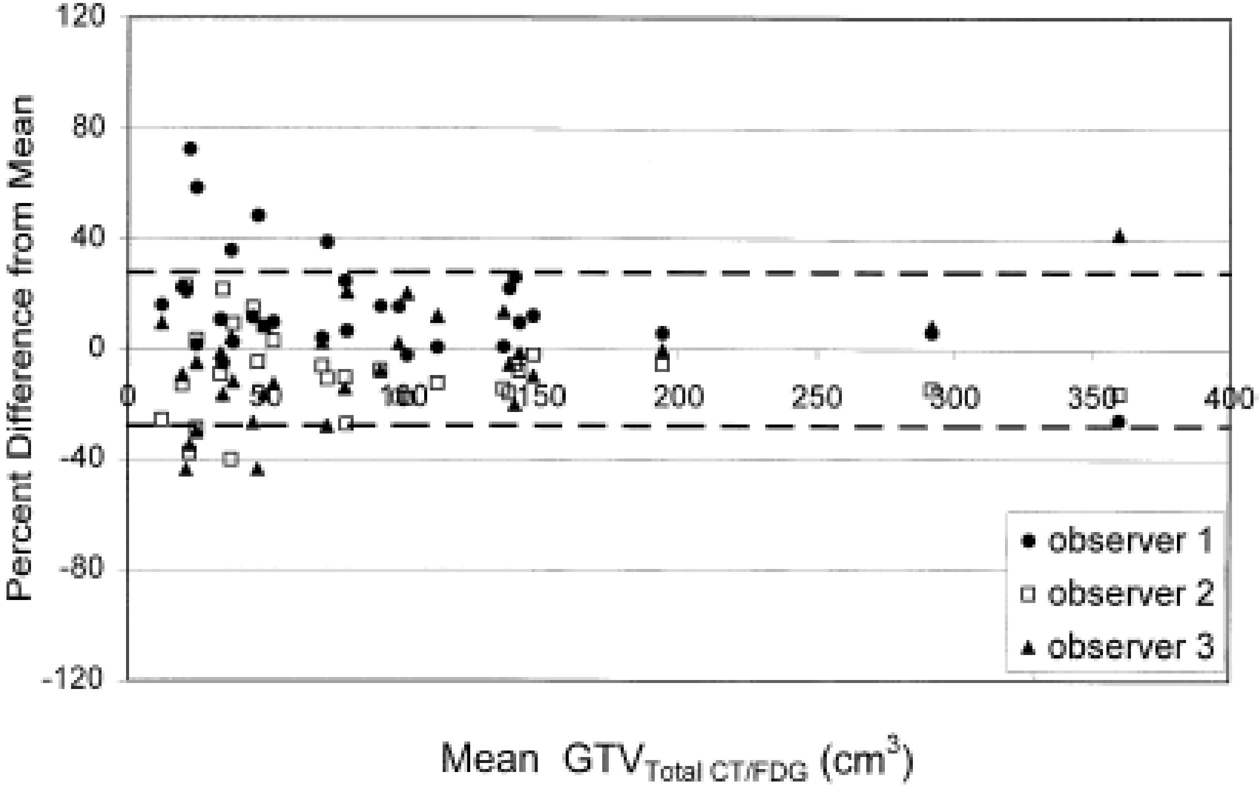

(b)

- With CT and PET, in 23 of 30 patients, all 3 observers’ volumes lie within 28% (the standard deviation of the variation in the group)

Caldwell et al. 2001; Int. J. Radiat. Oncol. Biol. Phys. 51:923-931

Different methods for tumor delineation on PET produce very different results

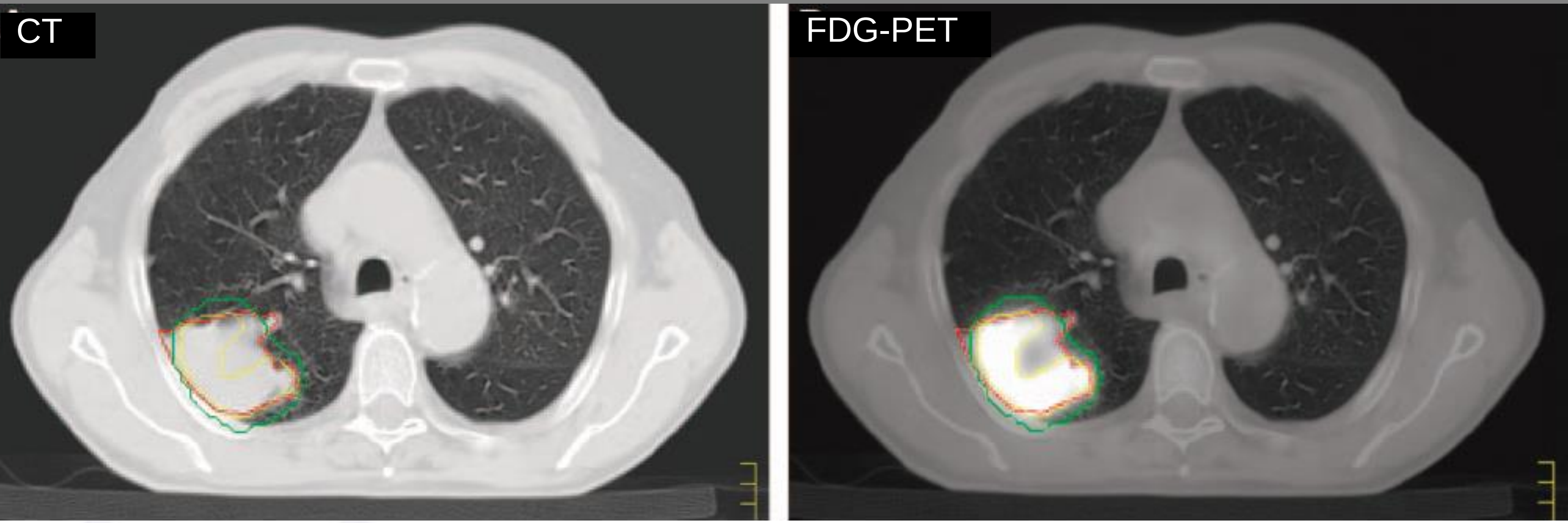

- GTV$_{40}$: take 40% of SUV$_{max}$ as threshold
- GTVbg: threshold based on mean within GTV$_{70}$ and background
- GTV$_{CT}$: delineation on CT

- GTV$_{40}$ is inadequate, but GTV$_{bg}$ also differs significantly from GTV$_{CT}$

Nestle et al. 2005; J. Nucl. Med. 46:1342-1348

Auto-contouring algorithms improve consistency

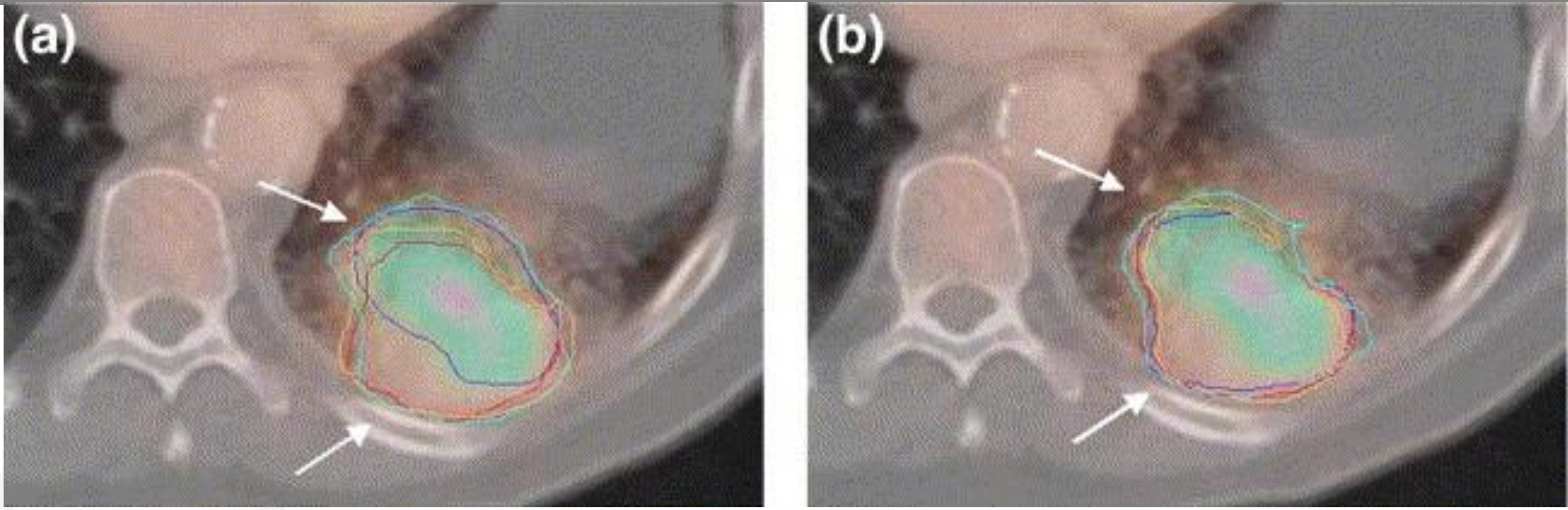

- Source to Background ratio (SBR) determines a threshold level, determined from phantom experiments (FDG-filled spheres in background)
- 5 observers delineated the tumor manualy (a) and edited an SBR-based contour if they deemed necessary (b)
- The SBR-based and edited contours show much less variability

Baardwijk et al. 2007; Int J Radiat Oncol Biol Phys. 68:771-778

Impact of FDG-PET on definition of PTV

- ↑ High sensitivity to positive lymph nodes
- ↓ High negative predictive value for lymph nodes
- ↓ Tumor can be differentiated from atalectasis
- ↓ Reduced inter-observer variability

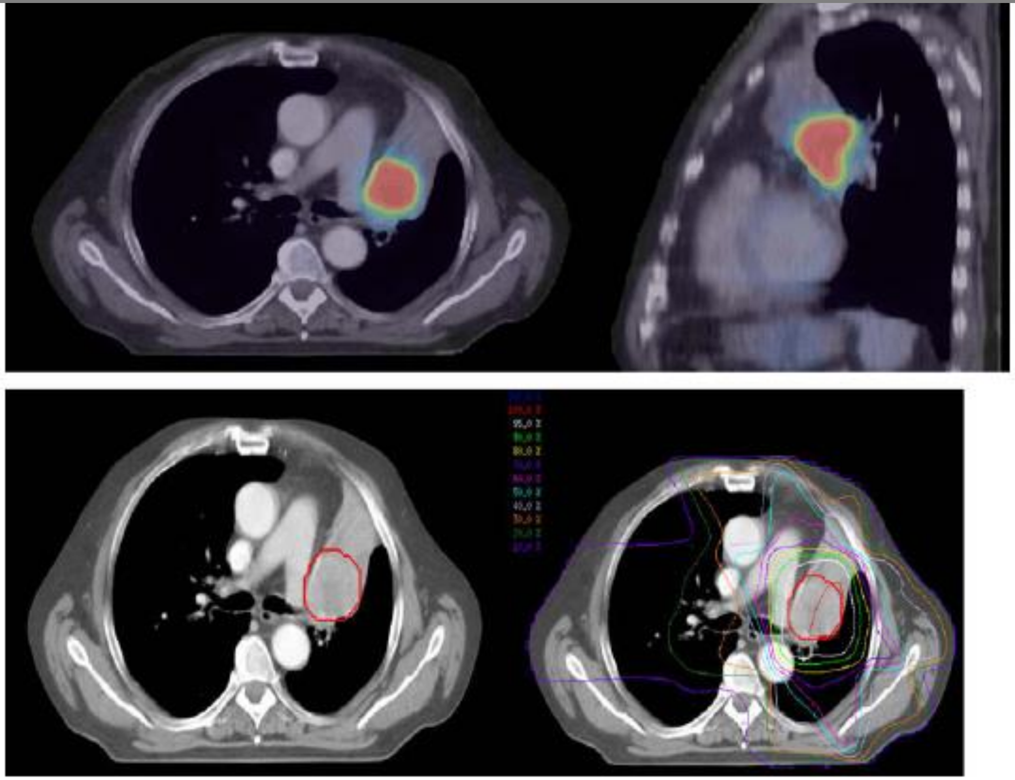

MacManus et al. 2009;
Radiother. Oncol. 91:85-94

Validation of PET contouring algorithms with pathology is essential

- Maximal diameter of SBR-based GTV compared with the maximal diameter of the primary tumor, after surgical resection

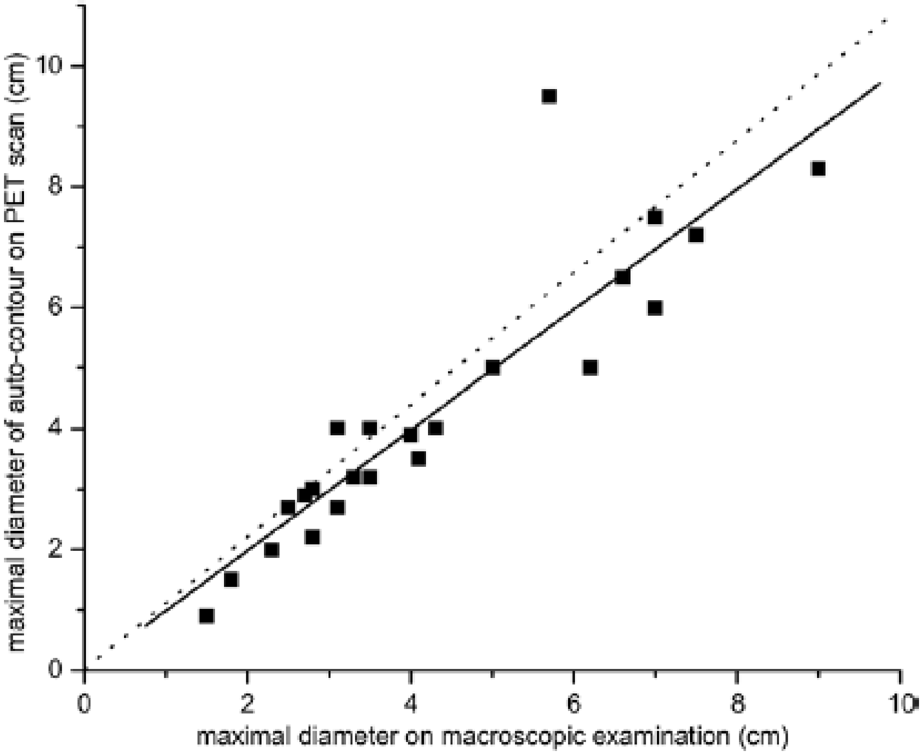

Baardwijk et al. 2007; Int J Radiat Oncol Biol Phys. 68:771-778

3D validation of contouring with pathology

- Large deformations of resection specimen make 3D correlation with pre-operative imaging is very difficult

- Lung lobes were inflated with formalin to approximate the CT volume
- Registration in two steps:
  1. find correct orientation of CT with sliced specimen; resample CT in the same plane
  2. match macroscopic slices to CT volume

- Verify GTV volume and shape
- Identify the extent of the CTV

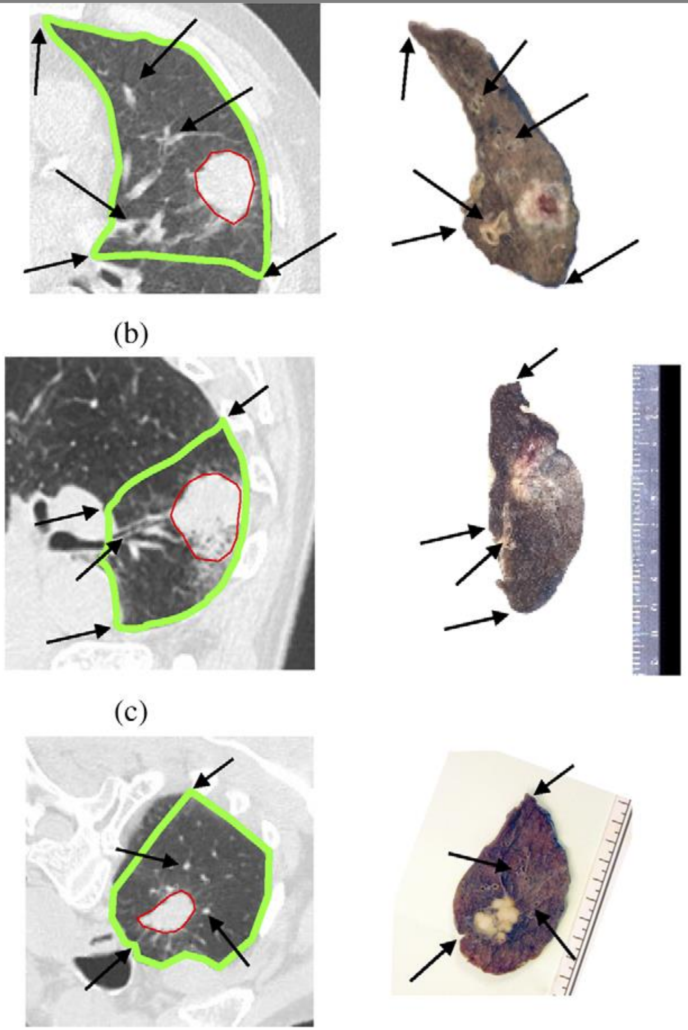

Stroom et al. 2007; Int J Radiat Oncol Biol Phys. 69:267-275

PET and CT registration: planning CT and CT of the PET-CT

- Is a specific planning PET-CT scan required? or can a PET-CT scan made for diagnostic purposes be used for delineation?

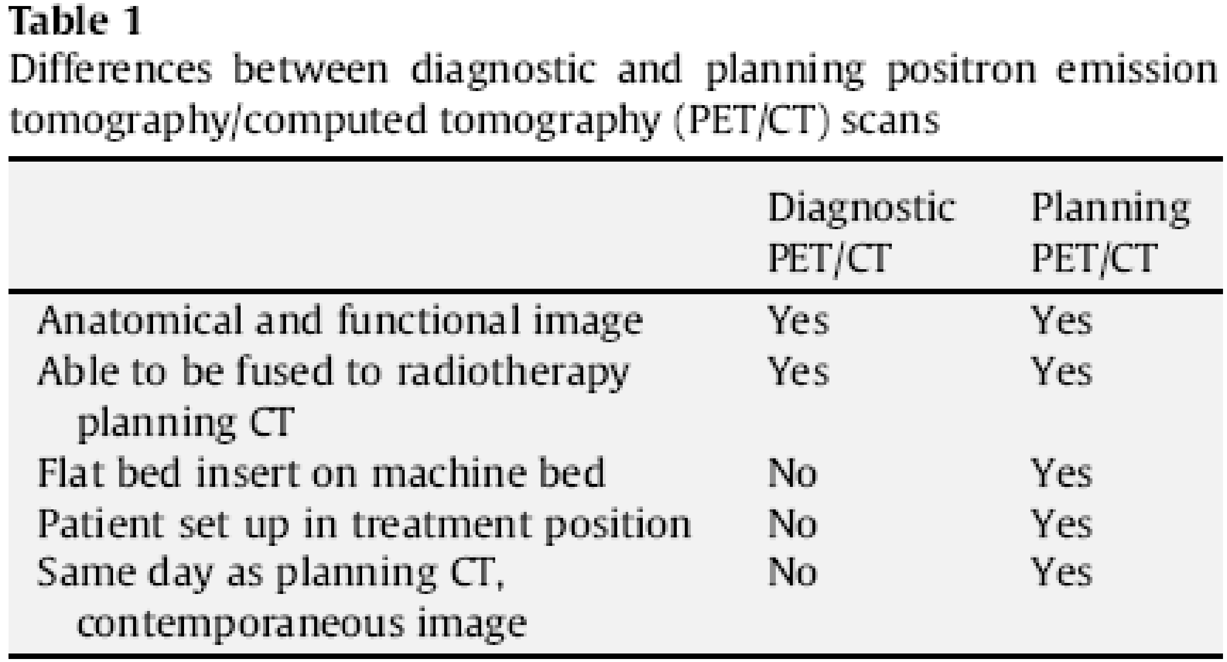

Table 1
Differences between diagnostic and planning positron emission tomography/computed tomography (PET/CT) scans

	Diagnostic PET/CT	Planning PET/CT
Anatomical and functional image	Yes	Yes
Able to be fused to radiotherapy planning CT	Yes	Yes
Flat bed insert on machine bed	No	Yes
Patient set up in treatment position	No	Yes
Same day as planning CT, contemporaneous image	No	Yes

Yap et al. 2010; Clin Oncol. 22:554-560

PET and CT registration: planning CT and CT of the PET-CT

- An average of 4 mm registration error between PET-CT to planning CT
- A diagnostic PET-CT has no larger registration errors than a planning PET-CT (if arms are positioned above the head)

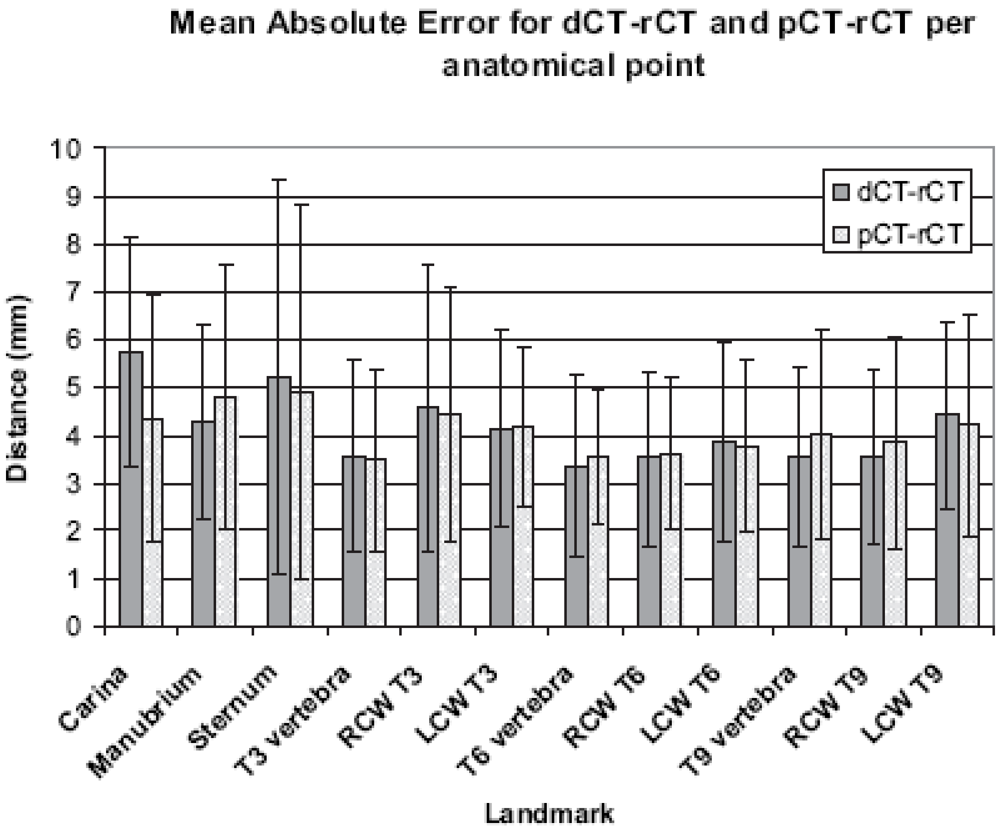

Yap et al. 2010; Clin Oncol. 22:554-560

how well are the PET and CT in a PET-CT registered?

- 19 lung cancer patients with 26 lesions
- 3D PET-CT exam
- Distance between center of lesions defined on PET and CT was 7.55 +/- 4.73 mm
- Baseline shift during the exam

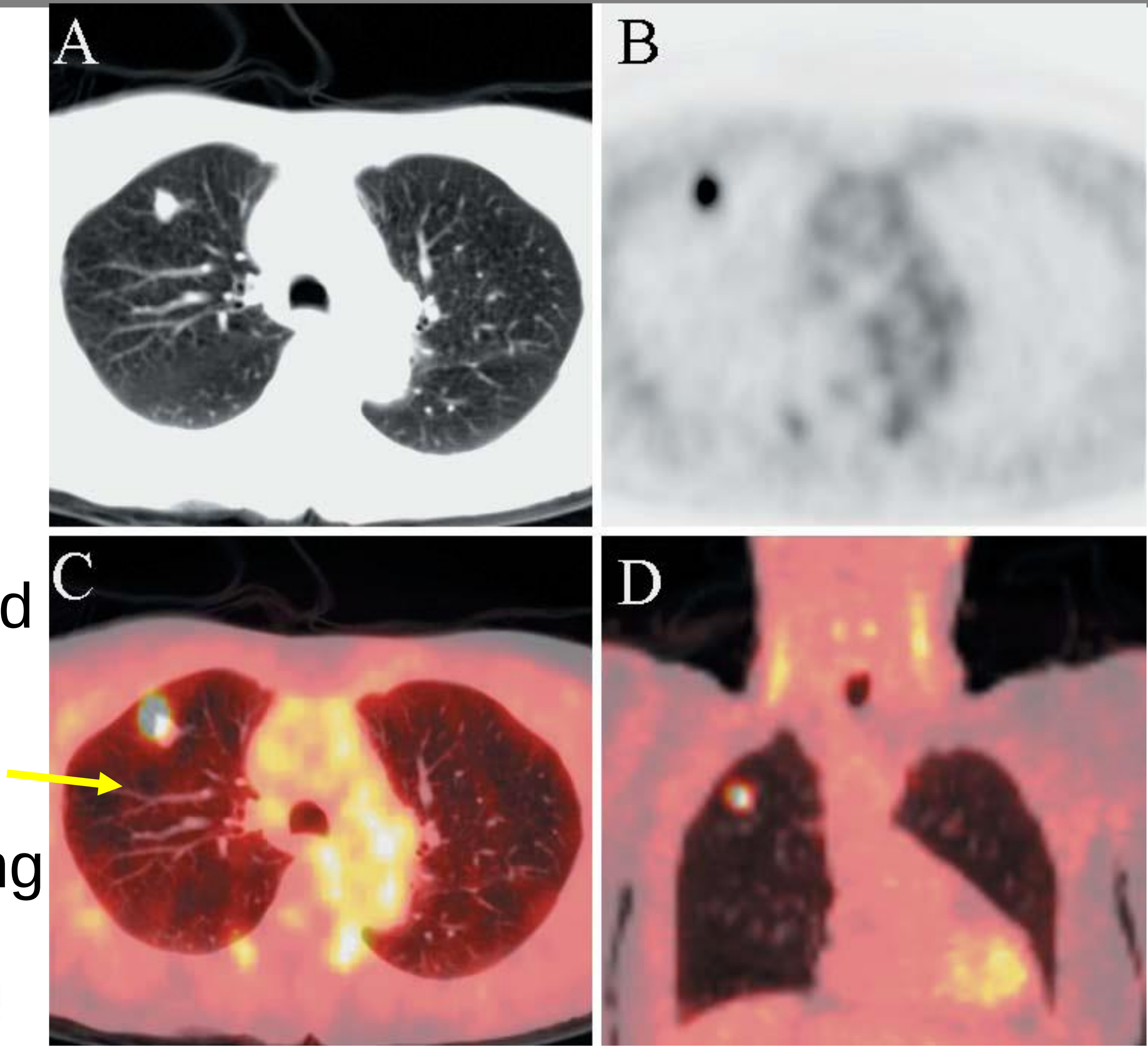

Cohade et al. 2002; Eur J Nucl Med Molec Imaging 30:721-726

Tumor motion during regular breathing

- Variety in observed behavior
- Large motion close to diaphragm
- Smaller motion towards top of lung
- hysteresis

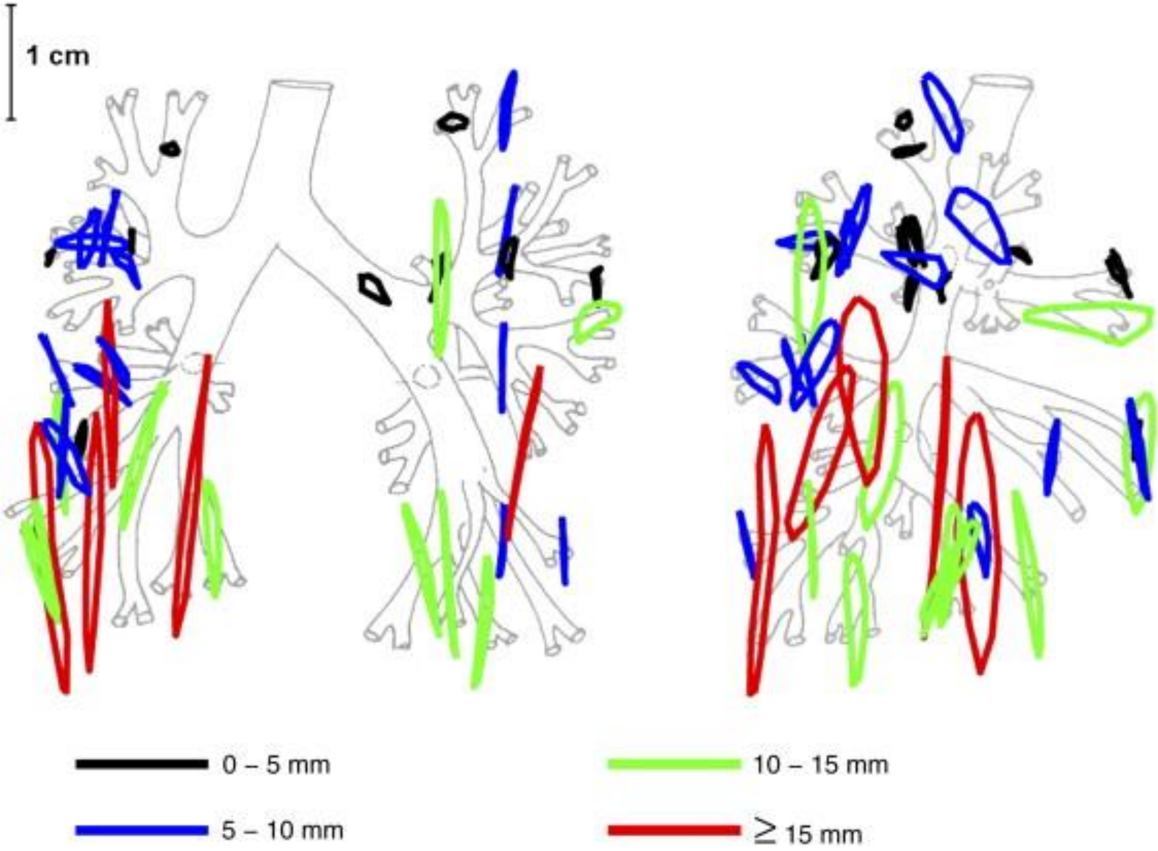
1 cm
0 – 5 mm
5 – 10 mm
10 – 15 mm
≥ 15 mm

Sonke et al., 2008. Int J Radiat Oncol Biol Phys. 70:590-598

4D PET-CT

- Acquire CT and PET signal with a signal reflecting the repiratory motion
- PET signal is sampled in 10 bins of ~0.5 s
- Reduced motion-induced blurring decreased the observed tumor volume by as much as 43%
- SUV values inside the tumor increase

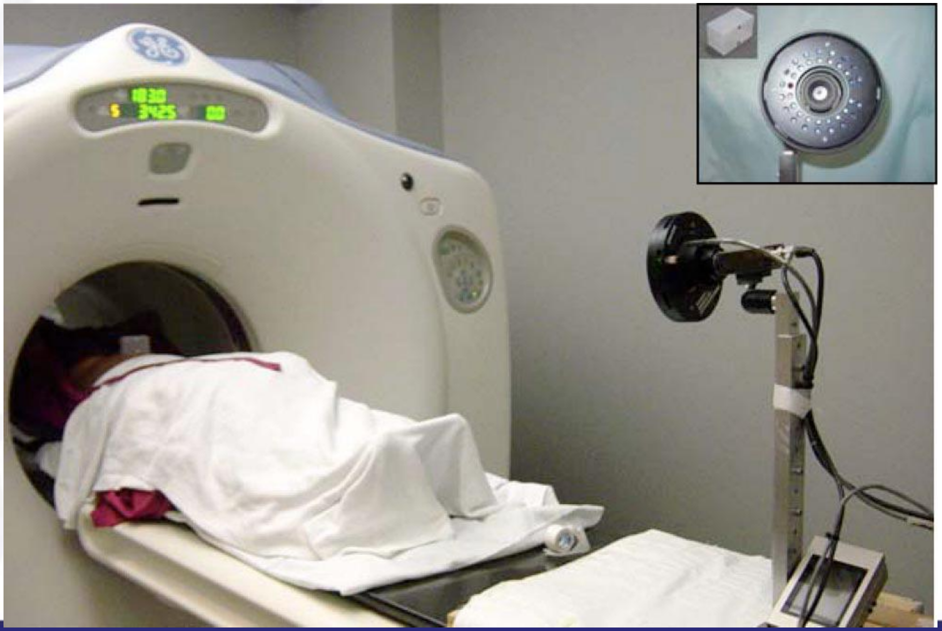

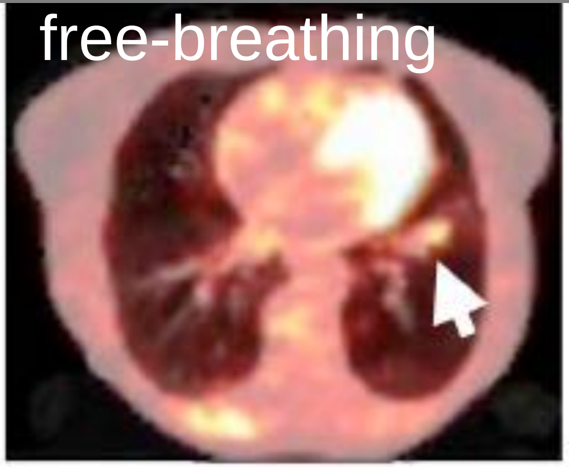

free-breathing

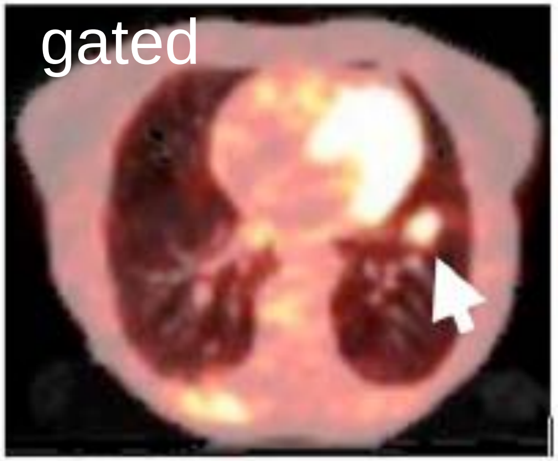

gated

Nehmeh et al. 2004; Med. Phys. 31:3179-3186

4D PET-CT

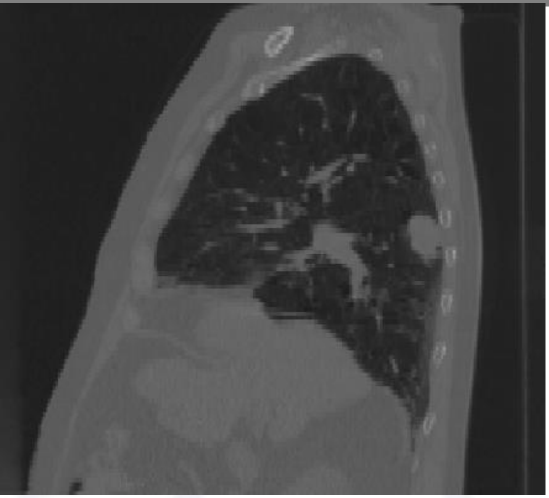

4D CT

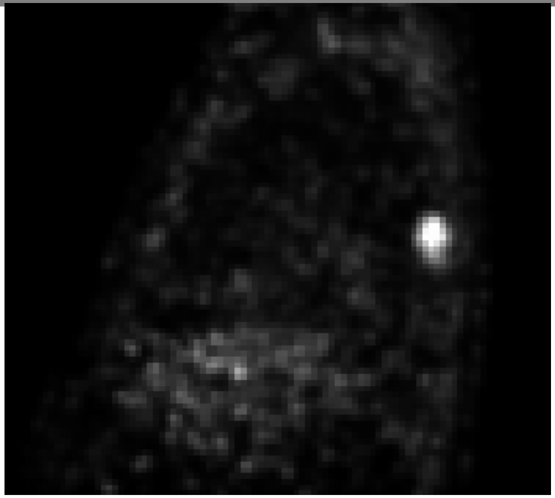

4D PET

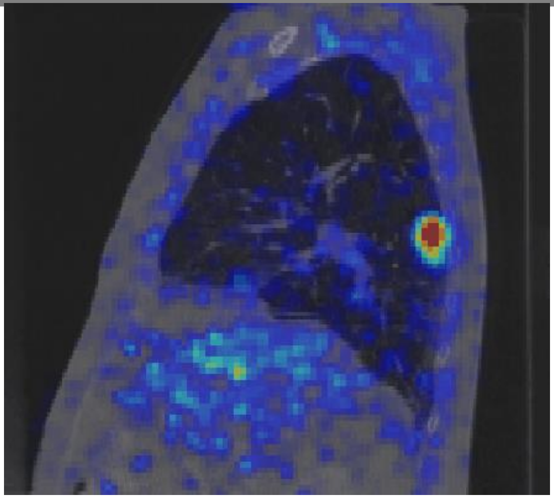

overlay

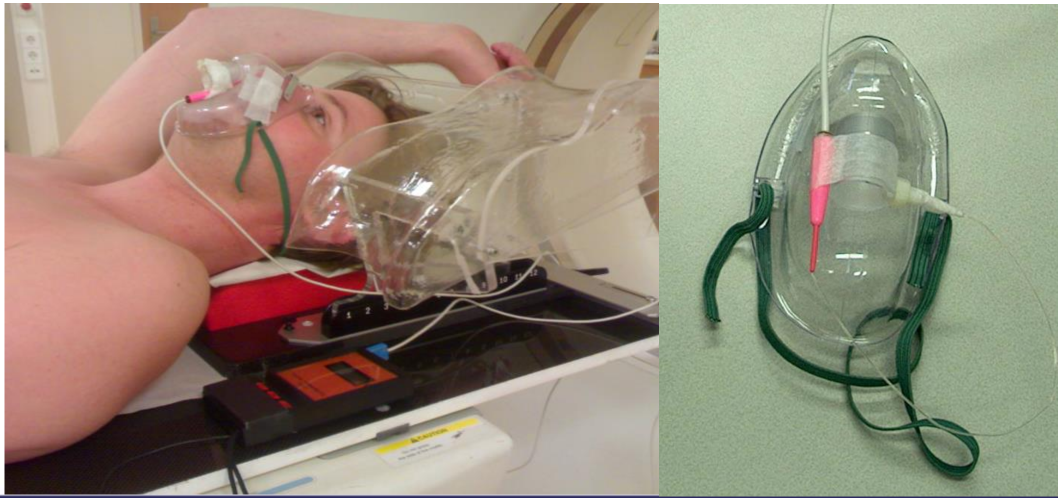

Attenuation correction for 4D PET

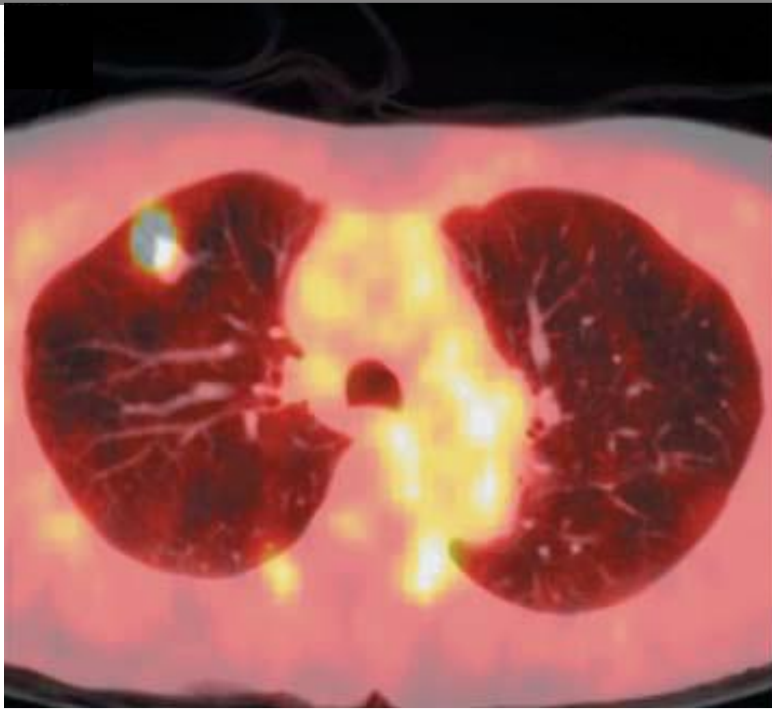

- A baseline shift between CT and PET results in an erroneous attenuation correction of the PET
- 4D PET attenuation correction with CT
  - standard 3D
  - average
  - mid-ventilation
  - 4D
- A baseline shift between CT and PET results in an erroneous attenuation correction of the PET

Attenuation correction for 4D PET

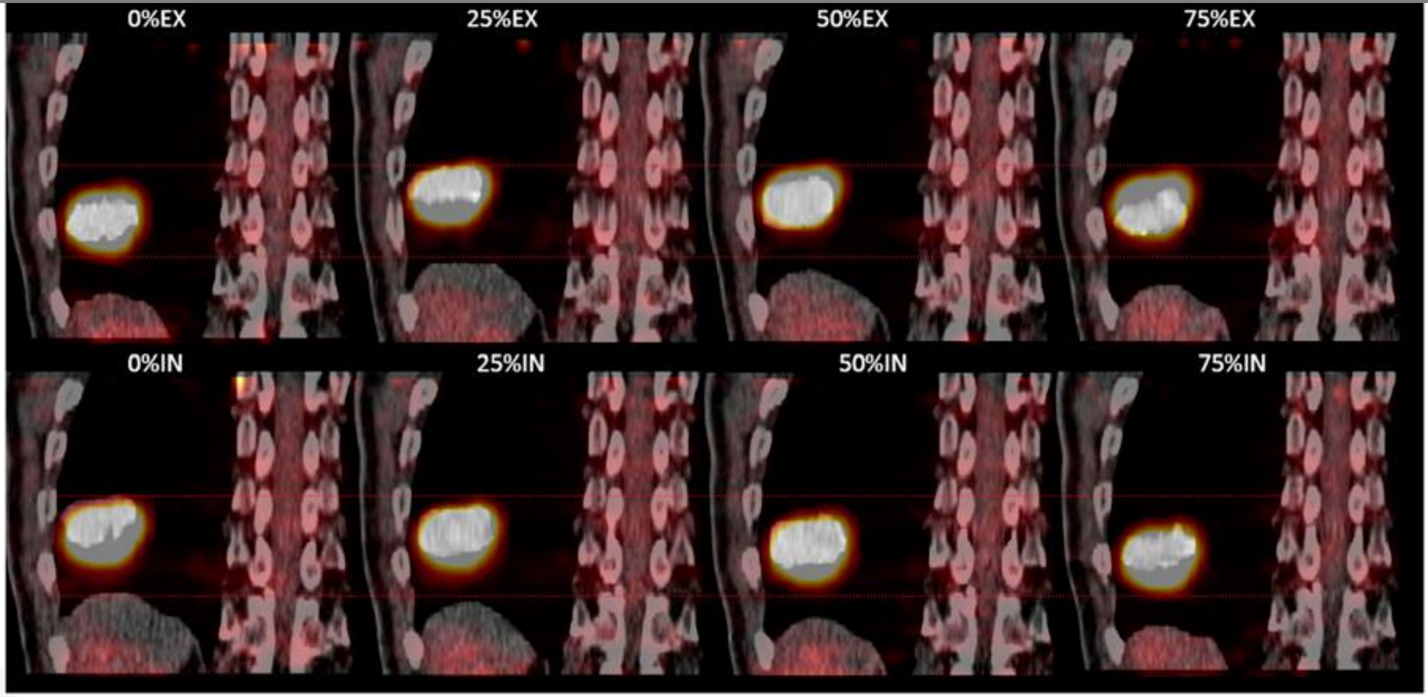
0%EX
25%EX
50%EX
75%EX
0%IN
25%IN
50%IN
75%IN

- in a 4D PET-CT scan, the phases of the 4D CT and 4D PET may not match
- What is a good strategy for attenuation correction?

Rosario et al. 2009; J Nucl Med Techn. 37:208-214

Attenuation correction for 4D PET

two methods for attenuation correction:

1. each individual phase of CT
2. 50% experation CT (mid-ventilation)

- Differences in SUV and volume are small

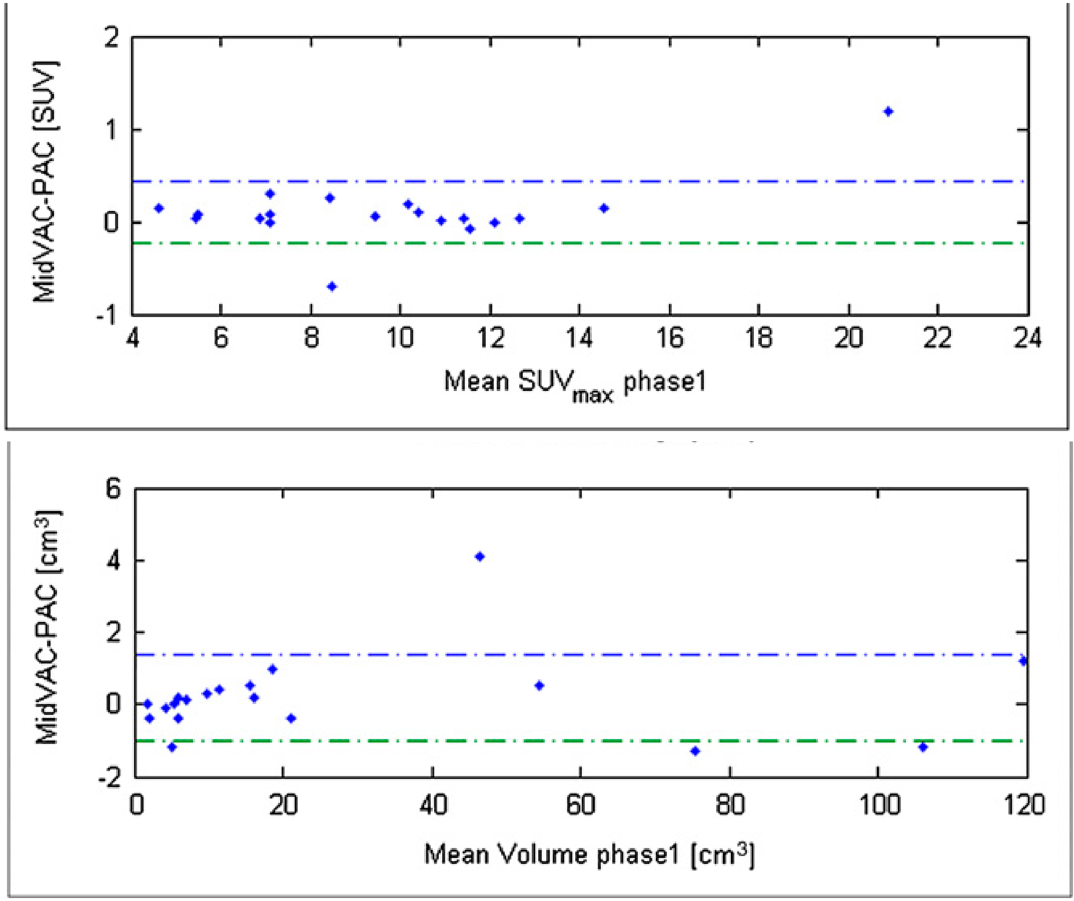

Rosario et al. 2009; J Nucl Med Techn. 37:208-214

Making a PET-CT for radiotherapy

- Registration of bony anatomy of a diagnostic PET-CT to planning CT is accurate
- baseline shift of tumor (shift relative to bony anatomy) frequently occurs

- gated (4D) PET-CT scan
  - SUV values higher than on blurred 3D scan
  - More precise imaging of tumor
- Attenuation correction on a single phase (mid-ventilation) of a 4D CT scan provides reliable SUV values

Target definition on a 4D CT scan

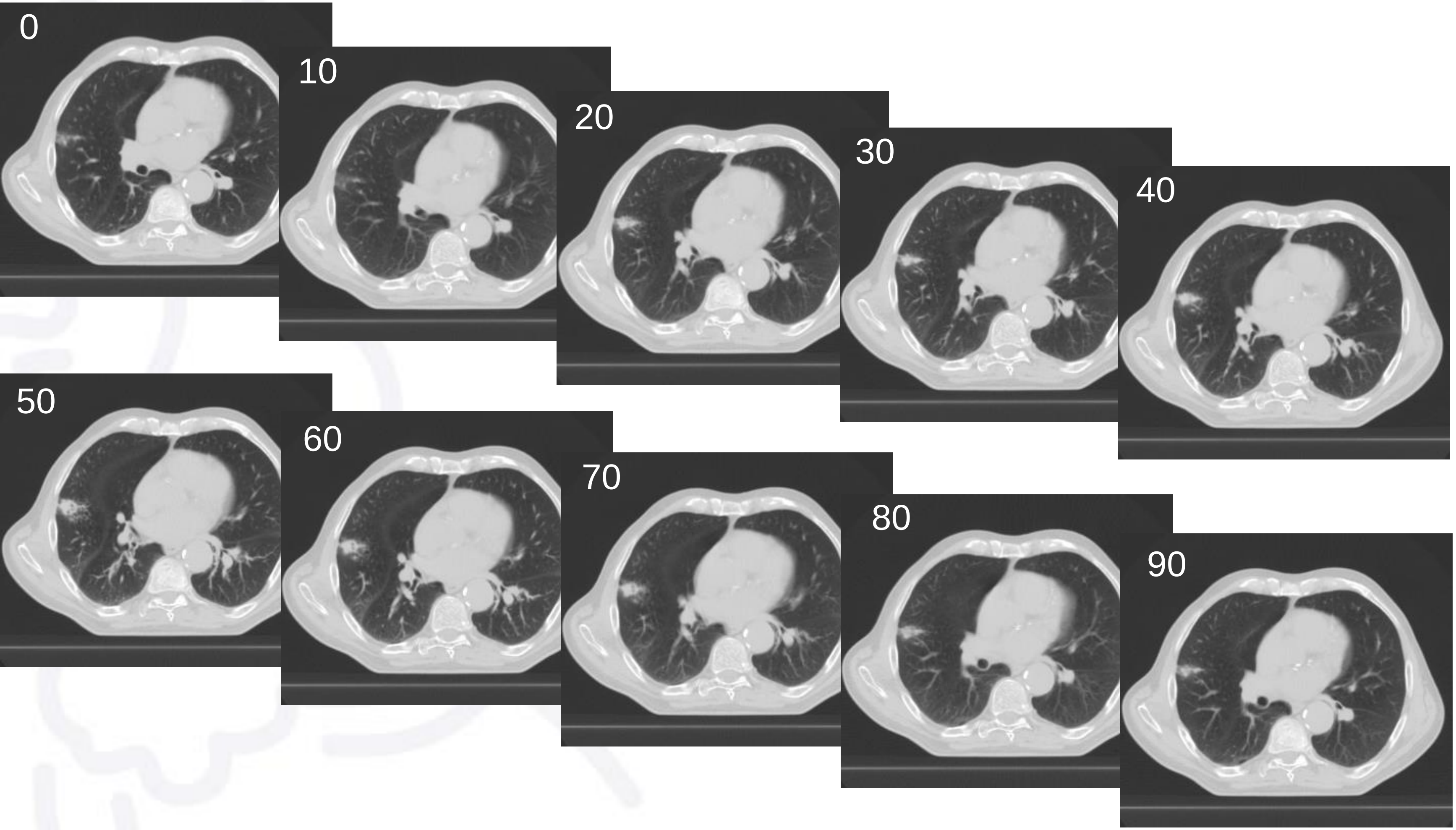
0
10
20
30
40
50
60
70
80
90

- How to define a target on a 4D CT scan

Target definition on a 4D CT scan

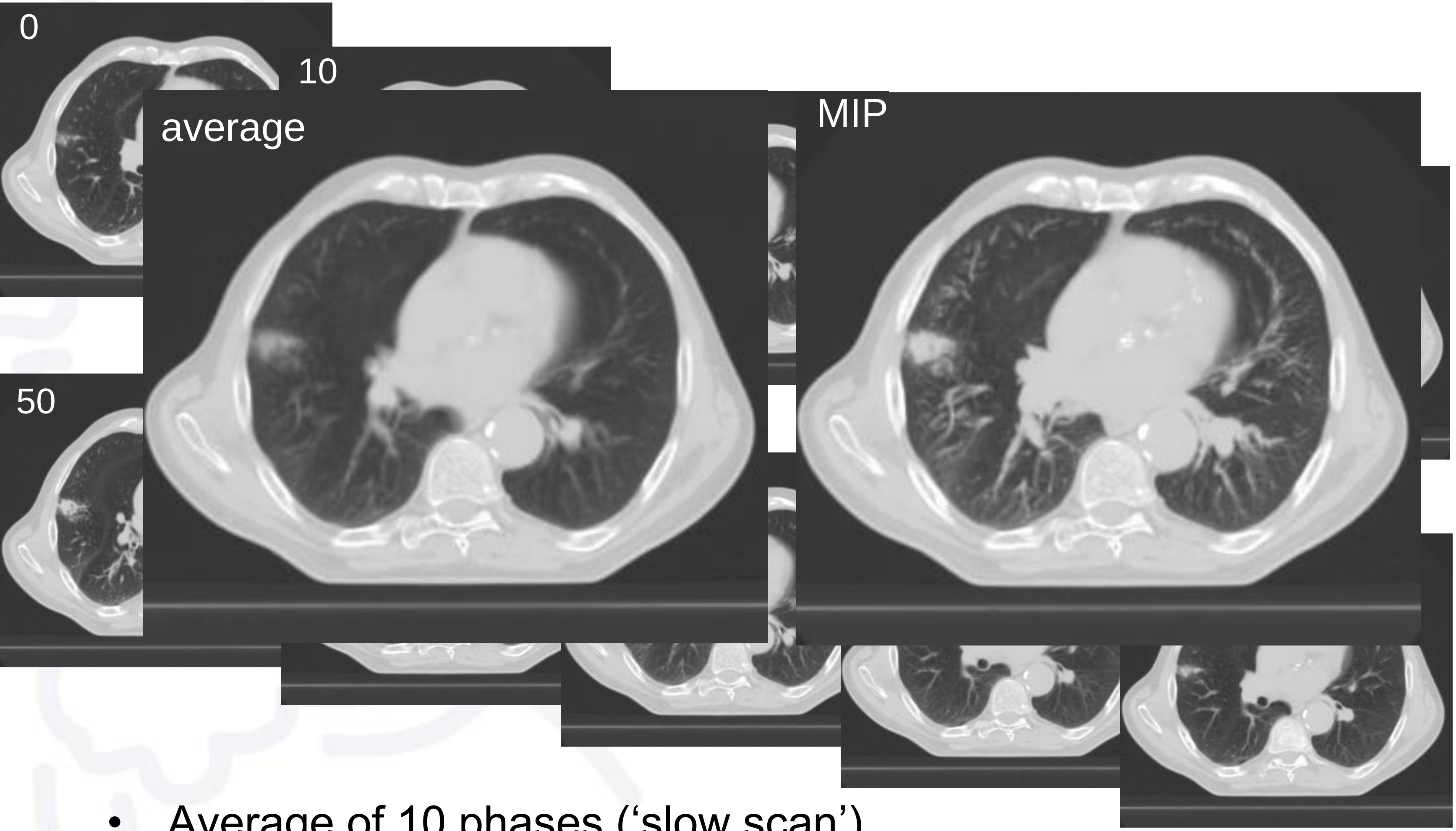
0
10
average
MIP
50

- Average of 10 phases (‘slow scan’)
- Maximum intensity projection of all phases

Internal Target Volume (ITV)

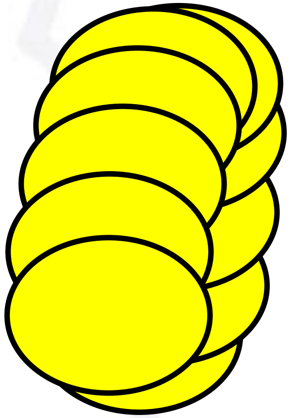

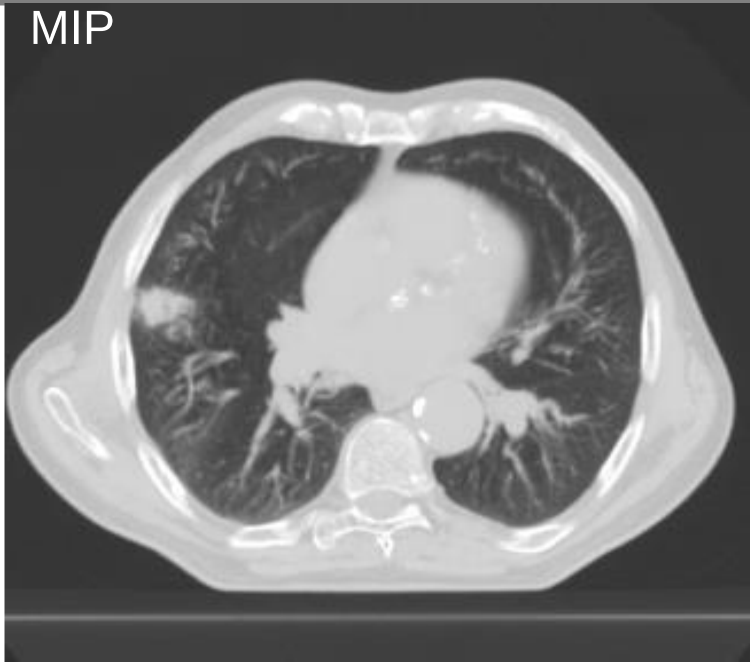

ITV is the combination of all volumes of all phases

= volume as shown on MIP

Internal Target Volume (ITV)

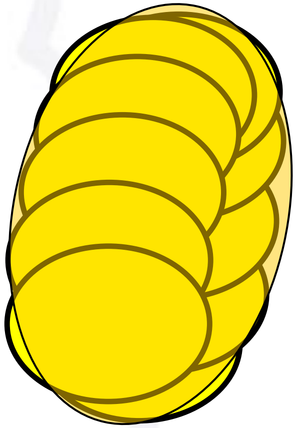

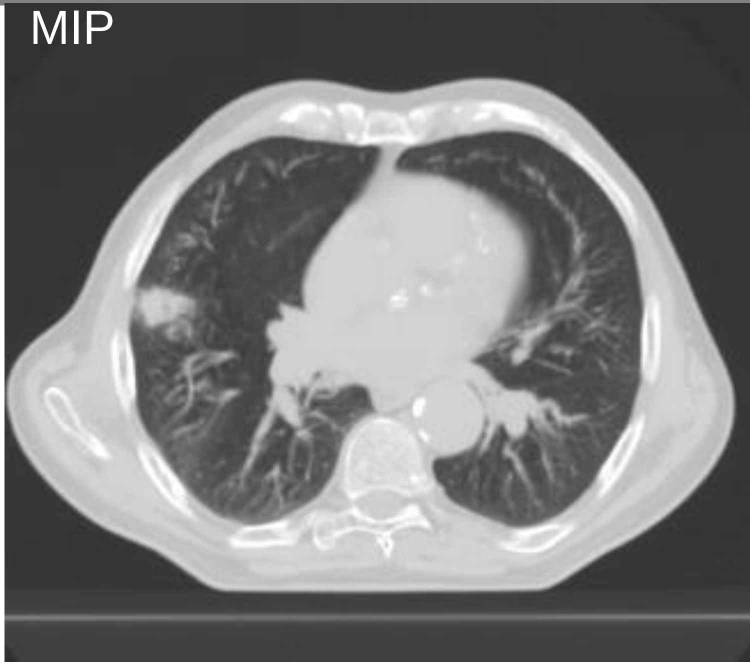

ITV is the combination of all volumes of all phases

= volume as shown on MIP

Internal Target Volume (ITV)

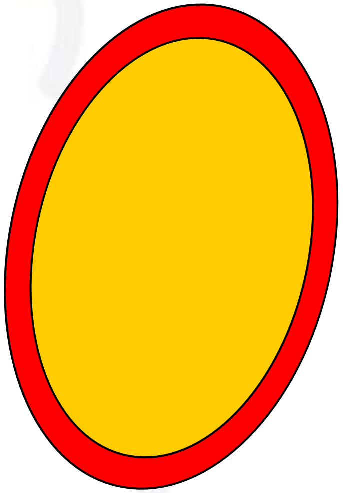

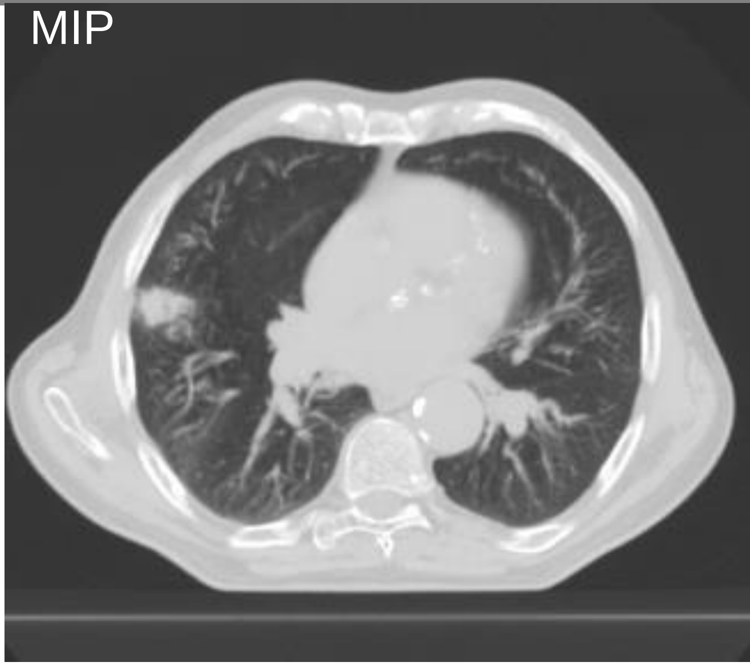

ITV is the combination of all volumes of all phases

= volume as shown on MIP

- Radiation treatment is possible during free breathing
- A PTV margin surrounds the ITV for delivery uncertainties

Maximum exhale phase

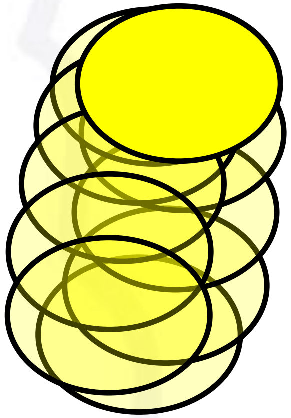

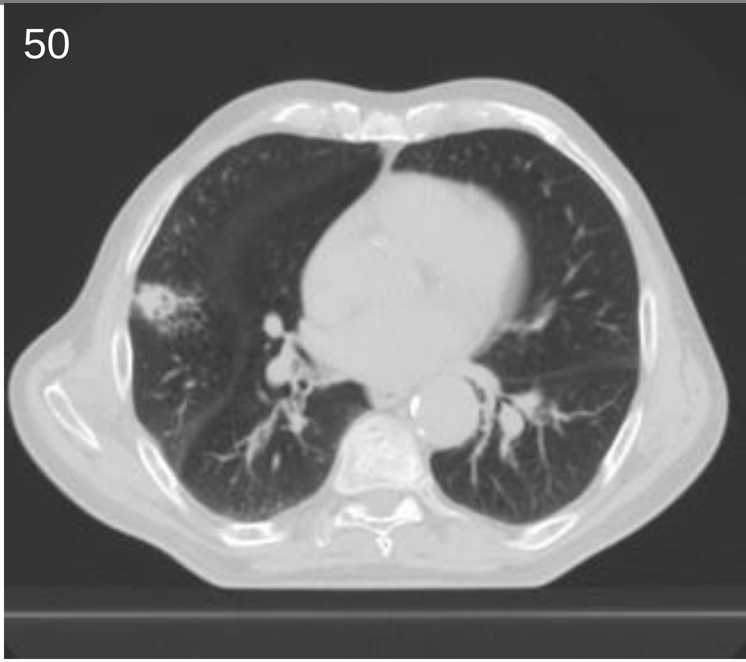

- GTV is the tumor as shown in a single phase; maximum exhale is most reproducible

Maximum exhale phase

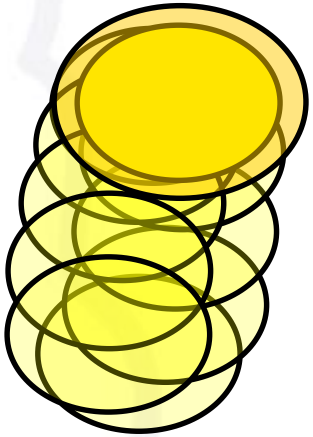

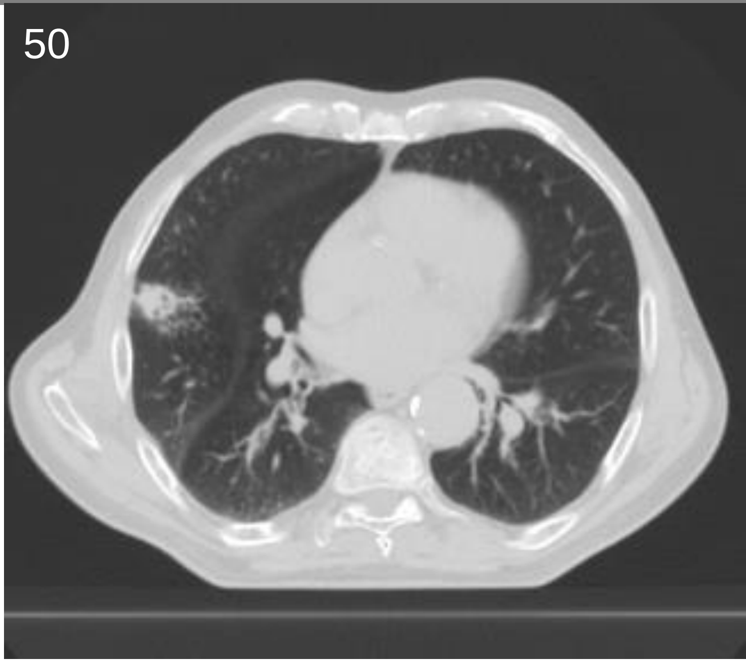

- GTV is the tumor as shown in a single phase; maximum exhale is most reproducible
- ITV is added to account for residual motion

Maximum exhale phase

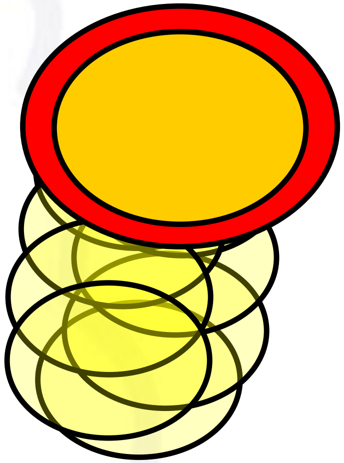

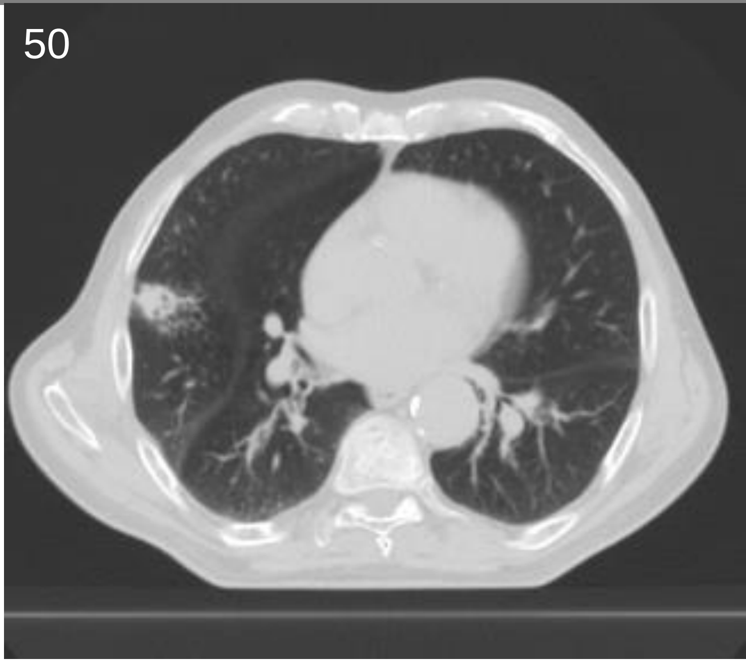

- GTV is the tumor as shown in a single phase; maximum exhale is most reproducible
- ITV is added to account for residual motion
- Gating is required: radiation treatment must be done during breath hold at maximum exhale; A PTV margin surrounds the ITV for delivery uncertainties

Mid-Ventilation scan

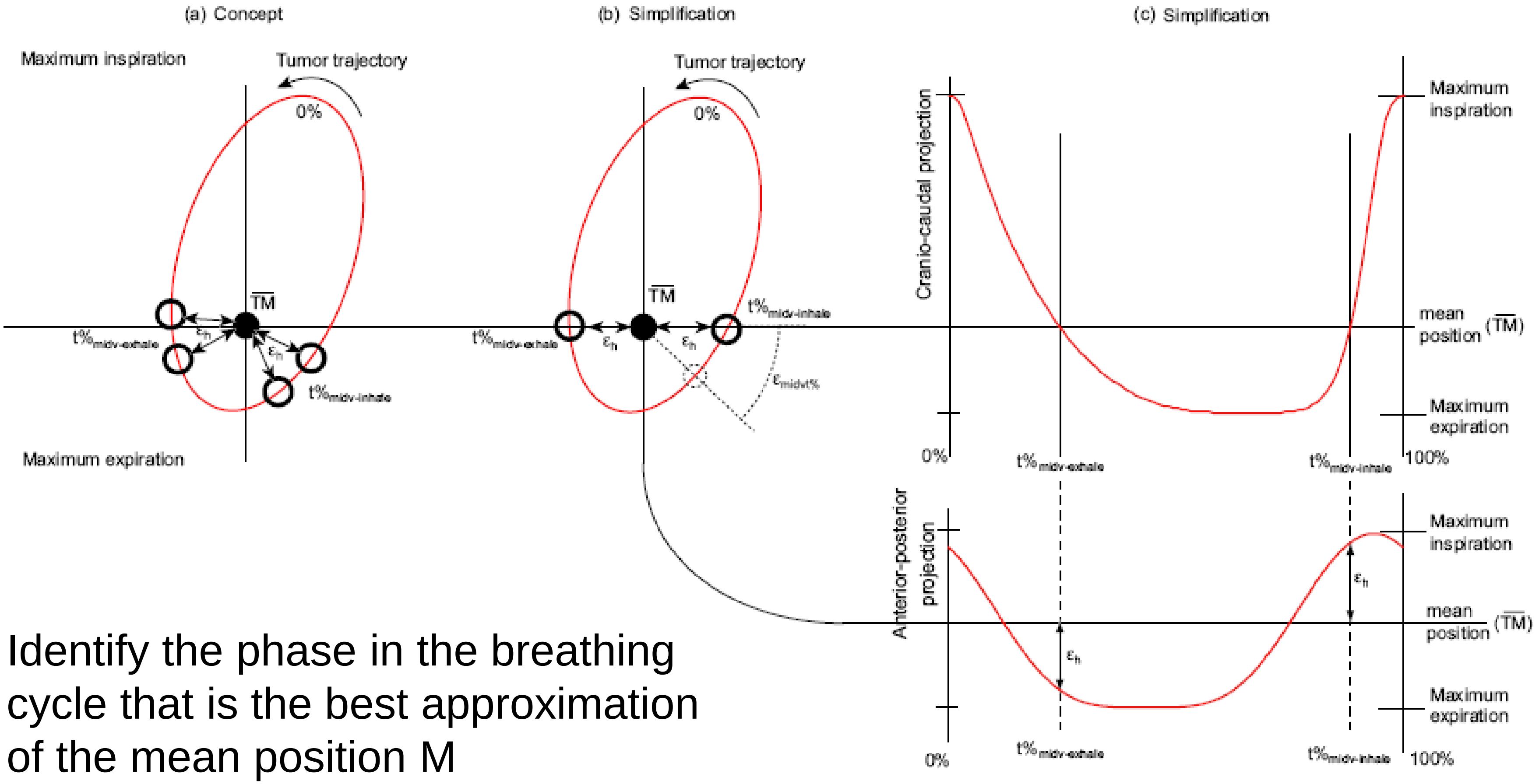
(a) Concept
Maximum inspiration
Tumor trajectory
0%
$\overline{TM}$
$t\%_{midv-exhale}$
ε_h
ε_h
$t\%_{midv-inhale}$
Maximum expiration
(b) Simplification
Tumor trajectory
0%
$\overline{TM}$
$t\%_{midv-inhale}$
$t\%_{midv-exhale}$
ε_h
ε_h
$\varepsilon_{midvt\%}$
(c) Simplification
Cranio-caudal projection
Maximum inspiration
mean position $(\overline{TM})$
Maximum expiration
0%
$t\%_{midv-exhale}$
$t\%_{midv-inhale}$
100%
Anterior-posterior projection
Maximum inspiration
ε_h
mean position $(\overline{TM})$
ε_h
Maximum expiration
0%
$t\%_{midv-exhale}$
$t\%_{midv-inhale}$
100%

Identify the phase in the breathing cycle that is the best approximation of the mean position M

Wolthaus et al. 2006. Int J Radiat Oncol Biol Phys. 65:1560-1571

Mid-Ventilation scan

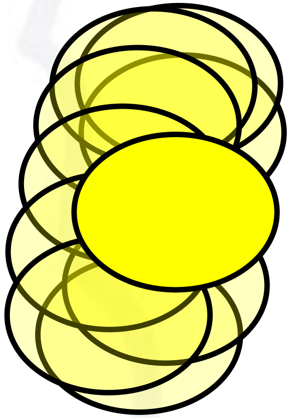

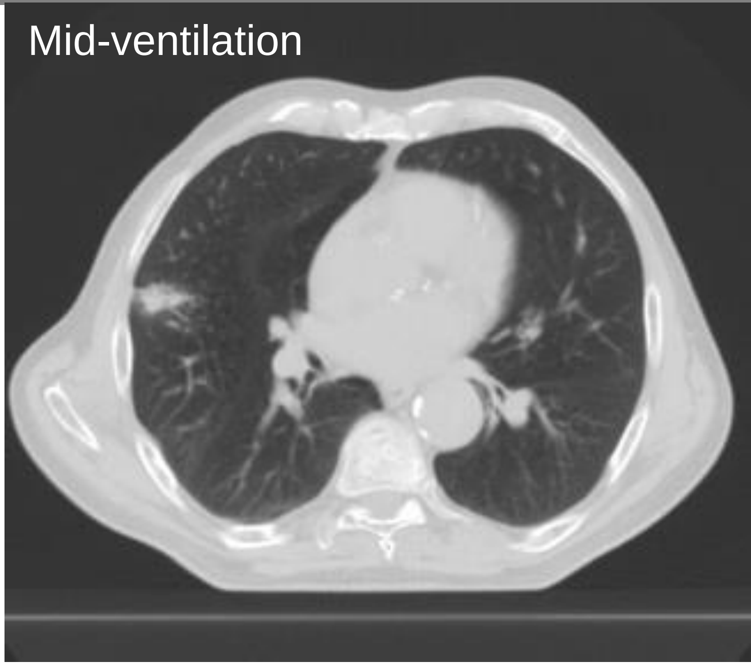

- GTV is defined on the mid-ventilation phase (phase closest to the mean position of the tumor)

Wolthaus et al. 2006. Int J Radiat Oncol Biol Phys. 65:1560-1571

Mid-Ventilation scan

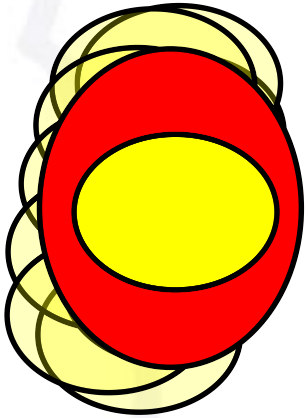

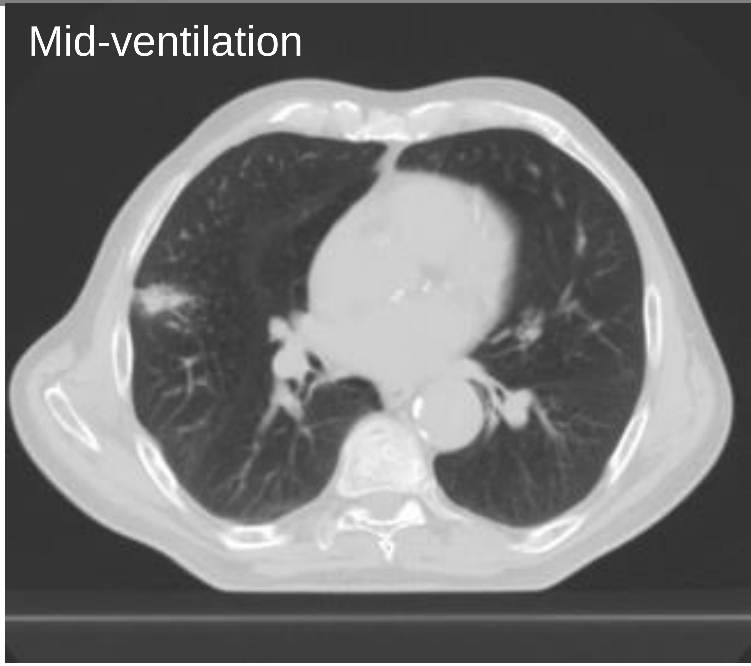

- GTV is defined on the mid-ventilation phase (phase closest to the mean position of the tumor)
- Radiation treatment is possible during free breathing
- A PTV margin surrounds the GTV for delivery uncertainties and breathing

Wolthaus et al. 2006. Int J Radiat Oncol Biol Phys. 65:1560-1571

Different PTV STRATEGIES

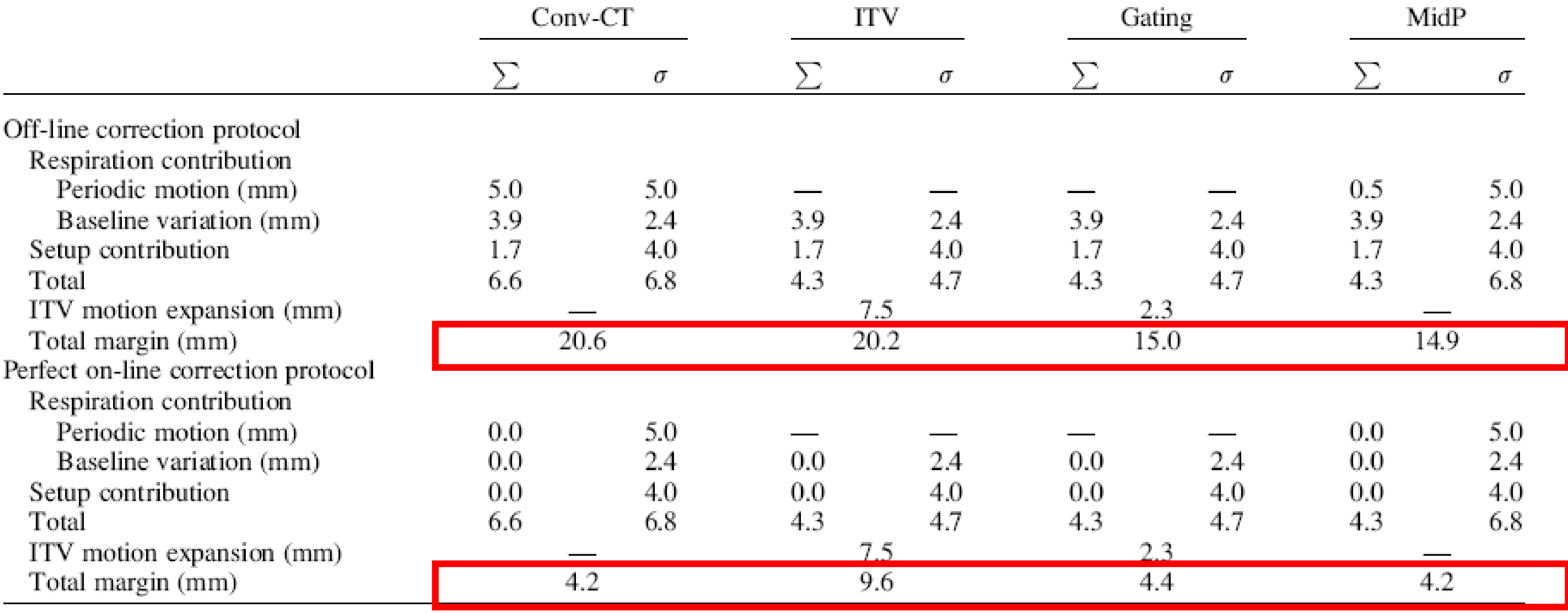

	Conv-CT		ITV		Gating		MidP	
	Σ	σ	Σ	σ	Σ	σ	Σ	σ
Off-line correction protocol								
Respiration contribution								
Periodic motion (mm)	5.0	5.0	—	—	—	—	0.5	5.0
Baseline variation (mm)	3.9	2.4	3.9	2.4	3.9	2.4	3.9	2.4
Setup contribution	1.7	4.0	1.7	4.0	1.7	4.0	1.7	4.0
Total	6.6	6.8	4.3	4.7	4.3	4.7	4.3	6.8
ITV motion expansion (mm)	—		7.5		2.3		—	
Total margin (mm)	20.6		20.2		15.0		14.9	
Perfect on-line correction protocol								
Respiration contribution								
Periodic motion (mm)	0.0	5.0	—	—	—	—	0.0	5.0
Baseline variation (mm)	0.0	2.4	0.0	2.4	0.0	2.4	0.0	2.4
Setup contribution	0.0	4.0	0.0	4.0	0.0	4.0	0.0	4.0
Total	6.6	6.8	4.3	4.7	4.3	4.7	4.3	6.8
ITV motion expansion (mm)	—		7.5		2.3		—	
Total margin (mm)	4.2		9.6		4.4		4.2	

- Off-line correction: based on bony anatomy
  - large margins required to account for baseline variation
- On-line correction: based on image of tumor

Wolthaus et al. 2008. Int J Radiat Oncol Biol Phys. 70:1229-1238

Different PTV STRATEGIES

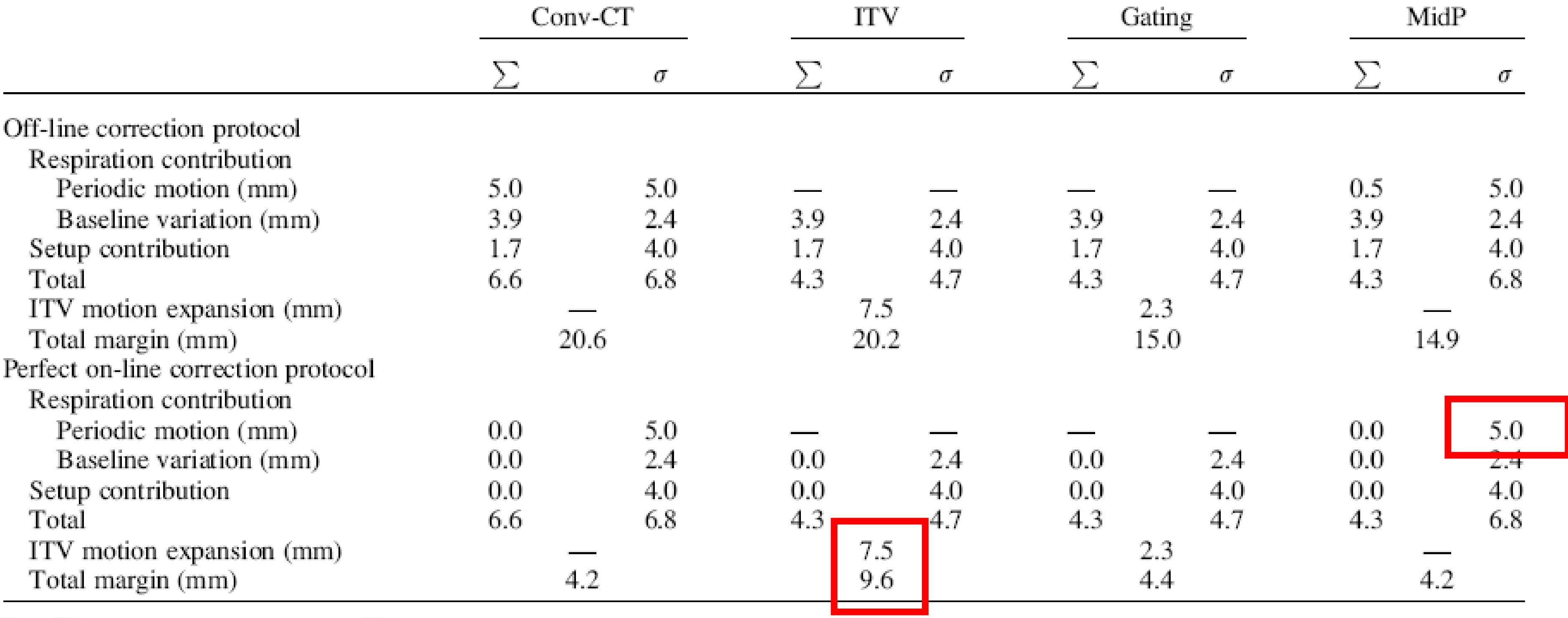

	Conv-CT		ITV		Gating		MidP	
	$\sum$	σ	$\sum$	σ	$\sum$	σ	$\sum$	σ
Off-line correction protocol								
Respiration contribution								
Periodic motion (mm)	5.0	5.0	—	—	—	—	0.5	5.0
Baseline variation (mm)	3.9	2.4	3.9	2.4	3.9	2.4	3.9	2.4
Setup contribution	1.7	4.0	1.7	4.0	1.7	4.0	1.7	4.0
Total	6.6	6.8	4.3	4.7	4.3	4.7	4.3	6.8
ITV motion expansion (mm)	—		7.5		2.3		—	
Total margin (mm)	20.6		20.2		15.0		14.9	
Perfect on-line correction protocol								
Respiration contribution								
Periodic motion (mm)	0.0	5.0	—	—	—	—	0.0	5.0
Baseline variation (mm)	0.0	2.4	0.0	2.4	0.0	2.4	0.0	2.4
Setup contribution	0.0	4.0	0.0	4.0	0.0	4.0	0.0	4.0
Total	6.6	6.8	4.3	4.7	4.3	4.7	4.3	6.8
ITV motion expansion (mm)	—		7.5		2.3		—	
Total margin (mm)	4.2		9.6		4.4		4.2	

- Off-line correction: based on bony anatomy
  - large margins required to account for baseline variation
- On-line correction: based on image of tumor
  - ITV motion expansion is much larger than the respiratory contribution in the margin for MidVentilation and gating

Impact of motion on dose

- Dose deposition in lung tumors is influenced by variations in electron density
- What happens to the dose if a tumor moves?
- Is a dose calculation per breathing phase necessary?

Impact of tumor motion on dose distribution

Dose moves with tumor

Plans based on ITV, with 0 mm margin

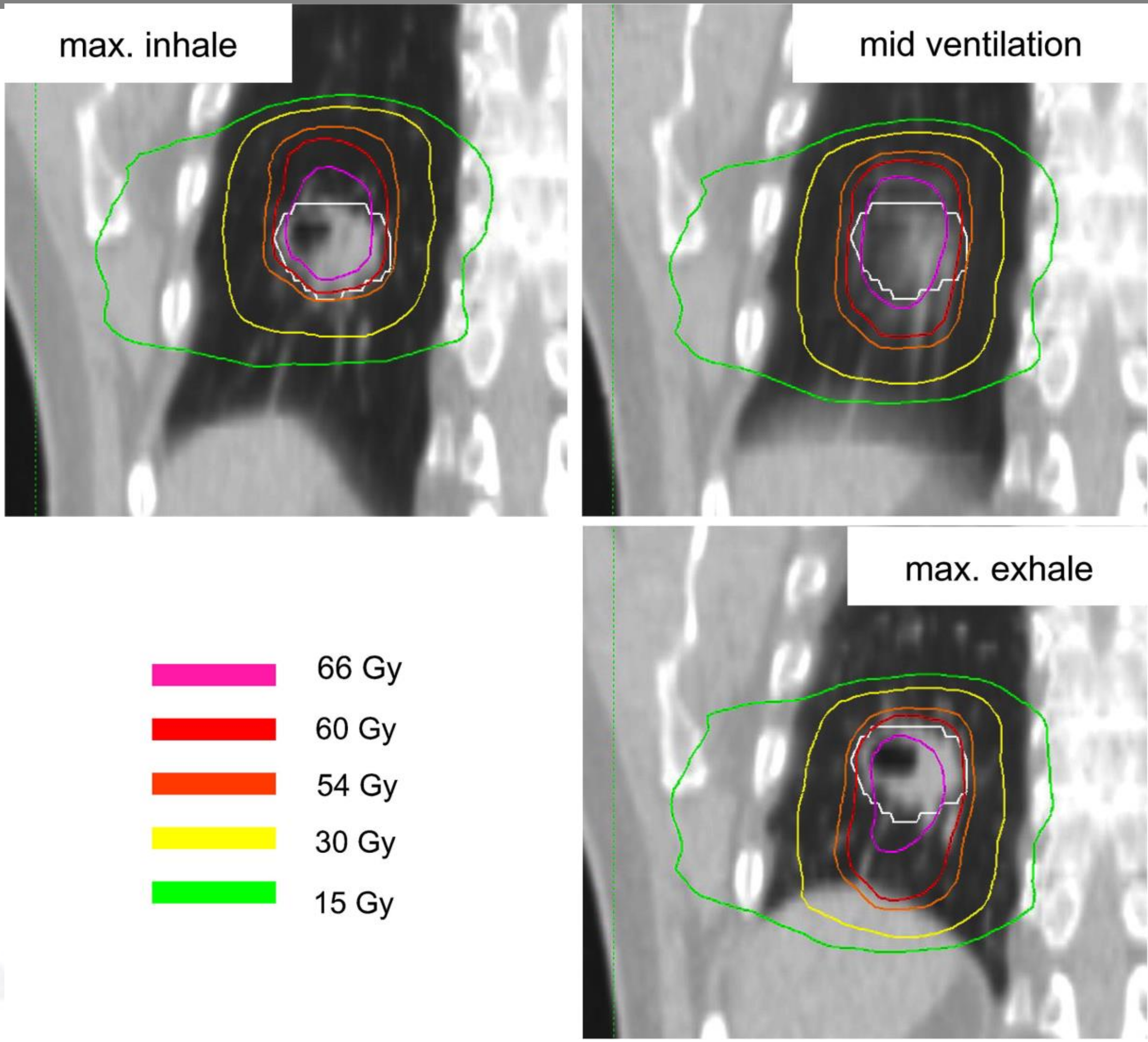
max. inhale
mid ventilation
max. exhale
66 Gy
60 Gy
54 Gy
30 Gy
15 Gy

Admiraal et al. 2008; Radiother Oncol 86:55-60

Impact of tumor motion on accumulated dose is very small

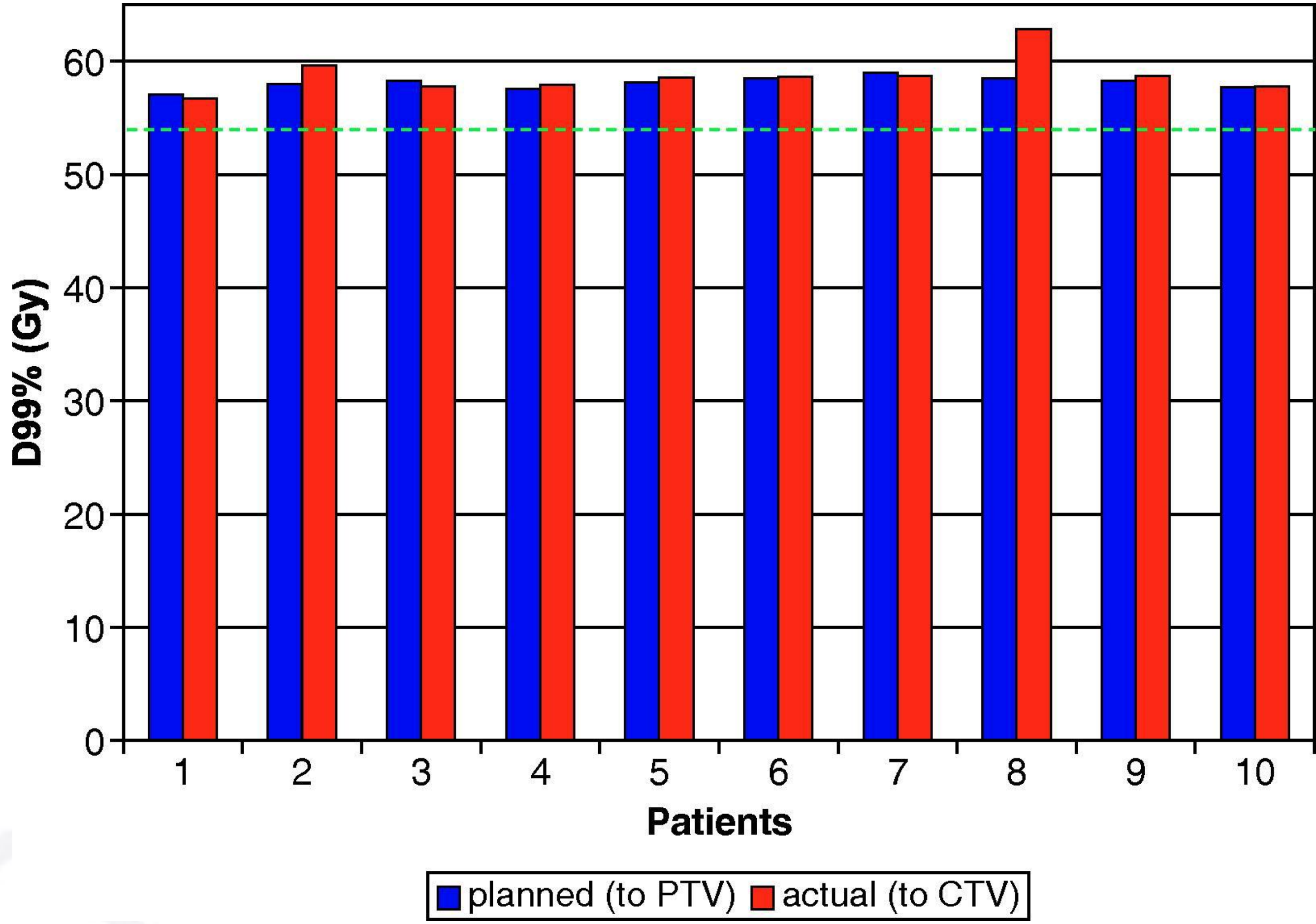

- Planned dose to 99% of the PTV
- Accumulated dose to 99% of the CTV, considering tumor motion

Admiraal et al. 2008; Radiother Oncol 86:55-60

From 4D CT to 3D Planning CT

4D CT

Detect Local Motion Vector field

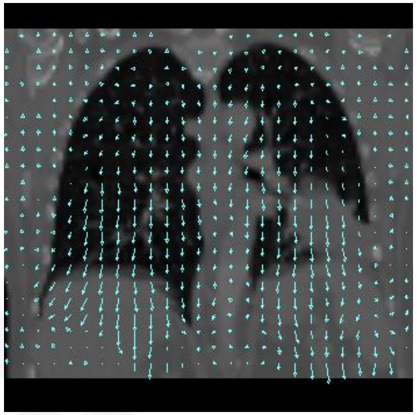

Reposition Motion vector field to average (MidP)

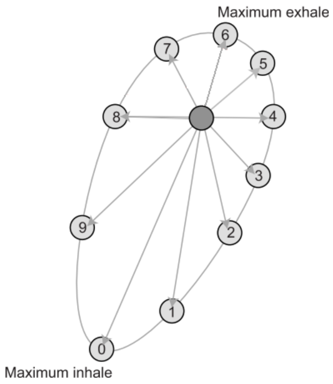
Maximum exhale
6
7
5
8
4
3
9
2
1
0
Maximum inhale

Deformation of CT to MidP

CT based Mid-Position PET

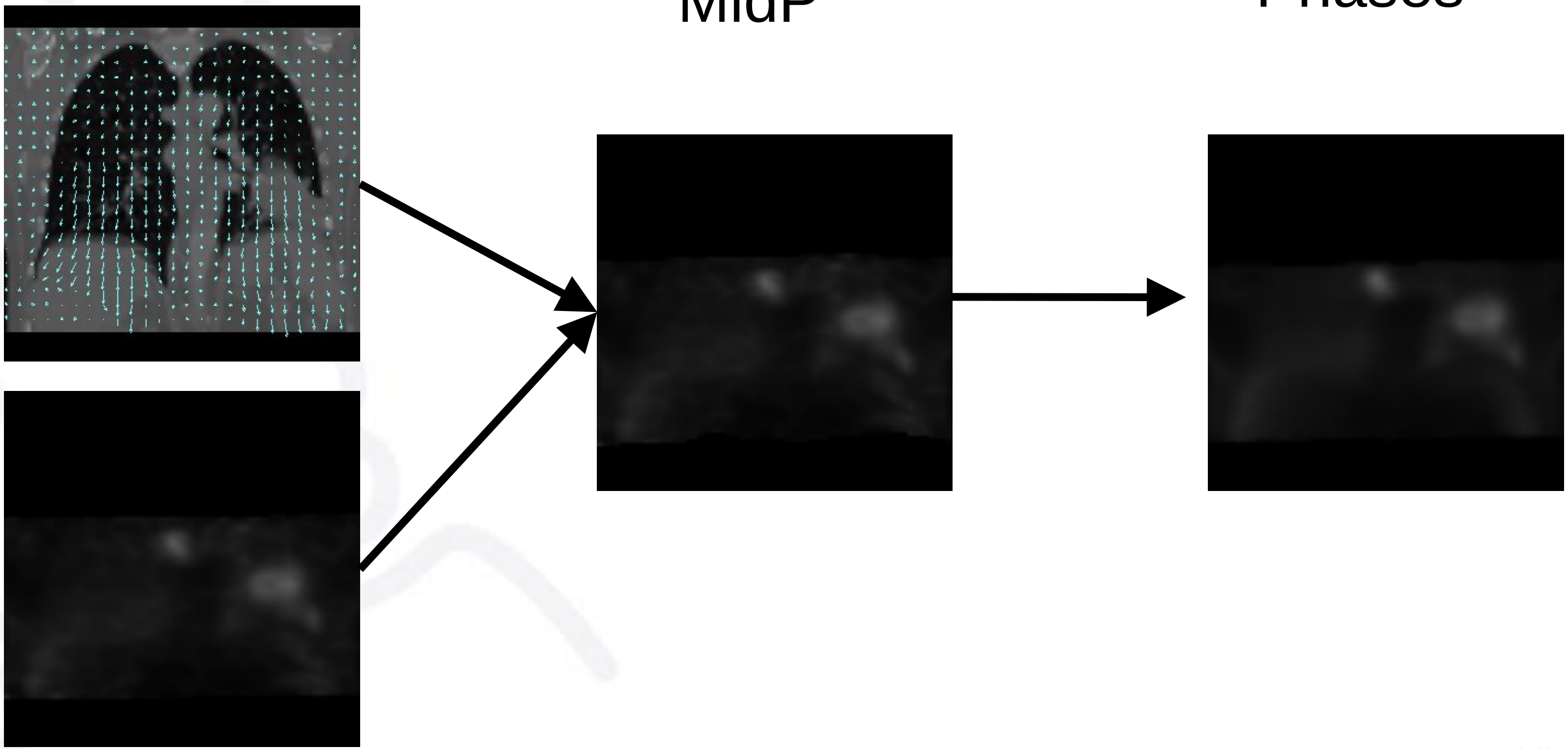

Motion detection in 4D CT

Deformation of 4D PET to CT MidP

Average of Respiration Phases

Courtesy Matthijs Kruis

From 4D PET to 3D Planning PET

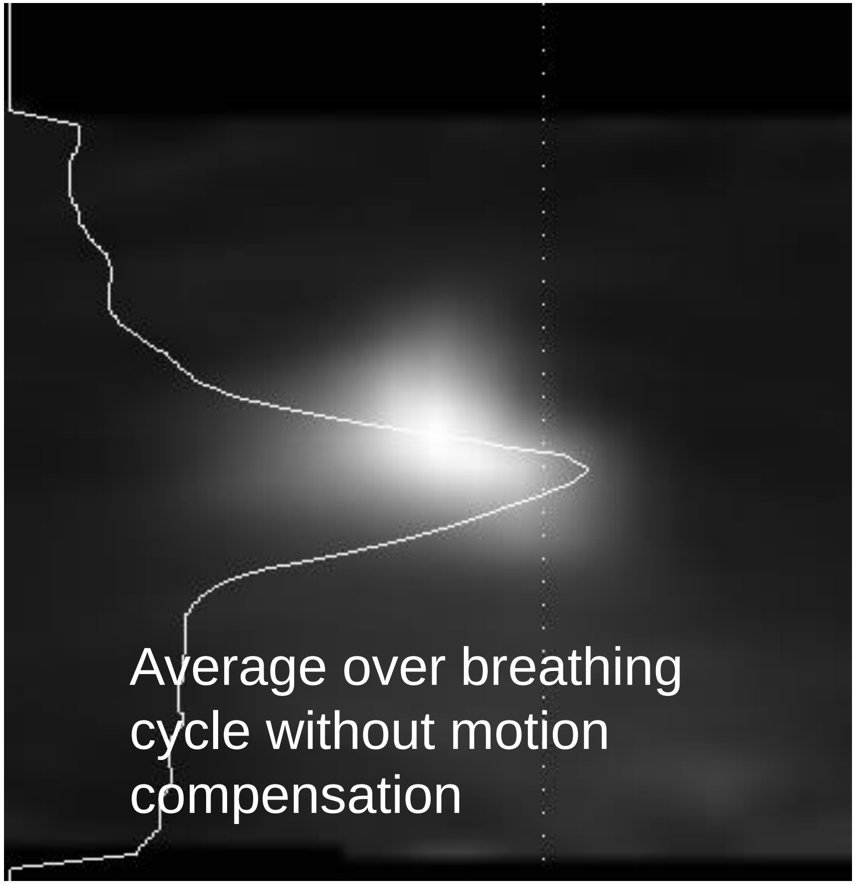

Average over breathing cycle without motion compensation

From 4D PET to 3D Planning PET

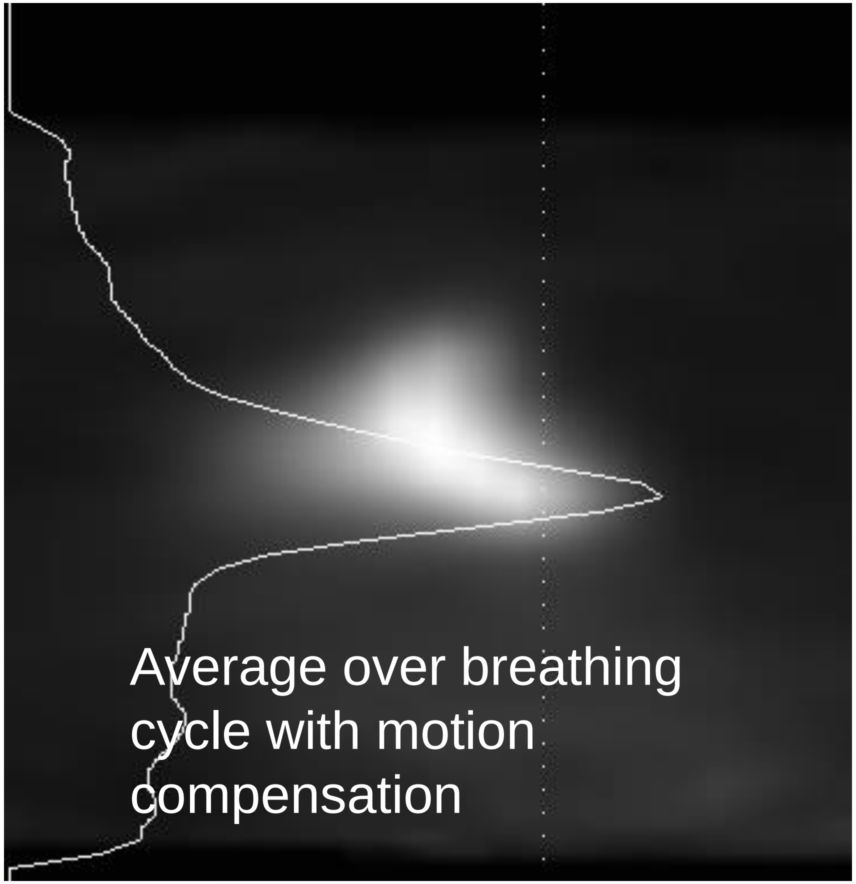

Average over breathing cycle with motion compensation

Use of in-room imaging for position verification

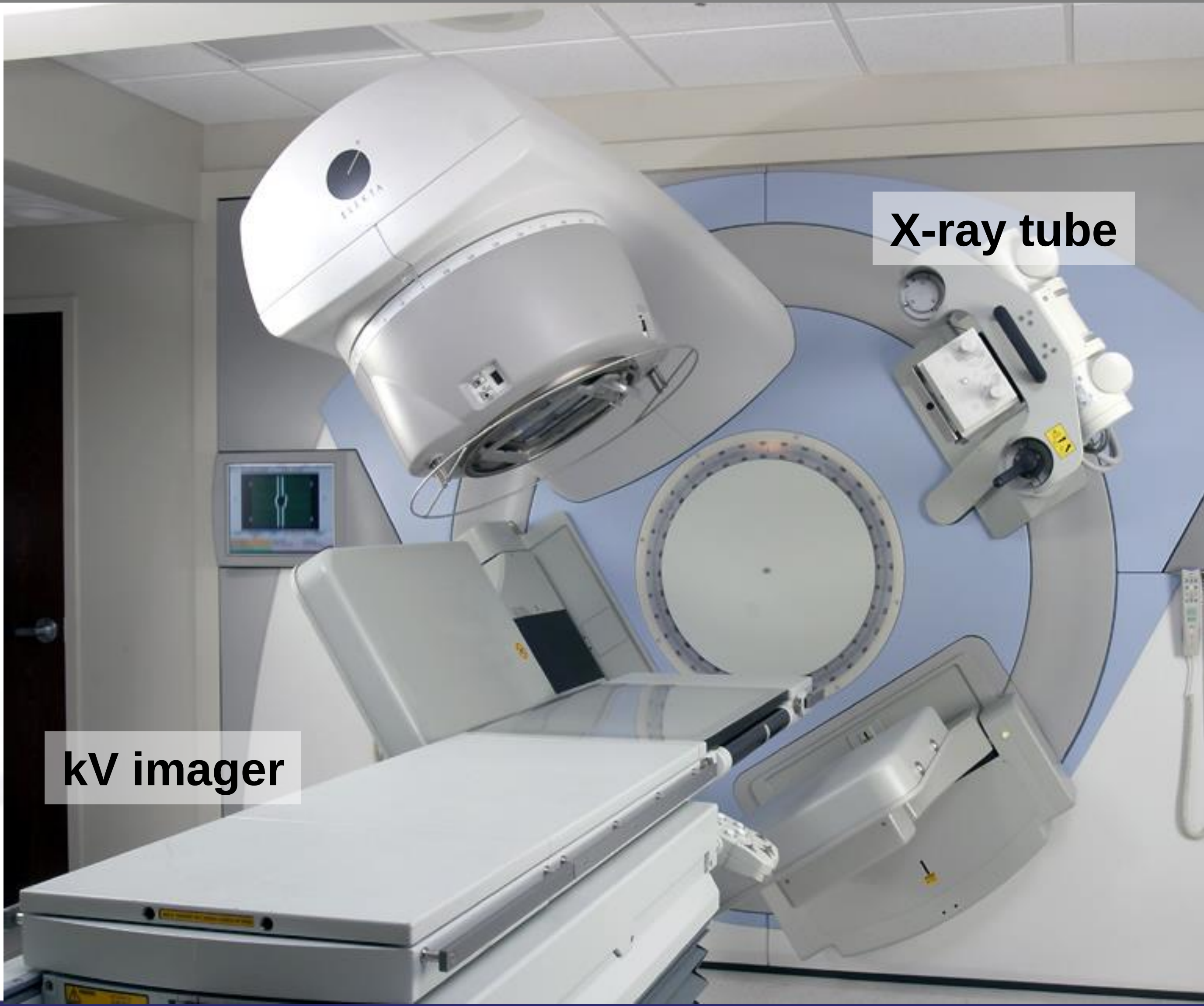

X-ray tube
kV imager

Baseline shifts

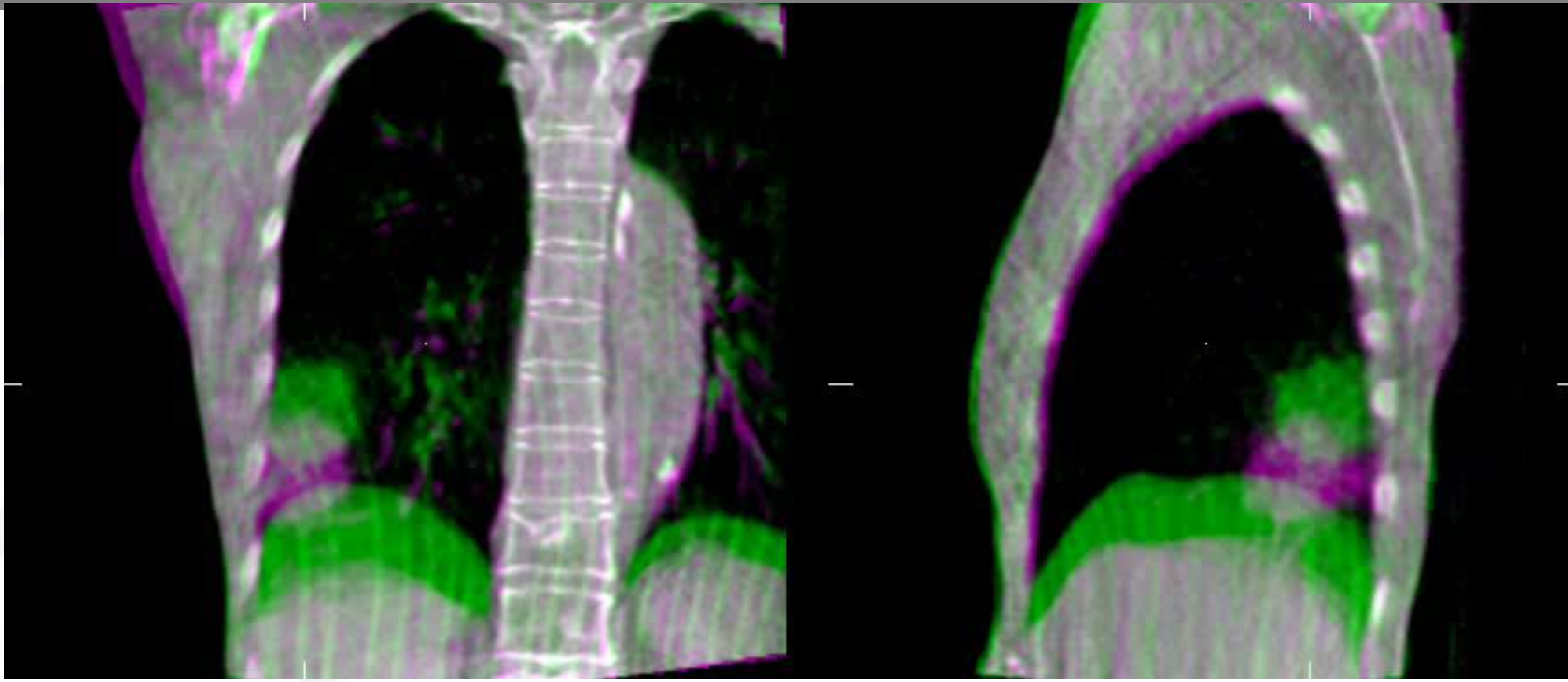

Two subsequent CBCT scans

- Good registration of bony anatomy
- Large displacement of average tumor position, close to diaphragm

Intra-fraction displacement of bone and tumor

- Displacement of tumor during treatment (40 minutes) can be up to 6 mm
- Part of this is due to motion of the patient’s bony anatomy
- Part is due to base-line shift
- Correlation is high in L-R direction, poorer in other directions

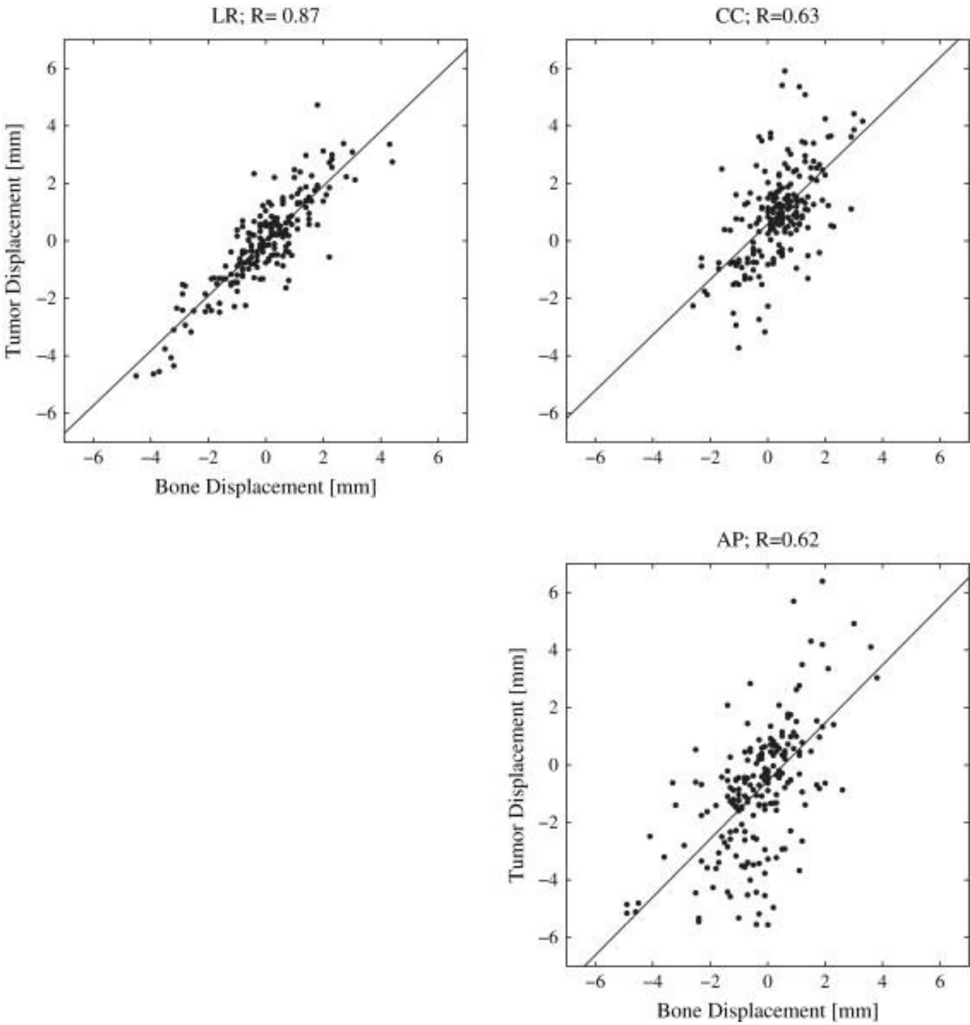

Sonke et al. 2008. Int J Radiat Oncol Biol Phys. 74:567-574

SBRT Lung protocol at NKI-AVL

- Acquire 4D CT scan
- Select mid-ventilation phase:
  Element of 4D scan closest to mid-position
- Optimize treatment plan on mid-ventilation

Planning

- Acquire 4D CBCT
- Bone match →Tumor match
- Apply correction
- Validate correction with 2nd scan
- Contact physician if
  - Shift > 1 cm
  - Anatomical changes

Treatment

SBRT lung: first scan (4 min for 4D)

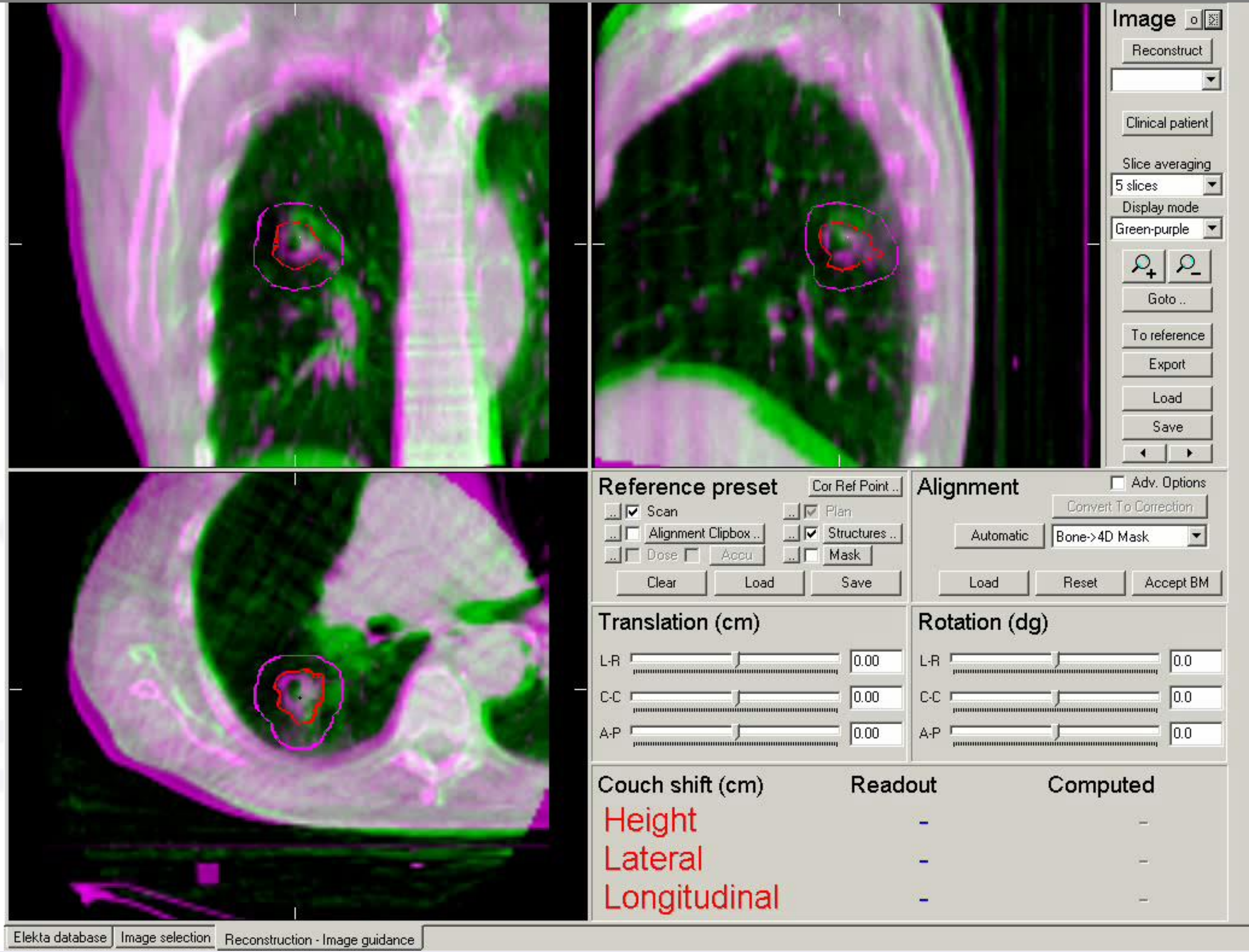

Slice averaging: 5 slices

Display mode: Green-purple

Reference preset

☑ Scan
☐ Alignment Clipbox ..
☐ Dose ☐ Accu
☑ Plan
☑ Structures ..
☐ Mask

Alignment

☐ Adv. Options

Bone->4D Mask

Translation (cm)

L-R 0.00
C-C 0.00
A-P 0.00

Rotation (dg)

L-R 0.0
C-C 0.0
A-P 0.0

Couch shift (cm)	Readout	Computed
Height	-	-
Lateral	-	-
Longitudinal	-	-

Image
Reconstruct
Clinical patient
Goto ..
To reference
Export
Load
Save
Cor Ref Point ..
Clear
Load
Save
Convert To Correction
Automatic
Load
Reset
Accept BM
Elekta database
Image selection
Reconstruction - Image guidance

SBRT lung: matched on bone

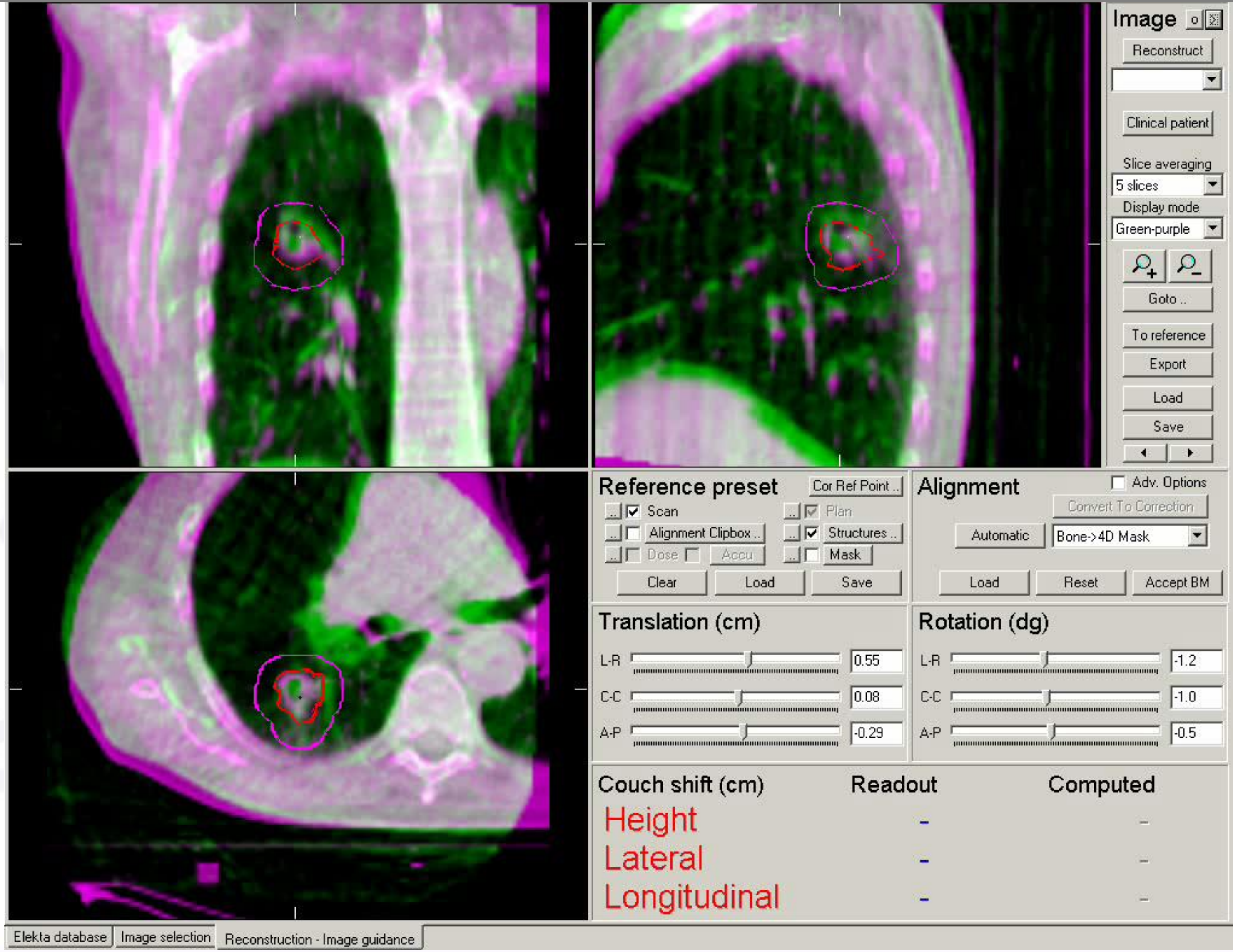
Image
Reconstruct
Clinical patient
Goto ..
To reference
Export
Load
Save
Cor Ref Point ..
Clear
Load
Save
Convert To Correction
Automatic
Load
Reset
Accept BM
Elekta database
Image selection
Reconstruction - Image guidance

Slice averaging: 5 slices

Display mode: Green-purple

Reference preset

☑ Scan
☐ Alignment Clipbox ..
☐ Dose ☐ Accu
☑ Plan
☑ Structures ..
☐ Mask

Alignment

☐ Adv. Options

Bone->4D Mask

	Translation (cm)	Rotation (dg)
L-R	0.55	-1.2
C-C	0.08	-1.0
A-P	-0.29	-0.5

Couch shift (cm)	Readout	Computed
Height	-	-
Lateral	-	-
Longitudinal	-	-

SBRT lung: matched on tumor

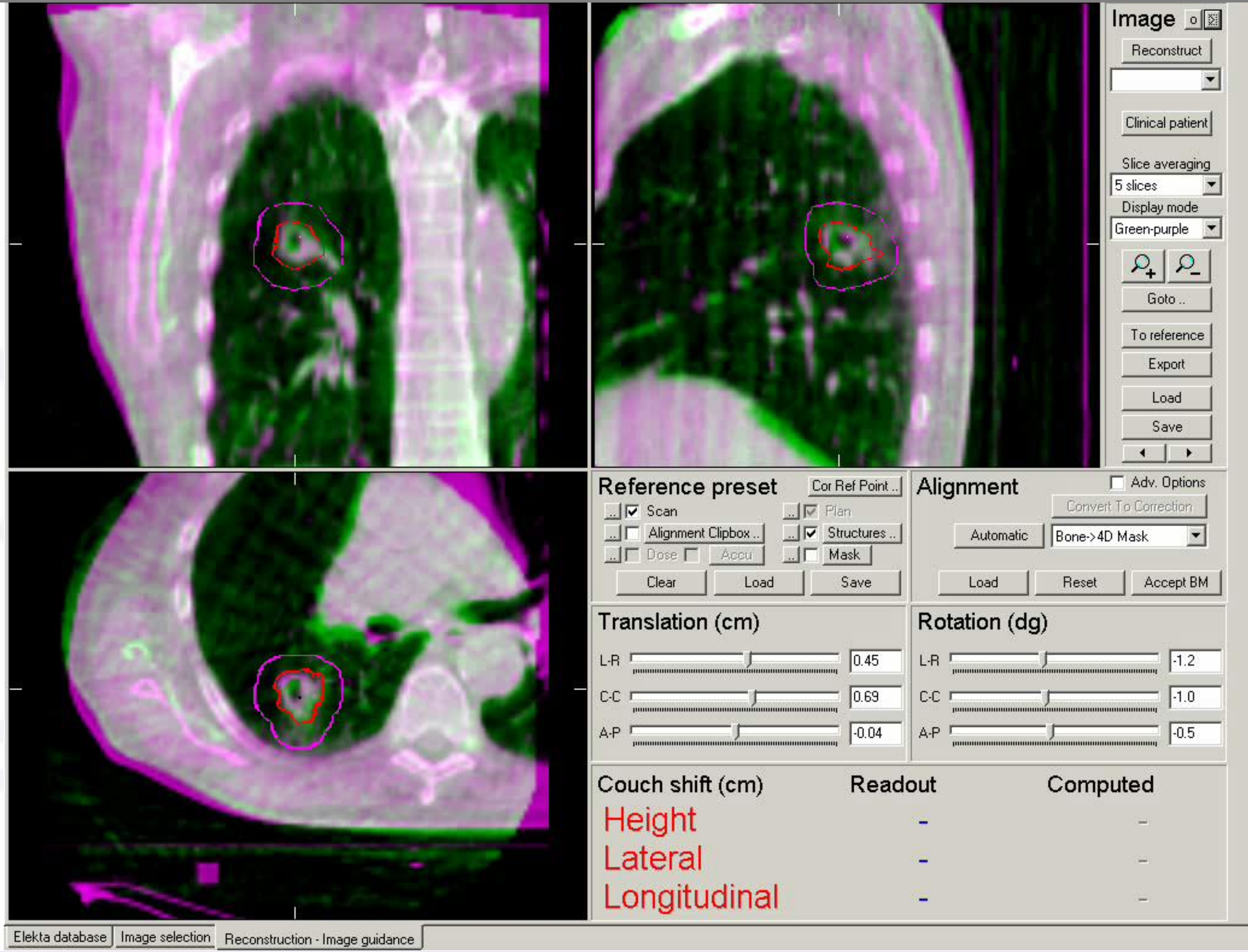
Image
Reconstruct
Clinical patient
Goto ..
To reference
Export
Load
Save
Cor Ref Point ..
Convert To Correction
Automatic
Clear
Load
Save
Load
Reset
Accept BM
Elekta database
Image selection
Reconstruction - Image guidance

Slice averaging: 5 slices

Display mode: Green-purple

Reference preset

- ☑ Scan
- ☐ Alignment Clipbox ..
- ☐ Dose ☐ Accu
- ☑ Plan
- ☑ Structures ..
- ☐ Mask

Alignment

☐ Adv. Options

Bone->4D Mask

Translation (cm)	
L-R	0.45
C-C	0.69
A-P	-0.04

Rotation (dg)	
L-R	-1.2
C-C	-1.0
A-P	-0.5

Couch shift (cm)	Readout	Computed
Height	-	-
Lateral	-	-
Longitudinal	-	-

Geometrical uncertainties

59 Patients, 3 fractions per patient

		LR (mm)	CC (mm)	AP (mm)
Residual Inter-fraction	GM	0.2	0.6	-0.6
	Σ	0.8	0.8	1.0
	σ	1.1	1.1	1.4
Intra-fraction	GM	0.0	1.0	-0.9
	Σ	1.2	1.3	1.9
	σ	1.2	1.4	1.7

Geometrical uncertainties

59 Patients, 3 fractions per patient

		LR (mm)	CC (mm)	AP (mm)
Residual Inter-fraction	GM	0.2	0.6	-0.6
	Σ	0.8	0.8	1.0
	σ	1.1	1.1	1.4
Intra-fraction	GM	0.0	1.0	-0.9
	Σ	1.2	1.3	1.9
	σ	1.2	1.4	1.7

Margins versus amplitude

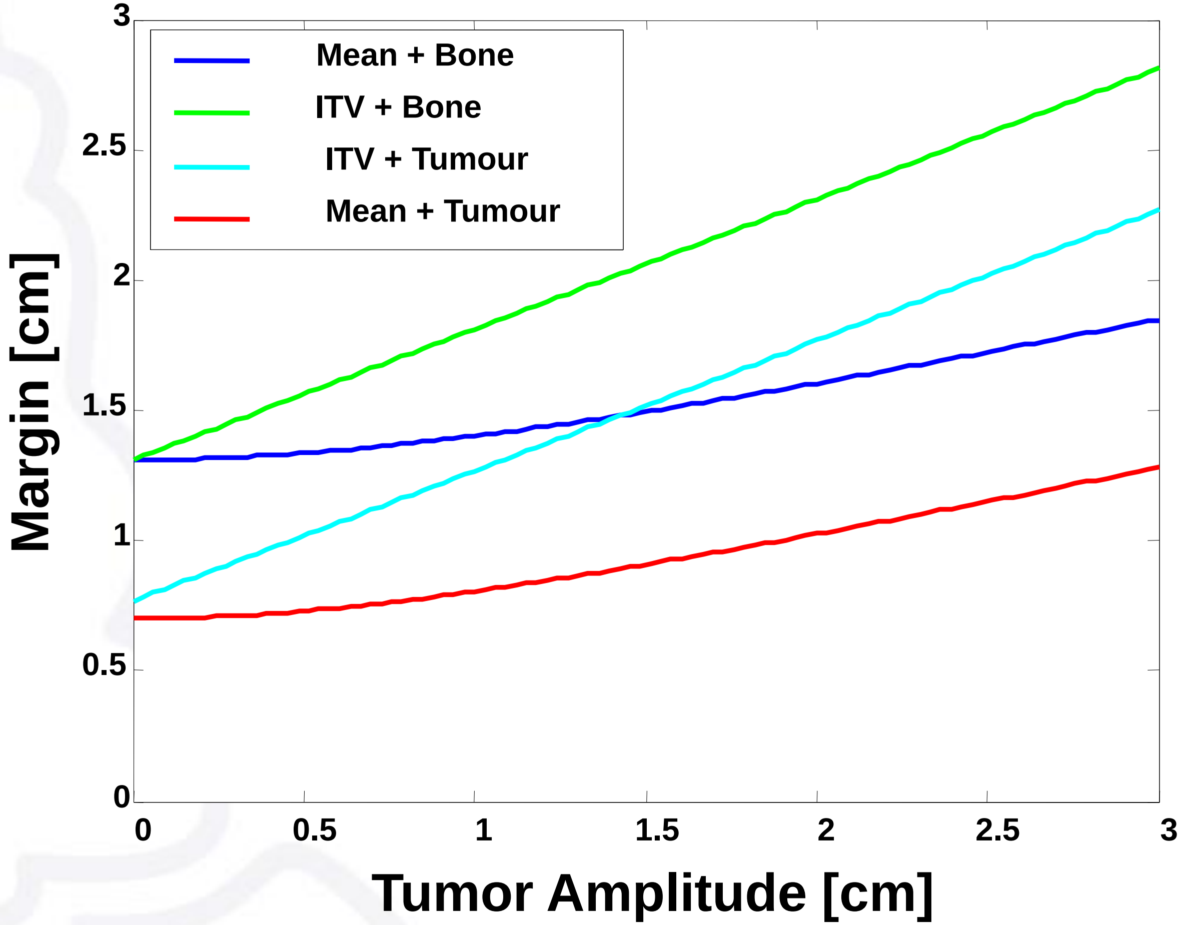

$$M = 2.5\Sigma + 0.84\sqrt{(\sigma_p^2 + \sigma^2)} - 0.84\sigma_p^2 \neq 2.5\Sigma + 0.7\sigma \qquad \sigma_p \approx 6.4 \text{ mm}$$

Assures 80% isodose encompasses GTV 90% of time in lung

Summary

- FDG-PET and CT are the prime imaging modalities in lung cancer

- PET improves the accuracy of staging
  - high negative predictive value for mediastinal lymph nodes

- More consistent contouring is possible with PET-CT
  - volume may increase (include lymph nodes) and decrease (avoid atalectasis)
  - systematic approach to thresholding (e.q. source-to-background ratio)
  - validation with pathology is essential

- 4D imaging CT is required for precise delineation of the tumor and characterizing the extent of motion
  - Tumor motion is not detected directly; surrogates are used

Summary

- Target definition
  - ITV, free breathing
  - Exhale – gating
  - Mid-ventilation, free breathing
- Dose calculation
  - Accurate dose model, also during IMRT/RapidArc optimization
  - In older studies: prescribed dose ≠ actual dose (deviations of up to 30%!)
- Position verification with cone-beam CT allows accurate targeting of the tumor (stereotactic body radiotherapy)

Acknowledgment

- Matthijs Kruis
- Peter Remeijer
- Jochem Wolthaus